INVESTIGATIONS OF A NOVEL PILE AND ANCHORAGE ~~SYSTEM~~ CONCEPT

by

David Joseph French, M.Sc D.I.C. C.Eng

April, 1990

A thesis submitted to the University of London
(Imperial College of Science, Technology and Medicine)

for the degree of
Doctor of Philosophy in the Faculty of Engineering

ABSTRACT

This thesis reports investigations into a new piling and anchorage concept that have taken place at Imperial College over the last four years. This new concept - called the Wedge-Pile - makes use of recent developments in the understanding of pile/soil behaviour in order to improve piling methods and design. The Wedge-Pile concept involves the radial expansion of a pile or anchorage along its length so as to increase the capacity of the pile in a reliable and predictable manner. The Wedge-Pile consists essentially of two components - an outer shell and an expander mandrel. The process consists of first installing the outer shell in the ground and then expanding the outer shell by driving through it the expander mandrel. Various different embodiments of Wedge-Pile are possible, but the underlying principle is the same in each case: expansion takes place locally and progressively, in the form of a wave moving down the outer shell. The key to the process is that the force required to expand a pile in this way is very much less than that required to expand a pile simultaneously over its whole length.

The purpose of the research carried out has been to demonstrate the effectiveness of the Wedge-Pile principle. Investigations using various types of Wedge-Pile have taken place in the field with 6m and 1.5m long piles, and in the laboratory with small scale models. A computer model has been developed in order to investigate theoretically the expansion process. The results of the investigations have shown that the load carrying capacity of a pile or anchorage can be increased many times by expansion. Relatively small expansions are required to achieve most of the gains in capacity possible, and the gains in capacity appear to be permanent with time. The large scale field trials have demonstrated that the Wedge-Pile principle is a practical and efficient method of producing a high performance pile or anchorage in a wide range of soils. It is thought that the load carrying behaviour of Wedge-Piles used in practice would be much more predictable than for conventional piles.

ACKNOWLEDGEMENTS

Firstly, I would like to thank Professor J. B. Burland for giving me the opportunity to work on this novel project, and for financial support during the latter part of my time at Imperial College.

Resources for the project were limited, and determined effort was required for the site work. In this respect, I would like to record my particular thanks to four people: Tim Fitch, Gerwyn Price, Reg Munford, and Brian Johnson.

Tim Fitch stayed on at Imperial College after completing his MSc studies, and assisted in the large scale testing at BRS and in the mini-pile work. His sense of humour lightened otherwise often tedious winter days. Gerwyn Price of the BRS fought through a bureaucratic quagmire to allow the use of BRS equipment and facilities, enabling the initial field trials to get off the ground. Reg Munford of the BRS single-handedly fabricated much of the equipment used in the field trials, and assisted at both of the main test sites. Brian Johnson of W.A. Dawson Ltd. put himself out to help during testing at the Luton site, even though more than fully occupied elsewhere.

I would like to thank past and present researchers of the Soil Mechanics Section of Imperial College, for useful discussions, assistance given to me, and for happy times: Tony Addis, Andrew Bond, Luiz Bressani, Mike Crilly, Rob Day, George Dounias, Teta Georgiannou, Jan Hellings, Nick Mapplebeck, Mike Leddra, Ioanis Lefas, Nigel Legge, Luis Lemos, 'Mac' Maccarini, Mahmoud Mahmoud, Justice Maswaswe, Nick Ninis, Dalmas Nyaoro, Chris Menkiti, Efrain Ovando-Shelley, Deneys Schreiner, Satoru Shibuya, Phil Smith, Theodora Tika, Dave Toll, Najwa Yassir and Richard Young.

I would also like to thank members of the academic staff: Dr R Chandler, Prof. J. Hutchinson, Dr R. Jardine, Dr M.N. Pavlovic, Dr D. Potts, Dr A. Skinner, and Prof. P Vaughan.

The assistance of the following members of the technical staff of the Department of Civil Engineering and the Soil Mechanics Section is appreciated: Steve Ackerley, Alan Bolsher, Eileen Gibbs, Roger Hare, Graham Keefe, Jack Neale, Chris Pitches, and Lou Spall (up the Palace). Thanks also to photographers Richard Packer and Andrew Chipling, librarians Kay Crooks and Jessica Underhill, and to secretary Kathy Evans.

The funding for the trials at BRS and Luton was provided jointly by the

Marine Technology Directorate of SERC and by Conoco (UK). Steel for the piles at these sites was donated by British Steel, and in-situ testing was carried out by Fugro (UK) Ltd. and Cambridge Insitu. W.A. Dawson Ltd. made their yard freely available and provided assistance and plant. The Geotechnics Division of the Building Research Establishment provided testing equipment throughout the trials. The trials at the Hermitage site were funded jointly by Conoco (UK) and by Cementation Piling and Foundations Ltd I am indebted to all these organisations for their assistance and encouragement. Peter Jones of CP&F Ltd. was of great help during the trials at Hermitage.

Finally, I would like to express gratitude to my parents for their support and to my dear friend, Pat Lucas, for her encouragement, advice, and particularly for reading the text of the thesis.

CONTENTS

CHAPTER 1
INTRODUCTION

This thesis reports investigations into a new piling and anchorage concept that have taken place at Imperial College over the last four years. This new concept - called the Wedge-Pile - is an attempt to make use of recent greater understanding of soil behaviour in order to improve piling methods and design. The concept involves the radial expansion of a pile or anchorage along its length in order to increase its shaft capacity in a reliable and predictable manner.

The work reported forms part of a continuing, long-term project. The eventual aim of the project is to make use of the Wedge-Pile concept in practice.

In this introductory Chapter the basic concepts of the Wedge-Pile process and the background soil mechanics theory are set down. The investigations that have been carried out are then outlined.

1.1 Basic Concepts

1.1.1 General background

The investigations concern both PILING PROCESS and PILE DESIGN. It is important to draw distinctions between the two.

Piling process is defined here as the means by which a load carrying member is introduced into the ground. There are many different pile types and installation methods. Piling existed long before the advent of soil mechanics and has evolved essentially on a trial and error basis. Even today, improvements in the understanding of pile behaviour usually follow behind developments in the piling process. Research is typically commissioned to justify existing design methods, rather than to develop new processes.

Pile design is largely an empirical process and is likely to remain so. This is because there are too many variables which are not under the control of the design engineer - the most important of these being the soil and the piling process. Pile-soil interaction behaviour is complicated and difficult to understand, even for homogeneous 'ideal' materials. In reality, soil deposits are highly heterogeneous and pile design must often be made on the basis of limited site

investigation data. The piling process is generally in the hands of the piling contractor, sometimes it is in the hands of individual operators.

Despite the fact that existing piling techniques and design methods will continue to be used successfully in many routine situations, it is important to continue the development of a sound understanding of the fundamental mechanisms of pile-soil behaviour, for two reasons:

(a) So that soundly based design procedures can be developed in order to extrapolate successfully from existing knowledge, when using piles and anchorages in new ground conditions or at a previously untried scale.

(b) So that it is possible to innovate successfully, both in the development of applications for piles and anchorages and in the piling process itself.

New piling processes and design methods based on sound theory should have much to offer. However, there are reasons why there may be resistance to introducing them in practice. For example:

- Cost: even if cost savings can be made in the long term, the time and cost of development work may be prohibitive if short term returns are a priority. Investment might have to be made in new piling plant, when there is already a big investment in traditional plant.

- Natural conservatism: the argument to stick with what has proved successful in the past is a powerful one.

- In the case of pile design, if major variables remain outside the control of the designer, sophisticated theories may be no better than empirical methods.

- In the case of new piling processes, it may not be in the financial interests of the piling contractor (or consultant) to reduce piling costs.

1.1.2 Theoretical Background

The function of a pile or anchorage is to transfer load from a structure into the ground. Load transfer takes place both along the shaft and at the base. The distribution of load between base and shaft will change during pile loading, especially if residual stresses remain after

driving. Shaft resistance is mobilised much more quickly than base resistance, and therefore often dominates at working loads.

The Wedge-Pile is concerned with increasing shaft resistance.

The shaft friction τ_{s_f} acting locally on the face of a pile at failure is given by the basic frictional equation

$$\tau_{s_f} = \sigma_r' \tan\delta' + c_a' \qquad (1.1)$$

where σ_r' is the radial effective stress, δ' is the effective angle of shearing resistance at the pile/soil interface, and c_a' is the effective adhesion intercept, which is usually neglected because of the local remoulding assumed to occur during driving.

δ', σ_r' and hence τ_{s_f} will generally vary along the length of the pile. Average values of shaft friction are more useful for design purposes.

Both δ' and σ_r' will be influenced to a greater or lesser extent by

(a) the soil type and geological history
(b) the type of pile and method of installation
(c) the type of loading prior to and leading up to failure.

These factors are discussed briefly in the next two Sections. Emphasis is placed on the behaviour of driven piles.

1.1.2.1 Factors influencing δ'

(a) Soil type and geological history:
The angle of shearing resistance δ' is a measure of the frictional interaction of the pile surface and the soil immediately surrounding it. This soil will have been intensely sheared and remoulded during pile installation, erasing any previous stress history. Much research has been carried out into interface shearing - recent work at Imperial College is reported in PhD theses by Lemos (1986) and Tika (1989).

In clays, the dominant factor determining shear response is the extent to which the clay particles align. Research has shown that:

- A remoulded sample of clay sheared slowly will exhibit an initial peak value of shear resistance, and then a drop to a residual value as clay particles align. The residual value of angle of interface friction, δ_r', is dependant on the precise type and rate of shearing

undergone.

- Rapid shear displacement can inhibit or disrupt particle alignment, causing an increase in shear resistance compared to residual values.

- Changes in shearing direction can also disturb particle alignment and cause increases in shearing resistance.

When a soil is sheared against another material, the effect of interface roughness depends on the size of the interface asperities in comparison with the size of the soil particles. In clays, the soil particle size is small, and δ' will be close to the corresponding angle of shearing resistance ϕ' unless the pile surface is very smooth.

In sands, the dominant factor determining peak shear resistance is relative density. Dense sands will exhibit dilatant strength. The tendency to dilate will be influenced by stress level. On continued shearing, the shear response of both initially loose and initially dense sands will tend to a constant volume value, ϕ'_{cv} , which will also be influenced by stress level.

When shearing sands against other materials, the roughness of interface will generally have a greater influence than in the case of clays because of the greater soil particle size. If the surface is rough enough $\delta' = \phi'$; for smooth surfaces δ' may be as low as $\phi'/2$ (Kishida and Uesugi, 1987).

In sands there is not the major influence of particle alignment found in clays, but δ' may be affected by particle comminution during driving.

Values of δ' can typically range from around 10° for high plasticity clays at residual to around 40° for granular materials. The corresponding factor of variation of $\tan\delta'$ is around five times. In practice, the variation in δ' and $\tan\delta'$ is usually much less than these values.

(b) Pile installation:
In clays, the limiting value of δ' operating at a given point along a pile shaft after installation depends on the extent to which remoulding and particle alignment have occurred during installation. For driven piles, there will be intense remoulding in the vicinity of the tip of the pile followed by shear displacement of the pile shaft against the adjacent soil. Depending on the rate of pile installation, the limiting

value of δ' after installation can lie between a peak value δ'_p and a residual value δ'_r. It may well vary along the length of the pile shaft.

In sands, the value of δ' operating at a given point along a pile after installation depends on the extent to which compaction, loosening, and shearing displacement have occurred. Compaction or loosening will dominate near the pile tip. Shearing effects will dominate along the shaft. The value of δ' acting on the pile face will tend to a constant volume value as continued shearing occurs. Changes in radial stress during pile installation may influence the value of δ' operating and δ' will generally vary along the pile shaft.

(c) Pile loading

During pile loading, the soil immediately adjacent to the shaft of a driven pile will experience strains of a basically similar nature to those experienced towards the end of installation. Important differences may be:

- slower and less violent shearing in the case of pile loading
- a reversal in the direction of shearing relative to installation in the case of tensile loading
- complicated changes of shearing direction and shearing rate in the case of other loading patterns, such as cyclic loading.

In clays, loading involving the slow displacement of a pile in the ground will encourage the development of residual values of δ'. Rapid shearing, or reversals in shearing direction, will give rise to values of δ' greater than δ'_r.

Recent research at Imperial College (Bond, 1989) has shown that the relationship between the shearing mode during installation and that during pile loading may determine whether the pile response is ductile or brittle. If pile installation was slow, as for a pile driven to refusal for example, δ' may be at residual prior to loading. In this case the loading response will rise to a peak and be maintained (provided there is no change in radial stress during loading). If installation was fast, or the pile loading involves a reversal in shearing direction relative to installation, the loading response may be brittle as δ' shows an initial peak and then tends to residual as continued slow displacement occurs. Repeated testing of piles may cause changes in δ' which are unlikely to occur during the initial loading of an in-service pile.

In sands, the influence of shearing rate on δ' will have less effect than in clays. Changes in radial stress during loading may be important however.

1.1.2.2 Factors influencing σ_r'

(a) Soil type and stress history:
In contrast to the angle of shearing resistance δ', which is a measure of the frictional response of the soil immediately adjacent to the pile surface, the radial effective stress σ_r' is controlled by the behaviour of the larger mass of soil surrounding the pile, and by the radial stresses existing in the ground before installation and operating at distance from the pile afterwards.

In-situ values of radial effective stress σ_{r_o}', expressed as a proportion of the corresponding in-situ vertical effective stress σ_{v_o}', can be highly variable according to the geological history of the soil. Values of $\sigma_{r_o}'/\sigma_{v_o}'$ range from about 0.3 for normally consolidated deposits to about 4 for highly overconsolidated deposits, a factor of variation of over ten times.

(b) Pile installation:
The action of pile installation will affect the radial effective stress acting on the pile afterwards. It is generally agreed that volume or radial displacement is an important factor. Displacement piles are likely to increase σ_r', replacement piles are likely to reduce σ_r'. A 'wished-in-place' pile would leave σ_r' unchanged. Only driven displacement piles are considered here.

Research has shown (Baligh 1985, 1986; Robinsky and Morrison, 1964) that in both clays and sands the action of driving a pile involves complicated stress paths which cause increases in radial stress in the vicinity of the pile tip, with subsequent reductions in radial stress along the shaft due to stress reversals and soil arching near and around the pile. Shearing at the fixed boundary of a pile shaft may suppress dilation or contraction of the soil, causing changes in radial stress. The intensely sheared and remoulded soil adjacent to a pile may respond differently to material at greater radius.

The installation of a driven pile is likely to be a partially drained event, but it is often convenient to think in terms of undrained behaviour for clays and drained behaviour for sands. In clays the process of installation will involve changes in effective radial

stress, σ'_r ; total radial stress, σ_r ; and pore water pressure, u. The final value of σ'_r acting against the pile face will depend on the relative changes of σ_r and u during consolidation.

Measurements of radial stresses acting on piles that have been made in recent years show that even for large displacement driven piles, values of σ'_r are often not much greater than the original value σ'_{ro} existing before pile installation (Jardine and Potts, 1988). This is thought to be due to the stress relief and arching of the soil that occurs during driving. The effect is particularly marked in sands, and gives rise to the phenomenon known as the 'critical depth' (Vesic, 1967), where increased pile penetration beyond a certain depth does not lead to a corresponding increase in unit shaft capacity. In certain situations, notably in the case of calcareous sands (see Chapter 4), σ'_r can be very low indeed due to contractant shear behaviour and soil arching effects caused by the process of installation.

The inherent strength of a soil, by allowing arching to occur, is often a factor working against the development of pile shaft friction. This suggests that pile design methods correlating shaft friction with soil strength may be misleading.

In contrast to the relatively low values of radial effective stress which have been measured around conventional piles, large values of radial stress can be generated by radial expansion into the soil. This is readily demonstrated by results from pressuremeter testing (Mair and Wood, 1987; Baguelin et al., 1978). A typical pressuremeter curve is shown in Figure 1.1. The available value of total radial stress in such tests, even at relatively small radial strains, is invariably well in excess of the 'lift-off' pressure, even for pressuremeters which have been pushed into the ground, rather than self-bored or lowered into a pre-bored hole. Following expansion, the eventual equilibrium value of radial effective stress will depend on stress changes during consolidation, but it has been shown that even for clays substantial increases in radial effective stress over in-situ values are possible. (Randolph et al., 1979; Wroth et al., 1979; see Chapter 9).

(c) Pile loading:
Changes in σ'_r , σ_r , and u may occur during loading. In general the magnitude of such changes will depend on how damaging the soil shearing regime during loading is, in comparison to that during installation:

- Static loading to failure will result in relatively small changes in σ'_r and u.

- Stress controlled, one-way cycling at stress levels below failure will have little effect in clays (eg. Ove Arup, 1986). Cycling at small strains in sands may cause a slow build up of pore pressures (eg. Bjerrum, 1973). The resulting drop in radial effective stress is often recoverable.

- Strain controlled cycling and two-way cycling involving reversals in shear direction are more damaging, in both clays and sands (eg. Poulos, 1989). Such cycling can cause rapid generation of pore pressures, and the large strain reversals involved can cause rearrangements in soil structure adjacent to the pile leading to permanent reductions in radial effective stress.

1.1.2.3 Conclusions on shaft resistance

In conclusion, both the angle of shearing resistance δ' and the radial effective stress σ_r' are influenced by the manner in which a pile is installed. Considering all soil types, the possible variation of δ' is no more than a factor of around five, and is usually less. The possible variation of σ_r' is at least a factor of 10, and hence σ_r' is the dominant variable in controlling shaft friction. Conventional piling techniques are not efficient at mobilising σ_r'. Much greater values of σ_r' can be generated by radial expansion into the ground. In clays, piling methods which avoid alignment of clay particles will give increased values of δ'.

1.1.3 Cavity expansion theory

It is known that displacement piles and other piling methods involving radial displacement or compaction of the ground give rise to greater radial effective stresses than other techniques, but such methods are largely uncontrolled and often operator dependant. The question that has not been addressed is:

'Can a piling method featuring controlled radial expansion be used to increase pile shaft capacity?'

The large body of available information on cavity expansion theory can be used to show differences between radial effective stresses acting on typical piles and limiting values potentially available. The shortfalls represent potential gains in capacity that might be available if a pile were to be expanded radially along its length.

Cavity expansion theory is discussed in more detail in Chapter 9. The body of information on cavity expansion falls into three main

categories:

(a) simple analytical theories for ideal soils

(b) complex numerical studies attempting to model conventional pile installation as cylindrical cavity expansion (e.g. Randolph et al., 1979; Wroth et al., 1979).

(c) data from pressuremeter and dilatometer testing, and associated developments of theory and analysis.

Analytical theories can be used to perform simple parametric studies on ideal soils, to give limiting values of radial stress available on expansion. An undrained, c_u , approach can be used for clays and a drained, ϕ' , approach for sands. By comparing these limiting values with typical values of radial stress acting on conventional piles at failure, the upper bound of any increases in pile capacity following expansion can be estimated. In the case of clays, assumptions need to be made regarding any loss of radial stress during consolidation.

Numerical work modelling conventional pile installation as cavity expansion has largely proved to be a failure in its original intention. However, this work is now directly relevant to the concept of an expanded pile, and can be used to indicate increases in pile capacity in clays.

Pressuremeter and dilatometer data can be used directly to estimate increases in pile capacity on expansion. This approach is suitable for sands, which exhibit near drained behaviour during expansion of a pressuremeter, such that upper bound increases in effective radial stresses can be forecast reliably. The approach is more complicated for clays because in this case expansion of a pressuremeter involves an increase in pore pressure that will not normally have dissipated by the end of the test, such that the long term value of radial effective stress is not known.

All three approaches outlined above and dealt with in more detail in Chapter 9 of this thesis indicate that by expanding a pile radially into the ground large increases in pile shaft capacity may be achievable.

1.2 The Wedge-Pile

1.2.1 The Process

Professor J.B. Burland of Imperial College has developed and

patented a simple mechanical means of expanding a pile after it has been driven or placed in the ground - the Wedge-Pile (Burland, 1988).

The process involves essentially two components (Figure 1.2):

(a) The outer shell
(b) The expander mandrel

The pile components may be of steel, concrete or other materials depending on the application. A variety of cross sections can be used.

The process consists of installing the outer shell in the ground either by driving or by placing it in a pre-bored hole. The expander mandrel is then passed through the outer shell, expanding it progressively throughout its length. The expander mandrel may be driven or jacked, pushed or pulled.

The key to the process is that the outer shell is expanded LOCALLY and PROGRESSIVELY by the shaped nose of the expander mandrel. This is shown diagrammatically in Figure 1.3. The force required to expand the outer shell in this way is very much less than that required to expand the outer shell simultaneously over its whole length. The expander mandrel may be left in place or removed. If it is removed, a means of retaining the outer shell in its expanded position must be provided.

From a soil mechanics point of view, the main potential advantages of the process over conventional methods are as follows:

(a) Increased pile shaft capacity due to the deliberate mobilisation of available radial effective stress by expansion.

(b) Possible further gains in capacity in clays arising from increased values of δ' caused by remoulding during expansion.

(c) Because the process is a controlled mechanical system, it should be possible to predict increases in pile capacity from basic theory or from the results of pressuremeter testing. This leads the way to more reliable and less empirical design methods.

(d) The actual carrying capacity of the installed pile can be directly estimated by measuring the forces required for expansion, if the frictional characteristics of the outer shell and the expander mandrel are known.

The Wedge-Pile concept has many possible embodiments, and has potential applications in a wide range of foundation and ground engineering problems. There are, in addition to the points listed above, advantages of the system from a wider engineering viewpoint - these are discussed later in this Chapter.

1.2.2 Key soil mechanics questions

The ability to generate high values of radial effective stress by radial expansion into the ground cannot be questioned. What is at issue is whether such high values can be generated by a simple mechanical system of pile driving, can be sustained throughout pile loading, and can be maintained in the long term.

A key feature of the mechanical system is that it must not allow even a slight amount of radial contraction following expansion. This would result in a large drop in σ_r', as demonstrated by the unloading curve of a pressuremeter test (Figure 1.1).

There are questions regarding the change in direction of shearing during pile loading, relative to that during expansion. Could this cause a significant drop in σ_r' during loading? In loose soils, would increases in σ_r' be meta-stable? Would cyclic loading cause the pile response to be brittle? The loss of any increase in σ_r' with time, due to stress relaxation or creep effects, is the most significant question of all. Would σ_r' tend towards the original in-situ value in the long term?

The answers to many of the detailed aspects of these questions are beyond the scope of this thesis and must await further research. The concern of the present research is to demonstrate the basic principles of the Wedge-Pile.

1.2.3 The Wedge-Pile Project

The stages involved in putting the Wedge-Pile concept into practice are shown in Figure 1.4.

The UNDERLYING CONCEPT is the mechanical process by which a pile is expanded by local and progressive deformation along its length.

The EMBODIMENT is the means by which the underlying concept can be put to practical use. The development of practical embodiments is the most important stage in the overall process. Ideas and testing will naturally be simple to start with and evolve to include detailed analysis and process details. In the next Section some of the ideas that have been considered so far are set down. Research at Imperial College to date has

concentrated on the development and testing of driven, pre-formed piles and tension piles.

ENGINEERING STUDIES involve the detailed appraisal of available embodiments and process details, design and member sizing, costing, and comparison with other available methods. Such studies are largely beyond the scope of this reseach.

1.3 Wedge-Pile Embodiments

This Section outlines the main ideas that have been considered in the application of the Wedge-Pile concept to driven piles and tension piles. All of the embodiments feature the concept of local and progressive expansion along the length of the pile. Some of the embodiments make use of standard piling sections and equipment, others are more innovative.

Firstly, the functions of the outer shell and the expander mandrel are considered, both during installation, and after installation when a wedge-pile acts as a permanent load carrying member. Factors influencing the acceptablity, cost and eventual choice of wedge-pile embodiment are then considered.

1.3.1 Functions of pile components during installation

1.3.1.1 Outer shell

The primary purpose of installing the outer shell is to introduce an expandable inclusion into the ground. It is the outer shell which determines the characteristics of the mechanical expansion process. Wedge-piles can be classified according to the mode of deformation of the outer shell as it is expanded locally. The mode of deformation will vary according to the material properties and the arrangement of the outer shell. The outer shell must be able to resist driving forces, including those during installation of the expander mandrel.

Research at Imperial College has focused on the use of an outer shell formed from steel. Some attention has been given to the use of plastic as an alternative.

There are a range of conventional pre-formed steel piles, from small displacement 'H' section piles to large displacement tubular or box sections driven with closed ends. The advantages of such steel displacement piles are well documented. The pile material can sustain high driving stresses and, when installed, high compressive and tensile loads. They are relatively light in weight for their load carrying

capacity. Also, they are not easily damaged by rough handling, can be inspected before driving and are easily cut down or extended. The two main drawbacks of steel piles are the high unit cost of the pile material and the effects of corrosion.

Steel H piles have additional advantages. Due to their small cross-sectional area they are easy to drive both to great depth and through intermediate hard strata. There is low risk of heave of surrounding ground and ease of driving in closely spaced groups. They are light to handle and particularly compact to store. However, H piles suffer from severe disadvantages. Their small cross-sectional area, although making driving easy, gives rise to low end resistance and low shaft resistance. 'Whipping' during driving may significantly reduce shaft resistance.

The ability to install easily in the ground a load carrying inclusion of small cross-sectional area is of particular relevance to the Wedge-Pile process.

Three main systems of wedge-pile incorporating a steel outer shell have been considered. These systems have all been given the general term 'steel wedge-piles', although the steel outer shell could be expanded by an expander mandrel of any appropriate material. The mode of deformation of the outer shell differs for each system, according to the flexural properties and configuration of the outer shell. This may have an influence on the increases in pile capacity achievable. The three main systems are as follows:

(a) The outer shell could be made up from steel sections temporarily held together and driven as one. Standard sections would normally be used (Figure 1.5). Appropriate connections would include bolts and tack welds. On driving the expander mandrel, the temporary connections would split apart and the separated elements be displaced radially into the ground. A variety of pile cross-sections could be employed, the most obvious being cruciform, box and channel. Depending on the configuration and size of the outer shell, it could be driven from the top, or from the bottom using an internal driving mandrel. Figure 1.6 shows a cruciform outer shell being split apart as the expander mandrel is driven.

    This system is defined as a 'multiple-element' outer shell. The expansion process involves flexural translation of the elements from their initial position to their fully displaced position. Depending on the steel sections used, the mode of bending may be

totally elastic or may involve some yielding such that contained plastic flow occurs.

It is clear from the outset that arrangements of this system which mobilise soil resistance in 3 or 4 directions may be more efficient than '2-way' versions.

(b) If a circular steel tube outer shell were to be used, one or more weak lines could be machined along the length of the tube. As the expander mandrel was driven, the outer shell would open up along one of the weak lines. If a single weak line were to be employed, the fully displaced configuration of the outer shell would involve substantial elastic bending (Figure 1.7). Further weak lines could be used to reduce the strain energy involved in the case of the single weak line, by promoting the formation of plastic hinges around the circumference of the outer shell during expansion. However, further weak lines would weaken the outer shell. A tubular shell system could be driven from the top or from the bottom.

The manner in which an expanded single split tube mobilises soil resistance is not as clear as in the case of the multiple-element system. This question is dealt with further in Chapters 7 and 8.

(c) A cruciform shaped outer shell could be formed by passing a thin tubular section through shaping rollers during the installation process. It would then be pulled into the ground by driving from the bottom. By driving a circular expander mandrel, the outer shell could be plastically deformed back into a near circular shape.

1.3.1.2 Expander mandrel

The expander mandrel displaces the outer shell radially into the ground, mobilising available radial effective stress. The expander mandrel comprises a nose section and a shank section.

The expander mandrel nose imparts the necessary radial force to displace the outer shell into the ground. The nose section must be so shaped to effect a smooth transition of the outer shell from its unexpanded position to its expanded position (Figure 1.3). In particular it is important that no radial contraction occurs (Section 1.2.2).

The shank section is the means by which the nose section is advanced into the outer shell. The shank maintains the outer shell in its expanded position after driving, unless some means is provided of holding the outer shell apart after driving the expander mandrel (a

system of spacers for example, as shown in Figure 1.8). In the latter case the expander mandrel could be removed.

The expander mandrel can be considered as a machine which moves a radial expanding force along the length of the outer shell. The velocity ratio of this machine is unity; the mechanical advantage depends on the shape of the nose and the frictional resistance between the outer shell and the expander mandrel. If the shank section of the expander mandrel is parallel sided and remains in contact with the outer shell, the mechanical advantage will decrease as the expander mandrel is advanced. If spacers were to be provided to hold the expanded outer shell in place, the shank could be of reduced section to eliminate friction between the shank and the outer shell, in order to increase the efficiency of the expansion process (Figure 1.8).

The expander mandrel could be formed from any suitable material, normally steel or concrete. A steel expander mandrel would be driven in the same manner as the outer shell. A concrete expander mandrel would probably be in the form of short precast segments. These could be installed consecutively by driving, or by jacking using the installed outer shell as reaction.

If a spacer system were to be provided, the expander mandrel could be removed and replaced with a permanent pile filling.

1.3.2 Structural functions of pile components after installation

Upon installation, the two main elements of a wedge-pile comprise:

(a) the outer shell
(b) an 'as driven' permanent expander mandrel, a replacement cementitious or low grade filler, or a combination of these two.

The outer shell is the interface with the ground and serves to transmit vertical loading into the soil mass.

If a permanent expander mandrel were to be employed, it would hold the outer shell in place and carry most of the bending moments arising from lateral loads. The outer shell would be the vertical load carrying member. At the top of the wedge-pile the two components would normally be structurally connected so as to act as a single unit.

If the wedge-pile were to be grouted up on installation, the pile would act as a single unit along its length and the outer shell would

not need to carry independently all the vertical load.

1.3.3 Acceptability and Cost

The fundamental questions that must be addressed when developing these new piling techniques are:

(i) Will the foundation be acceptable?
(ii) Can the technique be implemented more cheaply than other existing pile types ?

The following factors must be taken into account when assessing the various wedge-pile embodiments that have been described above:

(a) Acceptability.

The pile must satisfy load carrying and serviceabilty requirements, in both the long and short term. The load carrying characteristics of the various embodiments need to be determined. In the first instance this must be achieved by the load testing of prototype versions. Eventually, performance monitoring of working piles could be carried out.

The pile itself must be durable in the long term. As for conventional steel piles, a key question is the effect of corrosion. Also of importance is the integrity of any connection or grouting between the outer shell and the expander mandrel.

The piling technique must satisfy any environmental impact requirements, for example regulations and contractual obligations regarding noise and vibration control. Efficiency during driving will lead to the use of lighter plant, lower noise and vibration, and less general disturbance. Where competing with bored piles, the reduction of handling of removed soil would be a big advantage.

(b) Cost.

The cost of implementing the the Wedge-Pile technique, in comparison with other methods, is dependant on:

- The increase in load carrying capacity over existing methods, enabling the use of fewer or shorter piles to carry a given load. This factor must be considered in conjunction with the cost of installation.

- The reliability with which any increase in capacity can be predicted for design purposes. The underlying concept of the Wedge-Pile is that increases in pile capacity are accompanied by improved reliability and hence cost efficiency of design. In addition, measurement of the forces involved in expanding a wedge-pile could be used to estimate installed capacity. This information could then be used to give assurance of required capacity, or to provide feedback into the design process. Any changes in design thought desirable could be made 'on the spot', thus saving costs.

- Cost of installation. The total cost of installing a pile ultimately depends on the cost of the pile material; the driving energy required; the installation time required; together with the required amount of subsidiary handling of piles, equipment and any removed material.

1.3.4 Choice of system

Obvious initial objections to the use of steel wedge-piles that need to be addressed are the high cost of steel, the increased installation times due to two-stage driving, and the extra preparation and handling of piles required.

On the other hand, the two-stage installation process, with radial stress generated efficiently during the second stage, opens the door to process details which may reduce installation times and driving energies.

The most appropriate configuration of wedge-pile is likely to be the cruciform. The '4-way' expansion mode is likely to maximise increases in pile capacity. The small cross-sectional area of the outer shell would facilitate quick and easy installation using relatively light plant and equipment. Installation of the expander mandrel would create most of the volume of the pile, in an energy efficient manner. A cheap, cementitious material would be ideal for filling this volume. Permanent pre-cast concrete expander mandrel segments could be used or, in the case of a removable mandrel, the void created by expansion could be grouted up after withdrawal of the expander mandrel.

The outer shell of the cruciform pile would be the vertical load carrying member. Provision of corrosion protection would have to be made, particularly near to the ground surface. This might have a significant effect on pile material costs.

A large displacement box or tube type outer shell might be of benefit in weak or loose ground, as an efficient method of compacting the ground before expansion. In this case the pile could be grouted to form a single unit, and the outer shell need not be load carrying; hence corrosion of the outer shell would not be a problem. A thin-walled outer shell, driven from the bottom, could be used to reduce material costs. It might prove possible to use an outer shell of plastic tube to reduce material costs further still.

The installation energy of the outer shell could be reduced by using a slightly oversized driving shoe in order to reduce shaft friction during installation and concentrate driving energy at the toe of the pile. The resulting loss of radial effective stress would be easily recouped upon driving the expander mandrel. The installation energy of the expander mandrel could be reduced by appropriate choice of surface finish, and by lubrication between the outer shell and the expander mandrel shank. Pile capacity could be increased by the use of ribbing or corrugations on the outside of the outer shell. Such ribbing might reduce shaft friction during driving (in the same manner as the oversized driving shoe) and increase it after expansion.

1.4 Outline of Research

1.4.1 Objectives

The overall objectives of the research were as follows:

(a) to demonstrate the principle of the Wedge-Pile process

(b) to investigate the load carrying characteristics of a variety of wedge-pile embodiments at field and laboratory scale

(c) to determine whether any increases in pile capacity can be predicted by using cavity expansion theory or pressuremeter testing, or directly estimated by measuring expander mandrel installation force

(d) to assess the practicality of the Wedge-Pile system for civil engineering use, and to continue to develop new embodiments and essential process details.

Work was undertaken in the field, in the laboratory, and with computer models. The research was performed in stages, with specific objectives at each stage. This is summarised in Table 1.1.

1.4.2 Structure of thesis

CHAPTER 2 describes some simple model tests that were performed in the laboratory to assess the potential of the Wedge-Pile idea.

CHAPTER 3 describes the development of two types of 6m long steel wedge-pile, and associated equipment, used in large scale proving trials at two sites. The large scale trials and associated pressuremeter testing were performed at a weathered chalk site and a boulder clay site, and are described in CHAPTER 4 and CHAPTER 5 respectively.

CHAPTER 6 describes tests with 1.5m long steel 'mini-piles', carried out with the purpose of augmenting the large scale tests with results from a wider variety of soil types.

CHAPTER 7 summarises further simple model testing in the laboratory that was undertaken to investigate the importance of the mode of expansion, and to explore the potential of the Wedge-Pile in soil reinforcement processes.

CHAPTER 8 is a summary of large scale commercial trials which investigated the possible use of the Wedge-Pile concept for housing type foundations, and also for offshore use.

CHAPTER 9 reviews cavity expansion theory, and discusses increases in pile shaft capacity that might theoretically be possible by expanding a pile.

CHAPTER 10 describes numerical models that have been developed and used to perform a preliminary investigation into the importance of the shape of the expander mandrel nose.

The results from all of these investigations are drawn together and discussed in CHAPTER 11. A summary and overall conclusions are provided in CHAPTER 12.

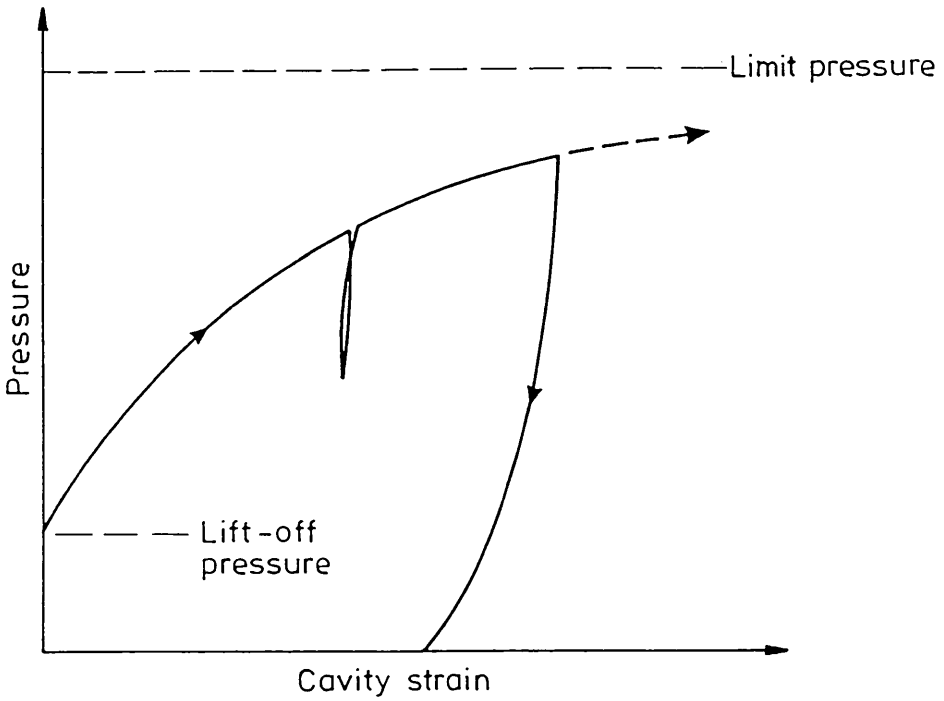

Figure 1.1 Typical pressuremeter pressure:strain curve

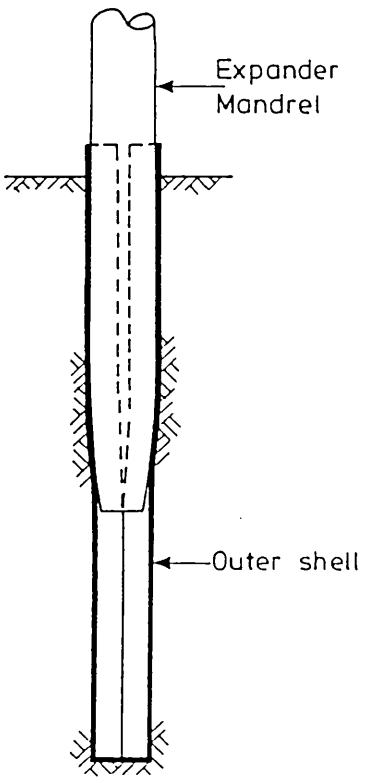

Figure 1.2 Components of the Wedge-Pile

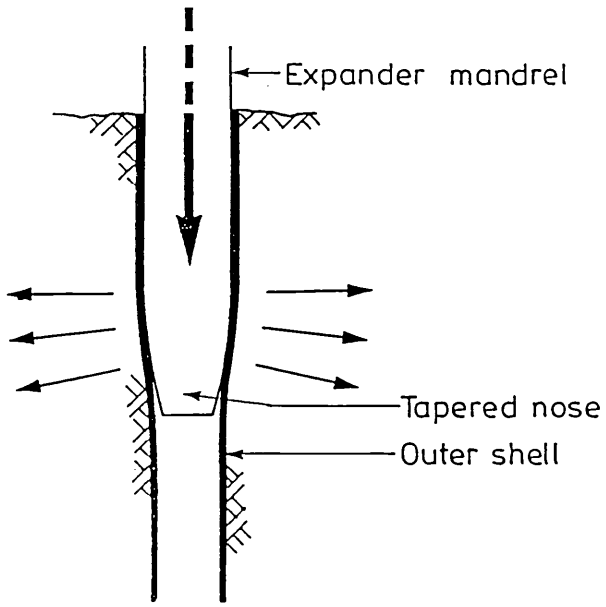

Figure 1.3 The Wedge-Pile principle:
local and progressive deformation

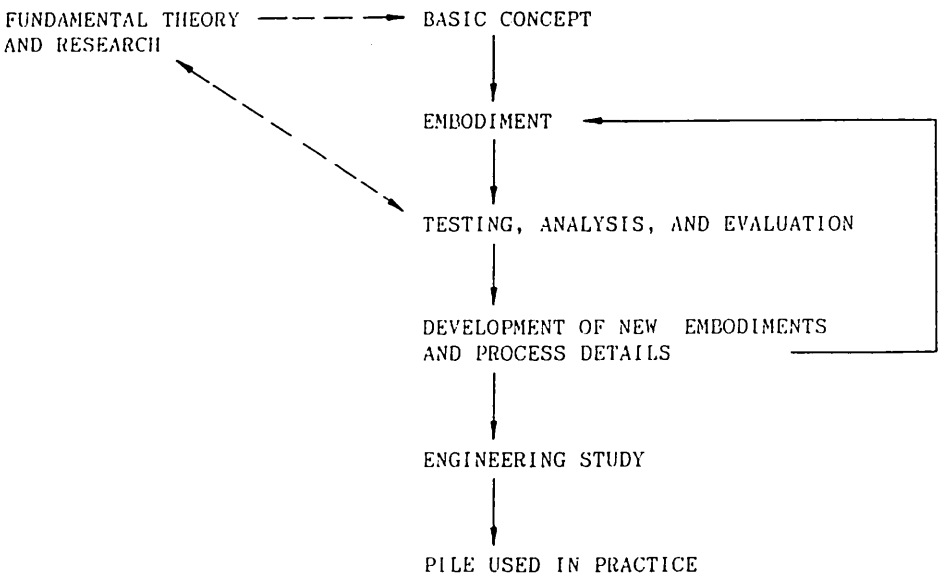

Figure 1.4 Wedge-Pile Project Structure

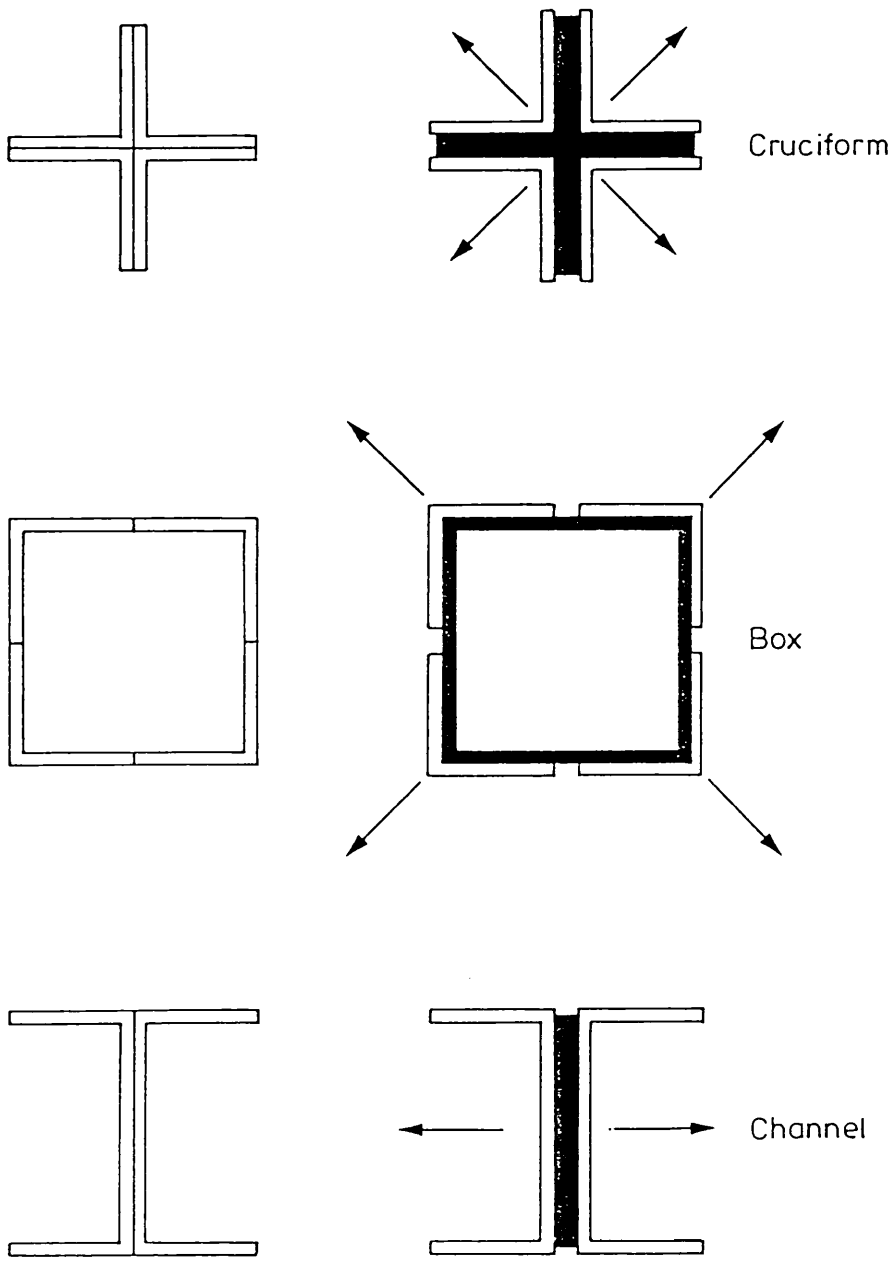

Figure 1.5 Types of 'multiple-element' wedge-piles

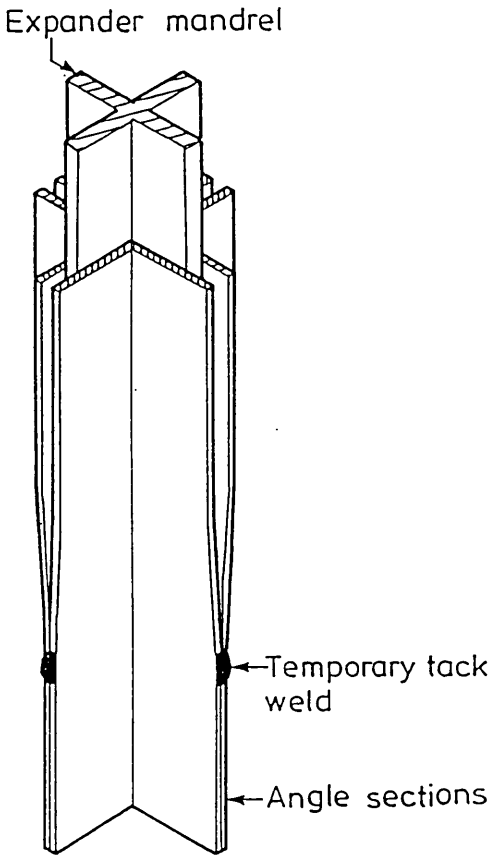

Figure 1.6 'Cruciform' wedge-pile during expansion

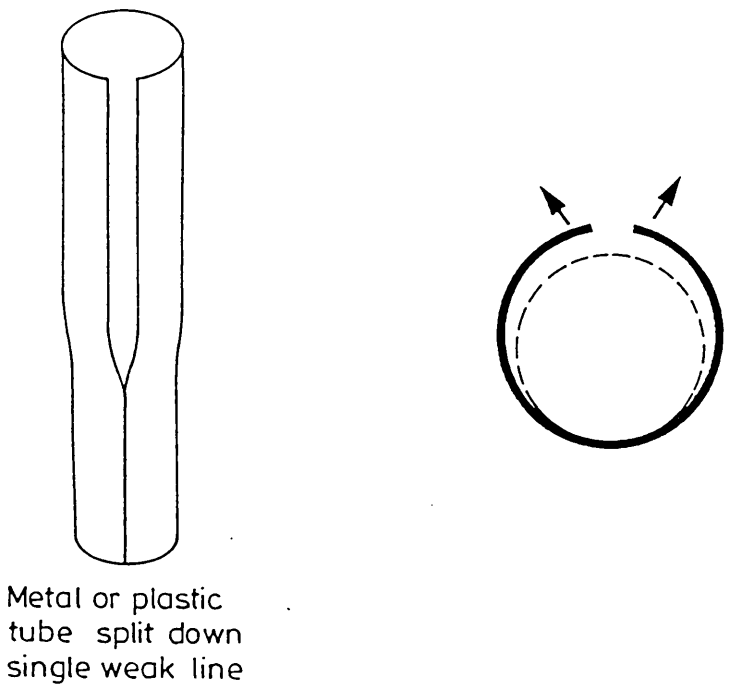

Figure 1.7 Circular tube type wedge-pile

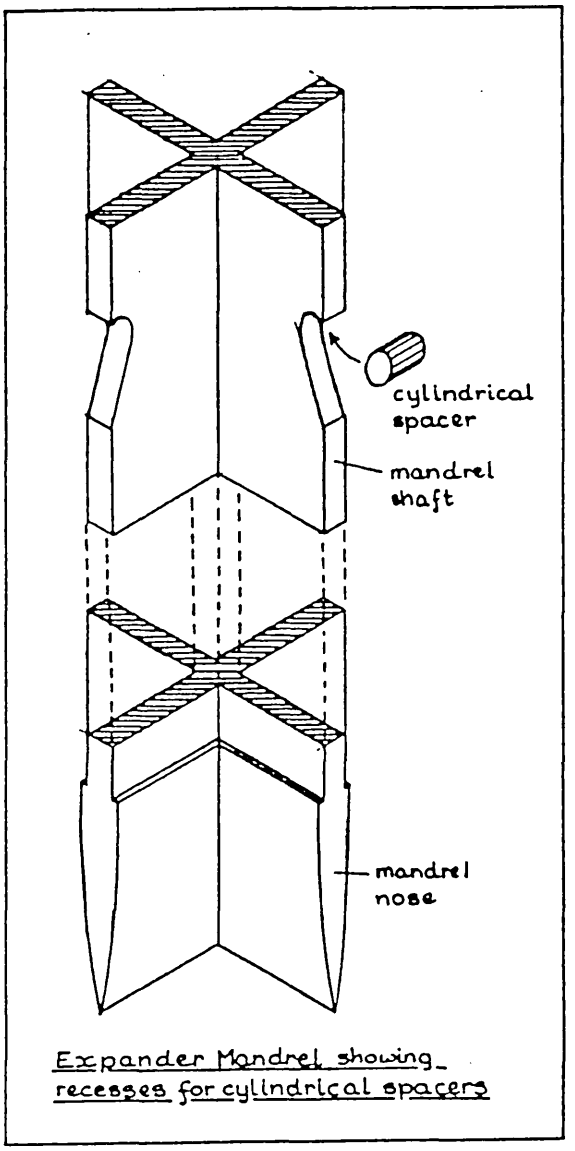

Figure 1.8 Example of retractable expander mandrel with spacer system

Description of Work	Main Objectives
Initial model tests	- Assess potential of idea
Large scale field trials	- Demonstrate principle at large scale - Compare with cavity expansion theory - Assess practicality
Mini-pile tests	- Extend data base of soil types tested
Further model tests	- Investigate effectiveness of different modes of expansion - Assess potential of concept for soil reinforcement and nailing
CP&F/Conoco trials	- Assess potential of concept for housing type foundations - Assess tubular pile relevant to use for offshore structures

Table 1.1 Summary of work carried out

CHAPTER 2
PRELIMINARY MODEL TESTS

2.1 Introduction

The first step in the Wedge-Pile project was to undertake some preliminary model tests in the laboratory in order to assess the potential of the idea. These model tests were the subject of an MSc project by French (1984). Additional work was subsequently performed in order to complete the test programme. The model tests were largely qualitative, intended to guide the way to further research. The time available for laboratory work was limited and emphasis was placed on obtaining a range of data from simple tests rather than limited information from more sophisticated testing.

This Chapter summarises the preliminary model tests. The test apparatus and results are described in more detail in the MSc report by French (ibid.).

2.2 Description of Model Piles and Apparatus

2.2.1 Summary

The test rig is shown schematically in Figure 2.1.

The experiments were performed on a large triaxial loading frame. Model wedge-piles were fabricated in mild steel and consisted of two components: an outer shell and an expander mandrel. The components were cruciform in shape, as shown in Plate 2.1. The pile components could be connected to a load cell, which was mounted on the stationary top ram of the loading frame. A carefully prepared and wetted sand bed in a circular container was mounted on the moving bottom ram of the loading frame.

To form a model wedge-pile, the pile components were pushed into the sand bed by raising the bottom ram. First, the outer shell was pushed into the sand. Then it was expanded by driving through it an expander mandrel. After expansion, the two components were clamped together at the top to form a single unit - the expanded pile. Both expanded piles and individual pile components could be tested in compression and in tension.

2.2.2 Outer shell

The cross-sectional area of the outer shell was made as small as possible in order to minimise driving energy and to make the outer shell as flexible as possible during expansion. Each outer shell was made up of four 250mm long 10x10mm angles bent up from 0.005inch mild steel shim with a smooth finish. Details of the outer shell are given in Figure 2.2. A large number of outer shells were made up, and a new outer shell was generally used for each test.

Before assembly, the angles were thoroughly cleaned with butanone to remove grease. The angles were then spot welded together at their bottom outside corners to form a single cruciform shaped unit. Finally, strips of adhesive tape were wrapped around the 'arms' of the cruciform, at the tip of the outer shell and at 100mm from the tip. The purpose of the bottom adhesive tape strips was to stop sand grains being forced up between the angles as the outer shell was pushed into the sand bed. The strips positioned near the middle of the outer shell prevented the angles bowing apart during driving. The spot welds held the tip of the outer shell together.

The outer shell was pushed into the sand by means of a load cell connector. This comprised a short length of 25mm diameter brass rod with slots in a cruciform shape cut at one end to receive the top of the outer shell. The slots were sufficiently narrow to locate the outer shell securely as it was pushed into the sand bed, but there was enough play to allow the connector to be subsequently pulled away from the top of the outer shell without a frictional force developing between the two. In order to apply tensile loads to the outer shell, it could be securely fixed within the connector by means of radial screws. At the top of the connector a threaded boss allowed connection to the load cell.

2.2.3 Expander mandrel

Four reusable expander mandrels of different flange sizes were fabricated, from 1mm, 2mm, 3mm and 4mm mild steel strip respectively. The expander mandrels were designated 'A' to 'D' respectively, and increased the initial width of the outer shell by 5%, 10%, 15%, and 20% respectively. Details are given in Figure 2.3. Each expander mandrel was cruciform shaped to match the outer shell and comprised a lower nose section, designed to ease apart the outer shell in a smooth and controlled manner; a central shank section; and an upper section to allow connection to the load cell. The total length of the expander mandrel was 305mm.

The load cell connectors for the expander mandrels were of similar construction to the connector for the outer shell. They featured single slots of the appropriate width to locate the tops of the expander mandrels. The expander mandrels were secured to the connectors by means of a single bolt passing through matching holes. This arrangement allowed both compressive and tensile loads to be applied to the expander mandrels.

2.2.4 Completed pile arrangement

Each expanded pile comprised an outer shell driven to 200mm depth, and an expander mandrel driven into the outer shell to a depth of 170mm. After the expander mandrel had been driven, the top of the outer shell was connected to it by means of four specially fabricated clamps, to form the expanded pile. The expanded pile could be driven further into the sand bed - or pulled out - by pushing or pulling on the expander mandrel, which extended above the top of the outer shell.

The cross-sectional areas of the expanded piles and the various pile components are given in Table 2.1.

2.2.5 Sand bed

An artificially graded fine to medium quartz sand was used for the study. The grading curve is given in Appendix 2.1.

The sand bed was prepared in a 255mm diameter, 385mm high circular plastic container using a simple sand raining technique (Hanna 1963; Chan and Hanna, 1980). Sand beds of different densities could be prepared by varying the intensity of rain and the height of drop (Kolbuszewski, 1948; Walker, 1964).

The ratio of the container diameter to the pile width was approximately 13:1. This ratio is lower than values reported for other model pile studies in rigid boundary containers (eg. Robinsky and Morrison, 1964; Chan and Hanna, 1980), but was considered acceptable bearing in mind the exploratory nature of the tests. The depth of the sand bed was typically 270mm. Some preliminary tests were performed in which model piles were driven very close to the bottom of the container, such that the resulting increase in base resistance could be observed. The depth of pile penetration for the test programme was selected such that there were no container base effects apparent.

After the test batch of sand had been discharged into the sand bed container, the top surface of the sand bed was smoothed flat with a special smoothing device. This gave a level datum from which depths of

penetration into the sand bed could be measured, and which allowed the average density of the sand bed to be calculated to within approximately 0.5%. Reproducibility of sand density was checked by performing identical installation tests with expander mandrel A. The results are shown in Appendix 2.1. The sand densities obtained using the sand raining apparatus were considered to be sufficiently reproducible for the model pile test programme.

In the early stages of the study dry sand was used, but it was found that dry sand poured through the gaps created as the four angles of the outer shell were opened up ahead of the expander mandrel nose. This was totally unsatisfactory, as sand filled the centre of the outer shell. This problem was overcome by the use of damp sand, which in any case is a better representation of real life conditions. A simple method was developed of dampening the sand after it had been placed.

The procedure for preparing a dampened sand bed was as follows. The sand bed container was itself contained within a similar container of greater diameter (Figure 2.1). The larger container was fitted with a tap near the base to allow de-aired water to be fed into the annulus between the two containers. An overflow pipe in the wall of the outer container maintained the maximum water level in the annulus approximately 10mm below the surface of the sand bed. Water entered the sand bed container at the bottom via 3mm diameter holes and was allowed to rise by capillary action until the sand was completely wetted. The annulus was then drained of water.

2.2.6 Test rig

The triaxial loading frame featured a motor driven bottom ram and a stationary top ram. The speed of the bottom ram could be adjusted with a gear box. Maximum clearance between the rams was 675mm; maximum throw of the bottom ram was 310mm. A standard 200lbf Imperial College load cell was used in conjunction with a digital voltmeter.

Depth of penetration of the pile components into the sand bed was governed by the movement of the bottom ram. Two methods of measuring the movement of the bottom ram were used. When pushing the pile components into the sand bed a vertical staff was used in conjunction with a pointer clamped to the bottom of the sand bed container. During loading tests on the installed piles a dial gauge extensometer was used.

2.3 Summary of Results

In this Section, outer shell and expander mandrel are referred to as

'shell' and 'mandrel' respectively.

2.3.1 Introduction

The main objective of the model pile test programme was to investigate the increase in load carrying capacity of expanded piles in comparison to the corresponding capacities of:

(a) mandrels driven alone (ie. driven into a sand bed, rather than into a shell)

(b) unexpanded shells.

Four suites of tests were performed - in medium-dense sand and in medium-loose sand, in compression and in tension. In each suite of tests the four differently sized expander mandrels were used.

Tests were performed in pairs, with a fresh sand bed being prepared for each test of the pair. The sand for each pair of tests was from the same sack of sand, and the two prepared sand beds were of very similar density (see Sections 2.3.2, 2.3.3). In the first test of a pair, a mandrel alone was installed and tested. In the second test, the same mandrel was used to form an expanded pile which was then tested. Each pair of tests allowed the comparison of an expanded pile with a 'conventional' pile of slightly less cross-sectional area (see Table 2.1). Each test consisted of an installation stage and a load test stage. Measurements of applied load and pile displacement were made in both stages. Tension tests were of most interest because in these tests base resistance was eliminated and any increase in pile capacity on expansion was due solely to an increase in shaft friction.

Because damp sand was used for the tests, it was neccessary to oven-dry the sand before reuse. This took a minimum of two days and as a result seven sacks of sand were required to enable testing to take place every day. Each sack, although containing identical sand, gave slightly different densities using the sand raining apparatus because of the effects of the drying process. Consequently, tests using sand from different sacks are not exactly comparable.

2.3.2 Tests in medium-dense sand

Two suites of tests were performed in medium-dense sand: one suite in compression and one suite in tension, with eight tests in total. The sand beds for the tests had relative densities before wetting within the range 58% to 79%. The relative densities for any two tests forming a 'pair' were within approximately 2% of each other. A small amount of

settlement of the sand bed occurred as a result of the wetting process - this was not measured. It is considered that the best indication of differences in sand density between test pairs is given by differences in installation loads of the shells.

In the first test of a pair, a mandrel alone was driven 200mm into a sand bed and then tested. In the second test of a pair a shell was driven 200mm into a sand bed and was then expanded by driving through it to a depth of 170mm the mandrel used in the first test. The pile components were installed at a rate of 16.51mm/minute. The piles were tested by pushing or pulling them a distance of 20mm at a rate of 1.10mm/minute. Typical results for a compression test and a tension test are presented in Figures 2.4 and 2.5 respectively.

The results from the two suites of tests are summarised in Table 2.2. Included in the Table are the final loads recorded during installation of the pile components, and the maximum test loads recorded. Comparison between loads is by means of load ratios, defined in Sections 2.3.2.1 to 2.3.3.2.

2.3.2.1 Compression tests
In Figure 2.6, three load ratios are plotted against mandrel size:

(a) mandrel alone : unexpanded shell
This load ratio is given by dividing the maximum test load of the mandrel alone by the final installation load of the shell.

(b) expanded pile : unexpanded shell
This load ratio is given by dividing the maximum test load of the expanded pile by the final installation load of the shell.

(c) expanded pile : mandrel alone
This load ratio is given by dividing the maximum test load of the expanded pile by the maximum test load of the mandrel alone.

The load carrying capacities of the mandrels alone and the corresponding expanded piles increase with mandrel size, in comparison to the shell installation loads (load ratios (a) and (b)). It is likely that most of this increase is due to the increase in base resistance associated with the increase in pile cross-sectional area.

The capacities of the expanded piles are greater than the capacities of the mandrels alone (load ratio (c)) by factors of over 1.75 for mandrels A and B. The increases in capacity for mandrels C and D are

less, probably because base resistance forms a greater proportion of overall pile capacity with increasing pile cross-sectional area.

2.3.2.2 Tension tests

In Figure 2.7, the ratio of the capacity of expanded piles to the capacity of mandrels alone is plotted. Factors of increase are in the range 2.75 to 4.73 with maximum increase for mandrel B. There appears to be a decreasing trend in load ratio for mandrel sizes greater than this. The load ratio for mandrel A may have been rather low due to the characteristics of this particular mandrel (see Section 2.3.3.2).

2.3.3 Tests in medium-loose sand

Two suites of tests were performed in medium-loose sand: one suite in compression and one suite in tension, with eight tests in total. The sand beds for the tests had relative densities before wetting within the range 29 to 38%. As before, the relative densities for the two tests forming a pair were within approximately 2% of each other.

The suite of tension tests were all performed using sand from a single sack, enabling the sand beds for these four tests to be prepared with very similar relative densities - between 33% and 38%. This set of tests was 'definitive' in the sense that installation loads and test loads from all the tests could be compared directly with reasonable confidence.

Tests were performed in pairs, as for the tests in medium-dense sand. The depths of penetration of the pile components, and the installation and testing rates were the same as before. Load-displacement behaviour was similar in overall form to that for the tests in medium-dense sand shown in Figures 2.4 and 2.5, except that overall loads were lower. There was a slight change in procedure for the tension tests, however. In these tests the outer shells were driven initially to 195mm at the installation rate of 16.51mm/minute; then withdrawn 5mm at the testing rate of 1.10mm/minute; and finally driven 10mm at 1.10mm/min to the final depth of 200mm. This enabled the tensile capacity of the shells to be measured.

The results from the two suites of tests are summarised in Table 2.3. The presentation of the data is the same as for the tests in medium-dense sand.

2.3.3.1 Compression tests

In Figure 2.8, three load ratios are plotted against mandrel size:

(a) mandrel alone : unexpanded shell
(b) expanded pile : unexpanded shell
(c) expanded pile : mandrel alone

The calculation of these ratios is as given in Section 2.3.2.1.

The pattern of behaviour of the model piles in compression is shown in Figure 2.8 and is the same as for the compression tests in medium-dense sand (Figure 2.6). The load carrying capacities of the mandrels alone and the corresponding expanded piles increase with mandrel size, in comparison to the shell installation loads, (load ratios (a) and (b)). As before, most of this increase is probably due to an increase in base resistance with mandrel size.

The capacities of the expanded piles in comparison to the mandrels alone (load ratio (c)) show a maximum increase in capacity of just over two times in the case of mandrel A. There is a gradual decrease in load ratio with mandrel size thereafter.

2.3.3.2 Tension tests
In Figure 2.9, two load ratios giving factors of increase in capacity of the expanded piles are plotted:

(a) expanded pile : mandrel alone
This load ratio is given by dividing the maximum test load of the expanded pile by the maximum test load of the mandrel alone.

(b) expanded pile : unexpanded shell
This load ratio is given by dividing the maximum test load of the expanded pile by the tensile capacity of the shell measured during installation (Section 2.3.3). This load ratio is a direct measure of the increase in shaft capacity obtained by expanding a pile after driving.

The factors of increase over mandrels alone (load ratio (a)) are in the range 3.06 to 3.77, with the exception of a large peak of 7.16 for mandrel B. Factors of increase over unexpanded shells (load ratio (b)) show a gradual increase from 2.57 for mandrel A to 3.76 for mandrel D.

In Figure 2.10 the actual tensile test loads for this definitive suite of tests are plotted against mandrel size. The installation loads are plotted in Figure 2.11. The unexpanded shell capacities lie within a fairly narrow band and expanded pile capacity increases with mandrel size, as might be expected. The pattern of behaviour for mandrel

capacities is rather odd, however. Firstly, for the most part, the capacities of the mandrels are below those of the unexpanded shells. As the shells have a smaller cross-sectional area than the mandrels, this is the reverse of what would be expected. Secondly, the capacity of mandrel A is greater than that of mandrel B - this again is the opposite of what would be expected, for the same reason given above.

The reasons for this behaviour are thought to be as follows. Firstly, the shim used to fabricate the shells had some inherent 'spring' - enough to give a small increase in radial stress along the pile shaft and a consequent increase in pile capacity. This effect would have been less marked in the case of the tests in medium-dense sand, where the overall test loads were higher. Secondly, examination showed that there were slight perturbations in the cross-section of mandrel A along its length, which were not present in the other mandrels. These perturbations were caused during the initial fabrication of mandrel A and were due to the flexibility of the 1mm thick mild steel strip used to fabricate this mandrel, in comparison to the thicker strips used for the other mandrels. The fact that mandrel A was not exactly parallel sided means that some passive resistance would have developed along the length of the pile, thereby increasing capacity.

The above effects should be borne in mind when considering the model pile test results. Increases in pile capacity of expanded piles in comparison to mandrels alone probably include a small element due to the springiness of the shells. Increases in expanded pile capacity in comparison to mandrel A would probably have been greater had mandrel A been perfectly straight sided.

2.3.4 Pile efficiency

This Section considers the concept of pile 'efficiency' - this is a measure of the return in load carrying capacity from the energy expended during installation of a pile. Efficiency is defined here as:

$$\frac{\text{Pile test load}}{\text{Energy expended during installation}} \qquad \frac{N}{J}$$

Tables 2.4 and 2.5 give details of:

(a) energies expended during installation of the model piles
(b) Efficiencies, as defined above
(c) increases in Efficiency of expanded piles in comparison to unexpanded shells.

Energy expended during installation has been obtained by calculating the area under the installation load:displacement plot - in the case of expanded piles the energy associated with pile expansion has been added to the energy associated with shell installation.

In Figure 2.12 Efficiency is plotted against mandrel size, for the compression tests in medium-dense and medium-loose sand. Values of Efficiency are greater for expanded piles in comparison to mandrels alone. For both expanded piles and mandrels alone, Efficiencies are greater in medium-dense sand than in medium-loose sand.

In Figure 2.13, Efficiency is plotted against mandrel size, for the tension tests in medium-dense and medium-loose sand. As for the compression tests, values of Efficiency are greater for expanded piles than for mandrels alone; and Efficiences are greater for both expanded piles and mandrels alone in medium-dense sand in comparison to medium-loose sand. In medium-loose sand, expanded piles show greater Efficiencies than for shells. Values of Efficiency for shells in medium-loose sand are greater than those for mandrels alone - this is due to the higher test loads of the shells in comparison to the mandrels, as explained in the previous Section.

In Figure 2.14, ratios of Efficiency for expanded piles in comparison to unexpanded piles are plotted against mandrel size. This Figure shows that expanded piles are more efficient than unexpanded piles. The maximum increase in Efficiency of an expanded pile in comparison to an unexpanded shell is 1.5 times in the case of mandrel A.

Expanded piles are more efficient than unexpanded piles, particularly at small expansions, even though two components are driven instead of one. Apart from the increase in capacity due to expansion, the reason for this greater efficiency is due to the low installation energies of the small displacement shells, and the low expansion energies at small expansions (see Tables 2.4 and 2.5).

2.4 Conclusions

With due caution in regard to the preliminary nature of the tests, two main conclusions can be drawn from the test results:

(a) All the test results indicate that a significant increase in load carrying capacity can be obtained by expanding a pile after driving. Results from the definitive suite of tests in medium-loose sand show increases in shaft capacity of between 2.5 and 3.75 times

by expanding an outer shell.

(b) All of the test results indicate that an expanded pile appears to be more efficient than a conventional pile - less energy is expended during pile installation for unit pile capacity, despite the fact that two components are driven instead of one. In the definitive suite of tests, expanded piles showed increases in Efficiency of up to 1.5 times in comparison to unexpanded outer shells. Most benefit in comparison to unexpanded piles was obtained at relatively low expansions.

The results from the preliminary model tests provided sufficient encouragement for a series of full scale wedge-pile field trials to be commenced.

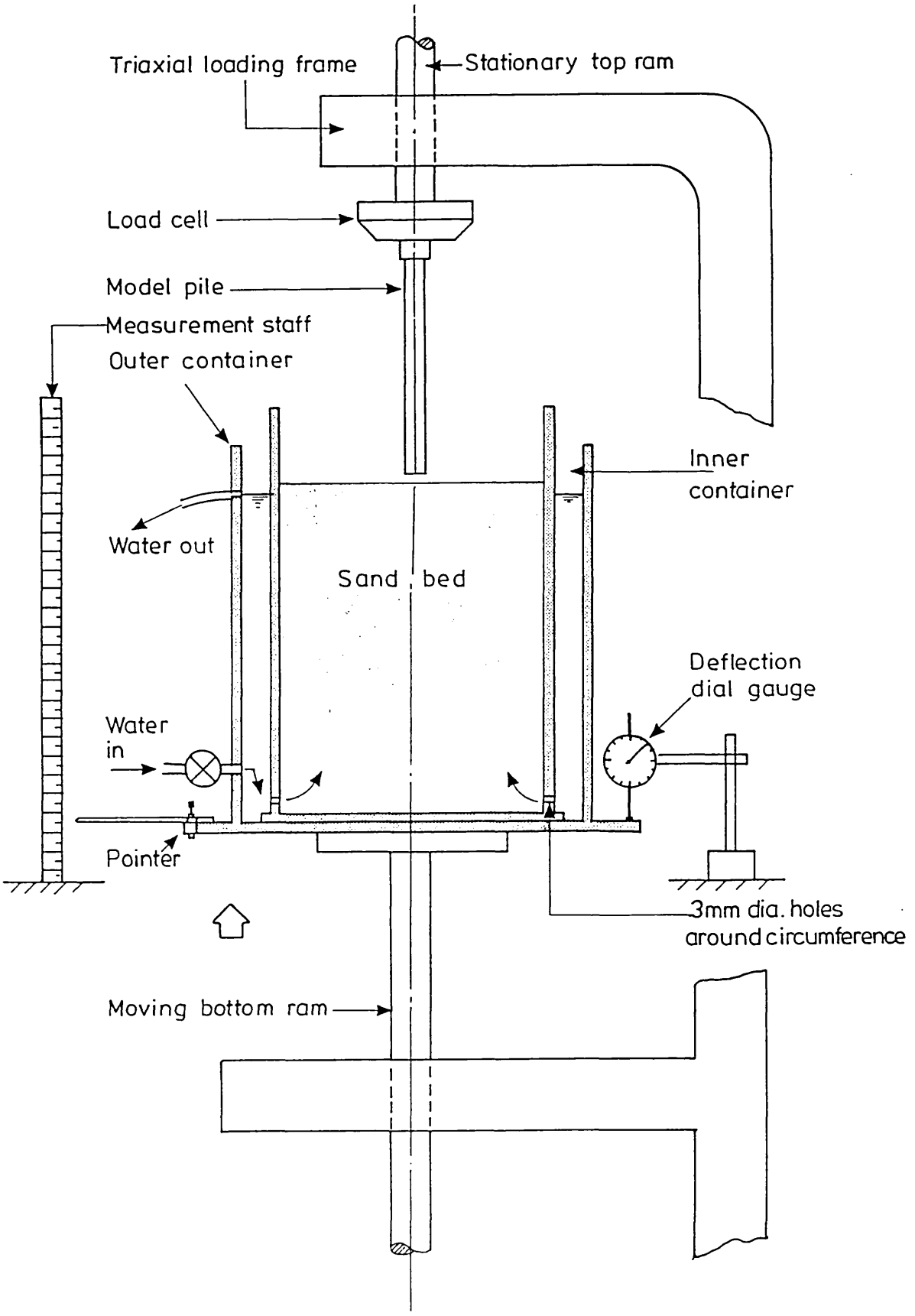

Figure 2.1 Schematic diagram of model pile test rig

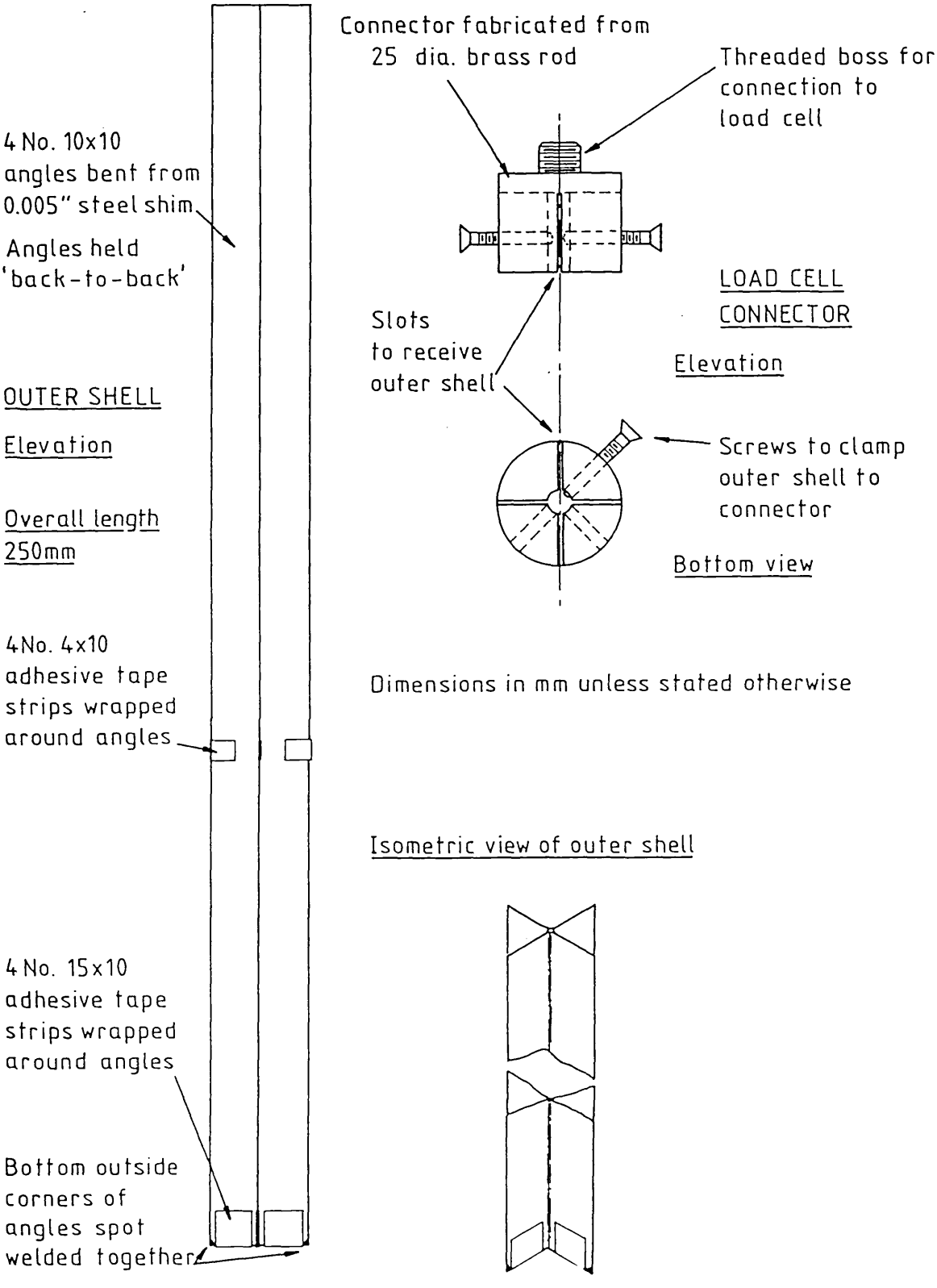

Figure 2.2 Model wedge-piles:
details of outer shell

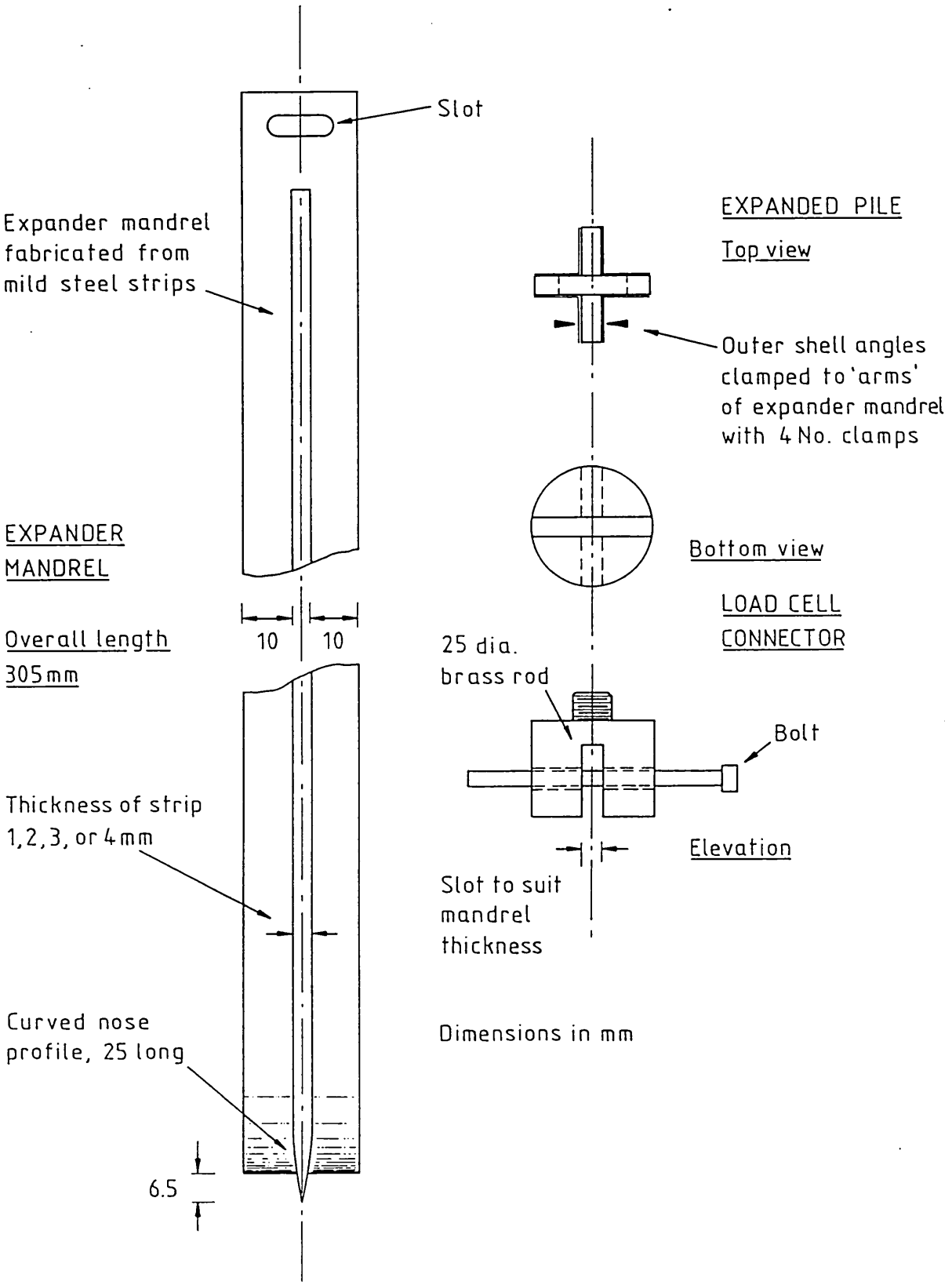

Figure 2.3 Model wedge-piles:
details of expander mandrel

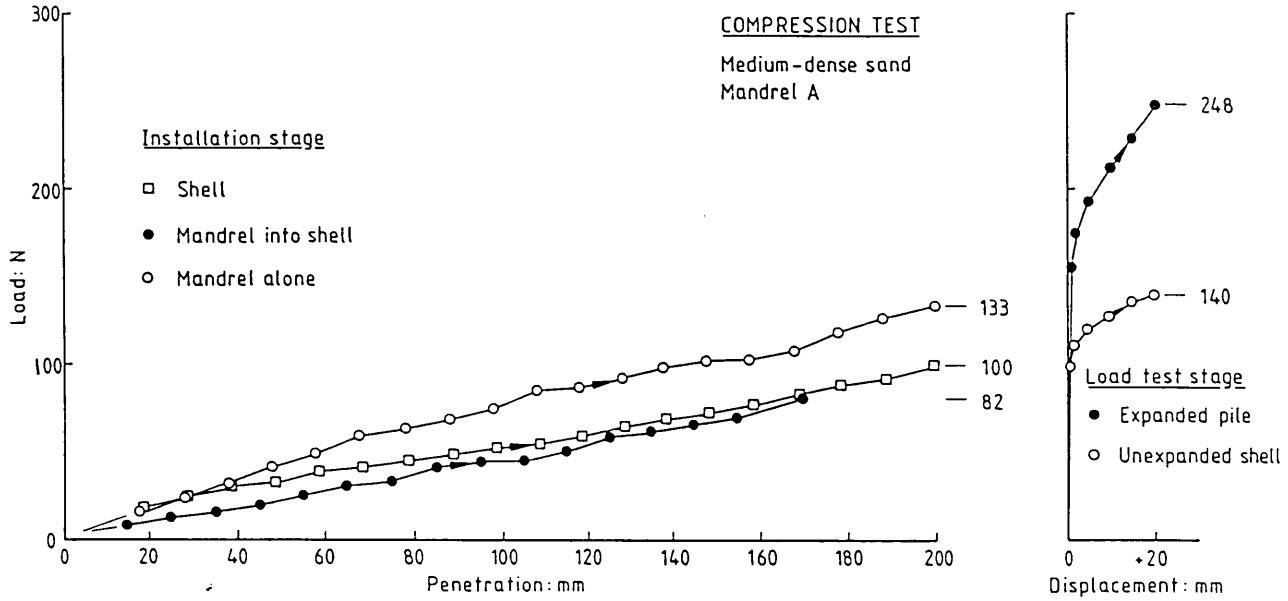

Figure 2.4 Typical results: compression test in medium-dense sand

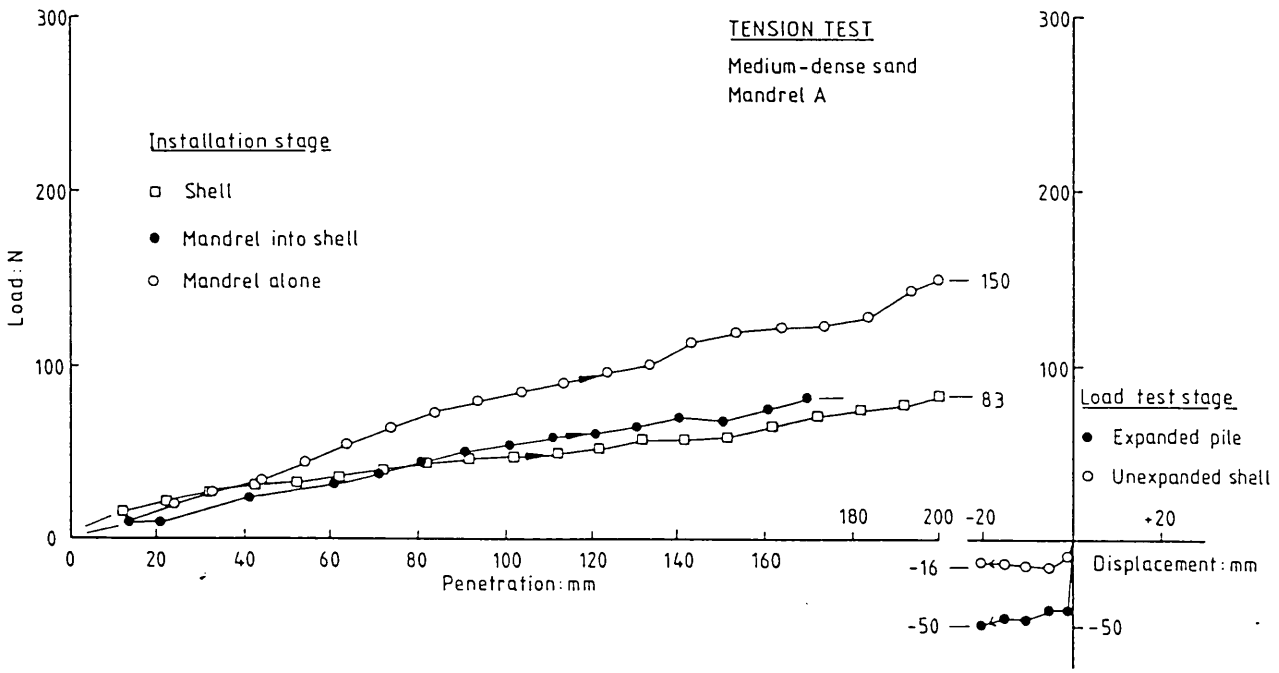

Figure 2.5 Typical results: tension test in medium-dense sand

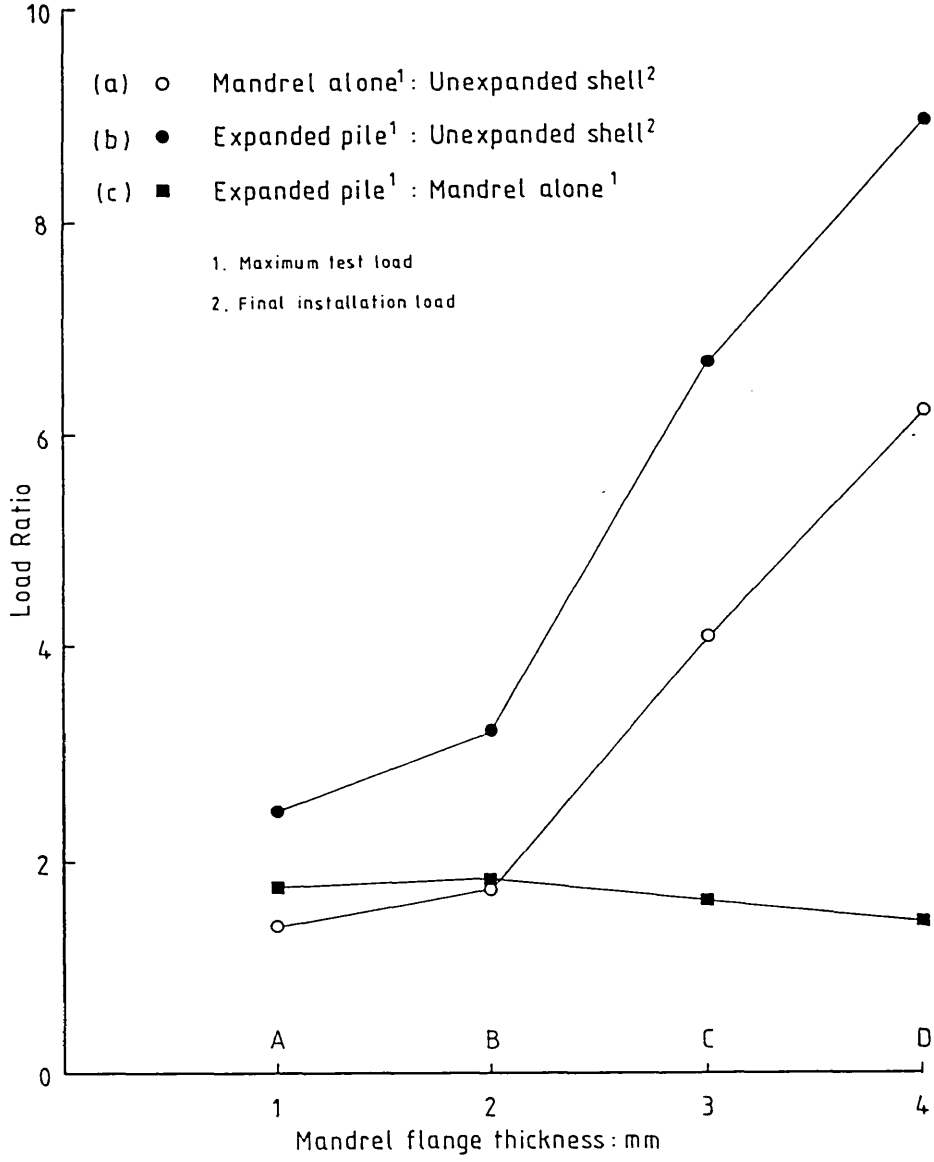

Figure 2.6 Load ratios against Mandrel size: medium-dense sand, compression

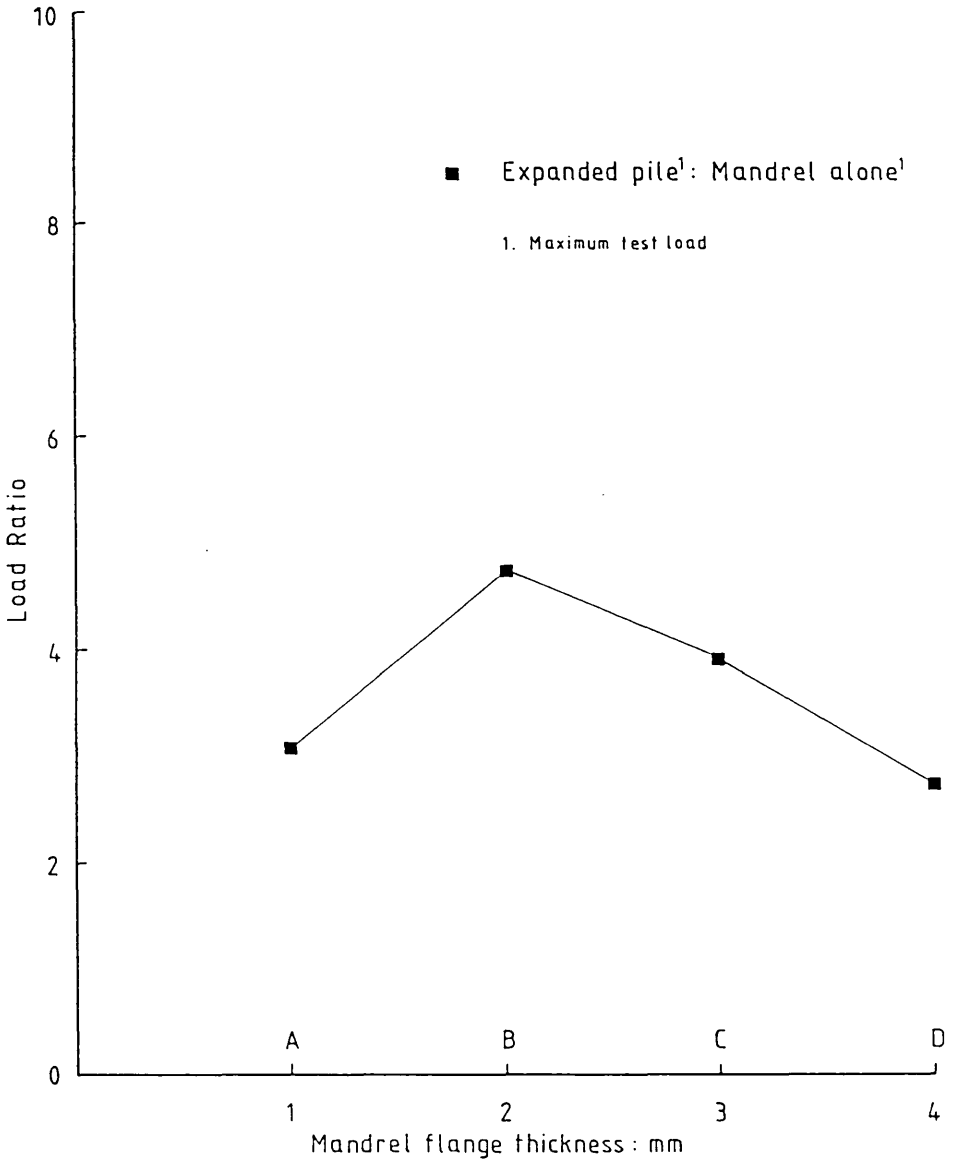

Figure 2.7 Load ratios against Mandrel size: medium-dense sand, tension

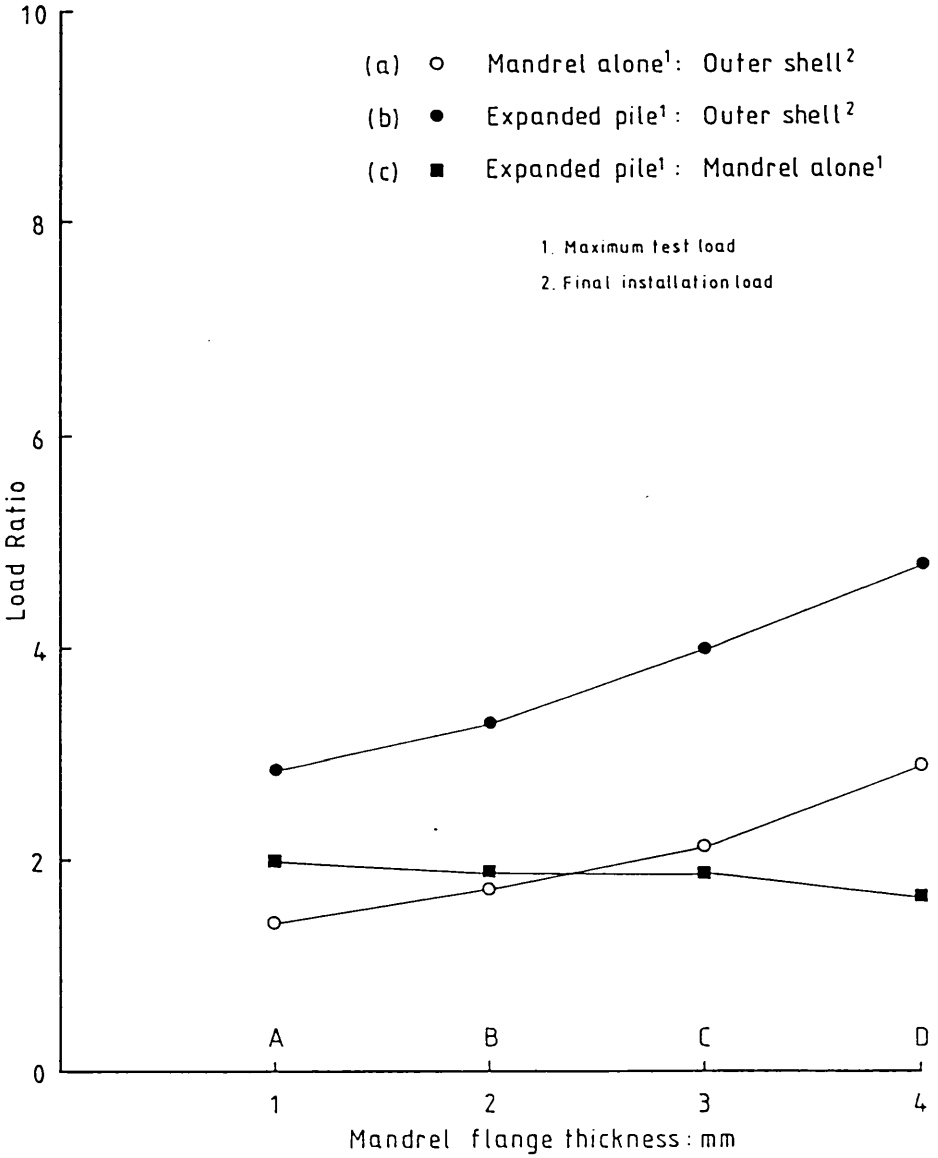

Figure 2.8 Load ratios against Mandrel size: medium-loose sand, compression

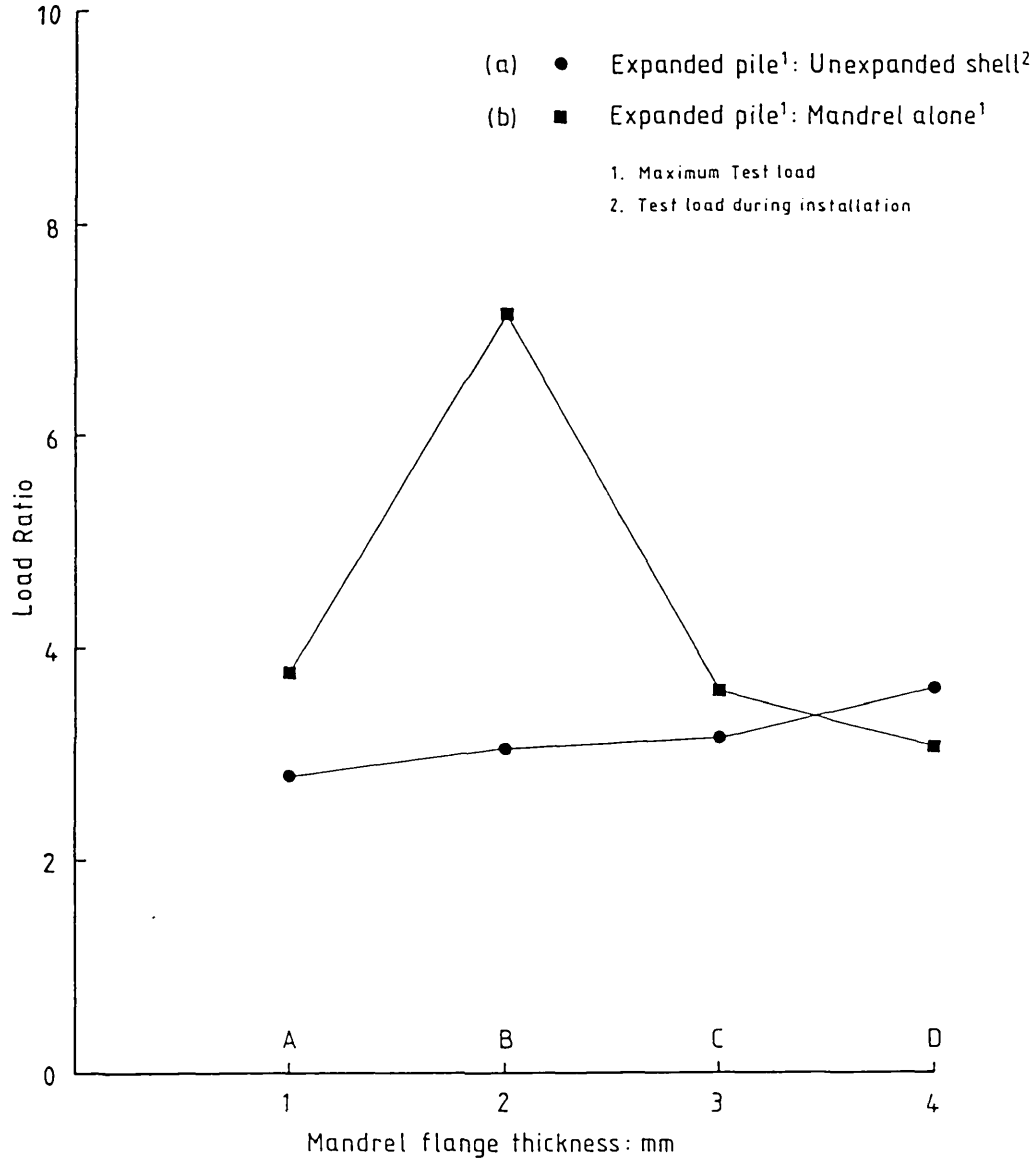

Figure 2.9 Load ratios against Mandrel size: medium-loose sand, tension

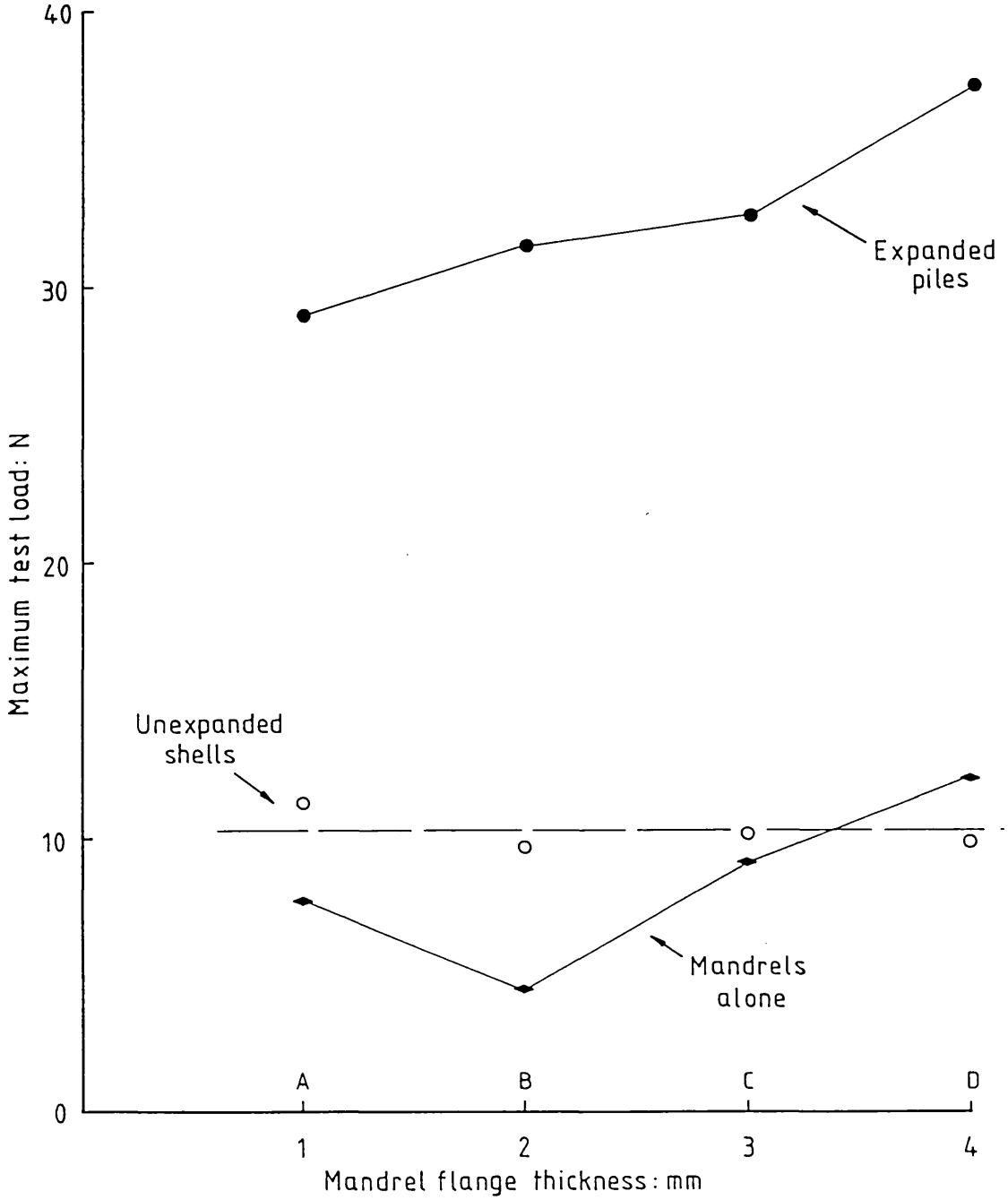

Figure 2.10 Test loads against Mandrel size: medium-loose sand, tension

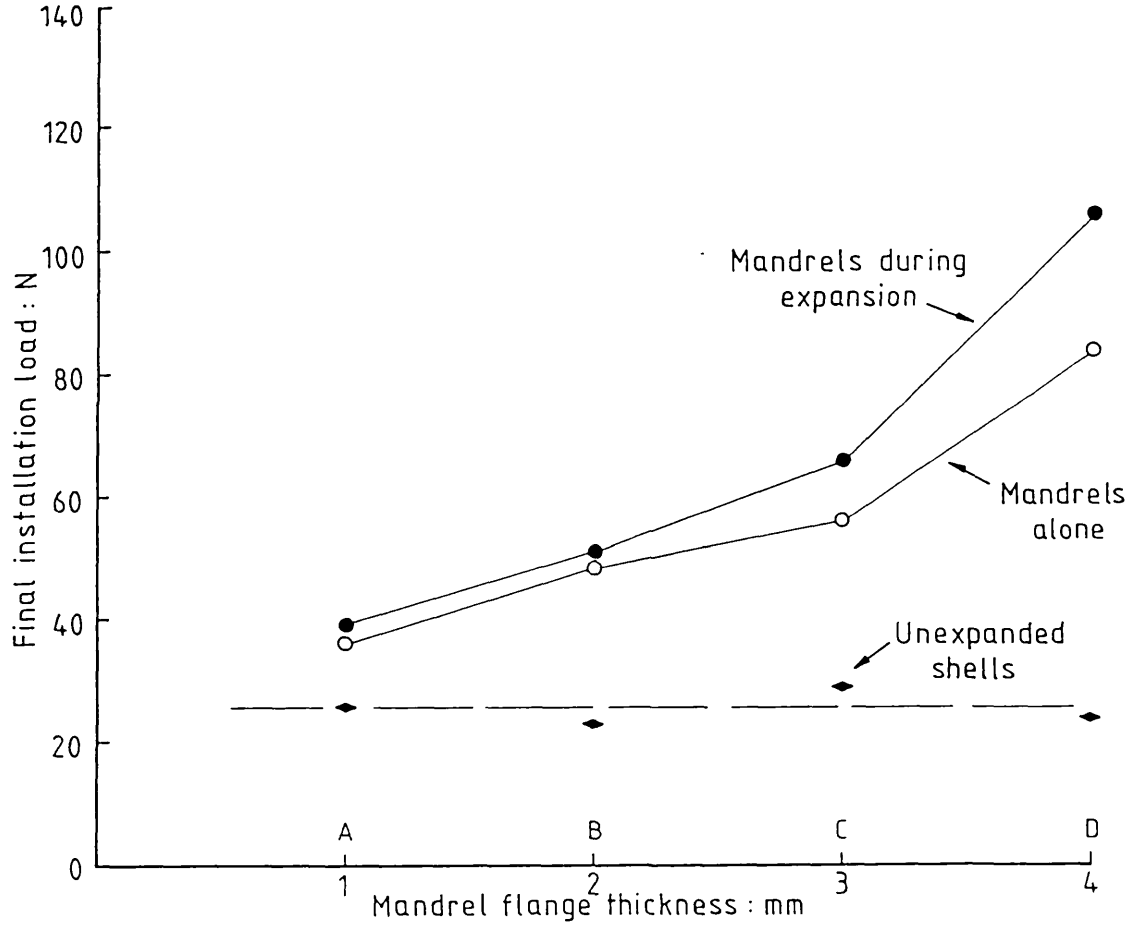

Figure 2.11 Installation loads against Mandrel size: medium-loose sand, tension

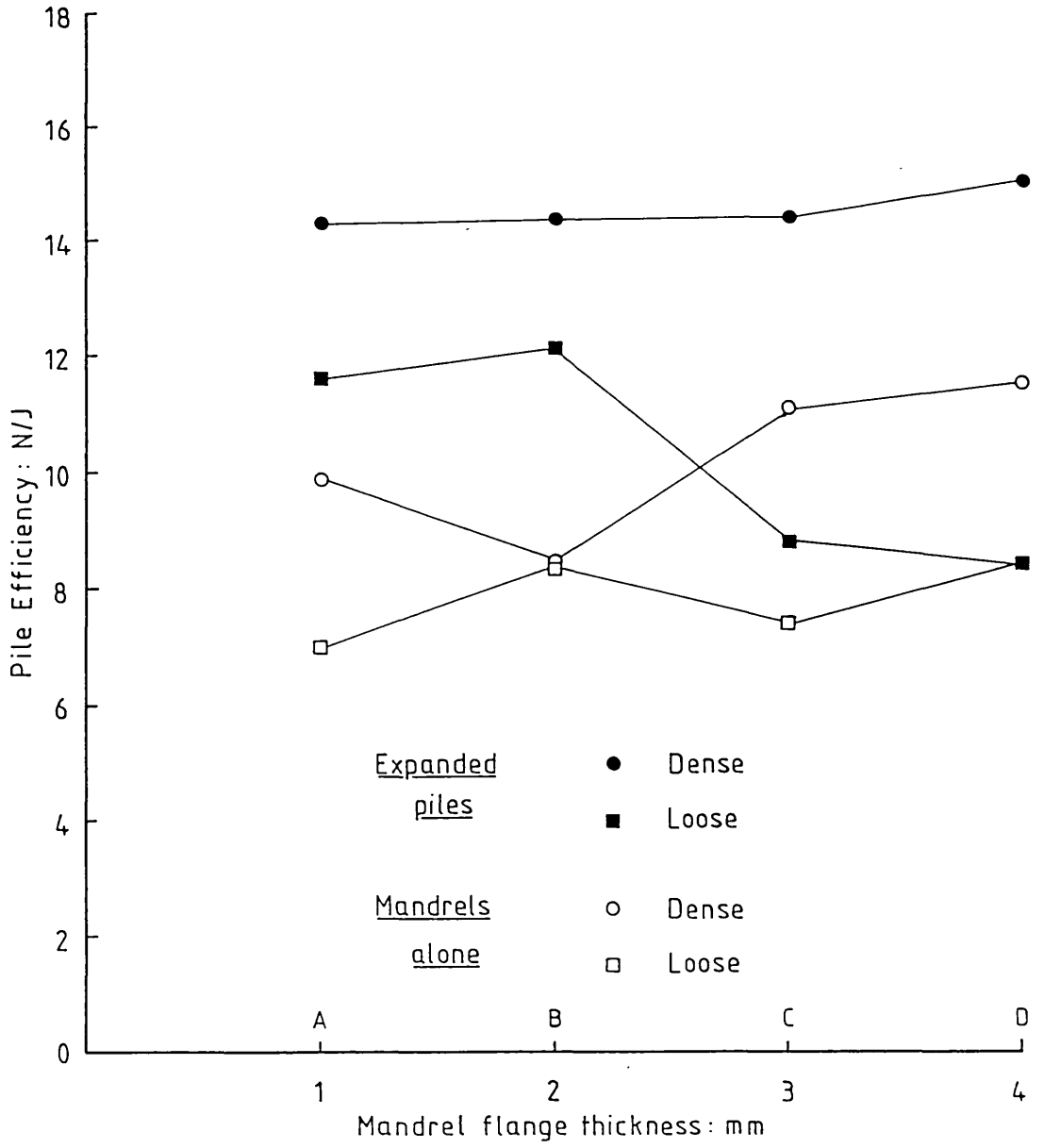

Figure 2.12 Pile Efficiency against Mandrel size: compression tests

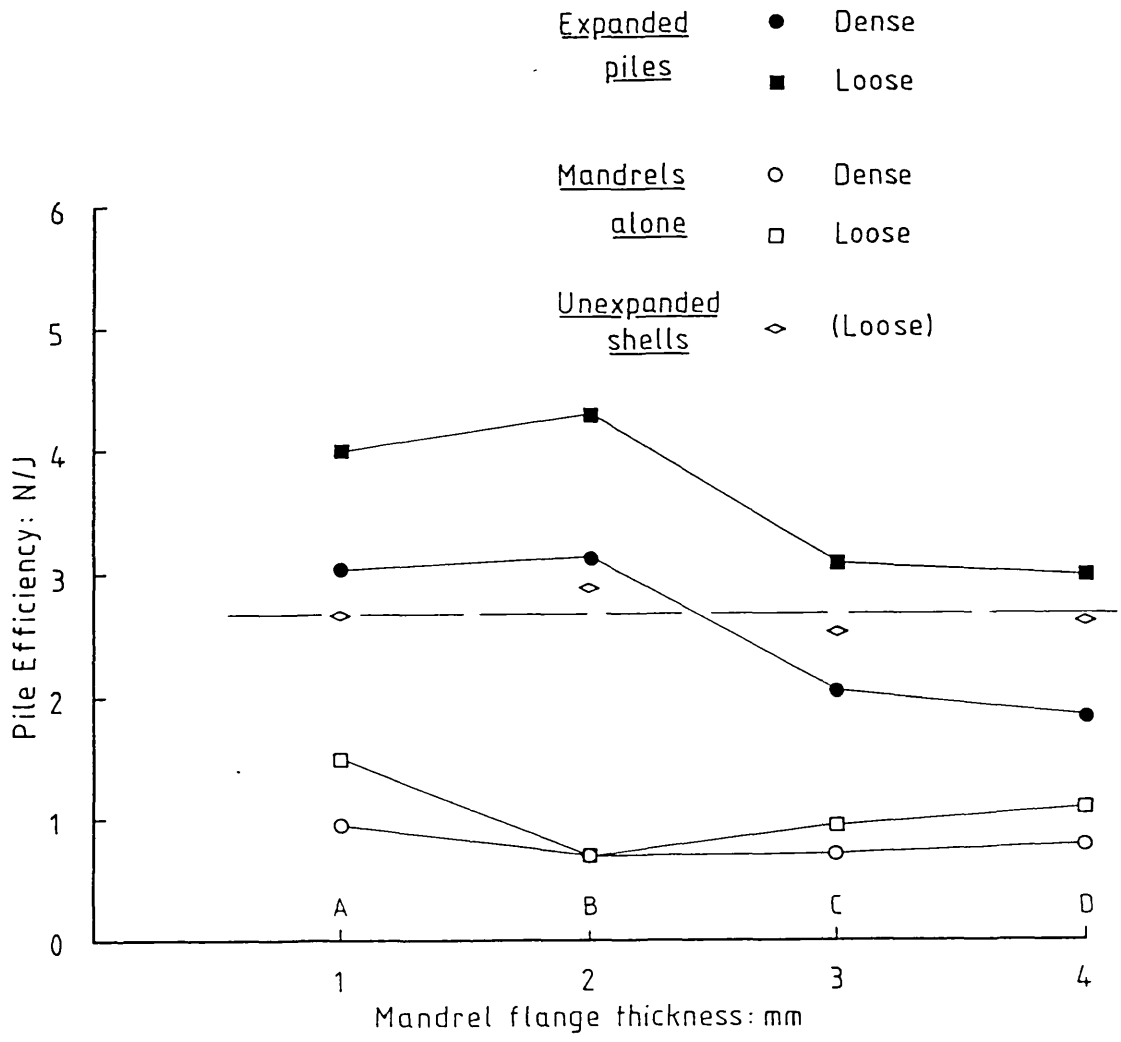

Figure 2.13 Pile Efficiency against Mandrel size: tension tests

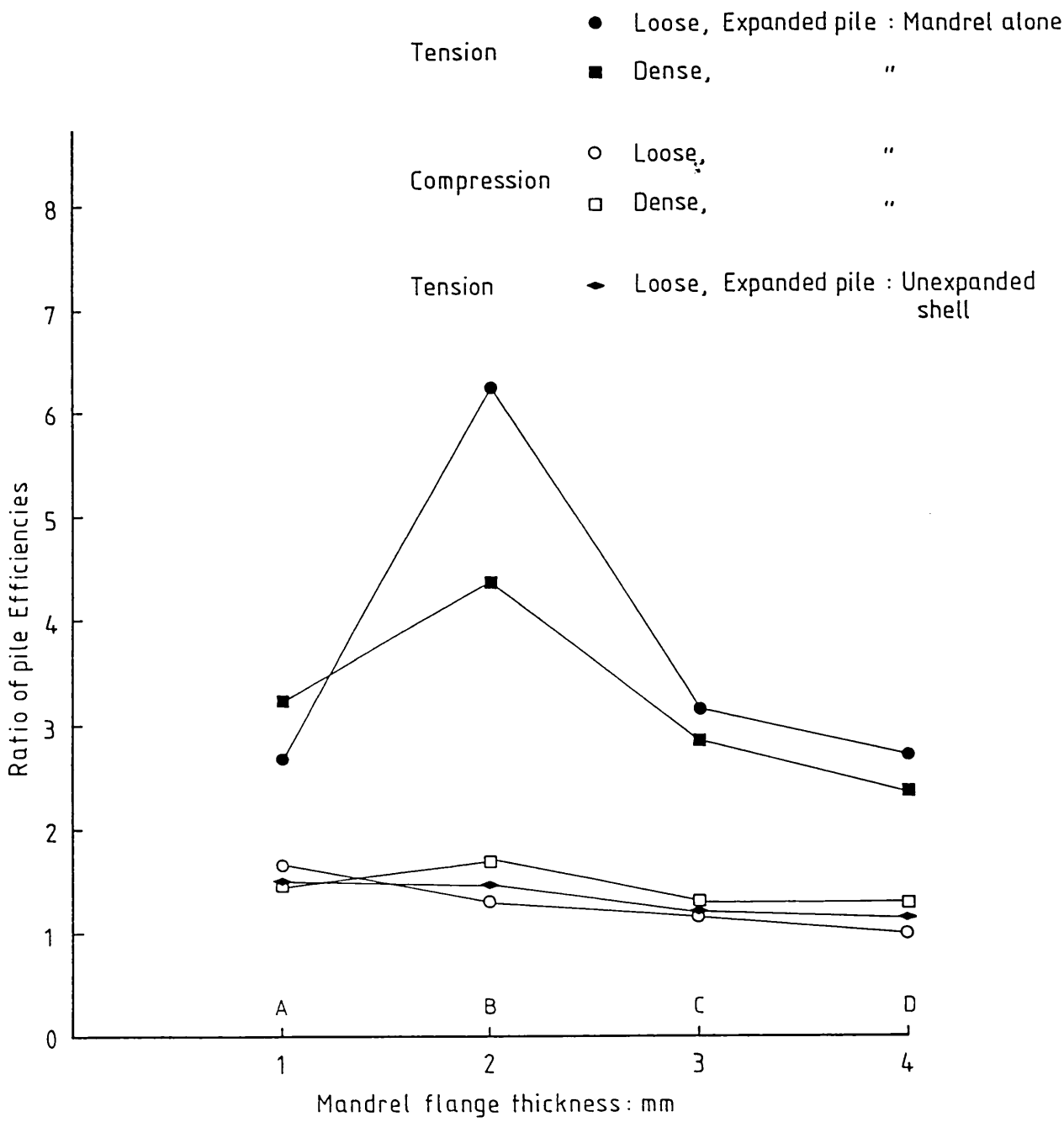

Figure 2.14 Increase in pile Efficiency against Mandrel size: all tests

Mandrel	Amount of expansion %	Shell mm^2	Nominal X-sect. areas Mandrel[A] mm^2	Mandrel+Shell[B] mm^2	Ratio B:A
A	5	10	41	51	1.24
B	10	10	84	94	1.12
C	15	10	129	139	1.08
D	20	10	176	186	1.06

Table 2.1 Cross-sectional areas of model piles

Mandrel	Amount of expansion	Final installation loads			Test loads		Ratio	Ratio	Ratio
		Mandrel alone	Expanded pile: Shell[A]	Mandrel	Mandrel alone[B]	Expanded pile[C]	B:A	C:A	C:B
	%	N	N	N	N	N			
Compression tests									
A	5	133.0	99.7	82.5	139.6	247.7	1.40	2.48	1.77
B	10	120.2	72.9	117.7	127.3	234.2	1.75	3.21	1.84
C	15	154.1	46.0	202.4	188.1	307.6	4.09	6.69	1.64
D	20	254.8	48.5	280.7	301.9	434.6	6.22	8.96	1.44
Tension tests									
A	5	150.0	83.5	82.7	-16.0	-49.5	-	-	3.09
B	10	155.4	83.5	126.6	-12.8	-60.6	-	-	4.73
C	15	280.0	179.3	329.7	-20.4	-80.0	-	-	3.92
D	20	232.0	79.3	307.3	-19.4	-53.4	-	-	2.75

Table 2.2 Model pile test results: medium-dense sand

Mandrel	Amount of expansion	Final installation loads			Max. Test loads			Ratio	Ratio	Ratio	Ratio
		Mandrel alone	Expanded pile: Shell[A]	Mandrel	Outer shell[B]	Mandrel alone[C]	Expanded pile[D]	C:A	D:A	D:C	D:B
	%	N	N	N	N	N	N				
Compression tests											
A	5	55.4	38.7	49.5	-	54.9	110.2	1.42	2.85	2.01	-
B	10	70.7	46.0	83.2	-	79.8	151.7	1.73	3.30	1.90	-
C	15	55.5	26.8	80.3	-	57.1	107.1	2.13	4.00	1.88	-
D	20	79.8	32.3	146.8	-	93.6	155.1	2.90	4.80	1.66	-
Tension tests											
A	5	36.2	25.9	38.6	-11.3	-7.7	-29.0	-	-	3.77	2.57
B	10	48.0	23.2	51.1	-9.7	-4.4	-31.5	-	-	7.16	3.25
C	15	56.0	29.2	65.7	-10.2	-9.1	-32.6	-	-	3.58	3.20
D	20	83.9	24.0	106.3	-9.9	-12.2	-37.3	-	-	3.06	3.76

Table 2.3 Model pile test results: medium-loose sand

Mandrel	Amount of expansion	Installation energies			Max. Test loads		Pile efficiencies		Ratio
		Mandrel alone	Expanded pile: Shell	Mandrel	Mandrel alone	Expanded pile	Mandrel alone[A]	Expanded pile[B]	B:A
	%	J	J	J	N	N	N/J	N/J	
Compression tests									
A	5	14.1	10.6	6.7	139.6	247.7	9.90	14.33	1.45
B	10	15.0	7.8	8.5	127.3	234.2	8.46	14.34	1.70
C	15	17.0	6.8	14.5	188.1	307.6	11.06	14.44	1.31
D	20	26.1	6.7	22.2	301.9	434.6	11.55	15.03	1.30
Tension tests									
A	5	16.9	9.5	6.6	-16.0	-49.5	0.95	3.07	3.23
B	10	17.8	10.0	9.4	-12.8	-60.6	0.72	3.13	4.35
C	15	28.3	18.4	20.6	-20.4	-80.0	0.72	2.05	2.85
D	20	24.6	8.7	20.0	-19.4	-53.4	0.79	1.86	2.35

Table 2.4 Model pile installation energies and Efficiencies: Medium-dense sand

Mandrel	Amount of expansion	Installation energies			Max. Test loads			Pile efficiencies			Ratio	Ratio
		Mandrel alone	Expanded pile: Shell	Mandrel	Shell	Mandrel alone	Expanded pile	Shell[A]	Mandrel alone[B]	Expanded Pile[C]	C:A	C:B
	%	J	J	J	N	N	N	N/J	N/J	N/J		
Compression tests												
A	5	7.8	5.1	4.3	-	54.9	110.2	-	7.0	11.6	-	1.66
B	10	8.5	5.9	6.6	-	79.8	151.7	-	9.4	12.2	-	1.30
C	15	7.7	3.9	8.3	-	57.1	107.1	-	7.4	8.8	-	1.18
D	20	11.0	4.6	13.8	-	93.6	155.1	-	8.5	8.4	-	1.00
Tension tests												
A	5	5.1	4.2	3.0	-11.3	-7.7	-29.0	2.68	1.50	4.03	1.5	2.69
B	10	6.4	3.3	4.0	-9.7	-4.4	-31.5	2.91	0.69	4.31	1.48	6.25
C	15	9.4	4.0	6.6	-10.2	-9.1	-32.6	2.54	0.97	3.08	1.21	3.16
D	20	11.0	3.8	8.6	-9.9	-12.2	-37.3	2.63	1.11	3.02	1.15	2.72

Table 2.5 Model pile installation energies and Efficiencies: Medium-loose sand

CHAPTER 3
DESCRIPTION OF LARGE-SCALE PILES AND EQUIPMENT

3.1 Introduction

Large scale field trials of the Wedge-Pile were undertaken using two types of 6m long steel piles. The piles were installed and tested at two different sites. This Chapter describes the piles and testing equipment developed for the field trials. Chapters 4 and 5 cover the investigations at the two sites.

3.1.1 Background to field trials

The overall aim of the field trials was to demonstrate the Wedge-Pile principle at large scale. Within this overall aim, the specific objectives were as follows:

(a) to establish what gains in pile capacity following expansion are possible under field conditions, and whether such gains are maintained with time.

(b) to investigate whether cavity expansion theory or pressuremeter test data can be used to predict the capacity of an expanded pile.

(c) to investigate the possibility of using expander mandrel installation energy or force as a method of predicting expanded pile capacity.

(d) to assess the practicality of the systems tested and to continue to develop new wedge-pile embodiments and process details.

A test programme involving different arrangements of steel wedge-piles in a range of soil profiles was proposed. Practical feasibility would be assessed by fabricating and installing the piles using standard engineering materials and techniques. Pile testing would be carried out to assess the load carrying characteristics of both unexpanded and expanded piles in the short and in the long term. To complement the pile tests, it was planned that pressuremeter testing would be performed to establish the limiting values of radial stress available by expansion into the ground.

A pile size of approximately 5m embedded length and 100 to 150mm width was envisaged - representing pilot scale for large civil engineering

structures and full scale for light industrial and domestic housing use. This size of pile was similar to the Imperial College instrumented pile (Jardine, 1985). Comparative testing of wedge-piles and the instrumented pile was tentatively planned. This size of pile was also thought to be about the maximum that could be conveniently handled in the college workshop.

It was hoped that installation of the piles would be undertaken on behalf of Imperial College by interested contractors or other organisations at minimal cost. The Geotechnics Division of the Building Research Establishment (BRE) agreed to assist in the provision and development of loading equipment for the pile tests. It was decided to test the piles in tension only. This would eliminate pile base resistance, making increases in shaft resistance easier to interpret. Tension tests would also obviate the need for heavy kentledge.

3.1.2 Types of pile tested
Two types of wedge-pile were fabricated and tested:

(a) large-displacement, closed-ended box section piles
- initial size 140x140mm, 6m long
- tested unexpanded, and expanded by 14% and 21% of initial width

(b) small-displacement, cruciform section piles
- initial size 140x140mm, 6m long
- tested unexpanded, and expanded by 11% and 21% of initial width.

The piles are described fully in Sections 3.2 and 3.3 respectively. The methods of installation, testing, and extraction of the piles are described in Sections 3.4 to 3.9.

The piles were fabricated from standard steel sections, and were designed to be extracted and reused at different sites. The pile length of 6m was a stock length for the steel sections and conveniently gave a depth of embedment of 5m. The two pile configurations chosen were easily made up using angle, box, and flat sections. The piles were intended to represent typical large and small displacement piles used in practice (Weltman and Little, 1977).

The amounts of expansion of the piles were selected on the basis of the results from the initial model tests in the laboratory, which had indicated an optimum expansion in the 10 to 20% range. Also, the results from pressuremeter tests typically exhibit a limiting radial stress in this radial strain range (see Chapter 9).

3.1.3 Choice of sites

The piles were installed and tested at two sites:

(a) a highly weathered chalk profile at the plant yard of piling contractor W. A. Dawson Ltd., Luton, Bedfordshire

(b) a medium plasticity boulder clay at the Building Research Station (BRS), Garston, Hertfordshire.

Full details of the test programmes at these sites are provided in Chapters 4 and 5.

There were two main reasons for selecting these particular sites.

Firstly, they provided extremes of soil type. Results from the two sites would provide an indication of the range of behaviour likely in other soil types. It was thought that the Wedge-Pile would be particularly appropriate for use in the chalk profile, with large increases in carrying capacity expected. This profile was also relevant to offshore piling in carbonate materials, where it was felt that there might be immediate applications for the Wedge-Pile. In contrast, the Wedge-Pile was thought to be rather unsuited to the clay till profile, with smaller increases in capacity expected. Another advantage of the BRS site was that various geotechnical testing had been performed there in the past.

The second main reason for selecting these two sites was to make maximum use of free offers of assistance from W.A. Dawson and BRE. As well as these organisations providing site facilities, W. A. Dawson allowed the use of their yard, craneage, and general workshop facilities; while BRE provided considerable assistance with transport, craneage, labour, and fabrication.

3.1.4 Resources and Methods

The methods used to fabricate and install the piles were intended to be representative of standard civil engineering practice. However, the system was not intended to be a 'commercial' prototype.

The project was subject to severely limited financial resources. Accordingly, there was great reliance on the assistance offered by BRE and W.A. Dawson, and other interested parties. This influenced the type of equipment developed and the site working methods adopted. For convenience, the BRS was gradually adopted as the base for the fabrication and storage of piles and equipment. Most of the fabrication

was undertaken at the BRE Fabrications Workshop, when staff were available. To maximise the use of this facility, simple fabrication techniques were adopted whenever possible. Drilling, welding, and flame cutting were relied on heavily, with machining being kept to a minimum and being carried out in the Imperial College workshops. Whenever possible, equipment was designed to make use of materials already available. Most site operations were organised to be performed by the author and one other person, with minimum use of craneage and other plant in order to cut down on hire costs.

3.2 Box Pile

3.2.1 Overall arrangement

The overall arrangement of the box pile is shown in Figure 3.1. It comprises two main components:

(a) outer shell
(b) expander mandrel

The outer shell was made up from four equal angle sections, held in a square configuration by temporary connections and driven as one. It was closed at the bottom by means of a driving shoe. The outer shell was driven by means of an internal driving mandrel acting against the driving shoe.

The expander mandrel was made up from box section. The outside dimensions of the expander mandrel were greater than the inside dimensions of the outer shell, such that the outer shell was split apart and expanded radially as the expander mandrel was driven into it. A nose section was provided at the bottom of the expander mandrel. The aim of the nose was to give a smooth transition of the outer shell from its unexpanded to its expanded position.

The piles were fabricated from Grade 43A hot rolled steel sections. Except in the case of one of the expander mandrels, the steel sections were not coated with mill varnish. The selection of section sizes for the various pile components was dependent upon the available combinations of angle and box section that would give expansions in the 10 to 20% range, and also allow an internal driving mandrel to be used. The combination of steel sections chosen was considered the most suitable amongst a number of other possibilities.

Two outer shells, one driving mandrel, and two expander mandrels were fabricated for use at the Luton site. After extraction at the end of

testing at this site the box piles were refurbished, and reused at the BRS site. An additional outer shell was fabricated for use at the BRS site. Plate 3.1 is an overall view of the box pile components.

3.2.2 Details of outer shell

Each outer shell was 6m long, made up from four uncoated 70x70x10mm equal angle sections (angles). The angles were held in a 140x140mm square configuration by means of temporary connections at 1m spacings. The temporary connections were required to be strong enough to hold the outer shell together prior to and during installation, but weak enough to be split apart when the expander mandrel was driven. Different arrangements were tried (Figure 3.2b, Plates 3.2, 3.3).

Initially, steel plates were used. These were bolted, pop-riveted or welded to the angles. It was found that this arrangement was liable to break apart when the pile was handled or transported, such that temporary clamping together of the outer shell was required prior to driving. Tack welding was adopted instead, this proved to be quicker and more robust. A light tack of about 10mm length was used. Both the plate connections and the tack weld connections performed satisfactorily during driving (Sections 3.4, 3.5).

The bottom of the outer shell was closed by means of a driving shoe, detailed in Figure 3.3 and shown in Plate 3.4. The driving shoe was machined from solid mild steel and comprised a conical tip, a neck section, and an anvil block. It was located and retained in the end of the outer shell by means of collar pieces welded to the angles, which interlocked with the neck of the driving shoe.

Because the driving shoe was an expensive item to machine and it was intended to use each pile more than once, the following measures were taken to prevent the driving shoe being lost when the pile was extracted (Figure 3.3):

(a) The dimensions of the driving shoe neck and anvil block were such that the driving shoe was still retained by the collar pieces after the maximum possible expansion of the outer shell.

(b) A cable anchorage point was provided on the driving shoe. This comprised a drilled and tapped hole to receive an eyebolt (Plate 3.4). A cable, passing down through the hollow pile elements, could be secured to the driving shoe. The cable remained in place throughout installation and testing of the pile, and could be used to pull the driving shoe from the ground in the event of it

slipping from the collar pieces during pile extraction. The cable arrangement was deployed at the Luton site, but it was not needed.

(c) At the BRS site the bottom 200mm length of the outer shell angles, enclosing the driving shoe, were welded together (Plate 3.5).

Shear lugs, formed from flat section, were welded to the angles near the top of the outer shell (Figure 3.2a). These formed part of the tension linkage between the the outer shell and the pile loading system, described in Section 3.6.4. They also provided lifting sling anchorage points.

3.2.3 Details of driving mandrel

It was anticipated that installation of the large-displacement box piles would involve high driving forces. To avoid damage to the head of the outer shell, the box piles were bottom driven by means of an internal driving mandrel bearing against the driving shoe. The driving mandrel comprised a 6m length of 100x100x10mm box section. The driving mandrel was contained within the outer shell and impinged against the anvil of the driving shoe. Packing strips welded to the driving mandrel kept it centrally positioned within the outer shell (Figures 3.1, 3.2c). Temporary lifting lugs were welded to the driving mandrel as required on site.

3.2.4 Details of expander mandrel

Two expander mandrels were fabricated from box section (box). The expander mandrels were classified on the basis of the amount of radial expansion they produced, expressed as a percentage of the initial outer shell width.

Expander mandrel 'A' was made up from 140x140x8mm box. This expanded the outer shell from 140x140mm to 160x160mm, an increase of 14.3%. The steel surface of this expander mandrel was uncoated.

Expander mandrel 'B' was made up from 150x150x8mm box. This expanded the outer shell from 140x140mm to 170x170mm, an increase of 21.4%. The steel surface of this expander mandrel was coated with mill varnish.

Each expander mandrel comprised a 5m long shank section of plain box and a 0.8m long nose section formed from box to give a curved profile over the bottom 0.7m. The nose section was detachable for easy fabrication and refurbishment, and was connected to the expander mandrel shank by means of internal bolted plates.

The sensitivity of wedge-pile performance on the shape of the expander mandrel nose formed an important part of the overall project. The initial approach adopted was to assess the performance of different nose profiles fabricated using simple workshop techniques. A nose length of 0.7m was selected for the box piles.

The nose section was fabricated as shown diagrammatically in Figure 3.4. A 0.8m length of box (Figure 3.4a) was flame cut over a length of 0.7m (Figure 3.4b). The four cantilever segments thus formed were displaced and clamped into position as shown in Figure 3.4c, to give end dimensions of 120x120mm - designed to fit inside the top of the outer shell. The nose was then welded up (Figure 3.4d), and finally smoothed with an angle grinder (Figure 3.4e). Figures 3.5 and 3.9 give further details of the expander mandrel nose arrangements. Plate 3.6 is an overall view of the nose of expander mandrel B.

The expander mandrels could be top driven, or bottom driven by means of the driving mandrel acting against an internally welded bearing plate at the bottom of the expander mandrel shank (not shown on the drawings). Various lugs were welded near the tops of the expander mandrels for lifting and pile loading purposes. The lugs were similar to the shear lugs at the tops of the outer shells. The arrangements varied and are not shown on the drawings.

3.2.5 Completed pile arrangement

The installed pile arrangement is shown in Figure 3.1. The outer shell of each box pile was driven to a depth of penetration of between 5.2m and 5.3m below ground level. The expander mandrel was driven to a depth of penetration such that the tip of the expander mandrel nose was 300mm short of the top of the driving shoe. The length of pile protruding above ground level allowed a tension connection to either the outer shell or the expander mandrel.

In civil engineering practice, the expander mandrel would be driven through to the bottom of the outer shell. The arrangement adopted for the field trials was designed to prevent damage to the expander mandrel nose and the bottom of the outer shell, and to make certain of retrieving the driving tip upon extraction of the pile.

3.3 Cruciform Pile

3.3.1 Overall arrangement

The overall arrangement of the cruciform pile is shown in Figure 3.6.

As with the box pile, it comprises two main components:

(a) outer shell
(b) expander mandrel

The outer shell was made up from four equal angle sections, held in a cruciform configuration and driven as one. It was held together at the bottom end by a welded driving shoe arrangement.

The expander mandrel was cruciform shaped, made up from flat sections welded together. The expander mandrel was driven into the outer shell, splitting it apart and expanding it radially. A nose section was provided, with the aim of providing a smooth transition between the unexpanded and the expanded positions of the outer shell.

The fabrication of the cruciform pile followed the same lines as that for the box pile. As before, the pile components were fabricated from Grade 43A hot rolled steel sections. The angles forming the outer shell were the same section as for the box pile. The two types of outer shell thus represented alternative arrangements of the same cross sectional area of steel. The flats forming the expander mandrel were selected to give similar expansions to those for the box pile - in the 10 to 20% range. The steel finishes of all the components were not coated with mill varnish.

Two outer shells and two expander mandrels were fabricated for use at the Luton site. After extraction at the end of testing at this site, the cruciform piles were refurbished and reused at the BRS site. Plate 3.7 is a general view of the cruciform piles at the Luton site.

3.3.2 Details of outer shell

The outer shell was 6m long, made up from four uncoated 70x70x10mm equal angle sections (angles). The angles were held back-to-back in a cruciform shape by means of temporary connections at 1m spacings. Tack welds were used. The detail was exactly the same as for the box pile and is shown in Figure 3.7a and Plate 3.8.

At the bottom of the outer shell a driving shoe arrangement was provided to hold the angles together as one and to prevent material being forced between the angles during driving. The driving shoe was formed by welding the angles together across the bottom of the outer shell, and up the sides for a distance of 150mm. This is shown in Figure 3.7b and Plate 3.9.

The outer shell was necessarily top driven. Relatively easy driving was expected for the small-displacement cruciform pile and consequently damage to the head of the outer shell during driving was not envisaged to be a major problem. However, precautions were taken (Figure 3.7a). Reinforcement blocks were provided, and the angles were also bolted together 400mm below the top of the outer shell to prevent the angles being forced apart during driving. Nylon insert nuts were used to prevent loosening of the bolts due to vibration during driving. The tops of the angles were chamfered to form a notch to receive the tip of the expander mandrel nose.

Shear lugs, formed from flat section, were welded to each angle (Figure 3.7a). These formed part of the tension linkage to the pile loading system described in Section 3.6.4. They also provided lifting sling anchorage points.

3.3.3 Details of expander mandrel

Two expander mandrels were fabricated. Each expander mandrel was 6m long, comprised of three flat sections (flats), made up into a cruciform. The expander mandrels were classified on the basis of the amount of radial expansion they produced, expressed as a percentage of the initial outer shell width.

Expander mandrel 'A' was made up from one 150x15mm flat and two 65x15mm flats. This expander mandrel expanded the outer shell from 140x140mm to 155x155mm, an expansion of 10.7%.

Expander mandrel 'B' was made up from one 160x30mm flat and two 65x30 mm flats. This expander mandrel expanded the outer shell from 140x140mm to 170x170mm, an expansion of 21.7%.

In all cases, the steel surfaces of the flats were not coated with mill varnish. The flats were held in a cruciform shape by means of welding at 500mm centres. The weld detail is shown in Figure 3.8.

The expander mandrels were top driven. The lengths of the 'arms' of the expander mandrel were slightly less than those of the outer shell (Figure 3.6) in order to reduce friction between the expander mandrel and the ground during driving.

A nose was formed at the end of the expander mandrel by flame cutting and angle grinding. Machining was not an available option. Because of the difficulty of forming a nose profile using hand held tools, the nose lengths for the cruciform piles were shorter than for the box piles. The

overall nose lengths were approximately 200mm for expander mandrel A and approximately 300mm for expander mandrel B. It was necessary for each nose to locate conveniently in the receiving notch at the top of the outer shell. This was achieved by slightly staggering and flaring the nose profile, and grinding to give sharp leading edges (Figure 3.8). Various lugs were welded to the top of each expander mandrel to provide lifting points or tension linkages to the pile loading system. Details were similar to the shear lugs at the top of the outer shell, and are not shown in the Figures.

Further details of the expander mandrel nose profiles for both the cruciform and the box piles are given in Figure 3.9. Plate 3.10 shows the nose of expander mandrel A.

3.3.4 Completed pile arrangement

The completed pile arrangement is shown in Figure 3.6. The outer shell of each cruciform pile was driven to a depth of 5.2m below ground level. The expander mandrel was driven to a depth of penetration such that the tip of the expander mandrel nose was approximately 200mm short of the bottom of the outer shell. The length of pile protruding above ground level allowed a tension connection to either the outer shell or the expander mandrel.

As with the box pile, the expander mandrel would in civil engineering practice be driven the whole length of the outer shell. A 'clip' type driving shoe might be developed, this being pushed off the end of the outer shell by the expander mandrel nose. A welded shoe arrangement was adopted in the field trials because it was imperative that there was no possibility of the outer shell splitting apart at the bottom during driving.

3.4 Pile Installation at Luton Site

In this Section, box piles and cruciform piles are treated together. Also, the term 'pile' is used to refer both to outer shells and to expander mandrels.

At the Luton site, piles were supported during driving within a simple piling frame and were driven using a 1.5t drop hammer with integral box guide. Craneage was provided by W.A. Dawson.

3.4.1 Piling frame

The piling frame is shown in Plate 3.11. Its purpose was to support the piles vertically during driving. The piling frame was 1.8m high and

comprised large steel beams stacked in a 'nest' and tack welded together. The pile to be driven was held at the top of the piling frame by a 'gate', formed by light steel sections welded to the large beams. The piling frame could be quickly dismantled and moved.

3.4.2 Pile installation procedure

Before pitching, the piles were marked off with chalk at 50mm intervals, to enable driving records to be made. The final penetration level was also marked off. When driving an outer shell, these marks were used in conjunction with a reference beam clamped across the piling frame beams. When driving an expander mandrel, the top of the outer shell was used as the reference.

The piles were lofted vertically during pitching by means of a fabric lifting sling wrapped around the top of the pile. The welded lugs at the top of the piles prevented the lifting sling from sliding off the pile. In the case of the box piles, the driving mandrel was inserted into the outer shells and expander mandrels before pitching. This operation was performed at ground level, with the pile components raised at one end on a trestle.

The outer shells were pitched as follows:

(a) The large beams of the piling frame were assembled and welded together.

(b) The outer shell was lowered through the piling frame and rested on the ground.

(c) With the outer shell resting on the ground but still being held by the crane, it was worked into a vertical position by hand. Verticality was checked by using a spirit level.

(d) The outer shell was held in this vertical position by means of the welded steel sections forming the 'gate'.

(e) The piling hammer was lowered onto the top of the outer shell or driving mandrel, ready for driving.

The outer shells were driven in two stages. In the first stage they were supported by the piling frame, and driven until the piling hammer guide was just clear of the top of the piling frame. The piling frame was then quickly dismantled and moved aside. In the second stage the piles were driven unsupported to their final depth of penetration. In

the case of the box piles, the driving mandrel was removed from the outer shell at this stage.

The procedure for pitching the expander mandrels was similar to that for the outer shells:

(a) The piling frame beams were reassembled around the driven outer shell.

(b) The expander mandrel was lowered through the piling frame and the nose tip was interlocked with the top of the outer shell.

(c) The expander mandrel was worked into a vertical position as before.

(d) The 'gates' were welded into position as before, but fitted more loosely, with timber packing if necessary, to allow the expander mandrel to follow the course of the outer shell during driving.

(e) The piling hammer was lowered onto the top of the expander mandrel or driving mandrel ready for driving.

The expander mandrels were driven in two stages as before, to the appropriate depth of penetration within the outer shells. It was necessary to weld a lightweight extension piece to the top of the expander mandrels at the very end of driving, to stop the piling hammer guide fouling the top of the outer shells.

3.4.3 Hammer arrangement and comments on pile driving

The piles were driven using a simple 1.5t drop hammer located on top of the piles by an integral box guide. The hammer was supplied and operated by W.A. Dawson. Hammer operation was by 'yard' cranes which did not have provision for the accurate setting of drop height. Reasonable control was available, but a number of different cranes and drivers were involved during the pile installation programme, making comparison of driving energies difficult. Also, because of the novelty of the system, the general philosophy during driving was to tap the piles gently into the ground, rather than to achieve maximum rate of penetration.

The temporary connection systems (Sections 3.2.2, 3.3.2) performed well. The outer shells were successfully held together as one during driving. A few of the connections were split apart at this stage, but this did not appear to affect driving. As the expander mandrels were driven the temporary connections appeared to split apart easily - there was no evidence of the connections affecting the penetration of the expander

mandrel into the outer shell.

The piles at the Luton site were all driven vertically to within an accuracy of approximately 1 in 100, based on measurements on the protruding lengths of the piles.

3.5 Pile Installation at BRS Site

As in the previous Section, box piles and cruciform piles are treated here as one. Outer shells and expander mandrels are both referred to as 'piles'.

At the BRS site it was decided to install the piles with a double-acting air hammer, this being the cheapest available system. It was too expensive to hire a crane with a drop hammer arrangement, and installation by jacking would have involved heavy kentledge for reaction and a large jacking frame. The piles were supported within a piling frame resting on large runway beams. The piling hammer was located on the top of the pile by leg guides. Craneage was either hired in, or provided by BRE.

Plate 3.12 is a general view of the piling frame during pile driving operations.

3.5.1 Piling frame and runway beams

The test bed was spanned by two 9m long, 914x419mm runway beams, supported clear of the ground by timber and steel grillages resting on 3.0x1.5m reinforced concrete spread foundations. The runway beams also formed part of the pile testing system (see Section 3.6).

The piling frame is shown in Figure 3.10. The basic frame was a braced double 'T' arrangement, box sections forming the base and 'I' beams forming the columns. The frame was fitted with four adjustable wheels, enabling it to be rolled along the runway beams into the appropriate position for pile driving. The frame having been rolled into position, the wheels were retracted so that the base of the frame rested on the runway beams. Final adjustments of the frame position could be made by pinching with a crowbar. The piling frame was then held in position during pile driving by bolted clamps bearing against the underside of the runway beams.

The pile was held in position during driving by two sets of adjustable guides mounted within the piling frame uprights. These were made up from drilled and slotted angle sections (Figure 3.11).

3.5.2 Pile installation procedure

The piles were prepared and handled in exactly the same manner as at the Luton site. The procedure for pitching the outer shells was as follows:

(a) The adjustable guides were loosely assembled within the piling frame to receive the outer shell.

(b) The outer shell was lowered into position within the guides and brought to rest on a steel plate at ground level. The plate made manoeuvring of the outer shell across the ground surface easier.

(c) With the outer shell resting on the steel plate but still being held by the crane, it was worked into a vertical position by hand, verticality being checked with a spirit level.

(d) The guides were bolted up tight against the outer shell and the steel plate was removed.

(e) The piling hammer was lowered onto the top of the outer shell, being guided into position by hand.

Prior to driving, one guide was positioned at the bottom of the piling frame, and one near the top. The top guide was lowered once during driving, then both guides were progressively removed in advance of the hammer. There was a pause in driving each time these adjustments were made. In the case of the box piles, the driving mandrel was removed after driving the outer shell.

The procedure for pitching the expander mandrels was similar to that for the outer shell:

(a) The adjustable guides were loosely bolted back in position, to receive the expander mandrel.

(b) The expander mandrel was lowered into the piling frame and the nose tip was interlocked with the top of the outer shell.

(c) With the expander mandrel resting on the outer shell it was worked into a vertical postion as before.

(d) The guides were tightened as before. However, to allow the expander mandrel to follow the course of the outer shell, the guides were loosened during driving if any signs of 'nipping' were

seen or heard.

(e) The piling hammer was lowered onto the top of the expander mandrel, as before.

Driving of the expander mandrel proceeded in the same manner as for the outer shell. Plate 3.13 shows a box expander mandrel being driven into an outer shell.

3.5.3 Hammer arrangements

Two types of double-acting air hammer were employed at the BRS site:

(a) Atlas-Copco PH5, overall weight 440kg
(b) BSP 500N, overall weight 1143kg

Details of the hammers are given in Appendix 3.1. The hammers were driven by standard air compressor units. To mount the piling hammers firmly and centrally over the top of the piles, driving caps and adjustable leg guides were designed and fabricated. These were fitted to the 'basic hammer', as supplied by the plant hire firm. The pile installation programme at the BRS site took place in three phases, with the PH5 hammer being used for the first and last phases, and the 500N hammer being used for the middle phase.

3.5.3.1 Leg guide arrangements: PH5 hammer

The PH5 hammer was used to drive one of the box outer shells, box expander mandrel B, and cruciform expander mandrel B.

The leg guide arrangements are shown in Figures 3.12 and 3.13. A two piece driving cap, shown in Figure 3.12, was used to protect the heads of the box driving mandrel and the box expander mandrel. The lower part of the driving cap was designed to interlock with the stub legs of the hammer. The driving cap was not used for the cruciform expander mandrel.

The hammer legs comprised four 1m long angle sections bolted to the hammer body (Figure 3.13). Adjustable bolt grips at the bottom of the legs, acting in conjunction with either the interlocked driving cap or a second set of bolt grips, located the hammer on top of the pile. Lengths of box section were bolted to the top of the cruciform expander mandrel to give a convenient cross-section for the bolt grips to act against.

3.5.3.2 Leg guide arrangements: 500N hammer

The 500N hammer was used to drive both of the cruciform outer shells,

one of the box outer shells, cruciform expander mandrel A, and box expander mandrel A.

The box pile driving cap used with the PH5 hammer was retained to aid comparison between the performances of the two hammers. A driving cap was not used for the cruciform piles, as these were already reinforced for driving (Section 3.3.2). The leg guide arrangements are shown in Figure 3.14. Guides or 'inserts', fabricated from angle section, were bolted to the standard adjustable insert holders. The inserts could be bolted in different positions according to the size of the pile being driven. Spacer blocks were welded to the cruciform piles; these were used in conjunction with the existing welded lugs to give a convenient cross section for the inserts to grip against.

3.5.4 General comments on pile driving

At the BRS site, the box piles were driven first. After discussions with piling hammer specialists, the Atlas Copco PH5 hammer was selected to drive the piles and the piling frame was designed accordingly. The first box outer shell was installed succesfully and the piling frame performed exceptionally well. However, driving was slow and the PH5 hammer appeared to be rather too light for the pile being driven.

During installation of the second box outer shell the driving shoe collar pieces failed during driving, after the rate of pile penetration had become very slow. As a result of this failure, it was necessary to change to the next heaviest available hammer - the 500N - in order to drive a replacement outer shell. The 500N was therefore used during the next phase of the pile installation programme, which included both box piles and cruciform piles. The 500N, although required for driving the box outer shells, proved to be unnecessarily heavy for the cruciform piles and the PH5 was reverted to for the third and final phase of pile installation.

The temporary connection systems (Sections 3.2.2, 3.3.2) performed very well during pile installation, showing only minor distress as the outer shells were driven but apparently splitting apart easily when the expander mandrels were driven.

Driving records were made in order to compare driving energies for the various piles. Comparisons were necessarily qualitative, due to the different hammers and air compressors that were used.

The box piles at the BRS site were driven vertically to within an accuracy of approximately 1 in 100, based on measurements on the exposed

lengths. The vertical driving accuracy of the cruciform piles was worse - approximately 1 in 50. This was due to the heavy 500N hammer disturbing the alignment of the outer shells within the piling frame guides during the early stages of driving.

3.6 Pile Testing System

3.6.1 Introduction

A 1000kN capacity pile testing system was developed. Its purpose was to enable the essential tensile load carrying characteristics of the unexpanded and expanded piles to be established. The system was designed initially for use at the Luton site and was subsequently refurbished and improved for use at the BRS site.

The loading and measuring equipment is described in Sections 3.6.2 to 3.6.5. The equipment was essentially the same for the two sites - the final arrangement used at the BRS site is described, with any differences from the Luton site being noted. Section 3.7 describes the setting up procedures for pile tests, with the Luton and BRS sites being dealt with separately. Test control procedures are described in Section 3.8 and pile extraction is described in Section 3.9.

The overall pile testing arrangement at the BRS site is shown in Figure 3.15 and Plate 3.14. The principal components are:

(a) jacking frame, mounted on runway beams
(b) jack crosshead assembly
(c) tension linkage assembly
(d) reference beam

An overall view of the testing arrangement at the Luton site is shown in Plate 3.15.

3.6.2 Jacking frame

The 4.4m high jacking frame was a double 'T' arrangement - the same basic frame as used for the piling frame at the BRS site. Sets of holes along the frame uprights received the crosshead.

At the Luton site, the jacking frame was mounted on spreader beams resting on the ground surface. The frame was maneouvred by crane and by crowbar pinching. At the BRS site, the jacking frame was fitted with wheels and mounted on the 9m long elevated runway beams (Section 3.5.1). Adjustment of the frame on the runway beams was achieved by using the frame wheels and by crowbar pinching. The jacking frame could

easily be tilted by screwing down the adjustable wheels as required. Screw jacks were fitted to hold the frame in position if so tilted, the wheels then being lifted clear of the runway beams. Any gaps between the base of the jacking frame and the runway beams were packed with metal shim prior to pile testing.

A block and tackle was used for lifting the crosshead assembly and tension linkage. This was mounted on a lightweight extension frame bolted to the top of the jacking frame. The extension frame provided sufficient headroom for the crosshead or other equipment to be lifted to the top of the jacking frame. At the BRS site a two level access scaffold was built around the jacking frame - this moved with the jacking frame as it was rolled along the runway beams.

3.6.3 Jack crosshead assembly

The jack crosshead assembly is shown in Figure 3.16 and Plate 3.16. It comprises, in ascending order:

(a) crosshead
(b) jack tilting platform
(c) hydraulic jack
(d) load cell
(e) bearing washer

All of the components include a central hole to allow the central tension rod to pass through the assembly.

3.6.3.1 Crosshead

The crosshead was fabricated from 300x200mm box section. Drilled and tapped blocks welded inside the ends of the crosshead enabled it to be bolted to the jacking frame columns. The crosshead was internally reinforced to allow a central 100mm hole. Lifting points were provided.

3.6.3.2 Jack tilting platform

The tilting platform enabled the jack to be aligned coaxially with a pile not in vertical alignment. It comprised a bearing platform and a tilting plate, as shown in Figure 3.17.

The bearing platform consisted of two main plates, separated by stiffening plates at each end and by tube reinforcement to a central hole. Adjusting bolts acted upwards from the top plate. The tilting plate, which was bolted to the bottom of the hydraulic jack, rested freely on the adjusting bolts. Both tilting movement and horizontal movement was thus possible.

3.6.3.3 Hydraulic jack

A 1000kN capacity annular shaped double-acting hydraulic jack was employed. The jack ram travel was 250mm. Hydraulic pressure was supplied either by a hand pump or by a large capacity electric pump with variable flow control unit. The hand pump was used to apply load during the pile tests, the electric pump was used whenever large and rapid movement of the jack ram was required - during pile extraction, for example.

3.6.3.4 Load cell

The applied load was measured with a standard 1000kN capacity annular shaped NCB/MRE Type 440 load cell in conjunction with a 'Peekel' monitoring gauge capable of measuring the load applied to the load cell within approximately 0.25kN. The load cell was calibrated regularly throughout the period of pile testing on hydraulic test machines at Imperial College and BRS.

3.6.3.5 Bearing washer

The bearing washer was a 200mm diameter, 60mm thick circular plate drilled and threaded to receive the central tension rod passing up through the crosshead assembly. Upward force was applied to the central tension rod by the hydraulic jack ram acting against the bearing washer, via the load cell. The inherent flexibility within the tension linkage ensured even seating between load cell/jack ram platen/bearing washer.

3.6.4 Tension linkage assembly

The tension linkage assembly enabled tensile loads to be applied to the pile heads. An adjustable system was required, in order to deal with the various pile configurations.

The system adopted applied loads to shear lugs welded to the pile components to be tested. In this way load could conveniently be applied to both box and cruciform piles, in any of the following cases:

(a) Unexpanded outer shell: load was applied to the tops of the four angle sections forming the outer shell.

(b) Expanded pile: load was applied to the tops of the four separated angle sections of the expanded outer shell, the angles constituting the vertical load carrying elements of the pile.

(c) Expander mandrel: load was applied to the top of the expander mandrel. The measurement of the force required to jack the expander mandrel relative to the outer shell can provide useful information

regarding the horizontal forces generated on expansion of the pile. The ability to jack out the expander mandrel from the outer shell also enabled expander mandrels to be extracted and then swopped between outer shells.

The shear lugs welded at the tops of the pile components were described in Sections 3.2 and 3.3. The tension linkage assembly is shown in Figure 3.18. It comprises:

(a) central tension rod
(b) loading box, featuring bolted loading blocks

3.6.4.1 Central tension rod
The central tension rod was a 50mm diameter high tensile steel rod, 1.8m long and threaded at both ends. It connected the loading box to the bearing washer of the jack crosshead assembly.

3.6.4.2 Loading box
Figure 3.18 shows an isometric view of the loading box which was constructed from 300x200mm box section, the internal dimensions of this section being sufficient to clear the largest expanded pile. A block, centrally drilled and threaded, was welded into the top of the loading box. This block received the central tension rod.

At the bottom of the loading box were two bolted loading block assemblies. These consisted of drilled and threaded rectangular blocks mounted on plates. The plates were bolted against the side of the loading box, the rectangular blocks passing through matching slots. The bolted lifting blocks overlapped beneath the shear lugs welded to the outer shells of the piles - or to the expander mandrels - and provided the tension linkage to the pile when the loading box was jacked upwards. Differently sized blocks and packing pieces were used to deal with the variously sized unexpanded and expanded piles.

Details of the loading box are shown in Figure 3.19. The procedures for mounting the loading box on the pile are described in Section 3.7.

3.6.5 Reference beam arrangement
The reference beam arrangement is shown in Figure 3.20. The reference beam comprised a 5m long tubular steel section supported by 2m long tubular steel piles driven 1.5m into the ground. One end of the beam was mounted within a channel guide to permit free expansion and contraction. The reference beam supports were positioned at least 2m from the pile being tested (Weltman, 1980).

Pile deflection was measured by long travel dial gauge extensometers. Two gauges were used, cantilevered from the reference beam using lightweight extensions and fixed so that the plungers were parallel to the pile axis. The dial gauge plungers impinged onto steel reference plates tack welded to two diametrically opposed outer shell angles. The plates were mounted perpendicular to the pile axis and the dial gauge plungers were set equidistant from the pile (Plate 3.17). The dial gauges were graduated at 0.01mm intervals; one revolution of the gauge represented 1mm movement. The reference beam system was protected against the direct influence of sunlight, wind and rain by the presence of the runway beams and jacking frame, and by tarpaulin covers.

In some of the early tests at the Luton site, an elevated reference beam was used, the dial gauges impinging against the top of the pile loading box (Plate 3.15).

3.7 Setting Up for Pile Tests

This Section briefly describes the procedures for setting up the jacking system and tension linkage prior to pile testing. There were two requirements to be met:

(a) the pile, tension linkage, and jack to be aligned coaxially
(b) the lifting blocks to bear evenly against the shear lugs.

The ease with which the jacking system could be set up succesfully depended on the verticality of the pile to be tested and the inherent flexibility of the testing system.

3.7.1 Procedure at Luton site

At the Luton site, all the piles were driven vertically to within an accuracy of approximately 1 in 100. For the purposes of pile testing, the piles and the jacking frame were assumed to act vertically. Flexibility within the jacking system was relatively high, with the spreader beams free to readjust slightly under load, and soil-pile stiffness being relatively low. The piles were being used for the first time - during fabrication of the outer shells the four shear lugs were correctly aligned and welded after the outer shell had been fixed together as one.

The procedure for setting up was as follows (refer to Figures 3.15 - 3.19):

(a) The loading box was lowered to rest on top of the pile to be tested.

(b) The appropriate lifting blocks were bolted in position.

(c) The jacking frame, with crosshead and jack, was lifted into position on the spreader beams, above the pile to be tested. The tilting platform was not used.

(d) The jacking frame was pinched into position centrally over the pile and loading box. The central tension rod was passed down through the jack and crosshead and screwed into the loading box.

(e) The load cell was mounted centrally on top of the jack ram platen.

(f) The bearing washer was screwed into place on the upstanding central tension rod.

(g) Slack in the system was taken up by raising the jack, with the tension linkage suspended, until the lifting blocks and shear lugs were within a few millimetres of each other.

(h) Final adjustments were made by pinching the jacking frame until the loading box was central over the pile. The jacking system was then ready for use.

3.7.2 Procedure at BRS site

The box piles at the BRS site were driven vertically to within an accuracy of approximately 1 in 100, the cruciform piles to within an accuracy of approximately 1 in 50. At the BRS site, flexibility within the testing system was lower than at the Luton site, with the runway beams resting on stiff foundation pads and soil-pile stiffness being relatively high. There were inevitably slight misalignments of the shear lugs on the outer shells, arising from pile reassembly.

At first, the same setting up procedure as at the Luton site was adopted. Problems were encountered in setting up the loading box coaxially and getting the lifting blocks to act evenly, particularly in the case of the cruciform piles. These problems were dealt with by means of the jack tilting platform, and by a change in procedure. The new setting up procedure that was adopted is described below (refer to Figures 3.15 to 3.19).

Jacking frame:

(a) A mounting spindle assembly was fixed centrally on top of the pile to be tested (Figure 3.21). The spindle fitted closely within the central threaded hole at the top of the loading box.

(b) The loading box was lowered onto the top of the pile, being held centrally by the mounting spindle.

(c) The lifting blocks were bolted into position.

(d) With the loading box held coaxially by the mounting spindle, the loading box was lifted until the lifting blocks and shear lugs engaged. The seating between the two could be observed through observation holes. Any gaps between the shear lugs and the lifting blocks were packed with steel shim.

(e) The loading box was held tightly in position with tack welded angle section (Figure 3.19, Plate 3.17), and the spindle was removed.

Tension linkage:

(a) The jacking frame, with crosshead and tilting platform in position, was rolled/jacked/tilted into position above the pile to be tested such that the required final adjustment of jack alignment was within the adjustment tolerance of the tilting platform.

(b) The central tension rod was passed down through the clearance hole in the crosshead and tilting platform and screwed into the central hole in the top of the loading box.

(c) The hydraulic jack was lowered onto the upstanding central tension rod. The tilting platform was then used to align the jack coaxially with the rod. There was sufficient clearance between the rod and the hole to be able to do this by eye.

(d) The load cell was mounted centrally on top of the jack ram platen.

(e) The bearing washer was screwed into position.

(f) Slack in the system was taken up by raising the jack ram until the load cell was within a few millimetres of the bearing washer. The jacking system was then ready for use.

3.8 Test Control

Loading and unloading of the pile using the hydraulic jack was achieved by means of the hand pump. Time, load, and displacement of the pile were recorded by hand.

The test control system was essentially the same as that used for the Imperial College instrumented pile tested at the BRE London Clay test site at Canons Park, Middlesex (Bond, 1989). In these tests, pile load and deflection were also continuously logged by means of electrical transducers and a computer logging system. Pile test logging data from the Canons Park programme are shown in Appendix 3.2, to indicate the typical accuracy of test control using the hand jack.

3.9 Pile Extraction

Piles were extracted in two stages - initially by jacking, and then by lifting with a crane. Expanded piles were usually extracted as one by pulling on the outer shell. Unexpanded piles were extracted in the same way. It was also possible to extract an expander mandrel from within an outer shell if required. The extraction procedures are outlined below.

(a) Jacking:
The pile jacking system was used (Section 3.6.3.3) The hydraulic jack was connected to the electric pump to enable extraction to take place quickly and easily.

The pile was extracted in a series of jack 'pushes', the jack crosshead assembly being advanced for each push. The jack ram was fully extended at each push and was then retracted, allowing the crosshead assembly to be moved up to the next set of mounting holes ready for the next push. The maximum applied load during each push was recorded.

Jacking continued until the applied load was safely within the capacity of the crane being used. The crosshead was generally near the top of the jacking frame at this stage.

(b) Lifting clear by crane:
The crosshead assembly and extension frame were removed. Lifting slings were attached to the pile, and it was pulled from the ground and lifted clear.

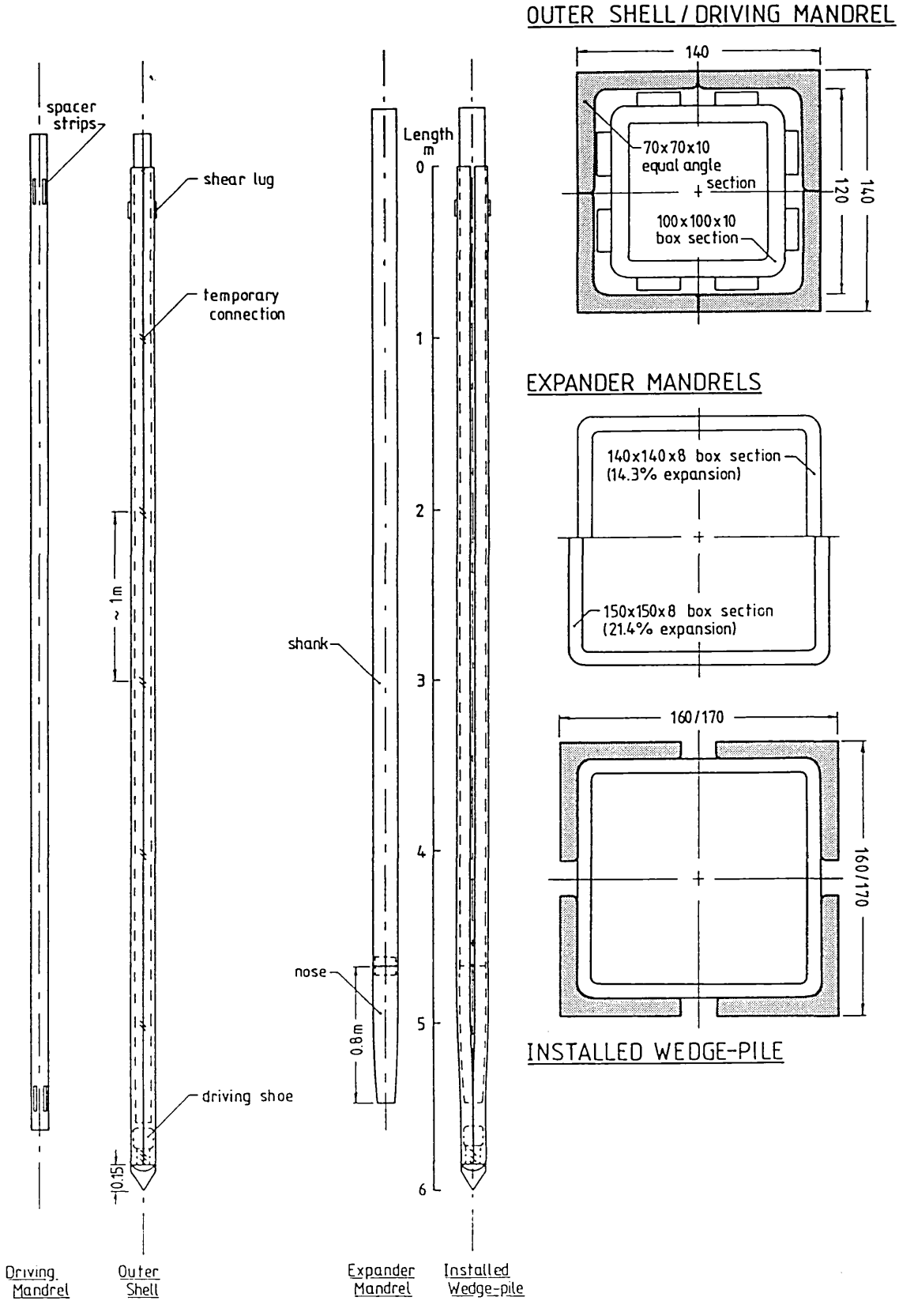

Figure 3.1 Box pile: general arrangement

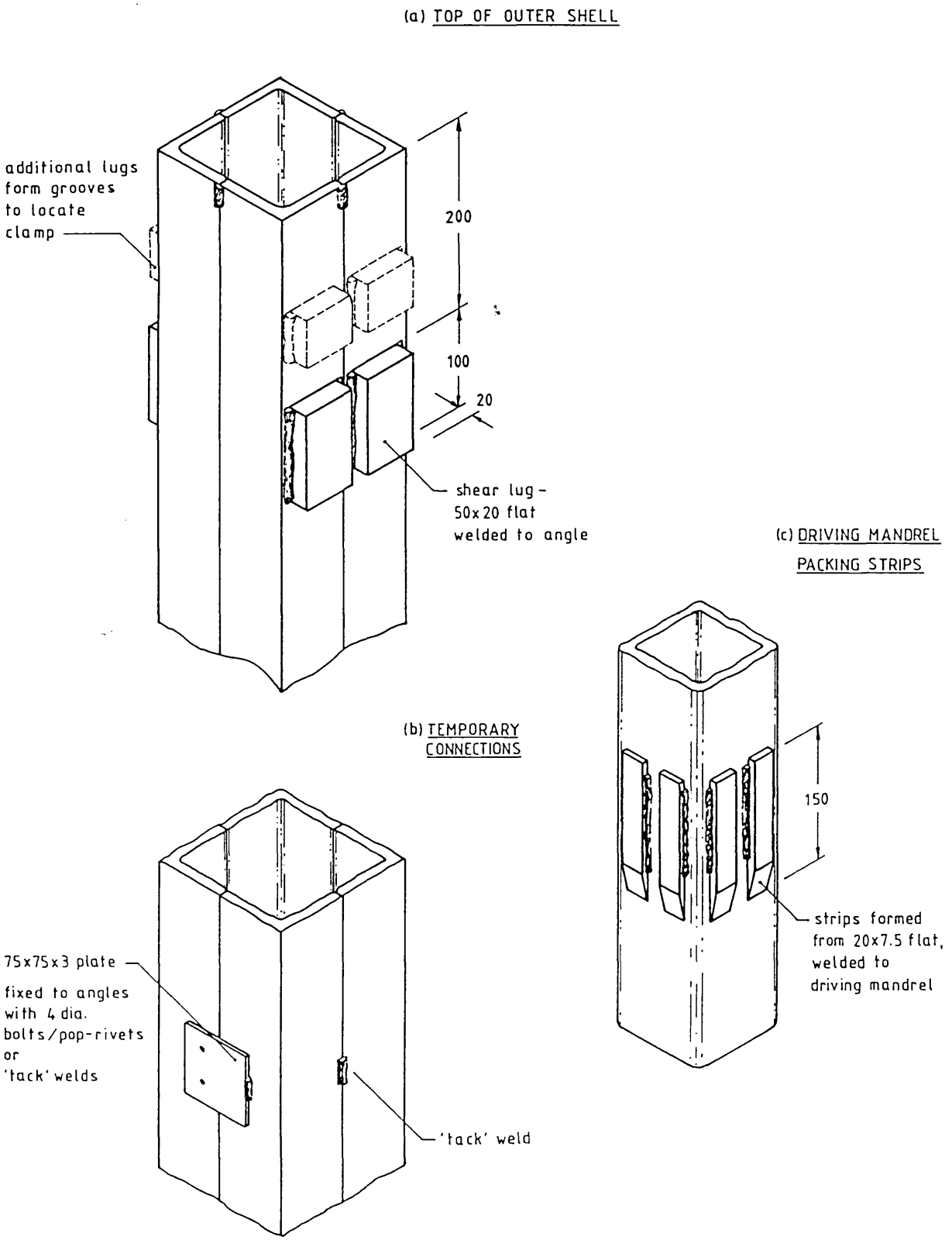

Figure 3.2 Box pile: details of outer shell

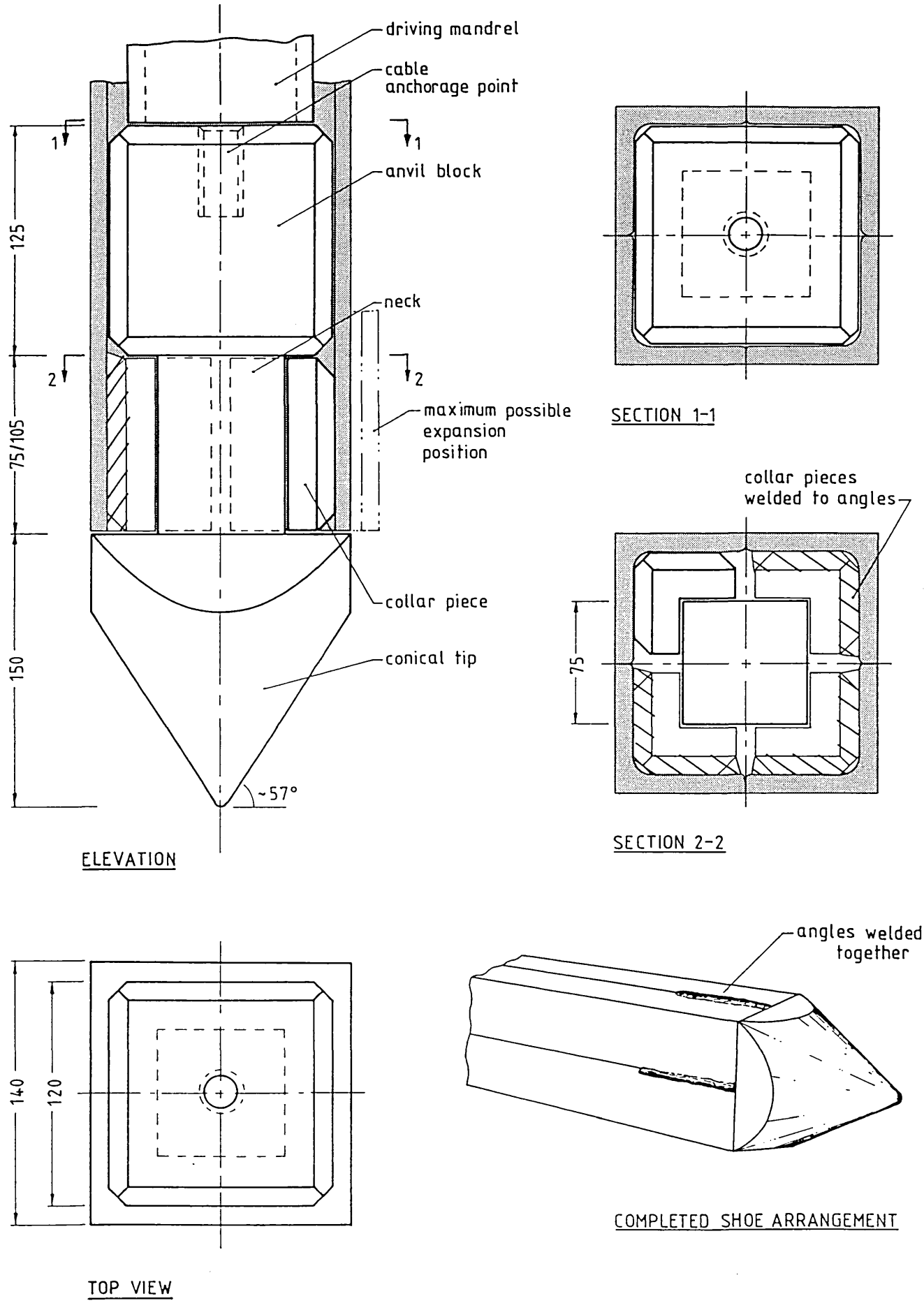

Figure 3.3 Box pile: details of driving shoe

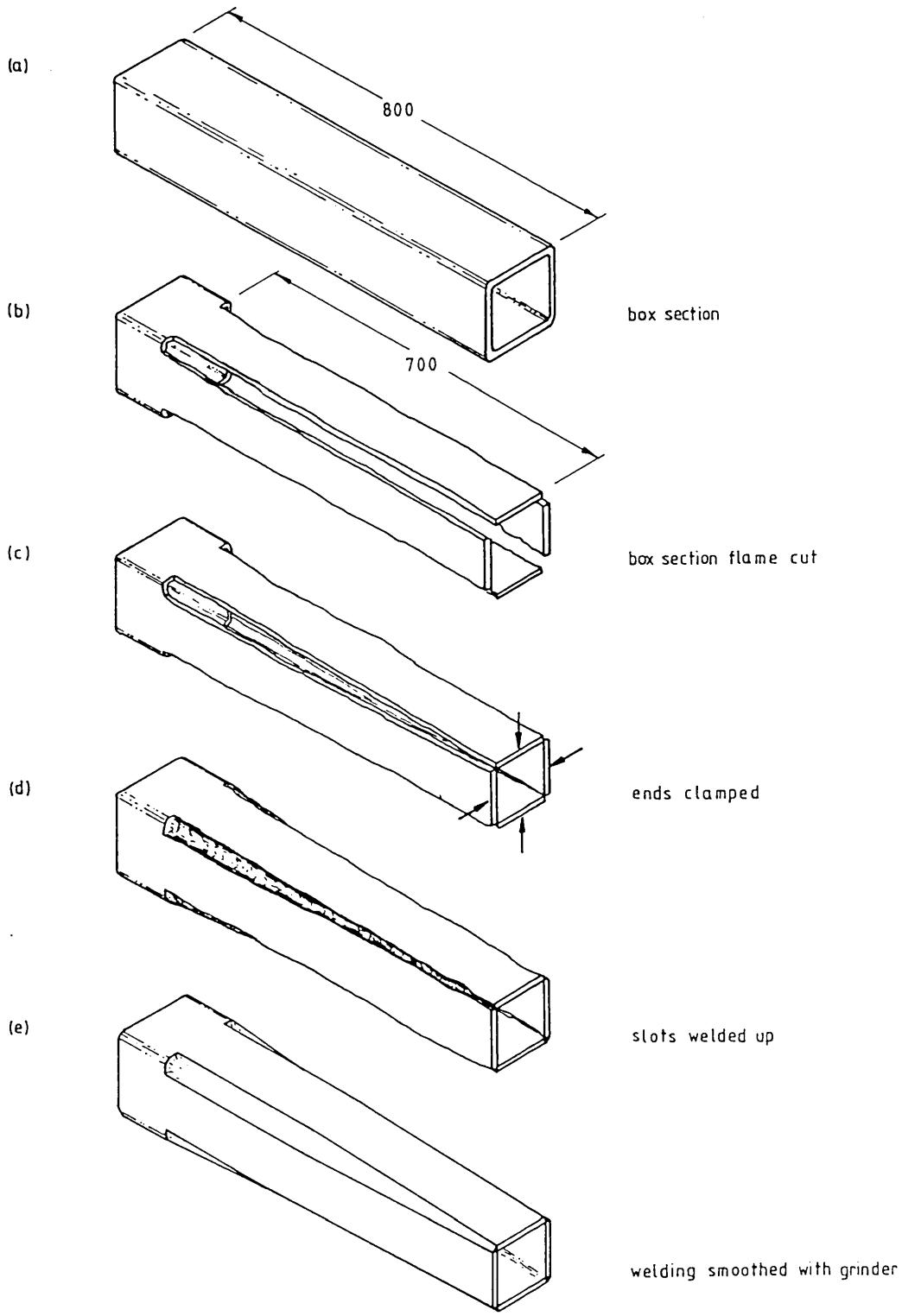

Figure 3.4 Box pile: expander mandrel nose fabrication

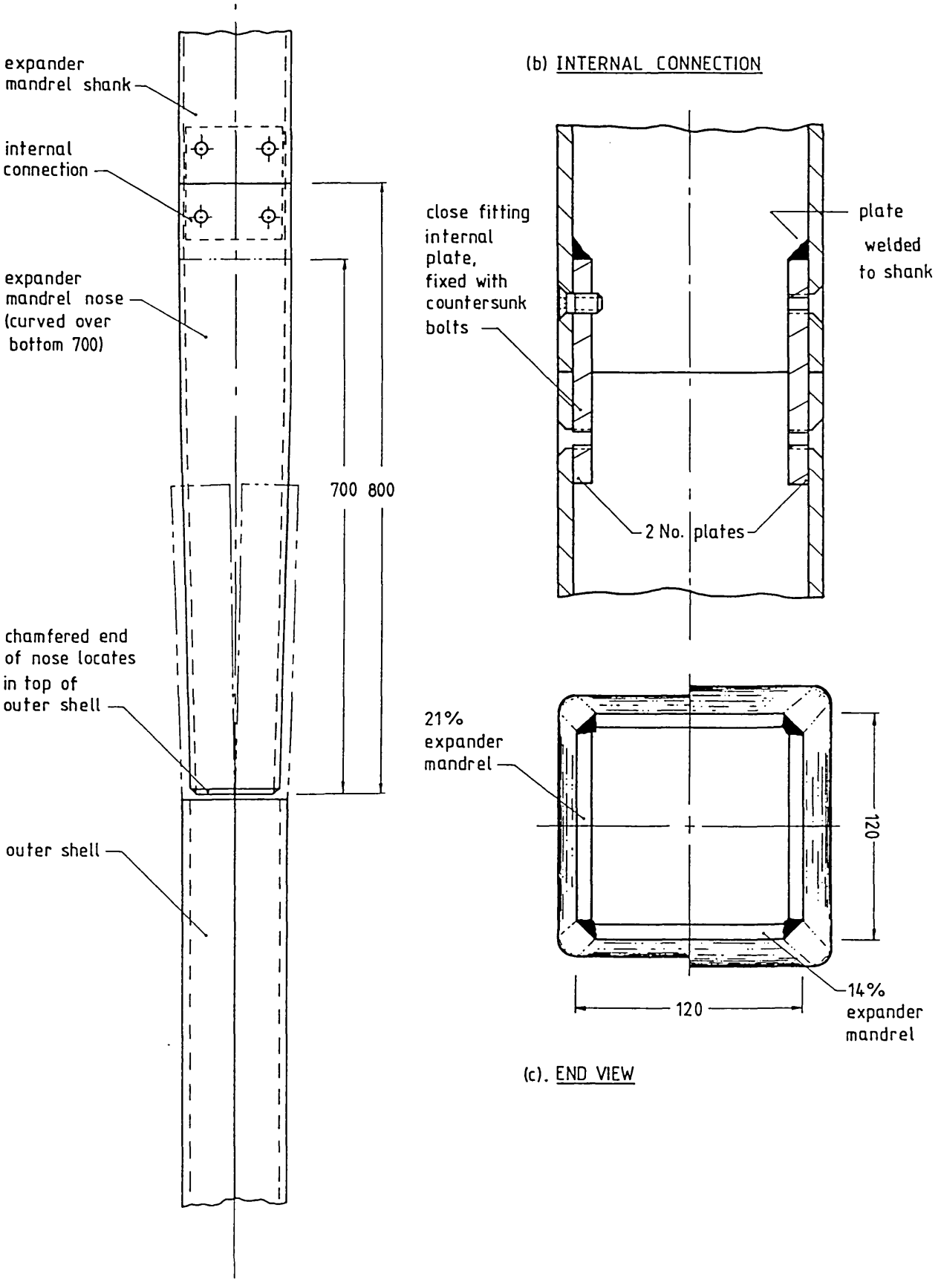

Figure 3.5 Box pile: details of expander mandrel nose

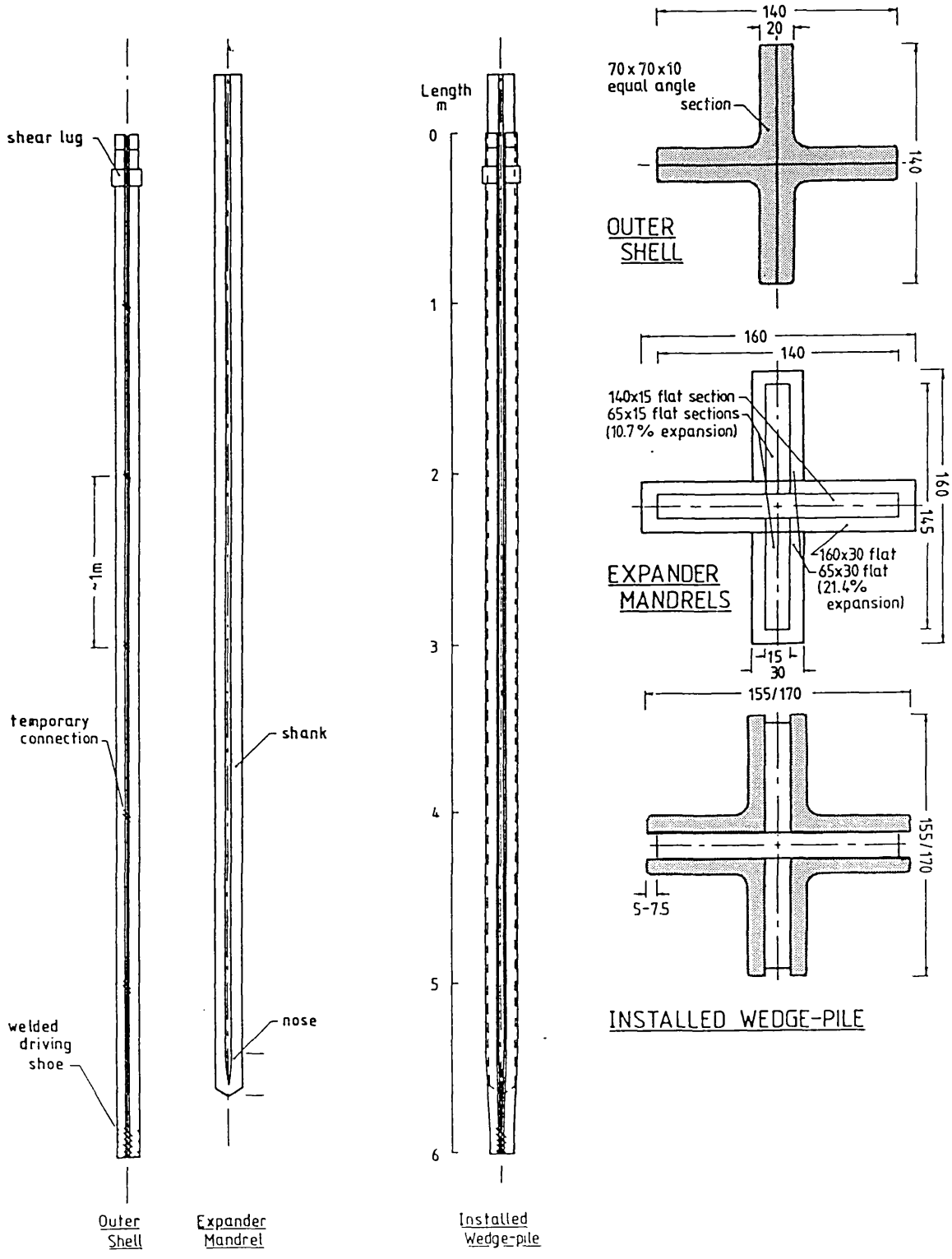

Figure 3.6 Cruciform pile: general arrangement

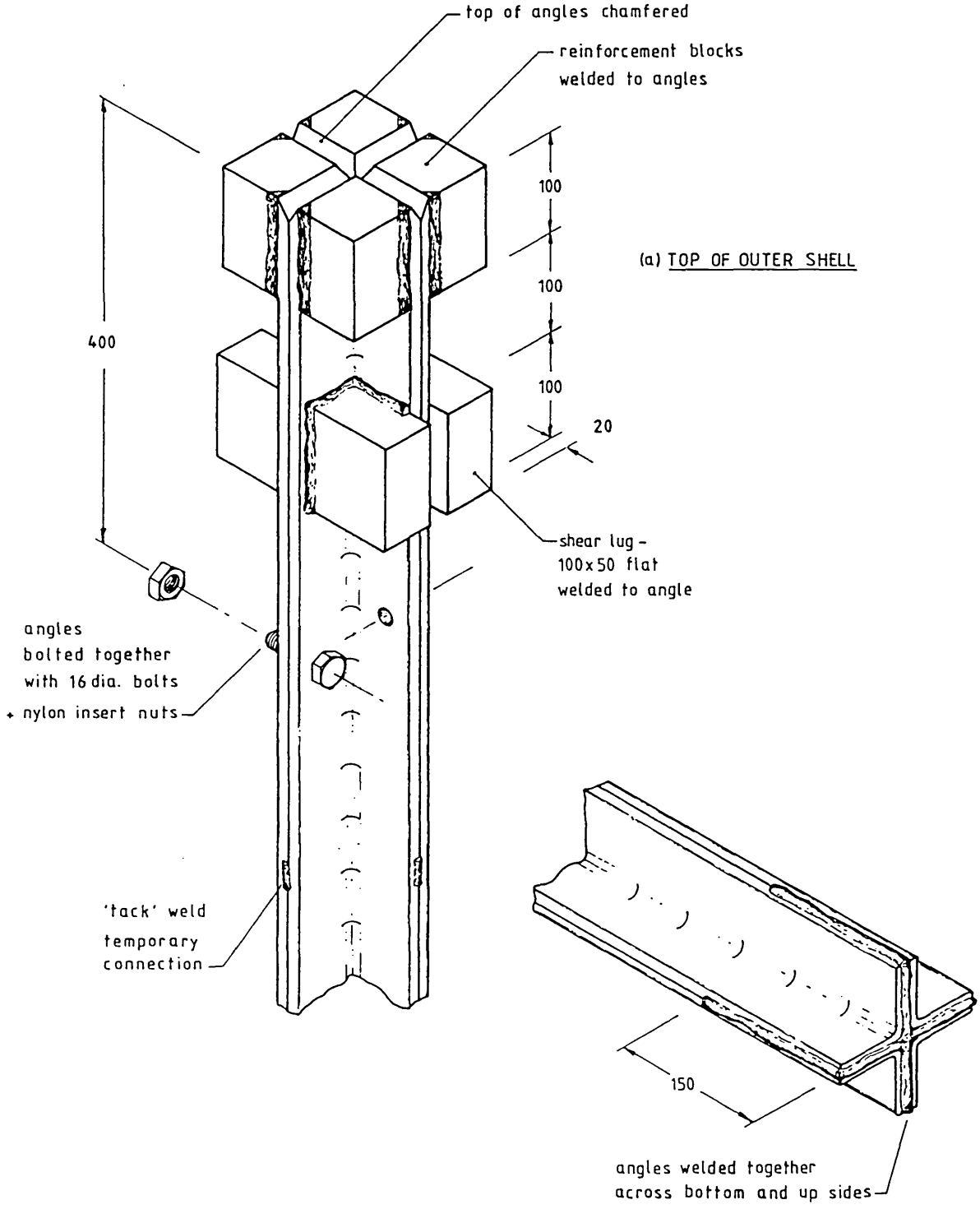

Figure 3.7 Cruciform pile: details of outer shell

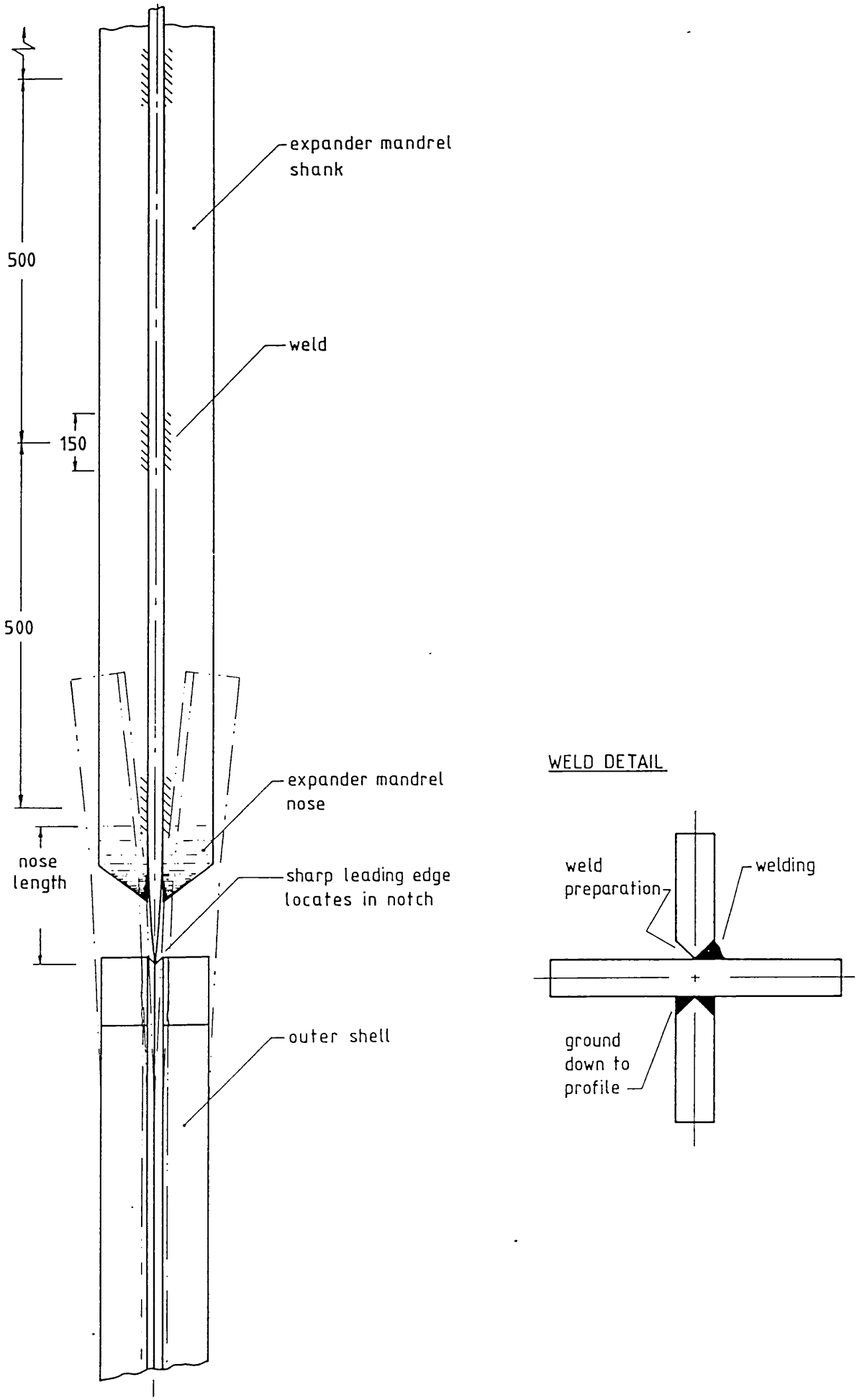

Figure 3.8 Cruciform pile: details of expander mandrel

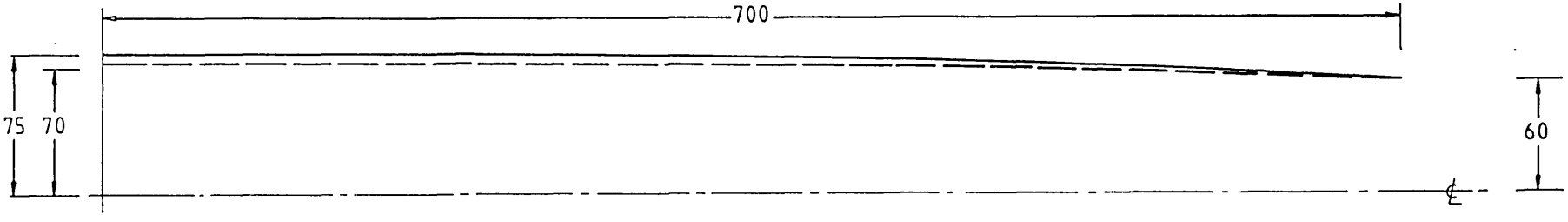

BOX EXPANDER MANDREL

Box segments bent elastically to give approximately cubic profile

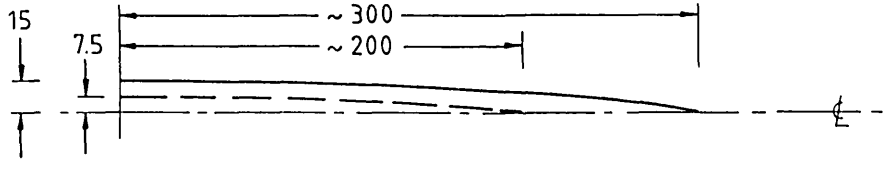

CRUCIFORM EXPANDER MANDREL

Expander mandrel flame cut and ground down to give approximately parabolic profile

Figure 3.9 Details of expander mandrel nose profiles

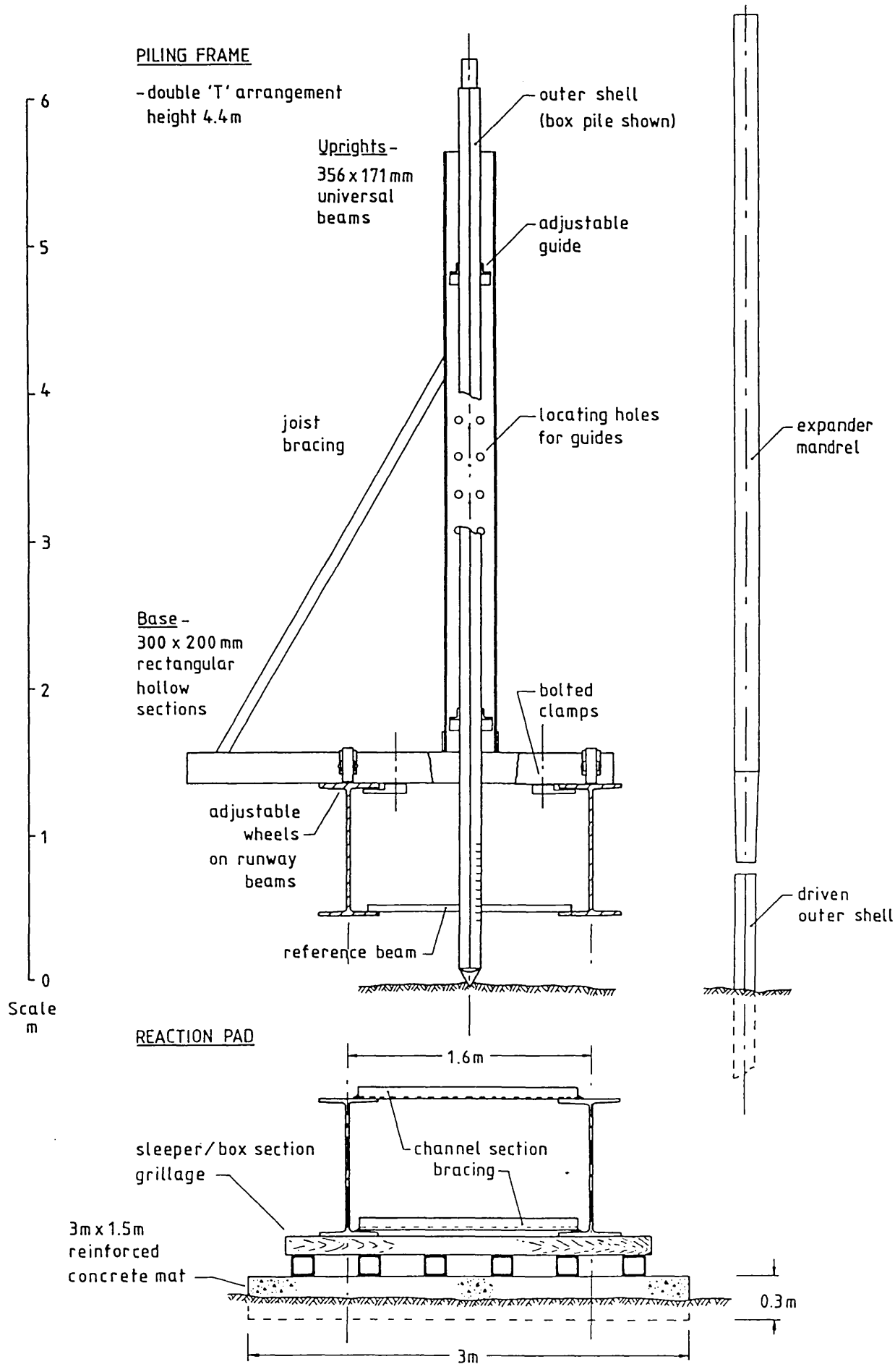

Figure 3.10 BRS piling frame: overall arrangement

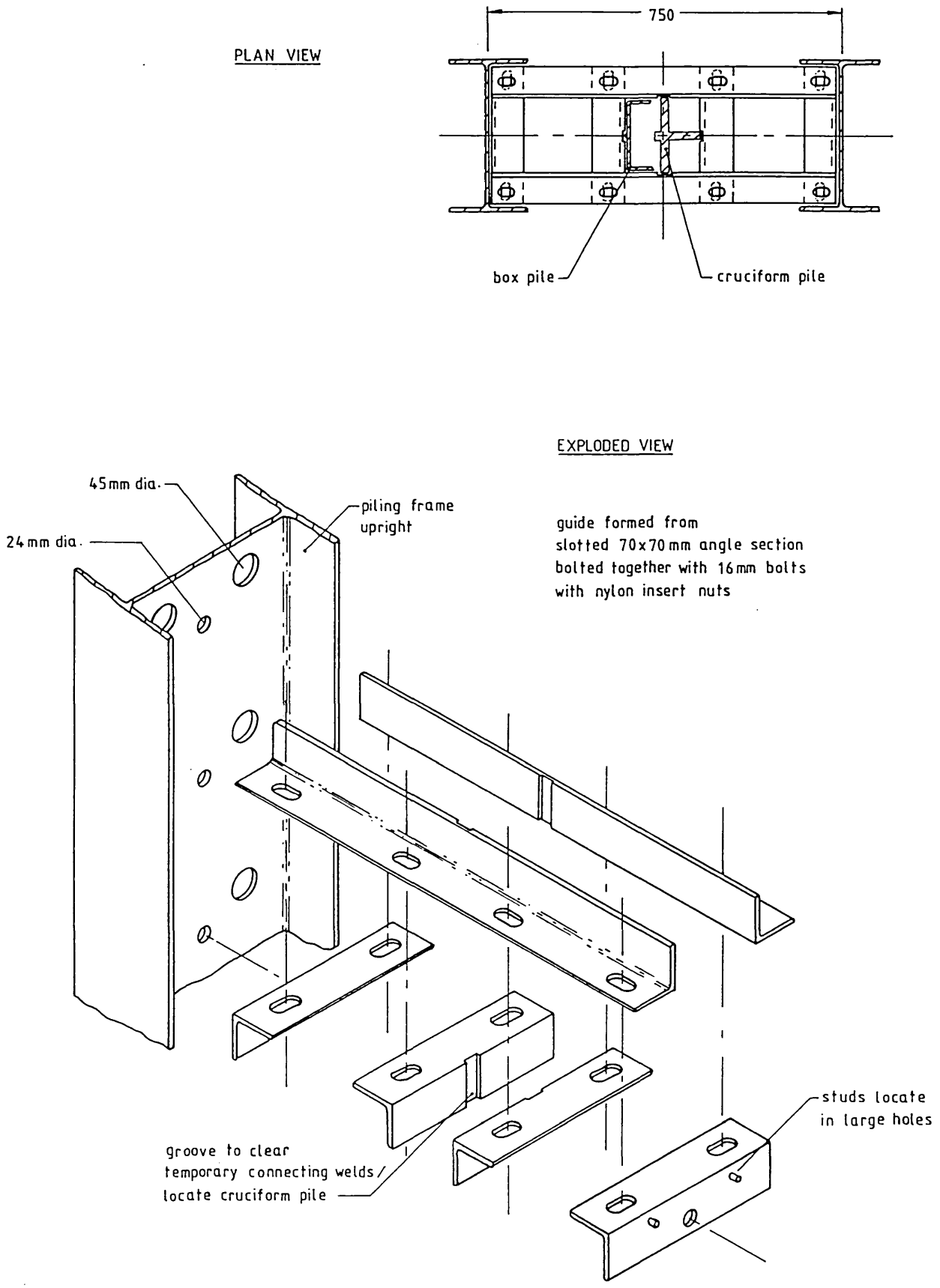

Figure 3.11 BRS piling frame: details of angle guides

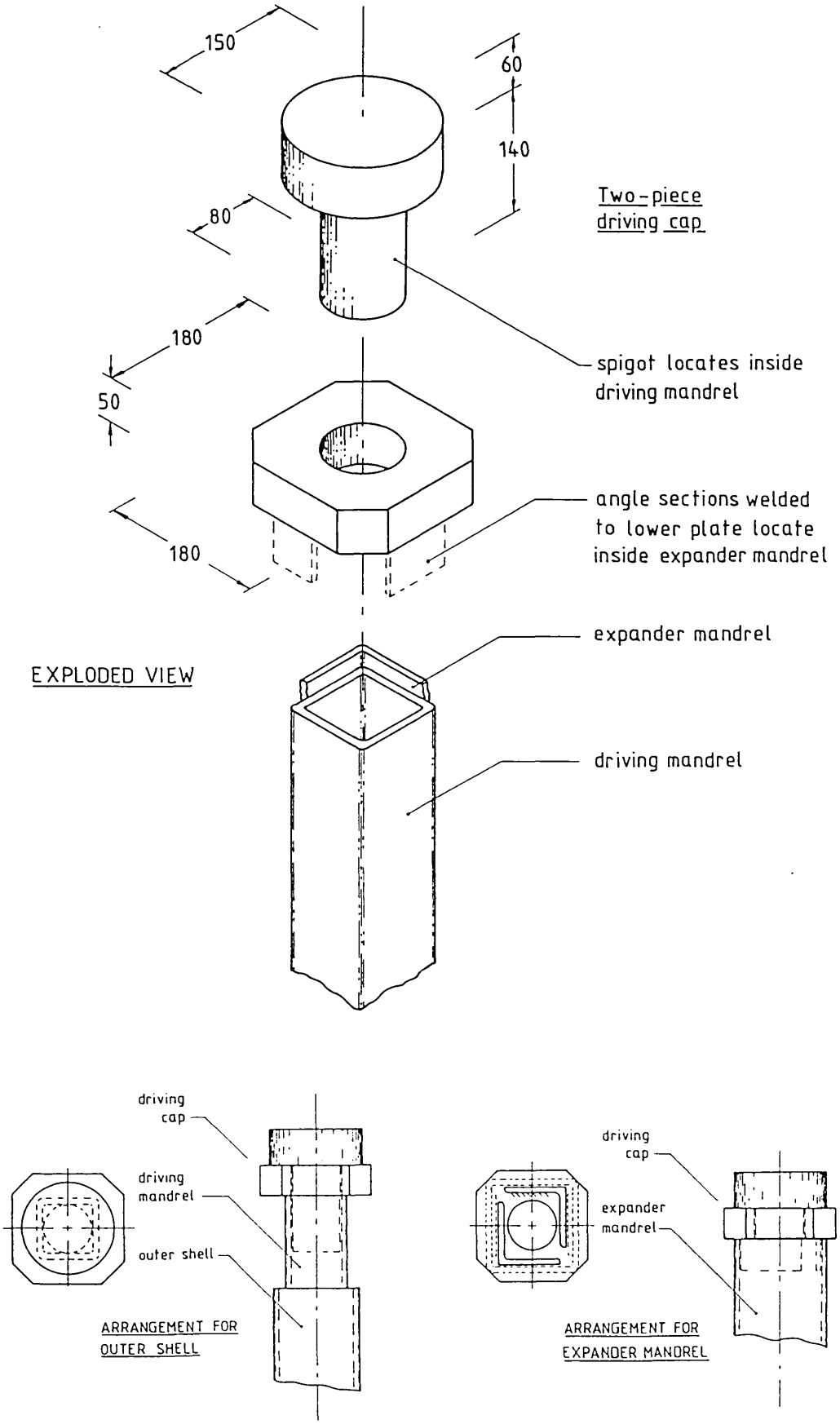

Figure 3.12 Details of pile driving helmets

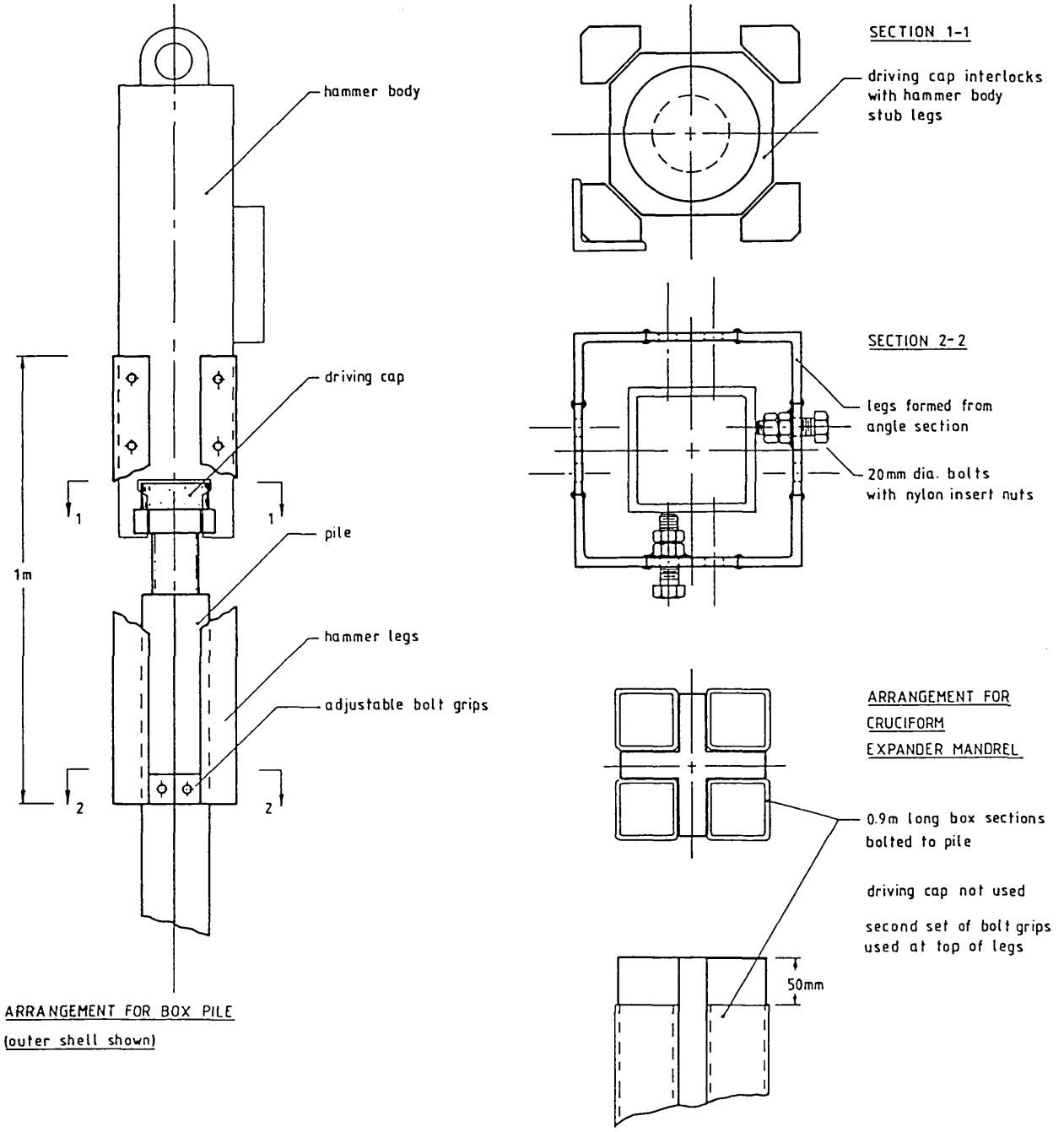

Figure 3.13 Details of PH5 hammer leg guides

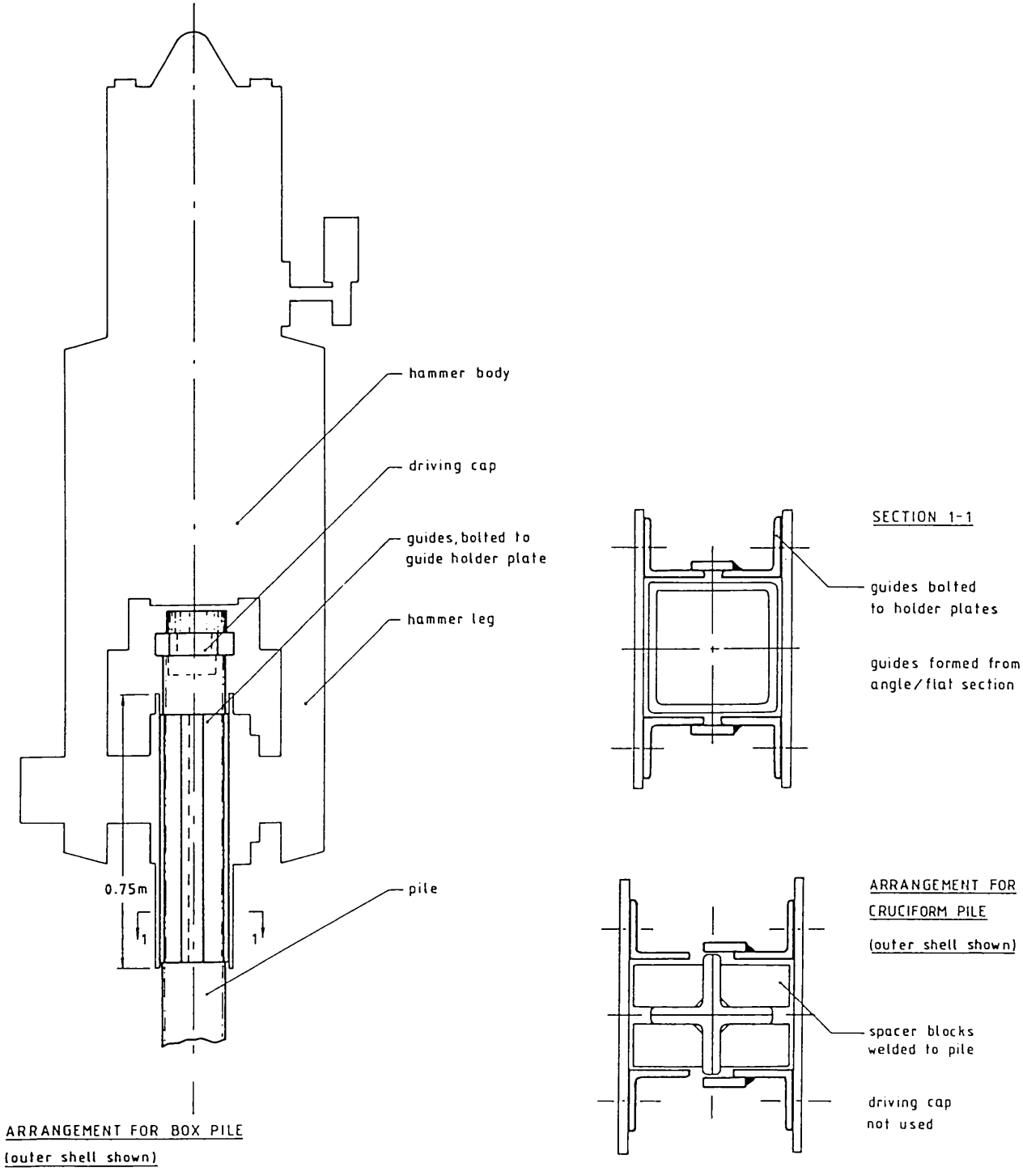

Figure 3.14 Details of 500N hammer leg guides

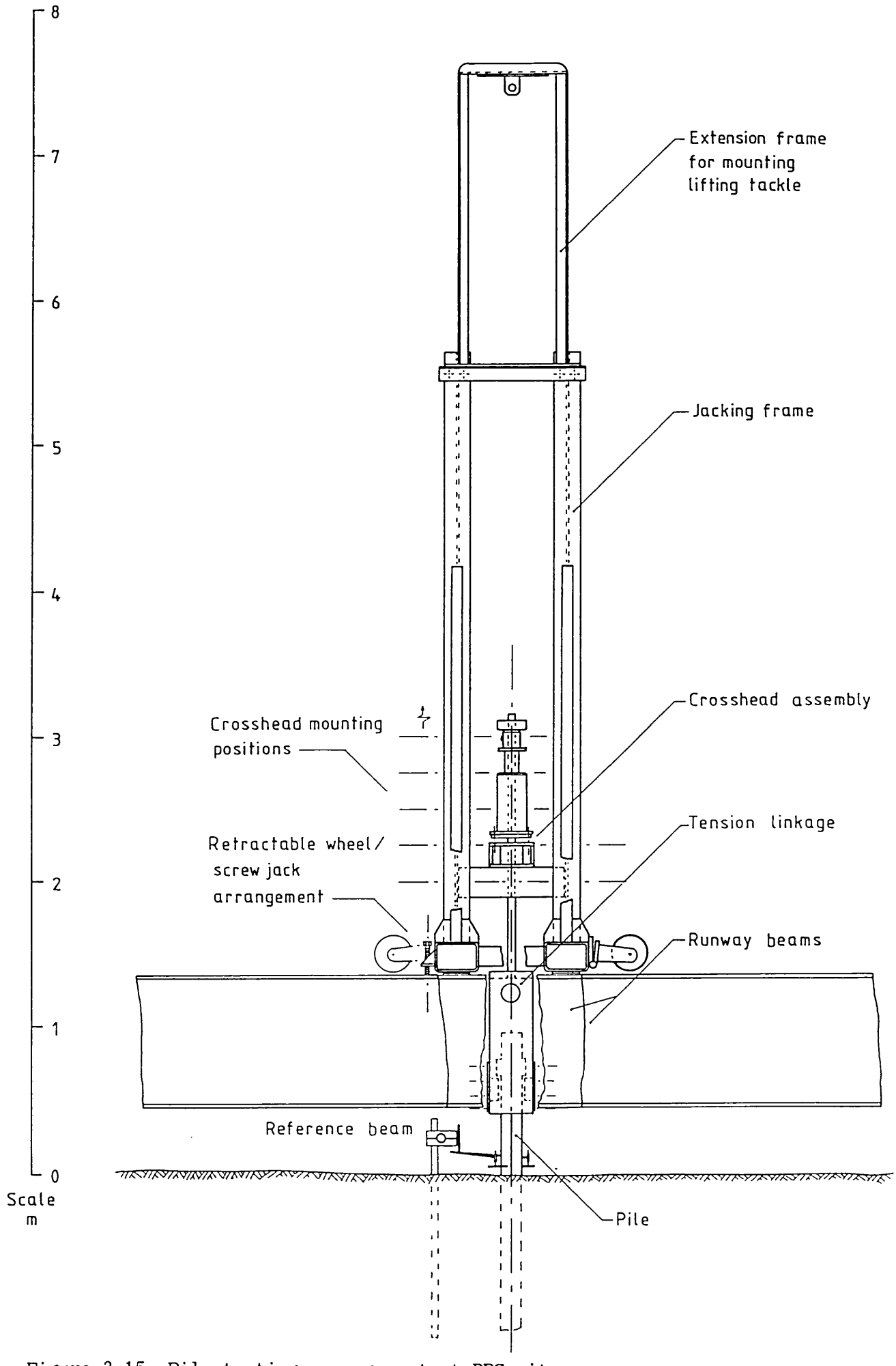

Figure 3.15 Pile testing arrangement at BRS site

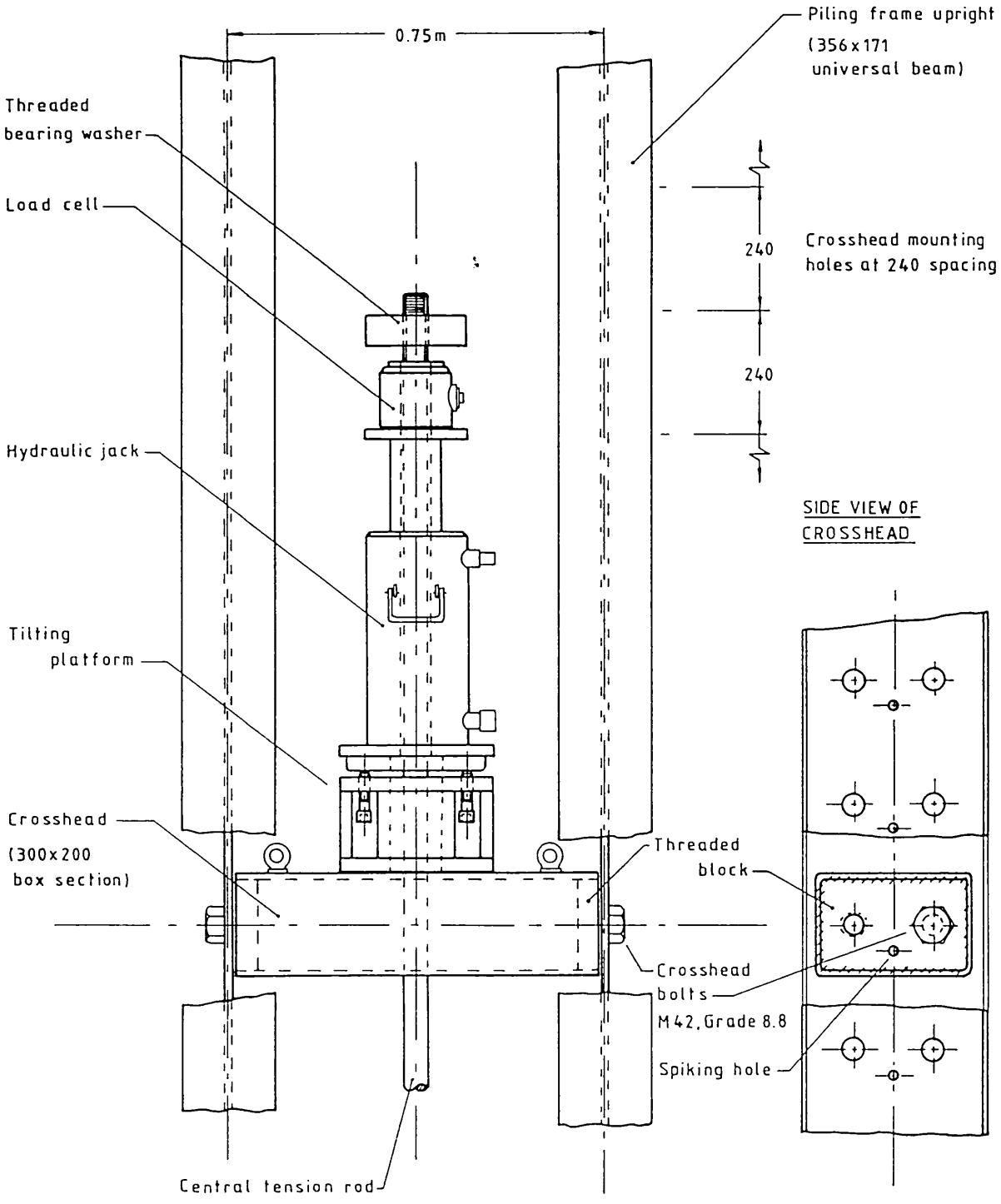

Figure 3.16 Jack crosshead: general arrangement

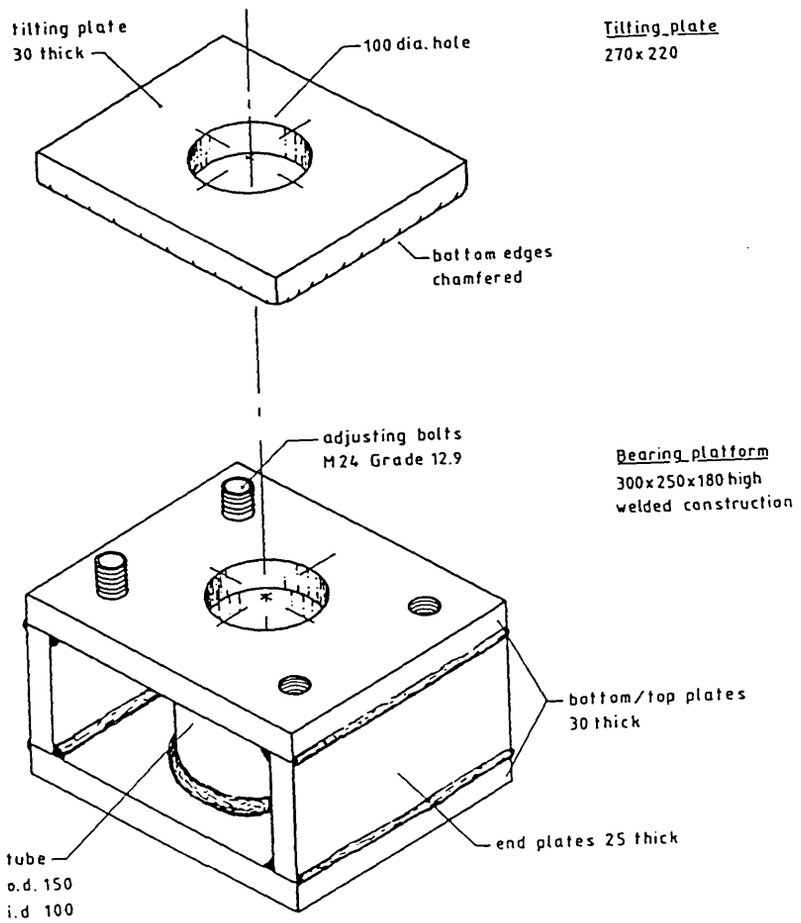

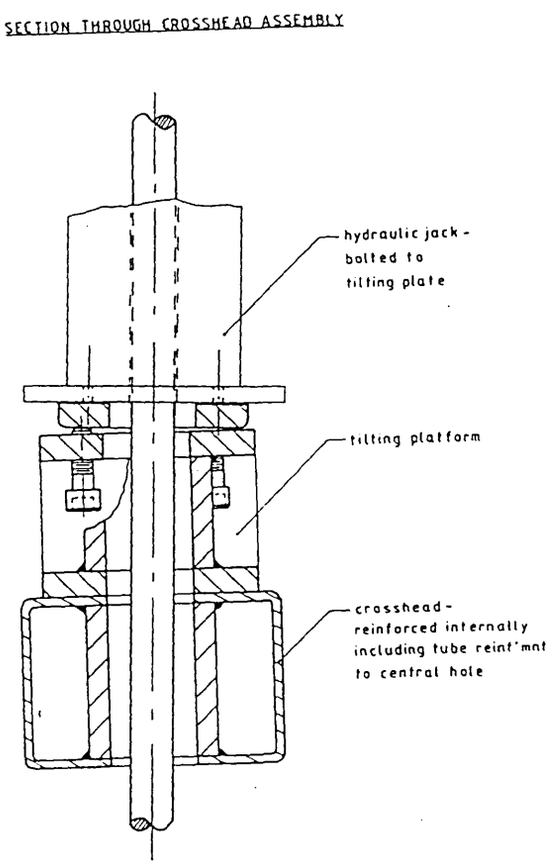

Figure 3.17 Details of tilting platform

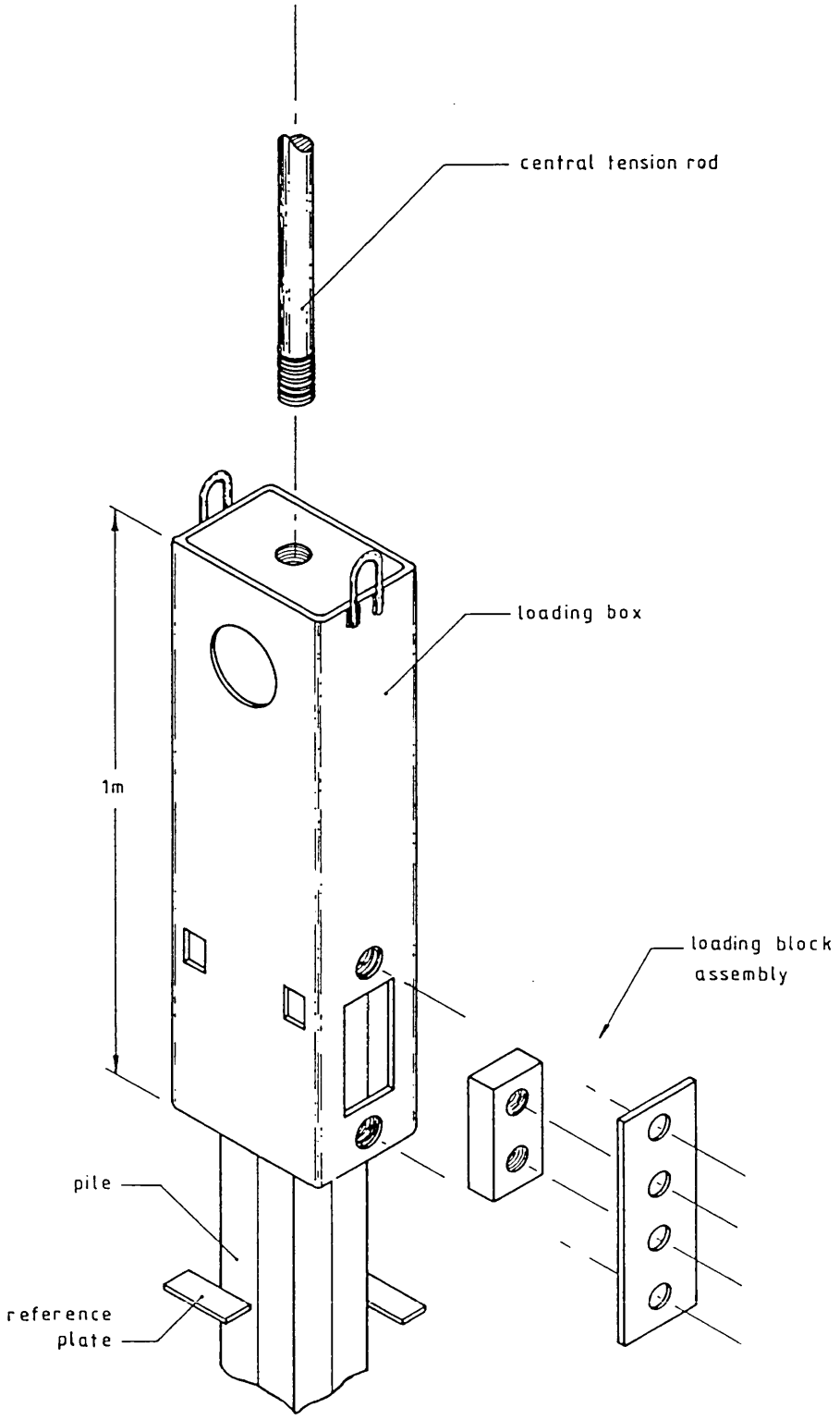

Figure 3.18 Tension linkage: overall arrangement

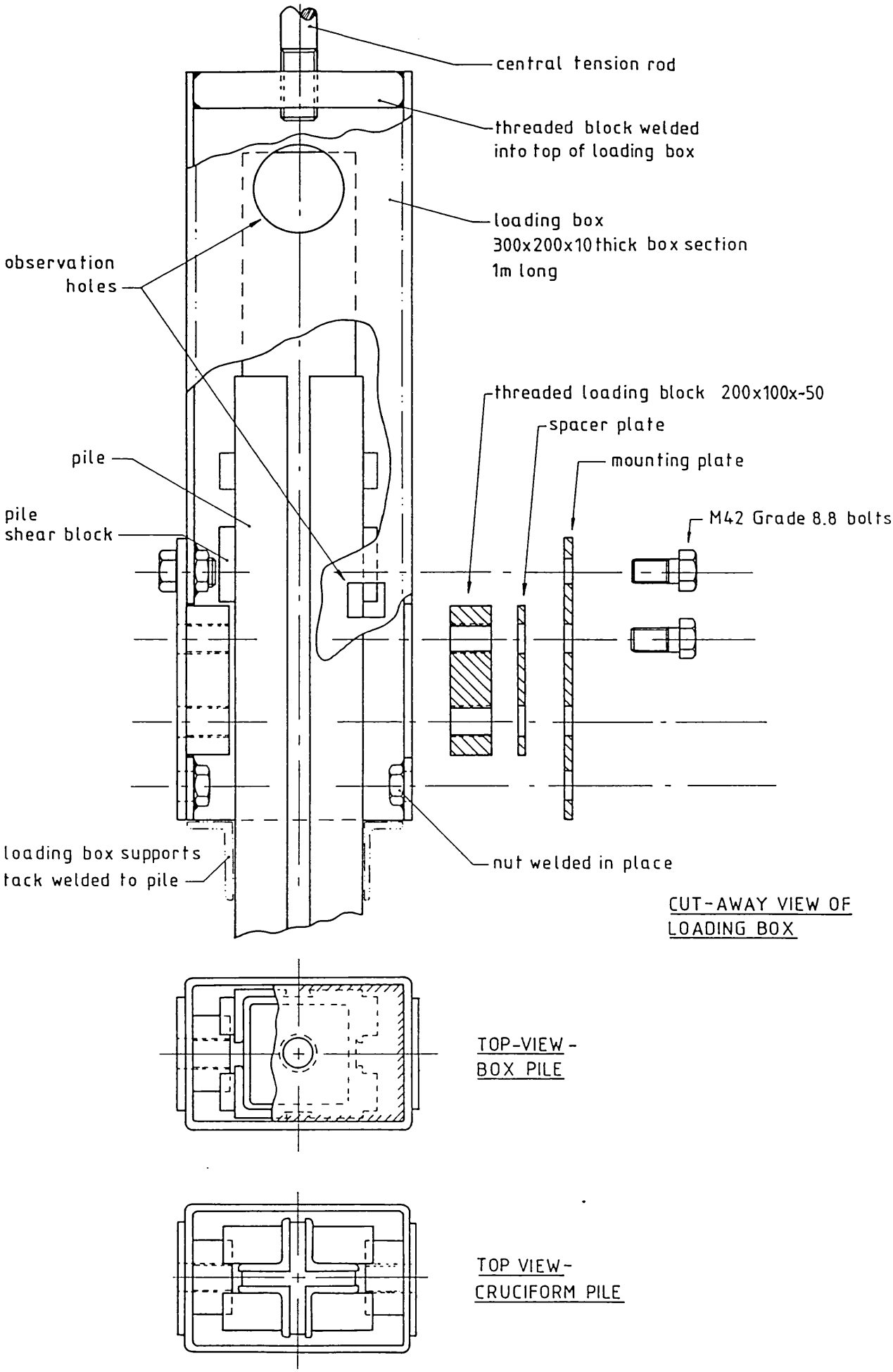

Figure 3.19 Details of loading box

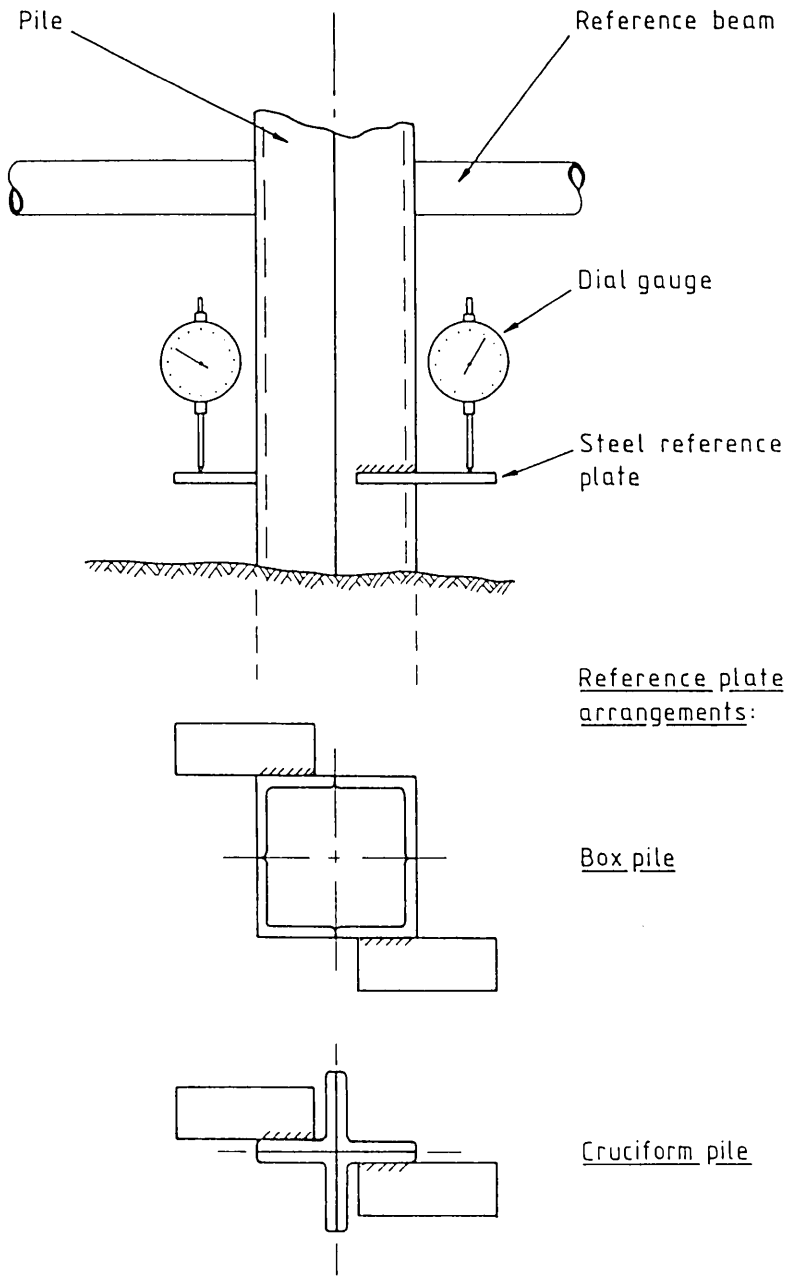

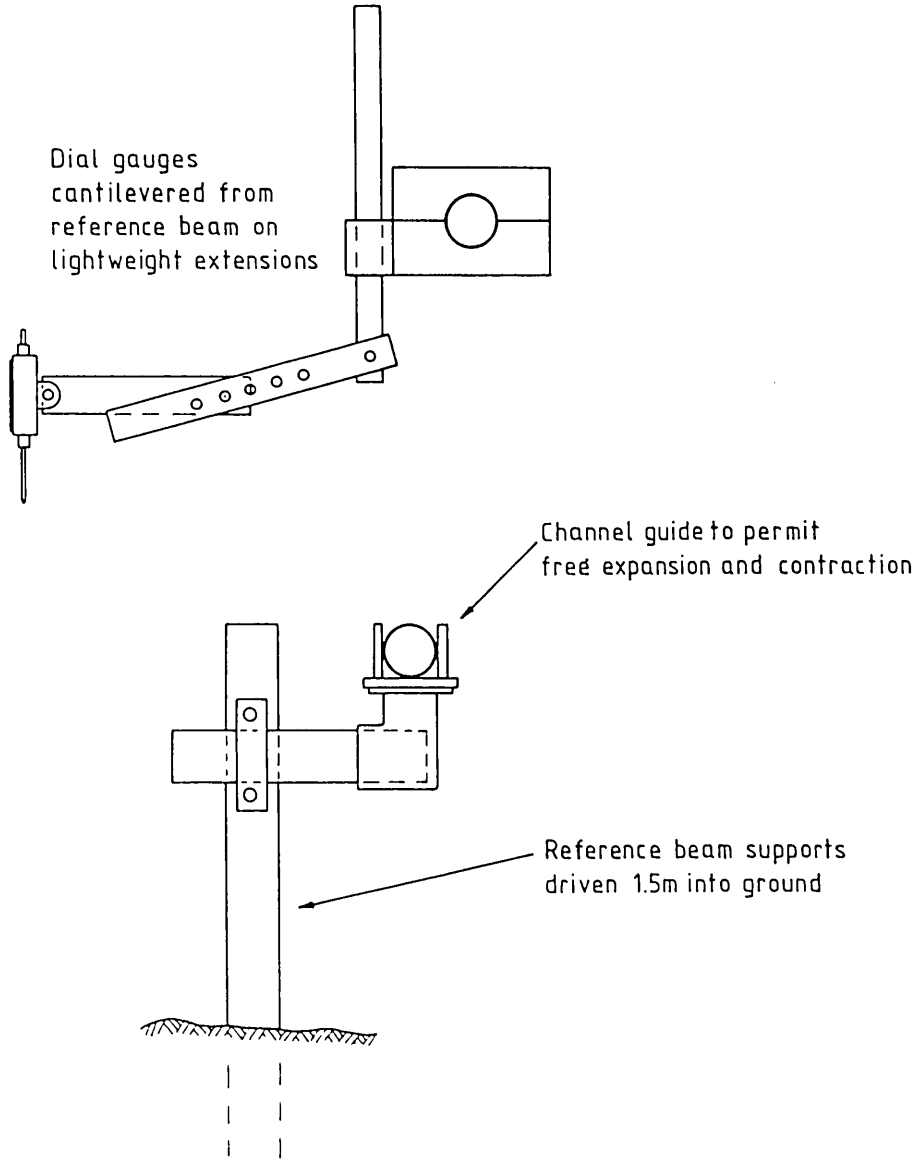

Figure 3.20 Reference beam arrangement

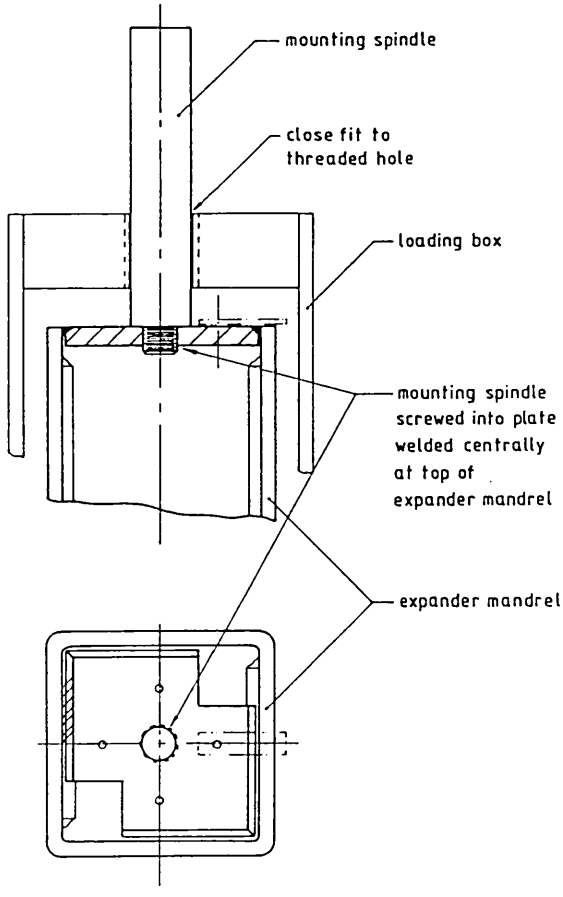

BOX WEDGE-PILE

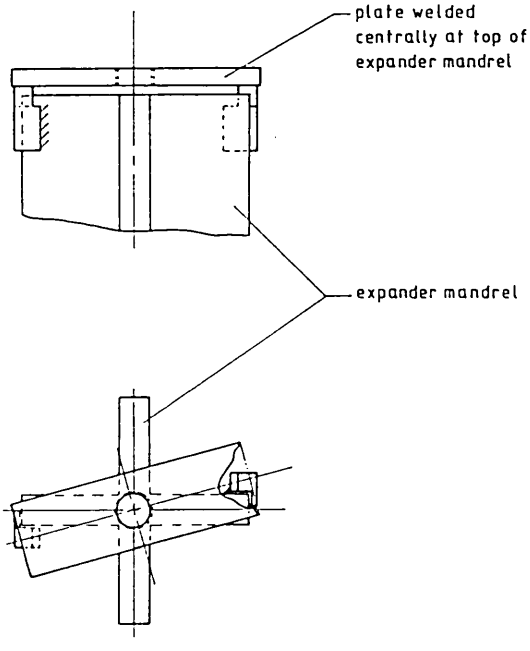

CRUCIFORM WEDGE-PILE

Figure 3.21 Details of centering spindles

CHAPTER 4
INVESTIGATIONS AT LUTON SITE

4.1 Introduction

This Chapter reports investigations undertaken in a highly weathered chalk profile at a site near Luton in Bedfordshire. The investigations were centred on a programme of tests on expanded and unexpanded steel wedge-piles, carried out over a period of nearly a year. The piles have been described in Chapter 3. In conjunction with the pile tests, in-situ soil tests were performed with a variety of instruments. These included tests with pressuremeter type devices, made in order to investigate the limiting radial stresses available upon expansion into the chalk. Shearbox tests were performed in order to determine the likely frictional behaviour between the piles and the chalk.

Chalk exhibits rather unusual engineering properties. In Section 4.2 some background is given to the behaviour of driven piles in chalk and the behaviour of carbonate sediments in general.

General details of the test site are given in Section 4.3. In Section 4.4, the results of the in-situ tests and shearbox tests are presented. Details of the configurations of the piles tested at the Luton site are given in Section 4.5. Driving information is dealt with in Section 4.6. The results of the pile testing programme are given in Section 4.7, with the main points of interest being summarised in Section 4.8.

The results of the investigations at the Luton site are discussed in Chapter 11.

4.2 Driven Piles in Chalk: Background

4.2.1 Composition of chalk

English chalk was deposited in a calm, warm, open sea environment. It is composed almost entirely of the remains of animal and plant life. The constituent particles of typical chalks consist almost exclusively of calcite (rhombohedral calcium carbonate - $CaCO_3$).

For typical soft white chalks, particle size analyses generally show a marked separation into a finer and a coarser fraction (Higginbottom, 1965; Clayton, 1983).

The finer matrix material is formed from coccoliths. These are minute calcareous bodies that formed part of the skeleton of the planktonic marine algae Haptophyceae. This matrix material commonly accounts for 70% or more of a typical sample and lies within the particle size range 0.5 to 4 micron. The matrix material was thus deposited as a fine lime mud, now generally referred to as micrite - a contraction of microcrystalline calcite (Fookes, 1988). The coccoliths themselves are composed of a large number of overlapping calcite crystals. After disintegration of the coccolith, these crystals appear to form the finest material normally present.

The coarser fraction, typically forming 20 to 30% of the material present, is mainly within the range 10 to 100 micron, equivalent to a coarse silt. It contains material from the skeletons of micro-organisms of the order Foraminifera and shell debris derived from other sea creatures.

In Britain the Chalk has been divided by geologists into three broad divisions by means of well-defined marker horizons. These broad divisions are termed Upper, Middle, and Lower Chalk. These divisions are further sub-divided on the basis of distinctive fossils. Hobbs (1976) distinguishes five types of chalk, within the three main divisions, based on their different engineering properties.

The most unusual feature of English Chalks is their generally high porosity, of up to 50% (Clayton, 1983). This is associated with a lack of reorganisation of the constituent particles and an absence of structures suggesting dewatering or compression. These characteristics are generally attributed to high initial porosity during deposition, followed by early cementing. This is supported by the fact that soft chalks can be found with natural water contents in excess of their remoulded liquid limits. Uncemented, such a structure could not have survived even modest overburden pressures.

The intergranular spaces of chalk have not normally been filled with any cementing medium. It seems likely that only minute quantities of cement are present (ibid.).

Superimposed on the effects of diagenesis are the effects of weathering. The main effect is a decrease in stiffness and strength of the chalk mass due to an increase in the number and openness of fissures and fractures (Ward et al, 1968). This effect increases with proximity to the ground surface, this being generally attributed to ice action. Near

the surface, severe frost shattering can occur, due to the susceptibility of chalk to frost heave. Apart from the in-situ products of ice action, transported products of this process have accumulated by solifluction (Higginbottom, 1965).

Ward et al (1968), in connection with investigations for the proposed CERN site at Mundford, Norfolk, made an engineering classification of the chalk at this site based on the fracture or fissure characteristics and the strength of the intact chalk. This scheme is now used generally as the basis for description of chalk, and for correlating the results of in-situ tests such as the SPT and CPT.

Because the natural moisture content of chalk will normally lie high in the plastic range, remoulding can cause the formation of a chalk slurry, often referred to as 'putty' chalk. The behaviour of such material is similar in some respects to that of 'quick' clays, as remoulding leads to an almost total loss of strength. Remoulding can be caused by natural mechanical disturbance, as in weathering and solifluction processes; or artificially, as in boring, sampling and pile driving.

4.2.2 Driven piles in chalk

The behaviour of piles installed in chalk is extensively reported in CIRIA Piling Development Group Report SP12 'Piling in chalk' (Hobbs and Healy, 1979) and in the proceedings of two ICE symposia - 'Chalk in earthworks and foundations' (1965) and 'Piles in weak rock' (1976).

These sources of information are based on work on land, in England. They predate the extensive recent research on carbonate soils outlined in the next Section. They are important, however, because they contain a large amount of well documented pile test data, highlight the particular problems of various types of piles in chalk, and set out the beginnings of an effective stress design approach.

Conventional driven piles in chalk are characterised by unpredictable behaviour and generally low shaft resistances, in comparison to piles in other soils. The reason for this is generally agreed to be the sensitivity of such piles to installation effects (Tomlinson, 1976). Installation effects associated with piles installed in chalk are discussed below.

Pile test results reported by Hobbs and Healy (1979) for pre-formed piles of different types installed in chalk suggest that the dominant factor in determining ultimate shaft resistance is the radial effective stress generated by installation of the pile. The radial effective

stress generated is a function of the volumetric displacement of the pile, and the response of the soil.

It is generally accepted that driving a pre-formed pile into intact chalk, in which the water content is generally near to the liquid limit, produces a sleeve of crushed and remoulded chalk around the pile during driving. This zone of material has a dominant influence on the frictional response of the pile shaft under load. A key feature is the ability of the chalk mass surrounding the pile to arch around this zone, such that in-situ stresses are not transmitted through it on to the pile. Consequently, shaft resistances for pre-formed piles are often not very sensitive to chalk depth or grade (Lord 1976). It is thought that piles driven into weathered chalk may behave differently. During driving, the weathered chalk might allow passage of the pile by acting as a granular material, or open fissures might allow freedom for lateral movement (Hobbs and Healy, 1979; Mallard, 1980).

It is also generally accepted that the crushing action caused by dynamic pile driving generates positive pore water pressures which considerably reduce shaft friction during driving. Evidence for pore pressure generation is essentially from pile driving records. Pauses in pile driving in chalk have been found to cause temporary increases in driving resistance, commonly known as 'soil set-up' or 'pile freeze' (Ellis, 1965; Fryett, 1976; Vijayvergiya et al 1977, 1978). The positive pore pressures generated during driving are dissipated rapidly (Hobbs and Healy, 1979). Palmer (1965) reports a case of a German bomb which managed to penetrate more than 50 feet into chalk, but which subsequently required extensive work with pneumatic tools over the whole of this length to extract. In contrast to driven piles, Hodges and Pink (1971), investigating piles slowly jacked into weak chalk, reported lower shaft loads under test than jacking loads recorded during installation.

Hobbs and Healy (1979) report shaft resistances for various pile types in chalk. Considerably higher shaft resistances are reported for driven cast- in-place piles of the Frankipile type than for pre-formed driven piles. These high shaft resistances are attributed mainly to the compacting action of the pile installation method exerting pressure on the chalk. Shaft resistances reported for large displacement driven piles are higher than those for small displacement driven piles.

4.2.3 Recent advances in the understanding of carbonate soils

In the last few years very extensive research has led to much greater understanding of the behaviour of carbonate soils. This has come about

because of problems associated with offshore oil and gas platform foundations constructed in such materials. The surge in research activity culminated in an international conference in Perth, Australia, devoted entirely to the subject: 'Engineering for Calcareous Sediments' (Jewell and Andrews, 1988). The proceedings of this conference represent the state-of- the-art on carbonate soils.

Carbonate sediments in offshore design and construction were first encountered in the Arabian Gulf in the 1960's. The first awakening to unusual behaviour was when piles were observed to 'free-fall' during driving (similar behaviour to that of the bomb mentioned earlier). Further problems with free-falling piles and very low shaft capacities in comparison with design predictions occurred during projects off Australia, Philippines and Brazil. These problems were generally overcome by employing expensive drilled and grouted pile systems, or by making use of high end bearing when available (McClelland, 1988).

The installation of the North Rankin structure on the Northwest Shelf of Australia added a new dimension to the problem. Despite extensive site investigation beforehand, when installed the large 72inch diameter driven piles failed to meet design requirements for axial load carrying capacity. The problems on this project in particular prompted the huge amount of recent research which has involved geologists and carbonate sedimentologists as well as soils engineers (ibid.).

A brief summary of some of the important aspects of carbonate soil behaviour is given below.

By definition, carbonate soils comprise over 50% carbonate minerals. The most common mineral is calcium carbonate $CaCO_3$, which is the principal component of limestone. Because of this, the descriptor 'calcareous' is often used to describe carbonate soils. This is not strictly correct (Fookes, 1988).

Carbonate sediments are formed in many marine environments. The location of their greatest abundance is on the floor of tropical marine seas. Carbonate minerals precipitate from carbonate rich seawater by biological or chemical processes, and accumulate in many ways, for example by skeletal remains or inorganic growths that nucleate on debris (ibid.)

The characteristics of carbonate soil structure can be divided into the following categories (after Celestino and Mitchell, 1983):

(a) Grain hardness and intragranular porosity -
The inherant softness of the calcite mineral (Moh hardness 3 in comparison to 7 for the quartz mineral), and often the presence of intragranular voids, causes the soil particles to crush easily, particularly when sheared.

(b) Soil fabric -
In carbonate soils, the soil particles are often angular or intricate in shape. This leads to high voids ratios during deposition, and low mean crushing pressures due to the low number of contact points between particles.

(c) Cementation -
This is perhaps the most distinguishing feature of carbonate soils. Cementation often occurs very early in the life of the sediment, preserving the open, high voids ratio structure arising during deposition. Carbonate soils are often only partly or weakly cemented.

These characteristics of carbonate soil structure give rise to a number of important features of mechanical behaviour (McClelland, 1988; Randolph, 1988):

Carbonate soils show high compressibility. This is attributed to a combination of particle crushing and skeleton collapse. The presence of light cementation at particle contact points will give rise to high void ratios and the capacity for large volume changes once the cementation is destroyed. During shearing, the combination of particle crushing and skeleton collapse leads to markedly contractant behaviour.

The presence of cementation may produce increased strength at low stresses, but it often gives rise to brittle behaviour. Carbonate soils characteristically exhibit yield points at small strains, after which stiffness is dramatically reduced and strains are largely irrecoverable.

Carbonate soils exhibit generally high friction angles in comparison to silica soils. This is attributed to the angular nature of carbonate soil particles. These high friction angles are not usually affected by crushing or by large strains (Noorany, 1985; Morrison et al, 1988). In contrast to silica soils, however, the tendency for crushing and skeleton collapse in carbonate soils means that they do not have a reliable tendency to dilate (Hull et al, 1988).

Piles, particularly driven piles, placed in carbonate soils usually give

inferior capacities to those in non-carbonate soils (McClelland, 1974). It is generally accepted that this is not due to low angles of pile/soil interface friction, but to low radial stresses acting on such piles. The low radial stresses are considered to be due to the compressible, contractant nature of carbonate soils. When a pile is driven into a carbonate material, a zone of crushed and remoulded soil is produced around the pile. Contraction in the remoulded zone will cause a zone of radial stress relief to form around the pile. It is the mechanism of transfer of radial stresses through this zone which determines pile skin friction. The high friction angles and presence of cementation which are characteristic of carbonate soils are usually associated with arching around the pile, following shear induced volume reduction and stress relief. The combination of these effects can lead to very low radial stresses acting against the pile. Skin friction may well decrease with increased soil strength (Lu, 1988).

Recent research on piles in carbonate soils has shown that they are very prone to significant reduction in capacity due to cyclic loading (Jewell and Andrews, 1988). It has been found that strength degradation is a function of cyclic displacements (Poulos and Chan, 1988). Stress cycling which does not cause large strains will not usually give rise to severe reductions in capacity. However, significant pore pressures can build up at negligible permanent strains (Fahey, 1988a).

There is widespread concern regarding driven piles in carbonate soils. The preferred alternative solution at the present time is the use of drilled and grouted piles. Tests have shown these to give high shaft frictions, but also to be prone to severe strain softening, particularly under cyclic loading. Drilled and grouted piles are very costly and require careful and expensive supervision and monitoring during construction. McClelland (1988) concludes 'there is an obvious need for other alternatives'.

4.3 Test Site

The test site was at the yard of W.A. Dawson Ltd., situated at Leagrave, near Luton, Bedfordfordshire (Grid reference TL 055248). The location of the site is shown on Figure 4.1.

The geology of the area in which the test site is located comprises Lower Chalk, overlain by glacial sands and gravels of variable thickness. A preliminary inspection of the test site, by means of a hand augered borehole and also a pit conveniently being dug nearby, indicated highly weathered chalk existing near ground level. The background

geology indicated that the chalk extended below the embedment depth of the piles to be installed.

4.4 Soil Testing

4.4.1 Scope

Because of limited resources, soil testing was focused on:

(a) In-situ testing; in particular the determination of the limiting radial effective stress available in the chalk upon expansion of pressuremeter type devices.

(b) The laboratory determination of simple frictional strength parameters relevant to the pile tests.

The soil testing was undertaken well after the pile tests were completed. Because of lack of space at the pile test site, the in-situ tests were made approximately 30m away.

Tests were performed with the following instruments:

- standard cone penetrometer
- piezocone
- Marchetti dilatometer
- full displacement pressuremeter.

The layout of the in-situ tests is shown in Figure 4.2. To provide a reference, one cone penetration test (CPT 1) was performed at the pile test site (Figure 4.17). The in-situ tests were performed between 3.6.88 and 5.7.88 by Fugro-McClelland Ltd.; and by Cambridge In-situ, who performed the pressuremeter tests.

4.4.2 Borehole

In conjunction with CPT 1, a hand-augered borehole was opened up to a depth of 2.8m at the pile test site. The soil collected from this borehole was used in the shearbox tests described in Section 4.4.7. Visual inspection of the chalk was made by means of 38mm and 76mm push-in tube samples at regular intervals. Intact pieces of chalk obtained from the sampling tubes were used to determine moisture contents. The moisture content profile is shown in Figure 4.3. The chalk moisture content of approximately 28% at the bottom of the borehole corresponds to a porosity of 43%, assuming full saturation and a specific gravity for the chalk of 2.7. The borehole revealed approximately 0.5m of made ground existing at ground level.

The water table (July 1988) was observed to be 2.7m below ground level in the open boreholes left by extraction of the test piles. Water levels in the box piles, recorded between October 1985 and April 1986, varied between 2.6m and 3.1m below ground level.

4.4.3 Standard cone tests

Three standard cone penetration tests were performed as a reference for the other in-situ tests. A $10cm^2$ cone was used, advanced at a rate of 20mm/sec. The results are shown in Figure 4.4 - the three traces are very similar. Between approximately 2m and 5m depth, cone and sleeve resistances are reasonably steady. The cone resistance values of 2 to 4MPa over this depth range correspond to a chalk grade of VI using the classifications of Power (1982). The higher cone resistances experienced above 2m depth are probably due to the presence of natural gravels and/or made ground, or possibly to desiccation effects in the chalk above the water table.

4.4.4 Piezocone tests

One piezocone test was performed. A $10cm^2$ Fugro cone was used, with the pore pressure element being located on the face of the tip. The piezocone was advanced at a rate of 20mm/sec. Dissipation tests were made at 1m intervals below the water table. In these tests, penetration of the piezocone was stopped and excess pore pressures were allowed to dissipate before penetration was resumed.

The piezocone profile is shown in Appendix 4.1. Positive pore pressures in excess of 1MPa were generated during insertion of the probe. The results of a typical dissipation test, performed at 5m depth, are given in Figure 4.5. These show the chalk to be relatively free draining, excess pore pressures dissipating to values approaching hydrostatic within a few minutes.

4.4.5 Marchetti dilatometer test

The Marchetti flat-blade dilatometer (DMT) is a relatively new instrument, developed in Italy in the late 1970's by Marchetti (Marchetti, 1980). It is a simple and robust in-situ testing device which can be rapidly deployed and advanced, making it potentially a very powerful profiling tool (Powell and Uglow, 1986; 1988a; 1988b). The instrument is currently the subject of much research and development (Luttenegger, 1988).

The DMT is a stainless steel blade 250mm long, 94mm wide and 14mm thick with a tip angle of about 16°. One face of the blade is recessed to take a 60mm diameter stainless steel membrane which lies flush with the face

of the blade (Figure 4.6). Tests are performed every 200mm down a profile with the blade being advanced at 20mm/sec between tests using conventional CPT equipment. Each test involves removing the driving load and inflating the membrane using gas pressure. Electrical sensors behind the membrane indicate the start of movement and 1mm displacement, when the gas pressures p_0 ('lift-off') and p_1 are recorded. Three standard index parameters can be derived from the test: Material Index I_D, Horizontal Stress Index K_D, and Dilatometer Modulus E_D. These parameters can be used empirically to estimate various soil properties.

A DMT profile was performed using the standard procedure. Of most interest are the pressures p_0 and p_1 against depth, which are plotted in Figure 4.7. The variations of the deduced index parameters I_D, K_D and E_D with depth are presented in Figure 4.8.

The DMT profile is similar in pattern to CPT's 2 and 3, with reasonably steady readings between 2m and 5m. Typical values of p_0 in this zone of between 100 to 200kPa are in good agreement with friction values of 50 to 100kPa at these depths in CPT's 2 and 3, bearing in mind the smooth surface finish of the friction sleeve (specified Centre Line Average (CLA) roughness <0.5 micron (ISSMFE, 1977; Lemos, 1986)).

4.4.6 Full displacement pressuremeter testing

4.4.6.1 Details of instrument

The Fugro Full Displacement Pressuremeter (FDPM) is a recent development. It has been developed primarily for offshore use, and is designed to be used in combination with continuous piezocone profiling. The instrument follows behind a standard Fugro piezocone.

The instrument employed at the Luton site was the prototype FDPM described by Withers et al (1986). The general arrangement of the FDPM is shown in Figure 4.9. Overall membrane length is 450mm; the outside diameter is 43.7mm - the same as that of the 15cm^2 cone. The length: diameter ratio is 10.3. The prototype FDPM has a differential pressure capability of 10MPa and a radial expansion limit of 50%.

The detailed design and manufacture of the Fugro FDPM is undertaken by Cambridge In-situ. The general form of the instrument and its control system is based on the Self Boring Pressuremeter (SBP) (Mair and Wood, 1987).

4.4.6.2 Testing at Luton site

The FDPM was employed at the Luton site with a dummy cone arrangement

(Figure 4.10). The distance between the centre of the membrane and the cone tip was 750mm. The FDPM was installed at a single location and three tests were made; at instrument depths of 3.5m, 5.5m and 7.0m. These are designated Tests 1, 2, and 3 respectively. The tests and instrument calibrations were performed by Cambridge In-situ. The instrument and control system being prototypes, the tests should be regarded as experimental in comparison to the other in-situ tests.

The FDPM is computer controlled. The strain rate for loading and unloading was selected as 2.5% per minute, with loading during the initial stages of the tests generally being by means of stress increments applied at a constant rate. It was originally intended to perform tests at a number of different strain rates, but this did not prove possible. A key feature of the control system was the 'hold' mode - designed to maintain radial strain at a target value. This feature was used to 'steady' tests before performing unload/reload loops; and to perform holding tests, in which it was the aim to maintain radial strain at a constant value while monitoring changes in total radial stress.

There were problems with the FDPM membranes, which split whenever unloadings were attempted from strains in excess of about 30%. As a result, no full unloading data were obtained from any of the tests, although unload/reload loops were performed in each test.

The tests are presented in Figures 4.11 to 4.13. Time, instrument pressure p, and average strain ε_c are plotted against each other. ε_c is given by the change in radius of the instrument, expressed as a percentage of the original radius. The average of the values from the three strain measuring arms has been taken and data in the strain range 0 to 20% are plotted. No useful data beyond this strain range were obtained because of the membrane problems.

Discussion is centred on these basic data. In general, derivation of soil parameters from the results has not been attempted because the test procedures employed were not standard.

4.4.6.3 Limiting total radial stress

In this Section, instrument pressure p is considered as total radial stress acting on the soil, σ_r .

σ_r appears to approach a limiting value at the end of all three tests: approximately 600kPa in Test 1, and approximately 1100kPa in Tests 2 and 3 . The stress:strain curves for Tests 2 and 3 are very similar. The

limiting values of σ_r in Tests 1 and 2 are in exact agreement with the values of p_1 obtained in the DMT test (Figure 4.7).

At the strain rate of 2.5%/minute adopted in the tests, expansion was likely to have been partially drained, given the dissipation characteristics indicated by the piezocone results. Consequently, consolidation would have taken place during the holding periods of the tests. Changes in σ_r and ε_c during the holding periods in Tests 2 and 3 are shown in more detail in Figures 4.14 and 4.15.

When the FDPM hold mode is selected (Point A), instrument pressure is slowly reduced. ε_c continues to increase, at a decreasing rate, as σ_r reduces. Consolidation will be occurring during this period, as the instrument slowly expands to a maximum value of ε_c (Point B). In Test 2, a drop in σ_r of 68kPa during 220 seconds occurred during this period. In Test 3 a drop in σ_r of 135kPa occurred during 90 seconds. If substantial consolidation during these periods is assumed, it suggests effective radial stresses after consolidation of about 10% less than the limiting pressures obtained during expansion of the FDPM. Further tests making use of slower strain rates and/or longer holding periods would be required to establish this accurately.

4.4.6.4 Constant radial strain tests

These are shown in Figures 4.14 and 4.15. As can been seen, after a maximum value of ε_c is reached at Point B , ε_c is not held at a constant value. Rather, uncontrolled unloading and reloading occurs. The reason for this phenomenom during strain controlled pressuremeter tests is due to ε_c overshooting the 'target' value. If this occurs, the computer control system unloads the instrument accordingly. Similar experiences are reported by Fahey (1988b).

Reductions in σ_r during the holding periods appear to be due solely to reductions in ε_c . The values of σ_r existing at the points of maximum ε_c prior to unloading are almost fully recovered when ε_c returns to these values (Points B, C). This would appear to indicate that the unloading and reloading during the holding periods were largely drained events.

4.4.6.5 Shear Moduli

Values of shear moduli G_{ur} obtained by the standard method of bisecting the unload/reload loops (Mair and Wood, 1987) are given in Table 4.1. As would be expected, G_{ur} increases with depth and decreases with the stress range of the unload/reload loop.

4.4.6.6 Lift-off pressures

The behaviour of all three strain arms during the initial stages of the tests was studied in detail but no clear pattern emerged. Values of p at lift-off ranged between 0kPa and 500kPa. The test in the weaker chalk at 3.5m depth exhibited a 'spongy' lift-off in comparison to the other two tests.

4.4.7 Shearbox testing

Drained, 60x60mm direct shearbox tests were undertaken using reconstituted samples of chalk obtained from the auger hole opened at the pile test site. General procedures for the tests were as set out by Head (1982). The majority of the tests were performed fully saturated. In addition to standard shearbox tests, interface tests were carried out in which the chalk was sheared against steel interfaces intended to represent the surface of the steel piles installed at the site.

4.4.7.1 Sample preparation

A test batch of chalk with a dry weight of about 10kg was made up from a selection of samples taken at depths of between 1.8m and 2.8m from the auger hole at the pile test site (Section 4.4.2). The test batch was thoroughly dried, and then ground in smaller batches for 2 minutes using a mechanical grinder. The grinding was broadly intended to simulate the crushing of chalk during pile driving. The grinding time was restricted, to prevent excessive comminution of the chalk particles (although Clayton (1983) reports that the method of crushing does not seem to affect the particle size distribution of chalks). The crushed material was then passed through a 1.18mm aperture sieve to remove stones, and larger lumps of chalk which could then be ground down for a further short period of time.

Four shearboxes were used for each suite of tests. The test batch of chalk was reduced to an appropriate size for each suite. Distilled water was then added to give a moisture content of between 27 to 28%, the approximate in-situ moisture content. The chalk was then thoroughly mixed, to a putty-like consistency. The samples were then lightly rammed into the shearbox moulds using a 15x15mm hardwood rammer. Samples for moisture content determinations were taken from the test batch.

4.4.7.2 Consolidation

After the samples had been placed in the shearbox moulds they were inundated with water and allowed to equalise for 15 to 20 minutes before normal loads were applied. Normal stresses adopted for the tests were in the range 60 to 493kPa. After applying the normal load, the samples were left to consolidate for at least 90 minutes (Hutchinson, 1971).

4.4.7.3 Shearing

The samples were tested with a single run of the shearbox. The rate of displacement of the lower half of the shearbox was in general 0.033mm/ minute. Shearing at faster and slower rates was carried out during some of the tests to check that the standard rate gave fully drained conditions (ibid.). Unloading and reloading tests were also performed. After shearing, the shearbox was quickly drained of water and the sample unloaded. The whole sample was then used for a moisture content determination.

4.4.7.4 Interface Tests

Suites of tests on two sets of steel interfaces were performed. The roughnesses of the interfaces were intended to be upper and lower bounds to the roughness of the surfaces of the piles at the Luton site. The interfaces comprised flat blocks of steel fitted tightly inside the shearboxes, with the top face of the block aligned exactly with the split between the upper and lower halves of the boxes. The test procedure for the interface tests was exactly the same as for the standard tests except that only the top half of the shear box was filled with chalk.

One set of interfaces was of standard cold finished machining steel, smoother than the hot finished steel sections used to fabricate the piles. The other set of interfaces was of identical blocks of steel, but with the shearing surfaces grit blasted to represent a rusted steel surface. Exactly the same technique has been found by Bond (1989) and Tika (1989) to give CLA roughness values of approximately 9 micron. This is in good agreement with values measured on a selection of rusted steel piles, including one of the wedge-piles used at the BRS site.

The interfaces were carefully degreased with butanone before each test.

4.4.7.5 Tests on dry chalk

A suite of tests on dry chalk was performed. The test procedure was exactly the same as for the standard shearbox tests on saturated chalk, except that the chalk was placed dry and the porous stones of the shear box were not used.

4.2.7.6 Results

Results from the tests are presented in Appendix 4.2. The following behaviour during shear was observed:

- although the shearbox was only given one run, shear response showed little or no tendency to fall from the peak value

- there was little apparent difference in shear response for strain rates varying between 0.0065 and 1.2mm/minute

- shear response was markedly stiffer on reloading

- the samples contracted during shear

- the moisture content of the chalk after shearing was between 23.9% and 24.5%.

The peak strength envelopes for the initial loadings are shown in Figure 4.16. An effective angle of friction ϕ' of approximately 36° for chalk:chalk shearing is indicated, with a reduction of up to 5° for chalk sheared against a steel interface. Slightly lower values of ϕ' for remoulded chalks are quoted by Clayton (1989).

4.5 Details of Pile Configurations

4.5.1 Dimensions and driven levels

Four steel wedge-piles were installed at the Luton site - two box piles and two cruciform piles. Details of the piles have been given in Chapter 3. The four piles were driven at spacings of 1.2 to 1.5m. The two box piles were numbered 1 and 2; and the two cruciform piles were numbered 3 and 4. The piles were driven into 300mm deep pitching holes, dug in order to remove hard core existing at ground level. Figure 4.17 shows the layout of the driven piles, and the general positioning of the loading frame spreader beams and the reference beam during testing.

Individual piles were generally tested in more than one configuration. The pile configuration is designated by the letter 'U' (unexpanded pile), 'A' (pile expanded by expander mandrel A), or 'B' (pile expanded by expander mandrel B).

The dimensions and driven levels of the box pile and cruciform pile configurations are summarised in Figures 4.18 and 4.19 respectively. Dates of installation are included. Details of driving are dealt with in Section 4.6, but a short summary is given below.

The outer shell of Box Pile 1 was driven and initially tested unexpanded (pile configuration 1U). It was then expanded by 14.3% of its width using expander mandrel A (pile configuration 1A), and

retested.

The outer shell of Box Pile 2 was driven and then expanded by 14.3% of its width using expander mandrel A (pile configuration 2A). After testing of this configuration was complete, expander mandrel A was extracted. The outer shell was then expanded by 21.4% of its original width using expander mandrel B (pile configuration 2B). The pile was then retested.

Figure 4.18 gives the driven levels of the bottom of the conical tip of the driving shoe, the bottom of the outer shell angles, the bottom of the expander mandrel nose, and the top of the expander mandrel nose. The small amount of dragdown of the outer shells which occurred as the expander mandrels were driven (typically 20 to 30mm) has been ignored (see Section 4.5.2).

The outer shell of Cruciform Pile 3 was driven and initially tested unexpanded (pile configuration 3U). It was then expanded by 21.4% of its width using expander mandrel B (pile configuration 3B), and retested.

The outer shell of Cruciform Pile 4 was driven and then expanded by 10.7% of its width using expander mandrel A (pile configuration 4A). It was then tested.

Figure 4.19 gives the driven levels of the bottom of the outer shell angles, the bottom of the expander mandrel nose, and the top of the expander mandrel nose. Also tabulated in Figures 4.18 and 4.19 are pile cross-sectional dimensions, pile weights, and the percentage amounts of expansion of the various pile configurations.

Simplified effective pile perimeters and cross-sectional areas have been assumed. These are indicated by the chain lines in Figures 4.18 and 4.19, and are shown in more detail in Figure 4.20. In the case of the cruciform piles, the failure surface is assumed to join the tips of the cruciform arms. This assumption is based on evidence obtained during pile extraction (see Section 4.7.9). The assumed pile perimeters have been used as the basis for calculating the pile shaft surface areas given in the next Section.

Two methods have been used to express the percentage amount of expansion of the pile configurations. In the first method, the amount of expansion is expressed as the percentage increase in pile width compared to the original width of the outer shell. In the second method, the amount of expansion is expressed as the percentage increase in the assumed pile

cross-sectional area compared to the original assumed cross-sectional area of the pile.

4.5.2 Shaft surface areas

Pile shaft surface areas are given in Figures 4.21 and 4.22. Four different surface areas are considered - the reasoning behind this is given below.

The limiting shaft friction, τ_{s_f} acting locally on the sides of steel wedge-piles of the types described in this Chapter is likely to vary, both around the perimeter of the pile and along the length of the pile.

Around the perimeter of the pile the angle sections will attract most of the effective radial stress σ_r' acting against the pile, 'dead' areas being likely to occur in the vicinity of the gaps opened up between the angles on expansion.

Along the length of the pile, σ_r' for a given vertical effective stress is likely to be affected both by over-expansion during installation of the expander mandrel, and by the effects of pile tapering. Over-expansion may cause a loss of σ_r' over the length of the expander mandrel shank. This possibility has been mentioned in Chapter 1 and is considered further in Chapters 10 and 11. The effect of the taper of the pile from its expanded to its unexpanded dimensions is likely to cause a reduction in σ_r' in the region of the expander mandrel nose, if upward pile displacements occur. This is discussed further in Chapter 11.

Because of these possible variations in σ_r', caution must be adopted when ascribing an overall 'active' shaft area to an expanded pile for the purposes of computing average shaft frictions. The approach adopted here is to set bounds to the active shaft surface area by defining four different surface areas, corresponding to different possible modes of shaft load mobilisation.

Two different pile perimeters and two different pile lengths have been considered:

- Full perimeter. This is defined as the full simplified perimeter of the pile, as indicated by the chain lines in Figures 4.18 to 4.22. For the expanded piles, shaft surface areas based on the full perimeter correspond to the assumption of uniform shaft resistance around the perimeter of the pile, including the areas of expander mandrel exposed by the split outer shell.

- Reduced perimeter. This includes only those portions of the simplified perimeter running along the outward facing edges of the angle sections. These portions are indicated by shading in Figure 4.20. Shaft surface areas based on the reduced perimeter correspond to the assumption of all shaft load being taken by the angle sections alone.

- Embedded length. This is defined as the length between the bottom of the pitching hole dug at ground level, and the bottom of the outer shell angles. Shaft areas based on the embedded length correspond to the assumption that the tapered portion of the outer shell contributes to shaft resistance. In the case of the box piles, the conical pile tip is assumed not to contribute to shaft resistance.

- Expanded length. This is defined as the length between the bottom of the pitching hole and the level of the top of the expander mandrel nose. Shaft areas based on the expanded length correspond to the assumption that the tapered portion of the expanded pile does not contribute to shaft resistance.

The four different shaft surface areas based on these pile lengths and perimeters are designated by the letters A to D. Figures 4.21 and 4.22 give the computed shaft surface areas for the box piles and cruciform piles respectively. The changes in pile embedment length due to downward displacement during expander mandrel installation and to upward displacement during pile testing correspond to changes in shaft surface areas of less than 1.5% and these have been ignored.

4.6 Pile Installation

Details of pile installation procedures have been given in Chapter 3. The installation process was not continuous, being interrupted by the need to rearrange and adjust the driving frame. The overall installation time for each pile component was typically about 1 hour. Further information on the installation of the piles at the Luton site is given in the next three Sections. The pile penetrations quoted refer to penetrations of the bottom of the pile component being driven (including any driving shoe) below ground level.

4.6.1 Installation of box piles

The box piles were transported to the Luton site from the BRS workshops just prior to installation. The condition of the pile surfaces was similar to the workshop condition shown in Plates 3.1 to 3.6.

Driving of the outer shell of Box Pile 1 commenced on the afternoon of 26.3.85. After 45 minutes driving, pile penetration had reached 3.82m below ground level. Driving was then stopped for the night and recommenced 21 hours later on 27.3.85. After 20 minutes driving the final penetration of 5.18m was achieved.

The outer shell of Box Pile 1 was expanded with expander mandrel A on 17.4.85, 21 days after the outer shell was driven (expander mandrel A having previously been extracted from Box Pile 2).

Driving of the outer shell of Box Pile 2 commenced on the afternoon of 27.3.85. After 15 minutes of driving, pile penetration had reached 3.44m below ground level. Driving was then stopped for the night. Driving recommenced 18 hours later on 28.3.85. After 30 minutes driving the final penetration of 5.26m was achieved. The outer shell was then expanded with expander mandrel A, this operation commencing within 30 minutes of the completion of driving of the outer shell. The expander mandrel installation time was approximately 1 hour. Dragdown of the outer shell as the expander mandrel was driven was approximately 25mm.

On 16.4.85 expander mandrel A was extracted from Box Pile 2 (see Section 4.7.8) to be replaced by expander mandrel B. Driving of expander mandrel B commenced the same day, being stopped for the night at a penetration of 4.25m. On the following day, 17.4.85, expander mandrel B was driven to final level. Dragdown of the outer shell during expansion was approximately 20mm.

4.6.2 Installation of cruciform piles

The cruciform piles were transported to the Luton site from the BRS workshops several weeks before installation. At the site, the piles were stored in the open where light corrosion occurred. The condition of the pile surfaces prior to installation can be observed in Plates 3.7 and 3.11.

The outer shells of Cruciform Piles 3 and 4 were installed on 4.10.85. Cruciform Pile 4 was expanded with expander mandrel A on 7.10.85, 3 days after the outer shell was installed. Cruciform outer shell 3 was expanded with expander mandrel B on 20.11.85, 47 days after the outer shell was driven.

4.6.3 Driving records

During pile installation, records were taken of pile penetration against number of hammer blows. The data must be considered to be highly qualitative because of the limitations of the pile driving system described in Section 3.4. The pile driving data are summarised in Figure 4.23. Pile penetration is plotted against cumulative drop height. A free-fall hammer drop is assumed, with drop height thus proportional to blow energy.

The driving data, although qualitative, appear to show some consistency. There is less driving resistance in the case of the cruciform piles than for the box piles. The driving resistance for the expander mandrel driven into Box Pile 2A (very soon after the outer shell was driven) is less than for the box expander mandrels driven after longer periods of consolidation subsequent to outer shell driving (Box Piles 1A, 2B).

The installation data are discussed further in Chapter 11.

4.7 Pile Testing

4.7.1 Rationale

In accordance with the overall objective of determining whether significant gains in pile shaft capacity can be achieved by means of expansion after driving, pile testing at the Luton site was focused on the determination of ultimate shaft resistances (Section 3.1). Tension only tests were adopted in order to eliminate base resistance. The capacity of expanded piles was compared with that of unexpanded piles.

In order to maximise the amount of information that could be obtained from each pile position, each pile was generally tested in more than one configuration. In addition, repeated testing of each pile configuration was performed in order to investigate some different aspects of pile behaviour, and to monitor changes in ultimate shaft capacity with time. A shortcoming of this approach was the possible effects of soil degradation around the piles due to repeated soil disturbance. This is discussed in Chapter 11.

For the bulk of the testing programme the Constant Rate of Extraction (CRE) test was adopted (Whitaker, 1963; Weltman, 1980). This displacement controlled method of testing provides a quick and convenient method of determining ultimate shaft capacity.

A displacement rate of 1mm/minute was adopted for the CRE tests (ibid). Given the piezocone results, this rate of displacement is likely

to have given rise to near drained conditions around the pile during testing. Upward pile displacement was maintained approximately at the 1mm/minute rate by hand pumping the hydraulic jack to 'pace' one of the pile deflection gauges (scale 1mm/revolution) with the sweep second hand of a clock. The pile displacement rate was usually less than the target rate during the early stages of a test due to fast rates of hand pumping being required to overcome stiff pile responses. Measurements of load and displacement were taken at least two times per minute. Post peak displacements were minimised to prevent excessive damage to the soil fabric around the pile.

In the later stages of the testing programme at the Luton site, an incremental system of pile loading (IL) was introduced in which loading was by means of discrete increments of load held over a series of increments of time (ibid.). This method of testing was introduced in order to investigate settlements and creep behaviour under sustained load, and to provide greater test control during the initial period of stiff pile response. Each increment of load was held until pile displacement was reasonably constant. Hold times varied, becoming longer towards the end of a test - periods of up to 32 minutes were employed. A CRE stage was included at the end of each incremental loading test in order to determine ultimate load. The incremental loading stage was generally stopped when the creep rate approached the 1mm/minute CRE displacement rate. There was usually a pause between the two stages when the loading pump was allowed to relax. This often caused a drop in load which can be observed on the load displacement plots.

Cyclic loading tests were carried out. The cyclic loads applied were intended to enable an overall assessment of the effect of repeated loading, rather than to reproduce a specific loading pattern. Tension only cycles were applied; cycling from near zero load to half the ultimate load in the previous static test was considered appropriate (Tomlinson, 1977). Cycle duration was made as short as possible, in order to maximise the number of cycles that could be applied in the testing time available. The time taken to apply a cycle ranged from 0.5 minute to 1.5 minutes, depending on the magnitudes of the loads applied.

4.7.2 Arrangement of reference beam and spreader beams

In the earlier stages of the testing programme at the Luton site the reference beam arrangement was not fully satisfactory. For convenience, an elevated reference beam arrangement was used with the deflection gauges acting against the top of the loading box (Section 3.6.5). This system gave rise to 'false zeros' on the load:displacement plots, and did not allow pile displacement during unloading to be accurately

measured. Also, the support system for the elevated reference beam was susceptible to vibrations from heavy goods trains running on the railway alongside the test site. Cumulative movements of the reference beam caused by these trains were of significance in the case of long duration cyclic loading tests.

The shortcomings of the reference beam system were overcome for the later stages of the testing programme by means of the arrangement described in Secton 3.6.5, with the deflection gauges acting against reference plates welded to the piles. The arrangement of the spreader beams and reference beam were such that interaction effects are not considered to have seriously affected the results of the pile tests given in the following Sections.

4.7.3 Summary of pile testing

The load:displacement histories of the four piles are summarised in Figures 4.24 to 4.27. Figure 4.28 is a calender history of the testing programme. Pile tests are referred to by means of the pile configuration, followed by a pile test number.

Individual tests are described in the following four Sections. The descriptions have been organised as testing histories for each pile position. In order to provide a complete description, some information regarding pile installation has been repeated. The test results are presented in Figures 4.29 to 4.58. The standard plot is of upward displacement of the pile head against applied tensile head load. Also presented are creep plots showing displacements during the holding periods of the incremental tests, and plots showing behaviour during cyclic loading. Upward displacement of the pile is taken as the average of the measurements made using the two dial gauges. Agreement between the two gauges was very good. Typical behaviour is shown in Appendix 4.3.

In the case of Tests 1U.1 to 1A.5 and Tests 2A.1 to 2B.5 the position of the vertical axis has been adjusted by eye to deal with false zeros. Data points in the region of the false zero are indicated by open circles. There is no unloading information for these tests (Section 4.7.2).

The load:displacement plots are accompanied by summary tables featuring key data from the tests. Shaft frictions calculated on the basis of the four shaft surface areas A to D and net failure loads are given. Information from these summary tables is brought together for each pile configuration in Tables 4.2 to 4.8. Included on the

load:displacement plots is the likely range of displacement due to elastic extension of the piles under load. The basis for the calculation of these elastic displacements is described in Section 4.7.10.

In order to compare pile capacities on a systematic basis, differences in capacity are defined in terms of factors. For example, an increase in capacity from 100 to 350kN is described as a factor of increase of 3.5.

4.7.4 Testing history: Box Pile 1

Pile Configuration 1U
The outer shell of Box Pile 1 was driven on 27.3.85 and was initially tested unexpanded.

Test 1U.1 Date: 2.4.85 Type: CRE Figure 4.29
Test 1U.1 was performed 6 days after driving. In this test, the first at the Luton site, control of the loading jack was by means of an electrically driven hydraulic pump (Section 3.6.3). At an applied load of 52.2kN, control of the loading jack was lost due to an error in operating the pump. The pile failed and was subjected to a sudden displacement of over 8mm. When control was regained, the recorded load was 52.6kN.

Test 1U.2 Date: 2.4.85 Type: CRE Figure 4.30
Test 1U.2 was performed immediately after Test 1U.1. Following the loss of control in the previous test, the electrically driven pump was replaced by a hand operated pump. Maximum recorded load was 66.4kN, at 1.8mm displacement. Further displacement to 2.7mm gave a drop in load to 64.3kN.

Test 1U.3 Date: 16.4.85 Type: CRE Figure 4.31
Test 1U.3 was performed 20 days after driving (14 days after the previous test). Maximum recorded load was 79.1kN, at 2.1mm displacement, representing a factor of increase of 1.19 over the previous test. Further displacement to 4.2mm gave a drop in load to 67.7kN.

Pile Configuration 1A
Box Pile 1 was expanded by 14.3% on 17.4.85, 21 days after the outer shell was driven.

Test 1A.1 Date: 22.4.85 Type: CRE Figure 4.32
Test 1A.1 was performed 5 days after expansion. Maximum recorded load was 302.8kN, at 14.0mm displacement; a factor of increase of 3.83 over

Test 1U.3. The test was stopped soon after the maximum load was reached. The shape of the load:displacement curve was markedly non-linear.

Test 1A.2 Date: 22.4.85 Type: Cyclic, CRE Figure 4.33, 4.34
Test 1A.2 was a cyclic loading test, performed immediately after Test 1A.1. In the first stage of the test, 25 cycles of loading between 15kN (average) and 150kN were applied (0.05 and 0.5 times the static capacity in Test 1A.1). There was a variation in the bottom of cycle load, which ranged from 0kN to 27kN. Each cycle of loading was applied over approximately 1.5 minutes. Load and displacement readings were taken at four points on the loading portion of each cycle.

The pile response during the loading portion of each cycle was very similar throughout cycling. In Figure 4.34 load is plotted against displacement, for cycles 8, 19 and 22. Reference displacement is taken as the displacement at the bottom of cycle load, which was 19kN for all three of these cycles. Because of problems with the reference beam arrangement (Section 4.7.2), the cumulative displacement of the pile during cycling could not be measured satisfactorily .

Immediately following the cycling stage, a CRE test was carried out (Figure 4.33). Maximum recorded load was 256.0kN, at 3.6mm displacement. The maximum load was a factor of 0.85 times the static failure load in Test 1A.1, carried out prior to cycling. Pile response was much stiffer than for Test 1A.1, the load:displacement curve being more linear. Further displacement after the maximum load to 4.9mm resulted in a drop in load to 249.7kN.

Test 1A.3 Date: 1.11.85 Type: IL, CRE Figures 4.35, 4.36
Test 1A.3 was performed 198 days after expansion (193 days after the previous test).

In the first stage of the test, load was increased in increments of 30kN (nominal), up to a load of 241.2kN. Load increments were maintained for up to 32 minutes. Total displacement at the end of the holding period for the 241.2kN increment was 2.6mm. The average creep displacement rate between 28 and 32 minutes of the final holding period was 0.81mm/min. Creep behaviour is presented in Figure 4.36.

In the second stage of the test CRE loading was applied (Figure 4.35). Maximum recorded load was 322.3kN at 5.4mm displacement. This represents a factor of increase of 1.26 over the maximum load in Test 1A.2 (performed immediately after cycling); and a factor of increase of 1.06 over the maximum load in Test 1A.1 (performed before cycling). The loss

in capacity that occurred as a result of cycling was thus fully recovered. The load:displacement curve up to maximum load followed closely that of the previous test. Further displacement to 9.9mm after the maximum load was reached resulted in a fall in load to 298.4kN.

4.7.5 Testing history: Box Pile 2

Pile Configuration 2A
The outer shell of Box Pile 2 was driven on 28.3.85 and was immediately expanded by 14.3%.

Test 2A.1 Date: 2.4.85 Type: CRE Figure 4.37
Test 2A.1 was performed 5 days after expansion. Maximum recorded load was 232.7kN, at 9.0mm displacement. Further displacement to 13.3mm resulted in a decrease in load to 224.1kN. The load:displacement curve was markedly non-linear.

Test 2A.2 Date: 16.4.85 Type: CRE Figure 4.38
Test 2A.2 was performed 19 days after expansion (14 days after the previous test). Maximum load recorded was 249.7kN, at 3.9mm displacement; a factor of increase of 1.07 on the maximum load in the previous test. Pile response was much stiffer and more linear than for Test 2A.1. Failure occurred quite suddenly, with little prior indication. After failure, further displacement to 6.3mm gave a decrease in load to 235.1kN.

Pile Configuration 2B
On 17.4.85, 1 day after Test 2A.2, expander mandrel A was extracted from Box Pile 2. Expander mandrel B was then driven in its place, expanding the pile by 21.4% of its original unexpanded width.

Test 2B.1 Date: 22.4.85 Type: CRE Figure 4.39
Test 2B.1 was performed 5 days after expansion. Maximum recorded load was 335.0kN, at 10.4mm displacement; a factor of increase of 1.34 over the maximum load in Test 2A.2. Further displacement to 14.6mm gave a drop in load to 328.8kN. The load:displacement curve was non-linear, similar to those for the initial loadings of expanded Piles 1A and 2A.

Test 2B.2 Date: 23.4.85 Type: Cyclic, CRE Figures 4.40, 4.41, 4.63
Test 2B.2 was a cyclic loading test, performed the day after Test 2B.1. 50 cycles of loading between 21kN (average) and 171kN were applied (0.06 and 0.51 times the static capacity in Test 2B.1). There was a variation in the bottom of cycle load, which ranged from 12kN to 27kN. Each loading cycle was completed in approximately 1.5 minutes. Load and

displacement readings were taken at four points on the loading portion of each cycle.

Pile response during the loading portion of each cycle was very similar throughout cycling. In Figure 4.41 load is plotted against displacement for cycles 3, 15, 40 and 50. Reference displacement is taken as the displacement at the bottom of cycle load, which was 19kN for all four cycles.

Cumulative displacement of the pile during cycling is shown in Figure 4.63, in which displacement at top of cycle load is plotted against cycle number. There is negligible difference in top of cycle displacement for cycle 1 and cycle 50 (1.7mm), although some minor fluctuations occur during the course of cycling (most probably because the deflection dial gauges were acting against the load box rather than against the pile).

Immediately after cycling, CRE loading was applied (Figure 4.40). Maximum recorded load was 272.6kN, at 4.6mm displacement; a factor of decrease of 0.81 times the maximum load in Test 2B.1 (carried out before cycling). The load:displacement response was characteristically stiffer and more linear up to failure than for Test 2B.1. Further displacement after failure to 6.4mm gave a drop in load to 262.2kN.

Test 2B.3 Date: 7.5.85 Type: CRE Figure 4.42
Test 2B.3 was carried out 20 days after expansion (14 days after the previous test). Maximum recorded load was 306.9kN, at 4.0mm displacement. This represents factors of increase of 1.13 over Test 2B.2 (carried out immediately after cycling) and 0.92 over Test 2B.1 (carried out before cycling). The load:displacement curve followed closely that of the previous test. After failure, further displacement to 5.7mm gave a drop in load to 266.8kN, a relatively marked loss in comparison to previous tests and close to the failure envelope for the previous test (although this is probably coincidental).

Test 2B.4 Date: 5.8.85 Type: CRE Figure 4.43
Test 2B.4 was performed 110 days after expansion (90 days after the previous test). Maximum recorded load was 314.2kN, at 4.1mm displacement; a factor of increase of 1.02 on the previous test. The factor of increase over Test 1B.1 was 0.94, the loss in capacity due to cycling being almost recovered. The load:displacement curve up to failure followed closely that of the previous two tests. After failure, further displacement to 5.0mm gave a drop in load to 303.8kN.

Test 2B.5 Date: 6.11.85 Type: IL, CRE Figures 4.44, 4.45
Test 2B.5 was performed 203 days after expansion (93 days after the previous test).

In the first stage of the test, load was increased in increments of 30kN (nominal) up to a load of 271.8kN. Load increments were maintained for up to 16 minutes. During the holding period at 271.8kN the rate of creep displacement increased suddenly and continued to accelerate. Between 4 and 6 minutes of the holding period, the creep displacement was 2.56mm (1.28mm/min). Pumping of the loading jack was stopped after 6 minutes and the load allowed to stabilise. The final incremental load was a factor of 0.87 times the maximum load in Test 2B.4. Creep behaviour is presented in Figure 4.45.

In the second stage of the test, CRE loading was applied (Figure 4.44). Pumping of the loading jack commenced at a stabilised load of 251.0kN. Maximum load recorded was 263.5kN, at 7.6mm displacement. The maximum load was less than the final load increment during the first stage of the test. Displacement to 12.0mm resulted in a further drop in load to 247.8kN.

4.7.6 Testing history: Cruciform Pile 3

Pile Configuration 3U
The outer shell of Pile 3 was driven on 4.10.85 and was initially tested unexpanded.

Test 3U.1 Date: 16.10.85 Type: IL, CRE Figures 4.46, 4.47
Test 3U.1 was performed 12 days after driving.

In the first stage of the test, two successive increments of 10kN (nominal) were applied, to give a load of 21.4kN. The second increment was maintained for 32 minutes, during which time substantial creep displacement of just under 3mm occurred. As a result, it was decided to proceed with the CRE stage of the test. Creep behaviour is shown in Figure 4.47.

During the CRE stage of the test (Figure 4.46) a slow increase in load occurred as a large displacement was applied to the pile. Maximum load recorded was 50.4kN, at 31.4mm displacement. The test was terminated shortly after this.

Test 3U.2 Date: 31.10.85 Type: Cyclic, CRE Figures 4.48, 4.49, 4.63
Test 3U.2 was a cyclic loading test performed 27 days after driving (15

days after the previous test).

50 cycles of loading between 1 and 25kN were applied (0.0 and 0.5 times the static capacity in the previous test). The time taken to apply each cycle was approximately 30 seconds. Load and displacement readings were taken at the top and bottom of each cycle. At 10 cycle intervals, a more accurately logged cycle (11 readings during the cycle) was performed, these cycles lasted approximately 60 seconds.

In Figure 4.49 load is plotted against displacement, for the accurately logged cycles. The loops appear similar, apart from the initially less stiff response in cycle 1. Cumulative displacement of the pile during cycling is shown in Figure 4.63, in which displacement at the top of cycle load is plotted against cycle number. Cumulative displacement at peak cycle load increases steadily from 0.7mm in cycle 1 to 2.2mm in cycle 50.

CRE loading was applied immediately after cycling (Figure 4.48). The maximum load recorded was 51.2kN at 10.7mm, almost identical to the maximum load in Test 3U.1 (before cycling). Displacement to failure was much less than for Test 3U.1 however.

Pile Configuration 3B
Cruciform Pile 3 was expanded by 21.4% on 20.11.85, 47 days after the outer shell was driven.

Test 3B.1 Date: 2.12.85 Type: IL, CRE Figures 4.50, 4.51
Test 3B.1 was performed 9 days after expansion. In the first stage of the test, load was increased in increments of 30kN (nominal) up to a load of 149.4kN. The load increments were maintained for up to 32 minutes. The ultimate creep displacement rate during the final load increment was an average of 0.04mm/min between 28 and 32 minutes of the holding period. Total displacement at 32 minutes was 10.2mm. Creep behaviour is shown in Figure 4.51.

In the second stage of the test, CRE loading was applied (Figure 4.50). Load increased slowly with continued displacement, reaching a maximum recorded value of 210.8kN at 24.0mm displacement. This represented a factor of increase of 4.12 on Test 3U.2 (carried out before expansion). Loading was stopped shortly after the maximum load was reached. The overall load:displacement curve was non-linear.

Test 3B.2 Date: 26.3.86 Type: CRE Figure 4.52
Test 3B.2 was performed 126 days after expansion (117 days after the

previous test). The maximum load recorded was 216.6kN at 8.3mm displacement, a small factor of increase of 1.03 on the previous test. Pile response was more linear, and displacement to failure was much less than for the previous test. Further displacement after the maximum load to 11.8mm gave a drop in load to 210.4kN.

4.7.7 Testing history: Cruciform Pile 4

Pile Configuration 4A
The outer shell of Cruciform Pile 4 was driven on 4.10.85. The outer shell was expanded 3 days later on 7.10.85.

Test 4A.1 Date: 16.10.85 Type: IL, CRE Figures 4.53, 4.54
Test 4A.1 was performed 9 days after expansion. In the first stage of the test, load was increased in increments of 25kN (nominal), up to a load of 125.3kN. The load increments were held for up to 32 minutes. Creep behaviour is shown in Figure 4.54.

The ultimate creep displacement rate during the final increment was an average of 0.06mm between 16 and 32 minutes of the holding period. Total displacement at 32 minutes was 2.7mm. At this point an attempt to start the CRE stage of the test was made. However, problems with the hand pump developed. In order to attend to the pump a total release of the applied load had to be made. Pile displacement after load release was 2.2mm.

In the second stage of the test CRE loading was applied (Figure 4.53). Problems with the hand pump continued to occur, resulting in a partial loss of load on three occasions. This did not appear to affect the load:displacement curve unduly, however, which was characteristically non-linear. Maximum recorded load was 304.4kN at 19.5mm. Further displacement to 34.5mm gave a small drop in load to 300.3kN.

Test 4A.2 Date:31.10-1.11.85 Type: Cyclic,CRE Figures 4.55, 4.56, 4.63
Test 4A.2 was a cyclic loading test, performed 24 days after expansion (15 days after the previous test).

Initially, load was cycled between 1kN and 150kN (0 and 0.50 times the static capacity in the previous test). 20 cycles of loading were applied, the time taken to apply each cycle was approximately 50 seconds. Load and displacement readings were taken at the top and bottom of each cycle. Cycles 1, 10 and 20 were more accurately logged (11 readings during the cycle); these cycles lasted approximately 1.5 minutes.

Cumulative displacement at top of cycle load increased with each cycle, from 2.1mm in cycle 1 to 11.8mm in cycle 20 (Figure 4.63). The rate of increase of displacement accelerated during cycles 10 to 20. At this point the pile was completely unloaded and testing was stopped for the night. Permanent displacement on unloading was 10.4mm.

The test recommenced approximately 17 hours later on 1.11.85. In the light of the degradation in pile performance the previous day, the cycling load was reduced. 30 cycles of loading between 1 and 121kN were applied (0 and 0.4 times the static capacity in Test 4A.1). These cycles were designated numbers 21 to 50. Logging was as for the first stage of cycling, with cycles 21, 30, 40 and 50 being more accurately logged. The time to apply each cycle was similar to the first stage of cycling.

Cumulative displacement at the top of cycle load increased at an accelerating rate throughout the cycling operation, from 12.0mm during cycle 21 to 26.9mm during cycle 50 (Figure 4.63). Total cumulative displacement of the pile after unloading at the end of cycle 50 was 25.6mm. The pile had obviously failed. At this point, a CRE test was immediately carried out (Figure 4.55). The pile failed at the cycling load. Maximum load recorded was 127.4kN, at 10.1mm displacement. The test was stopped at this point.

Load:displacement behaviour during cycling is shown in Figure 4.56. The accurately logged cycles have been plotted; reference displacement has been taken for convenience as the displacement at 31kN - this was a standard logging point for all the cycles. In both stages of cycling, there is a progressive loss of stiffness near the top of the loading cycle as the number of cycles applied increases. The loss in stiffness is associated with irrecoverable displacements.

Test 4A.3 Date: 25.3.86 Type: IL, CRE Figures 4.57, 4.58
Test 4A.3 was performed 169 days after expansion (145 days after the previous test).

In the first stage of the test, load was increased in increments of 30kN (nominal) up to a load of 150.9kN. The load increments were maintained for up to 16 minutes. Creep behaviour is shown in Figure 4.58. The creep rate increased suddenly when the final increment was applied, 1.2mm displacement occurring during the first minute of the holding period. Pumping of the loading jack was stopped at this point (total displacement 3.4mm) and the load allowed to stabilise. The final load increment was a factor of 1.18 times the final failure load in the previous test. The loss in capacity that occurred during cyclic Test

4A.2 was thus irrecoverable.

In the second stage of the test, CRE loading was applied (Figure 4.57). Pumping of the loading jack commenced at a stabilised load of 116kN. Maximum load recorded was 137.3kN, at 6.9mm displacement. Continued displacement to 10.9mm gave a small drop in load to 129kN. The maximum load was less than the final load increment during the first stage of the test, and represented a factor of 1.08 times the final failure load in Test 4A.2.

4.7.8 Extraction of expander mandrels

Measurements of applied load were taken during extraction of all the expander mandrels, except in the case of Cruciform Pile 3B. Details of the extraction process have been given in Section 3.9. The extraction data are presented in Table 4.9.

Measurements were taken of the initial peak jacking load, which occurred at the very start of extraction; and of the steady jacking load which occurred during the 10 to 20mm displacement following the peak load. In Table 4.9 these loads are compared with the maximum loads recorded in the final pile test performed before expander mandrel extraction.

There appears to be an increase in peak extraction load the longer an expander mandrel is left in place, presumably due to corrosion or pressure bonding between the outer shell and the expander mandrel with time. In the case of Cruciform Pile 4A, this bonding was sufficient to cause the pile to fail along the outer shell/soil interface as the expander mandrel was pulled.

The ratios of the post-peak steady extraction loads to the previous pile test maximum loads are between 0.26 and 0.34. Taking the angle of friction between steel and the chalk as 34° (Section 4.4.7), these values imply coefficients of friction μ between outer shell and expander mandrel of 0.18 to 0.23. The lowest value is that for Box Pile 2B, the expander mandrel in this case was coated with mill varnish. The deduced values of μ of 0.20 and 0.23 for Box Piles 1A and 2A, which had uncoated expander mandrels, agree well with published values for steel:steel friction (eg. Urquhart, 1940).

4.7.9 Removal of piles from ground

When the cruciform piles were removed from the ground (Section 3.9), chalk was found to be contained between the cruciform arms as shown in Plate 4.1. In the region of the expander mandrel nose there was a progressively smaller amount of chalk contained between the arms towards

the bottom of the pile.

4.7.10 Elastic deformation of piles

The displacement at the head of the piles due to elastic deformation of the steel pile members is now considered. The elastic displacement at the pile head depends on the relative deformations of the outer shell and expander mandrel. These in turn depend on the distribution of shaft resistance along the length of the pile, and the frictional behaviour along the interface between outer shell and expander mandrel. The frictional behaviour may well change with time, as indicated by the higher expander mandrel extraction loads for piles which had been left in the ground for longer periods of time (Section 4.7.8).

To provide simple lower and upper bounds to the elastic displacement of the piles near failure, two elastic lines have been plotted on the load:displacement plots. These are calculated as follows:

Lower bound -

(a) The outer shell and expander mandrel are assumed to act together as a single unit, i.e. the coefficient of friction between outer shell and expander mandrel is assumed to be greater than that between outer shell and soil.

(b) A uniform distribution of shaft resistance along the pile shaft at failure is assumed.

Upper bound -

(a) The load applied to the pile is assumed to be taken solely by the outer shell angles, i.e. the coefficient of friction between outer shell and expander mandrel is assumed to be zero.

(b) A triangular distribution of shaft resistance along the pile shaft at failure is assumed.

The total displacement of the pile head due to elastic deformation is made up of the displacement of the embedded pile length and the displacement of the exposed pile length at the top of the pile. Load transferred through the exposed pile length is assumed to be taken by the outer shell angles alone. Table 4.10 provides details of the calculation of the elastic lines for the various pile configurations. It lists cross-sectional areas of the pile members, embedded pile lengths, exposed pile lengths, and the corresponding elastic displacements at the pile head.

4.8 Summary of Pile Performances

The principal points of interest arising from the results of the pile tests at the Luton site are given in this Section. They are discussed in Chapter 11.

4.8.1 Initial increase in pile capacity

Initial loadings for the box piles and the cruciform piles are compared in Figures 4.59 and 4.60. Factors of increase in gross maximum load and in minimum/maximum average shaft frictions over the values for the unexpanded piles 1U and 3U are given. Because of the loss of control suffered in Test 1U.1, and the possible influence of this on Test 1U.2 carried out immediately afterwards, the reference test for Box Pile 1 is taken as Test 1U.3.

The unexpanded Box Pile 1U and Cruciform Pile 3U gave maximum loads of 79.1kN and 50.4kN respectively, corresponding to very similar average shaft frictions of 28.8kPa and 23.3kPa respectively.

For all the expanded box piles there were large increases in load carrying capacity in comparison to unexpanded Box Pile 1U. Box Pile 2B (expanded by 21.4%) performed best, showing a factor of increase of 4.23 in maximum load (5.37 in maximum average shaft friction). Box Piles 1A and 2A (both expanded by 14.3%) showed factors of increase in maximum load of 3.83 and 2.94 respectively. There were also large initial increases in load carrying capacity for both of the expanded cruciform piles, in comparison to unexpanded Cruciform Pile 3U. Cruciform Pile 4A (expanded by 10.7%) performed best, showing a factor of increase of 6.04 in maximums load (6.90 in maximum average shaft friction). Cruciform Pile 3B (expanded by 21.4%) performed less well than Cruciform Pile 4A, showing a factor of increase of 4.18 in maximum load. Average shaft friction values for all the piles are plotted against percentage expansion in Figure 4.61 (percentage increase in pile width); and Figure 4.62 (percentage increase in pile cross-sectional area).

4.8.2 Performance under cyclic loading

Details of the cyclic loading tests have been given in Sections 4.7.5 to 4.7.7. The behaviour of Box Pile 2B and Cruciform Piles 3U and 4A during cycling is compared in Figure 4.63.

Box Pile 1A (25 cycles of loading) showed no tendency to be pulled from the ground during cycling. The static test performed immediately after cycling showed a loss in capacity in comparison to the static test before cycling (factor of increase 0.85). This loss in capacity was more

than fully recovered with time (Figure 4.35).

Box Pile 2B (50 cycles of loading) underwent double the number of cycles applied to Box Pile 1A. The loss in capacity immediately after cycling (factor of increase 0.81) was greater than that for Box Pile 2B. The loss in capacity due to cycling was largely recoverable with time (Figure 4.43)

The unexpanded Cruciform Pile 3U (50 cycles of loading) suffered a permanent displacement of 1.9mm after cycling. However, the static capacity immediately after cycling was identical to that before cycling (Figure 4.48).

Cruciform Pile 4A performed badly during cycling. Large permanent displacements accumulated at an increasing rate during cycling. There was a progressive loss in stiffness near the tops of the loading cycles (Figure 4.56), and the pile failed at the cycling load. In contrast to the other piles which underwent cycling, the loss in capacity of Cruciform Pile 4A did not prove to be recoverable with time (Figure 4.57).

4.8.3 Overall pile performance in the long term

Testing histories have been presented in Figures 4.24 to 4.27. Selected tests for piles 1, 2 and 3 are also presented in Figures 4.64 to 4.66, plotted to a common displacement axis.

All the piles (except Box Pile 1U, for which only limited information is available) exhibit large displacements and non-linear load:displacement behaviour on initial loading, followed by much stiffer, more linear behaviour on subsequent loadings. It is important to note that the failure mode of both unexpanded and expanded piles is usually ductile, with only small gradual reductions in load after failure is reached.

The response of the box piles is stiffer than the cruciform piles. Values of displacement to failure for the expanded box piles (9.0 to 14.0mm on initial loading; 4mm on reloading) are less than those for the expanded cruciform piles (19.5 to 24.0mm on initial loading; <10mm on reloading). The softest pile response is that of the unexpanded Cruciform Pile 3U, with an initial displacement to failure of over 30mm, (8.8mm on reloading). The response of Pile 2A, expanded very soon after expansion, is less stiff than for Piles 1A and 2B, expanded after a longer period of consolidation subsequent to expansion.

Repeated reloadings generally seem to follow the same reloading line,

for example see Tests 2B.2 and 2B.4 in Figure 4.65. There is no indication of a general loss in capacity with time for piles subjected to a sequence of static CRE tests. In fact, small increases with time often occurred (Figures 4.24 to 4.27).

Losses in capacity associated with cyclic loading have been dealt with in the previous Section. Also worthy of note is the brittle pile response associated with incremental loading in Tests 2B.5 and 4A.3 (Figures 4.45, 4.58). In these tests, displacements 'ran away' during the final holding period of the incremental loading stage before the load was allowed to stabilise. The maximum loads during the subsequent CRE loadings were less than the final incremental loads previously applied.

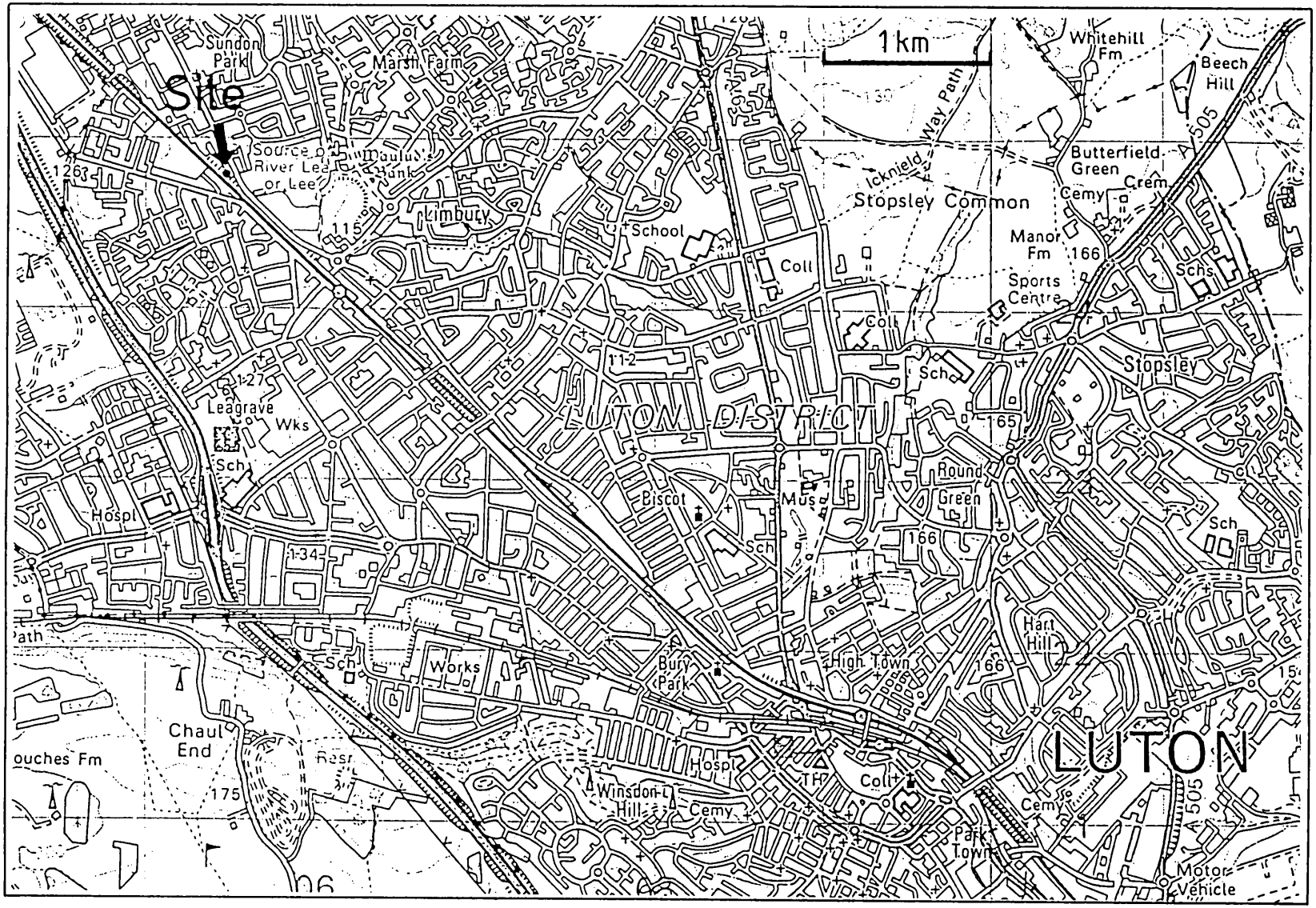

Figure 4.1 Location of Luton site

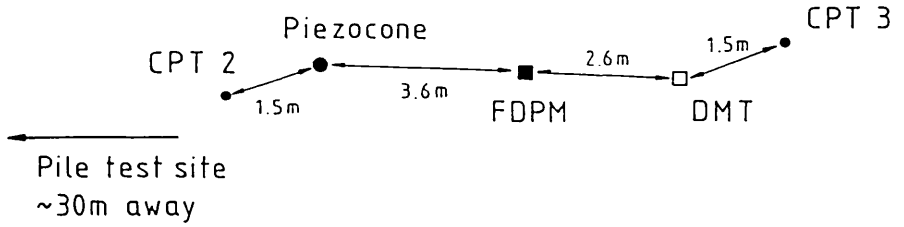

Figure 4.2 Layout of in-situ tests

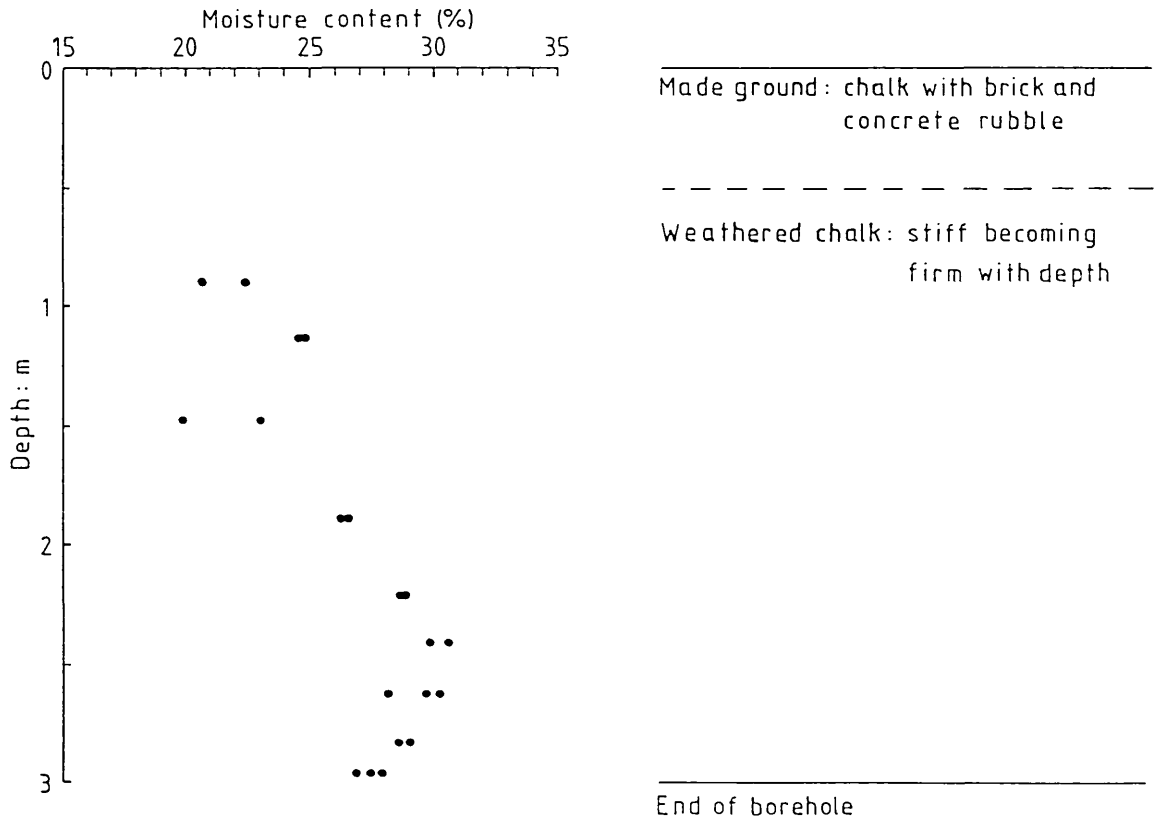

Figure 4.3 Moisture content of chalk against depth

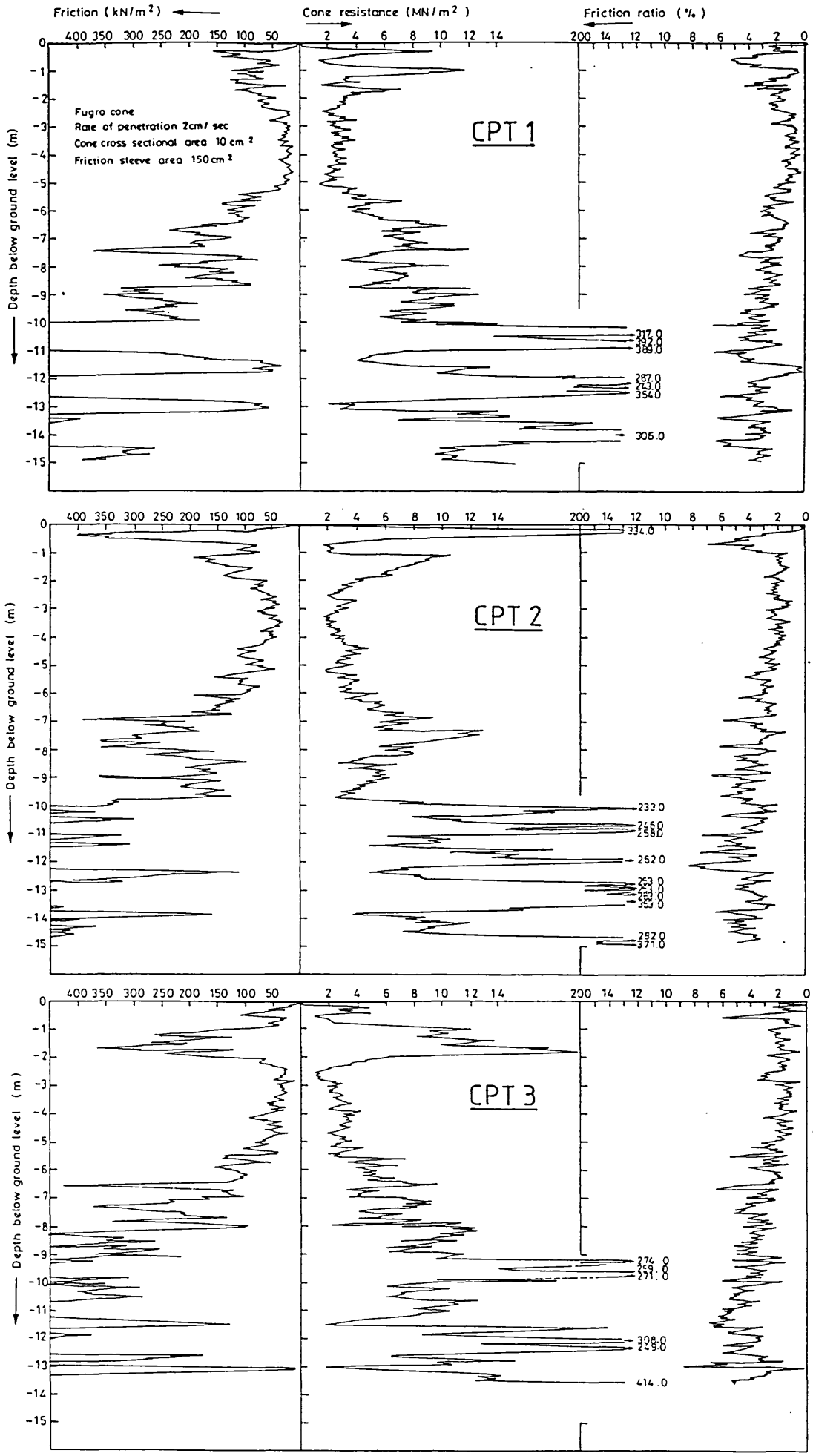

Figure 4.4 Results of Cone Penetration Tests

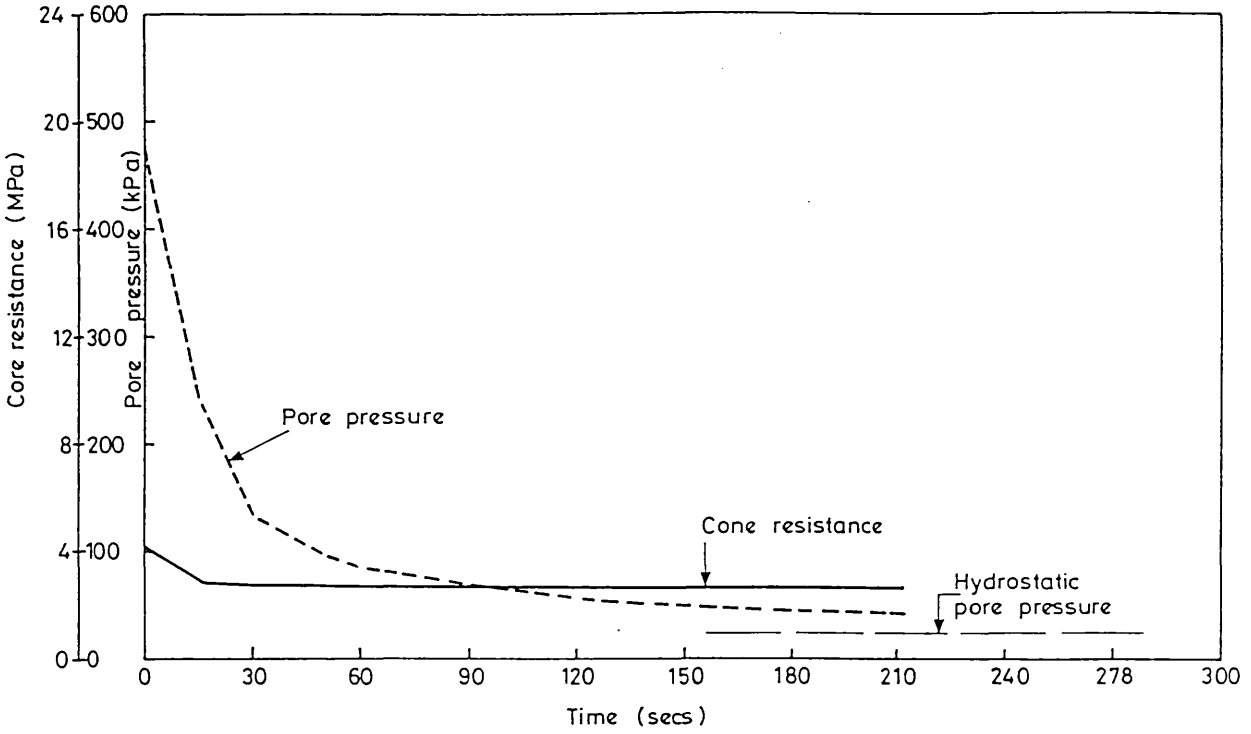

Figure 4.5 Result from typical Piezocone dissipation test

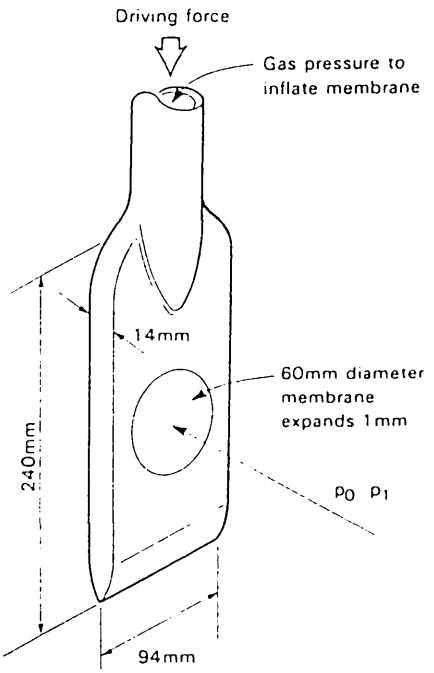

Figure 4.6 Sketch of Marchetti dilatometer
(after Powell and Uglow, 1988b)

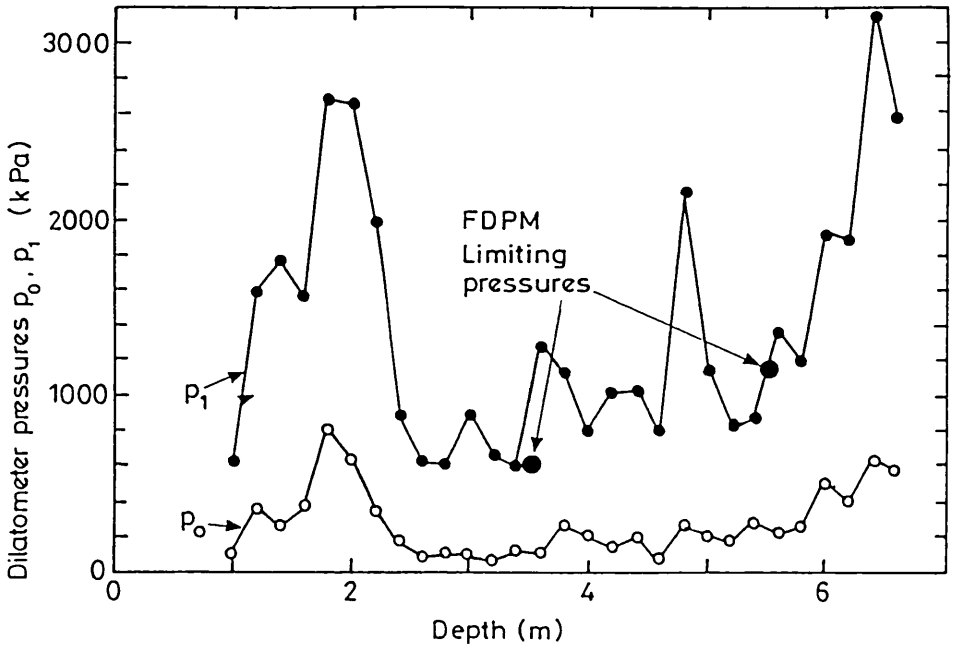

Figure 4.7 Dilatometer pressures p_0 , p_1 against depth

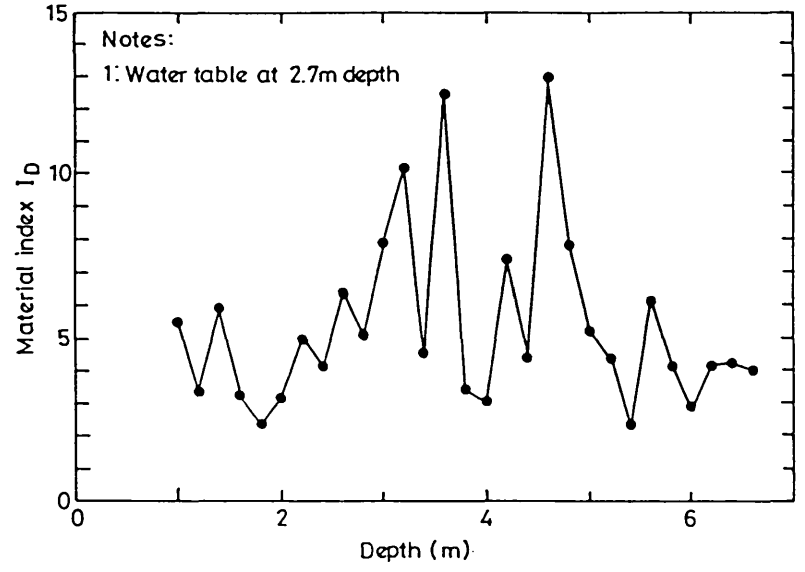

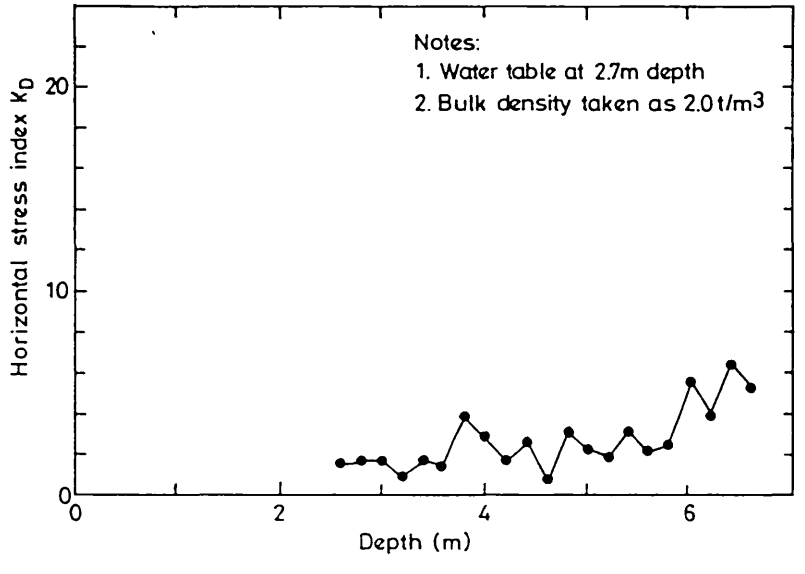

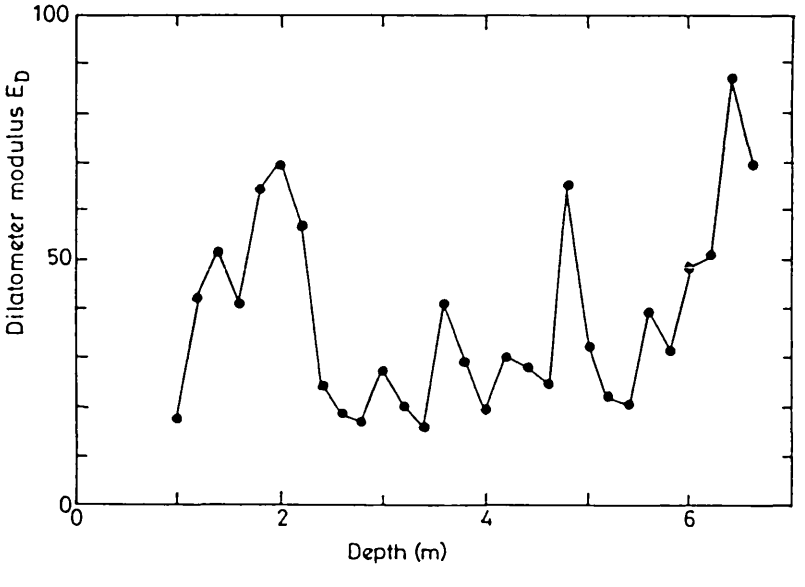

Figure 4.8 Dilatometer parameters I_D, K_D, E_D, against depth

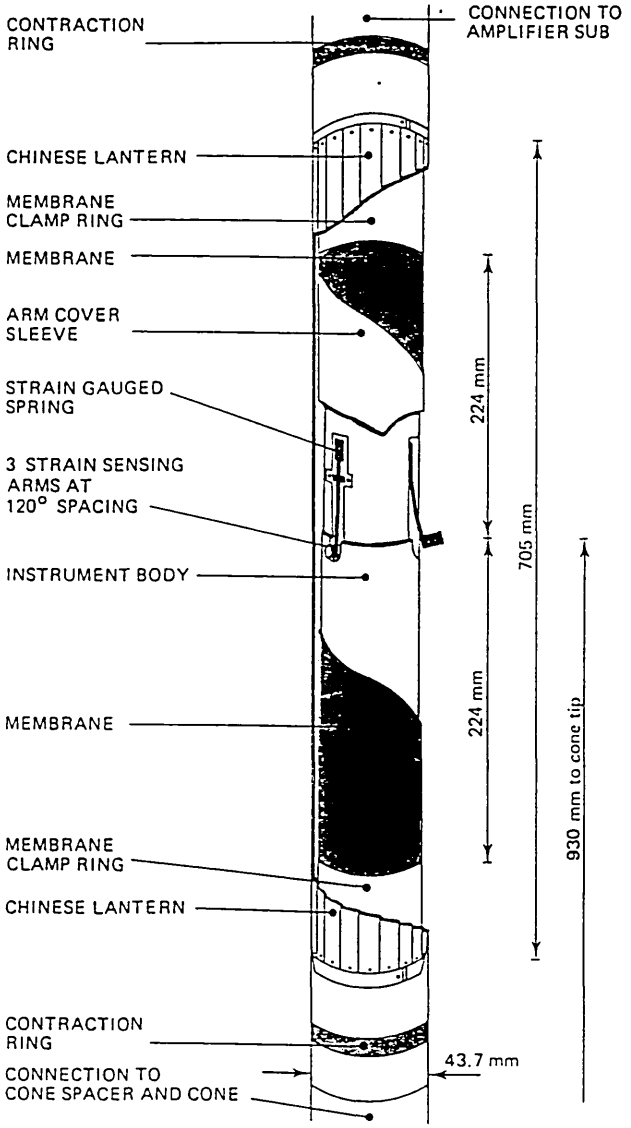

Figure 4.9 Details of FDPM
(after Withers et al, 1986)

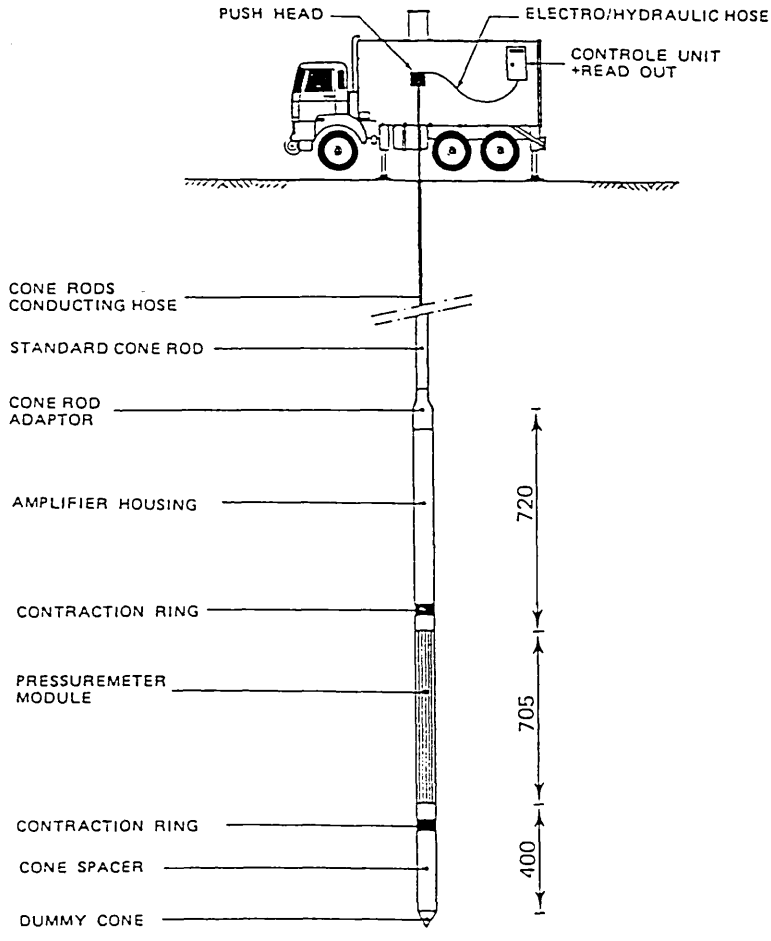

Figure 4.10 Set-up for FDPM testing
(after Withers et al, 1986)

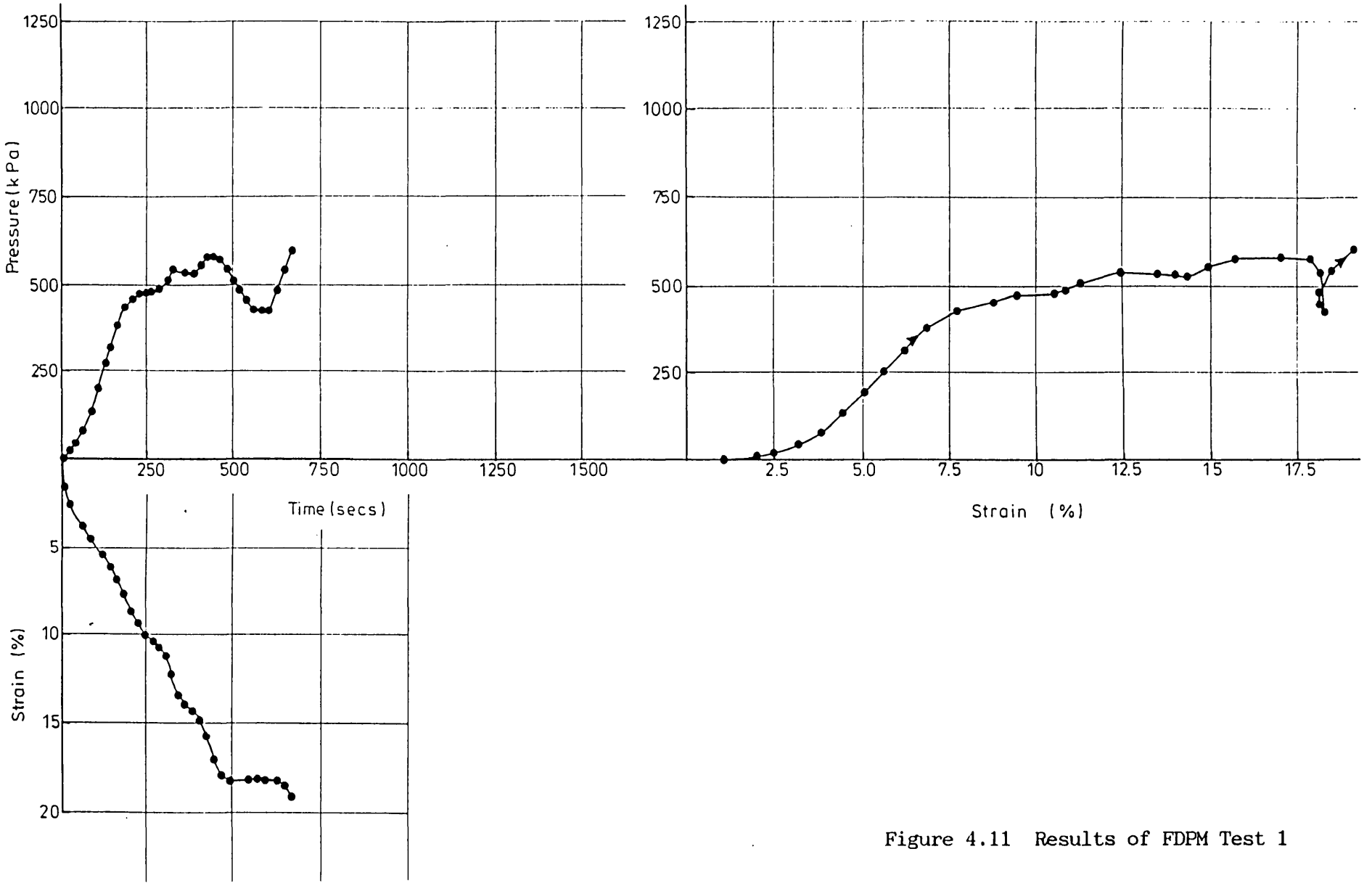

Figure 4.11 Results of FDPM Test 1

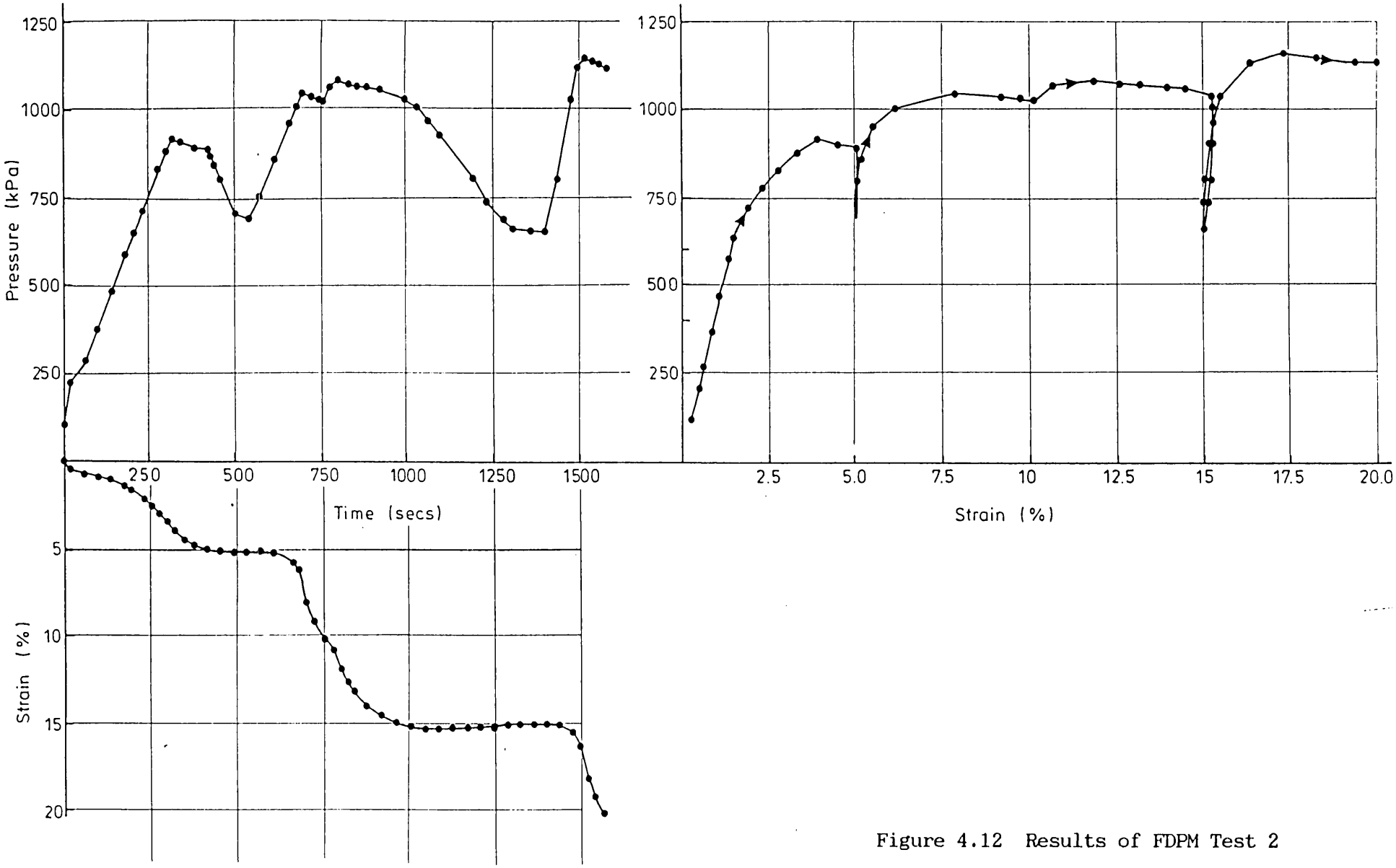

Figure 4.12 Results of FDPM Test 2

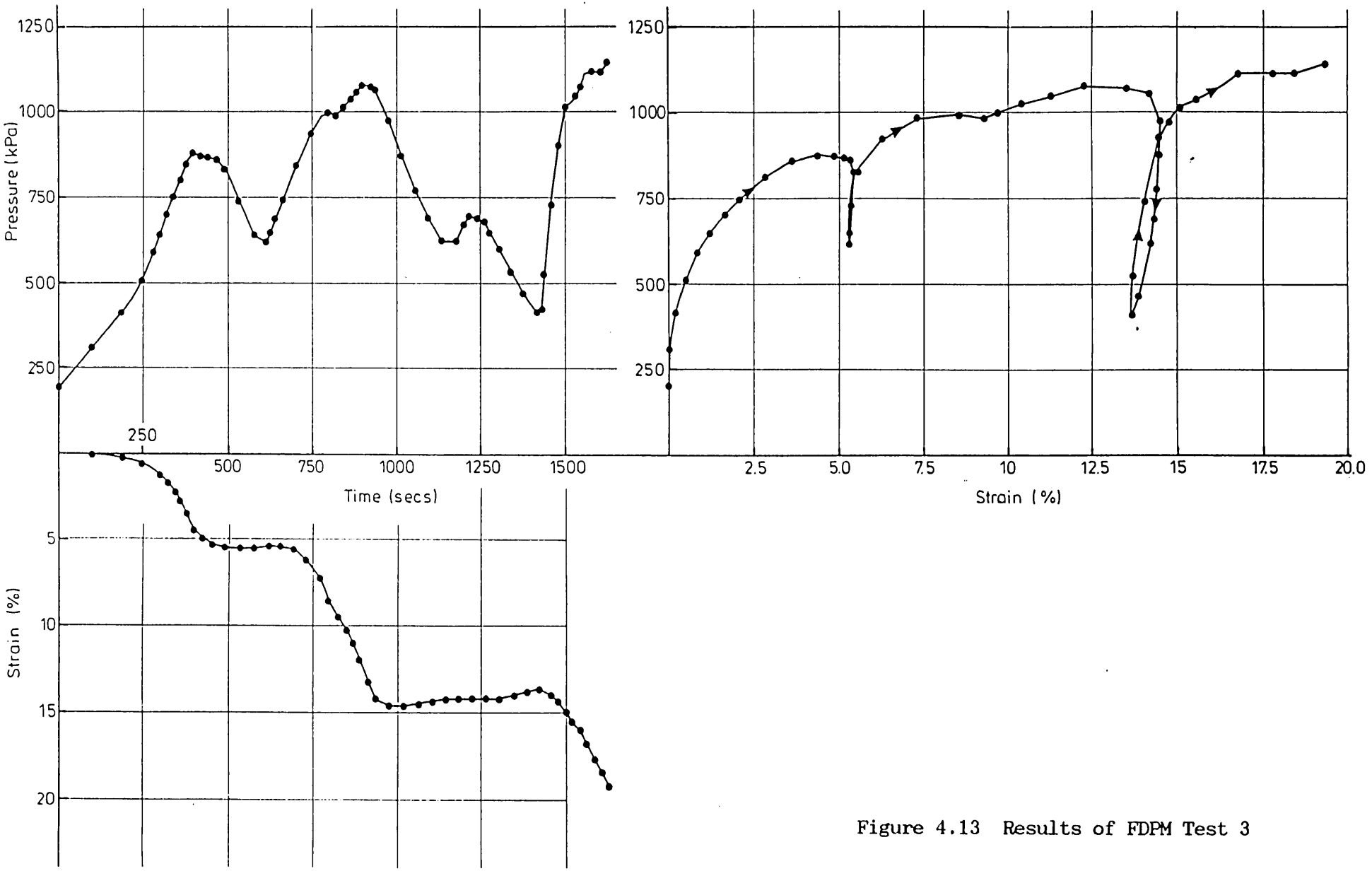

Figure 4.13 Results of FDPM Test 3

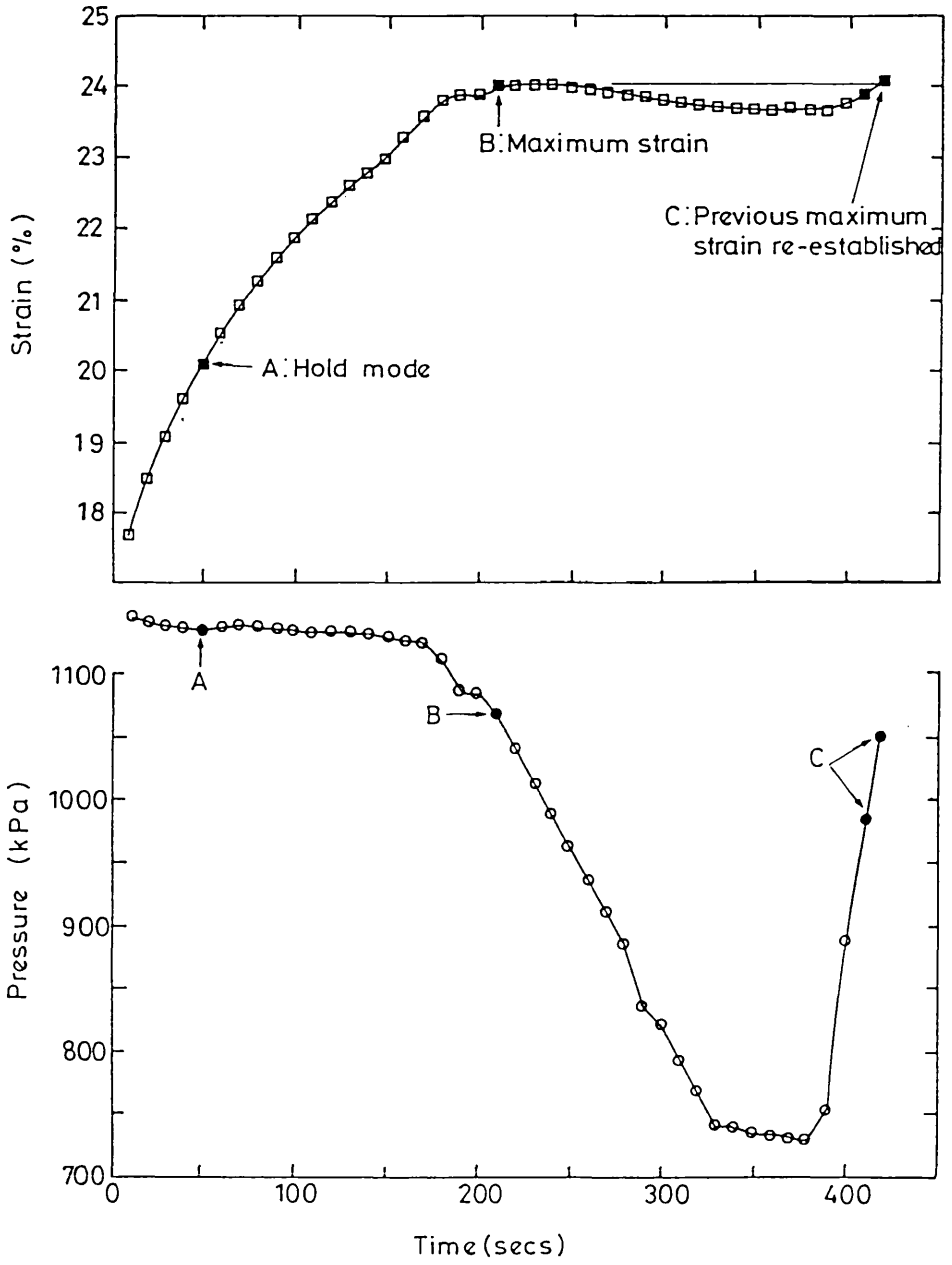

Figure 4.14 FDPM Test 2: Details of strain holding period

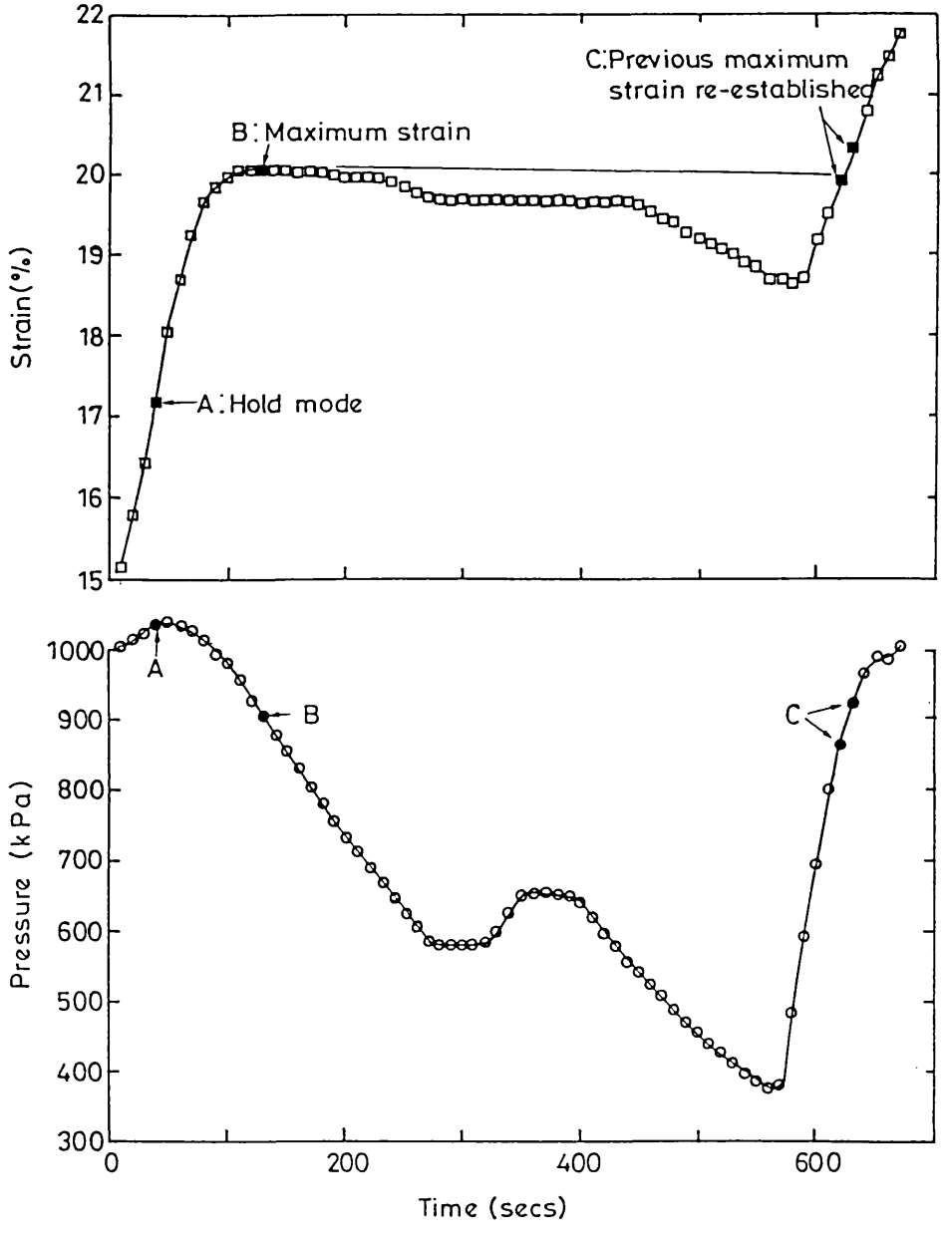

Figure 4.15 FDPM Test 3: Details of strain holding period

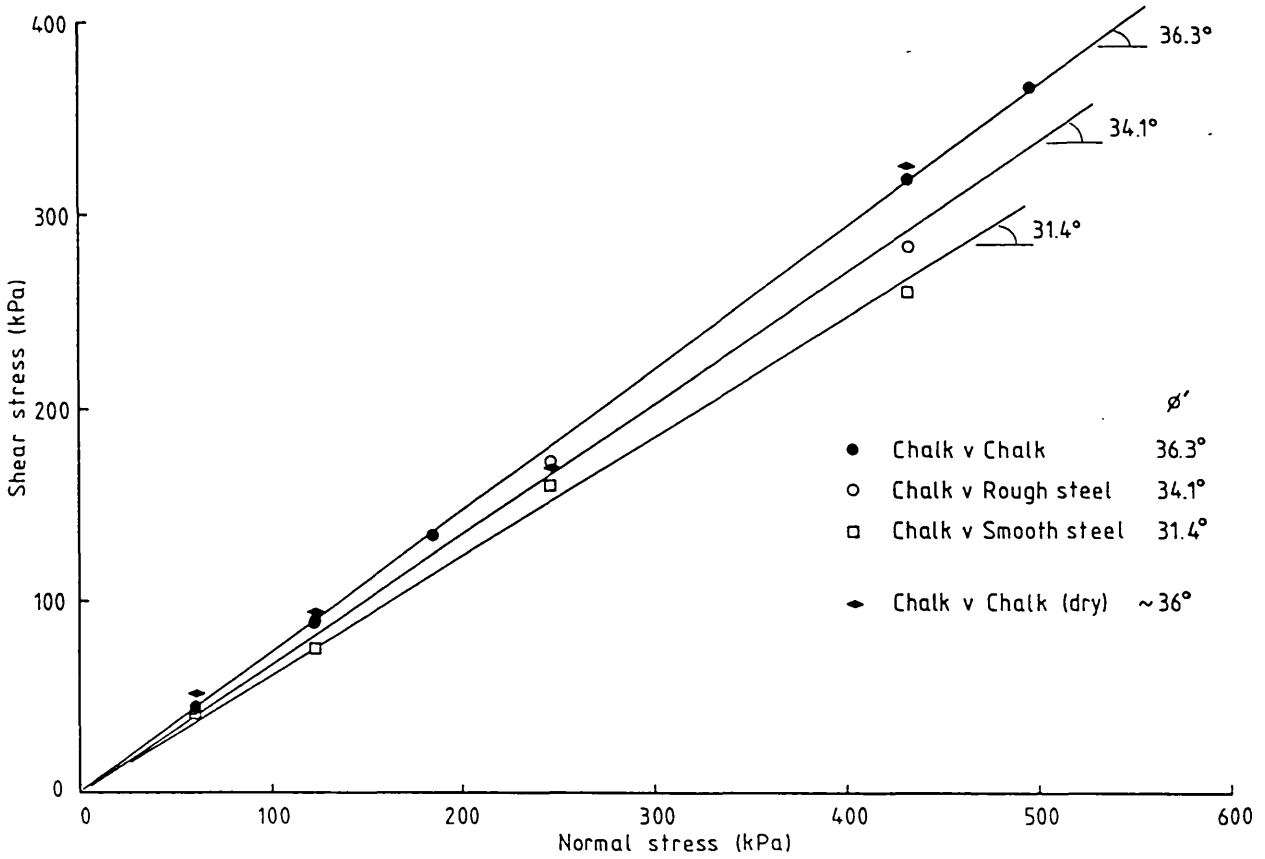

Figure 4.16 Shear box tests:
Shear strength - normal stress relationships

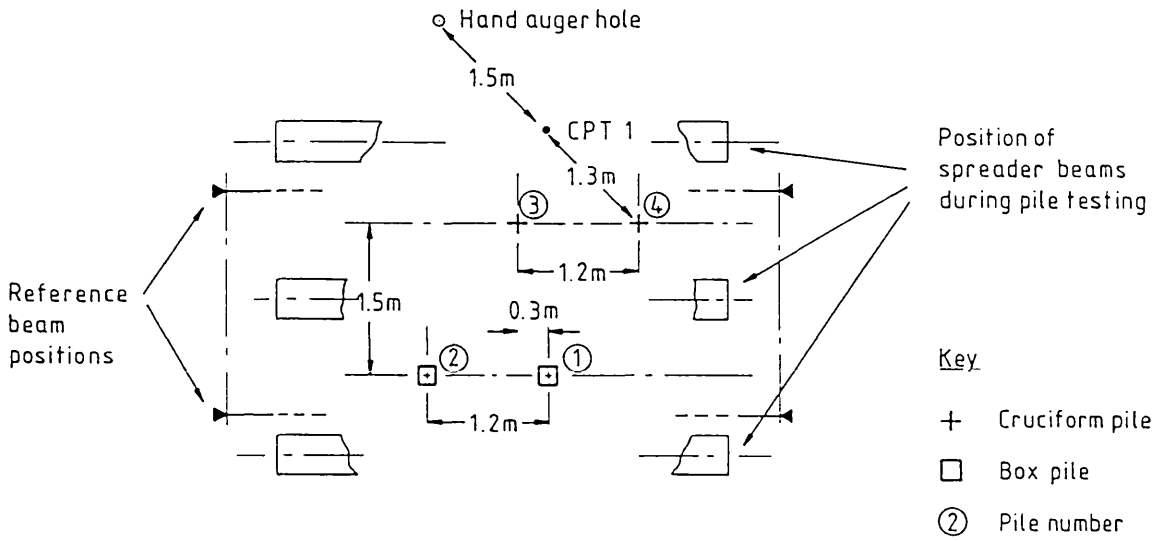

Figure 4.17 Layout of test piles at Luton site

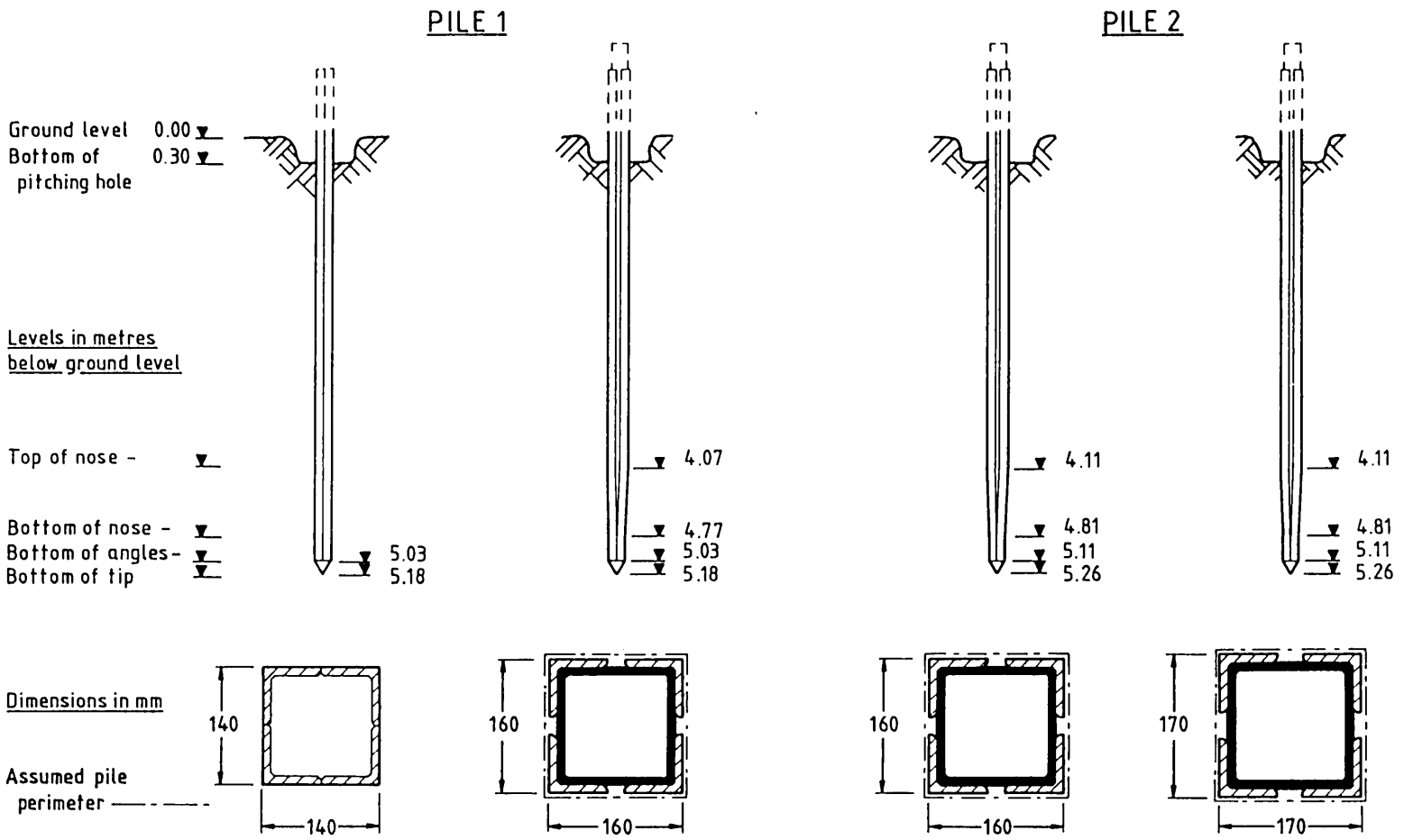

PILE CONFIGURATION	1U	1A	2A	2B
Outer shell driven:	27.3.85	27.3.85	28.3.85	28.3.85
Expander mandrel driven :	-	17.4.85	28.3.85	17.4.85
Days elapsed before expansion:	-	21	0	20
Pile width (m):	0.14	0.16	0.16	0.17
Pile X-sectional area (m^2):	0.0196	0.0256	0.0256	0.0289
% expansion of width:	-	14.3	14.3	21.4
% expansion of area:	-	30.6	30.6	47.4
Pile weight (kN):	2.7	4.6	4.6	4.8

Figure 4.18
Box piles: Details of dimensions and driven levels

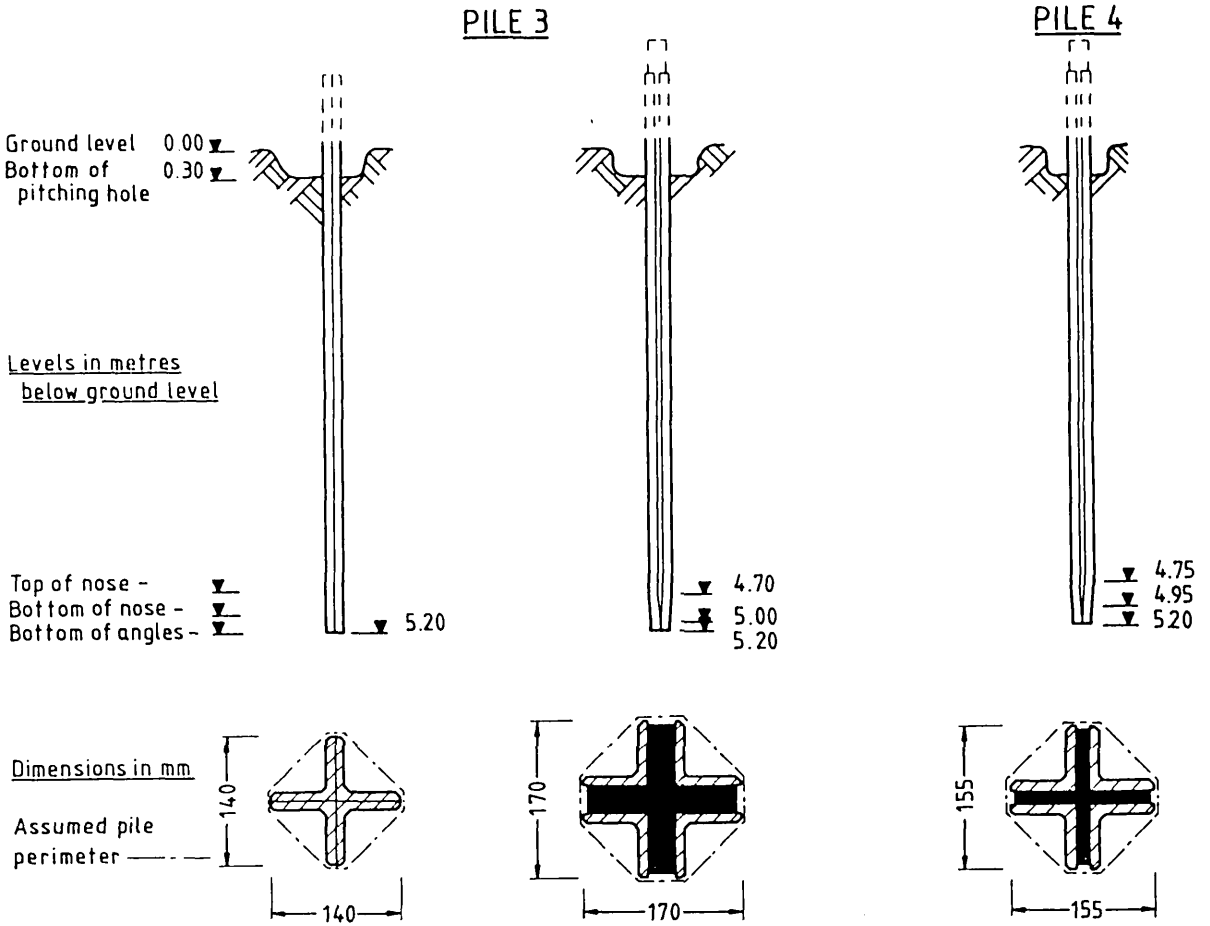

PILE CONFIGURATION	3U	3B	4A
Outer shell driven:	4.10.85	4.10.85	4.10.85
Expander mandrel driven:	-	20.11.85	7.10.85
Days elapsed before expansion:	-	47	3
Pile width (m) :	0.14	0.17	0.155
Pile X-sectional area (m^2):	0.0124	0.0217	0.0168
% expansion of width:	-	21.4	10.7
% expansion of area:	-	75.0	35.7
Pile weight (kN):	2.4	6.6	3.9

Figure 4.19
Cruciform piles:
Details of dimensions
and driven levels

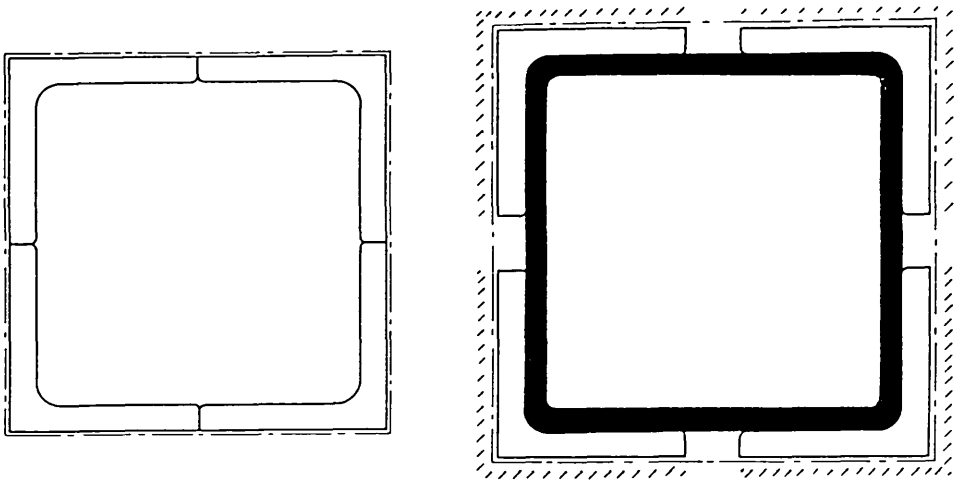

Figure 4.20 Details of 'full' and 'reduced' pile perimeters

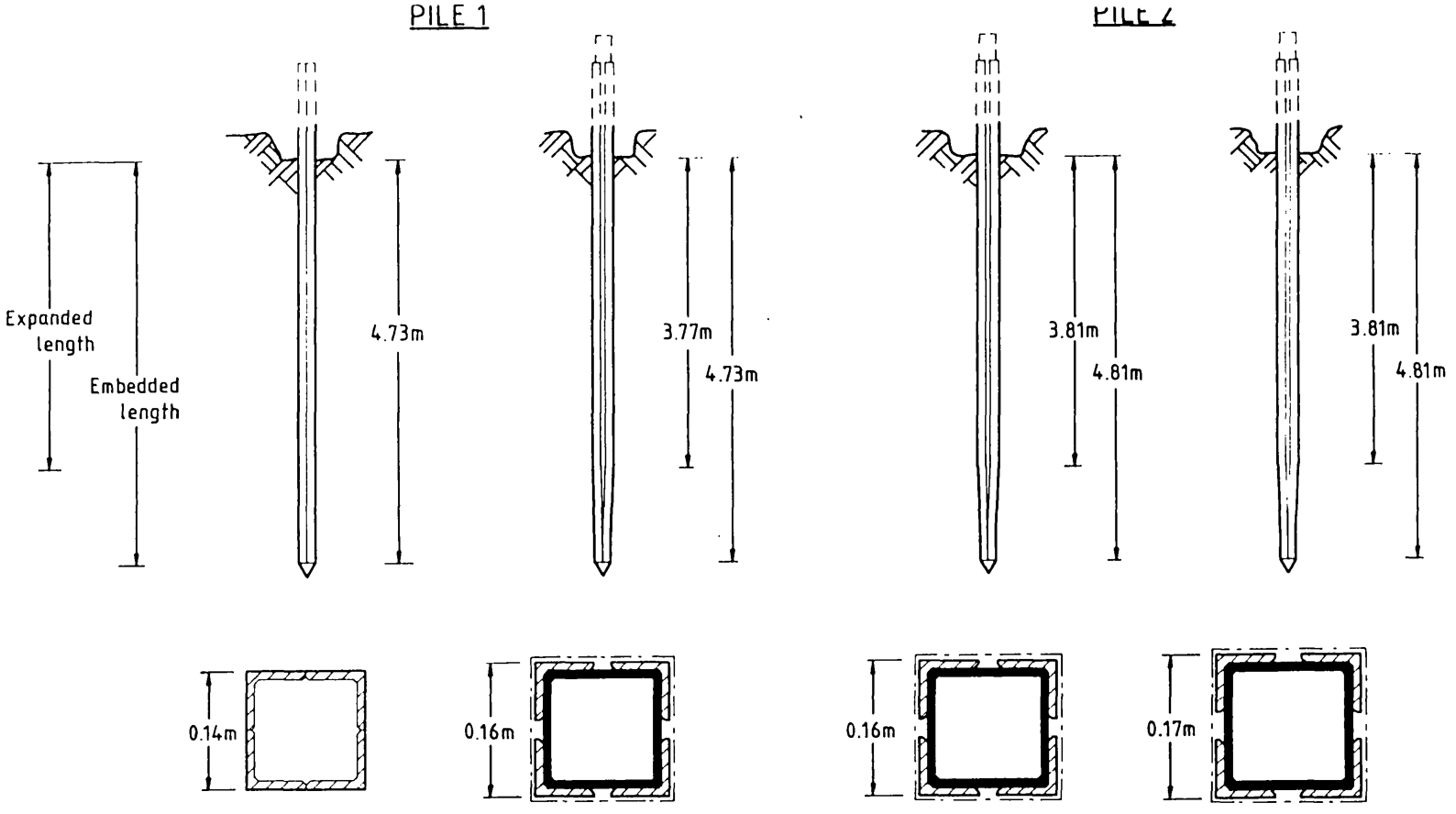

PILE CONFIGURATION	1U	1A	2A	2B
Pile Dimensions (m)				
Embedded length:	4.73	4.73	4.81	4.81
Expanded length:	-	3.77	3.81	3.81
Full perimeter:	0.56	0.64	0.64	0.68
Reduced perimeter:	-	0.56	0.56	0.56
Shaft Surface Areas (m^2)				
Embedded length,				
Full perimeter (A):	2.65	3.03	3.08	3.27
Reduced perimeter (B):	-	2.65	2.69	2.69
Expanded length,				
Full perimeter (C):	-	2.41	2.44	2.59
Expanded perimeter (D):	-	2.11	2.13	2.13

Figure 4.21
Box piles: Details of shaft surface areas

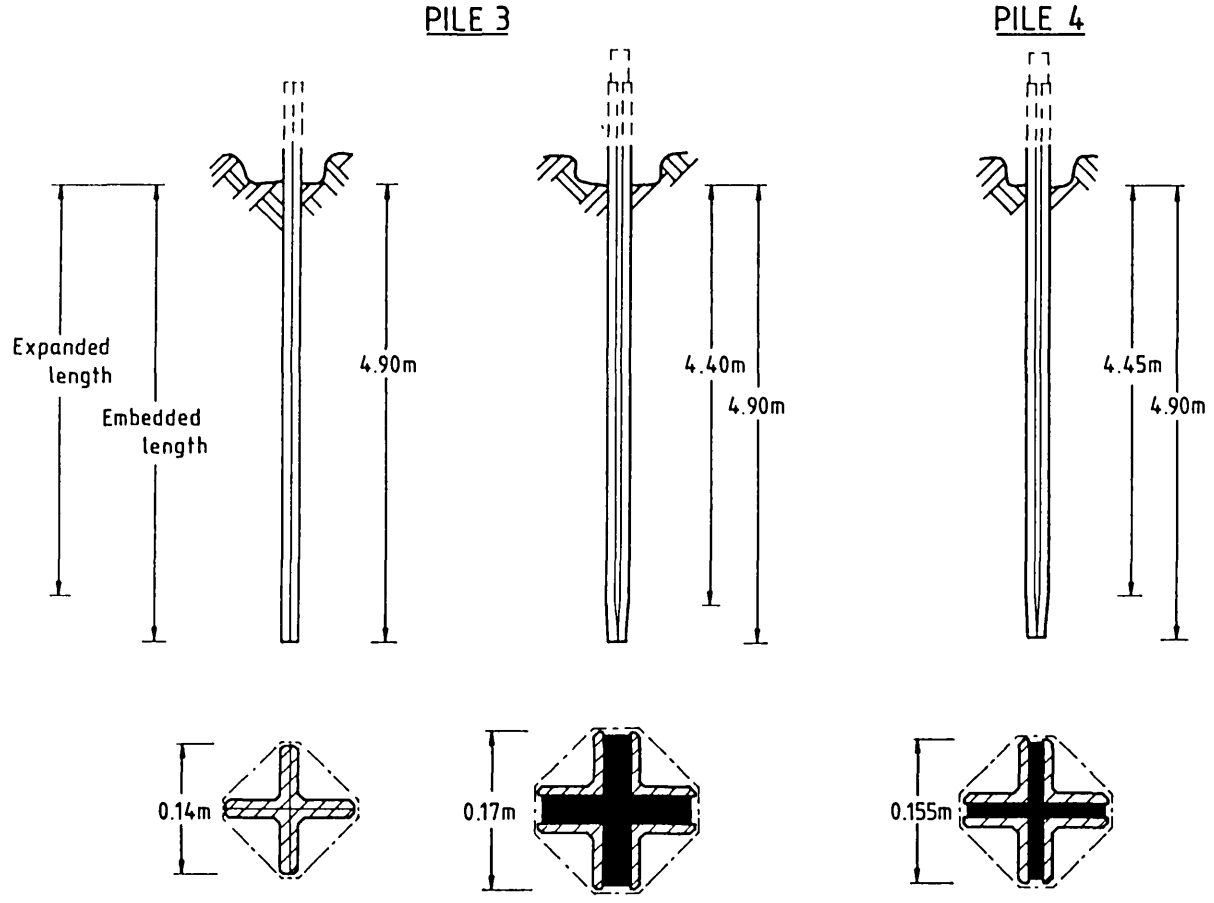

PILE CONFIGURATION	3U	3B	4A
Pile Dimensions (m)			
Embedded length:	4.90	4.9	4.90
Expanded length:	-	4.4	4.45
Full perimeter:	0.42	0.54	0.48
Reduced perimeter:	-	0.42	0.42
Shaft Surface areas (m^2)			
Embedded length,			
Full perimeter (A):	2.06	2.65	2.35
Reduced perimeter (B):	-	2.06	2.06
Expanded length,			
Full perimeter (C):	-	2.38	2.14
Expanded perimeter (D):	-	1.85	1.87

Figure 4.22
Cruciform piles:
Details of shaft
surface areas

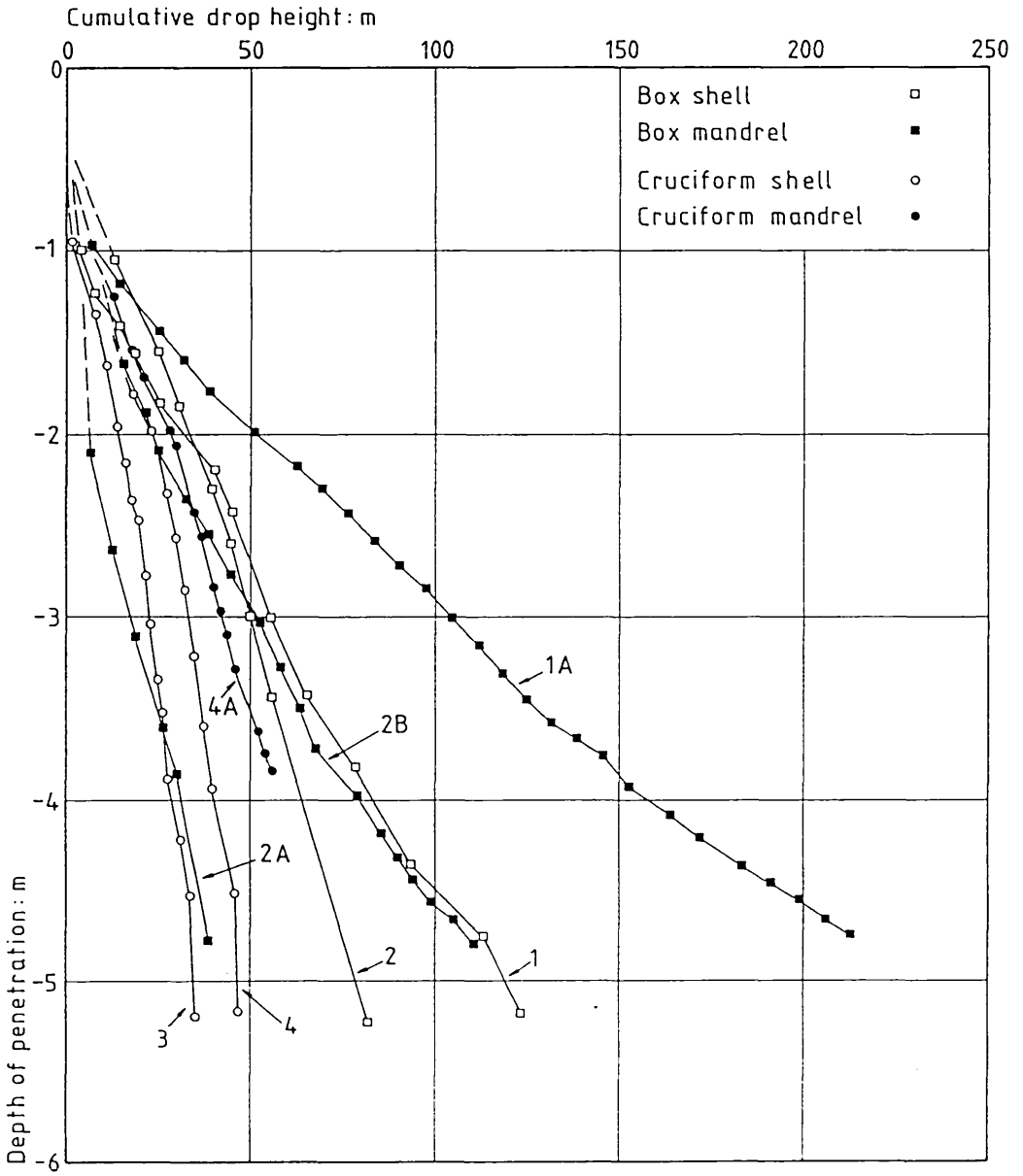

Figure 4.23 Pile driving records at Luton site:
Pile penetration against cumulative hammer drop height

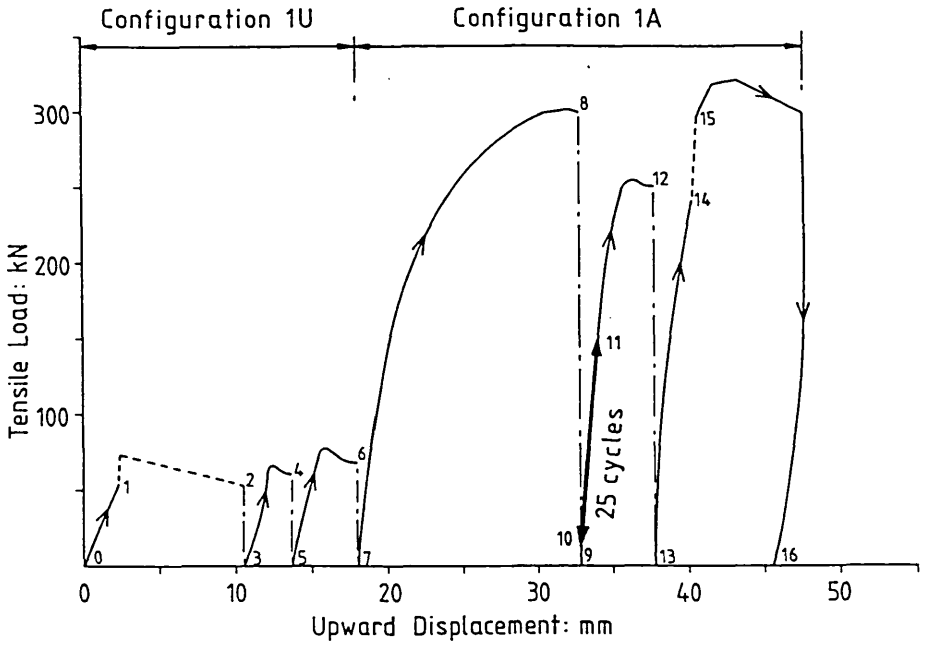

Test No.	Point Nos.	Date	Description of loading	Max. Load (kN)
PILE CONFIGURATION 1U				
1U.1	0-1	2. 4.85	CRE loading	73.5
	1-2		Loss of control	
1U.2	3-4	2. 4.85	CRE loading	66.4
1U.3	5-6	16. 4.85	CRE loading	79.1
PILE CONFIGURATION 1A				
1A.1	7-8	22. 4.85	CRE loading	302.8
1A.2	9,10-11	22. 4.85	Cyclic loading	150
	11-12		CRE loading	256.0
1A.3	13-14	1.11.85	Incremental loading	241.2
	15-16		CRE loading	322.3

Figure 4.24 Summary of pile testing: Pile 1

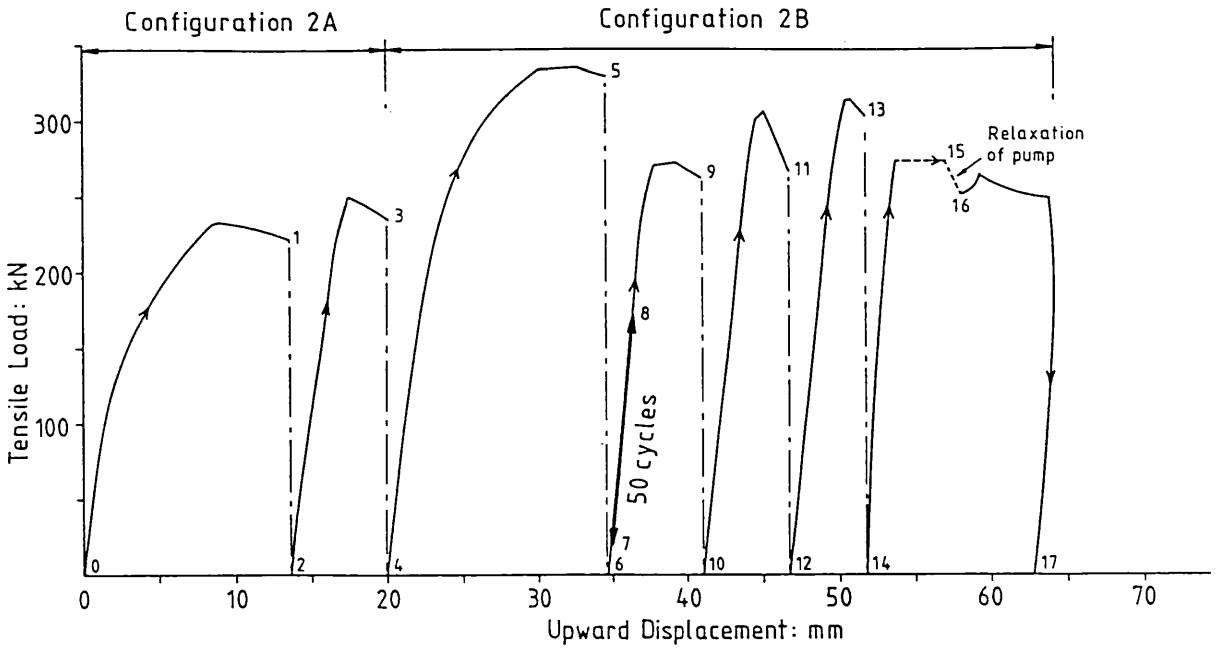

Test No.	Point Nos.	Date	Description of loading	Max. Load (kN)
PILE CONFIGURATION 2A				
2A.1	0-1	2. 4.85	CRE loading	232.7
2A.2	2-3	16. 4.85	CRE loading	249.7
PILE CONFIGURATION 2B				
2B.1	4-5	22. 4.85	CRE loading	335.0
2B.2	6,7-8	23. 4.85	Cyclic loading	171
	8-9		CRE loading	272.6
2B.3	10-11	7. 5.85	CRE loading	306.9
2B.4	12-13	5. 8.85	CRE loading	314.2
2B.5	14-15	6.11.85	Incremental loading	271.8
	16-17		CRE loading	263.5

Figure 4.25 Summary of pile testing: Pile 2

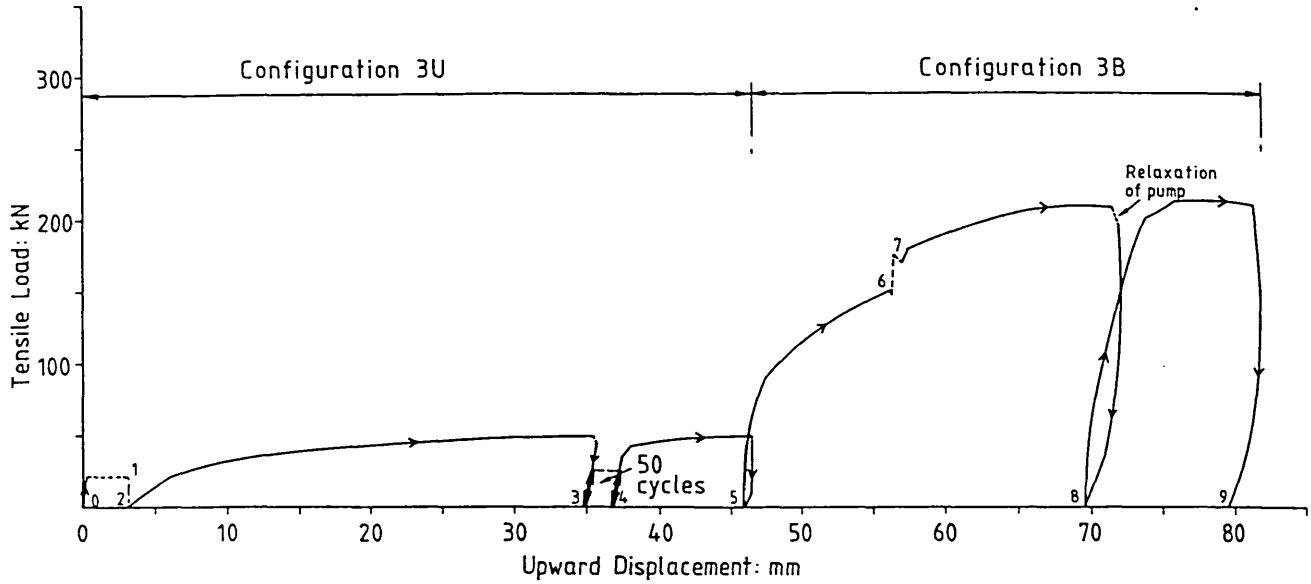

Test No.	Point Nos.	Date	Description of loading	Max. Load (kN)
PILE CONFIGURATION 3U				
3U.1	0-1	16.10.85	Incremental loading	21.4
	2-3		CRE loading	50.4
3U.2	3-4	31.10.85	Cyclic loading	25
	4-5		CRE loading	51.2
PILE CONFIGURATION 3B				
3B.1	5-6	2.12.85	Incremental loading	149.4
	7-8		CRE loading	210.8
3B.2	8-9	26. 3.86	CRE loading	216.6

Figure 4.26 Summary of pile testing: Pile 3

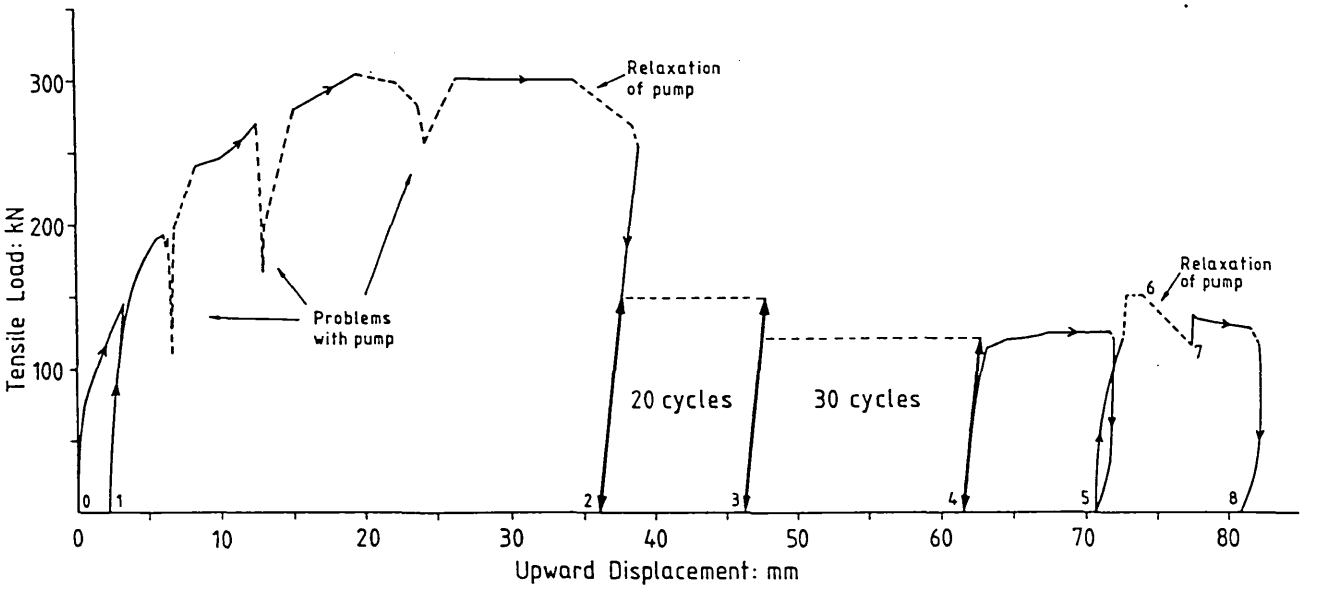

Test No.	Point Nos.	Date	Description of loading	Max. Load (kN)
PILE CONFIGURATION 4A				
4A.1	0-1	16.10.85	Incremental loading	125.3
	1-2		CRE loading	304.4
4A.2	2-3	31.10.85	Cyclic loading	150
	3-4	1.11.85	Cyclic loading	121
	4-5		CRE loading	127.4
4A.3	5-6	25. 3.86	Incremental loading	150.9
	7-8		CRE loading	137.3

Figure 4.27 Summary of pile testing: Pile 4

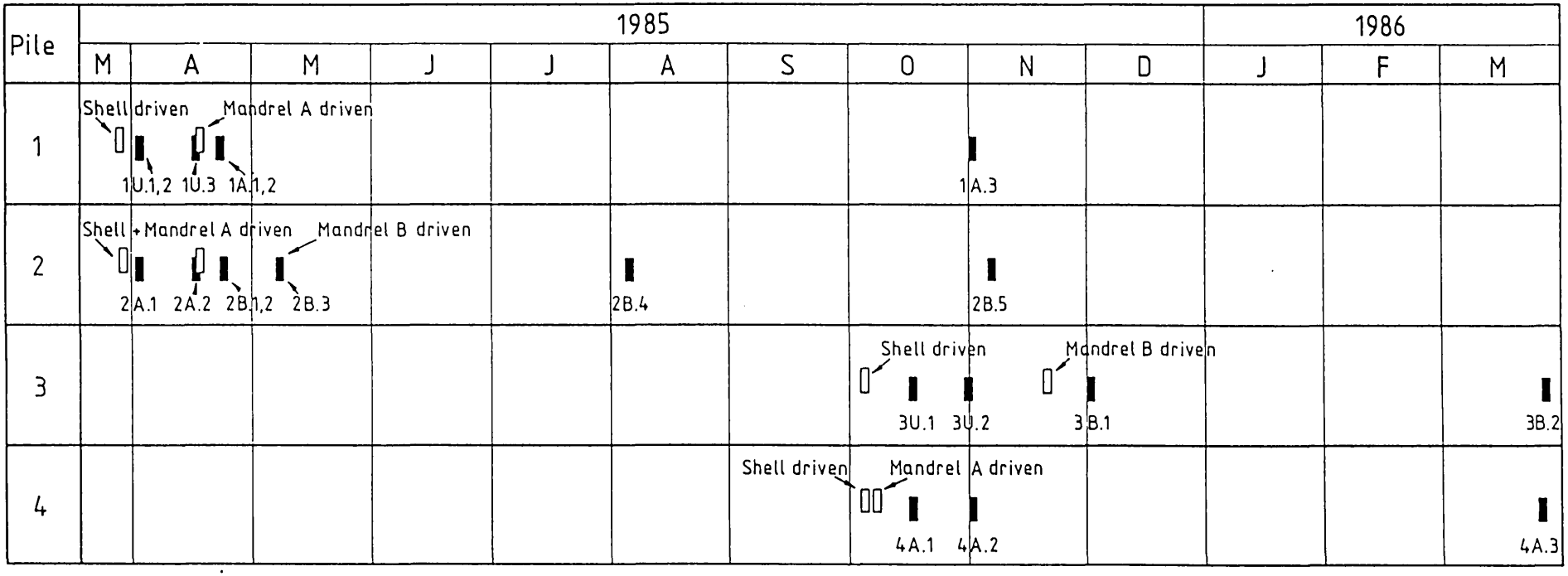

Figure 4.28 Summary of pile testing programme at Luton site

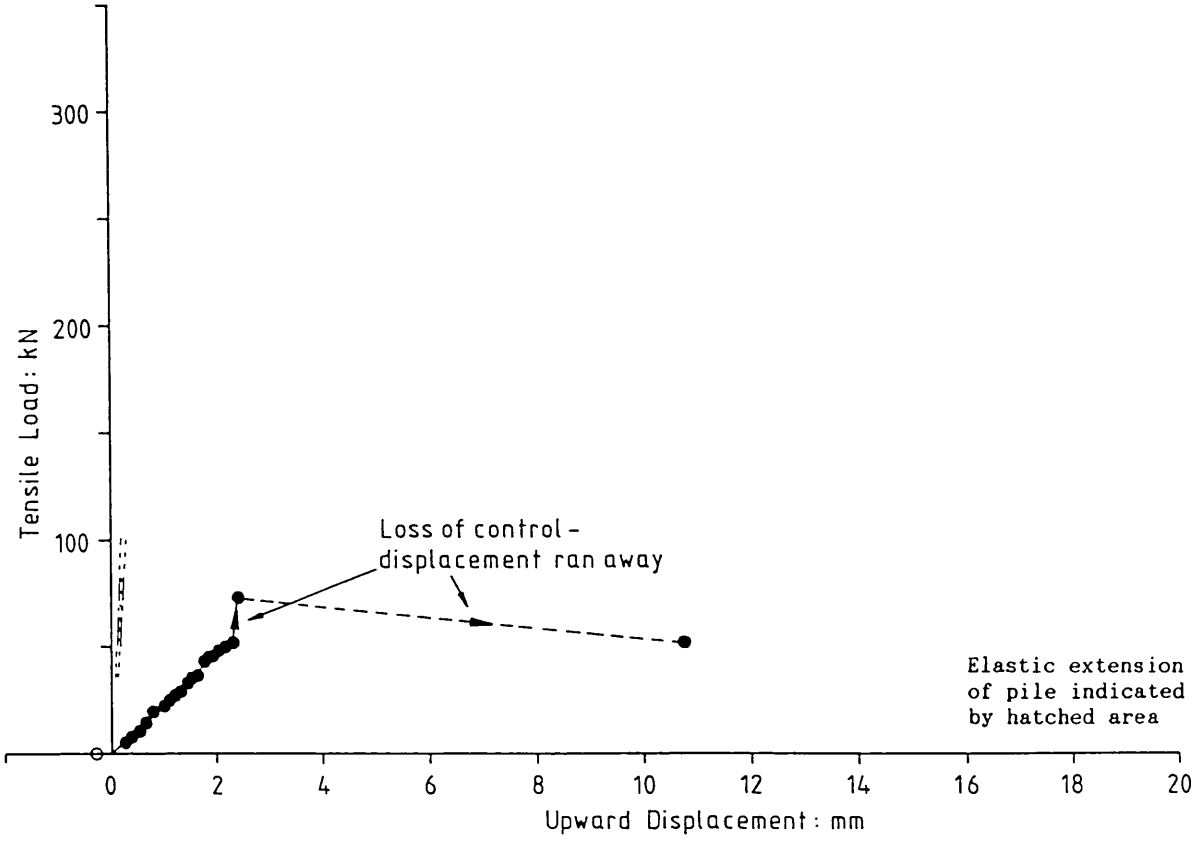

TEST 1U.1 Type: CRE Date: 2.4.85

Outer shell driven: 27.3.85 Expander mandrel driven: -
Days elapsed
prior to test: 6 -

Shaft areas: (m^2) Embedded length,
Full X-section (A): 2.65
Reduced X-section (B): -
Expanded length,
Full X-section (C): -
Reduced X-section (D): -

Pile weight: 2.7 (kN)

Test Stage	Maximum Load (Gross) (kN)	Maximum Load (Net) (kN)	Shaft Frictions (A) (kPa)	(B) (kPa)	(C) (kPa)	(D) (kPa)	Displacement at: Max. Load (mm)	Displacement at: End of stage (mm)
CRE	73.5	70.8	26.7	-	-	-	2.4	10.8

Notes: 1. Recorded during period of loss of control.

Figure 4.29 Results of Pile Test 1U.1

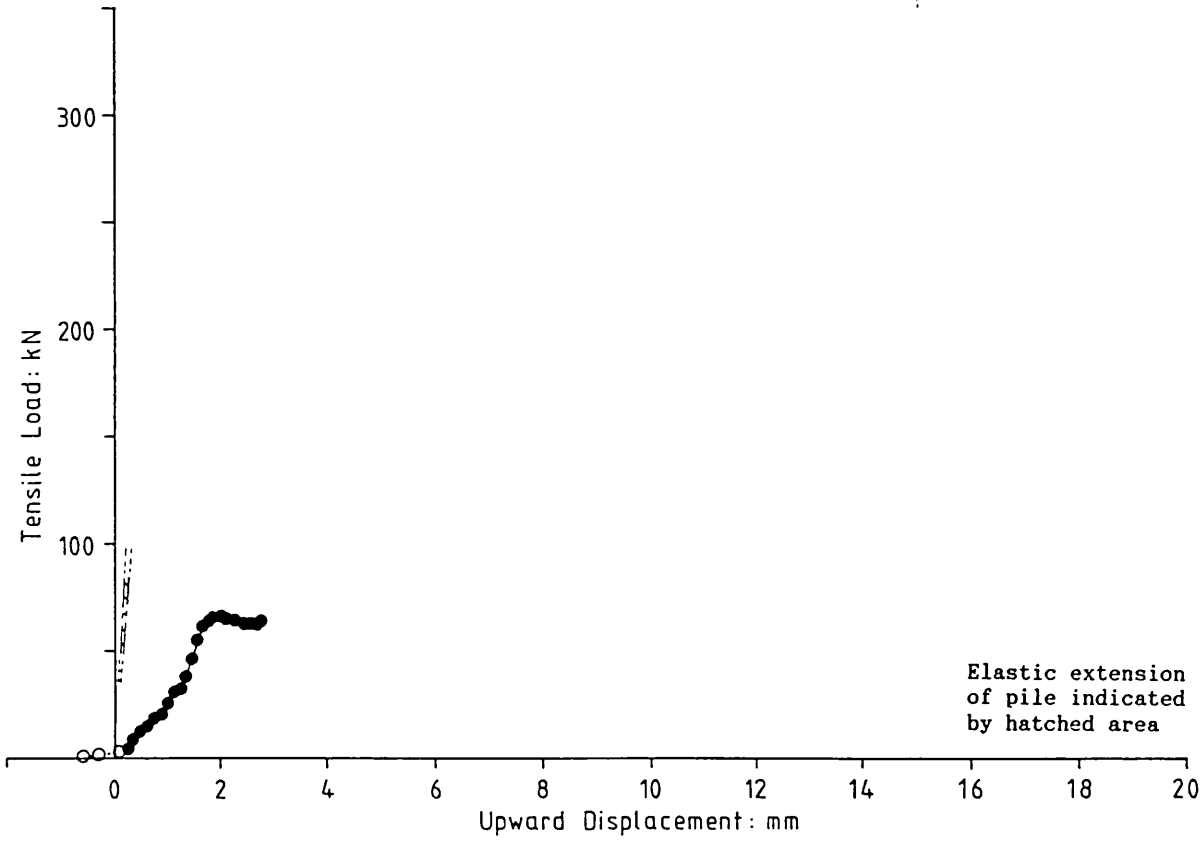

TEST 1U.2 Type: CRE Date: 2.4.85

Outer shell driven: 27.3.85 Expander mandrel driven: -

Days elapsed
prior to test: 6 -

Shaft areas: (m^2)

Embedded length,			Expanded length,		
Full X-section	(A):	2.65	Full X-section	(C):	-
Reduced X-section	(B):	-	Reduced X-section	(D):	-

Pile weight: 2.7 (kN)

Test Stage	Maximum Load (Gross)	(Net)	Shaft Frictions (A)	(B)	(C)	(D)	Displacement at: Max. Load	End of stage
	(kN)	(kN)	(kPa)	(kPa)	(kPa)	(kPa)	(mm)	(mm)
CRE	66.4	63.7	24.0	-	-	-	1.8	2.7

Figure 4.30 Results of Pile Test 1U.2

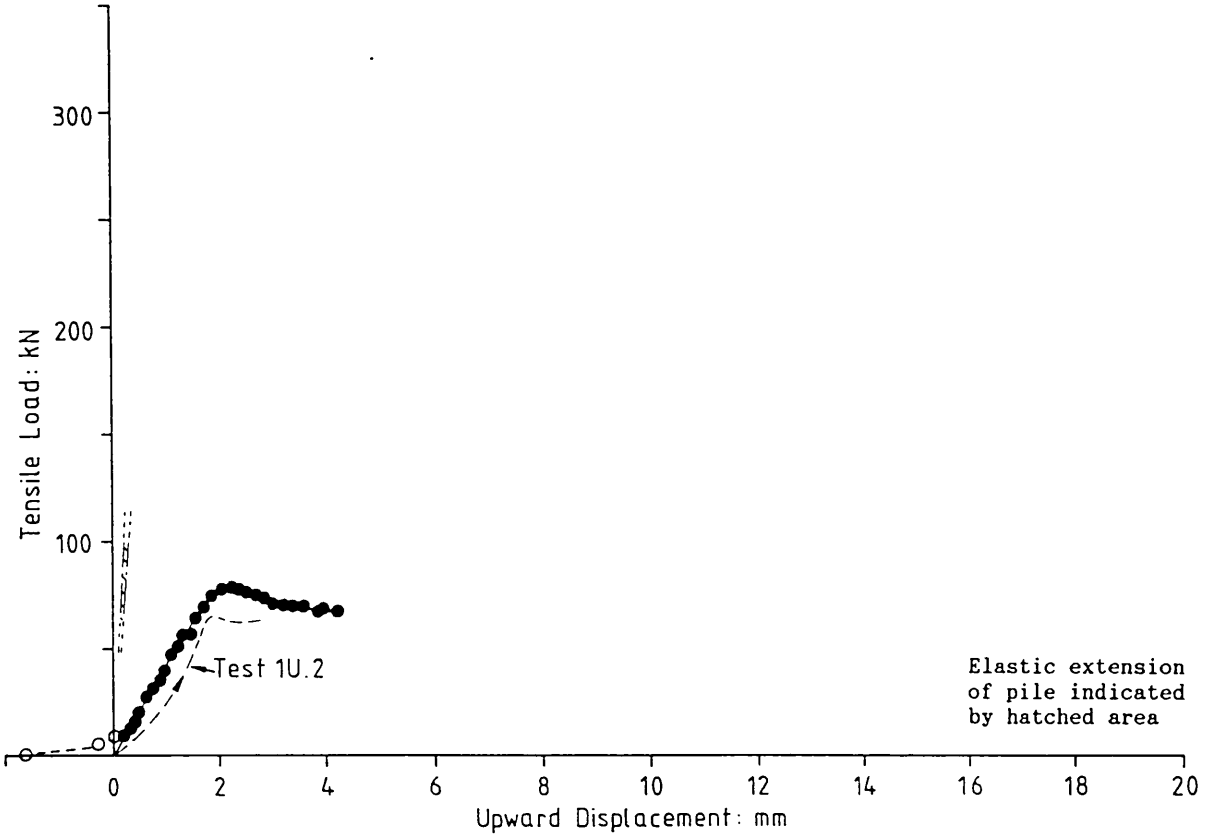

TEST 1U.3 Type: CRE Date: 16.4.85

Outer shell driven: 27.3.85 Expander mandrel driven: -
Days elapsed
prior to test: 20 -

Shaft areas: (m^2)
Embedded length,
Full X-section (A): 2.65
Reduced X-section (B): -
Expanded length,
Full X-section (C): -
Reduced X-section (D): -

Pile weight: 2.7 (kN)

Test Stage	Maximum Load (Gross) (kN)	Maximum Load (Net) (kN)	Shaft Frictions (A) (kPa)	(B) (kPa)	(C) (kPa)	(D) (kPa)	Displacement at: Max. Load (mm)	Displacement at: End of stage (mm)
CRE	79.1	76.4	28.8	-	-	-	2.1	4.2

Figure 4.31 Results of Pile Test 1U.3

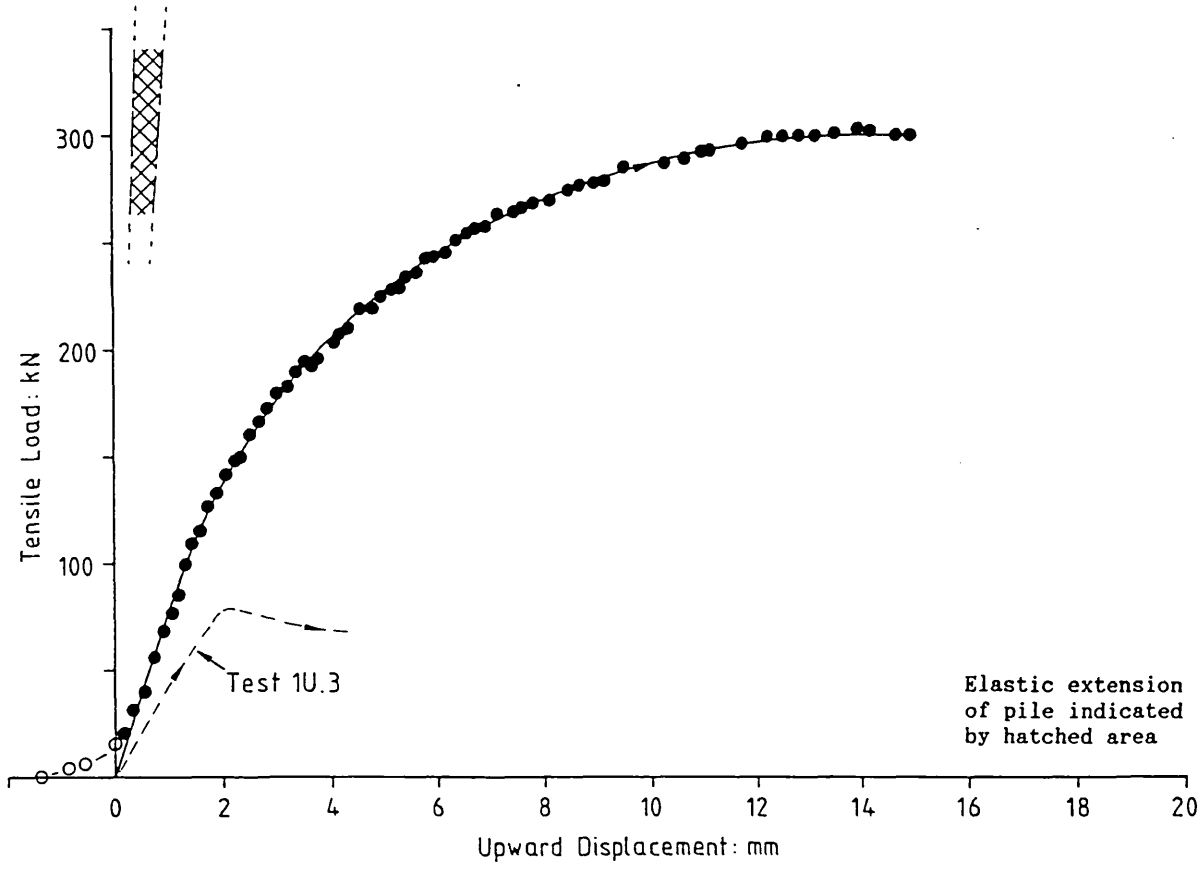

TEST 1A.1 Type: CRE Date: 22.4.85

Outer shell driven: 27.3.85 Expander mandrel driven: 17.4.85
Days elapsed
prior to test: 26 5

Shaft areas: (m^2)
Embedded length,
Full X-section (A): 3.03
Reduced X-section (B): 2.65
Expanded length,
Full X-section (C): 2.41
Reduced X-section (D): 2.11

Pile weight: 4.6 (kN)

Test Stage	Maximum Load (Gross) (kN)	(Net) (kN)	Shaft Frictions (A) (kPa)	(B) (kPa)	(C) (kPa)	(D) (kPa)	Displacement at: Max. Load (mm)	End of stage (mm)
CRE	302.8	298.2	98.5	112.6	123.6	141.3	14.0	14.9

Figure 4.32 Results of Pile Test 1A.1

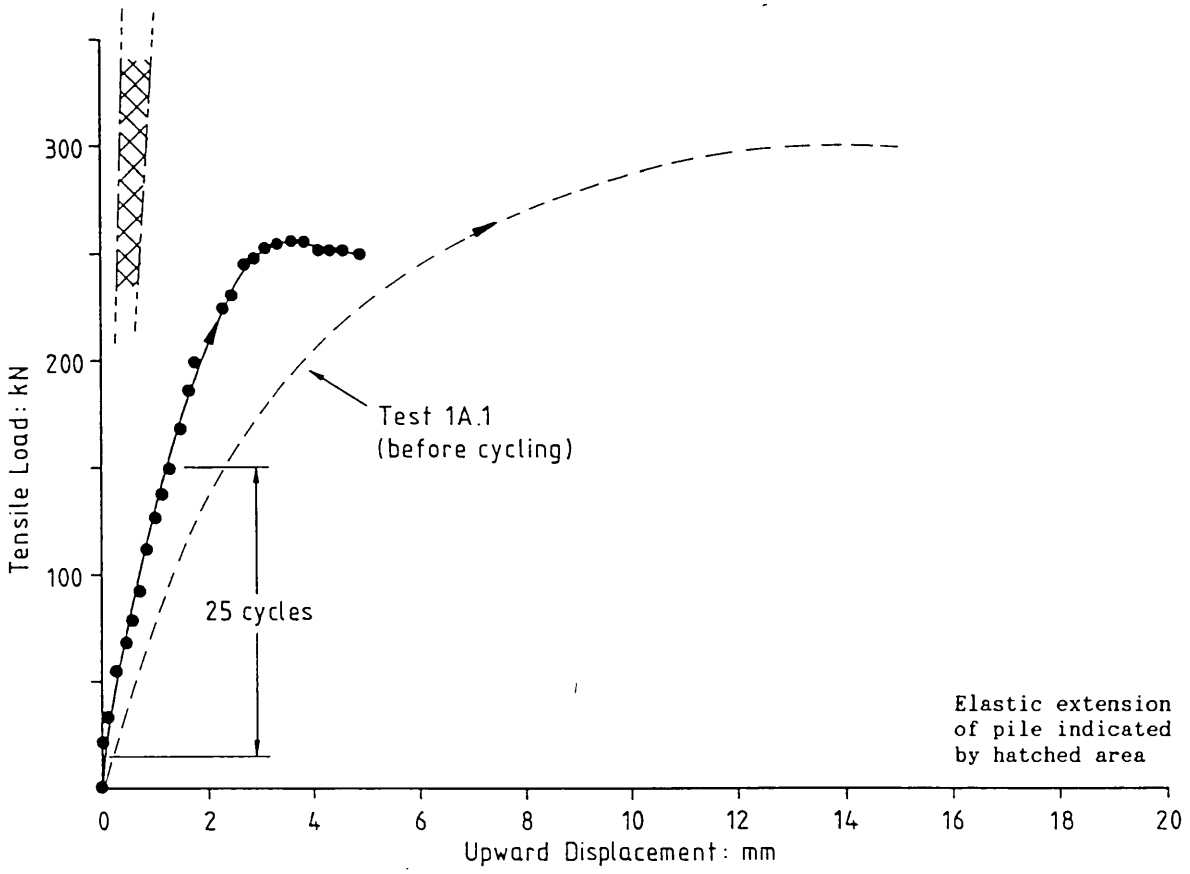

TEST 1A.2 Type: Cyclic, CRE Date: 22.4.85

Outer shell driven: 27.3.85 Expander mandrel driven: 17.4.85
Days elapsed
prior to test: 26 5

Shaft areas: (m^2)	Embedded length,		Expanded length,	
	Full X-section (A):	3.03	Full X-section (C):	2.41
	Reduced X-section (B):	2.65	Reduced X-section (D):	2.11

Pile weight: 4.6 (kN)

Test Stage	Maximum Load (Gross)	(Net)	Shaft Frictions (A)	(B)	(C)	(D)	Displacement at: Max. Load	End of stage
	(kN)	(kN)	(kPa)	(kPa)	(kPa)	(kPa)	(mm)	(mm)
Cyclic[1]	-	-	-	-	-	-	-	-
CRE	256.0	251.4	83.1	94.9	104.2	119.1	3.6	4.9

Notes: 1. 25 cycles, 15kN (approx) - 150kN

Figure 4.33 Results of Pile Test 1A.2

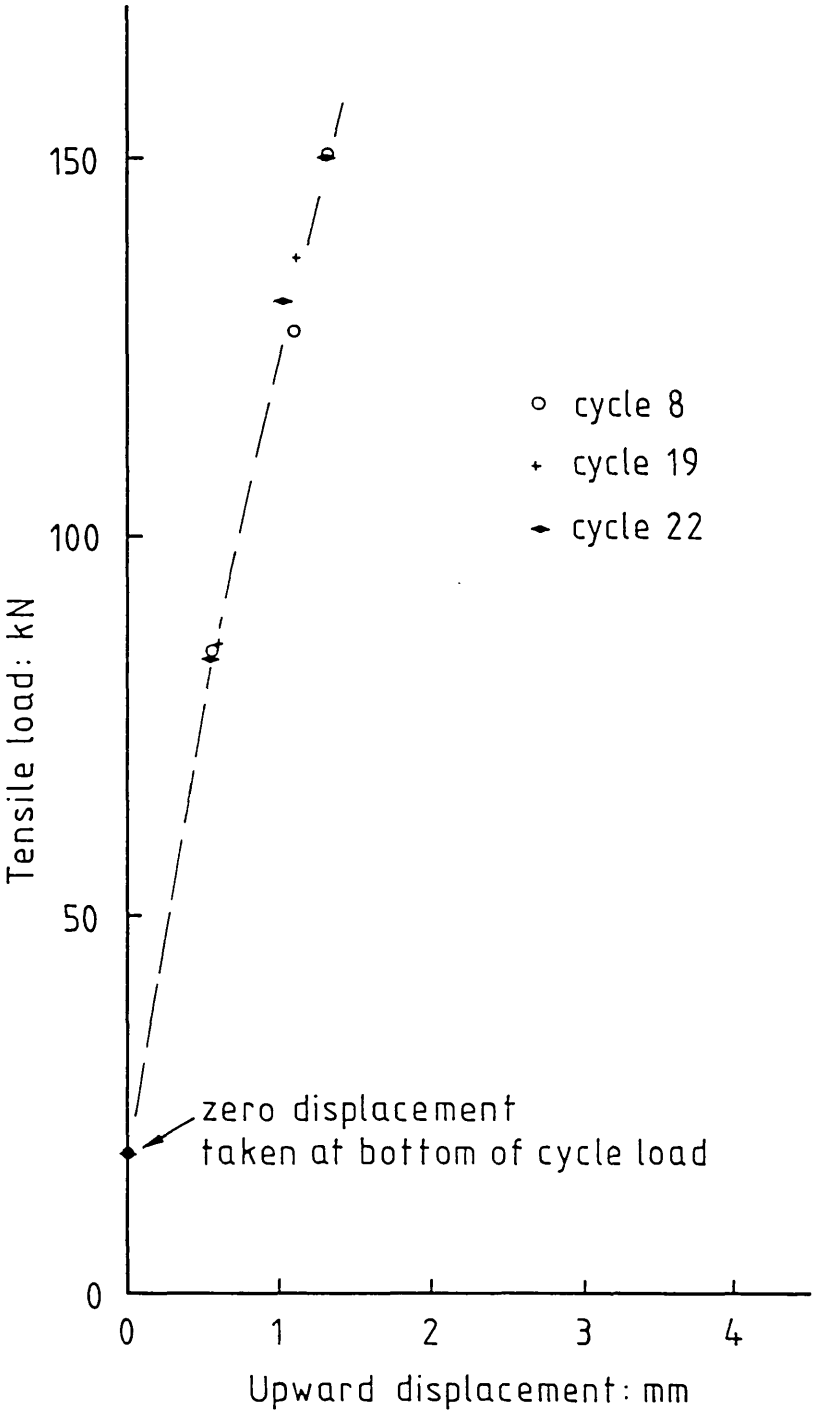

Figure 4.34 Pile Test 1A.2:
Load:displacement behaviour during cyclic loading

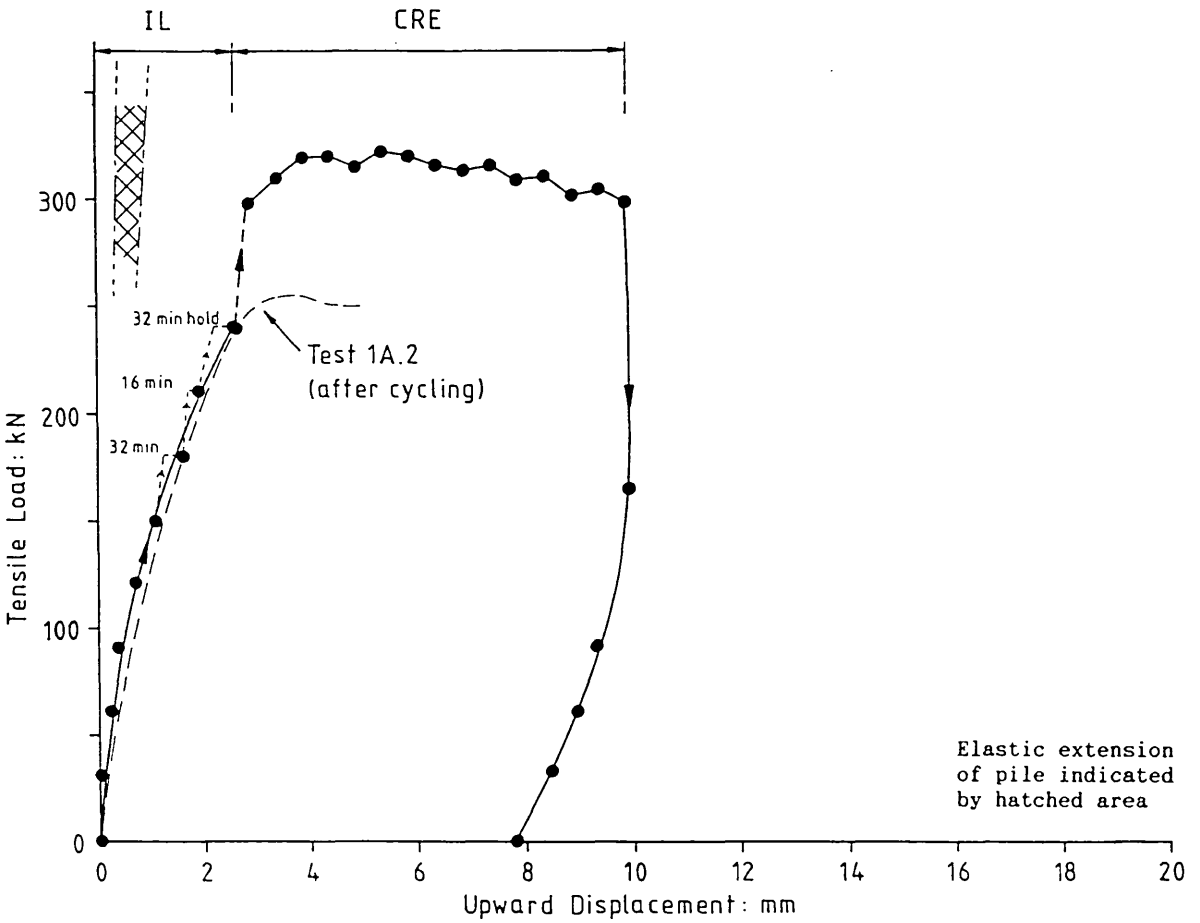

TEST 1A.3 Type: IL, CRE Date: 1.11.85

Outer shell driven: 27.3.85 Expander mandrel driven: 17.4.85

Days elapsed prior to test: 218 198

Shaft areas (m^2):

Embedded length,			Expanded length,		
Full X-section	(A):	3.03	Full X-section	(C):	2.41
Reduced X-section	(B):	2.65	Reduced X-section	(D):	2.11

Pile weight: 4.6 (kN)

Test Stage	Maximum Load (Gross) (kN)	Maximum Load (Net) (kN)	Shaft Frictions (A) (kPa)	(B) (kPa)	(C) (kPa)	(D) (kPa)	Displacement at: Max. Load (mm)	Displacement at: End of stage (mm)
IL	241.2	-	-	-	-	-	2.6	2.6
CRE	322.3	317.7	105.0	119.9	131.7	150.5	5.4	7.9

Figure 4.35 Results of Pile Test 1A.3

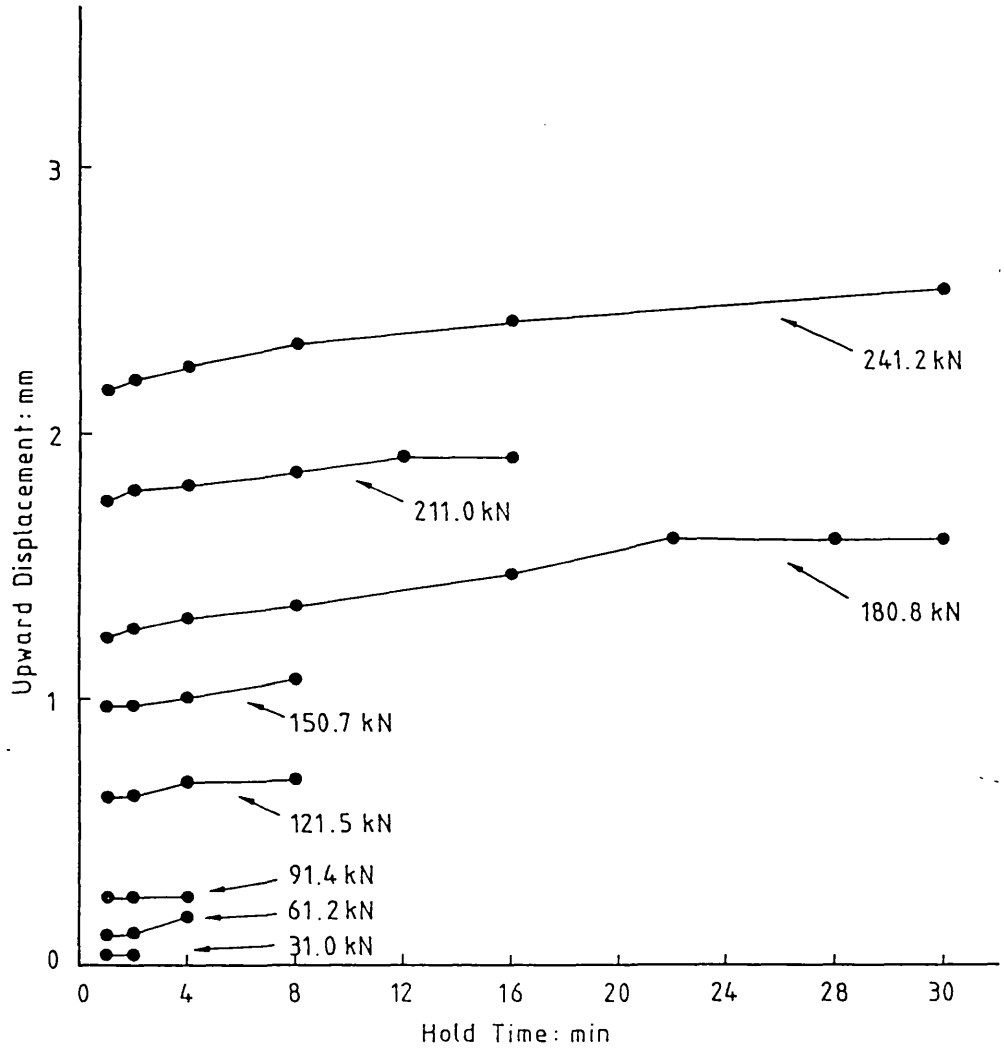

Figure 4.36 Pile Test 1A.3:
Creep behaviour during IL stage

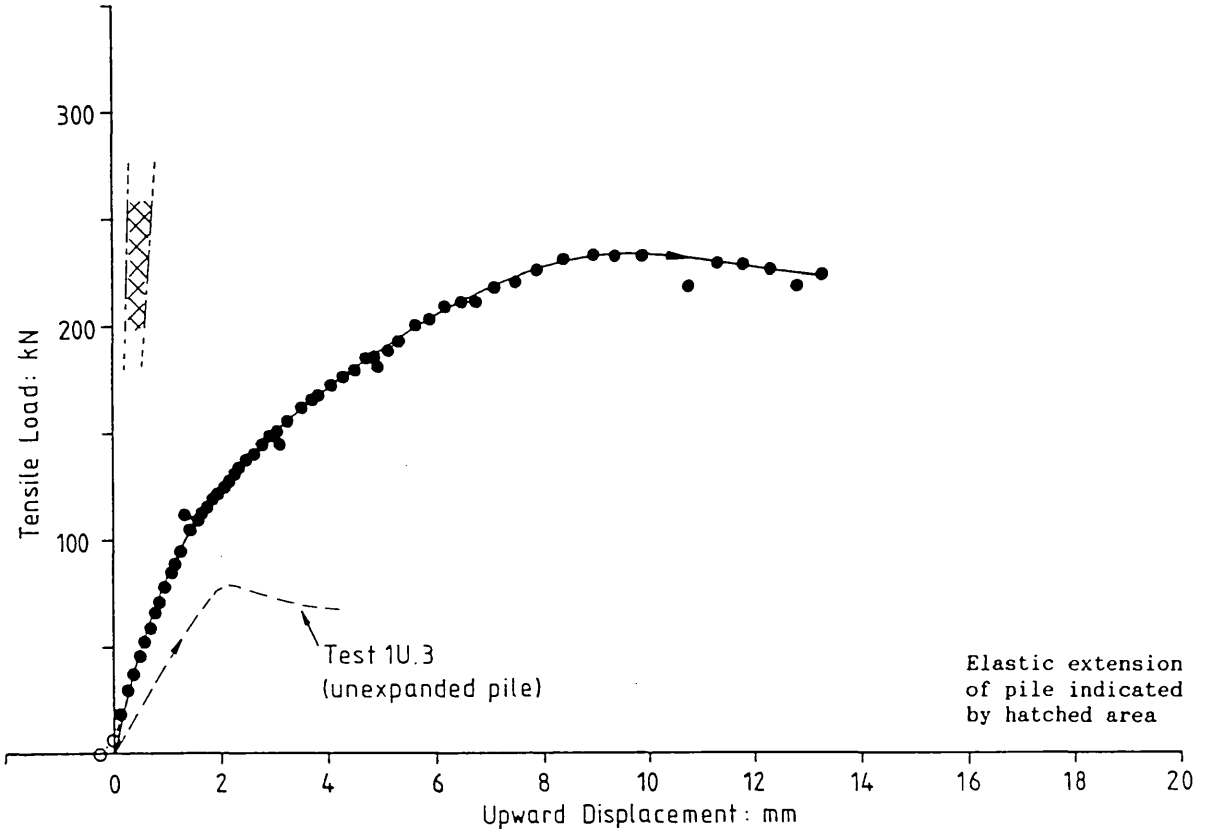

TEST 2A.1 Type: CRE Date: 2.4.85

Outer shell driven: 28.3.85 Expander mandrel driven: 28.3.85
Days elapsed
prior to test: 5 5

Shaft areas: (m^2)
Embedded length,
Full X-section (A): 3.08
Reduced X-section (B): 2.69
Expanded length,
Full X-section (C): 2.44
Reduced X-section (D): 2.13

Pile weight: 4.6 (kN)

Test Stage	Maximum Load (Gross) (kN)	Maximum Load (Net) (kN)	Shaft Frictions (A) (kPa)	(B) (kPa)	(C) (kPa)	(D) (kPa)	Displacement at: Max. Load (mm)	Displacement at: End of stage (mm)
CRE	232.7	228.1	74.1	84.7	93.6	106.9	9.0	13.3

Figure 4.37 Results of Pile Test 2A.1

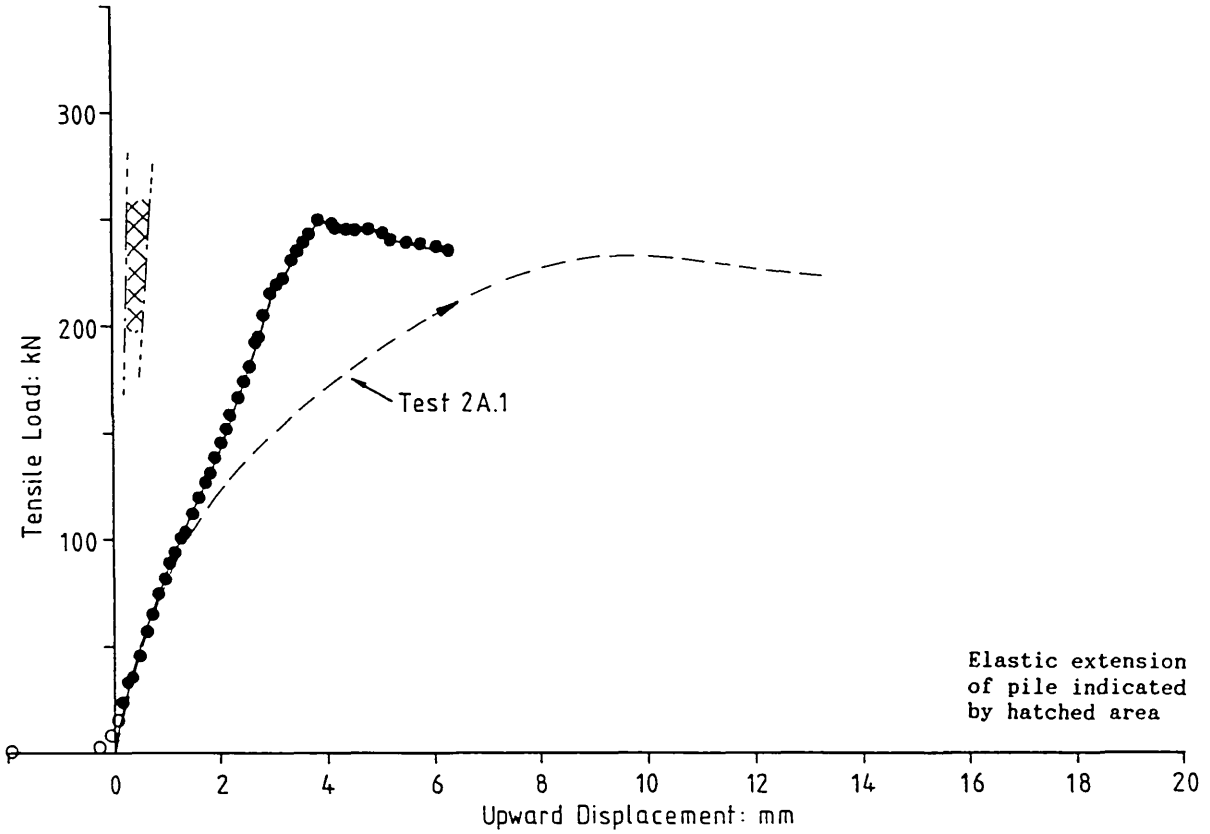

TEST 2A.2 Type: CRE Date: 16.4.85

Outer shell driven: 28.3.85 Expander mandrel driven: 28.3.85
Days elapsed
prior to test: 19 19

Shaft areas: (m^2)
Embedded length,
Full X-section (A): 3.08
Reduced X-section (B): 2.69
Expanded length,
Full X-section (C): 2.44
Reduced X-section (D): 2.13

Pile weight: 4.6 (kN)

Test Stage	Maximum Load (Gross) (kN)	Maximum Load (Net) (kN)	Shaft Frictions (A) (kPa)	(B) (kPa)	(C) (kPa)	(D) (kPa)	Displacement at: Max. Load (mm)	End of stage (mm)
CRE	249.7	245.1	79.6	91.0	100.5	114.9	3.9	6.3

Figure 4.38 Results of Pile Test 2A.2

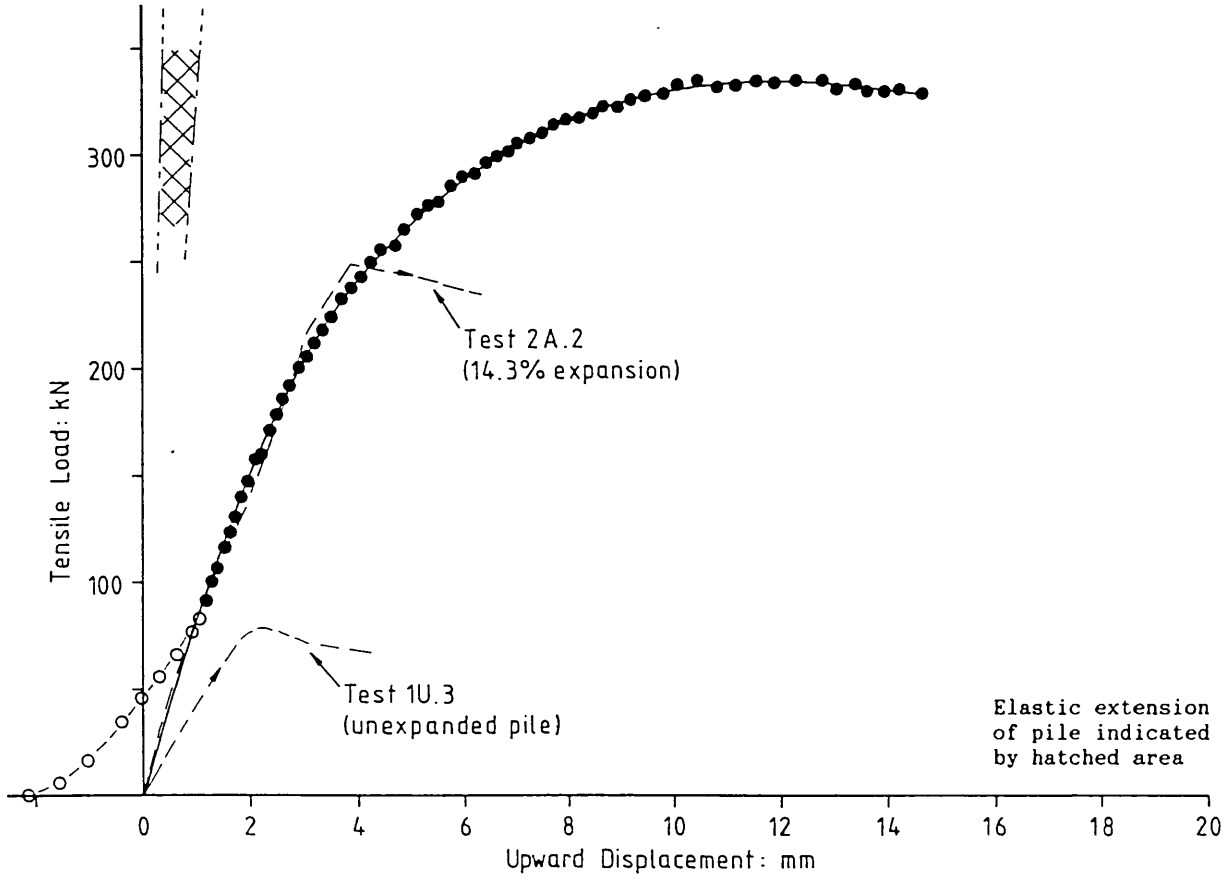

TEST 2B.1 Type: CRE Date: 22.4.85

Outer shell driven: 28.3.85 Expander mandrel driven: 17.4.85
Days elapsed
prior to test: 25 5

Shaft areas: (m^2) Embedded length, Full X-section (A): 3.27 Reduced X-section (B): 2.69
Expanded length, Full X-section (C): 2.59 Reduced X-section (D): 2.13

Pile weight: 4.8 (kN)

Test Stage	Maximum Load (Gross) (kN)	Maximum Load (Net) (kN)	Shaft Frictions (A) (kPa)	(B) (kPa)	(C) (kPa)	(D) (kPa)	Displacement at: Max. Load (mm)	End of stage (mm)
CRE	335.0	330.2	100.9	122.6	127.4	154.7	10.4	14.6

Figure 4.39 Results of Pile Test 2B.1

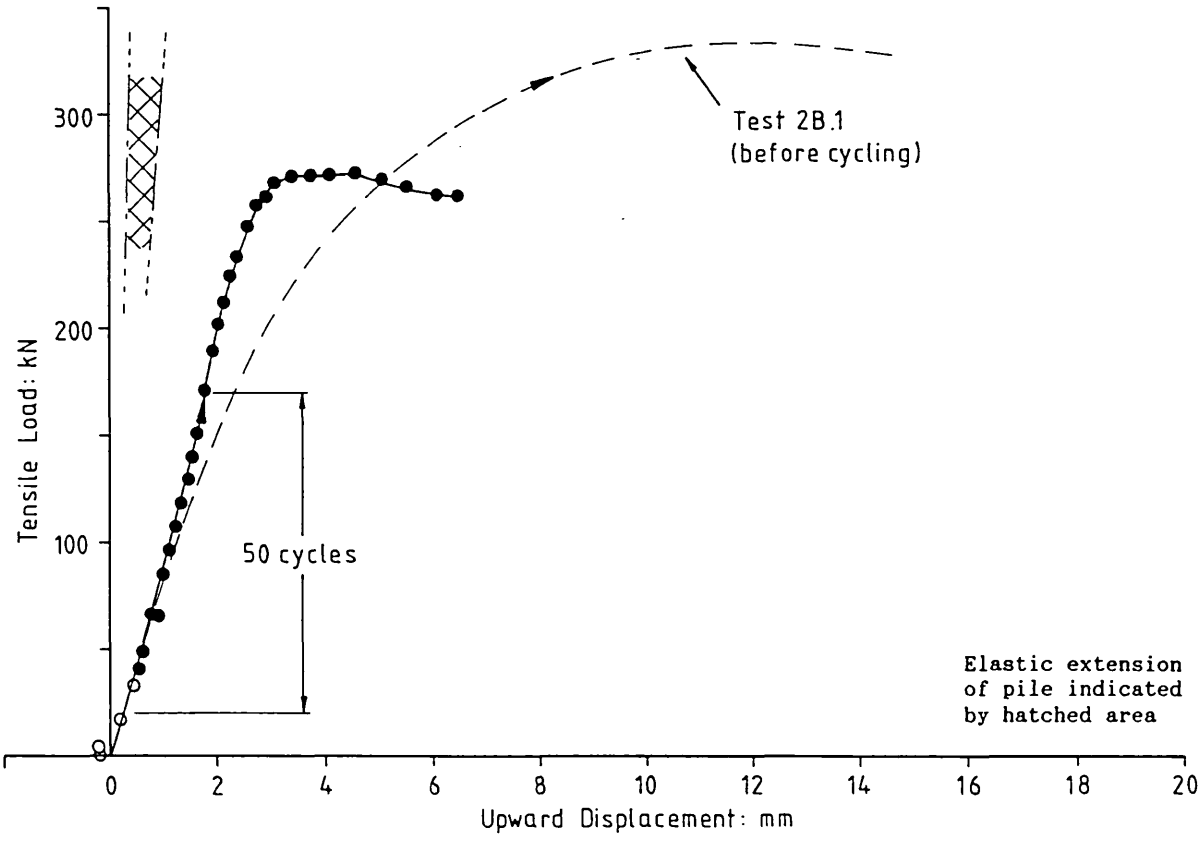

TEST 2B.2 Type: Cyclic, CRE Date: 23.5.85

Outer shell driven: 28.3.85 Expander mandrel driven: 17.4.85
Days elapsed
prior to test: 26 6

Shaft areas: (m^2)
Embedded length,
Full X-section (A): 3.27
Reduced X-section (B): 2.69
Expanded length,
Full X-section (C): 2.59
Reduced X-section (D): 2.13

Pile weight: 4.8 (kN)

Test Stage	Maximum Load (Gross) (kN)	Maximum Load (Net) (kN)	Shaft Frictions (A) (kPa)	(B) (kPa)	(C) (kPa)	(D) (kPa)	Displacement at: Max. Load (mm)	Displacement at: End of stage (mm)
Cyclic[1]	-	-	-	-	-	-	-	-
CRE	272.6	267.8	81.9	99.4	103.4	125.5	4.6	6.4

Notes: 1. 50 cycles, 21kN (approx) - 170.6kN

Figure 4.40 Results of Pile Test 2B.2

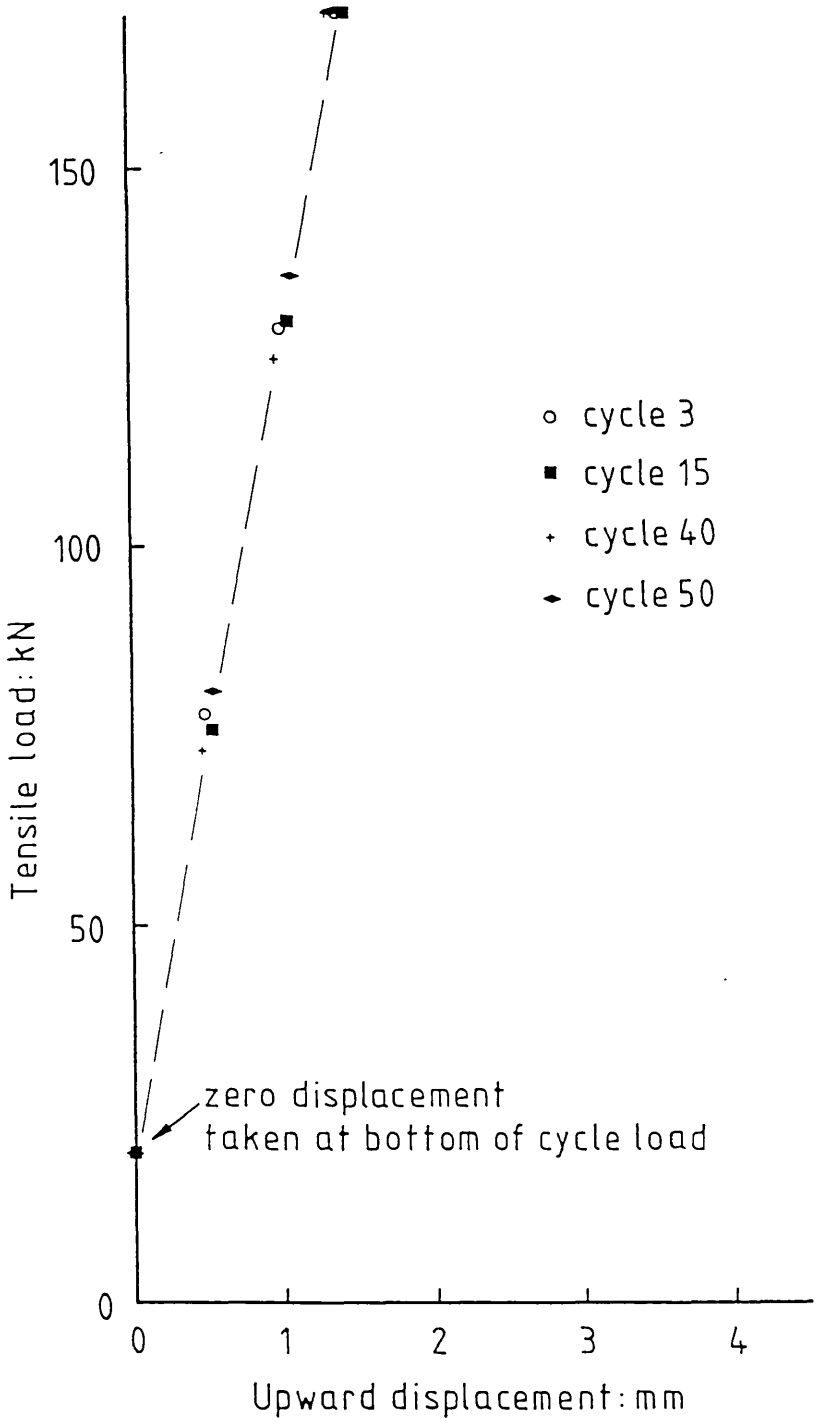

Figure 4.41 Pile Test 2B.2:
Load:displacement behaviour during cyclic loading

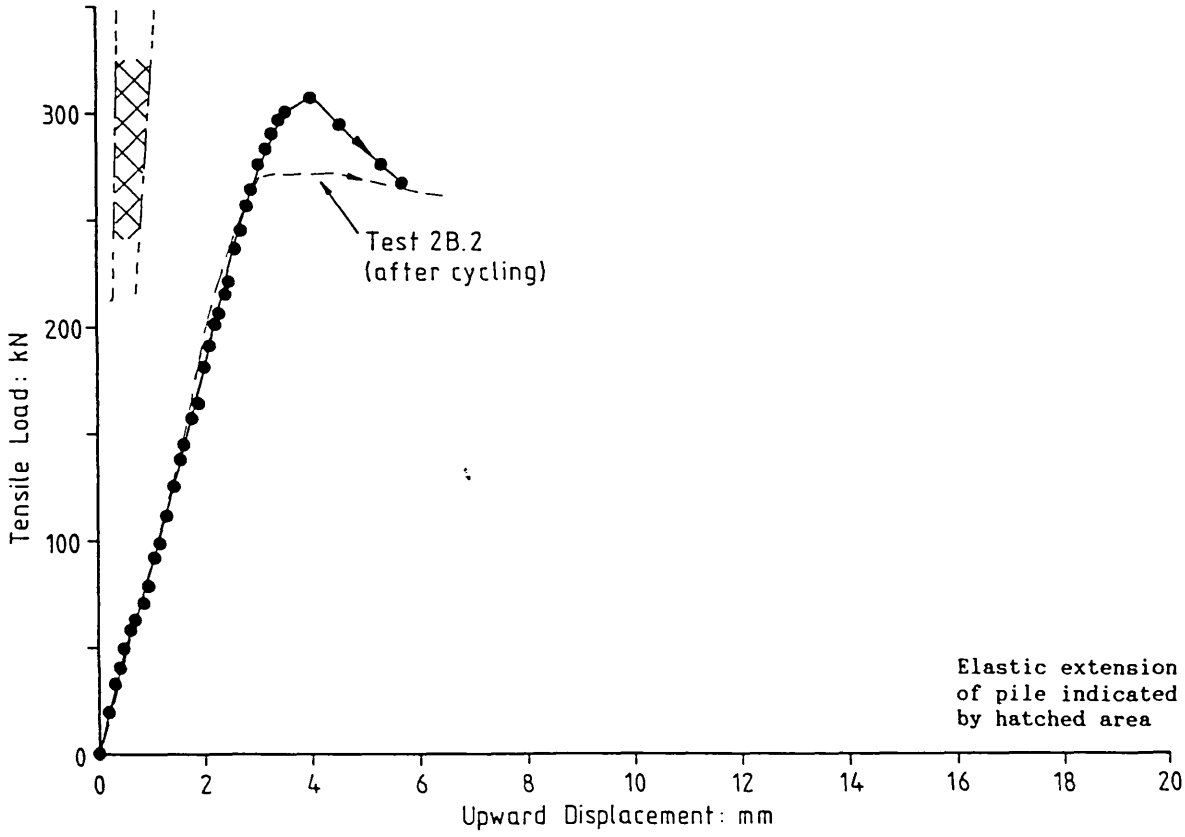

TEST 2B.3 Type: CRE Date: 7.5.85

Outer shell driven: 28.3.85 Expander mandrel driven: 17.4.85
Days elapsed
prior to test: 40 20

Shaft areas: (m^2)

Embedded length,			Expanded length,		
Full X-section	(A):	3.27	Full X-section	(C):	2.59
Reduced X-section	(B):	2.69	Reduced X-section	(D):	2.13

Pile weight: 4.8 (kN)

Test Stage	Maximum Load (Gross)	(Net)	Shaft Frictions (A)	(B)	(C)	(D)	Displacement at: Max. Load	End of stage
	(kN)	(kN)	(kPa)	(kPa)	(kPa)	(kPa)	(mm)	(mm)
CRE	306.9	302.1	92.4	112.1	116.1	141.6	4.0	5.7

Figure 4.42 Results of Pile Test 2B.3

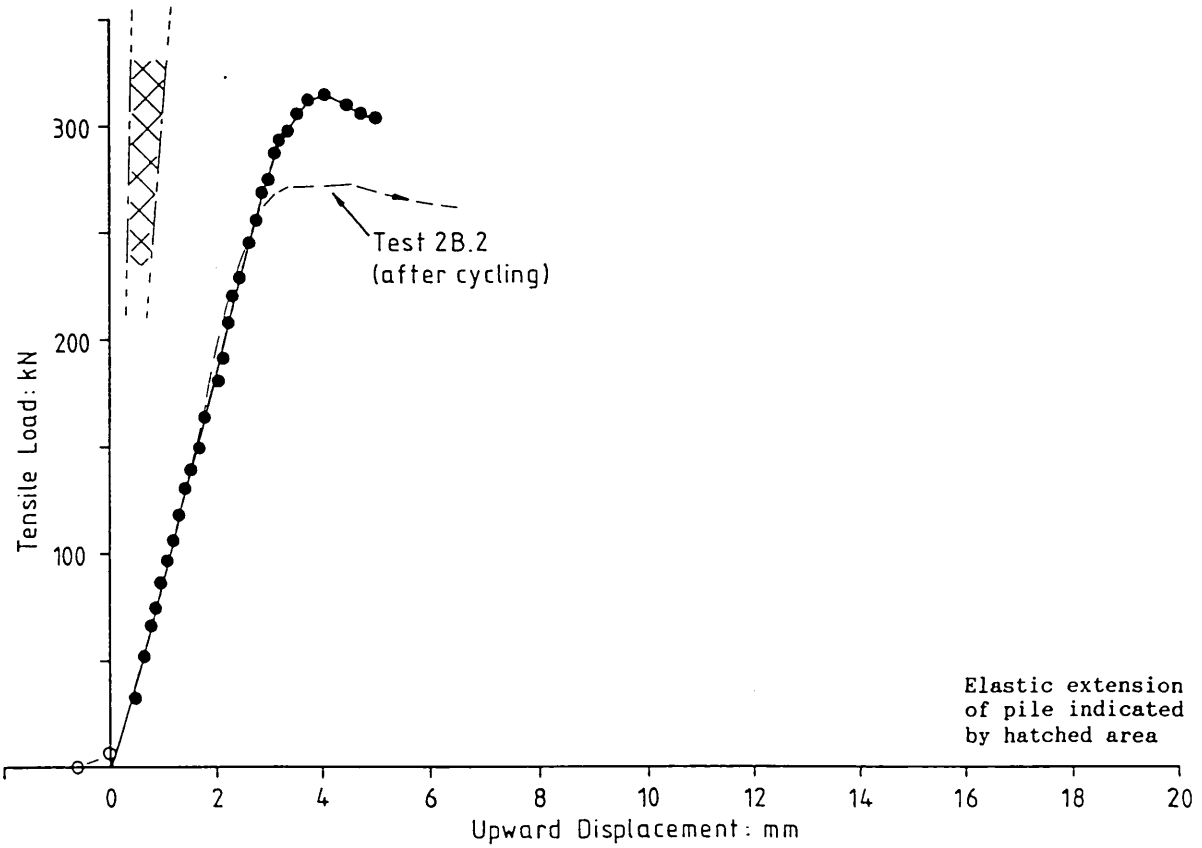

TEST 2B.4 Type: CRE Date: 5.8.85

Outer shell driven: 28.3.85 Expander mandrel driven: 17.4.85

Days elapsed prior to test: 130 110

Shaft areas (m^2): Embedded length, Full X-section (A): 3.27; Reduced X-section (B): 2.69. Expanded length, Full X-section (C): 2.59; Reduced X-section (D): 2.13

Pile weight (kN): 4.8

Test Stage	Maximum Load (Gross) (kN)	Maximum Load (Net) (kN)	Shaft Frictions (A) (kPa)	(B) (kPa)	(C) (kPa)	(D) (kPa)	Displacement at: Max. Load (mm)	Displacement at: End of stage (mm)
CRE	314.2	309.4	94.6	114.8	119.4	145.0	4.1	5.0

Figure 4.43 Results of Pile Test 2B.4

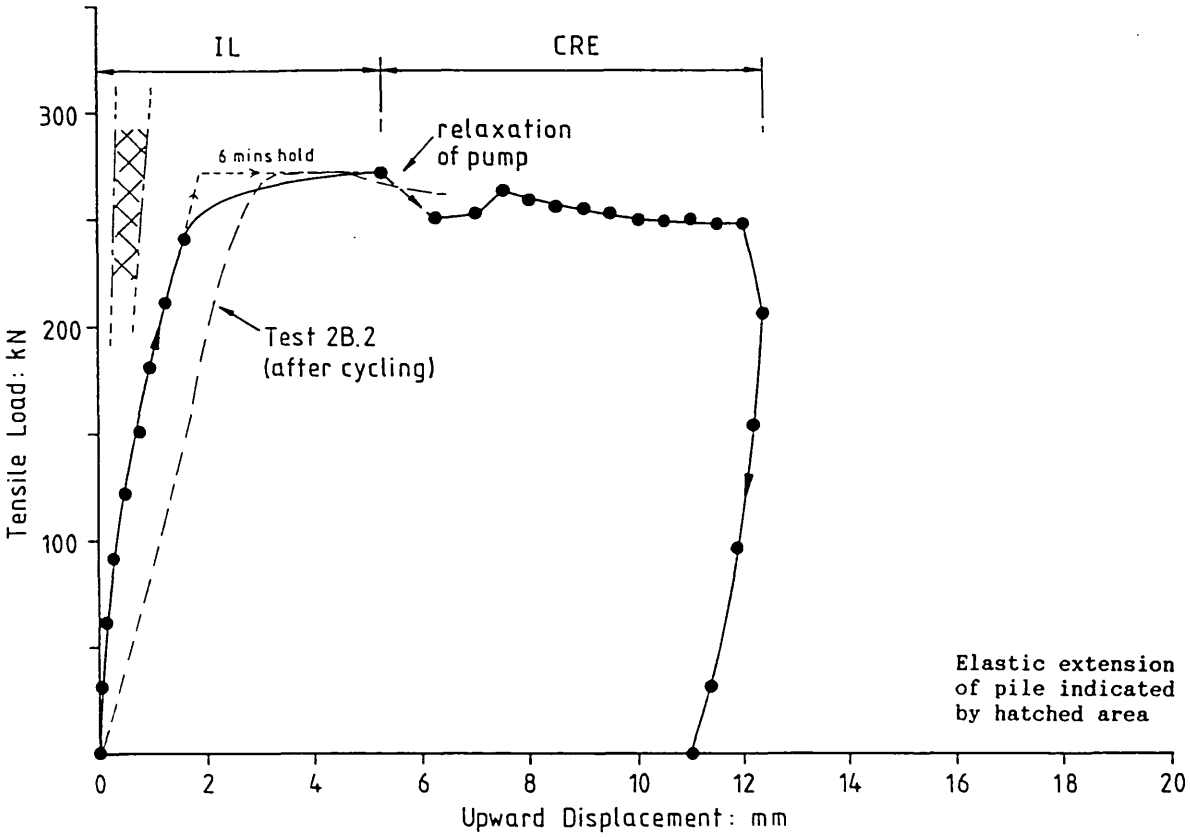

TEST 2B.5 Type: IL, CRE Date: 6.11.85

Outer shell driven: 28.3.85 Expander mandrel driven: 17.4.85
Days elapsed
prior to test: 223 203

Shaft areas: (m^2)
Embedded length, Full X-section (A): 3.27
Reduced X-section (B): 2.69
Expanded length, Full X-section (C): 2.59
Reduced X-section (D): 2.13

Pile weight: 4.8 (kN)

Test Stage	Maximum Load (Gross) (kN)	(Net) (kN)	Shaft Frictions (A) (kPa)	(B) (kPa)	(C) (kPa)	(D) (kPa)	Displacement at: Max. Load (mm)	End of stage (mm)
IL	271.8	-	-	-	-	-	5.3	5.3
CRE	263.5	258.7	79.1	96.0	99.8	121.2	7.6	11.0

Figure 4.44 Results of Pile Test 2B.5

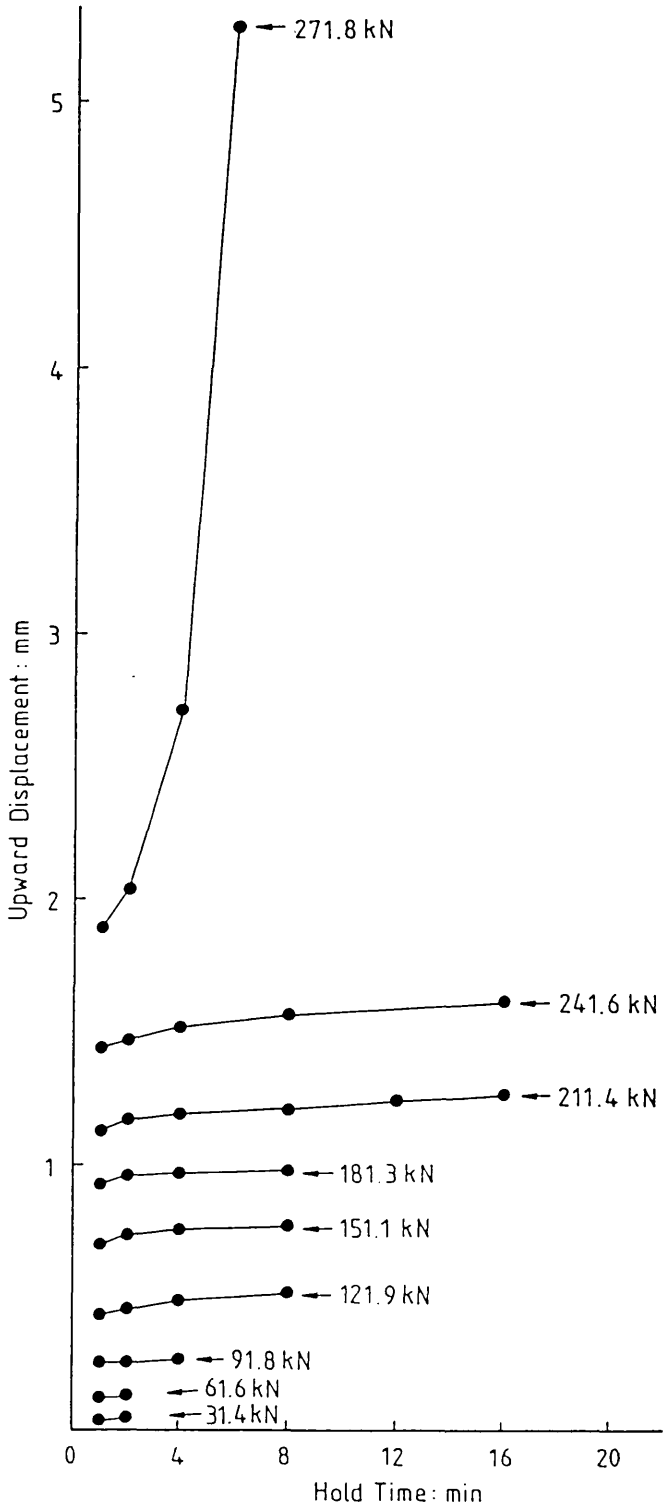

Figure 4.45 Pile Test 2B.5:
Creep behaviour during IL stage

TEST 3U.1 Type: IL, CRE Date: 16.10.85

Outer shell driven: 4.10.85 Expander mandrel driven: -
Days elapsed
prior to test: 12 -

Shaft areas: (m^2) Embedded length,
Full X-section (A): 2.06
Reduced X-section (B): -
Expanded length,
Full X-section (C): -
Reduced X-section (D): -

Pile weight: 2.4 (kN)

Test Stage	Maximum Load (Gross) (kN)	Maximum Load (Net) (kN)	Shaft Frictions (A) (kPa)	(B) (kPa)	(C) (kPa)	(D) (kPa)	Displacement at: Max. Load (mm)	End of stage (mm)
IL	21.4	-	-	-	-	-	3.0	3.0
CRE	50.4	48.0	23.3	-	-	-	31.4	31.8

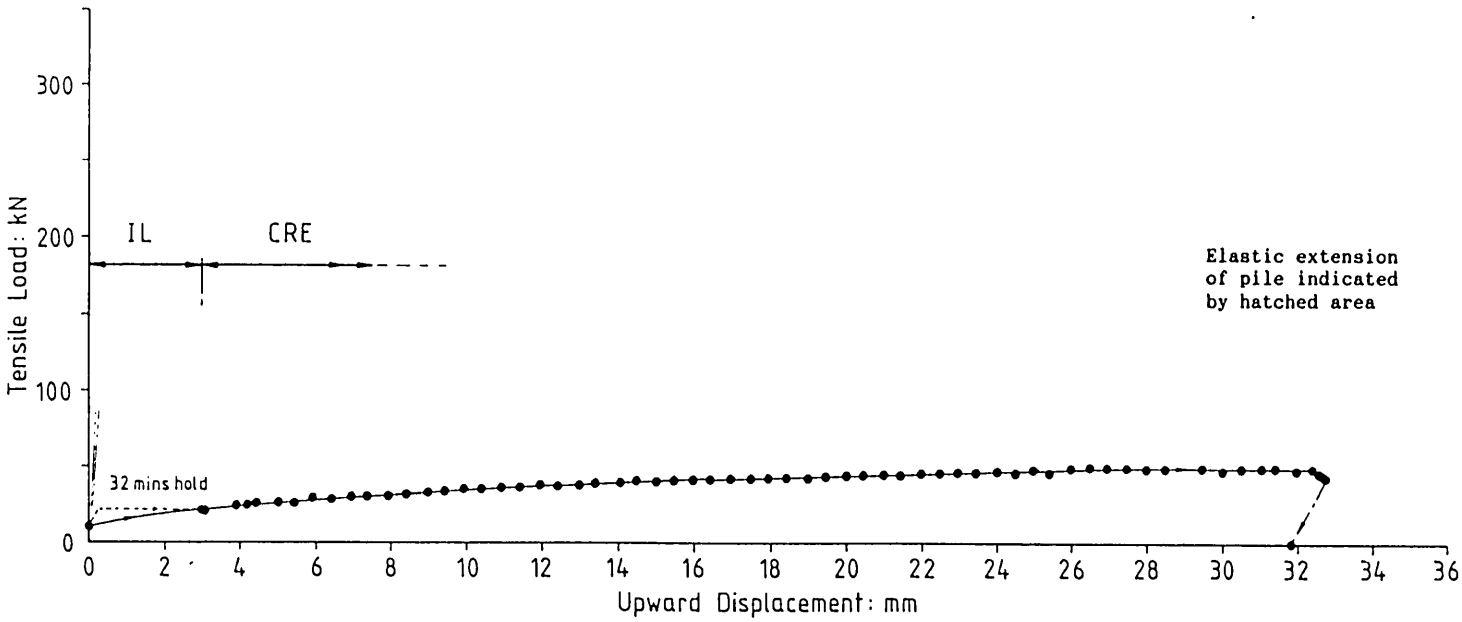

Figure 4.46
Results of Pile Test 3U.1

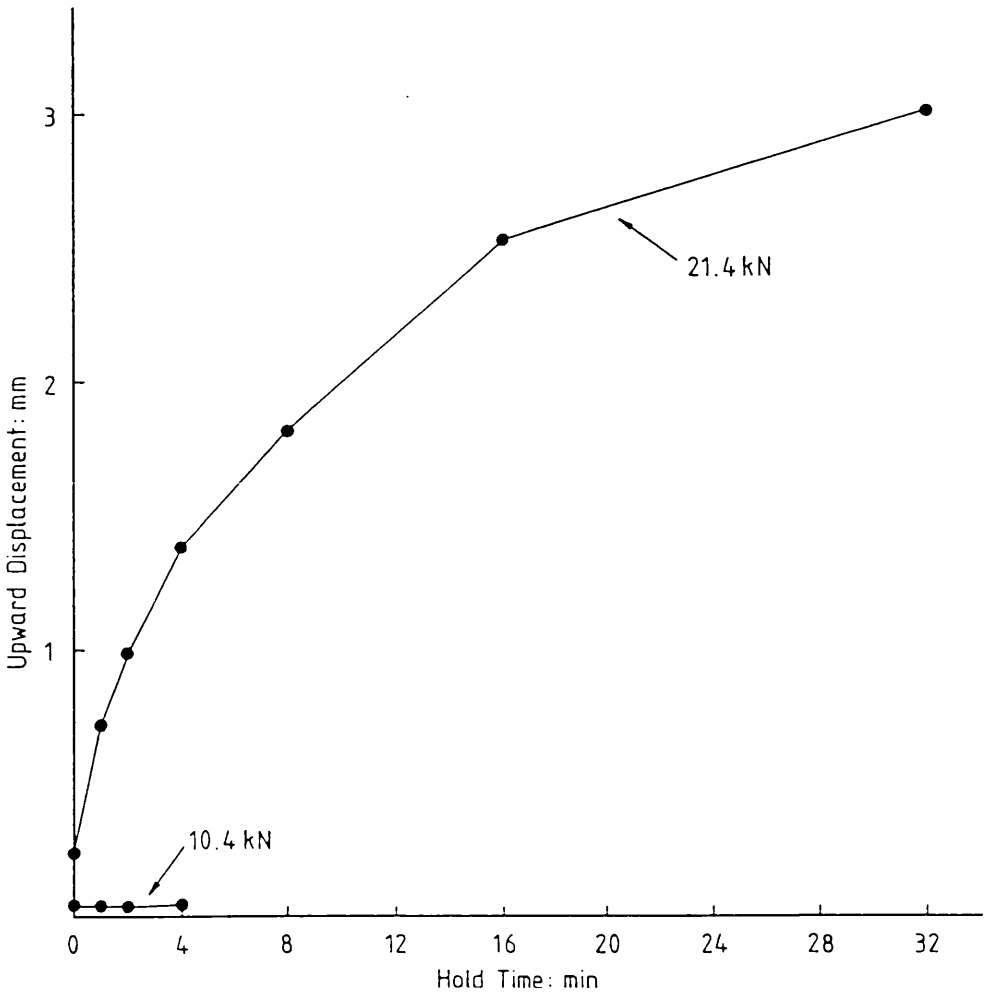

Figure 4.47 Pile Test 3U.1:
Creep behaviour during IL stage

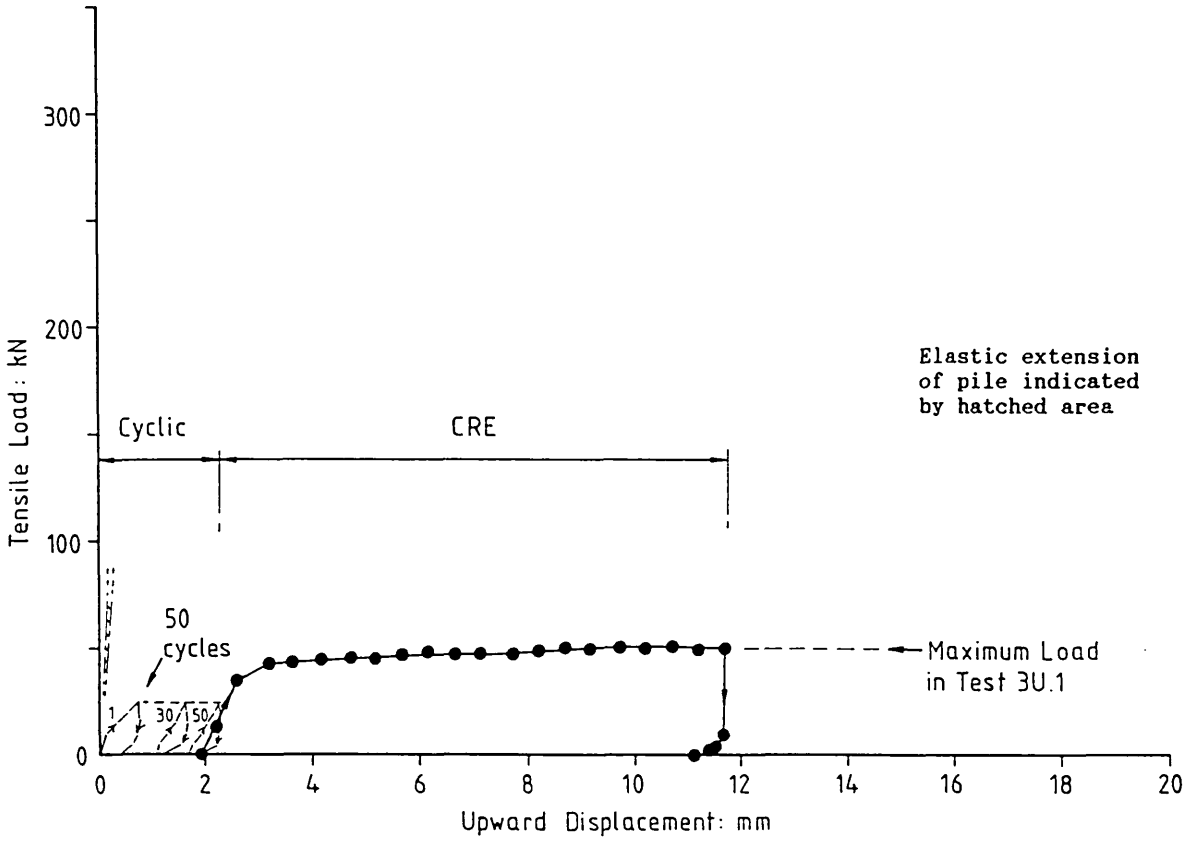

TEST 3U.2 Type: Cyclic, CRE Date: 31.10.85

Outer shell driven: 4.10.85 Expander mandrel driven: -
Days elapsed
prior to test: 27 -

Shaft areas: (m^2)
Embedded length,
Full X-section (A): 2.06
Reduced X-section (B): -
Expanded length,
Full X-section (C): -
Reduced X-section (D): -

Pile weight: 2.4 (kN)

Test Stage	Maximum Load (Gross) (kN)	(Net) (kN)	Shaft Frictions (A) (kPa)	(B) (kPa)	(C) (kPa)	(D) (kPa)	Displacement at: Max. Load (mm)	End of stage (mm)
Cyclic[1]	-	-	-	-	-	-	-	-
CRE	51.2	48.8	23.7	-	-	-	8.8	9.2

Notes: 1. 50 cycles 1kN - 25kN

Figure 4.48 Results of Pile Test 3U.2

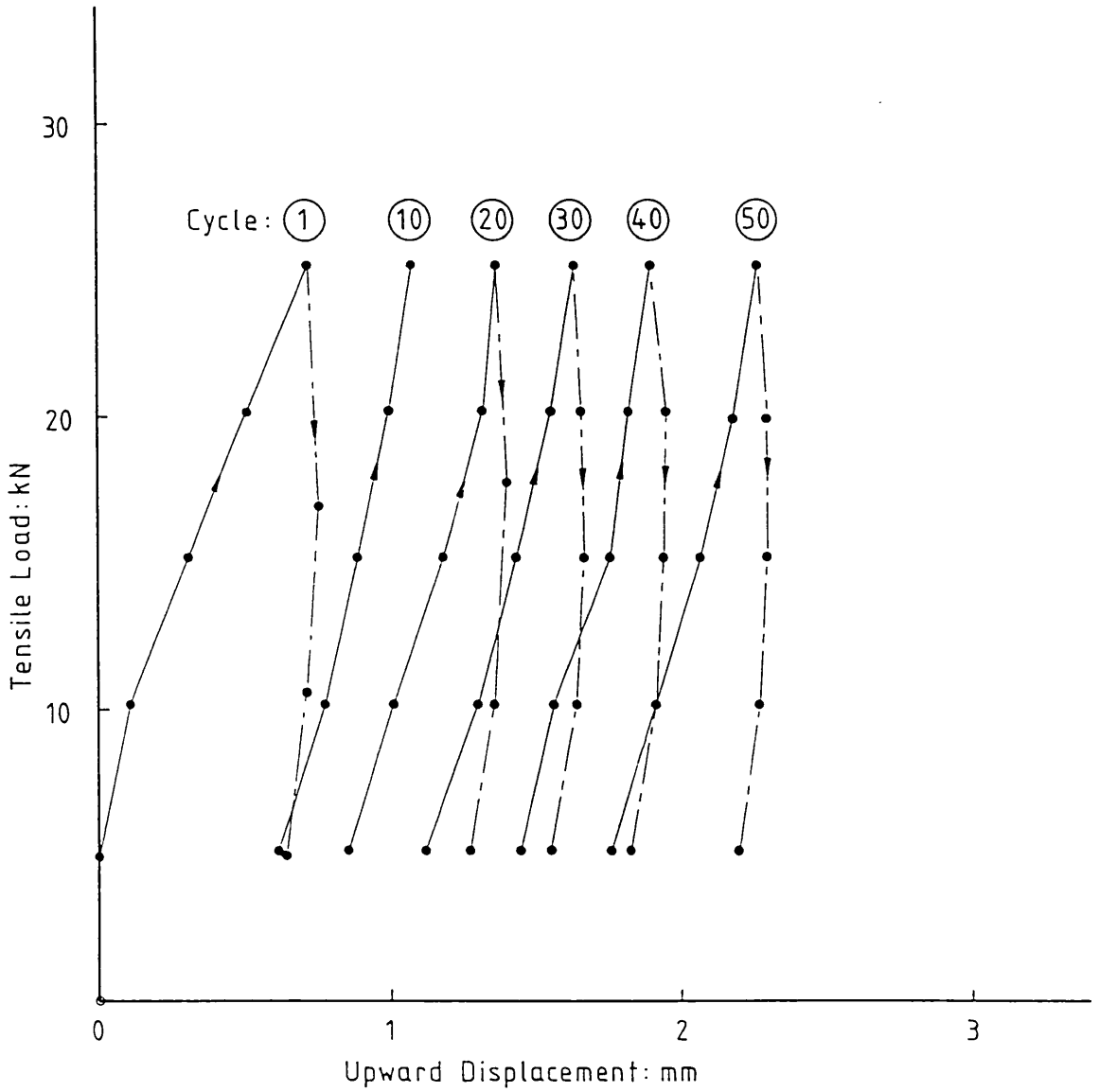

Figure 4.49 Pile Test 3U.2:
Load:displacement behaviour during cyclic loading

TEST 3B.1 Type: IL, CRE Date: 2.12.85

Outer shell driven: 4.10.85 Expander mandrel driven: 20.11.85
Days elapsed
prior to test: 12 9

Shaft areas: (m^2)
Embedded length,
Full X-section (A): 2.65
Reduced X-section (B): 2.06
Expanded length,
Full X-section (C): 2.38
Reduced X-section (D): 1.85

Pile weight: 6.6 (kN)

Test Stage	Maximum Load (Gross) (kN)	(Net) (kN)	Shaft Frictions (A) (kPa)	(B) (kPa)	(C) (kPa)	(D) (kPa)	Displacement at: Max. Load (mm)	End of stage (mm)
IL	149.4	-	-	-	-	-	10.2	10.2
CRE	210.8	204.2	77.2	99.2	85.9	110.5	24.0	23.7

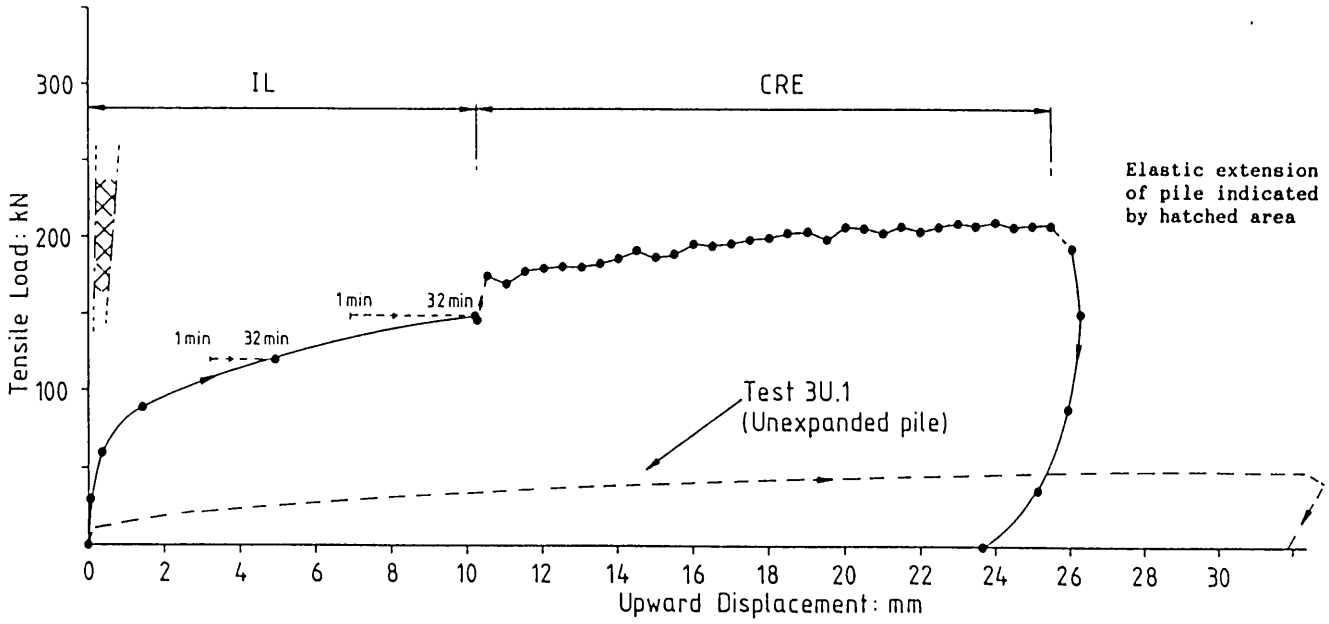

Figure 4.50
Results of Pile Test 3B.1

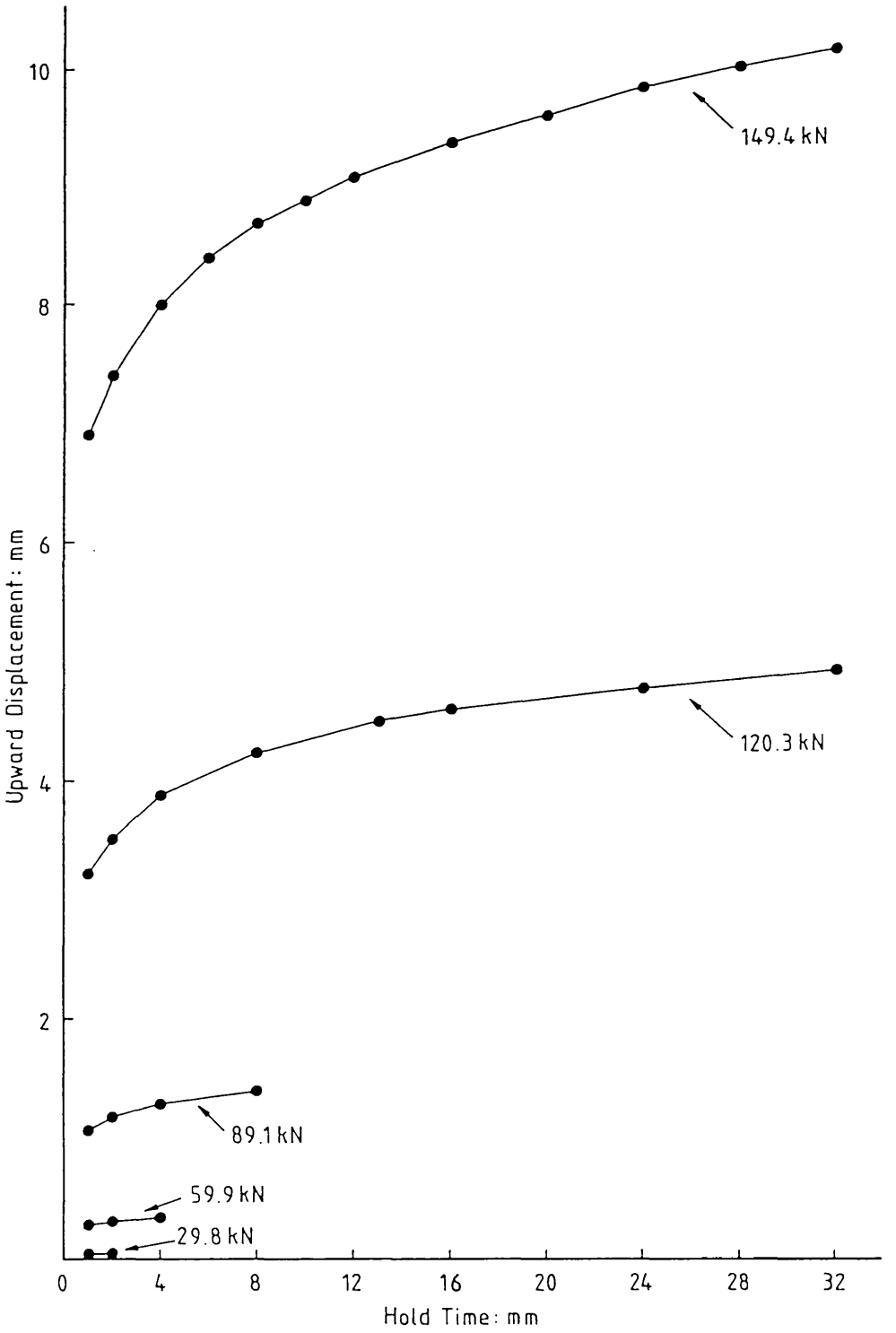

Figure 4.51 Pile Test 3B.1:
Creep behaviour during IL stage

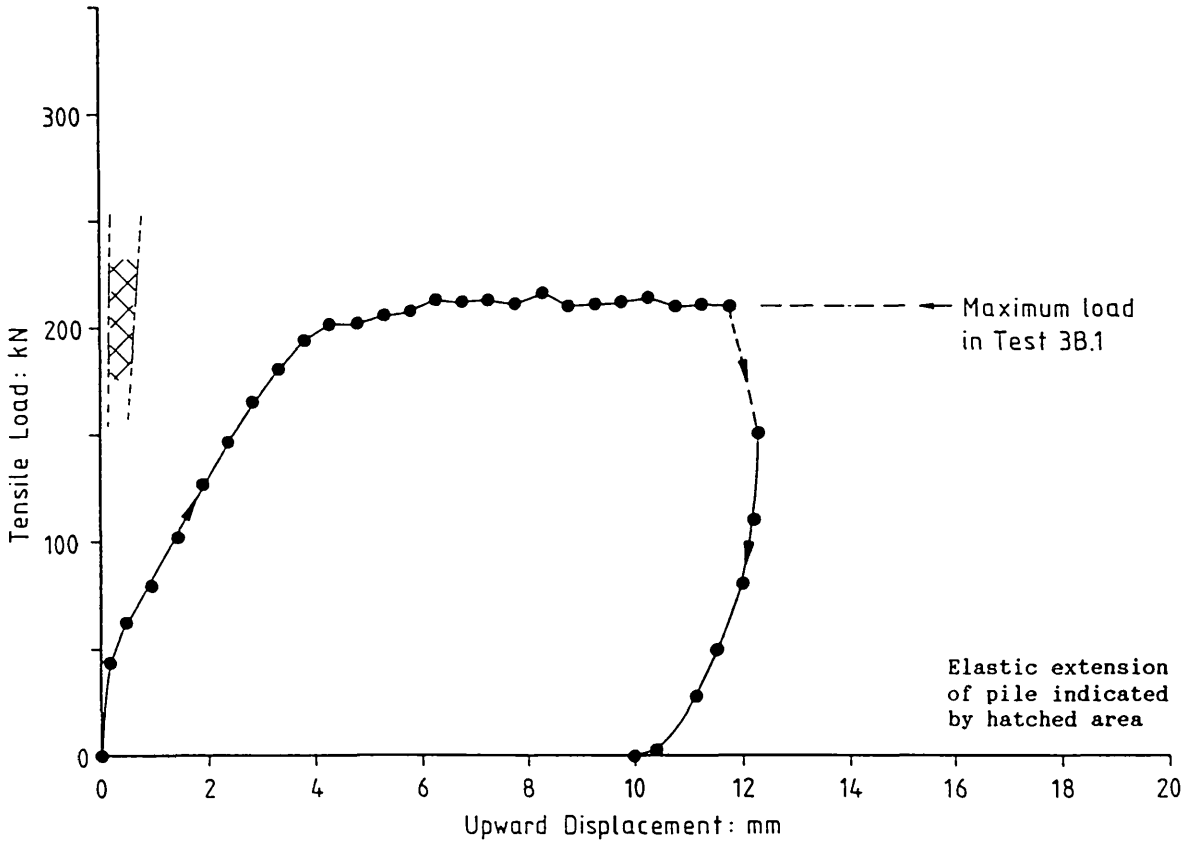

TEST 3B.2 Type: CRE Date: 26.3.86

Outer shell driven: 4.10.85 Expander mandrel driven: 20.11.85
Days elapsed
prior to test: 173 126

Shaft areas: (m^2)
Embedded length,
Full X-section (A): 2.65
Reduced X-section (B): 2.06
Expanded length,
Full X-section (C): 2.38
Reduced X-section (D): 1.85

Pile weight: 6.6 (kN)

Test Stage	Maximum Load (Gross) (kN)	Maximum Load (Net) (kN)	Shaft Frictions (A) (kPa)	(B) (kPa)	(C) (kPa)	(D) (kPa)	Displacement at: Max. Load (mm)	End of stage (mm)
CRE	216.6	210.0	79.4	102.0	88.4	113.6	8.3	10.0

Figure 4.52 Results of Pile Test 3B.2

TEST 4A.1 Type: IL, CRE Date: 16.10.85

Outer shell driven: 4.10.85 Expander mandrel driven: 7.10.85
Days elapsed
prior to test: 12 9

Shaft areas: (m^2)
Embedded length,
Full X-section (A): 2.35
Reduced X-section (B): 2.06
Expanded length,
Full X-section (C): 2.14
Reduced X-section (D): 1.87

Pile weight: 3.9 (kN)

Test Stage	Maximum Load (Gross) (kN)	(Net) (kN)	Shaft Frictions (A) (kPa)	(B) (kPa)	(C) (kPa)	(D) (kPa)	Displacement at: Max. Load (mm)	End of stage (mm)
IL	125.3	-	-	-	-	-	2.7	2.2
CRE	304.4	300.5	127.8	146.0	140.7	160.8	19.5	36.0

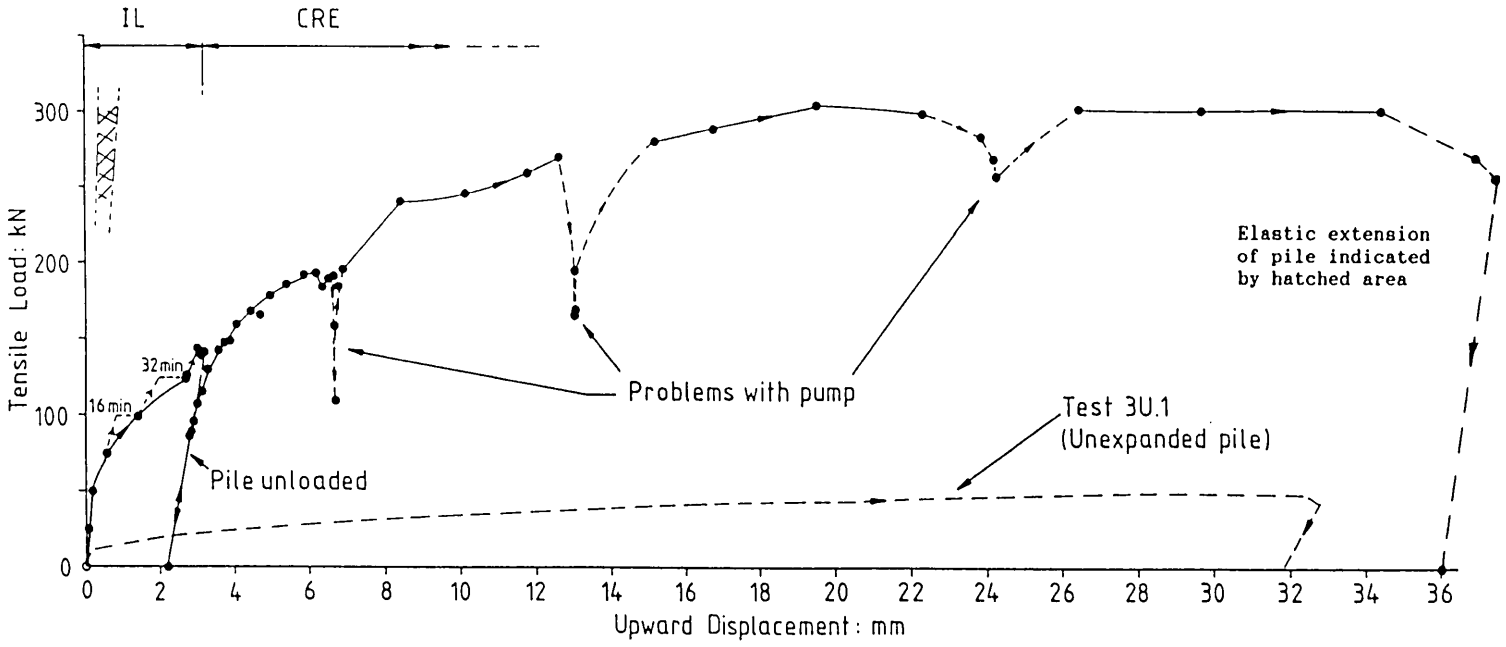

Figure 4.53
Results of Pile Test 4A.1

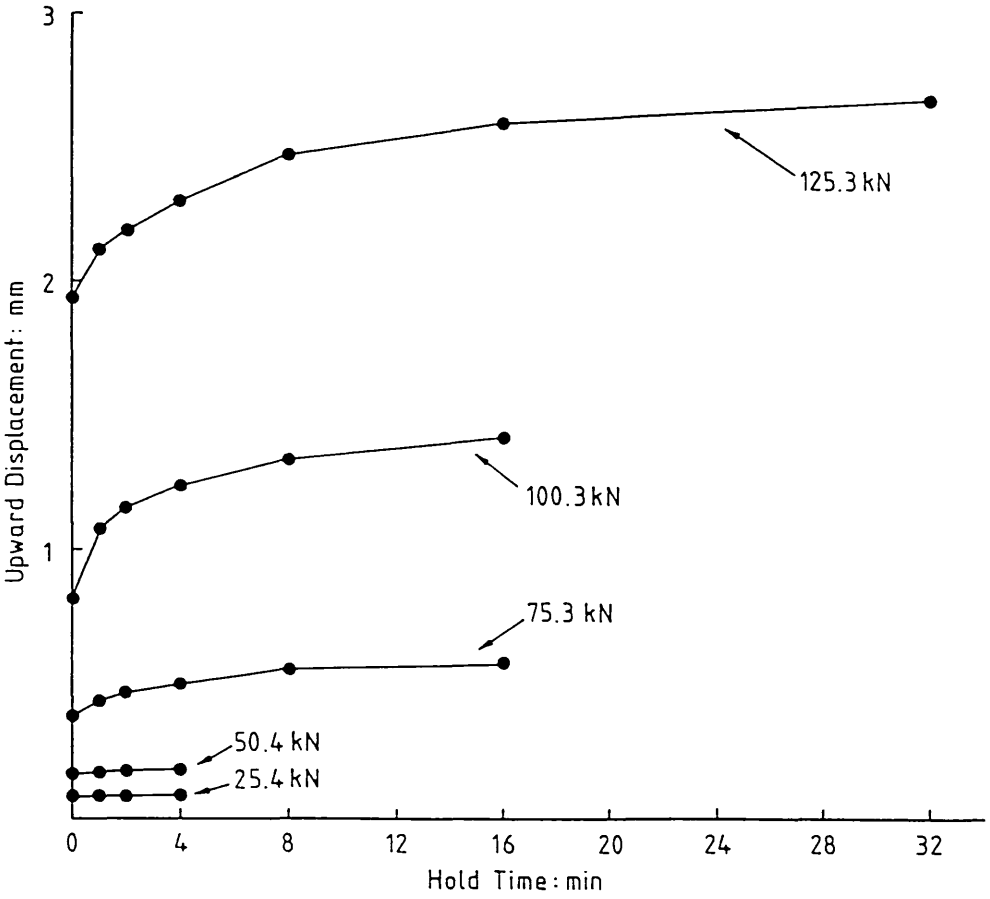

Figure 4.54 Pile Test 4A.1:
Creep behaviour during IL stage

TEST 4A.2 Type: Cyclic, CRE Date: 31.10 - 1.11.85

Outer shell driven: 4.10.85 Expander mandrel driven: 7.10.85

Days elapsed prior to test: 27 24

Shaft areas (m^2): Embedded length, Full X-section (A): 2.35; Reduced X-section (B): 2.06. Expanded length, Full X-section (C): 2.14; Reduced X-section (D): 1.87

Pile weight: 3.9 (kN)

Test Stage	Maximum Load (Gross) (kN)	Maximum Load (Net) (kN)	Shaft Frictions (A) (kPa)	(B) (kPa)	(C) (kPa)	(D) (kPa)	Displacement at: Max. Load (mm)	Displacement at: End of stage (mm)
Cyclic[1]	-	-	-	-	-	-	-	25.6
CRE	127.4	123.5[2]	52.5	60.0	57.8	66.1	35.7	34.7

Notes:
1. 20 cycles 1kN - 150kN
   30 cycles 1kN - 121kN
2. Failed at cycling load

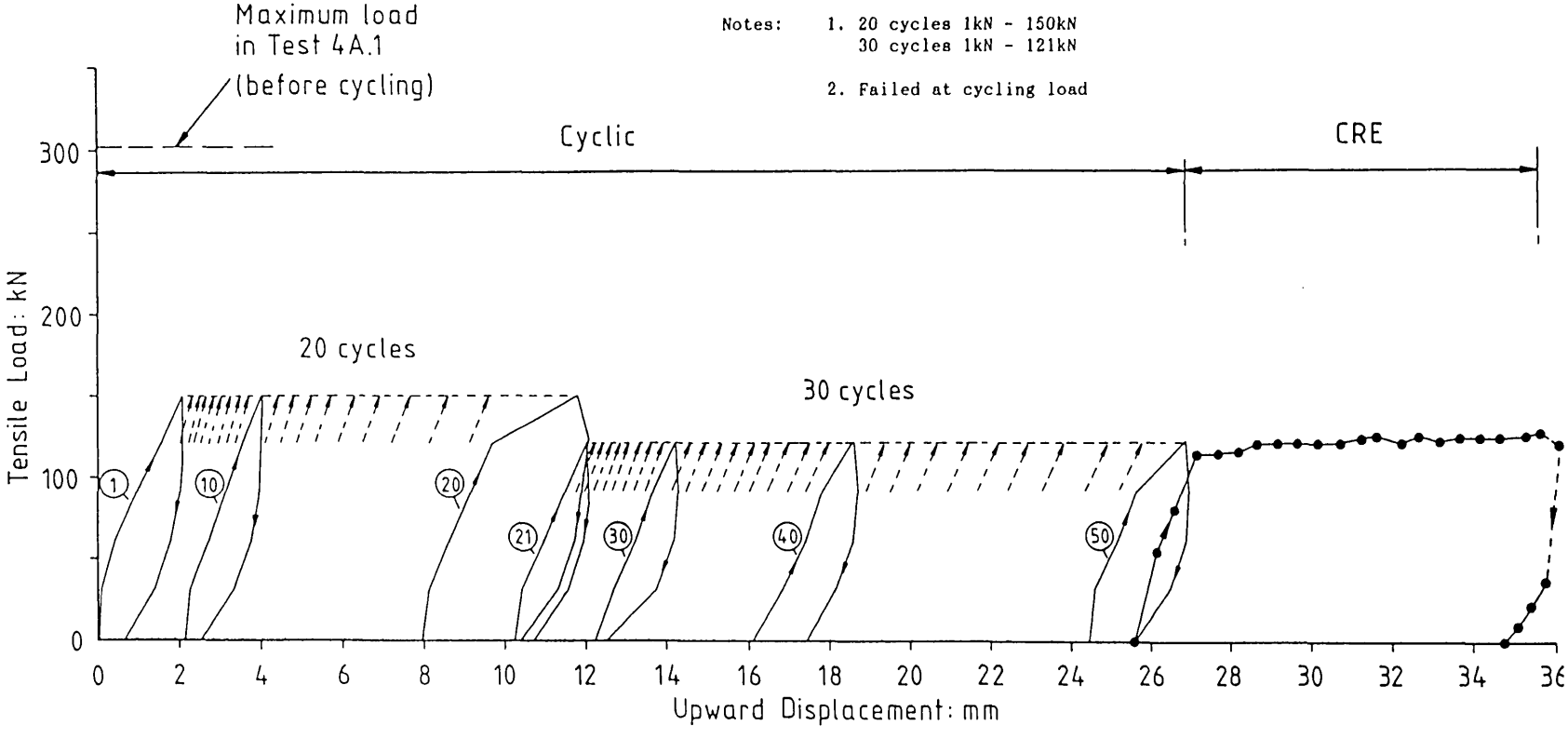

Figure 4.55 Results of Pile Test 4A.2

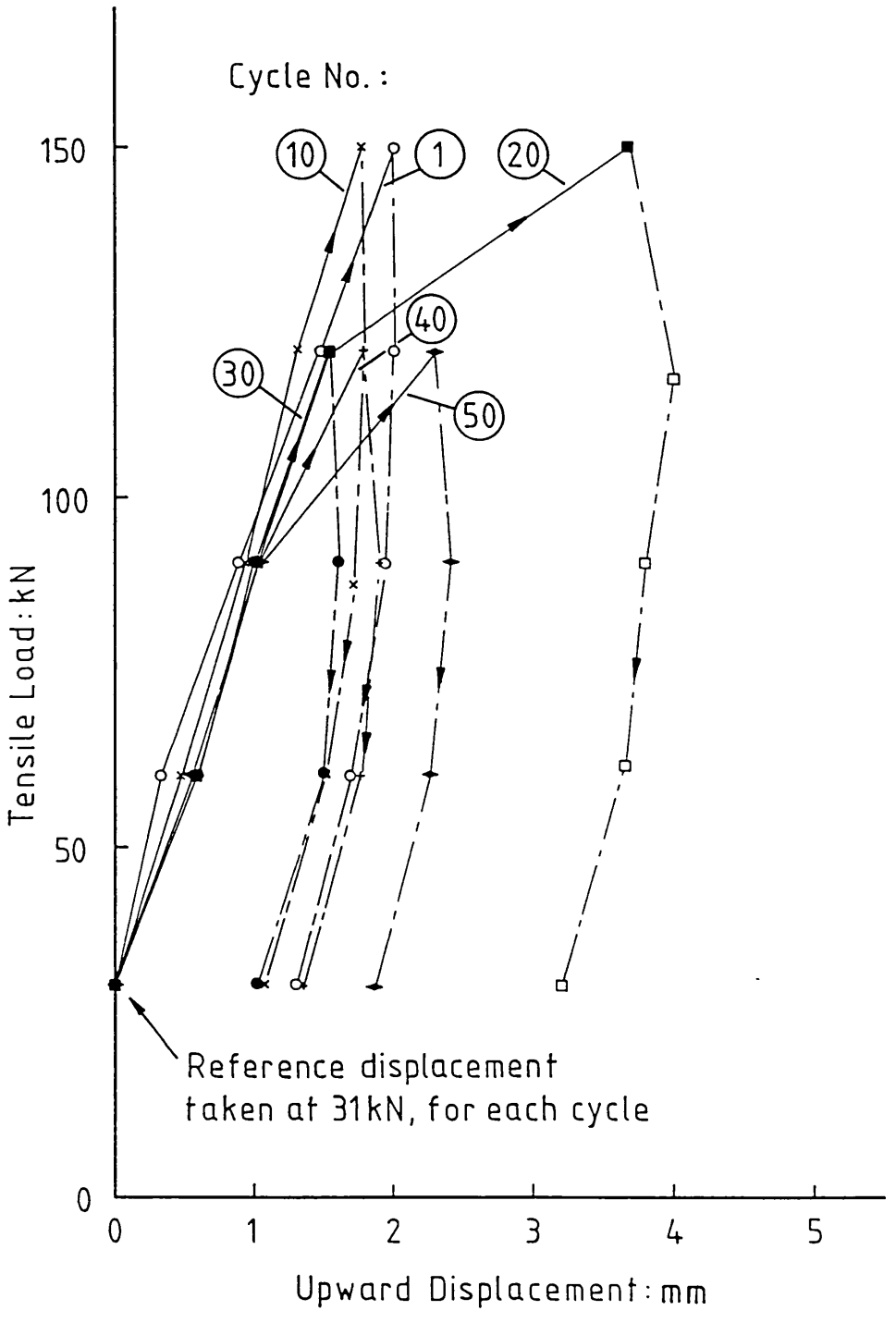

Figure 4.56 Pile Test 4A.2:
Load:displacement behaviour during cyclic loading

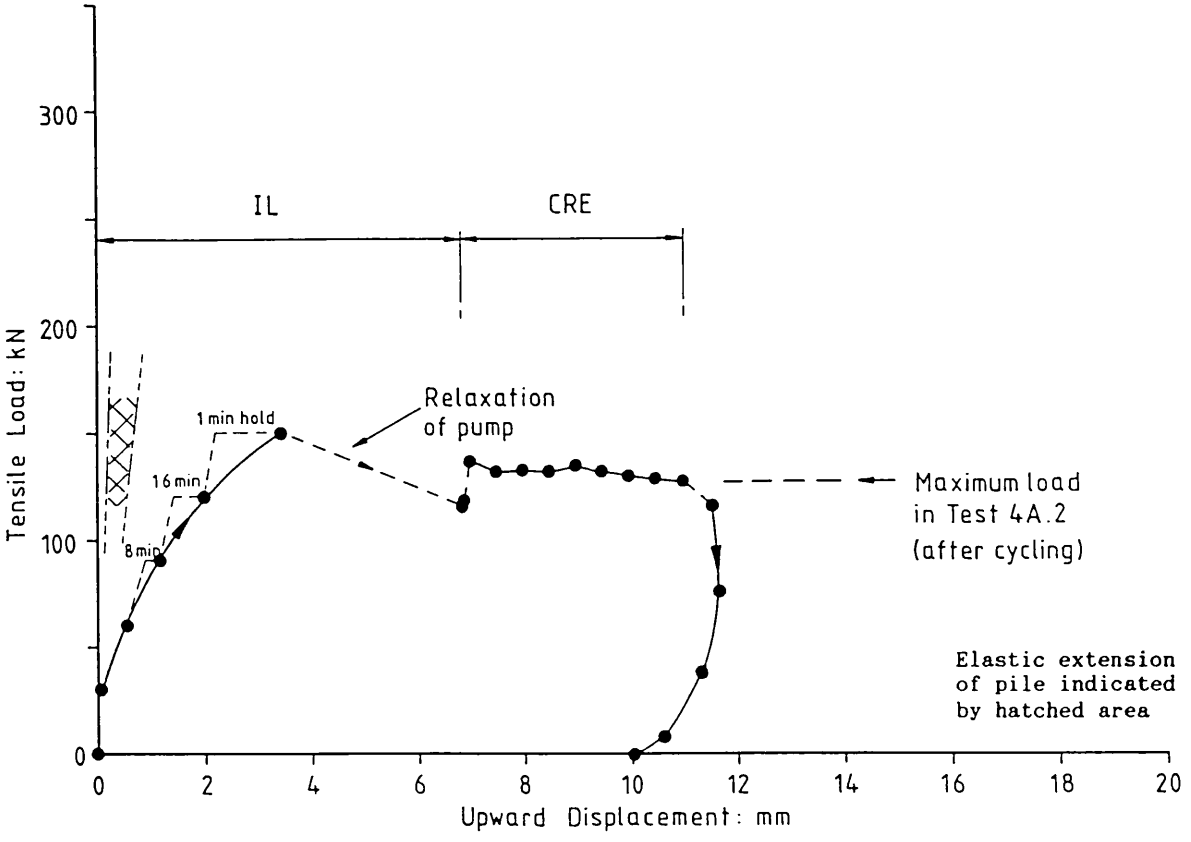

TEST 4A.3 Type: IL, CRE Date: 25.3.86

Outer shell driven: 4.10.85 Expander mandrel driven: 7.10.85

Days elapsed prior to test: 172 169

Shaft areas (m^2): Embedded length, Full X-section (A): 2.35; Reduced X-section (B): 2.06; Expanded length, Full X-section (C): 2.14; Reduced X-section (D): 1.87

Pile weight (kN): 3.9

Test Stage	Maximum Load (Gross) (kN)	Maximum Load (Net) (kN)	Shaft Frictions (A) (kPa)	(B) (kPa)	(C) (kPa)	(D) (kPa)	Displacement at: Max. Load (mm)	End of stage (mm)
IL	150.9	-	-	-	-	-	3.4	3.4
CRE	137.3	133.4	56.7	64.8	62.5	71.4	6.9	10.0

Figure 4.57 Results of Pile Test 4A.3

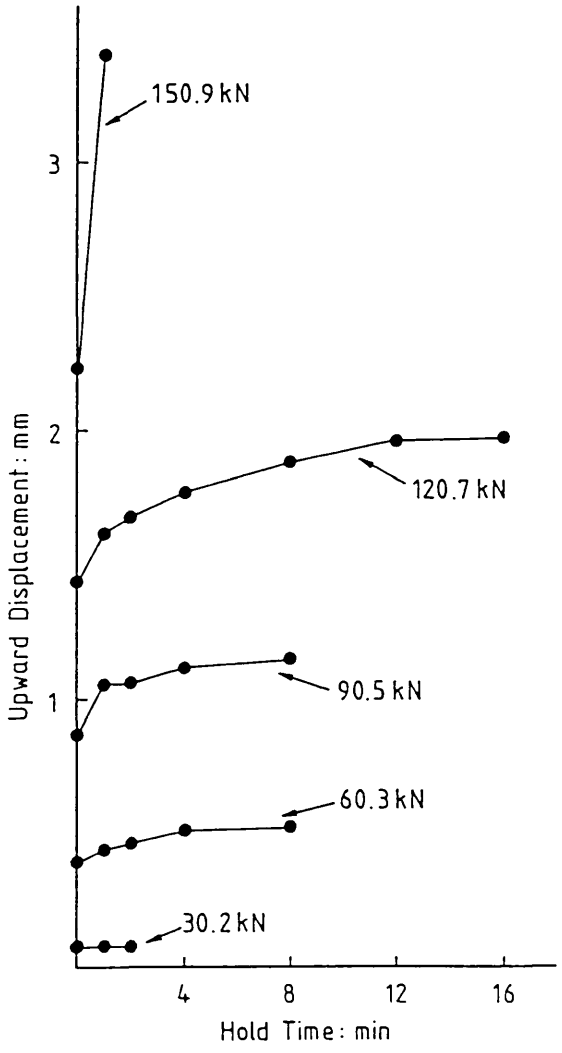

Figure 4.58 Pile Test 4A.3:
Creep behaviour during IL stage

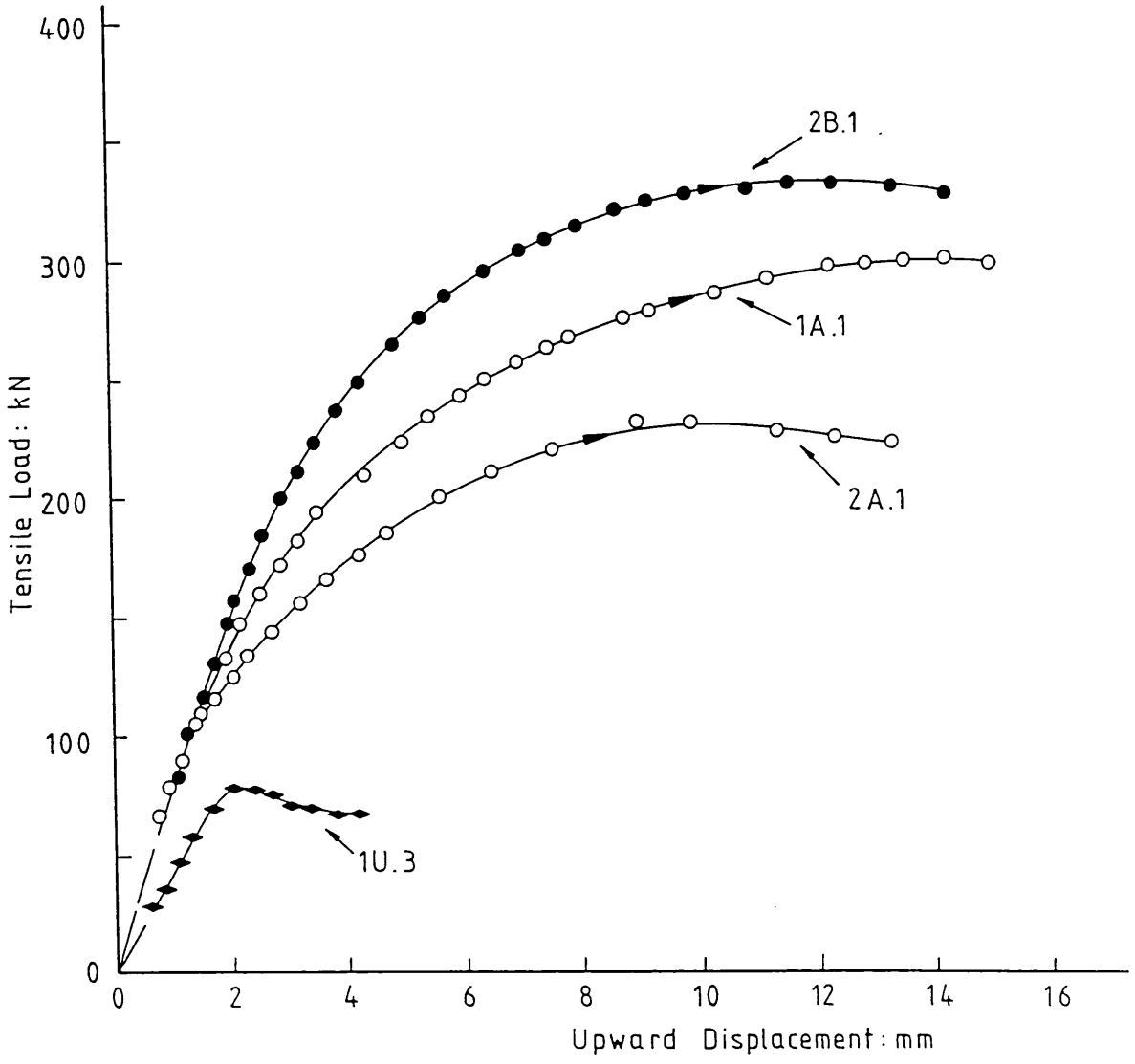

Pile No.	% expansion width	% expansion X-area	Test No.	Max. Load (Gross) (kN)	Shaft friction (A) (kPa)	Shaft friction (D) (kPa)	Factor of increase (Max. load)	Factor of increase (Shaft friction)
1U	-	-	1U.2	66.4	24.0	-	-	-
			1U.3	79.1	28.8	-	0.0	0.0
1A	14.3	30.6	1A.1	302.8	98.5	141.3	3.83	3.42 - 4.91
2A	14.3	30.6	2A.1	232.7	74.1	106.9	2.94	2.57 - 3.71
2B	21.4	47.4	2B.1	335.0	100.9	154.7	4.23	3.50 - 5.37

Figure 4.59 Summary of initial loadings of Box Piles

Pile No.	% expansion (width)	% expansion (X-area)	Test No.	Max. Load (Gross) (kN)	Shaft friction (A) (kPa)	Shaft friction (D) (kPa)	Factor of increase (Max. load)	Factor of increase (Shaft friction)
3U	-	-	3U.1	50.4	23.3	-	0.0	0.0
4A	10.7	35.7	4A.1	304.4	127.8	160.8	6.04	5.48 - 6.90
3B	21.4	75.0	3B.1	210.8	77.2	110.5	4.18	3.31 - 4.74

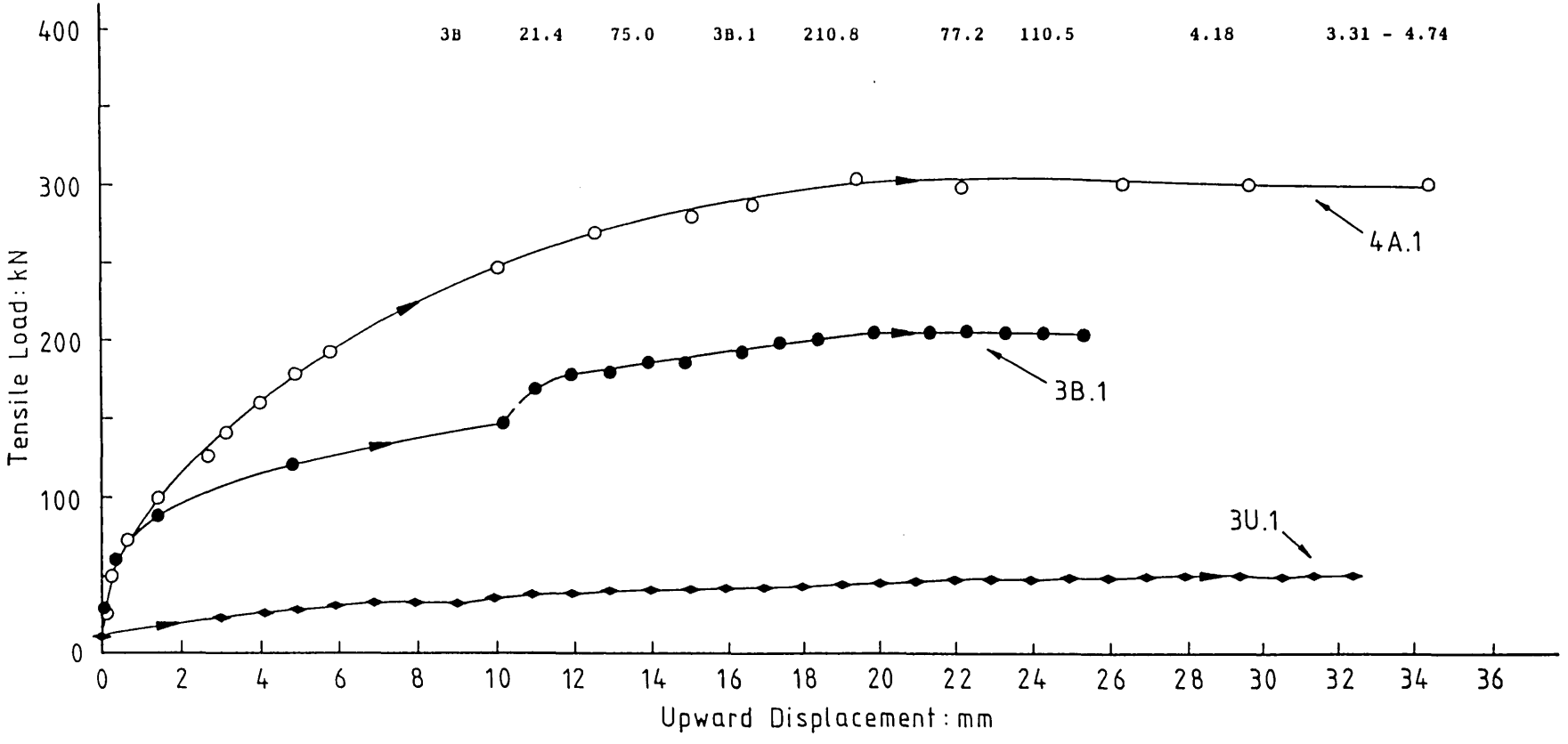

Figure 4.60 Summary of initial loadings of cruciform piles

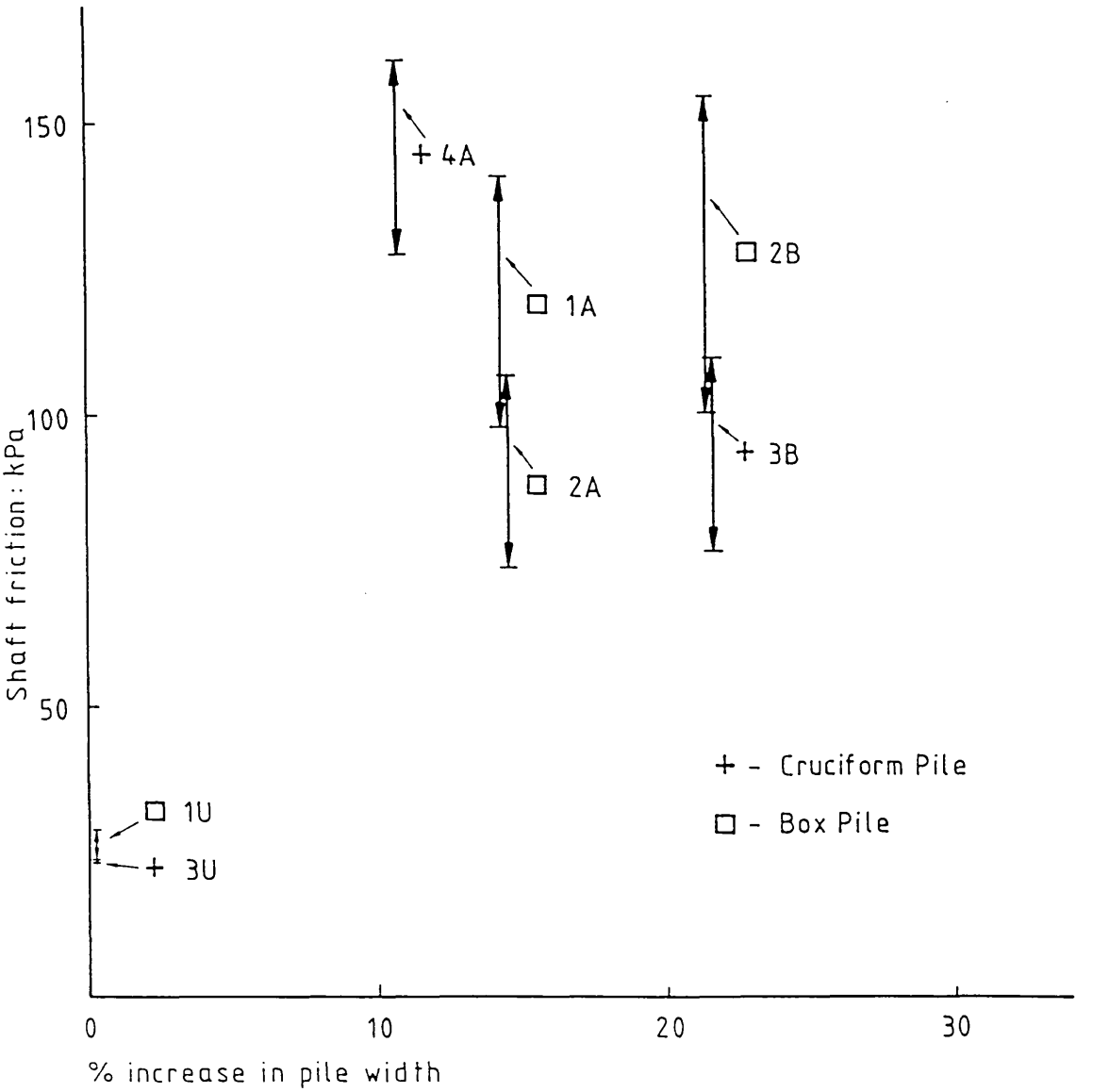

Figure 4.61 Deduced average pile shaft frictions against percentage increase in pile width

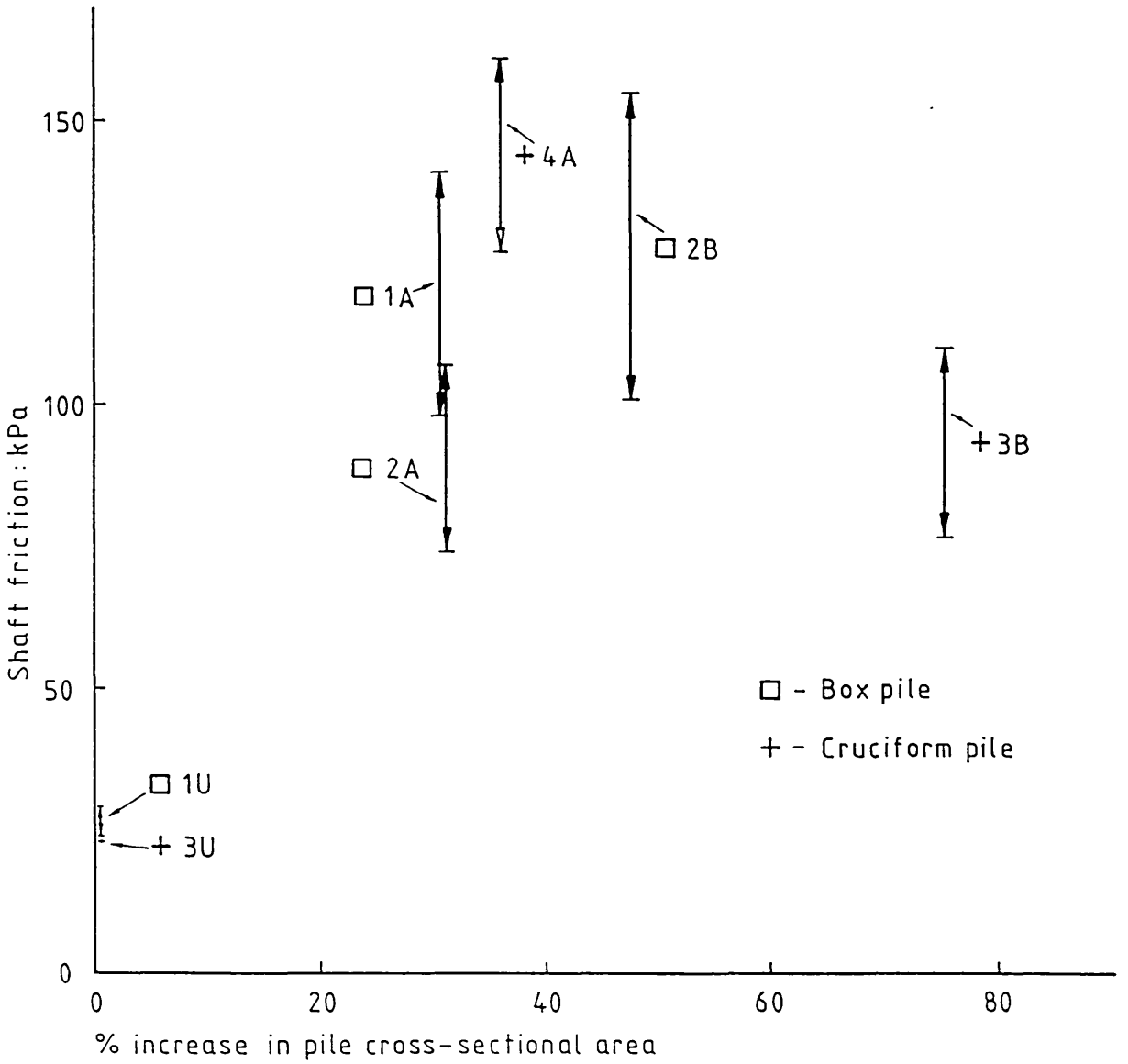

Figure 4.62 Deduced average shaft frictions against percentage increase in pile cross-sectional area

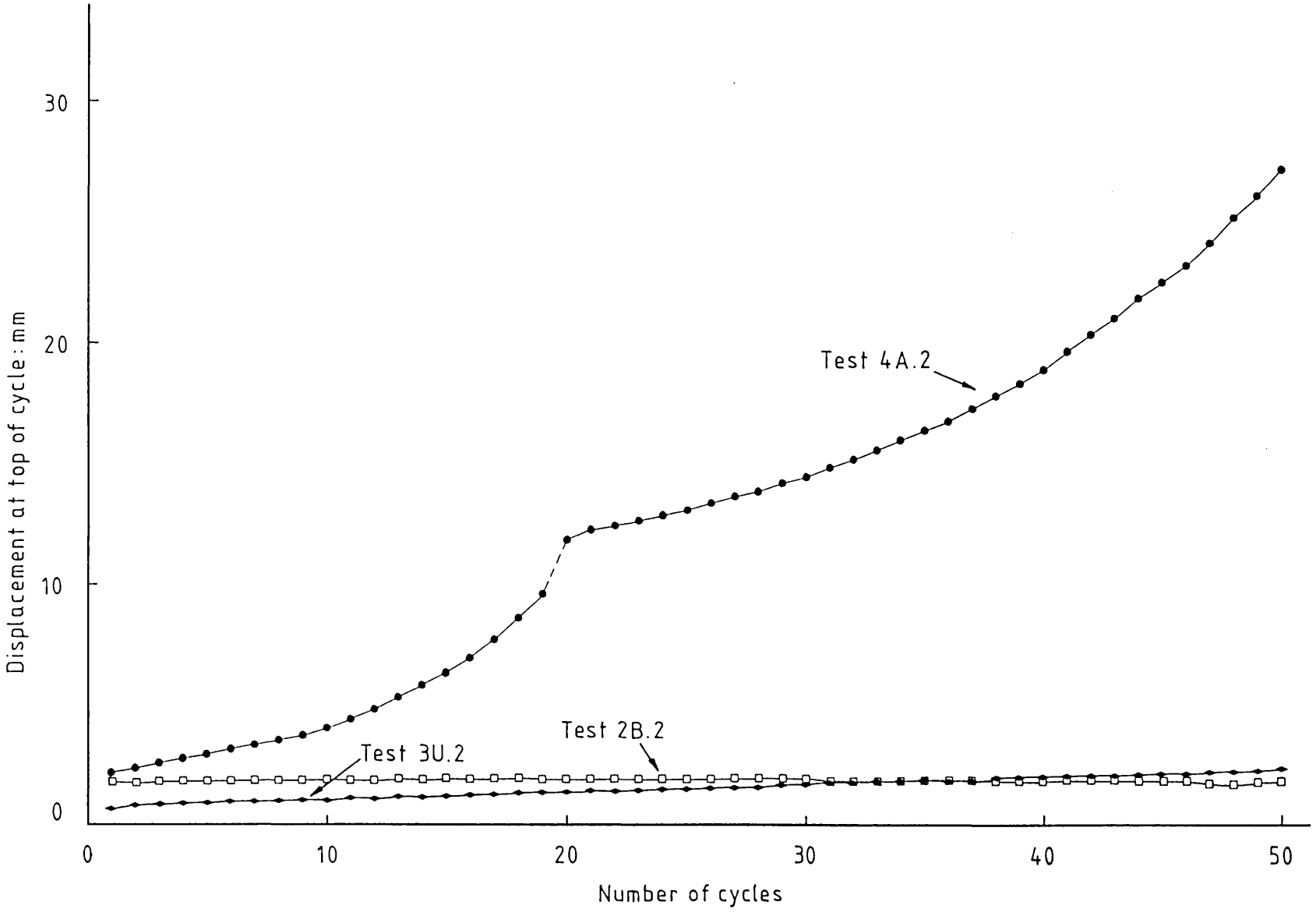

Figure 4.63 Performance of piles under cyclic loading

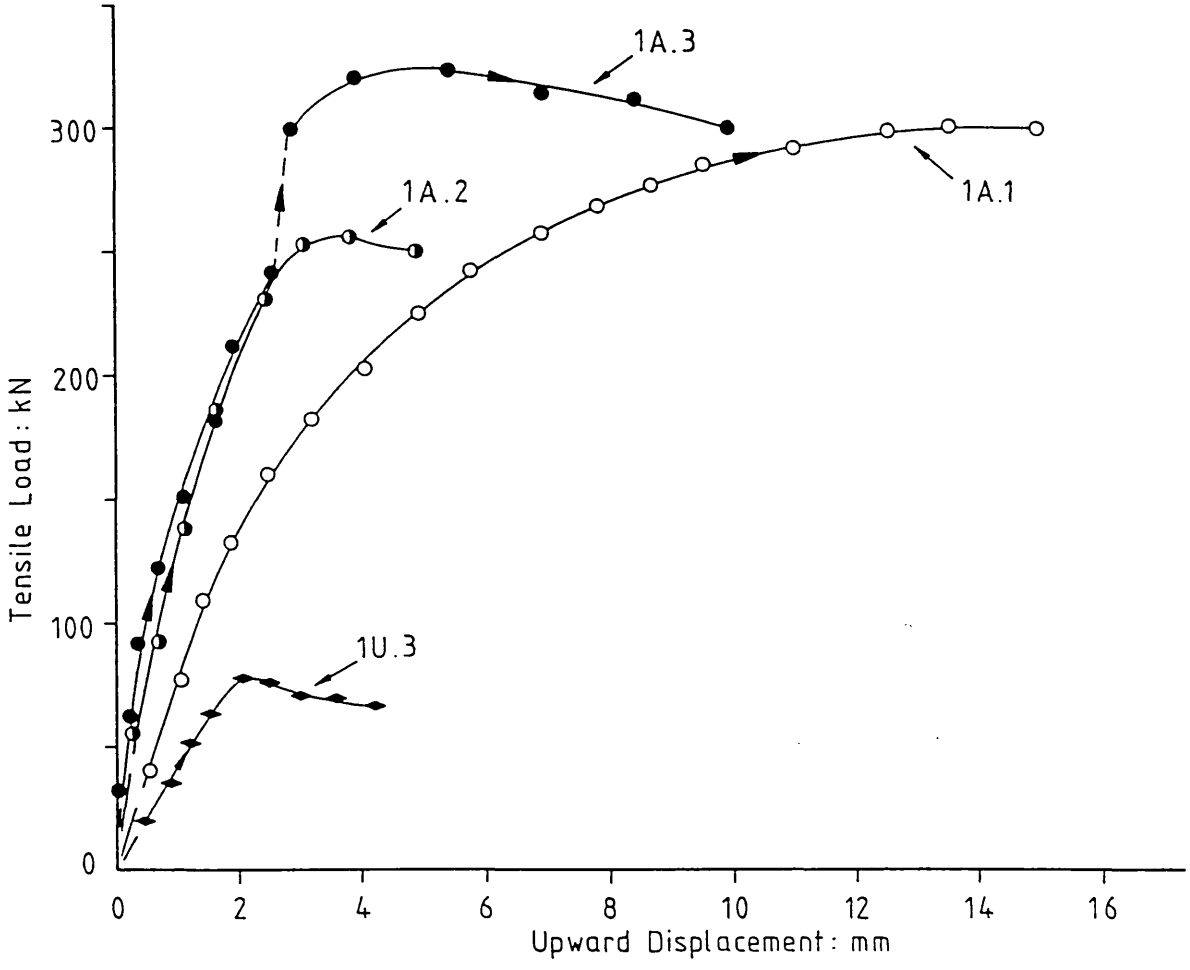

Figure 4.64 Summary of tests on Pile 1

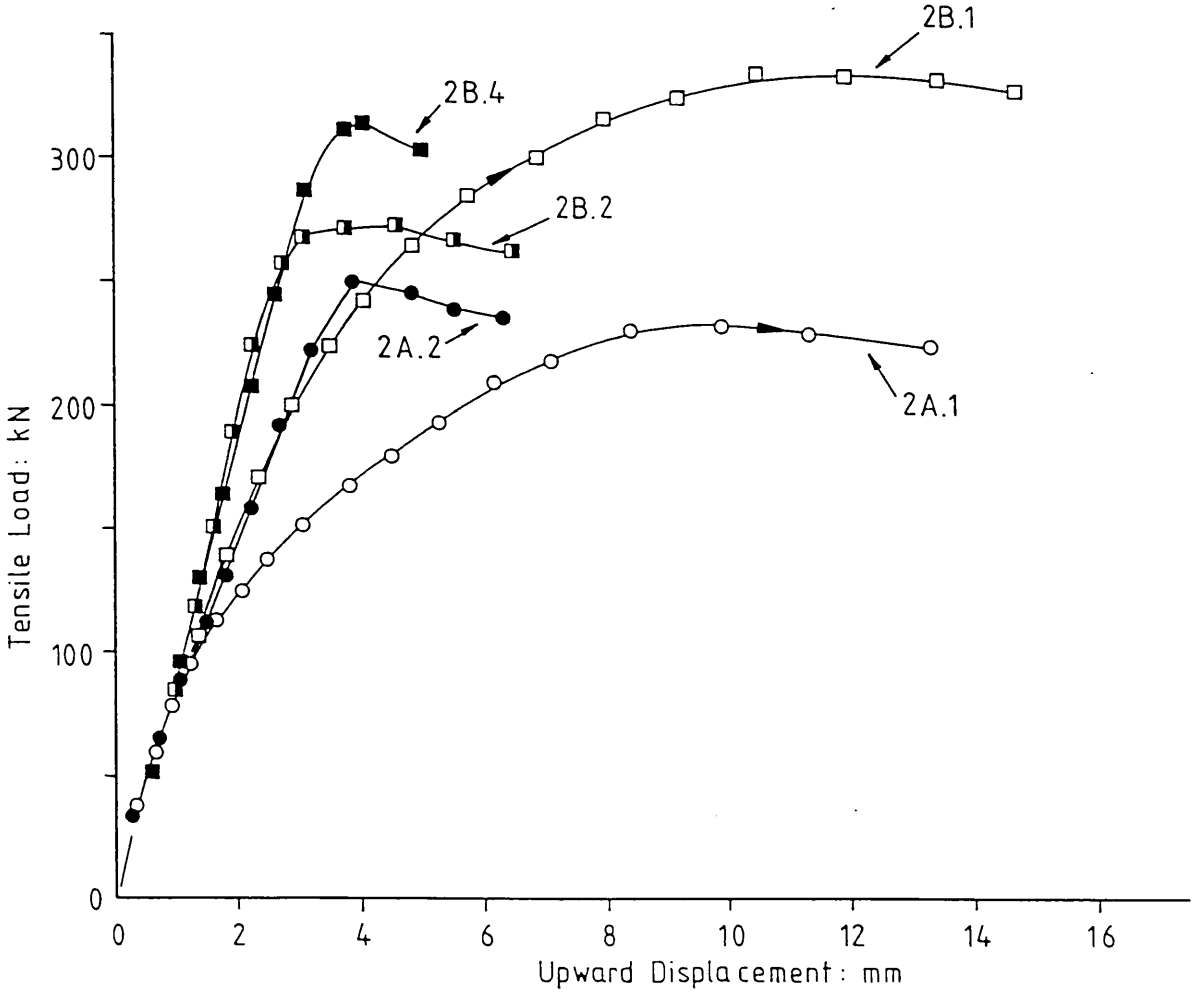

Figure 4.65 Summary of tests on Pile 2

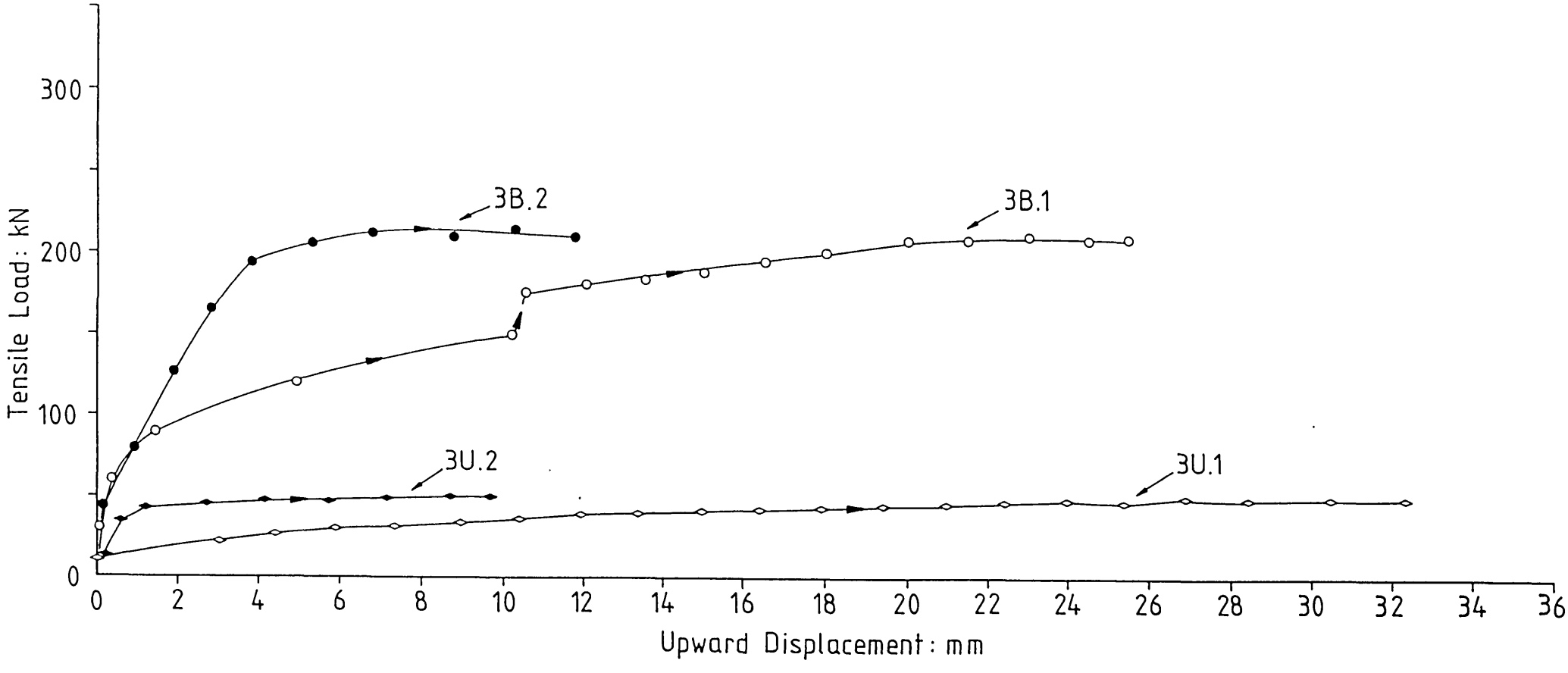

Figure 4.66 Summary of tests on Pile 3

Test No.	Depth (m)	Strain (%)	Arm No.	$\Delta\epsilon$ (%)	Δp (kPa)	Gur (arm) (MPa)	Gur (ave) (MPa)
1	3.5	18.2	1	0.087	85.6	49.2	
			2	0.064	85.1	66.5	63.5
			3	0.050	74.8	74.8	
2	5.5	5.1	1	0.032	173.4	270.9	
			2	0.069	173.0	125.4	165.3
			3	0.087	173.1	99.5	
3	7.0	5.4	1	0.073	208.6	142.9	
			2	0.100	208.1	104.1	113.9
			3	0.110	208.1	94.6	

Table 4.1 Values of shear modulus G_{ur} deduced from FPDM tests

Pile 1U

Outer shell driven: 27. 3.85 Expander mandrel driven: -

Shaft areas: (m^2)
Embedded length,
Full X-section (A): 2.65
Reduced X-section (B): -
Expanded length,
Full X-section (C): -
Reduced X-section (D): -

Pile weight: 2.7 (kN)

Test No.	Date	Days elapsed since driving: Shell	Mandrel	Test Stage	Maximum Load (Gross) (kN)	(Net) (kN)	Shaft Frictions (A) (kPa)	(B) (kPa)	(C) (kPa)	(D) (kPa)	Displacement at: Max. Load (mm)	End of stage (mm)
1U.1	2. 4.85	6	-	CRE	73.5	70.8	26.7	-	-	-	2.4	10.8
1U.2	2. 4.85	6	-	CRE	66.4	63.7	24.0	-	-	-	1.8	2.7
1U.3	16. 4.85	20	-	CRE	79.1	76.4	28.8	-	-	-	2.1	4.2

Notes:

Table 4.2 Summary of tests: Pile configuration 1U

Pile 1A

Outer shell driven: 27. 3.85 Expander mandrel driven: 17.4.85

Shaft areas: (m^2)	Embedded length,		Expanded length,	
	Full X-section (A):	3.03	Full X-section (C):	2.41
	Reduced X-section (B):	2.65	Reduced X-section (D):	2.11

Pile weight: 4.6 (kN)

Test No.	Date	Days elapsed since driving:		Test Stage	Maximum Load (Gross)	(Net)	Shaft Frictions (A)	(B)	(C)	(D)	Displacement at: Max. Load	End of stage
		Shell	Mandrel		(kN)	(kN)	(kPa)	(kPa)	(kPa)	(kPa)	(mm)	(mm)
1A.1	22. 4.85	26	5	CRE	302.8	298.2	98.5	112.6	123.6	141.3	14.0	14.9
1A.2	22. 4.85	26	5	Cyclic[1]	-	-	-	-	-	-	-	-
				CRE	256.0	251.4	83.1	94.9	104.2	119.1	3.6	4.9
1A.3	1.11.85	218	198	IL	241.2	-	-	-	-	-	2.6	2.6
				CRE	322.3	317.7	105.0	119.9	131.7	150.5	5.4	7.9

Notes: 1. 25 cycles, 15kN (approx) - 150kN.

Table 4.3 Summary of tests: Pile configuration 1A

Pile 2A

Outer shell driven: 28. 3.85 Expander mandrel driven: 28. 3.85

Shaft areas: (m^2)

Embedded length,			Expanded length,		
Full X-section	(A):	3.08	Full X-section	(C):	2.44
Reduced X-section	(B):	2.69	Reduced X-section	(D):	2.13

Pile weight: 4.6 (kN)

Test No.	Date	Days elapsed since driving: Shell	Mandrel	Test Stage	Maximum Load (Gross) (kN)	(Net) (kN)	Shaft Frictions (A) (kPa)	(B) (kPa)	(C) (kPa)	(D) (kPa)	Displacement at: Max. Load (mm)	End of stage (mm)
2A.1	2. 4.85	5	5	CRE	232.7	228.1	74.1	84.7	93.6	106.9	9.0	13.3
2A.2	16. 4.85	19	19	CRE	249.7	245.1	79.6	91.0	100.5	114.9	3.9	6.3

Notes:

Table 4.4 Summary of tests:
Pile configuration 2A

Pile 2B

Outer shell driven: 28. 3.85 Expander mandrel driven: 17. 4.85

Shaft areas: (m^2)

Embedded length,			Expanded length,		
Full X-section	(A):	3.27	Full X-section	(C):	2.59
Reduced X-section	(B):	2.69	Reduced X-section	(D):	2.13

Pile weight: 4.8 (kN)

Test No.	Date	Days elapsed since driving: Shell	Mandrel	Test Stage	Maximum Load (Gross) (kN)	(Net) (kN)	Shaft Frictions (A) (kPa)	(B) (kPa)	(C) (kPa)	(D) (kPa)	Displacement at: Max. Load (mm)	End of stage (mm)
2B.1	22. 4.85	25	5	CRE	335.0	330.2	100.9	122.6	127.4	154.7	10.4	14.6
2B.2	23. 4.85	26	6	Cyclic[1]	-	-	-	-	-	-	-	-
				CRE	272.6	267.8	81.9	99.4	103.4	125.5	4.6	6.4
2B.3	7. 5.85	40	20	CRE	306.9	302.1	92.4	112.1	116.6	141.6	4.0	5.7
2B.4	5. 8.85	130	110	CRE	314.2	309.4	94.6	114.8	119.4	145.0	4.1	5.0
2B.5	6.11.85	223	203	IL	271.8	-	-	-	-	-	5.3	5.3
				CRE	263.5	258.7	79.1	96.0	99.8	121.2	7.6	11.0

Notes: 1. 50 cycles, 21kN (approx) - 171kN

Table 4.5 Summary of tests: Pile configuration 2B

Pile 3U

Outer shell driven: 4.10.85 Expander mandrel driven: -

Shaft areas: (m^2) Embedded length, Full X-section (A): 2.06 Reduced X-section (B): -
Expanded length, Full X-section (C): - Reduced X-section (D): -

Pile weight: 2.4 (kN)

Test No.	Date	Days elapsed since driving: Shell	Mandrel	Test Stage	Maximum Load (Gross) (kN)	(Net) (kN)	Shaft Frictions (A) (kPa)	(B) (kPa)	(C) (kPa)	(D) (kPa)	Displacement at: Max. Load (mm)	End of stage (mm)
3U.1	16.10.85	12	-	IL	21.4	-	-	-	-	-	3.0	3.0
				CRE	50.4	48.0	23.3	-	-	-	31.4	31.8
3U.2	31.10.85	27	-	Cyclic[1]	-	-	-	-	-	-	-	1.9
				CRE	51.2	48.8	23.7	-	-	-	10.7	11.1

Notes: 1. 50 cycles 1kN - 25kN

Table 4.6 Summary of tests: Pile configuration 3U

Pile 3B

Outer shell driven: 4.10.85 Expander mandrel driven: 20.11.85

Shaft areas: (m^2)

Embedded length,			Expanded length,		
Full X-section	(A):	2.65	Full X-section	(C):	2.38
Reduced X-section	(B):	2.06	Reduced X-section	(D):	1.85

Pile weight: 6.6 (kN)

Test No.	Date	Days elapsed since driving:		Test Stage	Maximum Load (Gross)	Maximum Load (Net)	Shaft Frictions (A)	(B)	(C)	(D)	Displacement at: Max. Load	End of stage
		Shell	Mandrel		(kN)	(kN)	(kPa)	(kPa)	(kPa)	(kPa)	(mm)	(mm)
3B.1	2.12.85	12	9	IL	149.4	-	-	-	-	-	10.2	10.2
				CRE	210.8	204.2	77.2	99.2	85.9	110.5	24.0	23.7
3B.2	26. 3.86	173	126	CRE	216.6	210.0	79.4	102.0	88.4	113.6	8.3	10.0

Notes:

Table 4.7 Summary of tests: Pile configuration 3B

Pile 4A

Outer shell driven: 4.10.85 Expander mandrel driven: 7.10.85

Shaft areas: (m^2)

Embedded length,	Full X-section	(A):	2.35	Expanded length, Full X-section	(C): 2.14
	Reduced X-section	(B):	2.06	Reduced X-section	(D): 1.87

Pile weight: 3.9 (kN)

Test No.	Date	Days elapsed since driving: Shell	Mandrel	Test Stage	Maximum Load (Gross) (kN)	(Net) (kN)	Shaft Frictions (A) (kPa)	(B) (kPa)	(C) (kPa)	(D) (kPa)	Displacement at: Max. Load (mm)	End of stage (mm)
4A.1	16.10.85	12	9	IL	125.3	-	-	-	-	-	2.7	2.2
				CRE	304.4	300.5	127.8	146.0	140.7	160.8	19.5	36.0
4A.2	31.10 - 1.11.85	27	24	Cyclic[1]	-	-	-	-	-	-	-	25.6
				CRE	127.4	123.5[2]	52.5	60.0	57.8	66.1	35.7	34.7
4A.3	25. 3.86	172	169	IL	150.9	-	-	-	-	-	3.4	3.4
				CRE	137.3	133.4	56.7	64.8	62.5	71.4	6.9	10.0

Notes: 1. 20 cycles 1kN - 150kN.
30 cycles 1kN - 121kN.

2. Failed at cycling load.

Table 4.8 Summary of tests: Pile configuration 4A

Pile	Date of expander mandrel extraction	Days in place	Initial peak load	Steady load	Previous Pile Test		Steady load / Prev. Max.	Derived μ Shell/Mandrel
					Test No.	Maximum load		
			(kN)	(kN)		(kN)		
1A	12.11.85	239	195	93	1A.3	322	0.29	0.20
2A	16. 4.85	19	94	86	2A.2	250	0.34	0.23
2B	11.11.85	208	166	68	2B.5	264	0.26	0.18
4A	26. 3.86	170	-[1]	-	4A.3	137	-	-

Notes: 1. The expander mandrel and outer shell started to be pulled from the ground together, when the load applied to the expander mandrel was in the region of the maximum load recorded during the pile test the day before extraction.

Table 4.9 Details of pile extraction

Pile configuration	X-sectional areas of steel:			Embedded portion of pile				Exposed portion of pile	
				Lengths		Displacements[3]		Length[4]	Displacement[5]
	Shell	Mandrel	Shell+Mandrel	Shell	Shell+Mandrel[2]	Lower bound	Upper bound		
	(mm^2)	(mm^2)	(mm^2)	(mm)	(mm)	(mm $x10^{-3}$)	(mm $x10^{-3}$)	(mm)	(mm $x10^{-3}$)
1U	5240	-	-	4730	-	2.15P	2.87P	790	0.72P
1A	5240	4190	9430	4730	4600	1.16P	2.87P	790	0.72P
2A	5240	4190	9430	4810	4660	1.18P	2.91P	710	0.65P
2B	5240	4510	9750	4810	4660	1.14P	2.91P	710	0.65P
3U	5240	-	-	4900	-	2.23P	2.97P	200	0.18P
3B	5240	8700	13940	4900	4800	0.82P	2.97P	200	0.18P
4A	5240	4050	9290	4900	4775	1.22P	2.97P	200	0.18P

Notes:

1. For further details of pile dimensions and depths of embedments see Figures 4.18 and 4.19.

2. Depth of embedment in this case taken as the average of the embedment depths for the outer shell and the expander mandrel.

3. For lower bound, displacement = $\frac{L \times P}{2AE}$

   where: A = X-sect. area of outer shell + expander mandrel.
   L = Embedded length of outer shell + expander mandrel.
   P = Applied load.
   Uniform distribution of shaft resistance assumed.

   For upper bound, displacement = $\frac{2L \times P}{3AE}$

   where: A = X-sect. area of outer shell.
   L = Embedded length of outer shell.
   P = Applied load.
   Triangular distribution of load assumed.

   (Ref: Hobbs and Healy, 1979)

4. Exposed lengths taken as

   (a) Piles 1 and 2: Distance between bottom of pitching hole and bottom of pile lifting lug.

   (b) Piles 3 and 4: Distance between bottom of pitching hole and dial gauge reference plates. (Also applies to pile tests 1B.4 and 2B.6).

5. Displacement = $\frac{L \times P}{AE}$

   where: A = X-Sect. area of outer shell.
   L = Exposed length of outer shell.
   P = Applied load.

Table 4.10 Elastic displacements of piles under load

CHAPTER 5
INVESTIGATIONS AT BRS SITE

5.1 Introduction

This Chapter reports investigations performed a in stiff boulder clay profile at the Building Research Station (BRS) in Hertfordshire. Expanded and unexpanded steel wedge-piles were tested over periods of up to ten months. The pile testing was complemented by in-situ tests with various instruments.

The extensive geotechnical testing that has previously been carried out at the BRS site is summarised in Section 5.2. Details of the additional soil testing undertaken as part of the current research are given in Section 5.3. Details of the pile configurations tested at the BRS site are provided in Section 5.4, information on installation is given in Section 5.5, and the pile test results are provided in Section 5.6. A summary of the main findings of the investigations is given in Section 5.7.

The results from this Chapter are discussed in Chapter 11.

5.2 Test Site

5.2.1 Location

The site is located in the grounds of the BRS, approximately 30km northwest of central London (Grid reference TL 128014). The location of the site is shown in Figure 5.1.

5.2.2 Geology and soil properties

The site is situated in a chalky boulder clay area, near to the southern edge of the glaciated areas in the United Kingdom. The glacial deposits at the site consist of 11.5m of stiff, chalky, clay dominated lodgement till overlying 7.5m of glacial sandy gravels which rest on chalk bedrock at a depth of 18m. The glacial material was probably deposited by a lobe of ice extending in front of the main ice sheet during the Anglian glacial advance, which occurred between 300,000 and 500,000 years ago (Little and Atkinson, 1988). The material at the site was deposited after the ice had passed over the nearby Chiltern hills and contains a high percentage of chalk, in the form of irregular shaped lumps, probably originating from the weathered chalk of these

hills.

Detailed fabric studies have been carried out at the site and are reported by Marsland (1979) and Marsland et al (1982). An overall geotechnical assessment of the BRS site against the background of possible modes of deposition and depositional processes is given in a recent paper by Marsland and Powell (1989).

The fabric studies show that the till is divided into two distinct bands. A typical soil profile is shown in Figure 5.2, together with typical grading curves.

The upper 6m of till is reddish brown with grey mottling and contains numerous erratics with dimensions from less than 1mm to greater than 30mm. The till is of medium plasticity, with a liquid limit of around 47%, plastic limit of 19% and clay content of 41%. It contains numerous near vertical fissures enclosing relatively intact lumps of clay having typical dimensions of 30mm or more. The upper till has a natural moisture content of between 17% and 20%, close to the plastic limit.

The lower 6m of till is light to medium brown in colour. The average liquid limit, plastic limit and clay contents are 45%, 21% and 36% respectively; the percentage of sand is lower than for the upper till. The lower till is very shattered and breaks easily into small lumps of between 5 to 30mm in dimension. The most likely cause of this shattering is thought to be exposure to permafrost conditions during the period between a retreat and resurgence of the ice sheet, which then deposited the upper till. The natural moisture content of the lower till ranges between 22% and 24%, slightly higher than the plastic limit.

Chalk content as a percentage of total mass increases from 16% near the surface to 31% at a depth of 8m.

The groundwater pressure regime at the BRS site is complex, and the subject of continuing investigations (Powell, 1988). Recent measurements made about 100m from the pile test site with Casagrande piezometers indicate a near hydrostatic distribution from a depth of 0.5m to approximately 8m (this depth range presumably corresponding to that of the upper till at this particular site position). Below 8m depth, zero pore water pressures are indicated. This is interpreted as being due to underdrainage of the shattered lower till by the sandy gravels and chalk bedrock.

The pile test area is on the edge of a wood, and it is thought that the

upper till in this region may undergo seasonal variations in properties due to reductions in natural moisture content caused by evapo-transpiration. Moisture content determinations from push-in samples obtained from a hand auger hole opened at the pile test site in August 1988, albeit only to a depth of 2m, indicated natural moisture contents rather less than those quoted by Marsland (1977). The standing water levels in the box piles, observed throughout the pile test programme, were on average 625mm below ground level with seasonal variations of between 50mm and 100mm.

Investigations at the BRS site were undertaken in the 1970's as part of the programme of research on glacial clays undertaken by the Building Research Establishment (BRE) (Marsland, 1977; 1979; Marsland and Powell 1979). Large scale in-situ plate tests were a key feature of the research programme. These were used to determine operational soil parameters for design purposes and to calibrate smaller in-situ tests such as cones, pressuremeters and vanes. The results of the tests performed at the BRS site are summarised below.

In Figure 5.3, undrained strength c_u is plotted against depth, c_u being determined from 865mm diameter plate loading tests, 58mm diameter Menard pressuremeter tests, and 98mm diameter triaxial tests. The values of c_u from the plate tests are very consistent and show a slight tendency to increase with depth. The c_u values from the triaxial tests are more variable and show a tendency to decrease with depth. The c_u values from the pressuremeter tests, estimated by the limit pressure method (see Chapter 9), are rather higher than those given by the plate tests - this trend is similar to that experienced in similar test programmes in other glacial clays (Marsland, 1979).

Operational undrained moduli E_u determined from the initial loading curves of the plate tests for the stress range corresponding to loads from zero to half the ultimate are given in Figure 5.4, together with the corresponding values from the triaxial tests. In the upper till the two sets of E_u values are approximately the same. In the lower till the E_u values obtained from the large in-situ plate tests are about twice the corresponding values determined from the triaxial tests.

Four cone penetration tests were made in the 1970's study using a straight-sided Fugro cone with a projected cone area of $10cm^2$, a friction sleeve area of $150cm^2$, and a standard rate of penetration of 20mm/sec. The cone resistance, sleeve friction and friction ratio for a typical test are plotted in Figure 5.5. The cone resistances for all the tests are plotted in Figure 5.6, together with the ultimate bearing

pressures obtained from the 865mm diameter plate tests. The plate bearing pressures remain fairly constant with depth, whereas cone resistance reduces with increasing depth. In the upper till the cone resistances are about 3 times the plate bearing pressures, in the lower till this ratio drops to about 1.2. The corresponding cone factors N_k are 30 at a depth of 3m and 11 at a depth of 9m.

The differences in results from the large scale bearing capacity tests, the small scale in-situ tests and the triaxial tests are attributed to the differences in fabric down the soil profile (ibid., see also Marsland and Powell (1979); Marsland and Quarterman (1982)). The consistent pattern of strength and stiffness obtained from the plate tests is due to the large volumes of clay sheared in these tests. The high results obtained from the triaxial and cone tests in the upper till are due to the scale effects caused by the relatively widely spaced fissures. Conversely, the very low values obtained from the triaxial tests in the lower till result from sample disturbance of the closely fissured and friable clay. The shattered, loosely packed fabric of the lower till is also the most likely reason for the low N_k values obtained. The reasonable agreement of the pressuremeter c_u profile estimated using the limit pressure method with that from the plate tests may be due to the large strain capability of the Menard pressuremeter (up to 30%).

5.3 Soil Testing

5.3.1 Scope

As part of the present research, in-situ testing was undertaken to augment the existing geotechnical data. Tests were performed with the following instruments:

(a) standard cone penetrometer
(b) Marchetti dilatometer
(c) full displacement pressuremeter.

As was the case at the Luton site, the main objective of the in-situ tests was to investigate limiting radial stresses available by radial expansion into the ground. The tests were performed by Fugro-McClelland Ltd between 14-16 July 1986. The tests were performed in an area approximately 5m square and about 30m away from the pile test site, within the bounds of the BRE geotechnical testing area. Details of the Marchetti dilatometer (DMT) and the Full Displacement Pressuremeter (FDPM) have been given in Section 4.4.

To enable an estimate to be made of the effective angle of shearing resistance δ' likely to be operating on the sides of the test piles, a suite of drained direct shearbox tests was performed using a reconstituted sample of material from the upper till.

5.3.2 Standard cone tests

Two CPT tests were performed to provide a reference for the other in-situ tests. A $10cm^2$ Fugro cone was used, advanced at a rate of 20mm/sec. The two traces obtained were very similar and are shown in Figure 5.7. The cone resistances are in generally good agreement with the previous CPT profiles at the site, and show up the sharp division between the upper and lower tills. Sleeve frictions are generally higher than those shown by the typical profile given by Marsland (1977), particularly in the upper till. Both the sleeve friction values and the friction ratio values show up the division between the upper and lower till. The glacial gravels at this point at the BRS site were struck at a depth of 10m, as indicated by the sudden large increases in cone resistance.

5.3.3 Marchetti Dilatometer Tests

Two DMT profiles were performed using the standard procedure (Section 4.4.5). The pressures p_0 and p_1 are plotted against depth in Figure 5.8. Agreement between the two profiles is very good. A marked division between the upper and lower tills is again apparent, with a reduction occurring in p_0 and p_1 values in the lower till. Interestingly, the reduction in values of p_1 is greater than the reduction in values of p_0.

The deduced index parameters I_D, K_D and E_D are plotted against depth in Figure 5.9. These data are used below in conjunction with DMT data obtained by the BRE. The BRE data has been compared by Powell and Uglow (1986, 1988a, 1988b) with published correlations of DMT data against soil properties and soil types. These comparisons are shown in Figure 5.10.

The soil description chart, which classifies soils on the basis of E_D and I_D, has some success in identifying the upper and lower tills. It picks up the difference between the two tills and correctly identifies the reduced sand content of the lower till. The specific soil descriptions are not quite correct, the upper and lower till generally being identified as a dense to very dense clayey silt and a hard silty clay repectively.

Undrained shear strengths from 98mm triaxial samples, normalised by the effective overburden pressure, are plotted against K_D. The results from

the BRS site plot close to the Marchetti correlation line:

$$C_U = 0.22\sigma'_{v_o} (0.5K_D)^{1.25}$$

(Marchetti, 1980).

In-situ K_o values (measured by means of total stress spade cells, self-boring pressuremeters, and some suction tests) are plotted against K_D, for a number of British clays. On the basis of these results, Powell and Uglow (1988b) propose the following correlation for 'young' clays (younger than 70000 years before present):

$$K_o = 0.34K_D^{0.55}$$

Use of this correlation with the K_D values measured at the BRS site yields plausible values of K_o of 1.5 to 2.2 for the upper till, and 0.82 to 1.2 for the lower till.

It should be borne in mind that presentation of data on log:log plots such as in Figure 5.10 can mask the true size of any discrepancies (Powell and Uglow, 1988a).

5.3.4 Full Displacement Pressuremeter tests

The arrangement of the FDPM at the BRS site was as described in Section 4.4.6.2. The FDPM was installed in the ground at two locations. Five tests were performed, at three depths at the first location and at two depths at the second location. Four of the five tests were performed in the upper 6m of till. The tests were carried out at a strain rate of 2.5%/minute and the interval between data scans was 10 seconds. As at the Luton site, the tests should be regarded as experimental in comparison to the other in-situ tests. The principal details of the tests are given in Table 5.1. Plots of pressure p against radial strain ε_c are given in Appendix 5.1 - results from all three arms of the pressuremeter are given.

The pressure:strain curves shown in Appendix 5.1 typically show a distinct lift-off pressure, followed by a rise over a strain of a few percent to an almost constant limit pressure. This behaviour is in agreement with FDPM tests carried out in overconsolidated Gault clay at Madingley, Cambridge; reported by Houlsby and Withers (1988).

No information was obtained from strain arm 2 at the second FDPM location, and there were some problems with electronic 'noise' which was known to have affected at least the first two tests at the first FDPM location. This noise caused a scattering of results which occasionally made detailed interpretation of the p:ε_c curves difficult. The unloading curve for Test L1/T1 was invalid because the strain arms reached the limit of their travel and therefore the expanded radius of the FDPM

was unknown. There was a large discrepancy in strains measured by the two 'live' strain arms in Test L2/T2; this might have been caused by a boulder or a tree root adjacent to the expanding membrane.

The FDPM results are discussed below. Of most interest are the values of total radial stress σ_r generated on expansion. Soil parameters derived from the tests are also presented in order to provide comparisons with previous tests at the site. It is considered, however, that there are insufficient new data to enable general conclusions to be drawn regarding soil properties.

Values of shear modulus G are given in Table 5.2, estimated using two different methods:

(a) the standard method of bisecting unload-reload loops (Mair and Wood, 1987)

(b) The analytical method of Houlsby (Houlsby and Withers, 1988), which obtains c_u, G and σ_r from the unloading portion of the $p:\varepsilon_c$ curve.

The G values obtained by the Houlsby method are more consistent, and are about a third of the equivalent unload-reload values. Both sets of values are much higher than the values of G calculated from the previous plate tests and triaxial tests, which are mostly in the range 5 to 10MPa (assuming undrained conditions, $E_u = 3G$). Pressuremeter tests at the BRE glacial till site at Cowden showed a reasonably good agreement between shear moduli obtained from pressuremeters and from plate tests (Marsland, 1979; Powell and Uglow, 1985).

Values of undrained shear strength c_u are given in Table 5.3. These have been estimated using two different methods:

(a) the limit pressure method (Mair and Wood, 1987)
(b) the Houlsby method (Houlsby and Withers, 1988).

Because the tests exhibit clearly defined limit pressures, for convenience the maximum pressure recorded in each test has been taken as the limit pressure. In the calculation of c_u by the limit pressure method, the parameter

$$N_p = 1 + \ln(G/c_u)$$

has been taken as 6.18. This is consistent with a bearing capacity factor $N_c = 9.25$, as used to interpret the plate tests (Marsland, 1979). Values of K_o of 1.75 and 1.0 have been assumed for the upper and lower tills respectively, these being average values obtained from the DMT

tests (the c_u values obtained by the limit pressure method at this site are not sensitive to the assumptions regarding K_o).

Values of c_u obtained from the two methods are relatively consistent, but are higher than the values previously obtained by Marsland. The one test performed in the lower till (Test L2/T2) gave significantly lower values of c_u than for the upper till.

Details of the calculation of c_u and G by the Houlsby method are given by Legge (1987).

The discrepancy between the values of shear modulus and undrained shear strength obtained in the FDPM tests and the values obtained in previous tests is rather odd. Two possible reasons are seasonally low values of moisture content in the upper till, and strain rate effects. The time taken to reach maximum pressure in the earlier standard Menard pressuremeter tests was around 20 to 30 minutes (Marsland and Powell, 1989), corresponding to a strain rate of around 1%/minute. The strain rate for the FDPM tests was considerably faster at 2.5%/minute. Powell (1989) has reported that limit pressures obtained with the FDPM at a strain rate of 5%/minute in Gault Clay at the Madingley test site were around 10 to 20% higher than those obtained from corresponding standard Menard pressuremeter tests. On average, the limit pressures obtained from the Menard pressuremeter tests at the BRS site (Powell, 1989) are around 25% lower than the corresponding FDPM limit pressures.

In Table 5.4 the DMT pressures p_0 and p_1 are compared with the FDPM 'lift-off' and limit pressures. The FDPM lift-off pressures have been estimated by examining the $p:\varepsilon_c$ curves for the three arms at the start of each test and identifying for each arm a distinct change in slope of the $p:\varepsilon_c$ data (Mair and Wood, 1987). The average value for the three arms is given. The DMT p_1 pressures are on average around 20% higher than the corresponding limit (ie. maximum) pressures recorded in the FDPM tests (see also Figure 5.8). This behaviour is in agreement with correlations between DMT pressure p_1 and pressuremeter limit pressure discussed by Powell and Uglow (1986; 1988a) for tests in various UK soils.

Table 5.5 summarises the results of the FDPM holding tests. Further data are given in Appendix 5.1. In contrast to the FDPM tests at the Luton site the holding strains were closely maintained, enabling changes in total radial stress σ_r at constant strain to be monitored. In all the holding tests a steady decay of σ_r with time occurred. There was no tendency for σ_r to approach a plateau value within the period of the

tests. For holding periods varying between 34 and 51 minutes, reductions in σ_r varying between 12.4% and 13.3% occurred.

The holding data are discussed in Chapter 11.

5.3.5 Shearbox tests

A single suite of drained, 60mmx60mm direct shearbox tests was performed using a reconstituted sample of the upper till obtained from an auger hole opened at the pile test site. General procedures for the tests were as set out by Head (1982). The tests were performed fully saturated.

5.3.5.1 Sample preparation

A test batch of till with a dry weight of about 10kg was made up from samples taken between 0.8m and 2.0m depth from the auger hole. The test batch was thoroughly dried, and then ground down in smaller batches for 3 to 4 minutes using a mechanical grinder. The crushed material was then passed through a 2mm sieve to remove stones. Four shearboxes were used. The test batch of till was reduced to an appropriate size, and distilled water was then added to give a nominal moisture content of 30%. The sample was then thoroughly remoulded and worked into the shearboxes without compaction. Samples for moisture content determinations were taken from the test batch.

5.3.5.2 Consolidation

After the samples had been placed in the shearboxes, they were inundated with distilled water. Normal stresses in the range 60kPa to 432kPa were then applied. After application of the normal stresses the samples were left to consolidate for approximately 21 hours. Consolidation was monitored by plotting settlement readings against square-root of time.

5.4.5.3 Shearing

Times to failure and displacement rates required to give drained shearing were calculated using the equation

$$t_f = 12.7 \times t_{100} \text{ min}$$

(Gibson and Henkel, 1954)

Standard rates of displacement of the lower half of the shear boxes ranged from 0.0029mm/min to 0.0039mm/min, according to thickness of sample and shear load proving ring displacement at failure.

In two of the tests - those with normal stresses of 122kPa and 246kPa - reversals and reshearings were performed in order to establish drained residual strengths. In the limited time that was available, these tests could only be taken to approximately 12mm displacement. At these

displacements plateau shear stresses had not been clearly established, but sufficient information was obtained to enable a reasonable estimate of ϕ'_r to be made.

During the shear box tests, some shearing at slower rates was carried out to confirm that the standard rate gave drained conditions. The shearing rate during reversals was five times the standard rate. After shearing the shearbox was quickly drained of water and the sample unloaded. The whole sample was then used for a moisture content determination.

5.4.5.4 Results

Results from the tests are presented in Appendix 5.2. Peak values of ϕ' calculated from the results of individual tests, assuming $c' = 0$, range from 20° to 27°. For the two reversal tests at 122kPa and 246kPa normal stress, calculated values of ϕ' at the end of the final runs are 19.0° and 17.4° respectively. In the 246kPa normal stress test the shear stress was approaching a plateau value, and 17° is probably a reasonable estimate of ϕ'_r for this sample of till. The moisture content of the till after shearing decreased progressively from 16.3% to 11.4% for normal stresses increasing from 60kPa to 432kPa.

5.4 Details of Pile Configurations

5.4.1 Pile refurbishment

The piles used previously at the Luton site were reused at the BRS site. After removal from the ground at Luton the piles were thoroughly washed and brushed clean before being reassembled. During reassembly minor damage and bending that the pile components had sustained was repaired and straightened out.

5.4.2 Dimensions and driven levels

A total of five piles were installed at the BRS site - three box piles and two cruciform piles. Four of these piles were being reused, and another box pile was made up in addition. Details of the piles have been given in Chapter 3. The five piles were driven at spacings of 1.0 to 1.5m. The three box piles were numbered 5, 6 and 7; the two cruciform piles were numbered 8 and 9. Figure 5.11 shows the layout of the driven piles; and the positioning of the reaction pads, runway beams, and reference beam supports.

The pile configuration is designated by the letter 'U' (unexpanded pile), 'A' (pile expanded by expander mandrel A), or 'B' (pile expanded

by expander mandrel B). Two of the piles were tested in more than one configuration. The dimensions and driven levels of the box pile and cruciform pile configurations are summarised in Figures 5.12 and 5.13 respectively. Dates of installation are included. Details of driving are described in Section 5.5, but a short summary is given below.

The outer shell of Box Pile 5 was driven and initially tested unexpanded (pile configuration 5U). It was then expanded by 21.4% of its width using expander mandrel B (pile configuration 5B), and retested.

The outer shell of Box Pile 6 was driven short of the required depth due to a failure of its driving shoe. It was tested unexpanded before being extracted (pile configuration 6U).

The outer shell of Box Pile 7 was driven and then expanded by 14.3% of its width using expander mandrel A (pile configuration 7A). It was then tested.

Figure 5.12 gives the driven levels of the bottom of the conical tip of the driving shoe, the bottom of the outer shell angles, the bottom of the expander mandrel nose, and the top of the expander mandrel nose. Dragdown of the outer shells during driving of the expander mandrels was negligible and has been ignored.

The outer shell of Cruciform Pile 8 was driven and initially tested unexpanded (pile configuration 8U). It was then expanded by 21.4% of its width using expander mandrel B (pile configuration 8B), and retested.

The outer shell of Cruciform Pile 9 was driven and then expanded by 10.7% of its width using expander mandrel A (pile configuration 9A). It was then tested.

Figure 5.13 gives the driven levels of the bottom of the outer shell angles, the bottom of the expander mandrel nose, and the top of the expander mandrel nose.

As described in Section 4.5.1, simplified effective pile perimeters and cross-sectional areas have been assumed. These are indicated by the chain lines in Figures 5.12 to 5.15. As before, two methods have been used to express percentage expansion of the pile configurations: percentage increase in pile width, and percentage increase in pile cross-sectional area.

5.4.3 Shaft surface areas

Figures 5.14 and 5.15 give the shaft surface areas of the box piles and cruciform piles respectively. Four different shaft surface areas are given, designated by the letters A to D. These correspond to the different definitions of pile perimeter and pile length described in Section 4.5.2.

5.5 Pile Installation

5.5.1 Introduction

Details of pile installation procedures at the BRS site have been described in Section 3.5.

Driving records of pile penetration against air hammer driving time were taken and are presented in Figure 5.16. Pile penetration in Figure 5.16 refers to the penetration of the bottom of the pile component being driven (including any driving shoe) below ground level. The pile installation process was interrupted by breaks in order to adjust the piling frame guides and to lubricate the hammers. These breaks have not been included on Figure 5.16. The driving records commence at penetrations greater than zero, because it was not possible to obtain driving records during the early stages of pile installation when the rate of penetration was very fast.

The driving records provide qualitative information only. In some cases the driving records are incomplete, and the records are confused by the fact that different hammers and compressors were used. There is sufficient information, however, to draw important conclusions regarding the efficiency of the various pile configurations tested, in terms of the driving energy expended for given load capacity.

Two types of double-acting air hammer were used, the Atlas-Copco PH5 and the BSP 500N (Section 3.5.3). Details of the overall weights and the quoted air delivery pressures and blow rates for the two hammers are given below:

Hammer	Overall weight (kg)	Delivery pressure (psi)	Blows/min (max)
Atlas Copco PH5	440	85	310
BSP 500N	1150	90	330

The installation of each pile is described in the following five Sections.

5.5.2 Box Pile 5

(a) Outer shell

Driving of the outer shell of Box Pile 5 commenced on 12.3.86 using the PH5 hammer in conjunction with a 125cfm (cubic foot per minute air delivery) compressor supplied by BRS. The air delivery pressure recorded at the compressor was 82.5psi; the initial blow rate recorded was 260 blows/minute.

During approximately 75 minutes driving, the pile penetration rate slowed progressively. The hammer blow rate also slowed and the hammer eventually stalled at a pile penetration of 3.1m. An inspection of the compressor located a faulty valve. Driving recommenced 22 hours later on the following day, 13.3.86, with the hammer driven by a replacement 175cfm compressor. Air delivery pressure recorded at the compressor was 115psi, blow rate was on average 290 blows/minute and showed no tendency to drop off with time. Driving was very slow, approximately 190 minutes driving time being required to drive the outer shell to a final penetration of 5.04m. The average pile penetration rate during the last 10 minutes of driving was 6.0mm/min.

(b) Expander mandrel

The outer shell of Box Pile 5 was expanded with expander mandrel B on 12.8.86, 152 days after the outer shell was driven. The PH5 hammer was used, driven by the original BRS 125cfm compressor which by this time had been repaired. Air delivery pressure at the compressor was recorded as 92psi; the blow rate throughout driving was between 230 and 250 blows/minute, less than the blow rate when the hammer was driven with the 175cfm compressor. Expander mandrel B was driven to a final penetration of 4.59m in approximately 15 minutes of driving.

5.5.3 Box Pile 6

The outer shell of Box Pile 6 was driven on 14.3.86. The PH5 hammer driven by the 175cfm compressor was used. The air delivery pressure at the compressor was 115psi, the recorded blow rate was between 280 and 295 blows/minute and showed no tendency to fall with time. After 105 minutes of hard driving the penetration rate had become very slow. At a penetration of 3.92m the collar pieces securing the driving shoe failed, allowing the driving shoe to be pushed from the bottom of the outer shell. It was not possible to drive the pile any further. The average pile penetration rate during the last 40 minutes of driving was 4.25mm/min.

5.5.4 Box Pile 7

(a) Outer shell

Driving of the outer shell of Box Pile 7 commenced on 15.5.86. The 500N hammer was used, in conjunction with a 250cfm compressor. Air delivery pressure at the compressor was recorded as 70psi, blow rate was constant at 330 blows/min. After approximately 1 hour of driving, pile penetration fell quickly to a very slow rate. At a penetration of 4.4m the pile refused.

It was suspected that the capacity of the 250cfm compressor was marginally too low. Accordingly, it was replaced by a 350cfm compressor. Driving of the outer shell recommenced on 23.5.86 using the new compressor. The initial air delivery pressure was 84psi - this was gradually increased to 107psi by reducing the air delivery rate, the blow rate thereby being maintained between 338 and 350 blows/minute. Approximately 25 minutes driving was required to drive the outer shell to a final penetration of 5.11m. The average pile penetration rate during the last 2 minutes of driving was 15mm/min.

(b) Expander mandrel

The outer shell of Box Pile 7 was expanded with expander mandrel A on 29.5.86, 6 days after the outer shell was driven. The 500N hammer was used, driven by the 350cfm compressor. Air delivery pressure at the compressor and blow rate were recorded as 109psi and 309 blows/minute respectively. Driving was very easy; the expander mandrel was driven to a final penetration of 4.66m within approximately 5 minutes of driving.

5.5.5 Cruciform Pile 8

(a) Outer shell

The outer shell of Cruciform Pile 8 was driven on 13.5.86. The 500N hammer was used in conjunction with the 250cfm compressor. Driving was exceptionally easy and it was neccessary to deliberately under-power the hammer in the early stages of driving, by restricting the air supply, in order to maintain control of pile penetration. The pile penetration rate was too fast for accurate driving records to be made, the outer shell being driven to a depth of 5.05m within a few minutes. The pile penetration rate at the end of driving was of the order of 150mm/minute.

(b) Expander mandrel

The outer shell was expanded with expander mandrel B on 13.8.86, 92 days after the outer shell was driven. The PH5 hammer was used, driven by the BRS 125cfm compressor. The delivery pressure at the compressor was

92psi. The blow rate was initially around 250 blows/minute but fell towards the end of driving to around 180 blows/minute. The compressor was of slightly insufficient capacity for the job in hand and as a result driving was rather slow towards the end of driving, the hammer stalling on one occasion. The mandrel was driven to a final penetration of 4.89m in just under 50 minutes of driving.

5.5.6 Cruciform Pile 9

(a) Outer shell

The outer shell of Cruciform Pile 9 was driven on 13.5.86. The 500N hammer was used in conjunction with the 250cfm compressor. As with the outer shell of Cruciform Pile 8, driving was exceptionally easy and it was neccessary to deliberately under-power the hammer in order to maintain control during the early stages of driving. The pile penetration rate was too fast for accurate driving records to be made, the outer shell being driven to a penetration of 5.01m within a few minutes. The pile penetration rate at the end of driving was of the order of 150mm/minute.

(b) Expander mandrel

The outer shell was expanded with expander mandrel A on 14.5.86, the day after the outer shell was driven. The 500N hammer and 250cfm compressor were used. Driving was easy, and the hammer was deliberately under-powered in the early stages of driving. Driving records were taken towards the end of driving. The expander mandrel was driven to a final penetration of 4.74m within approximately 10 minutes. Driving seemed slightly slower than for the outer shell, but this was difficult to assess because the hammer was not fully powered throughout driving.

5.5.7 Summary of driving energies

Due to the different types of piling hammers and compressors used, it is difficult to assess driving energies. A qualitative summary is given below:

Of all the different pile components driven,

(a) the box outer shells required by far the greatest driving energy to install

(b) the driving energies required to install the box expander mandrels were very small in comparison to those for the box outer shells

(c) the cruciform outer shells required the least driving energy to

install

(d) the cruciform expander mandrels were also easy to drive, but on the basis of the limited information available they perhaps required rather more driving energy to install than the cruciform outer shells

(e) the box expander mandrels required less driving energy to install than the cruciform expander mandrels.

5.6 Pile Testing

5.6.1 Rationale

The overall objective of pile testing at the BRS site was the same as for the testing at the Luton site - the determination of ultimate shaft resistances. As at the Luton site, tension tests were employed to eliminate base resistance and the different expanded and unexpanded pile configurations were subjected to repeated testing.

An incremental system of pile loading (IL) was generally adopted at first, as described in Section 4.7.1. The reasons for this were as follows:

(a) An important consideration at the BRS site was the possibility of clay particle alignment effects (Section 1.1.2.1). Large pile displacements might cause reductions in pile capacity due to reductions in values of the effective angle of shearing resistance δ' operating along the pile shaft. This would confuse the analysis of the pile test results, which would be focused on the estimation of values of effective radial stress σ'_r operating against the pile shaft.

It was therefore decided to minimise pile displacements during the early testing history of the piles. This would be achieved by applying load increments so as to take the piles very near to failure, but not actually to failure, and by not applying CRE loading. A test of this type does not provide such a well defined failure as a CRE test, but allows the possibility of changes in shaft capacity with time to be monitored by means of repeated testing without the results being masked by a large drop in capacity due to particle alignment effects.

(b) To investigate creep behaviour during constant sustained loading.

Load increments during IL tests were selected on the basis of the likely pile failure load; increments were reduced as pile failure approached. Load increments were held until pile displacement was reasonably constant. Holding times varied, becoming longer towards the end of a test. Periods of up to 64 minutes were employed. Pumping of the loading ram hand pump was stopped when the rate of creep displacement continued undiminished.

Although the IL tests succeeded in the objective of controlling pile displacements, there were a number of disadvantages with this type of test. Failure was often ill-defined, and the load:displacement curve obtained could be irregular due to different load increments and holding times. The test duration could not be predicted accurately in advance, making it difficult to plan the loading pattern.

Consequently, a Constant Rate of (Incremental) Loading (CRL) test was introduced. In this test, constant increments of load were applied at a constant rate. Load increments and hold times were smaller than for the incremental tests - in general one increment was applied every 16 minutes. The advantages of the CRL test were that it was possible to select a loading rate or rates to suit the available testing period, the smaller increments led to a better defined failure, and the resulting load:displacement curves were smoother.

The original intention was to employ the CRL test method such that pile displacement could be stopped when a distinct change in creep behaviour occurred, at the 'creep limit' (Bustamante, 1982). The creep limit could then be related to ultimate capacity. Some success was achieved with this approach, but it was found to be best to continue the CRL test until the creep displacement rate approached that of the standard 1mm/rate of the CRE test. This enabled failure loads to be reasonably well defined.

Large displacement CRE tests, as described in Section 4.7.1, were reserved in the main for the end of the testing histories of the piles, prior to pile extraction. These tests enabled the ductility of the load:displacement response after expansion to be studied. The displacement rate for the CRE tests was 1mm/minute, as at the Luton site.

Cyclic loading tests were carried out - as at the Luton site these were performed to enable a general assessment of the effect of repeated loading. As before, tension only cycling was applied, from near zero load to half the previous static pile capacity. The cycles were of a

standard duration of 5 minutes each.

5.6.2 Summary of pile testing

The load:displacement histories of Piles 5, 7, 8 and 9 are summarised in Figures 5.17 to 5.20. Pile 6 was not driven to full penetration and is dealt with later. Figure 5.21 is a calender history of the testing programme. Pile tests in these Figures are referred to by means of the pile configuration, followed by a test number.

Individual pile tests are described in the following five Sections. The descriptions have been organised so as to provide testing histories for each pile position. In order to provide a complete description, some information already given regarding pile installation has been repeated.

Test data are presented in Figures 5.22 to 5.54. The main presentation of data for each pile test is in the form of three plots:

(a) applied tensile head load v time
(b) applied tensile head load v upward displacement of pile head
(c) upward displacement of pile head v time

The plots are accompanied by summary tables featuring key data from the tests. Shaft frictions are given, calculated on the basis of the four shaft areas A to D and net pile load at failure.

These main data are presented in Figures 5.22 to 5.39. Information from the summary tables accompanying the plots is brought together for each pile configuration in Tables 5.6 to 5.12. Creep behaviour during incremental loading is presented on a separate plot for each pile test. The creep plots have been grouped together as Figures 5.40 to 5.54, following the main data.

The upward displacement of a pile is taken as the average of the measurements made using the two dial gauges. Agreement between the two dial gauges during some of the early tests was not good due to bending of the top of the pile, caused by the applied load being non-axial. This problem was later solved. It is considered that where bending at the top of a pile occurred, this did not unduly affect the ultimate capacity of the pile. Appendix 5.3 gives typical pile load:displacement behaviour.

Included on the load:displacement plots is the likely range of pile head displacement due to elastic extension of the pile under load. Table 5.13 gives details of the calculation of the elastic lines. The basis for the calculation of this table is as described in Section 4.7.10.

In general, pile capacities are not compared quantitatively in the following five Sections - this is done in Section 5.7.1.

5.6.3 Testing history: Box Pile 5

Pile Configuration 5U
The outer shell of Box Pile 5 was driven on 13.3.86 and initially tested unexpanded.

Test 5U.1 Date: 25.4.86 Type: IL, CRE Figures 5.22, 5.40
Test 5U.1 was performed 43 days after driving. It was the first pile test at the BRS site.

In the first stage of the test, load was increased in increments. Initially, increments of 5kN were applied, up to a total load of 40kN. These increments were each held for 4 minutes, during which times negligible creep displacements occurred; apart for the 40kN increment which was held for 56 minutes, during which time approximately 0.1mm of apparent creep displacement occurred. It was concluded that this apparent creep was in fact relaxation of minor bending at the top of the pile.

At this point the load increments were increased to 10kN (nominal). These increments were maintained for up to 16 minutes. For load increments up to a total load of 135.3kN, neglible creep displacement occurred - less than 0.05mm during each holding period. Significant creep displacements, 0.25mm and 0.425mm respectively, occurred during the holding periods at 145.7kN and 156.1kN load. The final load increment of 156.1kN was held for 64 minutes, and the creep rate accelerated slightly towards the end of the holding period. The average creep rate between 56 and 64 minutes of the holding period was 0.0075mm/minute; final displacement was 1.28mm.

At this point it was decided to perform a CRE test. Maximum load recorded during this stage of the test was 201.8kN, at a displacement of 2.30mm. The maximum CRE load was a factor of 1.29 greater than the final incremental load. Further displacement to 7.30mm resulted in a drop in load to 187.1kN.

The pile was unloaded in nine increments of approximately 20kN, each unloading increment being maintained for between 2 and 4 minutes.

Test 5U.2 Date: 30.7.86 Type: IL Figures 5.23, 5.41
Test 5U.2 was performed 139 days after driving (96 days after the previous test).

Initially, five increments of 30kN (nominal) were applied, up to a total load of 156.5kN - very close to the final incremental load in Test 5U.1. These increments were held for up to 64 minutes each, during which times only small amounts of creep displacement occurred - less than 0.1mm during each holding period. A final increment of 20.8kN was then applied, to give an total applied load of 177.3kN. During the 32 minute holding period for this load increment, 1.20mm of creep displacement occurred. The average creep rate between 28 and 32 minutes was 0.049mm/minute. Displacement at the end of the final holding period was 2.16mm.

The pile was unloaded in four increments, held for two minutes each.

Pile Configuration 5B
Box Pile 5 was expanded by 21.4% on 12.8.86, 152 days after the outer shell was driven.

Test 5B.1 Date: 14.8.86 Type: IL Figures 5.24, 5.42
Test 5B.1 was performed 2 days after expansion. Six load increments of 50kN (nominal) were applied, up to a final load of 299.7kN. The increments were held for up to 32 minutes. Significant creep displacements, of up to 0.53mm during each holding period, occurred for the increments below the final load, but in all these cases displacements stabilised with time. The final load increment was maintained for 1.75 minutes, during which time large and accelerating creep displacements occurred. At this point pumping of the loading ram hand pump was stopped and the load allowed to stabilise. The creep displacement rate over the final 0.75 minutes was 1.47mm/minute. Total displacement at the end of the holding period was 4.92mm.

Unloading commenced from a stabilised load of 271.1kN, at 5.66mm displacement. Unloading took place in eight increments, held for 2 minutes each.

Test 5B.2 Date: 15.12.86 Type: CRL, CRE Figures 5.25, 5.43
Test 5B.2 was performed 122 days after expansion (120 days after the previous test).

In the first stage of the test CRL loading was applied. First, four increments of 50kN (nominal) were applied, up to a total applied load of

199.3kN. These increments were held for 16 minutes each. Apart from the first increment, total creep displacement during each holding period was under 0.1mm.

Increments of 10kN (nominal) were then applied, each increment being held for 16 minutes. For the increments up to a total load of 272.2kN, creep displacements continued to be small - within a total of 0.1mm during each holding period. Creep displacements during the holding periods of the final two load increments - 282.6kN and 293.0kN - were 0.22mm and 2.12mm respectively. The average creep rate between 12 and 16 minutes of the final holding period was 0.11mm/minute, final displacement was 3.64mm.

The CRE stage of the test commenced from a stabilised load of 278.0kN. Maximum load recorded during this stage was 297.4kN at 3.90mm displacement - a factor of increase of 1.02 on the final load in the CRL stage. Further displacement to 9.18mm gave a drop in load to 261.8kN. The load:displacement response was much stiffer than in Test 5B.1 (the initial loading of the expanded pile), the difference being associated with the greater creep displacements in Test 5B.1.

Unloading took place in seven increments, held for 2 minutes each.

Test 5B.3 Date: 17.12.86 Type: Cyclic, CRE Figures 5.26
Test 5B.3 was a cyclic loading test carried out 2 days after the previous test.

25 cycles of loading between 15.0kN and 149.4kN were applied (0.05 and 0.5 times the maximum load in the previous test). Each cycle lasted 5 minutes: the loading and unloading portions of the cycle lasted 2 minutes each, and the bottom and top of cycle loads were each held for 0.5 minute. Readings were taken at the beginning and at the end of the bottom/top of cycle holding periods. Some of the cycles were more accurately logged. The variation in bottom/top of cycle displacement during the 25 cycles was within 0.05mm - this small variation almost certainly being due to the characteristics of the loading/measurement system. The accurately logged cycles showed very little hysteresis.

25 minutes after the cycling stage of the test was completed, a CRE test was commenced. Maximum load recorded during this stage of the test was 276.3kN at 1.44mm displacement. Further displacement to 7.12mm resulted in a drop in load to 253.9kN.

The cyclic loading does not appear to have influenced the static

capacity of the pile. There is no change apparent in the slow downward trend of load with continued displacement in Tests 5B.1 to 5B.3, which can be observed in Figure 5.17.

Unloading took place in seven increments of 40kN approximately, each increment being held for 2 minutes.

5.6.4 Testing history - Box Pile 6

Pile Configuration 6U
The outer shell of Box Pile 6 was driven on 14.3.86, to a depth of 3.92m before failure of the driving shoe occurred. Before extraction the unexpanded outer shell was tested.

Test 6U.1 Date: 28.4.86 Type: CRL, CRE Figures 5.27, 5.44
Test 6U.1 was performed 45 days after driving. In the CRL stage of the test four increments of 20kN (nominal) were applied up to a final load of 103.8kN. In the second stage of the test CRE loading was applied. Maximum load recorded was 133.6kN, at 3.48mm displacement. Further displacement to 7.99mm resulted in a drop in load to 125.9kN.

Unloading commenced from a stabilised load of 92.2kN and took place in four increments, each held for 2 minutes.

5.6.5 Testing history - Box Pile 7

Pile configuration 7A
The outer shell of Box Pile 7 was driven on 23.5.86 and was expanded 6 days later on 29.5.86.

Test 7A.1 Date: 30.5.86 Type: IL Figures 5.28, 5.45
Test 7A.1 was performed the day after expansion. Initially, increments of 30kN (nominal) were applied up to a total load of 178.8kN. These increments were held for up to 32 minutes. Increments of 20kN were then applied, up to a final load of 303.6kN. The first four of the 20kN increments were held for 16 minutes each. Creep displacement during the holding periods of these increments increased steadily from 0.18mm at 199.6kN, to 0.42mm at 262.0kN. The last two increments, to 282.8kN and 303.6kN, were held for 64 minutes and 32 minutes respectively. Creep displacement during these holding periods was 1.07mm in both cases. The average creep displacement rate between 24 and 32 minutes of the final holding period was 0.022mm/min. Final displacement was 5.26mm.

Unloading took place in five increments of approximately 70kN. Each

increment was held for 2 minutes.

Test 7A.2 Date: 29.7.86 Type: IL Figures 5.29, 5.46
Test 7A.2 was performed 61 days after expansion (60 days after the previous test).

First, five increments of 62.5kN (nominal) were applied, up to a total load of 312.6kN. These increments were held for up to 64 minutes each. Creep displacement during the holding periods was much less than for the previous test - less than 0.4mm in all cases. A final increment of 31.2kN was applied, to give a final load of 343.8kN. During the holding period of this increment significant creep displacement of 1.38mm occurred, with the creep displacement rate increasing towards the end of the holding period. During the final minute of the holding period, 0.075mm displacement occurred; final displacement was 3.32mm. As in the case of Pile 5B, the reduced creep displacements during reloading of Pile 7A were associated with a much stiffer load:displacement response in comparison to the initial loading.

The pile was unloaded from a stabilised load of 338.4kN, in six increments held for 5 minutes each.

Test 7A.3 Date: 9.1.87 Type: CRL, CRE Figure 5.30, 5.47
Test 7A.3 was performed 225 days after expansion (164 days after the previous test).

In the CRL stage of the test, five increments of 50kN (nominal) were initially applied up to a total load of 249.5kN. Each increment was held for 16 minutes apart from the 99.7kN increment, which was held for 76 minutes while a break was taken from testing. Very little creep displacement occurred while these loads were maintained.

Seven increments of 12.5kN (nominal), each held for 16 minutes, were then applied up to a final applied load of 337.9kN. Creep displacements during holding periods were very small - less than 0.05mm - until the last three increments, when a gradual increase in creep displacements occurred. Total creep displacement during the final holding period was 1.3mm. Average creep displacement rate between 12 and 16 minutes of the final holding period was 0.10mm/min; final displacement was 3.49mm. The load:displacement plot of the CRL stage of the test followed very closely that of the previous test.

In the second stage of the test CRE loading was applied, commencing from a stabilised load of 319.0kN at 4.13mm displacement. Maximum load

recorded was 352.5kN at 4.63 displacement, representing a factor of increase in load of 1.04 in comparison to the final load increment in the CRL stage of the test. Further displacement to 10.13mm resulted in a gradual fall in load to 333.4kN.

Unloading commenced from a stabilised load of 316.5kN, and took place in six increments held for 2 minutes each.

5.6.6 Testing history - Cruciform Pile 8

Pile configuration 8U
The outer shell of Cruciform Pile 8 was driven on 13.5.86 and was initially tested unexpanded.

Test 8U.1 Date: 20.5.86 Type: IL Figures 5.31, 5.48
Test 8U.1 was performed on 20.5.86, 7 days after driving. Increments of 20kN (nominal) were applied up to a total load of 104.3kN. These increments were held for up to 32 minutes. Steadily increasing amounts of creep displacement occurred with increasing load - 0.60mm in the 32 minute holding period at 104.3kN. A final increment of 10.4kN was applied to give a final applied load of 114.7kN. The final increment was held for 8 minutes, during which time steady creep displacement of 1.02mm occurred. Average creep displacement rate between 4 and 8 minutes of the final holding period was 0.11mm/minute; final displacement was 2.79mm.

Unloading took place in five increments, each held for 2 minutes.

Test 8U.2 Date: 31.7.86 Type: IL Figure 5.32, 5.49
Test 8U.2 was performed 79 days after driving (72 days after the previous test).

The loading sequence was similar to the previous test. Four increments of 20kN (nominal) were applied up to a total load of 83.2kN; followed by three increments of 10kN (nominal) to a final load of 114.5kN - virtually identical to the final load in the previous test. The first three increments were held for 2 or 3 minutes only. The following three increments were held for 32 minutes, creep displacement increasing steadily with increasing load. Creep displacement at 104.0kN was 0.24mm.

The final load of 114.5kN was held for 14 minutes before pumping of the loading ram hand pump was stopped. During the holding period large and accelerating creep displacement occurred. Total creep displacement in 14 minutes was 2.92mm. Average creep displacement between 12 and 14 minutes

was 0.42mm/minute; final displacement was 4.40mm. The load:displacement plot was close to that of the previous test.

Unloading took place in five increments of approximately 20kN held for 2 minutes each, commencing from a stabilised load of 106.5kN.

Pile configuration 8B
Cruciform Pile 8B was expanded by 21.4% on 13.8.86, 92 days after the outer shell was driven.

Test 8B.1 Date: 18.8.86 Type: CRL Figure 5.33, 5.50
Test 8B.1 was performed 5 days after expansion. Three increments of 40kN (nominal) were initially applied, up to a total load of 119.0kN. Then, eight increments of 10kN (nominal) were applied up to a final load of 198.9kN. All of the load increments were held for 16 minutes, apart from the final increment which was held for 8 minutes. Creep displacement during the holding periods increased with load. Values were below 0.25mm per holding period for loads below 179.0kN. Creep displacements during the final three holding periods increased more rapidly. Creep displacement during the 8 minute final holding period was 1.26mm. Average creep displacement rate between 4 and 8 minutes was 0.15mm/minute; final displacement was 3.55mm. The load:displacement response was considerably stiffer than for the previous tests on the pile before it was expanded (Pile configuration 8U).

Unloading took place in eight increments held for 2 minutes each, commencing from a stabilised load of 194.2kN.

Test 8B.2 Date: 9.3.87 Type: CRL Figure 5.34, 5.51
Test 8B.2 was performed 208 days after expansion (203 days after the previous test).

The loading pattern was similar to the previous test: three increments of 50kN (nominal) were initially applied up to a total of 142.5kN, followed by ten increments of 10kN to a final load of 241.6kN. Increments were held for 16 minutes, apart from the final increment. For loads up to 211.6kN, creep displacements were very small - within 0.1mm/holding period. Creep displacement increased significantly after this - during the 221.6kN and 231.6kN holding periods, displacements of 0.18mm and 0.42mm respectively occurred. During the minute of the final holding period 0.38mm creep displacement occurred, and pumping of the loading ram hand pump was then stopped. Final displacement was 2.00mm. The load:displacement plot was much stiffer than for the previous test, this behaviour being associated with the reduced amount of creep

displacement.

Load was allowed to subside for approximately 20 minutes to a value of 217.9kN at 3.18mm, before unloading in a single increment took place.

Test 8B.3 Date: 10.3.87 Type: CRL, CRE Figure 5.35
Test 8B.3 was performed the day after Test 8B.2. The aim of the CRL stage of the test was to bring the pile quickly near to failure in order to perform a CRE test. Four increments of 50kN (nominal) were applied up to a total load of 200.8kN, followed by three increments of 10kN to give a final applied load of 231.2kN. The increments were generally held for 8 minutes. The final increment was held for 1 minute, during which time 0.64mm creep displacement occurred. Pumping of the hand jack was stopped. Total displacement at this point was 2.21mm. The load:displacement plot followed closely that of the previous day's test.

CRE loading commenced from a stabilised load of 211.2kN at 2.84mm. Maximum load recorded was 226.0kN at 4.82mm displacement, representing a factor of increase of 0.98 on the final incremental load in the CRL test. Further displacement to 7.82mm gave a drop in load to 215.2kN.

Load was allowed to stabilise to a value of 198.1kN before unloading commenced. Unloading took place in six increments held for two minutes each.

Test 8B.4 Date: 10.3.87 Type: Cyclic, CRL, CRE Figure 5.36
Test 8B.4 commenced 105 minutes after the completion of Test 8B.3. In the first stage of the test, 25 cycles of loading between 17kN and 114.0kN were applied (0.07 and 0.49 times the maximum load in Test 8B.3). Each cycle lasted 5 minutes: the loading and unloading portions of the cycle lasted 2 minutes each, and the bottom and top of cycle loads were held for 0.5 minute each. Some of the cycles were more accurately logged. The bottom/top of cycle displacements increased very slightly by 0.04mm during the 25 cycles. This may have been due to the characteristics of the loading/measurement system. The accurately logged cycles showed very little hysteresis.

10 minutes after the cycling stage was completed, a CRL stage was commenced with the purpose of bringing the pile quickly near to failure. Starting from a stabilised bottom of cycle load of 18.7kN, load increments - initially 50kN (nominal) and reducing to 10kN (nominal) - were applied to give a final applied load of 211.8kN. The increments were generally held for 8 minutes each. Creep displacement increased steadily with inceasing load. The final increment of 211.8kN was held

for 1 minute before pumping of the hand pump was stopped, during which time creep displacement of 1.00mm occurred. Final displacement was 2.80mm.

Load was allowed to subside to 198.9kN at 3.31mm displacement before a CRE test was carried out. Maximum load recorded was 207.7kN at 4.32mm displacement, falling to 197.5kN at 8.32mm displacement. The maximum load represented a factor of increase of 0.98 over the final increment in the CRL stage. The cyclic loading does not appear to have influenced the static capacity of the pile - there is no change apparent in the slow downward trend of load with continued displacement in Tests 8B.3 and 8B.4, which can be observed in Figure 5.19.

Unloading took place in six increments of approximately 40kN, commencing from a stabilised load of 187.1kN. The increments were held for 2 minutes each.

5.6.7 Testing history - Cruciform Pile 9

Pile configuration 9A
The outer shell of Cruciform Pile 9 was driven on 13.5.86 and was expanded by 10.7% on the next day, 14.5.86.

Test 9A.1 Date: 21.5.86 Type: IL Figure 5.37, 5.52
Test 9A.1 was performed 7 days after expansion. Initially, four increments of 30kN (nominal) were applied up to a total load of 124.9kN. The increments were held for 16 or 32 minutes. Creep displacement was significant - at 124.9kN it was 0.34mm during 32 minutes. Four increments of 20kN (nominal) were then applied to give a final applied load of 208.1kN. These increments were held for 32 or 64 minutes. Creep displacement increased steadily with applied load. During the final holding period 1.42mm displacement occurred in 32 minutes, average creep rate between 24 and 32 minutes was 0.059mm/min. Final displacement was 4.08mm.

Unloading took place in five increments, held for 3 minutes each.

Test 9A.2 Date: 1.8.86 Type: IL Figure 5.38, 5.53
Test 9A.2 was performed 79 days after expansion (72 days after the previous test).

Four increments of 40kN (nominal) were initially applied, up to a total load of 166.9kN. These increments were held for 8 minutes, apart from the 166.9kN increment which was held for 68 minutes while a break from

testing was taken. Creep displacement was less than for the previous test at corresponding loads - 0.2mm creep occurred during the holding period at 166.9kN.

Five increments of 10kN (nominal) were then applied, held for up to 53 minutes, to give a final load of 229.3kN. Creep displacement increased with applied load, but was less than for the previous test at corresponding loads. The final load of 229.3kN was held for 6 minutes during which time 1.26mm of creep displacement occurred. Creep displacement during the final minute was 0.3mm. Final displacement was 3.05mm. As for Cruciform Pile 8B, the load:displacement plot for this test was much stiffer than for the initial loading in Test 9A.1, this behaviour being associated with the reduced creep displacements.

Unloading took place in six increments of approximately 40kN each, commencing from a stabilised load of 222.0kN. The increments were held for up to 3 minutes each.

Test 9A.3 Date: 20.3.87 Type: CRL, CRE Figure 5.39, 5.54
Test 9A.3 was performed 310 days after expansion (231 days after the previous test).

In the CRL stage of the test, four increments of 40kN (nominal) were applied up to a total load of 160.9kN; followed by six increments of 10kN (nominal) to give a final load of 220.8kN. The standard holding period was 16 minutes. Creep displacements for loads up to 200.8kN were small - within 0.16mm per holding period. At 210.8kN load, 0.28mm creep displacement occurred during the holding period. At 220.8kN large and accelerating creep displacement occurred - 3.30mm before pumping of the loading ram hand pump was stopped after approximately 15.5 minutes of the holding period. Total displacement at the end of the final holding period was 4.8mm. Average creep displacement rate during the last 0.5 minute was 1.44mm/minute. The load:displacement plot for the CRL test was very similar to that for the previous test.

Load was allowed to subside to 192.9kN at 5.74mm displacement, and then a CRE test was performed. A maximum load of 209.8kN was soon recorded, at 6.14mm displacement. This represented a factor of increase in load of 0.95 in comparison to the final load in the CRL test. Continued displacement to 10.64mm resulted in a drop in load to 192.5kN.

Load was then allowed to subside to 177.3kN before unloading commenced. Unloading took place in six increments of approximately 40kN, each held for 2 minutes.

5.6.8 Tension test on expander mandrel

Before Cruciform Pile 9 was extracted, a test was performed in which tensile load was applied to the top of the expander mandrel. This test was performed on 20.3.87, immediately after pile Test 9A.3. Increments of load were applied to the top of the expander mandrel, up to a total of 187.7kN. The load increments were held for 5 minutes each, apart from the last increment which was held for 2 minutes. At the final increment of 187.7kN, very close to the load recorded at the end of Test 9A.3, the expander mandrel and outer shell were pulled steadily from the ground together as one.

5.6.9 Removal of piles from ground

The piles were removed from the ground as described in Section 3.9. When the cruciform piles were removed, soil was found to be contained between the cruciform arms of the outer shell angles. The material was contained within the cruciform arms in a similar way to the chalk at the Luton site, but not so uniformly. Soil may well have been pulled from the outer shell during extraction, bearing in mind the stony nature of the boulder clay. Vertical striations on the outer face of the contained material indicated a displacement surface.

When the box piles were removed from the ground, the outer shell was found to be covered with a thin layer of clay, approximately 0.5 to 1.0mm thick. Vertical striations indicated a displacement surface.

5.7 Comparison of Pile Performance

The main points regarding pile performance are outlined in this Section and discussed further in Chapter 11.

5.7.1 Increase in pile capacity

Because of the incremental testing that was employed, pile failure was sometimes ill-defined and care is needed in comparing pile capacities. The approach that has been adopted here is described below.

Table 5.14 lists, for all of the pile tests, the final incremental load applied, the final creep rate during that increment, and where appropriate the maximum CRE load. In the latter case the ratio of the final incremental load to the maximum CRE load is given. In Figure 5.55 final creep rate is plotted against this ratio.

Considering those tests with both an incremental and a CRE stage, for tests with a final creep rate of 0.10mm/minute or greater the final

incremental load is within 5% of the subsequent maximum CRE load. This observation has been used as the basis for defining 'incremental failure'. Incremental failure is deemed to have taken place if steady creep displacement of 0.10mm/minute or more occurred, and was maintained over several minutes. Incremental failure can be identified for tests where there was no CRE stage. The incremental failure load provides a good indication of ultimate pile capacity.

Table 5.14 indicates those tests in which incremental failure took place. Eighteen tests were carried out in all; in eight of these tests CRE failure occurred, in six of the remaining tests incremental failure occurred. In the remaining four tests (5U.2, 7A.1, 7A.2, 9A.1), in which failure did not occur, the final creep rate can be used in conjunction with Figure 5.55 to give an indication of the ultimate load that would have been obtained had the test been continued to failure. The final incremental loads and creep displacement rates in these tests suggest failure loads similar to those for other tests on the respective piles.

Maximum factors of increase in pile capacity are given in the last two columns of Table 5.14. In the first of the columns, the highest recorded failure load (incremental or CRE) for each pile configuration is compared with the highest recorded failure load for the unexpanded box or unexpanded cruciform pile, as appropriate. In the final column all the piles are compared with the unexpanded box pile. The tests in which the highest failure loads occurred are plotted in Figure 5.56 (box piles) and Figure 5.57 (cruciform piles).

Both the expanded box piles show increases in capacity over the unexpanded Pile 5U. Pile 7A (expansion 14.3%, factor of load increase 1.75) performed better than Pile 5B (expansion 21.4%, factor of load increase 1.47). The expanded cruciform piles show greater factors of increase, in comparison to unexpanded Cruciform Pile 8U. In this case Pile 8B (expansion 21.4%, factor of load increase 2.11) performed marginally better than Pile 9A (expansion 10.7%, factor of load increase 2.00).

Both the expanded cruciform piles show capacities greater than that of the unexpanded box pile, despite the fact that the combined energies of installation for the outer shells and expander mandrels of the expanded cruciform piles were very small in comparison to the installation energy for the outer shell of Box Pile 5U (Section 5.5.7).

The range of calculated average shaft frictions $\bar{\tau}_{s_f}$ for all the piles are plotted against percentage expansion in Figure 5.58 (percentage increase

in pile width) and Figure 5.59 (percentage increase in pile cross-sectional area).

5.7.2 Pile stiffness

Results from selected pile tests for all the piles are given in Figure 5.60. The following points emerge in regard to the stiffness of pile response under applied load:

(a) The unexpanded and expanded box piles have similar stiffnesses within the load range 0 to 150kN.

(b) The expanded cruciform piles are marginally stiffer than the box piles in the load range 0 to 150kN. In the case of Pile 8B this is most probably due to reduced elastic extension of the pile components under load.

(c) In comparison to the other piles, the unexpanded cruciform pile is markedly less stiff.

(d) Reloadings of the expanded piles are much stiffer than initial loadings, particularly in the load range 150 to 300kN.

5.7.3 Overall pile performance in the long term

Testing histories for the piles have been presented in Figures 5.17 to 5.20. As at the chalk site at Luton, there is no indication of a general loss in capacity with time for piles subjected to a sequence of static tests. Although it is difficult to be precise, because of the nature of the incremental testing, none of the piles showed any significant change in capacity with time, with the exception of Cruciform Pile 8B which showed a 21% increase in capacity from 198.9kN to 241.6kN in tests carried out 5 days and 208 days respectively after expansion.

The load:displacement plots of the CRE tests carried out at the end of the test programme all show a steady downward trend in load with displacement. Pile 5B shows a 14% drop in load during 12mm displacement; Pile 8B shows a 13% drop in load during 12mm displacement. This behaviour is similar to that of unexpanded Box Pile 5U, which showed a 7% drop in load during 5mm CRE displacement in Test 5U.1. Box Pile 6U, which was driven to refusal, showed only a 5% reduction in load during 8mm CRE displacement (Test 6U.1, Figure 5.27).

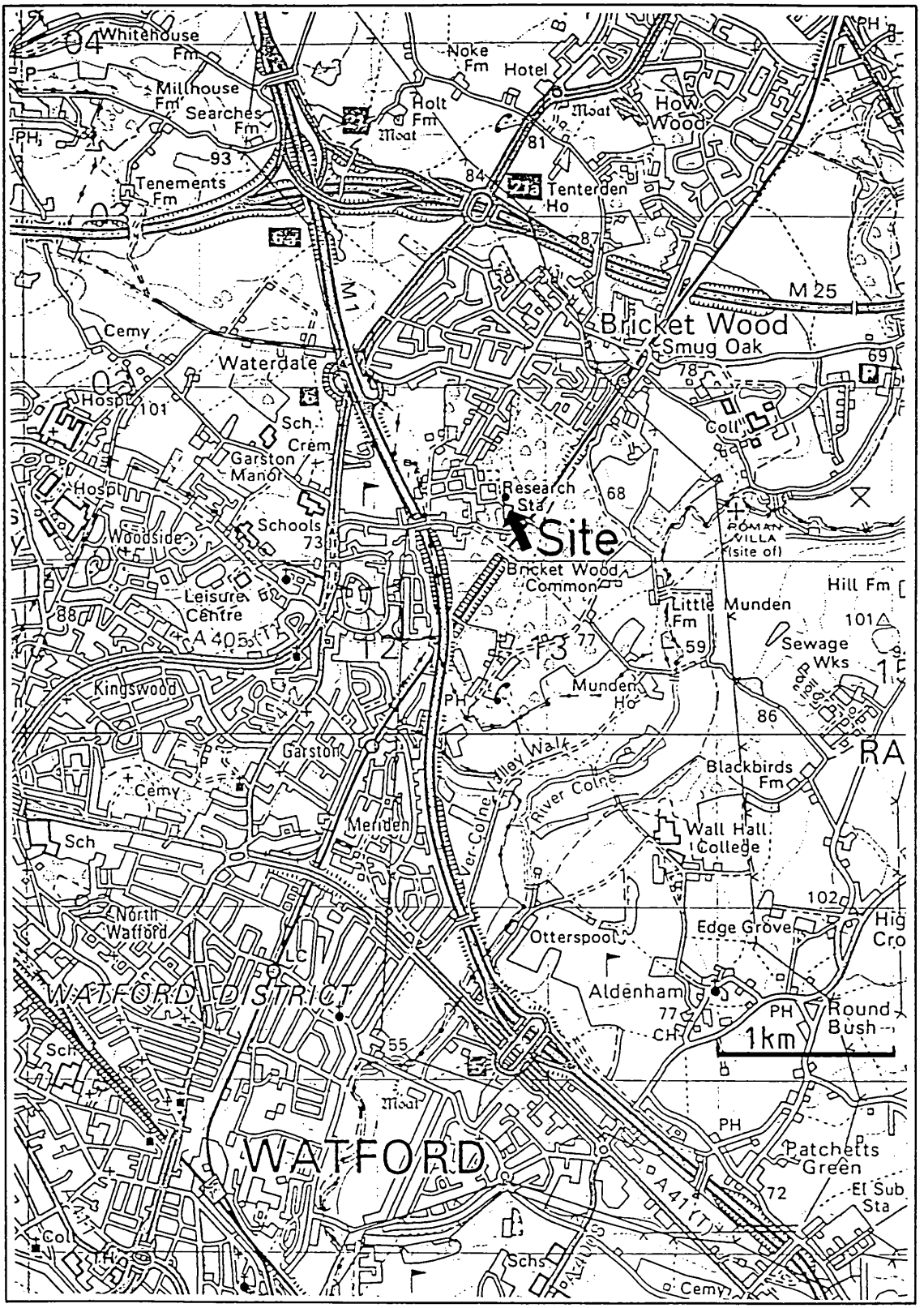

Figure 5.1 Location of BRS site

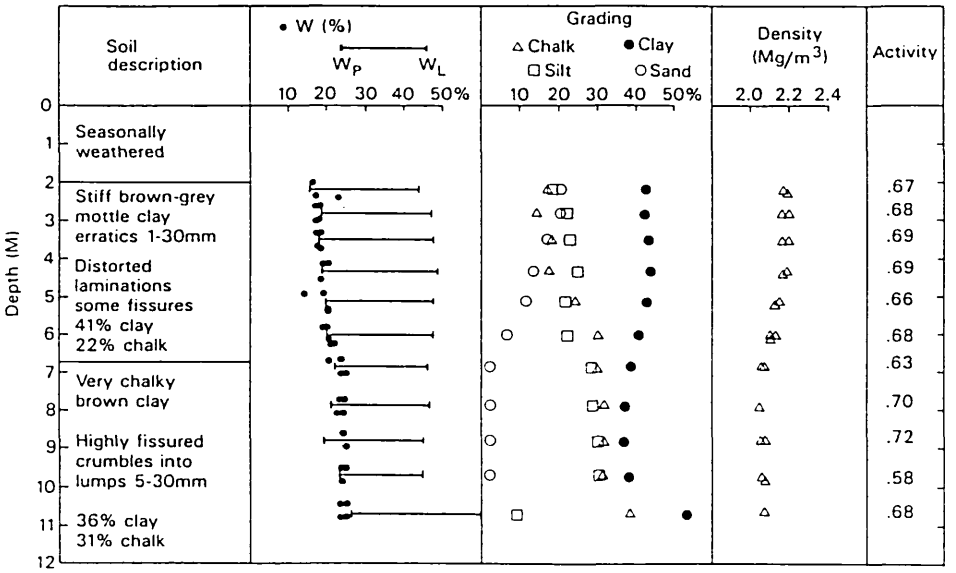

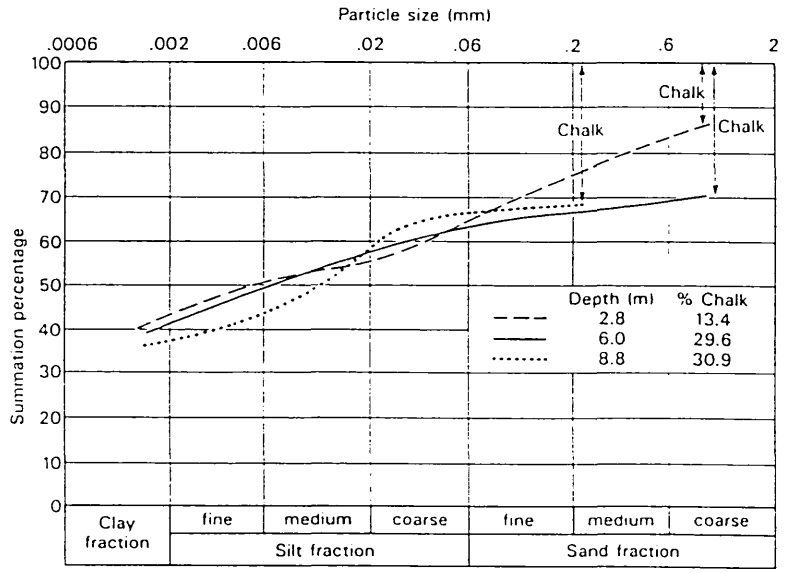

Figure 5.2 Soil profile and typical gradings (after Marsland and Powell, 1989)

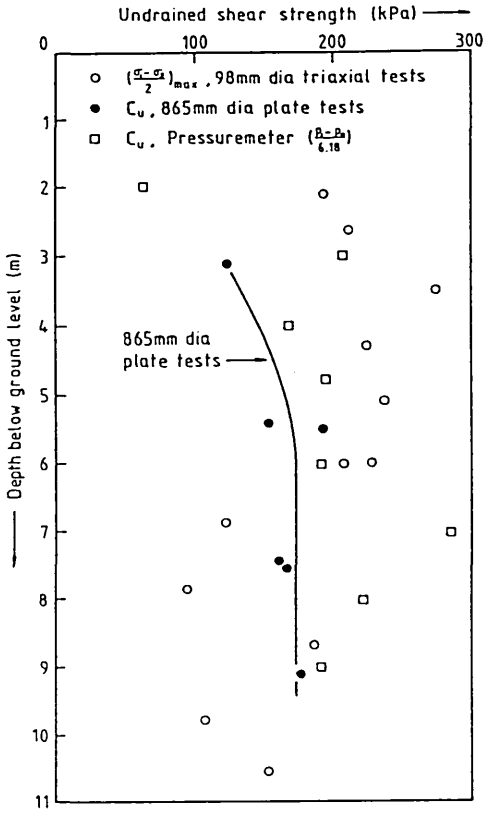

Figure 5.3 Variation of undrained shear strength with depth (after Marsland, 1977)

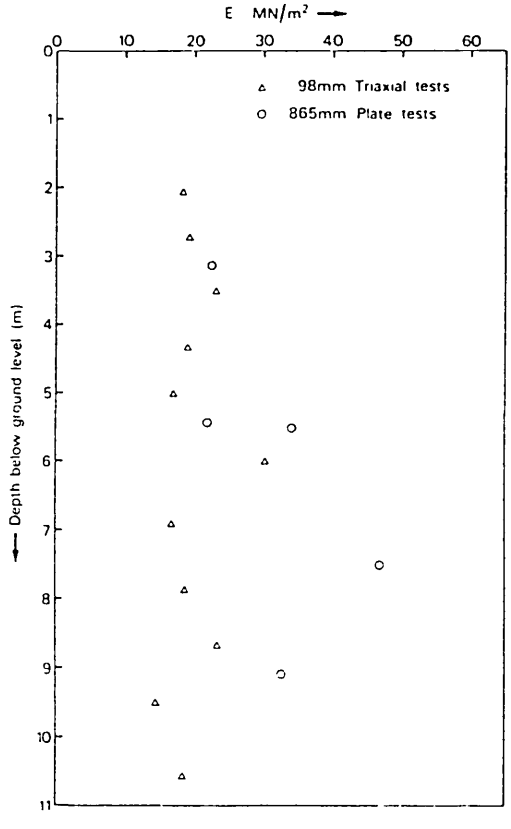

Figure 5.4 Variation of undrained modulus with depth (after Marsland, 1977)

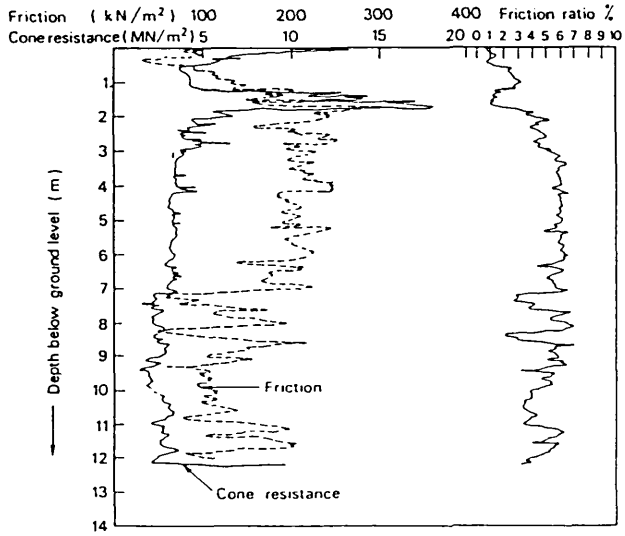

Figure 5.5 Typical profile from previous cone test at BRS
Speed of cone penetration 20mm/sec
(after Marsland, 1977)

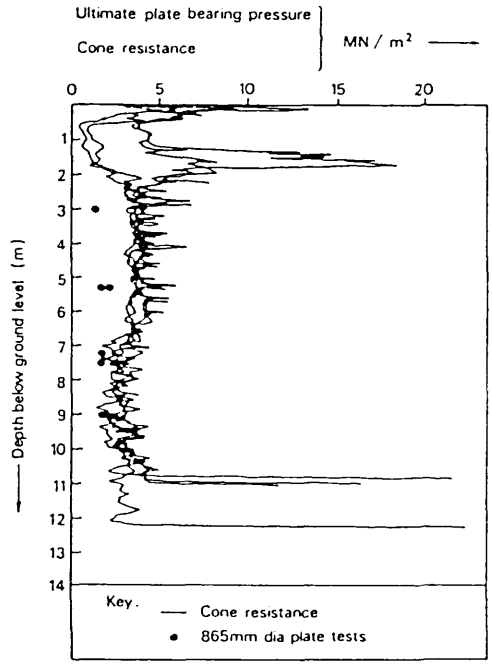

Figure 5.6 Cone profiles at 20mm/sec penetration compared with ultimate bearing pressures measured with 865mm plate
(after Marsland, 1977)

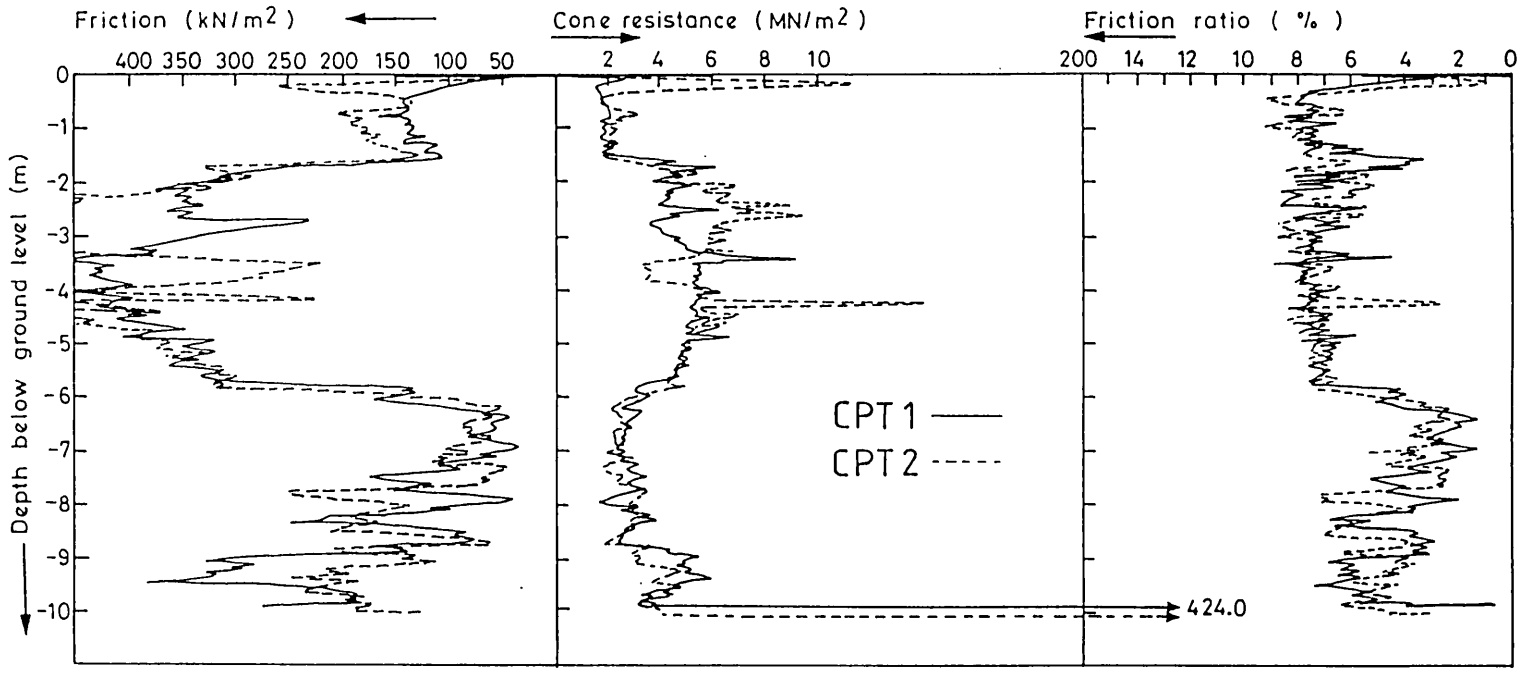

Fugro cone
Rate of penetration 2 cm / sec
Cone cross sectional area 10 cm²
Friction sleeve area 150 cm²

Figure 5.7 Results of Cone Penetration Tests

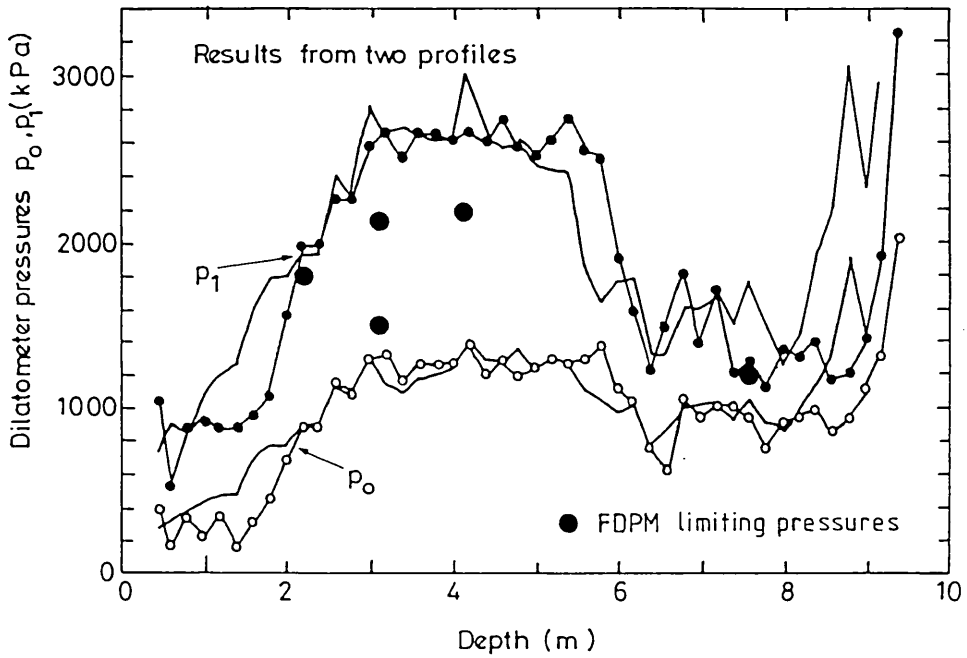

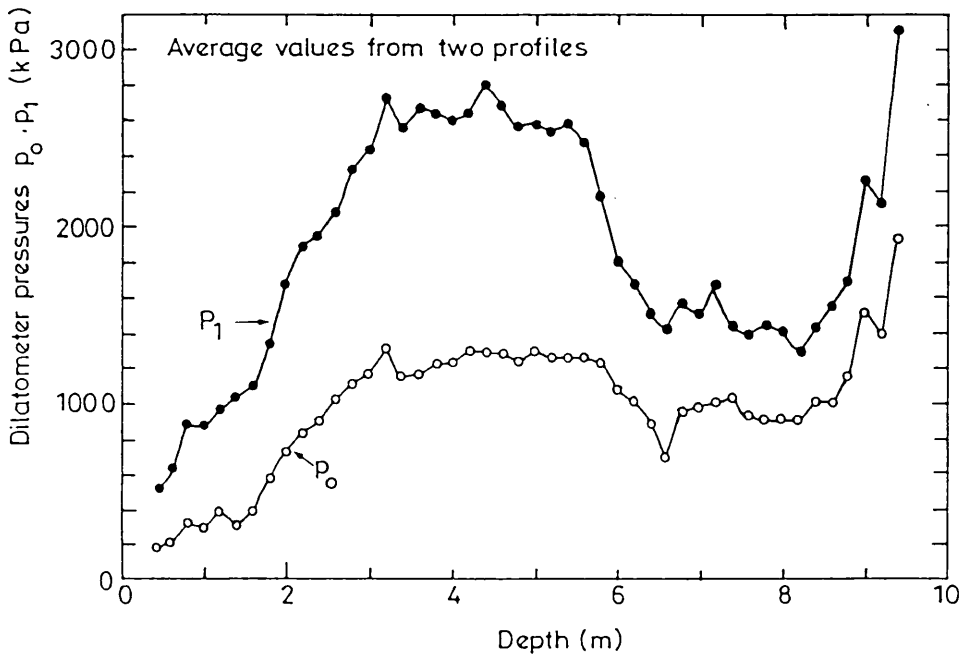

Figure 5.8 DMT pressures p_0 , p_1 against depth

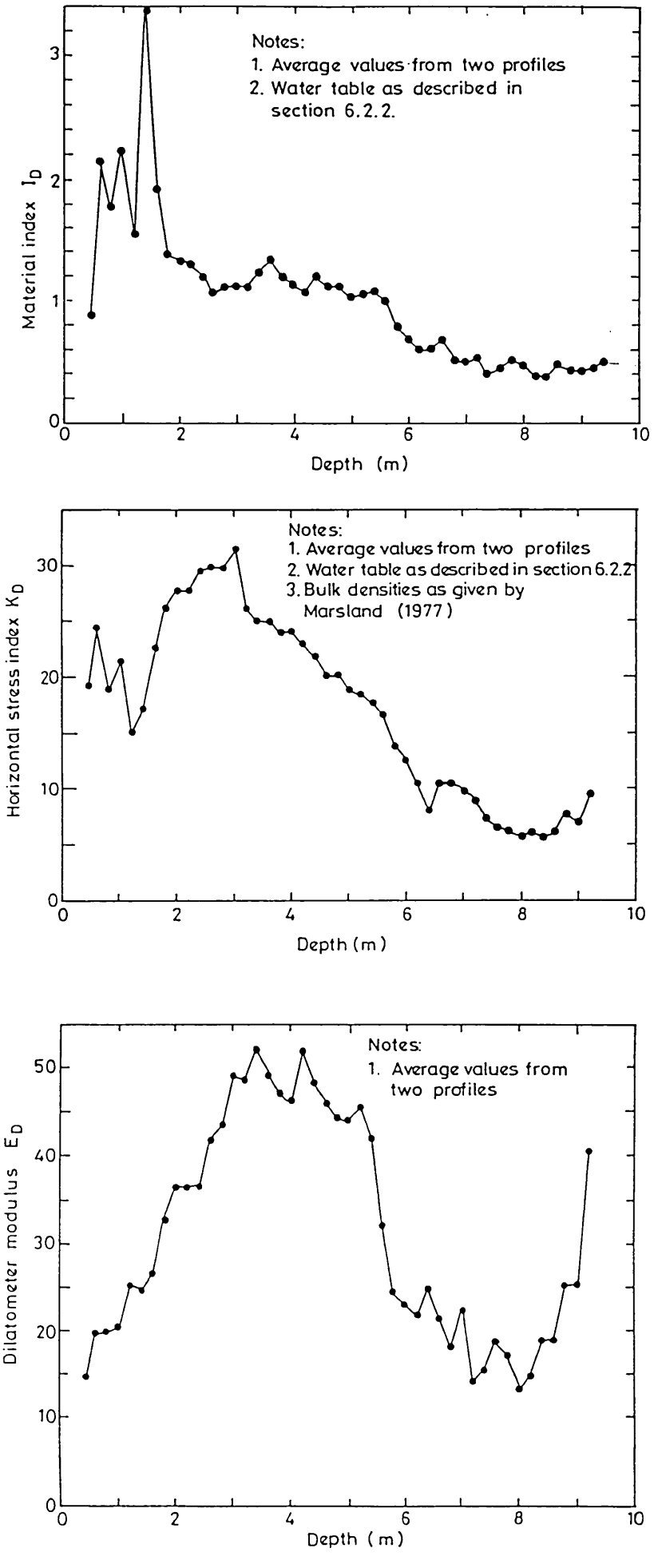

Figure 5.9 DMT index parameters I_D, K_D, E_D against depth

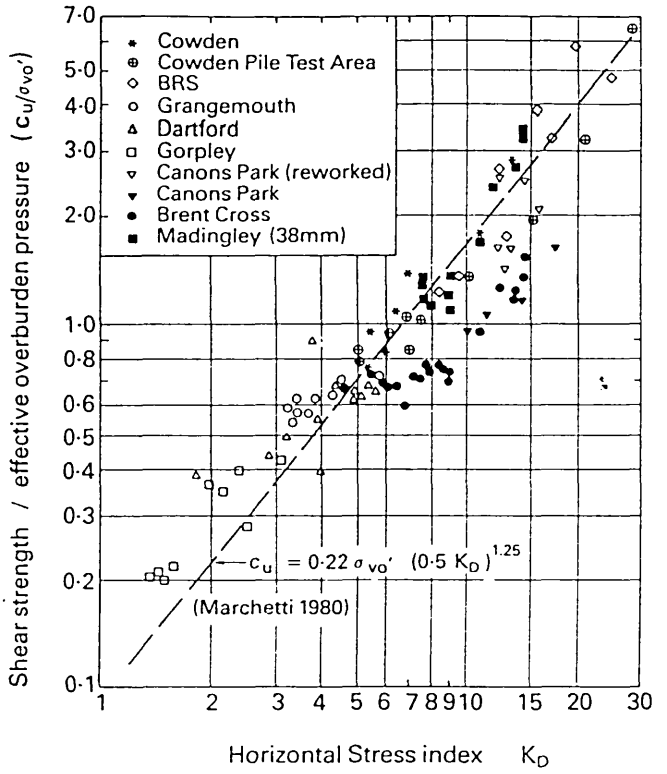

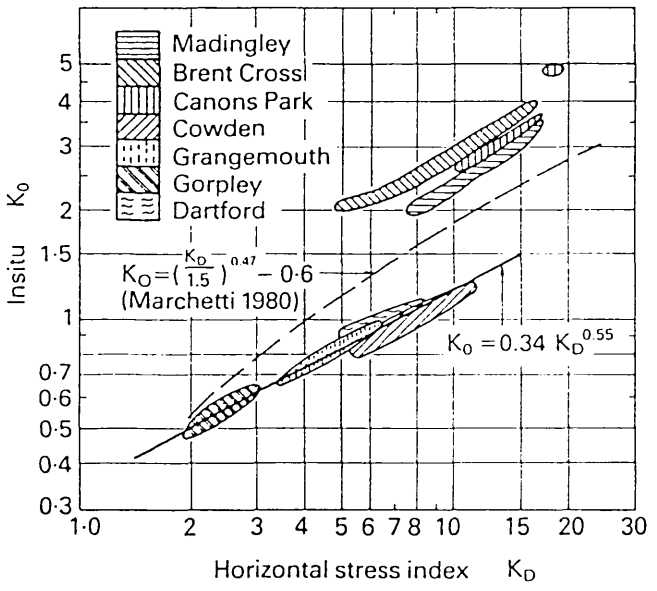

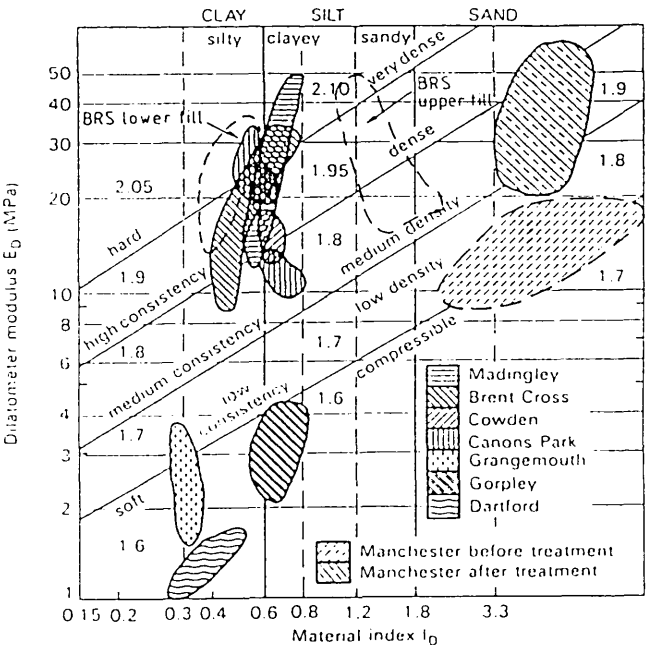

Figure 5.10 DMT identification charts

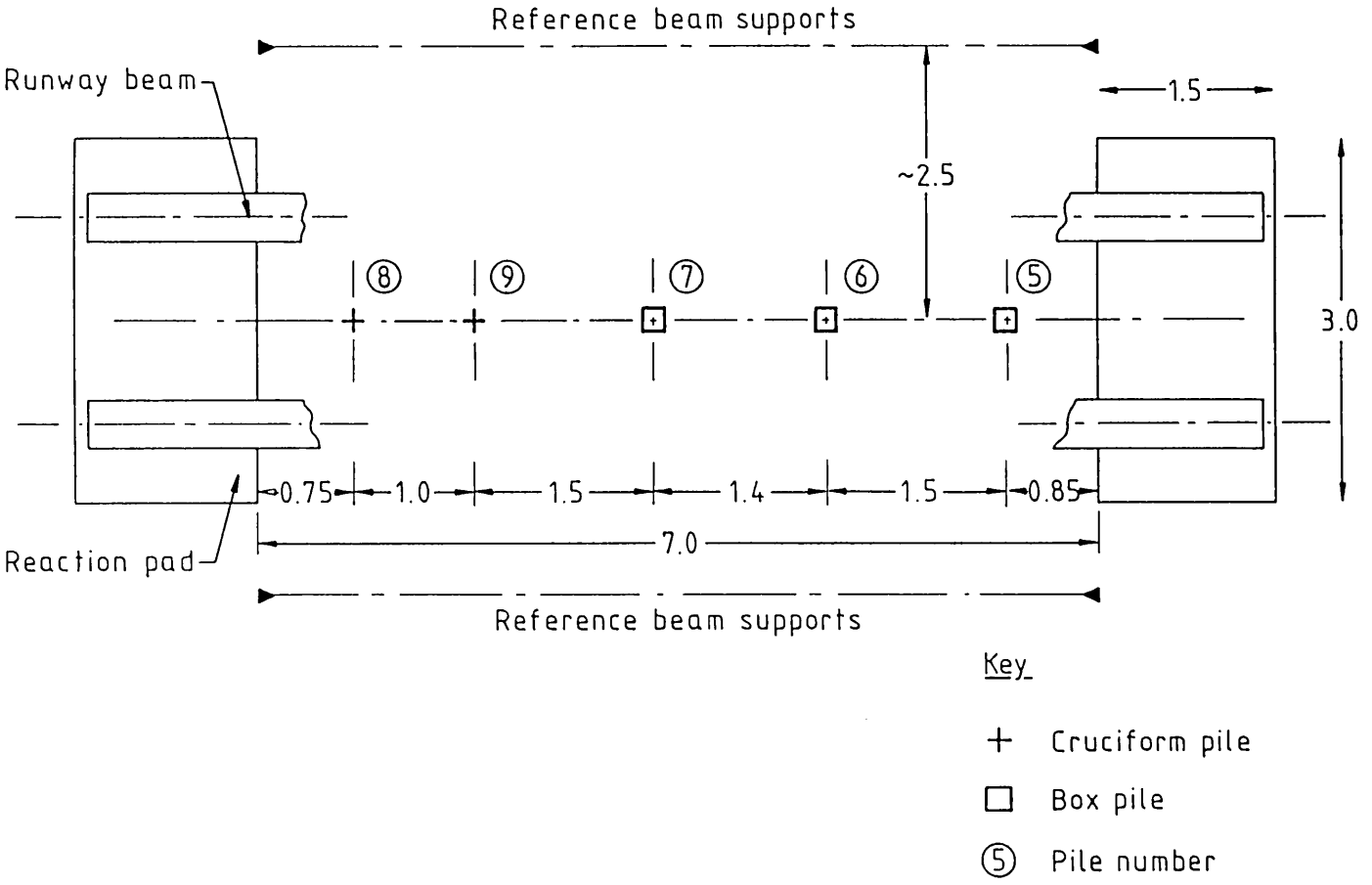

Figure 5.11 Layout of test piles at BRS site

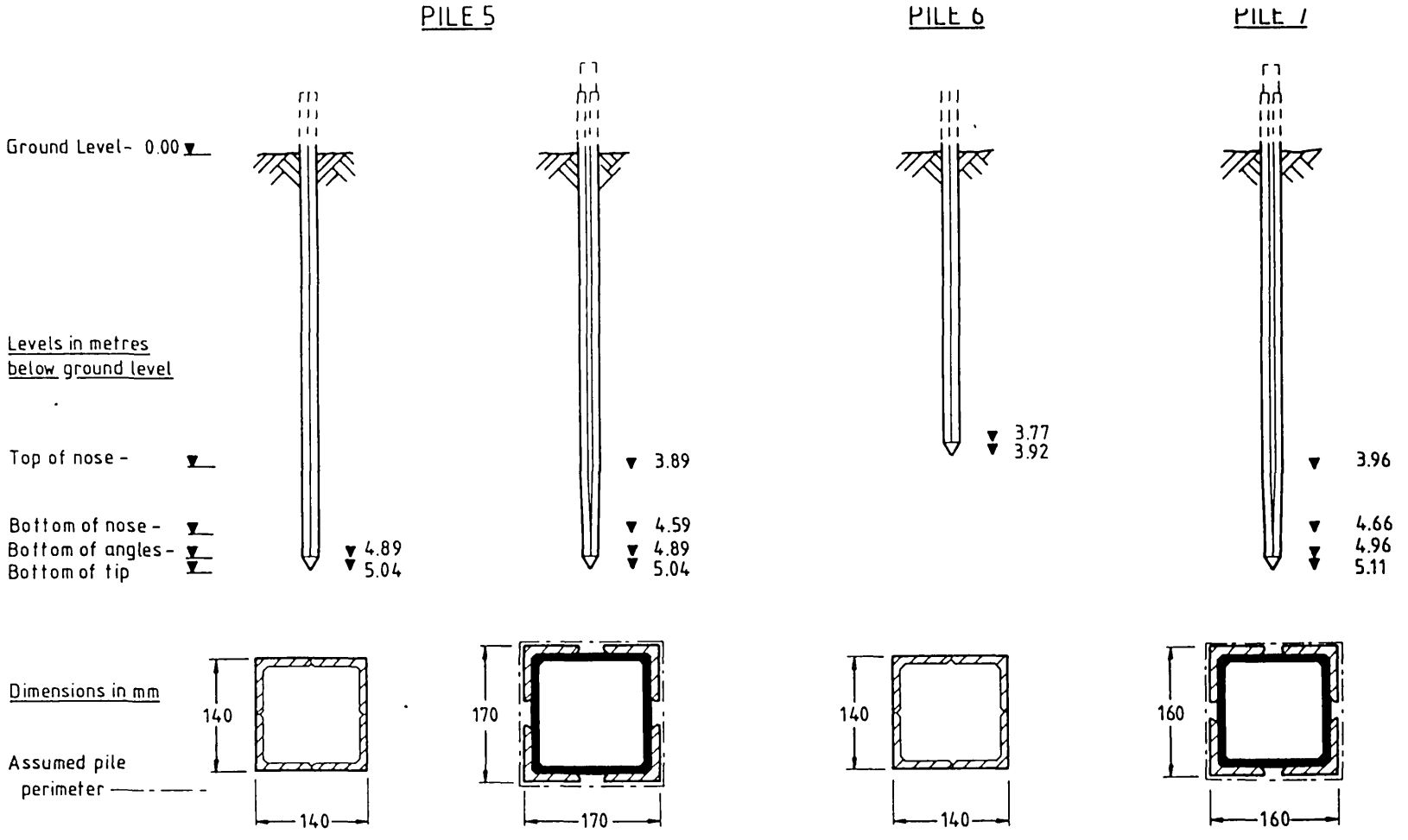

PILE CONFIGURATION	5U	5B	6U	7A
Outer shell driven:	13.3.86	13.3.86	14.3.86	23.5.86
Expander mandrel driven :	-	12.8.86	-	29.5.86
Days elapsed before expansion:	-	152	-	6
Pile width (m):	0.14	0.17	0.14	0.16
Pile X-sectional area (m^2):	0.0196	0.0289	0.0196	0.0256
% expansion of width:	-	21.4	-	14.3
% expansion of area:	-	47.4	-	30.6
Pile weight (kN):	2.7	4.8	2.7	4.6

Figure 5.12
Box piles: Details of dimensions and driven levels

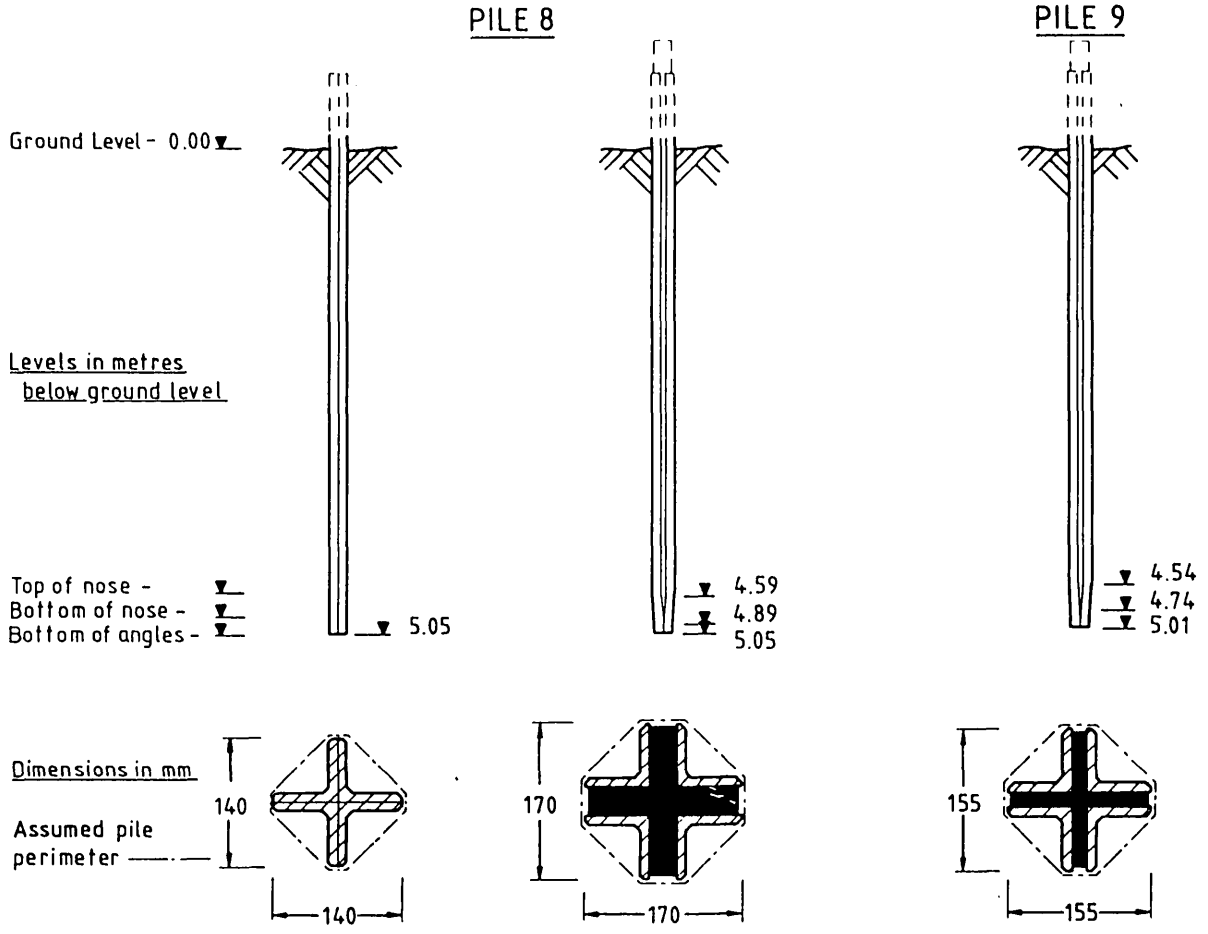

PILE CONFIGURATION	8U	8B	9A
Outer shell driven:	13.5.86	13.5.86	13.5.86
Expander mandrel driven :	-	13.8.86	14.5.86
Days elapsed before expansion:	-	92	1
Pile width (m):	0.14	0.17	0.155
Pile X-sectional area (m^2):	0.0124	0.0217	0.0168
% expansion of width:	-	21.4	10.7
% expansion of area:	-	75.0	35.7
Pile weight (kN):	2.4	6.6	3.9

Figure 5.13
Cruciform piles:
Details of dimensions
and driven levels

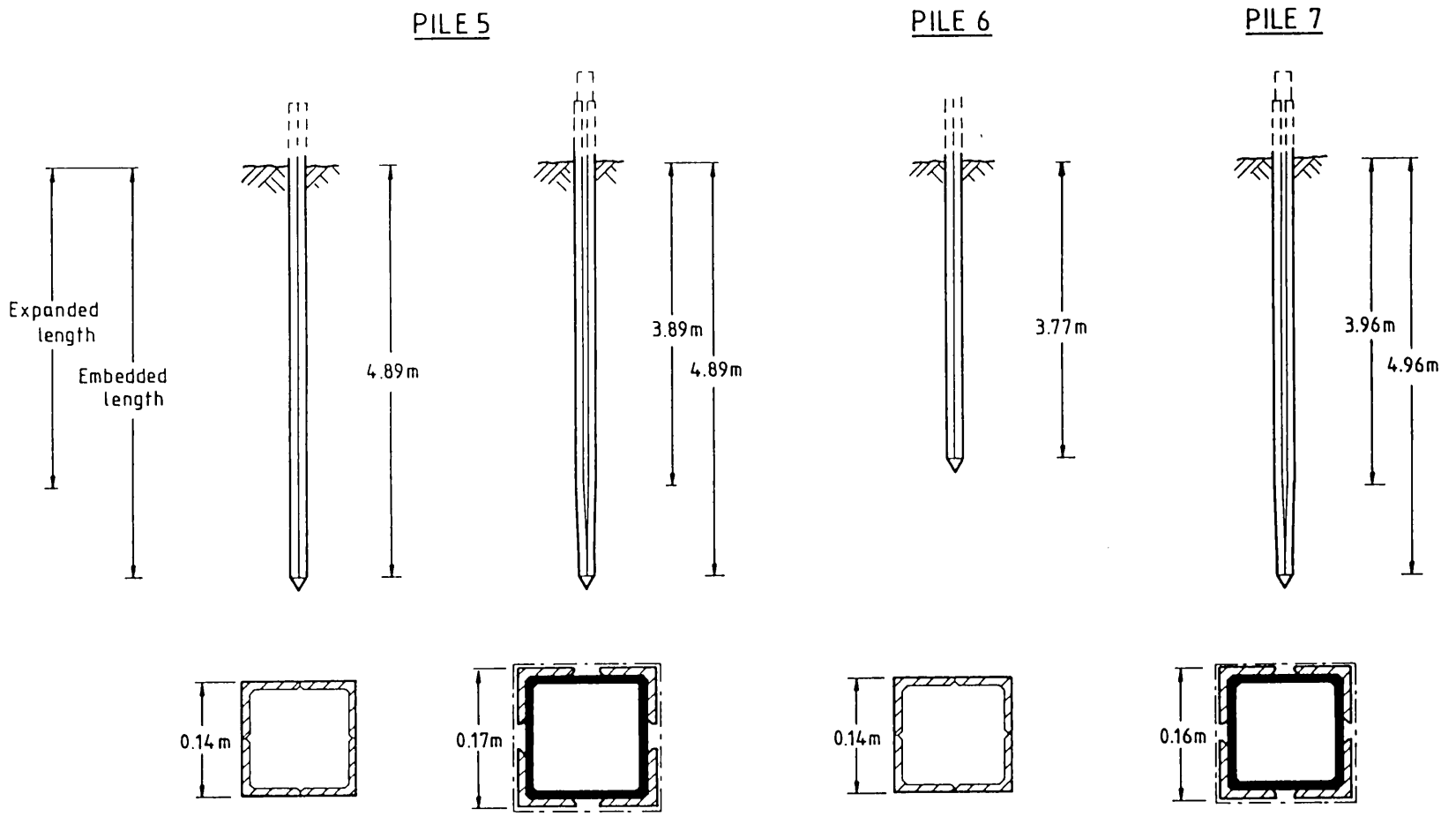

PILE CONFIGURATION	5U	5B	6U	7A
Pile Dimensions (m)				
Embedded length:	4.89	4.89	3.77	4.96
Expanded length:	-	3.89	-	3.96
Full perimeter:	0.56	0.68	0.56	0.64
Reduced perimeter:	-	0.56	-	0.56
Shaft Areas (m^2)				
Embedded length,				
Full perimeter (A):	2.74	3.32	2.11	3.17
Reduced perimeter (B):	-	2.74	-	2.78
Expanded length,				
Full perimeter (C):	-	2.64	-	2.53
Expanded perimeter (D):	-	2.18	-	2.22

Figure 5.14
Box piles: Details of shaft surface areas

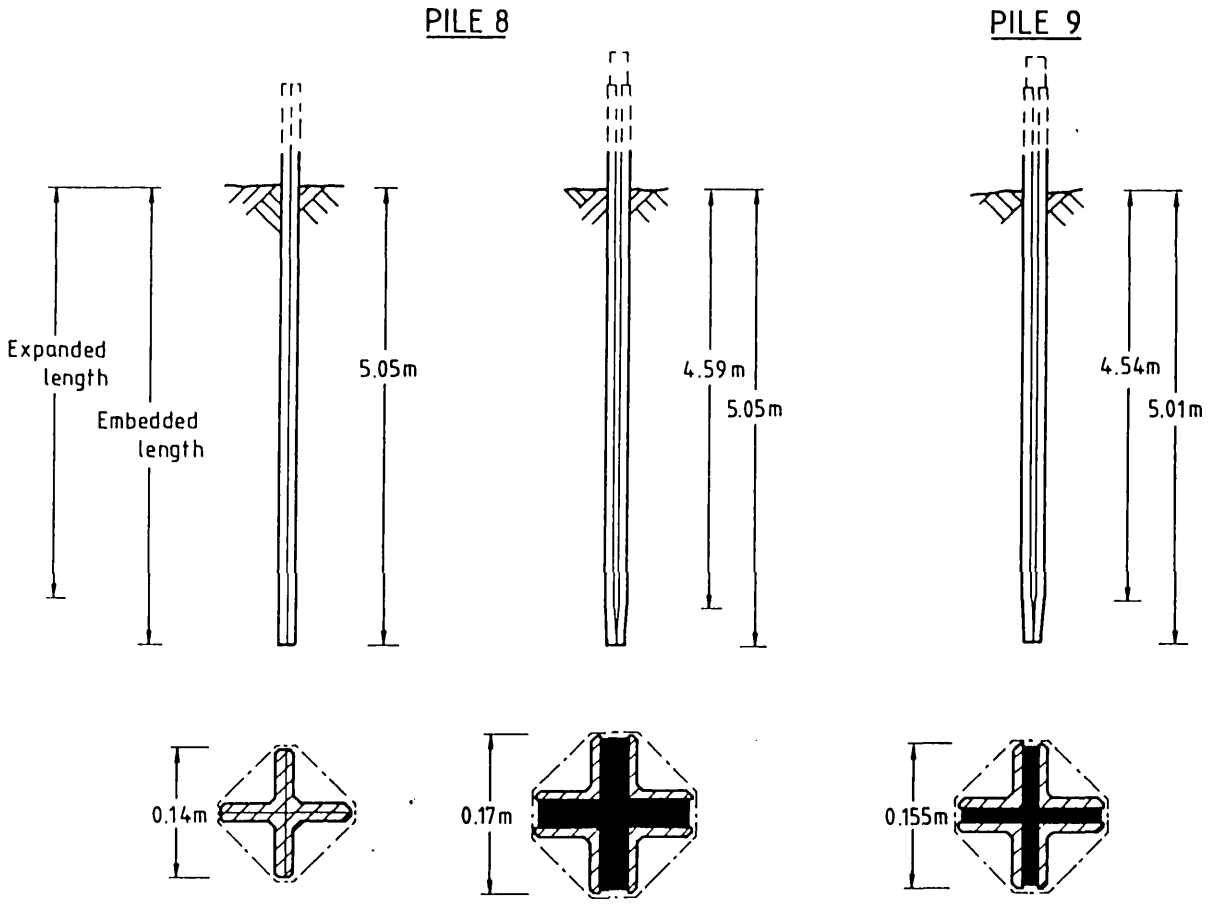

PILE CONFIGURATION	8U	8B	9A
Pile Dimensions (m)			
Embedded length:	5.05	5.05	5.01
Expanded length:	-	4.59	4.54
Full perimeter:	0.42	0.54	0.48
Reduced perimeter:	-	0.42	0.42
Shaft Areas (m^2)			
Embedded length,			
Full perimeter (A):	2.12	2.73	2.40
Reduced perimeter (B):	-	2.12	2.10
Expanded length,			
Full perimeter (C):	-	2.48	2.18
Expanded perimeter (D):	-	1.93	1.91

Figure 5.15
Cruciform piles:
Details of shaft
surface areas

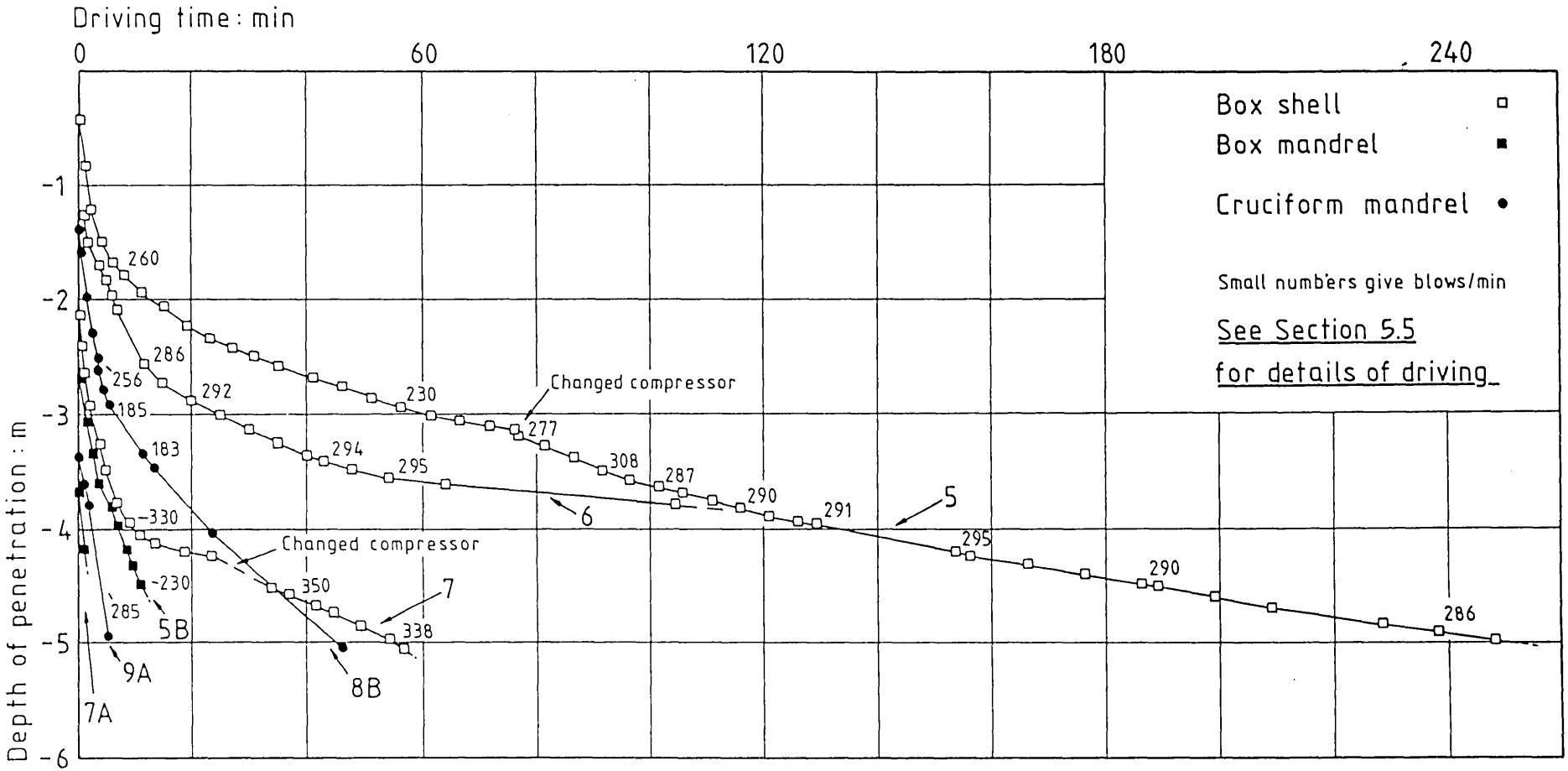

Figure 5.16 Pile driving records at BRS site:
Pile penetration against driving time

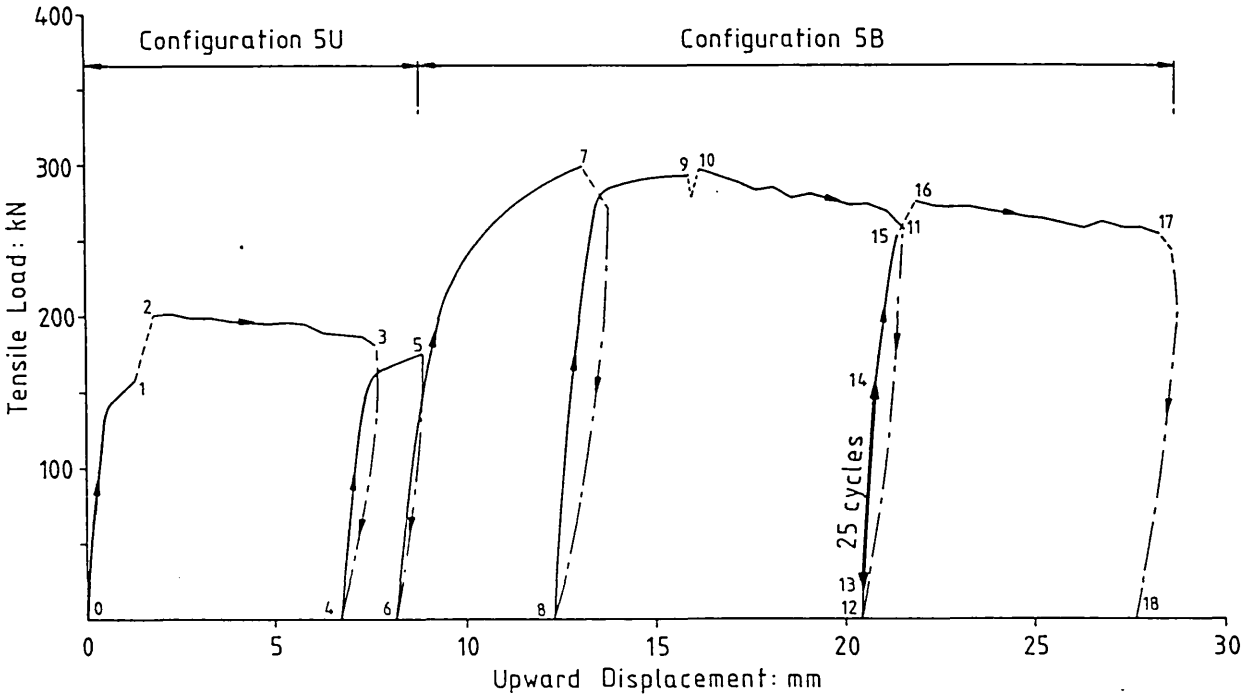

Test No.	Point Nos.	Date	Description of loading	Max. Load (kN)
PILE CONFIGURATION 5U				
5U.1	0-1	25. 4.86	Incremental loading	156.1
	2-3		CRE loading	201.8
5U.2	4-5	30. 7.86	Incremental loading	177.3
PILE CONFIGURATION 5B				
5B.1	6-7	14. 8.86	Incremental loading	299.7
5B.1	8-9	15.12.86	CRL loading	293.0
	10-11		CRE loading	297.4
5B.3	13-14	17.12.86	Cyclic loading	149.4
	14-17		CRE loading	276.3

Figure 5.17 Summary of pile testing: Pile 5

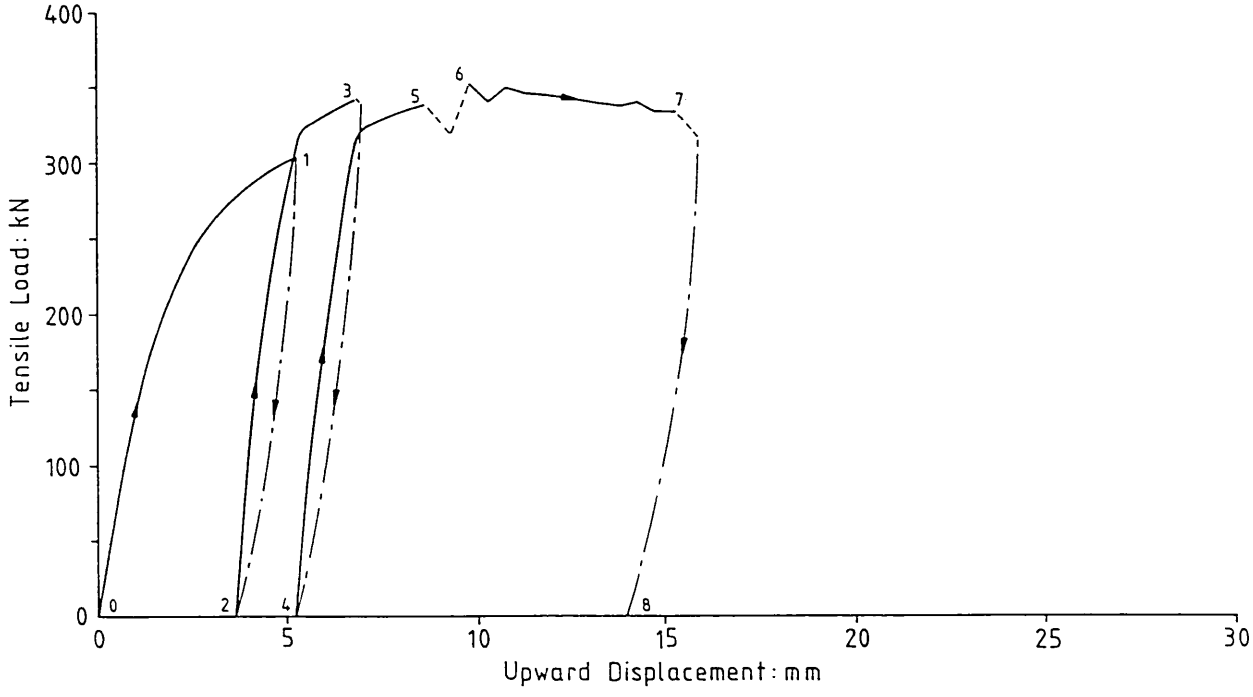

Test No.	Point Nos.	Date	Description of loading	Max. Load (kN)
PILE CONFIGURATION 7A				
7A.1	0-1	30. 5.86	Incremental loading	303.6
7A.2	2-3	29. 7.86	Incremental loading	343.8
7A.3	4-5	9. 1.87	CRL loading	337.9
	6-7		CRE loading	352.5

Figure 5.18 Summary of pile testing: Pile 7

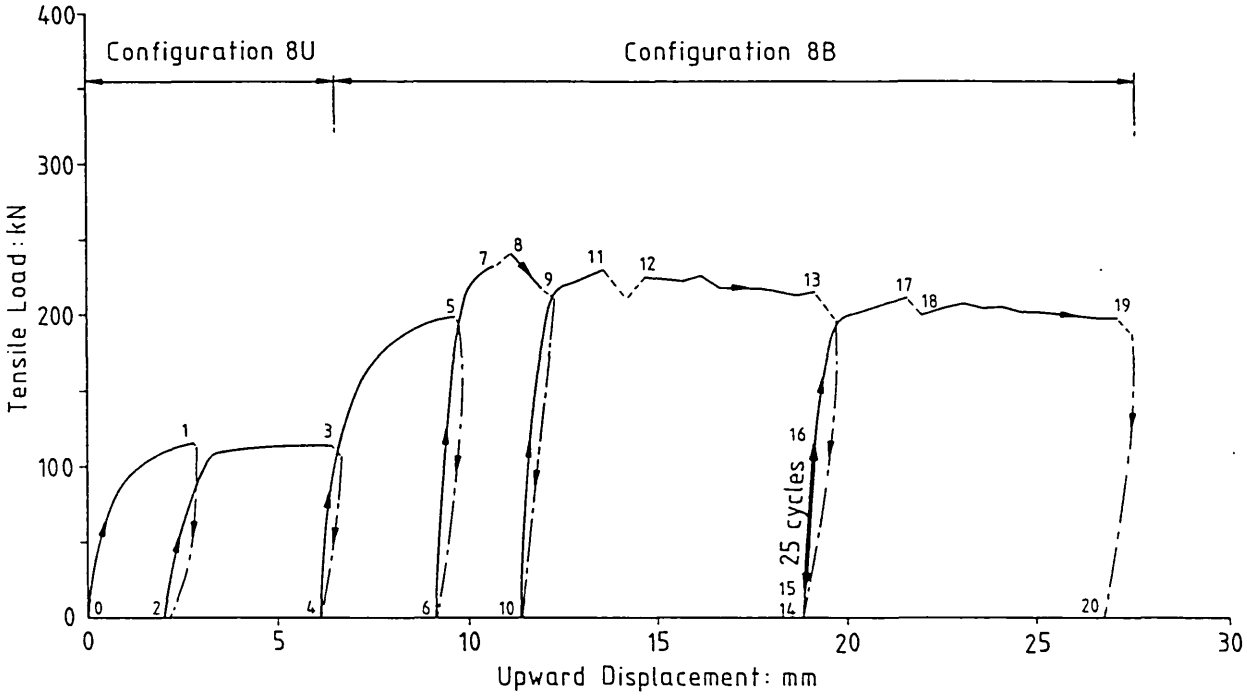

Test No.	Point Nos.	Date	Description of loading	Max. Load (kN)
PILE CONFIGURATION 8U				
8U.1	0-1	20. 5.86	Incremental loading	114.7
8U.2	2-3	31. 7.86	Incremental loading	114.5
PILE CONFIGURATION 8B				
8B.1	4-5	18. 8.86	CRL loading	198.9
8B.2	6-8 (8-9)	9. 3.87	CRL loading (Load relaxation)	241.6
8B.3	10-11 12-13	10. 3.87	CRL loading CRE loading	231.2 226.0
8B.4	15-16 16-17 18-19	10.3.87	Cyclic loading CRL loading CRE loading	114 211.8 207.7

Figure 5.19 Summary of pile testing: Pile 8

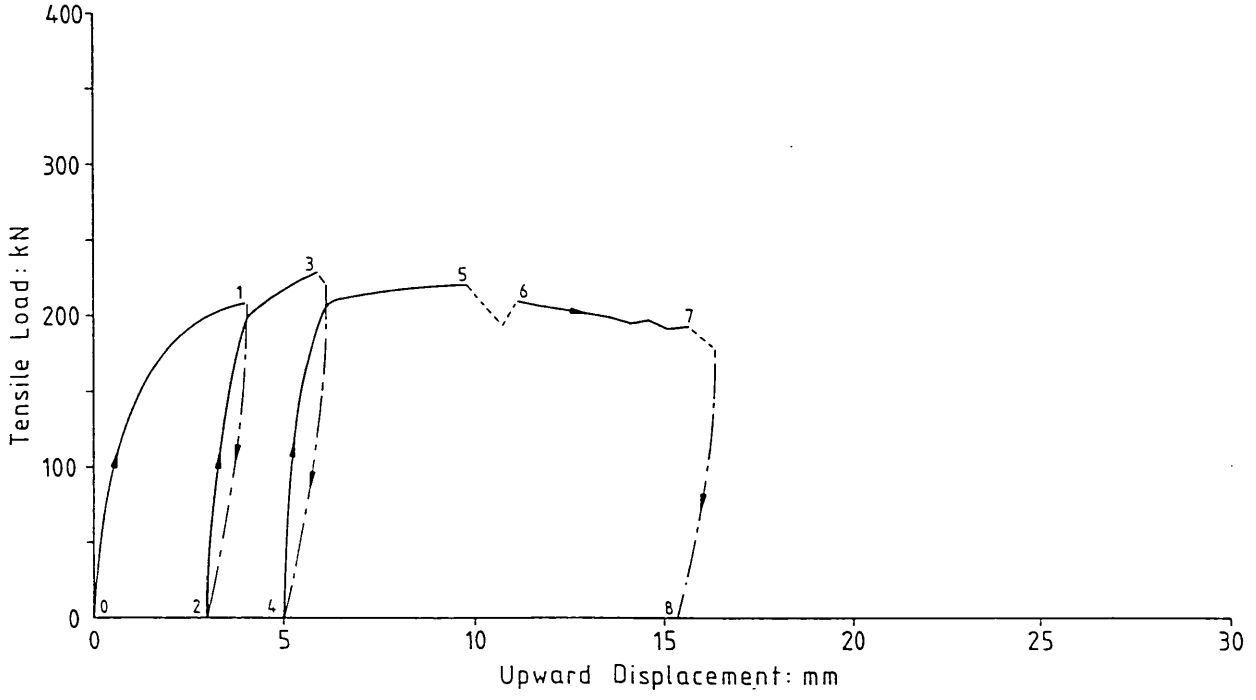

Test No.	Point Nos.	Date	Description of loading	Max. Load (kN)
PILE CONFIGURATION 9A				
9A.1	0-1	21. 5.86	Incremental loading	208.1
9A.2	2-3	1. 8.86	Incremental loading	229.3
9A.3	4-5	20. 3.87	CRL loading	220.8
	6-7		CRE loading	209.8

Figure 5.20 Summary of pile testing: Pile 9

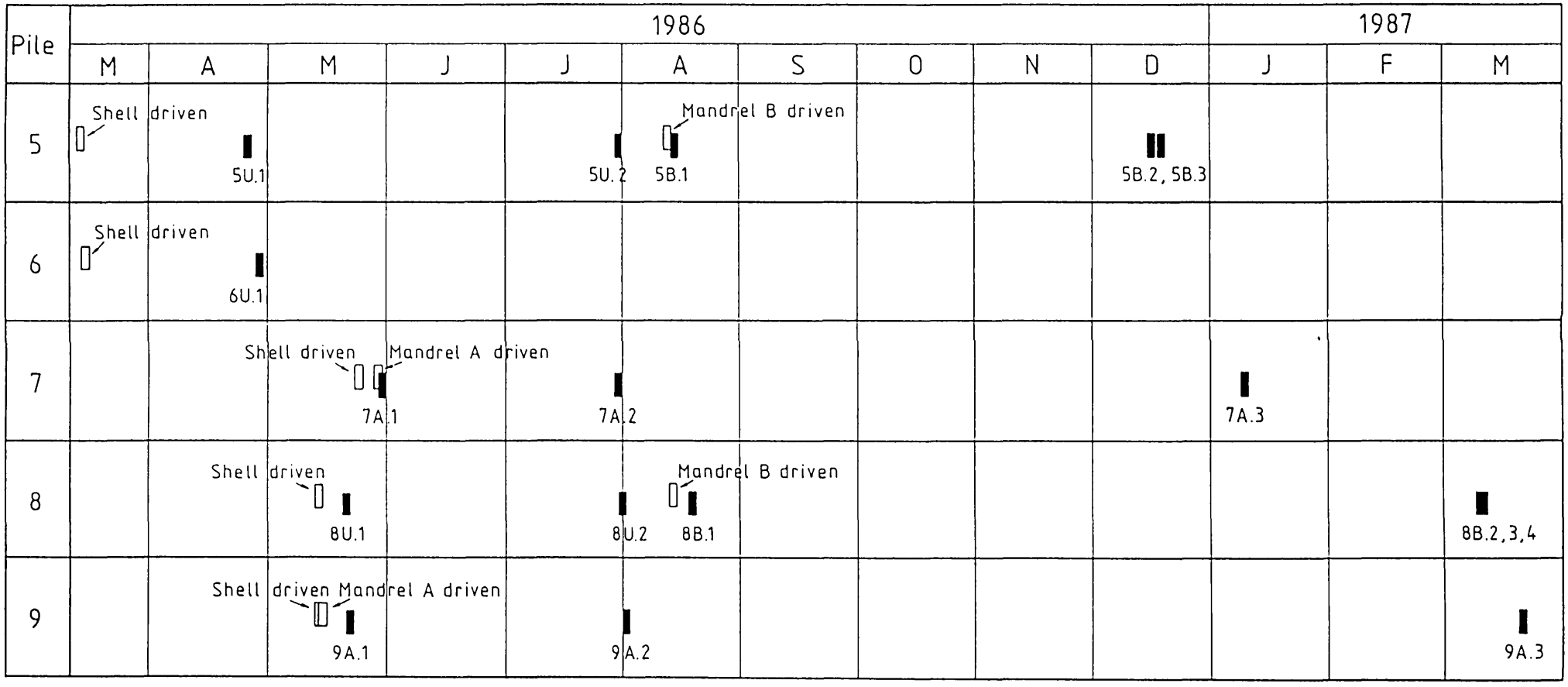

Figure 5.21 Summary of pile testing programme at BRS site

Figure 5.22 Results of Test 5U.1

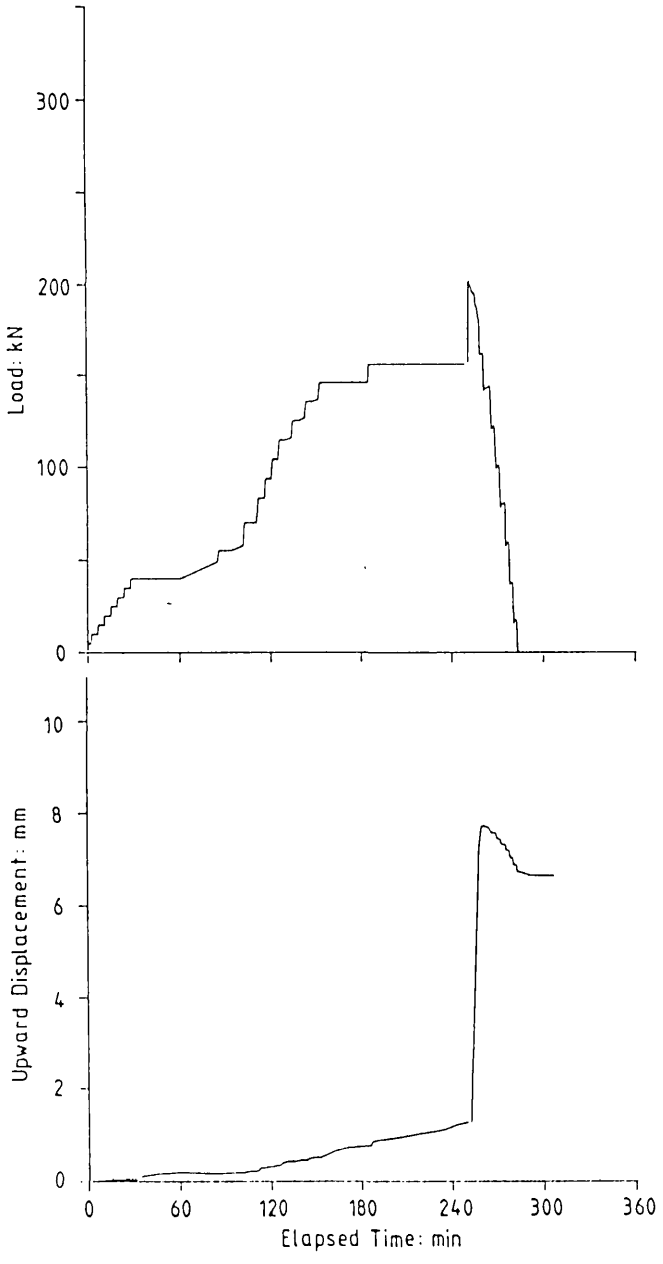

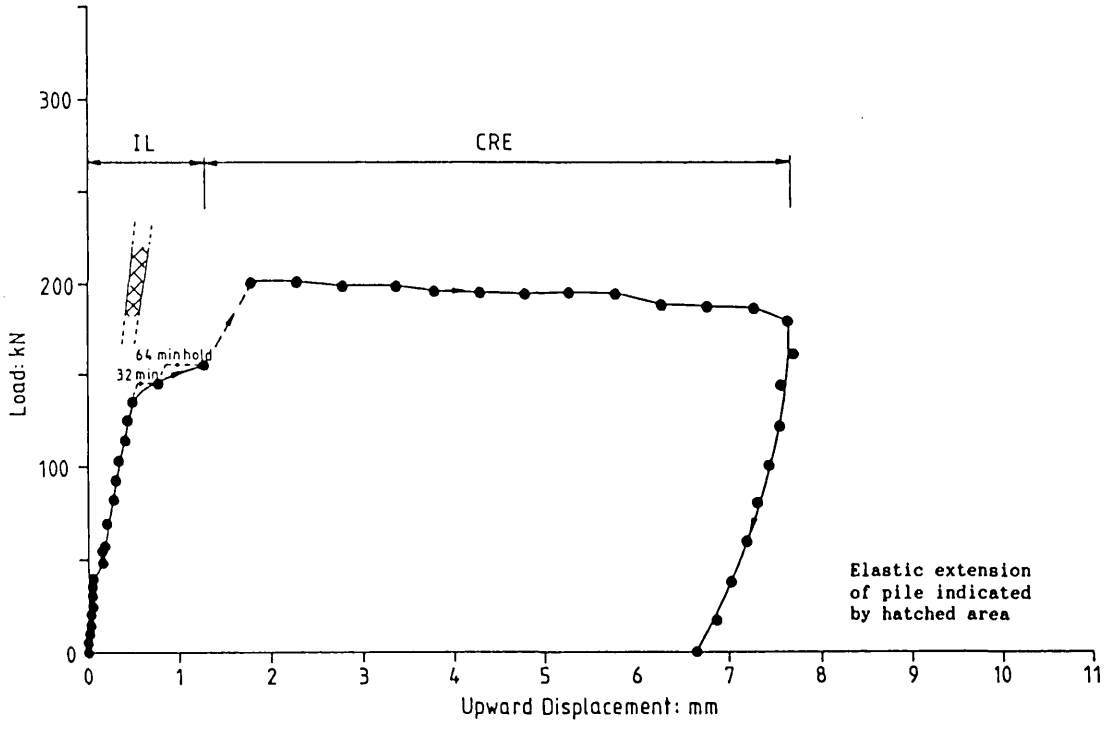

TEST 5U.1 Type: IL, CRE Date: 25.4.86

Outer shell driven: 13.3.86 Expander mandrel driven: -
Days elapsed
prior to test: 43 -

Shaft areas: (m^2) Embedded length, Full X-section (A): 2.74 Reduced X-section (B): - Expanded length, Full X-section (C): - Reduced X-section (D): -

Pile weight: 2.7 (kN)

Test Stage	Maximum Load (Gross) (kN)	(Net) (kN)	Shaft Frictions (A) (kPa)	(B) (kPa)	(C) (kPa)	(D) (kPa)	Displacement at: Max. Load (mm)	End of stage (mm)
IL	156.1	153.4	56.0	-	-	-	1.28	1.28
CRE	201.8	199.1	72.7	-	-	-	2.30	6.64

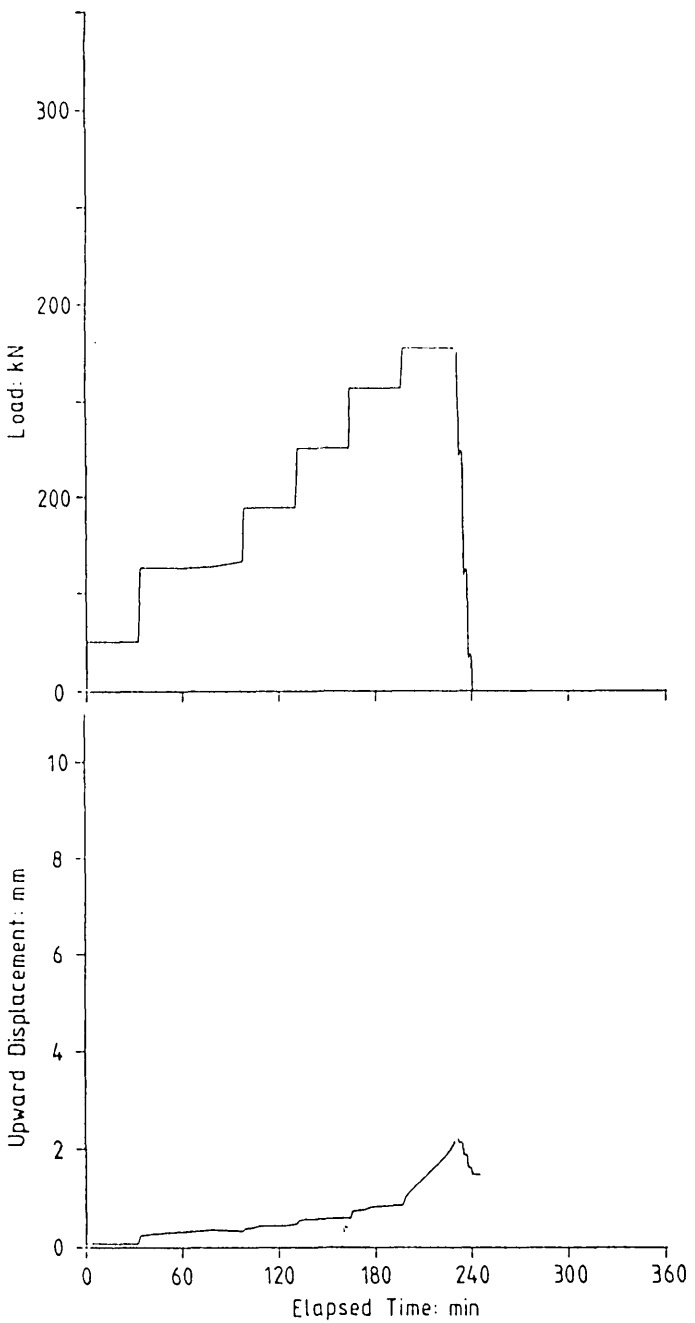

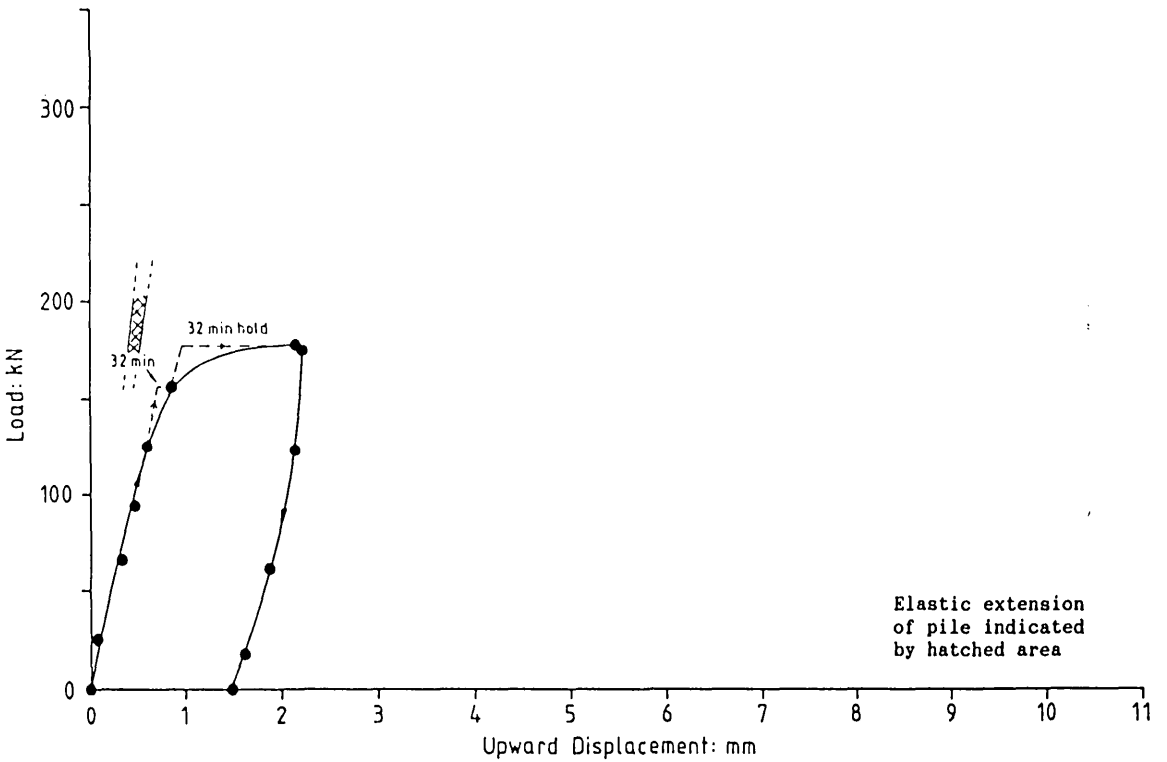

TEST 5U.2 Type: IL Date: 30.7.86

Outer shell driven: 13.3.86 Expander mandrel driven: -
Days elapsed
prior to test: 139 -

Shaft areas: (m^2) Embedded length, Full X-section (A): 2.74 Reduced X-section (B): - Expanded length, Full X-section (C): - Reduced X-section (D): -

Pile weight: 2.7 (kN)

Test Stage	Maximum Load (Gross) (kN)	(Net) (kN)	Shaft Frictions (A) (kPa)	(B) (kPa)	(C) (kPa)	(D) (kPa)	Displacement at: Max. Load (mm)	End of stage (mm)
IL	177.3	174.6	63.8	-	-	-	2.16	1.48

Figure 5.23 Results of Test 5U.2

Figure 5.24 Results of Test 5B.1

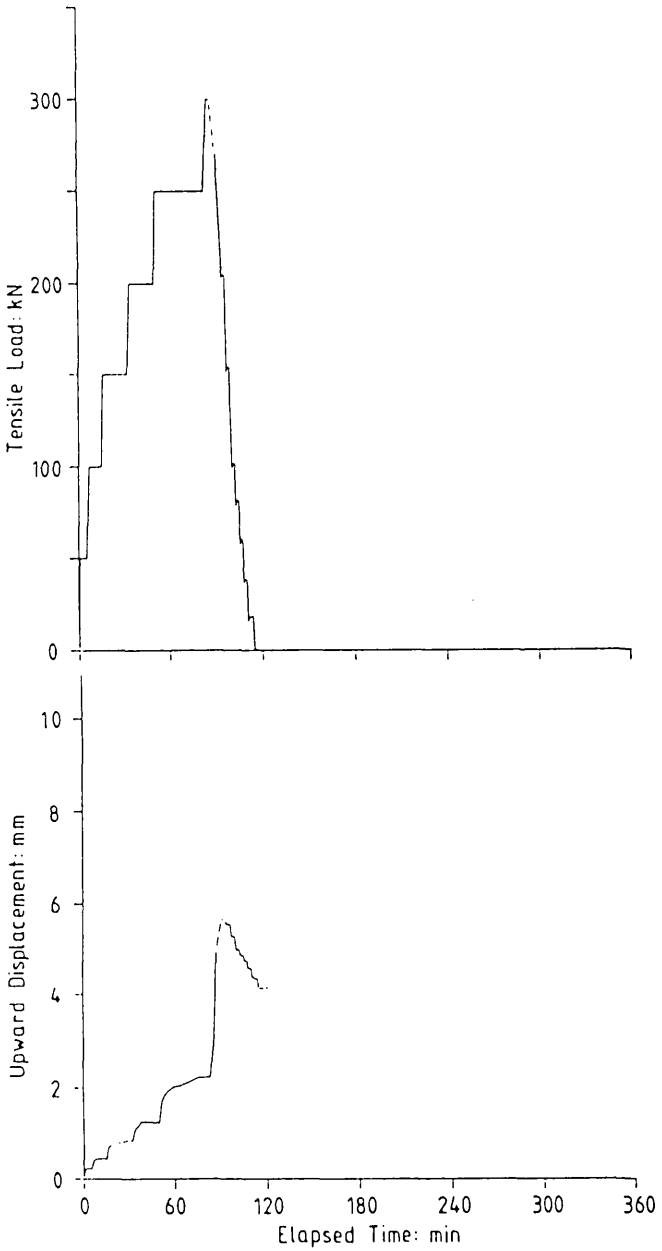

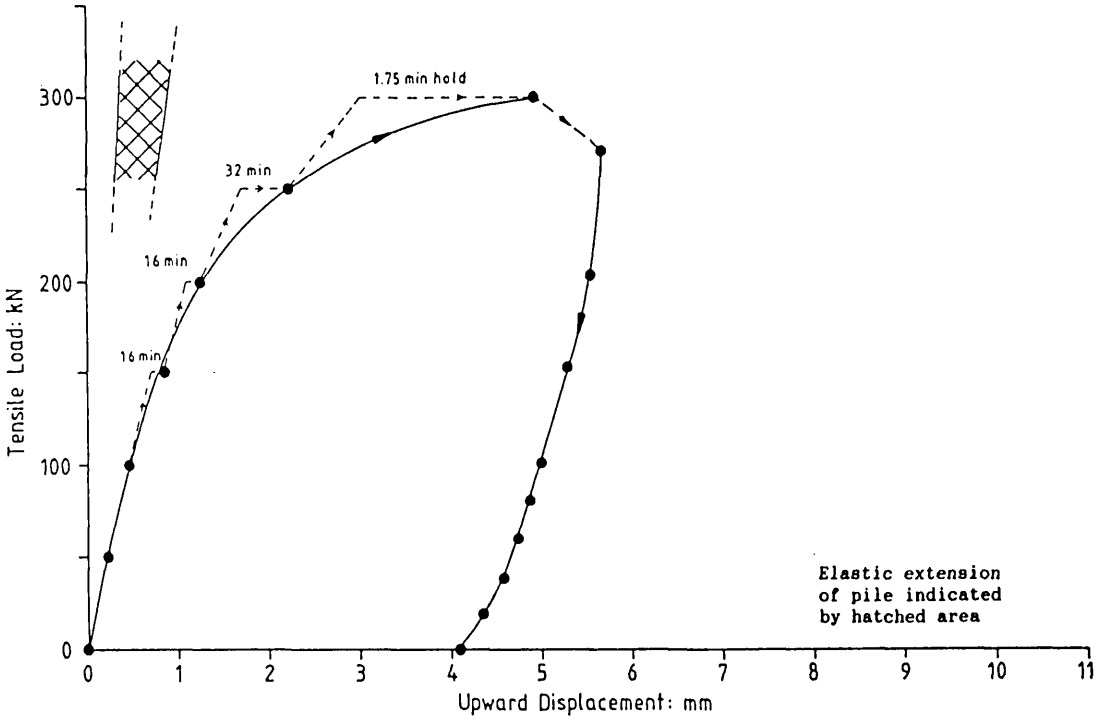

TEST 5B.1 Type: IL Date: 14.8.86

Outer shell driven: 13.3.86 Expander mandrel driven: 12.8.86
Days elapsed
prior to test: 154 2

Shaft areas: (m^2) Embedded length, Expanded length,
Full X-section (A): 3.32 Full X-section (C): 2.64
Reduced X-section (B): 2.74 Reduced X-section (D): 2.18

Pile weight: 4.8 (kN)

Test Stage	Maximum Load (Gross)	(Net)	Shaft Frictions (A)	(B)	(C)	(D)	Displacement at: Max. Load	End of stage
	(kN)	(kN)	(kPa)	(kPa)	(kPa)	(kPa)	(mm)	(mm)
IL	299.7	294.9	88.7	107.7	111.5	135.4	4.92	4.12

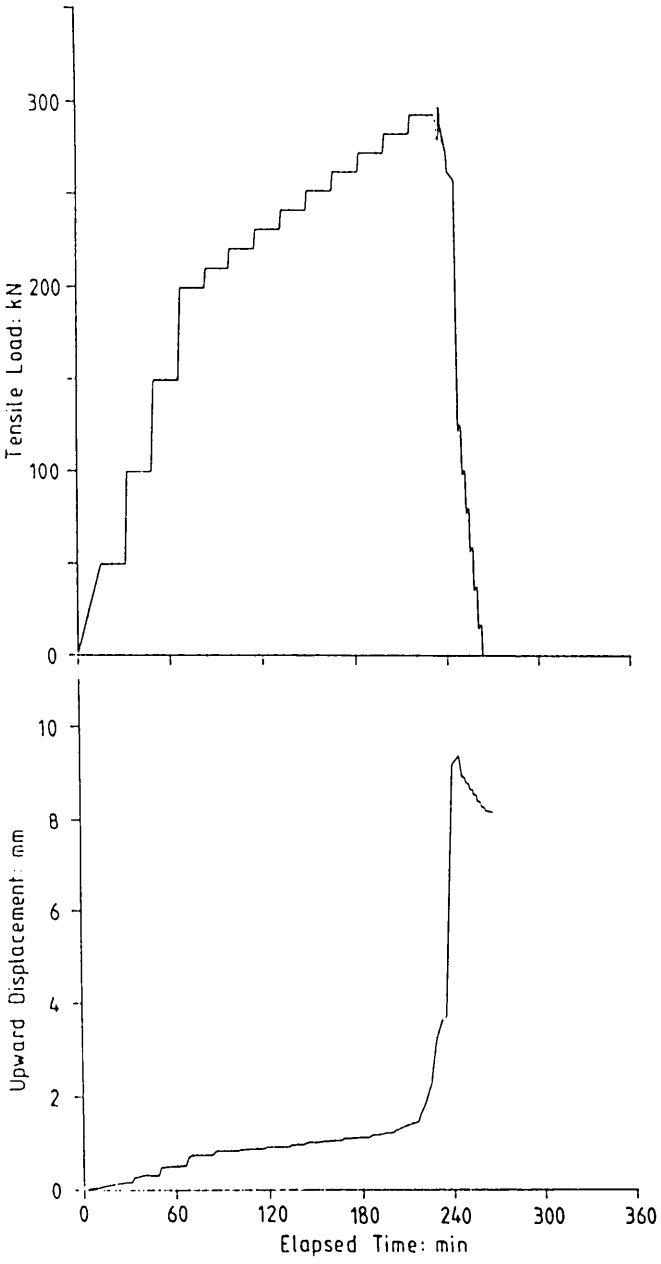

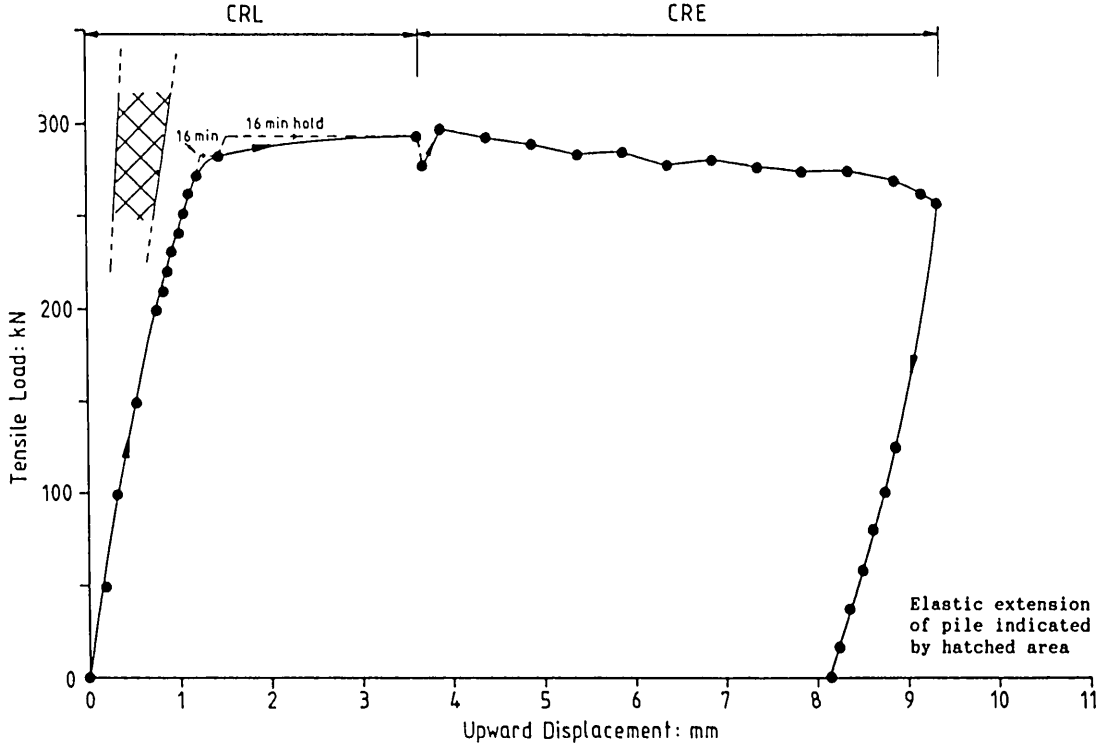

TEST 5B.2 Type: CRL, CRE Date: 15.12.86

Outer shell driven: 13.3.86 Expander mandrel driven: 12.8.86
Days elapsed
prior to test: .274 122

Shaft areas: (m^2)
Embedded length, Full X-section (A): 3.32
Embedded length, Reduced X-section (B): 2.74
Expanded length, Full X-section (C): 2.64
Expanded length, Reduced X-section (D): 2.18

Pile weight: 4.8 (kN)

Test Stage	Maximum Load (Gross) (kN)	Maximum Load (Net) (kN)	Shaft Frictions (A) (kPa)	(B) (kPa)	(C) (kPa)	(D) (kPa)	Displacement at: Max. Load (mm)	End of stage (mm)
CRL	293.0	-	-	-	-	-	3.64	3.64
CRE	297.4	292.6	88.0	106.9	110.6	134.3	3.90	8.15

Figure 5.25 Results of Test 5B.2

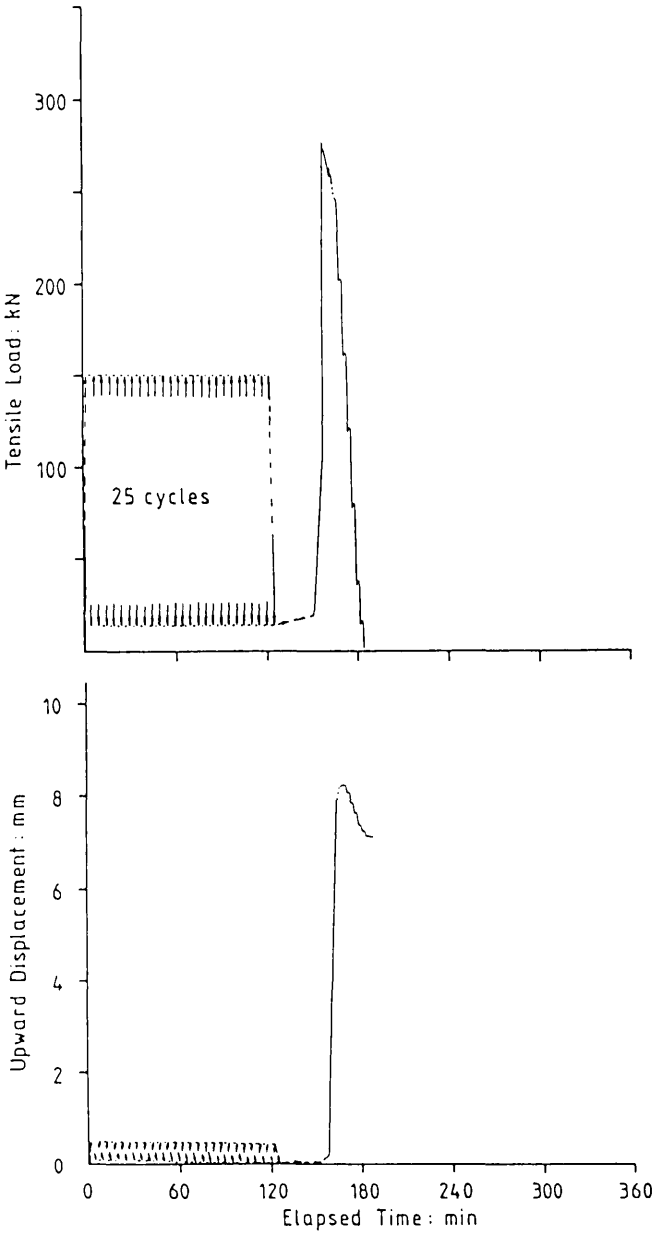

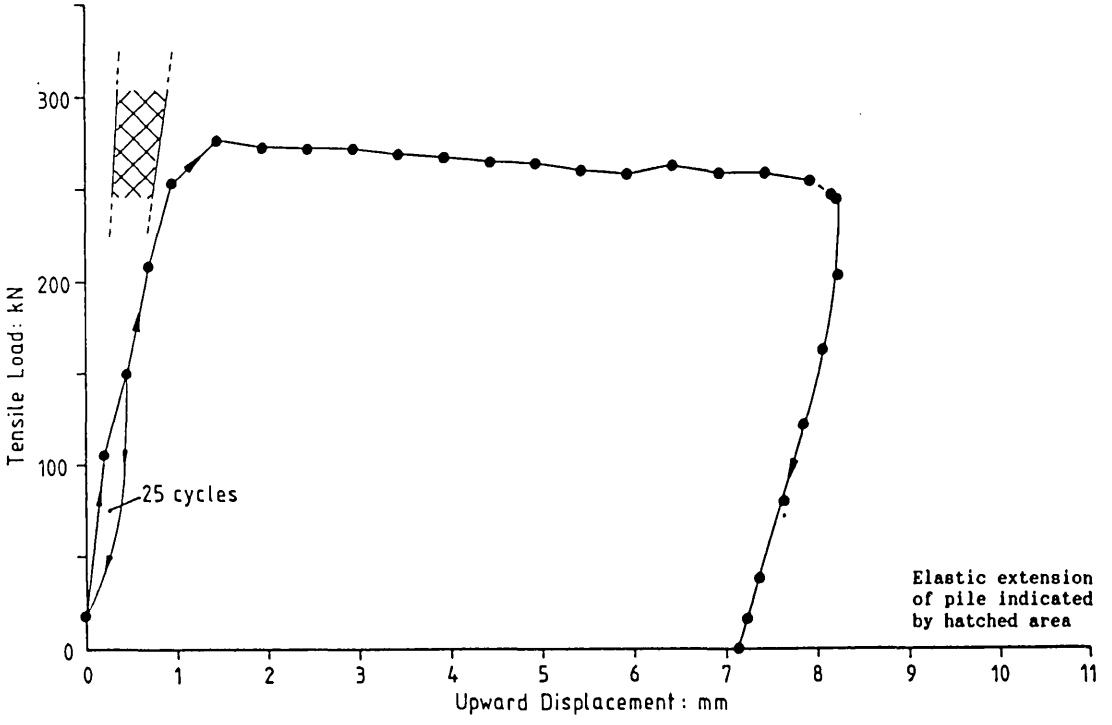

TEST 5B.3 Type: Cyclic, CRE Date: 17.12.86

Outer shell driven: 13.3.86 Expander mandrel driven: 12.8.86

Days elapsed prior to test: 276 124

Shaft areas (m^2): Embedded length, Full X-section (A): 3.32; Reduced X-section (B): 2.74. Expanded length, Full X-section (C): 2.64; Reduced X-section (D): 2.18

Pile weight: 4.8 (kN)

Test Stage	Maximum Load (Gross) (kN)	Maximum Load (Net) (kN)	Shaft Friction (A) (kPa)	Shaft Friction (B) (kPa)	Shaft Friction (C) (kPa)	Shaft Friction (D) (kPa)	Displacement at: Max. Load (mm)	Displacement at: End of stage (mm)
Cyclic[1]	-	-	-	-	-	-	-	-
CRE	276.3	271.5	81.6	99.2	102.6	124.7	1.44	7.12

Notes: 1. 25 cycles, 15kN - 149.4kN

Figure 5.26 Results of Test 5B.3

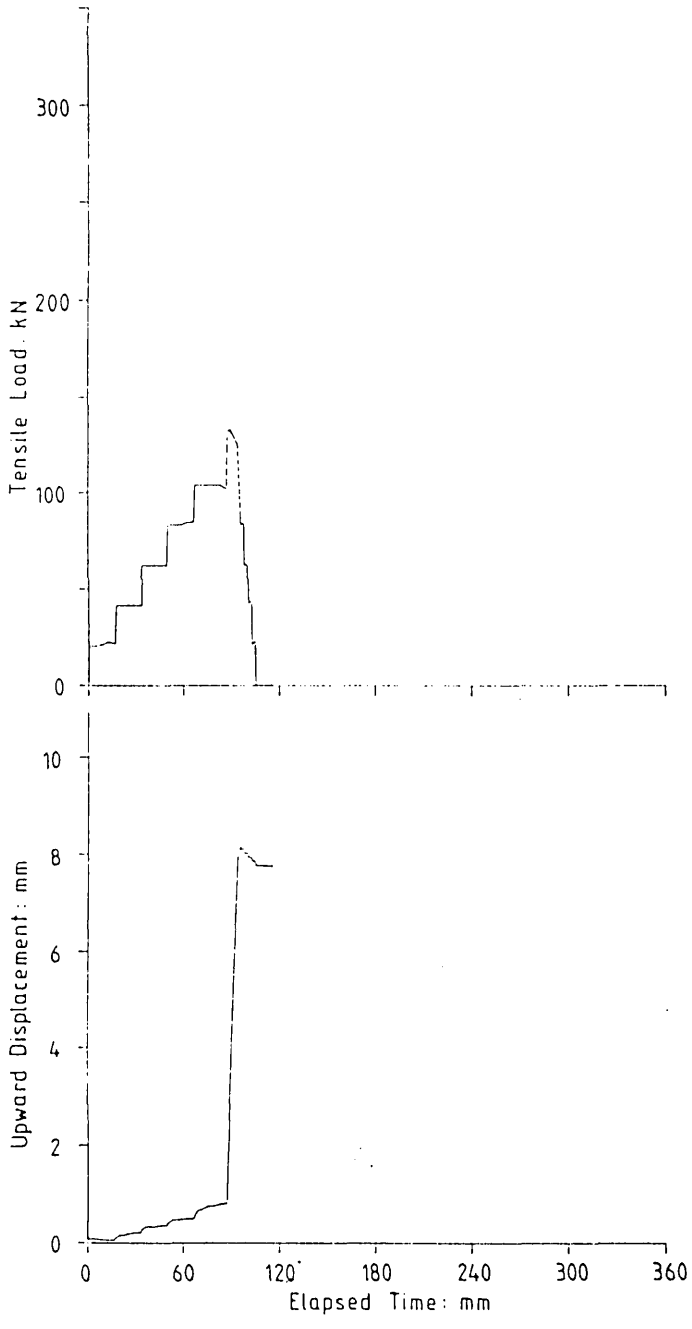

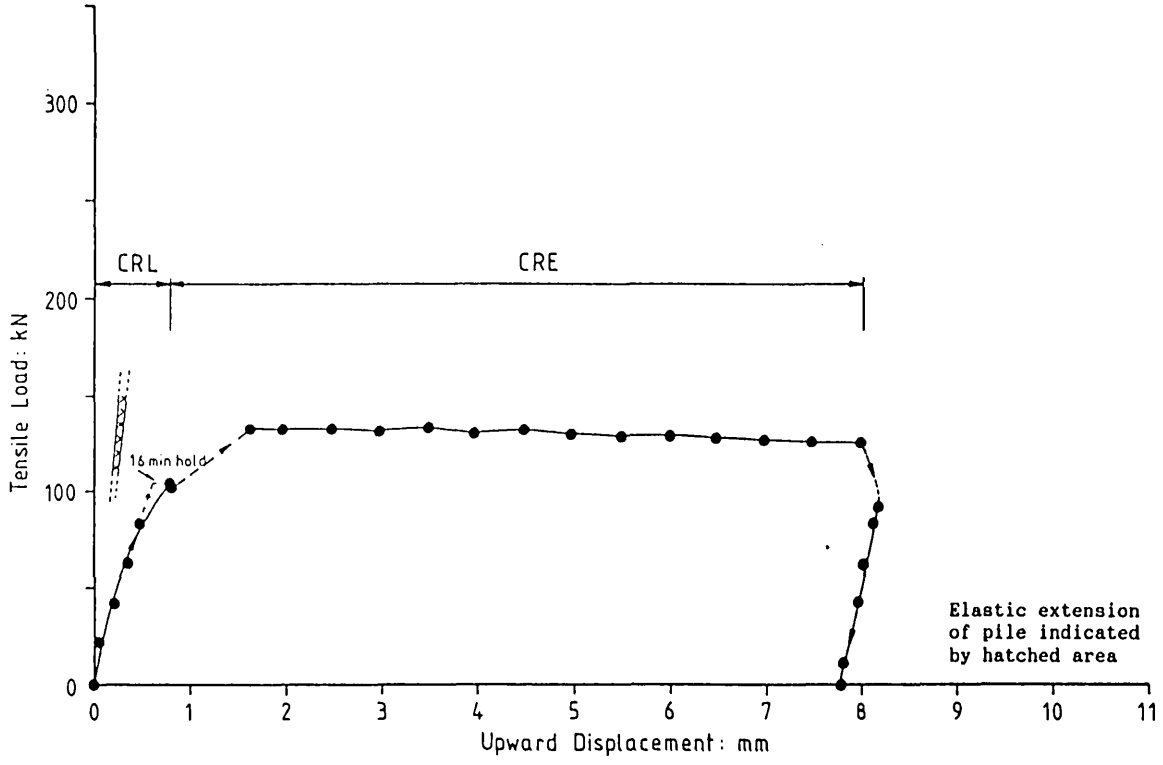

TEST 6U.1 Type: CRL, CRE Date: 28.4.86

Outer shell driven: 14.3.86 Expander mandrel driven: -
Days elapsed
prior to test: 45 -

Shaft areas: (m^2)
Embedded length,
Full X-section (A): 2.11
Reduced X-section (B): -
Expanded length,
Full X-section (C): -
Reduced X-section (D): -

Pile weight: 2.7 (kN)

Test Stage	Maximum Load (Gross) (kN)	Maximum Load (Net) (kN)	Shaft Frictions (A) (kPa)	(B) (kPa)	(C) (kPa)	(D) (kPa)	Displacement at: Max. Load (mm)	End of stage (mm)
CRL	103.8	-	-	-	-	-	0.79	0.79
CRE	133.6	130.9	62.0	-	-	-	3.48	7.76

Notes: 1. Pile not driven to full depth - driving shoe failed.

Figure 5.27 Results of Test 6U.1

Figure 5.28 Results of Test 7A.1

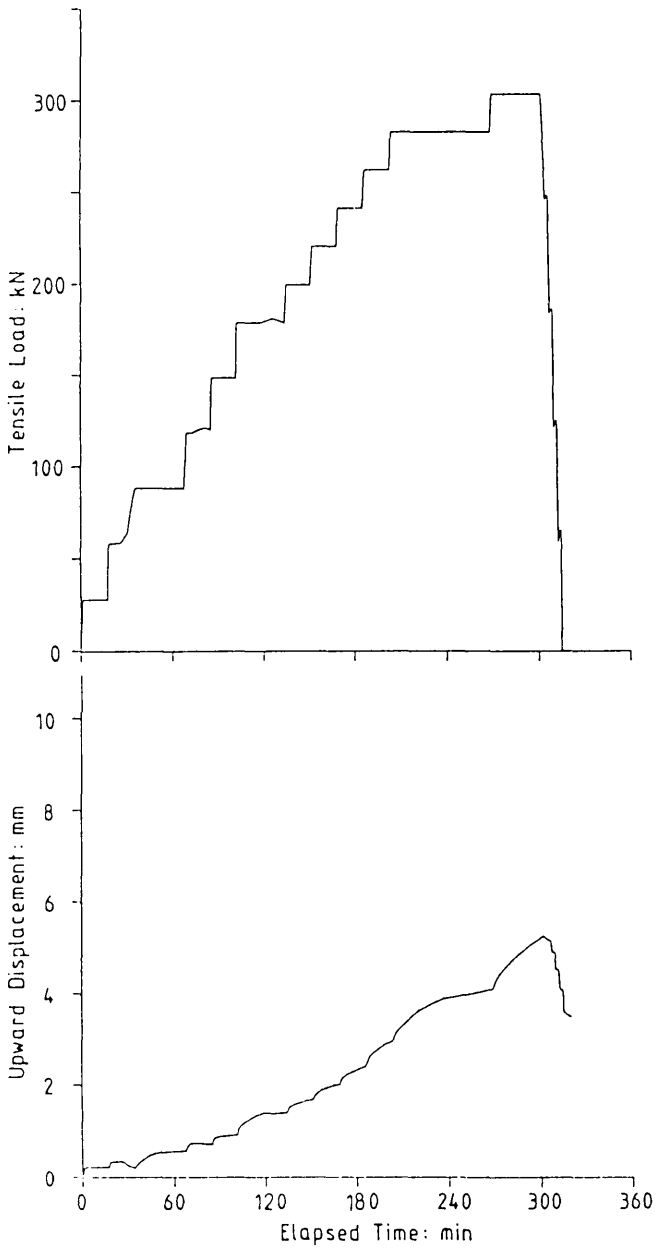

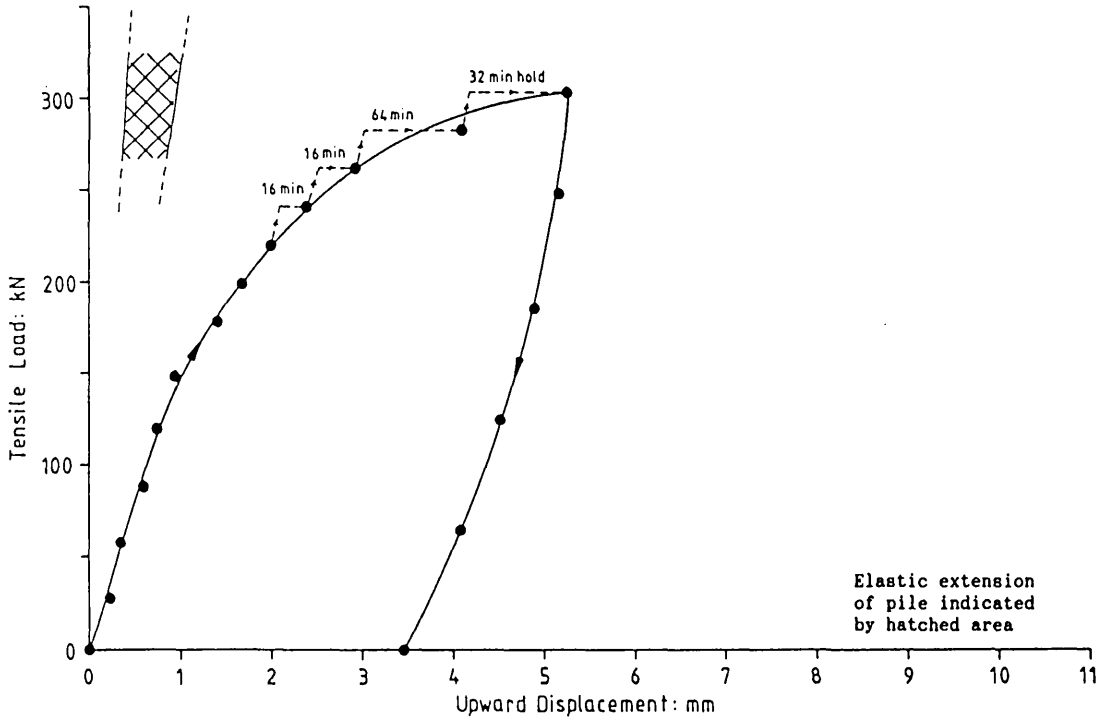

TEST 7A.1 Type: IL Date: 30.5.86

Outer shell driven: 23.5.86 Expander mandrel driven: 29.5.86

Days elapsed prior to test: 7 1

Shaft areas (m^2): Embedded length, Full X-section (A): 3.17; Reduced X-section (B): 2.78; Expanded length, Full X-section (C): 2.53; Reduced X-section (D): 2.22

Pile weight (kN): 4.6

Test Stage	Maximum Load (Gross) (kN)	Maximum Load (Net) (kN)	Shaft Frictions (A) (kPa)	(B) (kPa)	(C) (kPa)	(D) (kPa)	Displacement at: Max. Load (mm)	End of stage (mm)
IL	303.6	299.0	94.2	107.6	118.0	134.8	5.26	3.49

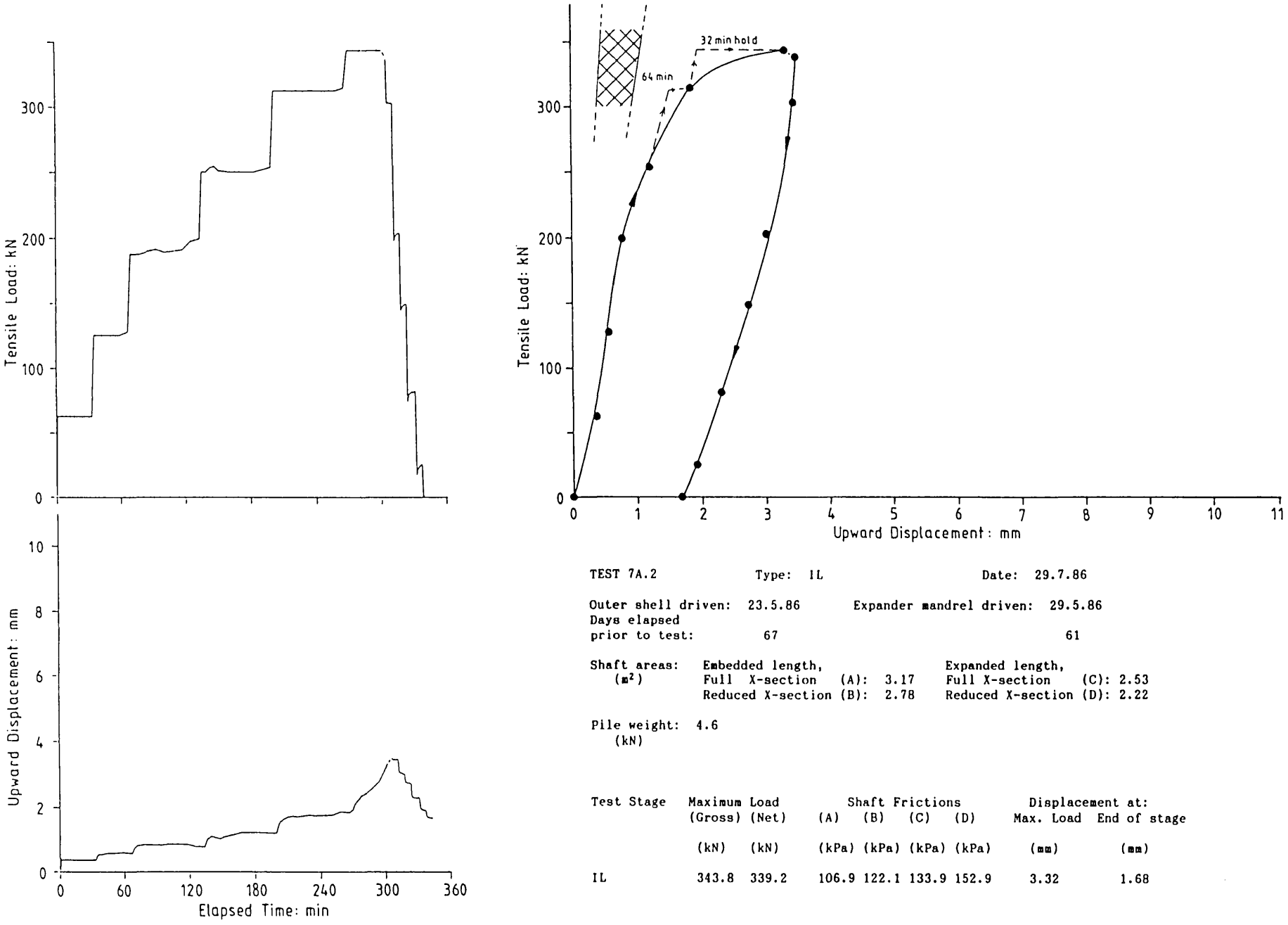

Figure 5.29 Results of Test 7A.2

TEST 7A.2 Type: IL Date: 29.7.86

Outer shell driven: 23.5.86 Expander mandrel driven: 29.5.86
Days elapsed
prior to test: 67 61

Shaft areas: (m^2)
Embedded length,
Full X-section (A): 3.17
Reduced X-section (B): 2.78
Expanded length,
Full X-section (C): 2.53
Reduced X-section (D): 2.22

Pile weight: 4.6 (kN)

Test Stage	Maximum Load (Gross) (kN)	(Net) (kN)	Shaft Frictions (A) (kPa)	(B) (kPa)	(C) (kPa)	(D) (kPa)	Displacement at: Max. Load (mm)	End of stage (mm)
IL	343.8	339.2	106.9	122.1	133.9	152.9	3.32	1.68

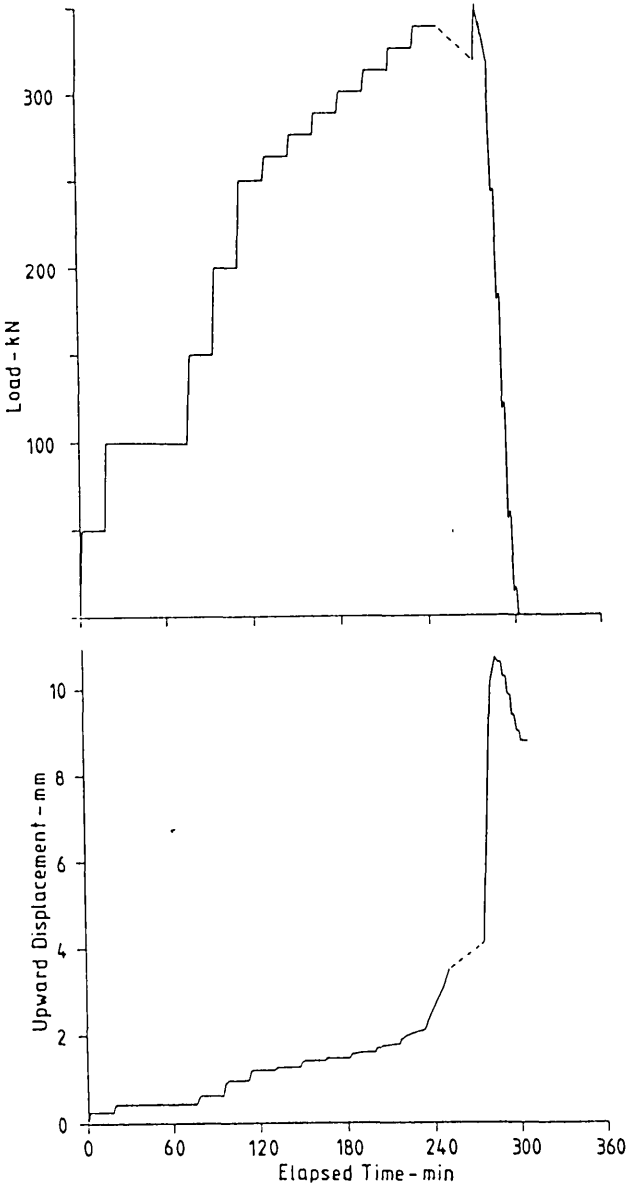

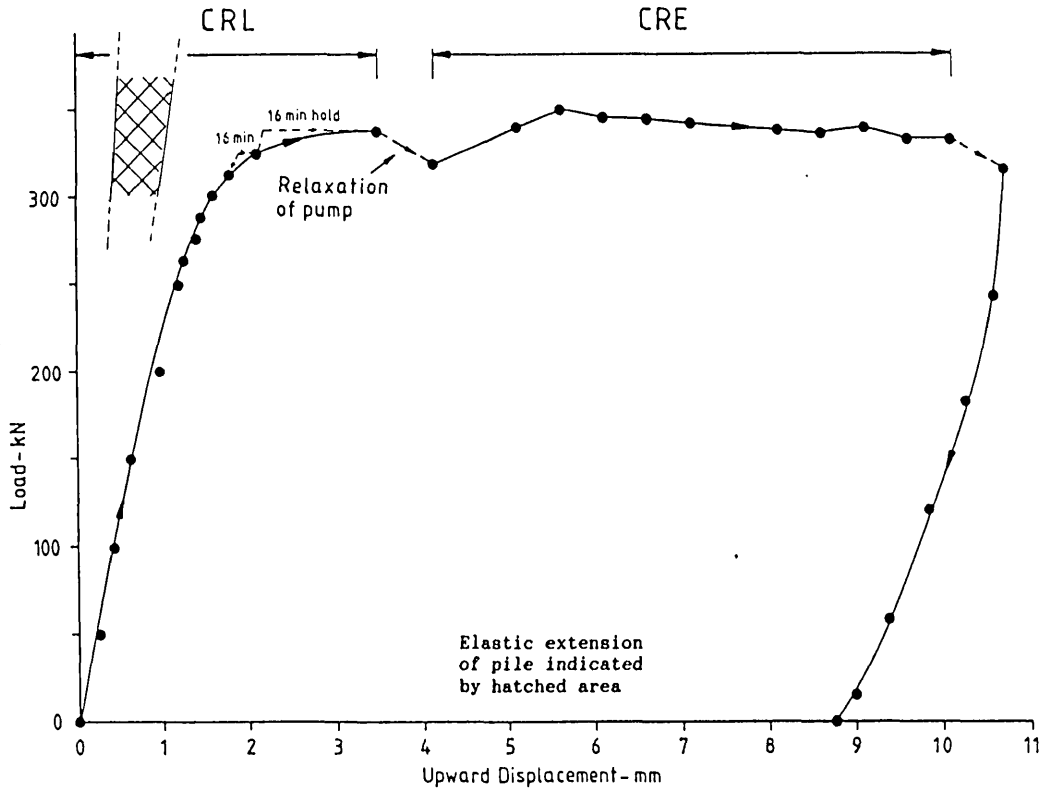

TEST 7A.3 Type: CRL, CRE Date: 9.1.87

Outer shell driven: 23.5.86 Expander mandrel driven: 29.5.86

Days elapsed prior to test: 231 225

Shaft areas (m^2): Embedded length, Full X-section (A): 3.17, Reduced X-section (B): 2.78; Expanded length, Full X-section (C): 2.53, Reduced X-section (D): 2.22

Pile weight (kN): 4.6

Test Stage	Maximum Load (Gross) (kN)	Maximum Load (Net) (kN)	Shaft Frictions (A) (kPa)	(B) (kPa)	(C) (kPa)	(D) (kPa)	Displacement at: Max. Load (mm)	End of stage (mm)
CRL	337.9	-	-	-	-	-	3.49	3.49
CRE	352.5	347.9	109.6	125.2	137.3	156.9	4.63	8.78

Figure 5.30 Results of Test 7A.3

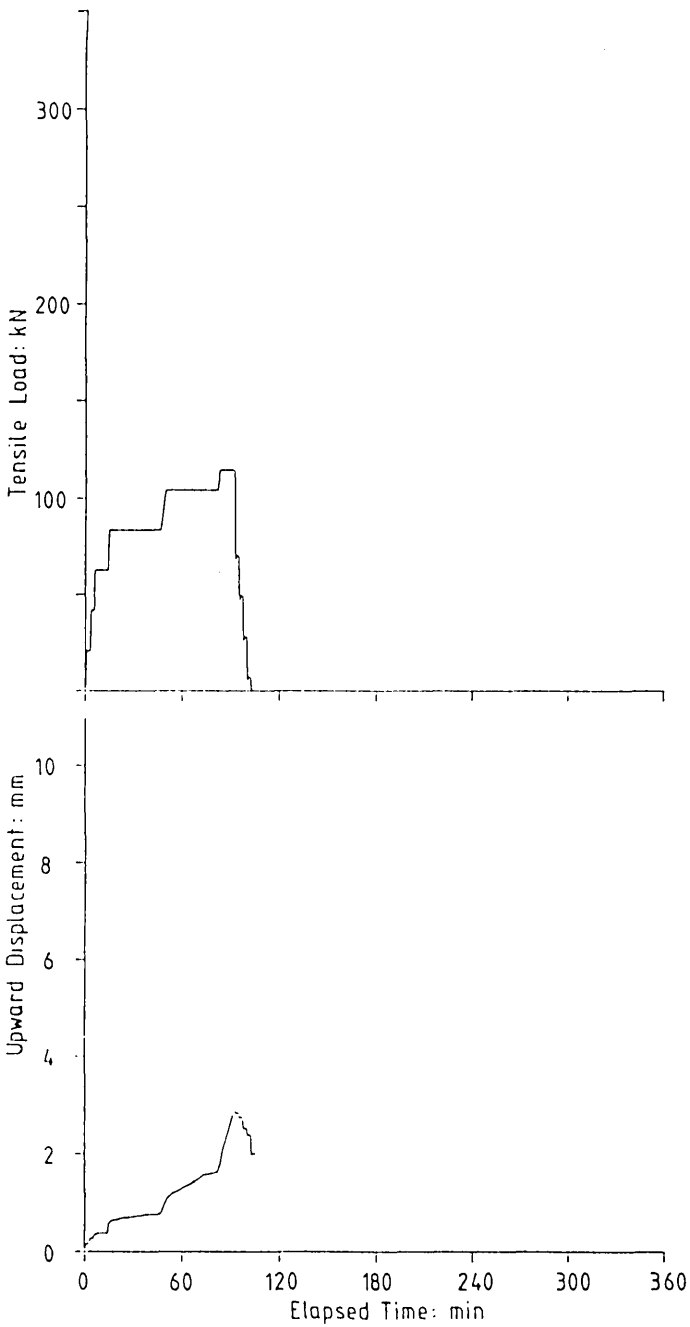

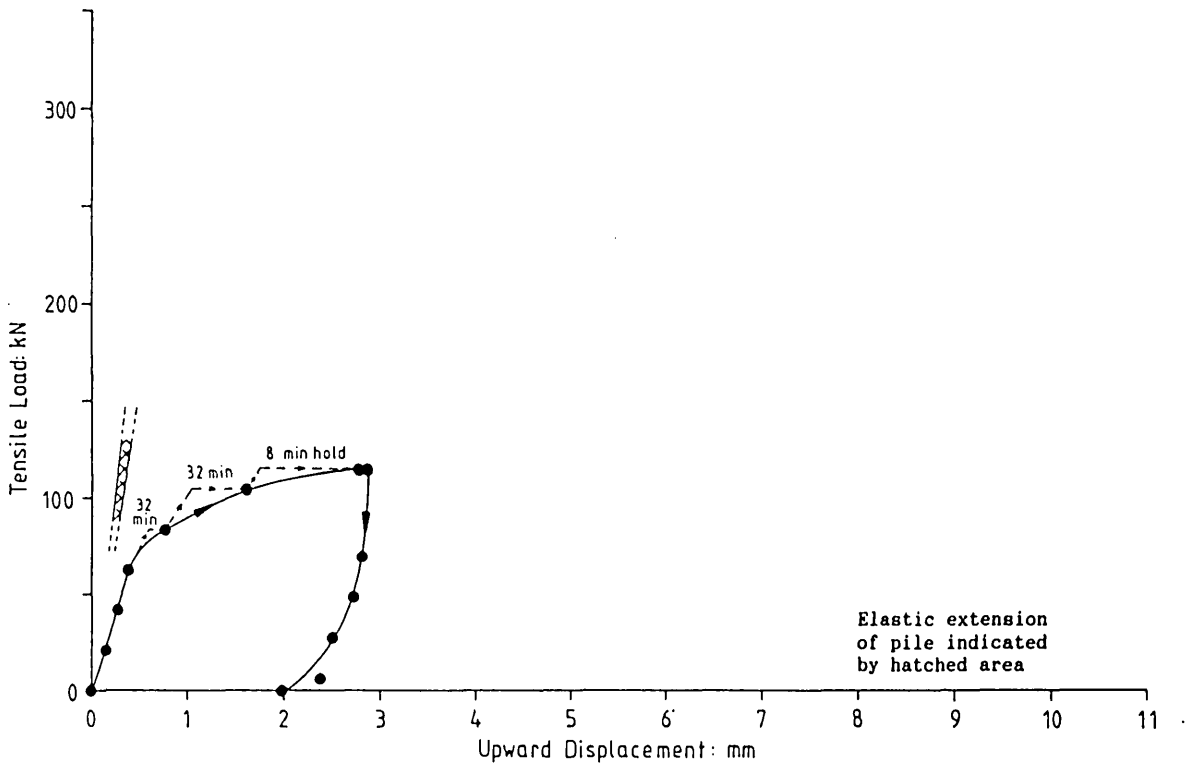

TEST 8U.1 Type: IL Date: 20.5.86

Outer shell driven: 13.5.86 Expander mandrel driven: -
Days elapsed
prior to test: 7 -

Shaft areas: (m^2)
Embedded length, Expanded length,
Full X-section (A): 2.12 Full X-section (C): -
Reduced X-section (B): - Reduced X-section (D): -

Pile weight: 2.4 (kN)

Test Stage	Maximum Load (Gross) (kN)	Maximum Load (Net) (kN)	Shaft Frictions (A) (kPa)	(B) (kPa)	(C) (kPa)	(D) (kPa)	Displacement at: Max. Load (mm)	Displacement at: End of stage (mm)
IL	114.7	112.3	53.0	-	-	-	2.79	2.00

Figure 5.31 Results of Test 8U.1

Figure 5.32 Results of Test 8U.2

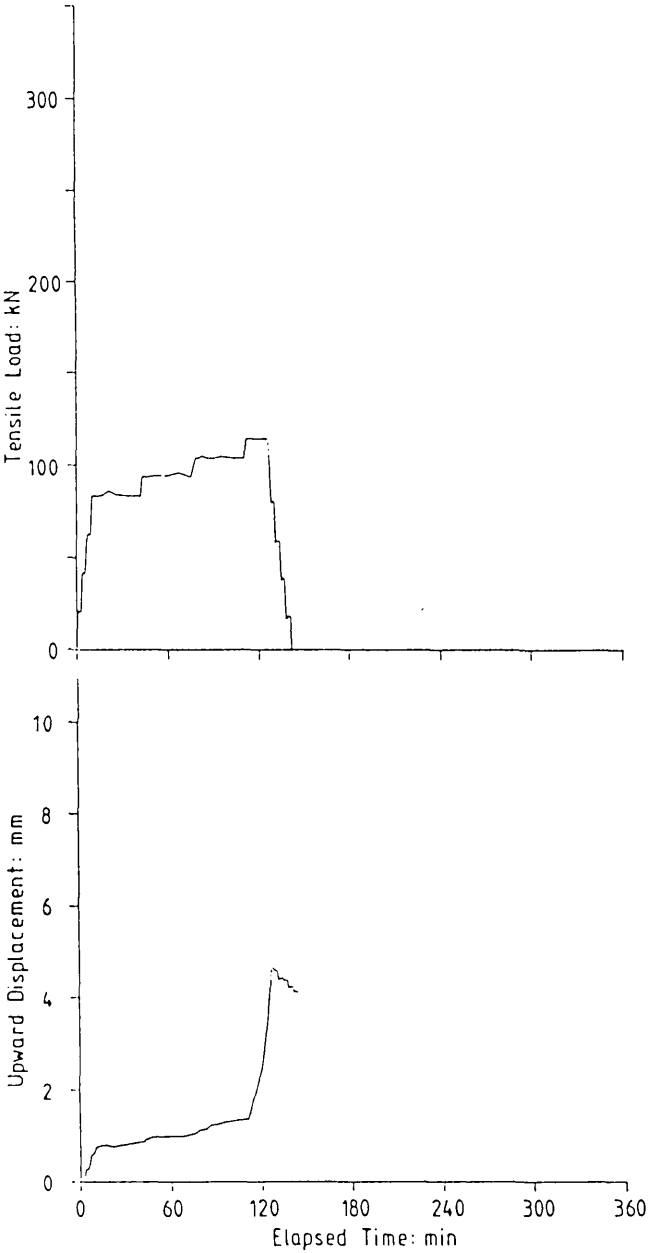

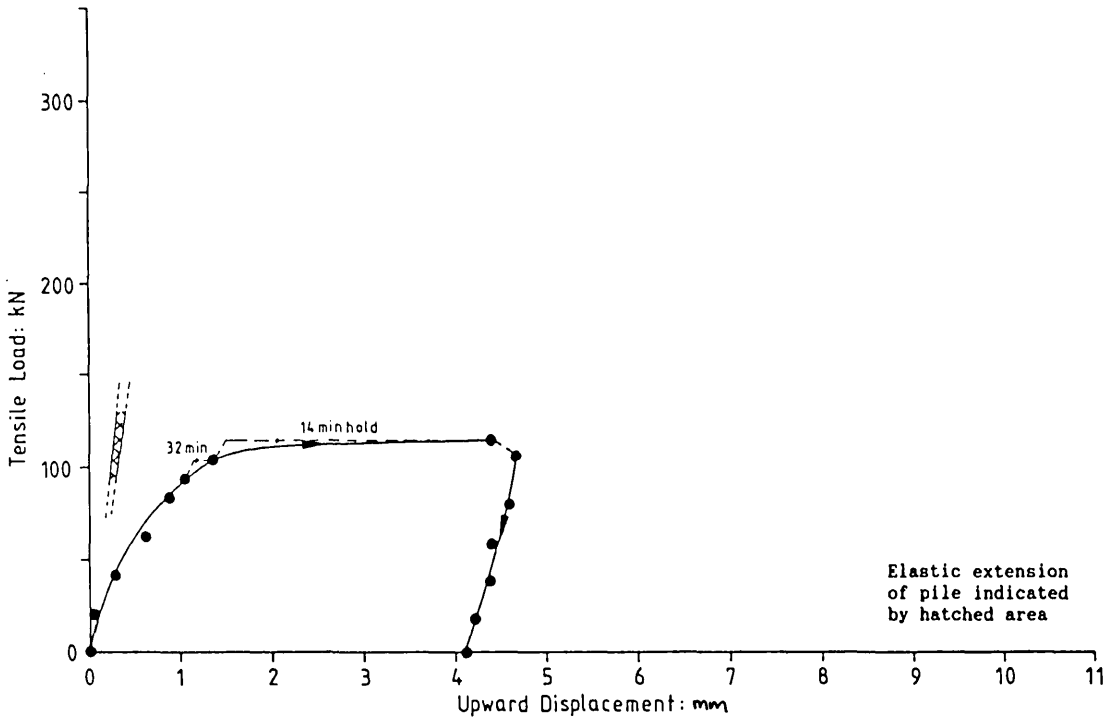

TEST 8U.2 Type: IL Date: 31.7.86

Outer shell driven: 13.5.86 Expander mandrel driven: -
Days elapsed
prior to test: 79 -

Shaft areas: (m^2) Embedded length, Full X-section (A): 2.12 Reduced X-section (B): - Expanded length, Full X-section (C): - Reduced X-section (D): -

Pile weight: 2.4 (kN)

Test Stage	Maximum Load (Gross) (kN)	Maximum Load (Net) (kN)	Shaft Frictions (A) (kPa)	(B) (kPa)	(C) (kPa)	(D) (kPa)	Displacement at: Max. Load (mm)	End of stage (mm)
IL	114.5	112.1	52.9	-	-	-	4.40	4.11

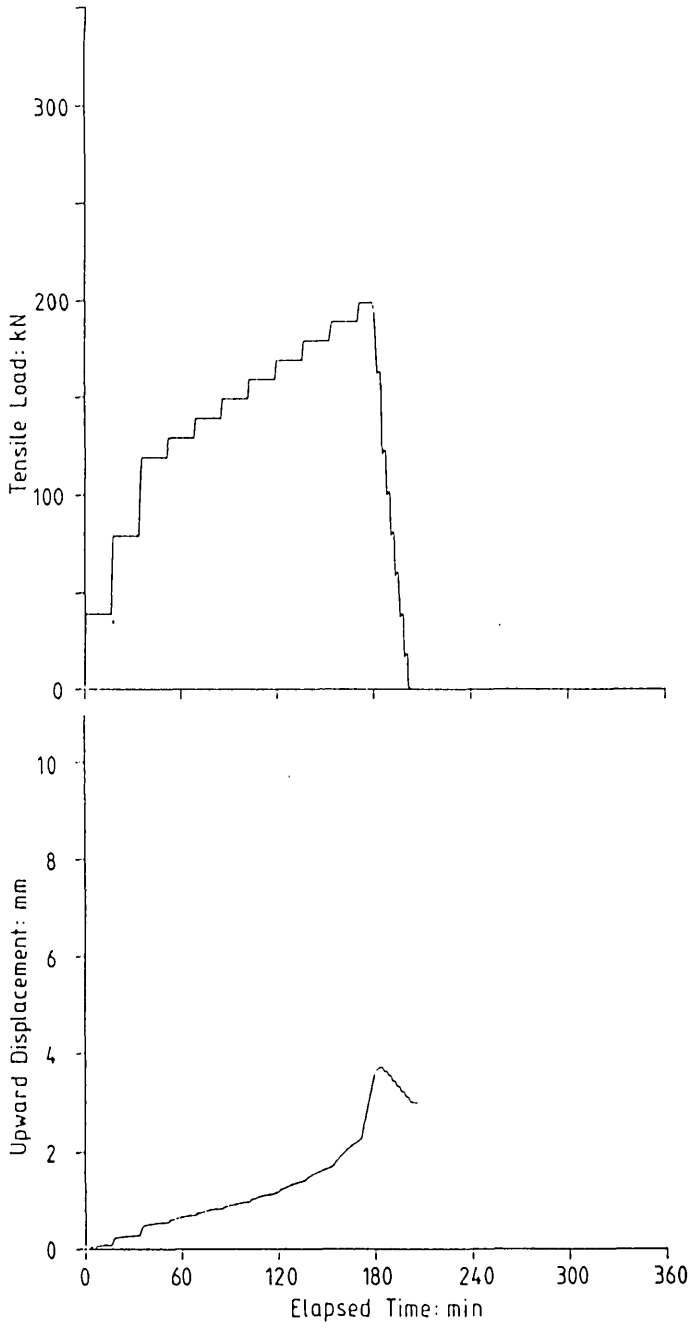

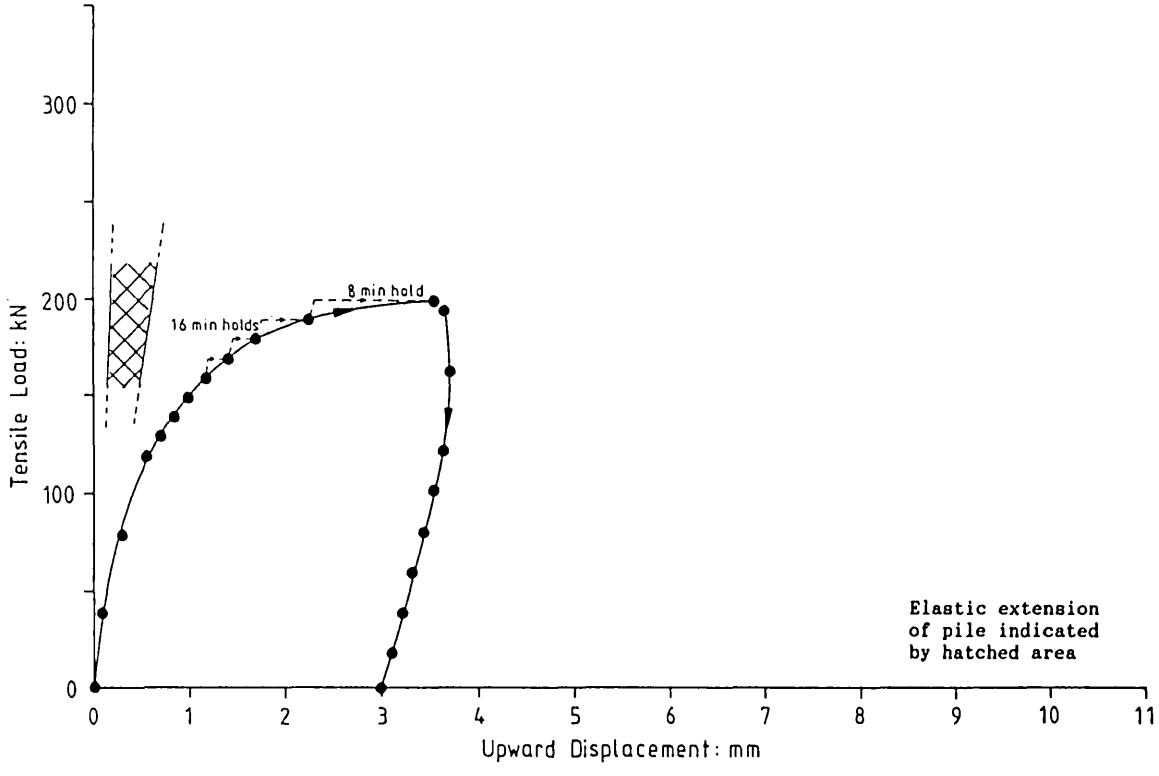

Figure 5.33 Results of Test 8B.1

TEST 8B.1 Type: CRL Date: 18.8.86

Outer shell driven: 13.5.86 Expander mandrel driven: 13.8.86

Days elapsed prior to test: 97 5

Shaft areas (m^2): Embedded length, Full X-section (A): 2.73; Reduced X-section (B): 2.12. Expanded length, Full X-section (C): 2.48; Reduced X-section (D): 1.93

Pile weight: 6.6 (kN)

Test Stage	Maximum Load (Gross) (kN)	Maximum Load (Net) (kN)	Shaft Frictions (A) (kPa)	(B) (kPa)	(C) (kPa)	(D) (kPa)	Displacement at: Max. Load (mm)	End of stage (mm)
CRL	198.9	192.3	70.5	90.7	77.6	99.7	3.55	3.00

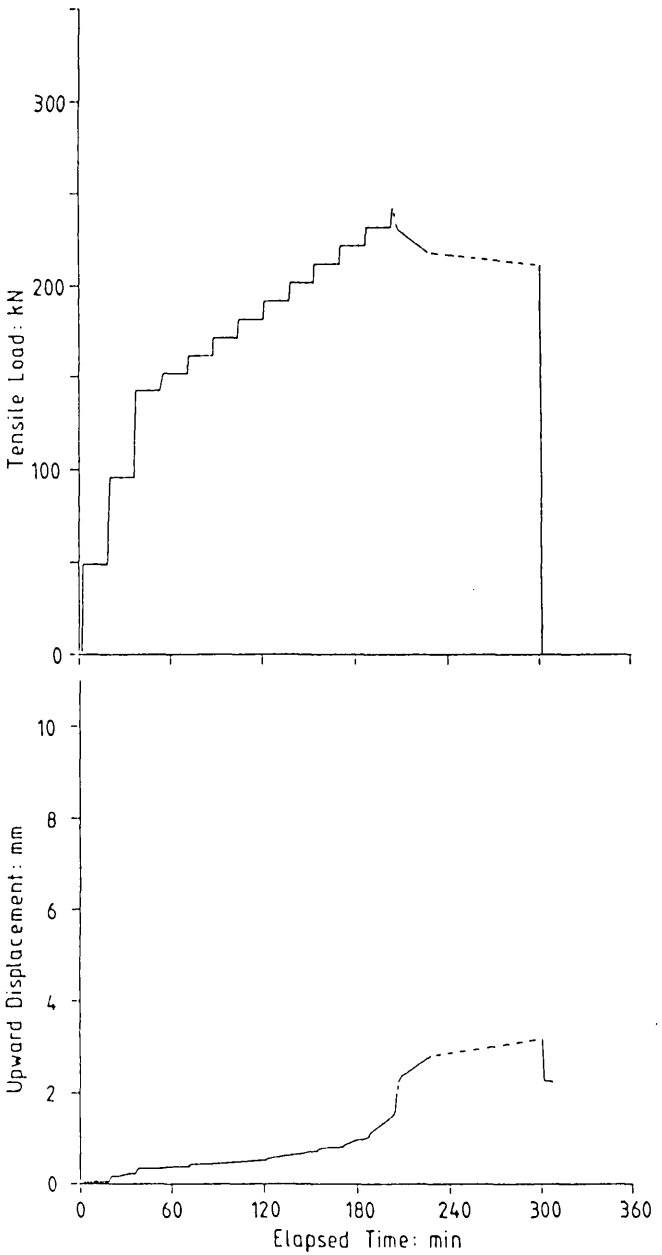

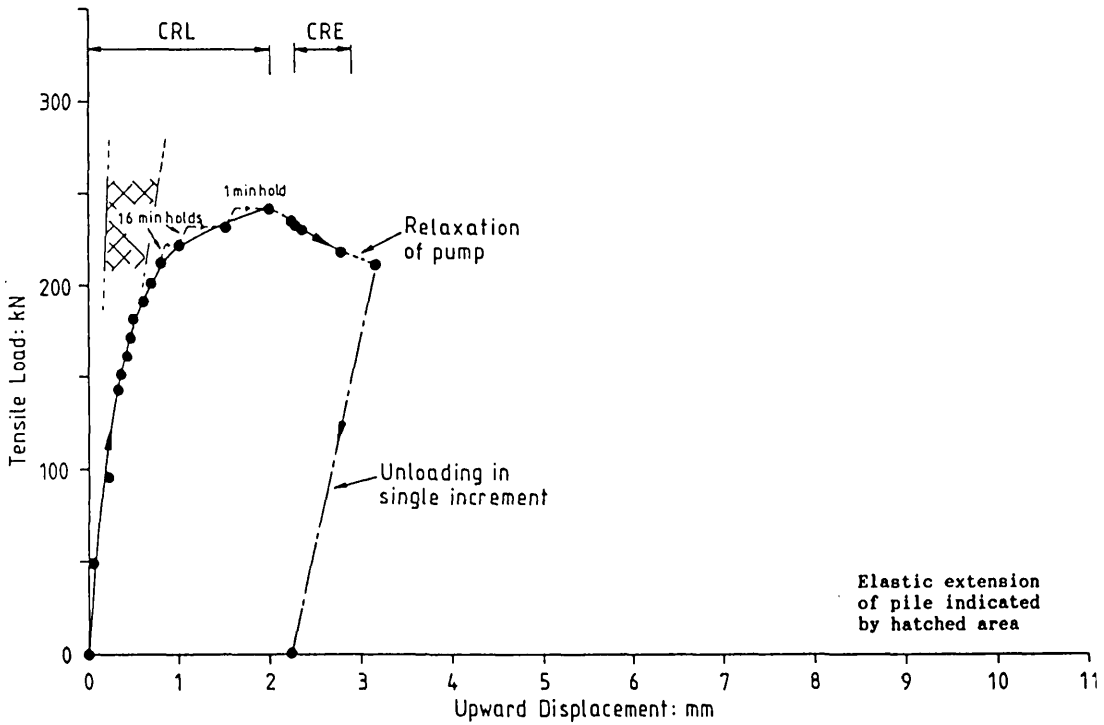

TEST 8B.2 Type: CRL Date: 9.3.87

Outer shell driven: 13.5.86 Expander mandrel driven: 13.8.86

Days elapsed prior to test: 300 208

Shaft areas (m^2): Embedded length, Full X-section (A): 2.73, Reduced X-section (B): 2.12; Expanded length, Full X-section (C): 2.48, Reduced X-section (D): 1.93

Pile weight: 6.6 (kN)

Test Stage	Maximum Load (Gross) (kN)	Maximum Load (Net) (kN)	Shaft Frictions (A) (kPa)	(B) (kPa)	(C) (kPa)	(D) (kPa)	Displacement at: Max. Load (mm)	End of stage (mm)
CRL	241.6	235.0	86.2	110.8	94.8	121.9	2.00	2.24

Figure 5.34 Results of Test 8B.2

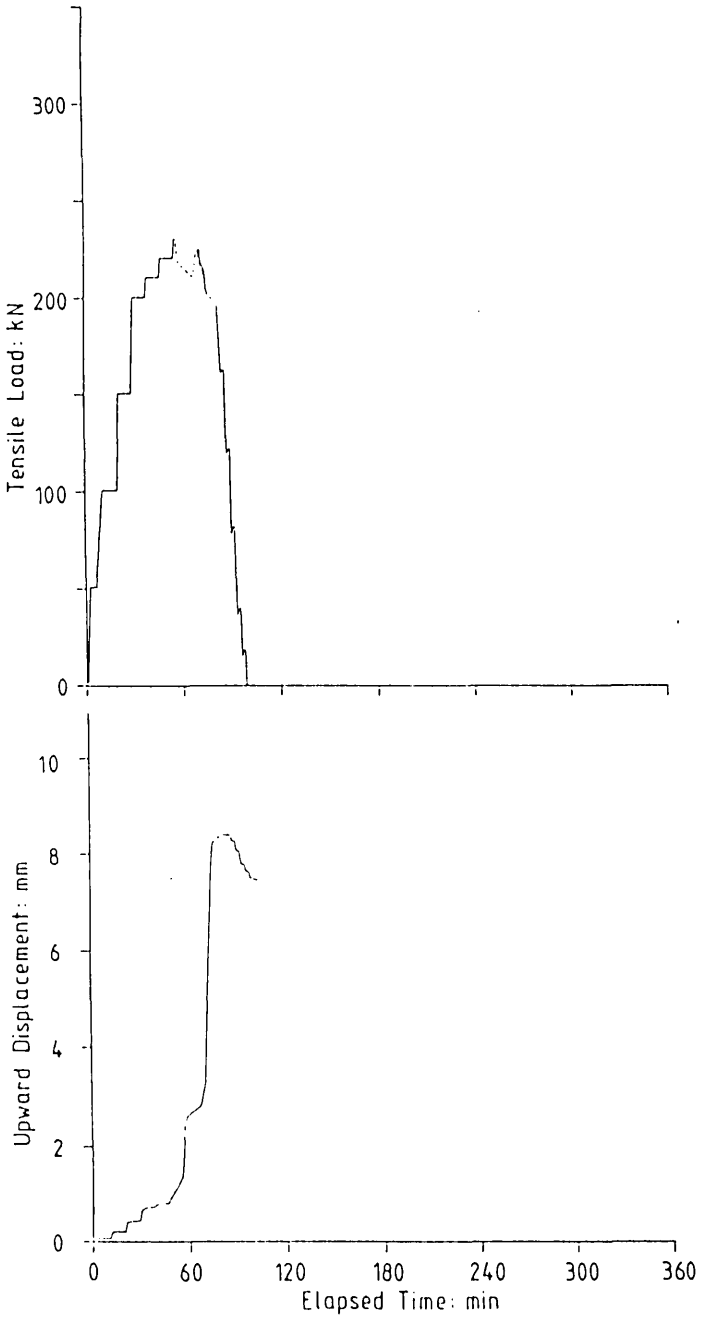

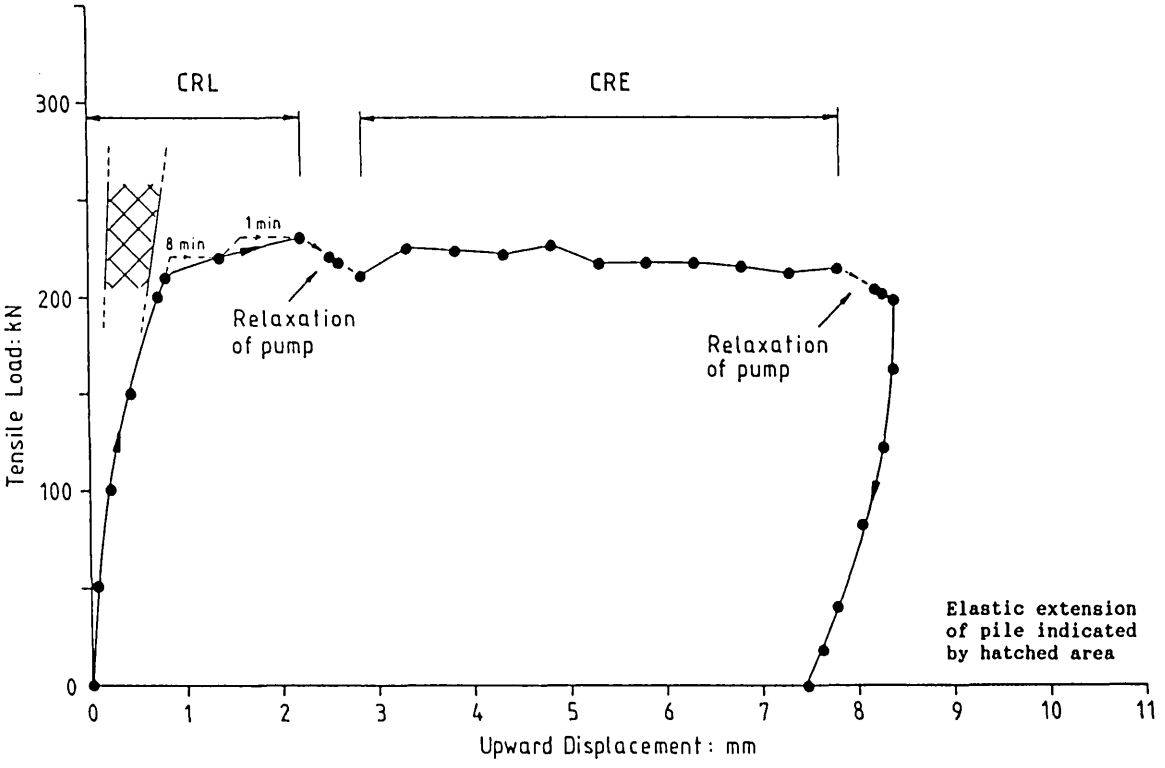

TEST 8B.3 Type: CRL, CRE Date: 10.3.87

Outer shell driven: 13.5.86 Expander mandrel driven: 13.8.86

Days elapsed prior to test: 301 209

Shaft areas (m^2): Embedded length, Full X-section (A): 2.73; Reduced X-section (B): 2.12. Expanded length, Full X-section (C): 2.48; Reduced X-section (D): 1.93

Pile weight: 6.6 (kN)

Test Stage	Maximum Load (Gross) (kN)	(Net) (kN)	Shaft Frictions (A) (kPa)	(B) (kPa)	(C) (kPa)	(D) (kPa)	Displacement at: Max. Load (mm)	End of stage (mm)
CRL	231.2	-	-	-	-	-	2.21	2.21
CRE	226.0	219.4	80.5	103.4	88.5	113.8	4.82	7.45

Figure 5.35 Results of Test 8B.3

Figure 5.36 Results of Test 8B.4

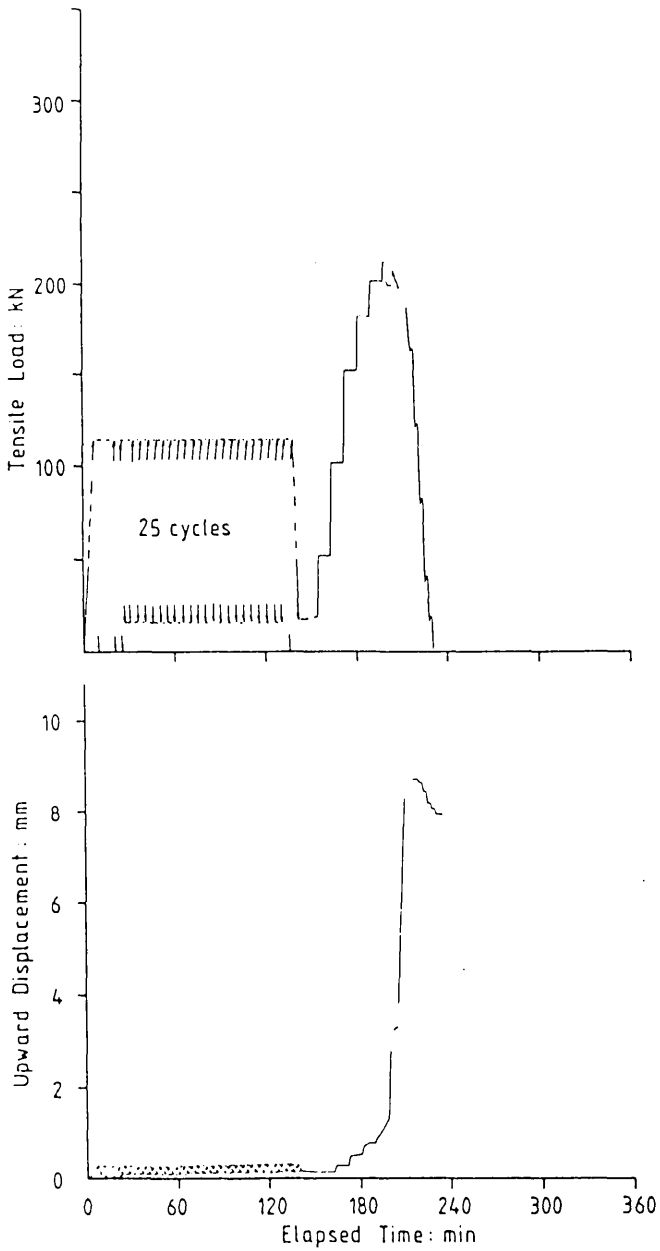

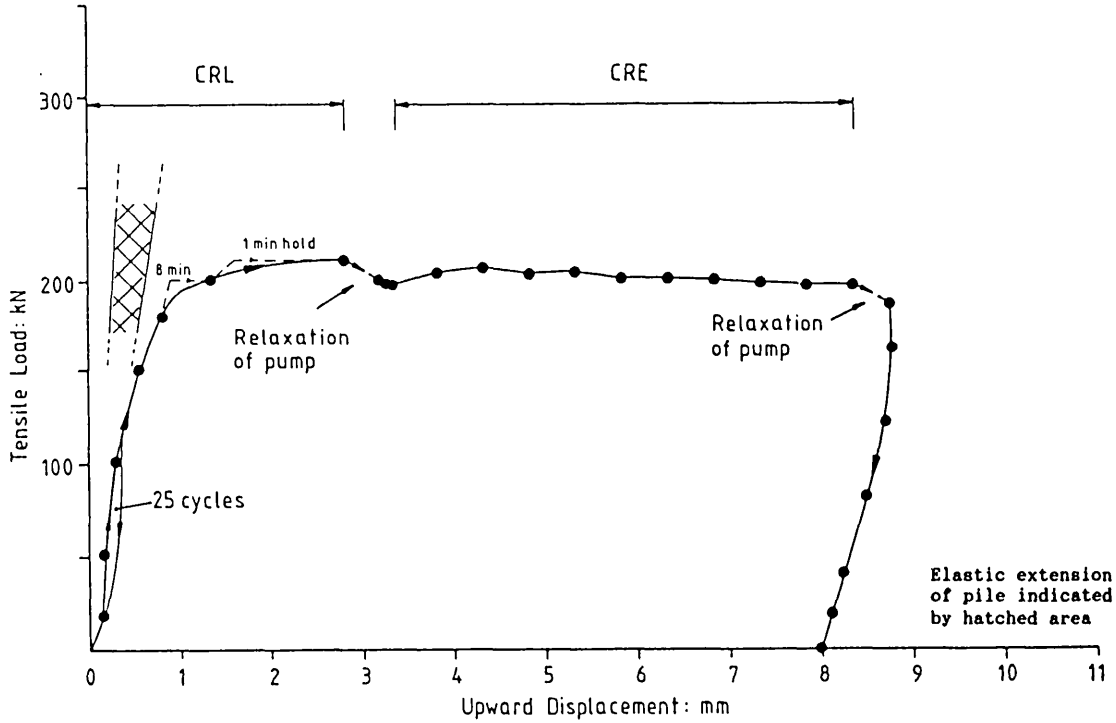

TEST 8B.4 Type: Cyclic, CRE Date: 10.3.87

Outer shell driven: 13.5.86 Expander mandrel driven: 13.8.86
Days elapsed prior to test: 301 209

Shaft areas (m^2): Embedded length, Full X-section (A): 2.73; Reduced X-section (B): 2.12. Expanded length, Full X-section (C): 2.48; Reduced X-section (D): 1.93

Pile weight (kN): 6.6

Test Stage	Maximum Load (Gross) (kN)	Maximum Load (Net) (kN)	Shaft Frictions (A) (kPa)	(B) (kPa)	(C) (kPa)	(D) (kPa)	Displacement at: Max. Load (mm)	End of stage (mm)
Cyclic[1]	-	-	-	-	-	-	-	-
CRE	207.7	201.1	73.7	94.8	81.1	104.3	4.32	7.96

Notes: 1. 25 cycles, 17kN - 114kN

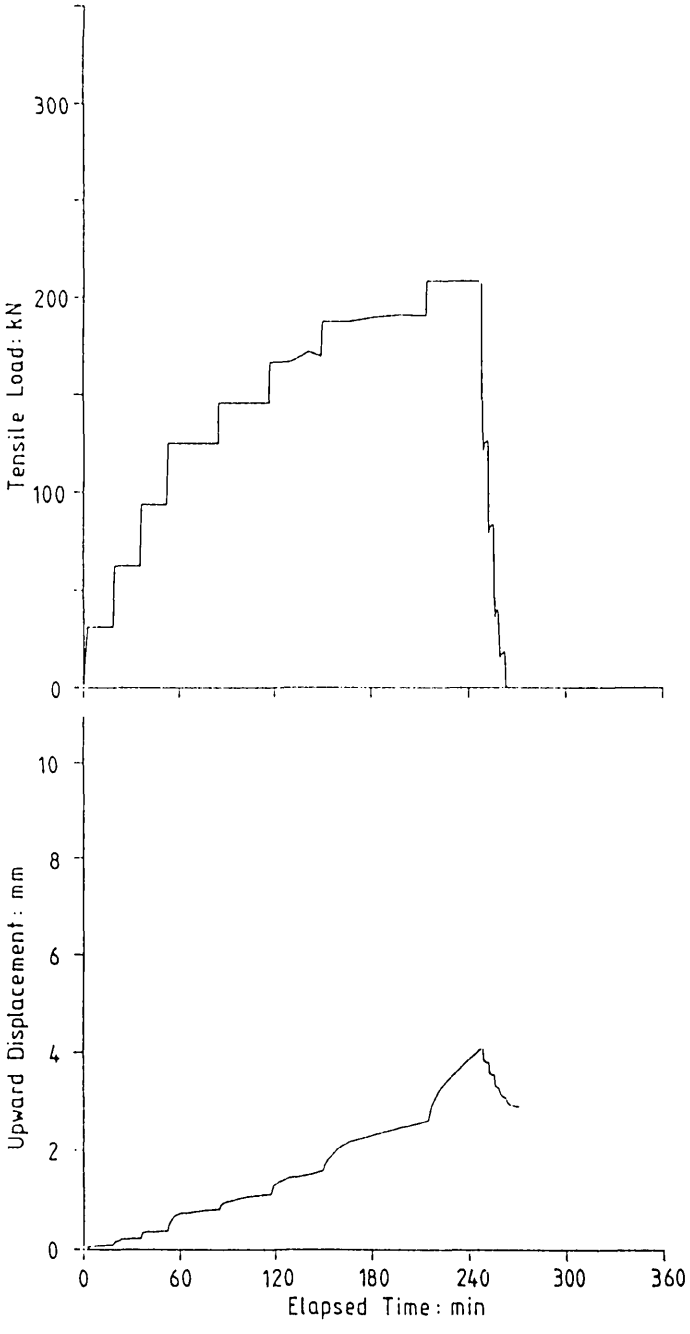

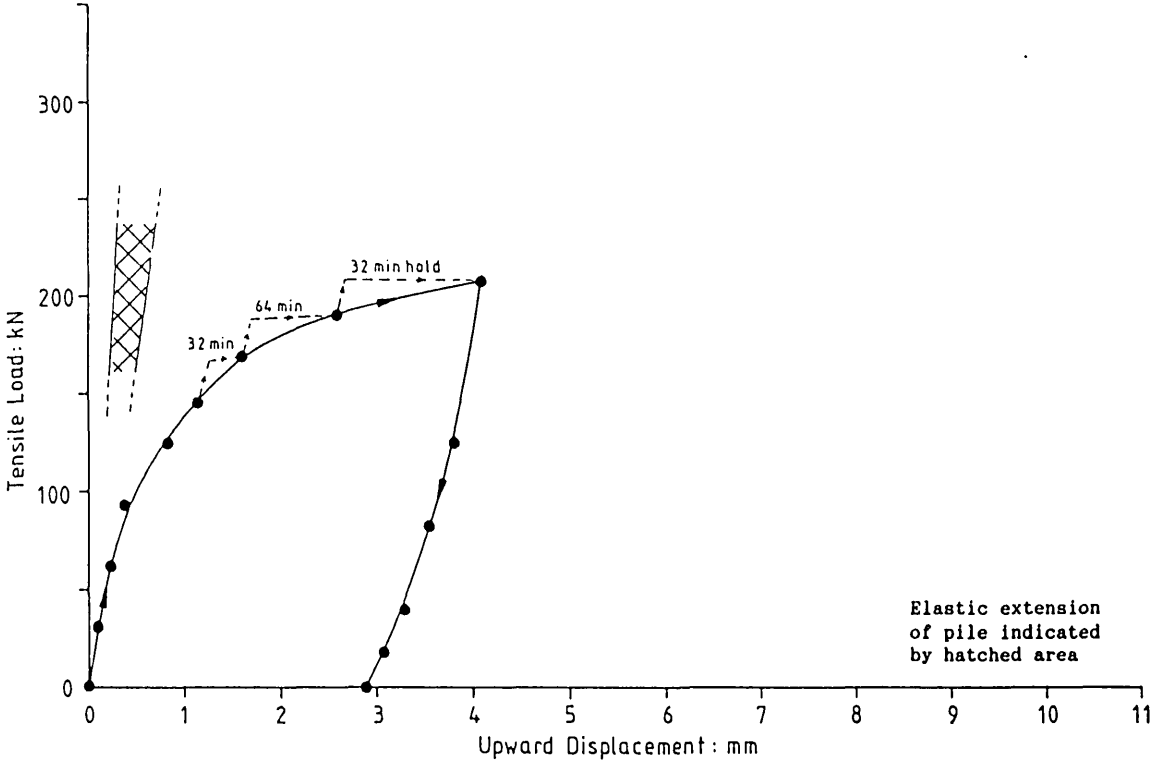

TEST 9A.1 Type: IL Date: 21.5.86

Outer shell driven: 13.5.86 Expander mandrel driven: 14.5.86

Days elapsed prior to test: 8 7

Shaft areas (m^2): Embedded length, Full X-section (A): 2.40; Reduced X-section (B): 2.10. Expanded length, Full X-section (C): 2.18; Reduced X-section (D): 1.91

Pile weight (kN): 3.9

Test Stage	Maximum Load (Gross) (kN)	Maximum Load (Net) (kN)	Shaft Frictions (A) (kPa)	(B) (kPa)	(C) (kPa)	(D) (kPa)	Displacement at: Max. Load (mm)	Displacement at: End of stage (mm)
IL	208.1	204.2	84.9	97.1	93.7	107.1	4.08	2.90

Figure 5.37 Results of Test 9A.1

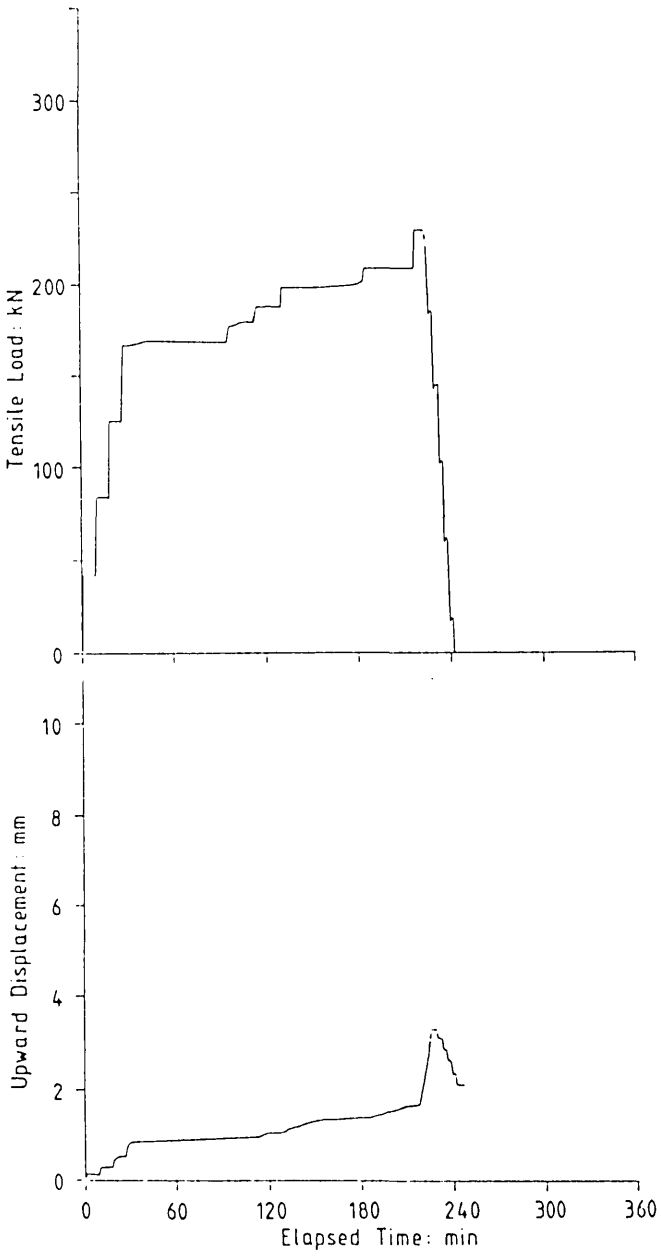

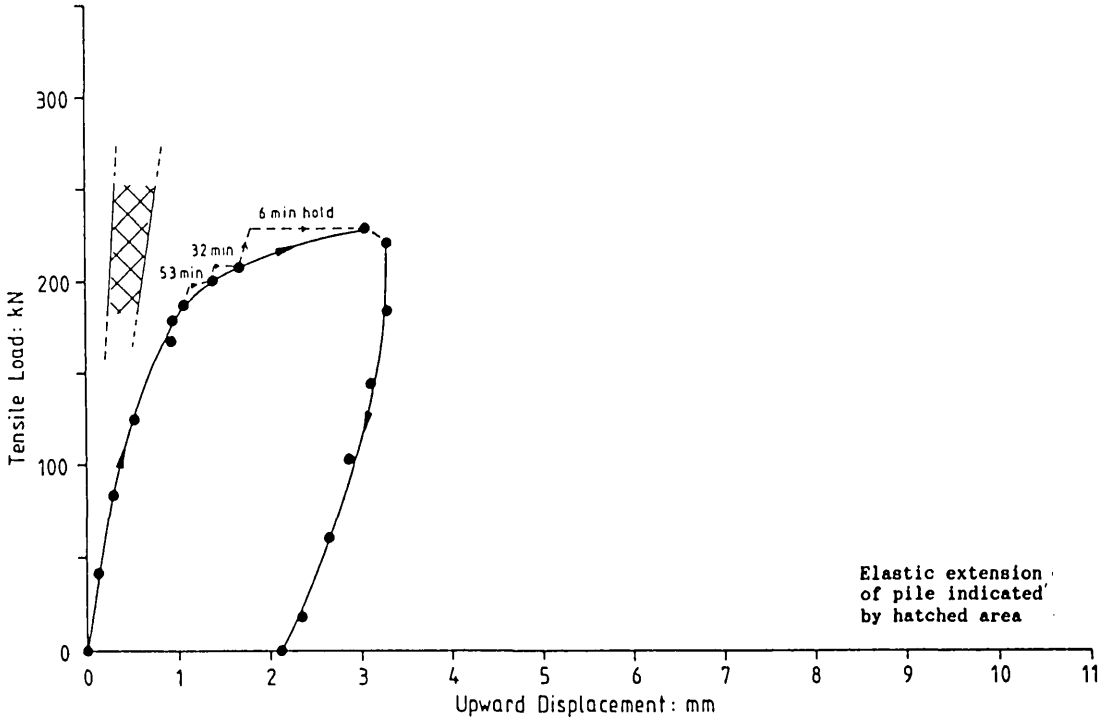

Figure 5.38 Results of Test 9A.2

TEST 9A.2 Type: IL Date: 1.8.86

Outer shell driven: 13.5.86 Expander mandrel driven: 14.5.86

Days elapsed prior to test: 80 79

Shaft areas (m^2): Embedded length, Full X-section (A): 2.40; Reduced X-section (B): 2.10. Expanded length, Full X-section (C): 2.18; Reduced X-section (D): 1.91

Pile weight: 3.9 (kN)

Test Stage	Maximum Load (Gross) (kN)	Maximum Load (Net) (kN)	Shaft Frictions (A) (kPa)	(B) (kPa)	(C) (kPa)	(D) (kPa)	Displacement at: Max. Load (mm)	End of stage (mm)
IL	229.3	225.4	93.7	107.1	103.4	118.2	3.05	2.10

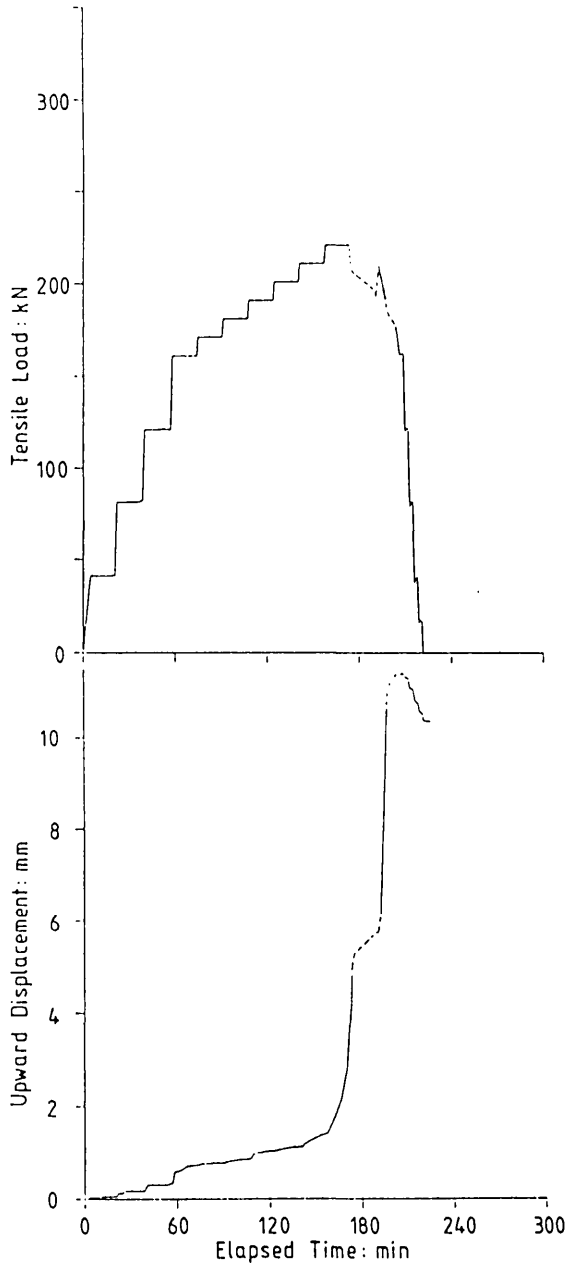

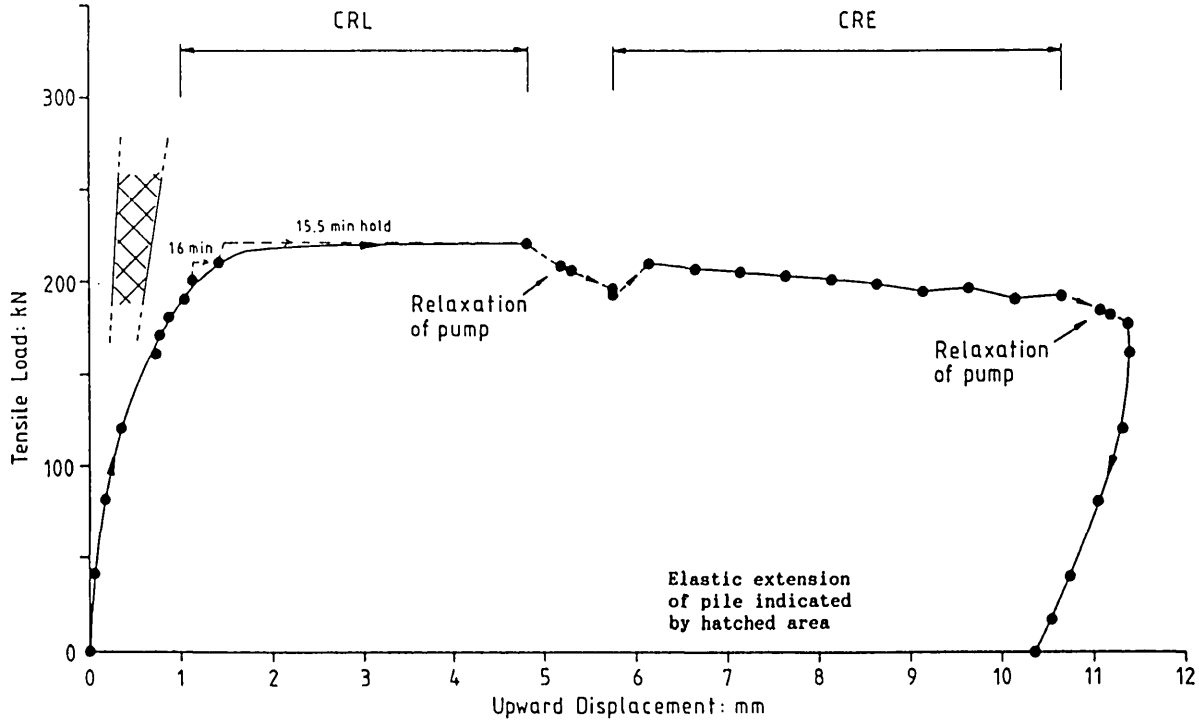

Figure 5.39 Results of Test 9A.3

TEST 9A.3 Type: CRL, CRE Date: 20.3.87

Outer shell driven: 13.5.86 Expander mandrel driven: 14.5.86

Days elapsed prior to test: 311 310

Shaft areas (m^2): Embedded length, Full X-section (A): 2.40; Reduced X-section (B): 2.10. Expanded length, Full X-section (C): 2.18; Reduced X-section (D): 1.91

Pile weight: 3.9 (kN)

Test Stage	Maximum Load (Gross) (kN)	Maximum Load (Net) (kN)	Shaft Frictions (A) (kPa)	(B) (kPa)	(C) (kPa)	(D) (kPa)	Displacement at: Max. Load (mm)	End of stage (mm)
CRL	220.8	-	-	-	-	-	4.80	4.80
CRE	209.8	205.9	85.6	97.9	94.5	108.0	6.14	10.34

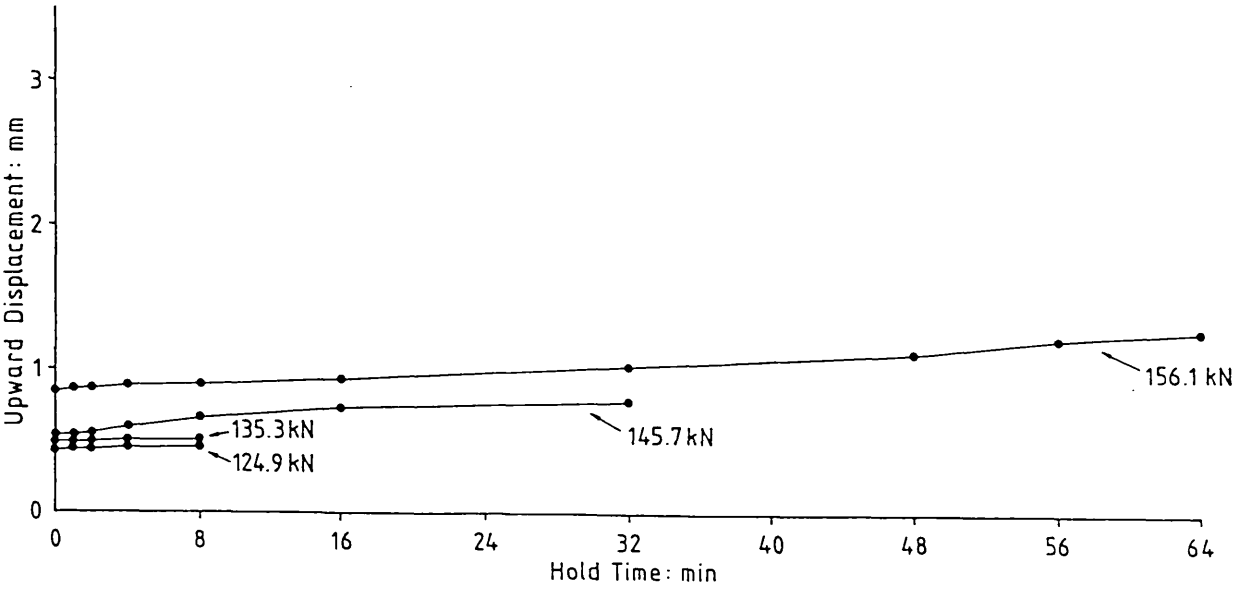

Figure 5.40 Pile Test 5U.1:
Creep behaviour during IL stage

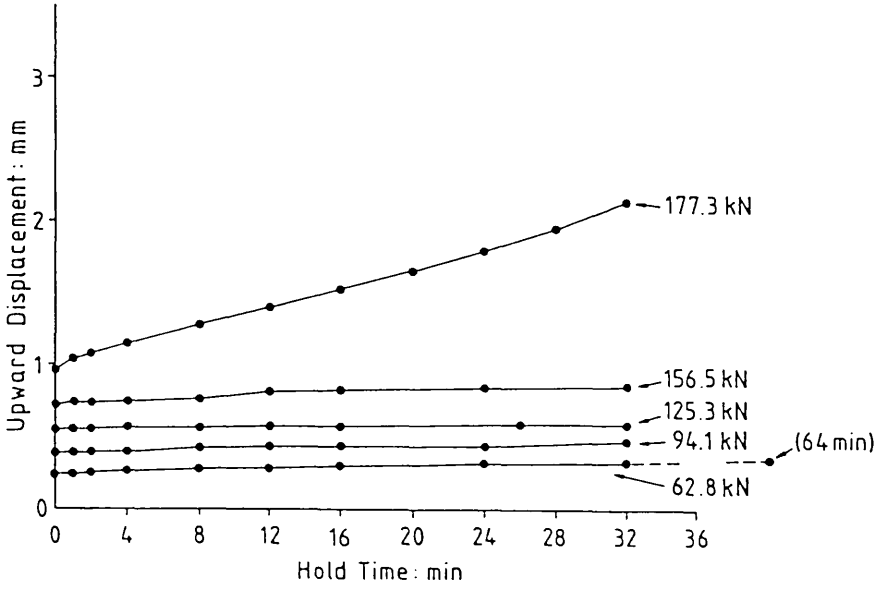

Figure 5.41 Pile Test 5U.2:
Creep behaviour during IL stage

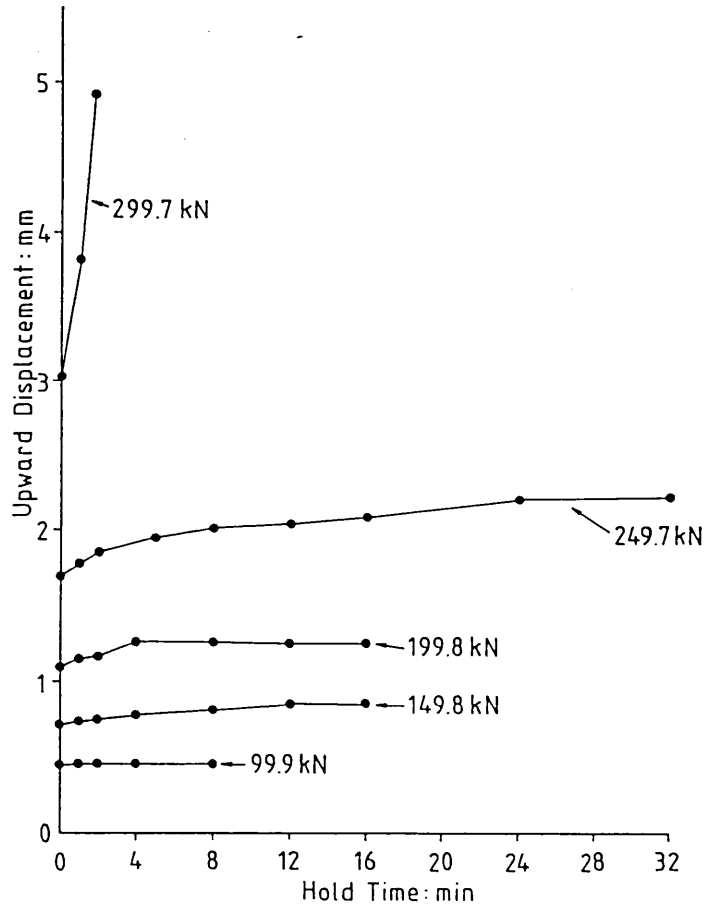

Figure 5.42 Pile Test 5B.1:
Creep behaviour during IL stage

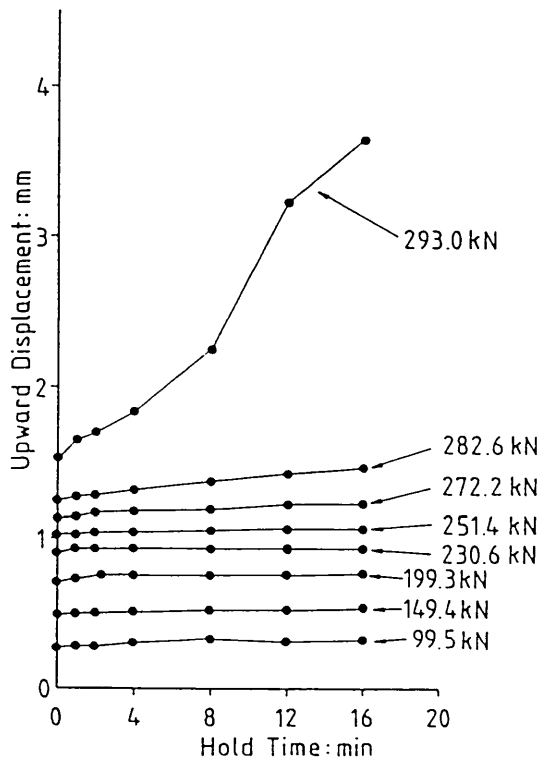

Figure 5.43 Pile Test 5B.2:
Creep behaviour during IL stage

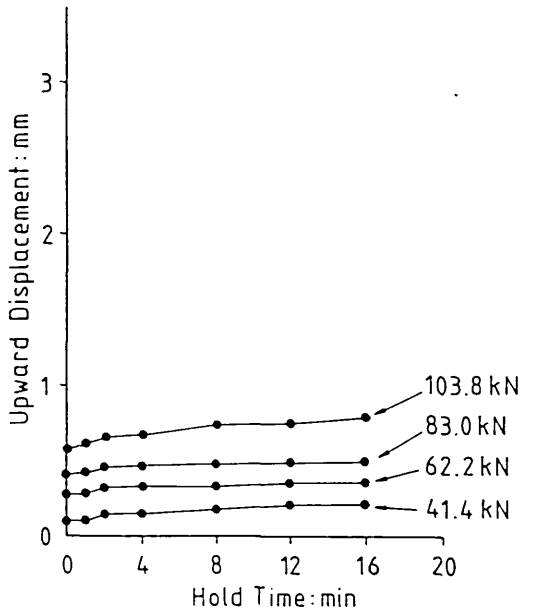

Figure 5.44 Pile Test 6U.1:
Creep behaviour during CRL stage

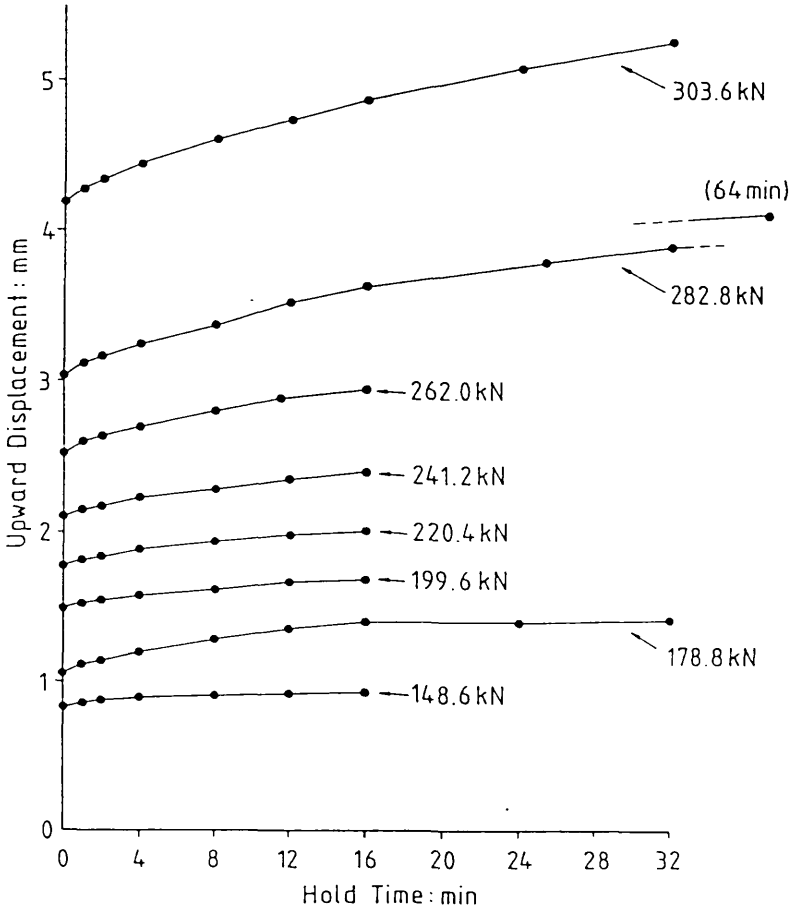

Figure 5.45 Pile Test 7A.1:
Creep behaviour during IL stage

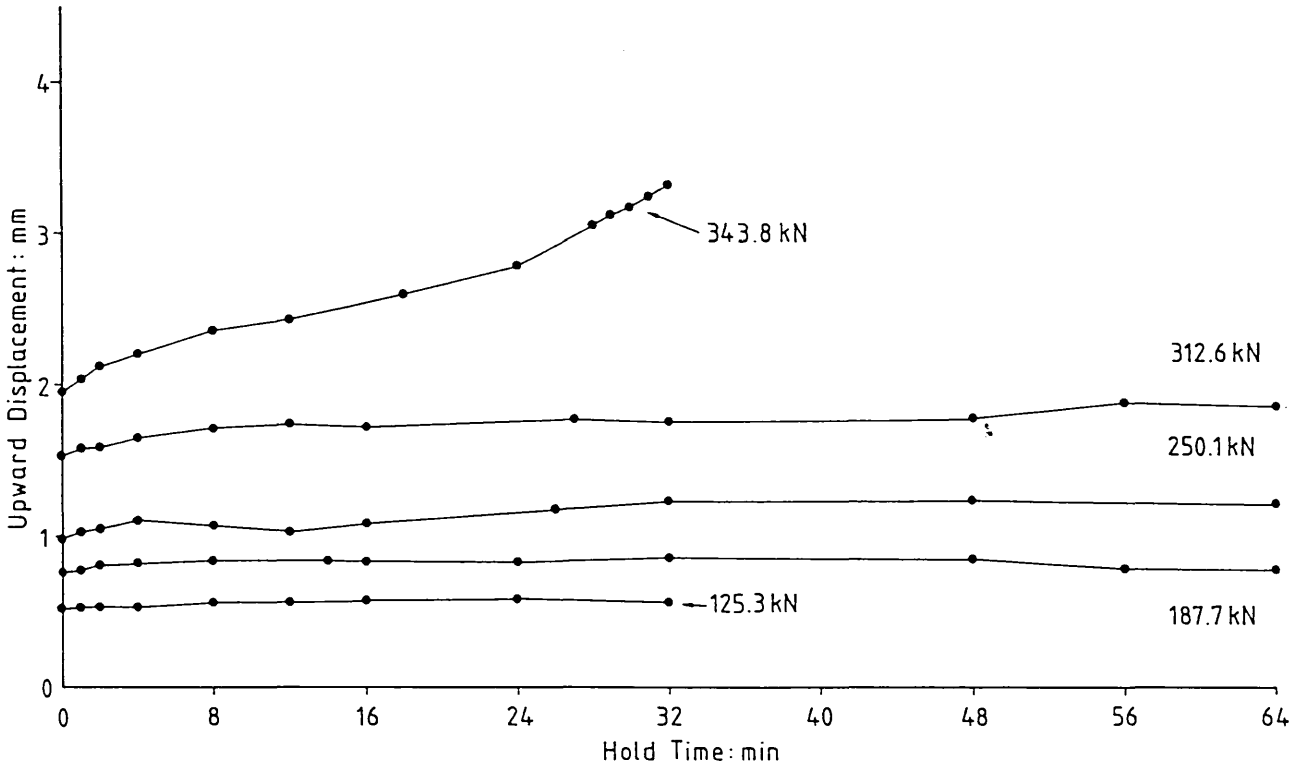

Figure 5.46 Pile Test 7A.2:
Creep behaviour during IL stage

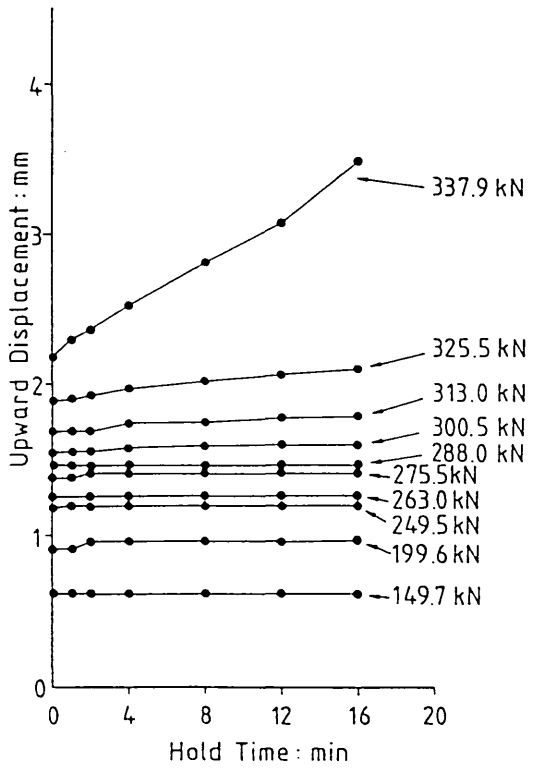

Figure 5.47 Pile Test 7A.3:
Creep behaviour during CRL stage

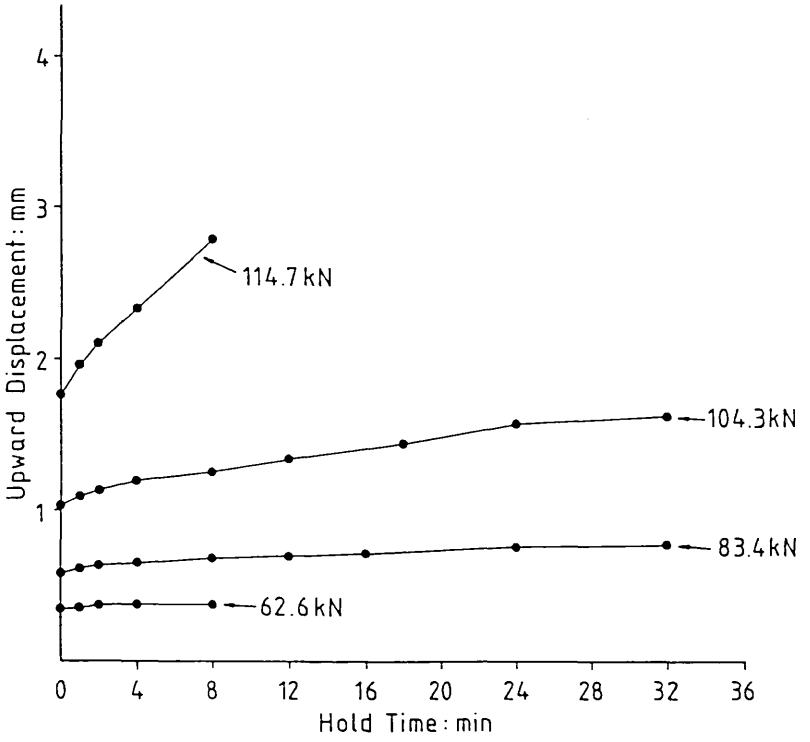

Figure 5.48 Pile Test 8U.1:
Creep behaviour during IL stage

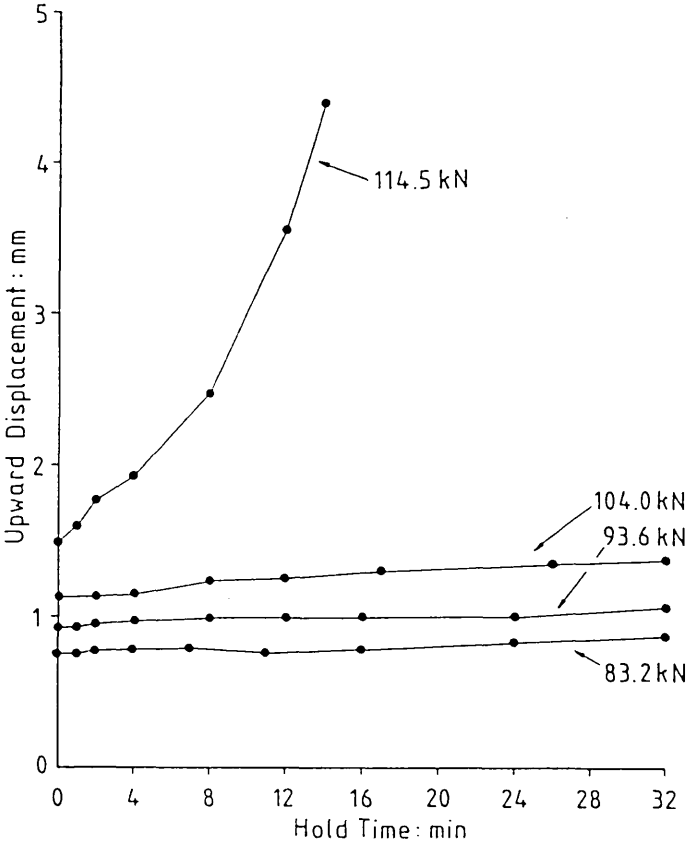

Figure 5.49 Pile Test 8U.2:
Creep behaviour during IL stage

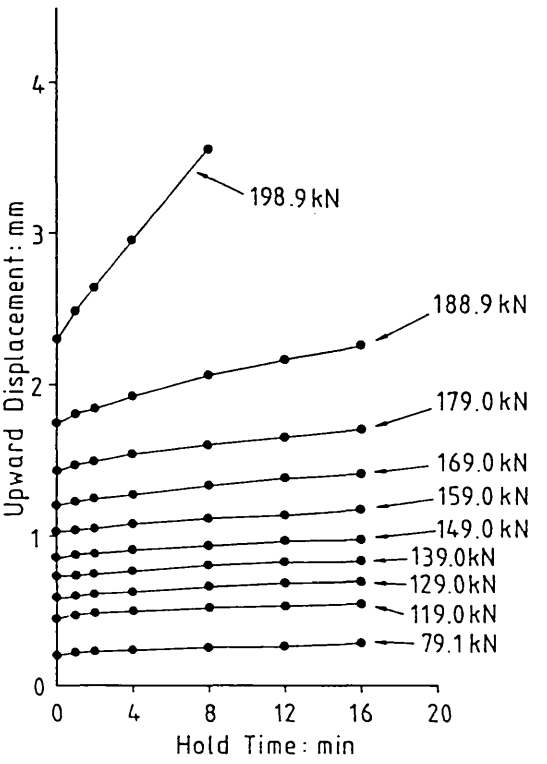

Figure 5.50 Pile Test 8B.1:
Creep behaviour during CRL stage

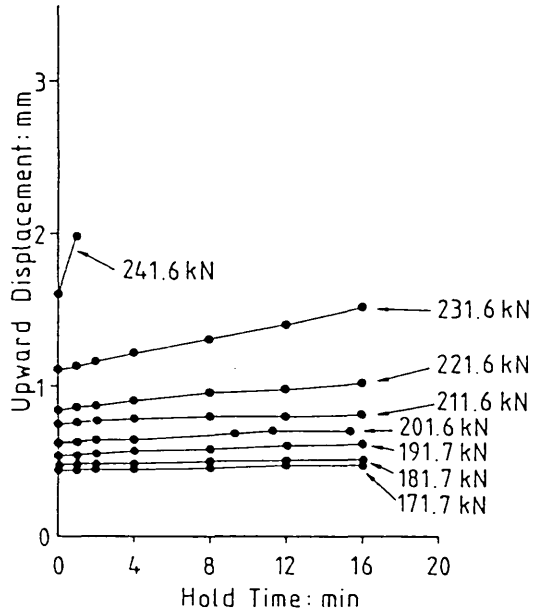

Figure 5.51 Pile Test 8B.2:
Creep behaviour during CRL stage

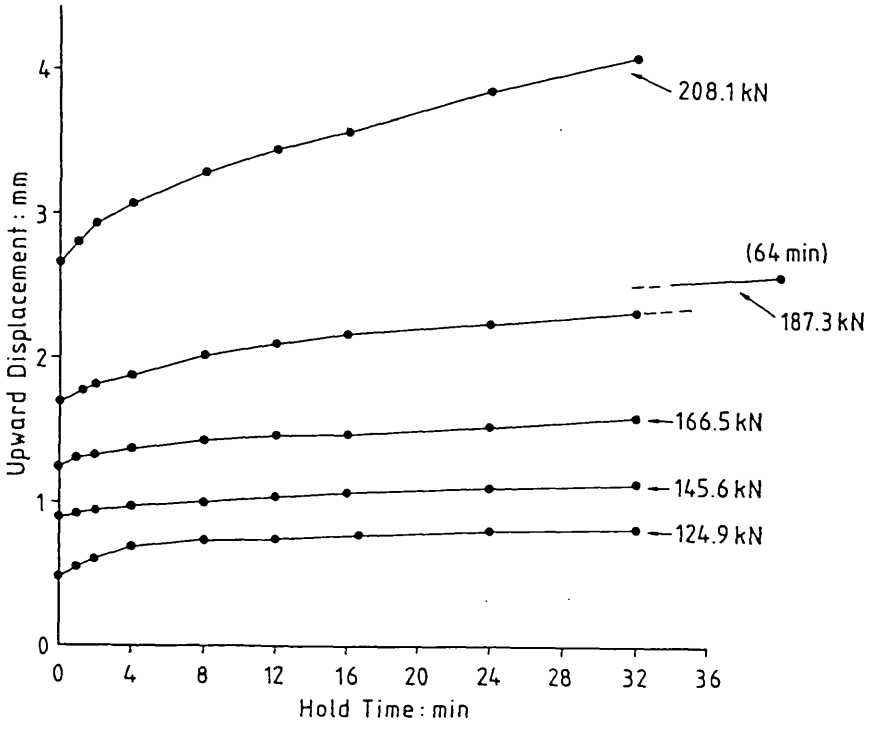

Figure 5.52 Pile Test 9A.1:
Creep behaviour during IL stage

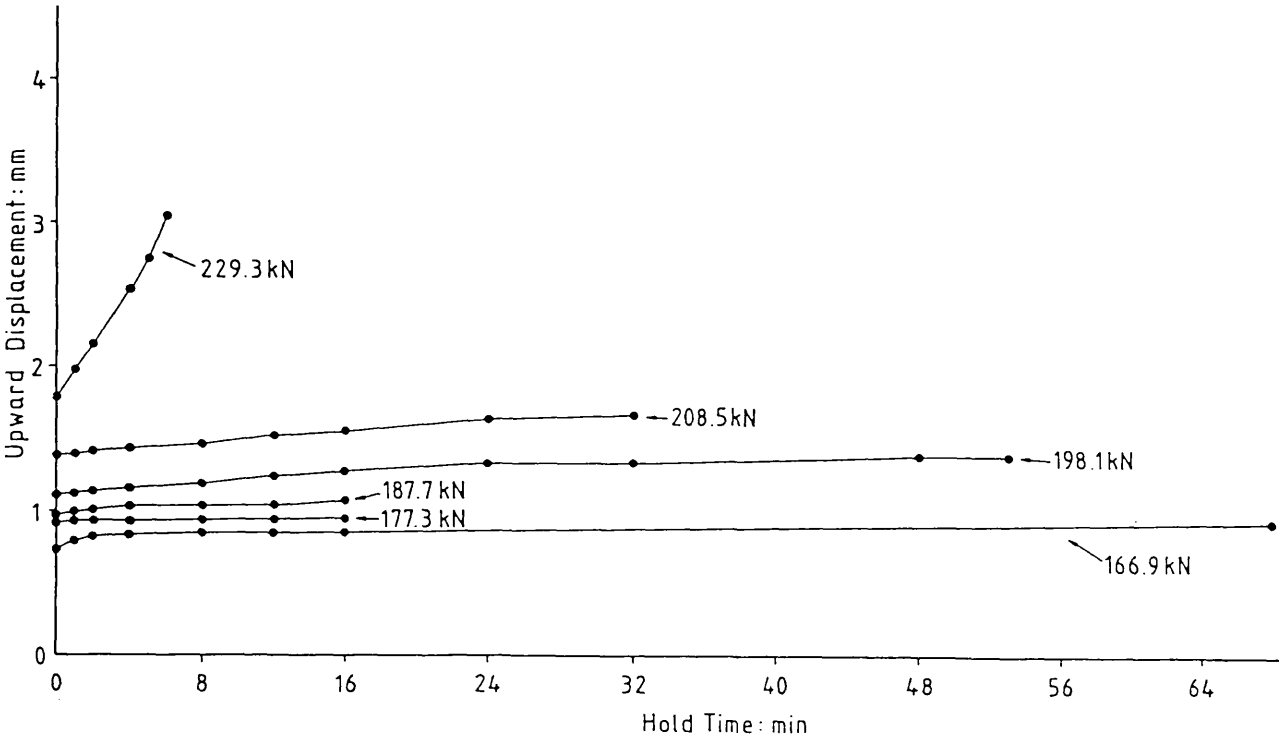

Figure 5.53 Pile Test 9A.2:
Creep behaviour during IL stage

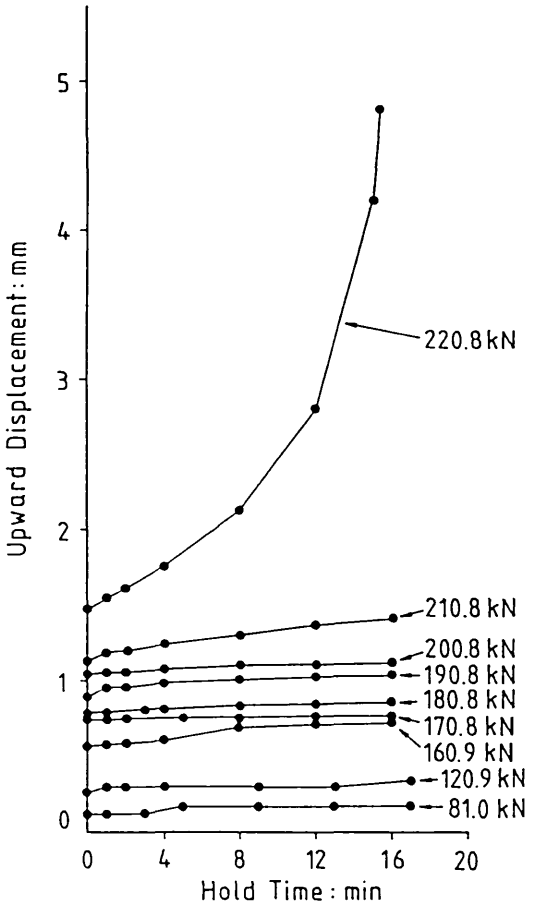

Figure 5.54 Pile Test 9A.3:
Creep behaviour during CRL stage

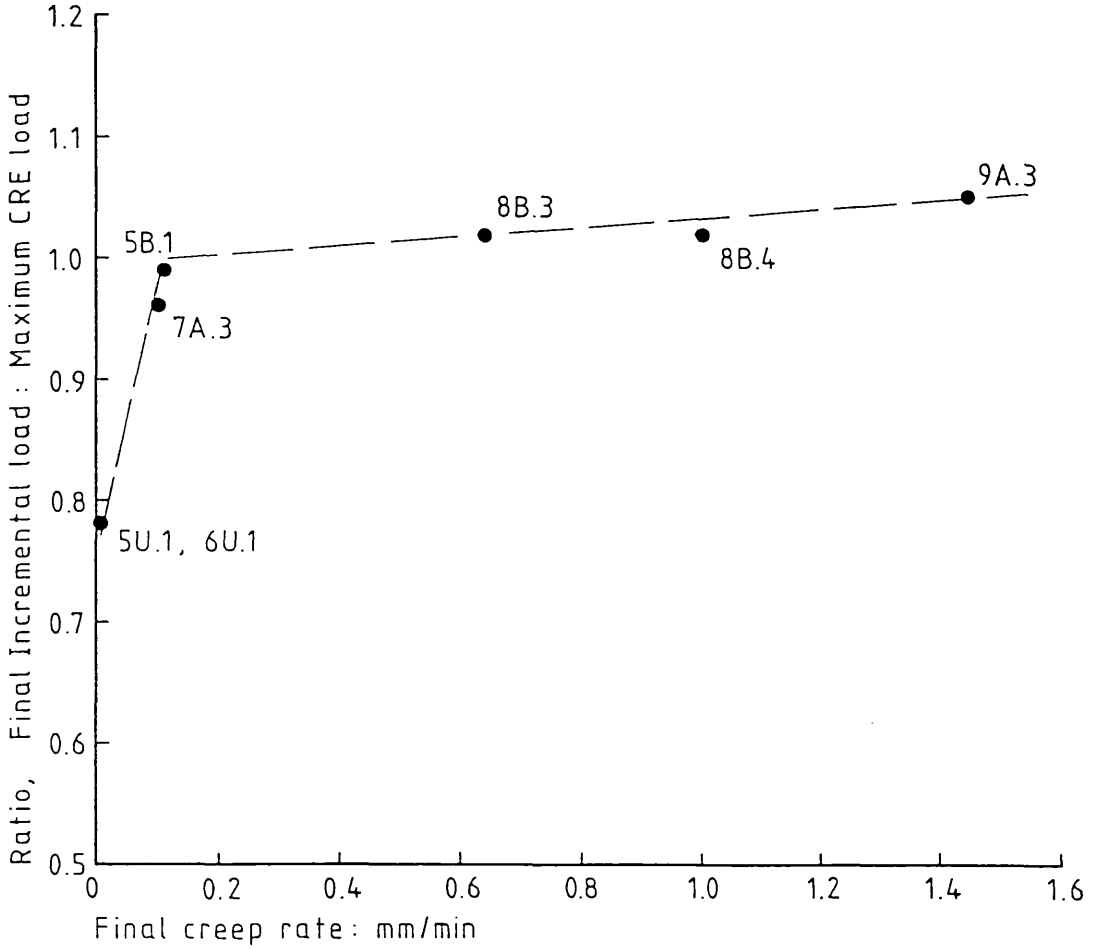

Figure 5.55 BRS pile tests:
'Creep ratio' against final creep displacement rate

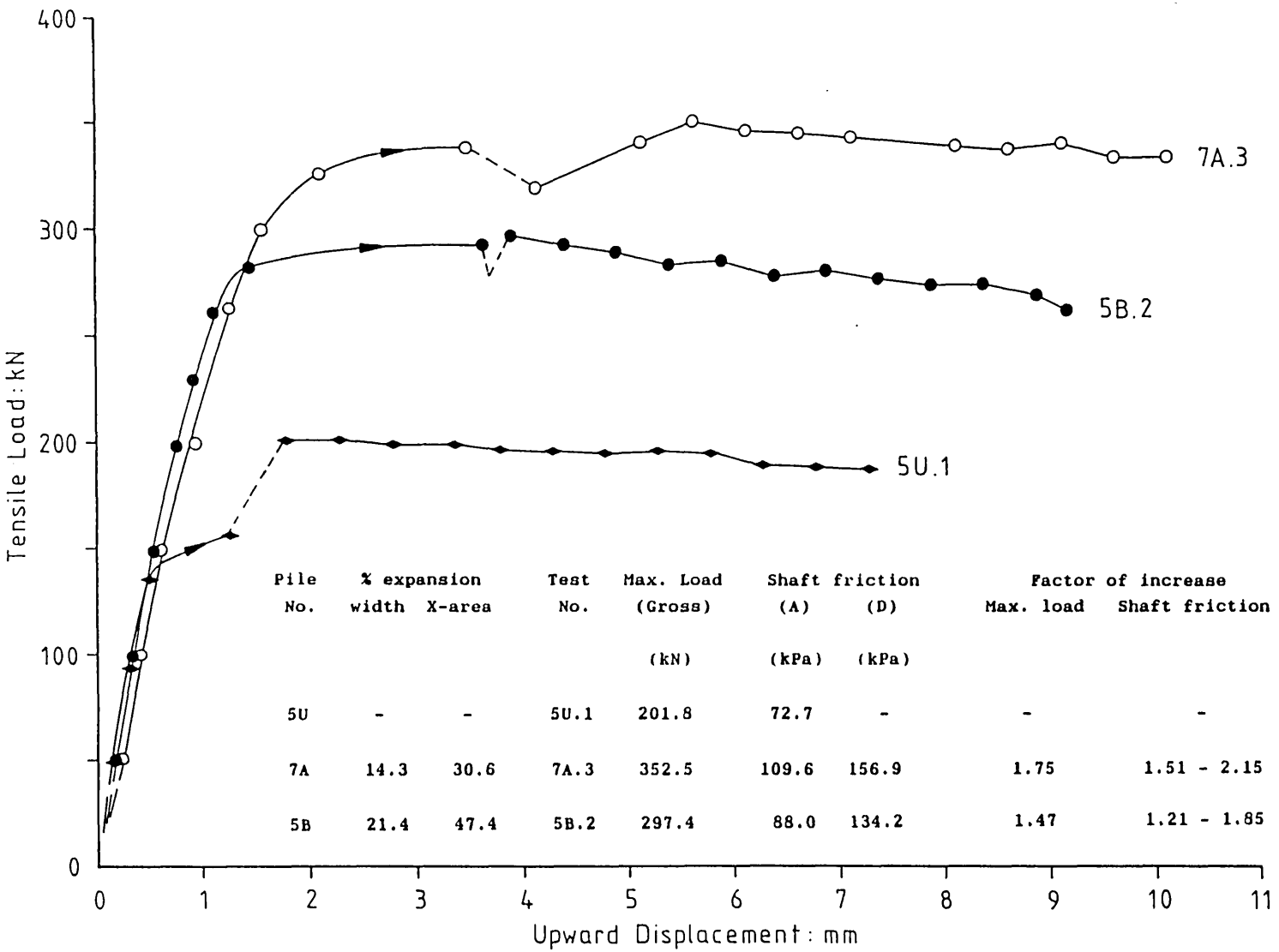

Pile No.	% expansion width	% expansion X-area	Test No.	Max. Load (Gross) (kN)	Shaft friction (A) (kPa)	Shaft friction (D) (kPa)	Factor of increase Max. load	Factor of increase Shaft friction
5U	-	-	5U.1	201.8	72.7	-	-	-
7A	14.3	30.6	7A.3	352.5	109.6	156.9	1.75	1.51 - 2.15
5B	21.4	47.4	5B.2	297.4	88.0	134.2	1.47	1.21 - 1.85

Figure 5.56 Summary of initial loadings of Box Piles

Pile No.	% expansion (width)	% expansion (X-area)	Test No.	Max. Load (Gross) (kN)	Shaft friction (A) (kPa)	Shaft friction (D) (kPa)	Factor of increase (Max. load)	Factor of increase (Shaft friction)
8U	-	-	8U.1	114.7	53.0	-	0.0	0.0
9A	10.7	35.7	9A.2	229.3	93.7	118.2	2.00	1.77 - 2.23
8B	21.4	75.0	8B.2	241.6	86.2	121.9	2.11	1.63 - 2.30

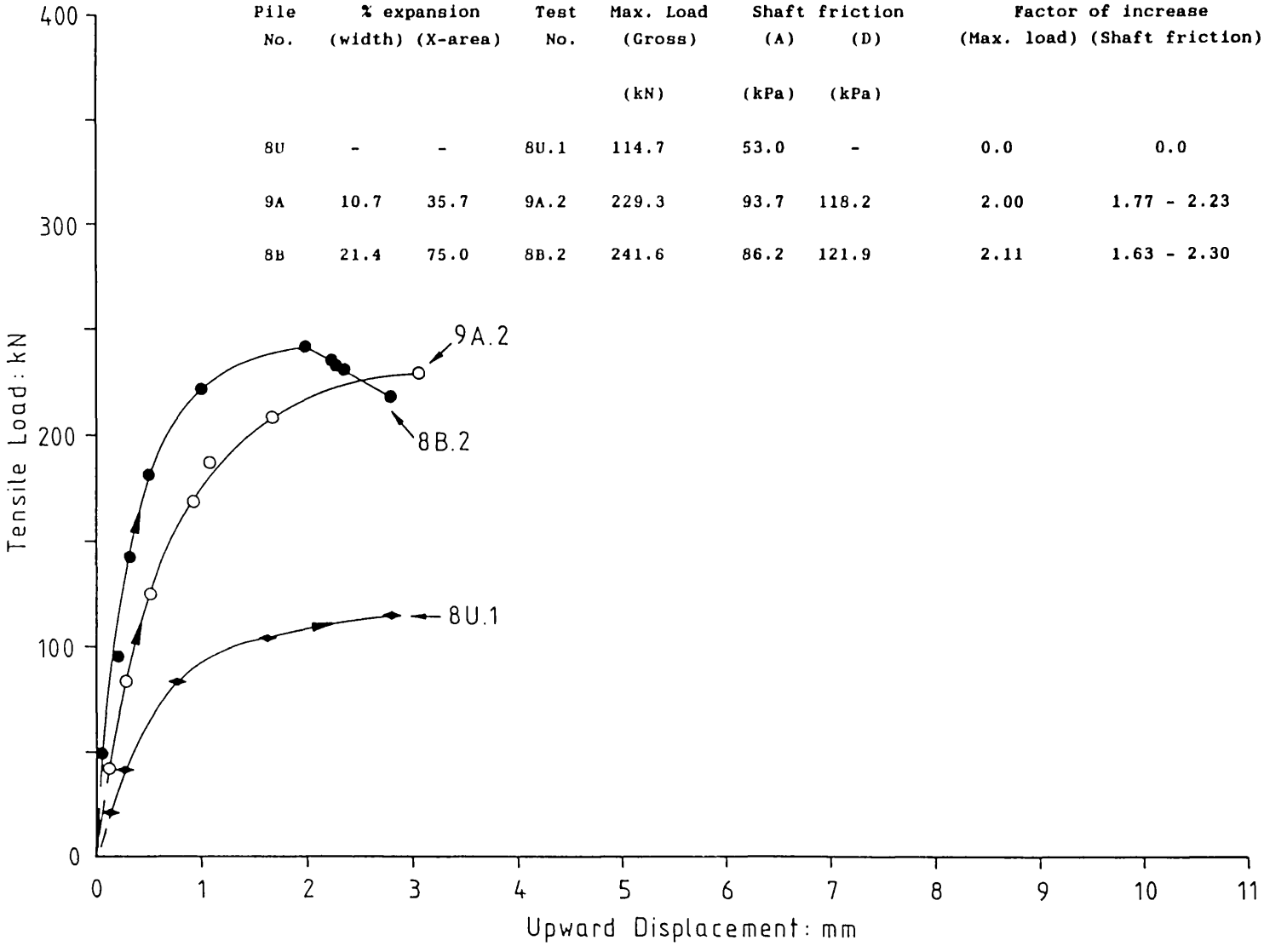

Figure 5.57 Summary of initial loadings of Cruciform Piles

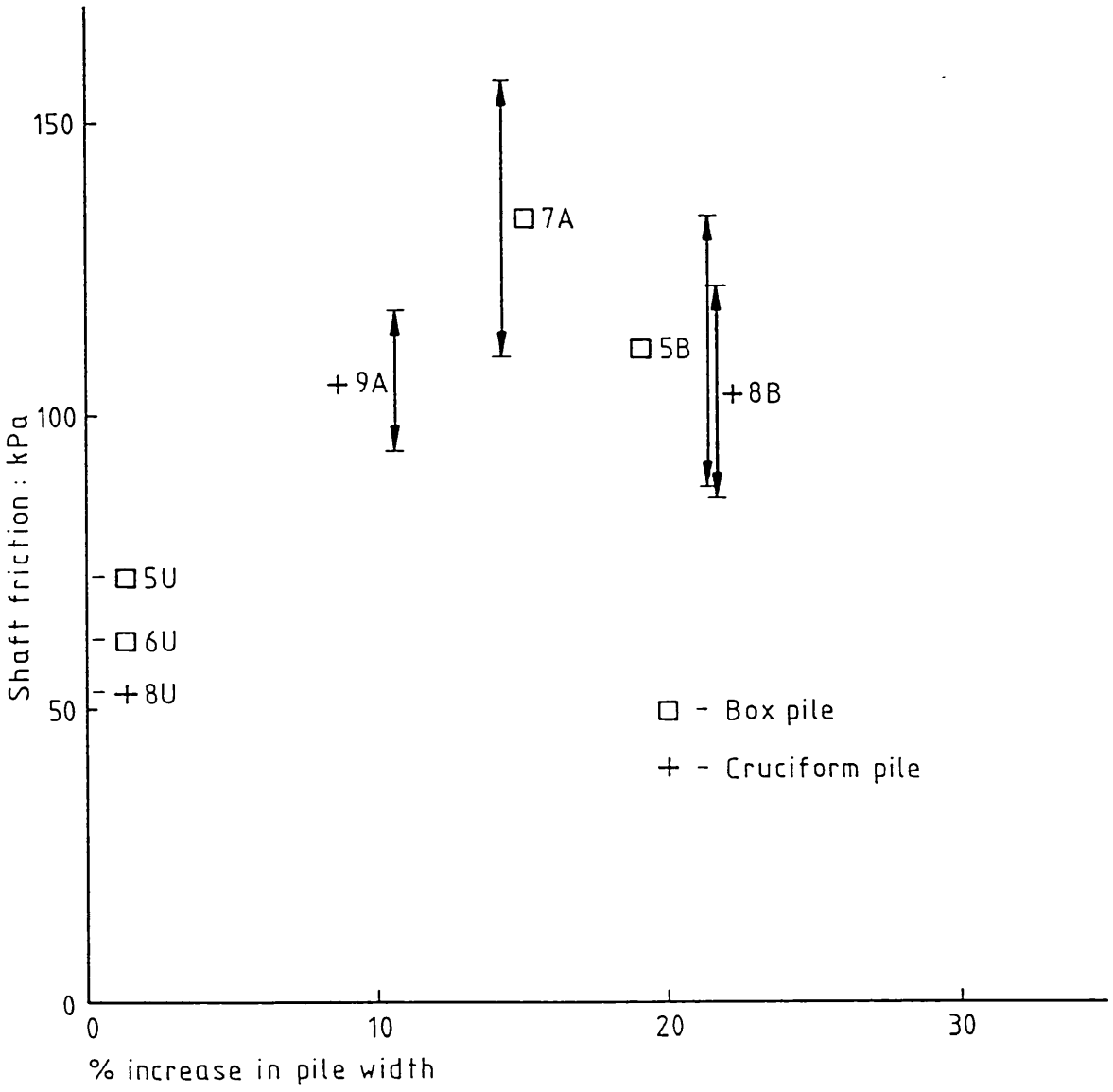

Figure 5.58 Deduced average pile shaft frictions against percentage increase in pile width

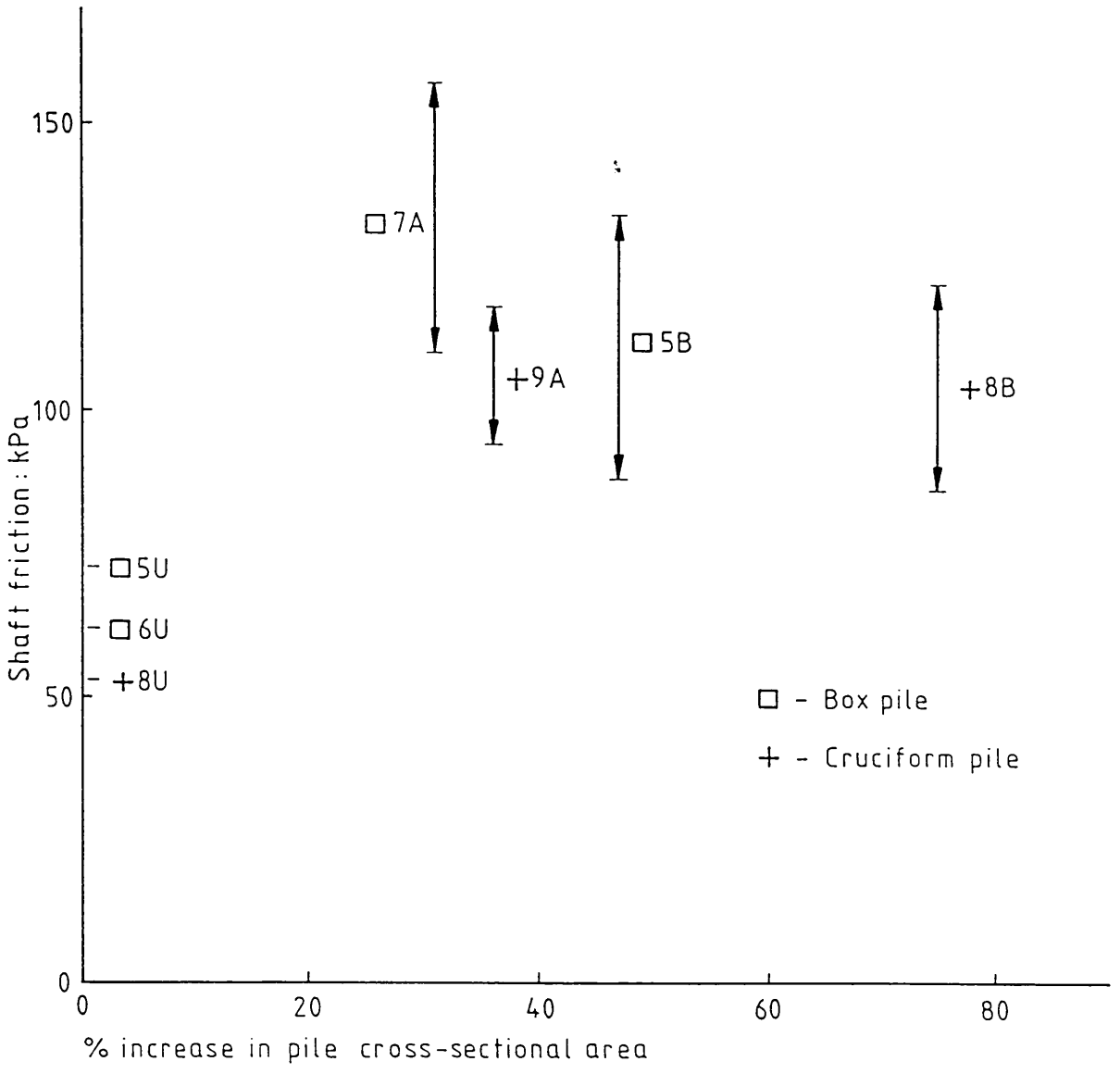

Figure 5.59 Deduced average pile shaft frictions against percentage increase in pile cross-sectional area

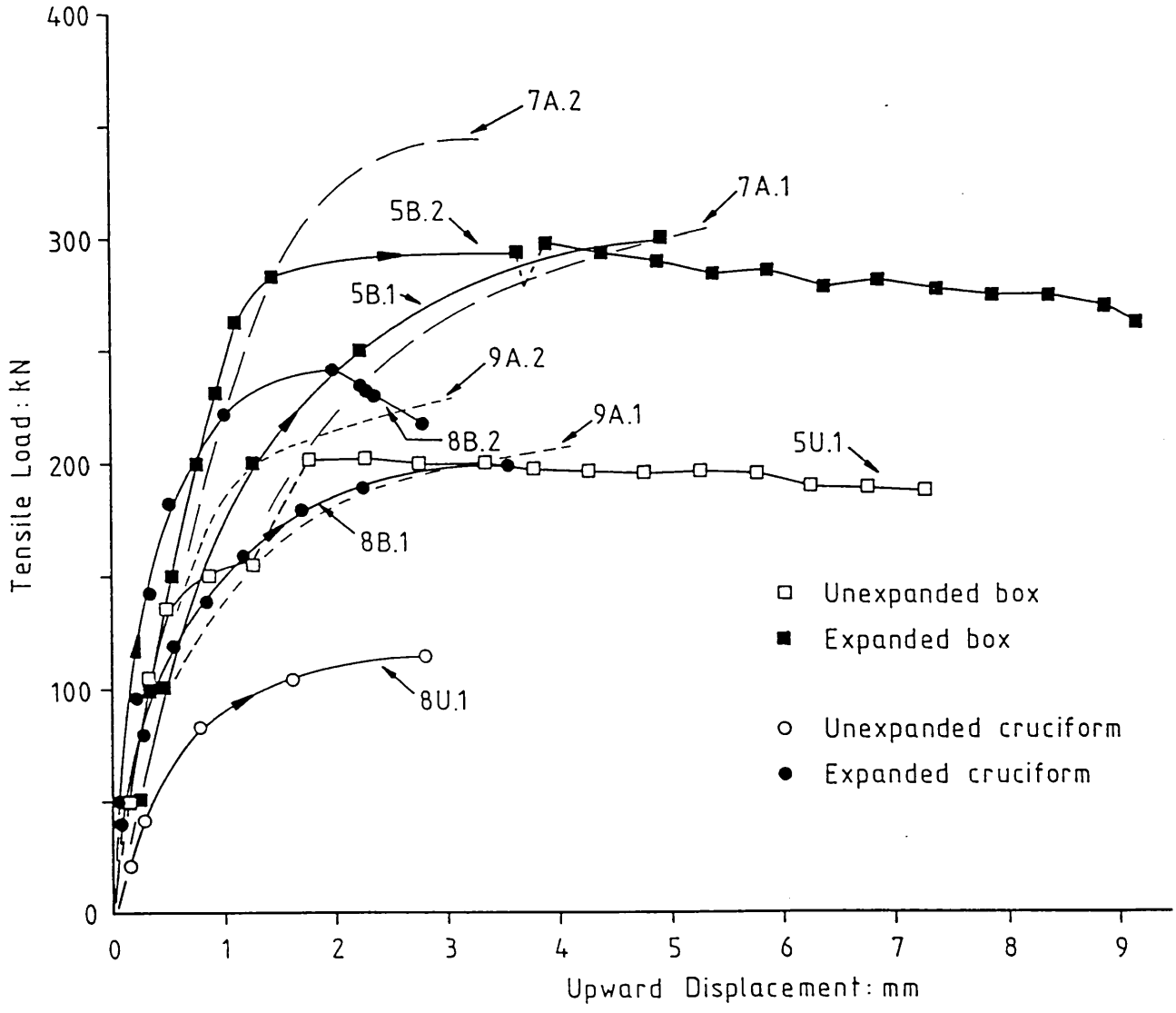

Figure 5.60 Results of selected pile tests at BRS

Test	Depth	Unload-reload data?	Strain	Holding test ?	Strain	Hold time	Max. strain	Max. pressure	Unload data ?
	(m)		(%)		(%)	(min)	(%)	(kPa)	
L1/T1	2.2	unreliable	-	no	-	-	49	~1800	no
L1/T2	3.1	yes	5.4	yes	21.8	51	37	2129	yes
L1/T3	4.1	yes	1.6	yes	8.1	34	36	2188	yes
L2/T1	3.1	yes	4.9	yes	12.5	40	37	1539	yes
L2/T2	7.6	yes	21.4	no	-	-	27	1201	yes

Table 5.1 Details of FDPM tests

Test	Depth	Arm	Strain	p/2Cu	Gur		Gh	
	(m)		(%)		MPa (Arm)	(Ave.)	MPa (Arm)	(Ave.)
L1/T2	3.1	1	5.1	0.69	85		23	
		2	4.8		65	67	24	23
		3	6.2		52		23	
L1/T3	4.1	1	1.5	0.36	94		37	
		2	1.9		90	90	26	33
		3	1.5		85		36	
L2/T1	3.1	1	5.1	0.52	107		33	
		3	4.7		54		14	24
L2/T2	7.6	1	35.2	0.31	78		76	
		3	7.2		33	56	19	26

Notes: 1. Gur calculated from FDPM unload-reload curve (Mair and Wood, 1987).
2. Gh calculated from unload curve, (Houlsby and Withers, 1988).

Table 5.2 Values of shear modulus G deduced from FDPM tests

Test	Depth	P_L	σ_v'	Cu (1)	Cu (2)
	(m)	(kPa)	(kPa)	(kPa)	(kPa)
L1/T1	2.2	2077	30	-	328
L1/T2	3.1	2647	40	366	332
L1/T3	4.1	2654	51	332	338
L2/T1	3.1	1823	40	228	237
L2/T2	7.6	1532	162	144	190

Notes: Cu (1) calculated by Houlsby method (Houlsby and Withers, 1988).
Cu (2) calculated by limit pressure method,
Np = 6.18 (Mair and Wood, 1987).

Table 5.3 Values of undrained shear strength c_u deduced from FDPM tests

Test	Depth	FDPM		DMT	
		$p_{lift-off}$	p_L	p_0	p_1
	(m)	(kPa)	(kPa)	(kPa)	(kPa)
L1/T1	2.2	830	2000	1796	2077
L1/T2	3.1	911	2129	1170	2430
L1/T3	4.1	645	2188	1235	2600
L2/T1	3.1	893	1539	1179	2430
L2/T2	7.6	568	1324	930	1370

Table 5.4 Summary of FDPM and DMT results

Test	Depth	Strain	Hold time	$P_{initial}$	P_{final}	ΔP	$\Delta P/P_{initial}$
	(m)	(%)	(min)	(kPa)	(kPa)	(kPa)	(%)
L1/T2	3.1	21.8	51	1877	1605	271	12.4
L1/T3	4.1	8.1	34	1668	1450	218	13.1
L2/T1	3.1	12.5	40	1151	998	153	13.3

Table 5.5 Details of FDPM holding tests

Pile 5U testing details

Outer shell driven: 13. 3.86 Expander mandrel driven: -

Shaft areas: (m^2)
Embedded length, Full X-section (A): 2.74 Reduced X-section (B): -
Expanded length, Full X-section (C): - Reduced X-section (D): -

Pile weight: 2.7 (kN)

Test No.	Date	Days elapsed since driving: Shell	Mandrel	Test Stage	Maximum Load (Gross) (kN)	(Net) (kN)	Shaft Frictions (A) (kPa)	(B) (kPa)	(C) (kPa)	(D) (kPa)	Displacement at: Max. Load (mm)	End of stage (mm)
5U.1	25. 4.86	43	-	IL	156.1	-*	-	-	-	-	1.28	1.28
				CRE	201.8	199.1	72.7	-	-	-	2.30	6.64
5U.2	30. 7.86	139	-	IL	177.3	174.6	63.8	-	-	-	2.16	1.48

Table 5.6 Summary of tests:
Pile configuration 5U

Pile 5B testing details

Outer shell driven: 13. 3.86 Expander mandrel driven: 12. 8.86

Shaft areas: (m^2)	Embedded length,		Expanded length,	
	Full X-section (A):	3.32	Full X-section (C):	2.64
	Reduced X-section (B):	2.74	Reduced X-section (D):	2.18

Pile weight: 4.8 (kN)

Test No.	Date	Days elapsed since driving: Shell	Mandrel	Test Stage	Maximum Load (Gross) (kN)	(Net) (kN)	Shaft Frictions (A) (kPa)	(B) (kPa)	(C) (kPa)	(D) (kPa)	Displacement at: Max. Load (mm)	End of stage (mm)
5B.1	14. 8.86	154	2	IL	299.7	294.9	88.7	107.7	111.5	135.4	4.92	4.12
5B.2	15.12.86	274	122	CRL	293.0	-	-	-	-	-	3.64	3.64
				CRE	297.4	292.6	88.0	106.9	110.6	134.3	3.90	8.15
5B.3	17.12.6	276	124	Cyclic[1]	-	-	-	-	-	-	-	-
				CRE	276.3	271.5	81.6	99.2	102.6	124.7	1.44	7.12

Notes: 1. 25 cycles, 15kN - 149.4kN

Table 5.7 Summary of tests: Pile configuration 5B

Pile 6U testing details

Outer shell driven: 14. 3.86 Expander mandrel driven: -

Shaft areas: (m^2)
Embedded length,
Full X-section (A): 2.11
Reduced X-section (B): -
Expanded length,
Full X-section (C): -
Reduced X-section (D): -

Pile weight: 2.7 (kN)

Test No.	Date	Days elapsed since driving: Shell	Mandrel	Test Stage	Maximum Load (Gross) (kN)	(Net) (kN)	Shaft Frictions (A) (kPa)	(B) (kPa)	(C) (kPa)	(D) (kPa)	Displacement at: Max. Load (mm)	End of stage (mm)
6U.1	28. 4.86	45	-	CRL	103.8	-	-	-	-	-	0.79	0.79
				CRE	133.6	130.9	62.0	-	-	-	3.48	7.76

Table 5.8 Summary of tests:
Pile configuration 6U

Pile 7A testing details

Outer shell driven: 23. 5.86 Expander mandrel driven: 29. 5.86

Shaft areas: (m^2)	Embedded length,		Expanded length,	
	Full X-section (A):	3.17	Full X-section (C):	2.53
	Reduced X-section (B):	2.78	Reduced X-section (D):	2.22

Pile weight: 4.6 (kN)

Test No.	Date	Days elapsed since driving:		Test Stage	Maximum Load (Gross)	(Net)	Shaft Frictions (A)	(B)	(C)	(D)	Displacement at: Max. Load	End of stage
		Shell	Mandrel		(kN)	(kN)	(kPa)	(kPa)	(kPa)	(kPa)	(mm)	(mm)
7A.1	30. 5.86	7	1	IL	303.6	299.0	94.2	107.6	118.0	134.8	5.26	3.49
7A.2	29. 7.86	67	61	IL	343.8	339.2	106.9	122.1	133.9	152.9	3.32	1.68
7A.3	9. 1.87	231	225	CRL	337.9	-	-	-	-	-	3.49	3.49
				CRE	352.5	347.9	109.6	125.2	137.3	156.9	4.63	8.78

Table 5.9 Summary of tests: Pile configuration 7A

Pile 8U testing details

Outer shell driven: 13. 5.86 Expander mandrel driven: -

Shaft areas: (m^2)
Embedded length, Full X-section (A): 2.12 Reduced X-section (B): -
Expanded length, Full X-section (C): - Reduced X-section (D): -

Pile weight: 2.4 (kN)

Test No.	Date	Days elapsed since driving: Shell	Mandrel	Test Stage	Maximum Load (Gross) (kN)	(Net) (kN)	Shaft Frictions (A) (kPa)	(B) (kPa)	(C) (kPa)	(D) (kPa)	Displacement at: Max. Load (mm)	End of stage (mm)
8U.1	20. 5.86	7	-	IL	114.7	112.3	53.0	-	-	-	2.79	2.00
8U.2	31. 7.86	79	-	IL	114.5	112.1	52.9	-	-	-	4.40	4.11

Notes:

Table 5.10 Summary of tests: Pile configuration 8U

Pile 8B testing details

Outer shell driven: 13. 5.86 Expander mandrel driven: 13. 8.86

Shaft areas: (m^2)

Embedded length,			Expanded length,		
Full X-section	(A):	2.73	Full X-section	(C):	2.48
Reduced X-section	(B):	2.12	Reduced X-section	(D):	1.93

Pile weight: 6.6 (kN)

Test No.	Date	Days elapsed since driving: Shell	Mandrel	Test Stage	Maximum Load (Gross) (kN)	(Net) (kN)	Shaft Frictions (A) (kPa)	(B) (kPa)	(C) (kPa)	(D) (kPa)	Displacement at: Max. Load (mm)	End of stage (mm)
8B.1	18. 8.86	97	5	CRL	198.9	192.3	70.5	90.7	77.6	99.7	3.55	3.00
8B.2	9. 3.87	300	208	CRL	241.6	235.0	86.2	110.8	94.8	121.9	2.00	2.24
8B.3	10. 3.87	301	209	CRL	231.2	-	-	-	-	-	2.21	2.21
				CRE	226.0	219.4	80.5	103.4	88.5	113.8	4.82	7.45
8B.4	10. 3.87	301	209	Cyclic[1]	-	-	-	-	-	-	-	-
				CRL	211.8	-	-	-	-	-	2.80	2.80
				CRE	207.7	201.1	73.7	94.8	81.1	104.3	4.32	7.96

Notes: 1. 25 cycles, 17kN - 114kN.

Table 5.11 Summary of tests: Pile configuration 8B

Pile 9A testing details

Outer shell driven: 13. 5.86 Expander mandrel driven: 14. 5.86

Shaft areas: (m^2)

Embedded length,			Expanded length,		
Full X-section	(A):	2.40	Full X-section	(C):	2.18
Reduced X-section	(B):	2.10	Reduced X-section	(D):	1.91

Pile weight: 3.9 (kN)

Test No.	Date	Days elapsed since driving: Shell	Mandrel	Test Stage	Maximum Load (Gross) (kN)	(Net) (kN)	Shaft Frictions (A) (kPa)	(B) (kPa)	(C) (kPa)	(D) (kPa)	Displacement at: Max. Load (mm)	End of stage (mm)
9A.1	21. 5.86	8	7	Incremental	208.1	204.2	84.9	97.1	93.7	107.1	4.08	2.90
9A.2	1. 8.86	80	79	Incremental	229.3	225.4	93.7	107.1	103.4	118.2	3.05	2.10
9A.3	20. 3.87	311	310	CRL	220.8	-	-	-	-	-	4.80	4.80
				CRE	209.8	205.9	85.6	97.9	94.5	108.0	6.14	10.34

Notes:

Table 5.12 Summary of tests:
Pile configuration 9A

Pile configuration	X-sectional areas of steel:			Embedded portion of pile				Exposed portion of pile	
				Lengths		Displacements[3]		Length[4]	Displacement[5]
	Shell	Mandrel	Shell+Mandrel	Shell	Shell+Mandrel[2]	Lower bound	Upper bound		
	(mm^2)	(mm^2)	(mm^2)	(mm)	(mm)	(mm x10^{-3})	(mm x10^{-3})	(mm)	(mm x10^{-3})
5U	5240	-	-	4890	-	2.22P	2.96P	230	0.21P
5B	5240	4510	9750	4890	4740	1.16P	2.96P	230	0.21P
6U	5240	-	-	3770	-	1.71P	2.28P	200	0.18P
7A	5240	4190	9430	4960	4810	1.21P	3.00P	160	0.15P
8U	5240	-	-	5050	-	2.29P	3.06P	-	-
8B	5240	8700	13940	5050	4970	0.85P	3.06P	-	-
9A	5240	4050	9290	5010	4875	1.25P	3.06P	-	-

Notes:

1. For further details of pile dimensions and depths of embedments see Figures 5.12 and 5.13.

2. Depth of embedment in this case taken as the average of the embedment depths for the outer shell and the expander mandrel.

3. For lower bound, displacement = $\frac{L \times P}{2AE}$

   where: A = X-sect. area of outer shell + expander mandrel.
   L = Embedded length of outer shell + expander mandrel.
   P = Applied load.
   Uniform distribution of shaft resistance assumed.

   For upper bound, displacement = $\frac{2L \times P}{3AE}$

   where: A = X-sect. area of outer shell.
   L = Embedded length of outer shell.
   P = Applied load.
   Triangular distribution of load assumed.

   (Ref: Hobbs and Healy, 1979)

4. Exposed lengths taken as distance between ground level and dial gauge reference plates.

5. Displacement = $\frac{L \times P}{AE}$

   where: A = X-Sect. area of outer shell.
   L = Exposed length of outer shell.
   P = Applied load.

Table 5.13 Elastic displacements of piles under load

Test No.	Final Inc. load (kN)	Final creep rate (mm/min)	Incremental failure ?	Maximum CRE load (kN)	Inc. fail. load / CRE fail. load	Load increase factor[1]	Load increase factor[2]
Box piles							
5U.1	156.1	0.0075	no	201.8	0.77	1.00	1.00
5U.2	177.3	0.049	no	-	-		
5B.1	299.7	1.47	yes	-	-		
5B.2	293.0	0.11	yes	297.4	0.99	1.47	1.47
5B.3	-	-	-	276.3	-		
6U.1	103.8	0.01	no	133.6	0.78		
7A.1	303.6	0.022	no	-	-		
7A.2	343.8	0.075	no	-	-		
7A.3	337.9	0.10	yes	352.5	0.96	1.75	1.75
Cruciform piles							
8U.1	114.7	0.11	yes	-	-	1.00	0.57
8U.2	114.5	0.42	yes	-	-		
8B.1	198.9	0.15	yes	-	-		
8B.2	241.6	0.38	yes	-	-	2.11	1.20
8B.3	231.2	0.64	yes	226.0	1.02		
8B.4	211.8	1.00	yes	207.7	1.02		
9A.1	208.1	0.059	no	-	-		
9A.2	229.3	0.30	yes	-	-	2.00	1.14
9A.3	220.8	1.44	yes	209.8	1.05		

Notes:

1. Ratio of the maximum recorded load for each pile configuration, to the respective maximum loads for the unexpanded box pile and unexpanded cruciform pile.

2. Ratio of the maximum recorded load for each pile configuration, to the maximum recorded load for the unexpanded box pile.

Table 5.14 Comparison of pile test results at BRS site

CHAPTER 6
MINI-PILE TESTING

6.1 Introduction

6.1.1 Background to miniature scale field trials

Work on the miniature scale system of steel wedge-piles commenced midway through the main programme of tests on 6m long piles at the Luton and BRS sites. Testing at Luton had been completed, and the Wedge-Pile principle had been demonstrated at large scale. At this stage it was decided to develop a smaller, more portable pile testing system which would provide the means to augment the 6m pile test data with information from a wider range of soil types.

The main criteria for such a system were as follows:

(a) the system should be easily transportable, by car or small van

(b) the piles should be easily extracted after testing, and easily reassembled for multiple re-use

(c) installation and testing of the piles should be able to be carried out by two people, without the need for craneage.

The cost advantage of such a system would allow many more sites to be visited than would be possible with the 6m piles. In addition, the fabrication and machining involved would be on a much smaller scale than before. This would mean that work could be conveniently based at Imperial College and there would be less reliance on help from other organisations, allowing modifications and developments to be made more readily than before.

Based on site experience with the 6m piles, an embedded pile length of approximately 1m was targeted as suitable for the new system. This length represents miniature scale for most civil engineering applications, but has direct relevance to certain anchorage situations, for example the semi-permanent anchoring of tension fabric structures.

It was decided to develop a cruciform type pile initially. This configuration was proving particularly successful in the large scale trials. Also, a small displacement pile such as the cruciform would be

easy to install. A cruciform pile with initial overall dimensions of 100x100mm was selected as appropriate. It was decided to make the cross sectional area of the outer shell as thin as possible. This decision was in line with the concept emerging at the time of a minimum displacement outer shell that would introduce an expandable inclusion into the ground with very low driving energy.

The overall aim of the miniature wedge-pile field trials would be to assess the gains in pile capacity possible in a range of different soil profiles. Unexpanded and expanded piles would be tested in tension, as with the 6m piles. The focus of the study would be on immediate gains in pile capacity. The behaviour of wedge-piles in the long term was more readily studied using the 6m piles at the secure sites at Luton and BRS.

6.1.2 Summary of piles tested

Three types of 'mini-pile' were eventually developed and tested. The principle characteristics of the piles are summarised below:

(a) Cruciform mini-pile, Type I:
- Initial size 100x100mm, 1.25m long; made up from 50x50x3mm angle sections.
- Tested unexpanded, and expanded by 6% and 10% of initial pile width.

(b) Cruciform mini-pile, Type II:
- Initial size 100x100mm, 1.5m long; made up from 50x50x1.5mm angle sections.
- Tested unexpanded, and expanded by 6% and 10% of initial pile width.

(c) '2-way', H section mini-pile:
- Initial size 100x100mm, 1.5m long; made up from two 100x50x1.5mm channels 'back-to-back'.
- Tested unexpanded, and expanded by 6% and 10%.

Development and testing of the mini-piles took place in two main phases. The initial development of the mini-pile system formed the subject of an MSc investigation by Fitch (1986), supervised by the author. The Type I cruciform mini-pile was developed and tested as part of this study. In the second phase of work, the Type II cruciform mini-pile and the H section mini-pile were developed and tested.

The mini-piles and installation procedures are described in Sections 6.2 to 6.4. Testing equipment and procedures, and pile extraction and

refurbishment, are described in Sections 6.5 to 6.7. The sites at which the mini-piles were tested are described in Section 6.8, and results from the testing programme are presented in Section 6.9.

6.2 Cruciform Mini-Pile, Type I

6.2.1 Introduction

The Type I cruciform mini-pile was the first of the mini-piles to be developed and tested. The various stages of development of the mini-pile are described by Fitch (1986). The final arrangement is described below.

The overall arrangement of the mini-pile is shown in Figure 6.1 and in Plate 6.1. The mini-pile was essentially a scaled down version of the 6m cruciform pile described in Section 3.3. Improvements in design based on experience with the larger pile were incorporated whenever possible.

As for the large cruciform pile, the mini-pile comprised two main components:

(a) outer shell
(b) expander mandrel

Four outer shells and two expander mandrels were fabricated. The system was used at three sites.

6.2.2 Details of outer shell

The outer shell was 1250mm long, with an initial cross section of 100x100mm, made up from four 50x50x3mm hot rolled equal angle sections (angles). The angles were not coated with mill varnish. The angles were held back-to-back in a cruciform configuration by temporary connecting bolts. 3mm diameter brass bolts at 475mm spacings were used, with nylon insert nuts to avoid loosening of the bolts during driving. The connections were designed to be split apart when the expander mandrel was driven into the outer shell.

The system of bolting was chosen in preference to tack welding. Although tack welding had proved more successful than bolting for the 6m piles, a system of replaceable connections allowed more control over the connecting forces on the outer shell during expansion. These were likely to be more critical in the case of the mini-piles because of the lower overall expansion forces. The bolted system also allowed repairs or adjustments to be made easily on site.

A welded driving shoe arrangement was provided by welding the angles

together across the bottom of the outer shell, and up the sides for a distance of 25mm.

The arrangement at the head of the outer shell was an improved version of that used for the 6m piles. Specially shaped loading blocks were welded to the top of each angle (Figure 6.2). The blocks reinforced the top of the outer shell during driving, and subsequently formed part of the loading system described in Section 6.5. Below the loading blocks, the angles were securely bolted together during driving by clamping bolts. 12mm diameter bolts in conjunction with nylon insert nuts were used.

6.2.3 Details of expander mandrel

Two differently sized expander mandrels were fabricated. Each expander mandrel was 1350mm long, made up from three cold rolled flat sections (flats) welded together in a cruciform shape. The form of construction was the same as for the 6m long pile.

As for the large piles, the expander mandrels were classified on the basis of the radial expansion they produced, expressed as a percentage of the initial dimensions of the outer shell. Expander mandrel 'A' was made up from one 100x6mm flat and two 50x6mm flats. It expanded the outer shell from 100x100mm to 106x106mm, an expansion of 6%. Expander mandrel 'A' is shown in Plate 6.1. Expander mandrel 'B' was made up from one 100x10mm flat and two 50x10mm flats. It expanded the outer shell from 100x100mm to 110x110mm, an expansion of 10%.

These amounts of expansion were selected on the basis of the large scale pile tests, which were showing large increases in pile carrying capacity at expansions of only 11%. It was decided to investigate the effect of expansions of lower than this amount in order to optimise expander mandrel size.

The flats forming the expander mandrel were held in a cruciform configuration by means of welding at 200mm spacings. The weld detail is shown in Figure 6.1. Reinforcement blocks were welded to the top of the expander mandrel. These were primarily designed to protect the expander mandrel during driving, but could also be used as loading blocks when load needed to be applied to the expander mandrel.

At the bottom of the expander mandrel, a nose was provided. The nose was accurately formed by using a shaping machine. The nose profile was formed at the ends of the individual flats comprising the expander mandrel, before assembly. The nose of expander mandrel B is shown in

Plate 6.2.

The design nose profile is shown in Figure 6.3. It is parabolic in form with a sharp leading edge to locate in the top of the outer shell. The profile is defined by expressing the length of the nose as a multiple of the thickness of the flat section forming the expander mandrel. A nose length of ten times the flat thickness was selected. The profiles were drawn out at full size so that template guides could be manufactured for use with the shaping machine.

The leading edge of the expander mandrel nose was staggered (Figure 6.1; Plate 6.2). This arrangement allowed the nose to be introduced easily into the top of the outer shell.

6.2.4 Completed mini-pile arrangement

The completed mini-pile arrangement is shown in Figure 6.1. The outer shell was driven to a depth of 1000mm. The expander mandrel was subsequently driven until the tip of the expander mandrel was 60mm short of the bottom of the outer shell.

6.2.5 Mini-Pile installation

The Type I cruciform mini-pile was hand driven using a two person operated post rammer or 'monkey', shown in Figure 6.4. The mass of the post rammer was approximately 50kg. Handles, and a box guide which located the rammer on top of the pile, allowed an 'up and down' driving action.

Before driving, the pile components were marked off with chalk at 50mm intervals, and at the final penetration position. The procedure for installing the pile was as follows:

Outer shell:

(a) The outer shell was held vertically prior to driving by means of a simple wooden trestle which supported the outer shell at approximately mid-height.

(b) The outer shell was driven into the ground, the trestle being removed at the appropriate time.

(c) After the outer shell was driven to final depth, the post rammer was lifted clear and the clamping bolts at the top of the outer shell were removed to allow the expander mandrel to be driven.

Expander mandrel:

(a) The nose of the expander mandrel was engaged in the top of the outer shell. The expander mandrel was then pushed into the outer shell by hand as far as possible so as to provide initial support for driving. Additional support was provided as before by using a trestle.

(b) The expander mandrel was driven into the outer shell by using the post rammer as before. The supporting trestle was removed once the expander mandrel was being firmly supported by the outer shell.

6.3 Cruciform Mini-Pile, Type II

6.3.1 Introduction

Following the initial trials of the mini-pile system using the Type I cruciform mini-piles, a further series of trials was started in a wider range of soil types, using improved versions of the mini-piles and equipment.

The main conclusions regarding the form of construction of the Type I cruciform mini-pile were as follows:

(a) The weakest point of the outer shell during driving was the region above the top clamping bolts. There was a tendency for the angles of the outer shell to be forced apart and distorted in this region during driving. This was mainly as a result of the rather crude post rammer striking the top of the outer shell unevenly.

(b) It was considered that it would be possible to install an outer shell formed from thinner angle sections, provided that an improved driving system was developed, designed to prevent damage to the top of the outer shell.

(c) The temporary bolted connections used to hold the outer shell together were time consuming to fix.

(d) The expander mandrels performed well.

The Type II cruciform mini-pile was developed in the light of these conclusions. The outer shell was redesigned, and is described in the next Section. The same expander mandrels were used as before. The overall arrangement of the Type II cruciform mini-pile is shown in Figure 6.5 and Plate 6.1. Seven of the new outer shells were fabricated. The improved mini-pile system was used at four sites.

6.3.2 Details of outer shell

The outer shell was 1500mm long, a small increase in length compared to the original version. The outer shell was initially 100x100mm in cross-section, made up from four 50x50x1.5mm angles.

The angles were bent up from 1.5mm thick cold rolled mild steel sheet. This form of fabrication allowed the use of thinner angles than those that were available as rolled sections. The thickness of angle was half that of the Type I outer shell, and the outer shell configuration represented what was considered to be the thinnest practicable cross-section that could be driven.

In the later stages of the testing programme the surfaces of some of the outer shells were roughened by means of grit-blasting. This process was carried out as part of the refurbishment of the mini-piles after use (Section 6.7.2).

A new system of temporary connections using pop-rivets was devised to hold the angles in the cruciform configuration. 3mm diameter aluminium/ 3.5% magnesium alloy pop-rivets were used at 150mm spacings. This system was quicker and more convenient than bolting, particularly when reassembling the outer shell for reuse.

A welded driving shoe was provided at the bottom of the outer shell. This was exactly the same as for the Type I outer shell.

A completely new arrangement was adopted at the top of the outer shell. A combined driving and loading head was devised, featuring a system of welded loading blocks and bolted stiffening boxes. The arrangement is shown in Figures 6.6 and 6.7 and in Plate 6.3. The specially shaped loading blocks were welded to the top of each angle. The blocks received the direct impact of driving, and subsequently formed part of the pile loading system described in Section 6.5. The blocks were shorter than those used for the Type I outer shell.

Beneath the welded blocks, the outer shell was held as one between the stiffening boxes, which were bolted together through the outer shell with 12mm diameter bolts in conjunction with nylon insert nuts. The stiffening boxes gave a convenient cross-section for a post driver to locate on. Extensions to the stiffening boxes allowed the location of a 75mm high anvil block, designed to spread driving impact evenly to the four angles of the outer shell (Figure 6.7).

6.3.3 Details of expander mandrel

The expander mandrels used were exactly the same as the Type I versions described in Section 6.2.3, except that they were extended at the top to an overall length of 1650mm.

6.3.4 Mini-Pile installation

The Type II cruciform mini-pile was installed using a commercial air driven post driver, shown in Plate 6.4. Details of the post driver are given in Appendix 6.1. This system of installation was adopted because it was lightweight and relatively cheap to operate; and because it was well controlled, allowing estimates of the relative driving energies of outer shell and expander mandrel to be made.

The standard arrangement of the post driver comprised:

(a) A main body, incorporating a reciprocating piston designed to strike the post directly.

(b) A guide or 'chuck' to locate the post driver centrally on the post to be driven. A variety of chucks were available.

The net weight of the post driver without chuck was 38kg. It was driven by a standard air compressor unit and was designed to deliver blows at up to 1700 blows per minute. A box guide was made up to fit to the main body of the post driver. The box guide fitted over the box stiffening arrangement at the top of the outer shell (Figure 6.7). During driving the post driver piston acted against the anvil block.

The rapid, vibratory type action of the post driver led to a smooth, well controlled mini-pile installation. The procedure for installation was as follows:

Outer shell:

(a) Before driving, the pile components were marked up with chalk as before. The outer shell was held vertically within a simple guide frame. Arrangements varied - the most common arrangement comprised two stacks of sleepers, with lengths of 50x50mm timber nailed between the top sleepers to form a 'gate' (Plate 6.5). The smooth action of the post driver enabled the pile to be supported at a lower level than for the Type I mini-piles.

(b) The post driver was located by hand on the top of the outer shell. It was operated by two people; one person steadied the post driver on the top of the pile, and the other controlled the air supply

valve.

(c) The outer shell was driven to final depth, the guide frame being dismantled just before the post driver guide began to foul it.

(d) After the outer shell had been driven, the post driver was lifted clear, and the outer shell box stiffeners were unbolted to allow the expander mandrel to be driven.

Expander mandrel:

(a) The nose of the expander mandrel was engaged in the outer shell and pushed to refusal by hand, as before. Because of the smooth action of the post driver no additional support was needed during driving.

(b) The post driver was lifted on to the top of the expander mandrel, and the expander mandrel was then driven to final depth.

6.3.5 Completed mini-pile arrangement

The completed mini-pile arrangement is shown in Figure 6.5. The outer shell was driven to a depth of 1250m. The expander mandrel was driven until the tip of the nose was 75mm short of the bottom of the outer shell.

6.4 H Section Mini-Pile

6.4.1 Introduction

The H section mini-pile was developed to investigate the expansion of wedge-piles in two directions only, rather than in four directions as in the case of cruciform and box piles.

In practice, the most convenient configuration for a '2-way' wedge-pile would be an outer shell comprised of two standard channel sections held 'back-to-back', with an expander mandrel formed from a single flat section (Section 1.3). The H section mini-pile was a version of this arrangement.

The H section mini-pile was developed during the second phase of mini-pile testing, in conjunction with the Type II cruciform mini-pile (referred to in this Section as the cruciform mini-pile). The general form of construction of the two mini-piles was the same.

The H section mini-pile is shown in Figure 6.8, and in Plates 6.6 to 6.8. Three outer shells and two expander mandrels were fabricated. The mini-piles were tested at two sites.

6.4.2 Details of outer shell

The outer shell was 1500m long, with an initial cross section of 100x100mm, made up from two 100x50x1.5mm channel sections (channels). The channels were bent up from 1.5mm thick cold rolled mild steel sheet. The overall cross sectional area of the pile was the same as for the cruciform mini-pile. The 2:1 aspect ratio of the channel sections was the same as that for standard rolled channel sections.

The channels were held back-to-back using pop-rivets, in exactly the same manner as for the cruciform mini-pile. Pairs of rivets at 100mm spacings were used. At the bottom of the outer shell a standard welded driving shoe arrangement was provided. At the top of the outer shell, a 2-way version of the driving and loading head developed for the cruciform pile was used (Figures 6.9, 6.10; Plate 6.7).

During expansion of the outer shell, the expander mandrel was located between the two channels by means of strips welded to one of the channels.

6.4.3 Details of expander mandrel

Two expander mandrels were fabricated. They were 1600mm long, formed from single lengths of cold rolled flat section (flat). As with the cruciform mini-pile, they were designated 'A' and 'B'. Expander mandrel A was made up from 100x6mm flat. It expanded the outer shell from a width of 100mm to 106mm, an increase of 6%. Expander mandrel B was made up from 100x10mm flat. It expanded the outer shell from a width of 100mm to 110mm, an increase of 10%.

At the top of each expander mandrel welded blocks were provided, as for the cruciform mini-piles. At the bottom of each expander mandrel parabolic nose sections were formed by means of a shaping machine. The nose lengths were ten times the width of the expander mandrel, as for the cruciform pile. The nose of expander mandrel B is shown in Plate 6.8.

6.4.4 Completed mini-pile arrangement

The completed mini-pile arrangement is shown in Figure 6.8. The outer shell was driven to a depth of 1250mm. The expander mandrel was driven until the tip of the nose was 125mm short of the bottom of the outer shell.

6.4.5 Pile Installation

The H section mini-pile was driven using the air operated post driver

described in Section 6.3.4. The procedure was exactly the same as before.

6.5 Mini-pile Testing

6.5.1 Introduction

A 200kN capacity testing system was developed for use with the mini-piles. In essence the system was a scaled down version of that used for the 6m piles. As before, the purpose of the testing system was to establish the essential load carrying characteristics of the mini-piles in tension. The testing system was developed initially as part of the MSc project by Fitch (1986). It was subsequently improved for the second phase of the field trials. The final arrangement is described below.

The overall arrangement is shown in Figure 6.11, and in Plate 6.9. The principal components are, in order of assembly:

(a) tension linkage
(b) reaction frame
(c) jack crossbeam assembly
(d) reference beam

The arrangement is described in the following Sections, together with the procedures for setting up the system prior to testing.

6.5.2 Tension linkage

The tension linkage comprised a loading box and a central tension rod.

6.5.2.1 Loading box

Two similar loading boxes were fabricated, one for the cruciform mini-piles and one for the H section piles. The loading boxes were smaller, redesigned versions of the loading box used for the 6m piles.

As before, the essential requirements to be met were that:

(a) the loading box should be adjustable, so as to deal with various mini-pile sizes and types

(b) the loading box should act coaxially with the mini-pile being tested and should pull evenly on the separate elements of the outer shell.

The cruciform loading box is shown in Figure 6.12, and in Plate 6.10.

Each loading box was fabricated from a 450mm length of 150x150mm box section, designed to fit over the mini-pile being tested. A centrally drilled and threaded block was welded or bolted into the top of the loading box. This received the central tension rod.

Specially shaped loading blocks were bolted inside the bottom of the loading box. These applied load by overlapping beneath the loading blocks welded at the top of the outer shell. The two sets of loading blocks formed 'matching pairs'.

The loading block arrangement for the cruciform mini-piles is shown in Figures 6.6 and 6.12. There were four matching pairs of blocks, with bearing faces inclined at 45° to the vertical. The arrangement for the H section mini-pile is shown in Figure 6.9. In this case there were two matching pairs of blocks, with bearing faces inclined at 30° to the vertical.

The geometry of each of these arrangements was such that as the loading box was pulled upwards, the loading blocks engaged and centred the loading box on top of the pile. Piles expanded by different amounts were dealt with without the need for packing blocks (Figure 6.12). An additional advantage of the system was that the lateral force generated by the action of the loading blocks gave a 'gripping' action that held the pile head together and reduced uneven pick-up of the angles.

6.5.2.2 Central tension rod

The central tension rod was a 600mm long 24mm diameter high tensile steel rod, threaded at each end.

6.5.2.3 Setting up procedure

The loading boxes were mounted coaxially on the pile to be tested as follows (Figure 6.12):

(a) An adjustable centering plate was placed on top of the mini-pile to be tested. In the centre of the plate was a spherical seating.

(b) An extension rod was screwed to the bottom of the central tension rod. The extension rod protruded into the loading box. A ball fixing at the bottom of the extension rod located in the spherical seating of the centering plate.

(c) The loading box, with central rods but without loading blocks, was lowered onto the mini-pile, the extension rod being located on the centering plate.

(d) The loading blocks were bolted in position.

(e) The central tension rod was screwed down into the loading box. This engaged and tightened the two sets of loading blocks such that the loading box was coaxial to the mini-pile.

6.5.3 Reaction frame

Reaction was provided by 1.25m long sleeper pieces stacked clear of the mini-pile. 1.4m long steel beams spanning between the top of the stacks provided support for the jack crossbeam.

6.5.4 Jack crossbeam assembly

The jack crossbeam assembly was set up coaxially over the upstanding central tension rod.

The jack crossbeam was 1.0m long, formed from box section. It spanned between the steel beams of the reaction frame. At the centre of the crossbeam was a clearance hole to the central tension rod. The crossbeam was mounted on adjusting bolts to enable it to be aligned correctly with the rod.

A 300kN capacity annular hydraulic jack was used, operated by a hand pump. The jack applied load to a bearing nut and washer at the top of the central tension rod. Applied load was measured by means of a standard 200kN NCB/MRE load cell in conjunction with a 'Peekel' monitoring gauge, capable of measuring the load to within approximately 0.05kN. The load cell and hydraulic jack were mounted centrally on the crossbeam.

6.5.5 Reference Beam

The reference beam arrangement is indicated in Figure 6.11. The reference beam was a shortened version of that used for the 6m tests (Section 3.6.5). The beam was 3m long, mounted on stakes driven 0.5m into the ground. Two dial gauge extensometers were used to measure pile deflection, as for the 6m piles.

The dial gauge plungers impinged onto reference plates fixed to the outer shell. In the case of the cruciform mini-piles, two reference plates were glued with epoxy resin to diametrically opposed outer shell angles. Studs located the plates in the correct position. In the case of the H section mini-pile, the two reference plates were bolted to the outer shell channels.

6.6 Test Control

The system was basically the same as for the 6m piles (Section 3.8). Loading and unloading of the pile was by the hand pump; time, load, and displacement of the mini-pile were recorded by hand.

6.7 Pile Extraction and Refurbishment

6.7.1 Extraction

The piles were extracted in two stages - first by jacking and then by levering.

If an expanded mini-pile was being extracted, the first stage involved jacking the expander mandrel relative to the outer shell by mounting the jack on top of the outer shell such that the jack ram acted against the underside of the expander mandrel reinforcement blocks. The expander mandrel was jacked approximately 300 to 400mm from the outer shell in a series of pushes, the jack being retracted and packing blocks being added after each push.

If an unexpanded mini-pile was being extracted, the first stage involved using the standard jacking system to pull the mini-pile from the ground. The mini-pile was pulled approximately 300 to 400mm from the ground in a series of pushes as before, this time with packing being placed beneath the jack crossbeam after each push.

In the second stage of extraction the mini-pile was levered from the ground. A 2.5m long box section lever was used, operated by two people with a sleeper stack acting as a fulcrum. The lever acted against the blocks welded to the top of the outer shell.

6.7.2 Refurbishment

After extraction the piles were thoroughly washed and cleaned with water and a stiff brush. Any deformities in the outer shells caused by installation or extraction were straightened out. The piles were then reassembled for use. Some of the outer shells were used at four sites, although others eventually became too damaged for reassembly and were discarded.

In the later stages of testing the Type II cruciform mini-piles were cleaned by means of grit-blasting, this being a very convenient method. Exactly the same grit-blaster was used as for the shearbox interfaces described in Section 4.4.7.

6.8 Test Sites

The mini-piles were tested at six different sites. The overall objective in selecting the sites was to test the mini-piles in a range of soil profiles. It was also important to use secure sites where equipment could be left unattended if necessary. It proved quite difficult to find convenient and secure sites where the soil profile was not disturbed in some way near ground level.

At each site a trial pit or hand auger hole was opened up and a visual description of the soil profile made. In the majority of cases particle size determinations of representative samples of soil were carried out; and measurements made with a specially fabricated probing rod in order to assess the uniformity of the soil profile.

The steel probing rod was approximately 2m long, comprising two lengths of rod which could be screwed together. The bottom rod featured a 0.75inch diameter, 60° taper conical tip of hardened steel, with a reduced shank of 0.5inch diameter. This rod could be extended by adding the top rod. The probing rod(s) was driven into the ground by means of a 7kg steel weight mounted on a slide rod. The sliding weight was repeatedly lifted by hand and dropped onto the top of the rod from a height of 250mm. Records were made of the number of blows against rod penetration.

The mini-pile testing sites have been numbered from 1 to 6. Table 6.1 is a summary of the sites, and gives details of which mini-pile types were tested at each site.

Site 1 was at the BRS in Hertfordshire, adjacent to the 6m wedge-pile test area. Below a depth of 0.5m this site consisted of undisturbed clay till, above 0.5m the clay had been disturbed and occasional pieces of hard-core and gravel were found.

Sites 2 and 3 were both at Silwood Park in Berkshire, the field station of Imperial College. Site 2 was loose undisturbed fine to medium silty sand. Site 3 was adjacent to a small lake and comprised badly drained made ground, consisting of a mixture of clay and granular material in all size ranges.

Site 4 was at a clay borrow pit on the Isle of Sheppey in Kent. This site was a very uniform profile of firm undisturbed weathered London clay.

Site 5 was at Holland House in central London. Mini-pile testing at this site was undertaken in connection with the proposed use of wedge-piles to anchor a tensile fabric canopy structure over the Holland House open air theatre. The test site was on a flat embankment in front of the House, and the soil profile was well drained made ground, consisting of a mixture of clay and granular material in all size ranges.

Site 6 was at a worked out sand extraction pit near Send in Surrey. The soil profile at this site was disturbed, and comprised very loose, very clayey sand overlying loose fine to medium sand.

Figures 6.13 to 6.18 provide details of the soil profiles at the six sites.

6.9 Mini-Pile Testing

The results of the mini-pile testing programme are presented in this Section. The results are discussed in Chapter 11.

6.9.1 Rationale

As for the 6m long wedge-piles, load testing was performed essentially to determine ultimate tensile capacities of the mini-piles. Expanded pile capacities were compared with those of unexpanded control piles. The standard mini-pile test consisted of a Constant Rate of (Incremental) Loading (CRL) test, normally followed by a Constant Rate of Extraction (CRE) test. The procedures for these tests were quicker versions of those described previously in Sections 4.7.1 and 5.6.1. The increments of load in CRL tests were selected on the basis of estimated failure load, to give around 6 to 10 increments to failure. Each increment was held for 5 minutes. Load increments were added until the creep displacement rate during the holding period approached 0.5mm/minute. The CRE displacement rate was 1mm/minute. The mini-piles were unloaded in increments, held for 1 minute each.

6.9.2 Tests on cruciform Type I mini-piles

The results of tests on Type I cruciform mini-piles at Sites 1, 2 and 3 are presented by Fitch (1986). The results are summarised in Table 6.2. As these tests were largely of a preliminary nature no further details are given here.

6.9.3 Tests on cruciform Type II / H section mini-piles

The results of tests on Type II cruciform and H section mini-piles at Sites 1, 4, 5 and 6 are summarised in Tables 6.3 to 6.6. These Tables

give dates of mini-pile installation, some information on driving, maximum test loads, and factors of increase in mini-pile capacity. Results from individual tests are plotted in Figures 6.19 to 6.34. Applied tensile head load is plotted against average upward displacement. Agreement between the two dial gauges used to measure displacement was excellent - typical behaviour is shown in Appendix 6.2.

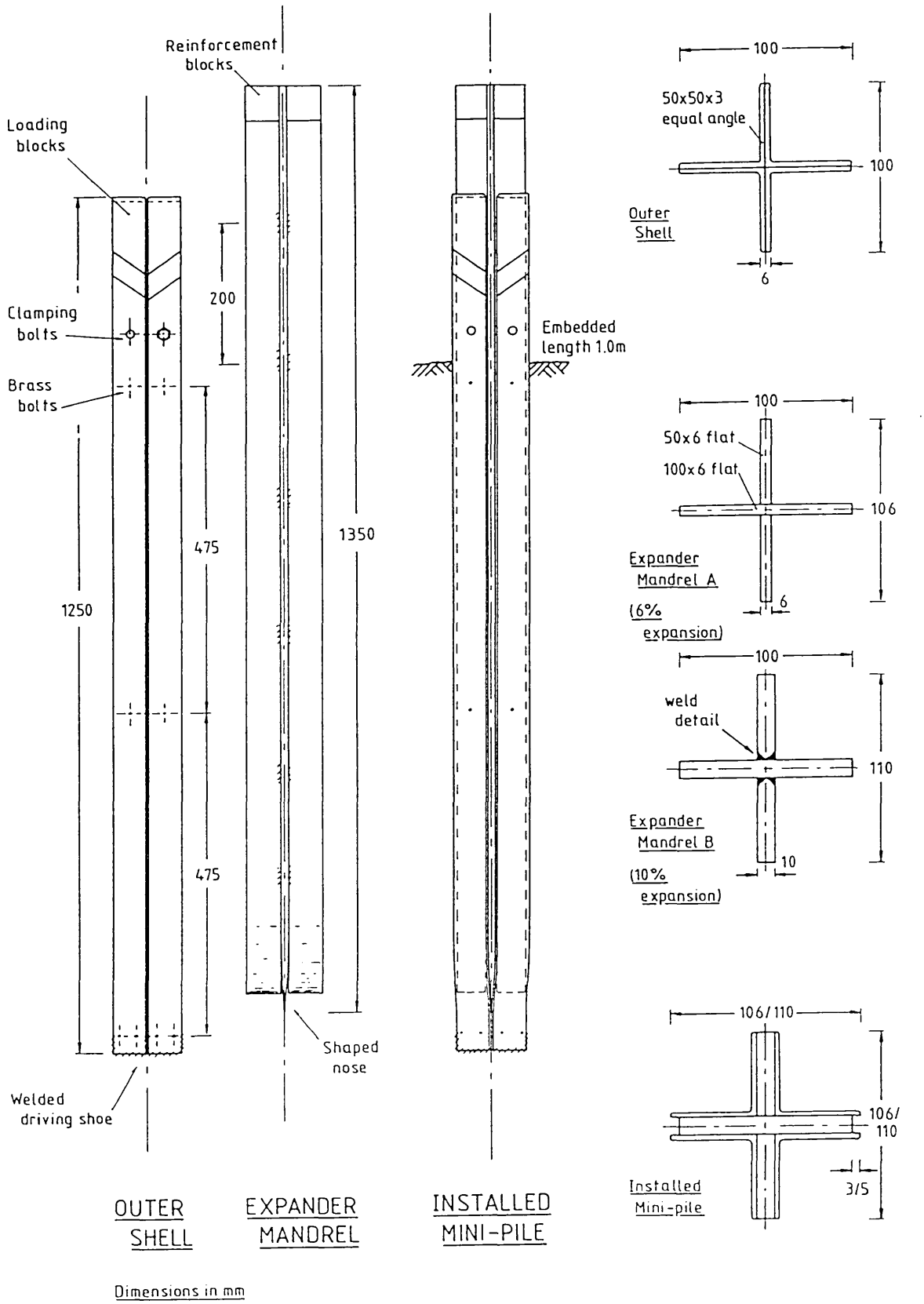

Figure 6.1 Type I cruciform mini-pile: overall arrangement

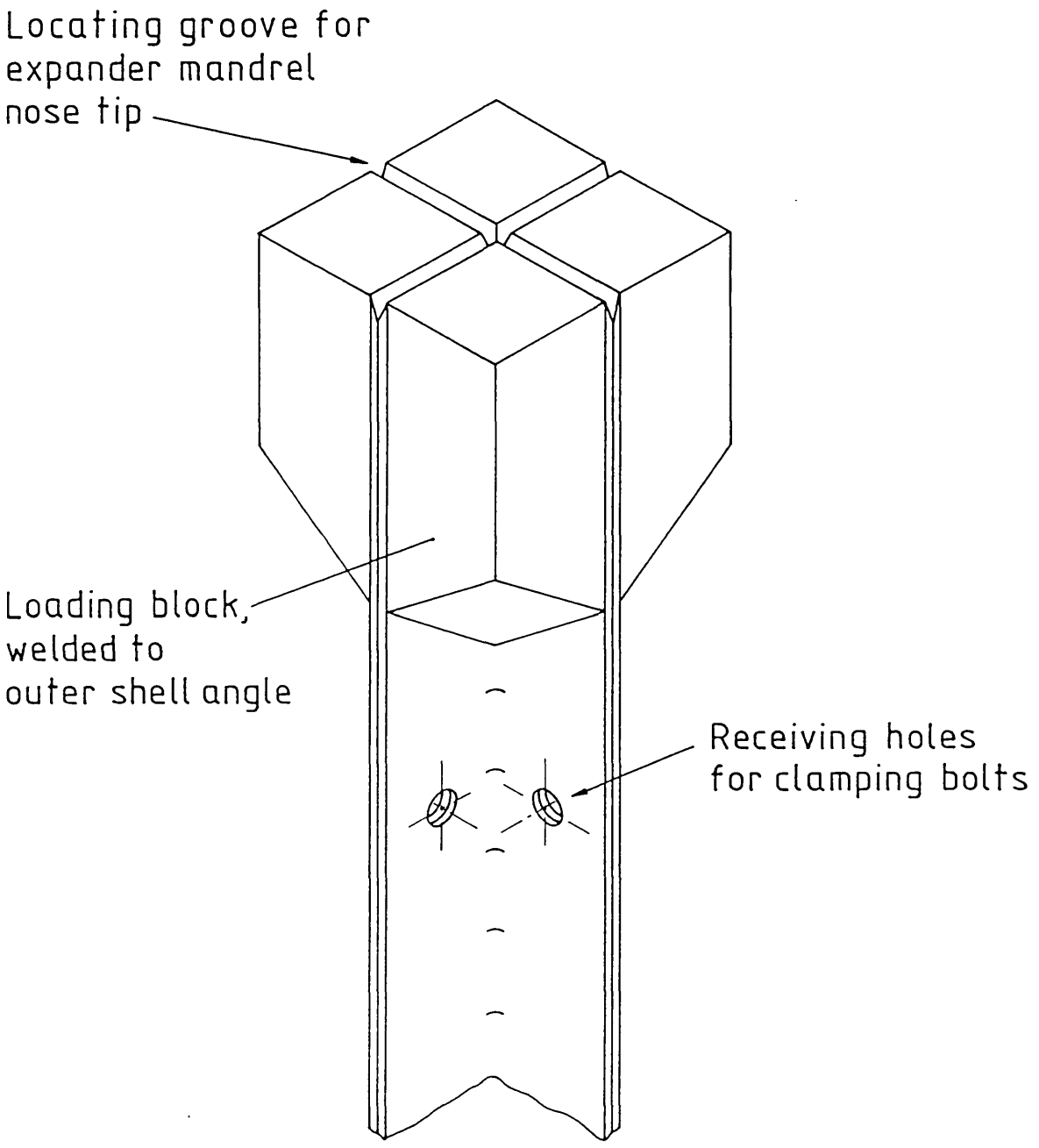

Figure 6.2 Type I cruciform mini-pile:
outer shell head detail

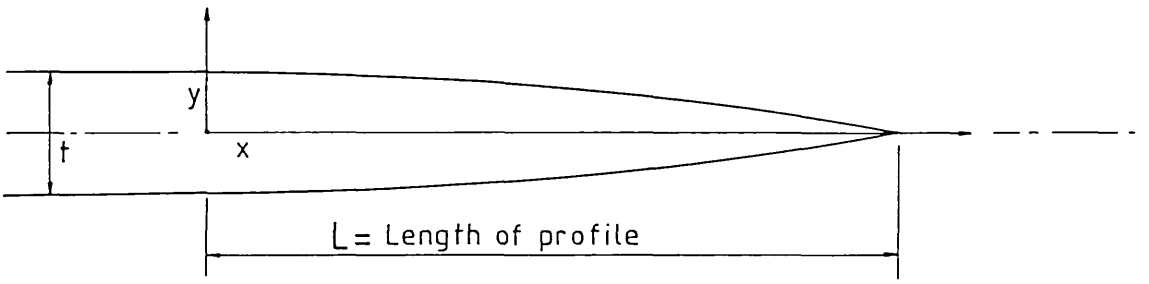

$$y = (t/2) - (t/2) . [(L-x)/L]^2$$

$t = 6mm ; 10mm$

$L = 10.t$

Figure 6.3 Details of expander mandrel nose profiles

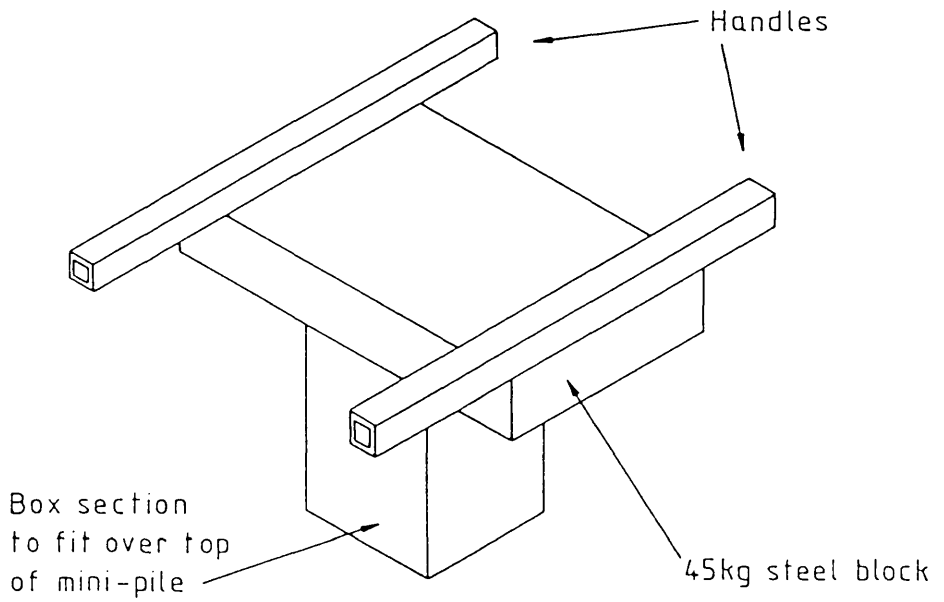

Figure 6.4 Driving 'monkey'

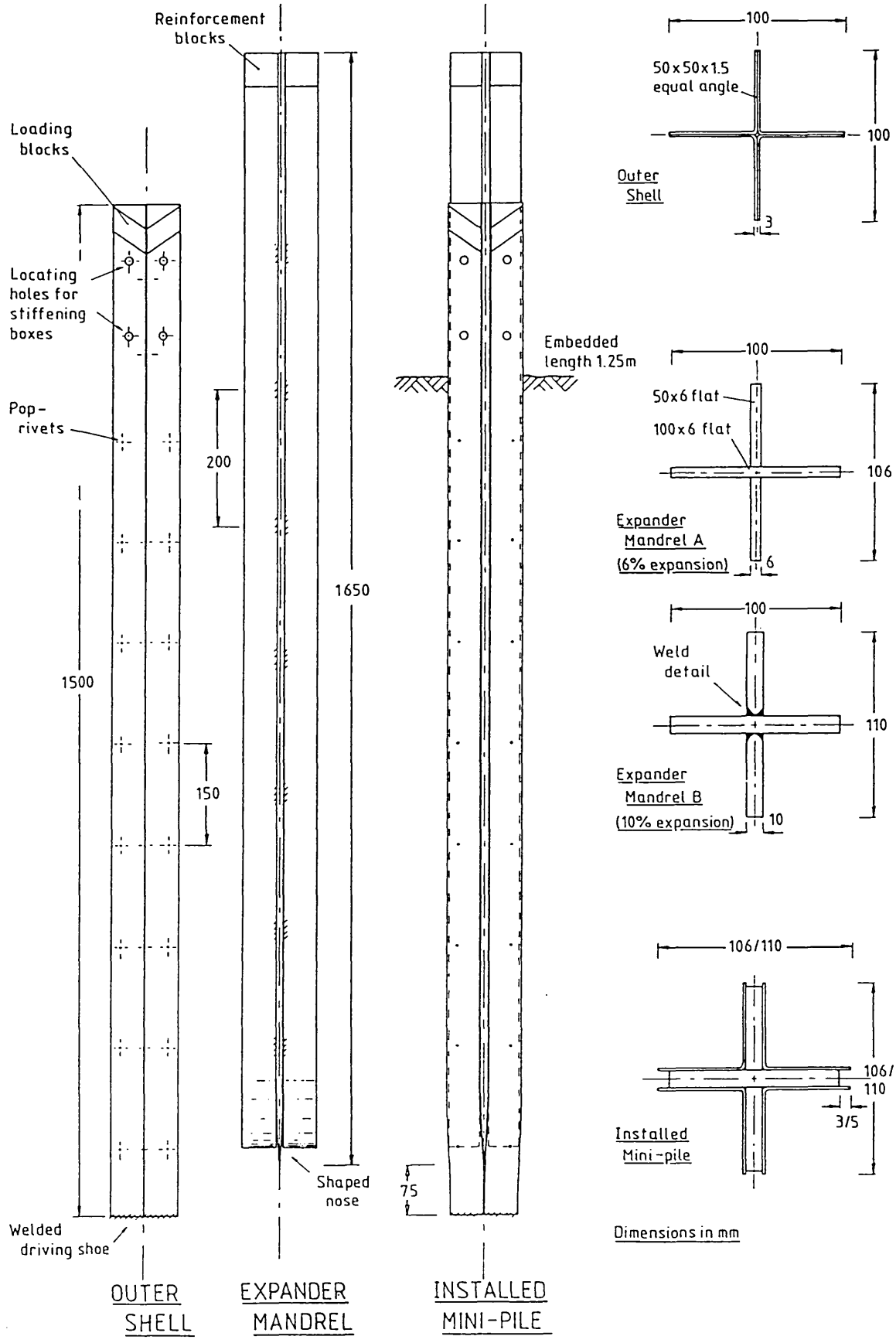

Figure 6.5 Type II cruciform mini-pile: overall arrangement

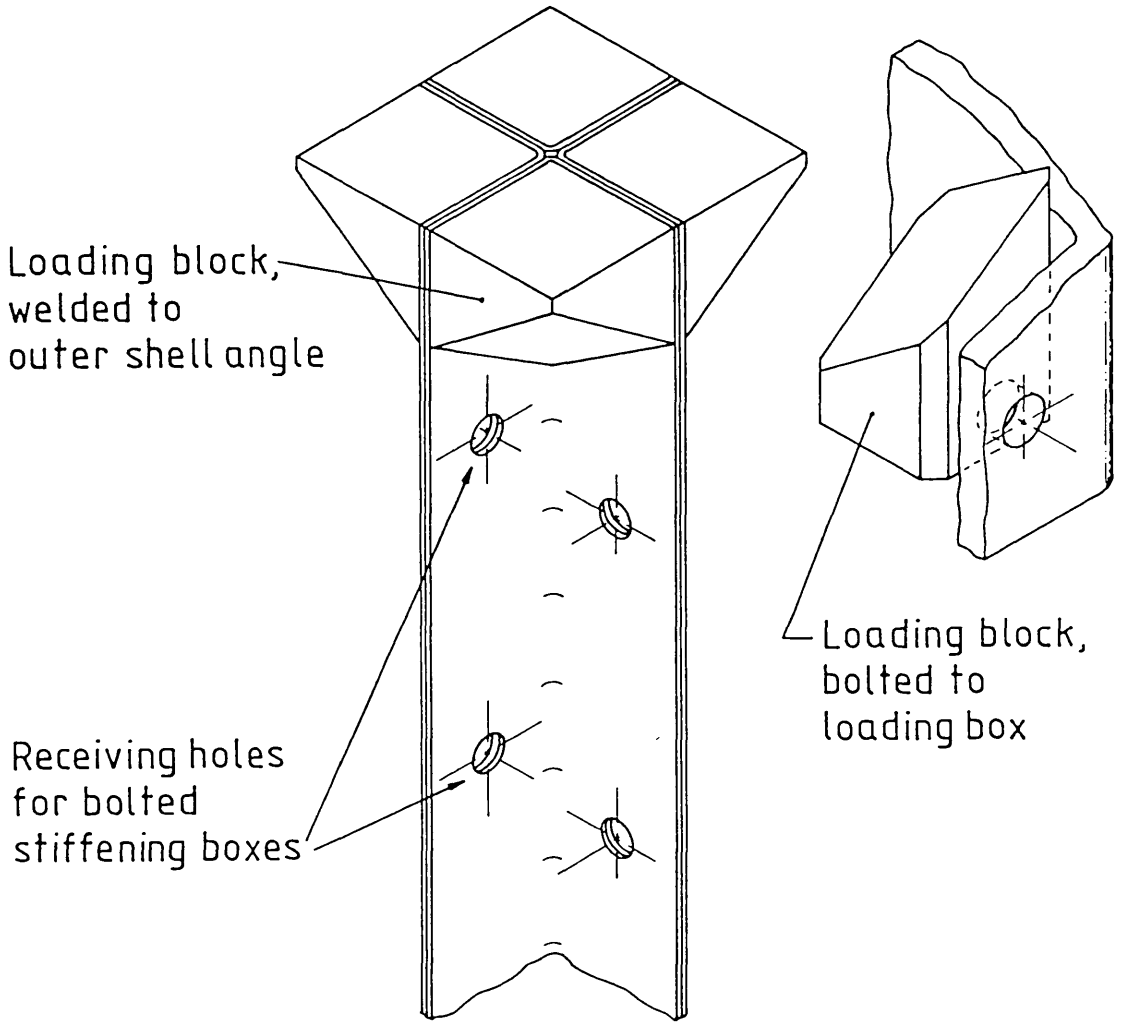

Figure 6.6 Type II cruciform mini-pile:
outer shell head detail

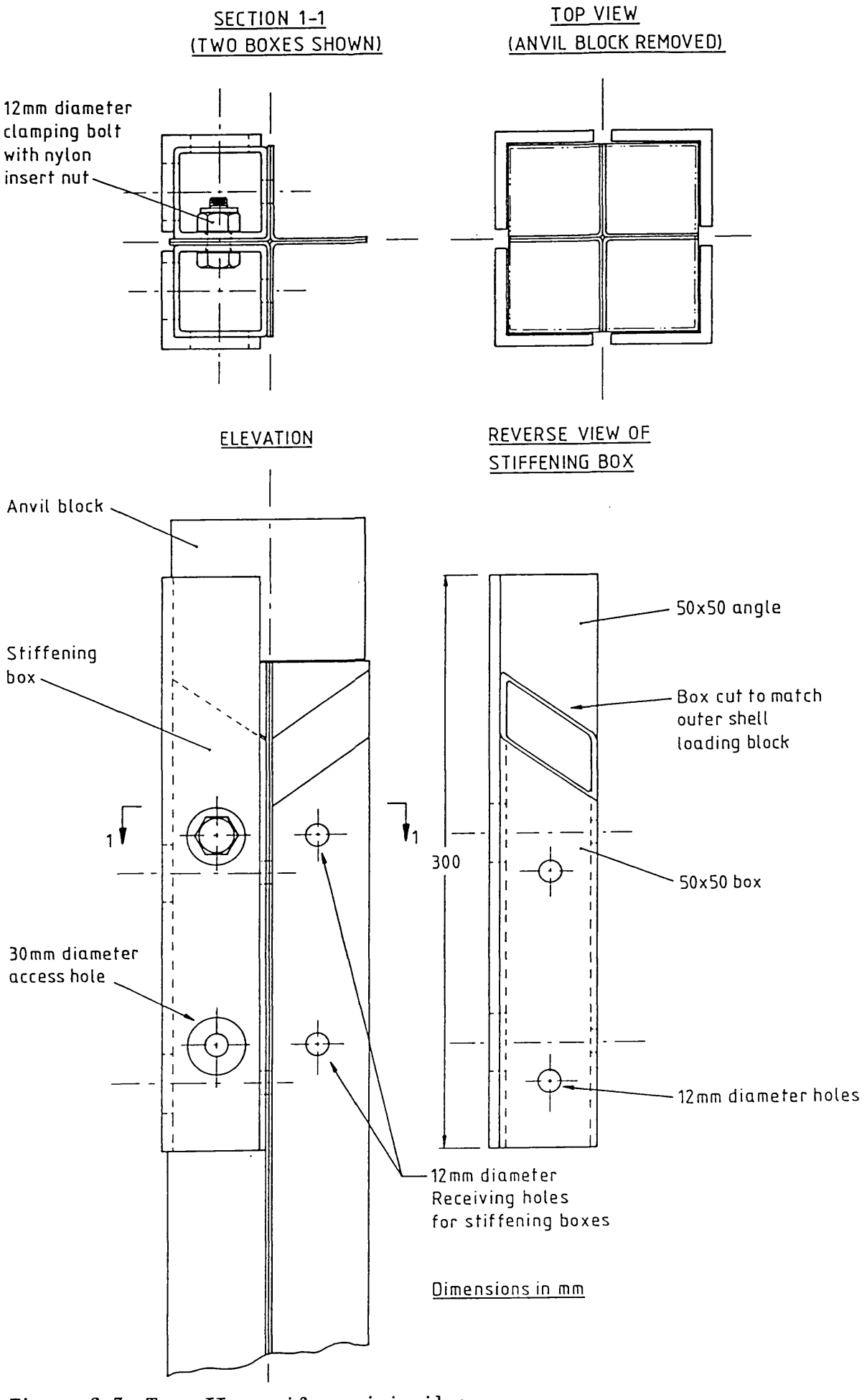

Figure 6.7 Type II cruciform mini-pile:
details of outer shell stiffening boxes

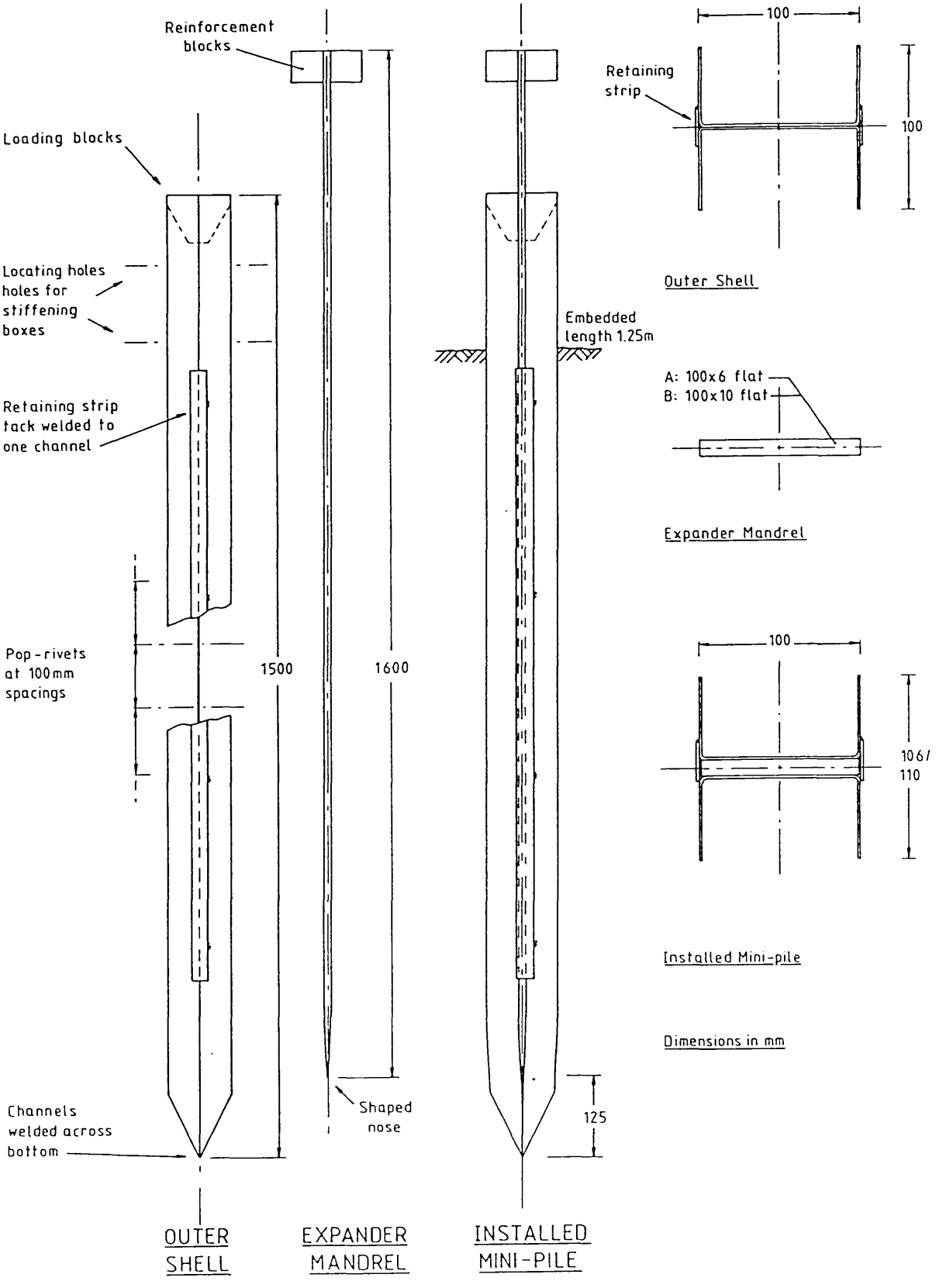

Figure 6.8 H section mini-pile: overall arrangement

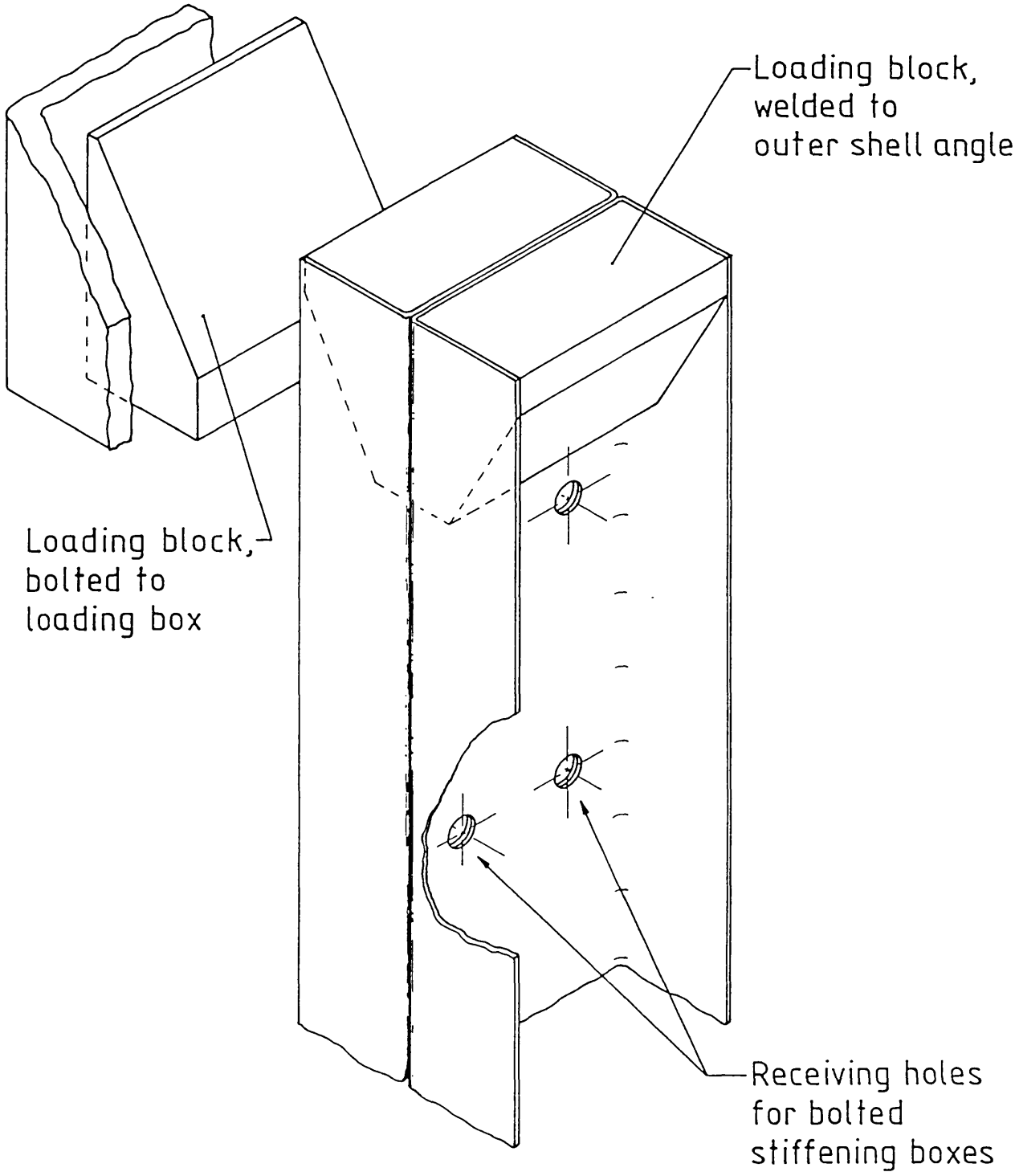

Figure 6.9 H section mini-pile:
outer shell head detail

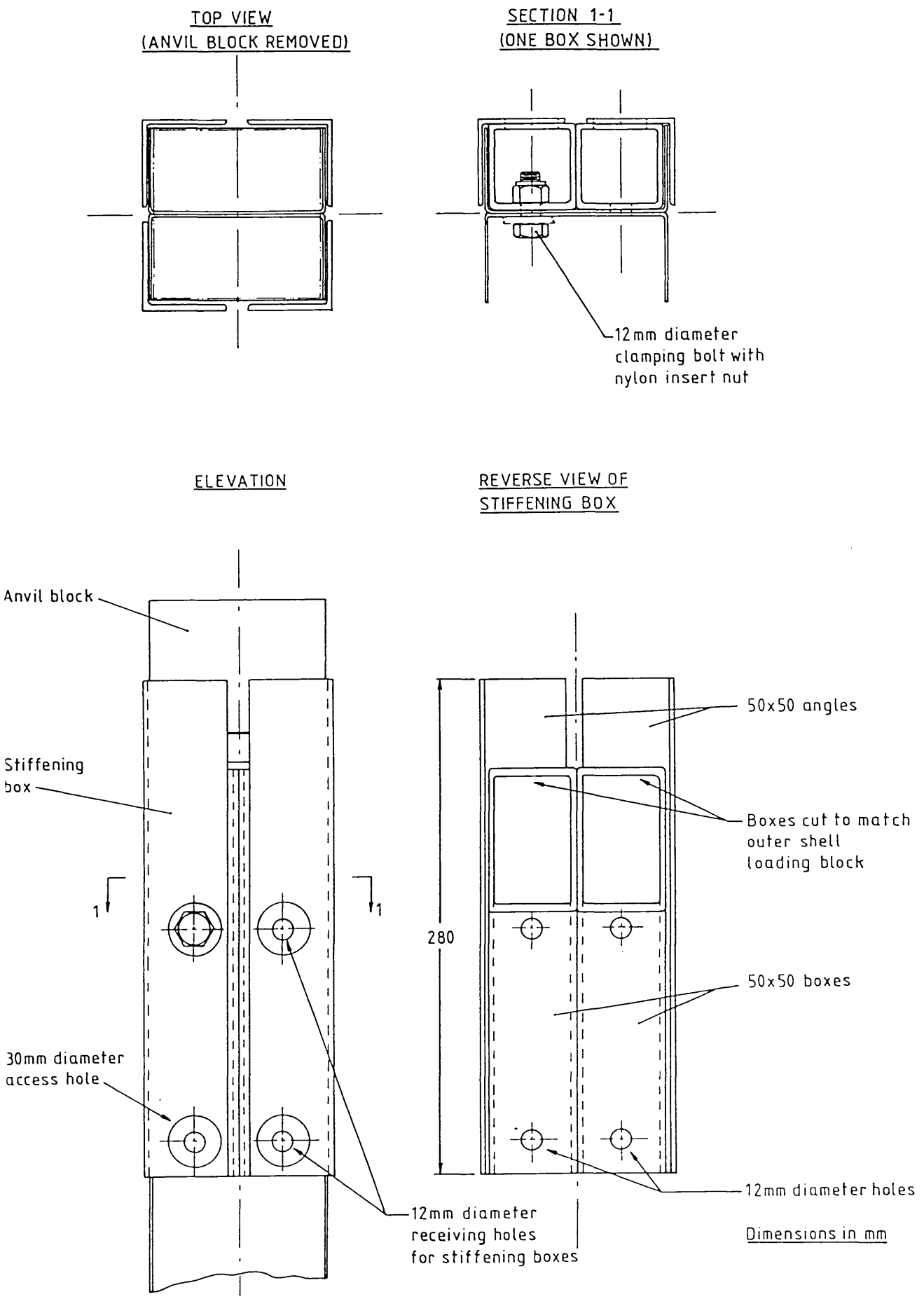

Figure 6.10 H section mini-pile:
details of outer shell stiffening boxes

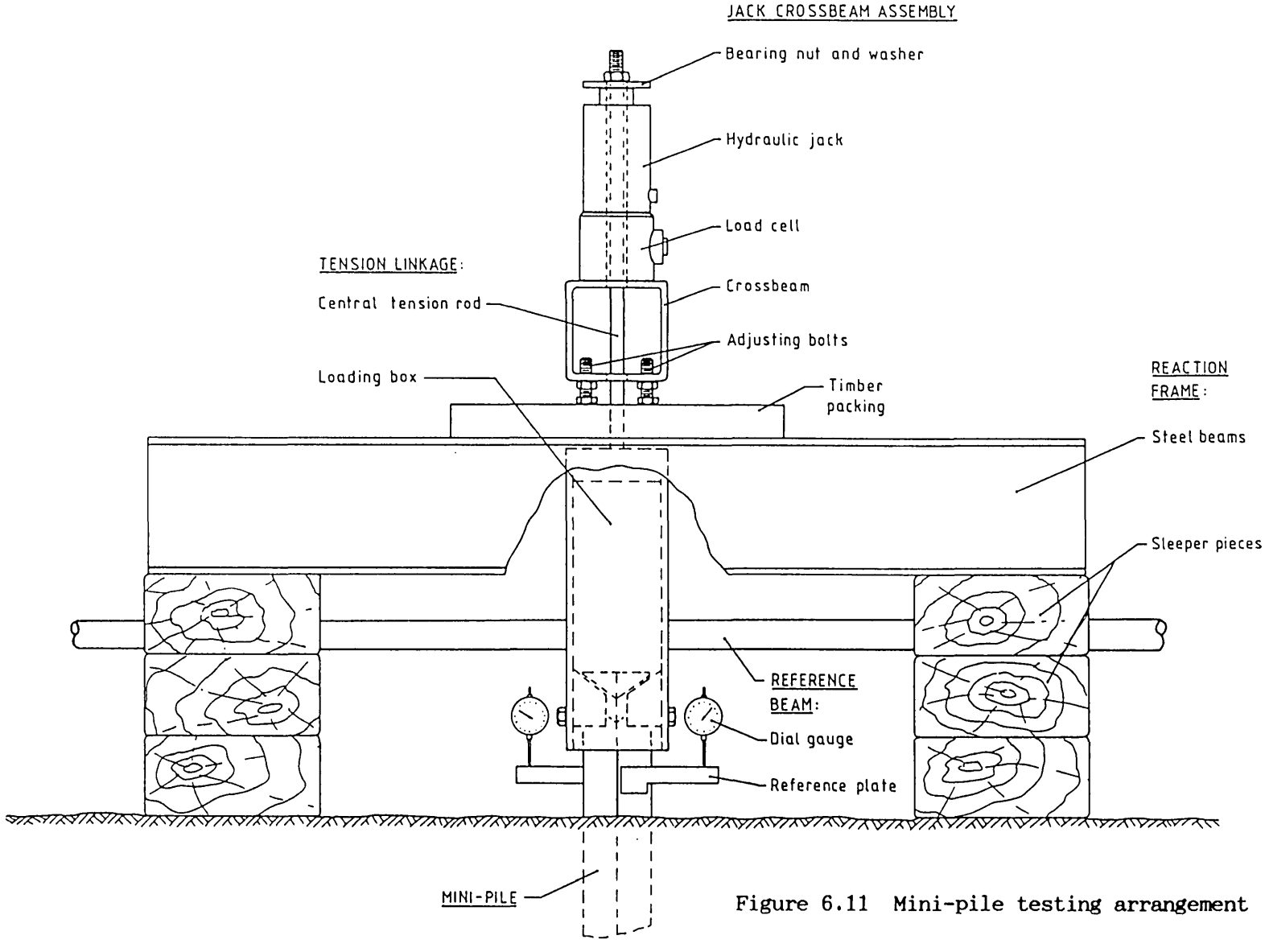

Figure 6.11 Mini-pile testing arrangement

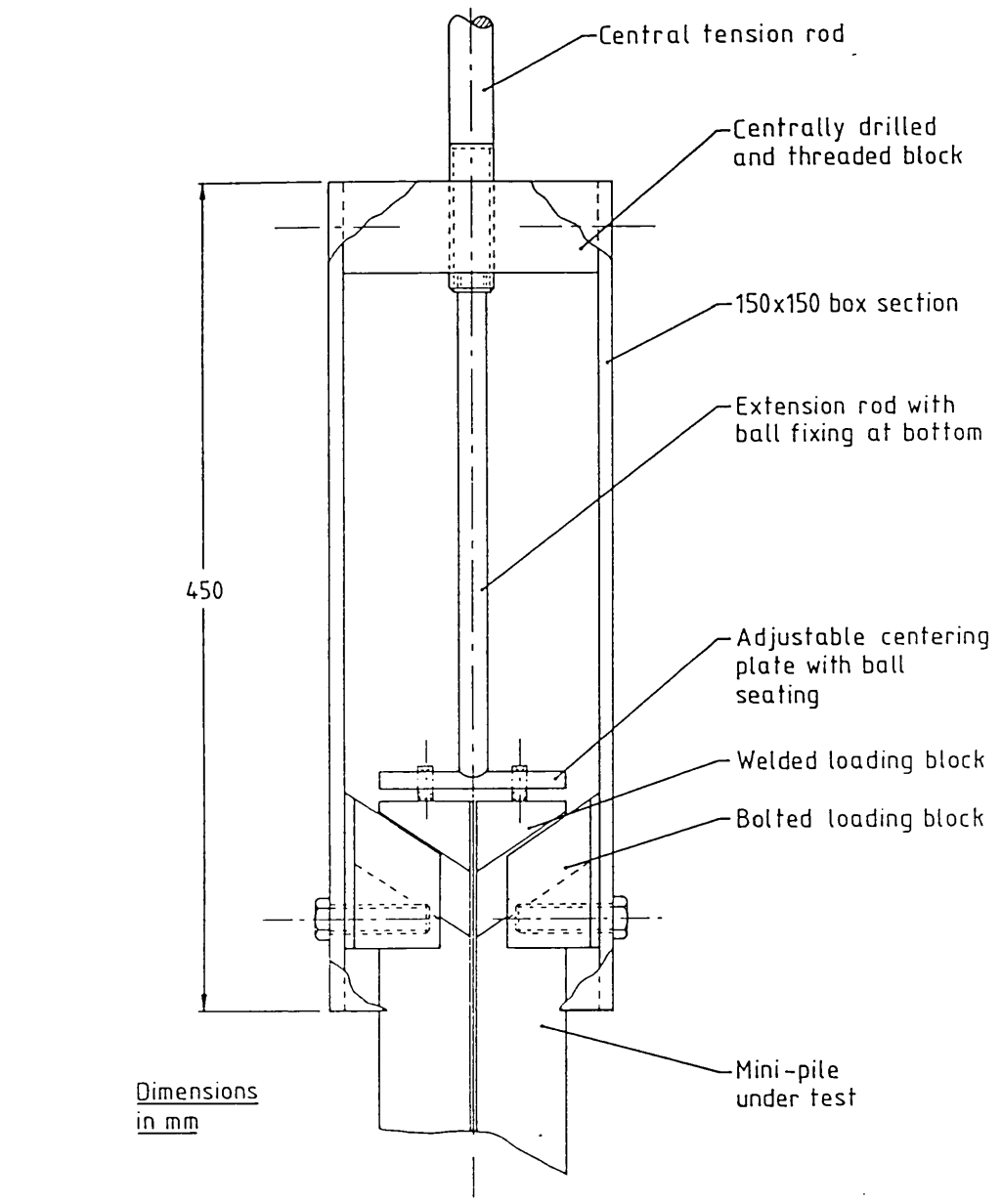

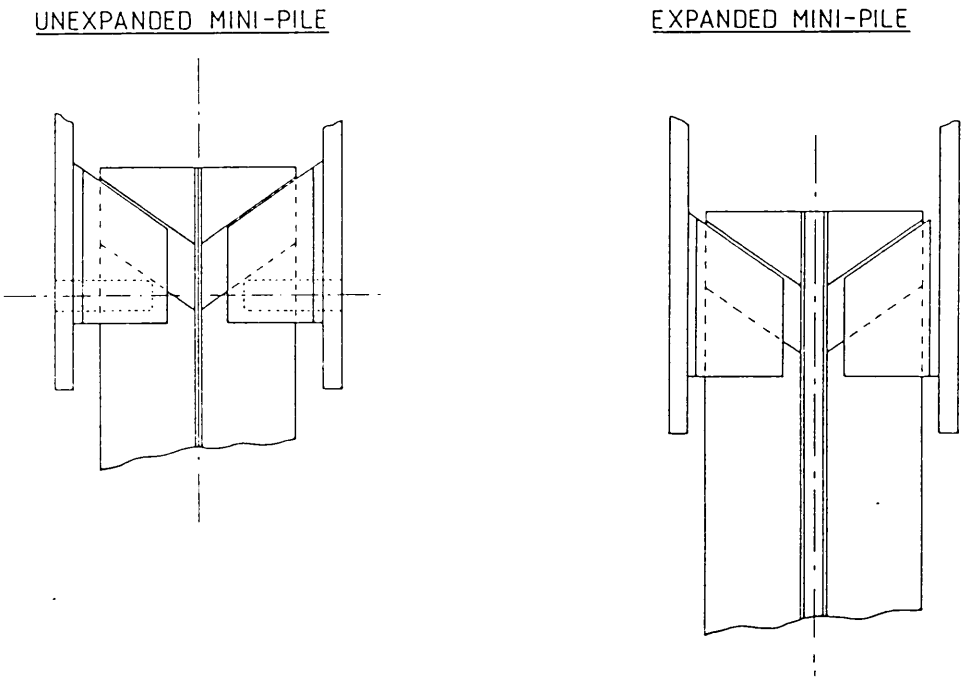

Figure 6.12 Cruciform loading box

Depth (m)	Visual description
	Hand auger hole 21/1/88
0.4-0.5	Reworked-ground: SOFT to FIRM brown CLAY with frequent medium to coarse sand and gravel sized fragments of brick, chalk and flint
0.5-1.1	FIRM reddish brown mottled grey slightly sandy CLAY with frequent fine to medium gravel (mostly chalk and flint) (End of borehole)

Notes:

1. Groundwater started to enter borehole at 0.64m. Water level at end of augering 1.08m below ground level

2. Moisture content determinations:

Depth (m)	Average m.c. (%)	
0.50	22.8	(Reworked ground)
0.70	29.0	(Upper Till)
0.85	29.7	(")
1.05	30.7	(")

Average Atterburg limits for upper till:
PL = 19 , LL = 47 (Marsland, 1977).

PROBE TEST RESULTS

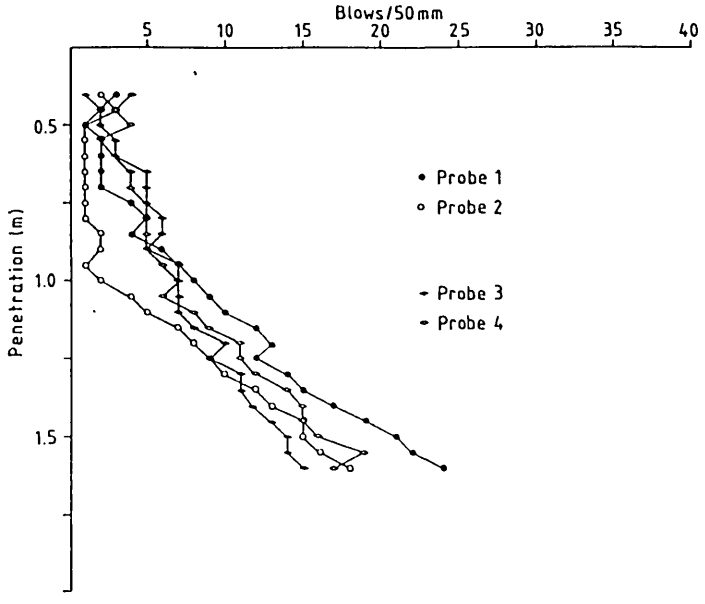

PLAN OF TEST SITE

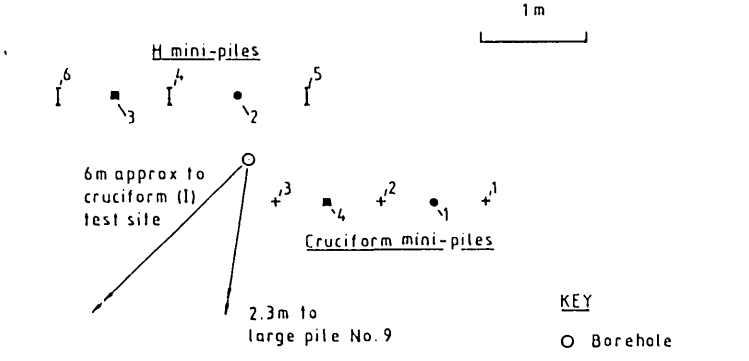

Figure 6.13
BRS site details

Depth (m)	Visual description
	Hand auger hole 12.8.78
0.25	Yellow brown fine to medium silty SAND with occasional fine to medium sub-rounded gravel
0.50	Yellow brown fine to medium silty SAND with occasional fine to coarse sub-rounded to sub-angular gravel
0.75	Yellow brown fine to medium silty SAND with occasional fine to coarse sub-rounded to sub-angular gravel
1.00	Yellow brown fine to medium clayey very silty SAND with occasional fine to medium sub-angular gravel
1.30	Yellow brown mottled grey fine to medium clayey very silty SAND with occasional fine to medium sub-angular gravel (End of borehole)

Notes: 1. Hole remained dry throughout augering.

PARTICLE SIZE DISTRIBUTION

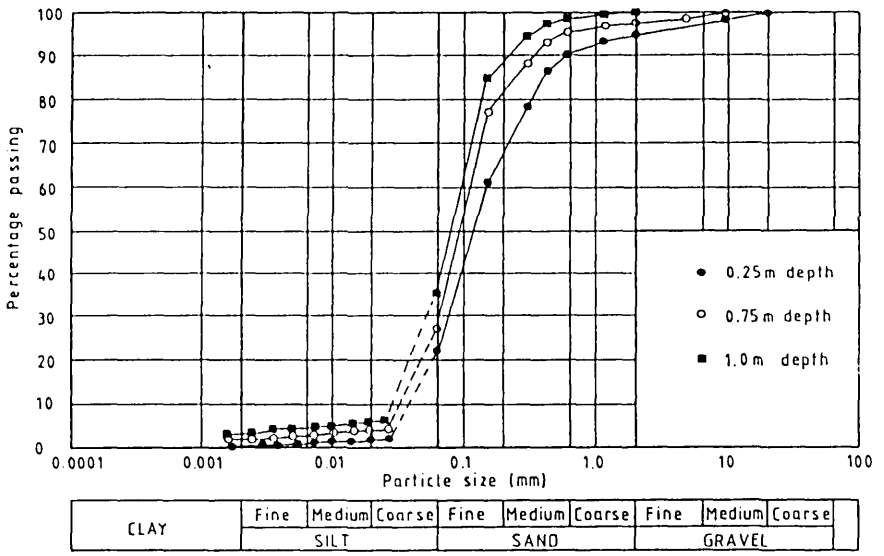

PROBE TEST RESULTS

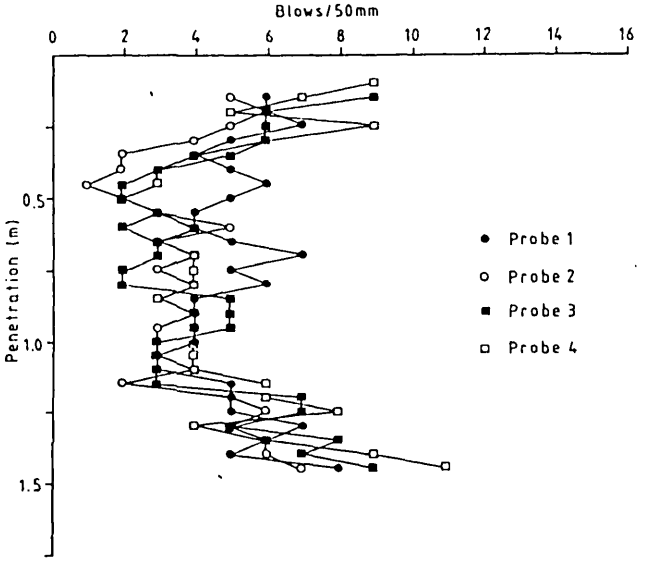

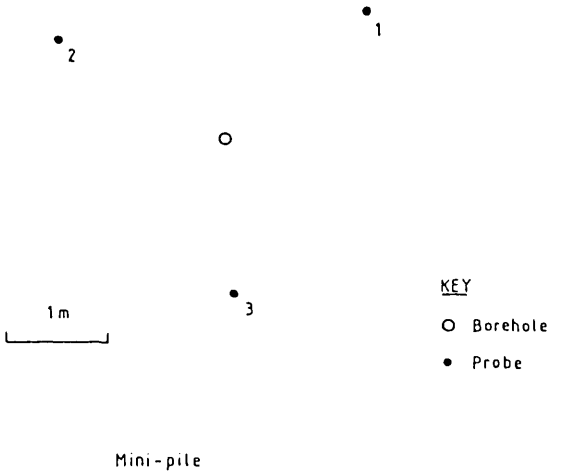

Figure 6.14
Silwood Park (A) site details

Depth (m)	Visual description
	Hand auger hole 12.8.87
0.25	Made ground: SOFT orangy brown very sandy CLAY with frequent fine to coarse sub-angular to sub-rounded gravel (including flint and brick)
0.50	Made ground: SOFT grey-black very sandy CLAY with frequent fine to coarse rounded to sub-rounded gravel (including flint and brick)
0.75	Made ground: VERY SOFT grey mottled black very sandy very silty CLAY with occasional fine to medium rounded gravel (mostly flint)
1.0	Made ground: Grey very clayey SAND with occasional sub-angular fine gravel (including flint and brick) and occasional rootlets
1.25	Made ground: Rounded to sub-rounded very sandy medium to coarse GRAVEL (mostly flint) in a matrix of silty sand (End of borehole)

Notes: 1. Ground water encountered at 1.1m, Water level at end of augering 1.17m.

PROBE TEST RESULTS

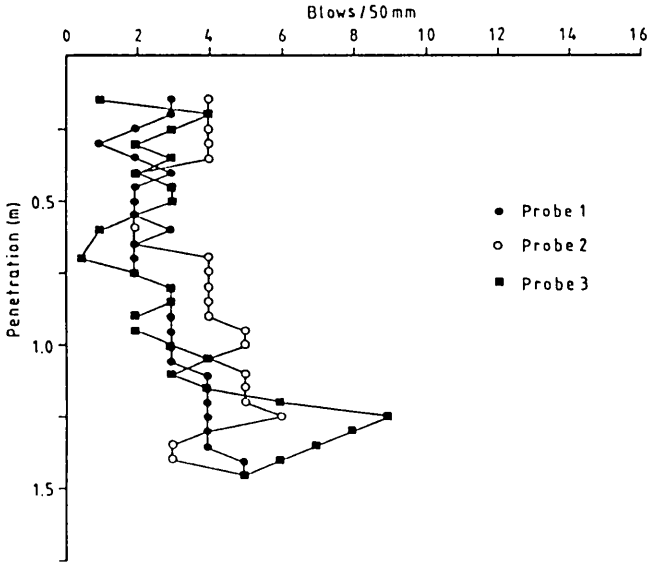

PLAN OF TEST SITE

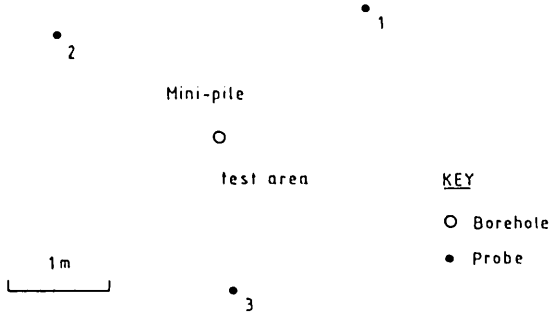

Figure 6.15
Silwood Park (B) site details

Depth (m)	Visual description
	Trial Pit 10.2.87
0.0-0.2	Topsoil
0.2-1.5	FIRM becoming STIFF fissured brown CLAY (London clay) Irregular fissuring, broadly horizontal/ vertical, spacing 5-40mm. Partially dried sample could be broken up into retangular blocks. Closed fissures, not polished but often damp, with rootlets. Fissures usually stained blue-grey. Occasional yellow sand lenses, 5-20mm thick, 50-100mm long. Occasional fragments of fossilised wood, rusty-black products of decomposition and clusters of selenite crystals. Frequent becoming occasional rootlets to c1.0m depth.
Notes	1. No groundwater encountered, trial pit remained dry overnight.

Hand penetrometer Cu values on intact samples of clay:

Depth (m)	Average Cu (kPa)
0.35	82
0.48	100
0.62	123
0.73	168
1.00	178
1.10	173

Moisture content determinations on intact samples of clay:

Depth (m)	Average m.c. (%)
0.35	40.8
0.60	37.4
0.92	32.4
1.14	33.0

Average determined Atterburg limit values:
PL = 29, LL = 76

PROBE TEST RESULTS

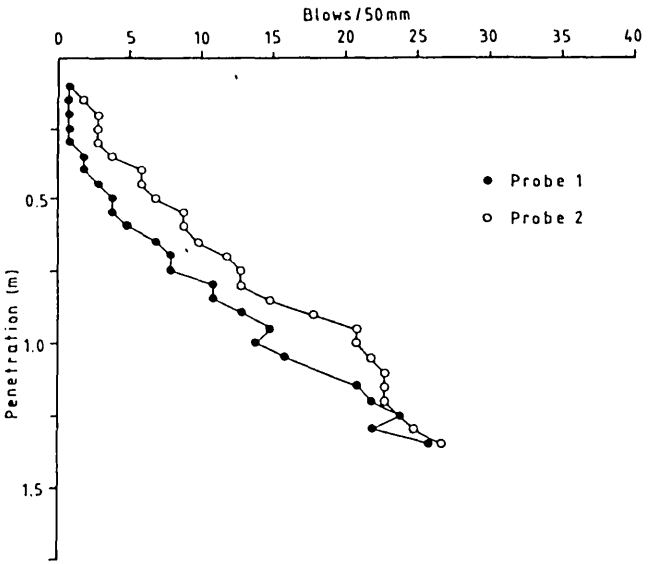

PARTICLE SIZE DISTRIBUTION

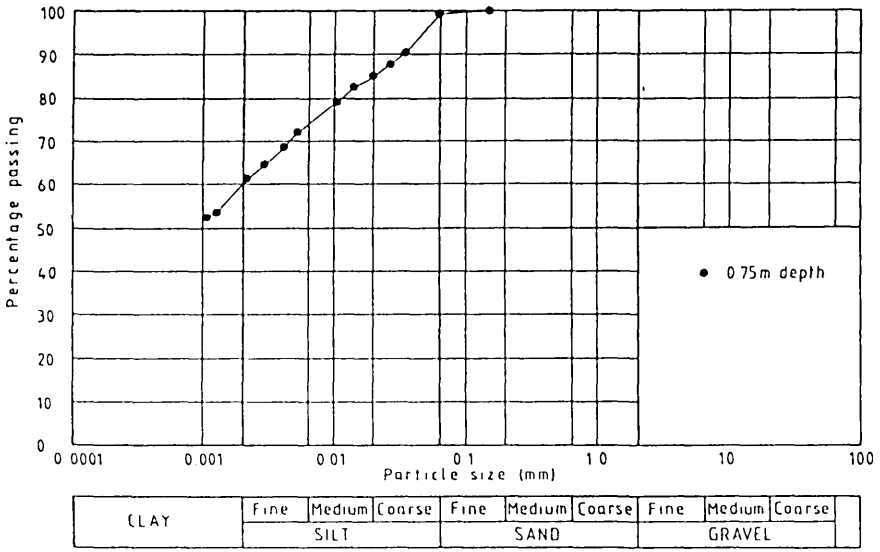

PLAN OF TEST SITE

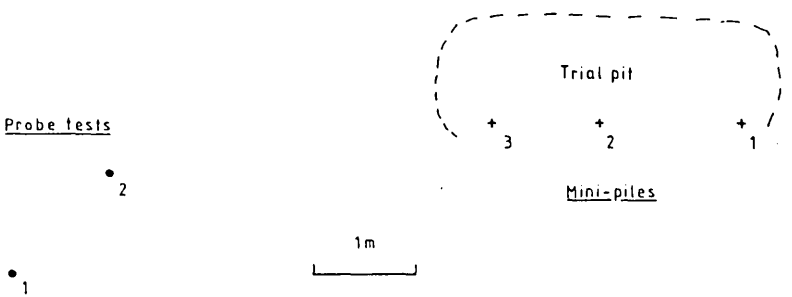

Figure 6.16
Sheppey Pit site details

Depth (m)	Visual description
	Hand auger hole 14.4.87
0.1	Made ground: Dark brown topsoil with frequent fine to coarse sub-angular gravel (including flint and hard-core) and frequent rootlets
0.5	Made ground: Dark brown topsoil with frequent fine to coarse round to sub-angular gravel (including flint and hard-core) and occasional rootlets
1.0	Made ground: Brown subsoil with frequent fine to medium gravel sized fragments of hard-core
1.5	Made ground: Brown subsoil with frequent fine to coarse gravel sized fragments of hard-core and occasional sub-rounded medium flint gravel (End of borehole)

Notes: 1. Hole remained dry throughout augering

PARTICLE SIZE DISTRIBUTION

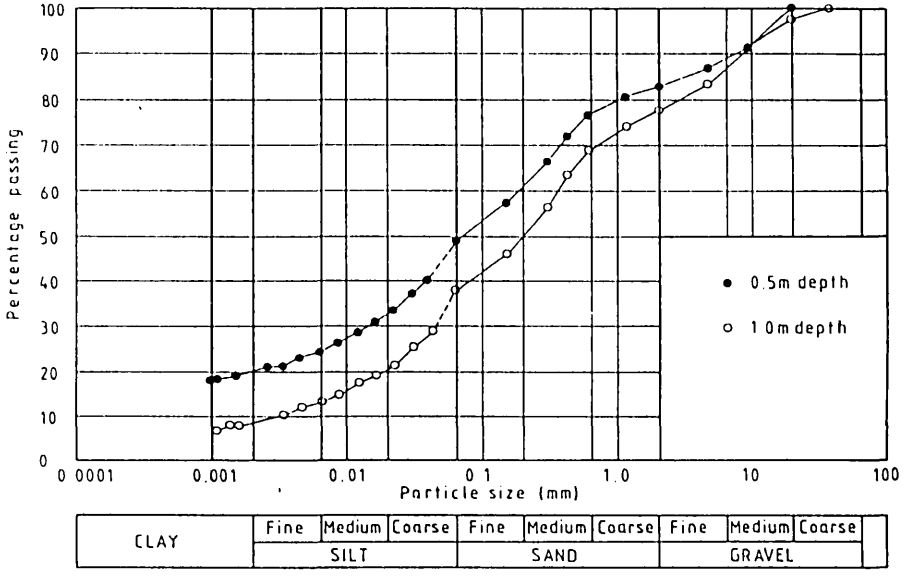

Figure 6.17
Holland House site details

Depth (m)	Visual description
	Trial pit 26.6.87
Above 0.7m¹	Reworked ground: VERY LOOSE yellowy brown very clayey very silty SAND with occasional lenses of grey mottled black silty clay
Below 0.7m¹	Reworked ground: LOOSE light grey fine to medium SAND

Notes:
1. Approximate depths - see probe tests for details.
2. No groundwater encountered.

PROBE TEST RESULTS

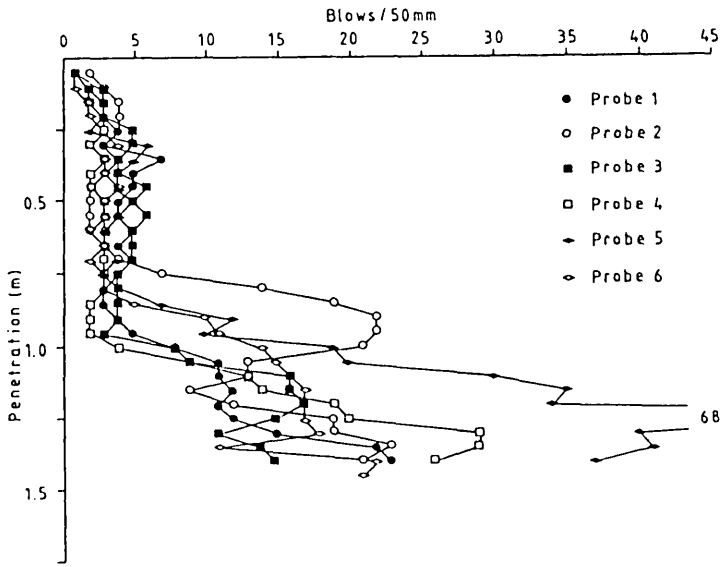

DRIVING RECORDS

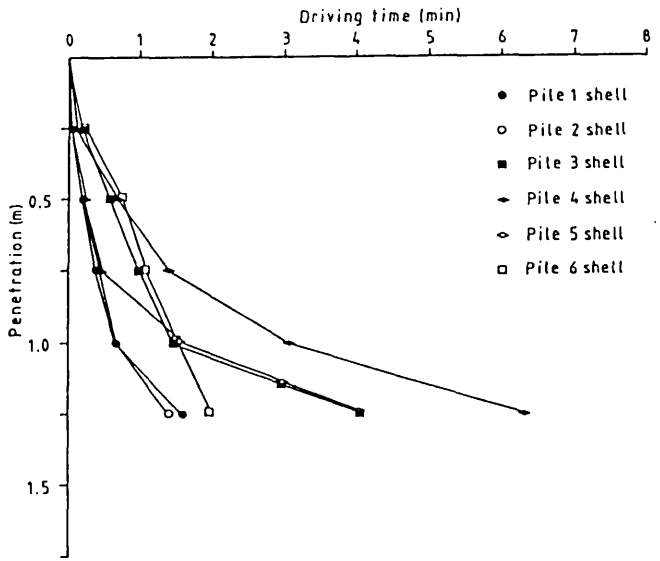

PARTICLE SIZE DISTRIBUTION

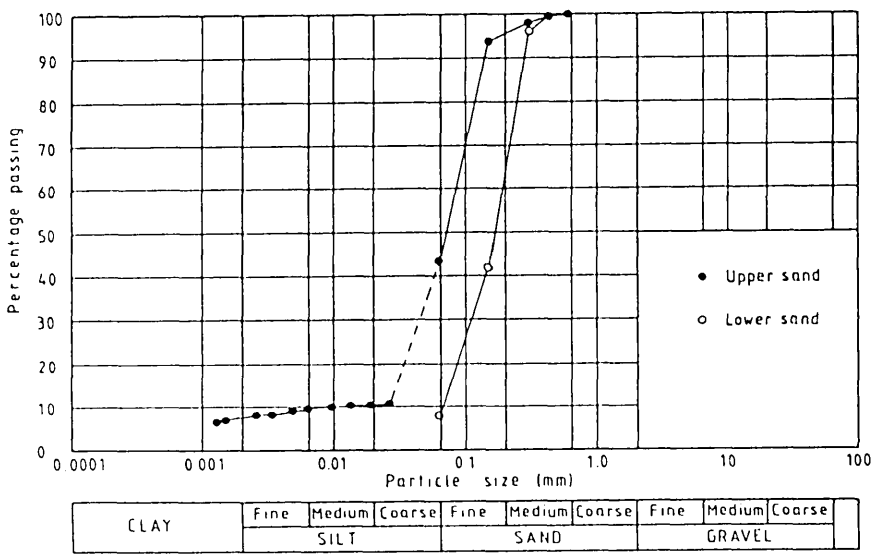

PLAN OF TEST SITE

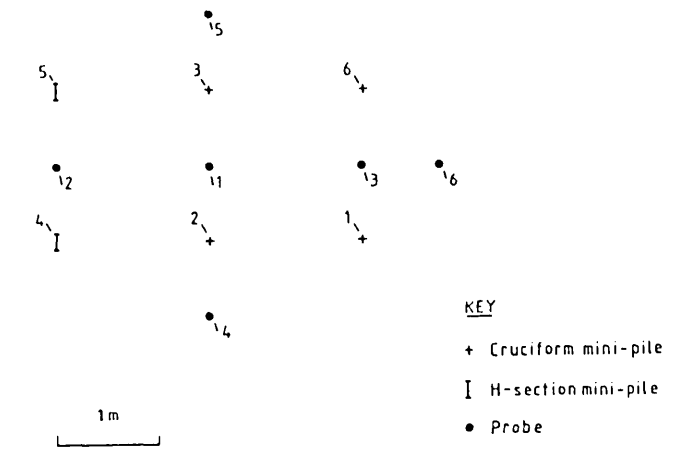

Figure 6.18 Send Court site details

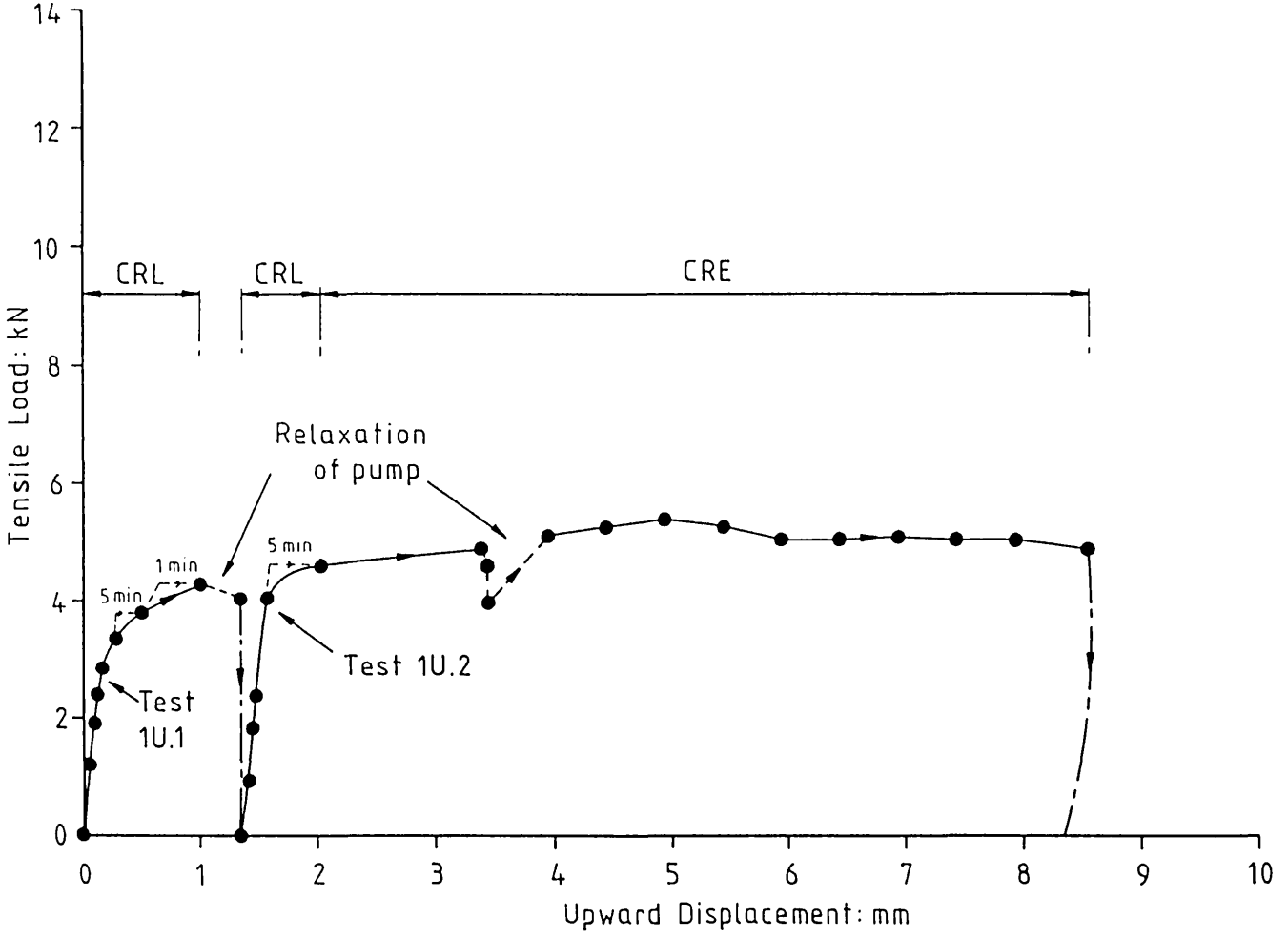

Figure 6.19 Test results: Cruciform mini-pile BRS/1U

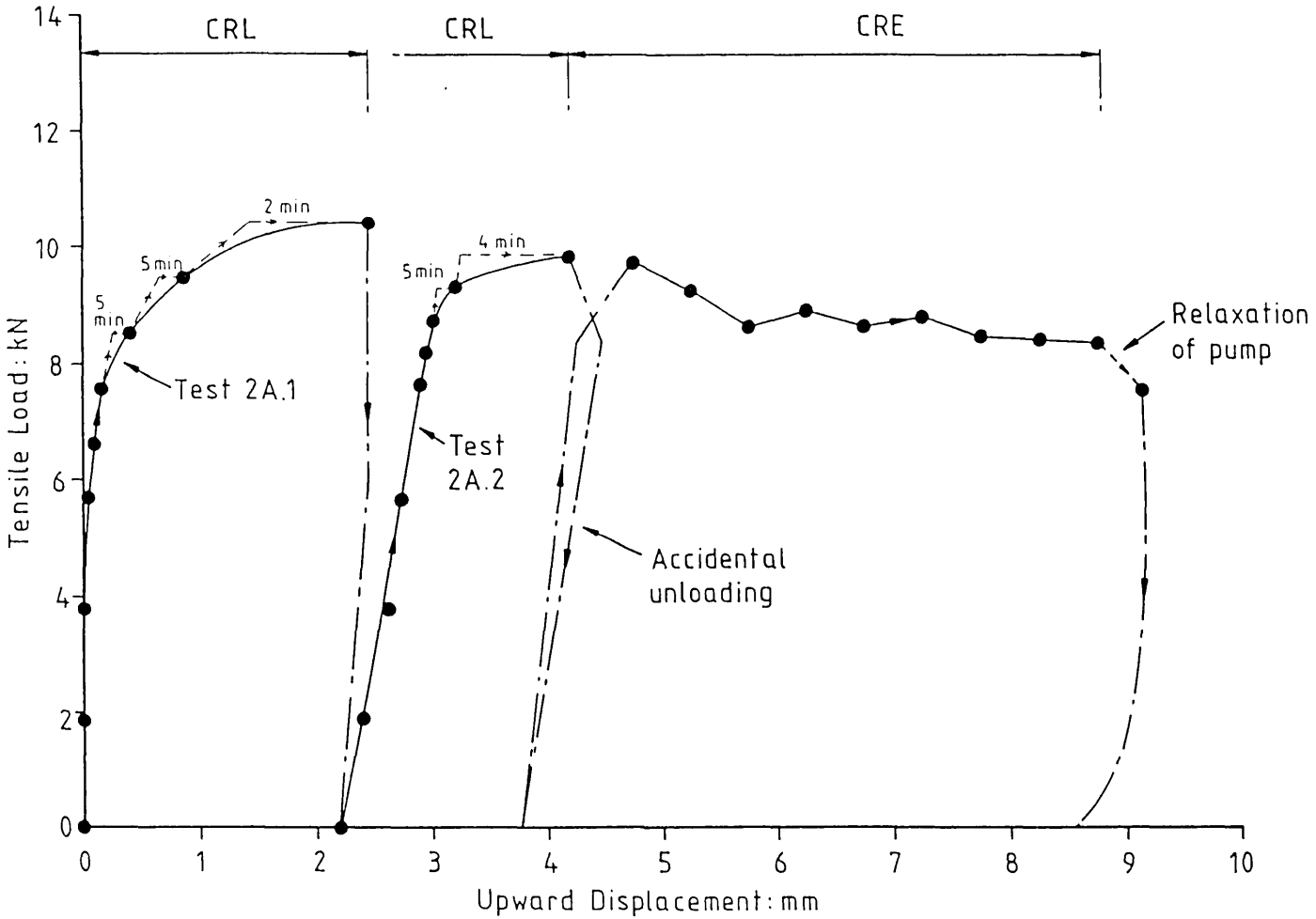

Figure 6.20 Test results: Cruciform mini-pile BRS/2A

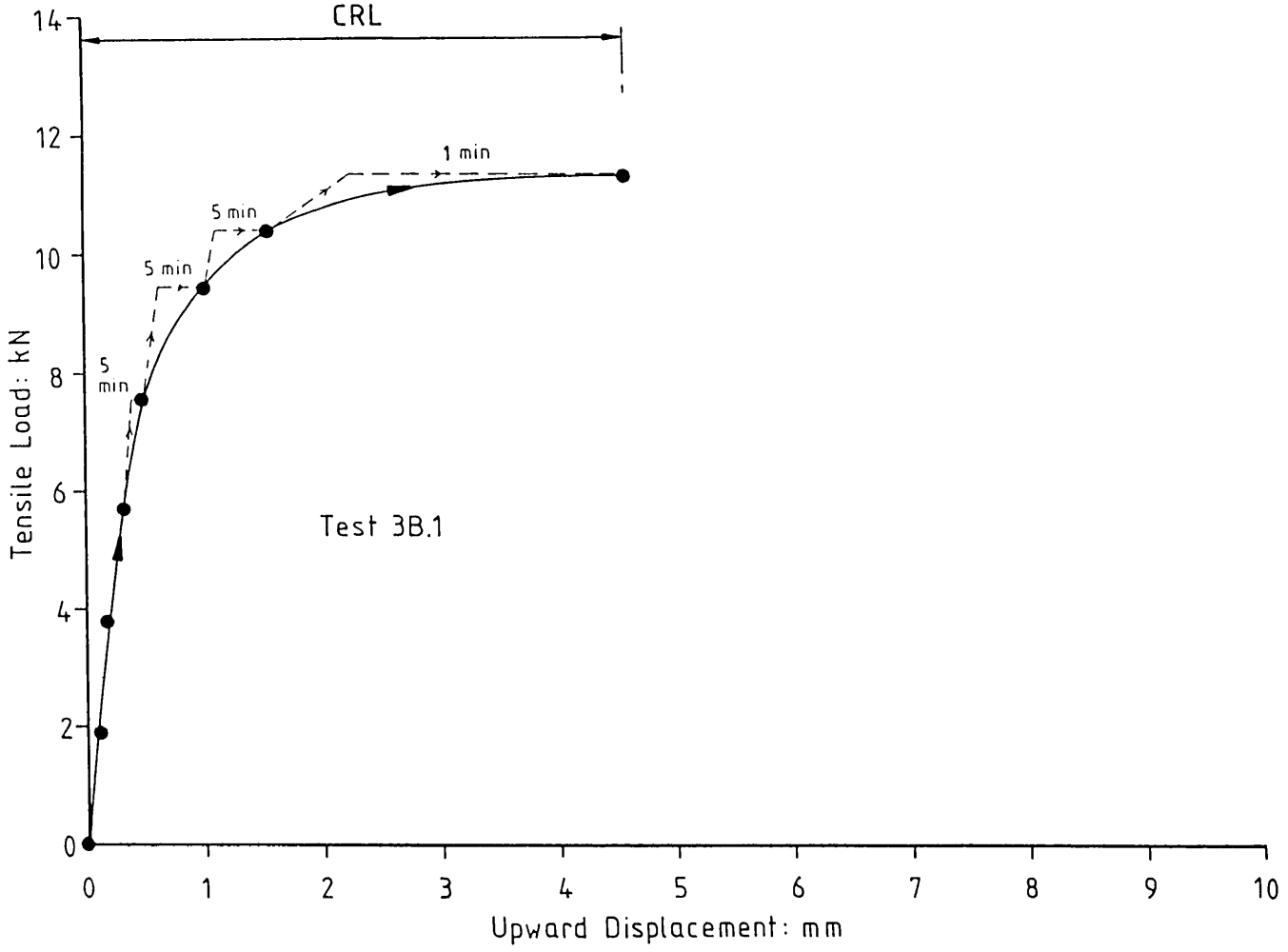

Figure 6.21 Test results: Cruciform mini-pile BRS/3B

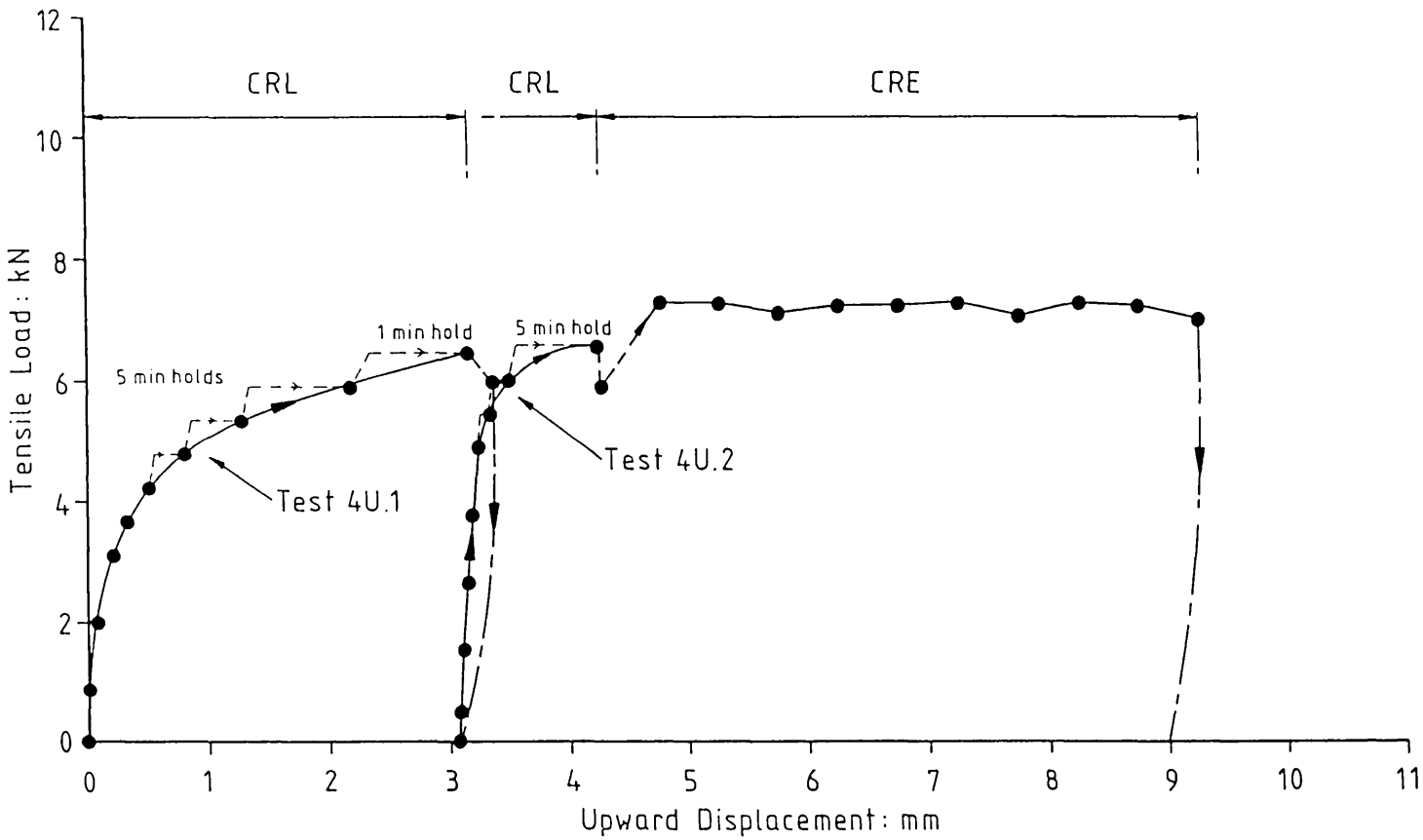

Figure 6.22 Test results: H section mini-pile BRS/4U

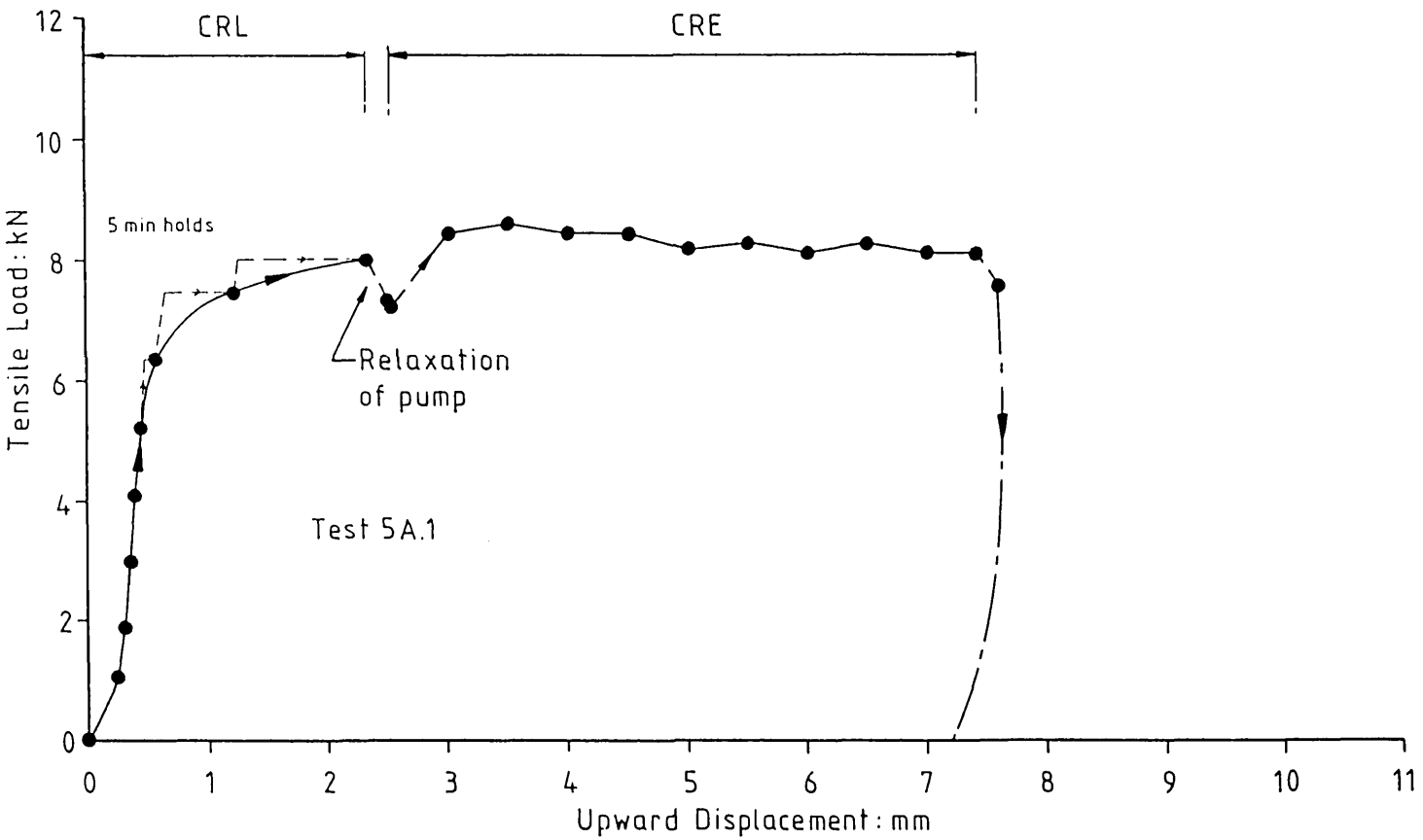

Figure 6.23 Test results: H section mini-pile BRS/5A

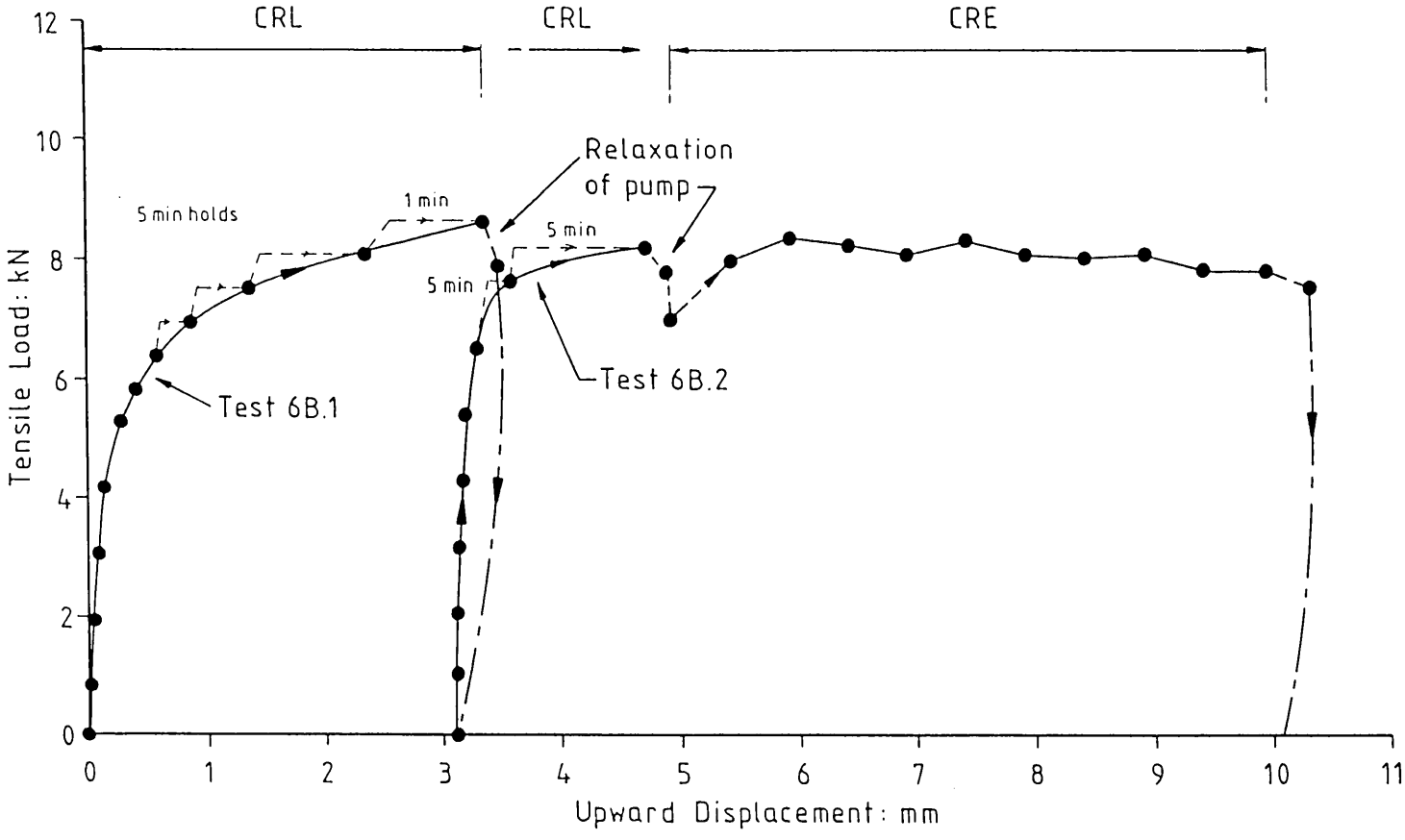

Figure 6.24 Test results: H section mini-pile BRS/6B

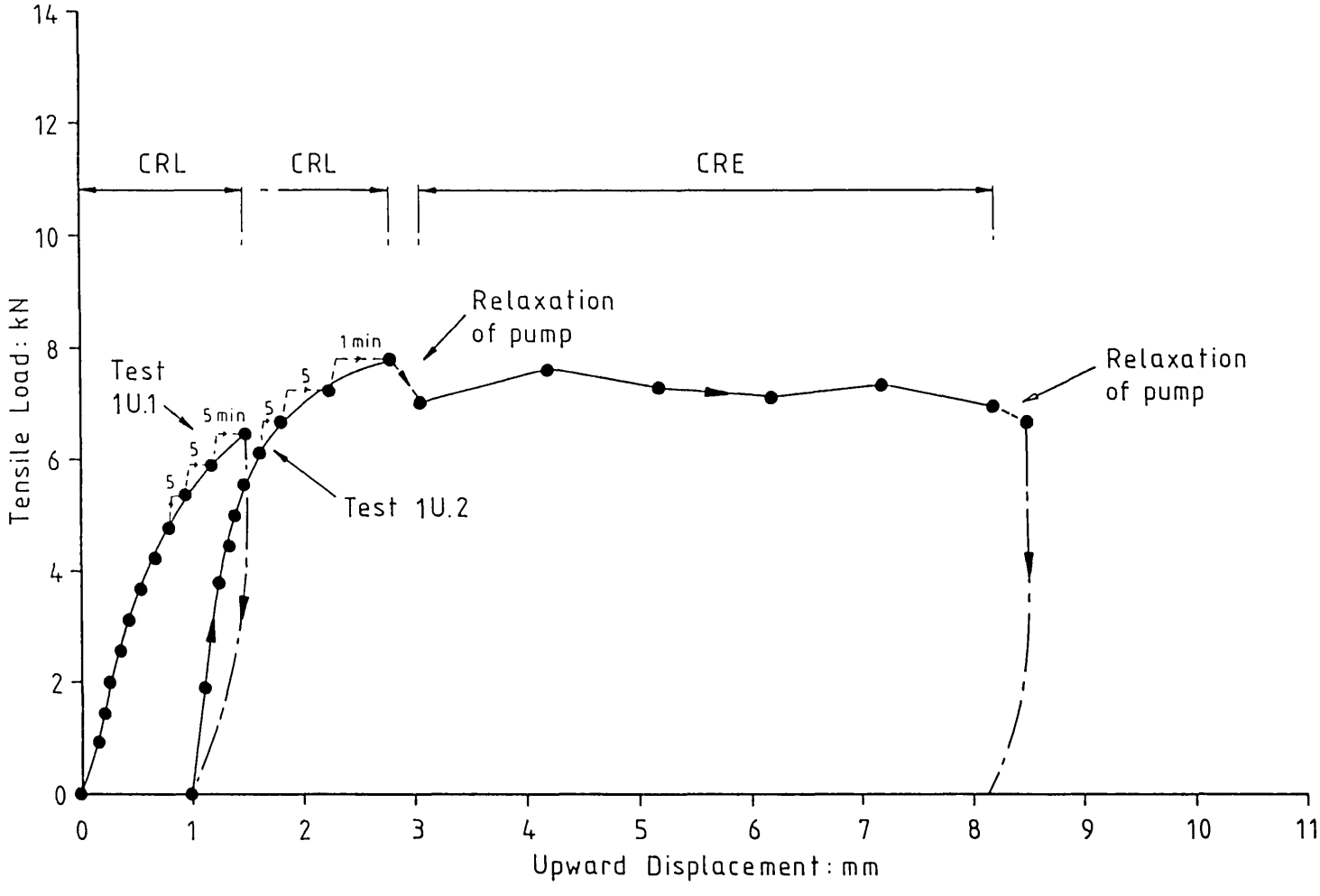

Figure 6.25 Test results: Cruciform mini-pile SHP/1U

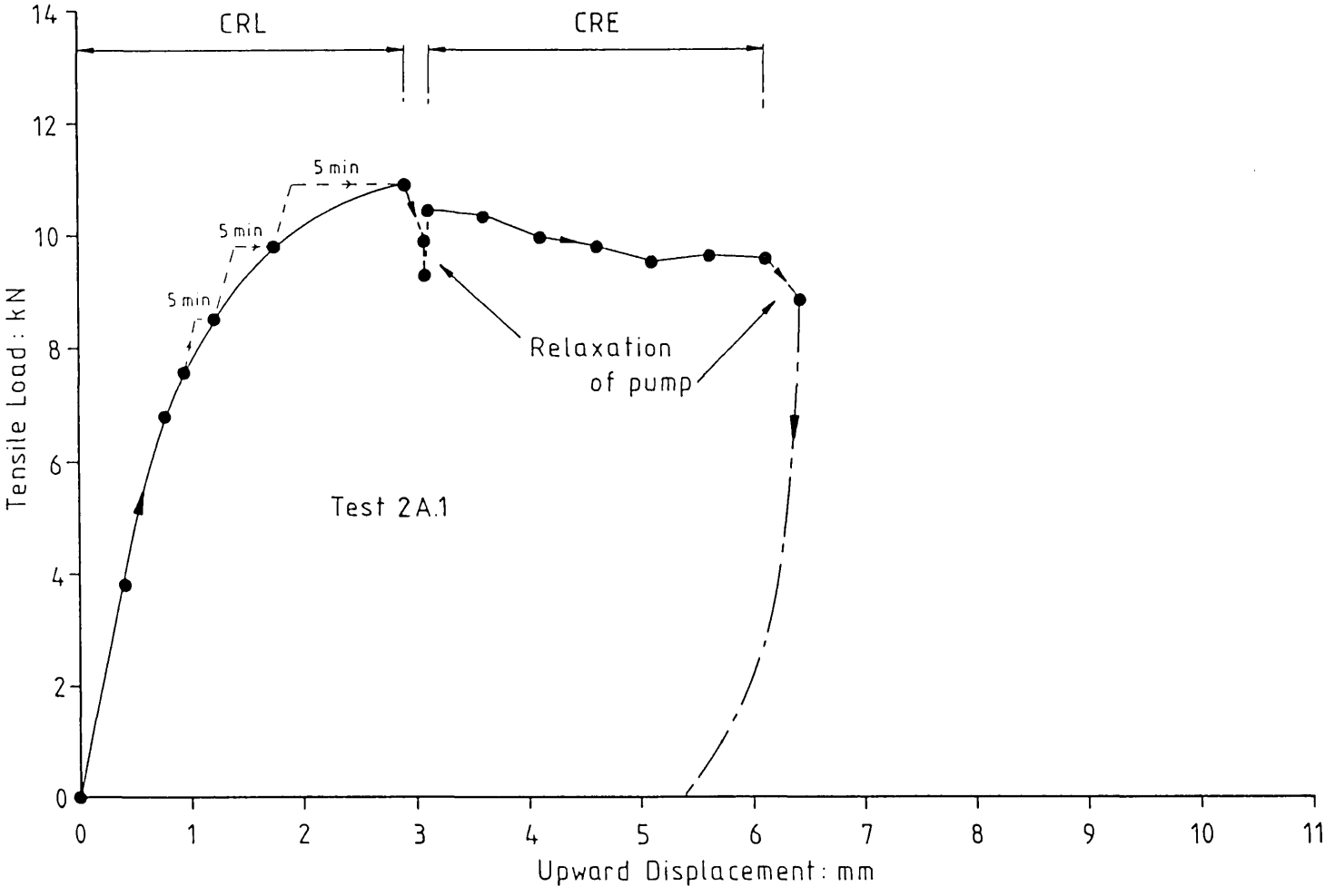

Figure 6.26 Test results: Cruciform mini-pile SHP/2A

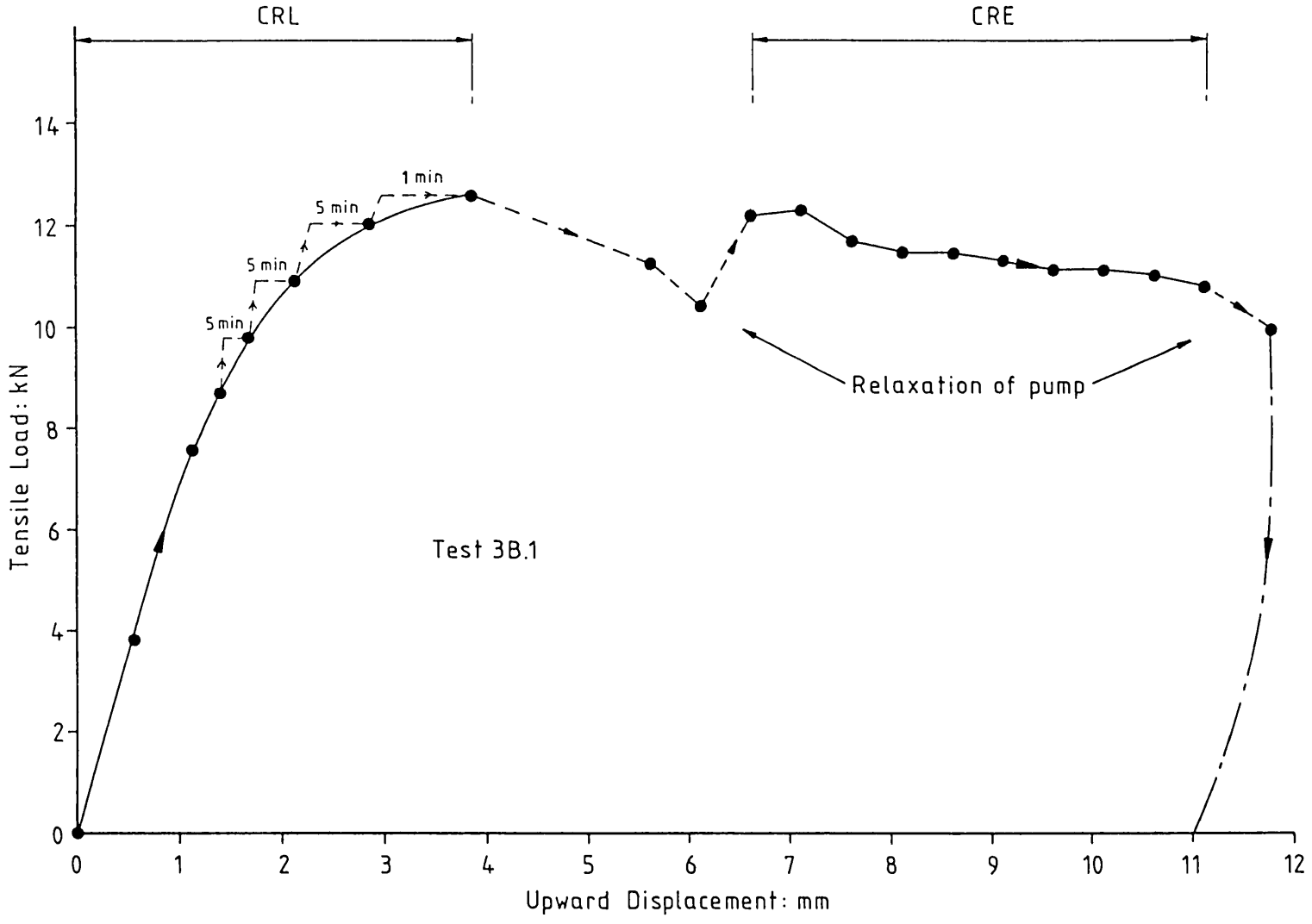

Figure 6.27 Test results: Cruciform mini-pile SHP/3B

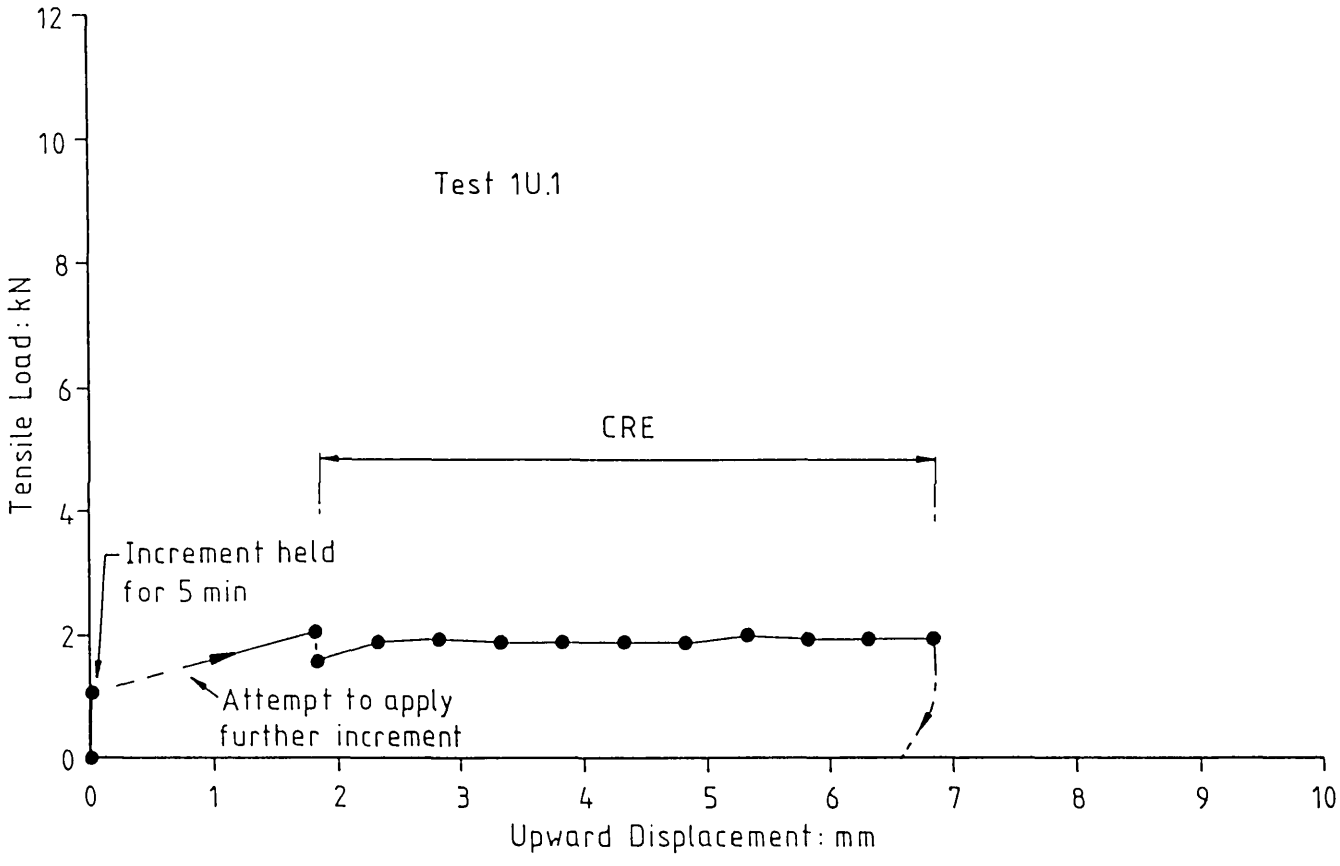

Figure 6.28 Test results: Cruciform mini-pile HH/1U

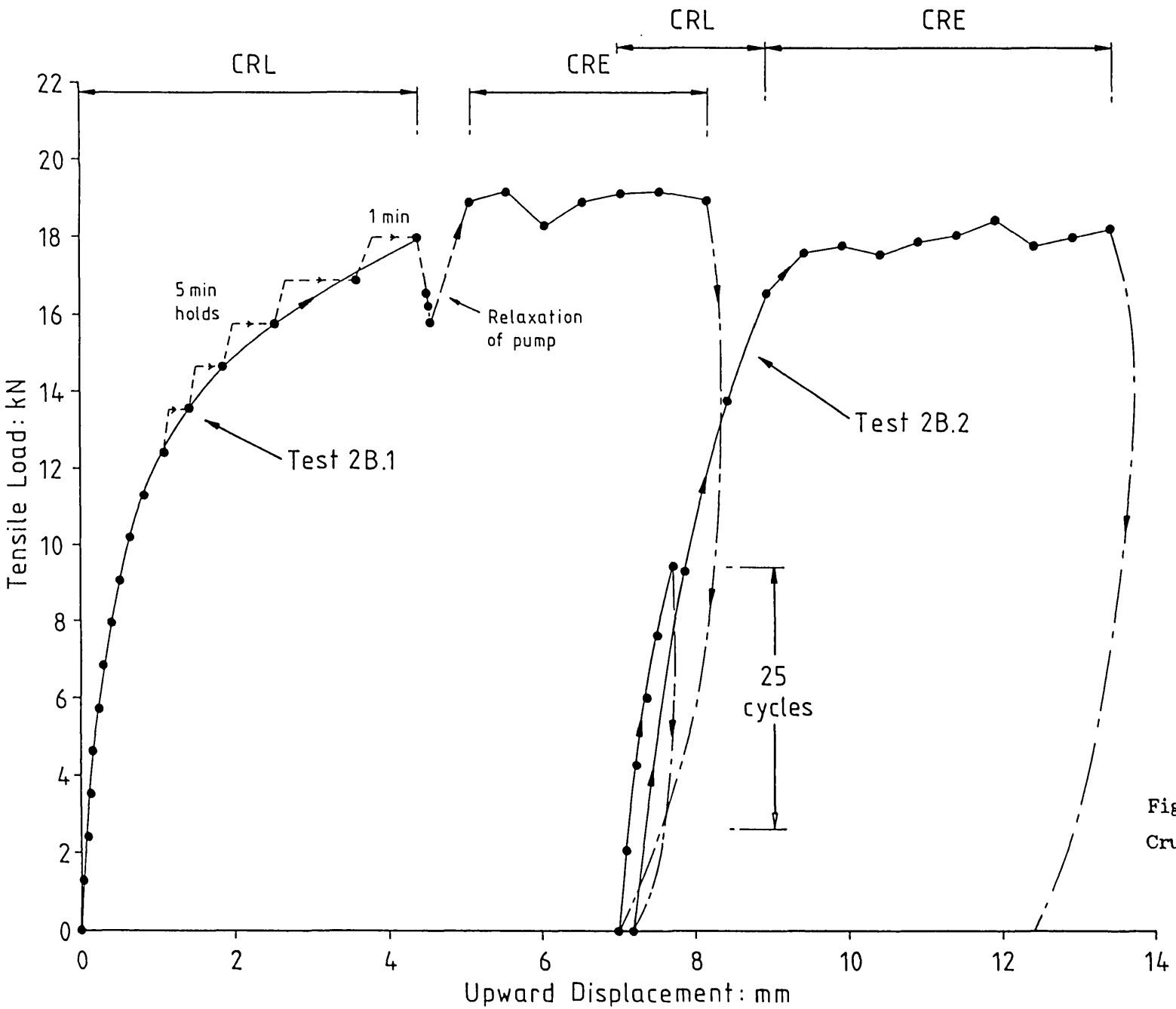

Figure 6.29 Test results: Cruciform mini-pile HH/2B

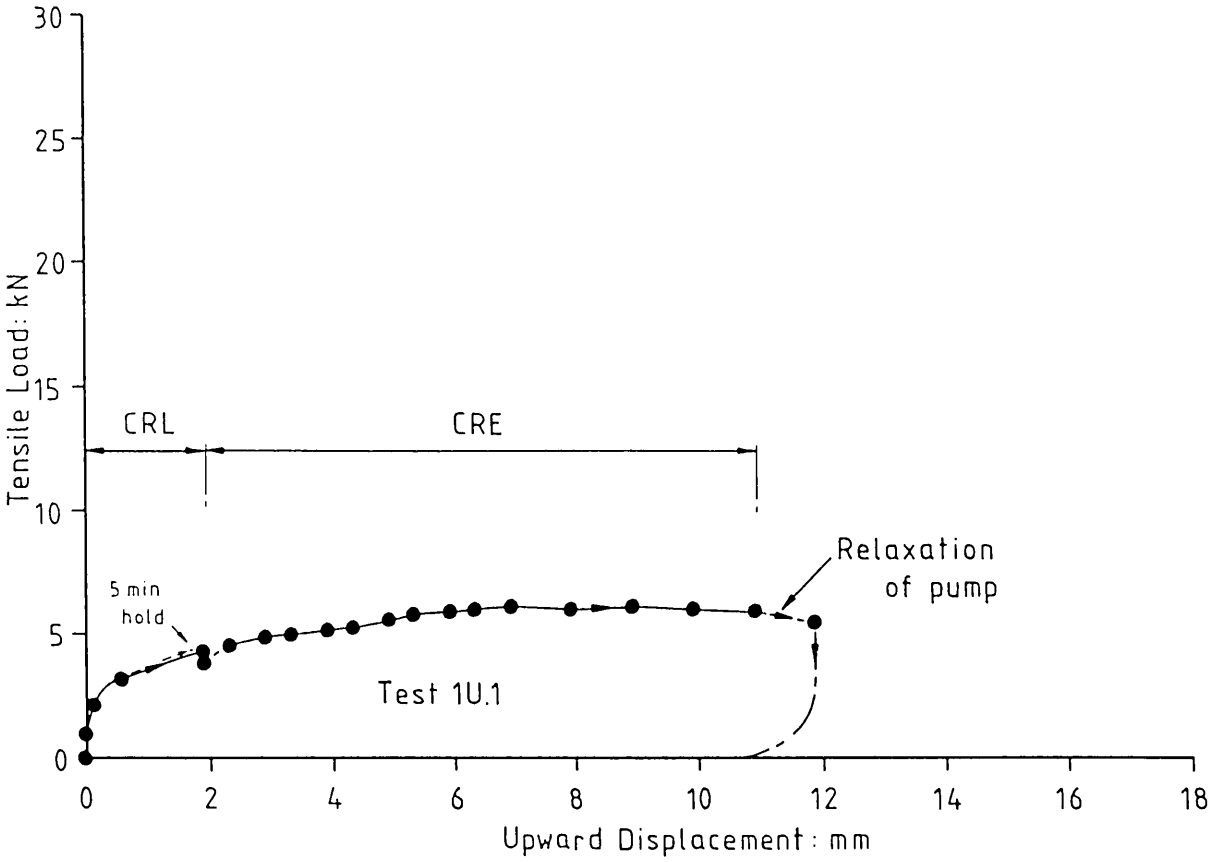

Figure 6.30 Test results: Cruciform mini-pile SC/1U

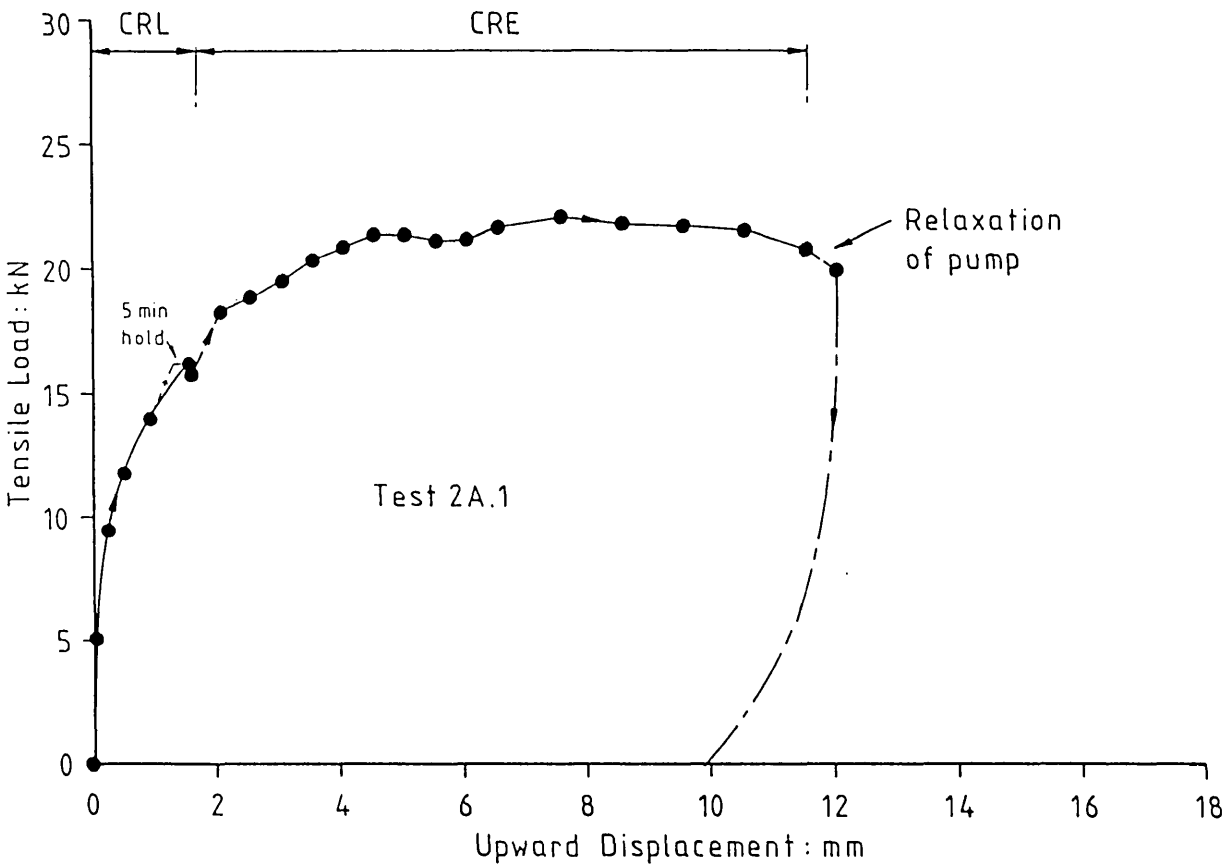

Figure 6.31 Test results: Cruciform mini-pile SC/2A

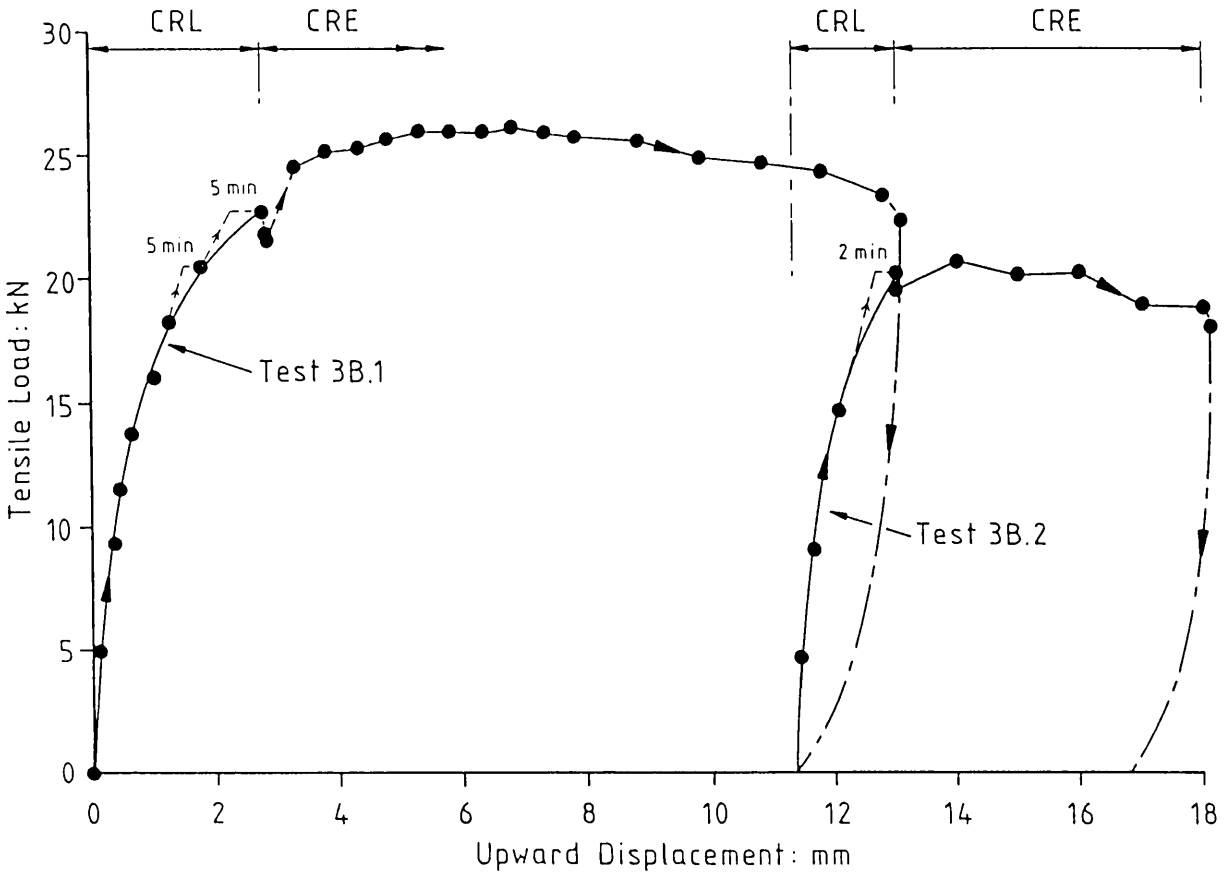

Figure 6.32 Test results: Cruciform mini-pile SC/3B

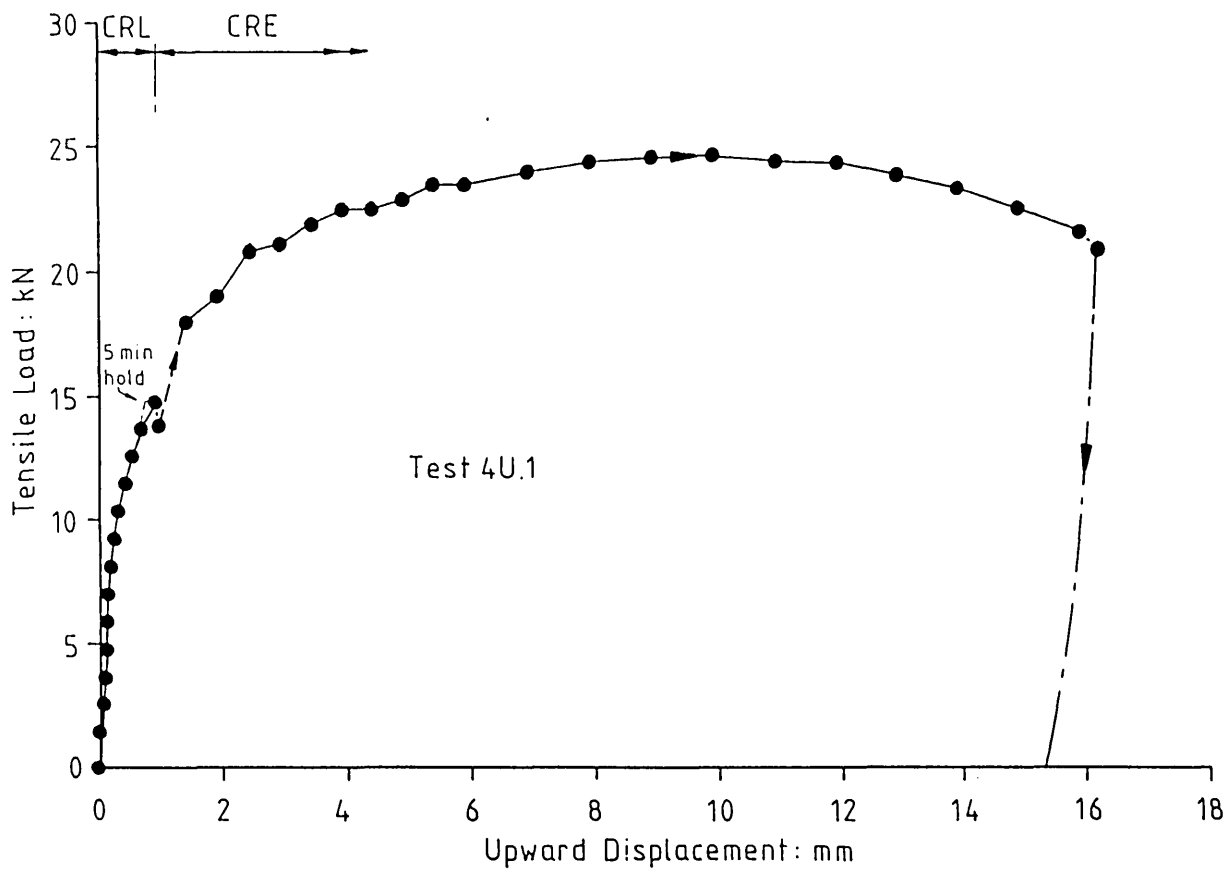

Figure 6.33 Test results: H section mini-pile SC/4U

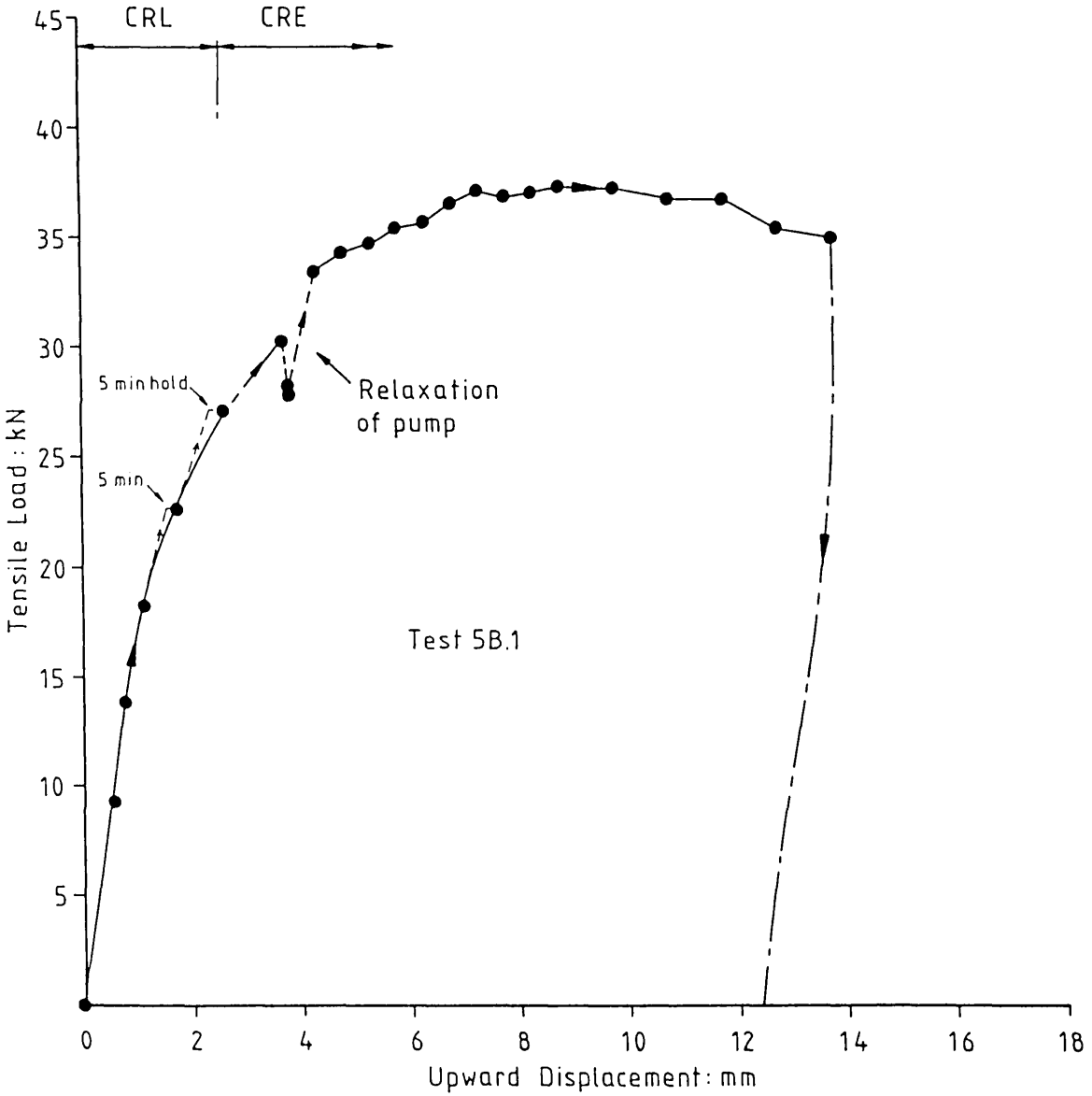

Figure 6.34 Test results:
H section mini-pile SC/5B

Site No.	Location	Brief description of soil profile	Mini-pile types tested
1	BRS	Firm clay till, overlain by reworked till containing occasional gravel and hard-core.	Cruciform type I Cruciform type II H section
2	Silwood Park (A)	Loose fine to medium silty sand.	Cruciform type I
3	Silwood Park (B)	Made ground: poorly drained mixture of clay and granular material.	Cruciform type I
4	Sheppey pit	Firm to stiff weathered London Clay	Cruciform type II
5	Holland House	Made ground: well drained mixture of clay and granular material.	Cruciform type II
6	Send Court pit	Disturbed ground: very loose clayey sand overlying loose fine to medium sand.	Cruciform type II H section

Table 6.1 Summary of mini-pile test sites

Site	Mini-pile failure loads (kN)			Factors of load increase over unexpanded mini-pile	
	amount of expansion:			amount of expansion:	
	unexp.	6%	10%	6%	10%
BRS	5.1	12.0	17.9	2.35	3.51
Silwood Park (A)	4.2	12.3	21.0	2.93	5.00
Silwood Park (B)	0.8	4.8	4.1	6.00	5.12

Notes: 1. Depth of embedment of outer shell = 1000mm
Depth of embedment of expander mandrel = 940mm

Table 6.2 Summary of tests on Type I cruciform mini-piles

SITE: BRS

Driving details:

Mini-Pile No.	Type	Expansion (%)	Dates of driving: Shell	Mandrel	Driving times (min:secs): Shell	Mandrel
BRS/1U	Cru. II	0	7.11.86	-	c3min	-
BRS/2A	Cru. II	6	7.11.86	7.11.86	c3min	0:25
BRS/3B	Cru. II	10	6.11.86	6.11.86	c4min	1:35
BRS/4U	H sect.	0	3. 3.87	-		
BRS/5A	H sect.	6	13. 3.87	13.3.87		
BRS/6B	H sect.	10	3. 3.87	3.3.87		

Testing details:

Test No.	Date	Test stage	Maximum load (kN)	Factor of load increase over unexpanded pile
CRUCIFORM MINI-PILES				
Mini-pile 1U				
1U.1	11.11.86	CRL	4.3	
1U.2	17.11.86	CRL	4.6	
		CRE	5.4	0.00
Mini-pile 2A				
2A.1	11.11.86	CRL	10.4	
2A.2	18.11.86	CRE	9.9	
		CRL	9.8	1.81
Mini-pile 3B				
3B.1	10.11.86	CRL	11.4	2.10

Notes: 1. Depth of embedment of outer shell = 1250mm
Depth of embedment of expander mandrel = 1175mm

2. Smooth finish to outer shells

Table 6.3 Test results: BRS site

Test No.	Date	Test stage	Maximum load (kN)	Factor of load increase over unexpanded pile
H-SECTION MINI-PILES				
Mini-pile 4U				
4U.1	4.3.87	CRL	6.5	
4U.2	26.3.87	CRL	6.6	
		CRE	7.3	0.00
Mini-pile 5A				
5A.1	27.3.87	CRL	8.0	
		CRE	8.6	1.18
Mini-pile 6B				
6B.1	5.3.87	CRL	8.6	
6B.2	26.3.87	CRL	8.2	
		CRE	8.4	1.15

Notes: 1. Depth of embedment of outer shell = 1250mm
Depth of embedment of expander mandrel = 1125mm

2. Smcoth finish to outer shells

Table 6.3 (continued)

SITE: SHEPPEY PIT

Driving details:

Mini-Pile No.	Type	Expansion (%)	Dates of driving: Shell	Mandrel	Driving times (min:sec): Shell	Mandrel
SHP/1U	Cru. II	0	25.11.87	-	c11min	-
SHP/2A	Cru. II	6	"	25.11.87	"	0:35
SHP/3B	Cru. II	10	"	"	"	1:05

Testing details:

Test No.	Date	Test stage	Maximum load (kN)	Factor of load increase over unexpanded pile
Mini-pile 1U				
1U.1	25.11.86	CRL	6.5	
1U.2	3.12.86	CRL	7.8	0.00
		CRE	7.6	
Mini-pile 2A				
2A.1	3.12.86	CRL	10.9	1.39
		CRE	10.5	
Mini-pile 3B				
3B.1	4.12.86	CRL	12.6	1.62
		CRE	12.3	

Notes: 1. Depth of embedment of outer shell = 1250mm
Depth of embedment of expander mandrel = 1175mm

2. Smooth finish to outer shells

Table 6.4 Test results: Sheppey pit site

SITE: HOLLAND HOUSE

Driving details:

Mini-Pile No.	Type	Expansion (%)	Dates of driving: Shell	Mandrel	Driving times (min:sec): Shell	Mandrel
HH/1U	Cru. II	0	29.4.87	-	c1min	-
HH/2B	Cru. II	10	29.4.87	29.4.87	c1min	1:00

Testing details:

Test No.	Date	Test stage	Maximum load (kN)	Factor of load increase over unexpanded pile
Mini-pile 1U				
1U.1	30.4.87	CRL	0.9	
		CRE	2.0	0.00
Mini-pile 2B				
2B.1	30.4.87	CRL	18.0	
		CRE	19.2	9.6
2B.2	1.5.87	Cyclic[2]		
		CRE	18.5	9.2

Notes:
1. Depth of embedment of outer shell = 1250mm
   Depth of embedment of expander mandrel = 1175mm
2. 25 cycles between approximately 3kN and 9.5kN.
3. Grit-blasted finish to outer shells

Table 6.5 Test results: Holland House site

SITE: SEND COURT PIT

Driving details:

Mini-Pile No.	Type	Expansion (%)	Dates of driving: Shell	Mandrel	Driving times (min:secs): Shell	Mandrel
SC/1U	Cru. II	0	24.6.87	25.6.87	1:37	-
SC/2A	Cru. II	6	"	"	1:47	0:47
SC/3B	Cru. II	10	"	"	4:04	1:17
SC/4U	H Sect.	0	"	"	6:21	-
SC/5B	H Sect.	10	"	"	4:05	1.23

Testing details:

Test No.	Date	Test stage	Maximum load (kN)	Factor of load increase over unexpanded pile
CRUCIFORM MINI-PILES				
Mini-pile 1U				
1U.1	25.6.87	CRL	4.3	
		CRE	6.2	0.00
Mini-pile 2A				
2A.1	26.6.87	CRL	16.2	
		CRE	22.1	3.56
Mini-pile 3B				
3B.1	25.6.87	CRL	22.7	
		CRE	26.1	4.21
3B.2	25.6.87	CRL	20.2	
		CRE	20.7	3.34

Notes: 1. Depth of embedment of outer shell = 1250mm
Depth of embedment of expander mandrel = 1175mm

2. Grit blasted finish to outer shells

Table 6.6 Test results: Send Court site

Test No.	Date	Test stage	Maximum load (kN)	Factor of load increase over unexpanded pile
H SECTION MINI-PILES				
Mini-pile 4U				
4U.1	26.6.87	CRL	14.8	
		CRE	24.7	0.00
Mini-pile 5B				
5B.1	26.6.87	CRL	27.1	
		CRE	37.3	1.51

Notes: 1. Depth of embedment of outer shell = 1250mm
Depth of embedment of expander mandrel = 1125mm

2. Grit blasted finish to outer shells

Table 6.6 (continued)

CHAPTER 7
SUMMARY OF FURTHER LABORATORY TESTING

7.1 Introduction

This Chapter briefly summarises the results of two MSc projects, supervised by the author, that formed part of the Wedge-Pile project. The projects involved laboratory model testing to investigate two different aspects of the Wedge-Pile concept:

(a) the behaviour of large-displacement circular wedge-piles employing 1, 3 or 4 weak lines

(b) the possible application of the Wedge-Pile principle to soil reinforcement techniques.

Full details of these projects are given in the respective MSc reports.

7.2 Model Tests on Circular Wedge-Piles

7.2.1 Introduction

A test programme on circular wedge-piles in sand was undertaken by Young (1988).

These tests were carried out in connection with the commercial field trials reported in Chapter 8. In the field trials, the performance of circular wedge-piles formed from both steel and plastic tubes was to be investigated. An important aspect of the work on circular piles was the influence of the number of expansion directions on the gain in pile capacity. In particular, it was important to establish any difference in behaviour between outer shells with just one weak line and the optimum arrangement, from a soil mechanics point of view, of expansion in 3 or 4 directions. From the point of view of fabrication, a 1-slit circular pile is relatively easy to produce. Circular piles with a greater number of slits are progressively more difficult and expensive to fabricate.

7.2.2 Description of model piles and apparatus

The model tests were performed in sand, using the same test rig as for the preliminary model tests described in Chapter 2. General test procedures were similar to those described previously.

The circular model piles comprised an outer shell and an expander mandrel (Figure 7.1). The outer shell was 21.5mm in diameter and 250mm in length, formed from PVC pipe. It was closed at its bottom end by means of a conical driving shoe machined from brass. The outer shell was free to move independently of the driving shoe during tension tests. Slits cut along the length of the outer shell allowed it to be expanded by the expander mandrel. Three expander mandrels were machined from steel rod. Each expander mandrel comprised a nose section and a shank section, and expanded the outer shell by 25% of its original diameter.

The mode of expansion could be varied by altering the number of slits cut in the outer shell. Arrangements employing 1, 3 and 4 slits were tested, in addition to the unexpanded outer shell with no slits. The slits were disposed symmetrically around the outer shell in all cases. The separated elements of the 3-slit and 4-slit piles were very much more flexible than the steel angles used to form the model cruciform piles (Section 2.2.2).

Tests were performed using both smooth sided piles and rough sided piles. The latter type were formed by cutting a screw thread along the length of the PVC outer shell.

Two different types of conical driving shoe were tried, in which the base of the cone was either flush, or oversized, in comparison to the outer shell. In the case of the oversized driving shoe, the outside diameter of the expanded pile was 12% greater than the maximum diameter of the driving shoe. Three different expander mandrel nose profiles were tried. Two of the profiles were uniform tapers and one was parabolic in shape.

Tests were carried out in both dry sand and damp sand. The sand used was the same as for the preliminary model tests (Section 2.2.5). The tests were performed in sand beds of the same nominal density; the average dry relative density was 69%, corresponding to the medium-dense tests described in Section 2.3.2. In the case of the tests in dry sand, a thin polythene membrane was glued to the inside of each outer shell in order to prevent sand pouring through the slits during expansion (refer to Section 2.2.5).

A large number of tests were performed to establish the tensile capacity of the various arrangements of pile that were possible. The piles were driven 250mm into the sand bed at 16.51mm/minute, and then pulled from it at a slower rate - usually five times slower than the installation rate.

7.2.3 Summary of results

Figure 7.2 covers all the pile tests in dry sand. Details of pile arrangements are given. Maximum tensile capacity of the model piles is plotted against the number of expansion slits. The main conclusions drawn from the tests in dry sand are given below:

(a) pile capacity for the expanded piles is significantly greater than for the unexpanded piles

(b) pile capacity for 1-slit expansion is significantly less than for 3-slit and 4-slit expansion

(c) there is no apparent increase in pile capacity for 4-slit expansion in comparison to 3-slit expansion

(d) average factors of increase in capacity, in comparison to the flush unexpanded piles, are 1.21 for the 1-slit piles and 2.05 for the combined results of the 3-slit and 4-slit piles

(e) for the 3-slit piles, there is little tendency for results for piles with oversized shoes to fall below results for piles with flush shoes; for the unexpanded piles the influence of driving shoe type is very marked, the results for the piles with oversize shoes falling well below the results for the piles with flush shoes.

Figure 7.3 covers all pile tests in damp sand - presentation is the same as for Figure 7.2. The main conclusions drawn from the tests in damp sand are basically the same as for the tests in dry sand, and are given below:

(a) overall, pile capacities are greater in damp sand than in dry sand, as to be expected due to the greater bulk weight and the apparent cohesion of the damp sand

(b) pile capacity for the expanded piles is significantly greater than for the unexpanded piles

(c) pile capacity for 1-slit expansion is significantly less than for 3-slit and 4-slit expansion

(d) there is no apparent increase in pile capacity for 4-slit expansion in comparison to 3-slit expansion

(e) average factors of increase in capacity, in comparison to the flush unexpanded piles, are 2.39 for the 1-slit piles, and 4.00 for the combined results of the 3-slit and 4-slit piles

(f) for the expanded piles, results for piles with oversized shoes tend to fall slightly below the results for piles with flush shoes; if comparative tests had been performed in the case of the unexpanded piles, the influence of driving shoe type would have been much more marked: an unexpanded pile with an oversize shoe would have given negligible tensile resistance, the sand being able to support itself clear of the pile shaft after driving.

Figure 7.4 covers all tests, in both dry sand and damp sand. Pile Efficiency (as defined in Section 2.3.4) is plotted against the number of expansion slits. The conclusions drawn from this Figure are given below:

(a) pile Efficiency for the 3-slit and 4-slit expanded piles is significantly greater than for the unexpanded piles

(b) pile Efficiency for 1-slit expansion is similar to that for the unexpanded piles

(c) there is a small increase in pile Efficiency for 4-slit expansion in comparison to 3-slit expansion

(d) average increases in Efficiency in comparison to the flush unexpanded piles are 0.96 for the 1-slit piles, and 1.54 and 1.76 for the 3-slit and 4-slit piles respectively

(e) pile Efficiencies for the 3-slit and 4-slit expanded piles are about half of those for the cruciform pile tests in medium-dense sand reported in Section 2.3.4, where Efficiencies of over 3 J/N were recorded.

Another significant finding from these model tests was that the expanded piles in both dry and damp sand exhibited much stiffer load-displacement behaviour than for the unexpanded piles, stiffness increasing with the number of expansion directions. Secant stiffnesses at peak load were up to ten times greater for expanded piles than for unexpanded piles.

There were insufficient data to prove if the shape of the expander mandrel nose had a significant effect on pile capacity, although the energy expended during expansion was found to be less in the case of the

parabolic nose profile than for the conical nose profiles.

7.2.4 Overall conclusions

The tests on model circular piles confirmed that large increases in load carrying capacity are possible by expanding a pile after driving - up to four times in this particular study. The number of expansion directions was shown to have an important influence on the increases in capacity. In particular, increases in capacity for 1-slit expansion were found to be significantly less than for 3-slit and 4-slit expansion.

The results for pile Efficiency are interesting. The Efficiencies for the 1-slit piles are approximately the same as for the unexpanded piles, the reason being that although capacities for the 1-slit piles are higher, driving energies are also higher. Efficiencies for the 3-slit and 4-slit piles are significantly higher than for the 1-slit piles. In addition to the greater pile capacities obtainable by expansion in 3 and 4 directions, this may reflect the greater strain energy involved in expanding the relatively stiff 1-slit outer shell in comparison to the relatively flexible 3-slit and 4-slit outer shells.

The lower Efficiencies for the large-displacement circular piles in comparison to those for the small-displacement cruciform piles confirms that the cruciform pile is likely to be the more successful wedge-pile configuration to adopt in practice.

7.3 Soil Nailing and Reinforced Earth Model Tests

Laboratory model tests in sand investigating the potential of the Wedge-Pile principle in soil reinforcement techniques were undertaken in an qualitative model study by Mapplebeck (1987).

7.3.1 Description of apparatus

The experiments were performed in sand beds of loose and of medium loose dry sand contained within a 0.86x0.17m, 168mm wide glass sided flume (Plate 7.1). The sand used was the same as for the preliminary model tests described in Chapter 2. Model retaining walls were constructed in the sand bed.

The methods used to construct the model retaining walls simulated the techniques used to construct retaining walls by soil nailing and reinforced earth techniques. In these methods, reinforcement strips are introduced into the soil mass and connected to wall panels. Stresses in the soil are transferred to the reinforcing strips by friction between the two, and the anchorage provided by the strips imparts

stability to the wall. The two techniques of soil nailing and reinforced earth share many common features, but there are also important differences. Soil nailing is a 'top down' construction technique; reinforced earth is a 'bottom up' technique. This is shown in Figure 7.5 (Bruce and Jewell, 1986).

In the model study, both types of soil reinforcement technique were investigated. Reinforcement strips formed from paper were used. These were 150mm long and 15mm wide, in the form of flat loops. They were installed horizontally into the sand bed, either by pushing with a 0.65mm thick aluminium pushing strip (soil nailing) or by placing (reinforced earth). After the reinforcement strips were installed, they could be expanded with 1.5mm thick plastic expander strips (Plate 7.2). The reinforcement strips were attached to 50mm deep wall panels formed from 1.5mm plastic strip. The wall panels were the same width as the testing flume and retained the sand mass (Plate 7.3).

Walls constructed with unexpanded reinforcement strips and with expanded reinforcement strips were tested by applying a surcharge just behind the top of the wall. Marker bands of sand enabled the resulting failure mechanism to be studied (Plate 7.4).

7.3.2 Summary of results

The load bearing capacity of walls with expanded reinforcement strips was found to be significantly greater than for walls with unexpanded reinforcement strips, for both soil nail walls and for reinforced earth walls. Gains in capacity of up to 1.7 times were possible in the case of reinforced earth walls.

Similarly, under a given load, walls with expanded reinforcement displaced less than walls with unexpanded reinforcement; displacements being up to 6 times lower in the case of reinforced earth walls and about 2 times lower for soil nail walls. Also, the expanded reinforcement had a beneficial influence on the locations of failure planes within the soil mass.

The results of the model studies gave encouragement to the belief that the Wedge-Pile principle has potential in soil reinforcement processes.

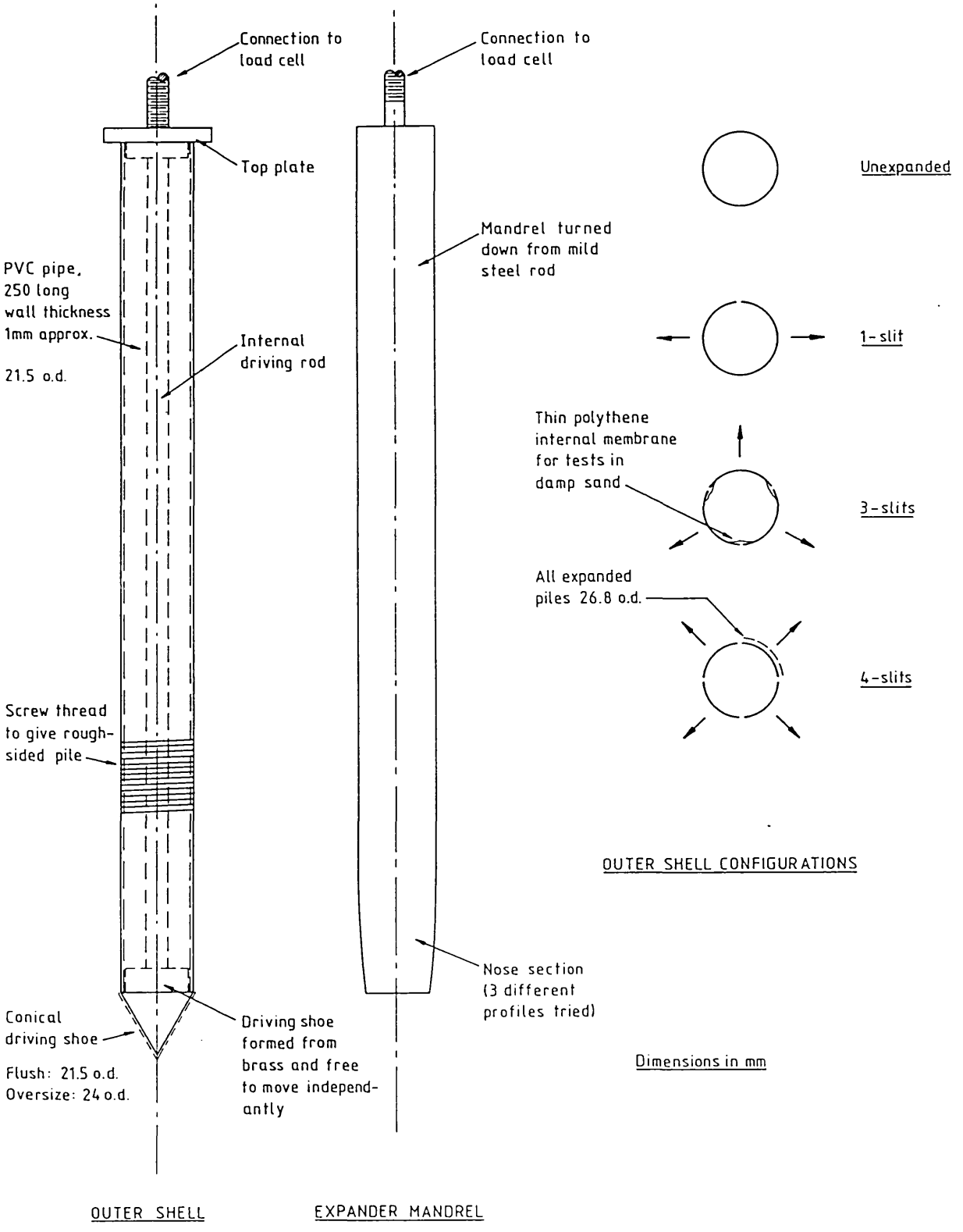

Figure 7.1 Circular model wedge-pile

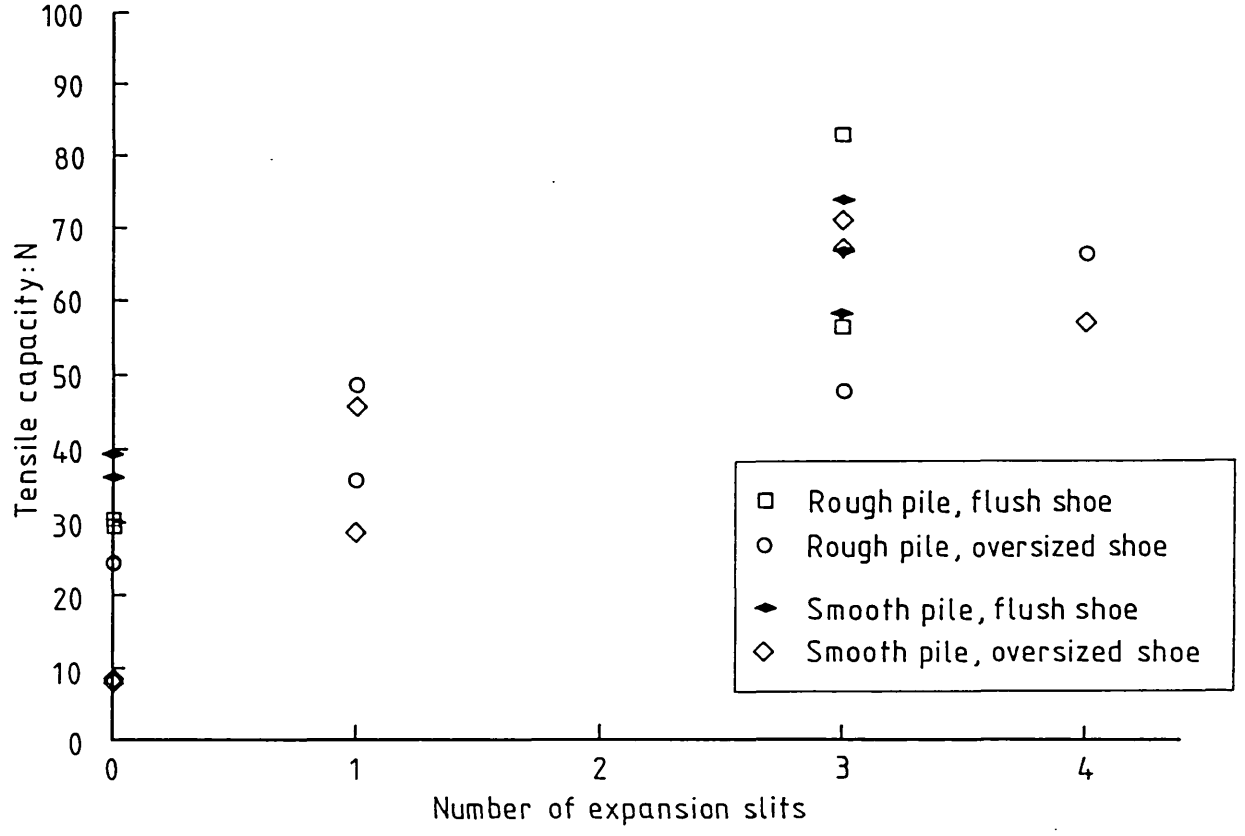

Figure 7.2 Summary of results: dry sand
Model pile capacity against Number of expansion slits

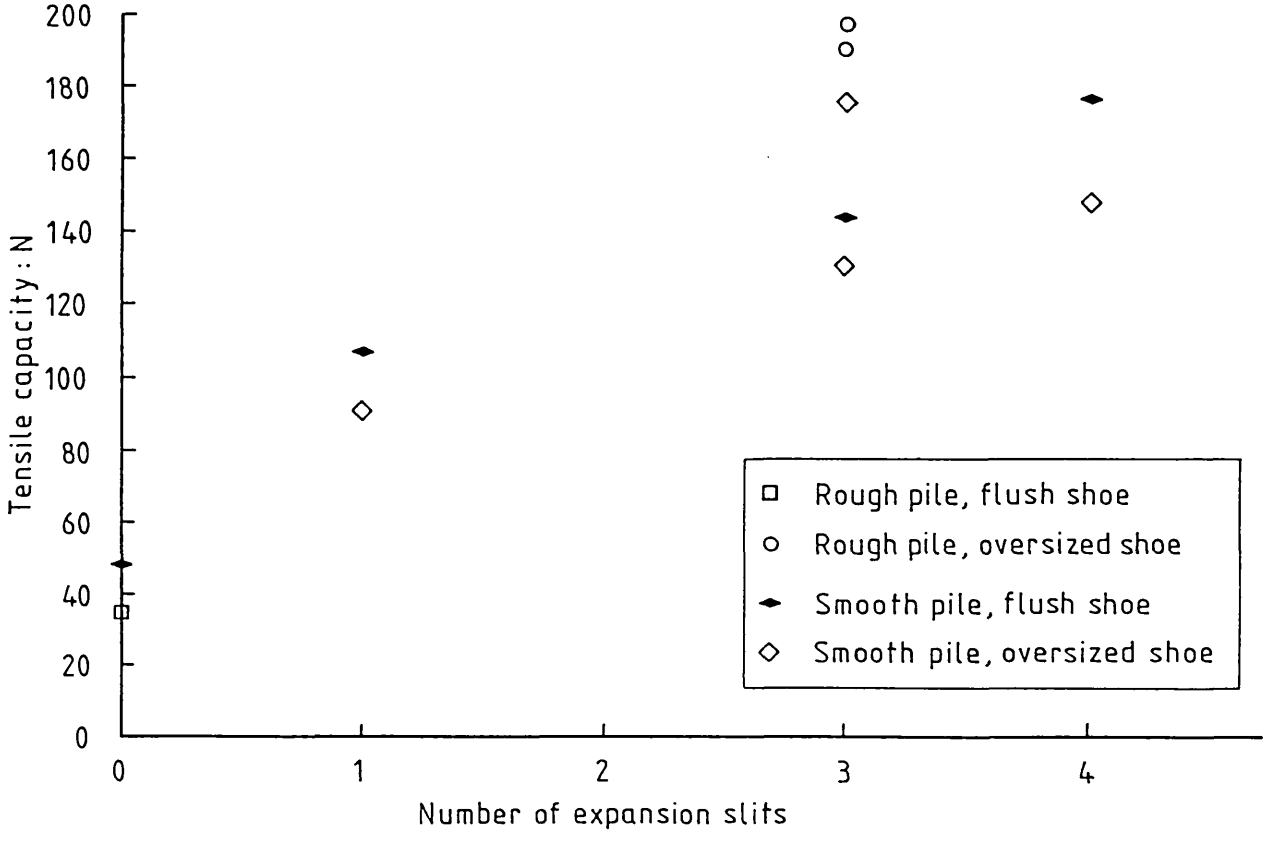

Figure 7.3 Summary of results: damp sand
Model pile capacity against Number of expansion slits

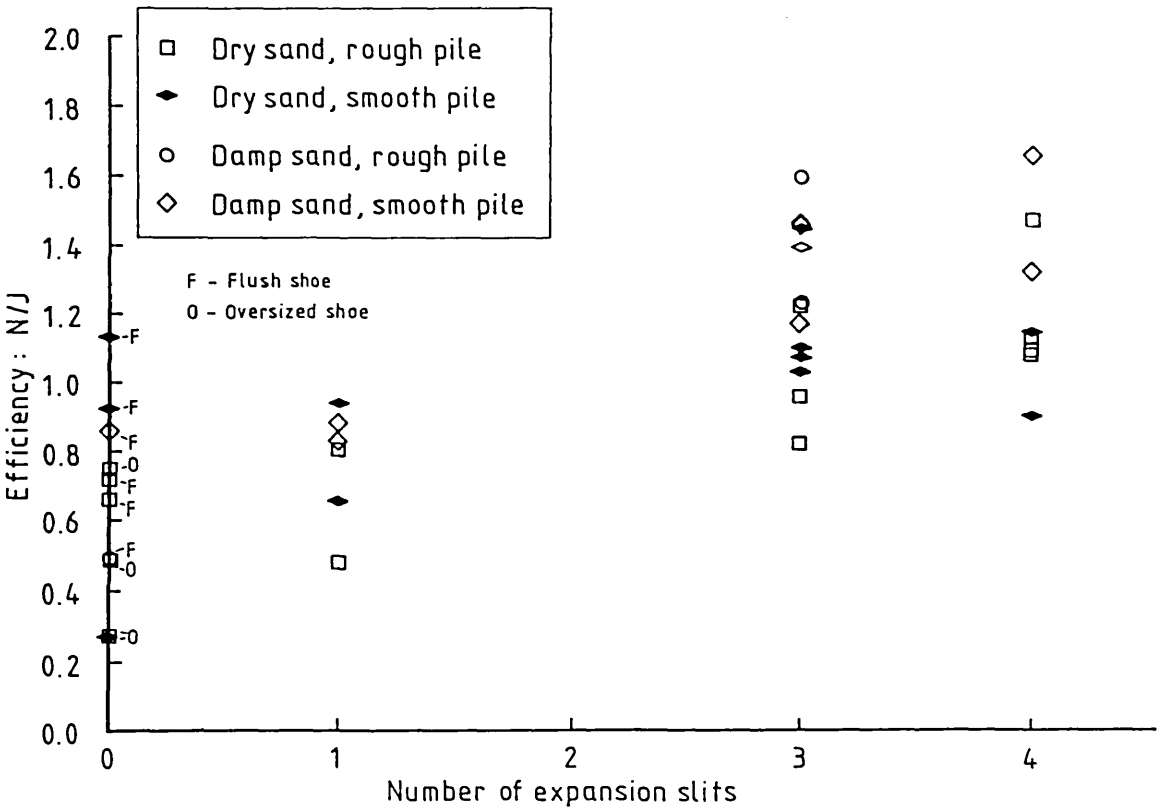

Figure 7.4 Summary of results: dry sand and damp sand
Pile Efficiency against Number of expansion slits

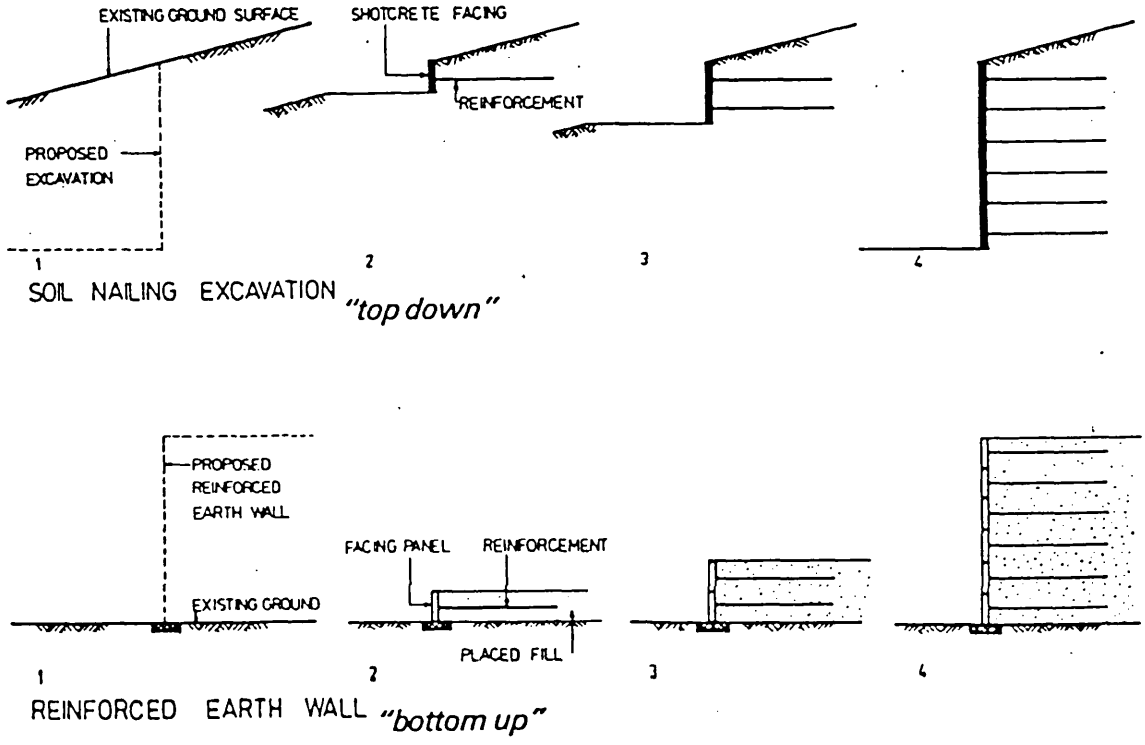

Figure 7.5 Contrast between soil nailing and reinforced earth (after Bruce and Jewell, 1986)

CHAPTER 8
CP&F/CONOCO FIELD TRIALS

8.1 Introduction

8.1.1 Background

While investigations into the Wedge-Pile were proceeding at Imperial College, Cementation Piling and Foundations Ltd (CP&F) showed interest in developing its commercial possibilities. The theoretical basis for the Wedge-Pile and the capability to predict pile load capacity were taken as confirmed by CP&F following the laboratory and field work described previously in this thesis. What was now at issue was whether or not the Wedge-Pile was a commercial proposition. This depended upon the suitability of CP&F's piling equipment and methods to exploit the Wedge-Pile system. Accordingly, CP&F were not primarily concerned with proving the Wedge-Pile, rather to prove the commercial viability of a chosen method of installation covering the whole process from procurement of materials to connection of the finished pile to the structure to be supported.

After various discussions with CP&F, it was decided that a wedge-pile developed for housing and light industrial foundations represented the easiest possible entry into the market. This would involve piles in the 5 to 6m length range with diameters between 100 to 250mm. The functioning of the foundation could range from that of a traditional pile to that of a ground treatment/soil reinforcing system (e.g. stone columns). A likely use of such a pile is in poor or made ground.

The building market in the United Kingdom is highly competitive and quantity surveyor dominated, with a character unlike that of civil or offshore engineering. Any proposed novel piling system will be judged solely on the basis of cost. In the light of this fact, it was considered by CP&F that a wedge-pile involving the use of steel would be far too expensive for a housing type pile, and it was therefore decided to explore the use of other materials. It was also considered by CP&F that a large-displacement circular cross-section pile was most suitable.

It was eventually decided by CP&F to proceed with full-scale trials of a wedge-pile involving the use of a 5 to 6m long, 200mm diameter circular plastic tube to form the outer shell; and low-grade concrete pipe

segments to form the expander mandrel. The inside of the wedge-pile would be lightly reinforced and grouted up after installation. The essential aim of the trials would be to prove equipment prior to further trials on a contract site, with the eventual aim of gaining approval for use of the system on an actual contract. The economics of the system can only be determined by assessing pile installation speeds under real contract conditions.

Shortly before the trials were due to commence, two developments took place.

Firstly, it was suggested by the author that thin gauge steel tubular outer shells should be tried in addition to the plastic tubes proposed. Steel tubes were only marginally more expensive than plastic tubes (at 1988 prices), and the engineering advantages of steel might well outweigh the small disadvantage in material cost.

The second development was the interest of Conoco (UK) Ltd in the CP&F trials, in connection with the possible use of the Wedge-Pile as a foundation technique for offshore oil and gas production platforms. This was a continuing interest - Conoco had helped to fund the work on the 6m box and cruciform piles at Luton and BRS. Despite the success of the work at these sites, field trials with circular type piles were considered essential by Conoco if the Wedge-Pile were to be promoted for offshore use, because circular tube piles are universal in the oil industry. The interest shown by Conoco developed into an involvement in the field trials. Two circular wedge-piles to Conoco's general specification, plus an unexpanded control pile, were included in the trials. These additional piles were of similar overall dimensions to the CP&F piles.

In contrast to the full-scale, 'commercial' nature of the CP&F trials, the Conoco trials were to be concerned only with the principle of circular tube expansion. The test piles would obviously not be full-scale, and details of the arrangements that would be used in practice offshore would only follow after a detailed engineering study made in the light of the results of the field trials.

In the main, the CP&F piles were to be tested in compression. The Conoco piles were to be tested in compression and in tension, with particular emphasis on cyclic loading.

8.1.2 Pile functioning

In the case of the CP&F piles, cost of pile material was an overriding

concern. Accordingly, the outer shells of the piles - formed from relatively expensive steel or plastic - were made as thin as possible. The bulky expander mandrel was formed from cheap cementitious material.

With this system of wedge-pile, the thin outer shell acts as an interface with the ground, transferring load along its length to the expander mandrel. Transfer of load from the structure being supported to the top of the pile is via the expander mandrel. In order to drive the expander mandrel, the frictional resistance between the outer shell and the expander mandrel must be less than that between the outer shell and the ground. After installation, it is required that a bonding agent be introduced between the outer shell and the expander mandrel, to enable load transfer to take place along the length of the pile. In the field trials this was achieved by grouting.

There were two main differences between the Conoco piles and the steel CP&F piles. Firstly, the Conoco piles were fabricated from steel throughout, including the expander mandrel. Secondly, the outer shell wall thickness of the Conoco piles was relatively thick in comparison to that for the CP&F piles. The reason for this was that in the offshore situation the outer shell would be the axial load carrying member of the wedge-pile. The expander mandrel would take most of the lateral loads on the pile.

The most important underlying question at issue in both the Conoco and the CP&F trials was the relative effectiveness of the various possible modes of wedge-pile expansion (Section 1.3). There is a crucial difference between the expanding action of a circular type wedge-pile and that of a 'multiple-element' wedge-pile. In the latter case, the geometry of the expander mandrel and the outer shell is such that the outer shell elements are forced to expand symmetrically, in two or more directions depending on the arrangement adopted. In the case of a circular wedge-pile, with weak lines machined along the length of the outer shell, there is no such constraining geometry. Although several weak lines might be employed, the pile would invariably open up along only one. Even if the weak lines were full depth cuts, such that the circular shell was made up from separate segments, the lack of a constraining geometry would mean that the outer shell would not necessarily be expanded symmetrically. The manner in which an outer shell with a single weak line mobilises radial effective stress is not so clear as for multiple-element piles. It probably involves the formation of a plastic hinge on the opposite side of the outer shell to the opened weak line, such that soil resistance is mobilised essentially in two directions (Figure 8.1).

As part of the CP&F/Conoco trials, laboratory experiments were carried out to determine the relative effectiveness of circular wedge-piles with 1, 3, and 4 slits in the outer shell. The results of these tests have been summarised in Chapter 7. The results indicate that greater increases in capacity are possible with 3 and 4 slits, in comparison to a single slit. The field trials were focused on the use of outer shells with a single weak line. The benefits of ease of fabrication and handling involved with this system outweighed any other considerations.

Another important aspect of the functioning of a circular wedge-pile is the influence of the outer shell wall thickness and its flexibility on the mode of expansion. If a circular tube outer shell is sufficiently flexible, it will expand by increasing its radius to that of the expander mandrel driven into it. In contrast, if the outer shell is relatively stiff, plastic hinges may develop in the outer shell as it is expanded such that portions of the outer shell will have radii less than the radius of the expander mandrel.

In the case of a 1-slit outer shell, the strain energy of bending involved in maintaining it in its expanded position may have a dominant influence on installation energy. The strain energy is proportional to the cube of the wall thickness. The stiffness of the outer shell is also likely to have a profound influence on behaviour in the zone of expansion, in the region of the expander mandrel nose. This aspect of behaviour is beyond the scope of this thesis, but it is clear from the work to be presented in Chapter 10 that a relatively stiff outer shell is more likely to over-expand than a relatively flexible one.

In the case of outer shells with relatively thick walls, the use of more than one weak line would have the advantage of reducing elastic bending in the expanded outer shell, even if the outer shell still opened up along only one weak line. This would reduce the driving energy required to install the expander mandrel. However, additional weak lines would increase the fabrication cost of the outer shell, and would progressively weaken it, making handling and installation more difficult.

The points raised in this Section are discussed in more detail in Chapter 11, in the light of the results from the field trials.

8.1.3 The field trials

The joint CP&F/Conoco field trials were carried out at CP&F's Hermitage depot near Newbury in Berkshire, between October and December 1988. The

author was responsible for most of the development of design details for the piles, and for all pile installation and testing operations. The investigations are described in the rest of this Chapter, with the aid of photographs.

Sections 8.2, 8.3 and 8.4 provide details of the CP&F plastic wedge-piles, the CP&F steel wedge-piles and the Conoco piles respectively. Section 8.5 describes the pile installation rig; pile installation procedures for the CP&F piles and the Conoco piles are described in Sections 8.6 and 8.7 respectively. Section 8.8 provides details of the test site and the arrangement of the driven piles, Section 8.9 gives notes on driving. Section 8.10 describes how the driven piles were prepared for testing. Pile testing arrangements are given in Section 8.11. The results of the field trials are provided in Section 8.12.

The results are discussed in Chapter 11.

8.2 CP&F Plastic Pile - Principal Components

8.2.1 Outer shell

Each outer shell comprised a 5m length of 200mm nominal o.d., 3mm nominal wall thickness polythene sewer pipe (to either DIN4102-B1 or DIN8077) (Plate 8.1). At its bottom end each outer shell was closed off by means of a steel driving shoe (Plate 8.2). Each driving shoe comprised a 10mm thick circular bottom plate of average overall diameter 210mm; a stub length of tube welded to the plate which located inside the polythene tube; and a 100mm long, 1.5mm thick outer sleeve welded to the plate, which located outside the polythene tube.

A single weak line was cut along the length of the polythene tube as it was installed in the ground. The method by which this was achieved is described in Section 8.5.

8.2.2 Expander mandrel

Each expander mandrel consisted of a steel nose section, and a shank section comprising lengths of concrete pipe.

The vertically cast concrete drainage pipes were unreinforced, parallel sided, and ogee jointed (Plate 8.3). The pipes were manufactured to BS5911:Part 3. The nominal outside diameter of the pipes was 210mm, length 1m, wall thickness 29mm, weight 38kg. Detailed measurements on a sample of a dozen pipes revealed average pipe diameters in the range 209mm to 215mm, and an average variation in diameter along the length of individual pipes of 3.5mm. Typical 28 day cube strengths of the

concrete mix for the pipes were quoted by the pipe manufacturers as 40 to 50N/mm^2. A pipe prepared with parallel ends and crushed axially at Imperial College failed at a load of 750kN.

The plastic pipes were very flexible and on expansion increased their radius to that of the concrete pipes. The outside diameter of the concrete pipes gave rise to an average increase in diameter of the plastic tube of 8%. The corresponding average increase in diameter in comparison to the diameter of the driving shoe was 3% - less than the target value of around 10% expansion. This was unavoidable, however, as the concrete pipes that were used were the only suitable ones available.

The nose section was machined from steel tube (Plate 8.4). The nose profile was designed with the aid of a computer model described in Chapter 10, and is shown in Figure 8.2. The overall length of the nose section was 350mm. At its top end the nose had a tapered joint to suit the concrete pipe joints, at its bottom end the nose was closed off with a plate. Two holes were drilled in the plate to allow grout to pass through it.

8.3 CP&F Steel Pile - Principal Components

8.3.1 Outer shell

Each outer shell comprised a 6m length of 195mm nominal i.d. helically welded HR4 mild steel tube (Plate 8.5). A number of tubes were purchased, with wall thicknesses of 16gauge, 14gauge and 10gauge (1.63mm, 2.03mm and 3.25mm) . A single weak line was formed along the length of the tube by flame cutting. The slag generated by the cutting prevented the tube from springing apart when the weak line was formed (Plate 8.6). The bottom of each steel tube was closed off by means of a steel driving shoe very similar to that for the plastic piles. In this case, however, the bottom plate was the same nominal outside diameter as the steel tube. Instead of an outer sleeve, three small 'prongs' were used to locate the outside of the tube (Plate 8.7).

8.3.2 Expander mandrel

The arrangement for the expander mandrel was exactly the same as for the plastic pile. On expansion, the outside diameter of the concrete pipes gave an average increase in diameter of the steel tubes of approximately 7.5%, assuming that the steel tubes opened out to the radius of the concrete pipes.

8.4 Details of Conoco Piles

8.4.1 Outer shell

Three outer shells were fabricated. Each outer shell was formed from a 7m length of 193.7mm o.d., 5.6mm wall thickness, hot finished seamless mild steel tube (BS 3601 HFS Grade 410, minimum yield stress 235N/mm^2) supplied without a coating of mill varnish (Plate 8.8). Each outer shell was closed at its bottom end by means of a 100mm long welded internal plug turned down from solid.

One of the outer shells had a single weak line along its length, one had three weak lines at 120° spacings around the perimeter, while the final outer shell was an unexpanded control pile and had no weak lines.

The weak lines were cut by means of a large milling machine in the CP&F workshops. Each weak line was approximately 3mm wide (the width of the cutting disc) (Plate 8.9). The depth of cut varied, because of slight irregularities and bends in the steel pipes. The maximum thickness of steel left after cutting was approximately 1mm. This arrangement provided sufficient strength to maintain the integrity of the outer shell during handling and installation. At full scale, it might not be economic to employ near full-depth weak lines in the outer shell. It is thought that it may be possible to employ instead relatively shallow 'scored' weak lines, along which a split would be propagated progressively as the expander mandrel was advanced. This possible technique was not investigated in the field trials.

In the case of the outer shell with three weak lines, over the top 2m of the tube the weak lines were cut through completely after machining, with a hand held disc cutter. Short lengths of 'intact' weak line were left at a few points over this length in order to hold the outer shell together. Three radial fins (fabricated from 50x10mm steel strip) were welded to the three outer shell segments over this length (Plate 8.10). The purpose of the full-depth cuts was to encourage the outer shell to expand symmetrically in three directions at the top of the pile. The purpose of the fins was to anchor the top 2m of the outer shell in the circumferential direction: this was intended to prevent the expansion process returning to a 'one-way' mode further down the pile.

8.4.2 Expander mandrel

Two identical expander mandrels were fabricated. The shanks were formed from 7.5m lengths of 203.2mm o.d., 6.3mm wall thickness hot finished seamless mild steel tube (DIN 17121 St52-3, minimum yield stress 335 N/mm^2). The tubes were coated with mill varnish. The nose sections were

1m in length and were turned down from 203.2x12.5mm tube (Plate 8.11). The nose profile used is shown in Figure 8.3. It was designed with the aid of the computer model described in Chapter 10, following the procedure given in Section 10.4.4. For the purposes of nose profile design it was assumed that the 3 weak line outer shell would split symmetrically into three separate segments during expansion. It was recognised that in practice this assumption might not be valid. In the absence of a more appropriate design method, and in order not to introduce a further variable into the tests, it was decided to use the same nose profile for the 1 weak line outer shell as for the 3 weak line outer shell.

The nose section was mounted coaxially on the end of the shank by means of a tight fitting internal sleeve. It was then welded to the shank section, the weld being ground down flush to the tube wall subsequently.

If the assumption is made that on expansion the internal diameter of the outer shells increased their radius to match that of the external diameter of the expander mandrel, the increase in diameter of the outer shells is calculated to be 10.7%. In the case of the 3 weak line outer shell, if the assumption is made that the radii of the three segments did not change on expansion, the 'crown' of each segment is calculated to move to a radial position 20% greater than that prior to expansion (Figure 8.4).

8.5 Description of Piling Rig

The rig used to install the test piles was designed and assembled at the Hermitage depot. It was built up on a 22-RB crawler mounted crane (Plate 8.12). The essential features of the rig are described below.

The principal component was a vertical mast, attached near its top to the crane jib and at its bottom to struts mounted on the crane body. At the top of the mast was a cathead with two sheave arrangements, over which two independent ropes passed. The first rope was connected to a 3.3t drop hammer. The drop hammer ran within guides running the whole length of the mast. The second rope was connected to a piling head (Plate 8.13) , which also ran within the mast guides. The piling head had a dual function, and featured a lifting pin arrangement and a hardwood dolly. The lifting pin arrangement enabled the pile being driven to be suspended and pitched. Once the pile was pitched, the piling head was lowered down onto the top of the pile. During driving the drop hammer acted against the hardwood dolly.

At the bottom of the mast a roller guide could be mounted (Plate 8.14). The roller guide was principally for use with the CP&F plastic piles and featured 3 tightly fitting rollers at 120° spacings. The roller guide initially located the bottom of the plastic tube during pitching, and was then left in place during driving. The three rollers were knurled, in order to roughen the outside of the plastic tube during installation. The roughening effect that was produced was largely cosmetic, the operation being designed to demonstrate only the principle of such a technique.

One of the rollers included a cutting disc, which cut a single weak line along the length of the plastic tube as it was driven. The disc cut most of the way through the wall of the tube. Details of the cutting and knurling roller are given in the next Section.

8.6 Pile Installation Procedure - CP&F Piles

8.6.1 Plastic outer shell

The plastic tubes were driven by means of a tightly fitting circular internal driving mandrel (Plate 8.15). The driving mandrel was first connected to the driving head, and lifted high up the mast. The light plastic tube was then pushed up by hand onto the driving mandrel from underneath, until it located inside a following ring welded near the top of the driving mandrel (Plate 8.16). At this point the driving mandrel protruded a few millimetres from the bottom of the plastic tube. The driving mandrel/outer shell was then lowered to the ground at the appropriate position for driving. As it was lowered it was located in the roller guide, and the driving shoe was fitted (Plate 8.17).

The driving mandrel/outer shell - held at the top by the piling head and at the bottom by the roller guide - was then driven into the ground. The driving shoe was driven by the driving mandrel acting against it. The plastic tube was driven by means of the following ring acting at the top (and to a limited extent the friction acting between the plastic tube and the tightly fitting driving mandrel). Plate 8.18 shows a plastic outer shell being driven through the roller guide, and shows the weak line being cut by the cutting disc. The usual driven level of the plastic tubes was approximately 4.9m below ground level. After installation was complete the driving mandrel was withdrawn from the plastic tube and disconnected from the driving head.

8.6.2 Steel outer shell

The driving procedure for the steel outer shells was very similar to that for the plastic outer shells.

The steel tubes were driven by means of a slackly fitting circular internal driving mandrel. The driving mandrel was first connected to the driving head, and lifted high up the mast. The steel tube was then pushed by two people onto the driving mandrel from underneath, until it located inside a following ring welded near the top of the driving mandrel. At this point the driving mandrel protruded a few millimetres from the bottom of the steel tube. The driving mandrel/outer shell was then lowered to the ground at the appropriate position for driving. As it was lowered it was located in the roller guide (which in this case was loosely fitting), and the driving shoe was fitted.

The driving mandrel/outer shell - held at the top by the piling head and loosely guided at the bottom by the roller guide - was then driven into the ground. The driving shoe was driven by the driving mandrel acting against it, the steel tube was driven by means of the following ring acting at the top. Plate 8.19 shows a steel outer shell being driven. The usual driven level of the outer shell was 5.9m below ground level. After installation was complete the driving mandrel was withdrawn from the steel tube and disconnected from the driving head.

8.6.3 Expander mandrel

After driving the plastic or steel outer shell, the weak line along the exposed length of outer shell was first fully opened out by hand. The steel expander mandrel nose section was then pushed by hand into the outer shell and positioned coaxially (Plate 8.20).

The expander mandrel was driven by means of a square section internal driving mandrel. This was first connected to the driving head and lifted up the mast.

The concrete pipe lengths following behind the nose section were driven two at a time. The first two concrete pipes were positioned by hand on top of the nose section - Plate 8.21 shows the first pipe being placed. Simple rope gaskets (Plate 8.22) were placed between the concrete pipes to minimise damage to the ends of the pipes during driving. At the top of the second pipe was a dolly arrangement (Plates 8.23, 8.24). This consisted, in ascending order, of a stiff nylon ring machined to match the concrete pipe joint; a ring cut from stiff foam rubber sheet; and a steel bearing plate.

After the first two concrete pipes and the dolly arrangement had been set up, the driving mandrel was lowered down inside the pipes until its bottom end rested against the bottom plate of the nose section. At this

point in the operation a bearing pin was fitted through a locating hole in the driving mandrel above the dolly (Plate 8.24). When the bottom of the driving mandrel was resting on the bottom plate of the nose section, there was a few millimetres clearance between the bearing pin and the dolly bearing plate.

Before driving, sand/cement grout was brushed onto the outside of the concrete pipes (Plate 8.23). The purpose of the grout was to provide a bond between the outer shell and the expander mandrel after installation. The nose section and the first two concrete pipes were then driven into the outer shell. The nose was driven from the bottom by the driving mandrel; the concrete pipes were driven from the top by the bearing pin.

After the first two concrete pipes had been driven, further pipes were driven in the same manner until the nose section met with the outer shell driving shoe. The driving mandrel was then withdrawn. As additional pipes were installed, the bearing pin was positioned in locating holes positioned progressively further up the driving mandrel.

8.7 Pile Installation Procedure - Conoco Piles

8.7.1 Outer Shell

The outer shells of the Conoco piles were driven from the top. Each outer shell was first connected to the driving head and lifted up the mast. The pile was then pitched vertically. The roller guide was not used. The outer shell - guided at the top only - was then driven.

8.7.2 Expander mandrel

After driving the outer shell, the driving head was disconnected from the outer shell and then connected to the expander mandrel. The expander mandrel was then lifted up the mast. 'Seeze-Free' metallic lubricant was sprayed on it beforehand, in order to reduce friction between the outer shell and the expander mandrel during driving. The expander mandrel was then lowered, and the nose section engaged in the top of the outer shell.

The expander mandrel - supported at the top by the driving head and at the bottom by the outer shell - was then driven from the top.

8.8 Details of Site and Pile Layout

8.8.1 Site

The piles were tested in ground at the CP&F Hermitage depot. The general

geology of the site area is Woolwich and Reading beds of silty sands to a depth of approximately 10m over chalk. The material at the test pile site had recently been excavated and replaced in order to exhume some other large piles. Particle size distibutions of samples of the excavated material are shown in Figure 8.5. No standing groundwater was encountered during the field trials.

After completion of the wedge-pile test programme, static cone penetration testing was carried out in order to characterise the site (Section 8.12.3).

8.8.2 Reaction piles

Before any test piles were driven, a grid of reaction piles was installed, designed to cope with a maximum test pile failure load of 1000kN. Nine 14m long, 600mm diameter Continuous Flight Auger (CFA) tension piles were installed, each with a design capacity of 500kN. The reaction piles were installed at 4m spacings in a square pattern which defined the test area.

8.8.3 Test piles

The test piles were driven between 26.10.88 and 2.11.88. Seventeen piles were driven in all, this number being made up of:

4 unexpanded CP&F plastic piles
2 unexpanded CP&F steel piles
6 expanded CP&F plastic piles
2 expanded CP&F steel piles
1 unexpanded Conoco pile
1 expanded, 1 weak line Conoco pile
1 expanded, 3 weak line Conoco pile.

Figure 8.6 shows the layout of the reaction piles and the test piles, and gives the driving dates of the test piles. Figure 8.7 shows diagrammatically the depths of embedment of the test piles.

8.9 Notes on Driving

8.9.1 Inconsistent ground conditions

As the test piles were driven it became apparent that instead of the piles being installed entirely in excavated and replaced material, as was the intention, piles in certain areas of the site were hitting virgin ground. This was obvious from the variation in driving resistances over the site, and was confirmed by the CPT tests that were carried out subsequently (Section 8.12.3).

8.9.2 CP&F piles

Difficulties were experienced in driving both the plastic outer shells and the concrete expander mandrel pipes of the CP&F piles. As can be seen from Figure 8.7, this resulted in many of the piles not being driven to design depth.

The problem often encountered during driving of the plastic tubes was splitting and buckling of the tubes. This usually occurred in the region of the roller guide as the weak line was cut, occasionally it occurred at the top of the tube in the vicinity of the following ring. The likelihood of this problem occurring was obviously greater during hard driving. Suprisingly, it often proved possible to complete the driving of damaged plastic pipes, even those quite badly split, provided the hammer drop height was reduced to a minimum.

Inspections with the aid of a torch inside the plastic tubes installed in the ground revealed that they were consistently in good condition - the diameters were not reduced at any point along the lengths of the tubes and it was usually possible to see the driving shoe at the bottom.

The problem often encountered during driving of the concrete pipes was one of shattering. Cracking usually propagated from the top pipe of each pair being driven, directly beneath the driving dolly. The problem was most likely to occur during hard driving. Because of the problem of shattering, the concrete pipes were driven to full depth on only 3 out of 8 occasions.

No problems were encountered when driving the steel outer shells of the CP&F piles.

The 'standard' hammer drop height for the installation of the CP&F piles was approximately 200 to 300mm, controlled by the eye of the crane driver. Blow rate was approximately 25 blows/minute. However, it was often necessary to reduce the drop height as driving progressed, in order to prevent damage to the plastic or concrete pipes. The total number of blows and the approximate average drop height for each of the CP&F piles are listed in Table 8.1. The variation in driving resistance can be observed.

Drawdown of the outer shell during expansion was typically in the range 50 to 100mm.

8.9.3 Conoco piles

Driving information for the Conoco piles is given in Figure 8.8 and Table 8.2. It can be seen that the unexpanded outer shell hit exceptionally dense ground, and that the two expanded piles were installed in relatively loose ground.

Problems occurred during driving of the expander mandrel into the 1-weak line outer shell. When the expander mandrel had penetrated to a depth of approximately 3.9m below ground level, it began to drag down the outer shell into the ground. Driving of the expander mandrel was stopped at a depth of penetration of 4.7m by which time the outer shell had been dragged down by a distance of 275mm, such that the top of the outer shell was at ground level.

Dragdown of the 3-weak line outer shell during expansion was negligible. On a visual inspection, it could be seen that at the top of the pile the outer shell had opened up along 2 of the 3 weak lines (Plates 8.25, 8.26).

8.9.4 Notes on preliminary trials

Some preliminary trials on the CP&F plastic piles were carried out before the main test programme, in relatively loose ground away from the test area. Some notes on these trials are given below, as these provide some background to the main trials.

8.9.4.1 Driving of plastic tube

6m lengths of 200mm diameter uPVC vent pipe were originally used to form the outer shells of the plastic piles. A flush driving shoe without an outer sleeve was tried at first. In this configuration the uPVC tubes invariably broke up during driving. Also, sand was forced into the uPVC tubes at the bottom. To overcome these problems, an oversized driving shoe with an outer sleeve was introduced. Various slightly oversized driving shoes were tried out. The greater the diameter of the driving shoe, the easier it was to drive the outer shell. It was eventually possible to pull or 'crowd' the outer shell into the ground, by means of one of the crane ropes acting downwards on the driving head via a sheave mounted at the bottom of the mast.

8.9.4.2 Cutting of weak line

The roller cutter was reasonably successful in cutting a weak line along the uPVC pipe, although there was a tendency for cracks to migrate away from the intended line.

8.9.4.3 Expansion of plastic pipes

In the relatively loose ground where the preliminary trials were carried out, it proved quite easy to drive the concrete pipes to full depth. However, when some installed concrete pipes were subsequently removed to inspect the inside of an expanded uPVC tube it was found that the tube had not opened up along the weak line. Instead, there was a crazed pattern of splitting, not near the weak line. After some experiments in the workshop, it was concluded that incomplete cutting of the uPVC tube by the roller disc had the effect of work-hardening the plastic in the region of the weak line, discouraging the opening up of the weak line on expansion.

In the light of this conclusion, polythene pipe was used to replace the uPVC pipe. The cutting of the weak line in polythene pipe was much 'cleaner' than for uPVC pipe, and the polythene pipe opened up along the weak line during expansion.

8.9.4.4 Driving expander mandrel

During the preliminary trials, a steel nose section without a bottom plate was used initially. This was not sucessful as it was found that the sharp leading edge of the nose tended to catch and ruck the plastic tube in the region of the weak line.

The design of the dolly arrangement for the concrete pipes evolved during driving trials. Attempts to drive the concrete pipes and nose section as one from the top were a failure. The 'two-pipe' system of driving proved to be the most convenient system possible in the circumstances - driving one pipe at a time involved twice as many retractions of the driving mandrel to load the pipes; driving three pipes at a time was usually not possible because the pipes often became unstable during driving.

8.10 Preparation of piles for testing

8.10.1 Grouting of CP&F piles

After installation, the 14 CP&F piles were filled with sand/cement grout (1:1 by weight), placed by means of a grout pump. Twelve CP&F piles were to be tested in compression only: a 25mm diameter ribbed reinforcing bar was placed inside these piles prior to grouting. The remaining two piles were to be tested in tension only: a 40mm diameter continuous thread Macalloy FT bar was placed inside each of these two piles, to act both as a reinforcing bar and as a load carrying tension bar. Both types of reinforcing bar were held centrally within the piles by means of spacers.

Each pile was grouted to a level that was 100 to 150mm below the level of the top of the outer shell. After the initial filling of the expanded piles with grout, it was observed that the grout levels often dropped with time, and needed to be topped up. This was particularly so in the case of the steel piles. This phenomenon was presumably due to grout passing through the grout holes in the bottom of the steel noses of the expander mandrels, to fill the voids beneath.

8.10.2 Pile head detail: CP&F piles
After grouting, the heads of the CP&F piles were prepared for testing as shown in Figure 8.9.

Where necessary, the top concrete pipe was broken back below the level of the top of the outer shell. The 25mm diameter reinforcing bars were also cut back below this level; the 40mm Macalloy bars were left extending upwards, so as to provide a tension connection with the pile testing system. Two slots were cut in the side of the pile to allow a reference plate mounting rod to be placed. Sand/cement grout was then placed by hand to fill the void at the top of the pile, short lengths of reinforcement being placed beforehand if considered necessary. In the case of the piles being tested in compression, a 10mm thick bearing plate was then worked down onto the grout, and bedded into contact with the top of the outer shell.

8.10.3 Pile head detail: Conoco piles
After driving, the tops of the 3 outer shells of the Conoco piles were between 0 and 500mm above ground level.

The tops of the two expander mandrels were first cut down to a level of 400mm above the top of the respective outer shells. The expander mandrels were then welded to the outer shells. In the case of the 3 weak line outer shell the welding was along the exposed edges of the three separated outer shell segments; in the case of the 1 weak line outer shell 'saw-teeth' were flame cut in the outer shell to facilitate the weld connection.

Tensile and compressive loads were applied to the Conoco piles by means of a load transfer tube (Figure 8.10). This was welded inside the top of the outer shell, saw-tooth cuts facilitating the welding. The load transfer tube featured top and bottom bearing plates. Tensile loads could be applied by means of a tension rod connected to the bottom bearing plate, compressive loads could be applied by means of a jack acting against the top bearing plate.

8.11 Pile Testing Arrangements

8.11.1 CP&F compression testing

Overall views of the arrangement for the CP&F compression tests are shown in Plates 8.27 and 8.28.

The CP&F piles that were to be tested in compression were installed in positions located centrally between a pair of reaction piles (see Figure 8.6). Reaction during compression tests was provided by means of a single test beam spanning between these two reaction piles, strapped down to 32mm diameter Macalloy tension bars cast into the reaction piles. Load was applied to the test pile by means of a hand operated jack, and measured by means of a load column. The test beam was supported at a level that enabled the jack and load column to be placed between it and the bearing plate at the top of the pile being tested.

Pile deflection was measured by means of two dial gauge extensometers, connected to a 6m long scaffold tube reference beam supported by 1.5m long scaffold tube piles driven into the ground. The dial gauge plungers acted against two symmetrically disposed reference plates welded to the mounting rod cast into the top of the test pile.

8.11.2 Conoco tension/compression testing

The Conoco piles were driven within quadrants formed by four reaction piles (see Figure 8.6). A reaction system employing four test beams enabled tensile or compressive loads to be applied to the piles (Plate 8.29).

Two primary beams were spanned between two pairs of reaction piles. The primary beams were carefully bedded down onto the tops of the reaction piles, with the aid of wooden packing, to enable compressive loads to be applied to the reaction piles. To enable tensile loads to be applied to the reaction piles, the primary beams were strapped down to the Macalloy tension bars.

Two secondary beams were spanned between the primary beams. The two sets of beams were strapped together to enable compressive or tensile loads to be transferred between them. The secondary beams were positioned either side of a central tension bar, comprised of 40mm diameter Macalloy bar, extending upwards from the pile being tested. The central tension bar was screwed into the load transfer tube at the top of the test pile.

Two hand operated jacks were used (Plate 8.30). The bottom jack applied compressive loads to the pile, and was mounted on top of the load transfer tube. It acted downwards against the load transfer tube and upwards against the secondary beams. The top jack applied tensile loads to the pile, and was mounted on top of the secondary beams. It acted upwards against a bearing washer screwed onto the top of the central tension rod, and downwards against the secondary beams.

The hydraulic jacks were annular in shape, to allow the central tension bar to pass through them to the top bearing washer. Tensile and compressive loads were measured by means of two separate annular shaped standard 1000kN NCB/MRE Type 440 load cells, in conjunction with 'Peekel' monitoring gauges. The two load cells were mounted on top of the tension and compression jacks. Large bearing plates were used to spread the loads from the jacks to the secondary beams.

Pile deflection was measured by means of three dial gauge extensometers, connected to two 6m long scaffold tube reference beams supported by 1.5m long scaffold tube piles driven into the ground. The dial gauge plungers acted against three symmetrically disposed reference plates welded to supporting bars welded to the top of the test pile (Plate 8.30).

8.11.3 CP&F tension testing

The CP&F piles to be tested in tension were driven within a quadrant formed by four reaction piles (see Figure 8.6). A reaction system employing four test beams was employed, as for the Conoco piles, enabling tensile loads to be applied to the Macalloy bars cast into the piles. The top tension jack only was used. Displacement measurement was as for the tests in compression.

8.12 Test results

8.12.1 CP&F pile tests

The standard pile loading procedure for the CP&F piles consisted of a Constant Rate of (Incremental) Loading (CRL) stage followed by a Constant Rate of Penetration or Constant Rate of Extraction stage (CRP or CRE) stage.

The loading increment for the CRL stage was selected on the basis of the estimated failure load, with a target of 6 to 10 increments to failure. Each increment of load was held for 5 minutes. CRL loading was continued until the creep displacement rate during the holding period was approximately 0.5mm/minute. At this point CRP or CRE loading was

applied, the standard rate of displacement was 1mm/min. CRP/CRE loading was continued for a pile displacement of approximately 20mm. It was observed during the tests on expanded piles that in all cases the outer shell and the expander mandrel were displaced as one.

Load displacement curves for the CP&F pile tests are given in Appendix 8.1. A summary of the pile tests is given in Table 8.1. Selected pile tests are discussed in Chapter 11.

8.12.2 Conoco pile tests

The Conoco piles were subjected to sophisticated patterns of loading based on suggestions by Conoco (Mueller, 1988), of relevance to offshore pile design. The loading patterns involved static testing to failure both in tension and in compression, load controlled tension cycling with a tension bias, and displacement controlled tension/compression cycling to subject the pile to severe strength degradation.

A summary of the results of tests on the Conoco piles is given in Table 8.2. The testing history of each Conoco pile is described below. Upward loads and displacements are considered to be positive, downward loads and displacements are considered to be negative.

Pile 13 Type:Unexpanded Date of test: 16-17.11.88 Figures 8.11, 8.12

(a) Testing of Pile 13 started on 16.11.88. The pile was first subjected to a static tension test to failure. Initially, CRL loading was applied. 9 increments of +50kN (nominal) were applied to a give a total load of +449.7kN. Each increment of load was held for 5 minutes, except the last increment which was held for 1 minute, during which time +0.81mm of creep displacement occurred.

At this point the hand pumping rate of the jack was increased to give a CRE displacement rate of +1mm/minute. CRE loading was applied for a displacement of +4.4mm during which time a peak tensile load of +458.1kN was recorded. The pile was then unloaded in 7 increments of approximately -75kN, each held for 3 minutes.

(b) Tension only cycling was then applied. First, 11 cycles of loading between +182.6kN and +274.4kN were applied (40% and 60% of the static capacity in the previous test). Then 10 cycles of loading between +136.7kN and +320.4kN were applied (30% and 70% of the previous static capacity). Each cycle of loading lasted approximately five minutes.

(c) After the tension cycling, a static test to tension failure was

performed. Commencing from a bottom of cycle load of +136.7kN, 4 increments of load to give a total load of +449.7kN were applied. Each increment was held for 2 minutes. CRE loading for a displacement of +3mm was then applied with a maximum load of +475.6kN being recorded, a 4% increase in load in comparison to the static test before tension cycling. The pile was then unloaded in 4 increments, each held for 1 minute. Testing was then stopped for the night.

(d) 18 hours later, on 17.11.88, tension/compression cycling was applied to the pile. The cycling was displacement controlled, 5 cycles of loading between +/- 5mm being applied. Top/bottom of cycle loads decayed during cycling (Figure 8.12). Energy loss per cycle tended towards a constant value, as indicated by the fact that the load:displacement plot followed similar hysteresis loops towards the end of cycling.

(e) After the tension/compression cycling, a static test to tension failure was performed. During 7mm of CRE loading a maximum load of +325.2kN was recorded, a drop in capacity of 32% in comparison to the static test performed before tension/compression cycling. The pile was then unloaded in 4 increments, each held for 1 minute.

(f) Finally, a static test to compression failure was carried out. First, 4 increments of -100kN (nominal) were applied to give a total load of -391.7kN. Each increment was held for 3 minutes. CRP testing was then applied. Approximately -33mm of CRP loading was applied, giving an overall displacement during the whole loading sequence of -18mm. The applied load at this point was -633.3kN. The pile was then unloaded in 6 increments of +100kN (nominal), each increment being held for 2 minutes.

Pile 4 Type: 1 weak line Date of test: 2.12.88 Figures 8.13, 8.14

(a) The pile was first taken to static tension failure. CRL loading was initially applied, 3 increments of +30kN (nominal) being applied to give a total load of +89.5kN. Each of these increments was held for 5 minutes. A further increment of +30kN was then added, but large displacements occurred as it was applied and it was decided to proceed with the CRE stage of the test. A peak load of +138.6kN was recorded during CRE loading of approximately +15mm. The pile was then unloaded in 6 increments, each held for 2 minutes.

(b) The pile was then taken to static compression failure. CRL loading was initially applied, 4 increments of -30kN (nominal) being applied to give a total load of -127.2kN. Each increment was held for 3 minutes.

Overall displacement at this point was approximately zero. CRP loading for a displacement of approximately -20mm was then applied. Maximum load recorded was -173.9kN. The pile was then unloaded in 5 increments, each held for 2 minutes.

Pile 11 Type: 3 weak lines Date of test: 1.12.88 Figures 8.15, 8.16

(a) The pile was first subjected to a static tension test to failure. Initially, CRL loading was applied. 2 increments of +75kN (nominal) were applied to give a total load of +149.6kN, this increment being selected on the basis of an expected failure load in the region of +500kN. Both increments of load were held for 5 minutes. During the holding period for the second load increment approximately +12mm of creep displacement occurred: the pile had obviously failed.

At this point the hand pumping rate was decreased to give a CRE displacement rate of +1mm/minute. CRE loading was applied for a displacement of +4.5mm during which time a peak tensile load of +162.2kN was recorded. The pile was then unloaded in 5 increments of approximately -30kN, each held for 2 minutes.

(b) Tension only cycling was then applied. First, 8 cycles of loading between +63.0kN and +95.4kN were applied (39% and 59% of the static capacity in the previous test. Then 8 cycles of loading between +47.4kN and +111.0kN were applied (29% and 68% of the previous static capacity). Each cycle of loading lasted approximately four minutes.

(c) After the tension cycling, a static test to tension failure was performed. During +3.5mm of CRE loading a maximum load of +158.8kN was recorded, a negligible decrease in load in comparison to the static test before tension cycling. The pile was then unloaded in 7 increments of -20kN (nominal), each increment being held for 1 minute.

(d) Tension/compression cycling was then applied to the pile. The cycling was displacement controlled, 5 cycles of loading between +/- 5mm being applied. Top of cycle loads showed a trend to decay during cycling, at a decreasing rate (Figure 8.16). The trend for bottom of cycle loads to decay was very much less. Energy loss per cycle, as indicated by the load:displacement loops, had not fully stabilised by the end of cycling.

(e) After the tension/compression cycling, a static test to tension failure was performed. During approximately +3mm of CRE loading a maximum load of +78.1kN was recorded, a drop in capacity of 51% in

comparison to the static test performed before tension/compression cycling. The pile was then unloaded in 4 increments of -20kN (nominal), each increment being held for 1 minute.

(f) Finally, compressive CRP loading was applied for a displacement of -28mm, until the compression jack ran out of travel. The applied load at this point was -172.0kN, the overall displacement during the whole loading sequence was approximately -5mm. The pile was then unloaded in 4 increments, each held for 1 minute.

8.12.3 CPT tests

The results of the CPT tests made on 28.11.88 are given in Appendix 8.2. It can be seen from these test results that ground conditions within the pile test area varied from very loose to very dense. The maximum cone resistances recorded in the top 6m of the profiles have been used to classify the density of the sand, following the scheme of Schmertmann (1970). This is shown in Figure 8.17.

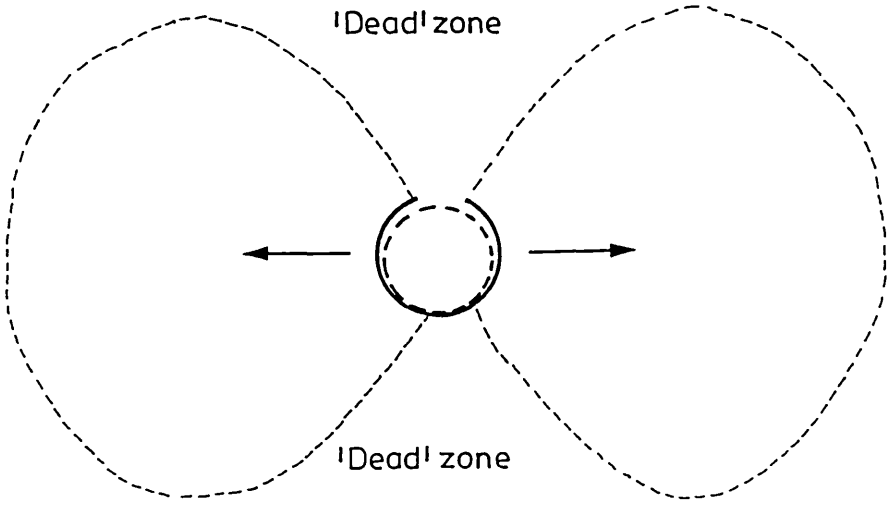

1 - slit outer shell

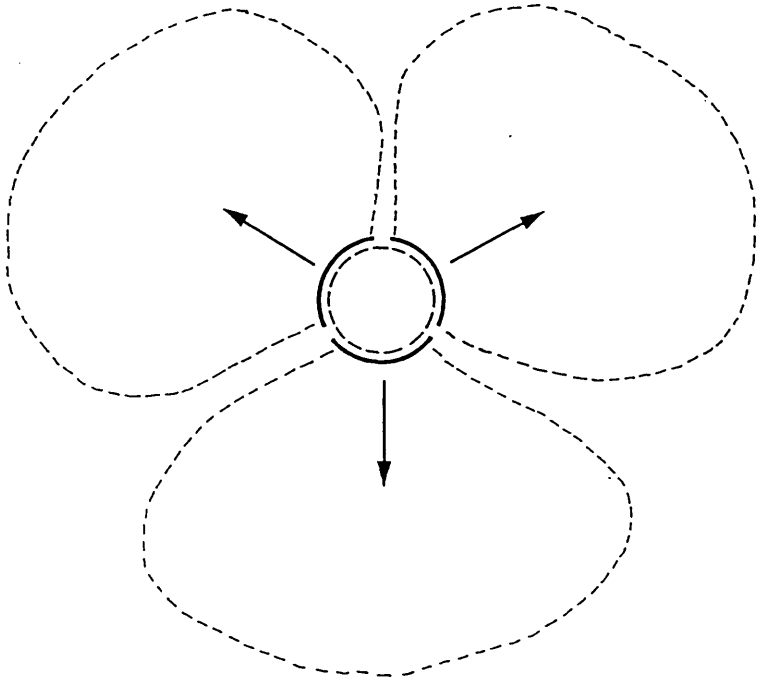

3 - slit outer shell

Figure 8.1 '1-slit' and '3-slit' expansion of a circular outer shell: Diagrammatic representation of mobilisation of soil resistance

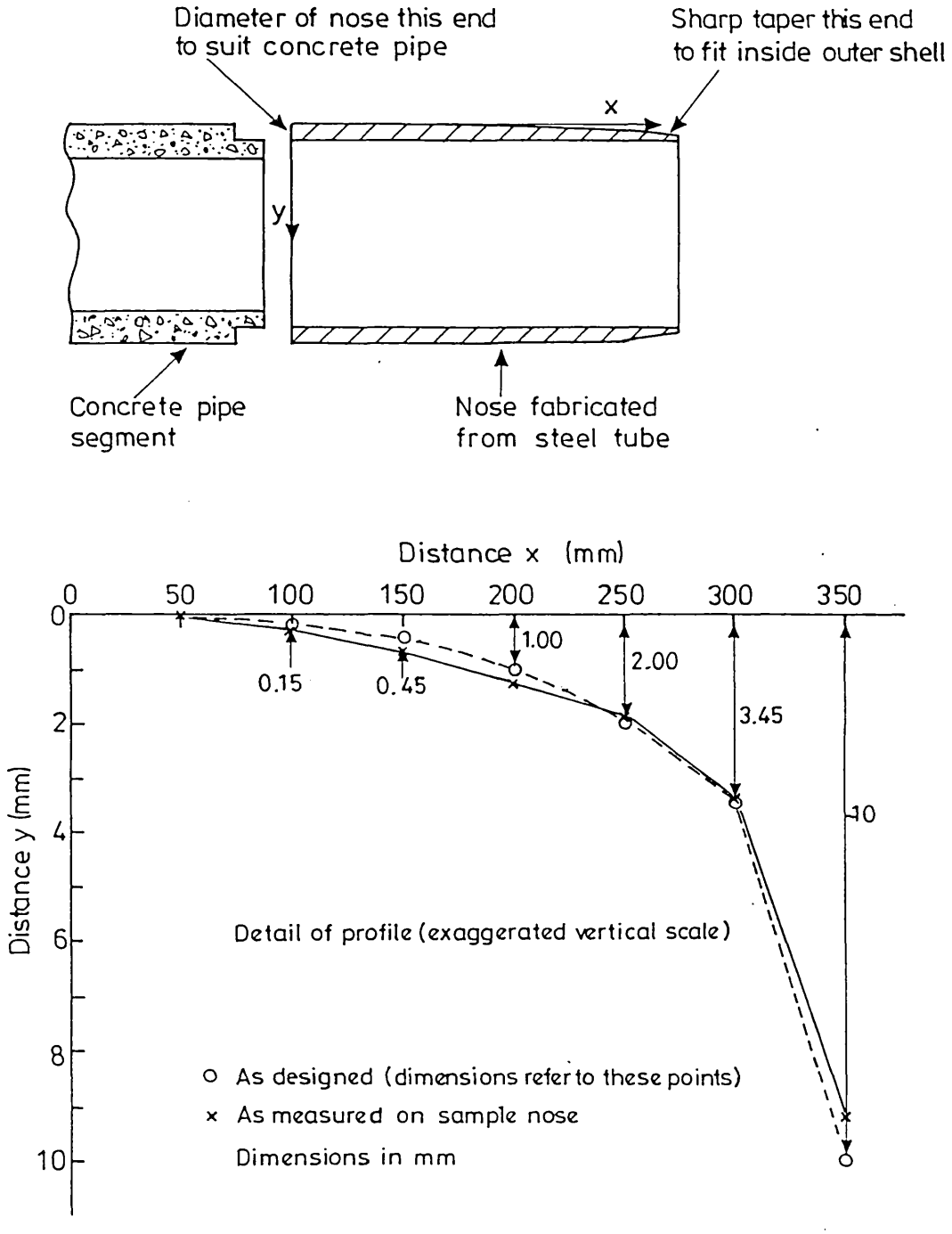

Figure 8.2 Details of CP&F pile expander mandrel nose

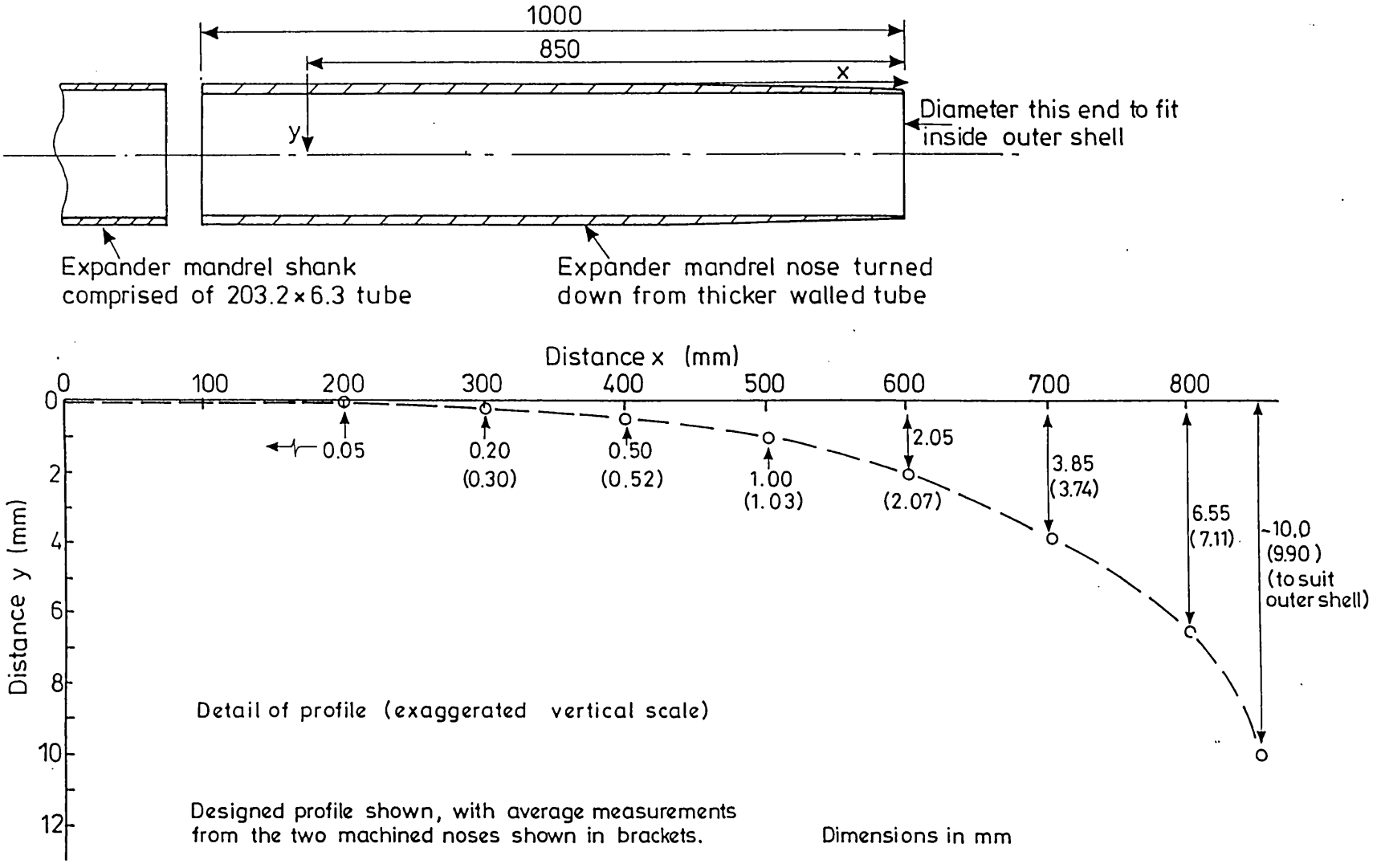

Figure 8.3 Details of Conoco pile expander mandrel nose

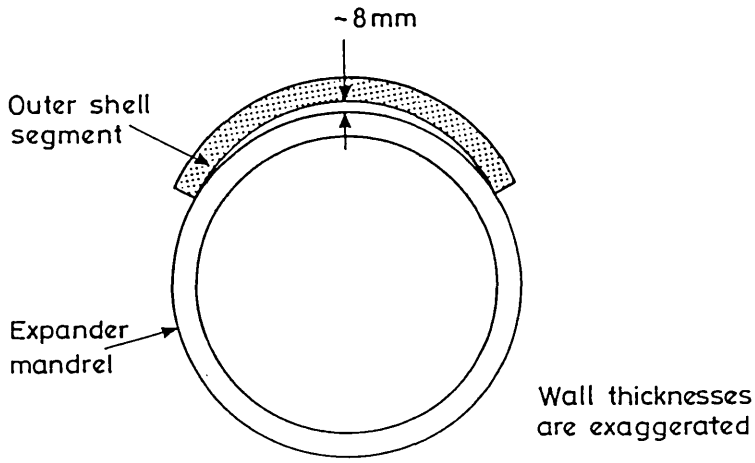

Figure 8.4 Expanded configuration of Conoco 3 weak line pile, assuming rigid outer shell

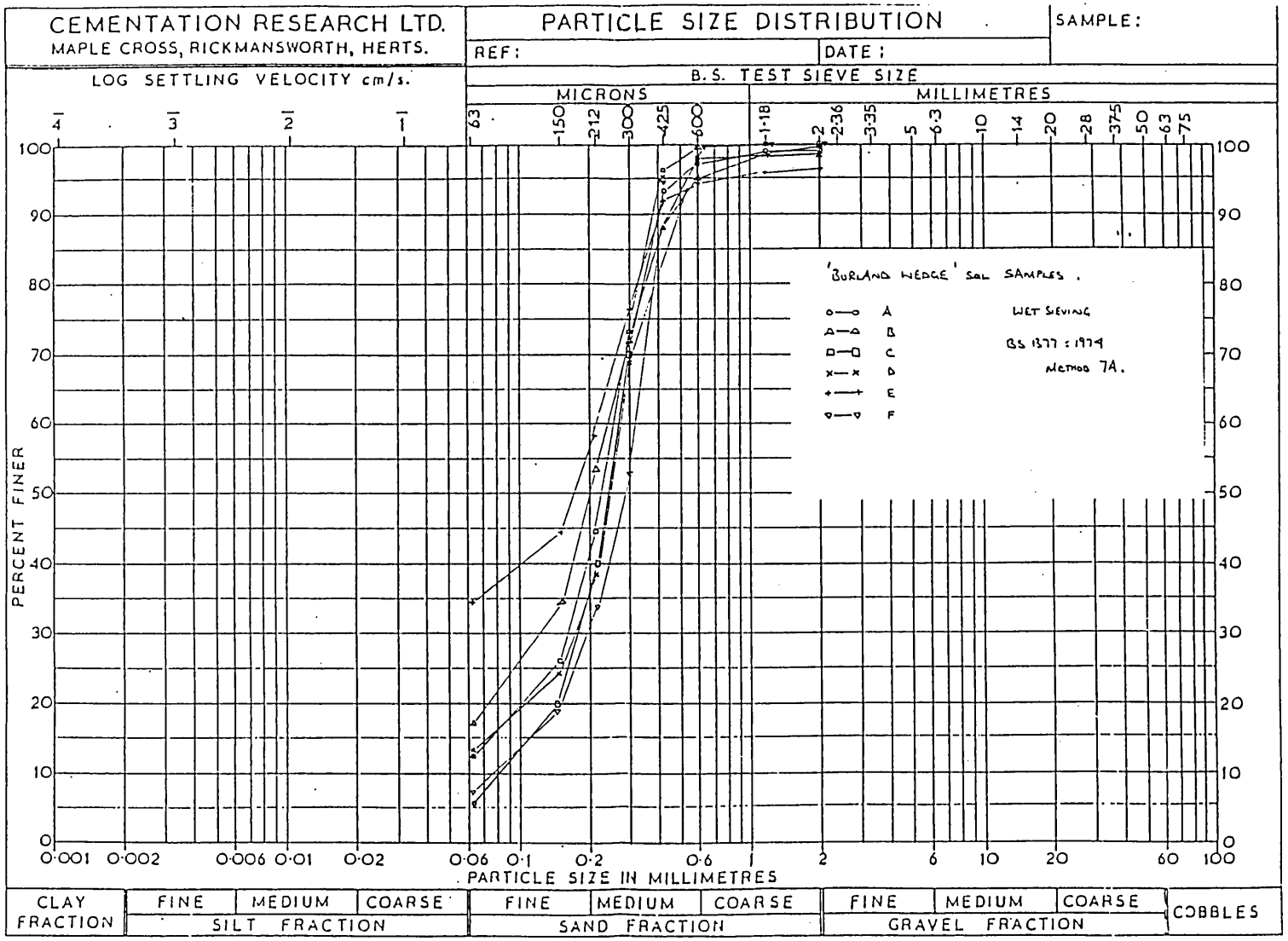

Figure 8.5 Typical grading curves for soil at test site

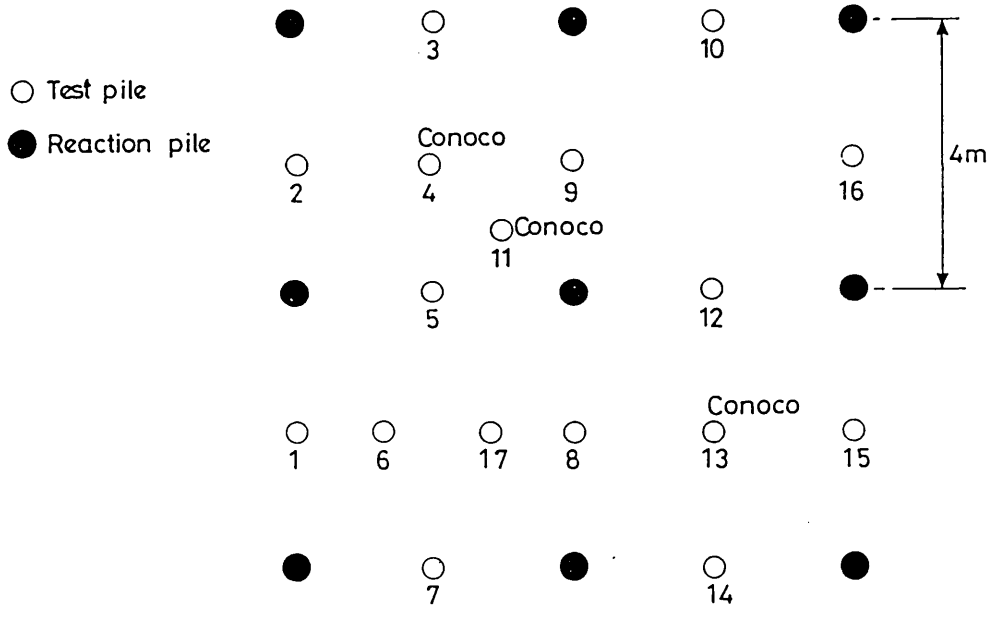

Pile No.	Type	Date driven
1	CP&F plastic, unexpanded	28/10/88
2	CP&F plastic, expanded	28/10/88
3	CP&F steel, unexpanded	26/10/88
4	Conoco, 1 weak line	31/10/88
5	CP&F plastic, expanded	28/10/88
6	CP&F steel, expanded	27/10/88
7	CP&F plastic, expanded	31/10/88
8	CP&F plastic, unexpanded	28/10/88
9	CP&F plastic, expanded	28/10/88
10	CP&F plastic, expanded	27/10/88
11	Conoco, 3 weak lines	2/11/88
12	CP&F plastic, unexpanded	27/10/88
13	Conoco, unexpanded	31/10/88
14	CP&F steel, unexpanded	26/10/88
15	CP&F plastic, unexpanded	28/10/88
16	CP&F steel, expanded	27/10/88
17	CP&F plastic, expanded	31/10/88

Figure 8.6 Layout of piles at Hermitage site

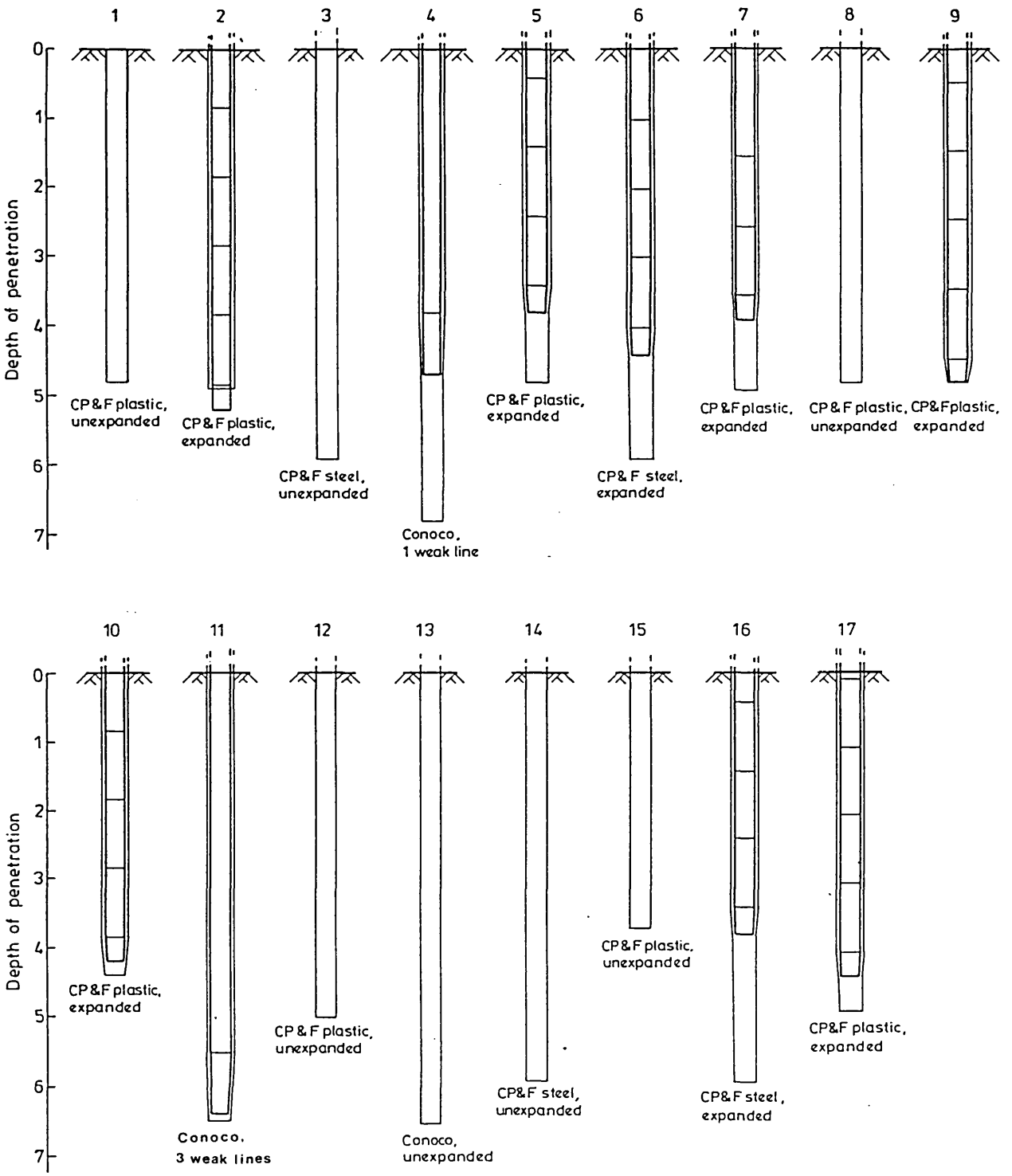

Figure 8.7 Driven depths of test piles

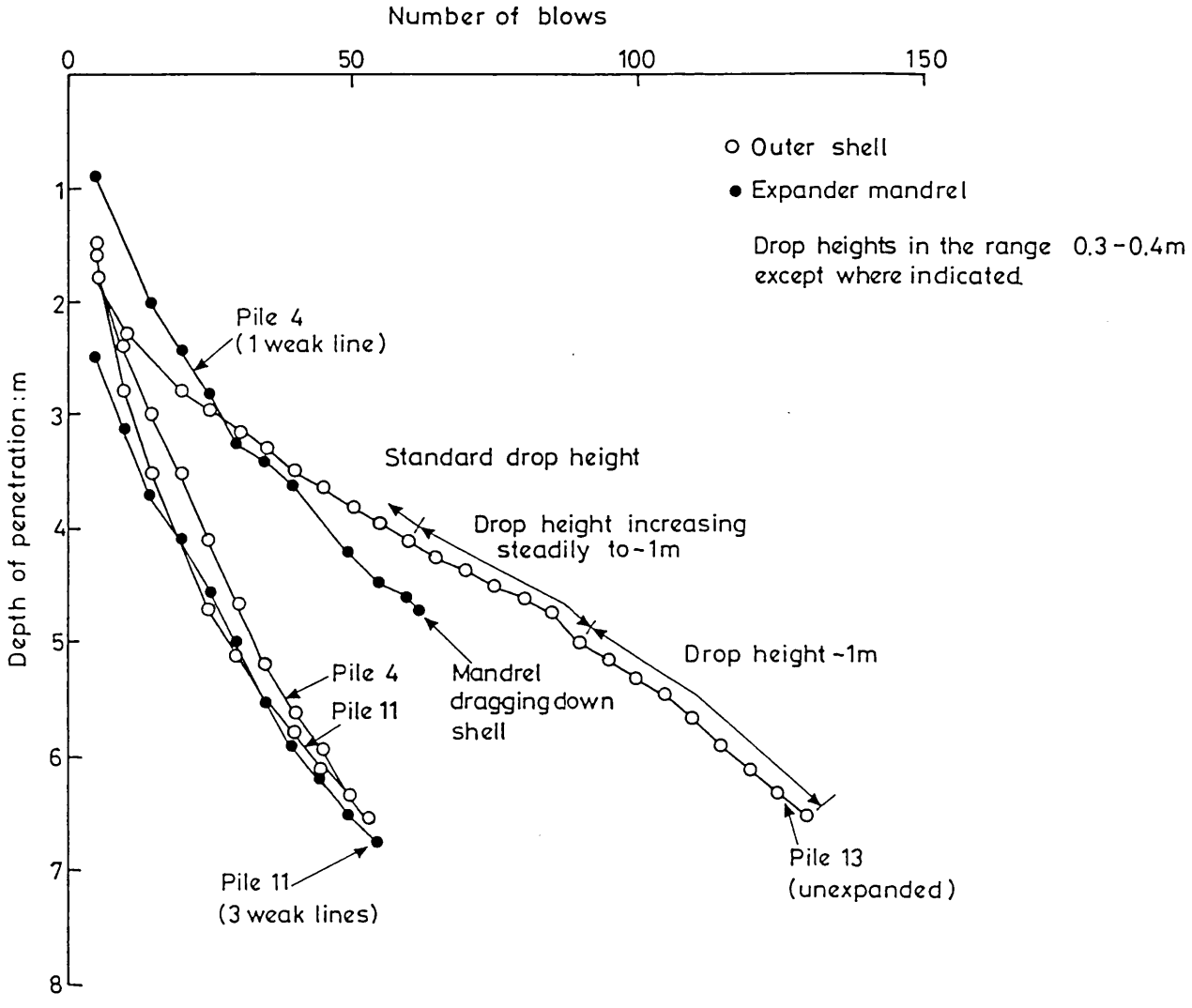

Figure 8.8 Driving records for Conoco piles

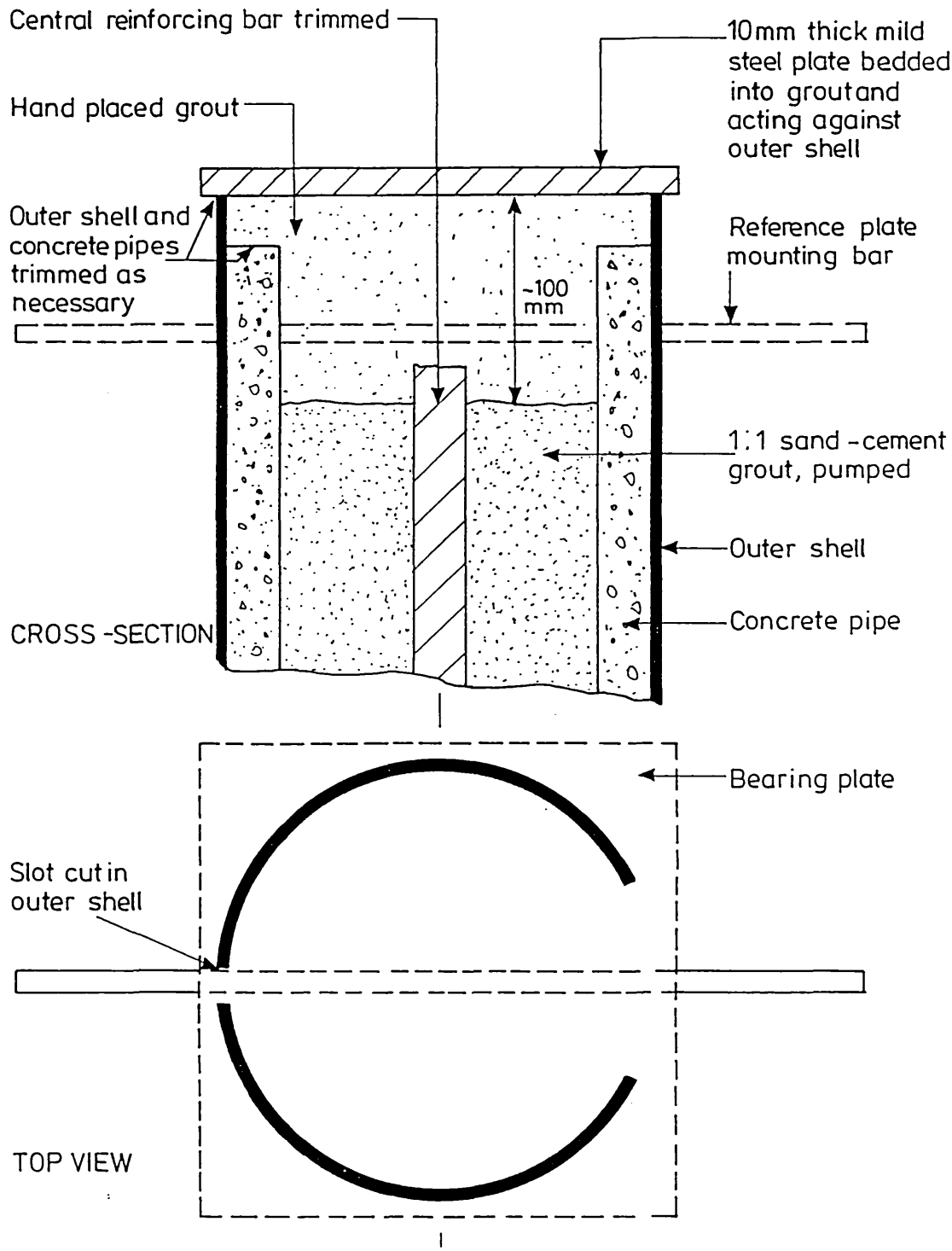

Figure 8.9 CP&F piles: grouting details

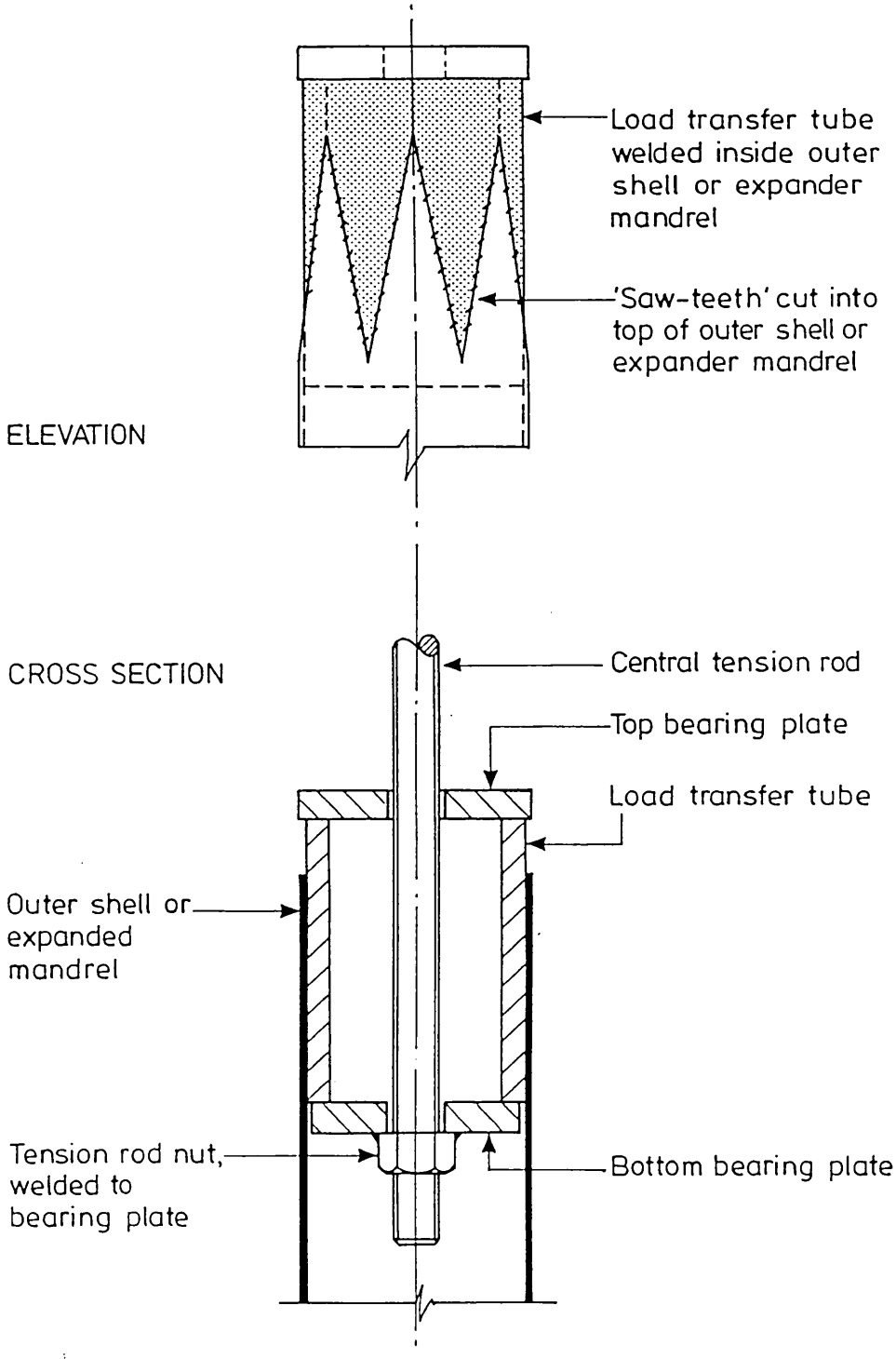

Figure 8.10 Conoco pile: details of load transfer tube

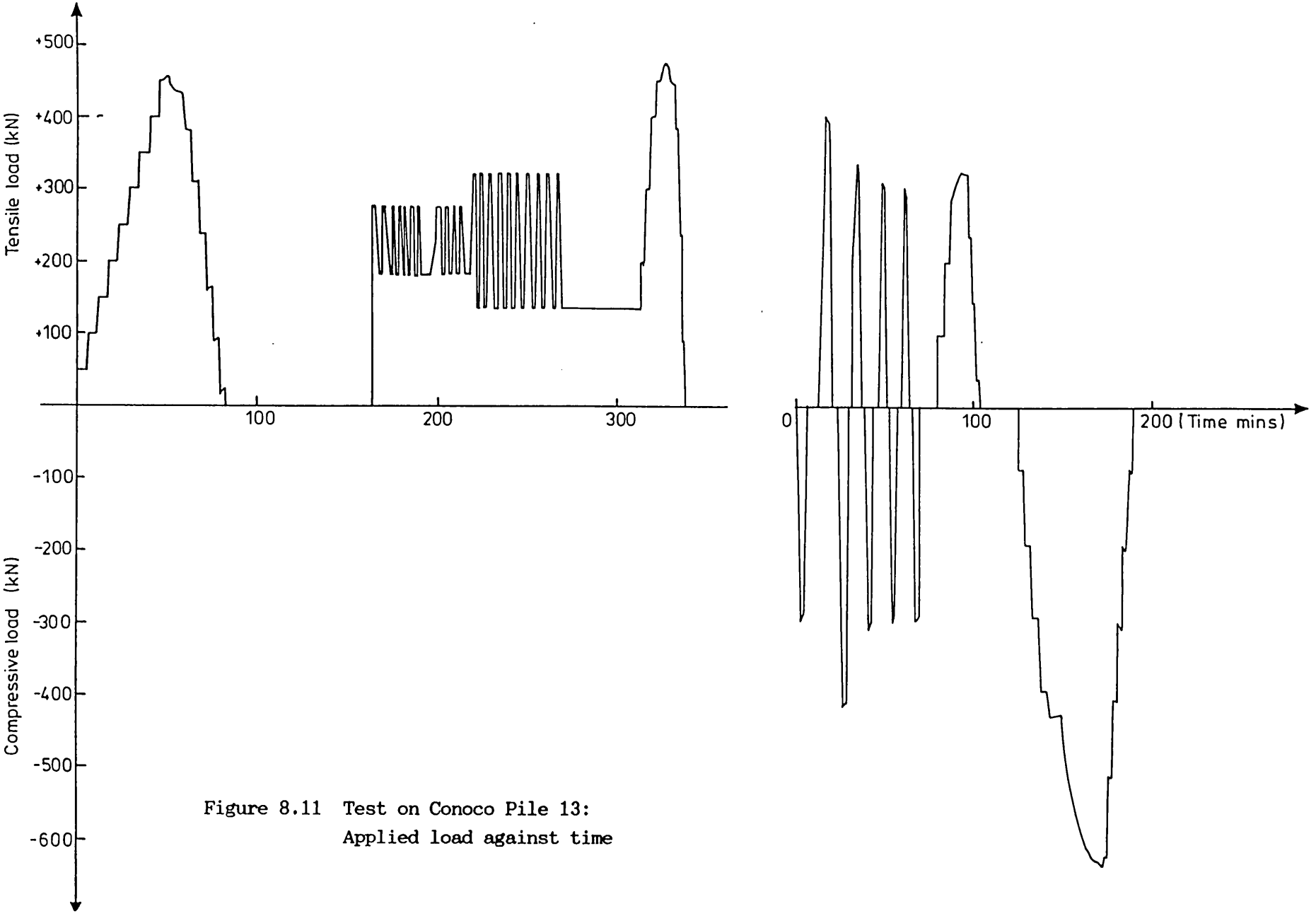

Figure 8.11 Test on Conoco Pile 13:
Applied load against time

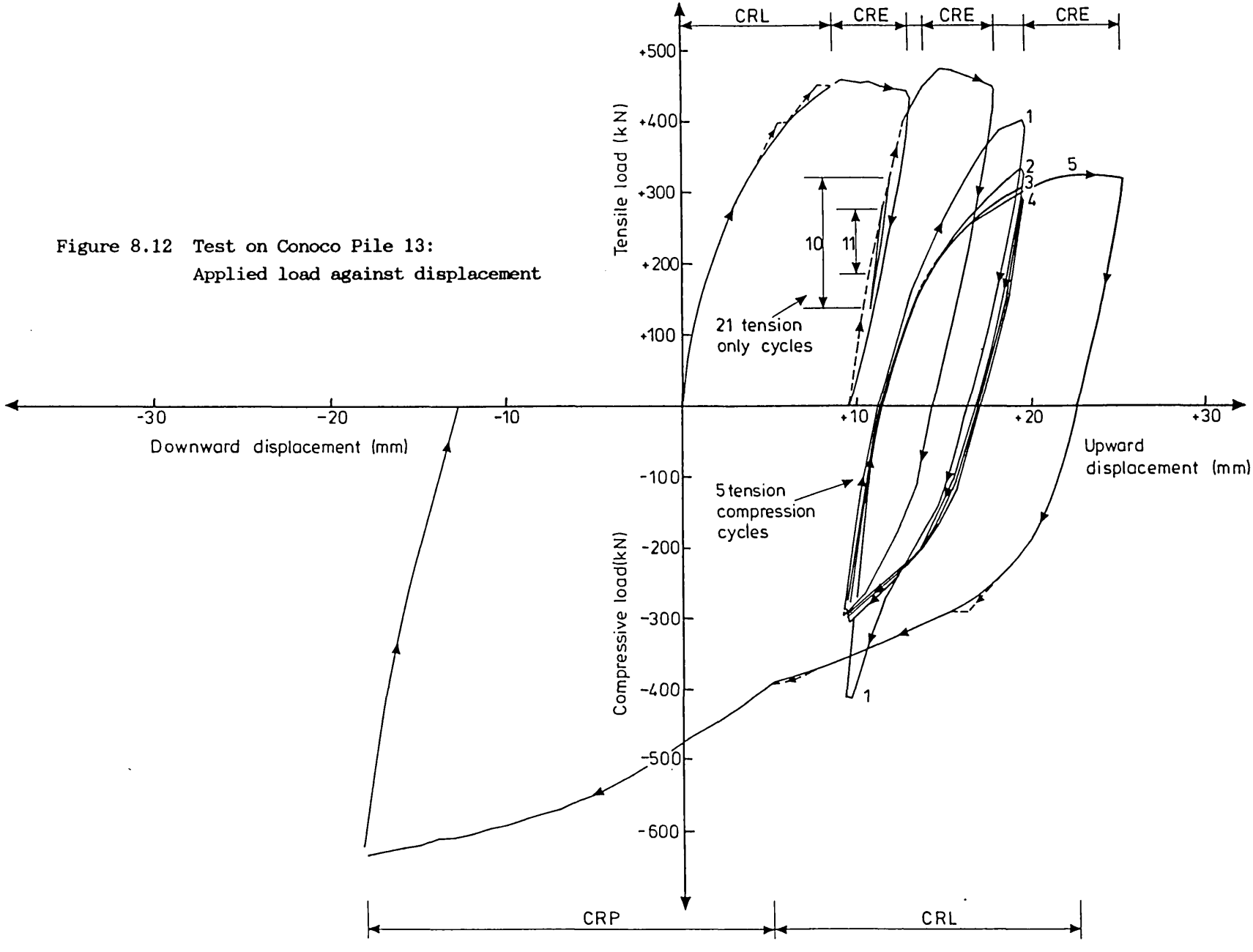

Figure 8.12 Test on Conoco Pile 13:
Applied load against displacement

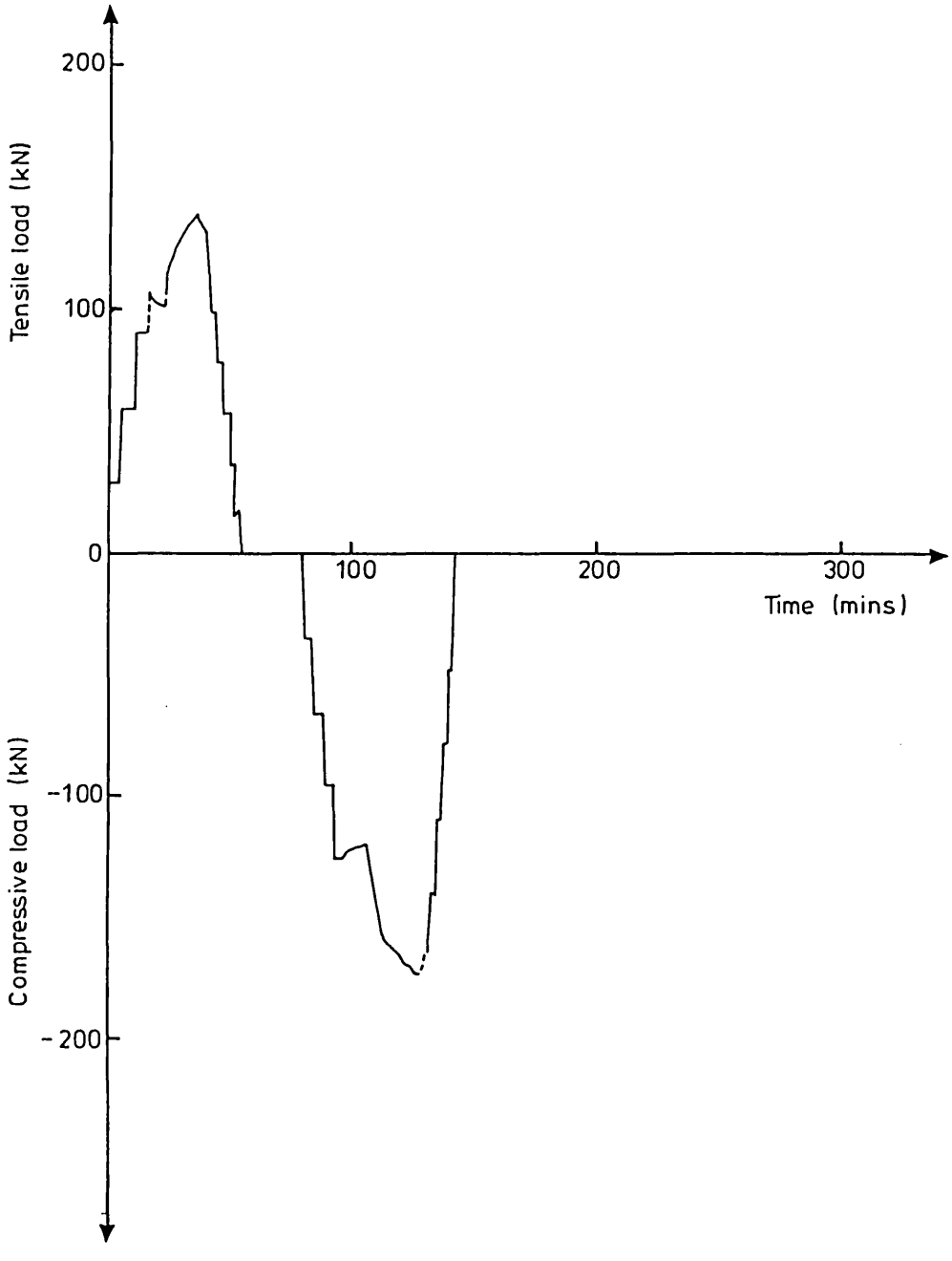

Figure 8.13 Test on Conoco Pile 4:
Applied load against time

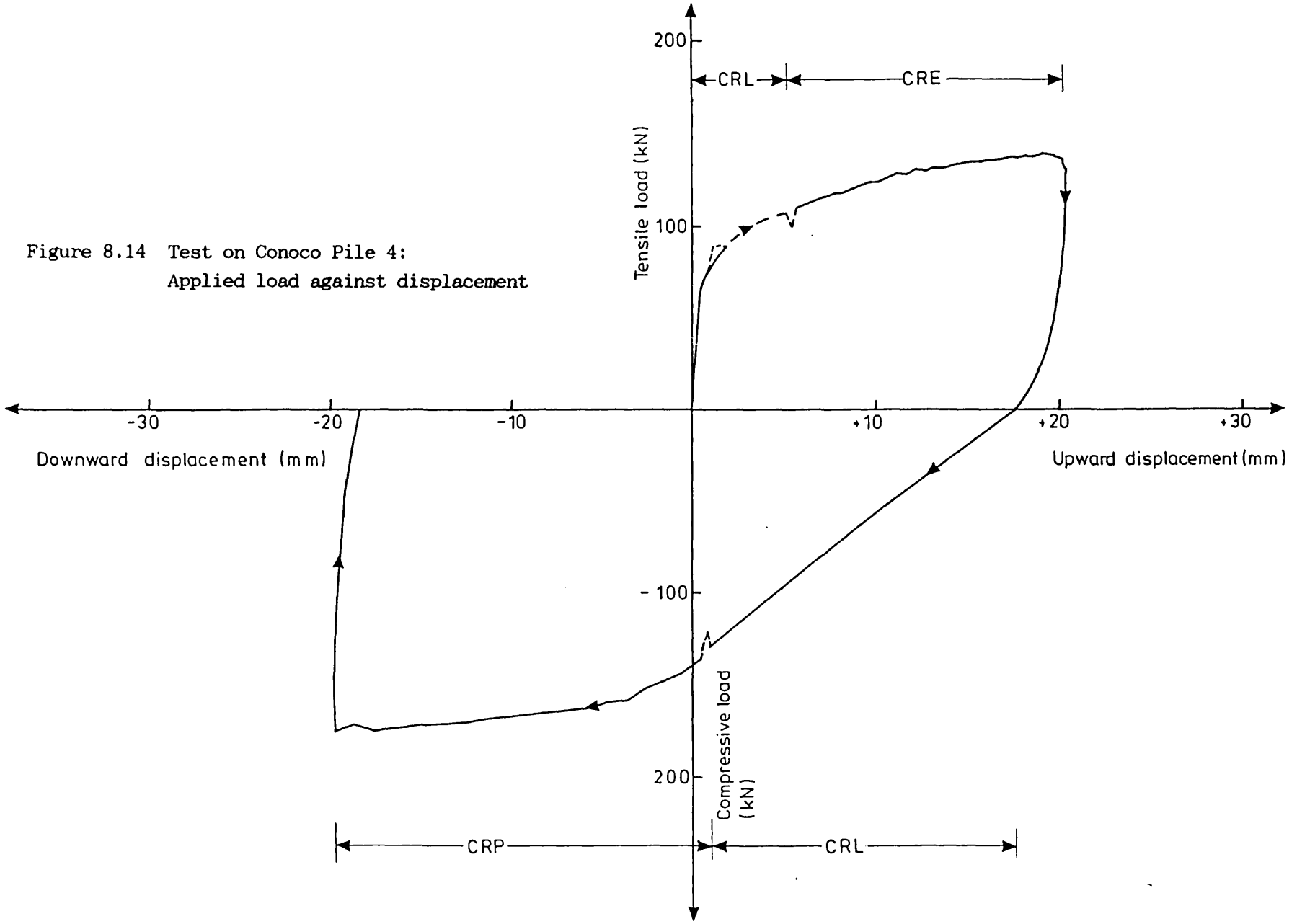

Figure 8.14 Test on Conoco Pile 4:
Applied load against displacement

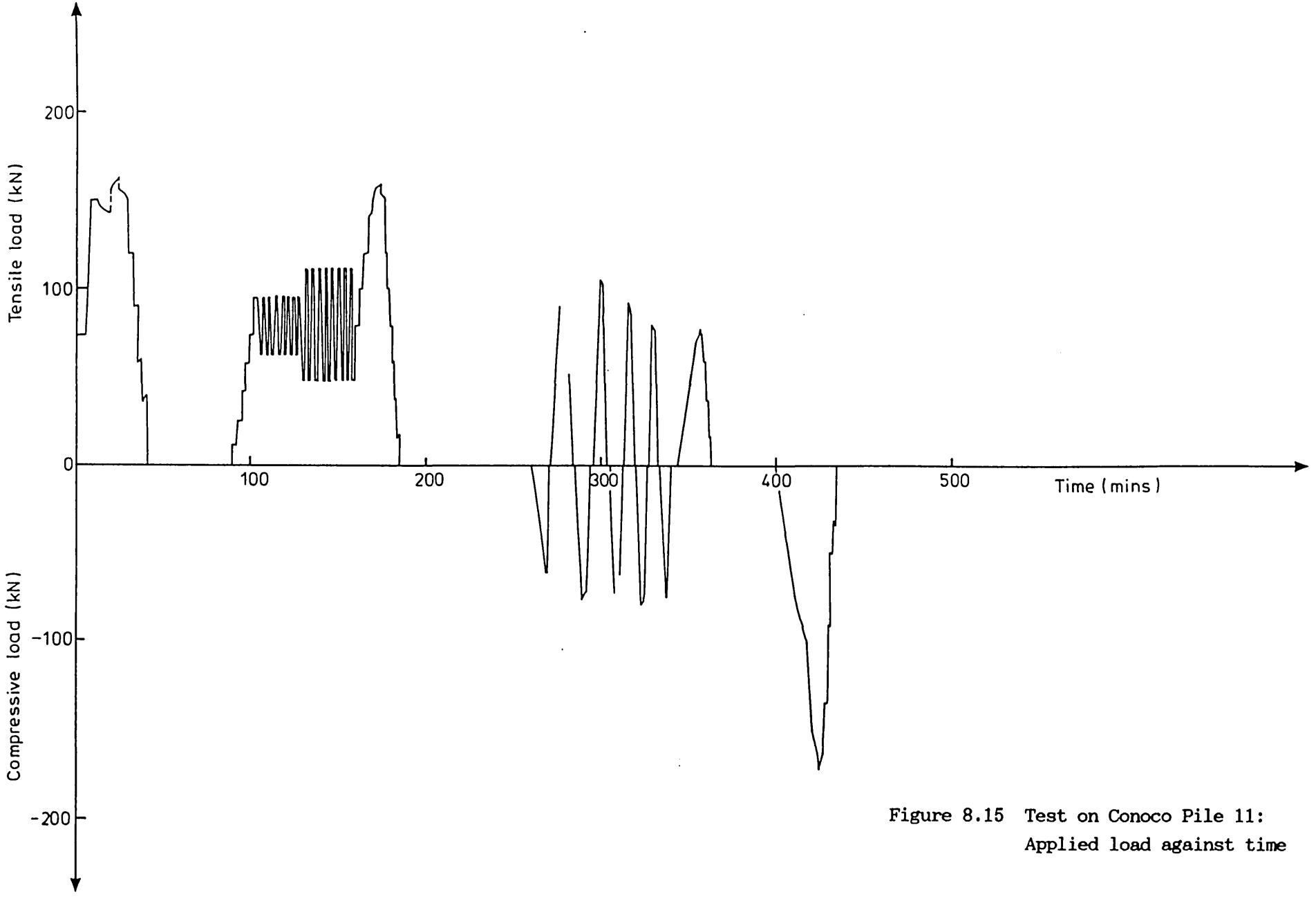

Figure 8.15 Test on Conoco Pile 11:
Applied load against time

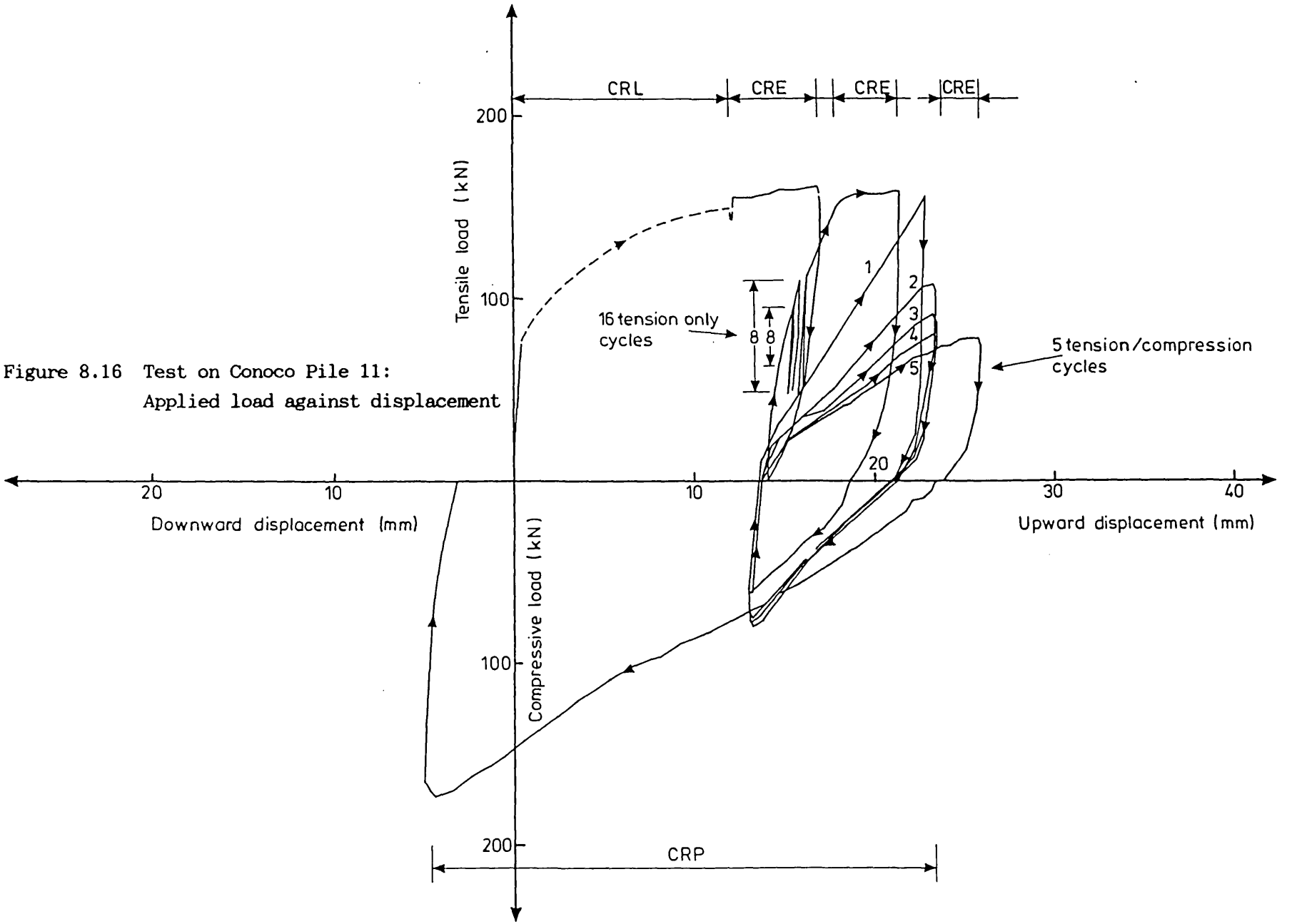

Figure 8.16 Test on Conoco Pile 11:
Applied load against displacement

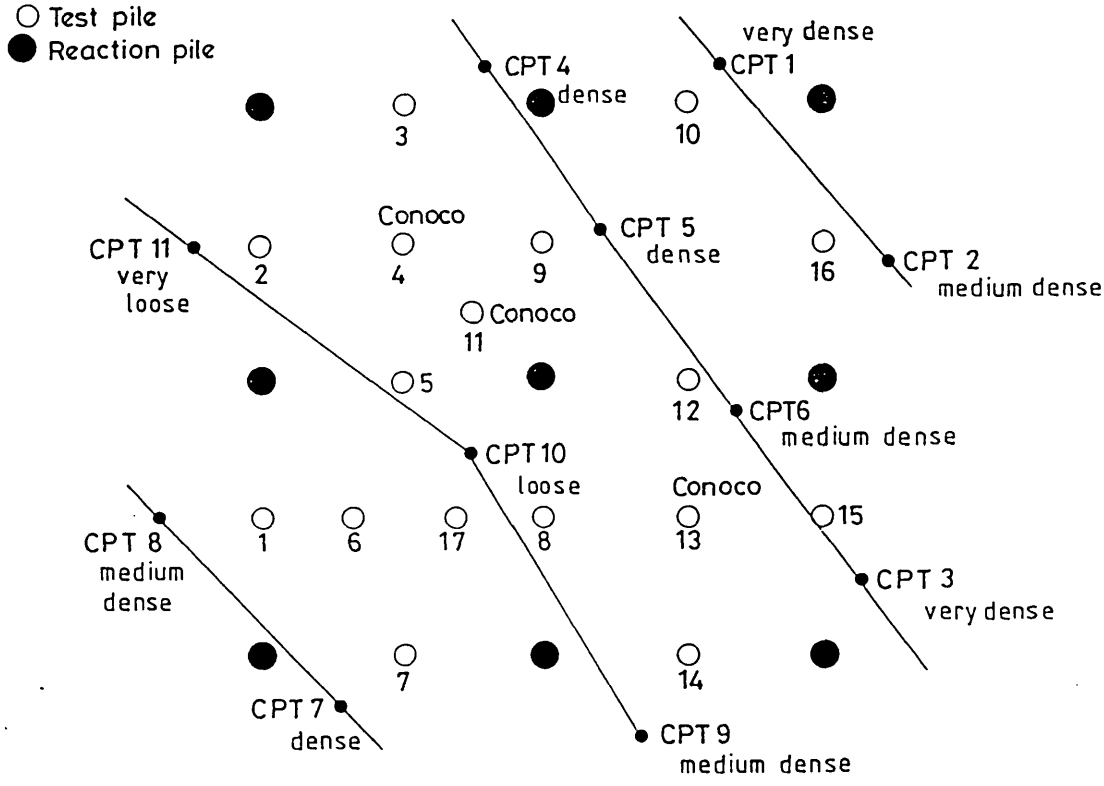

Figure 8.17 Location of CPT profiles

Pile No.	Type	Driven levels[1] Shell	Mandrel	Driving outer shell: Blows	Drop height[3]	Energy[4]	Test type	Maximum load (CRP or CRE)	Disp. at max. load
		(m below g.l.)			(mm)	(kJ)		(kN)	(mm)
1	Plastic unexpanded	4.8	-	40	300	388	Comp.	95	16.0
2	Plastic expanded	4.9	5.2[2]	24	300	233	Comp.	196	18.3
3	Steel unexpanded	5.9	-	85	200-250	619	Comp.	299	11.1
5	Plastic expanded	4.8	3.8				Comp.	100	14.3
6	Steel expanded	5.9	4.4	97	200-250	707	Ten.	199	20.0
7	Plastic expanded	4.9	3.9				Comp.	372	23.7
8	Plastic unexpanded	4.8	-	87	300-350	915	Comp.	296	21.5
9	Plastic expanded	4.8	4.8[2]	27	200-250	197	Comp.	182	13.7
10	Plastic expanded	4.4	4.2[2]	58	250	469	Comp.	390	21.1
12	Plastic unexpanded	5.0	-	98	200-300	793	Comp.	308	24.2
14	Steel unexpanded	5.9	-	59	200-250	430	Comp.	109	20.0
15	Plastic unexpanded	3.7	-				Comp.	169	22.0
16	Steel expanded	5.9	3.8	100	200-250	728	Comp.	402	17.1
17	Plastic expanded	4.9	4.4				Ten.	100	10.8

Notes:

1. *Does not include dragdown during expansion (typically 50-100mm).*
2. Expander mandrel nose met with outer shell driving shoe.
3. Average of drop height values estimated by eye.
4. Calculated using equation

   Driving energy = No. blows x average drop height x hammer weight

   (assumes no energy losses during driving)

Table 8.1 CP&F piles:
Summary of results

Pile No.	Pile type	Driven levels Shell	Mandrel	Driving outer shell: Blows	Drop height[3]	Energy[4]	Maximum loads Tension[5]	Comp.[6]	Disp. at max. loads Tension	Comp.
		(m below g.l)			(mm)	(kJ)	(kN)	(kN)	(mm)	(mm)
13	Unexpanded:									
	Outer shell	6.50		130	650	2735	+458	-633	+9.1	-18
4	Expanded, 1-split:									
	Outer shell	6.82[1]		53	300-400	601				
	Expander mandrel		4.70	62	300-400	702				
	Completed pile						+139	-174	+19.3	-20
11	Expanded, 3-split:									
	Outer shell	6.45		53	300-400	601				
	Expander mandrel		6.35[2]	55	300-400	623				
	Completed pile						+162	-172	+16.8	-5

Notes:
1. Includes 275mm dragdown during expansion.
2. Expander mandrel nose met with outer shell driving shoe.
3. Average of drop height values estimated by eye.
4. Calculated using equation

   Driving energy = No. blows x average drop height x hammer weight

   (assumes no energy losses during driving).
5. Initial static tension test.
6. Final static compression test.

Table 8.2 Conoco piles: Summary of results

CHAPTER 9
CAVITY EXPANSION BACKGROUND THEORY

9.1 Introduction

The aim of this Chapter is to provide a selective theoretical background to the Wedge-Pile project. The Chapter focuses on cavity expansion theories.

Analytical and numerical solutions have been found for both spherical and cylindrical expansion in various media, and these have been of much interest to geotechnical engineers. Solutions for spherical expansion have been applied to problems of bearing capacity (e.g. Gibson, 1950; Ladanyi, 1967; Vesic, 1972). Solutions for cylindrical expansion have been applied to such problems as the interpretation of pressuremeter tests (e.g. Gibson and Anderson, 1961; Palmer, 1972; Hughes et al, 1977; Carter et al, 1986), the installation of a cone penetrometer (Houlsby and Withers, 1988; Withers et al, 1989), and the installation of conventional driven piles (eg. Randolph et al 1979).

Sections 9.2 to 9.7 of this Chapter are concerned with behaviour in clay soils. Section 9.2 briefly summarises the available analytical solutions for undrained cylindrical cavity expansion. Section 9.3 considers the results from parametric studies carried out at Cambridge University employing a finite element technique to model the installation of a conventional driven pile as the creation of a long cylindrical cavity. Sections 9.4 to 9.7 review the application of cavity expansion theory to the analysis of the installation of both conventional piles and wedge-piles, in the light of recently developed methods of analysis and of data from instrumented piles. Section 9.8 summarises the analytical solutions available for drained cylindrical cavity expansion, and Section 9.9 considers their possible relevance to the behaviour of wedge-piles installed in sands.

9.2 Analytical Solutions for Undrained Cylindrical Cavity Expansion

Analytical solutions for the undrained expansion of a cylindrical cavity have been developed mainly for use in the interpretation of pressuremeter tests. It is assumed that the reader is familiar with the principles and basic details of pressuremeter testing (Mair and Wood, 1987).

9.2.1 Elastic-perfectly plastic analysis

The purpose of developing theories to analyse expansion during pressuremeter tests is to enable the determination of soil properties. This involves matching measurements of cavity pressure and change of cavity radius with a solution of the governing equations. Gibson and Anderson (1961), following the analyses of Bishop et el (1945) and Hill (1950), presented the first such interpretation of an expansion test. The test was modelled as the expansion of an existing cylindrical cavity in the ground. The pressuremeter was considered to be infinitely long such that the deformation of the surrounding soil was under conditions of axial symmetry and plane strain. Two analyses were presented, one of which was applicable to undrained expansion tests in clay. In this analysis the soil was assumed to undergo no volume change during expansion and to behave as an elastic-perfectly plastic material, characterised by a shear modulus G and an undrained shear strength c_u. The solution, referred to here as the Gibson/Anderson analysis, gives the displacement field and total stress distributions in the material around the cavity.

Expansion of a cavity in an elastic-perfectly plastic soil involves an expanding annulus of failed plastic soil near to the cavity, restrained by a surrounding mass of elastic soil. The stiffness of the pressuremeter response diminishes steadily as the elastic/plastic boundary is pushed further out, until a theoretical limiting condition is reached at infinite expansion, when

$$p_L = \sigma_{r_o} + c_u\{1 + \ln(G/c_u)\} \qquad (9.1)$$

where

p_L = limit pressure
σ_{r_o} = in-situ horizontal stress
c_u = undrained shear strength
G = shear modulus

Estimates of p_L, G, and σ_{r_o} can usually be made from the pressure:strain or pressure:volume curve of a pressuremeter test. Equation 9.1 can be rearranged to obtain c_u:

$$c_u = (p_L - \sigma_{r_o})/\{1 + \ln(G/c_u)\} \qquad (9.2)$$

This method of obtaining c_u is usually referred to as the 'limit pressure' method.

Marsland and Randolph (1977) defined the parameter

$$N_p = 1 + \ln(G/c_u) \qquad (9.3)$$

as the 'pressuremeter constant', analogous to the cone factor N_k used in the interpretation of the cone penetration test. N_p is relatively insensitive to changes in G/c_u. For example, a range of typical G/c_u values from 90 to 330 corresponds to a change in N_p of 5.5 to 6.8. A constant value of N_p is often assumed - a value of 6.18 is consistent with a bearing capacity factor N_c of 9.25 (ibid.).

Houlsby and Withers (1988) have recently extended the elastic-perfectly plastic analysis to include an unloading phase. Using this analysis, it is possible to make estimates of c_u, G and σ_{r_o} from the unloading curve of a Full Displacement Pressuremeter (FDPM) (Withers et al, 1986). In this new analysis, the initial installation of the FDPM is modelled theoretically as the expansion of a cylindrical cavity within the soil, and the expansion phase as a continued expansion of the same cylindrical cavity.

Houlsby and Withers have justified the use of cylindical cavity expansion theory to model the installation of the FDPM cone on the basis of work by Teh (1987), who implemented Baligh's strain path method (see Section 9.4) to analyse the 60° cone, and showed that the stress distribution far behind the cone tip was similar to the distribution created by the expansion of a cylindrical cavity from zero initial radius. The analysis thus predicts that the pressuremeter will 'lift off' at the limit pressure. It is difficult to reconcile this prediction with the usual observation of a 'lift-off' pressure well below the limit pressure, for pressuremeters pushed into the ground (e.g. Powell and Uglow, 1985; Houlsby and Withers, 1988).

9.2.2 General analysis

If it is assumed that the soil surrounding the pressuremeter is undrained and therefore does not change in volume during expansion, all elements of soil are subjected to deformations similar in mode and different only in magnitude. If it is also assumed that all soil elements have the same stress:strain response when subjected to this deformation, then elements of soil at different radii will have reached different points along a unique shear stress:shear strain curve. The pressuremeter pressure:deformation response is the integrated effect of the response of these soil elements, from infinite radius to the wall of the cavity.

In theory, the precise form of the unique shear stress:shear strain curve, which can take any form, can be deduced from the pressure: deformation curve. Very similar analyses were developed independently by Palmer (1972), Ladanyi (1972), Baguelin et al (1972); the analysis is referred to here as the Palmer analysis.

The shear stress, τ, at the wall of the cavity is given by the equation

$$\tau = \frac{dp}{d\{\ln(\Delta V/V)\}} \qquad (9.4)$$

where

p = current cavity pressure

V = current volume at pressure p

V_o = volume at reference pressure

$\Delta V = V - V_o$

Equation 9.4 states that τ at a particular cavity strain is equal to the current slope of the p:ln($\Delta V/V$) plot.

Although in theory the Palmer analysis is superior to the Gibson/ Anderson analysis, its practical application to the pressuremeter test is fraught with difficulties. The interpretation is very sensitive to disturbance caused by installation of the instrument, and on the choice of strain datum. In many soils stress:strain response is rate dependent; the strain rate surrounding an expanding pressuremeter varies inversely with the square of the radius and elements at different radii may therefore follow different stress:strain curves. The apparent peak strengths deduced from the results of pressuremeter tests using the Palmer analysis have generally proved unreliable, although less uncertainty surrounds the determination of the apparent large strain strength given by the slope of the p:ln($\Delta V/V$) at large deformations. A p:ln($\Delta V/V$) plot with an extended linear portion at large deformations is consistent with the soil tending to a condition of perfect plasticity, with τ remaining constant with continuing strain. The large strain strength is likely to give a better indication of the 'operational' strength of the soil around the pressuremeter (Marsland, 1977; 1979).

The problems involved in deducing a credible stress:strain curve from the results of a pressuremeter test have led to the general conclusion that the extra sophistication of the Palmer analysis is not justified and that the Gibson/Anderson analysis is satisfactory for design purposes in geotechnical engineering (Wroth, 1984; Mair and Wood, 1987).

9.3 Cavity Expansion Model of Conventional Pile Installation in Clays

9.3.1 Introduction

When a solid pile is driven, it must displace a volume of soil equal to the volume of the pile. At small depths ground heave will occur; at greater depths soil will be displaced predominantly radially. This has led to the installation process being modelled as the expansion of a cylindrical cavity, with the final radius of the cavity equal to that of the pile. In contrast to the expansion of a pressuremeter, which involves the expansion of a pre-existing cavity, the concept in the case of pile installation is that of the expansion of a cavity from zero radius. The most extensive exploration along this avenue of analysis was undertaken at Cambridge University in the late 1970's, previous analyses having been presented by Soderburg (1962), and Butterfield and Bannerjee (1970).

The work carried out at Cambridge (referred to here as the 'Cambridge theory') involved some new analytical methods and extensive parametric studies using a finite element method (Wroth et al, 1979; Randolph et al, 1979; Randolph and Wroth, 1982). It formed the central part of a programme of research into a general effective stress theory for the design of driven piles. The usual starting point for any such theory is the division of the problem into the following areas (Jardine, 1985):

(a) The general stress-strain and strength properties of soils.
(b) The evaluation of initial ground conditions.
(c) The process of pile installation.
(d) The equilibration of the soil after pile installation.
(e) The process of pile loading from fixed initial conditions.

The Cambridge theory is concerned with stages (c) and (d) of this sequence. Axial symmetry and plane strain conditions are assumed throughout, as before. The cylindrical expansion is assumed to occur at some distance away from end effects associated with the proximity of the ground surface and the tip of the pile. Randolph et al (1979) offer the results of other reported experimental work to support their assumption that displacements during installation, and subsequent excess pore water gradients during consolidation, are radial over most of the length of the pile.

Although in the pile installation problem the cavity must be created from zero radius, numerical modelling of this is not possible because of the infinite cavity strain that would occur at zero radius. Therefore,

the problem is simplified to that of the expansion of a cavity with initial radius a, to final radius 2a, where the radius of the pile r is related to a by the expression

$$r = \sqrt{3}\, a$$

such that the same volume of soil is displaced in both the real and the model cases. The solution for expansion from a finite radius ultimately gives the same limit solution as that which occurs immediately in the case of expansion from zero initial radius; after doubling the radius of a cavity the internal pressure is within 6% of the limit pressure and this provides a suitable approximate solution.

9.3.2 Elastic solution for consolidation

Randolph and Wroth (1979) presented an analytical solution for radial consolidation around a pile modelled as an expanded cylindrical cavity, assuming that the soil deforms elastically.

The Gibson/Anderson analysis can be used to predict the initial pore pressure distribution around the pile. If it assumed that, under undrained conditions, the mean effective stress in the plastic zone remains constant, the initial change in pore pressure Δu at the face of the pile is equal to the initial change in mean total stress Δp. From Equation 9.1:

$$\Delta\sigma_r = c_u\{1 + \ln(G/c_u)\} \qquad (9.5)$$

$$\Delta p = c_u \ln(G/c_u) \qquad (9.6)$$

$$\Delta u = \Delta p \qquad (9.7)$$

During elastic consolidation, changes in principal stresses occur as the pore pressure generated on installation dissipates. The change in radial effective stress, $\Delta\sigma_r'$, is governed by the equation

$$\Delta\sigma_r' = -\Delta u \qquad (9.8)$$

Thus the change in total stress during consolidation is predicted to be zero, implying that the full limiting pressure needed to expand the cylindrical cavity will eventually act as effective stress against the pile.

9.3.3 Finite element modelling of pile installation

In order to develop and use more complex and realistic soil models to represent the medium surrounding the pile, the researchers at Cambridge turned to a finite element method of analysis incorporating a version

of the work-hardening Modified Cam-clay soil model (Wroth et al, 1979; Randolph et al, 1979). Using this model, they were able to calculate stress and pore pressure changes immediately after driving and at any time during the period of soil equilibration. The co-ordinate system and the initial stress state in the soil that were adopted in the analyses are shown in Figure 9.1. The analyses considered stresses expressed in terms of the original undrained shear strength c_{u_i} .

A large number of parametric studies were performed using soil models representing London Clay and Boston Blue Clay, with additional studies using soil models representing a wide range of clay types. A range of overconsolidation ratios (OCRs) were considered. Jardine (1985) points out that some of the assumptions regarding the soil models that were used are contradicted by recent research.

The principal conclusions from the parametric studies were as follows:

(a) The total stress paths during expansion in the case of the Modified Cam-clay model are similar to those for the elastic-perfectly plastic model. This result is due to the geometric constraints on the strain path of each soil element - the elements are all at different stages on the same stress-strain path (Section 9.2.2). The increase in mean total stress is given closely by Equation 9.6 using secant values of G. Approximate stress paths during pile driving (ie. cavity expansion) for elements of soil near to the pile are shown in Figure 9.2.

(b) Although the total stress paths are largely independent of soil model, the effective stress paths - and hence pore pressures - differ between models, because in the work hardening model the value of the mean effective stress changes during shearing. The expression for the maximum pore pressure generated next to the pile, Δu, is given by the approximate expression

$$\Delta u = (p_i' - p_f') + c_{u_i} \ln(G/c_{u_i}) \qquad (9.9)$$

where
p_i' = mean effective stress prior to shearing
p_f' = mean effective stress after shearing
G = shear modulus
c_{u_i} = undrained shear strength

As the value of OCR increases so does G/c_{u_i} (for constant c_{u_i}), but (p_i' - p_f') decreases, becoming negative for values of OCR greater than 2 as the soil tends to dilate on shearing (Figure 9.2). These two effects

virtually cancel themselves out, with the result that the excess pore pressure distribution for a soil of given strength is scarcely affected by the stress history of the soil. The excess pore pressure (and total radial stress) is sensitive, however, to the value of shear modulus chosen in Equation 9.9; soils with larger values of shear modulus developing higher excess pore pressures and limiting total pressures. Choice of shear modulus has less influence on the final radial effective stress acting after consolidation (see (d) below). A typical stress distribution surrounding the pile immediately after installation is shown in Figure 9.3, for the cases of Boston Blue Clay with OCR = 1 and 8, and two different values of G. In the failed region of soil near to the pile the effective stresses for the two soil models are the same, regardless of the value of G. This is because the undrained strength is the same for each soil model.

(c) During consolidation, effective stresses increase as the excess pore pressures dissipate. Most of the soil surrounding the cavity (at radii greater than about twice the cavity radius) unloads in shear during consolidation. Near to the pile, however, the kinematic restraint of the relatively rigid pile causes the soil near to the pile to undergo further shear straining. Total radial stress is predicted to fall - this phenomenon has been observed during pressuremeter holding tests (Clarke et al, 1979).

(d) After consolidation, the stresses in the soil surrounding the driven pile are significantly altered, out to about 20 pile radii. A typical stress distribution surrounding the pile after consolidation is shown in Figure 9.4, for the case considered previously - Boston Blue Clay with OCR = 1 and 8, and two different values of G. Comparison of Figures 9.3 and 9.4 shows that whereas the ratio of the pore pressures generated on expansion for the two values of G is 1.8, the ratio of the final radial effective stresses acting after consolidation is only 1.13. The final radial effective stress acting on the pile in this case is about $5c_{u_i}$, the increase in effective stress during consolidation being around half of the initial excess pore pressure. From analyses using soil models representing a wide range of clays, σ'_r after consolidation is predicted by the Cambridge theory to be typically in the range 5 to $6c_{u_i}$.

In comparison with the more sophisticated numerical analyses subsequently carried out, the elastic solution for consolidation provides realistic estimates of the times necessary for consolidation to take place. This is because most of the soil is unloading in shear and the consolidation process is largely controlled by the flow of water

through the large volume of soil at intermediate radii. The stress changes near the pile are not well predicted by the elastic model, however.

(e) Near to the pile mean effective stress increases during consolidation, resulting in a significant increase in soil strength. After consolidation, the soil close to the pile is left normally consolidated with the major principal stress acting radially, and equal minor principal stresses acting vertically and circumferentially. The process of installation causes the soil to 'forget' its in-situ stress condition before driving.

9.4 Strain Path Approach for Pile Installation in Clays

Recently, an entirely different approach to the numerical modelling of pile installation has been developed at MIT under the direction of Baligh - the strain path method (Baligh, 1985; 1986). In the view of Baligh, cavity expansion methods - in which displacements, strains, stresses and pore pressures are dependent solely on the radial co-ordinate - are not appropriate for modelling penetration in soils, because they ignore two important aspects of vertical penetration:

(a) the dependence of soil deformations on the vertical co-ordinate during vertical penetration, i.e. the problem is two dimensional, not one-dimensional.

(b) the continuity of steady penetration.

(Baligh, 1986)

In order to develop a better understanding of the mechanisms of deep penetration, Baligh and his co-researchers have developed solutions such as that shown in Figure 9.5. Such solutions involve obtaining the velocity field around the pile (or other device) as it is installed in the soil. The basic hypothesis of the strain path method is that owing to the severe kinematic restraints in deep penetration problems, soil deformations and strains are essentially independent of the soil shearing characteristics. Consequently, the displacement field can be separated from the stress field without serious effect, and the problem can be reduced to a flow problem in which soil moves along streamlines around a fixed rigid body. The velocity fields obtained from the streamlines can be integrated to yield displacements and strain paths.

The strain path method has shown that deep penetration involves

significant reversals and reapplications of strain components and rotations of principal strain directions in the soil ahead of and surrounding the pile. These strain reversals have a profound influence on the state of stress acting on a pile after installation. The strain path method appears to offer great advantages over the cavity expansion approach, which cannot reproduce these important effects.

9.5 Comparison of Numerical Solutions with Observed Behaviour

Important research into the fundamentals of pile behaviour has been carried out at Imperial College in recent years. Much of this work is reported in PhD theses by Martins (1983), Jardine (1985) and Bond (1989).

Jardine (1985) and Jardine and Potts (1988) have carried out a thorough review of theoretical studies that have investigated the effects of pile installation, and have compared the results with predictions obtained by cavity expansion and strain path methods. Table 2.1 contains a summary of the data for the stress state at the end of consolidation obtained from these experiments (ibid.). These data provide an indication of the range of equilibrium radial effective stresses that might be expected close to a conventional driven pile. The final radial effective stress $\sigma'_{r\infty}$ is compared to the original undrained strength of the soil c_{u_i} and to the original in-situ radial effective stress σ'_{r_i} .

The full range for the ratio $\sigma'_{r\infty}/\sigma'_{r_i}$ falls between 0.6 and 2.1; the full range of $\sigma'_{r\infty}/c_{u_i}$ falls between 0.4 and 5.3. Taking simple unweighted averages of all the data yields mean values of $\sigma'_{r\infty}/\sigma'_{r_i}$ and $\sigma'_{r\infty}/c_{u_i}$ of 1.3 and 2.2 respectively. Cavity expansion theory, which predicts $\sigma'_{r\infty}/c_{u_i}$ values of around 5 to 6, therefore significantly overestimates the radial effective stresses that have been measured close to conventional displacement piles. Strain path solutions, which predict $\sigma'_{r\infty}/\sigma'_{r_i}$ values of around unity, appear to offer more satisfactory models of pile installation.

9.6 Stress Changes During Pile Loading in Clays

The axial loading of piles in clay soils can be conveniently divided into two main phases: an early stage during which no slip occurs between the pile and the soil, and a later stage during which the pile ruptures and plunges to failure.

9.6.1 Behaviour before pile slip

During the early stages of loading, the soil will adhere to the pile

until slip occurs. Kinematic continuity requires that the axial and circumferential strains in the soil adjacent to the pile will be zero (for a rigid pile), and that radial displacement at the pile/soil interface will be zero. The near pile soil behaviour will be dominated by its kinematic response to these boundary conditions (Martins, 1983). Complex stress changes may be required near to the pile as loading takes place (Potts and Martins, 1982).

Potts and Martins (ibid.) performed finite element analyses simulating pile loading using two variants, (A) and (B), of modified Cam-clay. Model (A) was the same as that employed by the Cambridge reseachers. A short segment of a long pile was modelled, well away from the influence of the pile tip and ground surface.

Some of the analyses simulated laboratory experiments on model piles installed in kaolin, reported by Chandler and Martins (1982). In these experiments, the model piles were carefully installed in beds of normally consolidated kaolin, such that there was minimal disturbance to the fabric and stress field surrounding the pile. Testing was under fully drained conditions. Good agreement of results was found between the model pile tests and the finite element prediction of model B, up to peak capacity. A slight fall in σ_r' during pile loading was predicted and measured. The soil model was not able to predict further reductions in shear stress after critical state conditions were reached and did not therefore simulate the marked reduction in model pile capacity on further displacement after peak, caused by the development of a residual failure surface (Martins, 1983).

A number of runs were carried out by Potts and Martins, to explore the effect of varying the initial stress conditions on pile loading behaviour.

Firstly, parametric studies were performed which simulated the model pile tests in normally consolidated kaolin. In these runs it was assumed that the initial stresses were uniform in the soil before pile loading and that the principal stresses were in the ratio $\sigma_r' = \sigma_\theta' = K\sigma_v'$. Values of K between 0.5 to 2.0 were considered. For drained loading, σ_r' was predicted to increase slightly as the initial stress ratio approached active conditions, but otherwise σ_r' was predicted to decrease, with the value at failure being within 20% of the initial value. These predictions were in good agreement with observed behaviour in the laboratory tests. The numerical studies predicted pile capacity to be only slightly dependent on drainage conditions during loading.

Further runs were then carried out in which the post-consolidation stresses from the results of two of the analyses of Randolph et al (1979) and Wroth et al (1979) (Section 9.3) were used to provide the initial stresses for pile loading simulation. Soil model (A) was used, soil parameters being chosen to represent (a) initially normally consolidated Boston Blue Clay, and (b) London Clay with OCR = 8.

Drained and undrained analyses were performed in the case of the normally consolidated Boston Blue Clay. In comparison to the previous parametric studies simulating the model pile tests, there were found to be greater reductions in σ_r' during loading, and increased differences between drained and undrained capacities. The reduction in σ_r' was around 40% and 50% for drained and undrained loading respectively, and the drained capacity was about 1.3 times greater than the undrained capacity. Maximum pore pressures during undrained loading were small in comparison to the pore pressures generated during pile driving (i.e. during cavity expansion). In a drained analysis on the overconsolidated London Clay, the reduction in σ_r' during loading was found to be around 30%.

Randolph and Wroth (1981) applied the results from simple shear tests to the undrained axial loading of piles, in an effort to relate the radial effective stresses predicted by cavity expansion theory to measured shaft capacities of conventional piles. Although good agreement was obtained, unrealistic reductions in σ_r' during loading were necessarily predicted because of the unrealistically high post-consolidation values of σ_r' predicted by cavity expansion theory. Jardine (1985) points out other inconsistencies in the simple shear approach.

Observations of real pile loading effects have to date been too limited to allow many general conclusions to be made (ibid.). Slight reductions in σ_r' are usually reported, less than the magnitude of the reductions predicted during pile loading for pile installation modelled as cavity expansion.

9.6.2 Behaviour during pile slip

As a pile is displaced in the ground - both during installation and during loading - plastic straining will be concentrated in a shear zone adjacent to the pile. The large relative displacements that occur give rise to important fabric changes in the shear zone, which will have an available strength between the residual strength and the remoulded strength, depending on the effective stresses in the soil, the method and rate of pile installation, and the type of soil. When the pile is loaded, slip will occur when the strength of the shear zone is exceeded.

Potts and Martins (1982) re-examined their drained finite element analyses of the model pile tests, and introduced reduced angles of shearing resistance on the vertical surface along the length of the pile. They found that the presence of a discontinuity suppressed reductions in σ_r' during loading, but that even so values of pile adhesion factor α were lower. The presence of such a discontinuity truncates the continuum analysis, and dictates pile capacity (the discontinuity is assumed not to affect the analysis until the threshold strength is reached). Adoption of residual friction angles on the discontinuity gave α values in good agreement with field data. Under undrained conditions, it was found that pile slip could occur before significant development of the pore pressures predicted by the continuum theory, as observed in practice (Bond, 1989). Potts and Martins concluded that even if pre-formed residual surfaces were assumed, the α values deduced from cavity expansion theory were unrealistically high.

Jardine and Potts (1988) describe an effective stress approach for the prediction of axial load:displacement relationships for large piled foundations. They applied the approach in a finite element analysis of the loading of the piled foundations of the Hutton Tension Leg Platform (TLP). The ground conditions at the Hutton TLP site comprise alternate layers of stiff to hard clays and dense to very dense sands.

Jardine and Potts concluded that the prediction of stresses acting after pile installation is the most difficult step in the prediction of pile capacity. In their analysis of the loading of the TLP foundation they used values of post-consolidation stresses based on the field measurements given in Table 9.1. The finite element analysis included modifications to allow an interface criterion along the length of the pile shaft, such that τ_{rz}/σ_r' values in the various clay and sand layers did not exceed specified values. Pile loading was assumed to be drained in the sand layers and undrained in the clay layers. Radial effective stresses during loading remained within 8% of the initial values before loading. Axial capacity was dominated by the distributions of σ_r' assumed to act prior to loading, and the assumed pile/soil frictional characteristics. The undrained shear strength profile prior to loading appeared to play a less direct role in determining shaft friction.

9.7 Cavity Expansion Model of Wedge-Pile Installation in Clay

9.7.1 Cylindrical expansion

The research outlined in the preceding Sections of this Chapter has shown that cylindrical cavity expansion is not a good model for

conventional pile installation, and seriously overpredicts the post-consolidation radial stresses acting against the side of a pile. It is far more likely to be successful in predicting the capacity of wedge-piles, provided that controlled radial expansion along the length of the pile shaft can be achieved. Accordingly, the theories and analysis presented previously can be used to predict likely increases in capacity due to expansion. At this early stage of the project only simple estimates are needed.

The shaft friction τ_{s_f} acting at failure on piles driven in clays is usually correlated either to the original undrained shear strength c_{u_i} :

$$\tau_{s_f} = \alpha \, c_{u_i} \qquad (9.10)$$

(e.g. Skempton, 1959; Tomlinson, 1970; 1977), or to the original vertical effective stress σ'_{v_o} :

$$\tau_{s_f} = \beta \sigma'_{v_o} \qquad (9.11)$$

(Burland, 1973).

The Cambridge solutions consider increases in effective stresses in terms of the original undrained strength, so the α approach is used here. A large amount of data has been accumulated which relates shaft adhesion to undrained strength, and α has been found to vary widely: between about 0.2 and 1.5 depending on the undrained strength, the length and type of pile, the rate of installation, and the succession of strata.

Pile capacity is only indirectly related to the original shear strength, being controlled by the effective radial stress acting at failure and the effective pile/soil interface friction. The field data from instrumented piles reproduced in Section 9.5 gives an indication of the post-consolidation radial stresses to be expected around driven piles. It is assumed here that the unweighted average value of $\sigma'_{r_\infty} / c_{u_i}$ = 2.2 from the data given in Table 9.1 is a typical average value for conventional driven piles. Assuming a possible range of δ' of between 10° and 30°, say, and the average $\sigma'_{r_\infty} / c_{u_i}$ value of 2.2, gives τ_{s_f} / c_{u_i} (α) values of between 0.4 and 1.3. Encouragingly, therefore, the average value of $\sigma'_{r_\infty} / c_{u_i}$ from the experimental data yields a possible range of α values within the range of published values. (Of course, variations in α are due to variations in σ'_r as well as δ').

Cavity expansion theory predicts post-consolidation radial stresses of

around 5 to $6c_{u_i}$, around 2 to 3 times greater than the average of measured values for conventional piles. However, Potts and Martins numerical work predicts greater reductions in σ_r' during loading if cavity expansion values are assumed for the initial stresses (Section 2.6). If the average post-consolidation values of σ_r' for conventional and expanded piles given in Section 9.5 are combined with reasonable assumptions regarding the drop in σ_r' during loading, a rough upper bound estimate can be made of the increase in radial effective stress that can be achieved by expanding a pile. Assuming that σ_r' drops by about 10% during loading in the case of conventional piles, and by about 30 to 40% in the case of expanded piles, the effective stress at failure is predicted to increase by a factor of around 1.8 (say 2). This factor also represents the increase in shaft capacity that would be expected if the pile/soil interface friction angle remains the same after expansion. If the action of expanding a pile disrupts residual surfaces formed during installation, the increase in shaft capacity may be greater.

9.7.2 Non-cylindrical expansion

In practice, a wedge-pile does not cause a uniform cylindrical expansion of a cavity as described by theory, rather it expands radially a number of separate longitudinal elements into the soil. A useful analogy to this situation is the lateral loading of piles; which has been studied in the case of cohesive soils by Broms (1964), Sullivan et al (1980), and Randolph and Houlsby (1984). The ultimate lateral resistance P developed on a pile is usually expressed in the form

$$P = N \cdot c_u \cdot D \qquad (9.12)$$

where

N = lateral bearing capacity factor

c_u = undrained shear strength

D = pile diameter

At depth, plastic flow mechanisms control the ultimate lateral resistance. Randolph and Houlsby (1984) developed solutions for a rigid, perfectly plastic soil and found values for N of between 9 and 12, depending on the pile/soil adhesion factor assumed. These values were in good agreement with reported experimental values obtained for N . However, the rigid-plastic analysis cannot deal with the effect of the plastic zone being fully confined by an outer elastic zone. This can be achieved by considering the lateral loading of a pile as similar to a pressuremeter test (Baguelin et al, 1978, Briaud et al, 1985).

It is reasonable to assume that the pressure in front of a laterally loaded pile will increase up to the limit pressure p_L obtainable from a pressuremeter test (Randolph and Houlsby, 1984). Randolph and Houlsby, assuming that the limit pressure p_L is given typically by the expression $p_L = \sigma_{r_o} + 6c_u$ (e.g. Marsland and Randolph, 1977), and making a small nominal allowance for the developed side shear on the pile that contributes to lateral pile resistance, suggested the expression

$$N = 7 + \sigma_{r_o} / c_u \qquad (9.13)$$

This approach can be extended to the case of the circular wedge-piles depicted in Figure 9.6, which are shown being expanded in 2, 3 and 4 directions. If it is assumed that the limiting pressure develops in front of each segment, and develops only in the direction of movement of the segment such that it acts over the segment chord length, the values of radial force/unit length developed on the sides of the expanded piles are in the same ratios as the effective perimeters, as given in Figure 9.6.

As can be seen from Figure 9.6, the foregoing assumptions lead to a prediction that 2, 3 and 4-way circular wedge-piles will develop between 64% and 90% of the radial force available by true cylindrical cavity expansion. There is less difference between the 3 and 4-way cases than between the 2 and 3-way cases. Exactly the same predictions can be shown to apply for piles of other shapes. These differences between 2, 3, and 4-way expansion will give rise to differences in the corresponding percentage increases in radial force in comparison to an unexpanded pile. In the case above, for example, if unexpanded pile capacity is taken as half that of the true cylindrical cavity expansion case, increases in radial force in comparison to the unexpanded pile of 28%, 66% and 80% are predicted for 2, 3, and 4-way expansion respectively. This simple calculation suggests that 2-way expansion will give significantly less increase in capacity in clays than for 3 and 4-way expansion.

9.8 Analytical Solutions for Drained Cylindrical Expansion

Analytical solutions have been presented for the expansion of a cylindrical cavity in sand. As was the case for clays, these solutions have been developed primarily for use in the interpretation of pressuremeter data. In contrast to the undrained, constant volume analysis adopted for clays, in the case of sands a drained analysis is appropriate and assumptions must be made regarding volume change in the sand surrounding the expanding cavity.

Gibson and Anderson (1961) extended their constant volume analysis to include a Mohr-Coulumb failure criterion. They did not obtain good agreement with experimental data when using this analysis. Subsequently, Ladanyi (1963) and Vesic (1972) presented analyses which incorporated more realistic assumptions regarding volume changes. The most widely used interpretation of the pressuremeter test is based on the analysis presented by Hughes et al (1977), referred to here as the Hughes analysis.

The Hughes analysis retains the assumption that deformation of the soil surrounding the pressuremeter takes place under conditions of axial symmetry and plane strain. It is assumed that after an initial stage of elastic deformation, the sand fails at a constant stress ratio, and at a constant rate of dilation. The mobilised angle of friction, ϕ', and angle of dilation ψ' are assumed to be related by Rowe's stress dilatancy equation:

$$\left[\frac{1 + \sin\phi'}{1 - \sin\phi'}\right] = \left[\frac{1 + \sin\phi'_{cv}}{1 - \sin\phi'_{cv}}\right]\left[\frac{1 + \sin\psi'}{1 - \sin\psi'}\right] \qquad (9.14)$$

Hughes et al show that once failure has been initiated at the wall of the cavity the following relationship exists between the cavity pressure p and the cavity strain ε_c, assuming small strains:

$$\ln(p-u_o) = s.\ln\{\varepsilon_c + c/2) + \text{constant} \qquad (9.15)$$

where

p = cavity pressure
u_o = static pore water pressure
$s = \dfrac{(1 + \sin\psi')\sin\phi'}{1 + \sin\phi'}$
ε_c = cavity strain
c = intercept on assumed volumetric strain v shear strain plot

The pressure:displacement curve is given by the expression

$$\varepsilon_c + c/2 = (\varepsilon_R + c/2)\{(p - u_o)/\sigma'_R\} \qquad (9.16)$$

where

ε_R is the strain associated with failure (i.e. the strain at the boundary of the failed zone).

σ'_R is the corresponding radial effective stress at the boundary of the failed zone.

A plot of $(p - u_o)$ against $(\varepsilon_c + c/2)$ on double logarithmic axes should give a straight line with slope s, from which values of ϕ' and ψ' can be derived from Equations 9.14 and 9.15 if ϕ'_{cv} for the sand is known or estimated. A value for c is also required, this is often assumed to be zero.

In order to give an example of the magnitude of increases in radial stress predicted by the Hughes analysis, the results of a simple parametric study are shown in Figure 9.7. Expansion is assumed to take place at 10m depth in dry sand with bulk soil weight γ = 15kN/m^3. Values of in-situ radial effective stress (σ'_{r_o}) given by taking K_o = 0.5, 1.0 and 1.5 have been assumed. Cavity pressures (σ'_r) at given radii have been calculated using Equation 9.16, with c assumed to be zero. The effect on σ'_r of varying ϕ', ψ', and G within typical ranges of values is shown. Cavity strains in the range 5 to 15% are considered; with ϕ' varying between 35° and 50°, ψ' varying between 0° and 10°, and G varing between 10MPa and 25MPa. For these ranges of parameters, the increase in radial effective stress over the in-situ values (σ'_r/σ'_{r_o}) is predicted to be about an order of magnitude. The potential gains in radial effective stress by expansion in sands are clearly greater than those in clays (Section 9.7.1).

Carter et al (1986) have presented combined analytical solutions for the expansion of spherical and cylindrical cavities in a cohesive frictional (c-ϕ) material. The solution assumes small strains. The solution for the pressure-expansion curve is considered appropriate for pressuremeter analyses, where strains do not usually exceed 10%. A numerical technique is required to give the entire pressure:displacement curve, including the large strain portion. However, the analytical solution does yield limit pressures at infinite expansion, thought by Carter et al to be relevant to the installation of a conventional pile. The analytical solutions for cylindrical cavities reduce down to the Gibson/Anderson expression in the case of purely cohesive soil, and (provided the soil is relatively stiff) to the Hughes expression in the case of a purely frictional material. Withers et al (1989) have presented cavity expansion/contraction analyses that have been developed for use with the FDPM in sands.

9.9 Cavity Expansion Model for Wedge-Pile Installation in Sands

Cavity expansion theories for sands predict large increases in radial

effective stress in comparison to in-situ values existing prior to expansion. These predictions are in agreement with the results of pressuremeter tests in sands (e.g. Baguelin et al, 1978; Mair and Wood, 1987). A large amount of pressuremeter data has been accumulated over recent decades in France; Table 9.2 gives a field guide to the density of sands based on the parameter $p_L^* = p_L - \sigma_{r_o}$, derived from the Menard pressuremeter.

Ignoring scale effects, and assuming that no over-expansion occurs, the radial effective stresses acting on a wedge-pile after expansion will be closely related to those given by a pressuremeter test taken to a similar radial strain.

The ultimate unit shaft friction τ_{s_f} acting on piles in sands, for penetrations less than the critical depth, is usually expressed by the relationship

$$\tau_{s_f} = K_s \sigma'_v . \tan\phi' \qquad (9.18)$$

where
σ'_v = effective overburden pressure
K_s = radial stress coefficient
δ' = effective angle of interface friction

The greatest uncertainty lies in the evalution of K_s. Values of K_s are usually back-analysed from the results of pile tests. Various empirical correlations have been published (e.g. Meyerhof, 1976; American Petroleum Institute (API), 1984) which give recommended values of K_s. It is usual to take K_s to lie between about 0.5 for loose sand and 1.0 for dense sand, although values of up to 3.0 have been quoted. A comprehensive review of published load test data and design methods for piles driven in sand was carried out by Lings (1985). He concluded that, in general, the API recommendation of K_s values of 1.0 and 0.8 for full displacement and open-ended piles respectively gave satisfactory results for piles up to 60 diameters penetration in normally consolidated sands. In overconsolidated sands the API predictions underestimated capacities.

Relatively little has been published concerning the stress states developed around piles driven in sand, and there is currently a need for much experimental and theoretical research in this direction (Jardine and Potts, 1988). Most of the reseach to date has been carried out in the laboratory and in testing pits (Szechy, 1961; Robinsky and Morrison, 1964; Kerisel, 1964; Vesic, 1967). Bond (1989) has recently performed field tests in sand with the Imperial College instrumented pile.

The seminal work by Robinsky and Morrison involved the use of lead shot to study sand displacements and compaction patterns ahead of and around a 1.5inch diameter model pile jacked into beds of loose and medium dense sand. They found that a complex sequence of density changes occurred in the sand, involving compaction below the pile, followed subsequently by stress relief as the pile toe passed by. The stress relief resulted in an increase in the void ratio of the sand immediately adjacent to the pile shaft, creating a thin sleeve of loose sand. Robinsky and Morrison concluded that a cylinder of dense sand, originally compacted beneath the pile toe, arched around the sleeve of loosened sand, preventing the development of the available lateral earth pressure. They further concluded that the load carrying capacity of piles in sand is controlled by the properties of the loosened zone, such that increases in lateral earth pressure have only a limited effect on capacity.

Hughes and Robertson (1985), made friction cone tests at the University of British Columbia (UBC) sand test site at McDonalds Farm. The results confirmed that when a probe is pushed into sand high stresses are developed at the tip, followed by large decreases as the tip passes. At McDonalds Farm, lateral stresses acting on the friction sleeve were almost two orders less than the stresses developed at the cone tip (Figure 9.8). Hughes and Robertson also presented data from tests in cone calibration chambers, previously reported by Baldi et al (1981). These data are shown in Figure 9.9, and show that for loose to medium dense sands at moderate stress levels (maximum dilation angle less than 6°), the average lateral stress in the region of the cone sleeve is close to the original in-situ lateral stress. In dense sands at shallow depths (dilation angle greater than 10°) greater lateral stresses acting on the cone sleeve have been observed. Hughes and Robertson suggest that lateral arching around an advancing cone in sand limits the lateral stresses that can act on the body of the cone - this suggestion is in agreement with the findings of Robinsky and Morrison (1964).

Clearly, both inferred and measured radial stresses acting on the sides of piles and probes driven or pushed into sand are many times less than the values predicted by cavity expansion theory, and measured in pressuremeter tests. Large increases in radial effective stress could reasonably be expected by expanding a driven pile in sand. This is clearly illustrated by the results of a FDPM test at the UBC test site presented by Hughes and Robertson (1985), shown here in Figure 9.10. The FDPM is an exact analogue of a pile driven into the ground and subsequently expanded. The results shown in Figure 9.10 indicate that after an expansion of only 9% the radial effective stress is around 7

to 8 times the value acting after installation of the FDPM (as indicted by the 'lift-off' pressure).

Any increases in pile capacity resulting from such increases in radial stress will depend crucially on reductions in radial stress that might occur during pile loading. In the case of a conventional pile driven in sand, in which the stress path followed during loading is usually a continuation of that followed during installation, it may be reasonable to assume that all reduction in σ_r' occurs during installation, with no further losses occurring during loading. In the case of an expanded pile, pile loading follows a different stress path to that during installation, and the assumption that no change occurs in σ_r' during loading is less reasonable. The influence of the further stress reversals that would occur during cyclic loading is likely to be important.

The radial force developed on the sides of a 2, 3 or 4-way wedge-pile expanded in sand may be less than that theoretically available by cylindrical cavity expansion, as outlined in Section 9.7.2.

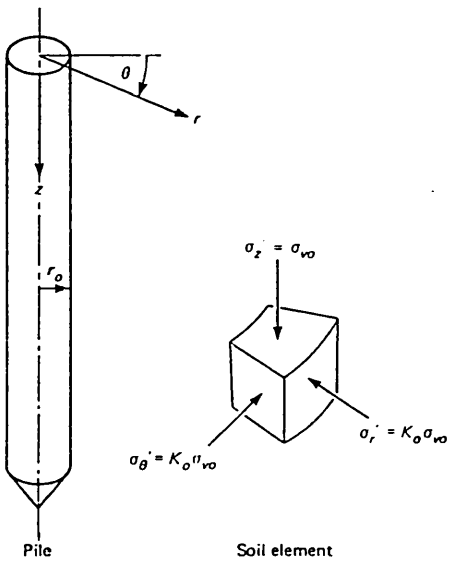

Figure 9.1 Cambridge Theory:
Co-ordinate system and initial stress state in the soil
(after Randolph and Wroth, 1982)

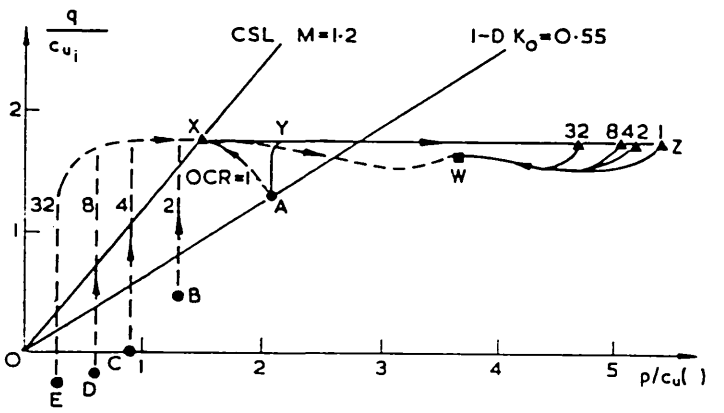

Figure 9.2 Stress paths during cavity expansion and subsequent consolidation for soil at r = 1.15r
(after Randolph et al, 1979)

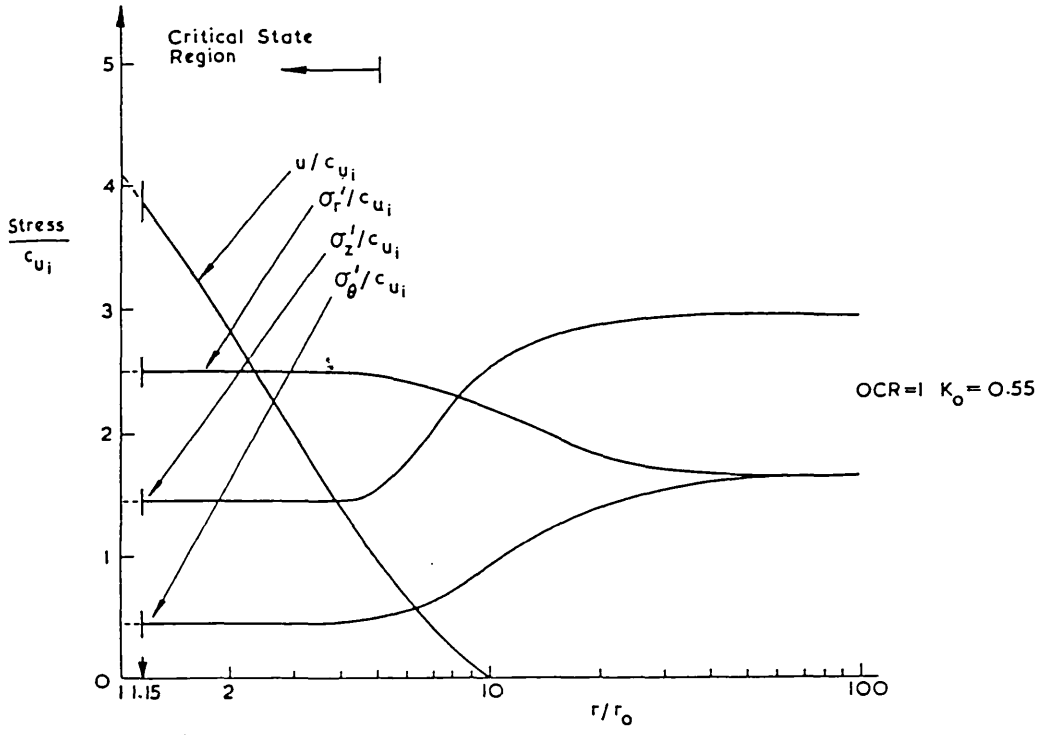

Stress distributions in the soil around the pile immediately after driving, OCR = 1

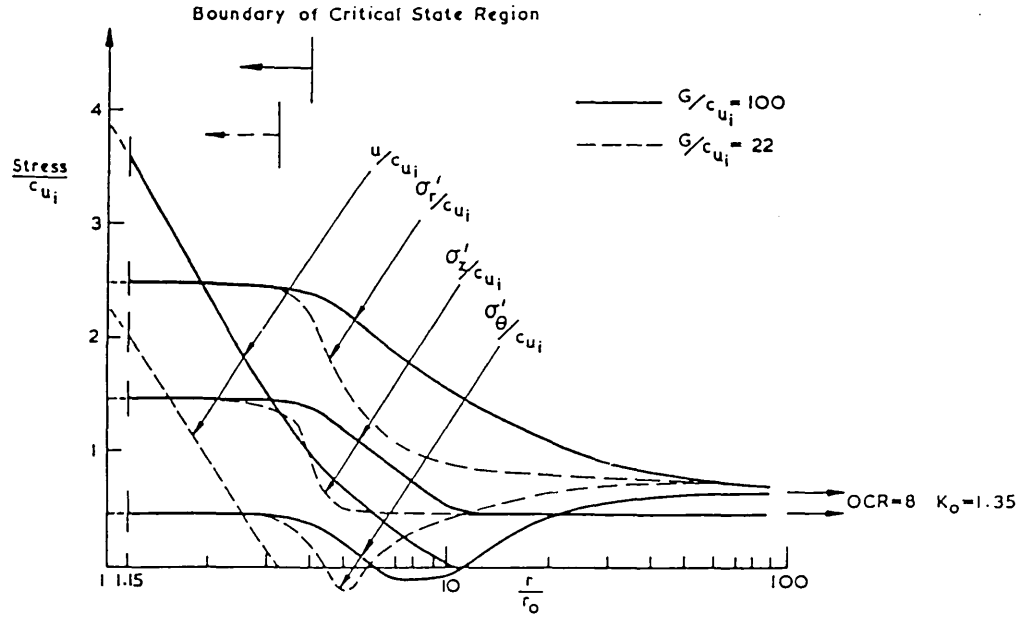

Stress distributions in the soil around the pile immediately after driving, OCR = 8

Figure 9.3 Stress distributions in the soil around the pile immediately after driving, OCR=1 and OCR=8 (after Randolph et al, 1979)

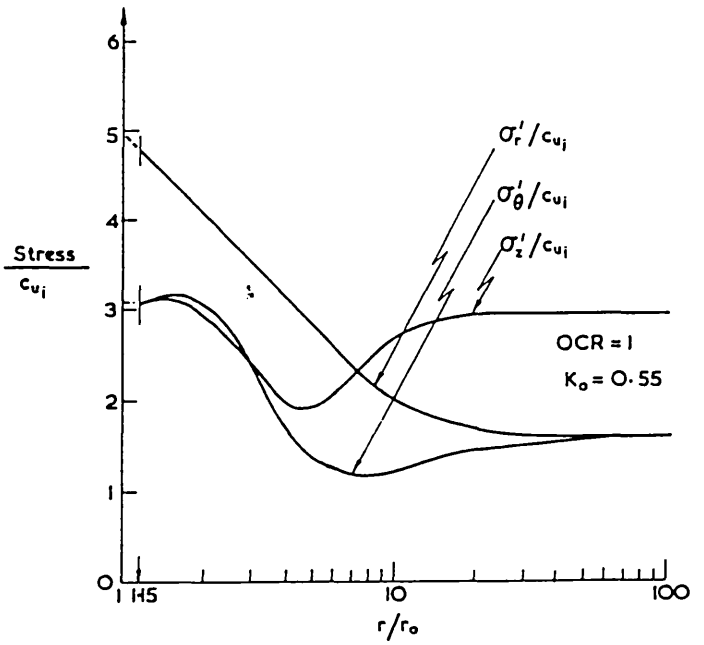

Distribution of stresses at end of consolidation for OCR = 1

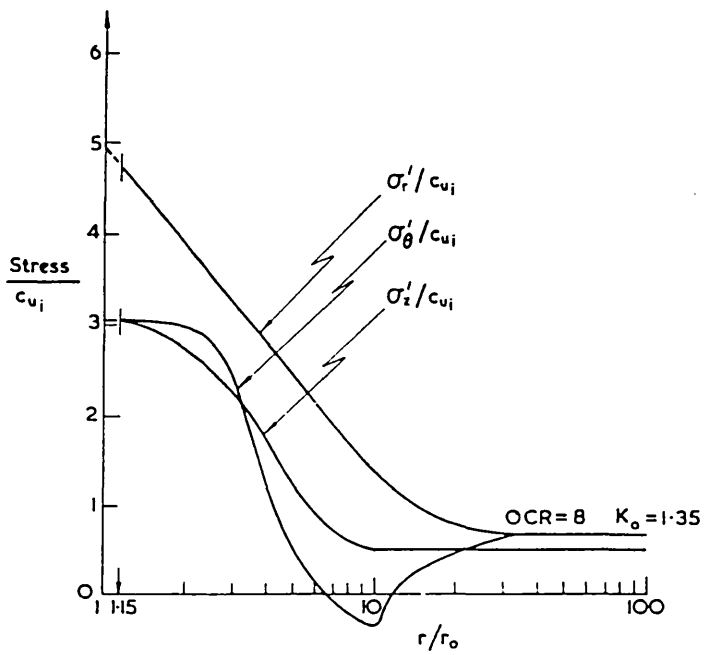

Distribution of stresses at end of consolidation for OCR = 8

Figure 9.4 Stress distributions in the soil around the pile at end of consolidation, OCR=1 and OCR=8 (after Randolph et al, 1979)

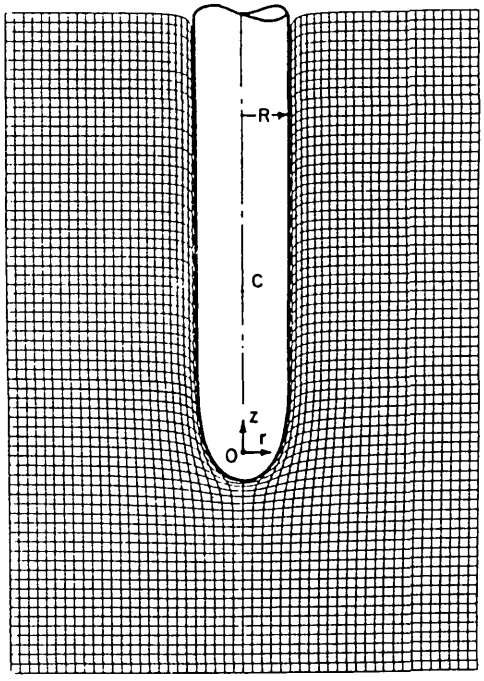

Figure 9.5 Typical strain path solution
(after Baligh, 1986)

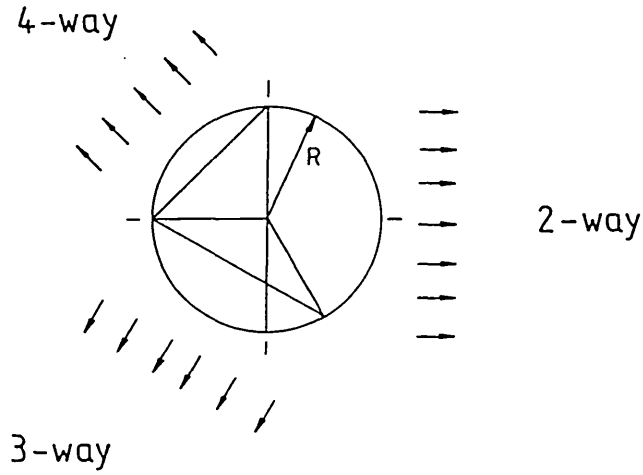

Pile type	Effective perimeter of expanded pile	Ratio of perimeter to that of expanded cavity
(Expanded cavity)	6.28R	1.00
2-way	4.00R	0.64
3-way	5.20R	0.83
4-way	5.66R	0.90

Figure 9.6 Non-cylindrical expansion of circular wedge-pile

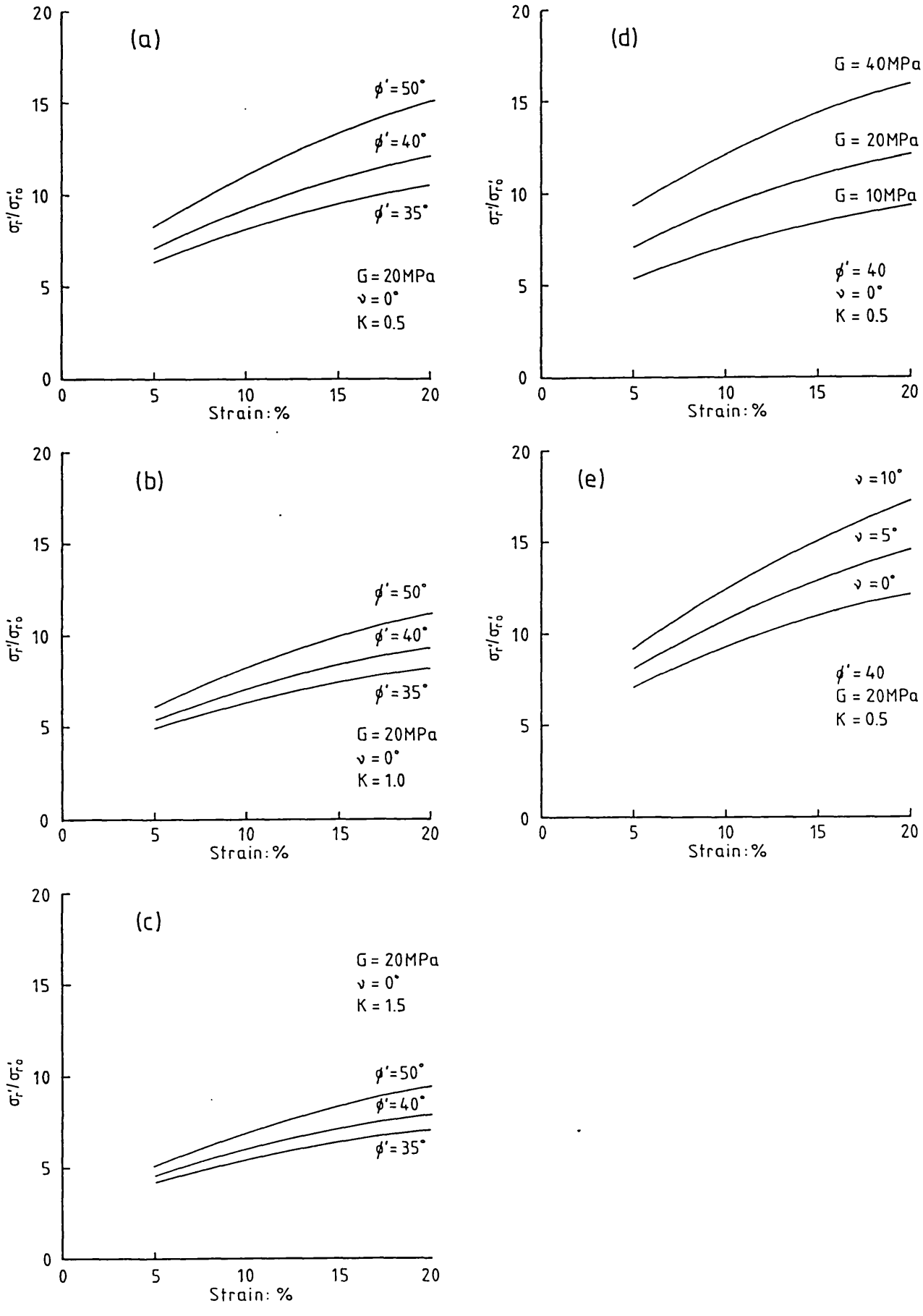

Figure 9.7 Parametric study using the analysis of Hughes et al (1977) (see Section 9.8)

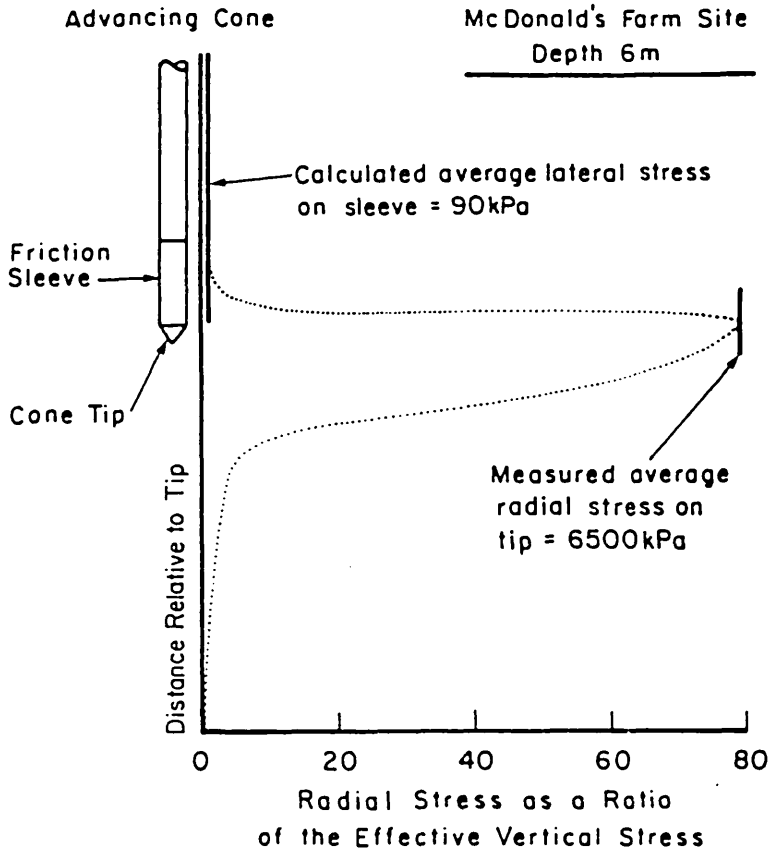

Figure 9.8 Qualitative evaluation of stress distribution around an advancing cone (after Hughes and Robertson, 1985)

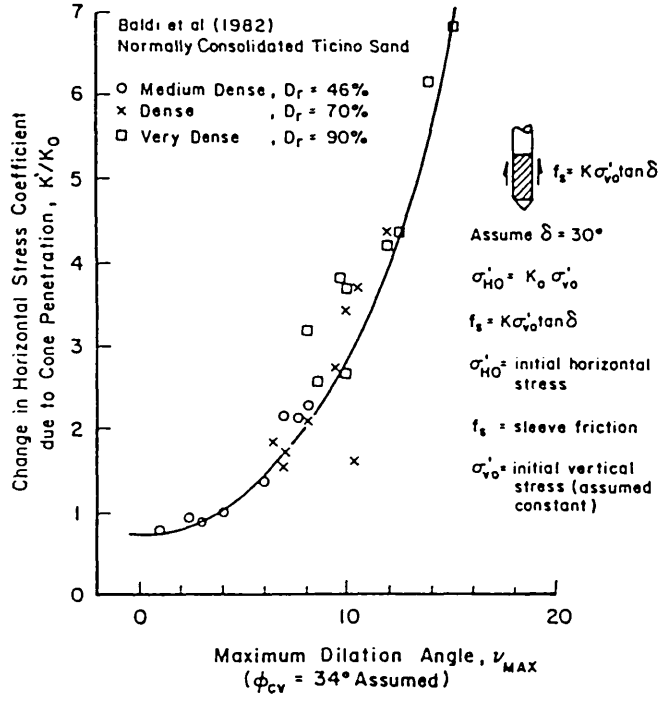

Figure 9.9 Change in horizontal stress coefficient due to cone penetration in sand (after Hughes and Robertson,1985)

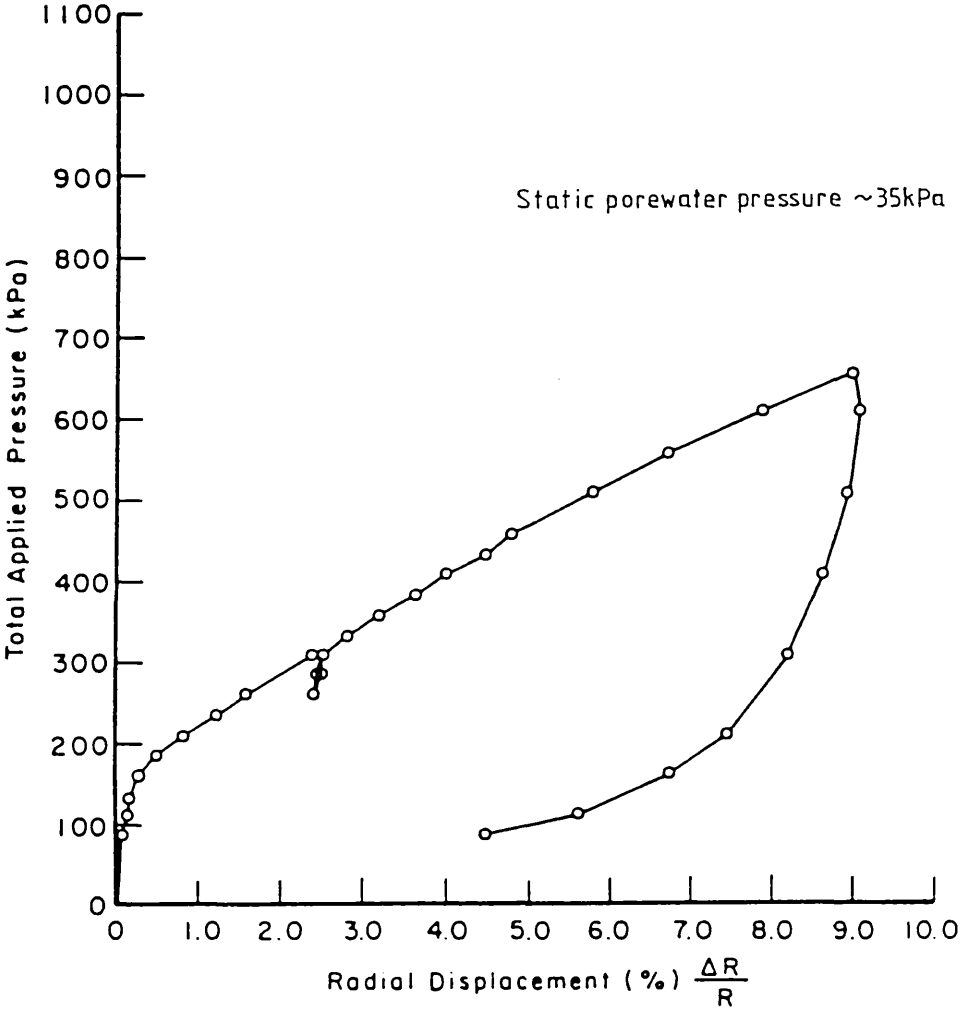

Figure 9.10 Typical result of full-displacement pressuremeter test at McDonalds Farm site (depth 5.5m) (after Hughes and Robertson, 1985)

Case	Soil	Apparent OCR	Depth: m	Degree of Equalization: %	Final $\sigma_{r\infty}'/C_{ui}$	$\sigma_{r\infty}'/\sigma_{ri}'$
1	*San Francisco Bay mud* $C_u \simeq 14$ kPa PI $\simeq 18\%$	$\simeq 1{\cdot}0$	3·5–6·5	$\simeq 100\%$	0·80–1·25	$\simeq 0{\cdot}60$
2	*Soft, plastic clay, Tokyo* $20 < C_u < 50$ kPa PI 50–60%	$\simeq 1{\cdot}8$ $\simeq 1{\cdot}5$	3·0 5·0	$\simeq 100\%$	1·30 1·43	1·00 1·43
3	*North Sea clays, Forties* $0 < C_u < 200$ kPa PI 14–65% below 40 m	$\simeq 1{\cdot}0$ $\simeq 1{\cdot}3$ $\simeq 1{\cdot}0$	41·0 55·0 70·0	incomplete $\simeq 15\%$ $\simeq 30\%$ $\simeq 43\%$	1·20 } inc. 1·30 } with 3·00 } time	0·62 } inc. 0·67 } with 1·50 } time
4	*Beaumont clay, Texas* $50 < C_u < 200$ kPa PI 45–55% (upper) 12–17% (lower)	6·3 5·2	5·0 10·0	incomplete (not quantifiable)	0·40 } prob. inc. with 1·10 } time	0·50 } prob. inc. with 1·40 } time
5	*Kaolin from slurry in model* $11 < C_u < 55$ kPa PI $\simeq 31\%$	1·0 2·0 4·0 8·0 17·0 25·0	–	$\simeq 100\%$	A B 4·00 3·00* 3·50 3·00 3·00 2·60 2·90 2·30 – 2·00 – 1·80	A B 1·25 0·94* 1·45 1·25 1·58 1·37 1·81 1·43 – 1·54 – 1·80
6	*Boston blue clay, Saugus* PI 12–25%	3·00 2·00 1·35	15·0 20·0 25·0	$\simeq 100\%$	1·80 3·20 2·50	1·00 1·50 1·10
	$40 < C_u < 65$ kPa	1·35 1·35	30·0 35·0		2·50 2·50	1·00 1·00
	MIT site PI 12–25% $60 < C_u < 100$ kPa	2·20 1·50 1·50	20·0 25·0 30·0	$\simeq 100\%$	2·00 2·00 1·90	0·90 1·10 1·10
7	*Haga leached marine clay, Norway* (within top 4·5 m) $30 < C_u < 65$ kPa PI $\simeq 15\%$	8·00 4·00	2·0 3·5	$\simeq 100\%$	0·87 1·34	0·89 1·23
8	*London clay Canons Park* $40 < C_u < 130$ kPa PI 42–58%	14·00 11·00	3·0 4·1	incomplete after 24 h	1·4– decr. 2·1 with time	1·3– decr. 2·1 with time
9	*Cran, France* Mixed profile plastic silts, silty clays $15 < C_u < 50$ kPa PI 40–60	'normally consolidated'	5·3 8·9 12·5	$\simeq 100\%$	decr. with time	2·05 → 1·0 1·95 → 1·22 1·85 → 1·50
10	*Empire clay* Zone I $C_u \simeq 65$ kPa PI 52–66 Zone II $C_u \simeq 90$ kPa PI 35–61	1·7 1·5	45 73	100% 100%	5·26 4·42	2·05 1·25

* Mean of several tests

Table 9.1 Data for stress state at end of consolidation obtained with instrumented piles (after Jardine and Potts, 1988)

p_l^* (kN/m²)	Description	SPT N
0 to 200	Very loose	0 to 4
200 to 500	Loose	4 to 10
500 to 1500	Medium dense	10 to 30
1500 to 2500	Dense	30 to 50
2500+	Very dense	>50

Table 9.2 Field guide to relative densities of sands related to net limit pressure from Menard pressuremeter tests (after Baguelin et al, 1978)

CHAPTER 10
A NUMERICAL MODEL FOR THE MECHANICAL EXPANSION PROCESS

10.1 Introduction

10.1.1 Aims

The primary aim of the numerical study was to develop an understanding of the mechanical expansion process of 'multiple-element' steel wedge-piles (Section 1.3). It was planned to model the essential features of the process by means of a simple numerical method. It was hoped that the model would assist in the analysis of the results of the field trials and could be used in the future as a design tool.

In this Chapter, outer shell and expander mandrel are referred to as shell and mandrel respectively.

For given soil behaviour and shell flexural properties, the key questions are:

(a) What is the radial effective stress generated on expansion for a given mandrel nose shape? In particular, what happens if there is over-expansion in the region of the nose?

(b) What is the displacement line of a shell element as it translates flexurally? What internal shear forces and bending moments are generated?

(c) What is the appropriate nose profile to effect a smooth transition of the shell without over-expansion?

(d) What effect do the temporary connections between the shell elements have ?

10.1.2 Problem description

Consider the 'long' wedge-pile shown in Figure 10.1. For simplicity a two element shell is considered, reducing the problem to a two dimensional problem rather than a three dimensional one. The process for shells comprising more than two elements is essentially the same, except that the soil forces generated on expansion will differ (Section 9.7). The soil is considered to be homogeneous so the problem is symmetrical.

The shell depicted has been installed in the ground and is undergoing expansion as the mandrel advances. The temporary connections which hold the shell together are ignored for the present. It is assumed that the displaced elements are held in position by the mandrel shank. The shell elements are assumed to behave fully elastically. The validity of this assumption is considered later. Any twisting of the shell elements is also ignored - the elements are assumed to bend in a single plane.

At some distance ahead of the mandrel nose, the shell elements have not been disturbed. The elements are held together in equilibrium by the radial effective stress, σ_1', generated as a result of installing the shell in the ground. This region is defined as the UNDISTURBED ZONE.

At some distance behind the mandrel nose, the shell elements have been displaced to their final position and are being maintained in that position by the advancing mandrel shank. The radial effective stress acting on the pile, σ_2', has been altered as a result of the expansion process. This region is defined as the FULLY DISPLACED ZONE.

There is no flexure of the shell elements in either the undisturbed or the fully displaced zones.

In the region of the mandrel nose, the shell elements are undergoing flexure as they are displaced radially into the soil. The elements are acted on by a system of soil forces and wedging forces. The radial effective stress will increase as the elements are displaced outwards, and decrease if there is any contraction behind the nose. This region is defined as the FLEXURE ZONE. The expansion process is confined to this zone and moves as a progressive wave of flexure along the shell as the mandrel is driven.

The mandrel nose acts as a wedge at some point or region along the flexure zone, applying a radial force or forces to the shell elements. The deflection line of the flexure zone depends on the shape of the nose, the soil forces generated and the flexural properties of the shell elements. Because the expansion process is displacement controlled it will be characterised by irreversible plastic straining of the soil mass surrounding the pile. Except for certain simple nose profiles the positions of the wedging forces are not known, and they may be distributed or concentrated depending on the shape and length of the nose. The position of the wedging forces, and the deflection line of the flexure zone, will in general vary with depth as the mandrel is driven.

The essential problem is to analyse the behaviour of the flexure zone. It is a problem of soil/structure interaction.

10.1.3 Possible solution strategies

The problem is highly non-linear since (for any given depth) it is not known ab initio what the length of the flexure zone is, where the wedging force(s) act, and over which part of the flexure zone the soil forces are increasing or decreasing. Therefore, all solution strategies will necessarily be iterative, making use of a computer or programmable calculator.

Three approaches were considered:

(a) A method based on standard analytical solutions for beams on elastic foundations. The shell elements are considered as beams, supported by an elastic foundation and being displaced by a system of wedging forces.

(b) Finite element or finite difference modelling. These methods involve dividing the shell elements up into segments and calculating the deflection of the beams at the nodal points between each segment. In the case of flexible beams, the numerical method usually adopted is the finite difference method. The deflection equation of the beam is represented by a finite difference approximation. Finite difference equations are obtained at each nodal point and are solved algebraically.

(c) A method that considers the shell elements as ordinary beams, supported by wedging forces and acted on by soil forces (Burgoyne and Aul, 1987). This approach can be regarded as the opposite of method (a). In this method, the soil forces are obtained by treating the soil as a discontinuous foundation (Hetenyi, 1946), with soil pressure at any point a function of displacement. The soil pressure is idealised as a series of point loads. The deflection line of the beam is initially guessed. The corresponding soil forces are calculated. These will result in a new displaced shape for which the soil forces can be reassessed, and so on until a solution is obtained.

Standard elastic foundation solutions can be useful in stress controlled problems where stress levels are such that the soil response is often reasonably elastic. This approach was rejected, however, because the problem under consideration is displacement controlled and the soil response is highly non-elastic. In particular, such an approach would

not model the non-elastic reduction in stress caused by over-expansion, which was one of the key areas of interest.

The finite difference method is a powerful technique capable of dealing with beams under complex loading conditions and with beam and soil properties varying along the beam. However, less computing time will normally be involved if beam properties and loading conditions are such that the superposition of standard analytical solutions can be used to achieve a solution. This can be demonstrated by means of an 'operational count'. Only multiplications and divisions will be counted since these are more time consuming on a computer or calculator than additions or subtractions.

For the case of a simply supported beam acted on by n vertical loads, the operational counts are as follows:

Finite difference method: this method involves solving n simultaneous equations. It can be shown that, using Gaussian elimination to solve the equations, the operational count is roughly proportional the cube of the size of the system, n^3 (de Vahl Davis, 1986).

Superposition method: this method essentially involves calculating n deflections for each of the n loads. The operational count is the square of the size of the system, n^2.

The superposition method is roughly n times quicker than the finite difference method. This is a particularly relevant point when considering the numerical analysis of beams on foundations, where the continuous support of the foundation is represented by a large number of point loads.

In theory, the iterative process of the ordinary beam approach should converge to a deflection line which causes support forces that are in equilibrium with soil forces, but in practice this is difficult to achieve. It has been found that the deflection line often tends to oscillate about the final solution as successive iterations are made (Burgoyne and Aul, 1987). Convergence only occurs if a proportion of the change in forces between iterations is applied to the beam. The determination of the proportion (the damping factor) to be used is critical, since if it is chosen too small convergence is very slow, and if too large, oscillation occurs.

Although the ordinary beam approach has been found in the past to be unsuitable for use in a general program (ibid.), it was decided to

explore this avenue of analysis because of its inherent simplicity.

10.2 Ordinary Beam Approach

The ordinary beam approach devised by the author consists of two stages:

(a) Definition of system -
The mathematical model for the soil is chosen. The beam properties and the support conditions are defined.

(b) Numerical solution -
The system is discretized and an iterative scheme is developed to converge to the final solution.

10.2.1 Definition of system

10.2.1.1 Soil model

The approach is based on the assumption of a discontinuous foundation (Hetenyi, 1946). It is obvious that a discontinuous foundation is not valid for soils. However, for flexible beams the errors involved in the use of the assumption are relatively small (Scott, 1981; Pavlovic and Tsikkos, 1982). The soil surrounding the pile is represented as a set of 'springs' which act independently, the depression of one spring having no effect on an adjacent spring (Figure 10.2). The more springs that are used the better is the representation of the soil.

Soil response is considered in terms of a radial stress : radial displacement relationship. Although the soil is represented by 'springs', the stress:displacement relationship can be as complicated as necessary. The concept is the same as for the t-z and p-y methods for axially and laterally loaded piles (Matlock and Reese, 1961; Smith, 1980; Sullivan et al, 1980). Drained expansion is assumed, with all stresses being effective stresses.

In reality, the stress:displacement relationship depends on the mechanical behaviour of the soil surrounding the wedge-pile and on the mode of deformation imposed on the soil as expansion takes place. The problem is complicated (Chapter 9). Both the mode of deformation and the behaviour of the soil will depend on the configuration of wedge-pile. The most readily available source of material on which to base the stress:displacement relationship is pressuremeter test data and associated cavity expansion theory. Typical soil response during expansion is illustrated in the stress:displacement relationship shown in Figure 10.3. If the stress:displacement curve is known or assumed, it

is a straightforward task to approximate the spring response of the discontinuous foundation to the desired degree of fidelity.

The models used in the study were intended to represent qualitatively the soil response at the BRS test site. The general approach was to develop the method using models of increasing complexity, until all the features of Figure 10.3 were taken into account. It was envisaged that quantitative analysis using site specific data could follow once the program was working satisfactorily.

The stress:displacement curves of the four models used are shown in Figure 10.4. The models are:

(a) linear-elastic
(b) linear-'elastic' with cut off
(c) non-linear 'elastic'
(d) non-linear non-elastic

Models (b) and (c) are 'elastic' in the sense that the loading and unloading paths for the the soil mass are the same.

10.2.1.2 Support conditions

The analysis considers the quasi-static expansion of a single shell element (Figure 10.5). The flexure zone of the element is treated as a free body, acted on by distributed soil forces and supported by concentrated wedging forces.

The simplest support system is considered. This comprises a single support R_0 acting at some point in the middle of the flexure zone, with end supports R_1, R_2 to maintain equilibrium. It is necessary for wedging forces to act outwards into the soil mass, as tensile forces between mandrel and shell are not admissible. By definition the bending moment at each end of the flexure zone is zero. Compatibility requires that the angular rotations θ_1, θ_2 at each end of the flexure zone are also zero. Axial forces are neglected.

The positions of the supports in the longitudinal direction are considered relative to the central support (L_1, L_2). The positions of the supports in the transverse direction are considered relative to the leading end support (d_0, d_2). d_2 is defined as the 'shank displacement'. The geometry of the supports sets constraints on the deflection line of the flexure zone such that the maximum displacement d_{max} is usually greater than the shank displacement d_2. This effect is defined as 'over-expansion'.

To achieve a solution to this beam system, three groups of unknowns need to be dealt with:

- Support geometry unknowns:
  It is not known ab initio the longitudinal positions of the end supports (L_1, L_2) or the transverse position of the central support (d_0).

- Soil force unknowns:
  The soil forces are a function of the deflection line, which is unknown. It is also not known which part of the beam is undergoing expansion and which part contraction.

- Reaction unknowns:
  Even for given support geometry and soil loads, the number of support reactions is greater than the number of equilibrium equations available. The system is statically indeterminate.

The study deals with two cases of the simple support system, defined as the 'Blunt' case and the 'Ideal' case. These are described below.

(a) Blunt case:
This is shown in Figure 10.6. It is the deflection line resulting from a 'Blunt' mandrel nose (see Section 10.4.1). In this case, over-expansion occurs:

$$d_0 < d_2 < d_{max}$$

The situation is represented as a beam carrying a distributed load, resting on simple supports at different levels. If:

$$d_0 = d_2 < d_{max}$$

the behaviour is described as 'fully-Blunt'. This is the deflection line resulting from expansion by a plain-ended mandrel, without a shaped nose.

(b) Ideal case:
This is shown in Figure 10.7. In this case there is no over-expansion:

$$d_0 < d_2 = d_{max}$$

Because the deflection line between the central and trailing supports curves in the same sense throughout, the trailing end reaction R_2 is zero.

The situation is represented as a beam carrying a distributed load, resting on two simple supports with an overhang. It can also be

considered in exactly the same way as for the Blunt case, but with R_2 set to zero.

The Ideal case is the deflection line associated with the lowest possible strain energy of expansion. It is further associated with the 'Ideal' mandrel nose profile (see Section 10.4.1).

The investigation concentrates on the fully-Blunt case and the Ideal case. These situations represent the extremes of the single support system. In the fully-Blunt case d_0 is known beforehand; in the Ideal case d_0 is given as part of the problem solution.

10.2.1.3 Beam properties

The flexural properties of the shell elements actually used in the field trials were readily available as standard information.

10.2.2 Numerical solution

Two similar programs were developed to deal with the two beam systems described in Section 10.2.1.2. The full solution method for each system is described separately, although much of the two methods is the same.

There are four main stages in the solution process:

(a) Discretization:
Soil and beam data are read into the program. The beam and soil are discretized.

(b) Core solution:
A statically determinate core solution is established, applicable for any given set of soil loads and supports.

(c) Iterative scheme - soil forces:
The support configuration and deflection line are initially guessed, corresponding soil forces are calculated. The core solution is used to recalculate the deflection line. The process is applied repeatedly to yield a solution satisfying equilibrium and soil constitutive law.

(d) Iterative scheme - support positions:
The support positions are systematically adjusted within a wider iterative scheme to yield a solution satisfying the compatibility requirements at the ends of the beam.

10.2.2.1 Blunt program

(a) Discretization

The shell element is considered as a beam (Figure 10.8). The length of the beam is specified such that it is greater than the likely length of the flexure zone. The beam is divided into segments. The distributed soil forces acting on the beam are idealised as a series of equivalent point loads acting at the middle of each segment. The end supports R_1, R_2 define the flexure zone and act at the end of their segments. The central support R_0 acts in the middle of its segment, in the opposite direction to the soil forces. The soil model is specified as a relationship between radial stress and radial displacement. The width of the beam and its flexural properties are also specified.

(b) Core solution

The beam system is rendered statically determinate by considering R_0 as a force identical to the soil forces but acting in the opposite direction (Figure 10.8). R_0 can then be brought within the iterative scheme. The problem is thus reduced to the case of a simply supported beam acted on by a series of concentrated loads - this can be readily solved by superposition.

(c) Iterative scheme - soil forces

So that the program can be of general application, it is important that the initial guess for the support geometry and the deflection line does not affect the final solution obtained. However, the convergence process can be speeded up if a good guess is provided. For the Blunt case, the transverse positions of all three supports d_0, d_1, d_2 are known; only L_1 and L_2 need to be guessed. An initial deflection line which simply joins the reaction positions by straight lines has proved satisfactory (Figure 10.8).

A displacement controlled iterative scheme has been adopted (see Section 10.2.3). Soil forces are calculated using the initial deflection line, and the deflected shape of the simply supported beam under the soil forces ONLY is calculated. The value of R_0 to give the correct value of d_0 is then calculated. The new deflection line is obtained by superimposing the deflection line due to the soil forces only, and the deflection line due to R_0. Soil forces are then recalculated and the process is repeated until a solution of the required accuracy is achieved.

The longitudinal position L_{max} at which d_{max} occurs (Figure 10.5) is used as a marker to separate the leading part of the flexure zone, where soil

forces increase, from the trailing part of the flexure zone where soil forces decrease. The stress:displacement loading curve is used for the leading part of the flexure zone, the unloading curve is used for the trailing part.

(d) Iterative scheme - support positions
Only L_1 and L_2 need to be considered. Having achieved a solution for the initial support configuration, the angular rotations θ_1, θ_2 are considered. Lengths L_1 and L_2 are then adjusted in the appropriate sense so as to move the overall solution towards a condition of $\theta_1 = \theta_2 = 0$ (Figure 10.9). The minimum possible adjustment is one increment length of the beam. The soil forces for the 'old' support configuration are carried forward to provide a good initial guess for the 'new' support configuration.

The solution process for soil forces is applied for the new support geometry, and θ_1 and θ_2 are again reassessed. The lengths L_1 and L_2 are readjusted and the process is repeated until compatibility is satisfied to the required degree of accuracy. At this point an approximate solution to the beam system is achieved, satisfying equilibrium, compatibility and soil constitutive law.

For presentational purposes, the solution is completed by:

- setting the beam displacement to d_1 and d_2 respectively throughout the undisturbed and fully displaced zones

- setting the soil stress in the undisturbed zone to p_1 and the soil stress in the fully displaced zone to the value p_2 existing at the trailing support.

10.2.2.2 Ideal program

(a) Discretization
The beam length is chosen, and beam and soil are idealised as before.

In the Ideal case there are by definition only two supports. However, a nominal trailing support R_2 is assumed, set to zero. R_1 and R_2 thus define the flexure zone as before, acting at the ends of their increments. R_0 acts in the middle of its increment, in the opposite direction to the soil forces.

(b) Core solution
In the Ideal case the beam system is statically determinate (Figure

10.7). The problem is thus one of a simply supported beam with an overhang, acted on by a series of concentrated loads - this is readily solved by superposition.

(c) Iterative scheme - soil forces
In this case d_0 is a further unknown, along with L_1 and L_2. All three are initially guessed. A straight line between the reaction positions defines the initial deflection line. The core solution is repeatedly applied to converge to a solution, as for the Blunt case.

(d) Iterative scheme - support positions
L_1, L_2 and d_0 need to be considered. Having achieved a solution for the initial support configuration, θ_1 and θ_2 are monitored as before. L_1 and L_2 are adjusted to give a full solution for a given d_0. At this stage d_0 is considered, and is then adjusted in the appropriate direction to move d_2 towards the correct position (Figure 10.9). The increment by which d_0 is adjusted can take any value. The solution proceeds with L_1, L_2 and d_0 being adjusted until a full solution to the beam system is obtained.

10.2.3 Features of the programs

There are three main types of routine in the programs:

(a) Core solution routines:
These routines use the core solutions to yield an iterative solution for a given support configuration. An iteration parameter is used to assess the accuracy of the solution. The iteration parameter is either a force, for example R_0; or a displacement, for example θ_1. As the solution process proceeds, the iteration parameter tends towards a final value. The difference in the value of the iteration parameter from one iteration to the next is a measure of the current accuracy of the solution. The core solution routines have as their arguments the percentage difference in iteration parameter required to terminate the solution. The solution is terminated when the change in the iteration parameter between successive iterations is within the specified value.

(b) Support adjustment routines:
These routines adjust the positions of the supports until compatibility at the end of the beam is satisfied. Accuracy of solution in these routines is defined by the increment of movement used to adjust the position of the support. In the case of the longitudinal positions L_1, L_2, the increment of movement is

expressed as a multiple of the beam segmental length. In the case of d_0, the increment of movement can be any value. These routines have as their argument the increment of movement of the support being adjusted.

(c) Master routine:
The master routine defines the overall iterative scheme. This routine specifies the order in which the core solution and support adjustment routines are called, along with the argument values which specify the accuracy of solution.

There are two main advantages of the program structure. Firstly, new core solution and support adjustment routines can be easily 'plugged-in' to the overall framework of the program to deal with different non-linearities or beam systems. Secondly, the argument values specified in the master routine can be used to vary the accuracy of solution at different stages of the overall iterative scheme and increase the efficiency of the program.

The art of the method is to design the overall iterative scheme such that the support positions are moved quickly towards the area of the final solution. During this stage coarse movements of the support positions are specified, and the accuracy of the core solution is specified such that only two or three iterations are required at each change of support position. As the support positions gravitate towards the final solution, the accuracy of solution is increased appropriately.

Listings of the program codes are given in Appendix 10.1.

10.3 Results and Discussion

10.3.1 Initial test runs

As the programs were developed, various test runs were performed using different soil models, beam properties and support configurations. The results from one of the Blunt program test runs is included to show the format of the data to be presented. This test run is of interest because it compares two types of soil model.

The stress:displacement curves for the two soil models are shown in Figure 10.10. Both the soil models have an initial stress p_1 of 112kPa and a limiting stress p_L of 224kPa, achieved after 20mm displacement. Model 'A' has a linear increase of stress with displacement between p_1 and p_L. Model 'B' is highly non-linear between p_1 and p_L, being a fifth-order curve. Both models are 'elastic' - soil response on loading and

unloading is given by the same curve. Figure 10.10 also gives details of the properties of the beam representing the shell element being expanded.

Figure 10.11 shows the deflection lines resulting from fully-Blunt expansion into the two types of soil. The flexure zone parameters are indicated on the plot. The shell is being expanded by a plain-ended mandrel with a shank displacement d_2 of 20mm. The central wedging force R_0 is acting halfway along the 10m long beam. End supports R_1, R_2 act at distances L_1, L_2 from R_0 and define the flexure zone. R_1 acts at zero displacement, R_0 and R_2 act at 20mm displacement. Maximum displacement d_{max} occurs at a distance L_{max} from R_0.

The deflection line appears to be insensitive to quite marked differences in the shape of the stress:displacement curve for given values of p_1 and p_L.

10.3.2 'BRS' soil model runs

A series of runs was performed using a soil model and beam properties that were intended to represent qualitatively conditions at the BRS site. The numerical investigation was carried out before the results of the pressuremeter testing at the BRS site were known. The soil stress: displacement curve and the beam properties are shown in Figure 10.12. Table 10.1 gives details of results.

The initial stress p_1 (=105kPa) of the stress:displacement curve was obtained by estimating the average normal effective stress acting on the unexpanded piles tested at the BRS site. A limiting stress p_L (=315kPa) of three times the initial stress was assumed, and a fourth order curve was used to model non-linear soil response between p_1 and p_L. Linear unloading behaviour was assumed, at a rate of 157.5kPa per 1mm displacement. The unloading gradient corresponded to a shear modulus of 11MPa. A 70x70x10mm thick equal angle beam was assumed, as used at the BRS site.

Two cases were considered - fully-Blunt expansion and Ideal expansion. The shank displacement was 10 mm in each case.

10.3.2.1 Deflection lines

Figure 10.13 shows the deflection lines for the two cases. The curves are similar over the leading part of the flexure zone, but differ over the trailing part. In the fully-Blunt case, there is a point of contraflexure between the central and trailing supports as the element over-expands. In the Ideal case, the deflection line curves in the same

sense between these two supports.

d_0 is 10mm for the fully-Blunt case and 8.9mm for the Ideal case. The difference between these values is small compared to the shank displacement. As the two cases considered are extremes of behaviour, the deflection line is obviously very sensitive to the position of the wedging force.

Length L_1 is similar for the two cases, approximately 1.1m. The difference in length L_2 is much more marked (0.43m in comparison to 0.71m). The maximum deflection in the fully-Blunt case is 10.57mm, an over-expansion of 0.57mm.

10.3.2.2 Shear forces and bending moments

Figures 10.14 and 10.15 show the shear forces and bending moments associated with Figure 10.13. The main difference between the Ideal and fully-Blunt cases occurs between the central and trailing supports, reflecting the difference in the two deflection lines. In the Ideal case $R_2 = 0$ and the bending moment remains negative between the two supports. In the fully-Blunt case $R_2 > 0$ and the bending moment changes sign between the two supports.

The length of the flexure zone, and the shear forces and bending moments (and hence the strain energy), are all greater for the fully-Blunt case. This is a consequence of the support geometry imposed on the beam system.

The peak bending moments are similar and occur at the central support. The peak values of -2.84kNm and -3.39kNm for the Ideal and fully-Blunt cases give maximum normal stresses in the beam of 352N/mm^2 and 420N/mm^2 respectively. The yield stress of the mild steel beam is 250N/mm^2. This suggests that in the field trials yielding may have occurred in the shell elements during expansion.

10.3.2.3 Radial stresses

Figure 10.16 shows the radial stresses acting on the shell in the two cases. Over the leading part of the flexure zone the radial stresses are similar, reflecting the similarity of the two deflection lines. At any given position the radial stress is slightly greater in the fully-Blunt case. Over the trailing part of the flexure zone the behaviour for the two cases is totally different. In the Ideal case the radial stress reaches a peak and is maintained. In the fully-Blunt case there is a large reduction in radial stress as the soil mass unloads.

The peak radial stress p_{max} for the Ideal case is 306kPa. p_{max} for the fully-Blunt case is 310kPa, followed by a reduction to 220kPa - this means that 44% of the gain in radial stress over the leading part of the flexure zone is lost over the trailing part.

10.3.2.4 Mandrel nose profile

Figure 10.17 shows the deflection line for the Ideal case in more detail. The approximate nose profile of box mandrel A used at the BRS site is shown for comparison. The nose profiles of box mandrel B and the cruciform mandrels were blunter than for box mandrel A (Figure 3.9). The mandrel nose profiles used at the BRS site appear to be far too blunt to have given rise to an Ideal deflection line and it would seem likely that over-expansion occured during mandrel installation.

10.3.2.5 Effect of different percentage expansion

Figures 10.18 to 10.23 deal with the effect of varying the percentage (%) expansion. The main points of interest are listed below:

(a) Figure 10.18 shows radial stresses for fully-Blunt expansions of 2.5mm, 5.0mm, 7.5mm and 10mm (corresponding to expansions of 3.6%, 7.1%, 10.7% and 14.2% in the field trials). The length of the flexure zone is not very sensitive to % expansion. Length L_1 varies from 0.83m to 1.09m; length L_2 varies from 0.51m to 0.71m.

(b) It can be seen from Figure 10.18 that p_{max} increases with % expansion, but at a decreasing rate. This behaviour is a result of the loading portion of the stress-displacement curve being non-linear.

In contrast, the amount by which radial stress decreases over the trailing part of the flexure zone increases proportionately with % expansion. This is because the unloading part of the stress: displacement curve is linear, so that the reduction in radial stress is directly proportional to the amount of over-expansion. Because the essential form of the deflection line is determined by the geometry of the supports, the amount of over-expansion - and hence the reduction in radial stress - is approximately proportional to the shank displacement. This is shown in Figure 10.19.

The value of p_2 generated by the passing of the mandrel nose depends on the relative values of the increase and decrease of stress along the length of the flexure zone. For small % expansions, the increases in radial stress over the leading part of

the flexure zone will dominate, and p_2 will increase with shank displacement. For large % expansions the reduction in radial stress over the trailing part of the flexure zone will dominate, and p_2 will decrease with shank displacement. (For very large % expansions, it is possible for p_2 to be less than p_1).

This is illustrated in Figure 10.20, which shows a progressive increase in p_2 for the 2.5mm, 5.0mm and 7.5mm cases, and then a decrease for the 10mm case. p_2 for the 10mm case is less than for the 5mm case. Figure 10.21 shows how the value of p_2 is controlled by the relative values of increase and decrease of radial stress along the flexure zone.

(c) Figure 10.22 shows the central propping force R_0 plotted against shank displacement d_2. The force required to expand the beam increases progressively with % expansion. Figure 10.23 shows p_2 plotted against R_0.

(d) Fully elastic behaviour occurs only in the 2.5mm case. For the three largest % expansions the maximum normal stress acting within the beam is greater than the yield stress, and the assumption of elastic behaviour becomes progressively less valid. However, the elastic solution provides a useful upper-bound for d_{max} and lower bound for p_2 (see Section 10.4.2).

10.3.3 Check runs

10.3.3.1 Convergence of solution

Figure 10.24 illustrates typical convergence behaviour within the core solution routine of the Blunt program. The iteration parameter in this case is R_0. This is plotted against the number of iterations. The effect of different damping factors is compared.

The solution conditioning is very good, convergence occurring even with a totally undamped system. For damping factors of 0.75 and 1.0 the iteration parameter (and deflection line) becomes sensibly indistinguishable after five or six iterations. For a damping factor of 0.5, the solution process takes longer, converging after 8 or 9 iterations. For a damping factor of 1.0 some oscillation of the solution occurs during convergence.

Good solution conditioning is to be expected with the displacement controlled iterative scheme used, in which an applied displacement is reimposed at each iterative step. Out of interest, some load controlled

iterative schemes were tried in which an applied LOAD was reimposed at each step. Damping factors as low as 0.25, and consequently a large number of iterations, were required to stop the solution oscillating. This is in line with the experiences reported by Burgoyne and Aul (1987).

The solution conditioning for the Ideal program was not as good as for the Blunt program - the solution became unstable when a damping factor near 1.0 was used. With a damping factor of 0.5, the solution conditioning was satisfactory. The difference in behaviour between the Blunt and Ideal systems was due to the fact that the Ideal system included a relatively flexible overhang from the central support.

10.3.3.2 Comparision with Hetenyi solution

The programs were checked against a closed form analytical solution. The core solution was changed to deal with a beam hinged at both ends, and supported by a linear elastic foundation. The analytical solution for this case is given by Hetenyi (1946). In Figure 10.25 two curves are plotted, the analytical solution and the numerical solution. It can be seen that the two solutions are indistinguishable.

10.3.3.3 Comparison between Ideal and Blunt programs

The Ideal deflection line shown in Figure 10.13 was checked by inputting the data obtained from the Ideal program into the Blunt program. The deflection line obtained using the Blunt Program was indistinguishable from that using the Ideal Program, and the trailing end reaction R_0 was found to be zero, which is correct.

10.4 Extensions of Method

This Section outlines refinements that could easily be made to the programs described, but which were not developed in full during the present investigation.

10.4.1 Mandrel nose profile

The analysis described so far has considered the expansion of the shell by the simplest possible system of wedging forces. Two extreme cases of this system have been dealt with - the fully-Blunt case and the Ideal case. It has been stated (Section 10.2.1.2) that the fully-Blunt case is associated with a plain ended, (or fully-Blunt) nose profile and that the Ideal case is similarly associated with an Ideal nose profile.

Some nomenclature is dealt with here (Figure 10.26):

- Nose shape:
  The nose shape is the form of the curve of the nose profile, eg. parabolic, or circular.

- Nose length:
  The nose length is a suitable characteristic length. The nose length can vary for a given nose shape, giving rise to a suite of profiles.

- General over-expansion:
  In this particular case of over-expansion, the central wedging force acts at a single point. Fully-Blunt expansion is the extreme of this behaviour.

- Local over-expansion:
  In this particular case of over-expansion, the shell is in continuous contact with the nose over part of its length, but lifts away over the trailing part of the nose, resulting in over-expansion. This behaviour is the result of local incompatibility between the deflection line of the shell and the profile of the nose: the nose profile is sufficiently long but is the wrong shape.

- Ideal nose profile:
  This is the nose profile giving rise to Ideal expansion. Two conditions apply - the maximum displacement of the shell elements is equal to the shank displacement, and the strain energy of expansion is a minimum. As a consequence, the length of the flexure zone will be at a minimum. The deflection line for Ideal expansion is defined by the simple system described in Section 10.2.1.

  In theory, Ideal expansion can be affected by a nose profile of similar shape to the Ideal deflection line. Note that the nose profile can be truncated ahead of the central support position. In reality however, soil forces will vary continuously with depth such that the Ideal deflection line will also continuously vary. Consequently, in practical terms there is no 'Ideal' nose profile - the profile will either be 'sub-Ideal' or 'super-Ideal'.

- Sub-Ideal or Blunt nose profile:
  In this case the length of the nose profile is shorter than for the associated Ideal nose profile. General over-expansion occurs. The strain energy of expansion is greater than for the Ideal case.

- Super-Ideal nose profile:
  In this case the length of the nose profile is longer than for the associated Ideal nose profile. The outer shell is 'over-supported' such that it is in continuous contact with the nose over part of its length. The length of the flexure zone and the strain energy of expansion are increased relative to the Ideal case. The shape of the nose may be such that local over-expansion occurs.

In the case of the field trials, it seems likely that the nose profiles used were Blunt, and general over-expansion occurred. A method to obtain the shell deflection line resulting from expansion by such nose profiles has been devised. It makes use of the principle of minimum potential energy, which states that of all possible displacement states of a loaded body that state of displacement which minimises the potential energy is the correct one.

To obtain the deflection line for the shell, the method already described is extended as follows:

(a) The nose profile is discretized as shown in Figure 10.27.

(b) The deflection line for the shell is calculated using the Blunt program. Different positions of the central wedging force are defined systematically using the discretized nose profile. There are a number of viable solutions for which the deflection line of the shell is compatible with the nose profile.

(c) The wedging force is initially considered to act at the trailing end of the nose (the fully-Blunt case) and is then moved towards the leading end. As the wedging force is moved down the nose, the strain energy of expansion decreases. The last viable solution in the direction of the leading end of the nose is the correct solution.

A generalised routine for this solution has not been written, although the solution process has been performed by 'hand' for a curved nose profile similar to the box mandrel nose used in the field trials. This exercise demonstrated that the wedging force migrated towards the tip of the nose. For the case considered ('BRS' soil model) the migration effect was small, and the expansion was virtually fully-Blunt.

10.4.2 Nose profiles - general considerations for design

10.4.2.1 Linear elastic behaviour of shell

In practice, a nose profile of fixed length and shape will be required to deal with different soil forces as it is advanced through the shell (although some consideration has been given to a 'tuning fork' nose which could respond to changes in soil forces). The key to designing the appropriate nose profile is to avoid over-expansion and thus maximise shank radial stress.

In general the Ideal nose profile will become shorter and more curved with depth, as the magnitude of soil forces increases. Conversely, the stiffer the shell elements are, the longer and less curved the nose profile will need to be. Design of a nose profile involves optimising the profile for a certain depth of penetration near the top of the pile, such that the expansion is super-Ideal below that depth. The shape of the optimum nose profile would be approximated by a suitable mathematical curve.

This approach will ensure that general over-expansion does not occur. However, except in the case of very long nose profiles, it is likely that there will always be slight incompatibilities between the nose profile and the deflection line of the shell elements, such that local over-expansion occurs.

10.4.2.2 Inelastic behaviour of outer shell

Although the consideration of inelastic bending in the flexure zone was beyond the scope of the study, some observations are set out below.

The bending moments in a given shell element will increase both with shank displacement and with depth, as soil forces increase. The increasing bending moments will eventually cause yielding in the outer fibres of the elements. For a given depth it is possible to identify the shank displacement at which yielding first occurs. Similarly, for a given shank displacement it is possible to identify the depth at which yielding first occurs. The mode of bending in the flexure zone can thus be controlled by selection of member properties. Whether or not yielding would be allowed to occur in practice would depend on the design philosophy adopted.

When yielding occurs, the moment:curvature relationship for the shell elements becomes non-linear. Curvature for a given moment is greater than if the beam were behaving linearly elastically. Therefore, for situations where a limited amount of yielding occurs, a nose profile

based on the assumption of linearly elastic behaviour would be useful for design purposes.

10.4.3 Connecting forces between shell elements

These can be easily dealt with by changing the core solution to deal with a fixed support at the leading end of the flexure zone. The limiting case is when the shear force at the fixed end equals the tensile strength of the fixing. Some runs were performed to investigate the effect of this shear force on the deflection line of the shell elements. As can be easily visualised, it had the effect of 'nipping' the shell elements together ahead of the nose such that L_1 was reduced and L_2 and d_{max} were increased.

10.4.3 Simple design approach

Some work not reported in this thesis, undertaken in connection with the commercial trials reported in Chapter 8, was performed with the programs that have been described. This work confirmed that the shape of the Ideal deflection line was not very sensitive to the soil model assumed (Section 10.3.1). It was more sensitive to the overall magnitude of the soil forces applied, and to the temporary fixing forces.

On the basis of this work, the following method for designing nose profiles is suggested for situations where the shell behaviour is reasonably elastic:

- Using the Ideal Program, the deflection lines associated with a number of very simple soil models are computed, for given shell type and percentage expansion. The soil models correspond to different depths, and likely extremes of soil response. A range of outer shell fixing forces are considered.

- From the range of L_2 and d_0 values obtained, the largest value of L_2 and the smallest value of d_0 are selected. These parameters define the nose length.

- The nose shape is defined by a suitable mathematical equation. The ideal shape would be a fourth order curve, as this is the shape of a cantilever subjected to a uniform load (Section 10.2.1). However, a simplified nose profile would obviously be easier to cast or machine.

10.5 Conclusions

10.5.1 Ordinary beam method

Programs based on an iterative numerical method have been developed to model the mechanical expansion process in 'multiple-element' wedge-piles. The behaviour of the outer shell elements is assumed to be linearly elastic. The soil surrounding the wedge-pile is assumed to behave as a discontinuous foundation. Non-linear soil response is easily dealt with.

10.5.2 The mechanical expansion process

Using the programs it is possible to calculate, for a given expander mandrel nose profile, the deflection line of the outer shell elements as they are expanded and the shear forces, bending moments, and radial stresses generated. A method of establishing the 'Ideal' profile has been developed.

Using the programs, it has been found that:

(a) The radial stresses generated on expansion are very sensitive to the profile of the expander mandrel nose.

(b) If over-expansion occurs as the expander mandrel is driven, the maximum radial effective stress that can be mobilised is less than that potentially available. When over-expansion occurs, radial stress increases ahead of the nose and then decreases behind the nose. The decrease behind the nose becomes dominant for large percentage expansions. Eventually, the radial stress generated by the passing of the nose does not increase with percentage expansion.

(c) The mandrel profiles used for the field trials were almost certainly too blunt and over-expansion probably occurred. Greater increases in load carrying capacity than those found may have been possible.

(d) In the field trials, it is likely that some yielding of the outer shell elements occurred, particularly at the larger expansions.

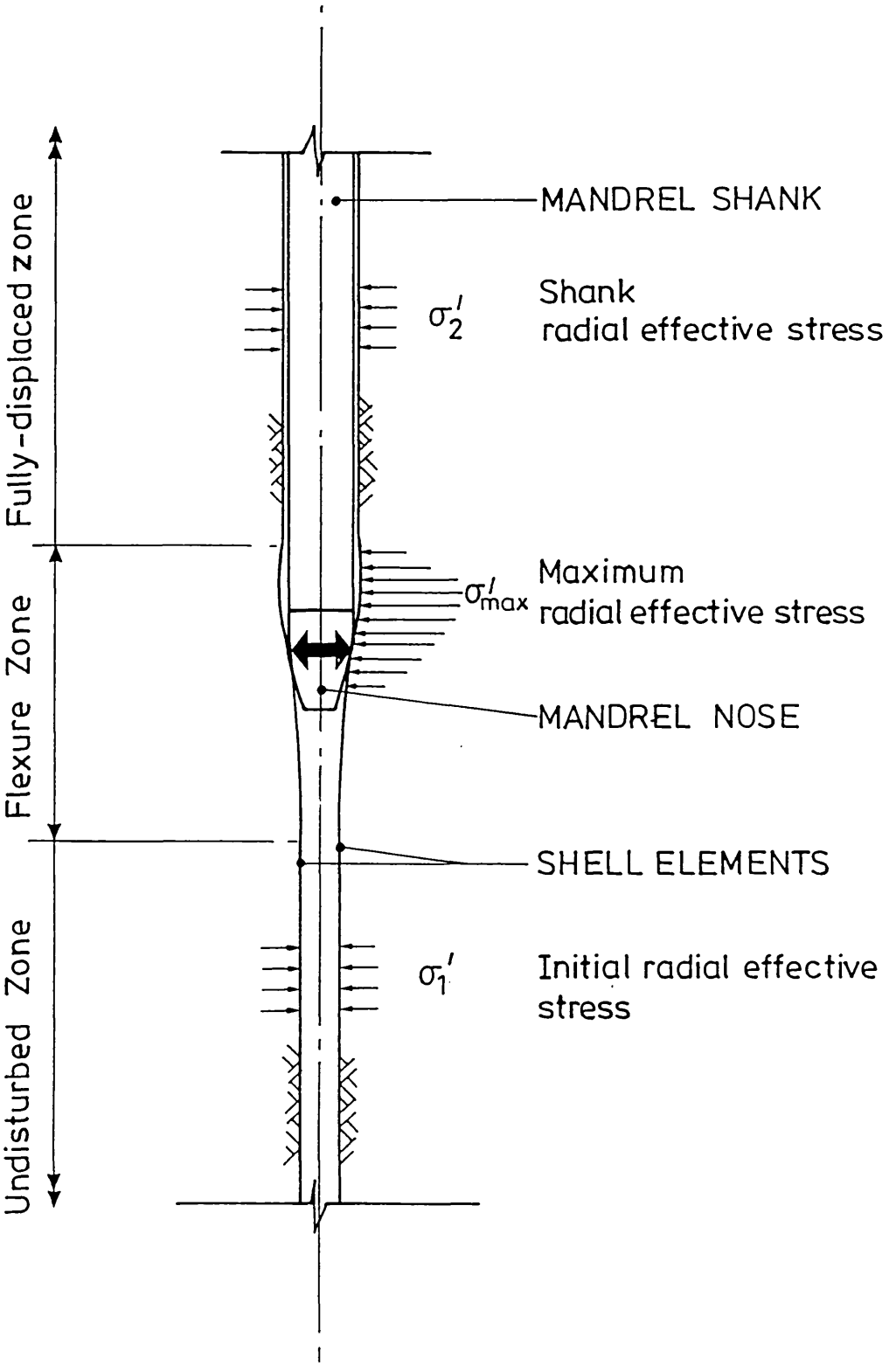

Figure 10.1 Problem description

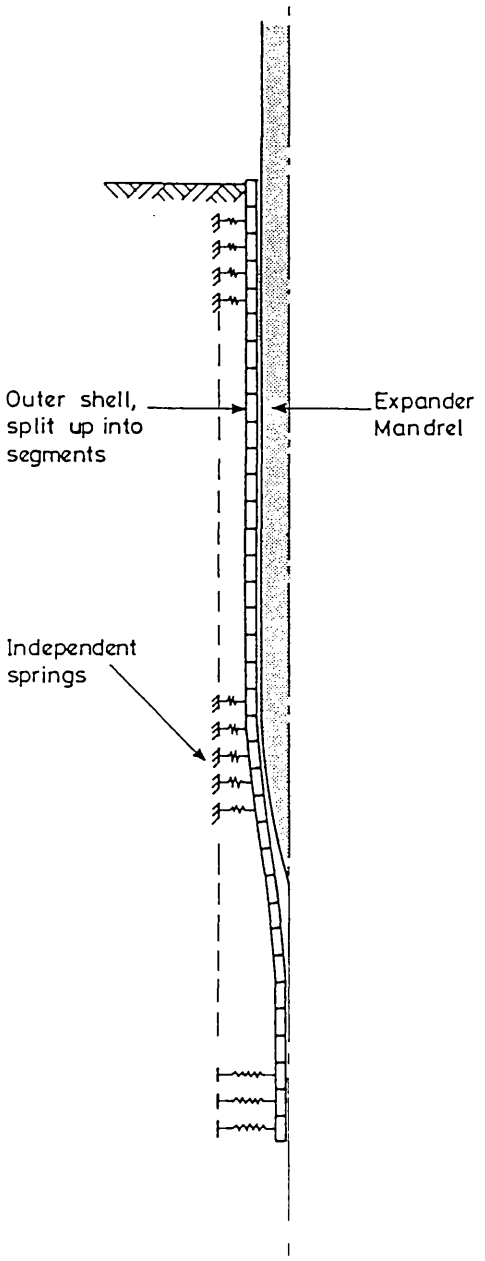

Figure 10.2 Concept of spring foundation

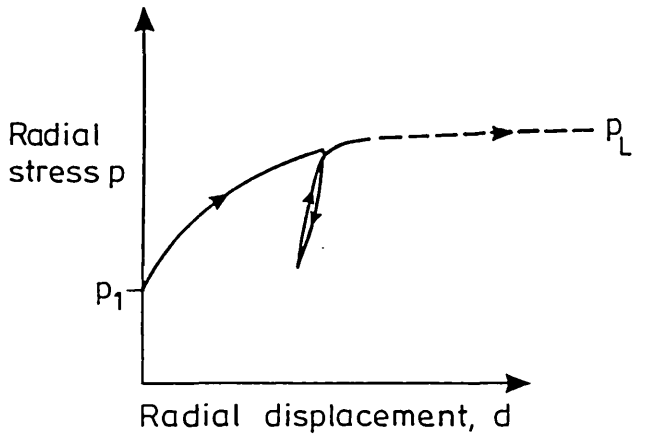

Figure 10.3 Typical pressuremeter stress:displacement curve

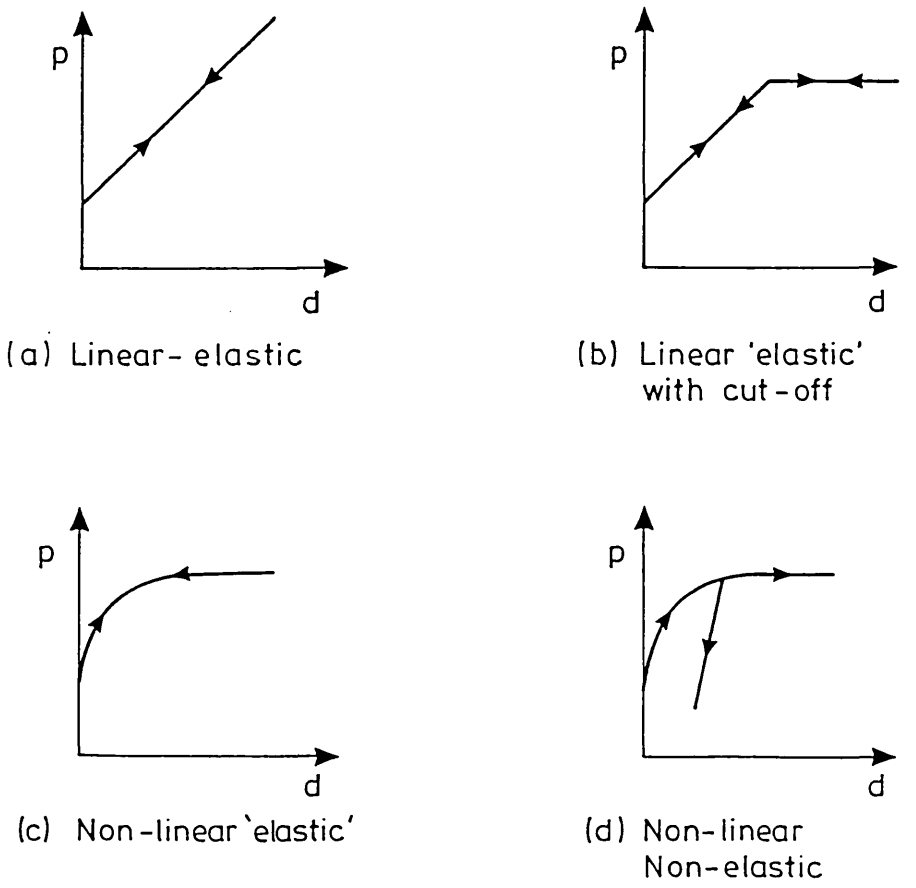

Figure 10.4 Soil models used in numerical study

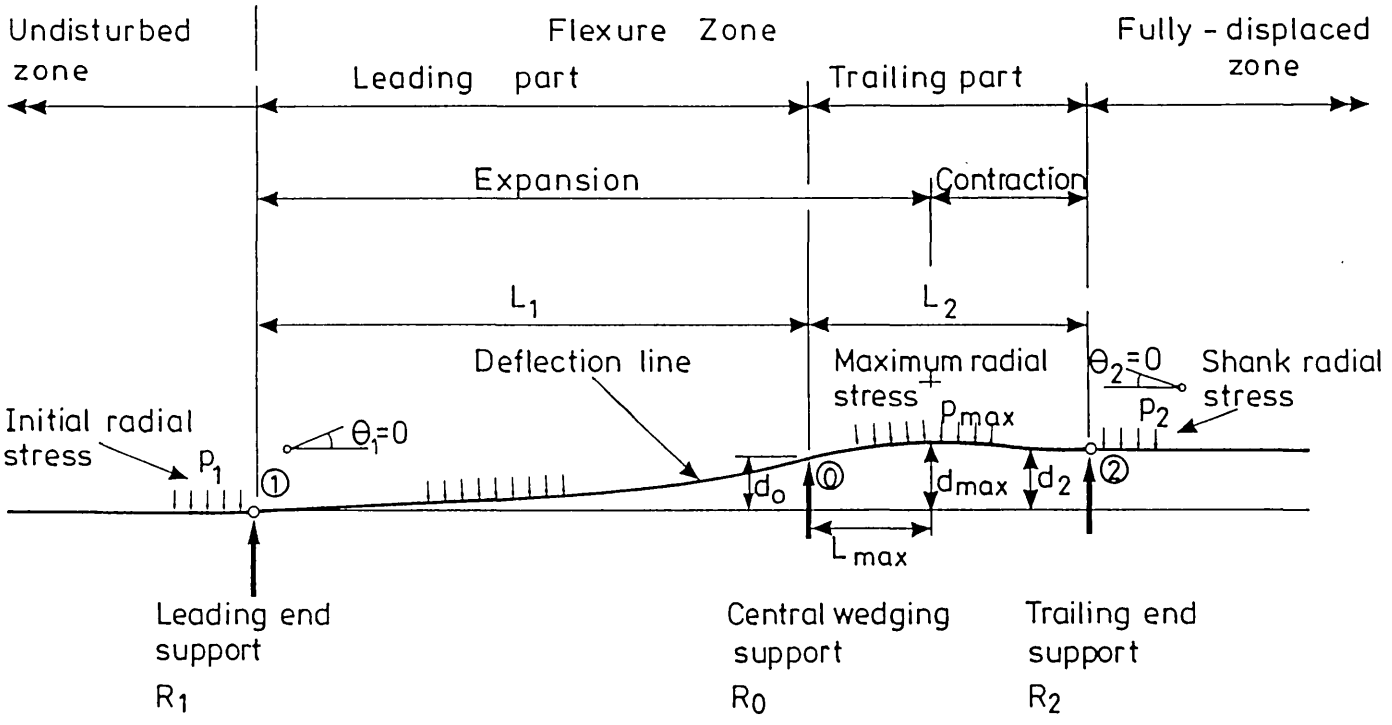

Figure 10.5 Definition of beam system

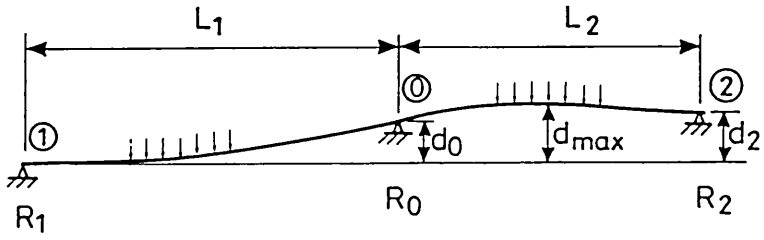

Figure 10.6 'Blunt' beam system

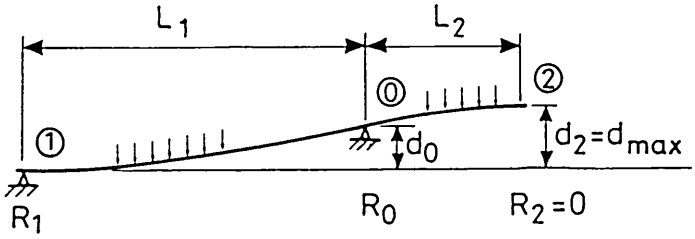

Figure 10.7 'Ideal' beam system

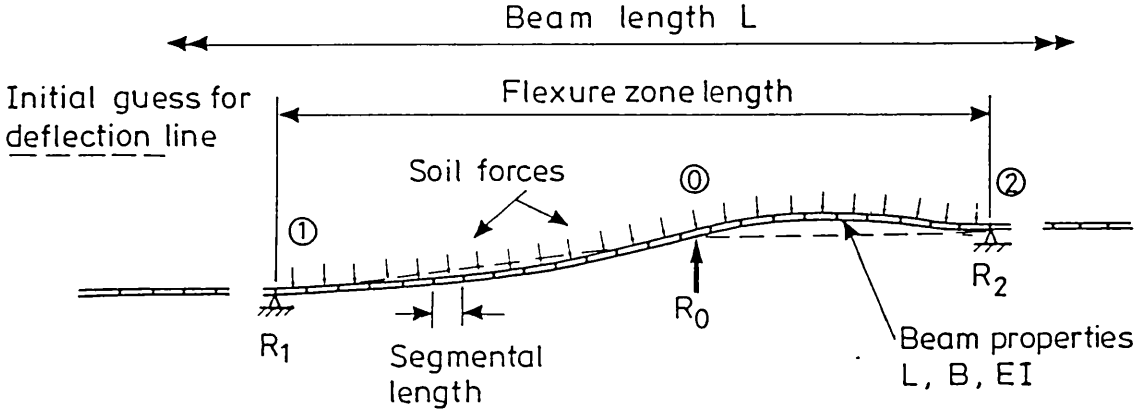

Figure 10.8 Discretisation of beam system

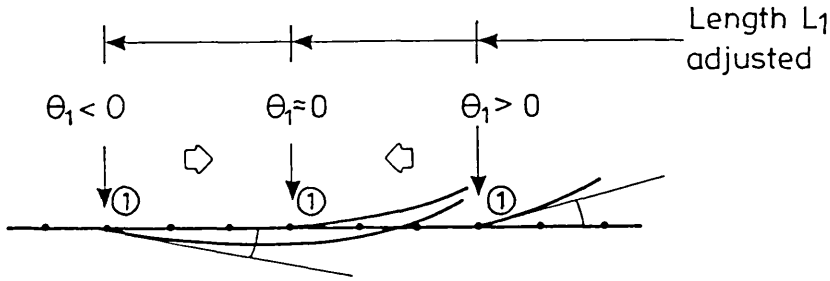

Adjustment of length L_1

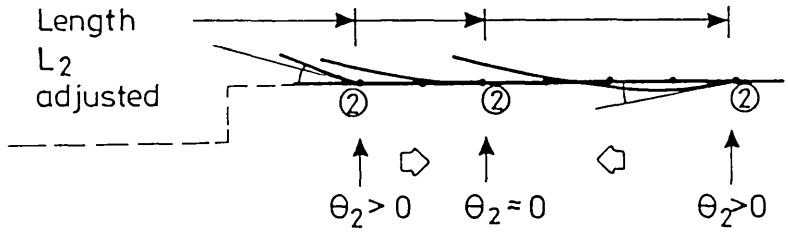

Adjustment of length L_2

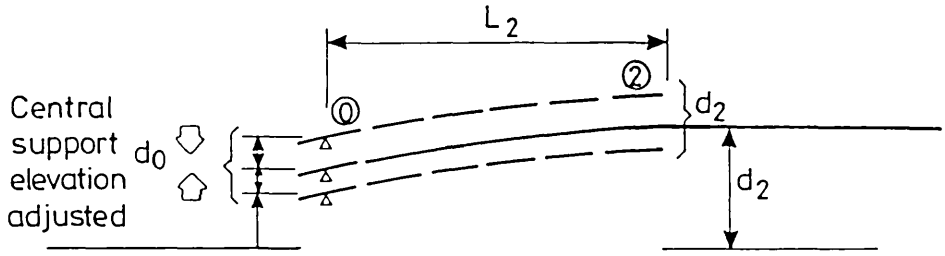

Adjustment of central support position do

Figure 10.9 Adjustment of support positions to give correct solution

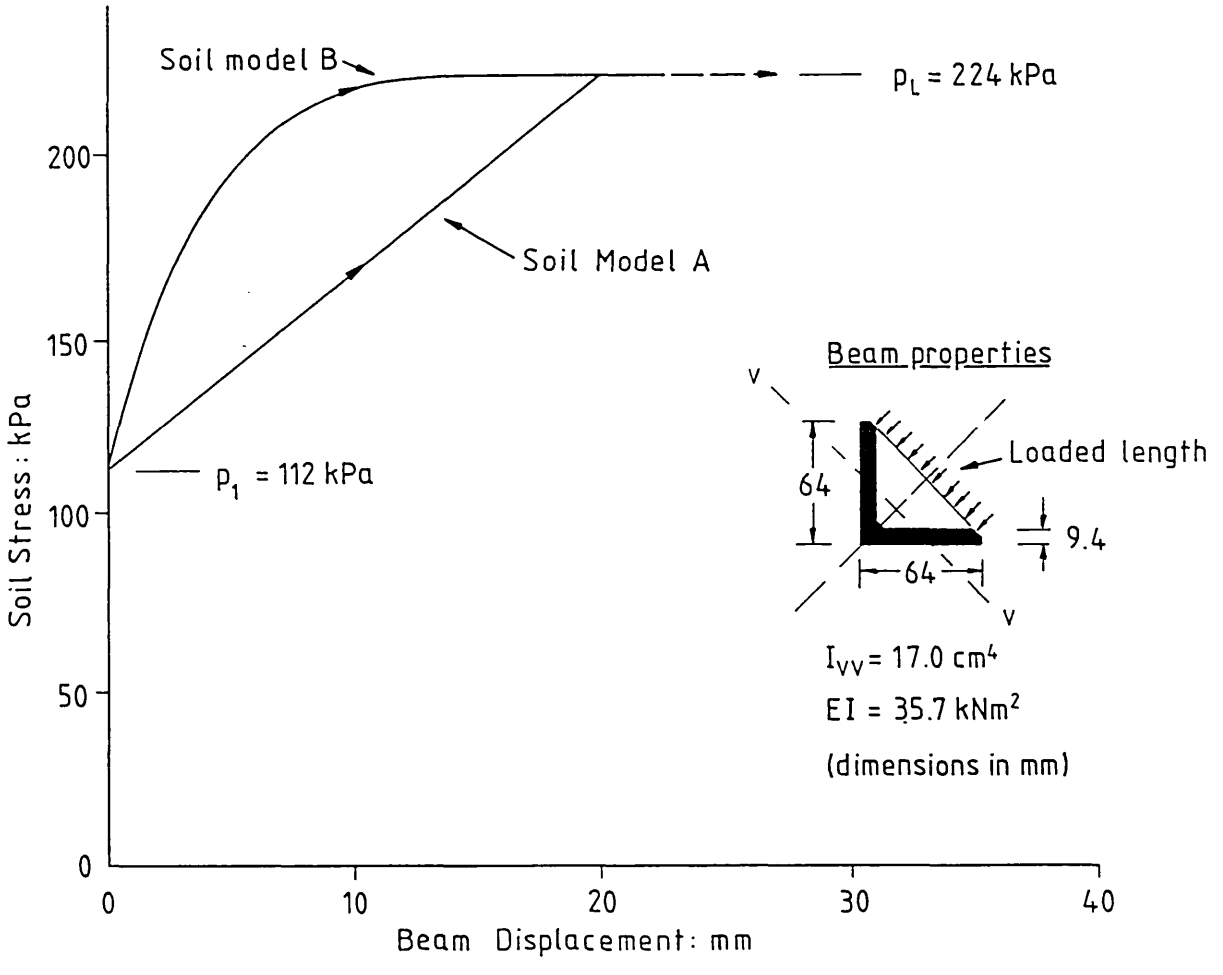

Figure 10.10 Soil models 'A' and 'B': stress:displacement curves

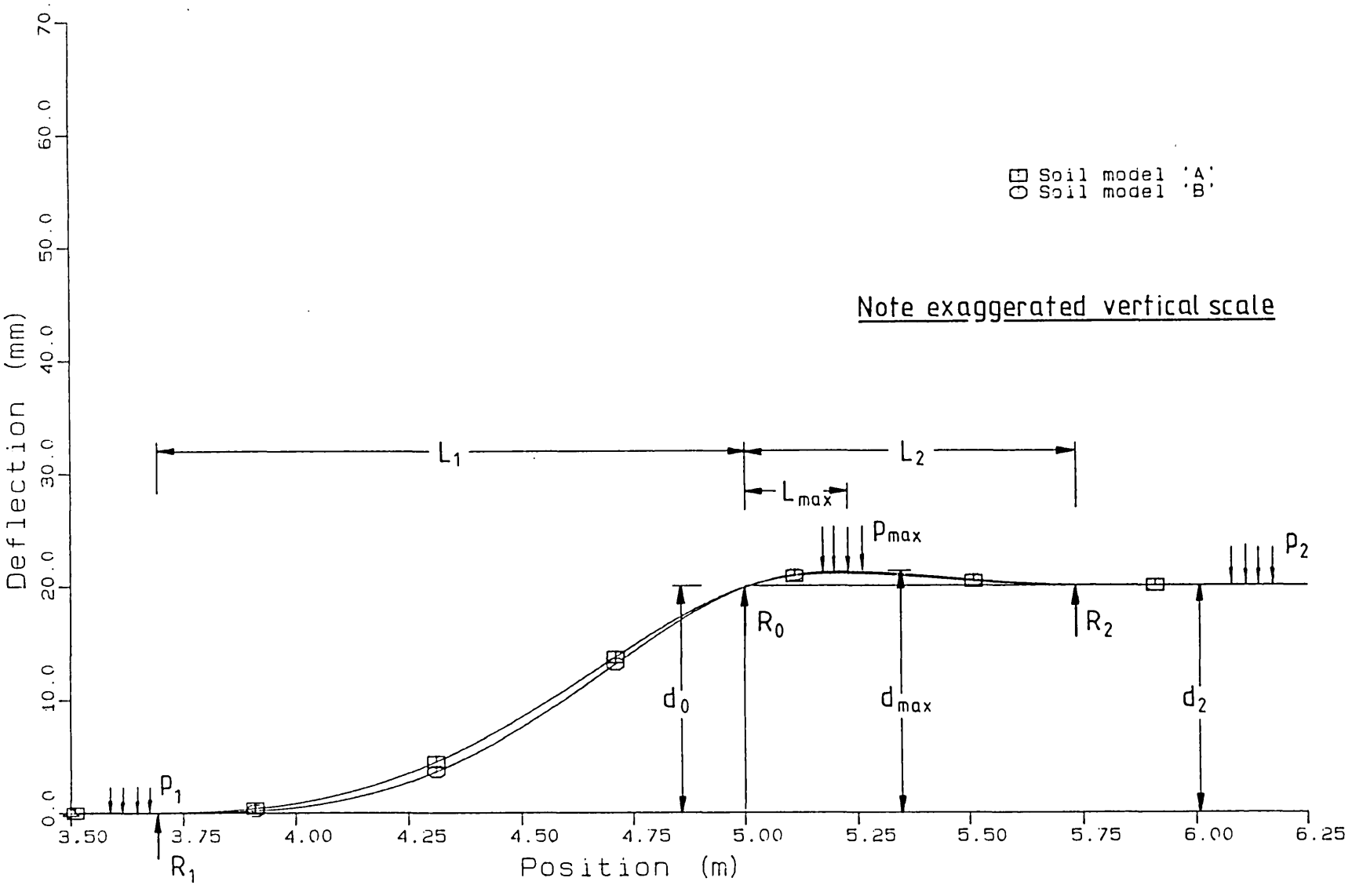

Figure 10.11 Soil Models 'A' and 'B', 'fully-Blunt' and 'Ideal' expansions: Deflection against Beam position

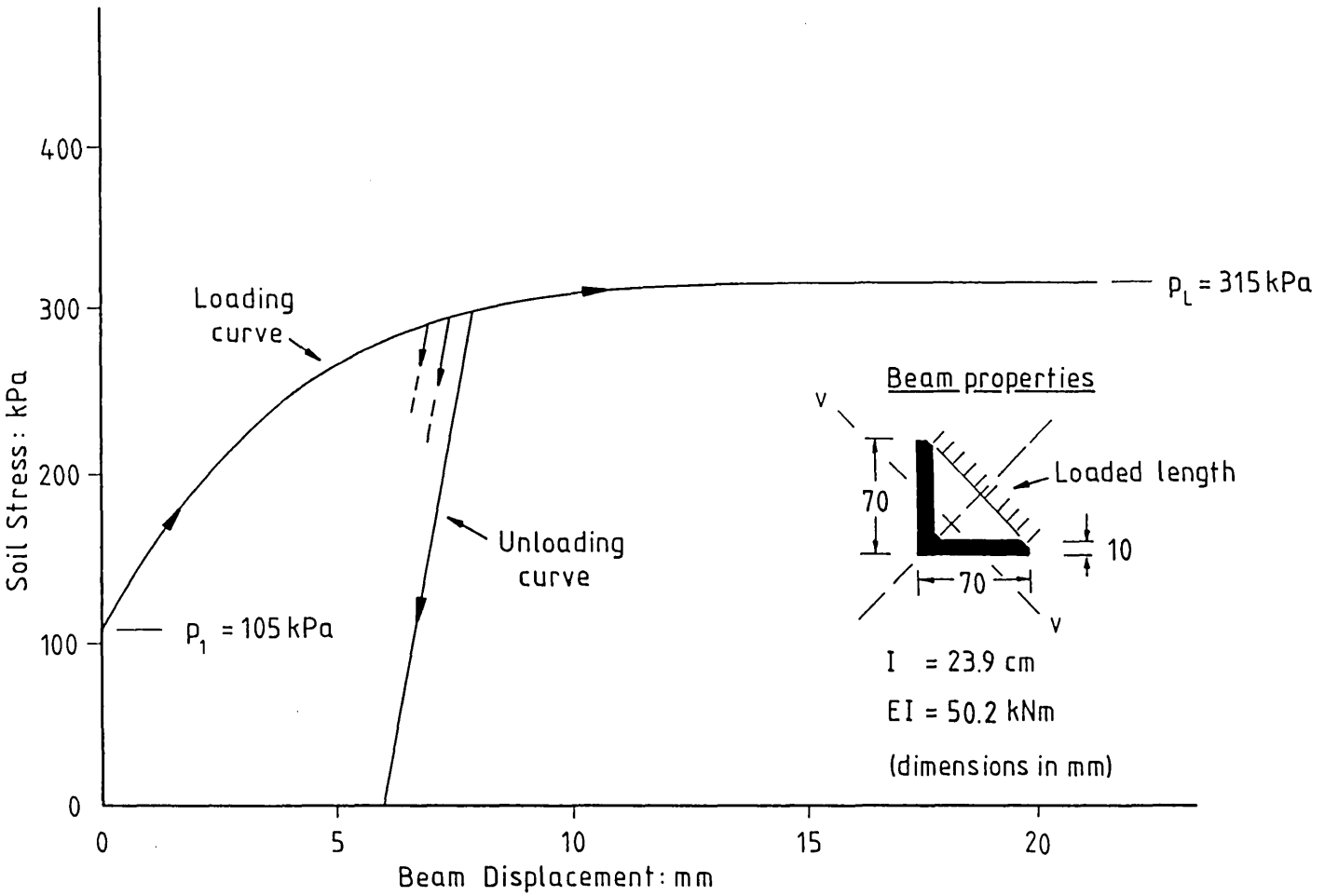

Figure 10.12 'BRS' soil model
stress:displacement curve

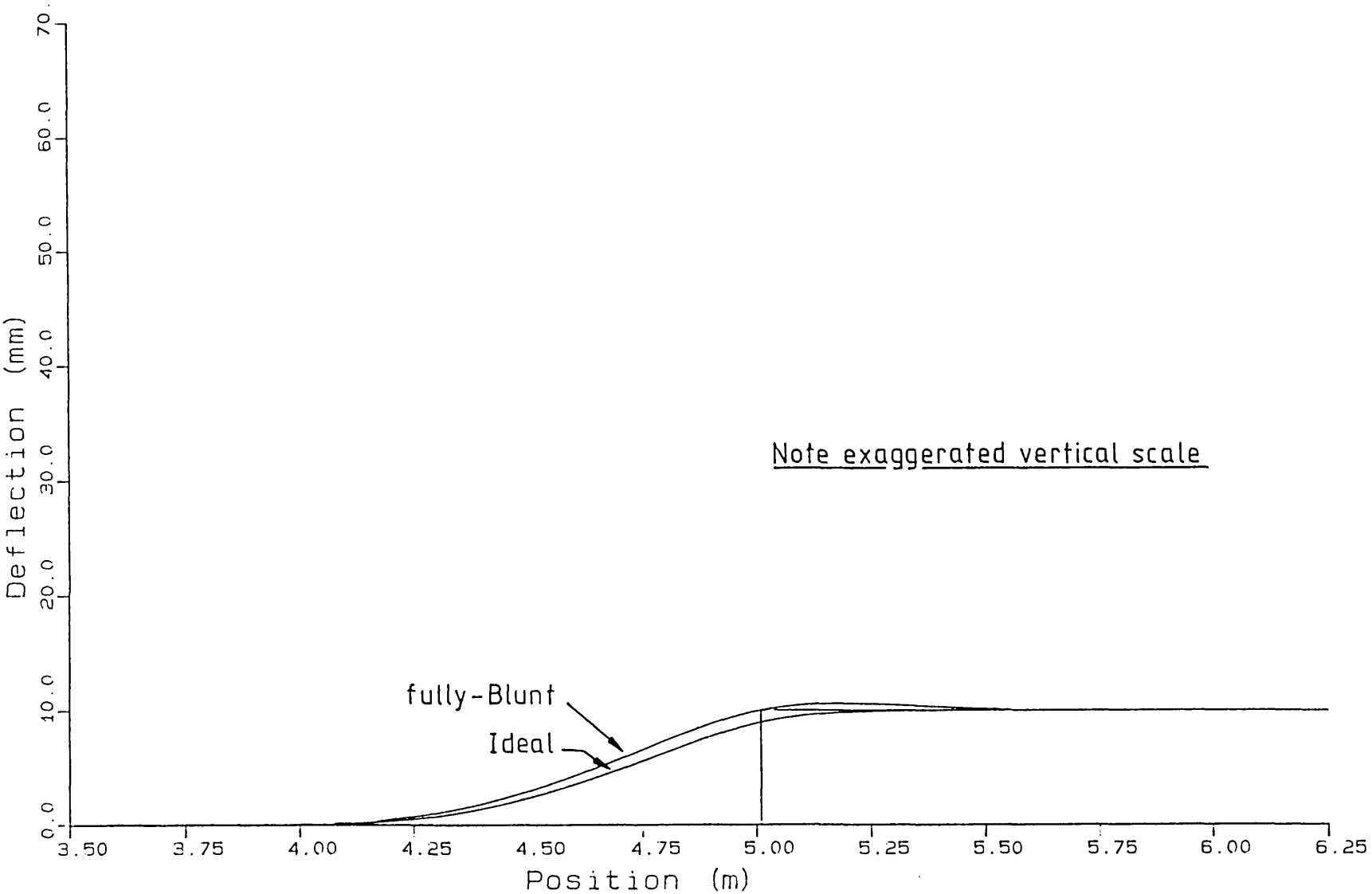

Figure 10.13 'BRS' soil model
'fully-Blunt and 'Ideal' expansions
Deflection against Beam position

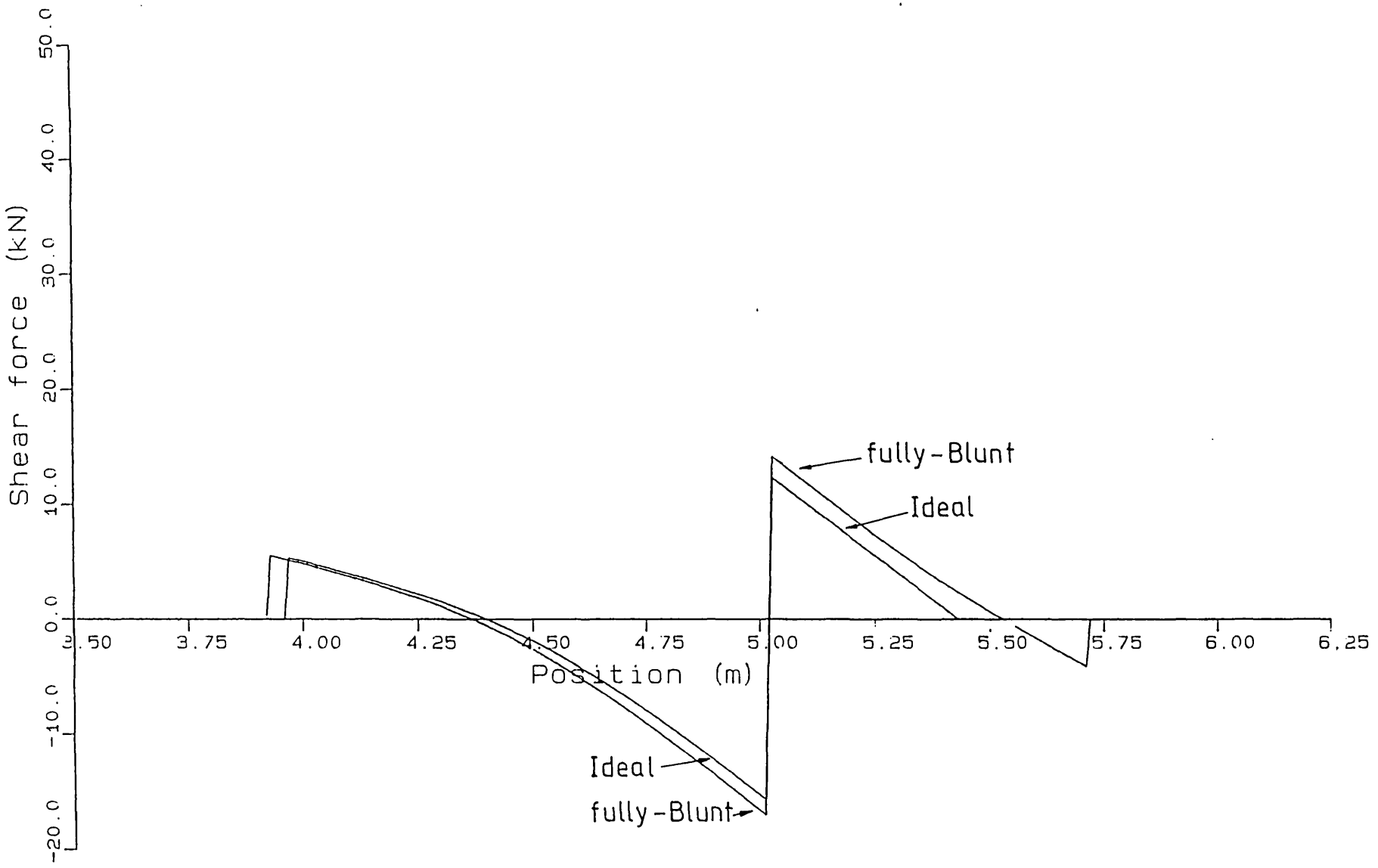

Figure 10.14 'BRS' soil model
'fully-Blunt and 'Ideal' expansions
Shear force against Beam position

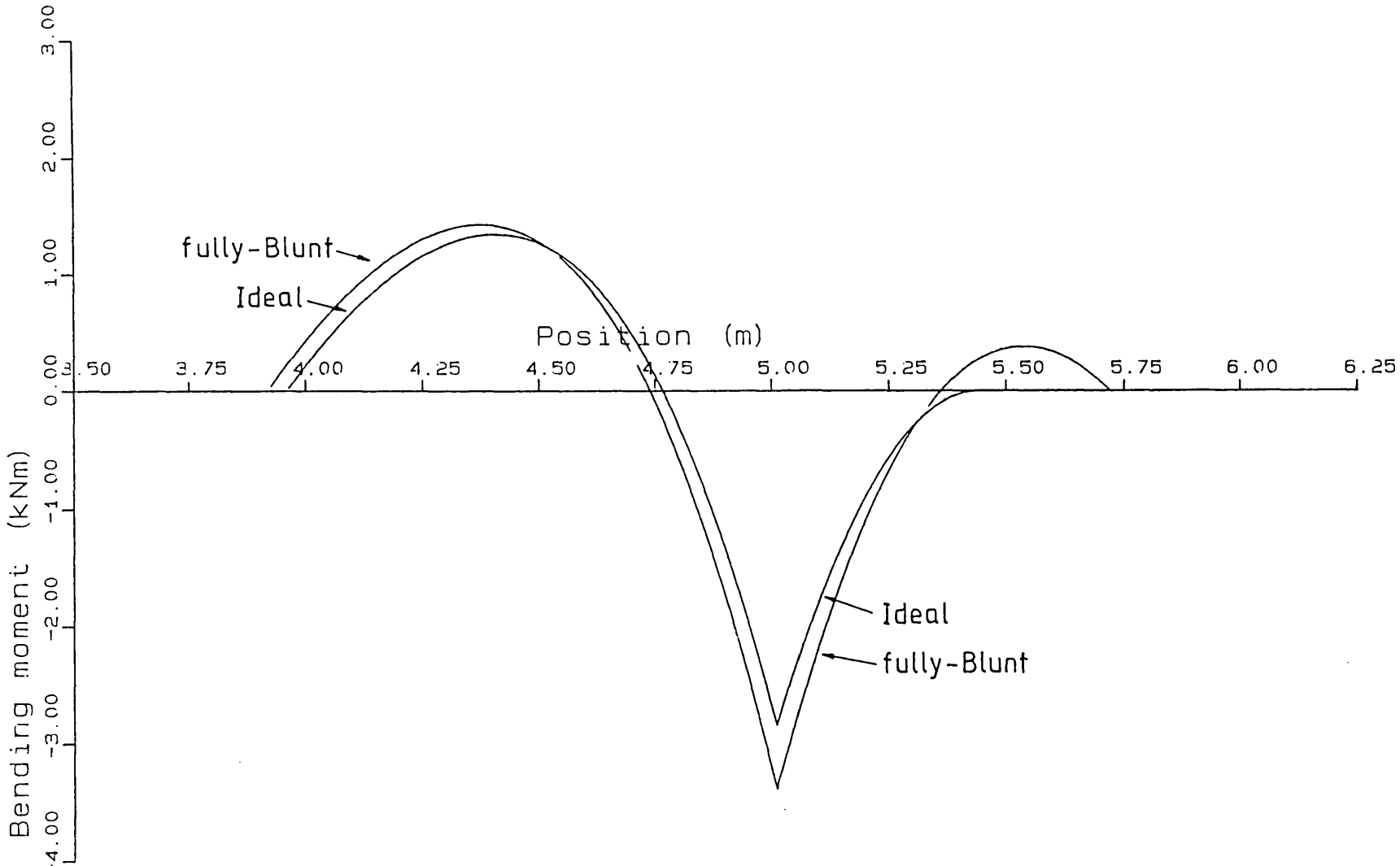

Figure 10.15 'BRS' soil model
'fully-Blunt and 'Ideal' expansions
Bending moment against Beam position

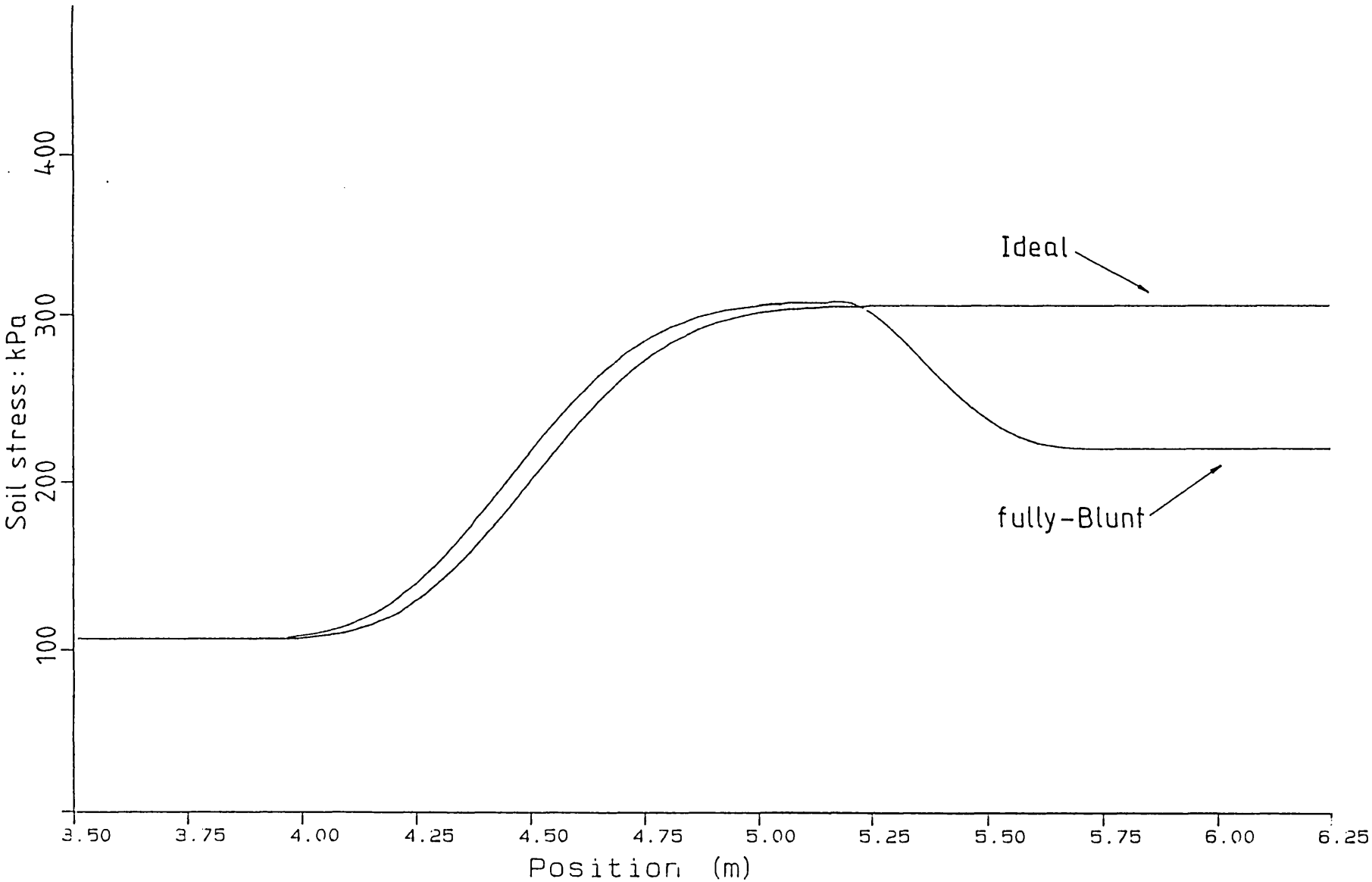

Figure 10.16 'BRS' soil model
'fully-Blunt and 'Ideal' expansions
Soil stress against Beam position

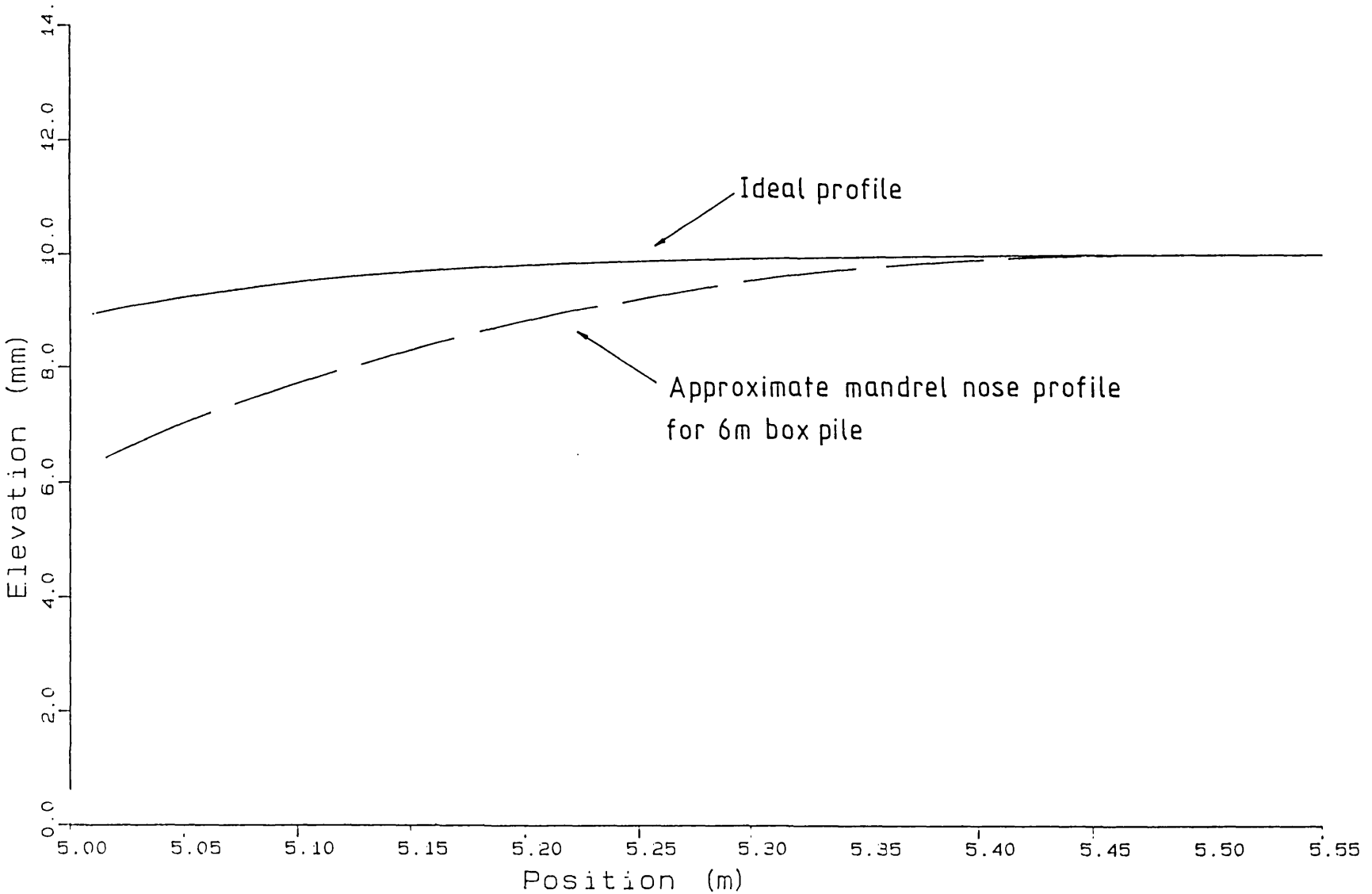

Figure 10.17 'BRS' soil model
Comparison of 'Ideal' deflection line with nose profile of box mandrel 'A'

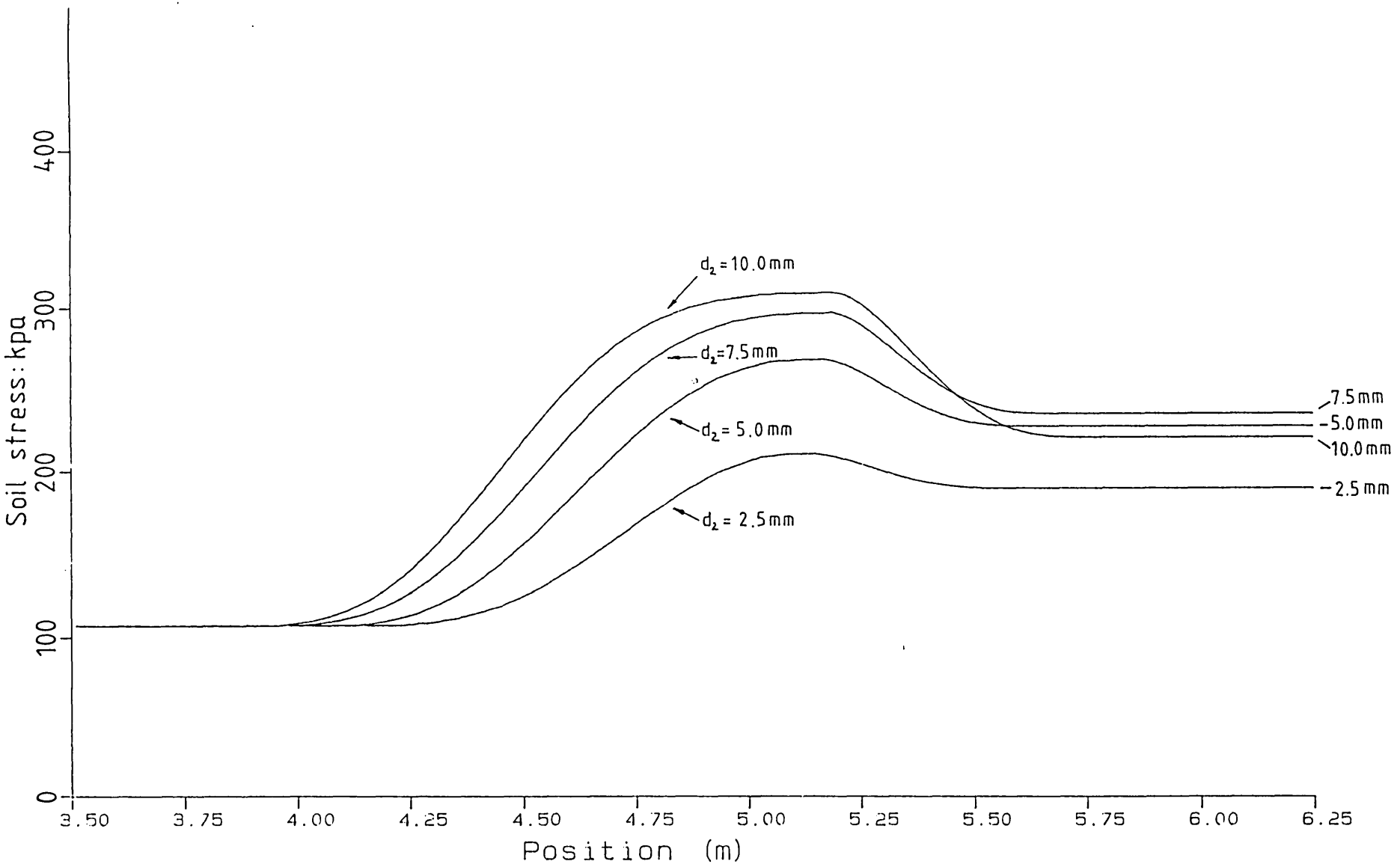

Figure 10.18 'BRS' soil model
'fully-Blunt' expansions of 2.5, 5.0, 7.5, and 10.0mm
Deflection against Beam position

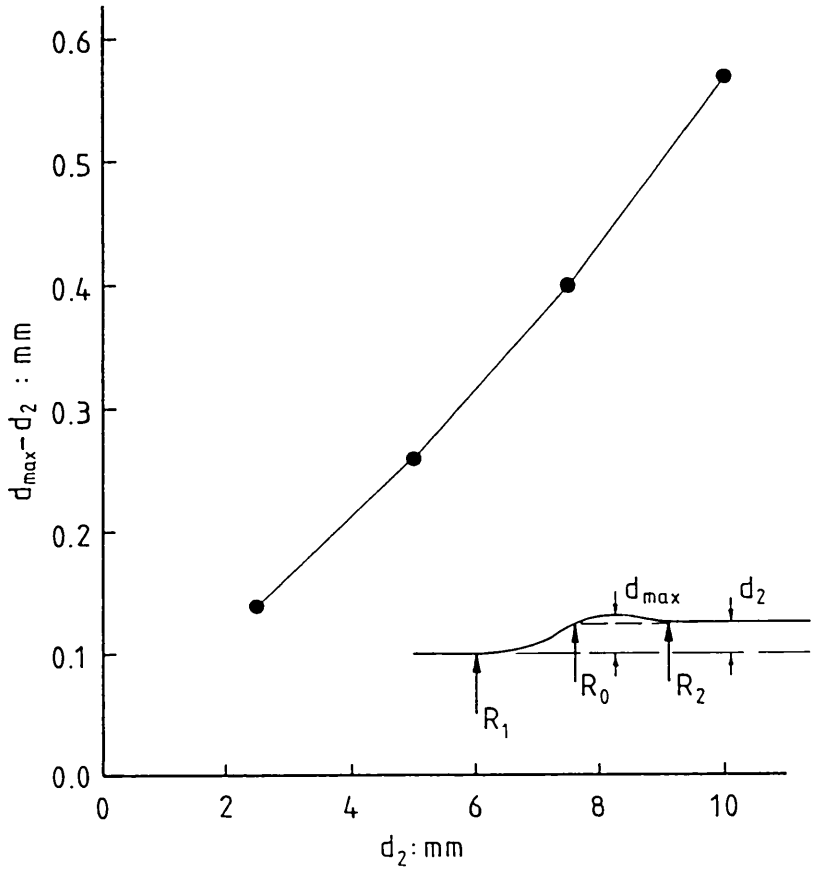

Figure 10.19 'BRS' soil model:
Over-expansion $d_{max}-d_2$ against Shank displacement d_2

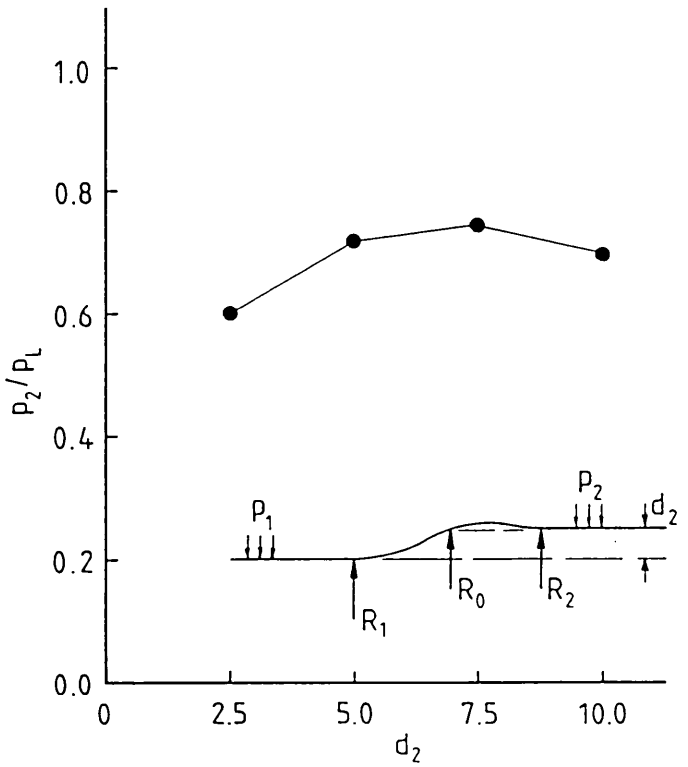

Figure 10.20 'BRS' soil model:
Normalised shank stress p_2/p_L against Shank displacement d_2

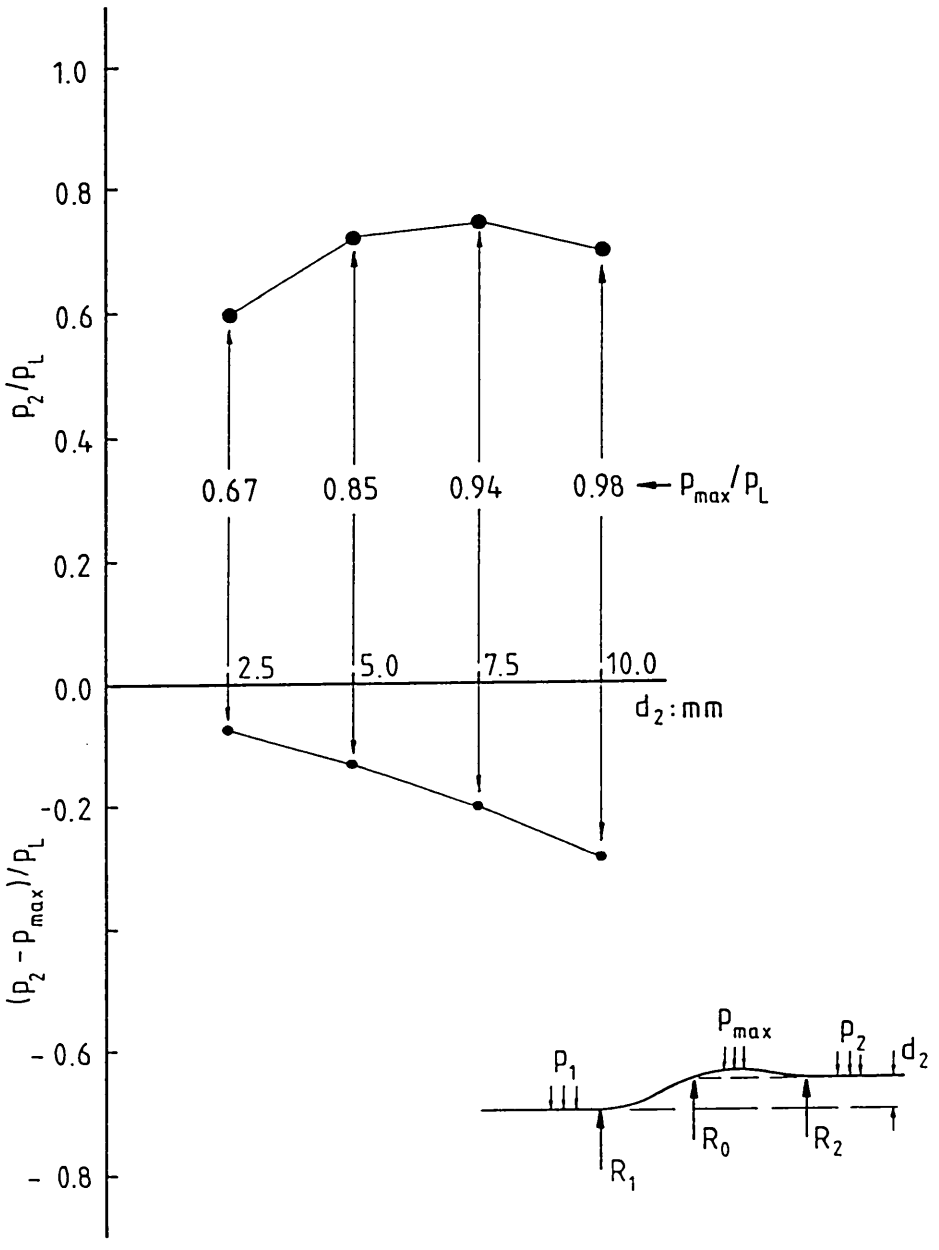

Figure 10.21 'BRS' soil model:
Influence of increase and decrease in stress, ahead of and behind mandrel nose, on the normalised shank stress p_2/p_L

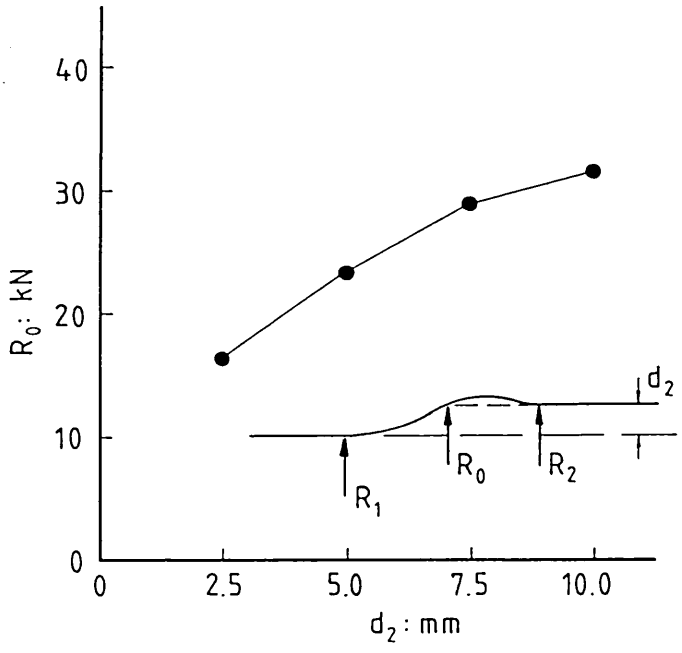

Figure 10.22 'BRS' soil model:
Central propping force R_o against Shank displacement d_2

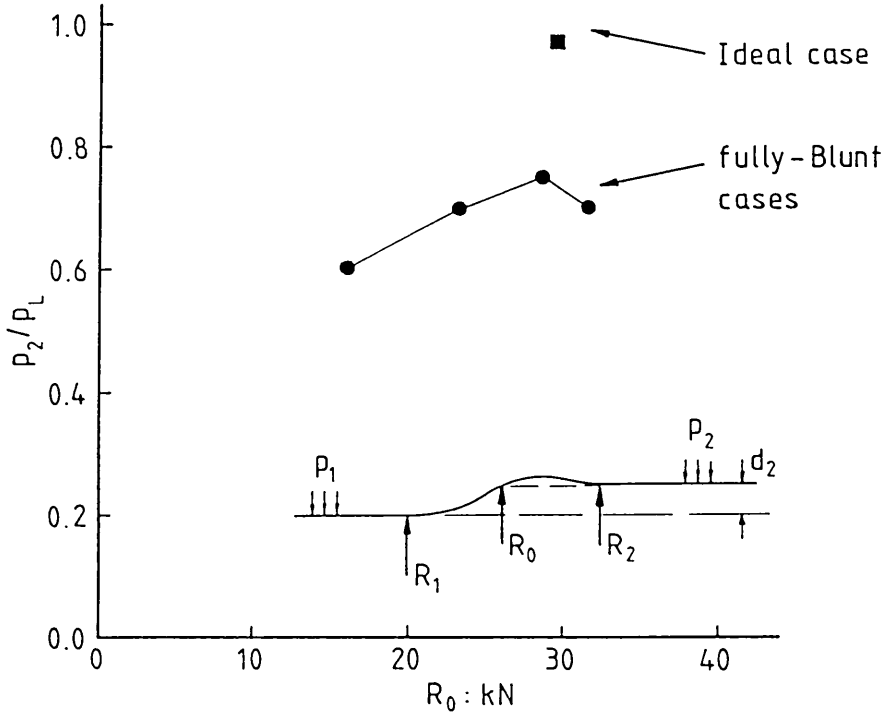

Figure 10.23 'BRS' soil model:
Normalised shank stress p_2/p_L against
Central propping force R_o

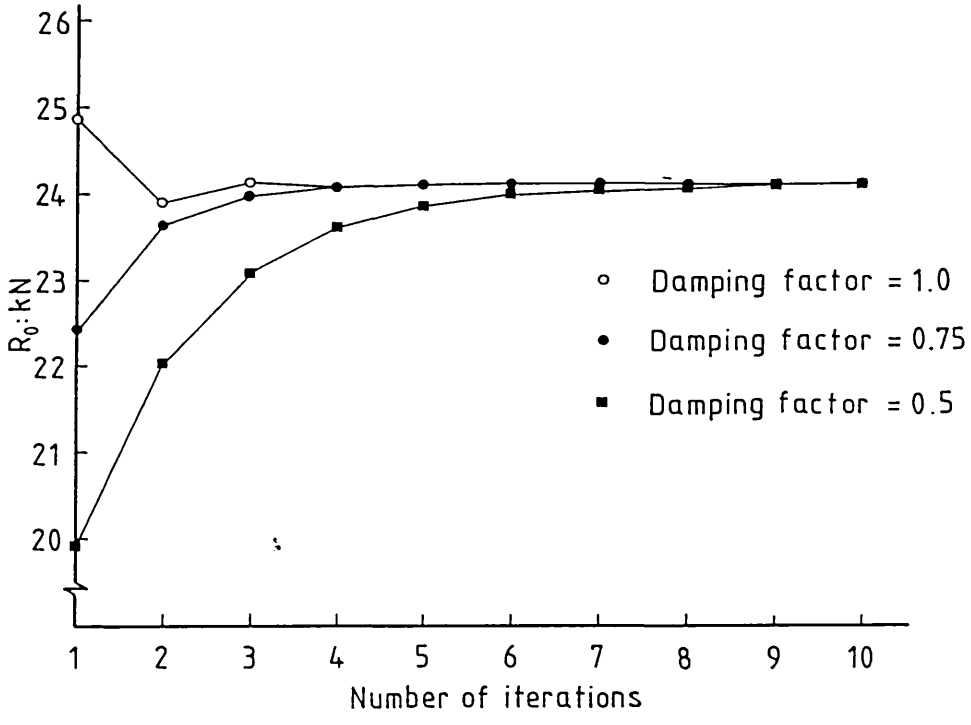

Figure 10.24 Example of solution convergence

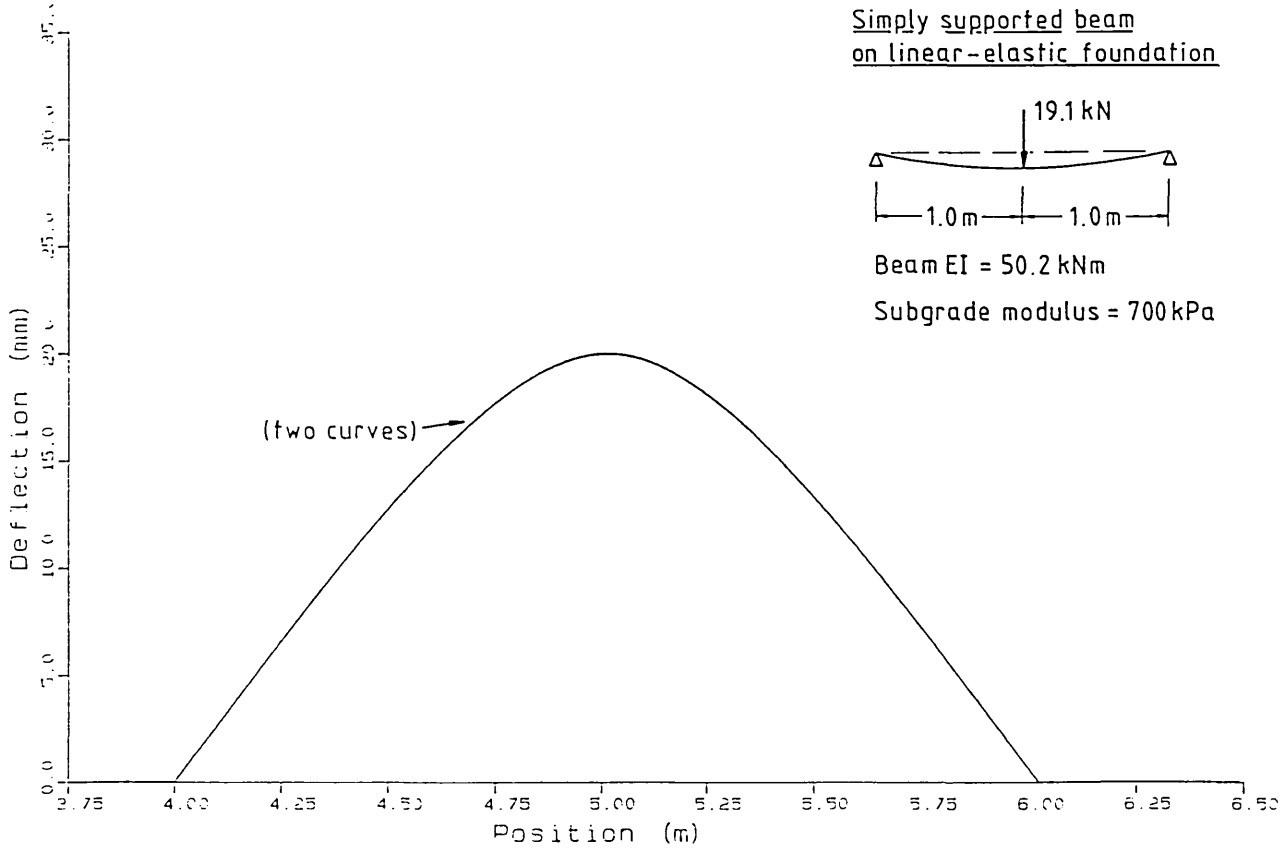

Figure 10.25 Comparison of numerical solution for simply supported beam on elastic foundation with standard Hetenyi solution

(a) Circular nose profiles - same SHAPE, different LENGTHS

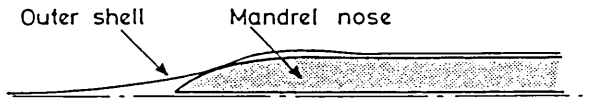

(b) General over expansion, sub-ideal nose profile

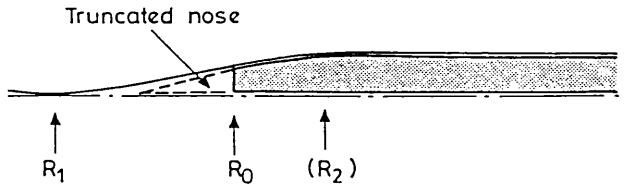

(c) No over-expansion, ideal nose profile

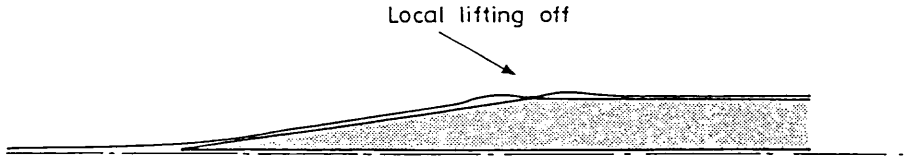

(d) Local over-expansion, super ideal nose profile

Figure 10.26 Nose profile design: nomenclature

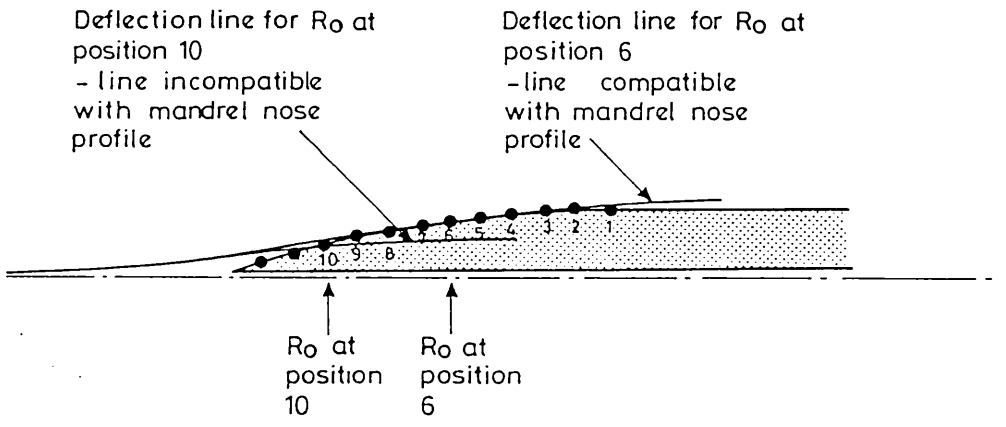

Figure 10.27 Nose profile design: discretization of nose profile

Type of expnsn.	Shank disp.	Seg. lngth.	L_1	L_2	L_{max}	d_1	d_2	d_e	d_{max}	R_1	R_e	R_2	p_1	p_c	p_{max}	p_2	Max. B.M.	Max σ_n
	mm	mm	m	m	m	mm	mm	mm	mm	kN	kN	kN	kN/m²	kN/m²	kN/m²	kN/m	kNm	N/mm²
Ideal	10.0	20.0	1.05	0.43	0.43	0.0	10.0	8.94	10.00	5.6	28.5	0.0	105	315	306	306	-2.84	352
Blunt	10.0	20.0	1.09	0.71	0.18	0.0	10.0	10.00	10.57	5.8	31.7	4.1	105	315	310	220	-3.39	420
Blunt	7.5	20.0	1.03	0.65	0.16	0.0	7.5	7.50	7.90	5.2	28.9	3.9	105	315	298	235	-2.83	350
Blunt	5.0	20.0	0.97	0.59	0.14	0.0	5.0	5.00	5.26	4.5	23.5	3.4	105	315	267	228	-2.19	271
Blunt	2.5	20.0	0.83	0.51	0.14	0.0	2.5	2.50	2.64	3.6	16.4	2.3	105	315	211	189	-1.37	170

Table 10.1 'BRS' soil model runs: results

CHAPTER 11
DISCUSSION OF RESULTS

11.1 Introduction

The majority of this Chapter comprises a discussion of the results of the various field trials reported in this thesis, consisting of the large-scale investigations at Luton and BRS (Chapters 4 and 5); the mini-pile testing (Chapter 6); and the CP&F/Conoco trials at Hermitage (Chapter 8). General aspects of the Wedge-Pile are also considered in this Chapter, and suggestions are given for further research.

Most of the work reported in this thesis concerns 'multiple-element' wedge-piles. In Section 11.2, a general overview of the results of all the tests on multiple-element wedge-piles is given.

The large scale trials at Luton and BRS constitute the most important part of the research described in this thesis. The results from the trials at Luton are discussed in detail in Sections 11.3 to 11.5; the results from the trials at BRS are discussed in detail in Sections 11.6 and 11.7. The results are considered within an effective stress framework. The basic frictional equation (Section 1.1.2) is employed in the form

$$\bar{\tau}_{s_f} = \bar{\sigma}'_r . \tan\bar{\delta}' + \bar{c}'_a \qquad (11.1)$$

where the 'bars' are used to indicate average values of skin friction, radial effective stress, angle of interface shearing, and effective adhesion intercept. Also employed in the analysis of the results is the equation

$$\bar{\tau}_{s_f} = \bar{K}_s . \bar{\sigma}'_v . \tan\bar{\delta}' + \bar{c}'_a \qquad (11.2)$$

where K_s is the radial stress factor and σ'_v is the vertical effective stress. As before, 'bars' are used to indicate average values of parameters.

Throughout the Chapter, 'bars' are used to indicate average values of parameters relevant to the pile tests. Where 'bars' are not used, values of parameters acting locally at a given point are indicated.

The results of the tests carried out with mini-piles are discussed in Section 11.8, while the CP&F/Conoco field trials are discussed in Section 11.9.

Some general aspects of the Wedge-Pile are discussed in Sections 11.10 to 11.12, in the light of the results of the research that has been undertaken. Suggestions for further research are given in Section 11.13.

11.2 Multiple Element Piles: Overview of Results

The principal results from all of the tests on multiple-element wedge-piles, at various scales, are summarised in Table 11.1. The following main points emerge:

(a) In all cases, expansion subsequent to initial driving increases pile capacity. This is a very significant result, which confirms the Wedge-Pile concept.

(b) There are larger increases in capacity in sands and in soils with an appreciable content of granular material, in comparison to gains recorded in clays. This finding is in accordance with the background theory presented in Chapter 9. There appear to be no inconsistencies between the gains in capacity found in the large scale, the miniature scale and the laboratory model scale tests.

(c) In tests on cruciform piles, the gains in capacity on expansion can be summarised broadly as follows:

- In clays, factors of increase in capacity are around 1.5 to 2.0, the lower values being found at the London Clay site and the higher values at the boulder clay site.

- In tests in sands, with mini-piles and with laboratory model piles, the maximum factor of increase in capacity is around 4. .

- In soils where the unexpanded pile capacity is low in comparison to the available soil strength (in the weathered chalk at Luton and in the clayey gravel at Holland House), expansion results in larger gains in capacity, of up to a factor of 10.

Because the various test piles were not expanded over their full lengths, increases in deduced average shaft friction are rather higher than the increases in pile capacity quoted above.

(d) The expanded box piles tested at Luton and at BRS generally performed rather better than the corresponding expanded cruciform piles. There is a more marked difference in capacities between unexpanded box piles and corresponding unexpanded cruciform piles; the unexpanded box piles giving higher capacities. Consequently, the factors of increase in capacity for the expanded box piles are lower than for the expanded cruciform piles.

(e) The H section mini-piles tested at BRS and at Send Court show significantly lower factors of increase in capacity than for the corresponding cruciform mini-piles.

11.3 Piles at Luton Site: Initial Increases in Capacity

The results of tests on 6m long box and cruciform piles in weathered chalk at Luton were presented in Chapter 4. The initial increases in pile capacity and in deduced average pile shaft friction were summarised in Section 4.8.1 and in Figures 4.59 and 4.60, which have been reproduced for convenience as Figures 11.1 and 11.2 of this Chapter.

11.3.1 Unexpanded piles

The unexpanded Box Pile 1U and Cruciform Pile 3U gave maximum loads of 79.1kN and 50.4kN respectively, corresponding to very similar average shaft frictions $\bar{\tau}_{s_f}$ of 28.8kPa and 23.3kPa respectively. These values are in good agreement with typical values of $\bar{\tau}_{s_f}$ of around 20 to 50kPa for driven piles in weathered chalk quoted by Hobbs and Healy (1979), and Lord (1989). These values of shaft friction are also very similar to the cone sleeve friction values recorded between 2 to 5m depth in CPT 1 (Figure 4.4), although the surface of the friction sleeve was smoother than the pile surface (Section 4.4.5). Reasonable agreement between cone sleeve frictions and steel pile shaft frictions in chalk has been reported by Mallard and Ballatyne (1977), and Lord (1976). Hodges and Pink (1971) reported cone frictions higher than pile shaft frictions.

The Cone Penetration Test performed at the pile test site (CPT 1) shows a profile which is reasonably consistent over much of the depth of embedment of the test piles, and it is considered that the chalk samples retrieved from the borehole opened up at the site are likely to be representative of the chalk adjacent to the test piles. Therefore, it is suggested that the following values of $\bar{\delta}'$ can be used in Equations 11.1 and 11.2:

$\bar{\delta}'$ chalk:chalk = 36°
$\bar{\delta}'$ chalk:rough steel = 34°

These are the values obtained from the shearbox tests described in Section 4.4.7.

The results from the shearbox tests show no tendency for δ' to degrade during continued displacement after maximum shearing load, so the $\bar{\delta}'$ values given above are considered to be relevant to the whole series of pile tests carried out. The value of $\bar{\delta}'$ for a chalk:chalk interface is appropriate for the cruciform piles, and the value of $\bar{\delta}'$ for a chalk:rough steel interface is appropriate for the box piles (Section 4.5.2).

Equation 11.1 has been used to calculate values of $\bar{\sigma}_r'$ associated with the values of $\bar{\tau}_{s_f}$ and $\bar{\delta}'$ given above. The effective adhesion intercept $\bar{c}_a'$ has been neglected because of the remoulding of the chalk surrounding the pile that will have occurred during driving. Adopting the $\bar{\tau}_{s_f}$ and $\bar{\delta}'$ values given above, and applying Equation 11.1, yields $\bar{\sigma}_r'$ values of 32.1kPa and 42.7kPa for the cruciform pile and the box pile respectively. The larger value of $\bar{\sigma}_r'$ in the case of the box pile is to be expected, because of the greater volume displacement of this pile. It is also worth noting that the form of construction of the unexpanded box pile was such that it would have acted as a drain in the ground. If excess pore pressures were generated during pile loading, it is possible for the draining potential of the box pile to have caused the capacity of the pile to be greater than if the pile had been impermeable. It is thought, however, that any excess pore pressures generated during static loading of the piles were small in comparison to the radial stresses acting (see Section 11.3.2).

Taking a porosity for the intact chalk of 43% (Section 4.4.2) gives plausible values of dry density, γ_D, and saturated density, γ_S, of 1.54t/m^3 and 1.97t/m^3 respectively. These values of porosity have been used to calculate values of $\bar{\sigma}_v'$. Applying these values of $\bar{\sigma}_v'$ in Equation 11.2, together with the deduced values of $\bar{\tau}_{s_f}$ and $\bar{\delta}'$ given above, yields values of $\bar{K}_s$ of 0.83 and 1.24 for the cruciform pile and the box pile respectively. These values of $\bar{K}_s$ are in good agreement with deduced values of $\bar{K}_s$ for driven piles given by Hobbs and Healy (1979).

11.3.2 Expanded piles

Deduced values of $\bar{\tau}_{s_f}$ at maximum pile load during initial loadings of the expanded box and expanded cruciform piles are given in Figures 11.1 and 11.2. Gains in shaft friction are up to 5.4 times in the case of the box

piles, and up to 6.9 times in the case of the cruciform piles. The enhancement of carrying capacity as a result of expansion is clearly very satisfactory. The shaft frictions of the expanded piles, of up to 161kPa, are near to the upper limits of ultimate values reported by Hobbs and Healy (1979) and Lord (1989), for traditional piles (of all types) in weathered chalk.

Adopting the $\bar{\delta}'$ values given in the previous Section, and applying Equation 11.1 with $\bar{c}'_a$ neglected as before, yields a range of $\bar{\sigma}'_r$ values for the expanded piles as shown in Table 11.2. Adopting values of γ_D and γ_S as before, and applying Equation 11.2, gives a range of $\bar{K}_s$ values as also shown in Table 11.2.

The actual values of $\bar{\tau}_{s_f}$, $\bar{\sigma}'_r$ and $\bar{K}_s$ for the expanded piles are considered to be near the top of the range of values given in Table 11.2; it being reasonable to assume that the outer shell angles attracted almost all of the radial effective stress acting on the expanded piles, and that rapid reductions in σ'_r occurred during initial loading along the tapered region at the bottom of the pile (Section 4.5.2).

The average of the deduced maximum $\bar{\sigma}'_r$ values for all the expanded piles is 194kPa. Overall, the expanded box piles show slightly greater values of deduced maximum $\bar{\sigma}'_r$ than the expanded cruciform piles; the average for the two cruciform piles 3B and 4A is 187kPa, the average for the three box piles 1A, 2A, and 2B is 199kPa. The closeness of these two values is in broad agreement with theory, which suggests that at large expansions, the radial stresses generated by the two types of pile should both tend to the same limiting value (provided that over-expansion does not occur). Two possible reasons for the small difference that was observed in the tests are the greater volume displacements of the box piles and/or greater over-expansion effects in the case of the cruciform piles, due to blunter expander mandrel nose profiles (Sections 3.3.3; 10.3.2.4; refer to Section 11.3.3).

It is important to note that the average values of $\bar{\tau}_{s_f}$ quoted above mask some significant variations between individual piles. These are discussed in Section 11.3.3.

In Figure 11.3, the deduced values of $\bar{\sigma}'_r$ at maximum pile load are plotted against percentage expansion of pile width. Also plotted in Figure 11.3 is the pressure:displacement plot from the FDPM test of most relevance to the analysis of the pile tests: Test 1, carried out at 3.5m depth in weathered chalk. The limiting value of pressure of around 600kPa developed during the FDPM test is about three times greater than

the deduced maximum values of $\bar{\sigma}_r'$ acting on the sides of the expanded piles under test.

It is not possible to give specific reasons for the large difference between the deduced radial effective stresses acting on the expanded piles at failure, and the measured radial total stresses generated during expansion of the FDPM. A number of different factors are likely to have had some effect. The main factors, and the possible magnitude of their effect, are given below:

(a) As discussed in Section 4.4.6, it is unlikely that expansion of the FDPM was under completely drained conditions and the limiting pressures obtained probably included an excess pore pressure component. If this component was large, significant reductions in σ_r' might have occurred around the FDPM if full consolidation had taken place at constant cavity strain.

However, the evidence from the piezocone dissipation tests (Section 4.4.4), in which near complete consolidation took place in a matter of minutes, suggests that the FDPM expansion rate of 2.5%/minute would have given substantially drained conditions. Evidence from the FDPM holding tests which were attempted is confused by the fact that the FDPM was not successfully held at a constant strain. As discussed in Section 4.4.6.4, however, the fluctuations in cavity pressure which occurred during the holding tests were closely associated with fluctuations in cavity strain. No large irrecoverable losses in cavity pressure were apparent during holding periods of up to 10 minutes, during which time consolidation was presumably substantially complete.

The FDPM cavity pressures recorded include small static pore pressure components. For the test made at 3.5m depth, this pressure is insignificant.

In summary, it is considered that the FDPM tests were substantially drained events, and that the pressures recorded during expansion of the FDPM must have been reasonably close to the effective radial stresses potentially available during expansion of the wedge-piles - within 10 to 20%, say.

(b) Stress relaxation or creep effects, resulting in a gradual reduction with time of the radial effective stress acting against the expanded piles, may have occurred in the period between the end of consolidation and the initial pile test. This aspect of

Wedge-Pile behaviour requires further research (Section 11.13). It is thought that stress relaxation or creep may be important in clay soils, but that in an essentially granular soil such as chalk these effects could not have resulted in reductions in radial stress that would account for the discrepancies between the FDPM tests and the pile tests described above.

(c) Following on from point (a) above is the question of the drainage conditions during pile loading. If pore pressures generated during pile loading were large in comparison to those generated during expansion of the FDPM, this might account for some of the difference between the deduced effective radial stresses acting during the pile tests and the total radial stresses measured during the FDPM tests. It is considered however, given the piezocone results, that any excess pore presures generated during static pile loading at a rate of 1mm/minute would have been very small in comparison to the radial stresses acting.

(d) It was shown in Chapter 9 that a '4-way' wedge-pile might generate less radial force/unit length than is potentially available by expansion of a true cylindrical cavity of the same effective diameter, the amount of reduction possibly being of the order of 10%.

(e) The results from the FDPM holding tests, during which inadvertent unloading of the FDPM occurred, provide a good indication of the magnitude of reductions in σ'_r that would have resulted if over-expansion took place during expansion of the wedge-piles. For example, in the FDPM test at a depth of 7m, a reduction in strain of 0.38% resulted in a drop in cavity pressure of 460kPa, almost half of that generated during expansion (Section 4.4.6.4). The same reduction in strain following expansion of a wedge-pile to a diameter of 150mm, say, implies a reduction in diameter of around 0.5mm. (The G_{ur} values recorded at a depth of 3.5m were lower than those measured at 7m (Section 4.4.6.5), so at this shallower depth rather larger reductions in strain would have been necessary to give the same magnitude of reductions in cavity pressure as given above.)

One of the main conclusions from the numerical study of the expansion process presented in Chapter 10 was that the expander mandrel nose profiles used for the large scale tests were very likely to have given rise to over-expansion. Large reductions in radial stress were predicted by the numerical model if such

over-expansion occurred. It is not possible to predict quantitatively the magnitude of any reductions which might have occurred at the Luton site, but certainly the results presented in Section 10.3.2 suggest that changes in pile diameter and consequent reductions in σ_r' of the magnitude quoted in the previous paragraph are entirely plausible.

(f) Reductions in σ_r' during initial pile loading are likely to have been significant. Again, it is not possible to be precise. The shearing regime during loading, in comparison to that during installation, has an important bearing here - this is discussed further in Section 11.5. Reductions in σ_r' during initial loading could reasonably be expected to be more significant than any of factors (a), (b), (c) and (d) above, but not as significant as factor (e).

In conclusion, it is considered that the most likely main cause of the large difference between deduced values of $\bar{\sigma}_r'$ acting on the expanded piles at failure, and those apparently available during expansion of the FDPM, is over-expansion in the region of the expander mandrel nose. This factor alone could easily account for all of the difference. A number of other factors may also have had an influence, the most important of these is probably reductions in σ_r' occurring during initial loading of the piles.

It is interesting to note that the results of the DMT tests carried out at the Luton site show the ratio of the DMT pressures p_1/p_0 to be in the region of 5 to 6 (Figure 4.7). The increases in σ_r' due to expansion of the piles is therefore apparently well predicted. As the DMT models closely the action of the wedge-piles, this is what might be expected. However, the DMT p_1 pressures are in excellent agreement with the corresponding FDPM limiting pressures, which have been shown not to be in good agreement with the results of the pile tests. This means that for the ratio p_1/p_0 to be correct, the values of p_0 must be higher than the deduced radial stresses acting on the unexpanded piles. This may well be the case, the reason being the positioning of the DMT pressure membrane near to the tip of the instrument. The p_0 pressure measured during a DMT test will be influenced by increases in radial stress occurring near the tip of the instrument as it is pushed into the ground (Figure 9.8). A pressure membrane situated some distance behind the tip would be likely to give p_0 values in better agreement with deduced radial stresses acting on the shafts of unexpanded piles. The good 'prediction' of the DMT results is therefore rather fortuitous. Despite this, it is thought that the DMT may have applications in the design of

wedge-piles (Section 11.12).

11.3.3 Effect of different percentage expansion

The deduced maximum values of $\bar{\tau}_{s_f}$ during the initial loadings of the expanded piles have been shown in Table 11.2, and in Figures 4.61 and 4.62. No clear pattern emerges in regard to the effect of the extent of expansion on pile capacity. An important point is that there were no large further increases in capacity obtained by expansion with the 'B' expander mandrels (21% expansion), in comparison to the 'A' expander mandrels (11% and 14% expansion). In the case of the box piles, Pile 2B (21.4% expansion) showed the best performance, with a factor of increase in maximum shaft friction of 5.4. Piles 1A and 2A (14.3% expansion) gave factors of increase of 4.9 and 3.7 respectively. In the case of the cruciform piles, Pile 4A (10.7% expansion) performed best, with a factor of increase in maximum shaft friction of 6.9; Pile 3B (21.4% expansion) performed less well, with a factor of increase of 4.7. These results are in general agreement with the results of the FDPM tests shown in Figures 4.11 to 4.13 - the pressure:expansion curves of the FDPM tests show only small increases in pressure for expansions between 10% and 20%.

The following points are relevant when considering the variation in results shown in Table 11.2:

(a) As described in Chapter 10, although increased percentage expansion may give rise to an increase in σ_r' ahead of the expander mandrel nose, it may also cause an increased loss in σ_r' behind the nose due to over-expansion. Eventually, losses in pile capacity with further increases in expansion are predicted to occur for 'blunt' nose profiles.

(b) Due to the fabrication difficulties mentioned in Section 3.3.3, the nose profile of cruciform expander mandrel B was very short and blunt. This may have caused particularly marked over-expansion to occur during installation of Cruciform Pile 3B, resulting in the lower capacity of this pile in comparison to Cruciform Pile 4A. The nose profile of this expander mandrel was later smoothed down for use at the BRS site.

(c) Box Pile 2A was expanded only 30 minutes after the outer shell was driven. The driving resistance met during expansion was significantly less than for the other piles (Figure 4.23), which were expanded after much longer time intervals following shell installation. Subsequent to driving, the load carrying capacity of

Box Pile 2A was significantly lower than for Box Piles 1A and 2B.

In contrast to the low excess pore pressures predicted during pile testing, large pore pressures are to be expected during driving of a large displacement pile in chalk, affecting a large radius of material around the driven pile. In the case of Box Pile 2A, pore pressures generated during expansion may not have fully dissipated before expansion took place.

The low driving energy for Box Pile 2A, and subsequent low capacity, suggests that after installation of the outer shell of a wedge-pile there may be benefits in allowing full consolidation and gain in soil strength before expansion is carried out.

The inherent limitations of the pile testing system - interference between adjacent test piles and/or the reaction system, for example - are not thought to have seriously influenced the measured pile capacities. However, such effects might be responsible in part for the differences observed between the capacities of the expanded piles. The effect of possible variations in ground conditions should also be borne in mind.

11.4 Piles at Luton Site: Overall performance

In this Section various aspects of the overall performance of the piles at the Luton site, summarised in Section 4.8.3, are considered. The performance of the piles under cyclic loading is considered in Section 11.5.

The stiffer reloading behaviour observed during the pile tests is characteristic behaviour for chalk, as demonstrated in the shearbox tests. The generally stiffer behaviour of the box piles in comparison to the cruciform piles can be attributed to the greater compacting action of the box piles giving rise to a more rigid material around these piles. The response of Box Pile 2A, expanded very soon after expansion, is less stiff than for Piles 1A and 2B, expanded after longer periods of consolidation. This softer response ties in with the lower capacity of Box Pile 2A discussed in the previous Section.

For conventional piles, it is reasonable to assume that the shearing regime during controlled static loading will be less severe than that during pile driving (e.g. Ebelhar et al, 1988). Consequently, it is to be expected that the load:displacement response during controlled static loading would be reasonably ductile after failure. This is

confirmed by the load:displacement curves for the unexpanded piles shown in Figures 11.1 and 11.2.

It is very encouraging that, in the main, the expanded piles also exhibited ductile behaviour after failure - as typified by the load: displacement curves for the expanded piles shown in Figures 11.1 and 11.2. However, sudden losses in capacity did occur during Tests 2B.5 and 4A.3 (Figures 4.44 and 4.57 respectively). As these tests were the last performed prior to extraction of the piles, it is not known whether these sudden losses in capacity would have been recoverable with time. The brittle behaviour observed in these two tests may have been the result of the previous large displacements of the piles having a damaging effect on the fabric of the chalk around the piles. Also, Box Pile 2 suffered disturbance, and a complete unloading of σ_r', when the expander mandrels were swopped around. It is interesting that Box Pile 1A, which showed by far the greatest driving resistance during installation and which underwent less disturbance during the testing programme than did Box Pile 2, showed no sign of any brittle behaviour.

Changes in pile capacity which might follow large pile straining are discussed further in the following Section.

No significant decreases in pile capacity with time were observed, for piles subjected to a series of static tests. This is obviously a very important result. It shows that the increases in radial effective stress and in pile capacity following expansion were sustainable and did not 'leak away' during the time span of the testing programme (up to 203 days). It is likely that any detrimental effects due to long term stress relaxation and creep would have manifested themselves over such a long period. This behaviour also suggests that during a series of static tests on expanded piles, any reductions in radial effective stress from values existing after driving and consolidation occur only during the initial loading of the pile.

Small increases in capacity often occurred, for piles subjected to a sequence of static CRE tests (Figures 4.24 to 4.27). The time spans over which these increases in capacity took place require the cause to be other than an increase in radial effective stress caused by consolidation after driving. Similar long term increases in the capacity of driven piles in weathered chalk have been reported by Hodges and Pink (1971), and Bustamente and Combarieu (1977). Hobbs and Healy (1979) suggest a 'general settling down of the chalk' as a possible reason. Another reason may be an increase in effective cohesion c_a' of the chalk with time: Clayton (1989) reports that, after remoulding, soft chalks

can recover apparent effective cohesion at least up to 13kPa.

11.5 Piles at Luton Site: Performance Under Cyclic Loading

In this Section the changes in pile capacity which occurred during cyclic loading, summarised in Section 4.8.2, are considered. First, a suggested framework of behaviour within which to discuss the results is presented. This framework is based on the reported behaviour of chalk and carbonate soils outlined in Chapter 4.

The chalk tested in the shearbox gave friction angles which were essentially unaffected by stress level or by continued large displacements. Therefore, the changes in pile capacity that occurred during cyclic loading were most probably caused by changes in effective radial stress. Such changes in σ_r' can be temporary or permanent.

Temporary changes in σ_r' tend to be associated with the generation of excess pore pressures, which subsequently dissipate. Pore pressures may gradually accumulate at small strains while total radial stress remains constant.

Permanent reductions in σ_r' tend to be associated with contractant behaviour during shear. The propensity for this to occur depends on the severity of the current shearing regime in relation to that previously experienced by the chalk surrounding the pile. Permanent reductions in σ_r' are generally associated with large shear strains and/or strain reversals. Reductions in σ_r' can take place rapidly as the chalk structure collapses, and these reductions will usually be associated with the rapid generation of pore pressures. Dissipation of these pore pressures will not result in increases in σ_r'.

Complicated patterns of behaviour may take place during cyclic loading. Pore pressures may accumulate during small strain cycling, but these will not affect the pile load:displacement response if the severity and number of the loading cycles applied is within certain threshold values. Reductions in σ_r' under these circumstances will usually be recoverable. Alternatively, the slow development of pore pressures may eventually cause a softening of the pile response, causing larger strains to develop, in turn giving rise to rapid increases in pore pressures and strains. Under these circumstances permanent losses in σ_r' may occur.

During driving of a pile in chalk, there is intense shearing along the shaft of the pile, resulting in the generation of large pore pressures and reductions in σ_r'. The greater the shearing action during driving,

the greater the reductions in σ'_r, and the less is the scope for subsequent reductions in σ'_r during pile loading. Shearing and compaction is more thorough in the case of large displacement piles than for small displacement piles.

The results of the cyclic loading tests are now considered in the light of the framework of behaviour suggested above.

Unexpanded Cruciform Pile 3U suffered 1.9mm of permanent displacement during 50 cycles of loading, but the static capacity after cycling was virtually identical to that before cycling. The cyclic loading apparently had little or no effect on either pore pressures or $\bar{\sigma}'_r$. This suggests that either the shearing regime during testing was less severe than that experienced during driving of the pile, or that $\bar{\sigma}'_r$ had already degraded to a 'minimum possible' value during driving.

Box Piles 1A and 2B suffered no permanent displacement during cycling, and showed no softening of load:displacement response. However, the static tests performed immediately after cycling showed reductions in capacity of up to 19% in comparison to the static tests before cycling. These losses in capacity were largely recoverable with time. This behaviour suggests that the losses in capacity were associated with the steady accumulation of pore pressures during cycling, which subsequently dissipated. This is supported by the fact that Box Pile 2B (50 cycles) suffered a greater loss in capacity than Box Pile 1A (25 cycles). Whether further cycling would have eventually triggered permanent reductions in $\bar{\sigma}'_r$ is a matter for conjecture.

Cruciform Pile 4A suffered large permanent displacements during cycling. The progressive softening of load:displacement response near the top of the loading cycles, and the fact that the pile subsequently failed at the cycling load, suggests that large increases in pore pressure occurred during cycling. In contrast to the other piles, the loss in capacity on cycling was not recoverable: the large strains during cycling must have given rise to permanent reductions in $\bar{\sigma}'_r$.

The much better performance under cyclic loading of the expanded box piles in comparison to the expanded cruciform piles can be attributed to the greater compacting action of the box piles during driving. Two reasons are suggested here. Firstly, the greater compactive effort of the box piles gave rise to a stiffer load:displacement response under test (Section 11.4). As a result, the strains during the stress controlled cycling, and the pore pressures generated, were less for these piles. Secondly, as stated above, the greater the compaction

during pile installation, the less scope there is for subsequent shear induced reductions in σ_r'. It appears that in the case of Cruciform Pile 4A, the compaction of the chalk prior to expansion was insufficient to prevent shear induced reductions of σ_r' during cycling.

An interesting question is why the reduction in capacity of Cruciform Pile 4A during cycling did not manifest itself during the initial static loading of the pile, when the pile was displaced by over 30mm. During this displacement, the chalk close to the pile must have been thoroughly sheared. The reason may be that the cyclic loading caused contractant behaviour to occur a short distance from the pile, in a region not thoroughly compacted during driving of the outer shell, or sheared during static loading.

11.6 Piles at BRS Site: Initial Increases in Capacity

The results of tests on 6m long box and cruciform piles in boulder clay at BRS were presented in Chapter 5. Increases in capacity and in shaft friction have been summarised in Table 5.14 and in Figures 5.56 and 5.57. For convenience, these have been reproduced as Table 11.3 and Figures 11.4 and 11.5 of this Chapter.

11.6.1 Unexpanded piles

Whereas appropriate values of $\bar{\delta}'$ at failure can be estimated with reasonable confidence for the piles at the Luton site, the selection of $\bar{\delta}'$ values for the piles at the BRS site is more difficult, for two reasons:

(a) The nature of boulder clay means that large samples are required in order to reproduce representative behaviour. Ideally, large (305x305mm) shearbox tests are required for the testing of materials containing coarse gravel.

(b) Clay particle alignment effects: the value of δ' operating at failure will be somewhere between peak and residual values, depending on the current rate of displacement, and the previous mode and rate of displacement during installation. Expansion of a pile may disrupt residual surfaces formed during initial installation.

The results from the single suite of standard (60x60mm) shearbox tests on a small sample of the till, in which all material not passing a 2mm size seive was removed, indicate that significant particle alignment occurs during shearing of the till (Section 5.3.5). A residual value of

δ' of around 17° was found, with peak values varying between 20° and 27°. The residual values of δ' obtained from the shearbox tests are rather lower than values normally associated with medium plasticity clays (eg. Chandler, 1984).

Peak values of $\bar{\tau}_{s_f}$ for the unexpanded cruciform pile and unexpanded box pile during initial loadings have been calculated as 53kPa and 73kPa respectively (Figures 11.4, 11.5). Equation 11.2 has been used to calculate values of the radial stress factor $\bar{K}_s$ corresponding to the values of shaft friction given above. The effective adhesion intercept $\bar{c}_a'$ has been neglected because of the remoulding of the soil adjacent to the pile that will have taken place during installation. In order to deduce appropriate values of $\bar{\sigma}_v'$, the value of γ for the upper till has been taken as 2.15kN/m^3 (Figure 5.2) and the level of the water table has been taken as 0.5m below ground level (Section 5.2.2). Applying Equation 11.2 with deduced values of $\bar{\sigma}_v'$ and with a range of $\bar{\delta}'$ values, yields $\bar{K}_s$ values as shown in Table 11.4.

Values of $\bar{K}_s$ derived by assuming $\bar{\delta}'$ to be equal to the (near) residual values of δ' indicated by the shearbox tests are well in excess of maximum in-situ values of $\bar{K}_s$ that can be expected in this deposit, even for the low-displacement cruciform pile, the installation of which presumably did not cause a large increase in radial effective stress above in-situ values. The assumption of a value of $\bar{\delta}'$ of around 25° operating during the pile tests implies more plausible values of $\bar{K}_s$.

Although interface tests were not carried out, it is considered that the limiting (i.e. peak and residual) values of δ' for till:till shearing and till:rough steel shearing would be very similar, because clay was found adhering to the steel piles on extraction (Section 5.6.9). If the values of $\bar{\delta}'$ acting at initial failure for the cruciform and box piles are taken to be the same, a larger value of $\bar{\sigma}_r'$ is implied for the box pile than for the cruciform pile (Table 11.4), as was the case at the weathered chalk site. As at the Luton site, this may be due to the larger volume displacement of the box pile. In practice, the values of $\bar{\delta}'$ acting at initial failure for the two types of pile may have been different - the cruciform piles were installed at a faster rate than the box piles (Section 5.5) and this might have resulted in higher values of $\bar{\delta}'$.

As at the Luton site, another possible reason for the larger deduced values of $\bar{\sigma}_r'$ in the case of the unexpanded box pile is that this pile would have acted as a drain during loading (Section 11.3.1). However, as discussed previously, any excess pore pressures generated during

loading are thought to have been small in comparison with the radial stresses acting.

11.6.2 Expanded piles

Maximum loads and deduced shaft frictions for the pile tests on the expanded piles are shown in Table 11.3, and in Figures 11.4 and 11.5. Gains in deduced shaft friction are up to 2.15 times in the case of the box piles, and up to 2.3 times in the case of the cruciform piles. These gains in shaft friction are considered to be very satisfactory for a medium-plasticity clay. As discussed in Section 11.3.2, the actual values of $\bar{\tau}_{s_f}$ operating in the pile tests are considered to be near the top of the range of values quoted in Table 11.3. Taking these maximum values of $\bar{\tau}_{s_f}$, and lower and upper bound values of $\bar{\delta}'$ at initial failure as 17° and 25° respectively, and applying Equation 11.1 with $\bar{c}'_a$ neglected as before, yields a deduced range of $\bar{\sigma}'_r$ values for the expanded piles as shown in Table 11.5.

If the same value of $\bar{\delta}'$ at failure is assumed for both the box and the cruciform piles, the expanded box piles show on average deduced values of $\bar{\sigma}'_r$ around 20% greater than for the expanded cruciform piles. This difference is rather larger than that found at the Luton site. The most likely cause of the larger values of $\bar{\sigma}'_r$ in the case of the box piles is either the greater volume displacement of the box piles, or greater losses in σ'_r due to overexpansion during expansion of the cruciform piles. It is considered that in the case of the expanded box and cruciform piles the assumption of a similar value of $\bar{\delta}'$ is a reasonable one, because the remoulding action of the expansion process in the case of the two different types of pile is likely to have been similar.

Even assuming the lower bound, residual value of $\bar{\delta}' = 17^\circ$, the deduced values of $\bar{\sigma}'_r$ obtained from the pile tests are many times lower than the limiting total pressures obtained from the FDPM and DMT tests reported in Chapter 5, which were typically in the region of 2000kPa. As was the case with the results of the pile tests at the Luton site, it is not possible to give specific reasons for this large discrepancy. The main possible reasons, and the possible magnitude of their effect, are outlined below:

(a) There is a discrepancy between the limit pressures obtained from the FDPM and DMT tests, and the limit pressures from the earlier Menard pressuremeter tests reported by Marsland. The average of the limit pressures obtained from the earlier tests (over the depth range corresponding to the FDPM tests) is approximately 1400kPa (Powell, 1989), in comparison to an average of around 1800kPa for

the FDPM. As discussed in Section 5.3.4, this may be due to the fact that the FDPM test is performed at a much faster rate than the Menard Pressuremeter test. However, it is also possible that the higher limit pressures measured in the FDPM tests may have in part been due to seasonally high moisture contents in the till. This requires further research.

(b) The FDPM was expanded under nominally undrained conditions, and excess pore pressures would have been generated during expansion. According to the Cambridge theory presented in Section 9.3.3, reductions in total radial stress σ_r should occur during consolidation following the undrained expansion of a cylindrical cavity in clay. Reductions in σ_r did occur during the FDPM holding tests, of around 12 to 13% during holding periods of between 34 to 51 minutes.

The problem here is one of assessing the extent to which consolidation occurred during the holding periods. The fissured fabric of the till would have encouraged relatively quick consolidation. However, there is no evidence of a slowing down of the rate of reduction in σ_r during the holding periods, suggesting that consolidation was not near completion and that further reductions in σ_r would have taken place if the holding tests had been continued for longer periods. As a comparison to the FDPM tests reported here, holding tests with the Self Boring Pressuremeter (SBP) in soft organic and silty clays reported by Clarke et al (1979) showed consolidation times t_{50} generally less than 30 minutes. The radius of the SBP instrument prior to holding was approximately 0.0350m, in comparison to values of about 0.025m in the case of the FDPM tests. It might reasonably be speculated that the falls in radial stress that occurred during the holding periods of the FDPM tests were around half of the reductions that would have occurred if full consolidation had taken place.

The static pore water pressures acting on the FDPM during the tests were insignificant in comparison to the radial pressures measured.

(c) Stress relaxation or creep effects may have caused significant reductions with time in the value of $\bar{\sigma}_r'$ acting on the expanded piles, during the period between the end of consolidation after driving and the initial pile test. Further experimental work would be required to determine the magnitude of this possible reduction (see Section 11.13).

(d) As discussed in Chapter 9, '4-way' wedge-piles may generate lower values of radial force/unit length than those available by expansion of a true cylindrical cavity.

(e) As also discussed in Chapter 9, unloading information from the FDPM tests can be used to provide an indication of the magnitude of reductions in radial stress that would have taken place if over-expansion occurred. The values of shear moduli obtained from the FDPM tests at BRS (Table 5.2) are broadly similar to those at the Luton site (Table 4.1), and so the same conclusions as before can be made: it is possible that large reductions in σ_r' occurred due to over-expansion. Decreases in σ_r' of around half the increase resulting from expansion, for example, are quite feasible.

(f) The theory presented in Section 9.6.1 predicts that reductions in σ_r' will occur during the initial loading of a pile that has been expanded radially in the ground. The theory suggests that in clays the magnitude of the reduction is around a third of the value of σ_r' existing after expansion and subsequent consolidation.

In summary, it is considered that reductions in σ_r' caused by over-expansion during pile installation are likely to have been responsible for a large part of the discrepancy between the deduced values of effective radial stress acting on the expanded piles at failure, and the measured values of total radial stress in the FDPM tests.

Moisture content changes in the till may have caused pressures measured in the FDPM tests to be unusually high. Previous Menard pressuremeter tests gave lower values of total radial stress on expansion, but these values are still around 5 to 6 times the deduced values of σ_r' acting on the piles.

Significant reductions in σ_r', due to consolidation and creep effects, are likely to have occurred during the period between expansion and initial pile testing. Further significant reductions in σ_r' are likely to have occurred during initial pile loading.

11.6.3 Effect of different percentage expansion

Because of the uncertainties regarding the values of $\bar{\delta}'$ that are appropriate to the pile tests, in this Section pile capacities are compared on the basis of shaft frictions.

Calculated values of $\bar{\tau}_{s_f}$ for the four expanded piles have been given in

Table 11.3, and in Figures 5.58 and 5.59. As was found at the chalk site, there were no large further increases obtained by expansion with the 'B' expander mandrels (21% expansion), in comparison to the 'A' expander mandrels (11% and 14% expansion). This result is in agreement with the results of the FDPM tests - the plots of pressure against radial strain shown in Appendix 5.1 show little increase in pressure for radial strains above 10%.

Cruciform Pile 8B gave a maximum deduced value of $\bar{\tau}_{s_f}$ of 121.9kPa, a small increase over Cruciform Pile 9A which gave a value of 118.2kPa. Box Pile 5B gave a maximum deduced value of $\bar{\tau}_{s_f}$ of 134.2kPa, a rather large drop in comparison to Box Pile 7A which gave a value of 156.9kPa.

As discussed in Section 11.6.2, over-expansion effects may have been significant. Interestingly, the maximum value of $\bar{\tau}_{s_f}$ (Box Pile 7A) was obtained with the least blunt expander mandrel nose profile (Figure 3.9). Also, the very blunt nose profile of cruciform expander mandrel B - as used at the Luton site - was smoothed down for use at the BRS site, and this time gave a slightly higher pile capacity than for expander mandrel A, in contrast to the experience at the Luton site (Section 11.3.3). These observations tend to support the hypothesis that over-expansion effects may have been significant in the pile tests at Luton and BRS.

As previously discussed in Section 11.3.3, the possible variations in ground conditions at the test site, and the inherant limitations of the pile testing system, may also be responsible in part for differences in capacity of the expanded piles.

11.7 Piles at BRS site: Overall Performance

In this Section, some aspects of the overall performance of the piles at the BRS site described in Section 5.7 are discussed.

The most notable feature regarding the load:displacement behaviour of the expanded piles is the stiffer response during reloading, in comparison to initial loading. The unexpanded piles do not exhibit this behaviour. The less stiff response of the expanded piles on initial loading is associated with greater creep displacements under maintained loads. Two possible reasons for this behaviour may be:

(a) The change of direction of shearing during initial loading, in comparison to that during expansion.

(b) Large plastic strains during initial loading. These would be expected during shearing of a normally consolidated clay, as the stress path during shear will traverse the state boundary surface. Cavity expansion theory predicts the clay surrounding an expanded pile to be normally consolidated after pile installation. For normally consolidated clays, after plastic straining occurs during initial loading, subsequent unloading and reloading falls within the current yield locus for the clay and is essentially elastic.

As was found at the chalk site, the expanded piles showed no reduction in capacity with time, during periods of up to 300 days. This is a very encouraging result, which demonstrates that - over this time span at least - increases in effective radial stress due to pile expansion in clay soils are not subject to degradation due to stress relaxation and creep effects.

Although it is difficult to be precise, because of the nature of the incremental testing performed, none of the piles at the BRS site exhibited any significant change in capacity with time, with the exception of Cruciform Pile 8B which showed a 21% increase in capacity in tests carried out 5 days and 208 days respectively after expansion. (The initial tests on the other expanded piles were carried out after intervals of at least 7 days after driving). This suggests that consolidation of the till after pile installation was completed quickly - in a matter of a few days at most. This can be attributed to the fissured fabric of the till allowing relatively quick dissipation of excess pore pressures. An alternative but less likely explanation for the increase in capacity of Pile 8B with time is that initially there were spaces between the soil and the sides of the expander mandrel, in the region of the gaps opened up between the outer shell angles on expansion (Figure 3.6). Such gaps may have closed up with time, resulting in an increase in the radial force/unit length acting on the pile.

The results from the CRE tests on the expanded piles performed at the end of the test programme show reasonably ductile behaviour. Slow reductions in load occur with continued displacement after failure. Pile 5B shows a 14% drop in load during 12mm displacement (Figure 5.17); Pile 8B shows a 13% drop in load during 12mm displacement (Figure 5.19). This is similar behaviour to that of unexpanded Box Pile 5U, which showed a 7% drop in load during 5mm displacement (Figure 5.22). The most likely reason for such reductions in load is reductions in $\bar{\delta}'$ towards residual values due to clay particle alignment. This implies that the installation process for the expanded piles and for unexpanded Box Pile

5U gave rise to initial values of $\bar{\delta}'$ which were greater than residual. The deduced values of $\bar{K}_s$ given in Table 11.4 suggest values of $\bar{\delta}'$ greater than residual during initial testing

The load:displacement curve for Box Pile 6U did not exhibit such a marked trend of load reduction after failure as the other piles, suffering only a 5% drop in load during 8mm displacement (Figure 5.27). This pile was driven to refusal, and the rate of advance of the pile into the ground was very slow at the end of driving. This may have given rise to conditions nearer to residual at the pile/soil interface.

The one-way stress cycling had no apparent effect on pile capacity. This is normal behaviour for conventional piles in stiff clays (eg. Ove Arup, 1986).

11.8 Mini-Pile Testing

11.8.1 Increases in capacity

The results from the tests on cruciform Type II mini-piles at Sites 1, 4, 5 and 6 are summarised in Figure 11.6. The four soil profiles have been arranged in order of increasing percentage of granular material. The approximate percentage clay content for each soil profile is given.

Capacities of the expanded cruciform mini-piles increase with increasing granular content. The increase in capacity from the high plasticity London Clay to the very sandy clay is approximately 2 times. This factor of increase could easily be accounted for by a corresponding increase in values of $\bar{\delta}'$. For example, a quite plausible increase in $\bar{\delta}'$ from 15° to 30° from the London Clay site to the very sandy clay site gives an increase in $\tan\bar{\delta}'$ of just over 2 times. This suggests that at the four test sites, the radial effective stresses generated on expansion were broadly similar.

The capacities of the unexpanded cruciform piles at the four sites vary by a factor of just under 4, compared to the variation of approximately 2 times for the expanded piles. There is no trend of greater capacity with increasing granular content for the unexpanded piles. This suggests that values of $\bar{\sigma}_r'$ acting on the unexpanded mini-piles at the four sites varied by a factor greater than 4.

Figure 11.6 shows that, as a result of the different trends in mini-pile capacity with soil type described above, there are greater gains in capacity in granular soils than in clay soils. This finding is consistent with theory, and is due to the more effective mobilisation of

soil strength in the radial direction in the case of the expanded mini-piles. The fact that the results also show that the mobilisation of $\bar{\sigma}_r'$ is more consistent in the case of expanded mini-piles is an important finding: it suggests that wedge-piles would give increased reliability over conventional piles in variable or uncertain ground conditions.

The factors of increase in capacity for the cruciform mini-piles expanded by 10% range from 1.61 to 9.8 (Figure 11.6, Table 11.1). Expansion by 10% gives greater capacities than expansion by 6%, but the difference is small in comparison to the overall gains in capacity, suggesting that most of the benefit of expansion can be obtained at relatively small percentage expansions. The gains in capacity for the cruciform mini-piles are consistent with the gains in capacity for the large scale cruciform piles. As the effective radial stresses acting at failure in the case of the large scale piles were found to be substantially less than those potentially available, this is also likely to be the case for the mini-piles. Although the outer shell angles of the mini-piles were more flexible than the angles of the large scale piles, it is still considered that the most likely cause of this shortfall in radial effective stress is the effect of over-expansion.

The results from the tests on cruciform Type I mini-piles at Sites 1, 2 and 3 (summarised in Table 6.2) show increases in capacity in good general agreement with the results from the tests on the Type II cruciform mini-piles. Greater increases in capacity were found at the BRS site for the Type I tests (performed in August 1986) than for the Type II tests (performed in November 1986). The probable reason for this is seasonal variation in moisture content near ground level. There was a significant difference in the results of comparative probe tests carried out in April and September 1987, with much higher blow counts being recorded in the latter case.

At the two sites where they were tested, the H section mini-piles showed much lower factors of increase in capacity in comparison to the cruciform Type II mini-piles (Table 11.1). At the BRS site, the maximum increase in capacity was 1.28 in comparison to 2.10 for the cruciform mini-piles. At the Send Court site, the increase in capacity was 1.51 in comparison to 4.21 for the cruciform mini-piles, although this result may have been affected by variations in mini-pile penetration into the denser sand existing at this site (see below). These results indicate that '2-way' expansion is not as efficient as '4-way' expansion. The probable reason for this has been discussed in Section 9.7.2 - 'dead' areas, where radial effective stress is not fully mobilised, are likely

to occur around a '2-way' pile.

At the Send Court site, the H section mini-piles were found to have penetrated into the denser underlying sand to a greater extent than the cruciform piles. This was confirmed by the probe tests, and by the greater driving times for the H section piles. As a result of the denser ground conditions, the capacities of both the unexpanded and the expanded H section mini-piles are significantly greater than for the cruciform piles. Also, the driving records suggest that the outer shell of the unexpanded H section mini-pile was installed in denser ground than the outer shell of the expanded H section mini-pile. This may be part of the reason for the low '2-way' increase in capacity at the Send Court site.

11.10.2 Other points of interest

The details of mini-pile driving times given in Tables 6.3 to 6.6 show that the driving times for expander mandrels were in most cases very much less than those for outer shells. This is a very significant result (see Section 11.10).

Reloadings of both unexpanded and expanded mini-piles at Sites 1, 4 and 5 show stiffer responses than for initial loadings (Figures 6.19 to 6.34).

There is no clear pattern in regard to changes in mini-pile capacity with time. It is worth noting that a trial pit at the Sheppey site was opened up around the mini-piles after testing and this revealed that surface water had drained and accumulated between the outer shell angles of the mini-piles in the two months that they had been in the ground. This had caused softening of the clay surrounding the mini-piles, which might have had some effect on pile capacity. Such softening may also have taken place around the Type II cruciform mini-piles at the BRS site. The H section mini-piles at the BRS site were covered with plastic sheeting between tests.

There were distinct post-peak drops in capacity with continued displacement for tests on the expanded cruciform mini-piles at the London clay site at Sheppey (Figures 6.26, 6.27). The most likely cause of this is clay particle alignment of the high plasticity clay. Supporting evidence for this hypothesis was discovered during careful exhumation of one of the expanded cruciform mini-piles at this site. Imprints of the outer shell angles on the surrounding clay showed that failure had not taken place along the pile/soil interface. A slickensided displacement surface was discovered at one point along the

shaft of the mini-pile. The displacement surface joined the tips of the cruciform 'arms'. In contrast to the expanded mini-piles, the unexpanded mini-pile did not show a significant post-peak drop in capacity (Figure 6.25), suggesting that $\bar{\delta}'$ for the unexpanded pile was near to residual at initial failure. Part of the increase in mini-pile capacity at the London Clay site might therefore have been due to remoulding of soil around the mini-pile during expansion, giving rise to greater $\bar{\delta}'$ values at initial failure for the expanded piles in comparison to the unexpanded pile.

The good performance under cyclic loading of the expanded cruciform mini-pile at the Holland House site accords with the behaviour under cyclic loading of the Cruciform Pile 8B at the BRS site.

11.9 CP&F/Conoco Field Trials

11.9.1 CP&F piles

A summary of the driven levels, outer shell driving records, and test failure loads for the CP&F piles has been given in Table 8.1.

Considering the results as a whole, on first inspection there appears to be no generalised increase in pile capacity on expansion: capacities of the unexpanded piles range from 95 to 308kN, capacities of the expanded piles range from 100 to 390kN. However, as described later in this Section, on detailed inspection a different pattern emerges.

The following factors will have influenced the results:

(a) Variable ground conditions -
As indicated by the wide range of driving energy values (197 to 915kJ for the plastic shells, 430 to 728kJ for the steel shells) and the CPT results (Section 8.12.3), the ground conditions were very variable, ranging from very loose to very dense on the basis of the CPT tests.

(b) Oversized driving shoe -
The oversized driving shoe used in the case of the plastic outer shells will have reduced shaft friction on the sides of the unexpanded plastic piles, in comparison to the unexpanded steel piles which had nominally flush driving shoes.

(c) Small percentage expansion -
The percentage increases in diameter of the piles on expansion (3%

for the plastic piles, 7.5% for the steel piles), were rather low in comparison to what is considered to be the optimum value of around 10%.

(d) Expander mandrel not driven to full depth -
The expander mandrels were driven to full depth, such that the nose met with the driving shoe of the outer shell, on only 3 out of 8 occasions. In those cases where the expander mandrel was driven short of full depth, for full base resistance of the pile to have been mobilised during testing it would have been necessary for grout to have fully filled the void beneath the nose. From observations made during grouting (Section 8.10.1), this is believed to have occurred in the case of the steel Piles 6 and 16, but possibly not in the case of plastic Piles 5 and 17.

The steel tubes almost certainly would have remained intact in the region beneath the expander mandrel nose; the plastic piles may have crumpled, allowing loose sand to enter and block the void above the driving shoe.

(e) Surface roughness -
The effective angles of interface friction for the plastic piles and the steel piles are likely to have been different. This aspect of pile behaviour is beyond the scope of this discussion.

The best means of characterising the density of the ground into which each pile was driven is considered to be the driving energy of the outer shell. Therefore, only those piles for which good driving records are available have been included in the analysis of results given in the following two Sections.

11.9.1.1 CP&F plastic piles
The load:displacement curves for the 6 tests on plastic piles for which reliable driving records exist are plotted in Figure 11.7. The driving energy for the outer shell of each pile is given. All of these tests were in compression, the applied load being taken both in base resistance and in shaft resistance. The expander mandrels of Piles 2, 9 and 10 were driven to full depth.

On the basis of the data shown in Figure 11.7, there appears to be a broad relationship between the driving energy of the outer shell and subsequent pile capacity. In the case of the unexpanded piles, Piles 8 and 12 have reasonably similar driving energies of 915kJ and 793kJ respectively, and give similar test capacities of 296kN and 308kN; Pile

1 has a driving energy of 388kJ, much less than that for Piles 8 and 9, and a correspondingly lower capacity under test of 95kN. In the case of the expanded piles there is a similar trend. Piles 2 and 9 have reasonably similar driving energies of 233kJ and 197kJ respectively, and give similar test capacities of 196kN and 182kN; Pile 10 has a driving energy of 469kJ, more than twice that for Piles 8 and 9, and has a correspondingly greater capacity under test of 390kN.

If the results for the unexpanded plastic piles are compared with those for the expanded plastic piles, it becomes clear that expansion had a very significant effect on pile capacity. Pile failure load is plotted against outer shell driving energy in Figure 11.8. For given outer shell driving energy, greater capacities were achieved with expanded piles than with unexpanded piles. The factor of increase is approximately 3 times.

The factor of increase of 3 quoted above compares the expanded plastic piles with unexpanded piles that were driven with over-sized driving shoes. The over-sized driving shoes presumably reduced the capacity of the unexpanded piles, in comparison to the capacities that would have been obtained if the piles had been fitted with flush driving shoes. No plastic test piles with flush driving shoes were driven, but the results of the unexpanded steel piles driven with flush shoes are also shown on Figure 11.8, and these can be compared with the results for the expanded plastic piles. For given outer shell driving energy, greater capacities for expanded plastic piles in comparison to unexpanded steel piles are apparent.

It is clear from these results that substantial increases in shaft resistance are possible by expansion of a 'thin' tubular outer shell along a single weak line.

11.9.1.2 CP&F steel piles

The load:displacement curves for the 4 tests on steel piles are plotted in Figure 11.9; driving energies are given. Three of the tests (Tests 3, 6 and 16) show reasonably similar driving energies, in the range 619 to 728kJ. The respective tests on these three piles were a compression test on an unexpanded pile, a compression test on an expanded pile, and a tension test on an expanded pile.

If it is assumed that these three piles can be compared on a like-with-like basis, an estimate of the increase in shaft capacity on expansion can be made. The capacities of the expanded pile in compression (402kN) and the expanded pile in tension (199kN) suggest

that around half of the capacity of the compression pile was taken in base resistance and half in shaft resistance. Following on from this, if a value of base resistance of 200kN is assumed for both piles 3 and 16 (unexpanded and expanded compression piles respectively), it can be deduced that shaft resistance for expanded Pile 16 is about twice that for unexpanded Pile 3. As for the results from the plastic piles, this suggests that significant increases in shaft resistance are possible by expanding a thin-tube, single weak line outer shell. A doubling of shaft friction for '1-slit' expansion is in good agreement with the results of the model tests (Figure 7.3) - greater capacities may have been possible if 3 or 4-slit expansion had been carried out.

The expanded pile tested in tension (Pile 6) performed exceptionally well in comparison to unexpanded Pile 14 tested in compression, giving twice the capacity. However, the lower outer shell driving energy for Pile 14 suggests that it was driven into looser ground in comparison to the other steel piles.

The capacities of the CP&F steel piles tested in compression are plotted against outer shell driving energy in Figure 11.8. There are much less data for the steel piles than for the plastic piles. On the basis of the limited data available, the increases in capacity for the steel piles seem rather less than for the plastic piles. Possible reasons for the lower increases in capacity are the flush driving shoe that was used in the case of the steel piles; or greater over-expansion effects in the case of the steel piles, due to the stiffer outer shells.

11.9.1.3 Overall conclusions on trials

The Hermitage trials were carried out at the time of writing this thesis, and some of the more general implications of the results may take some time to emerge, after consultation with industry. In discussions with CP&F immediately after the trials, the following comments were made by CP&F:

- It was accepted that the trials had amply demonstrated that the Wedge-Pile expansion process significantly enhances pile skin friction.

- The system was thought to be practical.

- Steel tubes were considered to be more appropriate for commercial use than plastic tubes, which were thought to be too fragile.

- A cruciform type wedge-pile was thought likely to prove more

commercially viable than the circular tube system tested, due to the ease of driving of a low-displacement pile such as the cruciform. Also, a system featuring a retractable expander mandrel (Section 1.3) would reduce handling times and material costs. Further trials at the Hermitage site with cruciform piles are being considered.

11.9.2 Conoco piles

The driven levels, driving records and maximum test loads for the Conoco piles have been summarised in Table 8.2. Load:displacement plots for the pile tests have been given in Figures 8.11 to 8.16.

11.9.2.1 Driving energies

The two expanded piles (Piles 4 and 11) were driven at positions within 1m of each other. The number of blows required to drive the outer shells of these piles was 53 in each case, corresponding to a driving energy of 601kJ. The driving energy required to install the unexpanded outer shell (Pile 13) was very large in comparison, at 2735kJ being more than four times greater.

The relatively easy driving of Piles 4 and 11 is in accordance with the easy driving of nearby CP&F Piles 2 and 9, and with the indication of loose ground in this area by CPT Tests 10 and 11. CPT Test 3 indicates very dense ground in the region of Pile 13; also, hard driving in this area prevented CP&F Pile 15 being driven to full depth.

The energy required to expand the 3 weak line outer shell of Pile 11 was very similar to that required to initially drive the outer shell (outer shell 600kJ, expander mandrel 623kJ). Significantly greater driving energy was required to expand the 1 weak line outer shell of Pile 4 (outer shell 600kJ; expander mandrel - to 4.7m depth only - 702kJ). The greater expansion energy in the case of the 1 weak line outer shell is thought to be due to the forces (independent of soil forces) involved in opening up the outer shell and then maintaining it elastically in its expanded configuration. The 'gripping' action of the expanded outer shell on the shank of the expander mandrel, in combination with the constricting action of the unexpanded outer shell ahead of the advancing expander mandrel nose, are thought to be the most likely causes of the dragdown of the 1 weak line outer shell during expansion.

An indication of the magnitude of the forces involved in opening up a 1 weak line outer shell can be obtained by considering the situation shown in Figure 11.10. Opening out of a relatively stiff outer shell, such as for the Conoco piles, will involve the formation of plastic mechanisms.

Figure 11.10 shows a unit length of a 'stiff' outer shell, not under the action of any soil forces, being opened up by a rigid expander mandrel that is slowly increasing in size. During the early stages of expansion, the geometry of the situation is such that expanding forces P and 2P will act as shown. Bending moment/unit length in the outer shell is given by the expression

$$M = \{P\sin\theta\,(\cos\phi + \cos\theta) + P\cos\theta\,(\sin\phi - \sin\theta)\} \times R$$

(for definitions see Figure 11.10)

Maximum bending moment M_{max} is given by the expression (PxR). Plastic hinges will form initially in the region of points B and C. Further expansion will eventually result in a plastic hinge at D, at which point there is a full mechanism. A lower bound to the force required for the elastic deformation that occurs during opening out of the outer shell is given by the force needed to give first yield. For the Conoco outer shells, at first yield P = 13N/mm^2. At full expansion, this is equivalent to a radial force/mm length of pipe of 50.4N, or a radial stress of 83kPa. This radial stress is clearly substantial, being of the same order of magnitude as the radial soil stresses generated during expansion. Forces of this magnitude are likely to have acted along the shanks of the Conoco piles as the expander mandrels were advanced.

Gaps will tend to develop between the expander mandrel and the outer shell on expansion, because of their different radii. Radial soil forces will act to close these gaps, but it can be shown that for relatively stiff outer shells, such as for the Conoco piles, small gaps are likely to remain after pile installation.

11.9.2.2 Pile capacities

The fact that the expanded piles and the unexpanded pile were driven into completely different types of ground precludes any sensible comparison between them. It can be seen from Table 8.2 that the static capacity of the unexpanded pile was much greater than for the expanded piles, both in tension and in compression.

The initial static tensile capacity of the 3 weak line Pile 11 (162kN) was 17% greater than for the 1 weak line Pile 4 (139kN). The maximum load recorded in static compression for Pile 4 (174kN) is slightly lower than those for the nearby expanded CP&F piles 2 and 9 (196kN and 182kN), despite both the depth of embedment and the percentage expansion of the Conoco pile being greater. It would seem that the much stiffer outer shells of the Conoco piles had a detrimental effect on the generation of increased shaft resistance, presumably because of greater over-expansion

effects.

At the top of Pile 11 the outer shell opened up along 2 of the 3 weak lines (Section 8.9.3). It is not known whether this pattern of deformation continued along the length of the pile. It is planned to exhume the piles at a future date. This will throw some light on questions regarding the modes of deformation of the 1 weak line and 3 weak line piles.

Under cyclic loading, the unexpanded and the expanded piles responded in a similar manner. There were no losses in static capacity following tension only cycling, but large losses in capacity following strain controlled tension/compression cycling (a 32% loss for the unexpanded pile, 51% loss for the 3 weak line expanded pile). This behaviour accords with other reported cyclic loading tests on piles in sands (eg. Poulos, 1989).

11.9.2.3 Overall conclusions on trials

As for the CP&F piles, some of the more general implications of the results of the Conoco pile tests have yet to be fully developed. This will require discussions with industry. However, the very poor performance of both the 1 weak line and 3 weak line piles, in comparison to nearby CP&F piles, suggests that there is little future in a wedge-pile system featuring a relatively stiff circular outer shell. Systems featuring relatively flexible, multiple-element outer shells are far more promising.

For offshore use, the functioning of a wedge-pile could be separated into two areas. A lower, cruciform shaped part of the pile would serve solely to resist axial loads. At the top of the pile, the outer shell could be stiffened in order to deal with lateral loads. Indeed, the top part of the pile could be a different shape to the lower part: this approach could serve to maintain conventional techniques for pile/structure connection. It would be necessary to overcome established thinking within the offshore oil and gas industry in order to successfully promote such a novel piling solution.

11.10 Expander Mandrel: Driving Forces and Driving Efficiency

The results from the expander mandrel extraction tests at the Luton site (Section 4.7.8) show that (for multiple-element piles) the limiting shear stress between expander mandrel:outer shell is related to the limiting shear stress between outer shell:soil by the ratio of the coefficients of friction of the two displacement surfaces. This is

readily apparent from a consideration of the basic frictional Equation 11.1.

If the frictional characteristics of the pile components and the soil are known, estimates of shaft capacity can therefore be made by measuring the force or energy required to install the expander mandrel. In the case of driven expander mandrels, such estimates would contain an element of empiricism, but the relationship between driving energy and pile capacity would be very much more direct than is the case for conventional piles. More accurate estimates could be made if the expander mandrel was jacked into place, and measurements were made of the jacking forces. Alternatively, piles could be easily proof tested after installation by jacking the expander mandrel a short distance against the reaction of the outer shell.

At the weathered chalk site at Luton, driving resistances for the outer shells were generally less than for the expander mandrels subsequently driven into them (Figure 4.23). The low driving resistances for the outer shells are consistent with large pore pressures being generated by the crushing action of the outer shell on the chalk during driving, resulting in reductions in radial effective stress. This is normal for driven piles in chalk. There was less driving resistance for the small-displacement cruciform shells than for the large-displacement box shells, as is to be expected. The greater driving resistances recorded for the expander mandrels in comparison to the outer shells are due to the large increases in radial effective stress that took place during expansion.

As discussed in Section 11.3.2, the driving resistance for expander mandrel 2A - driven very soon after the outer shell was driven - was less than for the box mandrels driven after longer periods of consolidation subsequent to outer shell driving. This lower driving resistance appears to be associated with a subsequent lower capacity under test. Although the driving records are highly qualitative, this finding provides some evidence of a relationship between expander mandrel driving energy and subsequent pile capacity.

The most important conclusion that can be drawn from the driving records at the BRS site is that high efficency in the generation of shaft capacity can be achieved by cruciform wedge-piles. This was dramatically shown by the driving records for unexpanded Box Pile 5U, in comparison to the driving records for expanded Cruciform Piles 8B and 9A (Section 5.5.7). The combined driving energy for the shell and mandrel of piles 8B and 9A was very much less than the driving energy for the

shell of Box Pile 5U. Under test, however, both of the expanded cruciform piles gave higher capacities than the unexpanded box pile. This finding confirms the basic Wedge-Pile principle of local and progressive expansion.

The results of the mini-pile tests given in Chapter 6, and the laboratory model tests reported in Chapters 2 and 7 , confirm that the wedge-pile is more efficient than conventional piles in generating shaft resistance.

11.11 Choice of Wedge-Pile Type

The choice of the appropriate type of wedge-pile for a given situation will be influenced by engineering and commercial considerations largely beyond the scope of this thesis. Some of these were discussed in Chapter 1. Important conclusions of the present research that are of relevance to the choice of wedge-pile type are described below:

(a) For given energy of installation, the cruciform pile is the most efficient pile configuration for developing shaft capacity. Shaft capacities achieved with the cruciform piles at the Luton and BRS sites were only slightly less than those achieved with the box piles, but the overall driving energies involved were much less, particularly at the stiff clay site.

(b) The trials at Hermitage show that it is possible to reduce the driving energy of the outer shell by making use of an over-sized driving shoe.

(c) In weathered chalk, the greater compacting action of the box piles in comparison to the cruciform piles gave rise to stiffer pile response and better pile performance under cyclic loading. This behaviour was in large measure due to the nature of chalk, but similar benefits may well result from the use of large-displacement type wedge-piles in loose sands or poor ground.

(d) It is clear from the mini-pile and the laboratory model tests that 2-way expansion or 'split tube' expansion gives rise to significantly lower increases in capacity than 3 or 4-way expansion.

(e) The results from the numerical model study show that the nose profile of the expander mandrel plays a very important part in determining the shaft capacity of wedge-piles, because of the

effect of the nose profile on the amount of over-expansion of the outer shell.

(f) The more flexible the outer shell, the less the likelihood of severe over-expansion. Thin outer shells which act solely as an interface with the ground will be relatively flexible. If the outer shell is required to act as a load carrying member, however, a stiffer outer shell will be needed and the load carrying requirements will conflict with the desire for member flexibility. In this situation, the member size must be selected to give an optimum solution.

(g) A question that has regularly been raised in discussions with industry, and which is relevant to (f) above, is the problem of corrosion of steel outer shells. The traditional method of corrosion protection in the case of steel piles is to increase pile member thicknesses, in order to provide 'sacrificial' steel. It has been found that if such an approach is adopted for wedge-pile design, and the corrosion rates adopted are conservative, the outer shell member sizes required are often such that they would be too expensive for the Wedge-Pile to be competitive with other piling methods. Two points are relevant here. Firstly, research has shown that the underground corrosion of steel piles driven into undisturbed soils is negligible, irrespective of the soil type and characteristics (British Steel Corporation (BSC), 1978). Secondly, relatively cheap and durable painted coatings are now available to protect reliably steel piles near ground level or in circumstances where corrosion may be more significant than is normally the case (e.g. in marine environments) (BSC, 1979; 1987).

(h) The 'split-tube' type pile has advantages over other wedge-pile types in terms of fabrication and installation. However, there appear to be two major disadvantages of the split-tube idea. Firstly, the capacity of a 1 weak line pile has been shown to be significantly less than that of an equivalent 3 or 4 weak line pile. Secondly, the use of a thick walled tube requires large forces, independent of soil forces, to open out the outer shell and maintain it in position. These forces will result in high driving energies, which may make successful installation of the expander mandrel impossible.

11.12 Wedge-Pile Design

The essential requirements for economic and reliable pile design are a

sound underlying theoretical framework, together with sufficient supporting pile test data.

The Wedge-Pile concept is based on sound soil mechanics theory. In the medium to long term - given sufficient resources - this underlying theory, in combination with an increasing amount of test data, should enable much more reliable and predictable pile design than is currently possible with conventional piling techniques. At the present time, however, test data on the Wedge-Pile are still insufficient by industrial standards; and some key soil mechanics questions remain to be answered.

In the short to medium term, it is proposed that wedge-pile design should be on the basis of 'factors of increase'. With this system, the shaft capacity of a wedge-pile would be calculated initially as for a conventional pile. A factor of increase in shaft capacity due to expansion would then be applied. The value of the factor of increase would depend on the soil type and would be higher in the case of sands than for clays. A design chart akin to Figure 11.6 could be devised. The reliability of such a chart would improve as the amount of available test data increased.

In the medium to long-term, it is proposed that the shaft capacity of a wedge-pile could be related to the limiting pressure available by cavity expansion in the soil. The limiting pressure could be estimated theoretically if strength parameters and in-situ stresses were known, or could be measured directly by pressuremeter tests. It is thought that a promising line of approach is the development of a semi-empirical method making use of DMT profiles. The successful application of such methods of design will require a more extensive range of test data than is available at present, including data from instrumented piles on the detailed state of stress around an expanded pile after installation and during loading (see Section 11.13 below).

11.13 Suggestions for Further Research

The research described in this thesis has demonstrated the basic principles of the Wedge-Pile process. In the light of the work to date, there are several areas in which it is considered that more detailed research is now merited. Some suggestions for further research are given below:

(a) Pressuremeter testing:
Pressuremeter testing provides a ready means of investigating the stress

changes that occur during and after the expansion of a cavity in the ground. However, because most testing undertaken with pressuremeters is designed for the measurement of soil properties, tests that would be of particular relevance to the Wedge-Pile concept are usually either not performed or else not reported. A specially designed, thorough programme of tests with the FDPM could answer many of the questions regarding the Wedge-Pile expansion process raised earlier in this Chapter. Such a test programme would include tests at different strain rates, and would pay particular attention to strain holding tests in order to model the installation of an expanded pile and to investigate stress changes occurring during consolidation after expansion. 'Long-term' strain holding tests, particularly in clay soils, could be performed in order to investigate possible reductions in σ_r' with time due to creep effects. The length of time over which such tests could be held would depend upon the capabilities of the FDPM control system.

An FDPM instrument incorporating a pore pressure transducer would allow direct measurement of changes in effective stress around the expanded cavity. This was not possible with the instrument used at the Luton and BRS sites.

It was initially envisaged that the FDPM testing programmes at Luton and BRS would be more extensive. This was not possible, however, because the high overhead costs of the Fugro testing truck meant that Fugro could only allow it to be used free of charge for a very limited period. If funds could be found to hire the truck and FDPM for 1 to 2 weeks, say, it is felt that invaluable data could be gathered.

(b) Expander mandrel nose profile:
The essence of the Wedge-Pile process is that it is a controlled method of maximising pile shaft capacity: the means of achieving this control is the expander mandrel nose profile. Design of the nose profile therefore holds the key to the process. It is suggested that - with the aid of the numerical model described in Chapter 10 - 'standard' nose profiles should be developed, in order to standardise future test data and to provide the basis for prototype nose profiles for use in civil engineering practice.

It is suggested that attention should be concentrated on developing relatively simple and easily fabricated nose profiles. Comparative field trials should be carried out using different nose types. A 'fully-Blunt' plain-ended expander mandrel could be used to provide a suitable control in such trials.

(c) Tests on instrumented wedge-piles:
In combination with (a) and (b) above, it is suggested that carefully instrumented laboratory model tests should be performed to investigate the stress changes that occur around a wedge-pile during initial installation, expansion, and subsequent testing. Another important study which could be made in the laboratory is the investigation of the relative patterns of failure in the soil alongside expanded and unexpanded piles. The laboratory testing might possibly be augmented in due course by tests in the field with an instrumented wedge-pile. Such laboratory and field tests would involve the development and detailed design of appropriate instrumentation for the piles.

(d) Development of new wedge-pile embodiments:
There is much scope for the further investigation and development of different types of Wedge-Pile. Discussions with piling specialists has been found to be very useful when developing new ideas.

Some of the different possible embodiments of Wedge-Pile have been outlined in Section 1.3 of this thesis. An important area for future research is considered to be the development of a 're-usable' expander mandrel (Sections 1.3.1.2, 1.3.4). If a re-useable expander mandrel could be developed, large savings in pile material costs could be made, in comparison to wedge-pile systems employing a permanent expander mandrel. It is thought that the development of a re-useable mandrel system would probably best be undertaken at near full scale, in conjunction with a piling contractor.

(e) Development of design methods:
Different design approaches that could adopted for the Wedge-Pile were given in Section 11.12. Field trials of wedge-piles at established geotechnical test sites, where in-situ soil testing and tests on conventional piles have been carried out previously, would provide the best means of providing the data necessary to develop such design methods in detail.

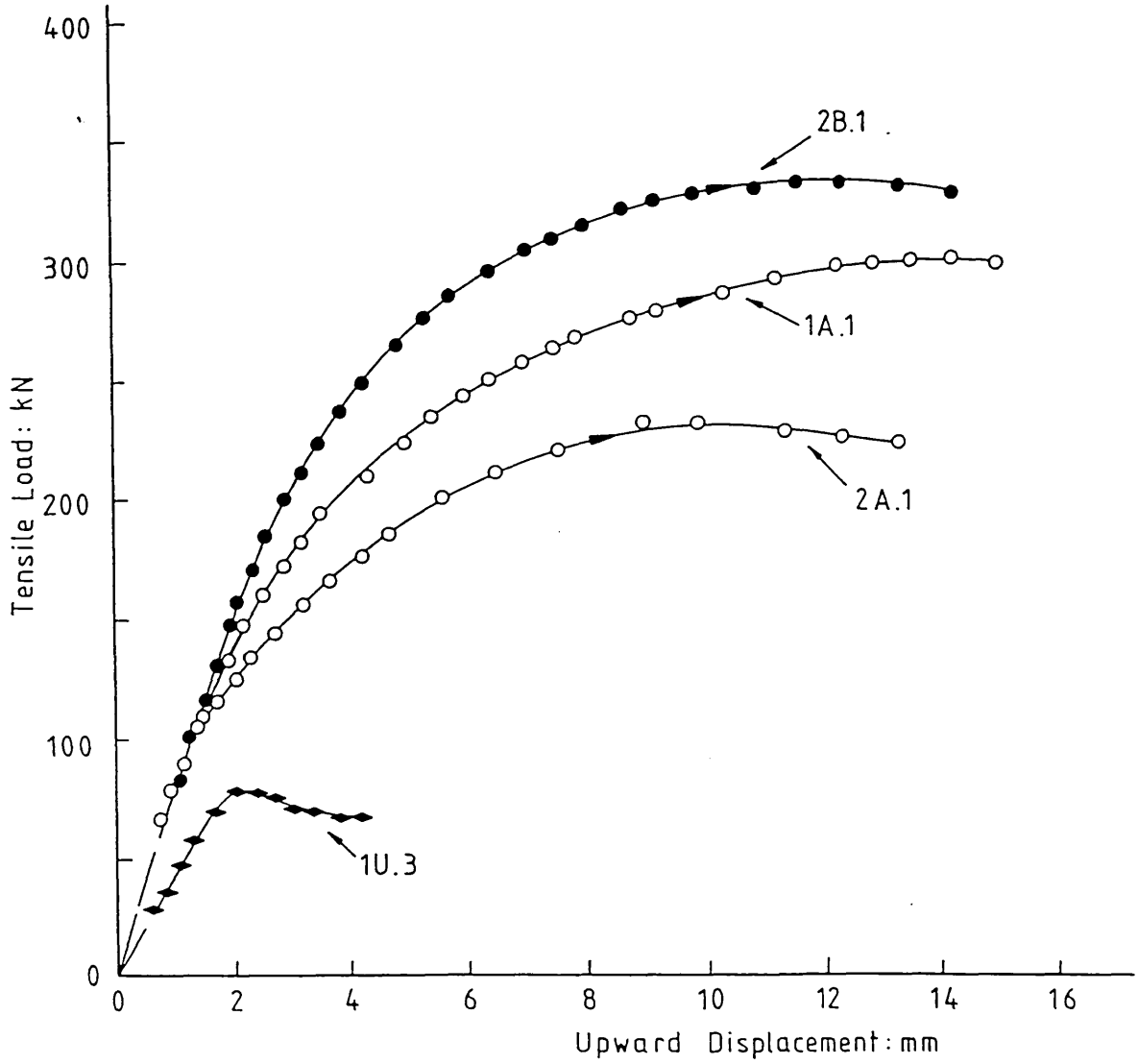

Pile No.	% expansion width	% expansion X-area	Test No.	Max. Load (Gross) (kN)	Shaft friction (A) (kPa)	Shaft friction (D) (kPa)	Factor of increase Max. load	Factor of increase Shaft friction
1U	-	-	1U.2	66.4	24.0	-	-	-
			1U.3	79.1	28.8	-	0.0	0.0
1A	14.3	30.6	1A.1	302.8	98.5	141.3	3.83	3.42 - 4.91
2A	14.3	30.6	2A.1	232.7	74.1	106.9	2.94	2.57 - 3.71
2B	21.4	47.4	2B.1	335.0	100.9	154.7	4.23	3.50 - 5.37

Figure 11.1 Luton site:
Summary of initial loadings of Box Piles

Pile No.	% expansion (width)	(X-area)	Test No.	Max. Load (Gross) (kN)	Shaft friction (A) (kPa)	(D) (kPa)	Factor of increase (Max. load)	(Shaft friction)
3U	-	-	3U.1	50.4	23.3	-	0.0	0.0
4A	10.7	35.7	4A.1	304.4	127.8	160.8	6.04	5.48 - 6.90
3B	21.4	75.0	3B.1	210.8	77.2	110.5	4.18	3.31 - 4.74

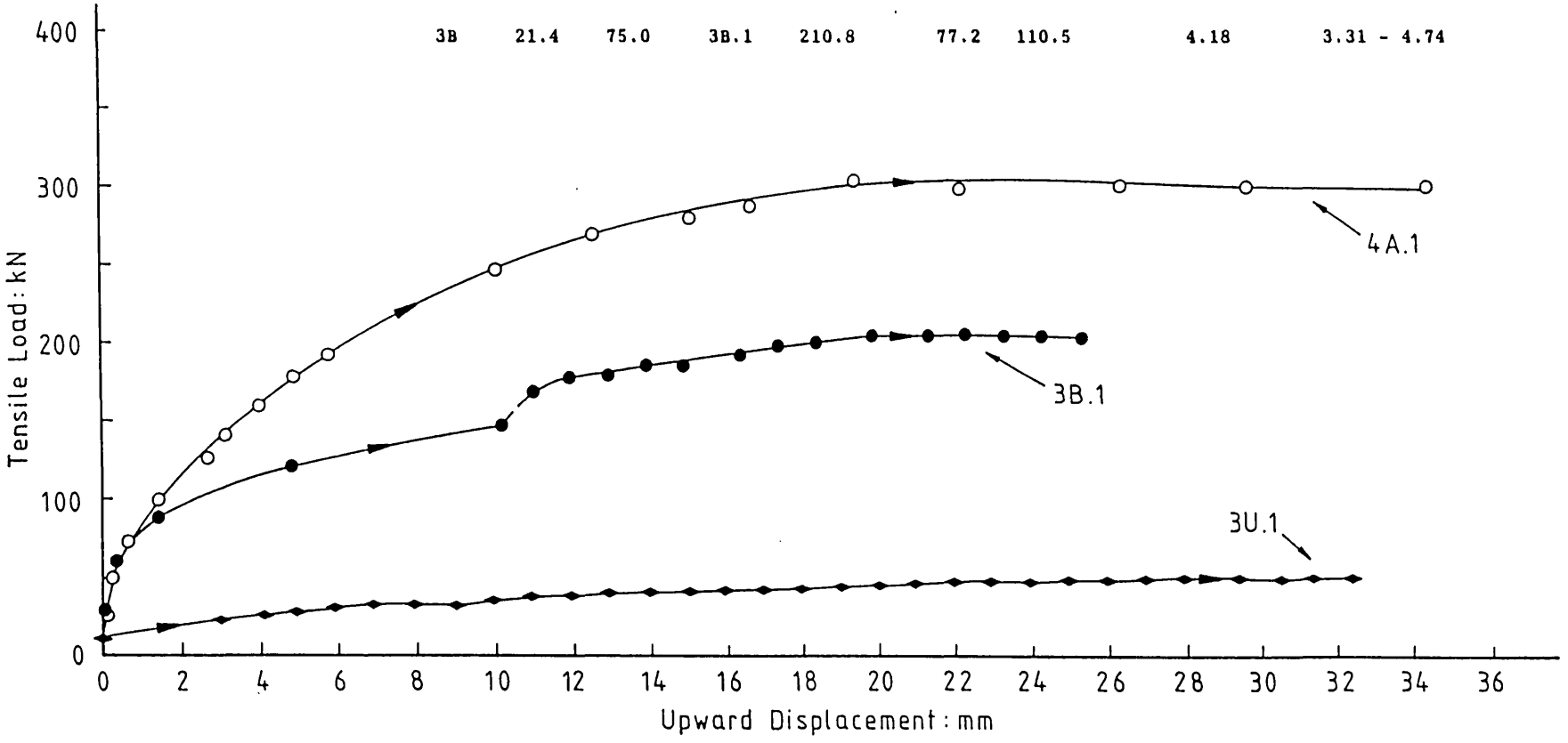

Figure 11.2 Luton site:
Summary of initial loadings on cruciform piles

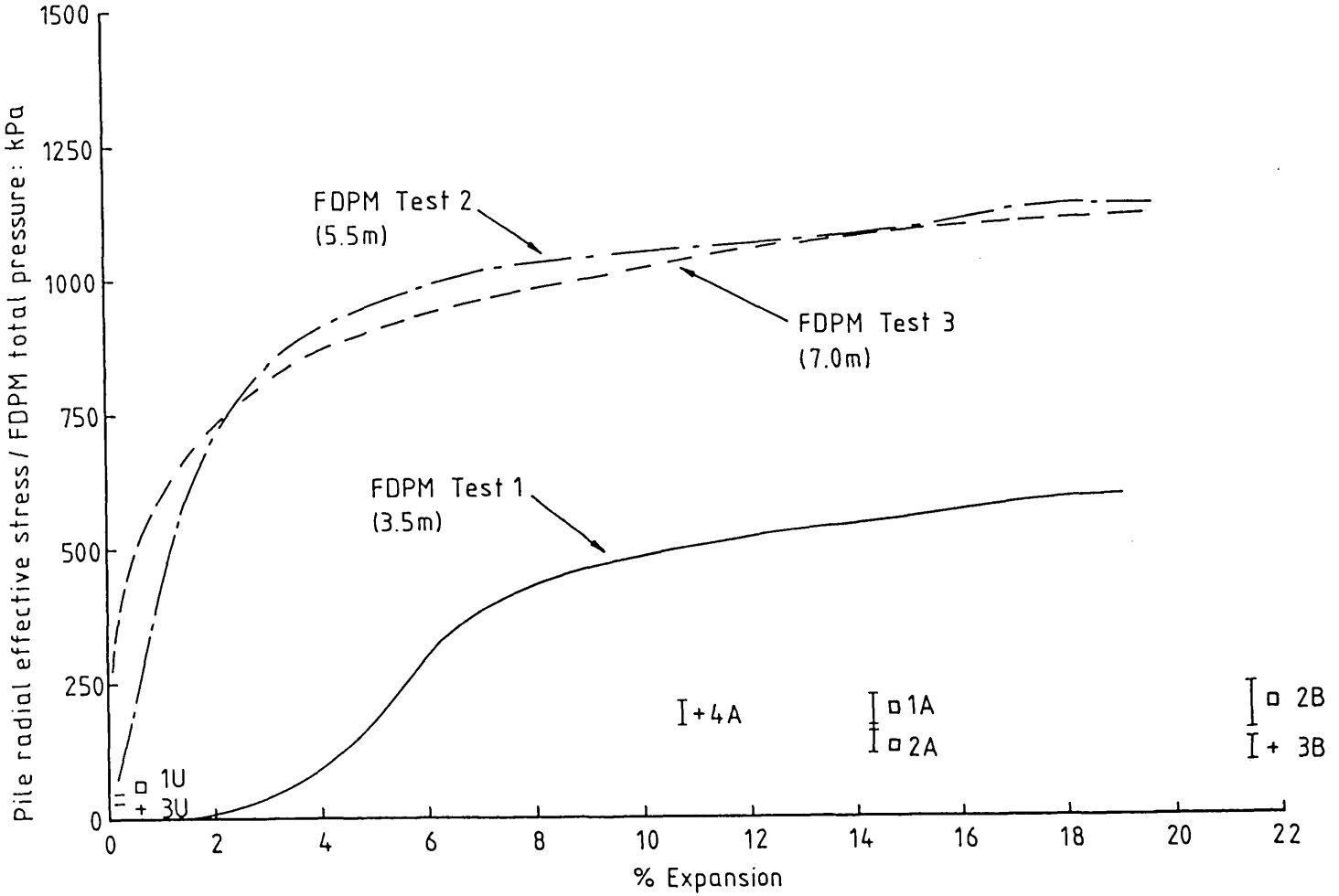

Figure 11.3 Comparison of deduced values of σ_r' acting on piles and total radial stresses measured in FDPM tests

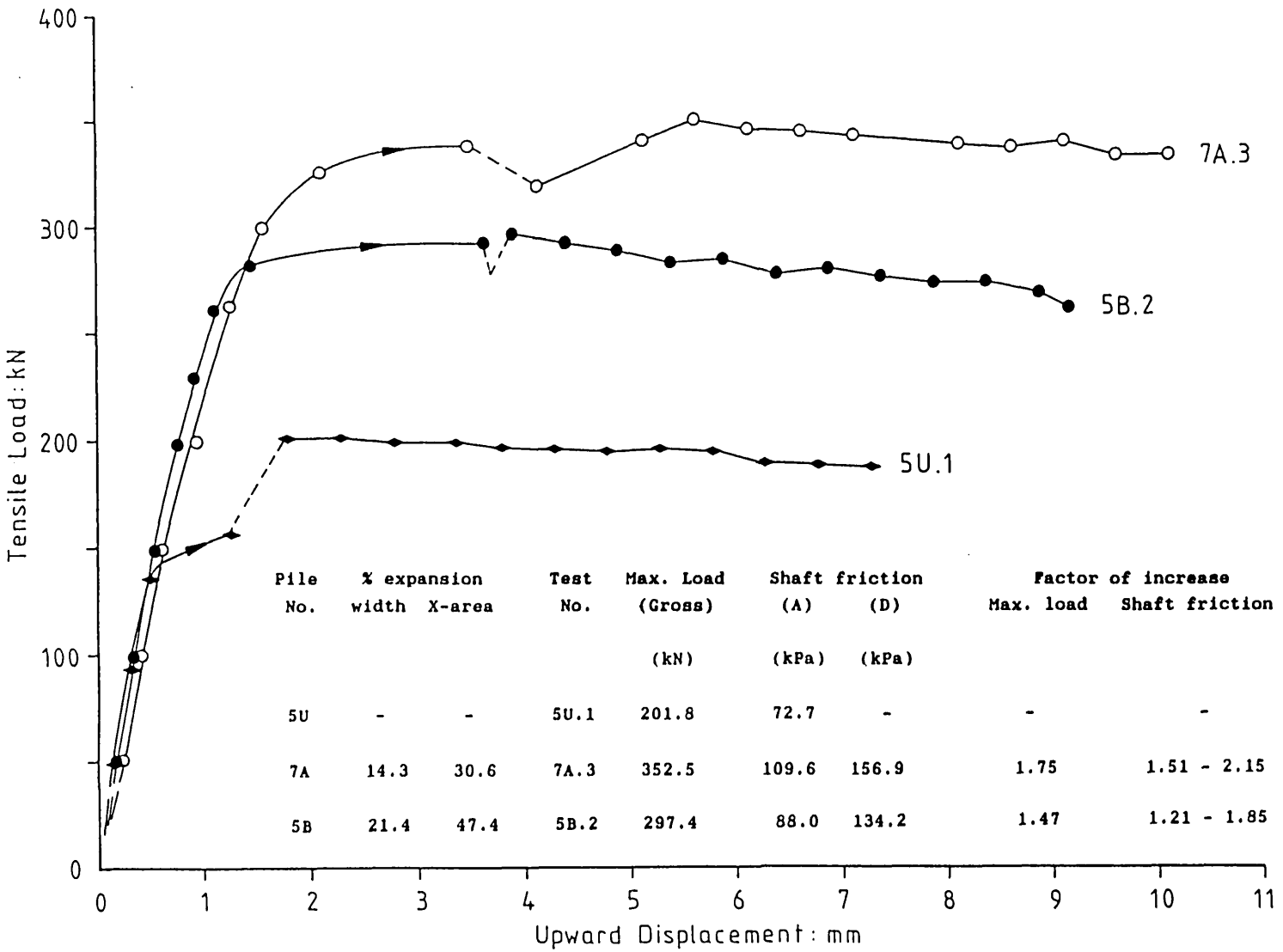

Pile No.	% expansion width	% expansion X-area	Test No.	Max. Load (Gross) (kN)	Shaft friction (A) (kPa)	Shaft friction (D) (kPa)	Factor of increase Max. load	Factor of increase Shaft friction
5U	-	-	5U.1	201.8	72.7	-	-	-
7A	14.3	30.6	7A.3	352.5	109.6	156.9	1.75	1.51 - 2.15
5B	21.4	47.4	5B.2	297.4	88.0	134.2	1.47	1.21 - 1.85

Figure 11.4 BRS site:
Summary of initial loadings on box piles

Pile No.	% expansion (width)	% expansion (X-area)	Test No.	Max. Load (Gross) (kN)	Shaft friction (A) (kPa)	Shaft friction (D) (kPa)	Factor of increase (Max. load)	Factor of increase (Shaft friction)
8U	-	-	8U.1	114.7	53.0	-	0.0	0.0
9A	10.7	35.7	9A.2	229.3	93.7	118.2	2.00	1.77 - 2.23
8B	21.4	75.0	8B.2	241.6	86.2	121.9	2.11	1.63 - 2.30

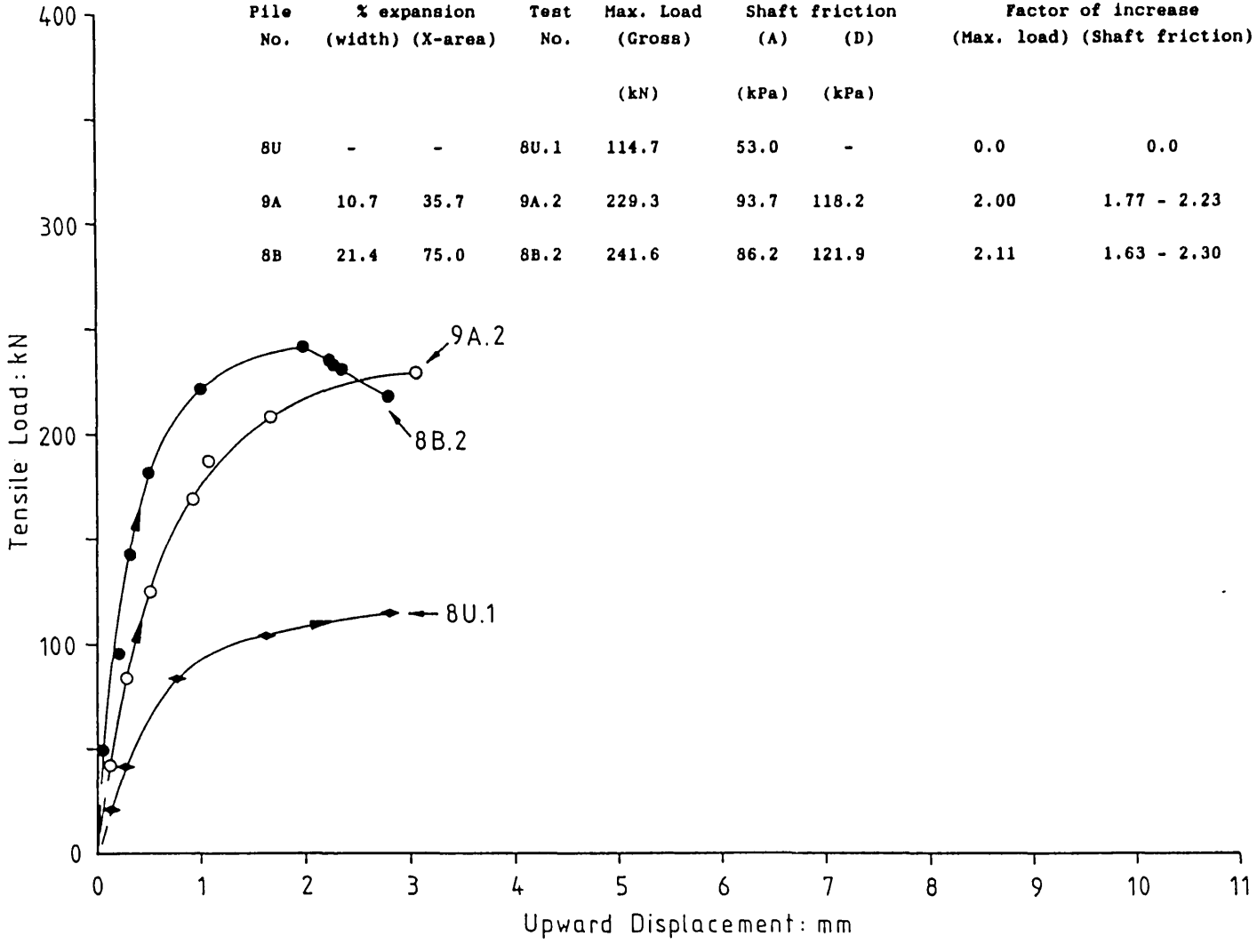

Figure 11.5 BRS site:
Summary of initial loadings on cruciform piles

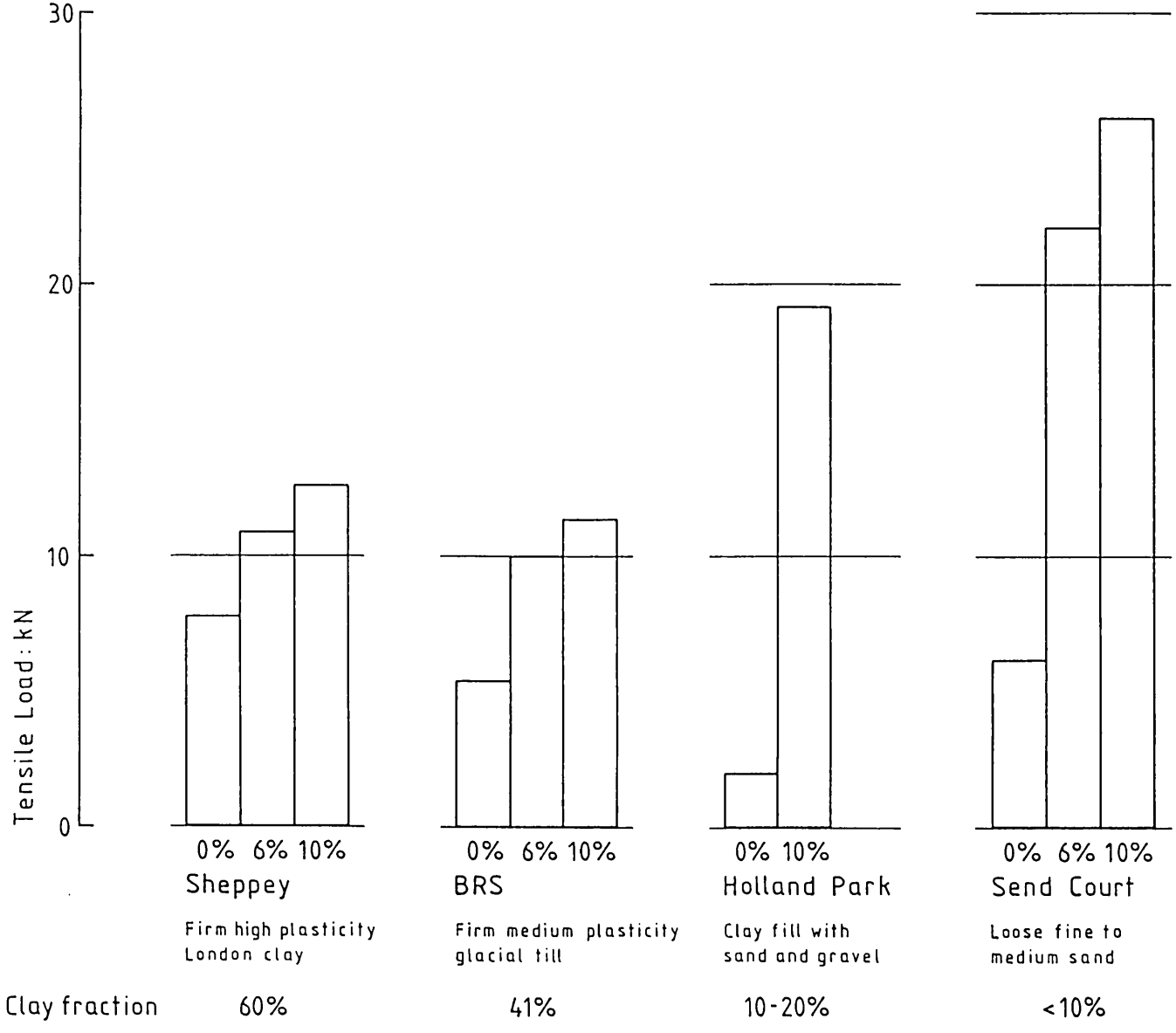

Figure 11.6 Cruciform Type II mini-pile tests: Summary of results

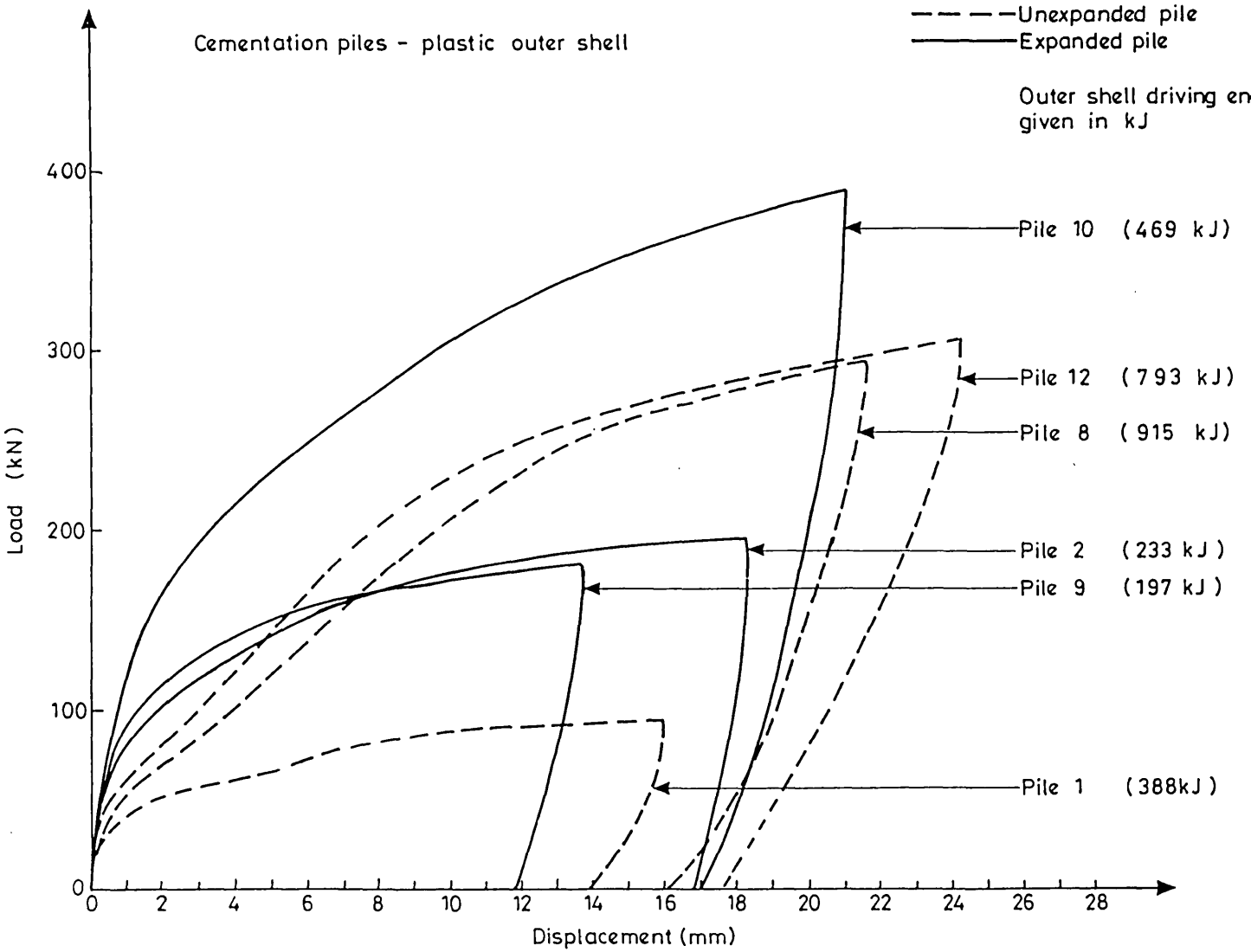

Figure 11.7 CP&F plastic piles: load:displacement curves

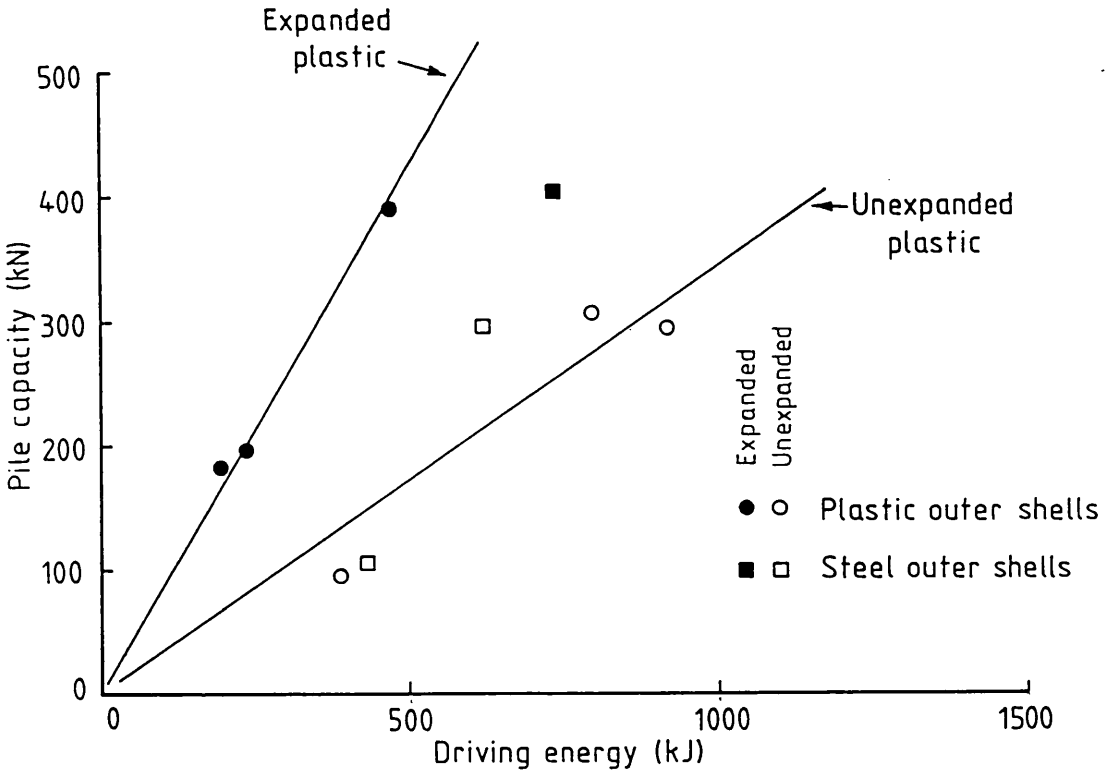

Figure 11.8 CP&F piles:
Pile capacity against Pile driving energy

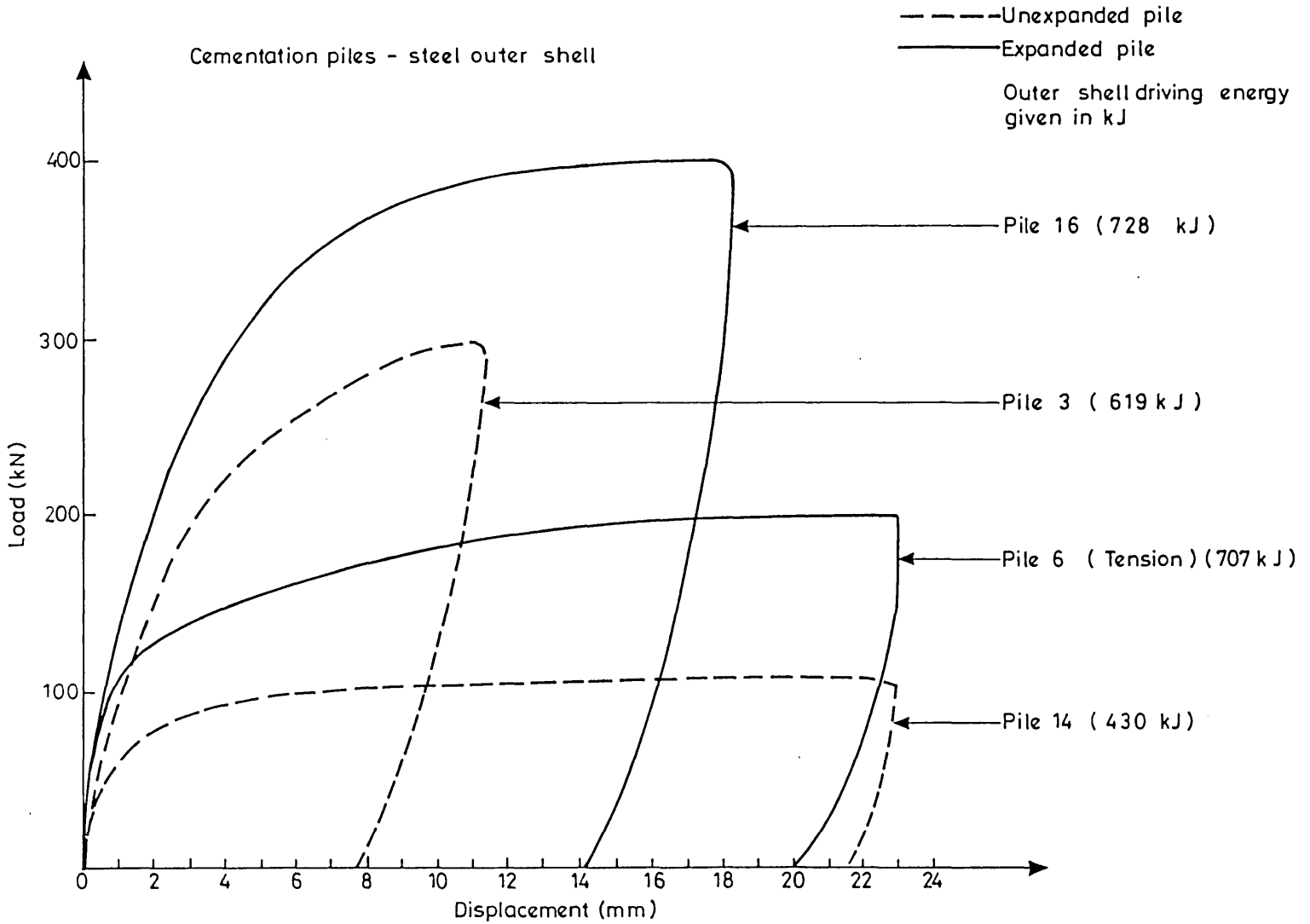

Figure 11.9 CP&F steel piles: load:displacement curves

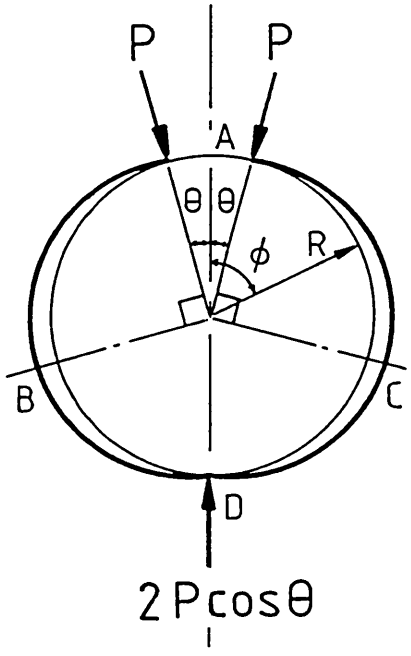

For a completely 'flattened' outer shell,

$$\theta_{min} = \left[\frac{\text{outside perimeter of mandrel - inside perimeter of shell}}{\text{2 x outside perimeter of mandrel}}\right] \text{ x } 360$$

$$= \left[\frac{203.2 - 182.5}{2 \text{ x } 203.2}\right] \text{ x } 360 = 18.3^\circ \text{ say } 20^\circ$$

For $\theta = 20^\circ$

M_{max} = P x R , occuring at $\phi = 110^\circ$

M_{yield} = 1.23 $x10^3$ Nmm/mm

P = 13N/mm

Resultant force/mm = 13 x (2 + 2cos20°) = 50.4 = say 50N/mm

This is equivalent to a radial stress acting of

$50.4/\pi$ x 193.7 = 0.083N/mm^2 = 83kPa at yield

Figure 11.10 'Stiff' circular outer shell: expansion forces

Soil type	Pile type	Pile width (mm)	Pile length (m)	Length fully expanded (%)	Amount of expansion (%)	Unexpanded capacity (kN)	Expanded capacity (kN)	Factor of increase
Luton site								
Weathered chalk	Box	140	5.0-5.1	80	14.3, 21.4	79	233-335	2.94-4.23
	Cruciform	140	5.2	90	10.7, 21.4	50	211-304	4.18-6.04
BRS site								
Stiff boulder clay	Box	140	4.9-5.0	80	14.3, 21.4	202	297-352	1.47-1.75
	Cruciform	140	5.0	91	10.7, 21.4	115	229-242	2.00-2.11
Mini-piles								
Firm weathered London clay	Cruciform II	100	1.25	94	6, 10	7.8	10.9-12.6	1.39-1.62
Firm boulder clay (partly reworked)	Cruciform II	100	1.25	94	6, 10	5.4	9.8-11.4	1.81-2.10
	H section	100	1.25	90	6, 10	7.3	8.4-8.6	1.15-1.18
Clayey gravel	Cruciform II	100	1.25	94	10	2.0	19.2	9.60
Very loose clayey sand overlying denser fine sand	Cruciform II	100	1.25	94	6, 10	6.2	22.1-26.1	3.56-4.21
	H section	100	1.25	90	10	24.7	37.3	1.51
Model piles								
Fine sand	Cruciform	20	0.20	85	5-20			2.6-3.8

Table 11.1 Multiple-element wedge-piles: overview of results

	$\bar{\tau}_{s_f}$		$\bar{\sigma}'_r$		$\bar{K}_s$	
	min (kPa)	max (kPa)	min (kPa)	max (kPa)	min	max
Box Piles						
1U	28.8		42.7		1.1	
1A	98.5	141.3	146.0	209.5	4.0	5.7
2A	74.1	106.9	109.9	158.5	3.0	4.4
2B	100.9	154.7	149.6	229.4	4.1	6.2
Cruciform Piles						
3U	23.3		32.1		0.8	
4A	127.8	160.8	175.9	221.3	4.8	6.0
3B	77.2	110.5	106.3	152.1	2.9	4.1

Notes: 1. Minimum values correspond with pile perimeter 'A'
Maximum values correspond with pile perimeter 'D'

2. $\bar{\delta}' = 34^\circ$ assumed for box piles
$\bar{\delta}' = 36^\circ$ assumed for cruciform piles

Table 11.2 Luton site:
Deduced values of radial effective stress $\bar{\sigma}'_r$
and radial stress factor $\bar{K}_s$ acting on test piles

Test No.	Final Inc. load (kN)	Final creep rate (mm/min)	Incremental failure ?	Maximum CRE load (kN)	Inc. fail. load / CRE fail. load	Load increase factor[1]	Load increase factor[2]
Box piles							
5U.1	156.1	0.0075	no	201.8	0.77	1.00	1.00
5U.2	177.3	0.049	no	-	-		
5B.1	299.7	1.47	yes	-	-		
5B.2	293.0	0.11	yes	297.4	0.99	1.47	1.47
5B.3	-	-	-	276.3	-		
6U.1	103.8	0.01	no	133.6	0.78		
7A.1	303.6	0.022	no	-	-		
7A.2	343.8	0.075	no	-	-		
7A.3	337.9	0.10	yes	352.5	0.96	1.75	1.75
Cruciform piles							
8U.1	114.7	0.11	yes	-	-	1.00	0.57
8U.2	114.5	0.42	yes	-	-		
8B.1	198.9	0.15	yes	-	-		
8B.2	241.6	0.38	yes	-	-	2.11	1.20
8B.3	231.2	0.64	yes	226.0	1.02		
8B.4	211.8	1.00	yes	207.7	1.02		
9A.1	208.1	0.059	no	-	-		
9A.2	229.3	0.30	yes	-	-	2.00	1.14
9A.3	220.8	1.44	yes	209.8	1.05		

Notes:

1. Ratio of the maximum recorded load for each pile configuration, to the respective maximum loads for the unexpanded box pile and unexpanded cruciform pile.

2. Ratio of the maximum recorded load for each pile configuration, to the maximum recorded load for the unexpanded box pile.

Table 11.3 BRS site: Comparison of pile test results

Assumed values of $\bar{\delta}'$	Deduced values of $\bar{K}_s$	
	Cruciform pile	Box pile
17°	4.6	6.3
20°	3.8	5.3
25°	3.0	4.1
30°	2.4	3.3
35°	2.0	2.7

Table 11.4 BRS site, unexpanded piles:
Deduced values of $\bar{K}_s$ for range of assumed values of $\bar{\delta}'$

Pile test	$\bar{\tau}_{s_f}$ min (kPa)	$\bar{\tau}_{s_f}$ max (kPa)	$\bar{\sigma}_r'$ min (kPa)	$\bar{\sigma}_r'$ max (kPa)
Box Piles				
5U.1	72.7		155.9	237.8
7A.3	109.6	156.9	235.0	513.2
5B.2	88.0	134.2	188.7	438.9
Cruciform Piles				
8U.1	53.0		113.7	173.4
9A.2	93.7	118.2	200.9	386.6
8B.2	86.2	121.9	184.9	398.7

Notes:
1. $\bar{\tau}_{s_f}$ min refers to pile perimeter 'A'
   $\bar{\tau}_{s_f}$ max refers to pile perimeter 'D'
2. $\bar{\sigma}_r'$ min given by assuming $\bar{\tau}_{s_f}$ min, $\bar{\delta}' = 25°$
   $\bar{\sigma}_r'$ max given by assuming $\bar{\tau}_{s_f}$ max, $\bar{\delta}' = 17°$

Table 11.5 BRS site:
Deduced values of radial effective stress $\bar{\sigma}_r'$
and radial stress factor $\bar{K}_s$ acting on test piles

CHAPTER 12
SUMMARY AND CONCLUSIONS

12.1 The Wedge-Pile

12.1.1 Measurements and predictions of radial effective stresses acting on conventional piles at failure have shown that they are usually much less than those values potentially available, particularly in sands. Even for large-displacement piles, values of radial effective stress existing after pile installation are often not much greater than the original values existing before installation. Greater values of radial effective stress can be mobilised by radial expansion into the ground. This is readily demonstrated by pressuremeter tests. Simple theory suggests that increases in pile capacity of around two times in clays and in excess of ten times in sands are possible, by radially expanding a pile along its length.

12.2.2 Professor J.B. Burland has devised and patented a simple means of expanding a pile or anchorage after it has been installed in the ground - the Wedge-Pile. The process involves two main components:

(a) The outer shell
(b) The expander mandrel

The process consists of installing the outer shell in the ground, and then expanding it radially along its length by passing an expander mandrel through it. Various different embodiments of wedge-pile are possible, but the underlying principle is the same in each case. Expansion takes place locally and progressively, in the form of a wave moving down the shell. The key to the process lies in the fact that the force required to expand the shell in this way is very much less than the force required to expand the shell simultaneously over its whole length. The magnitude of the force required to progress the expansion can be controlled by the profile of the nose of the expander mandrel and by the flexibility of the outer shell.

12.2 Summary of Work Undertaken

12.2.1 Investigations have been undertaken at Imperial College in order to demonstrate the principle of the Wedge-Pile. These have taken place in the the field with 6m and 1.5m long piles, in the laboratory with

small-scale models, and with computer models.

12.2.2 Three types of 'multiple-element' wedge-pile have been investigated. This type of wedge-pile has an outer shell comprised of separate elements, initially held together temporarily and driven as one, and then subsequently split apart during expansion. The three types investigated were the cruciform pile, in which the outer shell is comprised of four equal angle sections held 'back-to-back'; the box pile, in which four equal angles are held in a box configuration; and the H-pile, in which two channel sections are held 'back-to-back'. Investigations have also been carried out on circular tube wedge-piles. This type of wedge-pile features an outer shell comprised of a circular tube, with one or more longitudinal weak lines or splits in the tube which can be opened up to allow expansion.

12.2.3 Laboratory tests with small model cruciform piles in beds of sand showed factors of increase in pile capacity after expansion of around 3 to 4. The expanded piles required significantly less energy to install for given pile capacity than did traditional driven piles.

12.2.4 Tests with 6m long, 140mm wide steel cruciform and closed-ended box piles have been performed in a highly weathered (Grade VI) chalk profile. It was found that the shaft capacity of piles in this soil profile could be greatly increased by radial expansion. The unexpanded cruciform and box piles gave average shaft frictions of less than 30kPa. When expanded by between 11% and 21% of initial pile width, however, average shaft frictions in excess of 100kPa and as high as 160kPa were obtained. The static shaft friction of the expanded cruciform piles was similar to that of the expanded closed-ended box piles, but the cruciform piles had advantages in their ease of driving. The expanded box piles tended to be stiffer in their response to load than the expanded cruciform piles, however. Under large one-way cyclic loads (of the order of half the static capacity), the expanded cruciform pile showed significant degradation of carrying capacity wheareas the expanded box pile appeared to be unaffected. This is thought to be due to the compaction of the high porosity chalk structure during driving of a box pile. Any pile or anchor in chalk which does not compact the surrounding chalk during installation is likely to be prone to significant loss of shaft capacity under large cycles of load. Tests on expanded piles left in the ground for between 110 days and 198 days showed that there was no obvious tendency for load carrying capacity to decrease with time.

12.2.5 Tests with 6m long, 140mm wide steel cruciform and closed-ended

box piles have been performed in a stiff boulder clay profile of medium plasticity. Increases in shaft capacity on expansion (by between 11% and 21% of initial pile width) of around 2 times were found in this soil profile: the unexpanded piles giving average shaft frictions of between 50kPa and 75kPA and the expanded piles giving average shaft frictions between 100kPa and 150kPa. As for the tests in the chalk profile, the expanded cruciform piles showed major advantages over the expanded box piles in their ease of driving. Also as before, tests on expanded piles left in the ground for between 124 and 310 days showed no obvious tendency for load carrying capacity to decrease with time.

12.2.6 At the two test sites described above, the deduced radial effective stresses acting on the expanded piles at failure were much less than those apparently available when expanding a pressuremeter in the same soil profile. There are a number of possible reasons for these differences, but a major factor is thought to be over-expansion effects as summarised in Section 12.2.9 below. At each of the sites, there was relatively little difference in load carrying capacity for the expanded piles for expansions ranging between 11% and 21% of initial pile width.

12.2.7 Tests with 1.5m long, 100mm wide steel cruciform and H-section mini-piles have been made in a range of soil profiles. Expansion by 6% and 10% of initial mini-pile width gave increased capacity in all soil profiles, the amount of increase being greater in sands and in soils with a significant granular content, in comparison to clays. Tests on cruciform mini-piles gave increases in capacity ranging from 1.6 times in weathered London clay to 9.6 times in a clayey gravel. Expanded mini-pile capacity showed significantly less variation between sites in comparison to unexpanded mini-pile capacity. The '2-way' H-section mini-pile gave significantly lower increases in capacity than the '4-way' cruciform mini-pile.

12.2.8 Laboratory model tests have been undertaken which have demonstrated the potential of the Wedge-Pile principle in soil reinforcement processes.

12.2.9 Computer programs based on an iterative numerical method have been developed in order to model the mechanical expansion process of multiple-element wedge-piles. Using these programs it has been found that the radial stresses generated on expansion are sensitive to the shape of the expander mandrel nose and the flexibility of the outer shell. If the nose is too blunt, it may cause the outer shell to over-expand just behind the nose and then to contract back onto the

shank of the expander mandrel. Such radial contraction after initial expansion will significantly reduce the radial effective stresses acting on the pile. It is thought that the nose profiles employed in the investigations were too blunt, and increases in load carrying capacity greater than those found may have been possible.

12.2.10 Field trials of various types of 6m long, 200mm diameter circular piles have been undertaken in sand. Two types of pile with a thin walled outer shell of either steel or plastic tube were tested - the design of these piles was aimed at the housing and light industrial foundation market. The outer shell featured a single weak line to allow expansion by driving into the tube a succession of 1m long concrete pipes. Trials were also carried out with all-steel piles with the same overall dimensions as the piles just mentioned, but with thicker walled outer shells. The design of these piles was aimed at the offshore structure foundation market and in these trials outer shells both with a single weak line and with three weak lines were tested. The thin walled piles proved successful in terms of increased capacity, ease of driving, and practicality, although it is thought that the cruciform pile may prove more viable commercially. The thicker walled piles were not as succesful in terms of increased pile capacity as the thin walled piles. This is believed to be because the increased stiffness of the outer shells gave rise to increased over-expansion effects. Supporting work with laboratory models has demonstrated that a '1-split' outer shell will give significantly less capacity on expansion than a 3 or 4-split outer shell.

12.3 Critique of Work Undertaken

12.3.1 The experiments carried out with laboratory models were intended to be solely qualitative. The limitations of such small scale tests in relation to large scale field behaviour are obvious.

12.3.2 The trials with box and cruciform piles at the Luton and BRS sites had the major advantage of large scale. However, because of limited resources, the piles, equipment, and testing methods were rather basic. Results from the repeated testing of a single pile are open to criticism, and the loading applied to the piles did not include two-way cycling - such cycling might have resulted in more significant losses in capacity than those found for one-way cycling. It appears that the capacities of the expanded piles must have been heavily influenced by the expander mandrel nose profiles that were used: in other words, the expansion process was not well controlled. Of necessity, the analysis of the results has been rather generalised and has involved

some conjecture. Despite these shortcomings, however, the effectiveness of the Wedge-Pile process has been amply demonstrated at large scale.

12.3.3 The mini-piles were fabricated to a high standard, but the load testing equipment was relatively basic in comparison. The piles were tested in the top 1m of ground - at most sites this was variable or disturbed, and was often made ground. Interpretation of the test results has been on an empirical basis. The results from the mini-pile trials, however, have successfully demonstrated the Wedge-Pile principle in a wider range of soil profiles than was possible at a larger scale.

12.3.4 The development of the computer models to investigate the importance of the expander mandrel nose shape fulfilled the objective of a 'first step' approach to the problem. Only a simple spring foundation soil model was employed, however.

12.3.5 The CP&F trials of a housing type wedge-pile were succesful. However, the highly variable ground conditions at the test site has made analysis of the Conoco pile tests very difficult.

12.4 Concluding Remarks

12.4.1 The investigations described in this thesis have shown that the load carrying capacity of a pile or anchorage can be increased many times by expanding it radially along its length. Relatively small expansions are required to achieve most of the potential gains in capacity. The gains in capacity appear to be permanent with time.

12.4.2 Field trials have demonstrated that the Wedge-Pile principle is a practical and efficient method of producing a high performance pile or anchorage in a wide range of soils.

12.4.3 Qualitative measurements have shown the scope for accurately predicting wedge-pile capacity after installation. Further work is needed in order to determine whether wedge-pile capacity can be reliably related to the limiting pressures obtainable in pressuremeter tests. It is thought that design of wedge-piles will eventually be much more reliable than for conventional piles because of the improved control of the installation process that will be possible.

12.4.4 It is important to appreciate that production wedge-piles and anchorages may differ in many important details from the experimental piles described in this thesis, which were designed purely to demonstrate the principle of the Wedge-Pile. Having proved the

principle, many developments both in equipment and use are possible.

12.4.5 The field trials of circular wedge-piles arose because of an understandable desire by some civil engineering organisations to promote wedge-pile embodiments which resemble piles and anchorages that have been succesfully used in practice. The overall performance of circular piles has not proved to be as good as that of cruciform piles, however. It is considered that the cruciform pile is the type of wedge-pile most likely to give greatest all round benefit over conventional driven piles. It may be necessary to overcome established thinking within the civil engineering industry if such a pile is to be used commercially.

12.4.6 The research described in this thesis has demonstrated the basic principles of the Wedge-Pile. There are several areas in which more detailed research is now appropriate.

PLATES

Plate 2.1 Laboratory model cruciform wedge-pile:
expander mandrel (left) and outer shell (right)

(Note: outer shells used in tests tack-welded at bottom outside corners only)


0 10 20 30 40 50
MM

Plate 3.1 Box Pile: overall view
driving mandrel (left), outer shell (centre) and
expander mandrel (right)

Plate 3.2 Box Pile: outer shell plate connection

Plate 3.3 Box Pile: outer shell weld connection

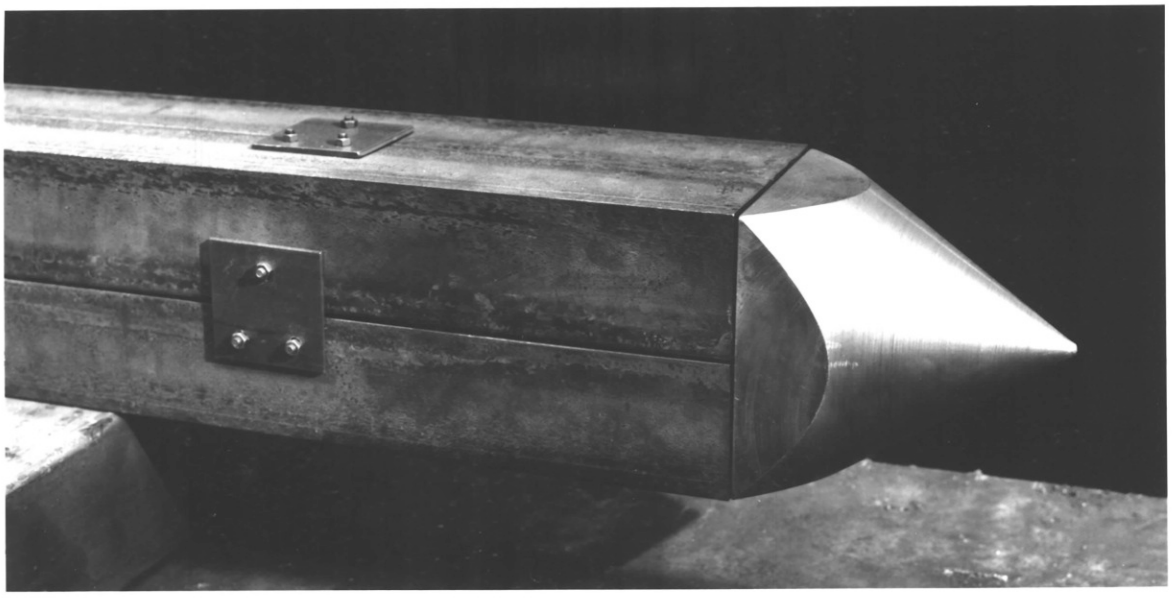

Plate 3.4 Box Pile: driving shoe

Plate 3.5 Box Pile: driving shoe with outer shell assembled

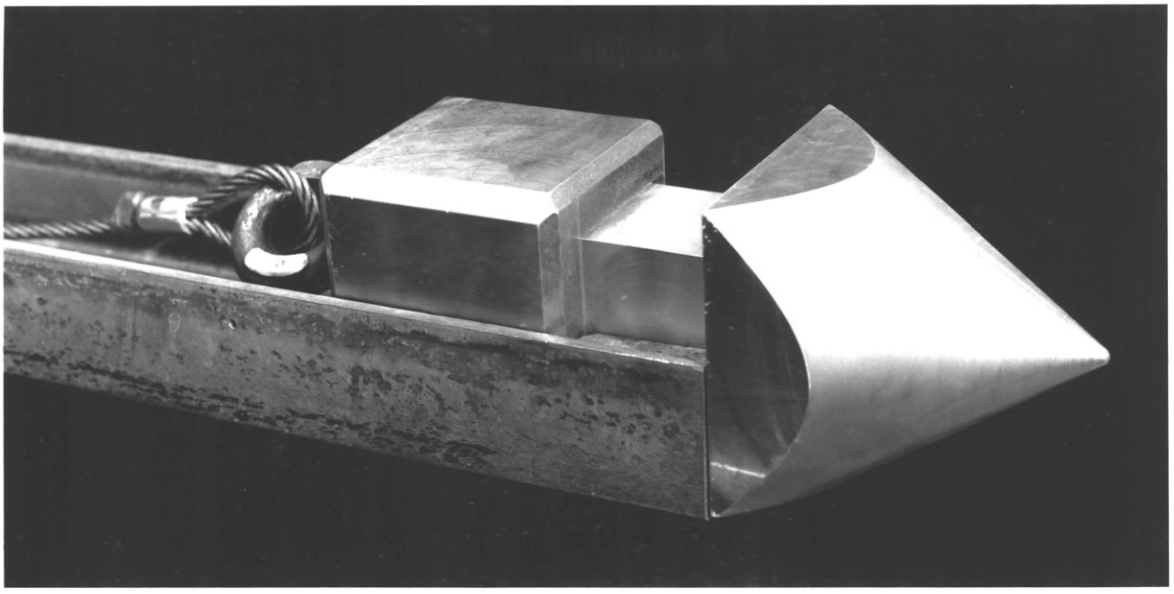

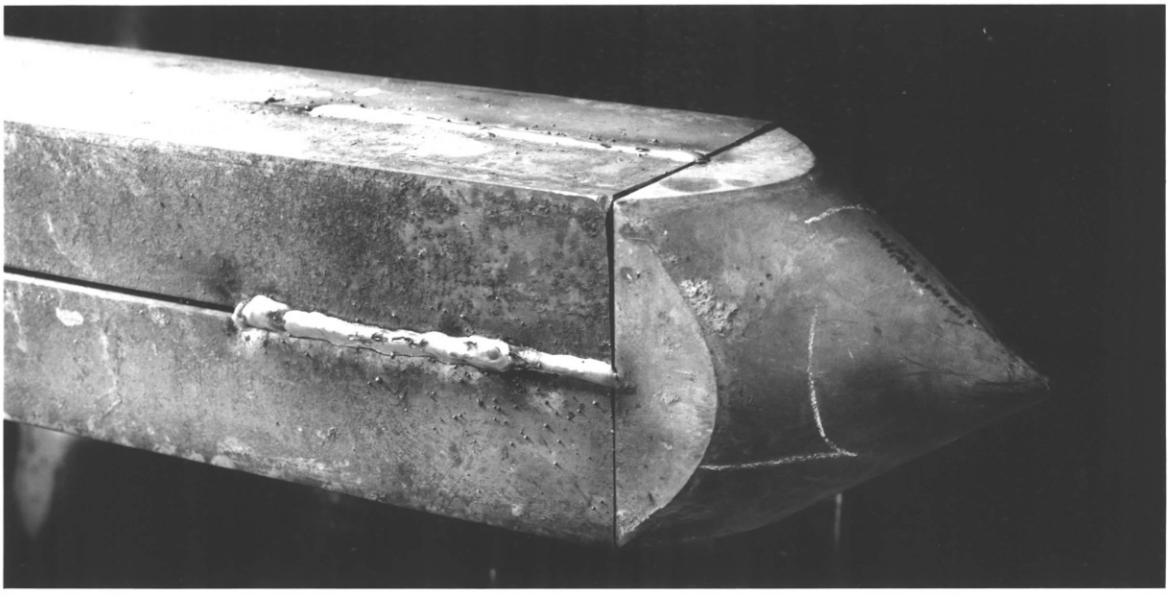

Plate 3.6 Box Pile: expander mandrel nose

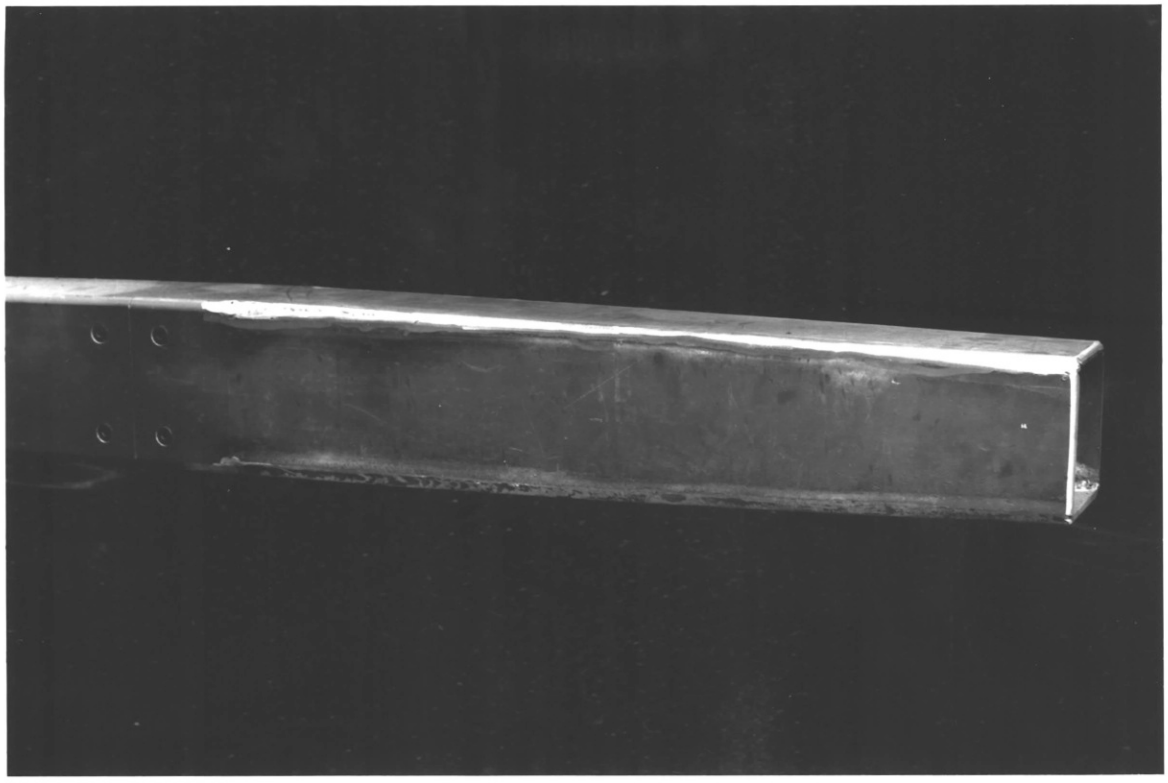

Plate 3.7 Cruciform Pile: overall view

Plate 3.8 Cruciform Pile: weld connection

Plate 3.9 Cruciform Pile: driving shoe arrangement

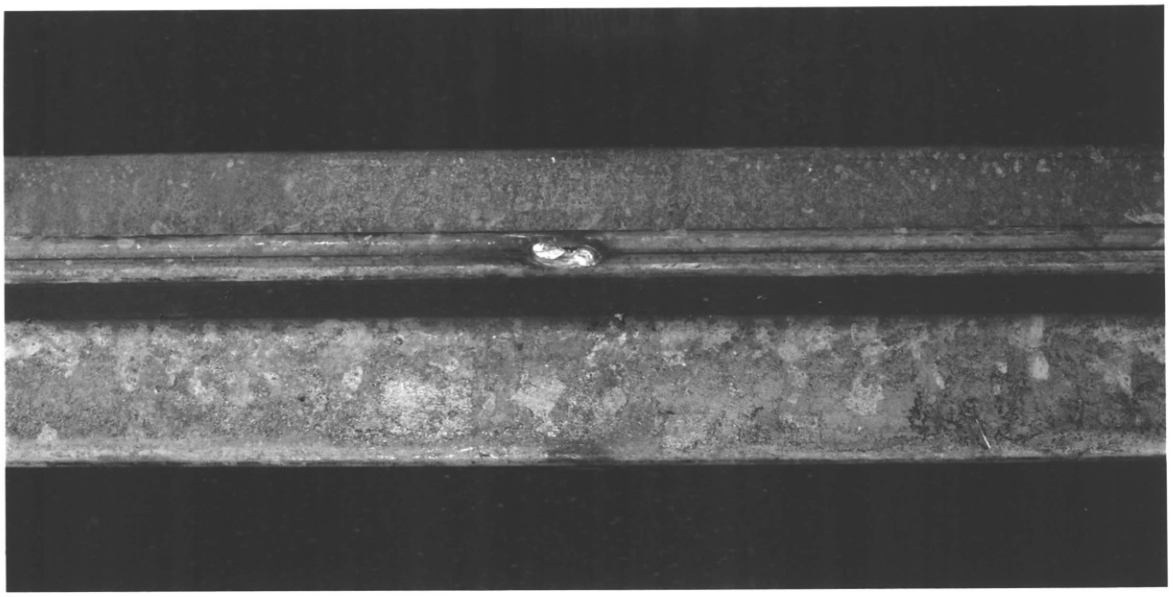

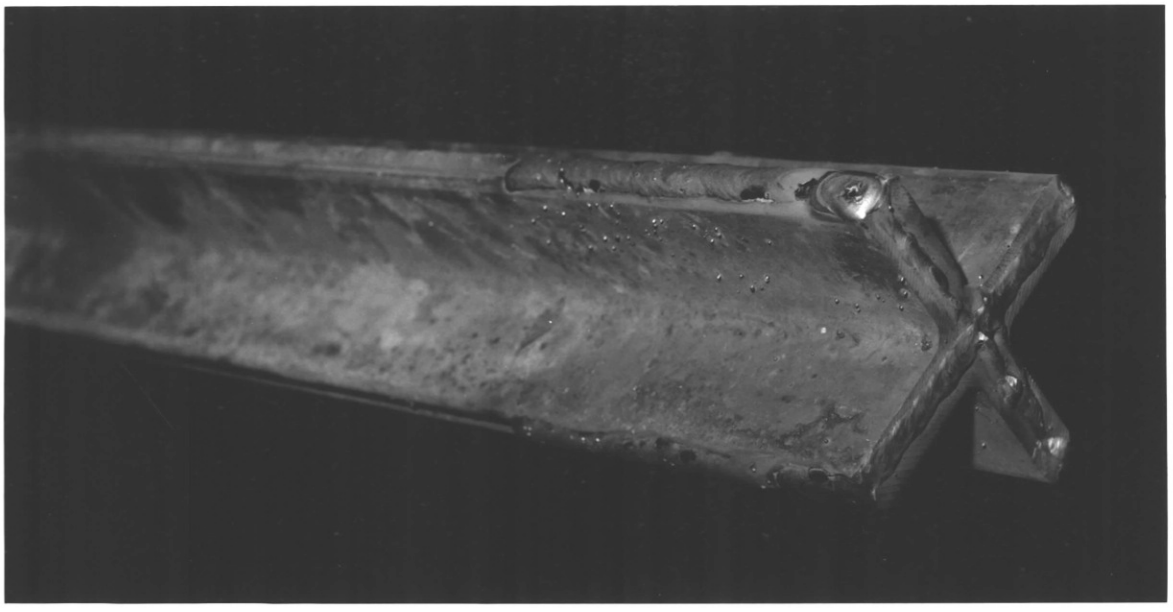

Plate 3.10 Cruciform Pile: expander mandrel nose

Plate 3.11 Luton site: driving frame

Plate 3.12 BRS site: driving frame

Plate 3.13 Box Pile: Expander mandrel being driven into outer shell

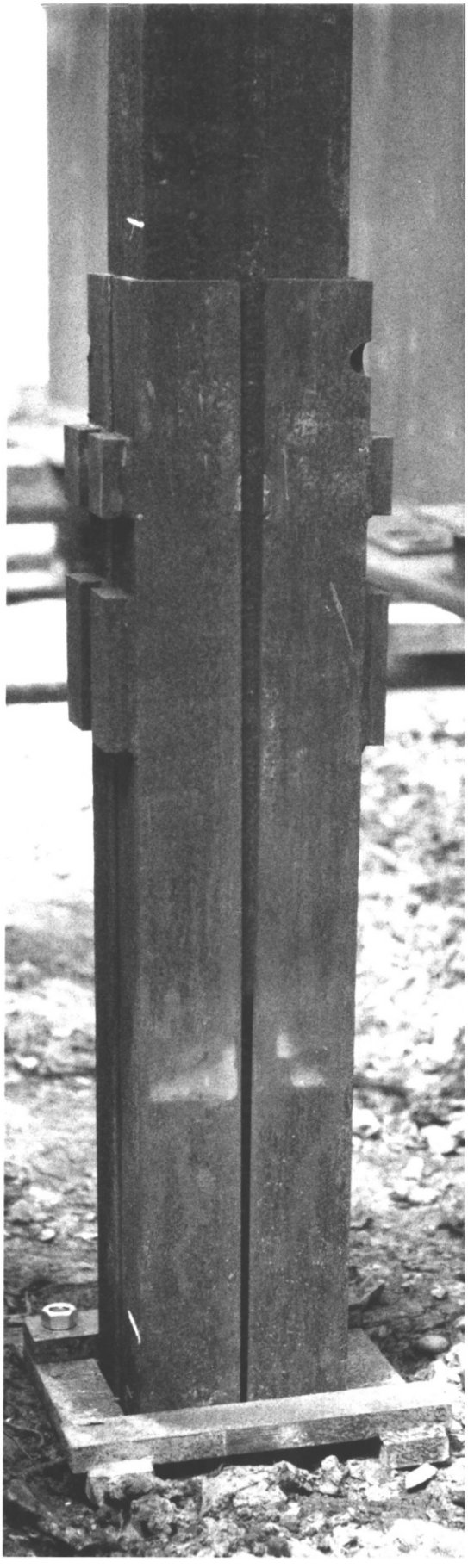

Plate 3.15 Luton site: pile testing arrangement

Plate 3.14 BRS site: pile testing arrangement

Plate 3.16 Pile testing frame crosshead

Plate 3.17 Cruciform Pile under test

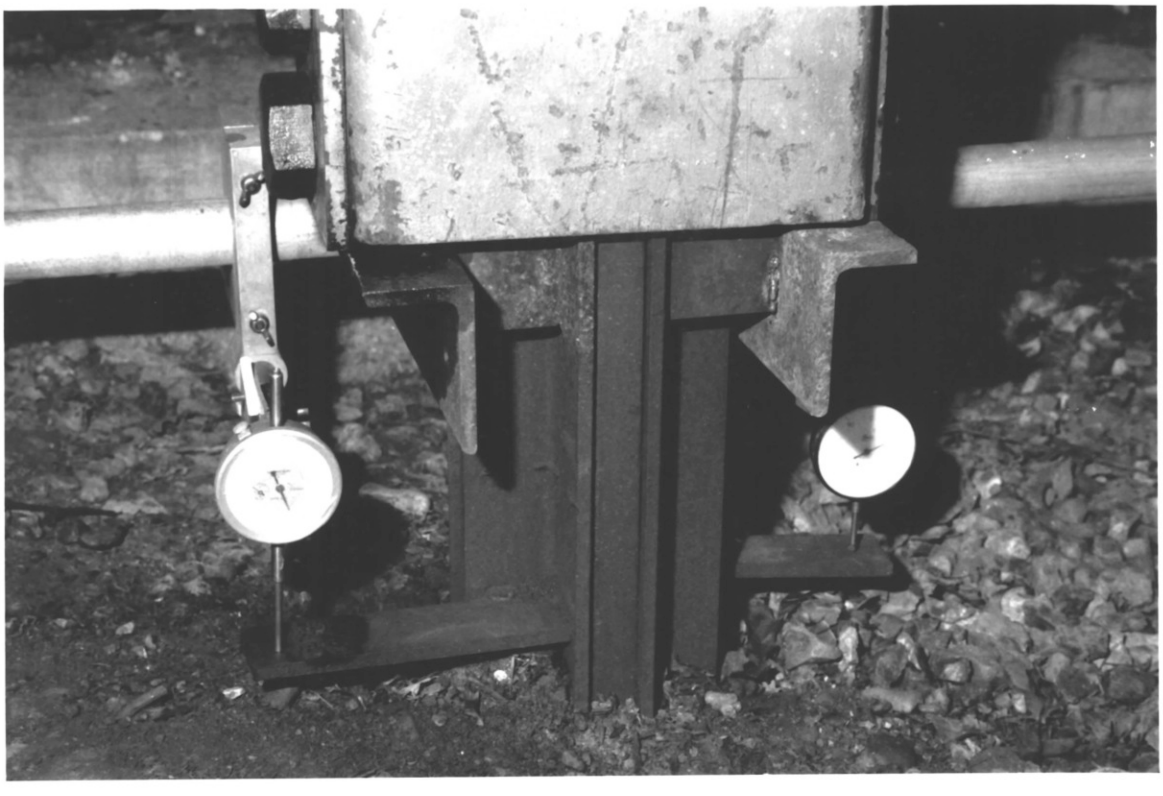

Plate 4.1 Luton site: Cruciform Pile after extraction

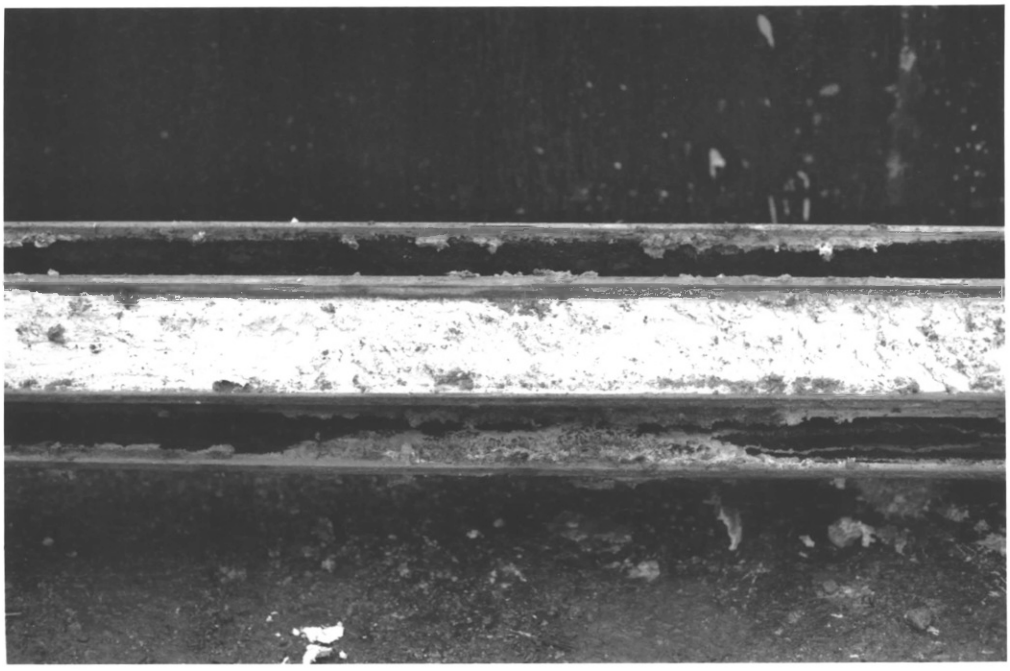

Plate 6.1 Cruciform mini-piles Types I and II: overall view
Type I outer shell (background), expander
mandrel (centre), Type II outer shell (foreground)

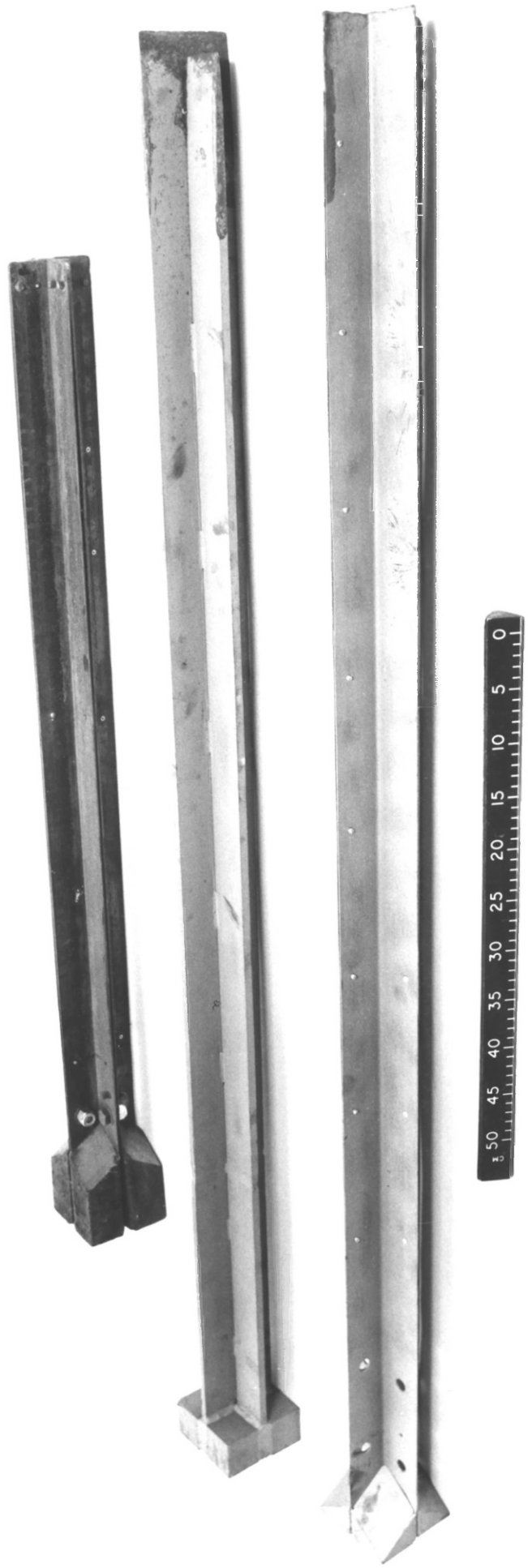
0
5
10
15
20
25
30
35
40
45
50

Plate 6.3 Cruciform mini-pile Type II:
detail of driving head

Plate 6.2 Cruciform mini-pile Type II:
detail of expander mandrel nose

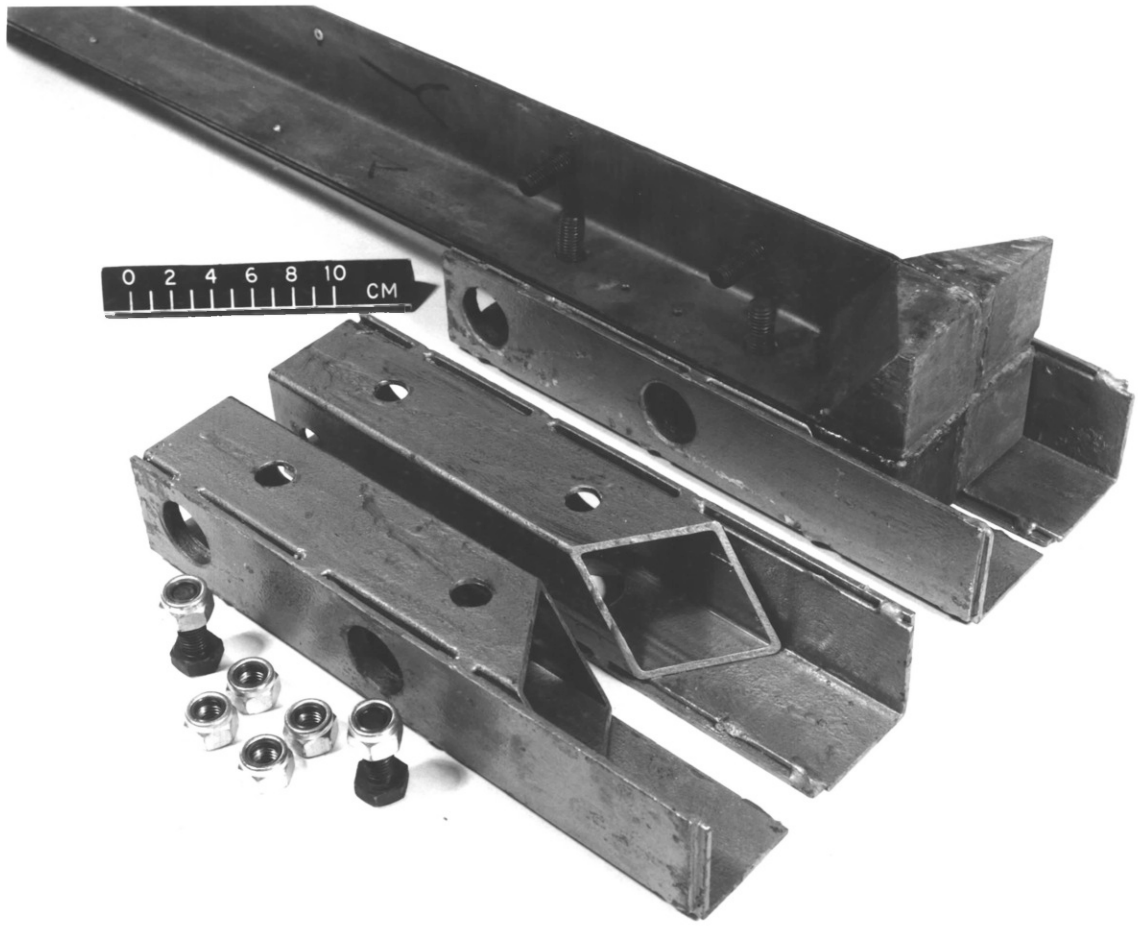
0 2 4 6 8 10
CM

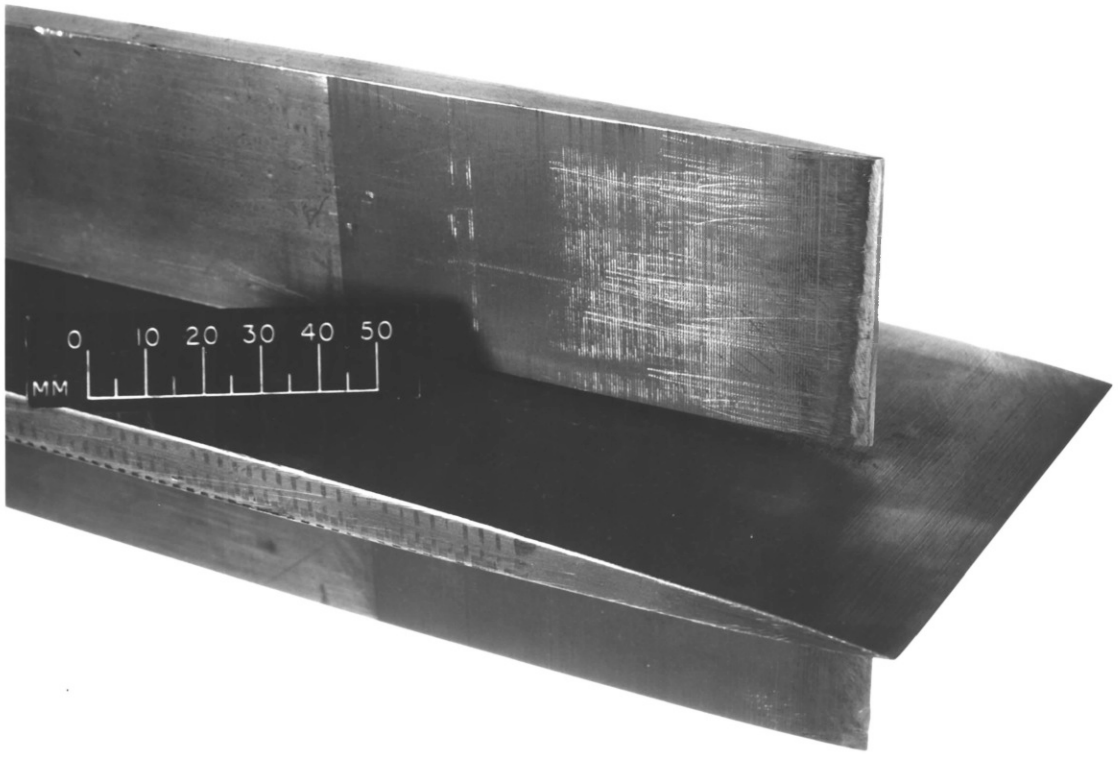
0 10 20 30 40 50
MM

Plate 6.4 Air driven post-driver in operation

Plate 6.5 Support trestle for mini-pile

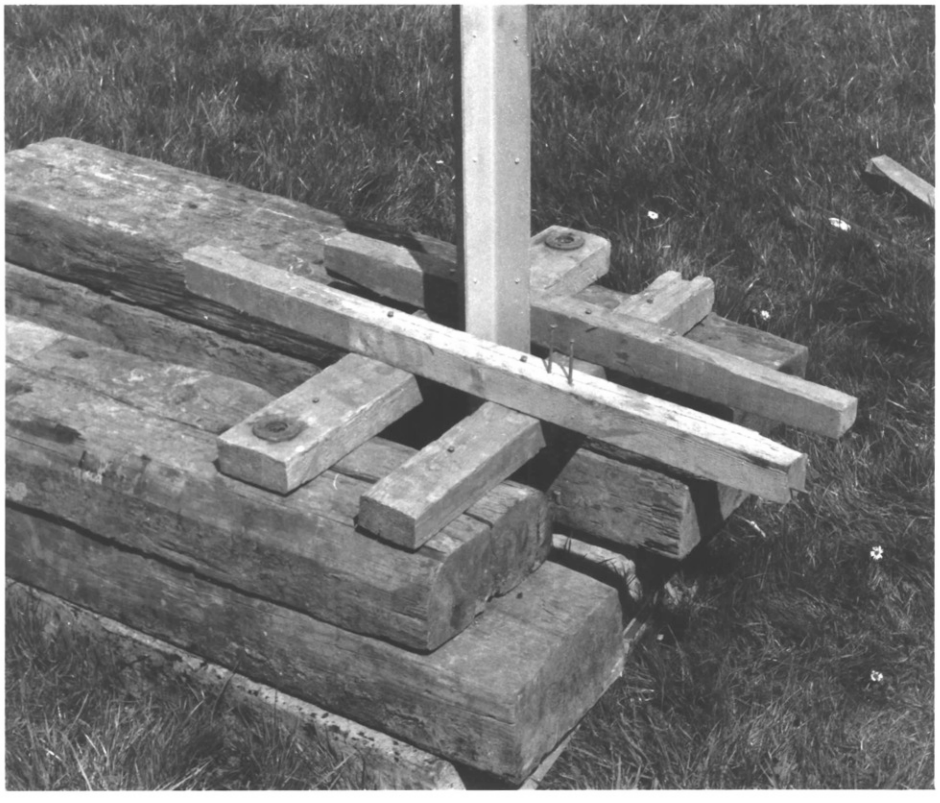

Plate 6.6 H section mini-pile:
Outer shell (background), expander mandrel (foreground)


0
5
10
15
20
25
30
35
40
45
50

Plate 6.7 H section mini-pile: detail of driving head

Plate 6.8 H section mini-pile: detail of expander mandrel nose

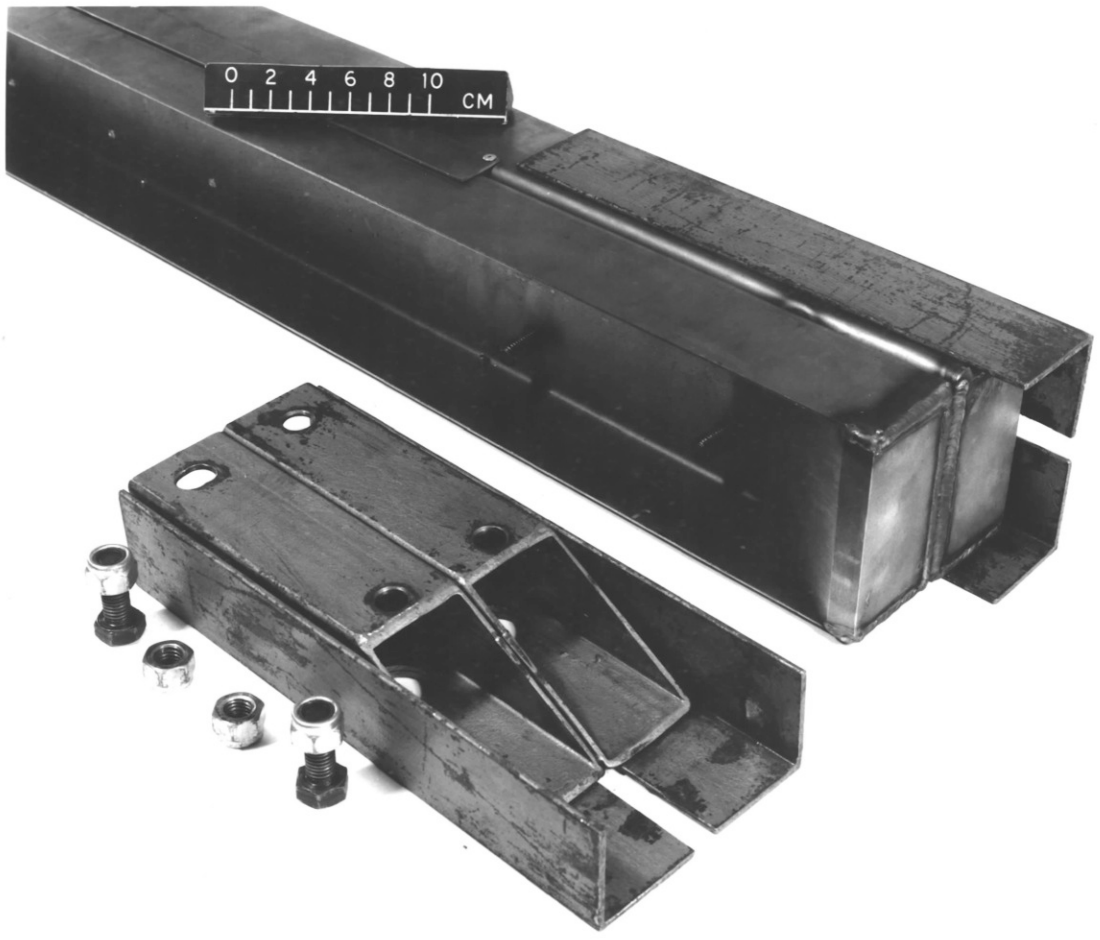
0 2 4 6 8 10
CM

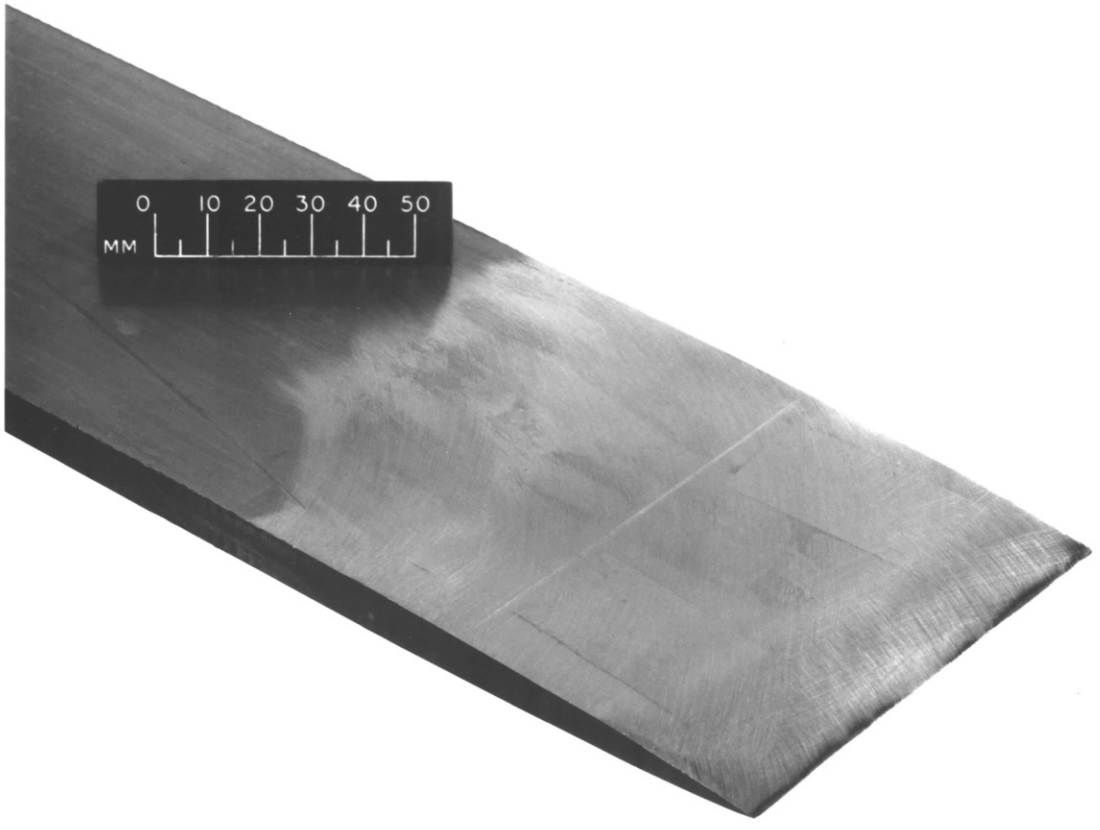
0 10 20 30 40 50
MM

Plate 6.9 Mini-pile testing set-up

Plate 6.10 Cruciform loading box

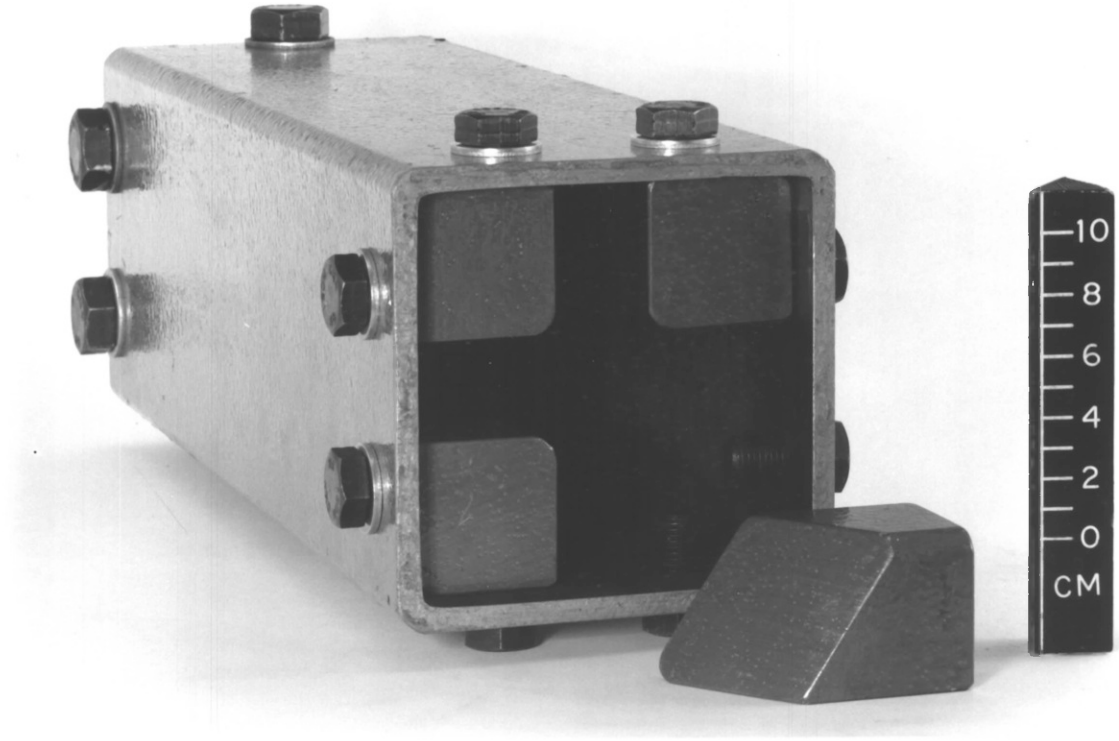
10
8
6
4
2
0
CM

Plate 7.1 Testing flume for soil reinforcement model tests

Plate 7.2 1.5mm thick plastic nail being inserted into retained sand

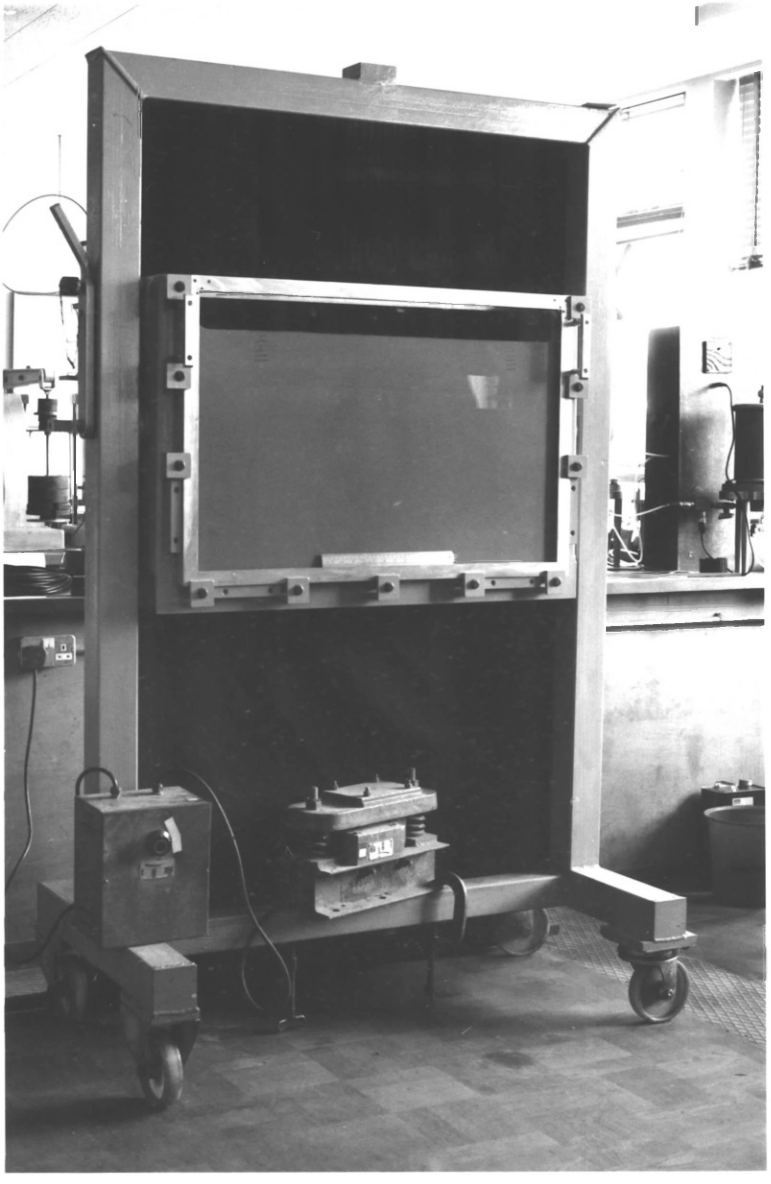

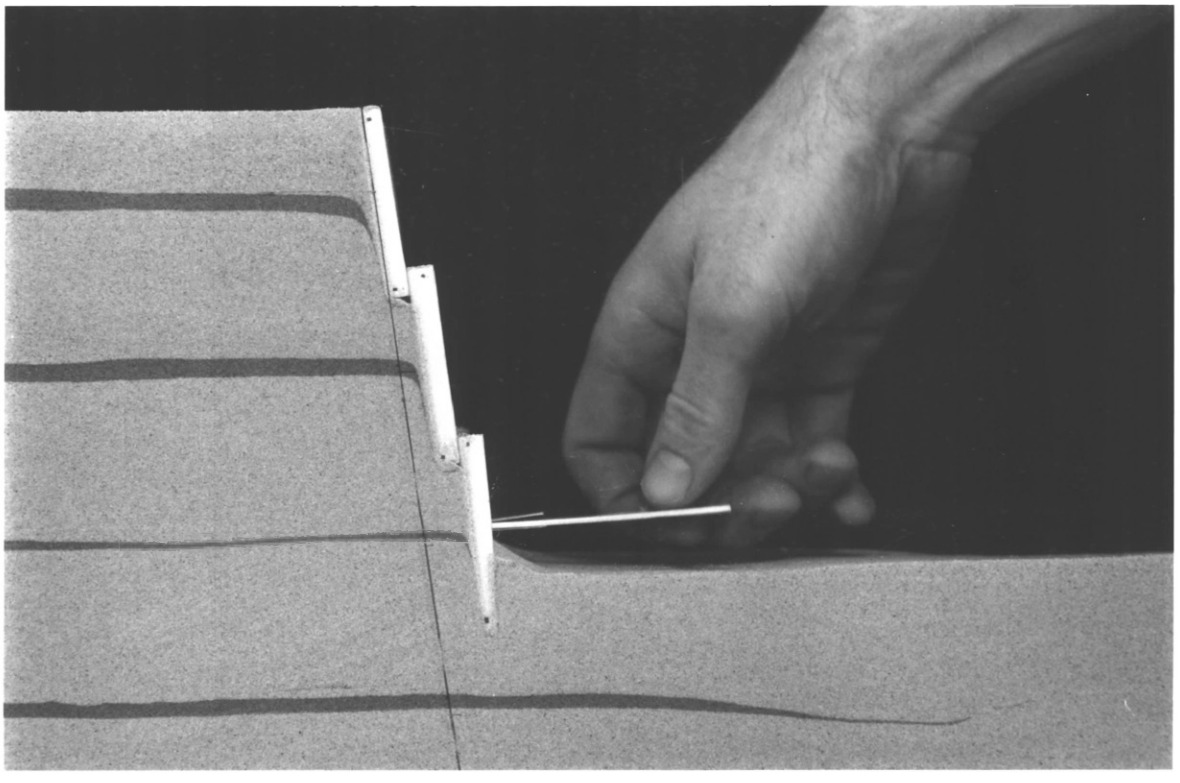

Plate 7.3 Completed soil nail wall showing marker bands of dyed sand

Plate 7.4 Soil nail wall under test

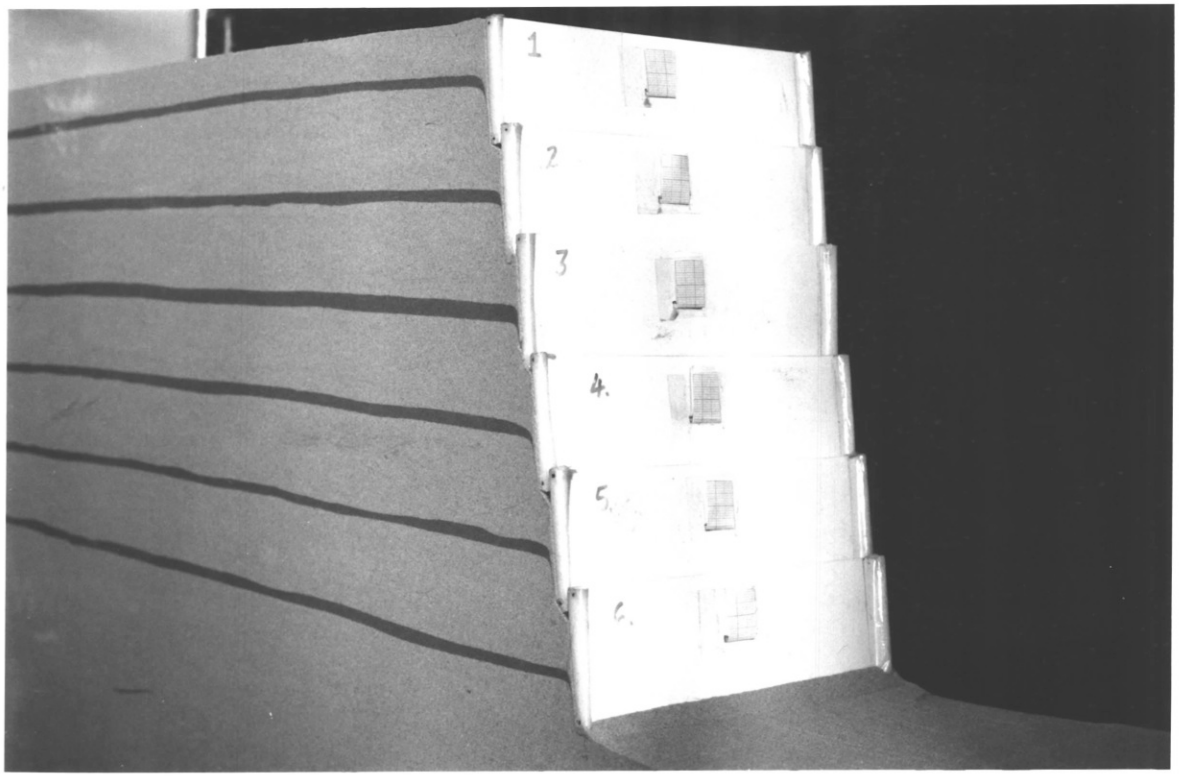
1
2
3
4.
5.
6.

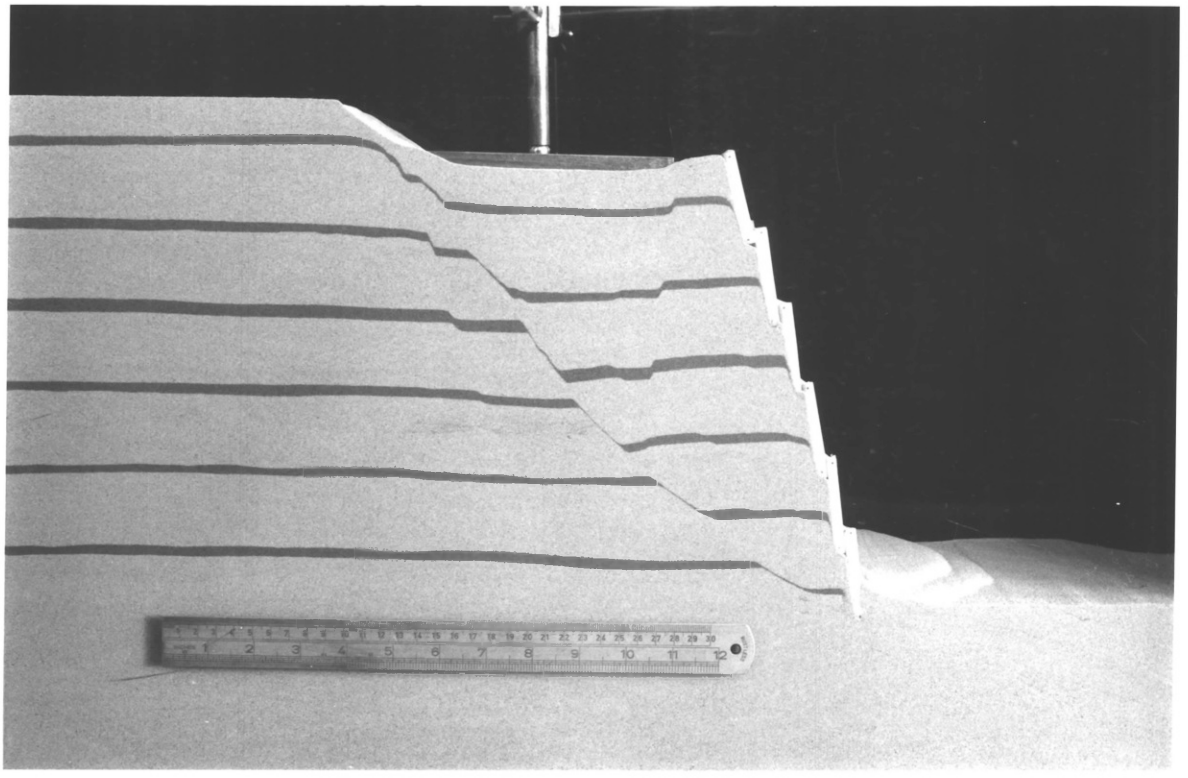

Plate 8.1 CP&F plastic piles:
plastic tube outer shells

Plate 8.2 CP&F plastic piles:
outer shell driving shoe

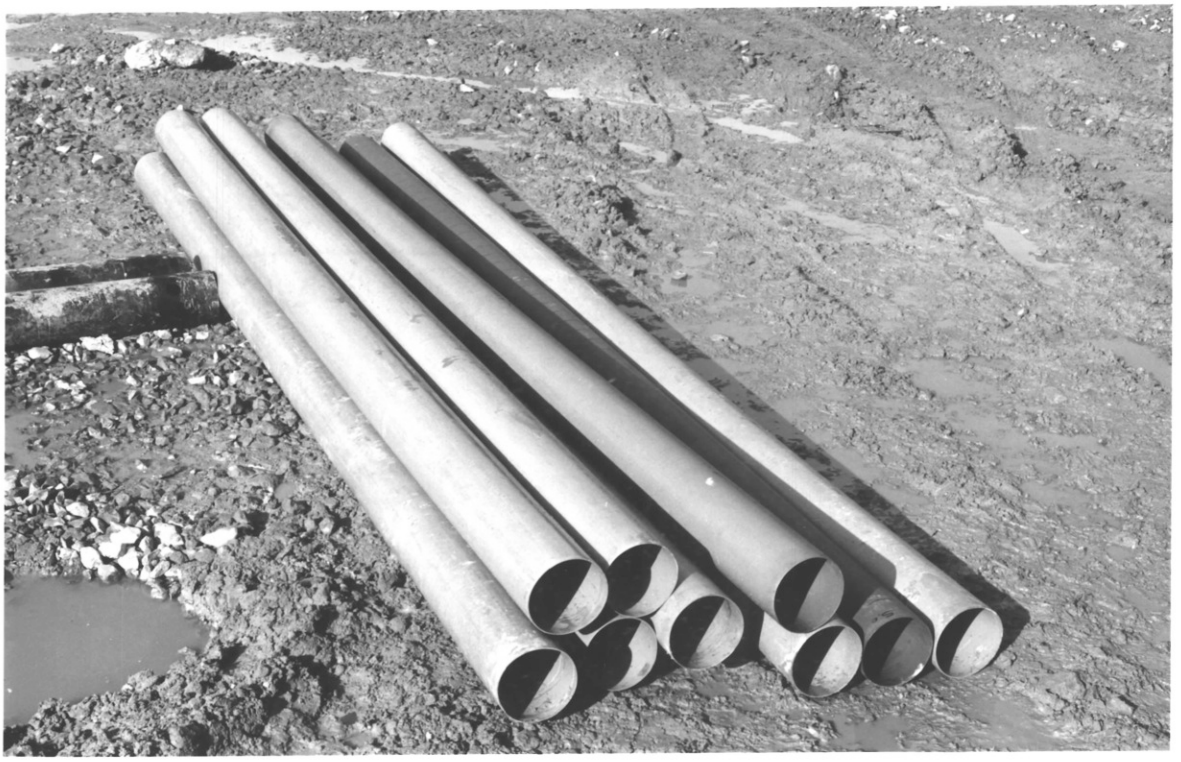

Plate 8.3 CP&F piles:
concrete pipe expander mandrel segments

Plate 8.4 CP&F piles:
expander mandrel nose

Plate 8.5 CP&F steel piles:
steel pipe outer shells

Plate 8.6 CP&F steel piles:
detail of flame cut weak line

Plate 8.7 CP&F steel piles:
outer shell driving shoe

Plate 8.8 Conoco piles:
outer shells

Plate 8.9 Conoco piles:
detail of machine cut weak line in outer shell

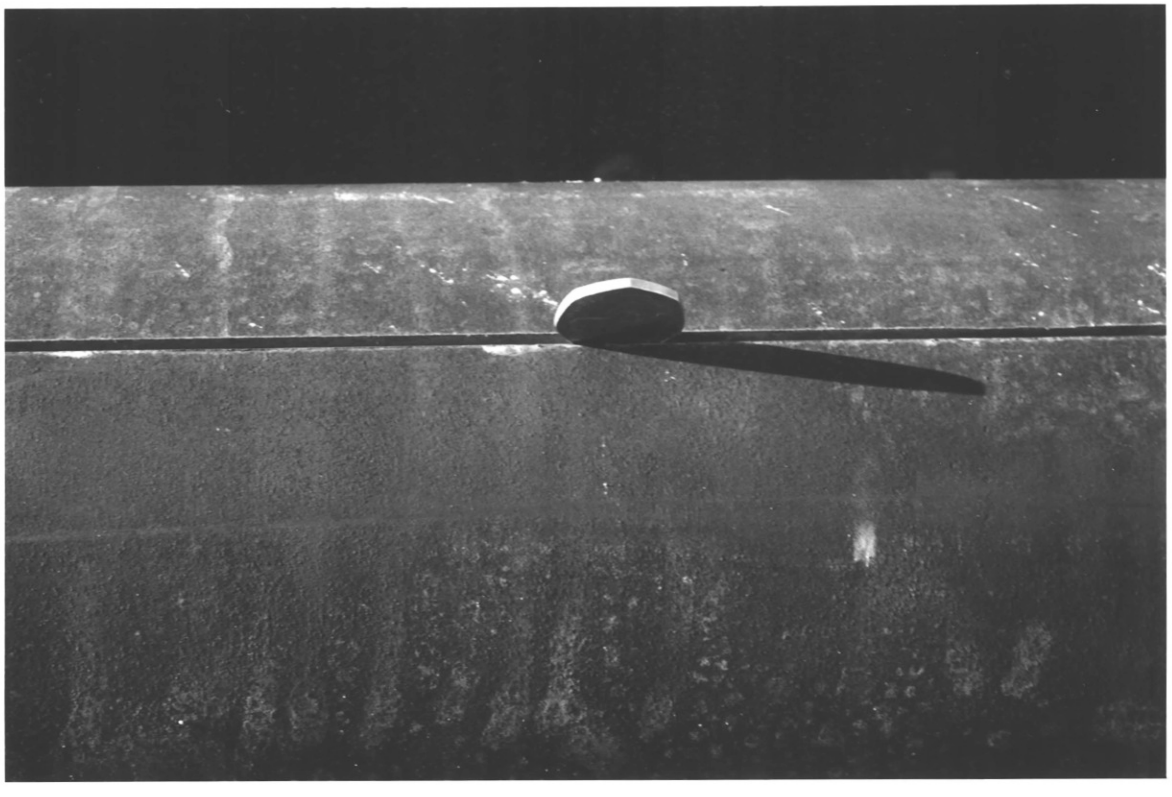

Plate 8.10 Conoco 3 weak line outer shell:
detail of 'fins' at top of outer shell

Plate 8.11 Conoco piles:
detail of expander mandrel noses

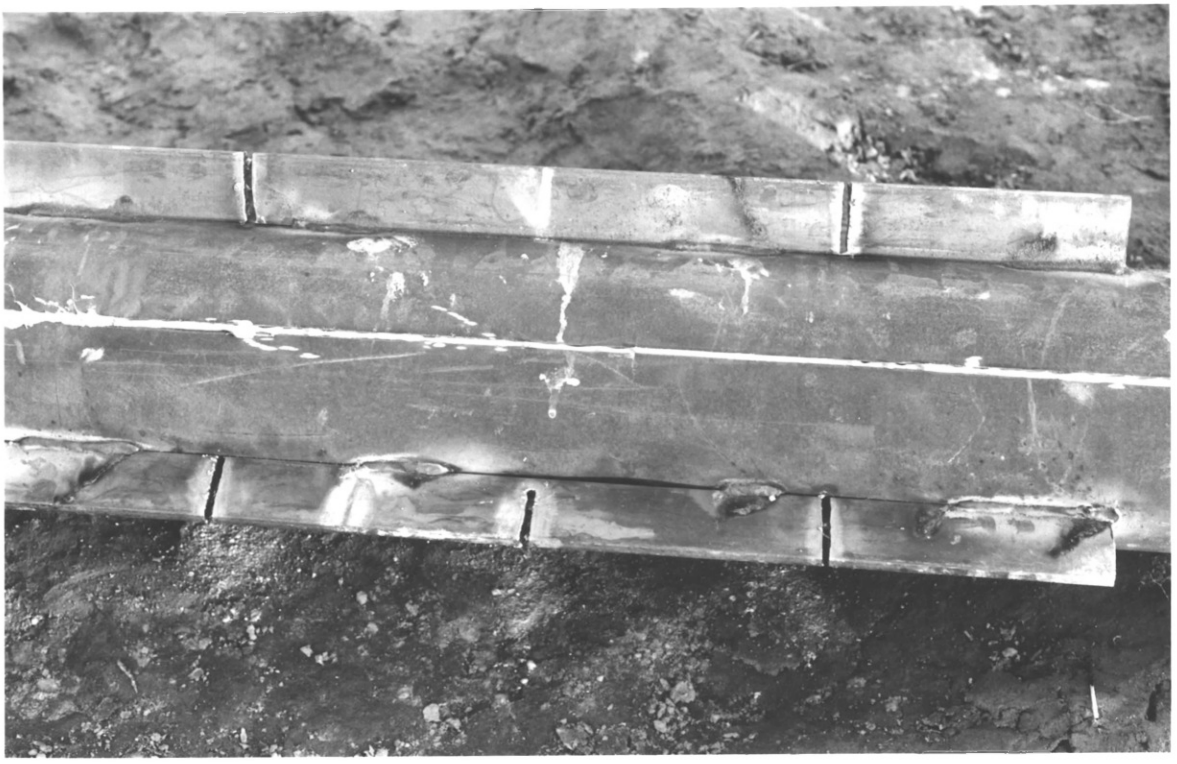

Plate 8.12 General view of piling rig used for field trials

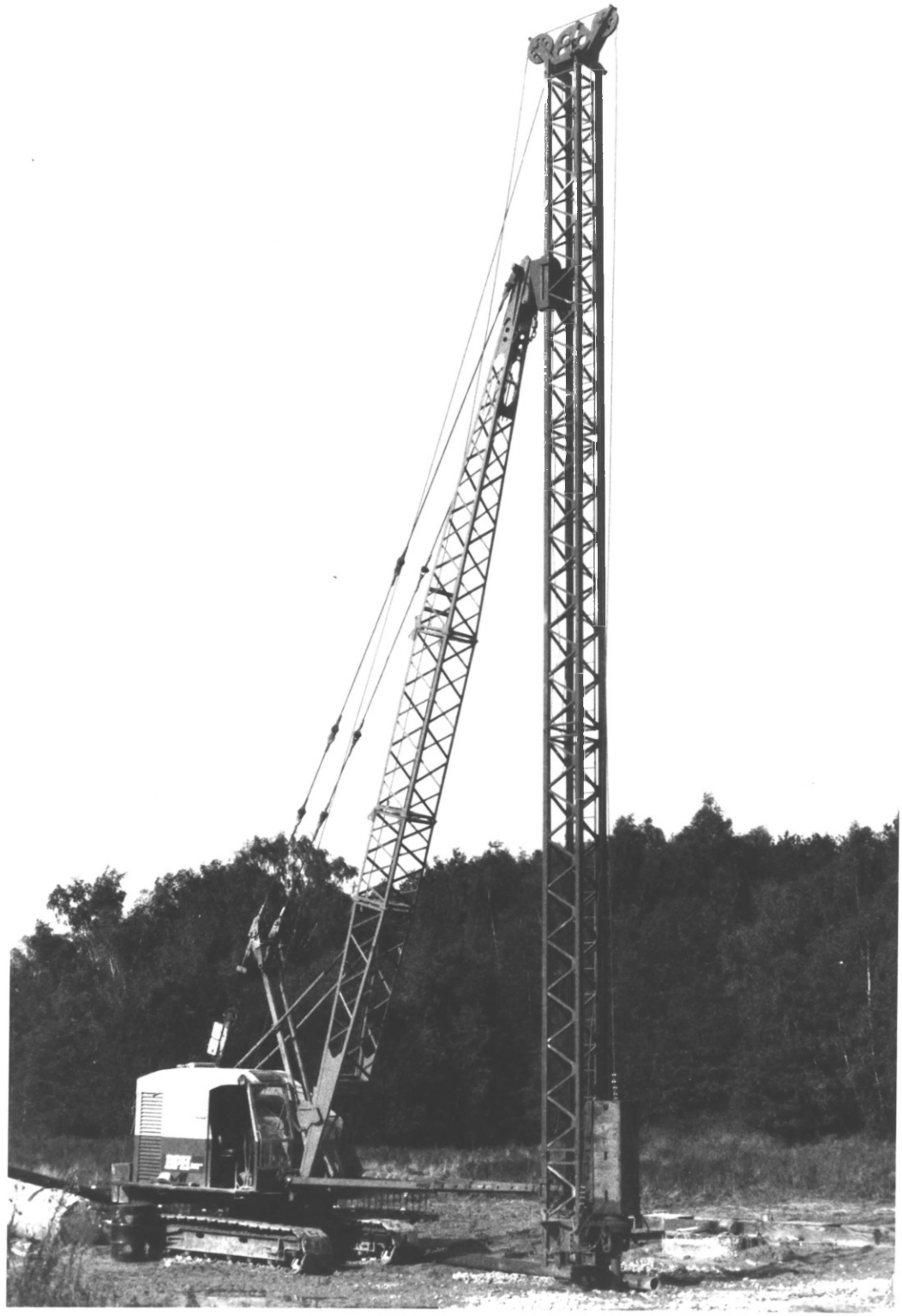

Plate 8.13 Piling rig:
View of piling head

Plate 8.14 Piling rig:
Detail of roller guide

Plate 8.15 Driving mandrel within plastic outer shell (bottom)

Plate 8.16 Driving mandrel within plastic outer shell (top)

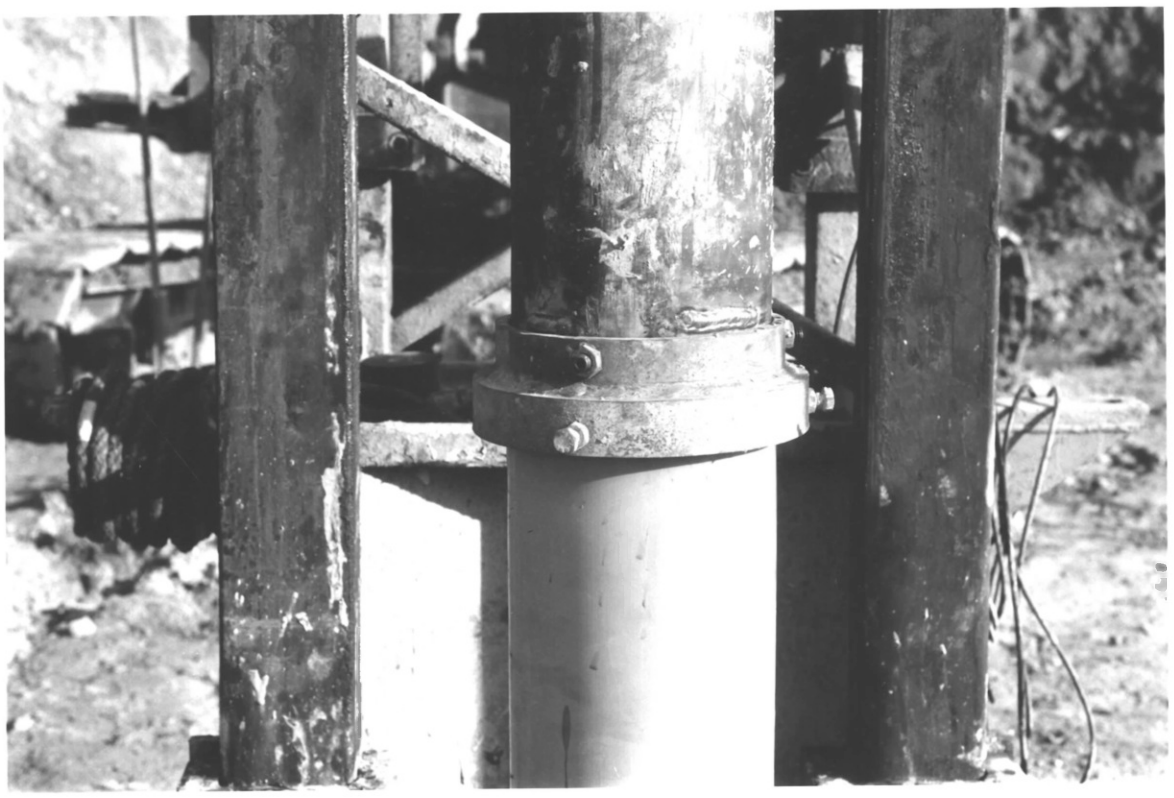

Plate 8.17 CP&F plastic pile:
driving shoe being fitted

Plate 8.18 CP&F plastic pile:
weak line being cut

Plate 8.19 CP&F steel pile:
outer shell being driven

Plate 8.20 CP&F plastic pile:
expander mandrel nose engaged in outer shell

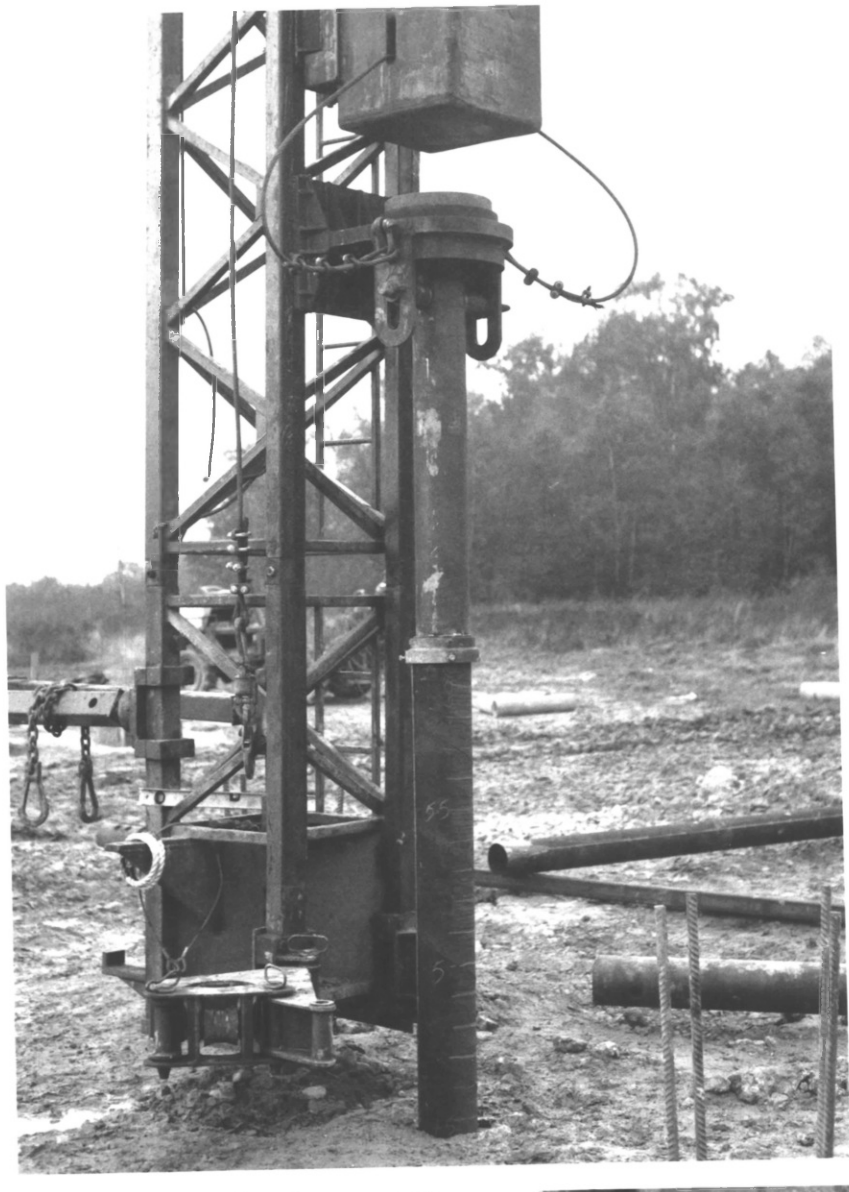

Plate 8.21 CP&F piles:
loading concrete pipe segment

Plate 8.22 CP&F piles:
detail of rope gasket between concrete pipes

Plate 8.23 CP&F piles:
applying grout to concrete pipes

Plate 8.24 CP&F piles:
detail of driving dolly


209


STATION

Plate 8.25 Conoco 3 weak line pile:
view of unopened weak line

Plate 8.26 Conoco 3 weak line:
view of opened weak line (other opened weak line similar)

Plate 8.27 CP&F piles:
overall view of compression testing set-up

Plate 8.28 CP&F piles:
view of compression pile under test

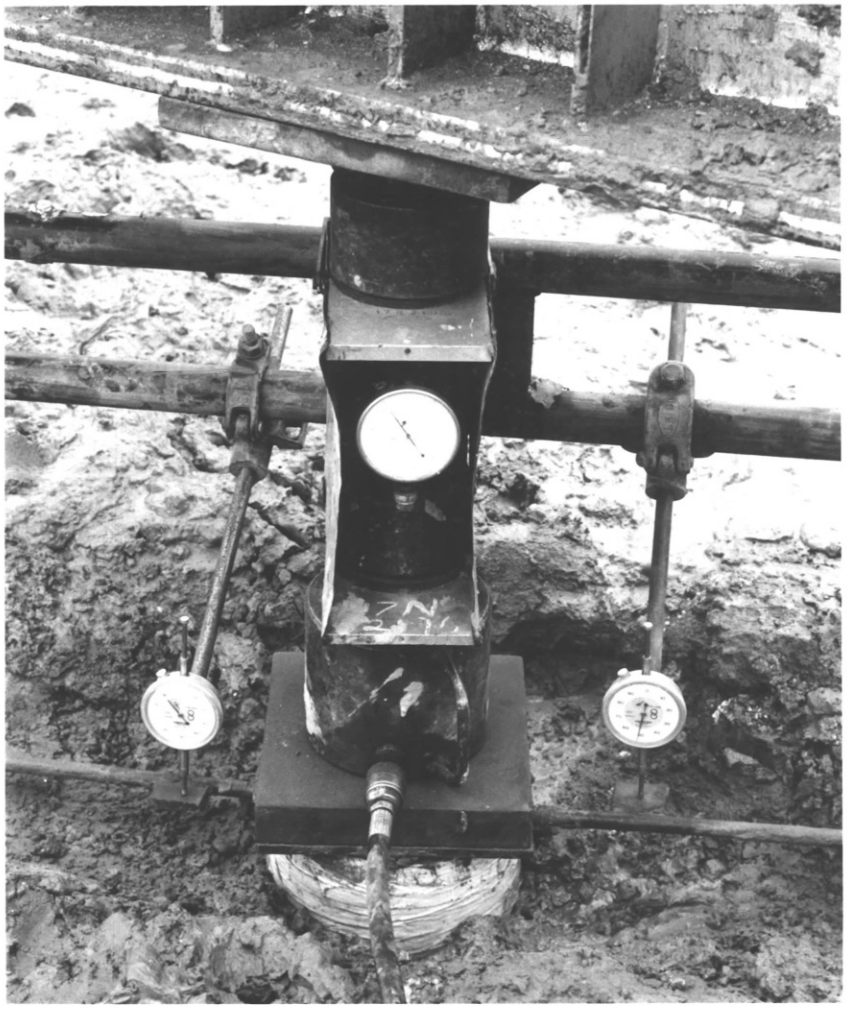

Plate 8.29 Conoco piles:
overall view of testing set-up

Plate 8.30 Conoco piles:
view of unexpanded pile under test

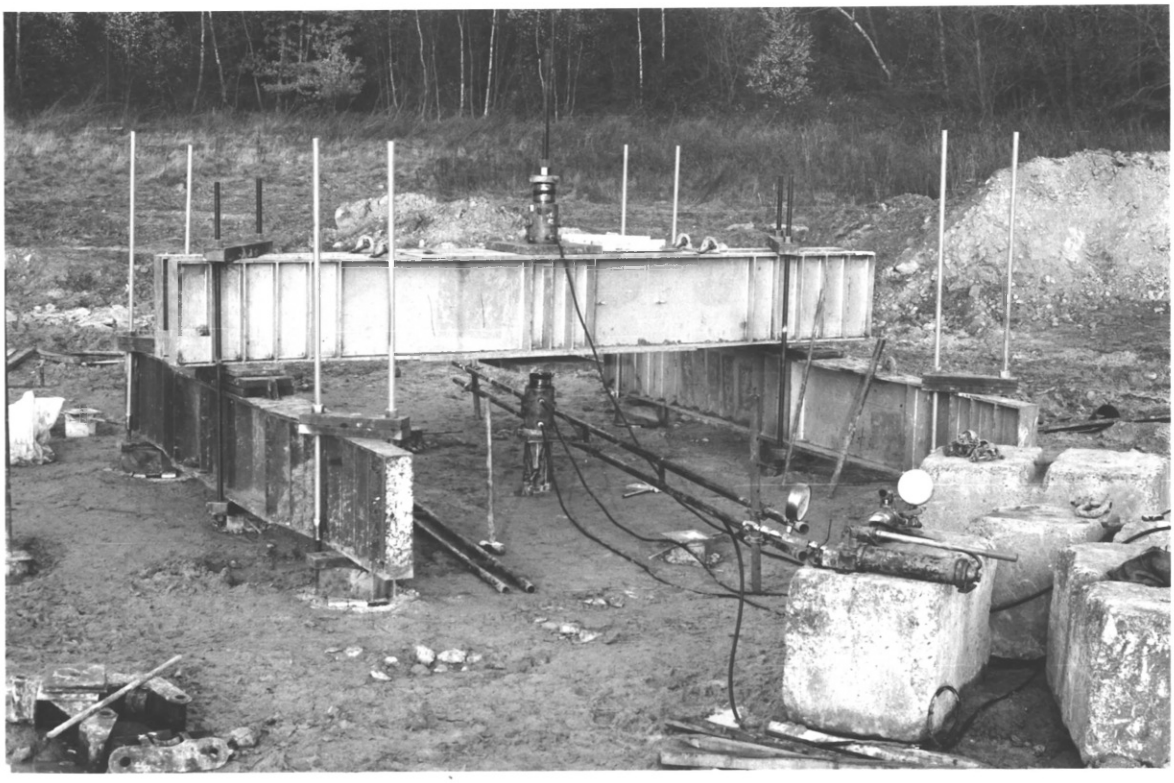

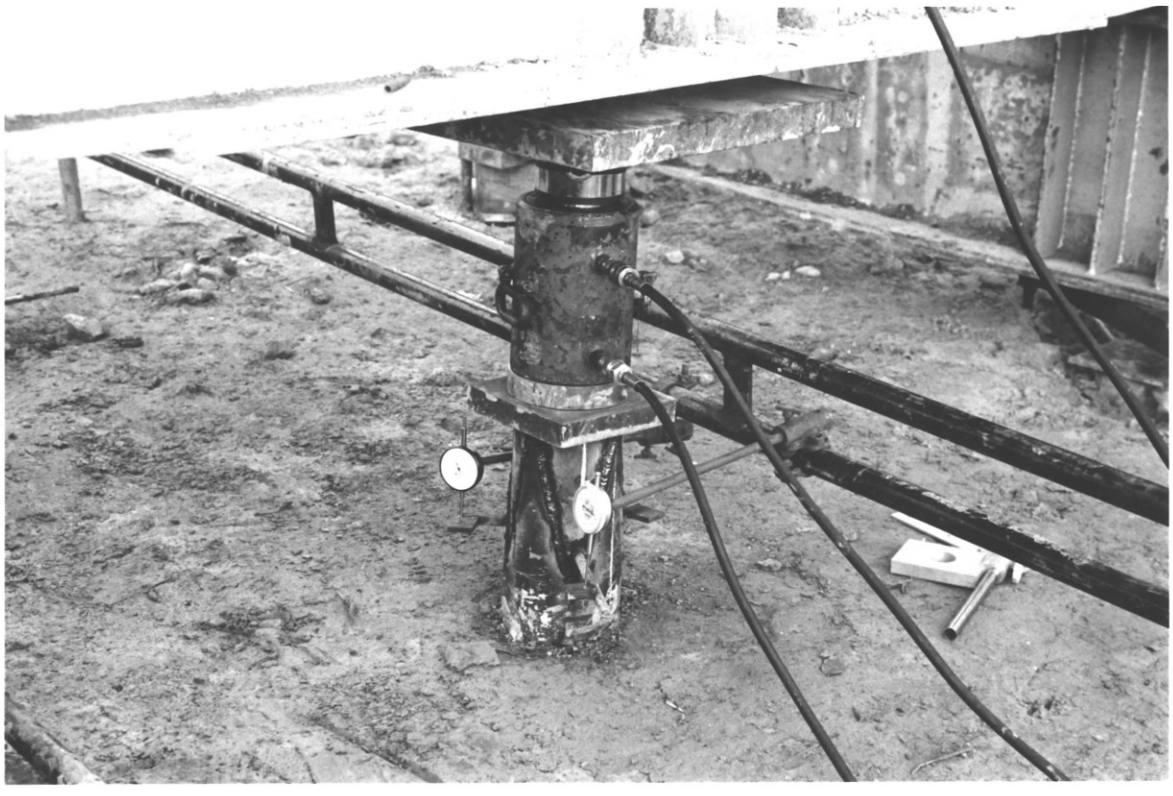

REFERENCES

American Petroleum Institute (1984). Recommended practice for planning, designing and constructing fixed offshore structures. API RP 2A, 44-47.

Baguelin, F., Jezequel, J.F. and Shields, D.H. (1978). The pressuremeter and foundation engineering. Trans. Tech. Publications, Clausthal (W. Germany), 1978.

Baguelin, F., Jezequel, J.F., Le Mee, E. and Le Mehaute, A. (1972). Expansion of cylindrical probes in cohesive soils. J. Soil. Mech. Fdn. Div., Am. Soc. Civ. Engrs 98, SM11, 1129-1142.

Baldi, G., Bellotti, R., Ghionna, V., Jamiolkowski, M. and Pasqualini, E. (1981). Cone resistance of a medium dry sand. 10th Int. Conf. Soil Mech. Fdn. Engng., Stockholm 2, 427-432.

Baligh, M.M. (1985). Strain path method. J. Geotech. Engng. Div. Am. Soc. Civ. Engrs 111, GT9, 1108-1136.

Baligh, M.M. (1986). Undrained deep penetration, I: shear stresses (and) II: pore pressures. Geotechnique 36(4), 471-502.

Bishop, R.F., Hill, R. and Mott, N.F. (1945). The theory of indentation and hardness tests. Proc. Phys. Soc. 57(3), 147-159.

Bjerrum, L (1973). Geotechnical problems involved in foundations of structures in the North Sea. Geotechnique 23(3), 319-358.

Bond, A.J. (1989). Behaviour of displacement piles in overconsolidated clays. PhD thesis, Imperial College, University of London.

Briaud, J.L., Smith, T.D. and Tucker, L.M. (1985). A pressuremeter method for laterally loaded piles. Proc. 11th Int. Conf. Soil Mechs. Fdn. Engng., San Francisco, 1353-1356.

British Steel Corporation (1978). A review of the underground corrosion of steel piling. Report No. T/CS/1114/1/78/C, June 1978.

British Steel Corporation (1979). The corrosion and protection of steel piling. Report No. T/CS/1115/1/79/C, November 1979.

British Steel Corporation (1987). Coating of steel piling products. Report No. BSC S 810 2,87.

Broms, B.B. (1964). Lateral resistance of piles in cohesive soils. J. Soil Mech. Fdns. Div. Am. Soc. Civ. Engrs. 90, SM2, 27-63.

Bruce, D.A. and Jewell, R.A. (1986). Soil nailing: application and practice. Ground Engineering, Part I: 19(8), Part II: 20(1).

Burgoyne, C.J. and Aul, M. (1987). Prestressed beams lifting off elastic supports. The Structural Engineer, 65B(2).

Burland, J.B. (1973). Shaft friction of piles in clay - a simple fundamental approach. Ground Engineering 6(3), 30-42.

Burland, J.B. (1988). Improvements in and relating to piles and anchorages. UK Patent GB 2170847B; US Patent 4, 768,900; European Patent 0 179 836.

Burland, J.B. (1987). Personal communication.

Bustamante, M. (1982). The pile loading test. Presses de l'ecole nationale des Ponts et Chaussees, 1982.

Bustamante, M. and Combarieu, O. (1977). Bearing capacity of piles driven in weathered chalk. Int. Symp. on the geotechnics of structurally complex formations, Capri, 1977.

Butterfield, D. and Bannerjee, P.K. (1970). The effect of pore water pressures on the ultimate bearing capacity of driven piles. Proc. 2nd S.E. Asian Conf. Soil Engng., Bangkok, 385-394.

Carter, J.P., Booker, J.R. and Yeung, S.K. (1986). Cavity expansion in cohesive frictional soils. Geotechnique 36(3), 349-358

Celestino, T.B. and Mitchell, J.K. (1983). Behaviour of carbonate sands for foundations of offshore structures. Proc. Brazil Offshore '83, Rio de Janeiro, 85-102.

Chan, S.F. and Hanna, T.H. (1980). Repeated loading on single piles in sand. J. Geotech. Engng. Div. Am. Soc. Civ. Engrs. 106, GT2, 171-188.

Chandler, R.J. (1984). Recent European experience of landslides in over-consolidated clays and soft rocks. State of the Art Report, 4th Int. Symp. on landslides, Toronto.

Chandler, R.J. and Martins, J.P. (1982). An experimental study of skin friction around piles. Geotechnique 32(2), 119-132.

Clarke, B.G., Carter, J.P. and Wroth, C.P. (1979). In situ determination of the consolidation characteristics of saturated clays. Proc. 7th Eur. Conf. Soil Mech. 2, 207-213.

Clayton, C.R.I. (1983). The influence of diagenesis on some index properties of chalk in England. Geotechnique 33(3),225-241.

Clayton, C.R.I. (1989). The Mechanical Properties of the Chalk. Keynote Address: Int. Chalk Symposium, Brighton (To be published)

Ebelhar, R.J., Young, A.G. and Stieben, G.P. (1988). Cone penetrometer and conductor pullout tests in carbonate soils offshore Africa. Engineering for calcareous sediments, Proc. Int. Conf. Calcareous Sediments, Perth, Balkema, 1988, 155-163.

Ellis, L.G. (1965). Discussion. Proc. Symp. on Chalk in earthworks and foundations, ICE, London, 60-67.

Fahey, M. (1988a). The response of calcareous soil in static and cyclic triaxial tests. Engineering for calcareous sediments, Proc. Int. Conf. Calcareous Sediments, Perth, Balkema, 1988, 61-68.

Fahey, M. (1988b). Self-boring pressuremeter testing in calcareous soil. Engineering for calcareous sediments, Proc. Int. Conf. Calcareous Sediments, Perth, Balkema, 1988, 165-172.

Fitch, T.R. (1986). Field testing of Burland mini wedge-piles. MSc dissertation, Imperial College, University of London.

Fookes, P.G. (1988). The geology of carbonate soils and rocks and their engineering characterisation and description. Engineering for calcareous sediments, Proc. Int. Conf. Calcareous Sediments, Perth, Balkema, 1988, 787-806.

French, D.J. (1984). Tests on model wedge-piles in sand. MSc dissertation, Imperial College, University of London.

Fryett, J.W.P. (1976). Discussion. Piles in Weak Rock, ICE, London, 1977, 193-196.

Gibson, R.E. (1950). Correspondence. J. Instn. Civ. Engrs. 34, 382-383.

Gibson, R.E. and Anderson, W.F. (1961). In situ measurement of soil properties with the pressuremeter. Civ. Engng. Publ. Wks. Rev. 56, 615-618.

Gibson, R.E. and Henkel, D.J. (1954). Influence of duration of tests at a constant rate of strain on measured 'drained' strength. Geotechnique 4(1), 6-15.

Hanna, T.H. (1963). Model studies of foundation groups in sand. Geotechnique 13.

Head, K. (1982). Manual of soil laboratory testing, Vol. 2, Pentech, London, 1982.

Hetenyi, M. (1946). Beams on elastic foundation, University of Michigan Press, 1946.

Higginbottom, I.E. (1965). The engineering geology of Chalk. Proc. Symp. on Chalk in earthworks and foundations, ICE, London, 1-13.

Hill, R. (1950). The mathematical theory of plasticity. Oxford University Press, 1950.

Hobbs, N.B. (1976). Behaviour and design of piles in Chalk. Proc. Symp. on piles in weak rock, ICE, London, May 1976, 149-175.

Hobbs, N.B. and Healy, P.R. (1979). Piling in Chalk (full version). DoE/ CIRIA Piling Development Group Report PG12, September 1979.

Hodges, W.G.H. and Pink, S. (1971). The use of penetrometer soundings in the estimation of pile bearing capacity and settlement for driven piles in highly weathered chalk in Portsmouth areas as an alternative to site investigations by borehole sampling and laboratory testing. Proc. Roscoe Mem. Symp., Cambridge University, 707-723.

Houlsby, G.T. and Withers, N.J. (1988). Analysis of the cone pressuremeter test in clay. Geotechnique 38(4), 575-587.

Hughes, J.M.O. and Robertson, P.K. (1985). Full-displacement pressuremeter testing in sand. Can. Geotech. J. 22, 298-307.

Hughes, J.M.O., Wroth, C.P. and Windle, D. (1977). Pressuremeter tests in sands. Geotechnique 27(4), 455-477.

Hull, T.S., Poulos, H.G. and Alehossein, H. (1988). The static behaviour of various calcareous sediments. Engineering for calcareous sediments,

Proc. Int. Conf. Calcareous Sediments, Perth, Balkema, 1988, 87-96.

Hutchinson, J.N. (1971). Field and laboratory studies of a fall in Upper Chalk cliffs at Joss Bay, Isle of Thanet. Proc. Roscoe Mem. Symp., Cambridge University, 692-706.

ISSMFE (1977). Penetration test for use in Europe. Report of sub-committee.

Jardine, R.J. (1985). Investigations of pile soil behaviour, with special reference to the foundations of offshore structures. Ph.D. Thesis, Imperial College, University of London.

Jardine, R.J. and Potts, D.M. (1988). Hutton tension leg platform foundations: prediction of driven pile behaviour. Geotechnique 38(2), 231-252.

Jewell, R.J. and Andrews, D.C. (Editors) (1988). Engineering for Calcareous Sediments, Perth, Balkema, 1988.

Kerisel, J. (1964). Deep foundations basic experimental facts. Conf. Deep Fdns., Mexico 1, 5-44.

Kishida, H. and Uesugi, M. (1987). Tests of the interface between sand and steel in the simple shear apparatus. Geotechnique 37(1), 45-52.

Kolbuszewski, J. (1948). An experimental study of the maximum and minimum porosities of sand. Proc. 2nd Int. Conf. Soil Mech. Fdn. Engng., Rotterdam 1, 158-165.

Ladanyi, B. (1963). Evaluation of pressuremeter tests in granular soils. 2nd Panamerican Conf. Soil Mech. Fdn. Engng 1, 3-20.

Ladanyi, B. (1967). Expansion of cavities in brittle media. Int. J. Rock Mech. Min. Sci. 4, 301-328.

Ladanyi, B. (1972). In-situ determination of undrained stress-strain behaviour of sensitive clays with the pressuremeter. Canad. Geotech. J. 9(3), 313-319.

Legge, N.B. (1988). Analysis, interpretation and application of full displacement pressuremeter data to the wedge-pile concept. MSc dissertation, Imperial College, University of London.

Lemos, L.J.L.L. (1986). The effect of rate on residual strength of soil. Ph.D Thesis, Imperial College, University of London.

Lings, M.L. (1985). The skin friction of driven piles in sand. MSc dissertation, Imperial College, University of London.

Little, J.A. and Atkinson, J.H. (1988). Some geological and engineering characteristics of Lodgement Tills from the Vale of St Albans Hertfordshire. Quart. J. Engng. Geol. 21(2), 183-199.

Lord, J.A. (1976). A comparison of three types of driven cast-in-situ piles in chalk. Geotechnique 26(1), 73-93.

Lord, J.A. (1989). Design and construction in chalk. Keynote address: Int. Chalk Symposium, Brighton (To be published).

Lu, W.T.D. (1988). Effects of grain crushing on axial behaviour of driven piles in calcareous sand. Engineering for calcareous sediments. Proc. Int. Conf. on Calcareous Sediments, Perth, Balkema, 231-238.

Luttenegger, A.J. (1988). Current status of the Marchetti dilatometer test. Proc. 3rd Eur. Symp. on Penetration Testing, Birmingham, 137-155.

Mair, R.J. and Wood, D.M (1987). Pressuremeter testing: methods and interpretation. CIRIA ground engineering report: in-situ testing, Butterworths, Sevenoaks, Kent, 1987.

Mallard, D.J. (1980). Technical note: An examination of piles in upper chalk. Geotechnique 30(3), 295-302

Mallard, D.J and Ballatyne, J.L. (1976). The behaviour of piles in Upper Chalk at Littlebrook 'D' power station. Geotechnique 26(1), 115-132.

Mapplebeck, N.J. (1987). Experiments on the use of wedge anchorages in soil nailing and earth reinforcement. MSc dissertation, Imperial College, University of London.

Marchetti, S. (1980). In-situ tests by flat dilatometer. J. Geotech. Engng. Div. Am. Soc. Civ. Engrs. 2, 255-259.

Marsland, A. (1977). The evaluation of the engineering design parameters for glacial clays. Quart. J. Engng. Geol. 10(1), 1-26.

Marsland, A. (1979). The interpretation of in-situ tests in glacial clays. Proc. Int. Conf. Offshore Site Investigation, Society for Underwater Technology, London, 218-228.

Marsland, A. and Powell, J.J.M. (1979). Evaluating the large-scale properties of glacial clays for foundation design. Proc. 2nd Conf. on Behaviour of Offshore Structures, MIT, I, 193-214.

Marsland, A. and Powell, J.J.M. (1988). Investigation of cone penetration test in British clay carried out by the Building Research Establishment 1960-86. Penetration Testing in the UK, Thomas Telford, London, 1988.

Marsland, A. and Powell, J.J.M. (1989). Field and laboratory investigations of the clay tills at the test bed site at the Building Research Establishment, Garston. To be published.

Marsland, A., Prince, A. and Love, M.A. (1982). The role of soil fabric studies in the evaluation of the engineering parameters of offshore deposits. Proc. 3rd Int. Conf. on the behaviour of offshore structures, MIT, I, 181-202.

Marsland, A. and Randolph, M.F. (1977). Comparisons of the results from pressuremeter tests and large in situ plate tests in London clay. Geotechnique 27(2), 217-243.

Marsland, A. and Quarterman, R.S.T. (1982). Factors affecting the measurement and interpretation of quasi static penetration tests in clays. Proc. 2nd Eur. Symp. on Penetration Testing, Amsterdam, II, 697-702.

Martins, J.P. (1983). Shaft resistance of axially loaded piles in clay. Ph.D thesis, Imperial College, University of London.

Matlock, H. and Reese, L.C. (1961). Generalised solutions for laterally loaded piles. Proc. Am. Soc. Civ. Engrs. 86, SM5, 673-694.

McClelland, B. (1974). Design of deep penetration piles for ocean structures. J. Geotech. Engng. Div. Am. Soc. Civ. Engrs. 100, GT7, 709-747.

McClelland, B. (1988). Calcareous sediments: an engineering enigma. Engineering for calcareous sediments. Proc. Int. Conf. on Calcareous Sediments, Perth, Balkema, 777-784.

Meyerhof, G.G. (1976). Bearing capacity and settlement of pile foundations. J. Soil Mech. Fdn. Div., Am. Soc. Civ. Engrs. 102, GT3, 197-228.

Morrison, M.J., McIntyre, P.D., Sauls, D.P. and Oosthuizen, M. (1988). Laboratory tests for carbonate soils from offshore Africa. Engineering for calcareous sediments. Proc. Int. Conf. on Calcareou Sediments, Perth, Balkema, 109-118.

Mueller, J.L. (1988). Burland Wedge-Pile: suitablility for offshore installations and loading conditions. Conoco interoffice communication.

Noorany, I. (1985). Side friction of piles in calcareous sands. Proc. 11th Int. Conf. on Soil Mech. Fdn. Engng., San Francisco 3, 1611-1614.

Ove Arup and Partners (1986). Comparison of British and Norwegian research on the behaviour of piles as anchors for buoyant structures. Department of Energy Offshore Technology Report, OTH 86 218, HMSO, London, 1986.

Palmer, A.C. (1972). Undrained plane-strain expansion of a cylindrical cavity in clay: a simple interpretation of the pressuremeter test. Geotechnique 22(3), 451-457.

Palmer, D.J. (1965). Discussion. Proc. Symp. on Chalk in earthworks and foundations, London, 67-69.

Pavlovic, M.N. and Tsikkos, S. (1982). Beams on quasi-winkler foundations. Engng. Struct., 4.

Potts, D.M. and Martins, J.P. (1982). The shaft resistance of axially loaded piles in clay. Geotechnique 32(4), 369-386.

Poulos, H.G. (1989). Pile behaviour - theory and practice. Geotechnique 39(3), 365-415.

Poulos, H.G. and Chan, K.F. (1988). Tests on model instrumented piles in calcareous soil. Engineering for calcareous sediments. Proc. Int. Conf. on Calcareous Sediments, Perth, Balkema, 245-254.

Powell, J.J.M. (1988). Personal communication.

Powell, J.J.M. (1989). Personal communication.

Powell, J.J.M. and Uglow, I.M. (1985). A comparison of Menard, self-

boring, and push-in pressuremeter tests in a stiff clay till. Proc. Conf. on Advances in Underwater Technology and Offshore Engineering, London, 1985, Vol. 3, Offshore Site Investigation, 201-217.

Powell, J.J.M. and Uglow, I.M. (1986). Dilatometer testing in stiff overconsolidated clays. 39th Canadian Geotech. Conf. on In-situ testing and field behaviour, Carleton University, Ottawa, 317-326.

Powell, J.J.M. and Uglow, I.M. (1988a). Marchetti dilatometer testing in UK soils. Proc. 3rd Eur. Symp. on Penetration Testing, ISOPT, Birmingham, 555-562.

Powell, J.J.M. and Uglow, I.M. (1988b). The interpretation of the Marchetti dilatometer test in UK clays. Penetration testing in the UK, Thomas Telford, London, 1988.

Power, P.T. (1982). The use of the electric cone penetrometer in the determination of the engineering properties of chalk. Proc. 2nd Eur. Symp. on Penetration Testing, Amsterdam, 1982, 769-774.

Randolph, M.F. (1988). The axial capacity of deep foundations in calcareous sands. Engineering for calcareous sediments. Proc. Int. Conf. on Calcareous Sediments, Perth, Balkema, 837-858.

Randolph, M.F., Carter, J.P. and Wroth, C.P. (1979). Driven piles in clay - the effects of installation and subsequent consolidation. Geotechnique 29(4), 361-393.

Randolph, M.F. and Houlsby, G.T. (1984). The limiting pressure on a circular pile loaded laterally in cohesive soil. Geotechnique 34(4), 613-623.

Randolph, M.F. and Wroth, C.P. (1979). An analytical solution for consolidation around a driven pile. Int. J. Numer. Anal. Methods in Geomech. 3(3), 217-229.

Randolph, M.F. and Wroth, C.P. (1981). Application of the failure state in undrained simple shear to the shaft capacity in driven piles. Geotechnique 31(1), 143-157.

Randolph, M.F. and Wroth, C.P. (1982). Recent developments in understanding the axial capacity of piles in clay. Ground Engineering 15(7), 17-25

Robinsky, E.I. and Morrison, C.F (1964). Sand displacement and compaction around model friction piles. Can. Geotech. J. 1(2), 81-93.

Scott, R.F. (1981). Foundation Analysis. Prentice-Hall, 1981.

Schmertmann, J.H. (1970). Static cone to compute settlement over sand. J. Soil Mech. Found. Div. Am. Soc. Civ. Engrs. 96, SM3, 1011-1043.

Skempton, A.W. (1959). Cast in-situ bored piles in London Clay. Geotechnique 9(4), 153-173.

Smith, I.M. (1980). A survey of numerical methods in offshore piling. Proc. Conf. on Numerical Methods in Offshore Piling, ICE, London, 1980, 1-8.

Soderburg, L.O. (1962). Consolidation theory applied to foundation pile time effects. Geotechnique 12(3), 217-225.

Sullivan, W.R., Reese, L.C. and Fenske, C.W. (1980). Unified method for analysis of laterally loaded piles in clay. Numerical methods in offshore piling, ICE, London, 1980, 135-146.

Szechy, C. (1961). The effects of vibration and driving upon the voids in granular soils surrounding a pile. Proc. 5th Int. Conf. Soil Mech. Fdn. Engng. 2, 161-164.

Teh, C.I. (1987). An analytical study of the cone penetration test. DPhil thesis, University of Oxford.

Tika, T. (1989). The effect of rate of shear on the residual strength of soil. PhD thesis, Imperial College, University of London.

Tomlinson, M.J. (1970). Adhesion of piles in stiff clays. CIRIA report 26, November 1970.

Tomlinson, M.J. (1976). Preface to Proc. Conf. on Piles in weak rock. Geotechnique 26(1), 1-4.

Tomlinson, M.J. (1977). Pile design and construction practice. Viewpoint Publication (Cement and Concrete Association), 1977.

Tomlinson, M.J. (1980). Foundation design and construction, 4th edn., London, Pitman, 1980.

Urquhart, L. C. (1940). Civil Engineering Handbook. McGraw-Hill, 1940.

de Vahl Davis, G. (1986). Numerical methods in engineering and science, Allen and Unwin, 1986.

Vesic, A.S. (1967). A study of bearing capacity of deep foundations. Project B-189 (final report), Georgia Institute of Technology, Atlanta, Georgia.

Vesic, A.S. (1972). Expansion of cavities in infinite soil mass. J. Soil Mech. Fdns. Div. Am. Soc. Civ. Engrs. 98, SM3, 265-290.

Vijayvergiya, V.N., Cheng, A.P. and Kolk, H.J. (1977). Effect of soil set up on pile drivability in chalk. J. Geotech. Engng. Div. Am. Soc. Civ. Engrs. 103, GT8, 908-913.

Vijayvergiya, V.N., Cheng, A.P. and Kolk, H.J. (1978). Design and installation of piles in chalk. Ground Engineering 11(2).

Walker, B.P. (1964). Experiments on model pile foundations in sand. PhD thesis, Imperial College, University of London.

Ward, W.H., Burland, J.B. and Gallois, R.W. (1968). Geotechnical assessment of a site at Mundford, Norfolk, for a proton accelerator. Geotechnique 18(4), 399-341.

Weltman, A.J. (1980). Pile load testing procedures. DoE/CIRIA Piling Development Group Report PG7, March 1980.

Weltman, A.J. and Little, J.A. (1977). A review of bearing pile types.

DoE/CIRIA Piling Development Group Report PG1, January 1977.

Whitaker, T. (1963). The constant rate of penetration test for the determination of the ultimate bearing capacity of a pile. Proc. Instn. Civ. Engrs. 26, 119-123.

Withers, N.J., Howie, J., Hughes, J.M.O. and Robertson, P.K. (1989). Performance and analysis of cone pressuremeter tests in sands. Geotechnique 39(3), 433-454.

Withers, N.J., Schaap, L.H.J. and Dalton C.P. (1986). The development of the full displacement pressuremeter. Proc. 2nd Int. Symp. The Pressuremeter and Its Marine Applications. ASCE Special Technical Publication 950, 38-56.

Wroth, C.P. (1984). The interpretation of in-situ soil tests. Geotechnique 34(4), 449-489.

Wroth, C.P., Carter, J.P. and Randolph, M.F. (1979). Stress changes around a pile driven into cohesive soil. Recent developments in the design and construction of piles, ICE, London, 1980, 345-354.

Young, R.H. (1988). Tests on large displacement wedge-pile models in sand. MSc dissertation, Imperial College, University of London.

APPENDICES

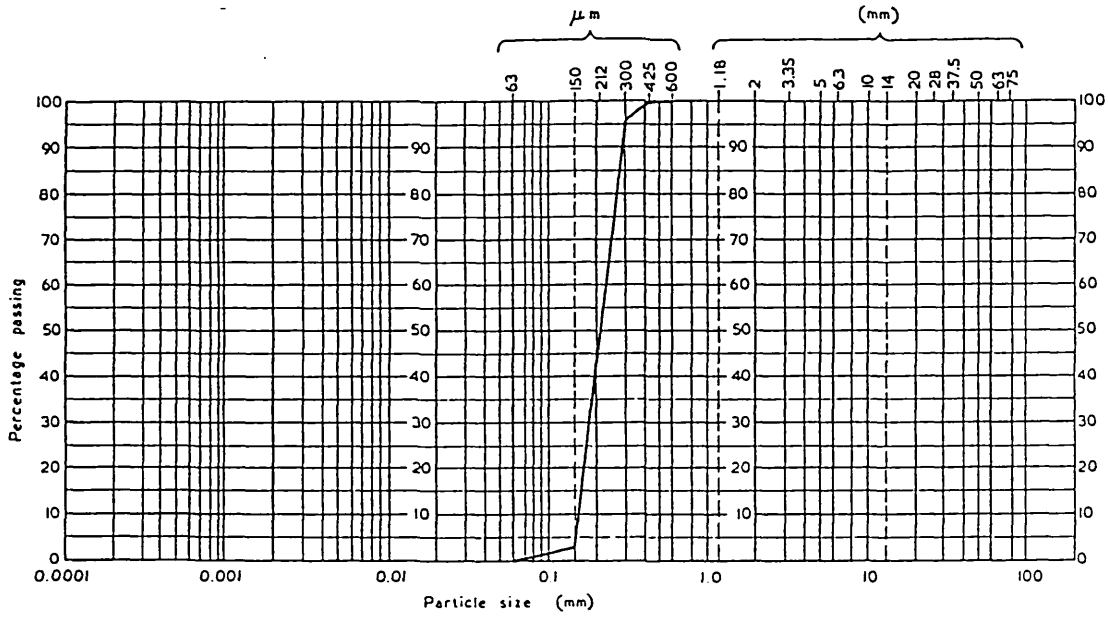

D52/100 nominal grading, supplied by David Ball Company, Cambridge
G_s = 2.66, e_{max}= 0.99, e_{min} = 0.71

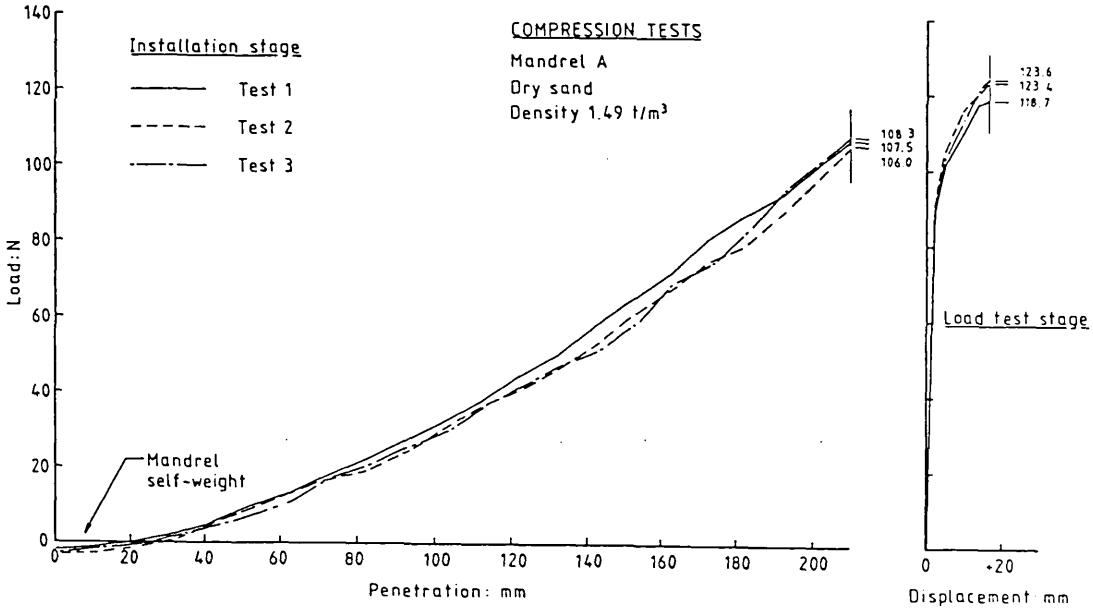

Tests to demonstrate reproducibility of sand density

Appendix 2.1 Laboratory model tests: details of sand used for tests

PH5 ATLAS COPCO Double Acting Air Hammer

(lightweight range)

Introduction

Atlas Copco double-acting sheeting driver type PH5 weighs 390 kg (860 lbs) and has an impact rate of 310 blows per minute. It is recommended for plank and light steel sheeting. Below is an example of a portable arrangement.

Sheeting driver PH5 is also provided with bolt holes to be used for guides and attachments. The spacing of the holes along the sides and in the head is given below.
Dimensions in mm.

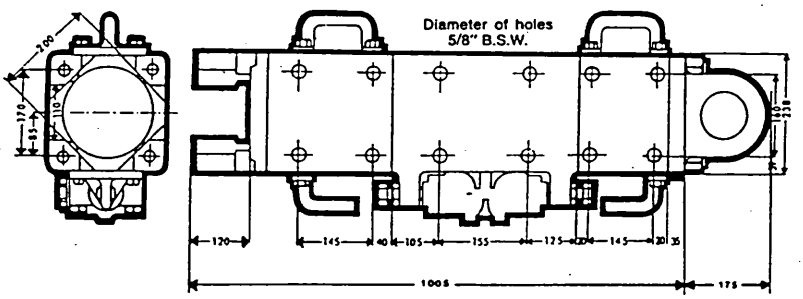

Type	Air consumption at 6 kg/cm² (85 psi)		Piston diameter		Length of stroke		Blows per minute	Maximum thickness of pile		Maximum thickness of sheeting		overall length		net weight		Hose
	m³/min	cfm	mm	in	mm	in		mm	in	mm	in	mm	in	kg	lb	nipple
PH5	2.6	92	150	529/32	190	7 1/2	310	200	8	110	4 3/8	1,180	46 1/2	390	860	3/4"

WATSON and HILLHOUSE (PLANT HIRE) LTD.

Whitehouse Road, Ipswich IP1 5NT, Suffolk
Tel: Ipswich (0473) 48652-5 Telex 988775 G

Northern Depot: North Florida Road, Haydock Industrial Estate, St. Helens, Merseyside WA11 9UB *Tel: Ashton-in-Makerfield (0942) 711501*

Appendix 3.1 Details of piling hammers used at BRS site

N. Series
MkII Double Acting Air Hammers

Models 500N 600N 700N

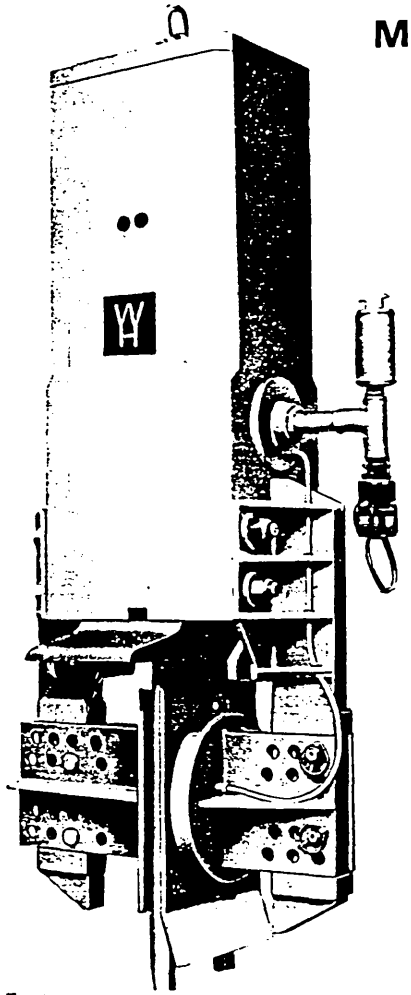

This range of air operated Double Acting Hammers has been designed to operate at maximum efficiency when used with the standard sizes of compressors normally available to contractors. The three sizes of hammer are suitable for driving a wide range of sheet steel and bearing piles of all types.

Their robust design with only two moving parts and a simple lubrication system allows the hammer to be run for long periods, under severe conditions, with the minimum of attention. A new design of pneumatically operated leg grip ensures that the hammer retains a strong grip on the pile allowing the introduction of a patented high pressure bounce chamber at the upper end of the ram stroke, which enables the frequency and energy of the blow to be much increased.

Description
The hammer body is a one piece casting. The ram and valve spool are the only two moving parts in the whole hammer. The ram operates against the anvil block which in turn is in direct contact with the top of the pile. The hammer is designed to drive pairs of piles and the anvil block extends beyond the hammer body to give complete coverage of the pile heads. Alternative anvils can be quickly fitted if it is desired to drive single sheet piles or bearing piles.

Basic Features

Pneumatic grip
A circular diaphragm assembly is an integral part of one insert holder. This is fitted with a pressure operated diaphragm fed by airline direct from the inlet manifold. A pad on the back face of the insert fits into a circular recess in the diaphragm holder. When the hammer is operating air pressure acting on the rubber diaphragm forces the insert outwards to grip the pile firmly. As soon as the air supply is turned off the diaphragm releases, allowing the hammer to be lifted from the pile.

Legs
The hammer legs are bolted directly on to the hammer body. The lower end of the legs are drilled for attachment of the insert holders. Matching holes in the insert holders are staggered to give a wide range of adjustment to suit all types of inserts.

Inserts
Each set of inserts consists of two halves. These are fitted to the insert holders by only two bolts. In many cases several sections of piling can be driven by the same set of inserts by altering the pin positions in the insert holders to widen or close the gap into which the pile fits. Many other sections of piling can be driven by changing one half of the inserts only.

Anvil Blocks
With the **N series** hammers, it is essential that the correct anvil block is used. Generally when driving pairs of piles, a wide anvil block is recommended but a narrow anvil block should be used when driving piles singly. For the 600N an intermediate anvil block is also available for certain sections.

WATSON and HILLHOUSE (PLANT HIRE) LTD.

Whitehouse Road, Ipswich IP1 5NT, Suffolk
Tel: Ipswich (0473) 48652-5 Telex 983775 G

Northern Depot North Florida Road, Haydock Industrial Estate, St. Helens, Merseyside WA11 9UB *Tel: Ashton-in-Makerfield (0942) 711501*

Appendix 3.1 (cont.)

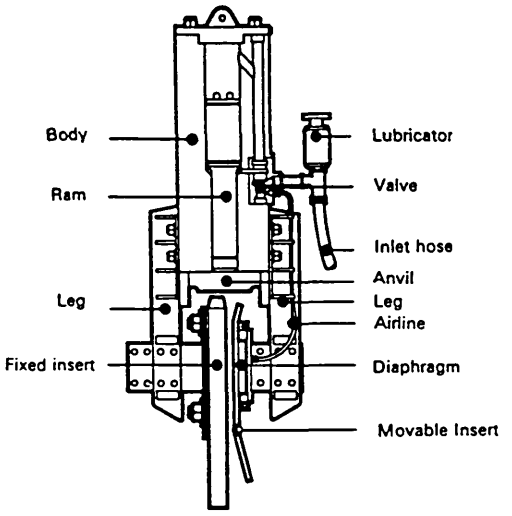

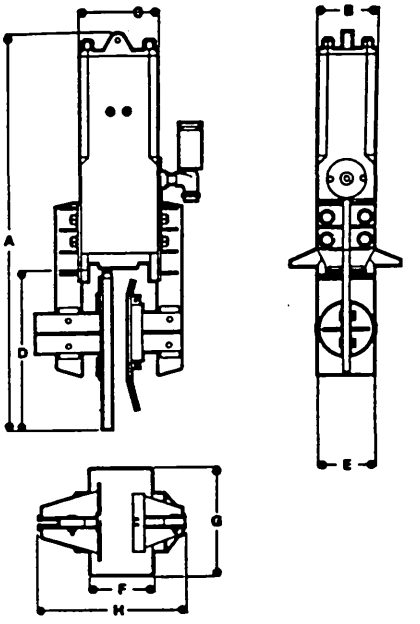

Hammer size	500N		600N		700N	
Weight of ram	90.7 kg	200 lb	227 kg	500 lb	385 kg	850 lb
Stroke of ram	229 mm	9 in.	305 mm	12 in.	330 mm	13 in.
Weight of anvil (wide flat)	104 kg	230 lb	227 kg	500 lb	281 kg	620 lb
Maximum No. of blows/min		330		250		225
Maximum kinetic energy	165 Kgm	1200 lb/ft	415 Kgm	3000 lb/ft	650 Kgm	4700 lb/ft
Size of hose	38 mm	1½ in.	38 mm	1½ in.	51 mm	2 in.
Recommended size of compressor	7.07 m^3/min	250 ft^3/min	10.3 m^3/min	480 ft^3/min	17 m^3/min	600 ft^3/min
Overall weight of hammer complete with legs and inserts and wide flat anvil	1143 kg	2520 lb	2177 kg	4800 lb	3006 kg	6630 lb
Above information based on 6.3 kg/cm^2 (90 lb/in^2) at hammer						
A Overall height to bottom of inserts Frodingham pairs, Larssen singles	1933 mm	76⅛ in.	2273 mm	89½ in.	2419 mm	95¼ in.
A Larssen pairs	1794 mm	70⅝ in.	2184 mm	86 in	2261 mm	89 in
B Width of cylinder	317 mm	12½ in.	356 mm	14 in.	432 mm	17 in
C Depth of cylinder	381 mm	15 in.	508 mm	20 in.	510 mm	24 in.
D Distance of inserts below top of piles Frodingham pairs, Larssen singles	756 mm	29¾ in.	768 mm	30¼ in.	768 mm	30¼ in.
D Larssen pairs	616 mm	24¼ in.	629 mm	24¾ in.	629 mm	24¾ in.
E Diameter of diaphragm assembly	304 mm	12 in.	381 mm	15 in.	381 mm	15 in.
F Width of anvil	229 mm	9 in.	292 mm	11½ in.	356 mm	14 in.
G Length of anvil narrow	359 mm	14⅛ in.	381 mm	15 in.	457 mm	18 in.
G wide	559 mm	22 in.	711 mm	28 in.	711 mm	28 in.
G intermediate	457 mm	18 in.	457 mm	18 in.		
H Maximum over insert holders	896 mm	35¼ in.	1152 mm	45⅜ in.	1397 mm	55 in.

WATSON and HILLHOUSE (PLANT HIRE) LTD.

Appendix 3.1 (cont.)

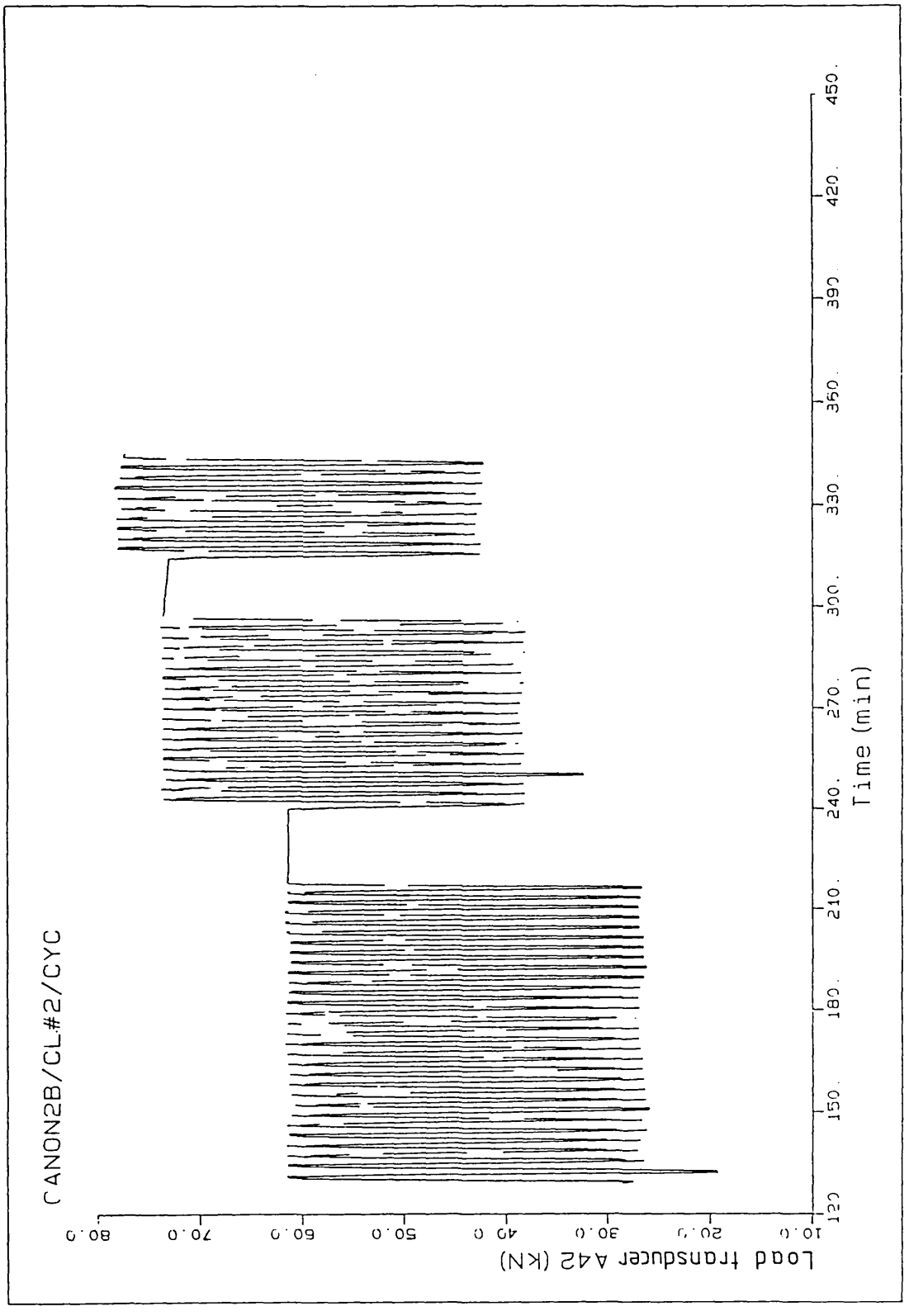

Appendix 3.2 Typical test data from IC instrumented pile (Bond, 1989)

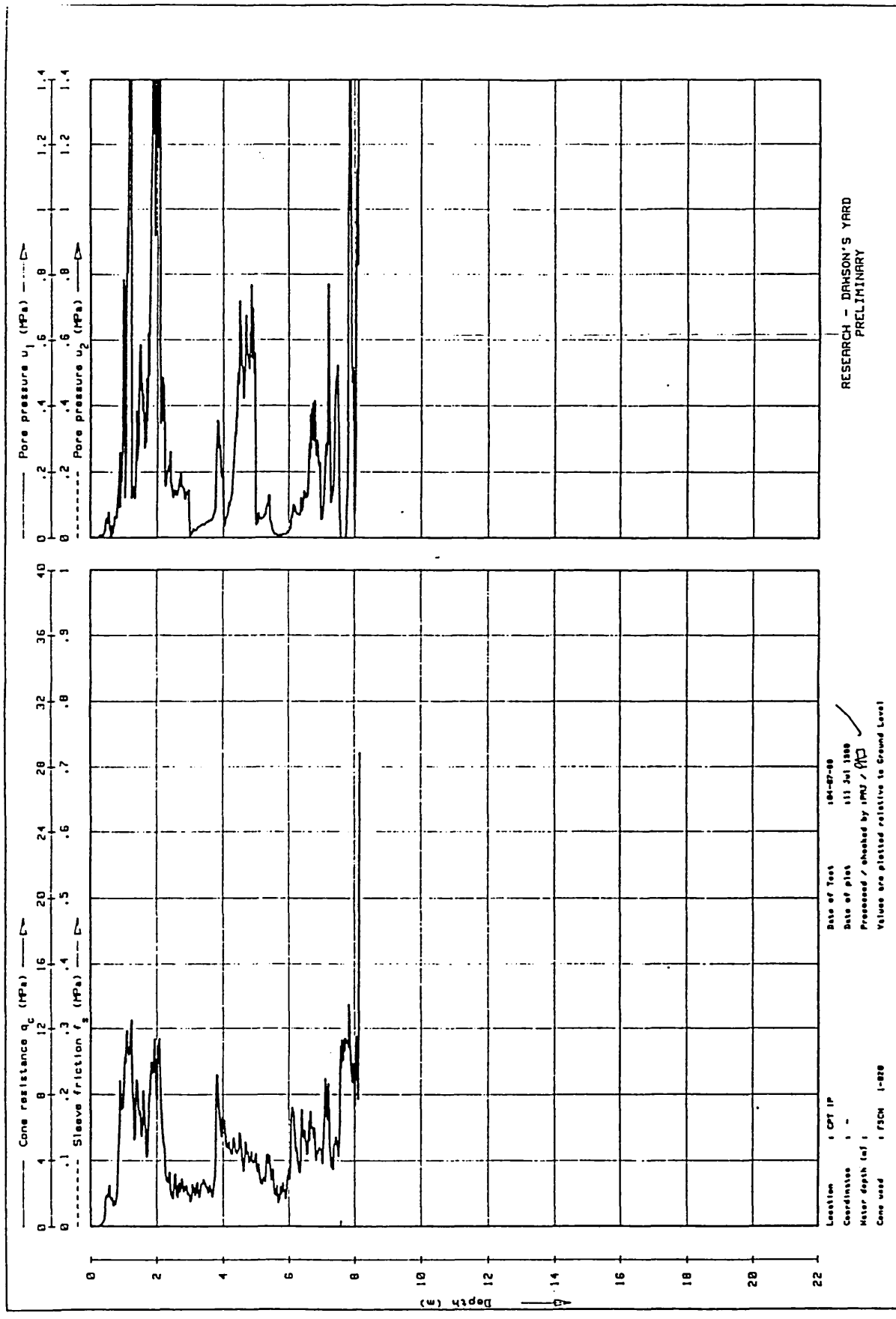

Appendix 4.1 Luton site: results of piezocone test

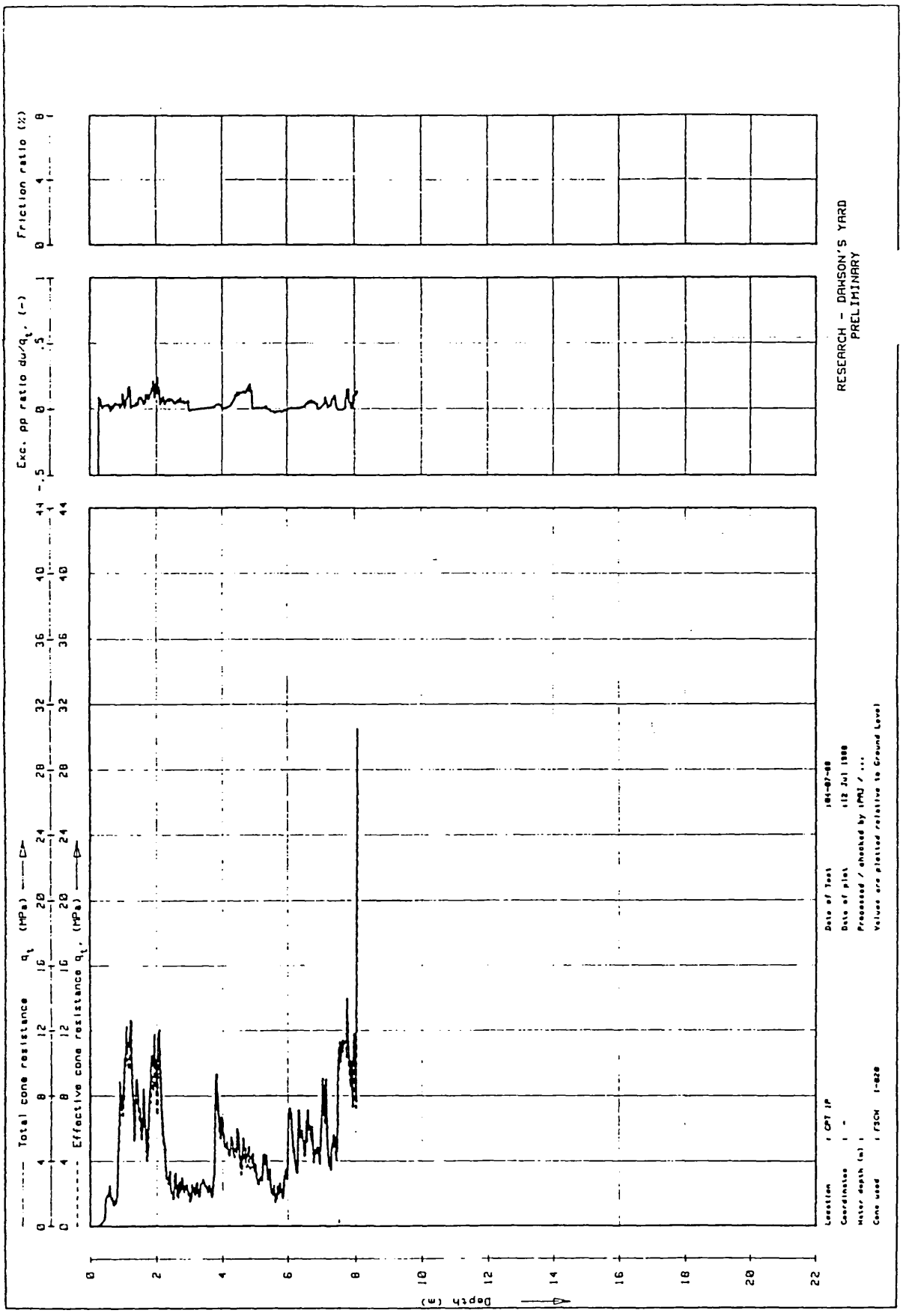

Appendix 4.1 (cont.)

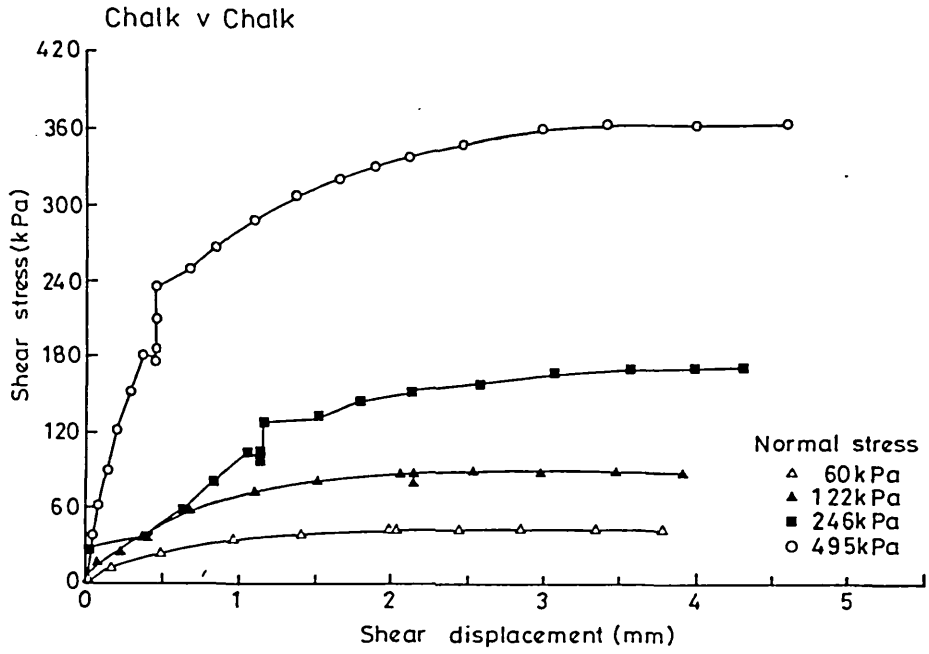

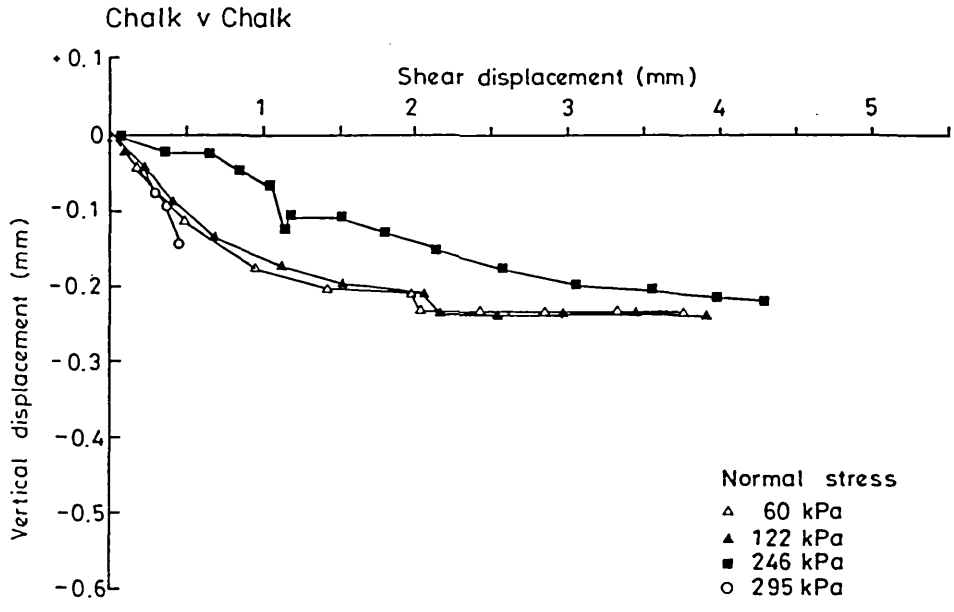

Appendix 4.2 Luton site: shearbox test results

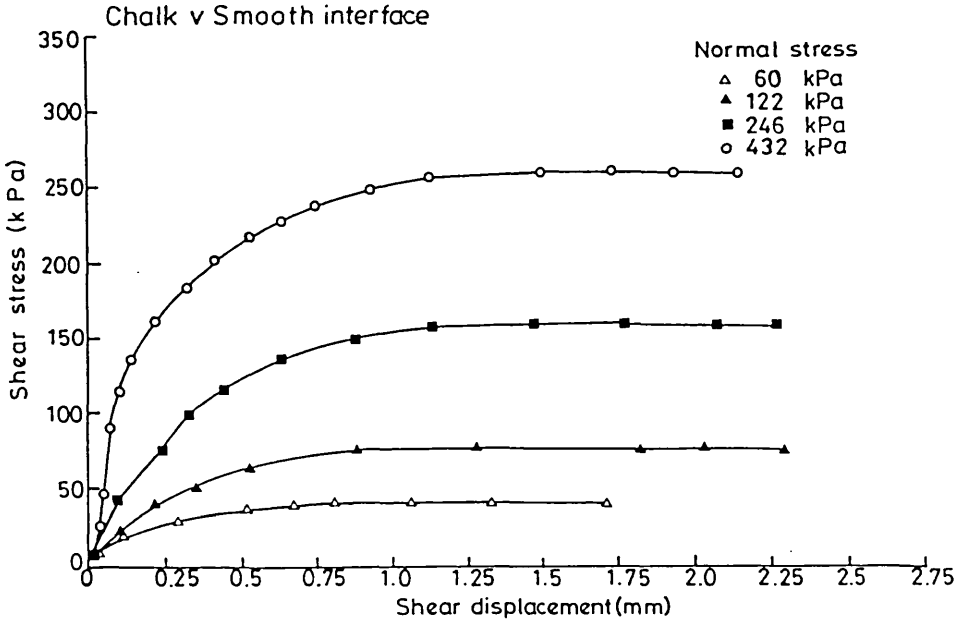

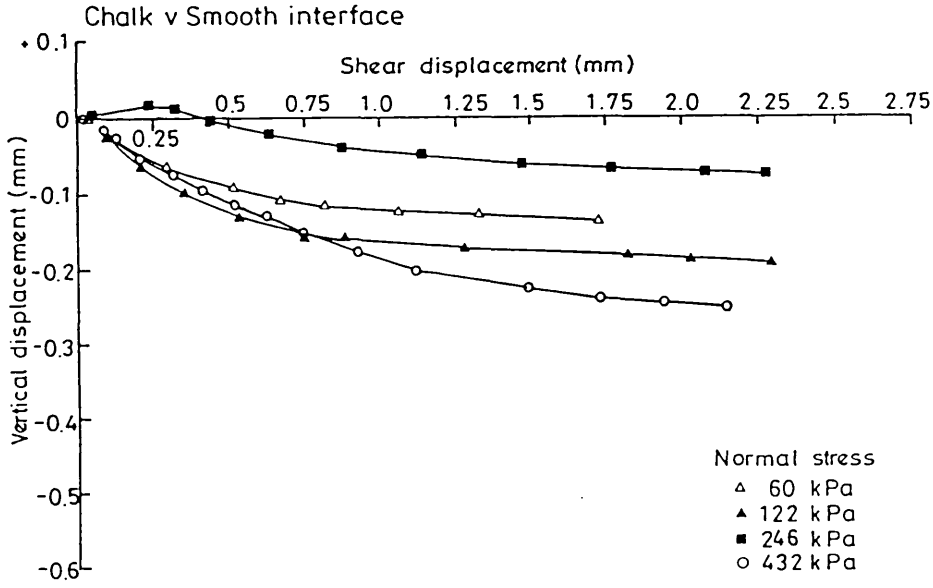

Appendix 4.2 (cont.)

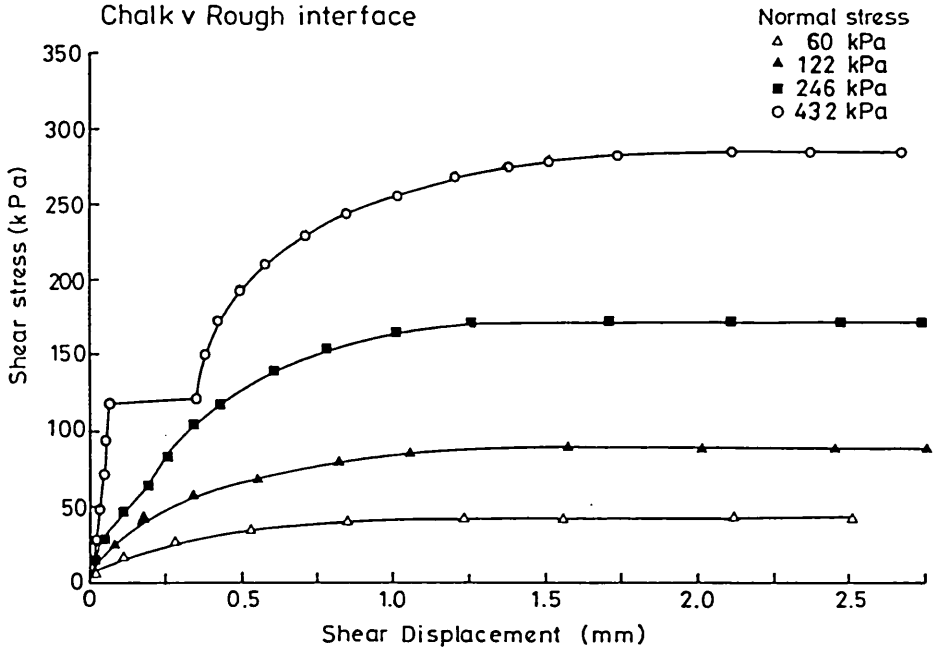

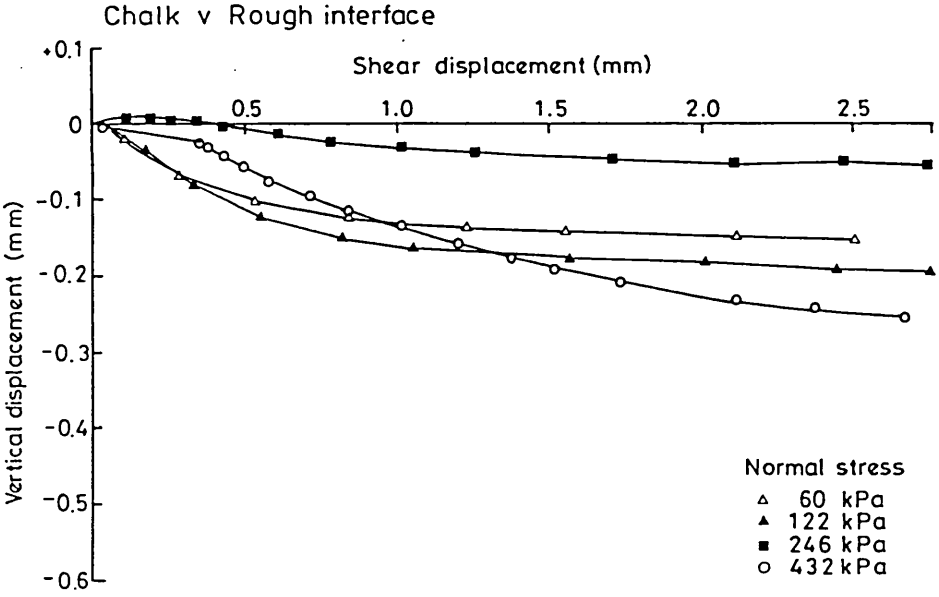

Appendix 4.2 (cont.)

Typical re-load behaviour
Chalk v Chalk 122 kPa

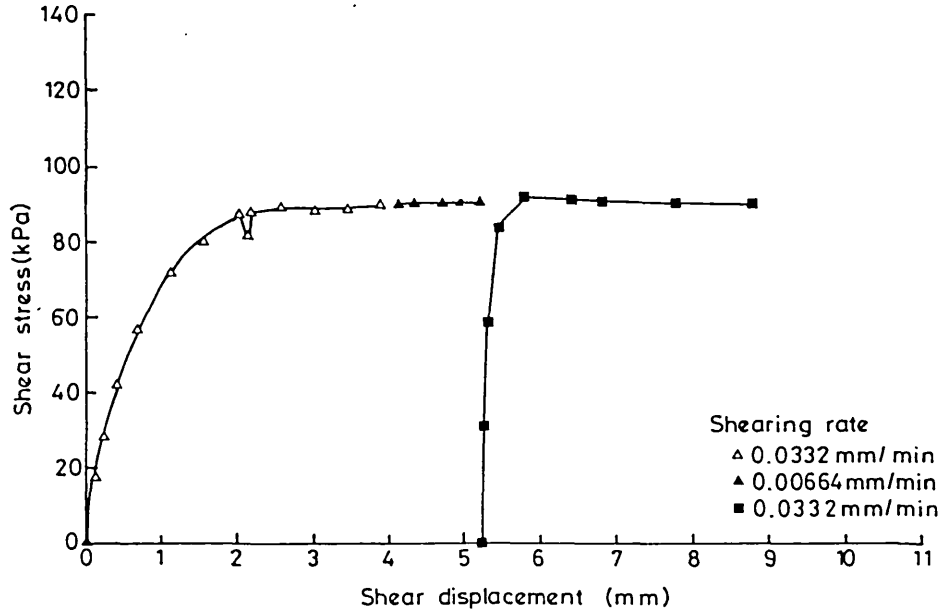

Typical reload behaviour
Chalk v rough interface - 122 kPa normal stress

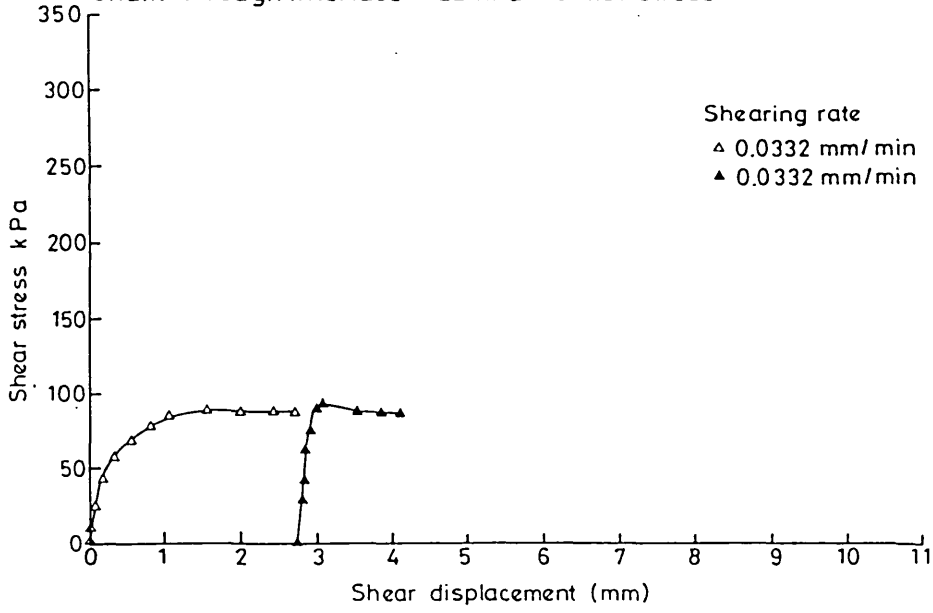

Appendix 4.2 (cont.)

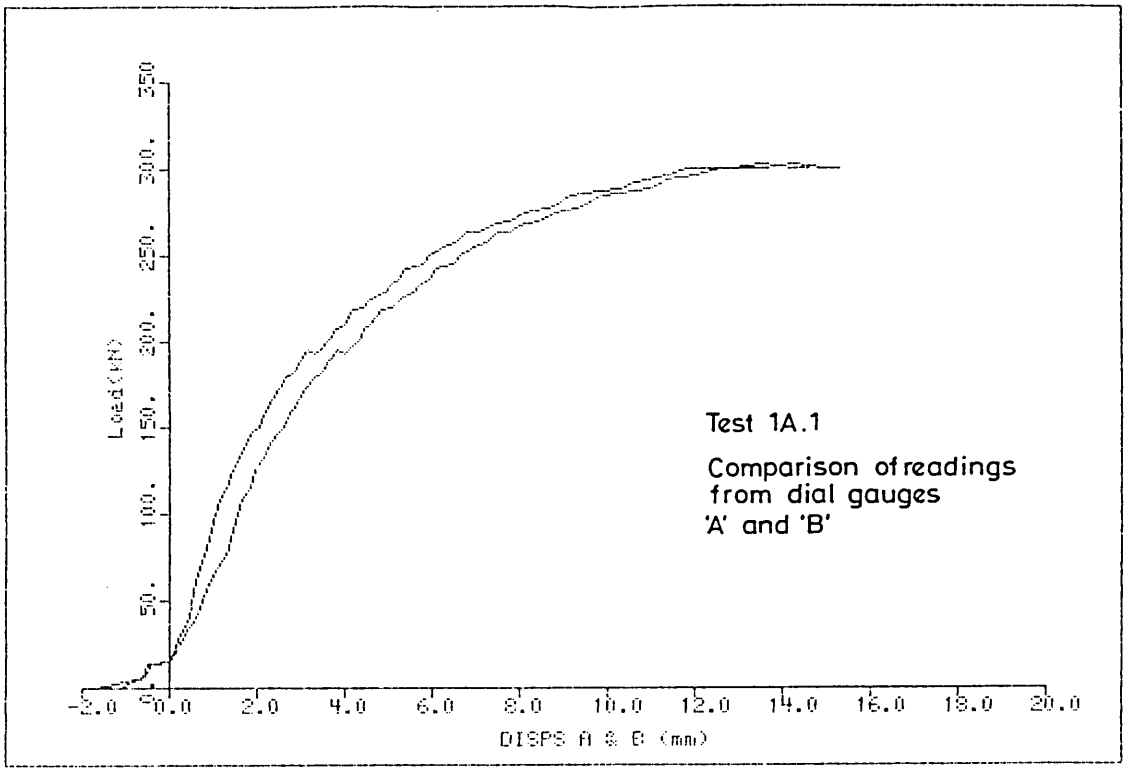

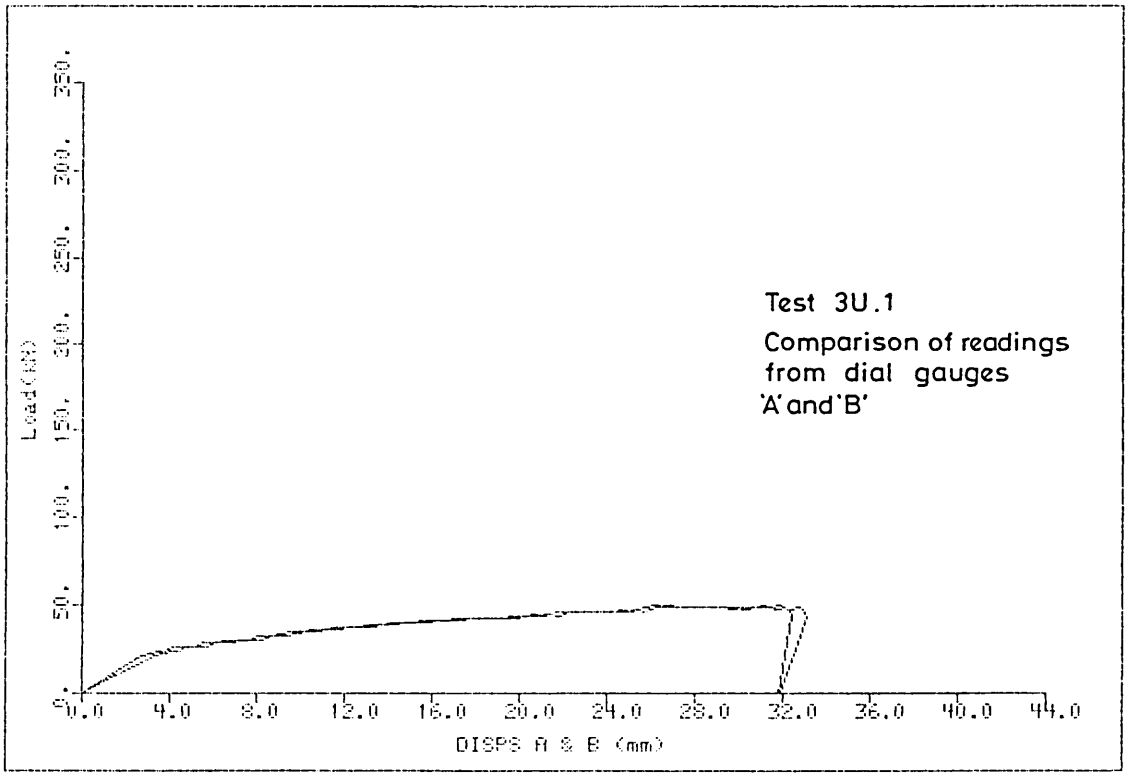

Appendix 4.3 Luton site: typical results from pile tests

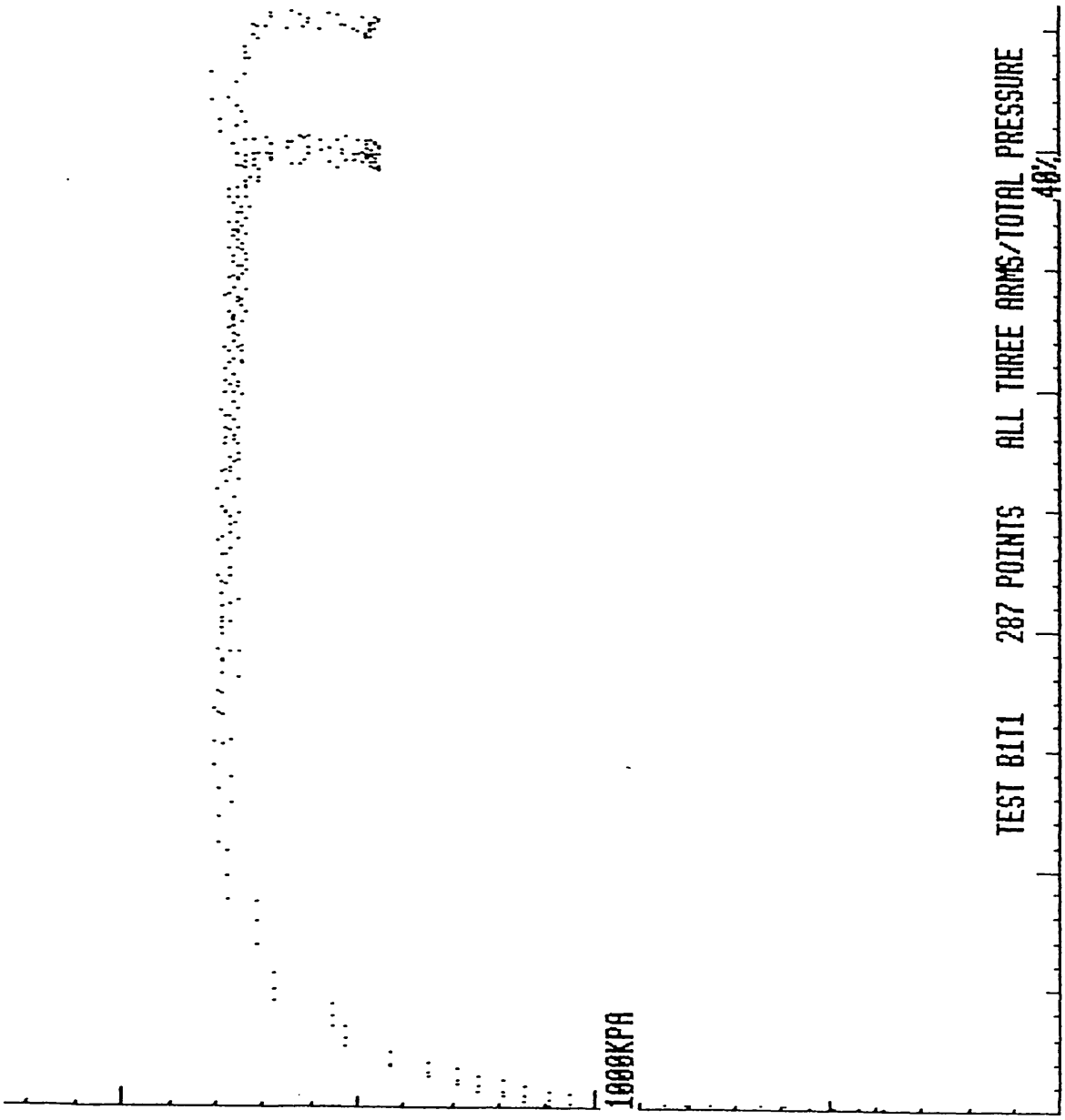

Appendix 5.1 BRS site: data from FDPM Test L1/T1

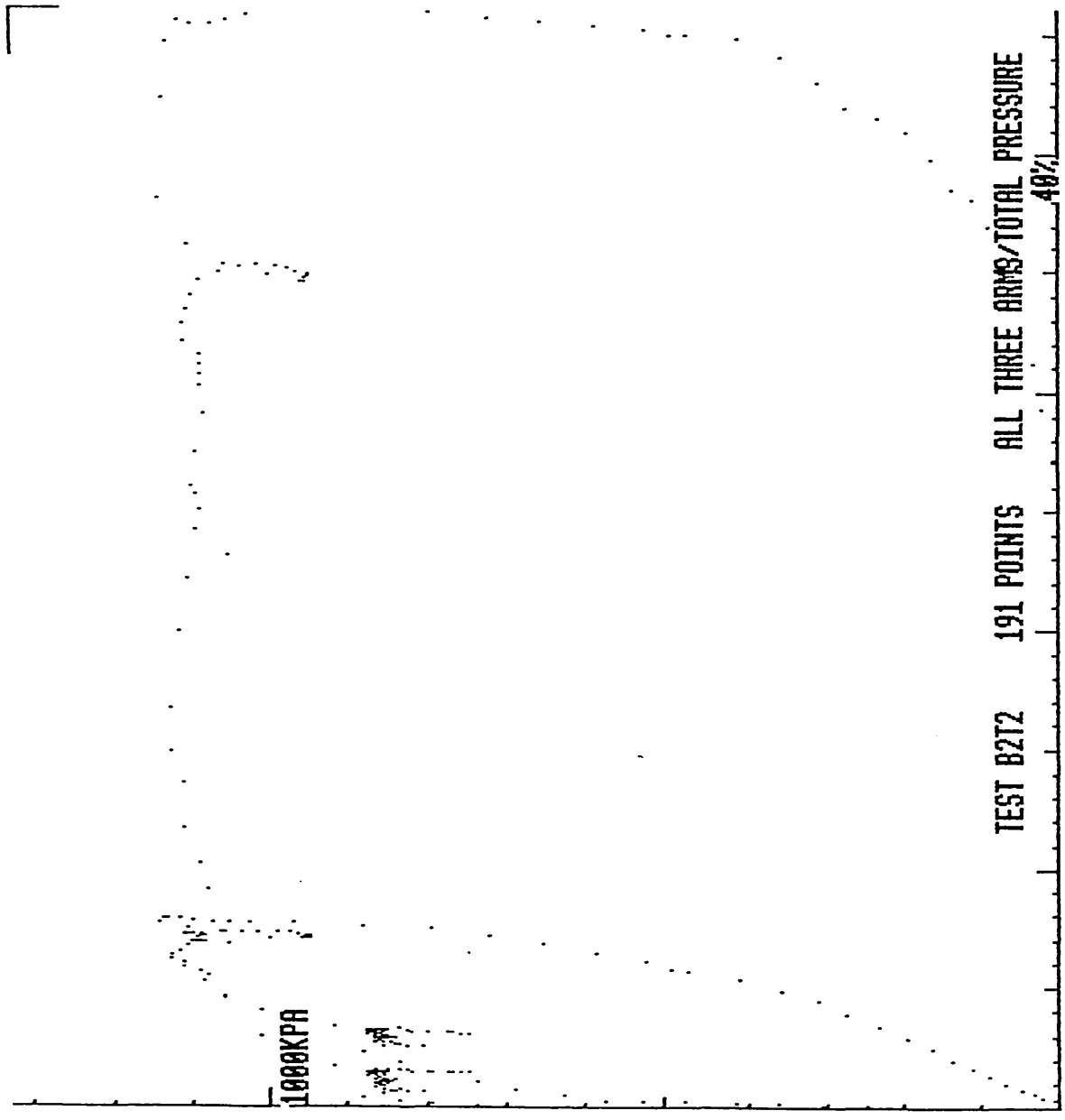

Appendix 5.1 (cont.) BRS site: data from FDPM Test L1/T2

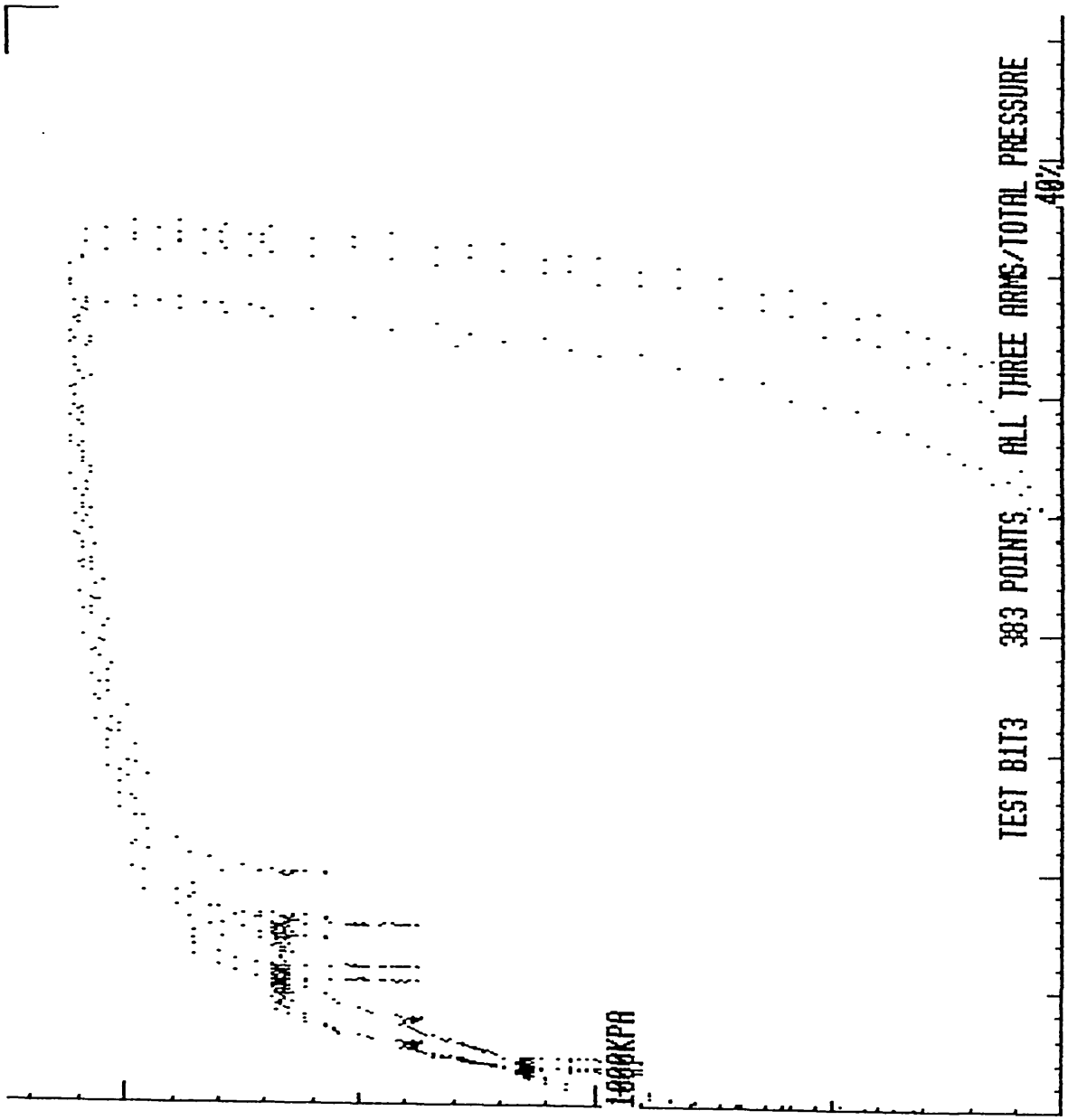

Appendix 5.1 (cont.) BRS site: data from FDPM Test L1/T3

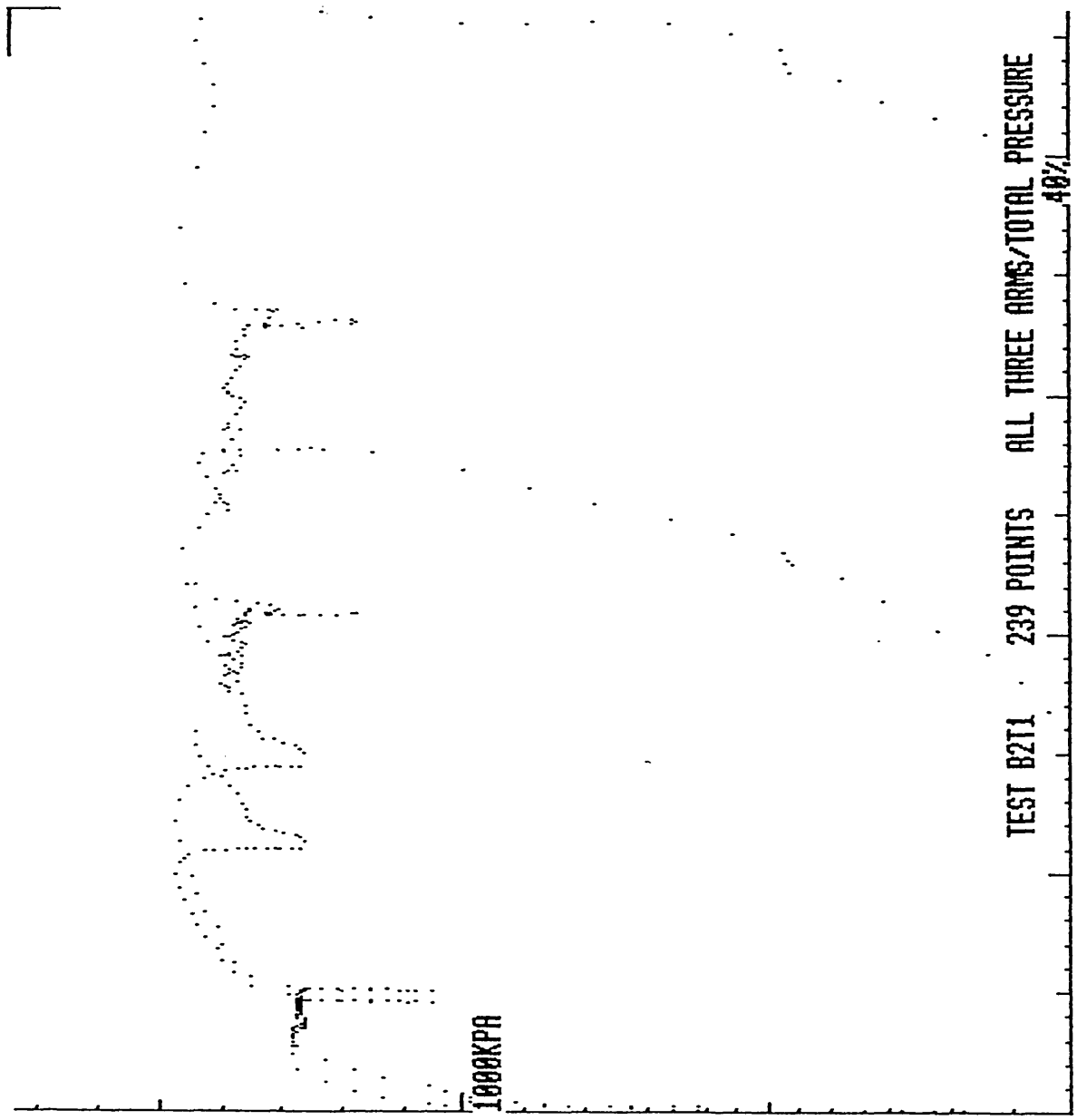

Appendix 5.1 (cont.) BRS site: data from FDPM Test L2/T1

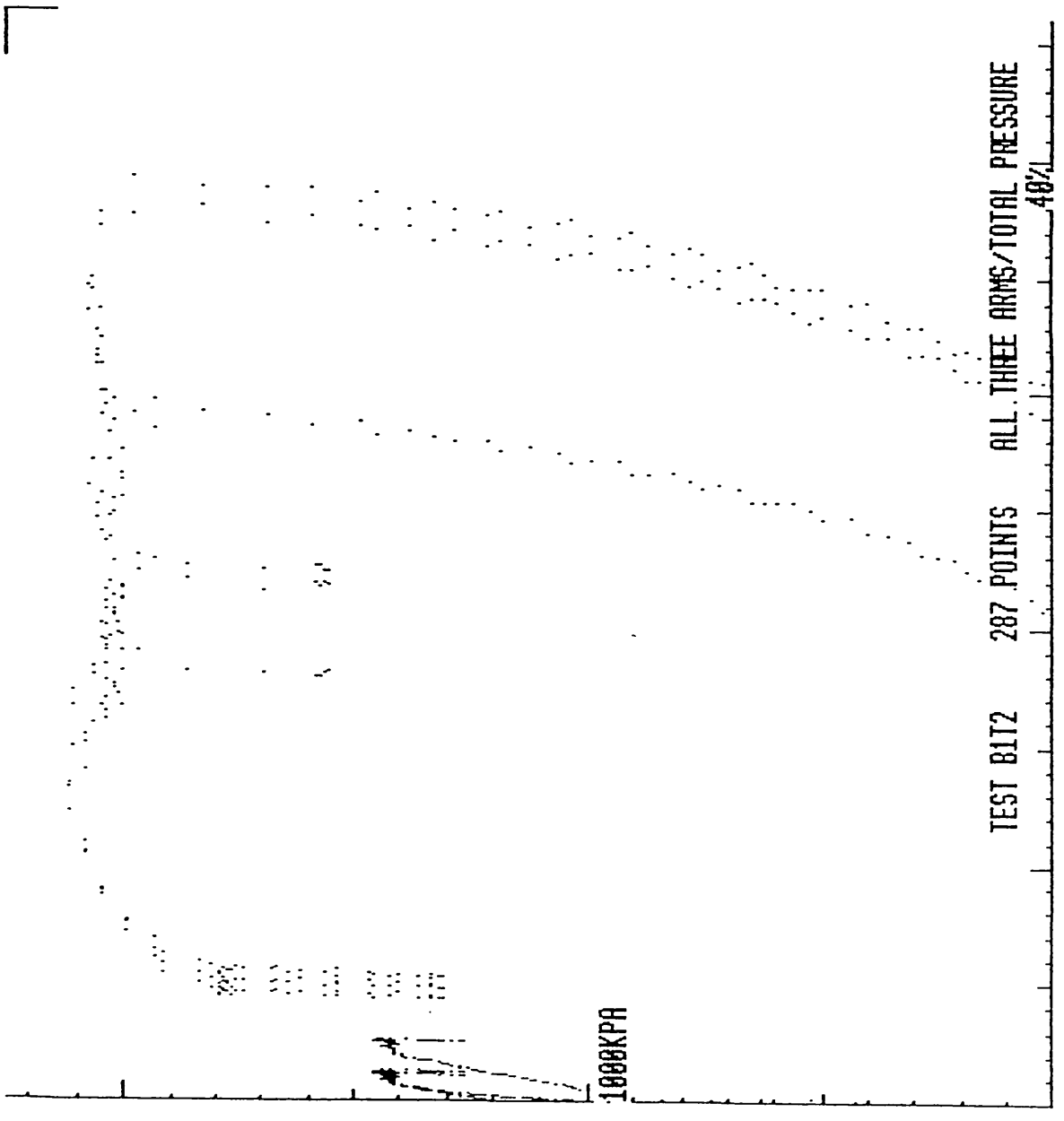

Appendix 5.1 (cont.) BRS site: data from FDPM Test L2/T2

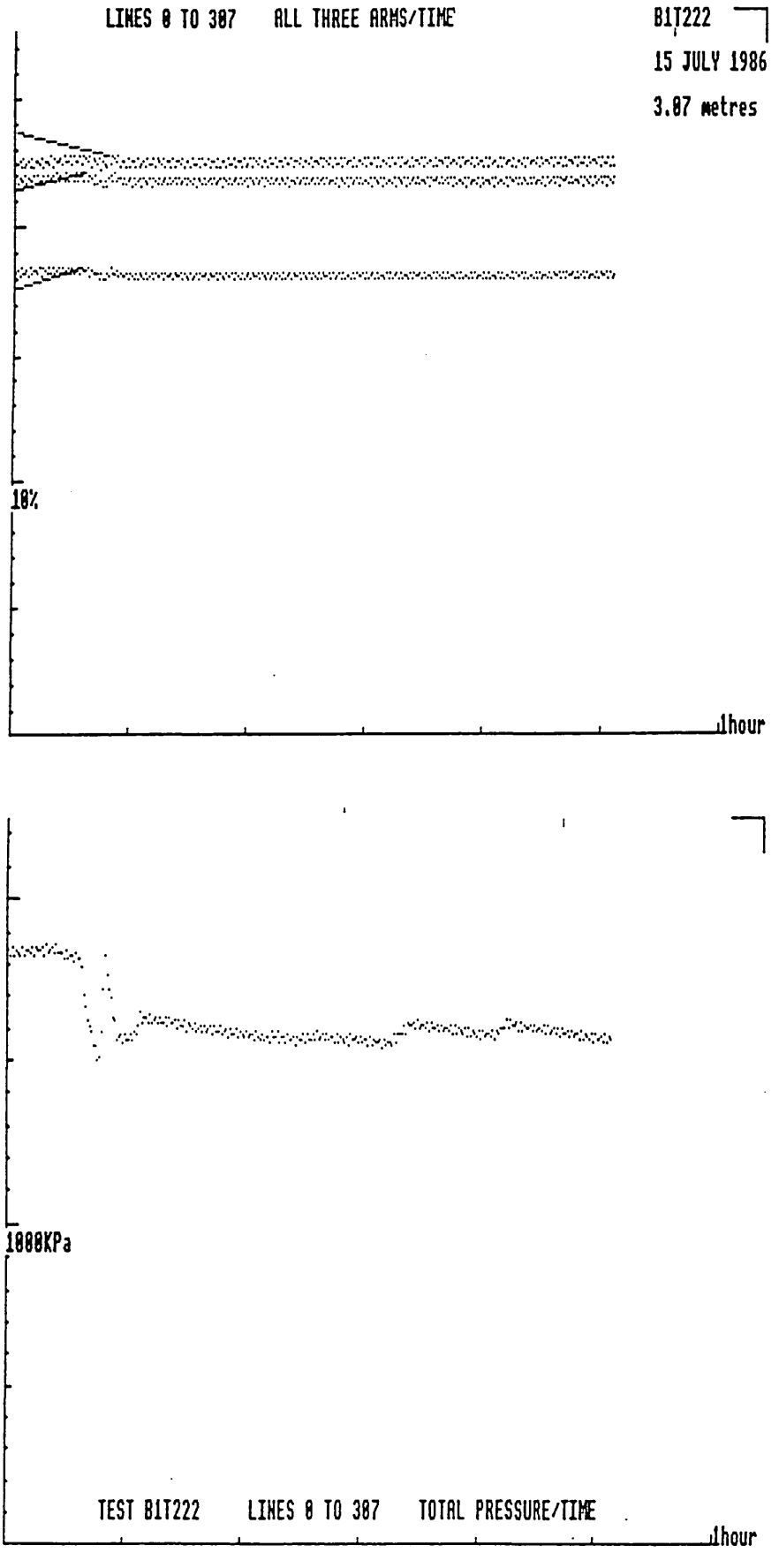

Appendix 5.1 (cont.) BRS site: FDPM Test L1/T2 holding data

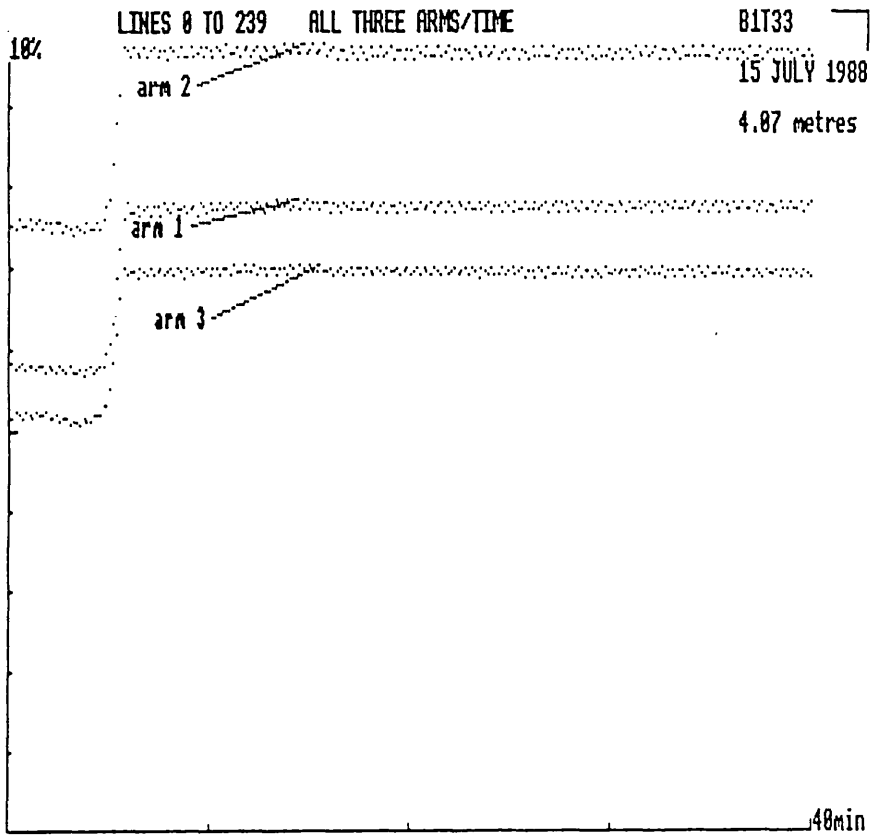

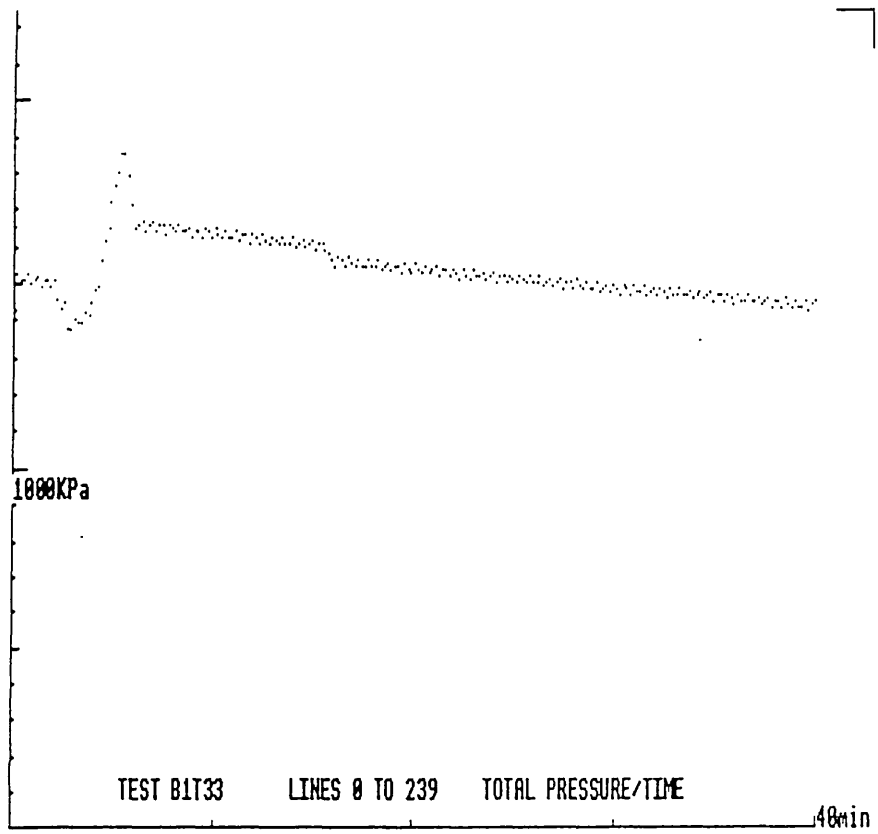

Appendix 5.1 (cont.) BRS site: FDPM Test L1/T3 holding data

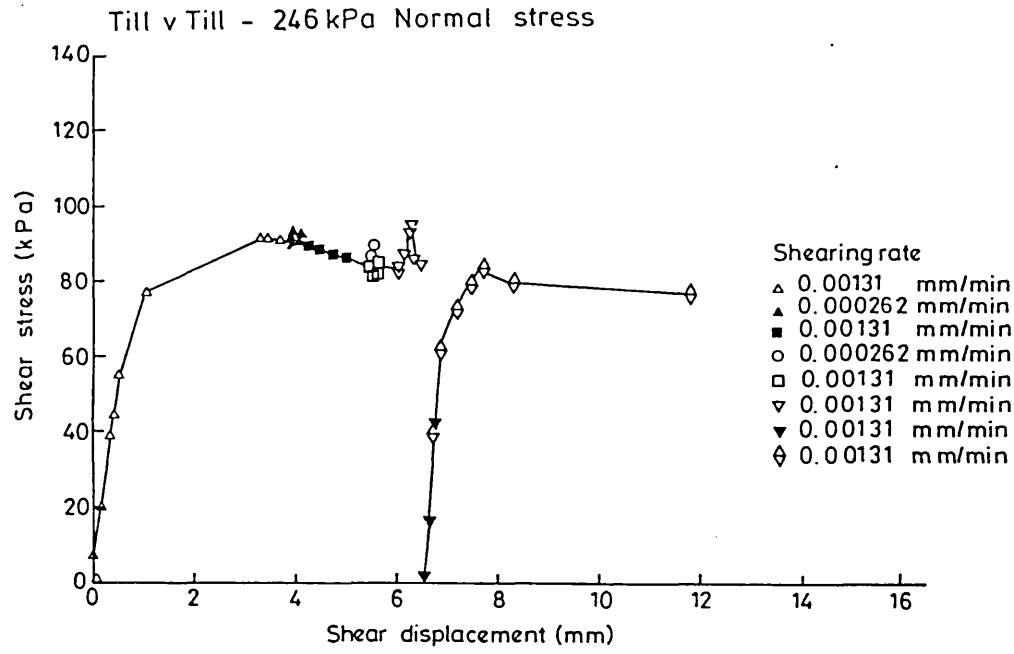

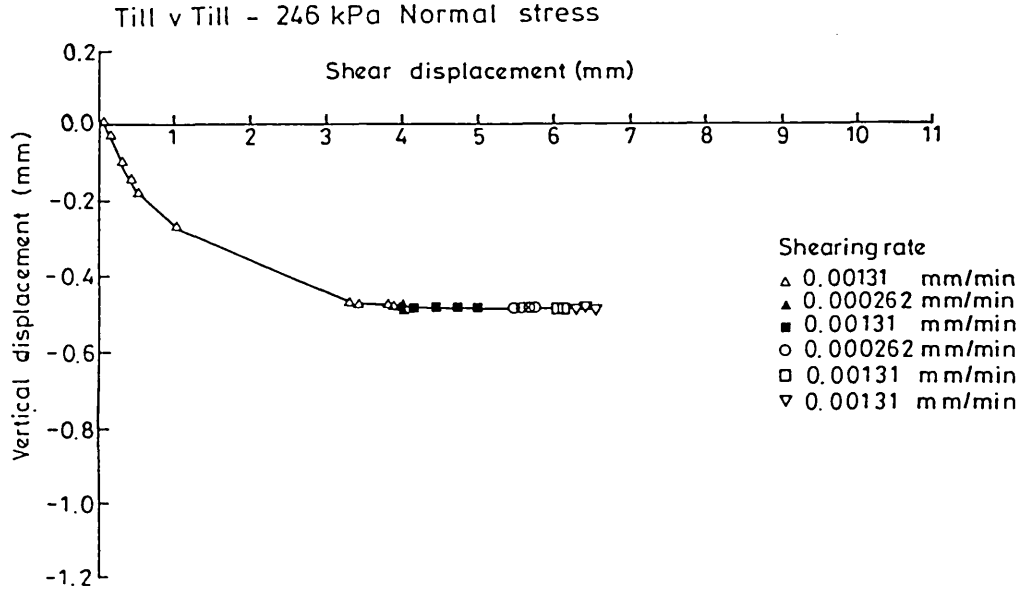

Appendix 5.2 BRS site: shearbox test results

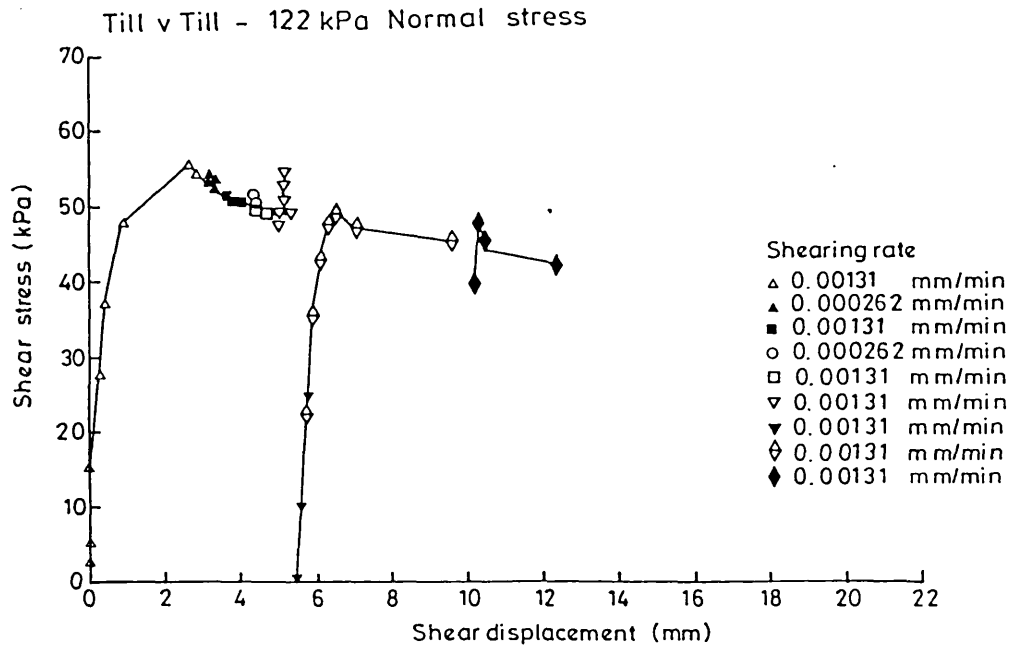

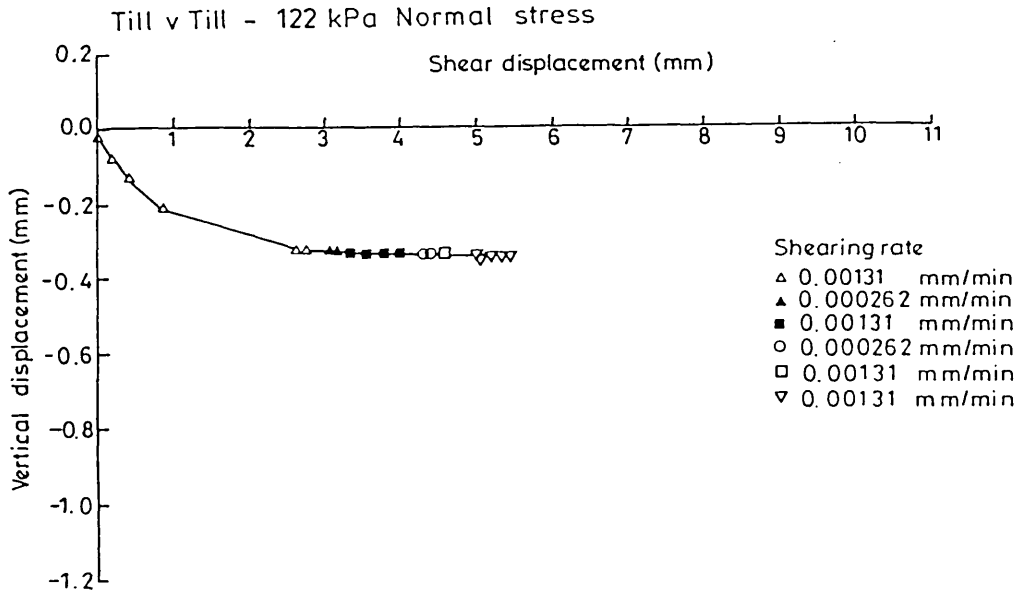

Appendix 5.2 (cont.)

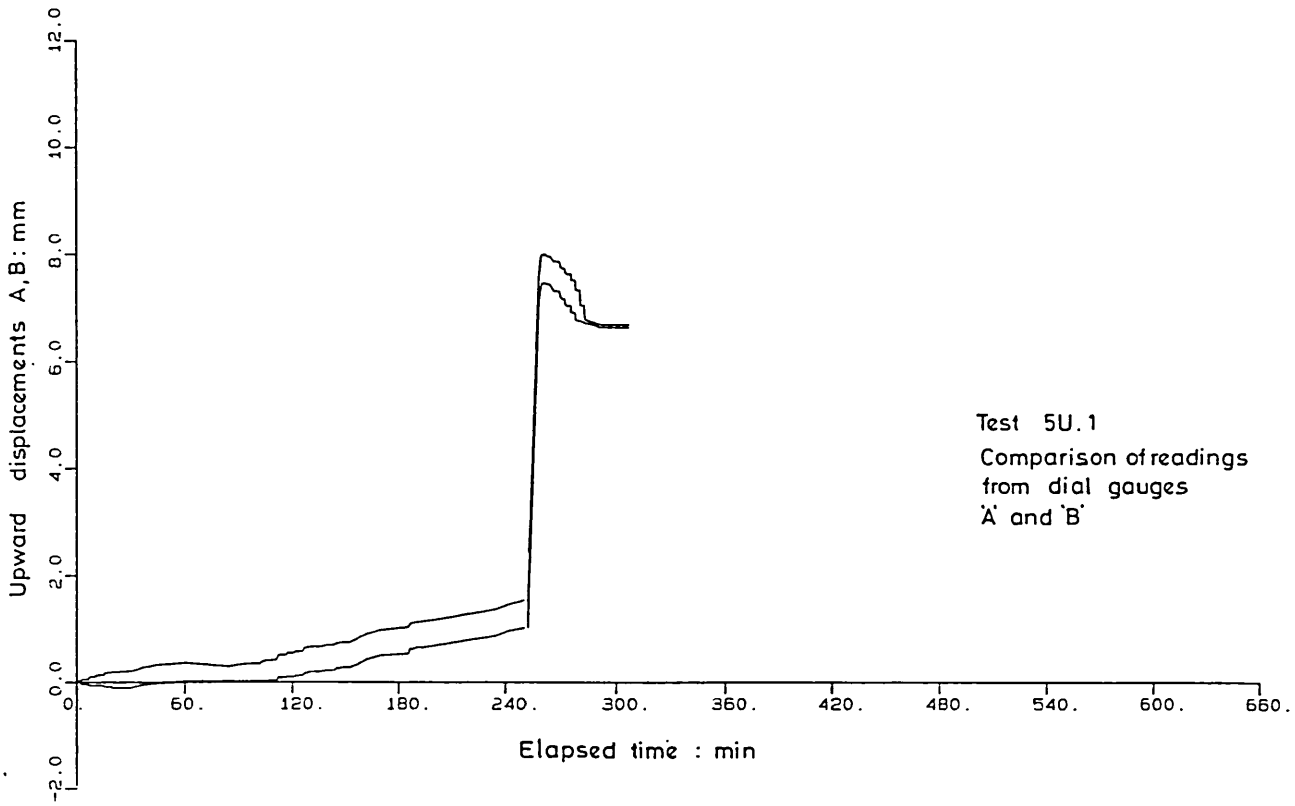

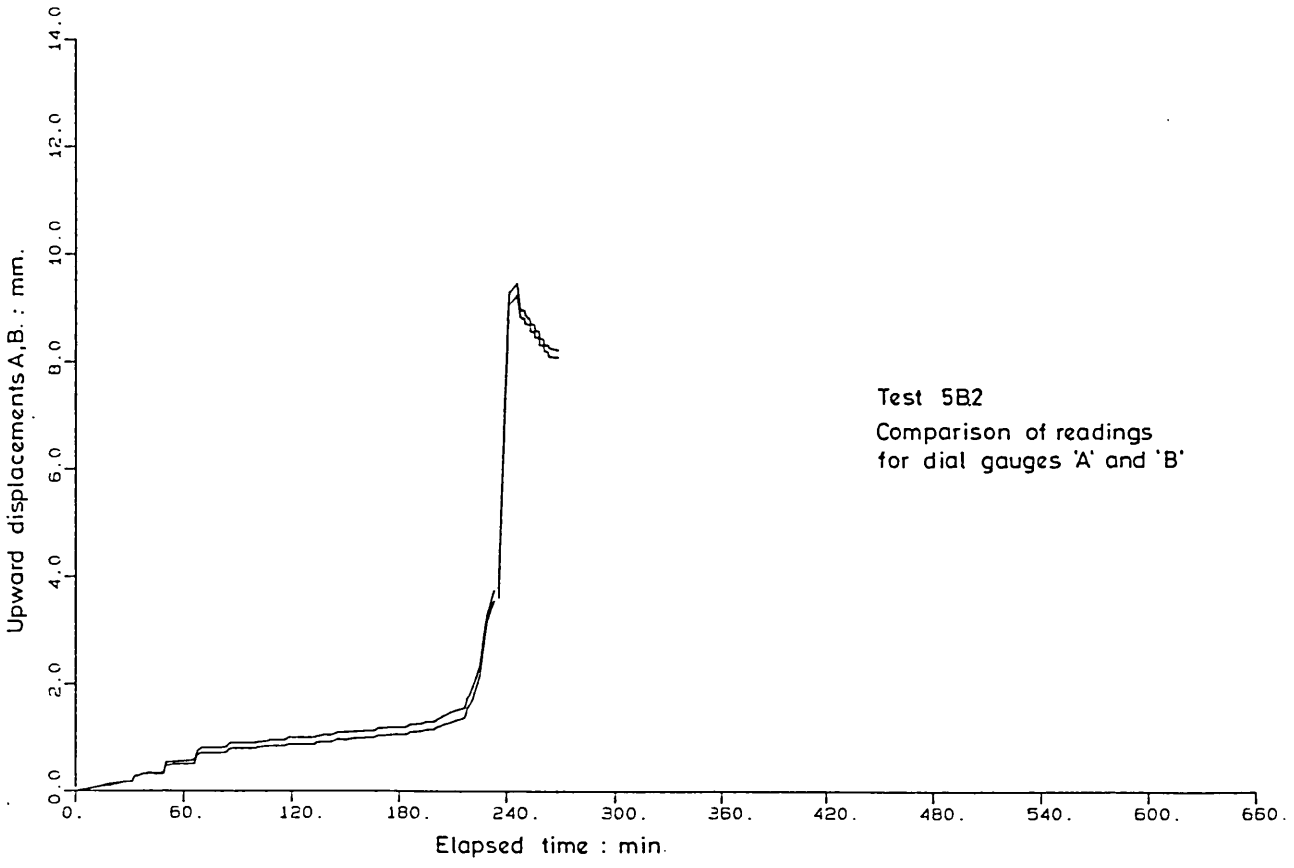

Appendix 5.3 BRS site: typical results from pile tests

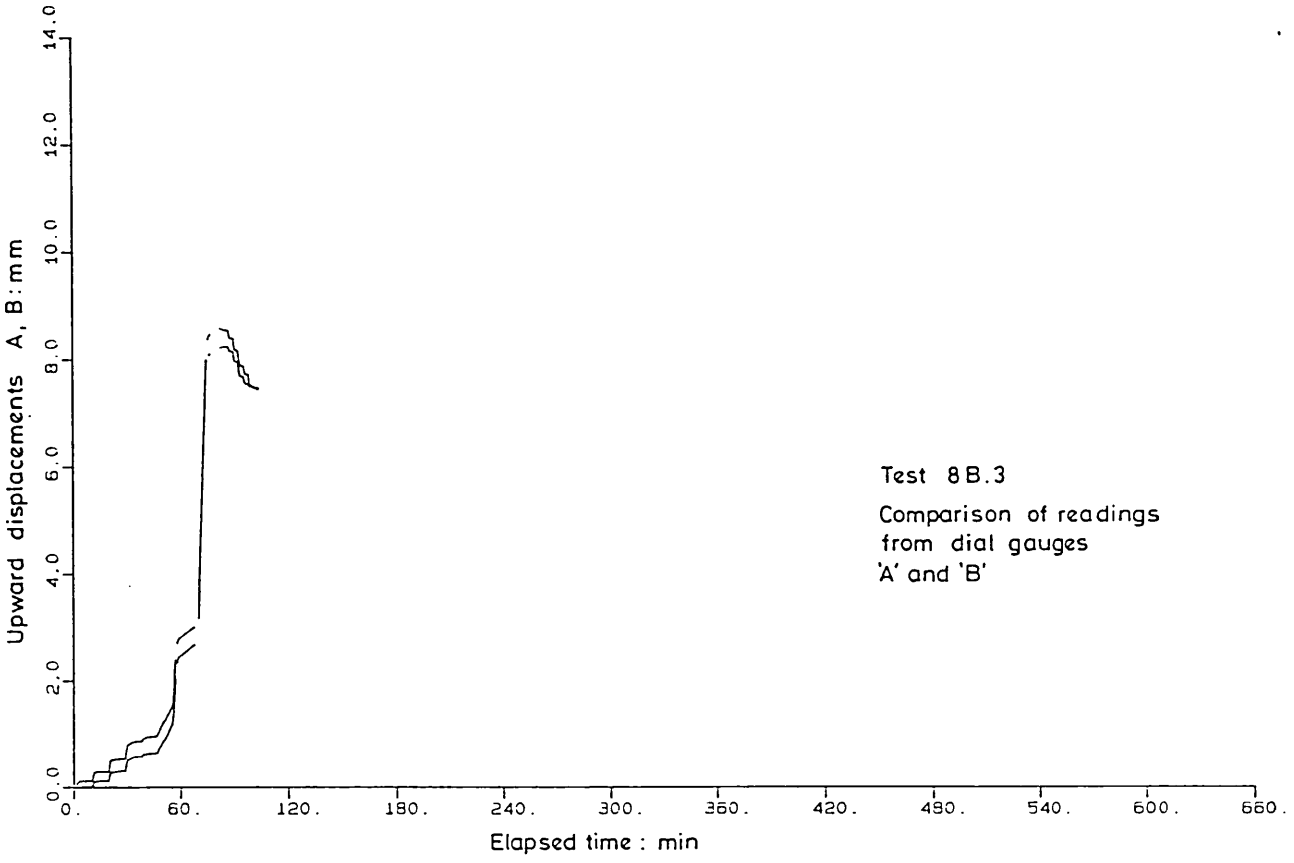

Appendix 5.3 (cont.)

Rhino Sales Corporation has a policy of continuous product improvement and reserves the right to change specifications, design, or prices at any time without notice or the incurring of obligations.

Rhino

air operated post drivers

Four, Low Cost, Rhino Post Drivers let you pick the right size for your job. In seconds, you can drive Telespar, Channel Posts, Delineator Posts, Pipe, Sand Points, Ground Rods, T Posts, Anchors, Z Posts, Large Tent Pegs, I Posts, W Posts, Concrete Form Pins, Beams, Round, Square or Rectangular Tubing, Wood Posts, Stakes or any shape up to 4". Sheet Piling and Guard Rail Posts are driven with adapters.

Rhino®

PD-95 drives 12 ft. Telespar road sign post.

Rhino Sales Corporation / P.O. Box 367 / 620 Andrews Avenue / Kewanee, Illinois 61443 U.S.A. / Phone 309/853-4461

Appendix 6.1 Mini-pile testing: details of post driver

low cost efficient trouble-free operation

Easily operated by one man, they deliver up to 1700 blows per minute. One moving part, a reciprocating piston, strikes directly on the Post or Driving Adapter. The Drivers have low air consumption rates, are light-weight and hand portable, ideal for driving in places that are hard to reach. All you need is enough air capacity, the recommended air pressure, a Filter-Regulator-Lubricator to assure clean air, plus ten drops of oil per minute, and your Rhino Post Driver will give you Fast, Low Cost driving. Alloy Steel Pistons and other features insure little or no maintenance.

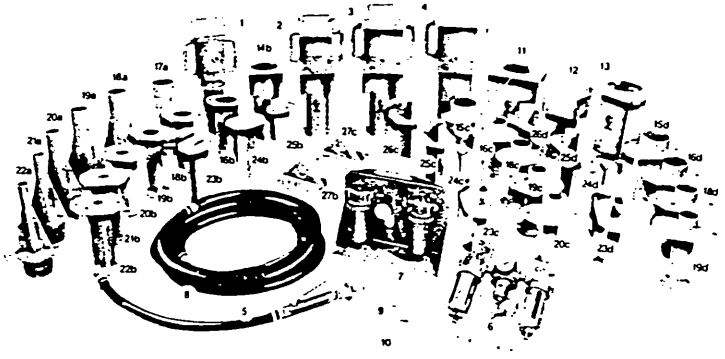

▲ PD-135 with special chuck drives 4" x 6" guard rail post.

▲ PD-50 driving a farm T-post.

◀ PD-50 drives chain link fence post.

▼ PD-40 drives ground rod for power poles.

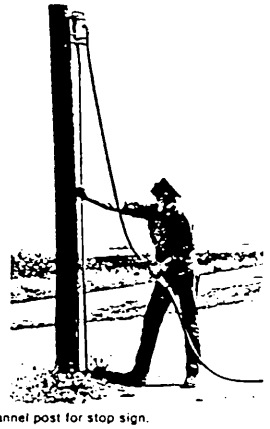

▲ PD-50 driving 12 ft. channel post for stop sign.

◀ PD-50 drives channel post break-away base.

POST DRIVER AND ACCESSORY SPECIFICATIONS

(All Drivers are equipped with the exclusive Rhino Alloy, Double Valve Piston)

NO.	MODEL OR PART NO.	SPECIFICATIONS
1	PD-40	Light Duty Post Driver with one Chuck 2.9" (73.6 mm) to 1" (26.6 mm), Uses 30 CFM (.83 m³/min) @90 PSI (6.5 kg/cm²). Approx. Wt. 48.4 lbs. (21.9 kg)
2	PD-50	Medium Duty Post Driver with 3 5/8" (92 mm) Master Chuck, Uses 42 CFM (1.17 m³/min) @90 PSI (6.5 kg/cm²). Approx. Wt. 57.5 lbs. (26.1 kg)
3	PD-95	Medium/Heavy Duty Post Driver with 4 1/4" (107.9 mm) Master Chuck, Uses 59 CFM (1.64 m³/min) @100 PSI (7 kg/cm²). Approx. Wt. 100 lbs. (45.4 kg)
4	PD-135	Heavy Duty Post Driver with 4 1/4" (107.9 mm) Master Chuck, Uses 64 CFM (1.78 m³/min) @100 PSI (7 kg/cm²). Approx. Wt. 136 lbs. (61.7 kg)
5	600000	Throttle Valve Kit with 2' (609 mm) Hose Whip, (Used with all Drivers)
6	601000	Filter-Regulator-Lubricator (Post Driver Protection)
7	225000	Carrier for Filter-Regulator-Lubricator
8	605006	3/4" (19 mm) Extra Air Hose for Valve Kit or Air Line Extensions
9	606600	Air Line Coupler
10	606601	Coupler Safety Clip
11	070061	4" x 6" (101 mm x 152 mm) H Column Chuck for PD-135
12	070062	4" x 6" (101 mm x 152 mm) H Column Driving Cap
13	070063	4" x 4" (101 mm x 101 mm) Wood Post Chuck for PD-135

STANDARD CHUCKS, CHUCK ADAPTERS, AND LIFT EYE TOPS

(Select the proper Chuck I.D. or Shape from Chuck Sizing Techdata (Form No. 121-1), then order the Part No. in the column under your Post Driver's Model No. (S/O means Special Order)

NO.	CHUCK I.D. OR DESCRIPTION	POST DRIVER MODEL NO. PD-40 (a)	PD-50 (b)	PD-95 (c)	PD-135 (d)
14	4 1/4" (107.9 mm)	—	070060	Standard	Standard
15	3 5/8" (92 mm)	—	Standard	070051	070056
16	3" (77.9 mm)	—	070035	070052	070057
17	2.9" (73.6 mm)	070024	—	—	—
18	2 1/2" (62.7 mm)	070025	070036	070053	070058
19	2" (52.5 mm)	070026	070037	070054	070059
20	1 1/2" (40.8 mm)	070027	070038	070055	S/O
21	1 1/4" (35.0 mm)	070028	070040	S/O	S/O
22	1" (26.6 mm)	070029	070048	S/O	S/O
23	Channel Post Adapter	—	070066	070069	070073
24	Channel Post Adapter	—	070067	070070	070074
25	Channel Post Adapter	—	070068	070071	070075
26	Channel Post Adapter	—	—	070072	070076
27	Lift Eye Top	—	070064	070065	Standard

Special Chuckes can be designed for your job. Available for Models PD-50, PD-95, PD-135.

Appendix 6.1 (cont.)

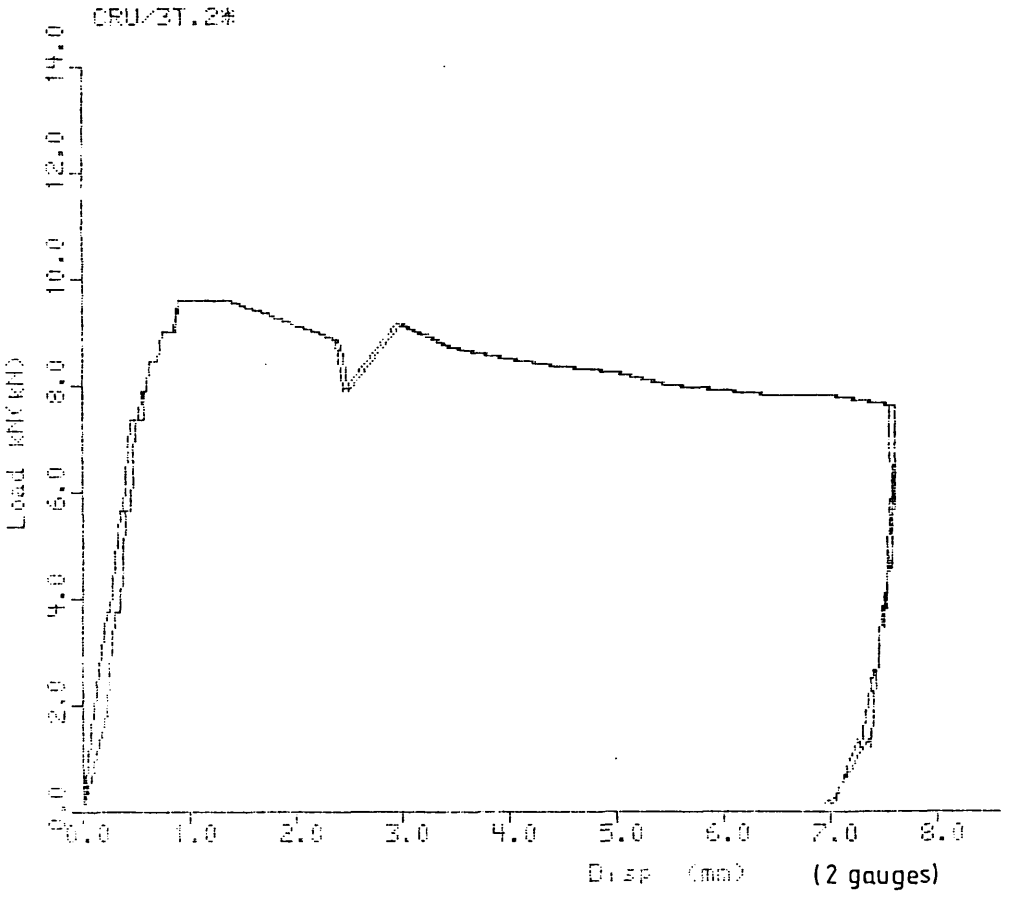

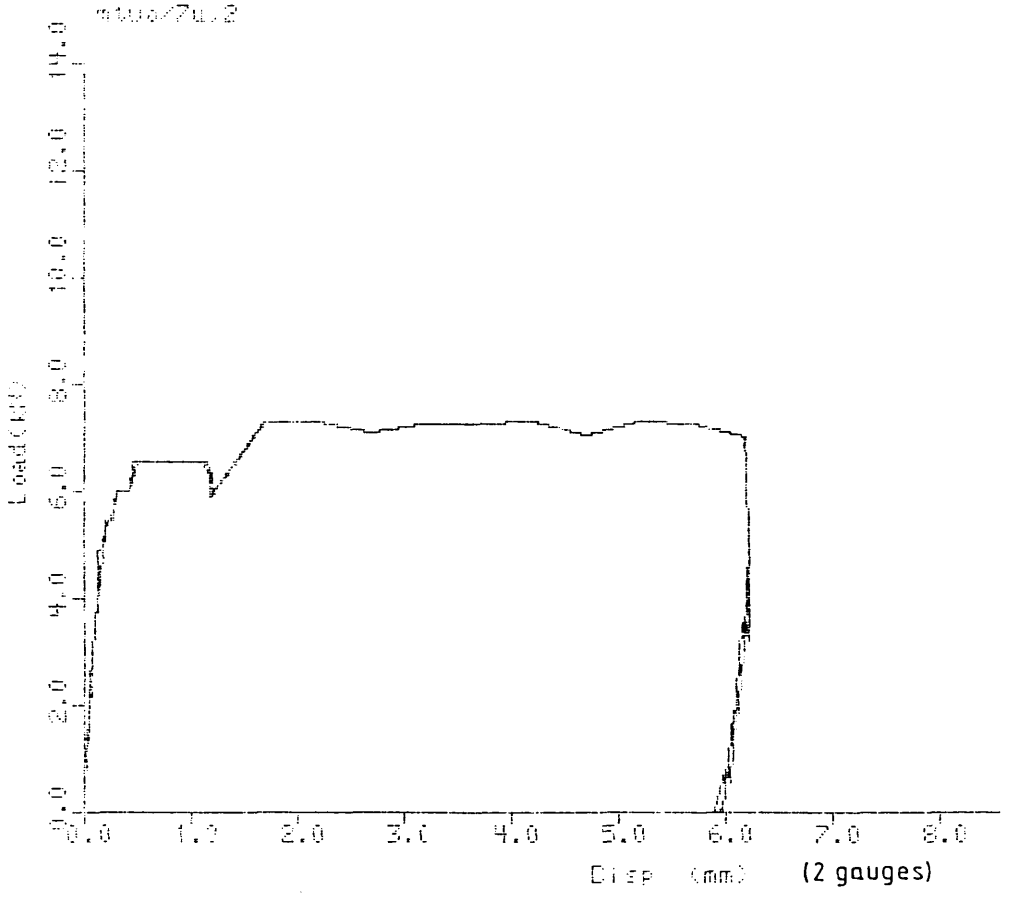

Appendix 6.2 Mini-pile testing: typical results from tests

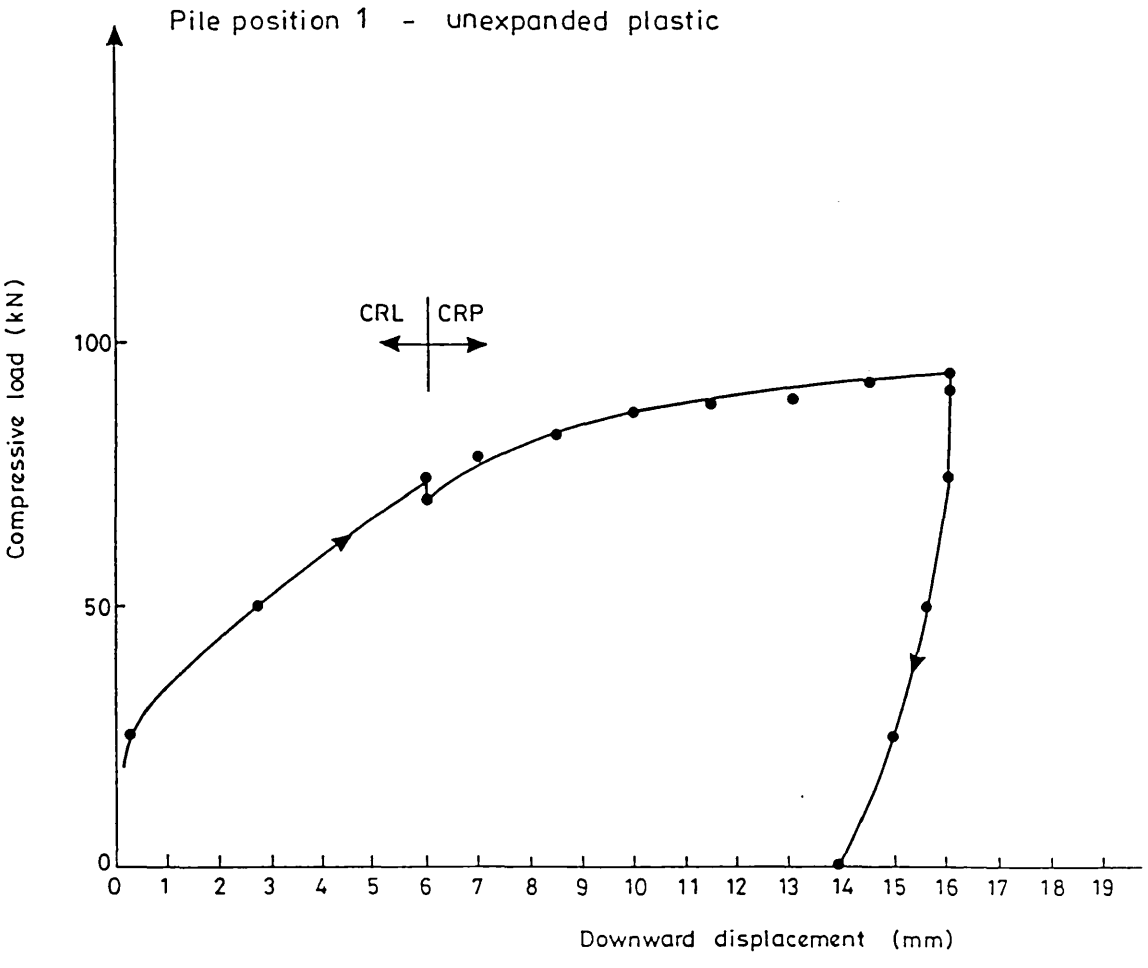

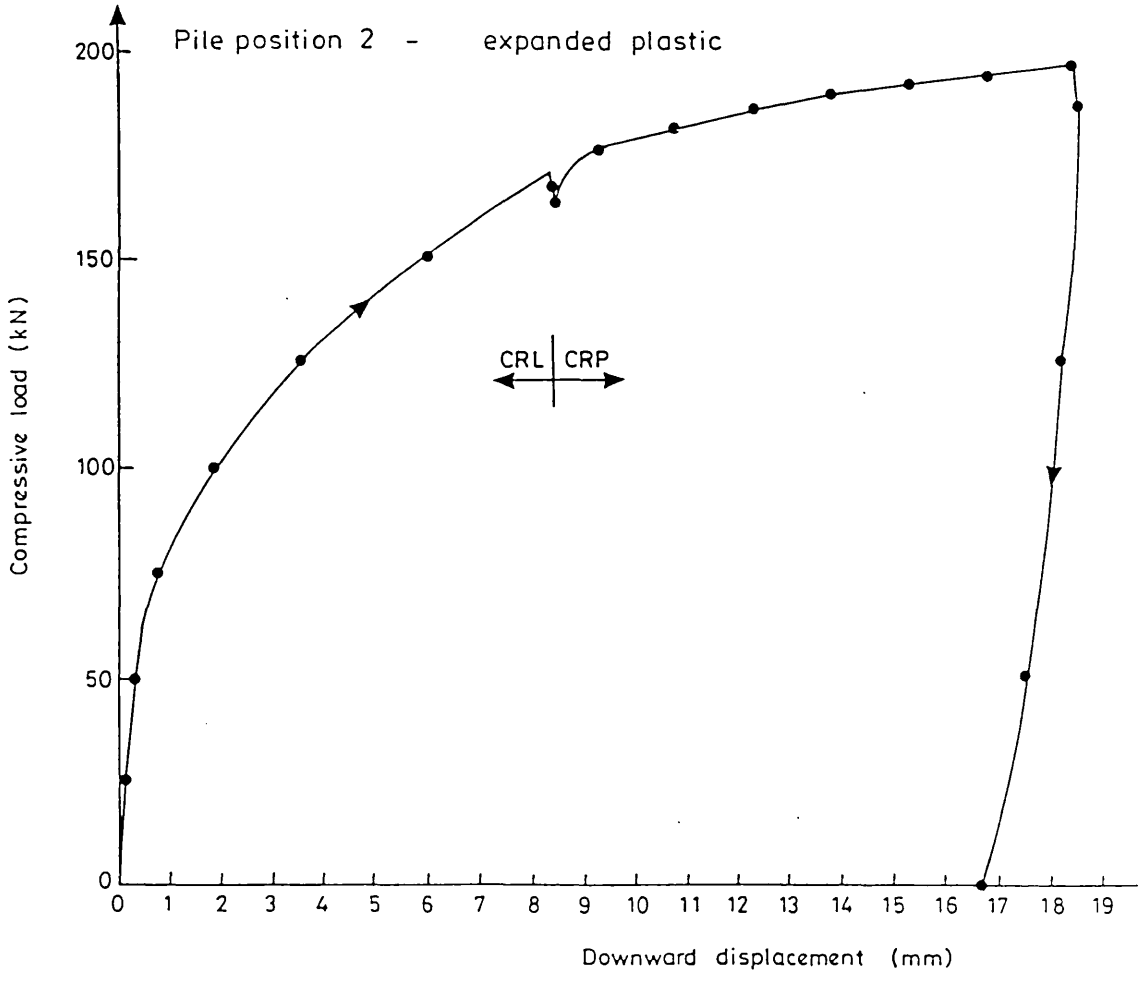

Appendix 8.1 CP&F/Conoco field trials: results of CP&F pile tests

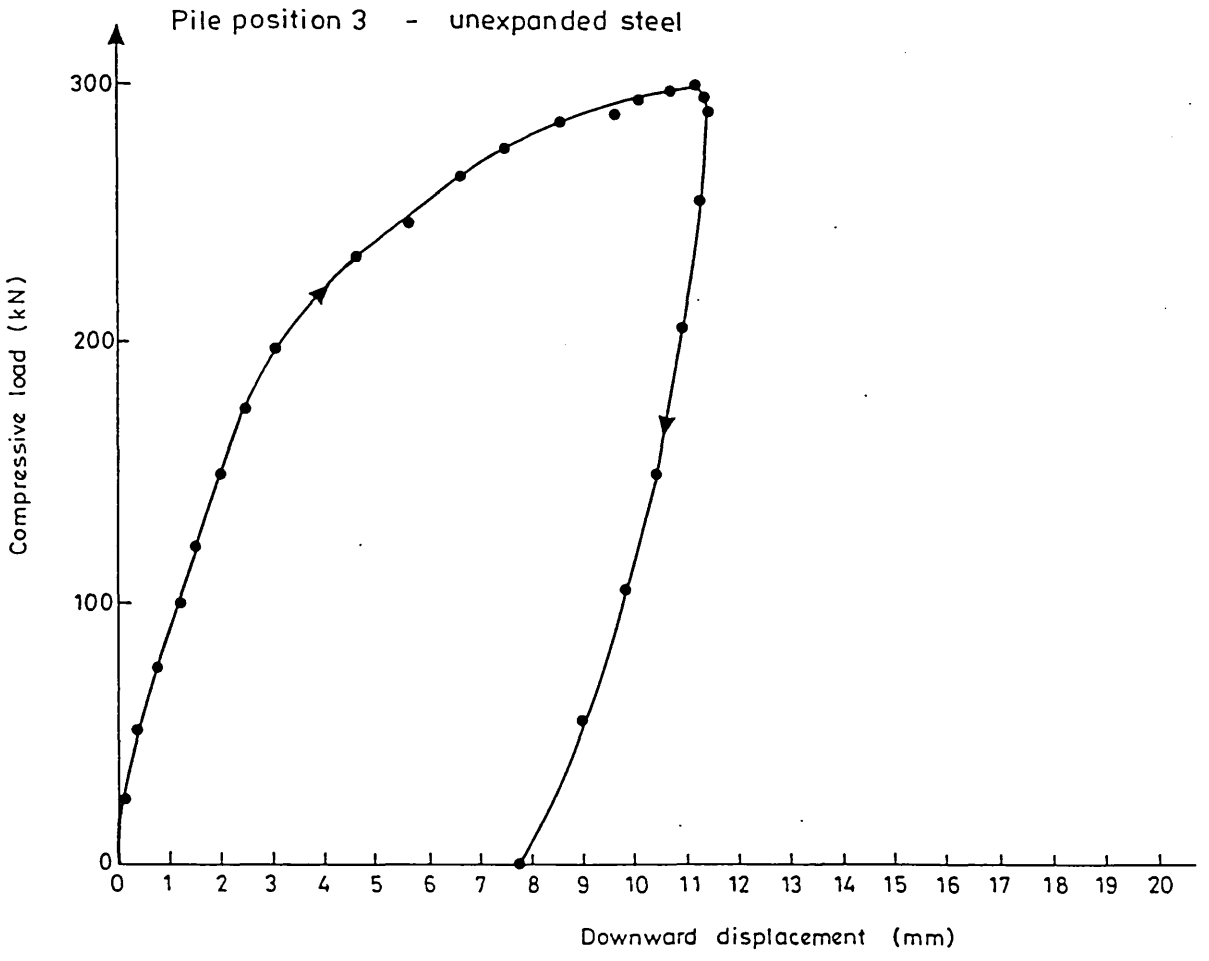

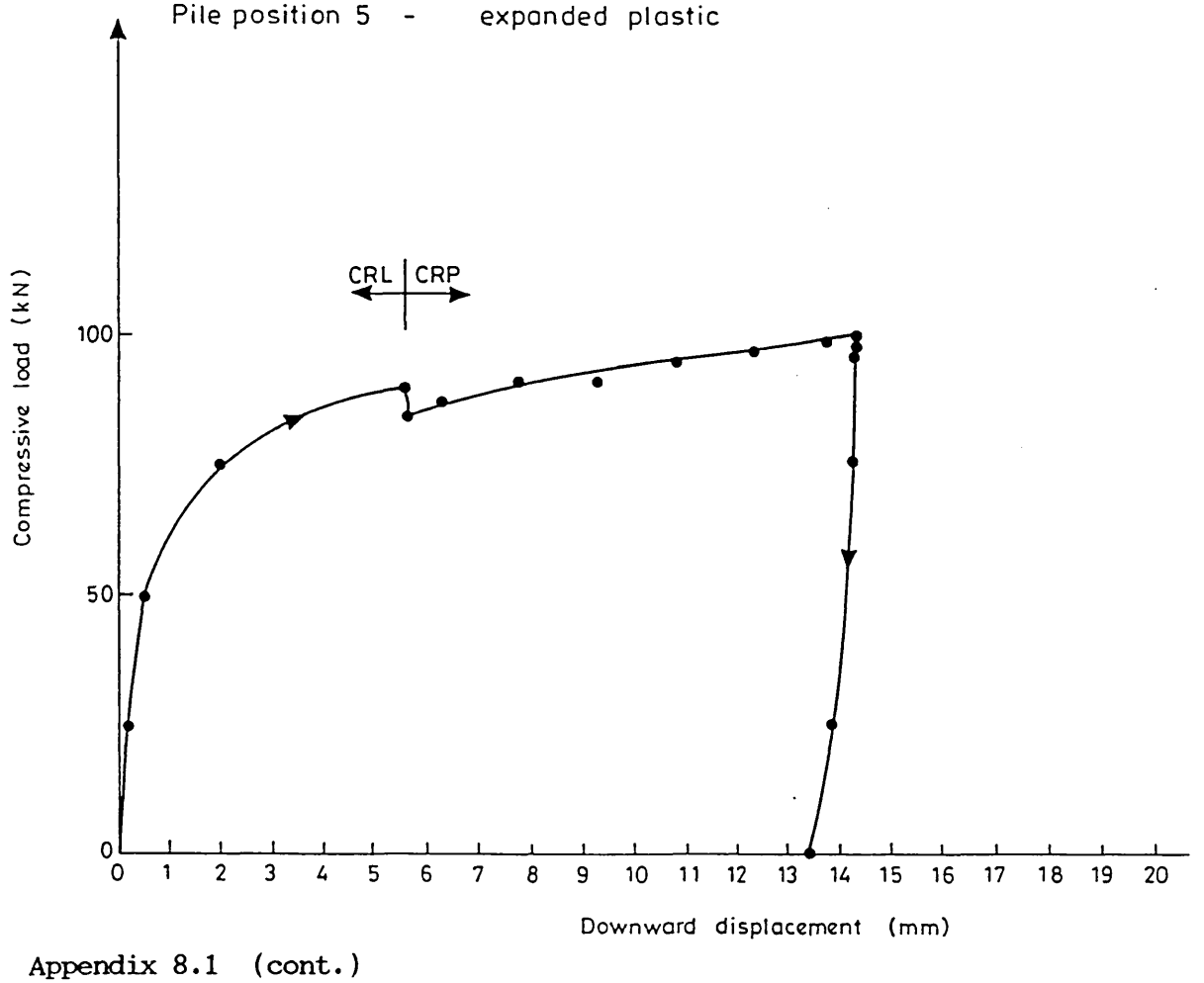

Appendix 8.1 (cont.)

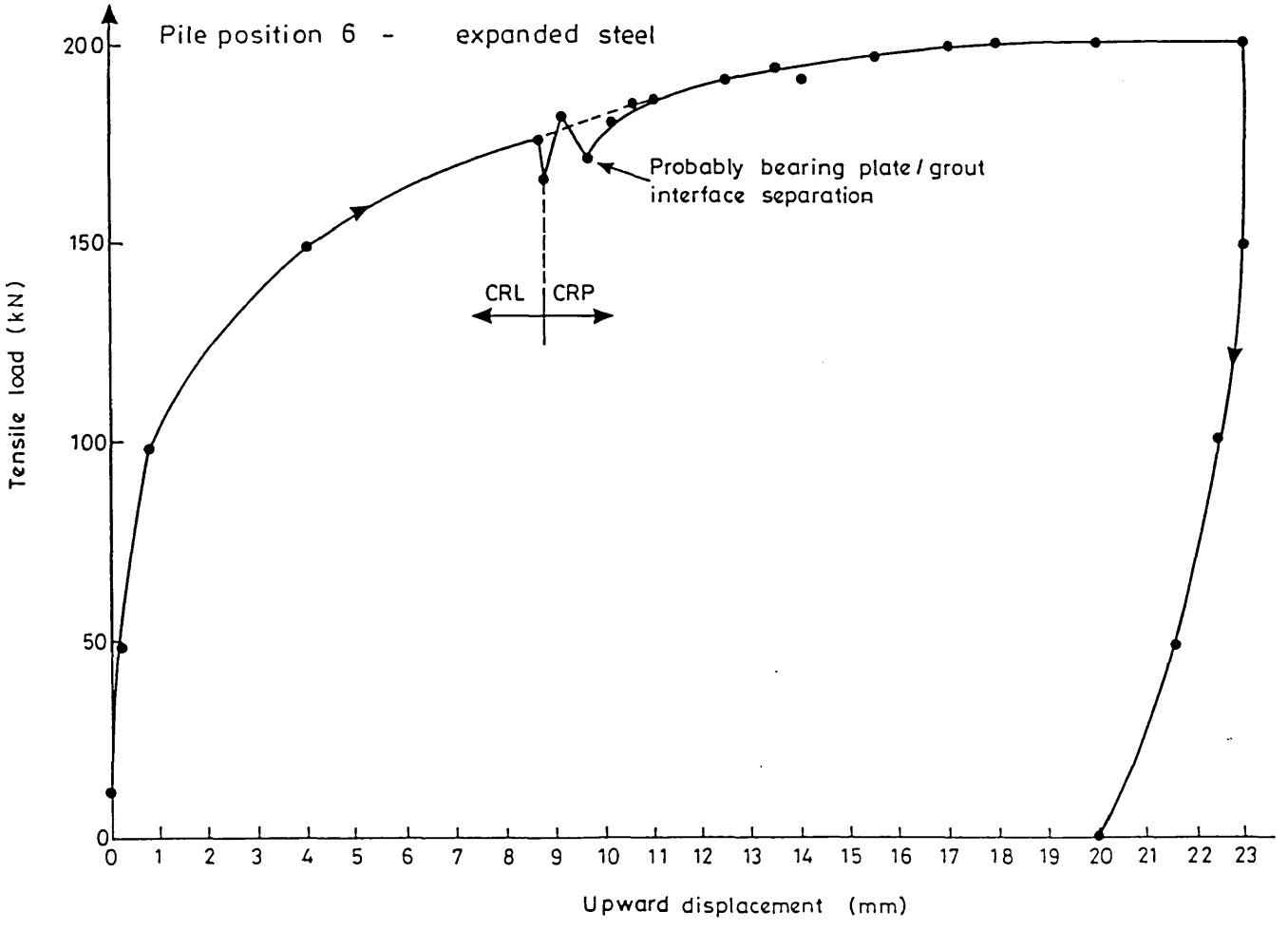

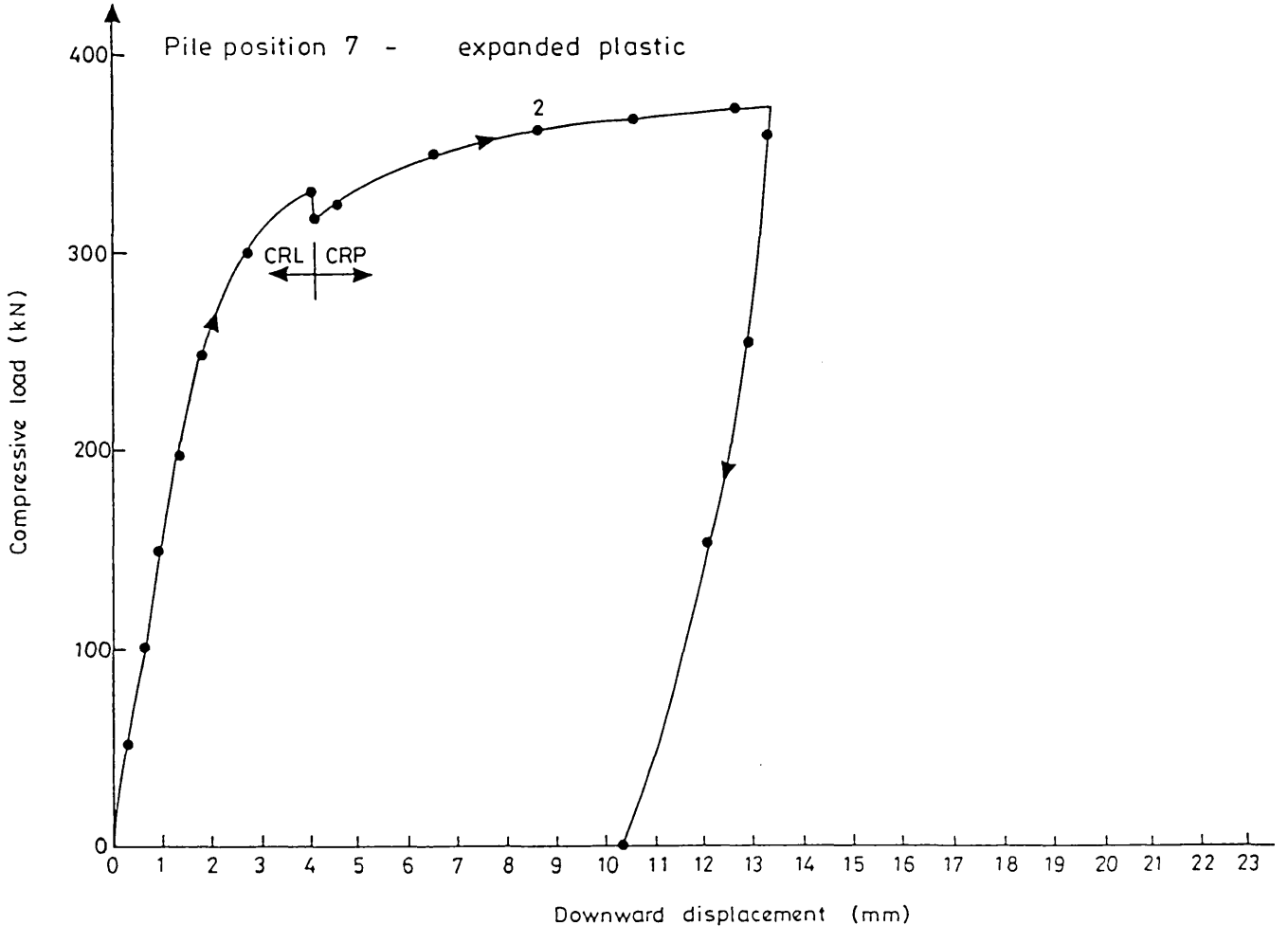

Appendix 8.1 (cont.)

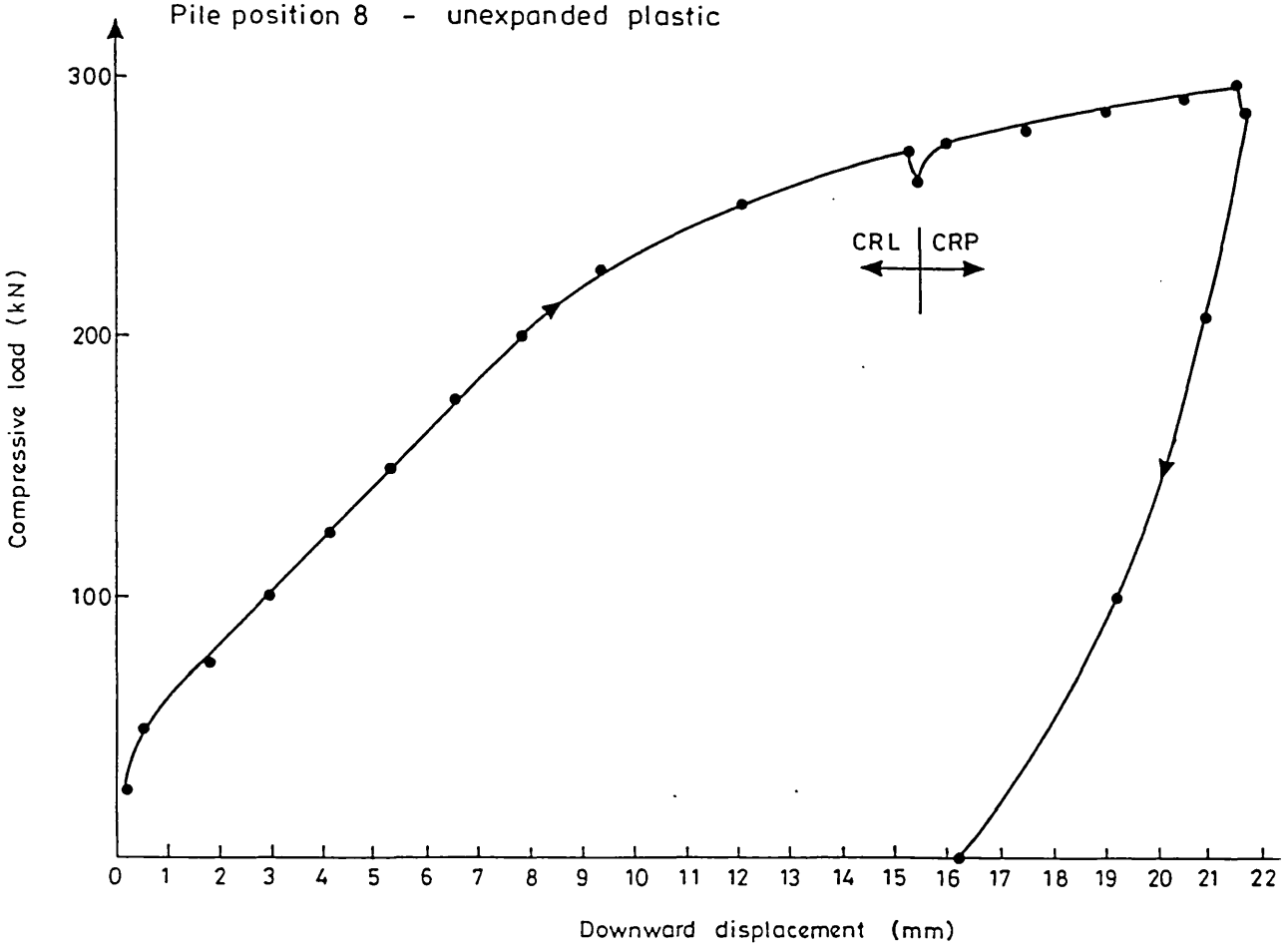

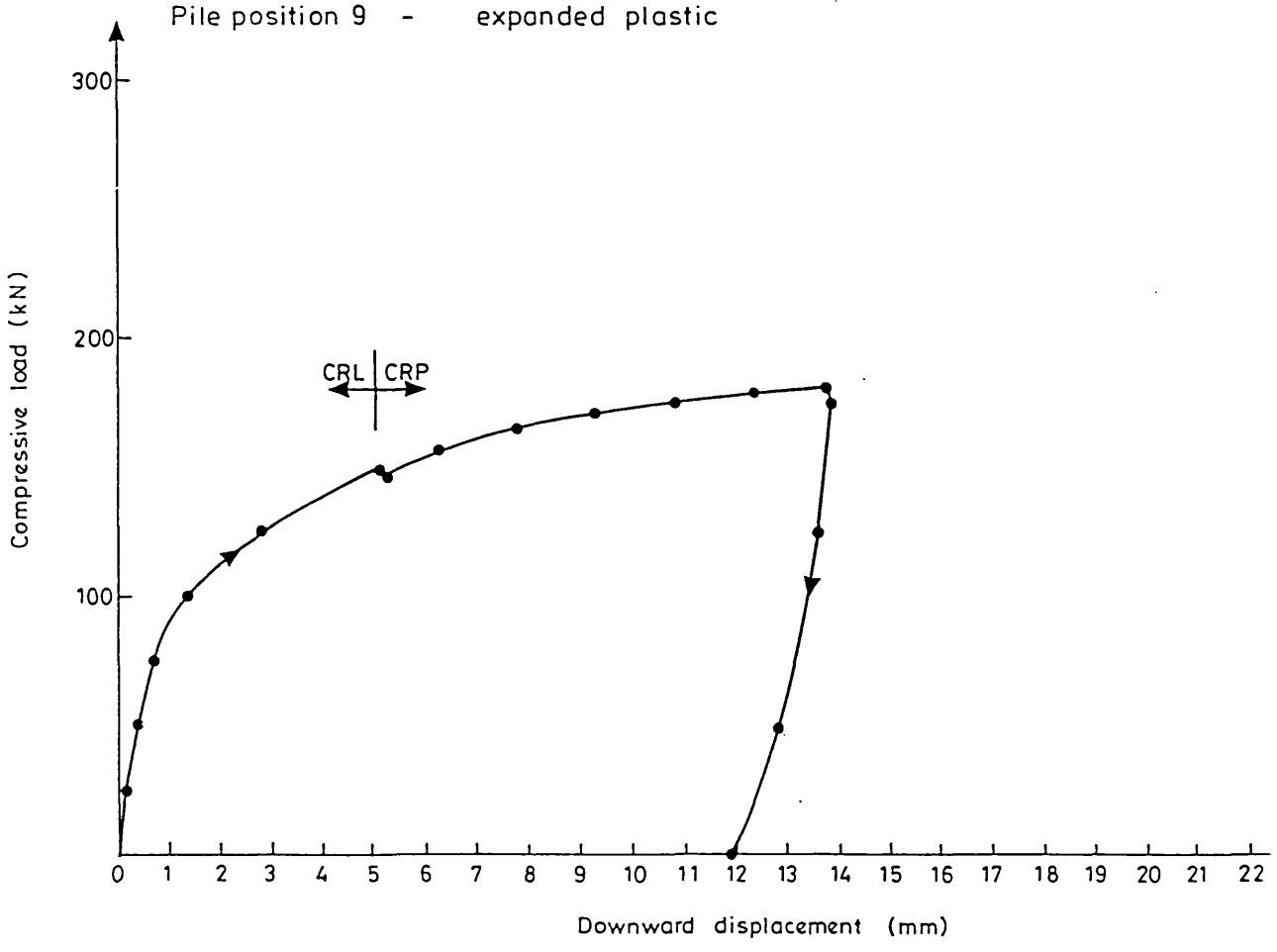

Appendix 8.1 (cont.)

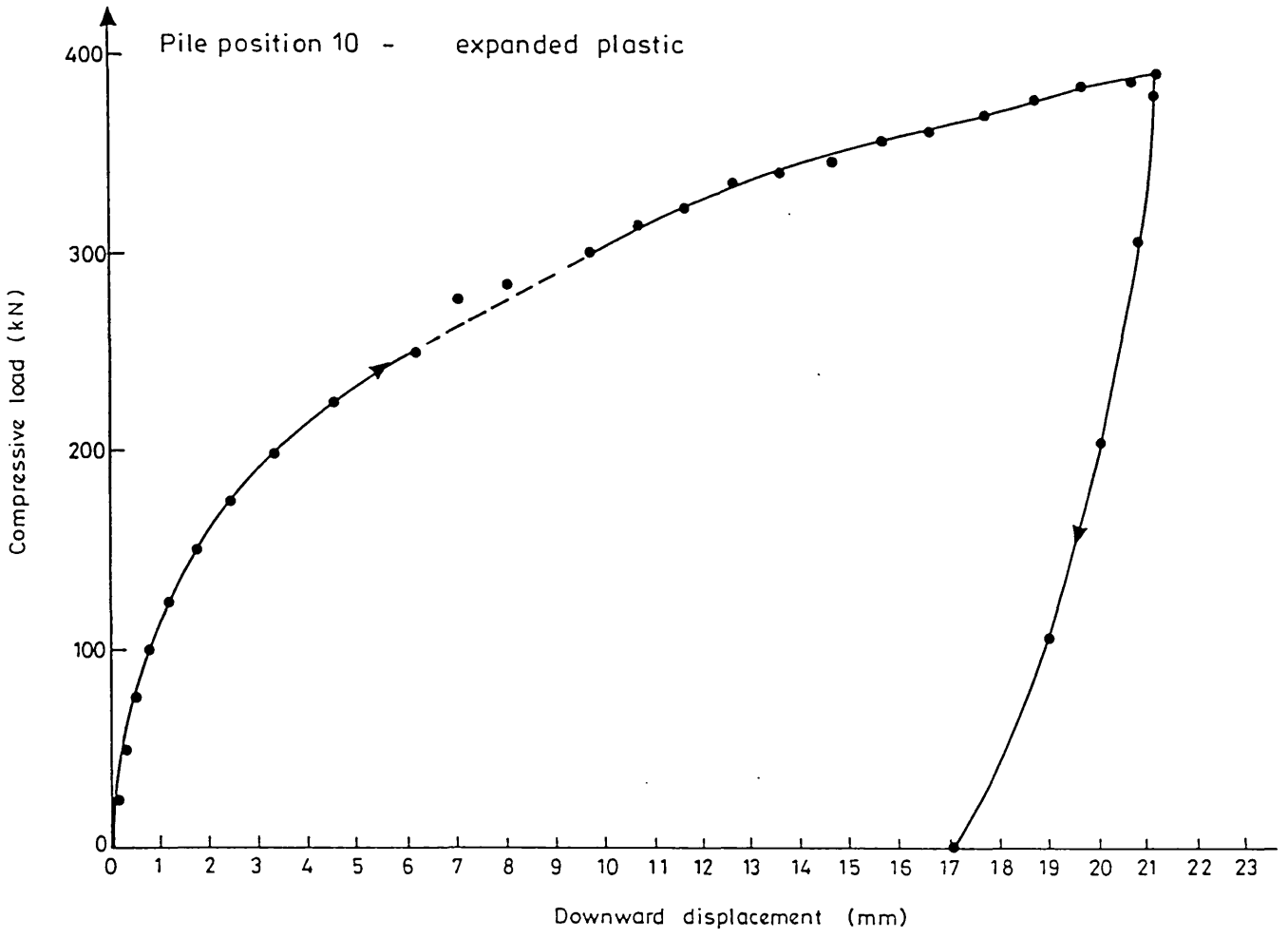

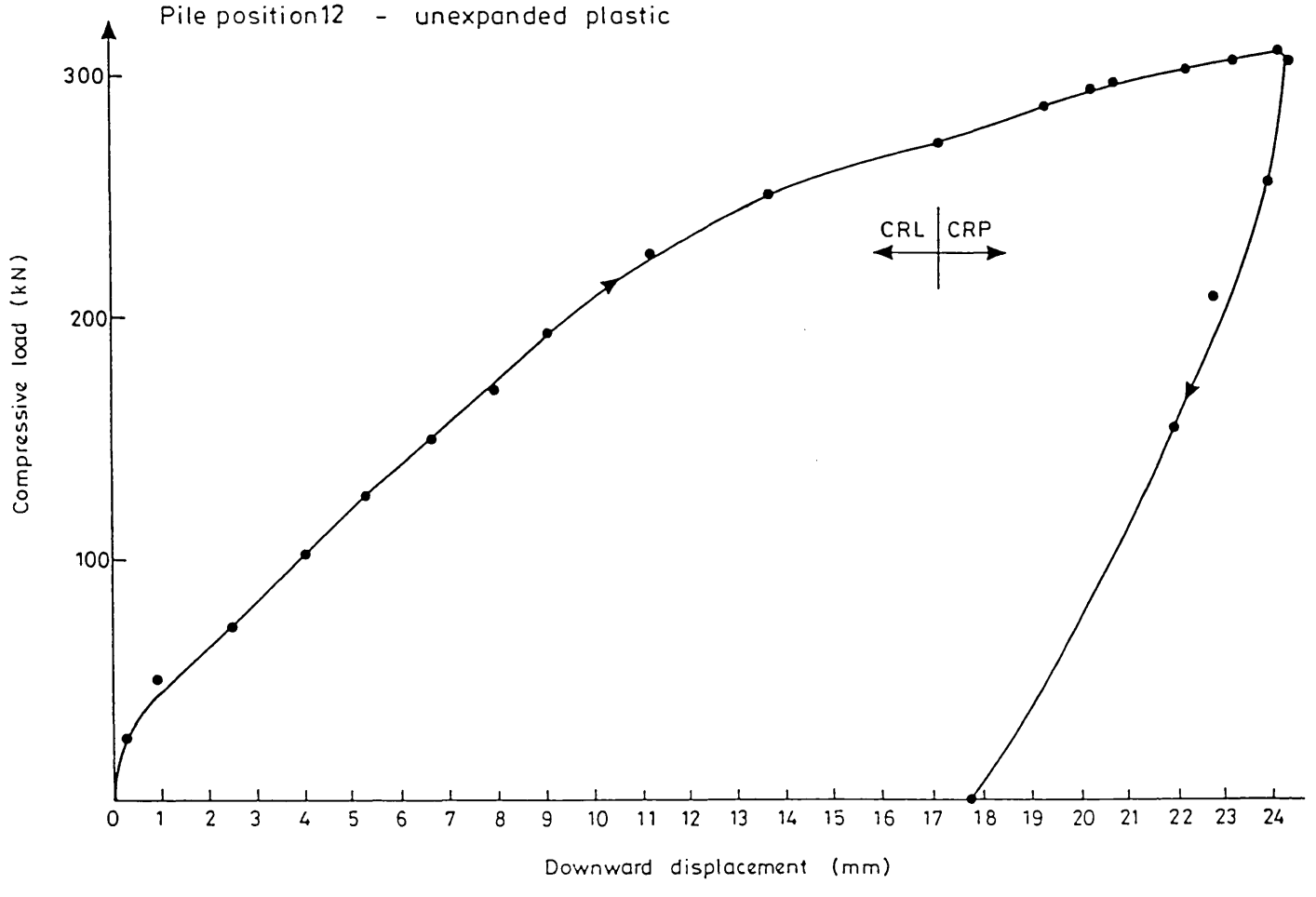

Appendix 8.1 (cont.)

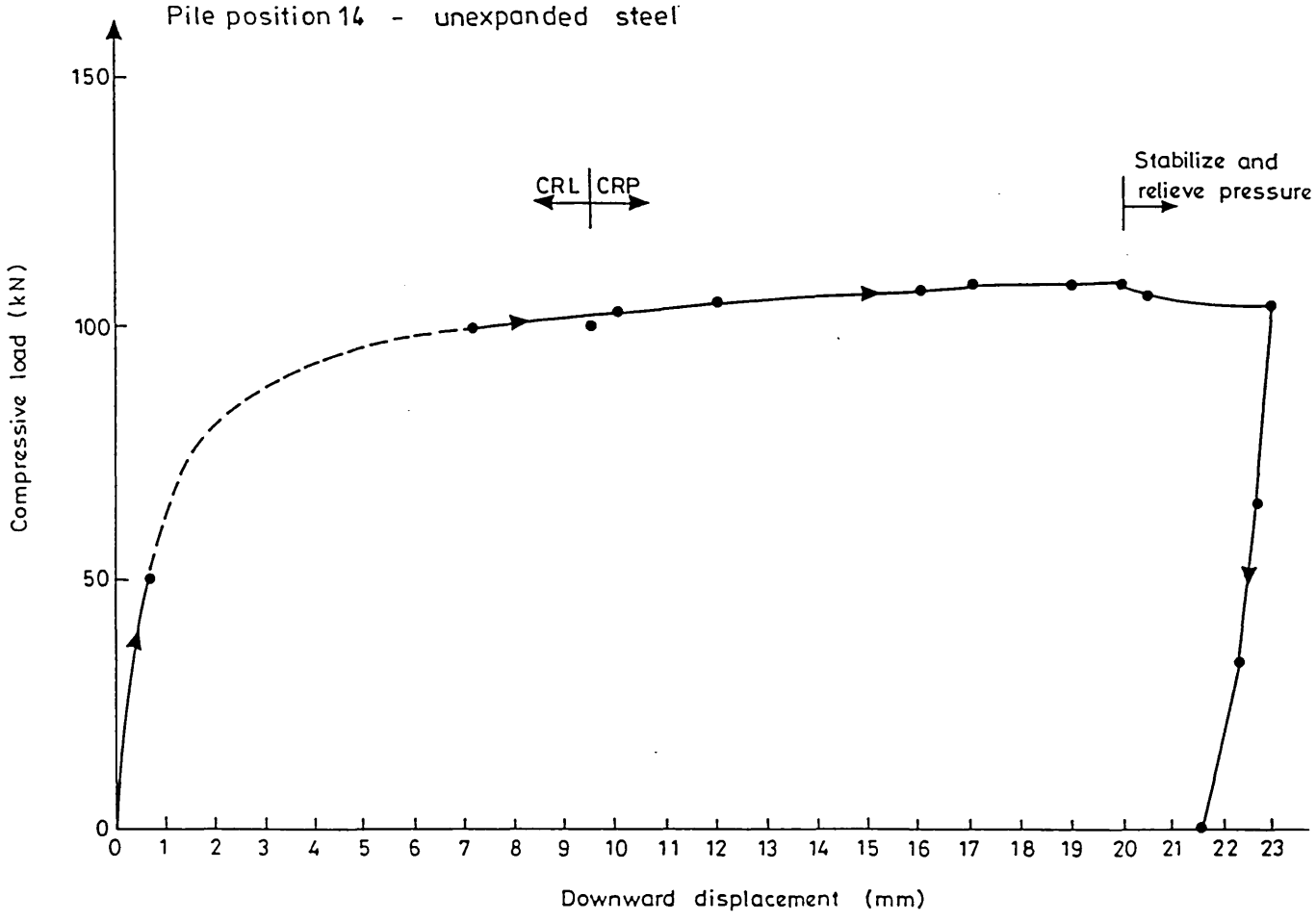

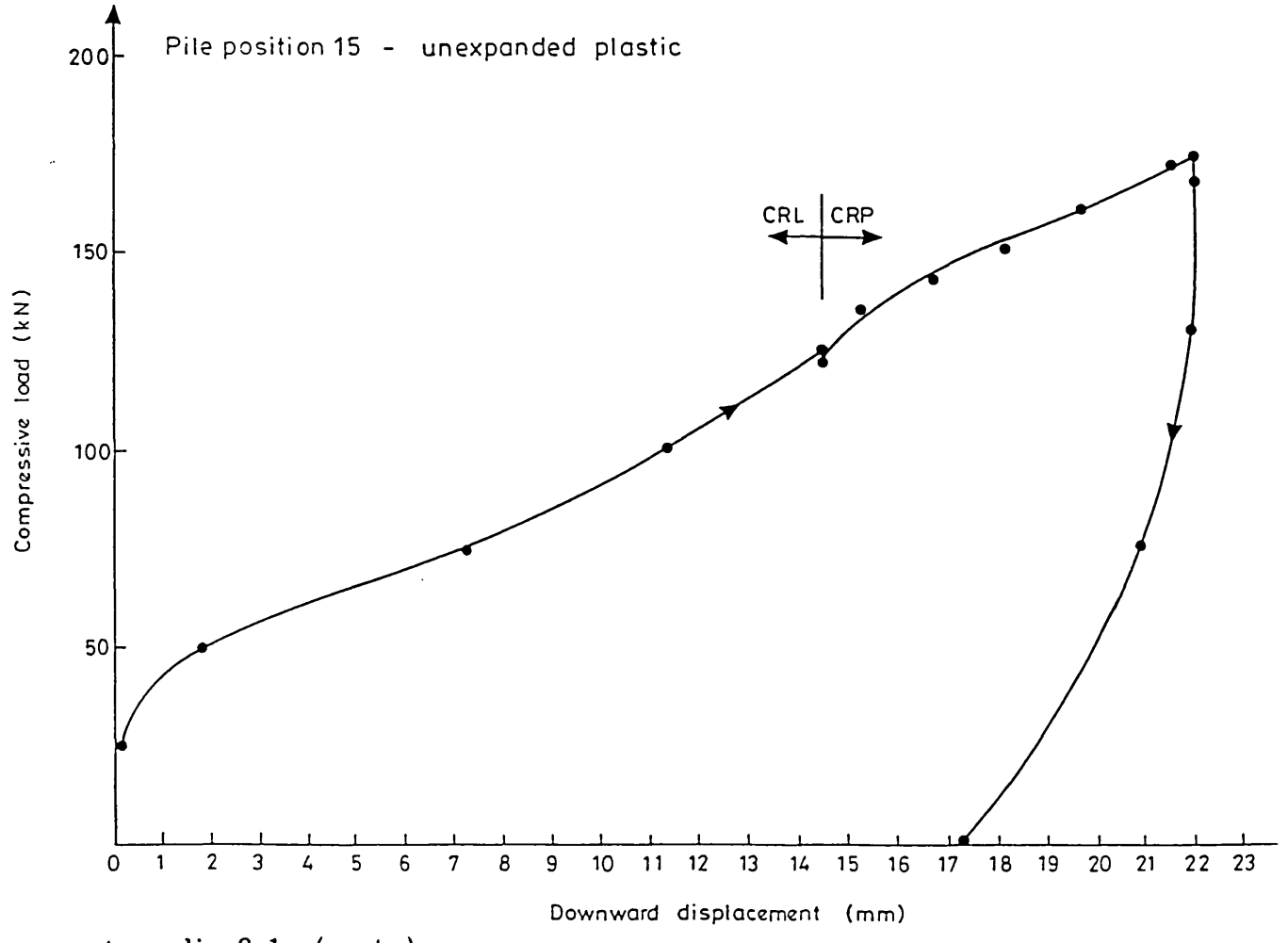

Appendix 8.1 (cont.)

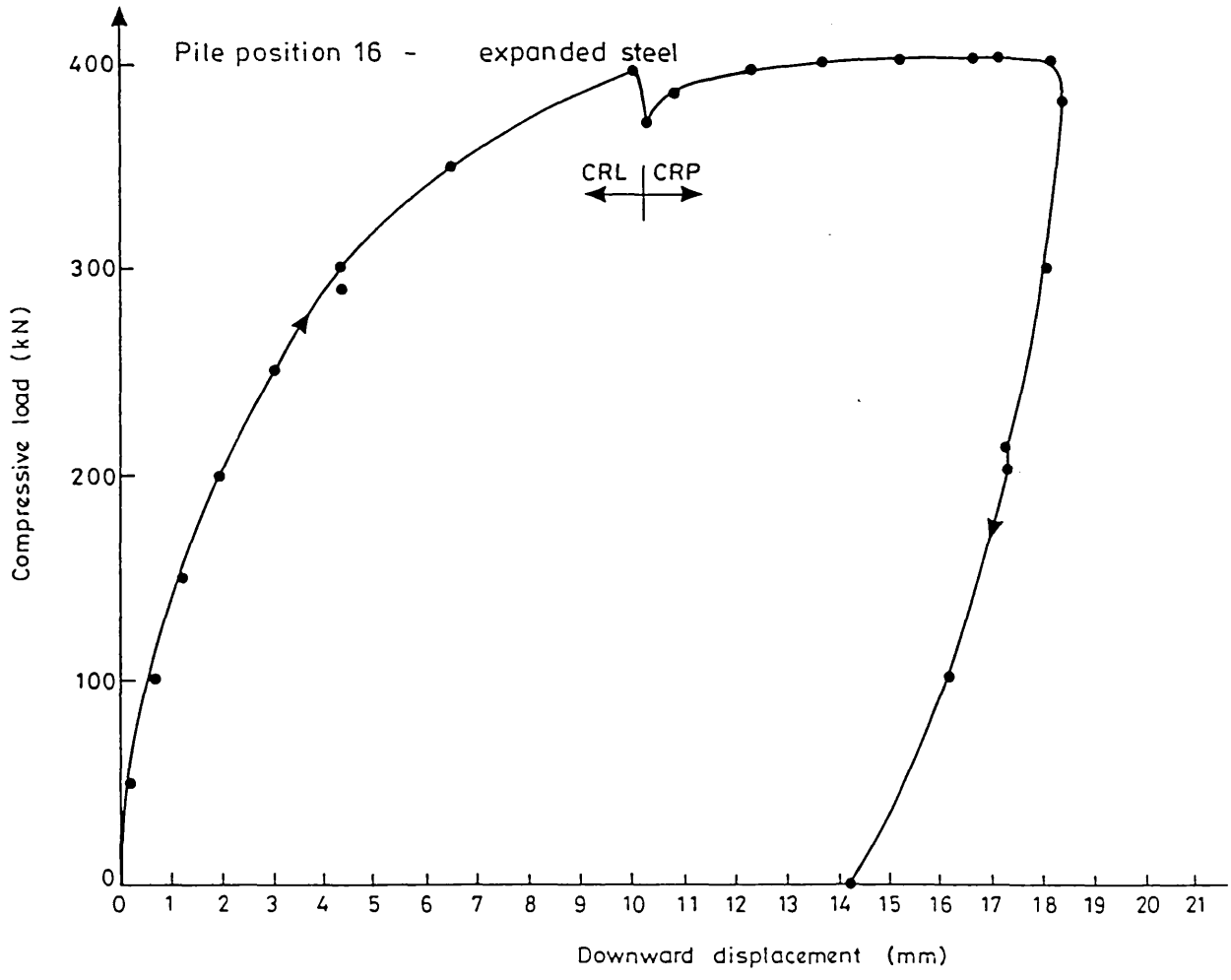

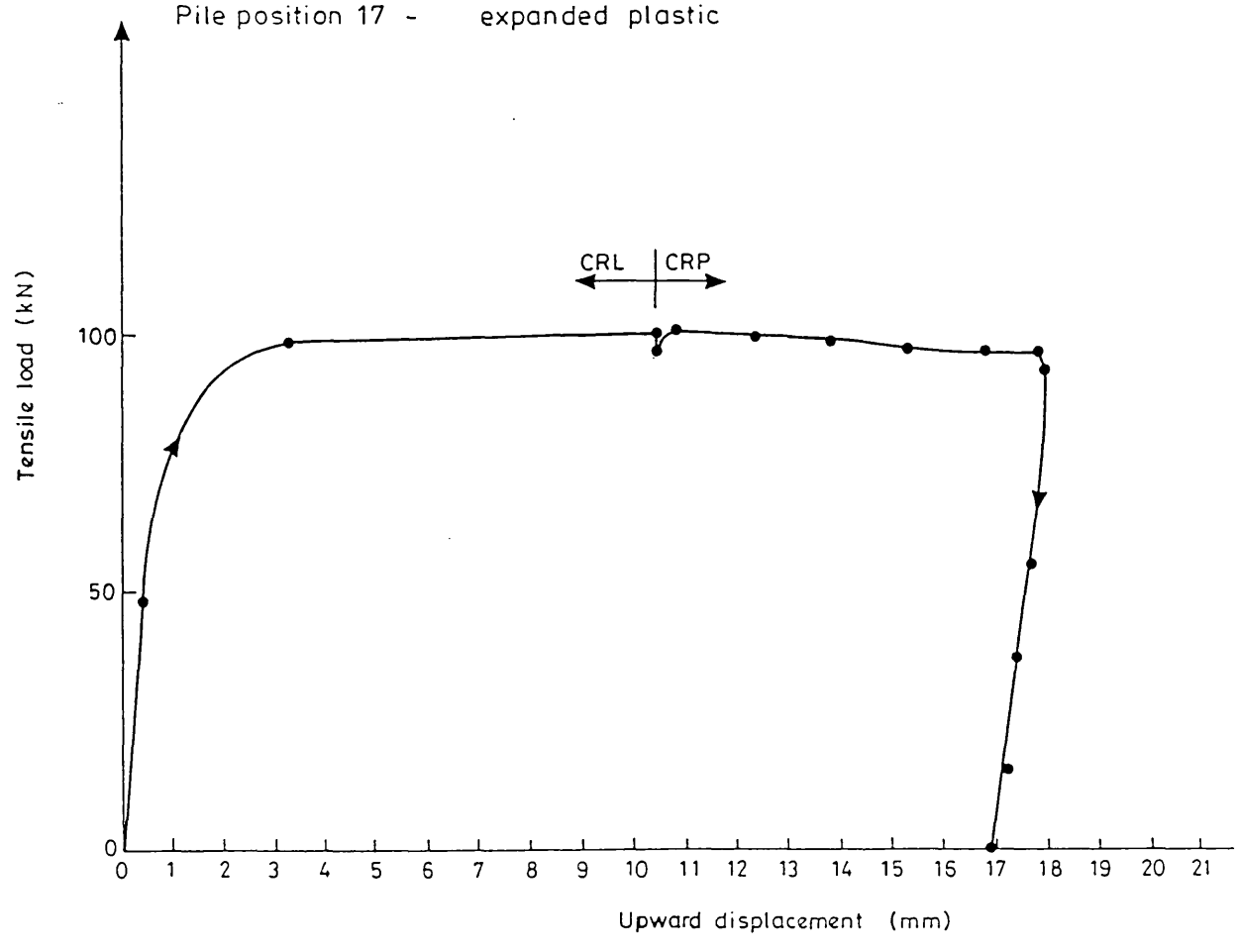

Appendix 8.1 (cont.)

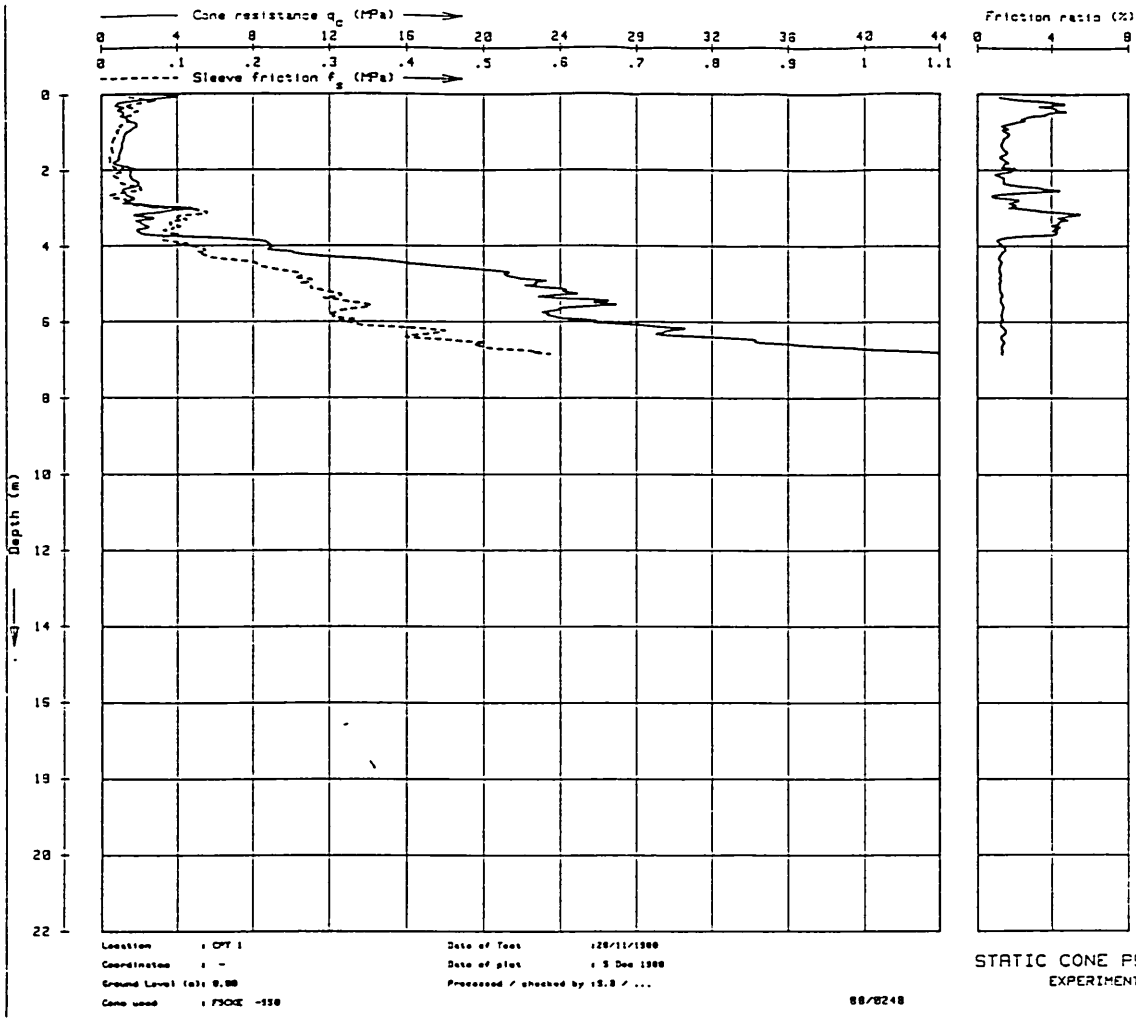

STATIC CONE PENETRATION TEST CPT 1
EXPERIMENTAL SITE - HERMITAGE

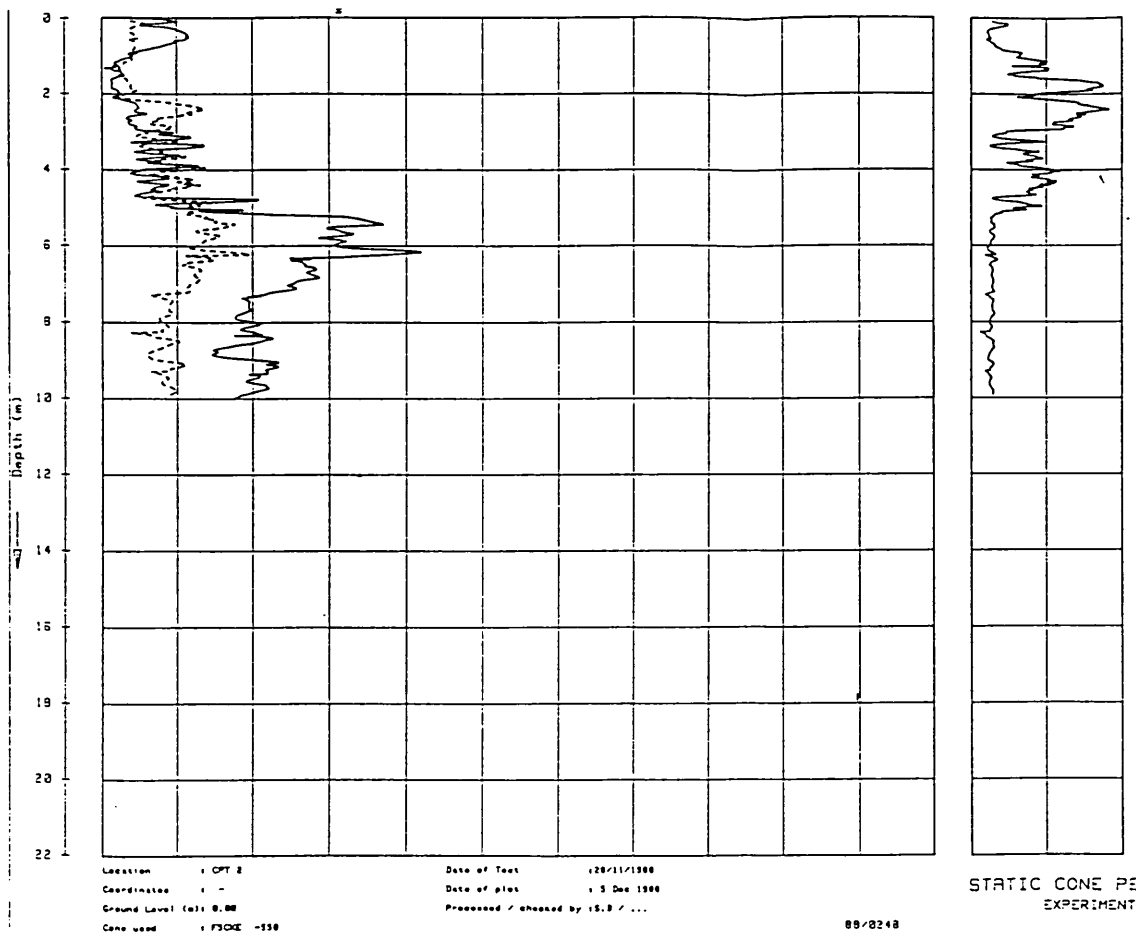

STATIC CONE PENETRATION TEST CPT 2
EXPERIMENTAL SITE - HERMITAGE

Appendix 8.2 CP&F/Conoco field trials: results of CPT tests

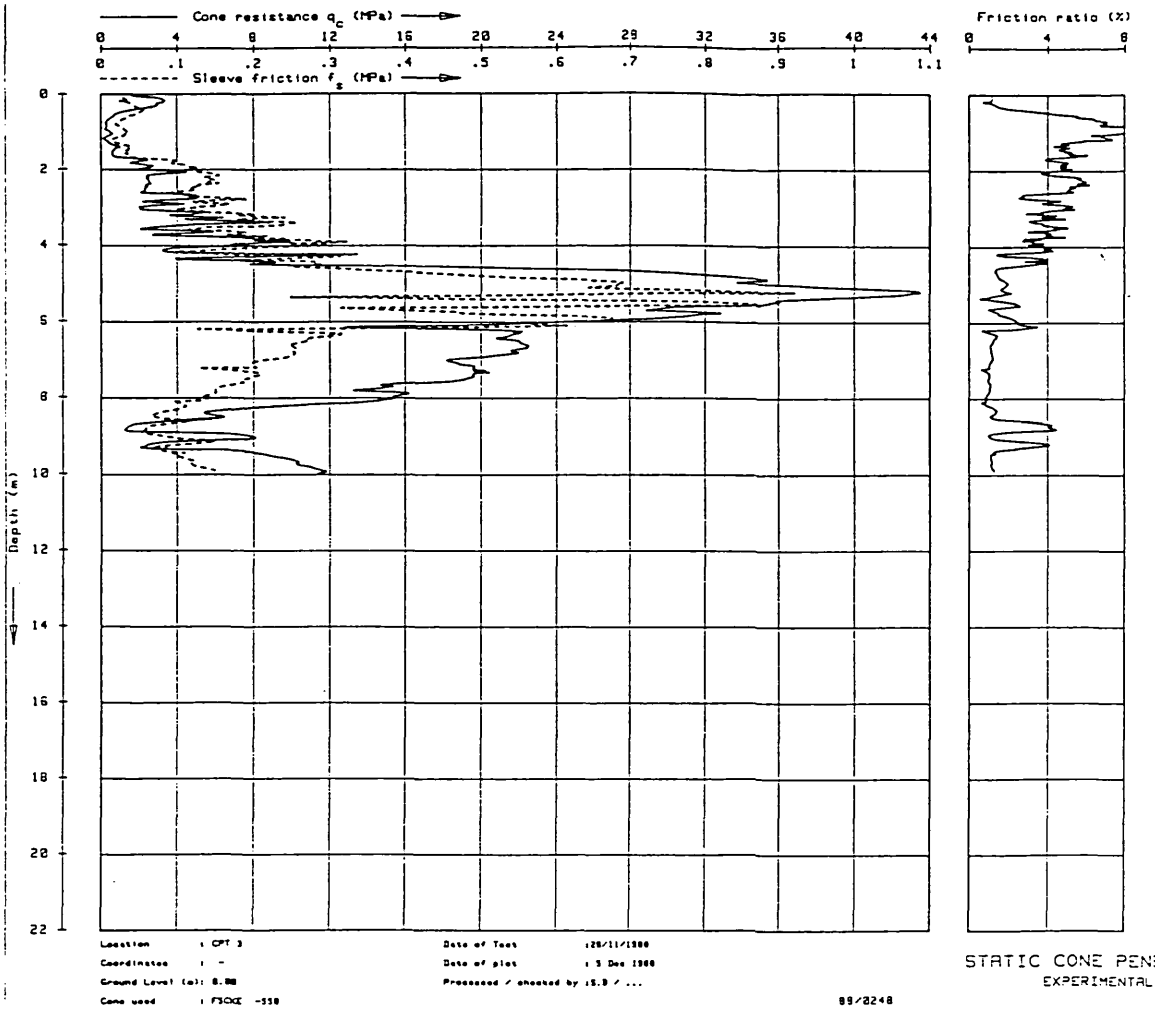

STATIC CONE PENETRATION TEST CPT 3
EXPERIMENTAL SITE - HERMITAGE

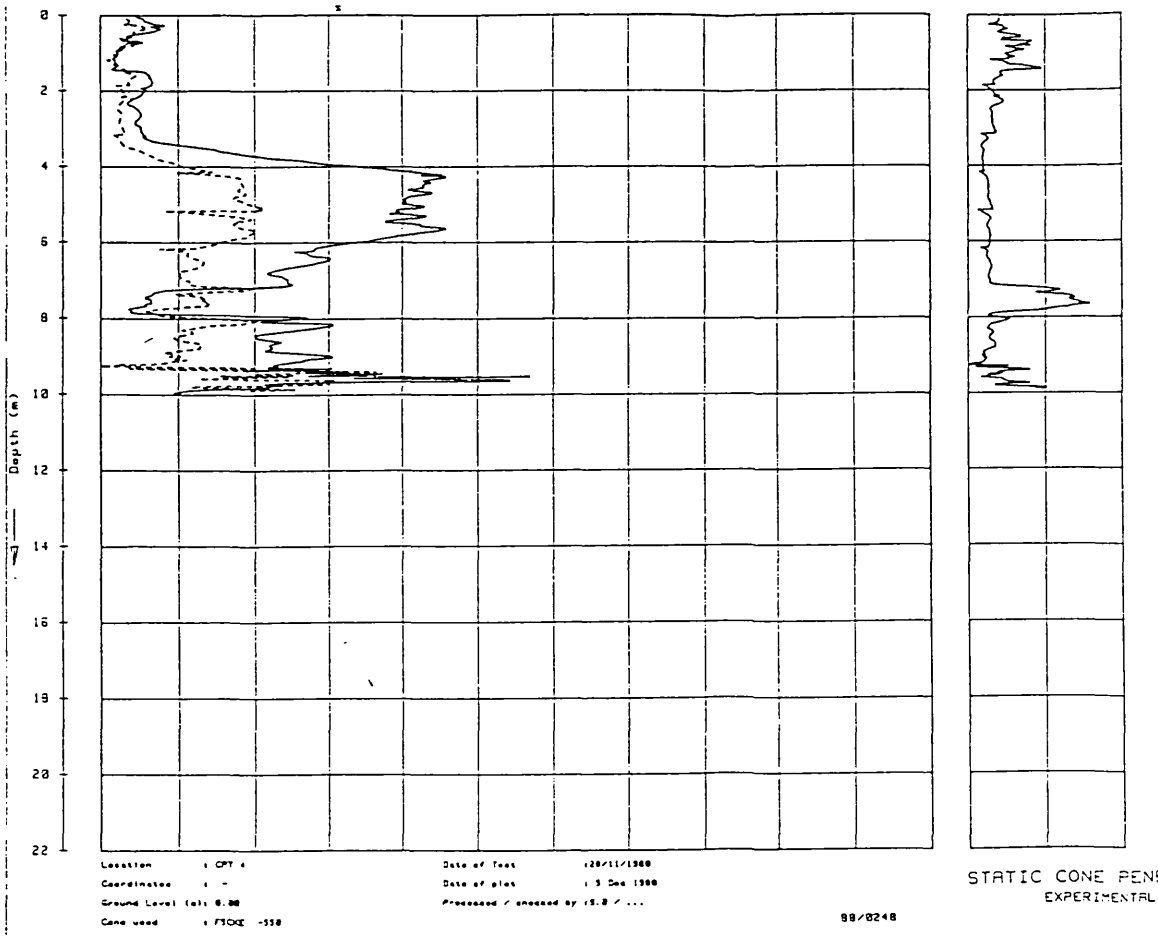

STATIC CONE PENETRATION TEST CPT 4
EXPERIMENTAL SITE - HERMITAGE

Appendix 8.2 (cont.)

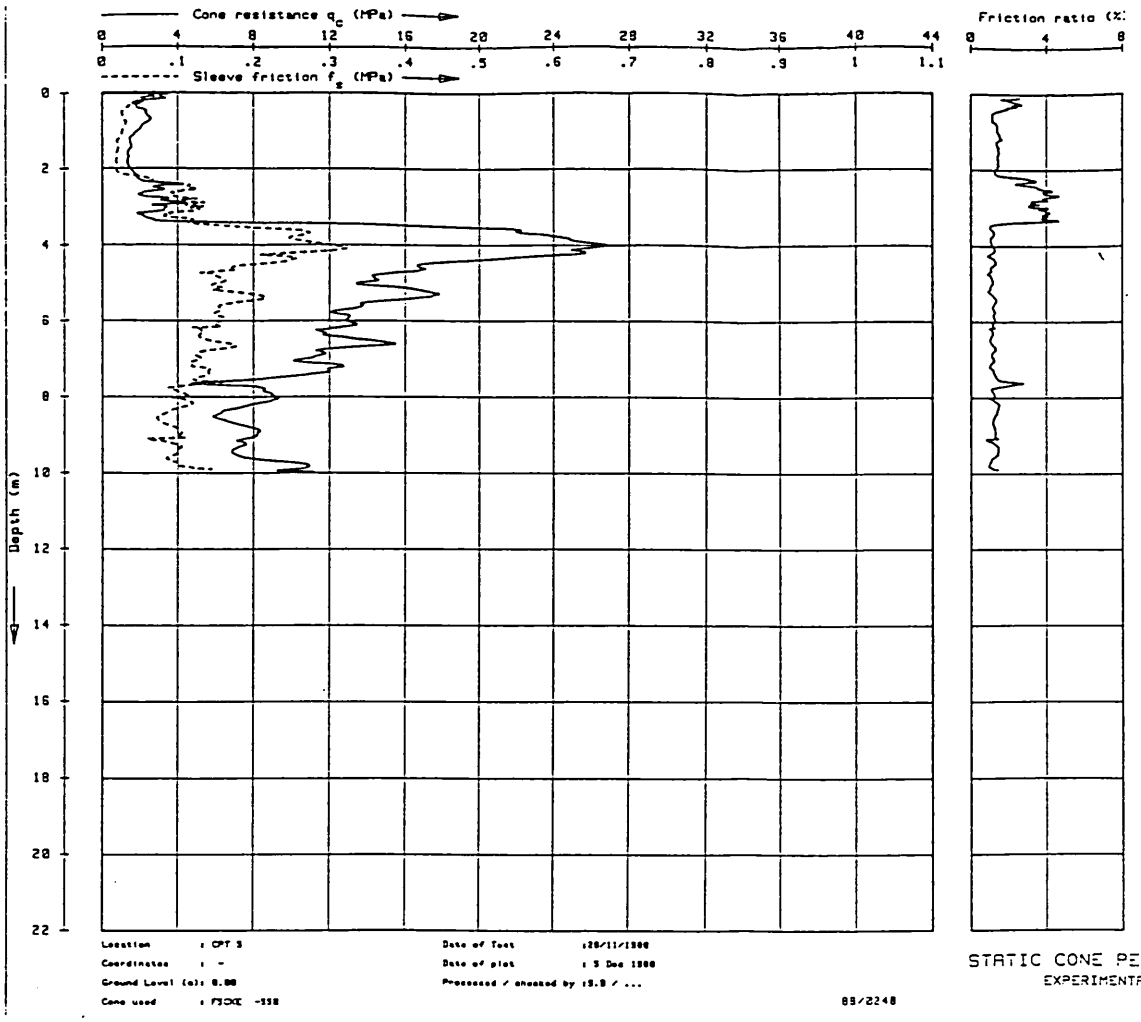

STATIC CONE PENETRATION TEST CPT 5
EXPERIMENTAL SITE - HERMITAGE

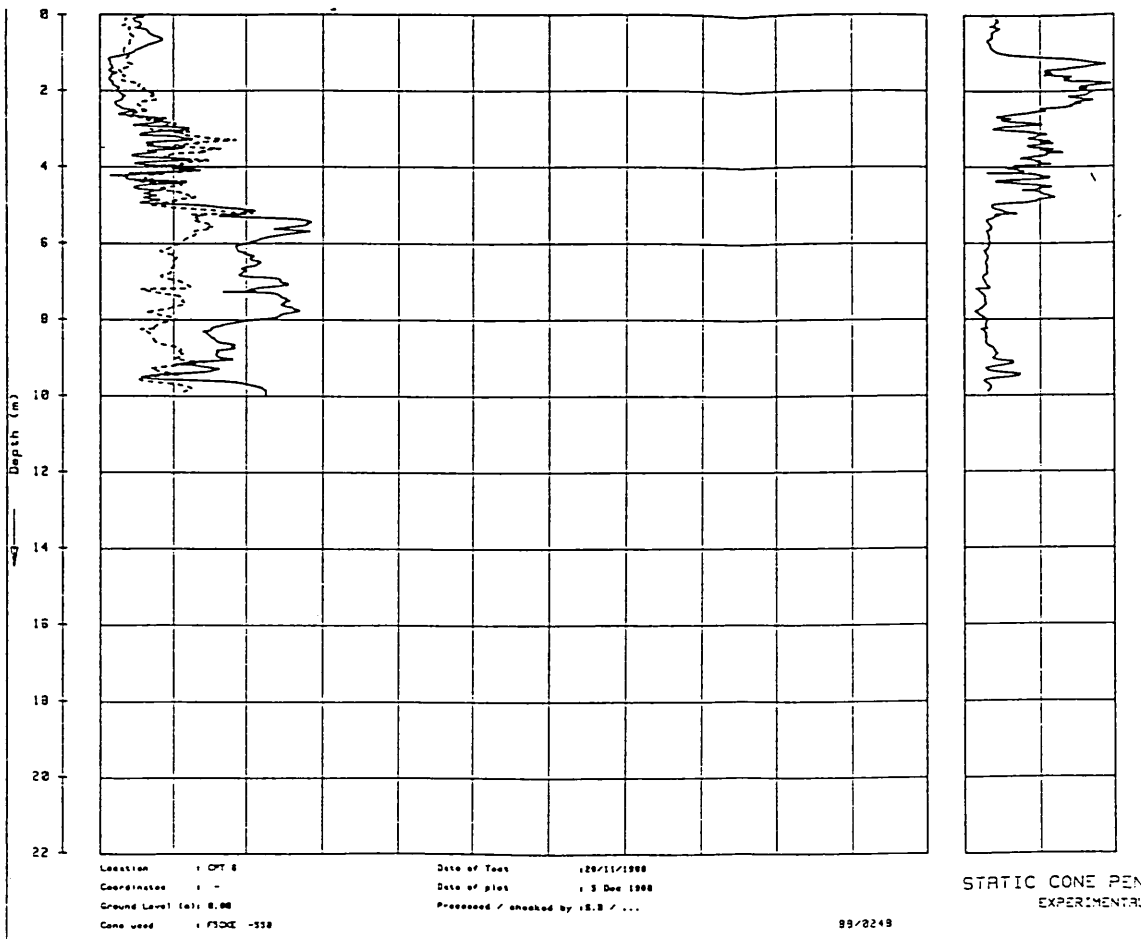

STATIC CONE PENETRATION TEST CPT 6
EXPERIMENTAL SITE - HERMITAGE

Appendix 8.2 (cont.)

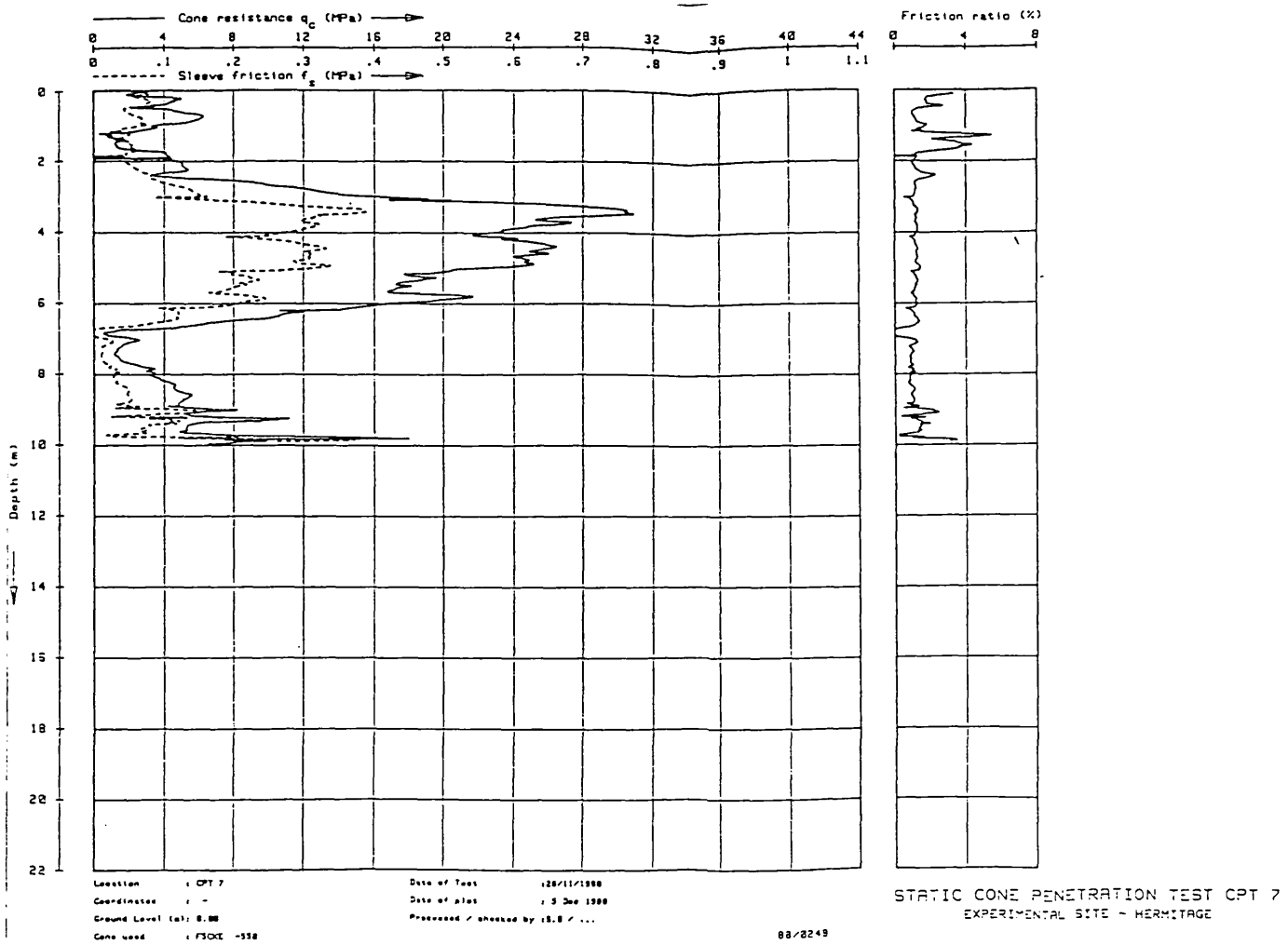

STATIC CONE PENETRATION TEST CPT 7
EXPERIMENTAL SITE - HERMITAGE

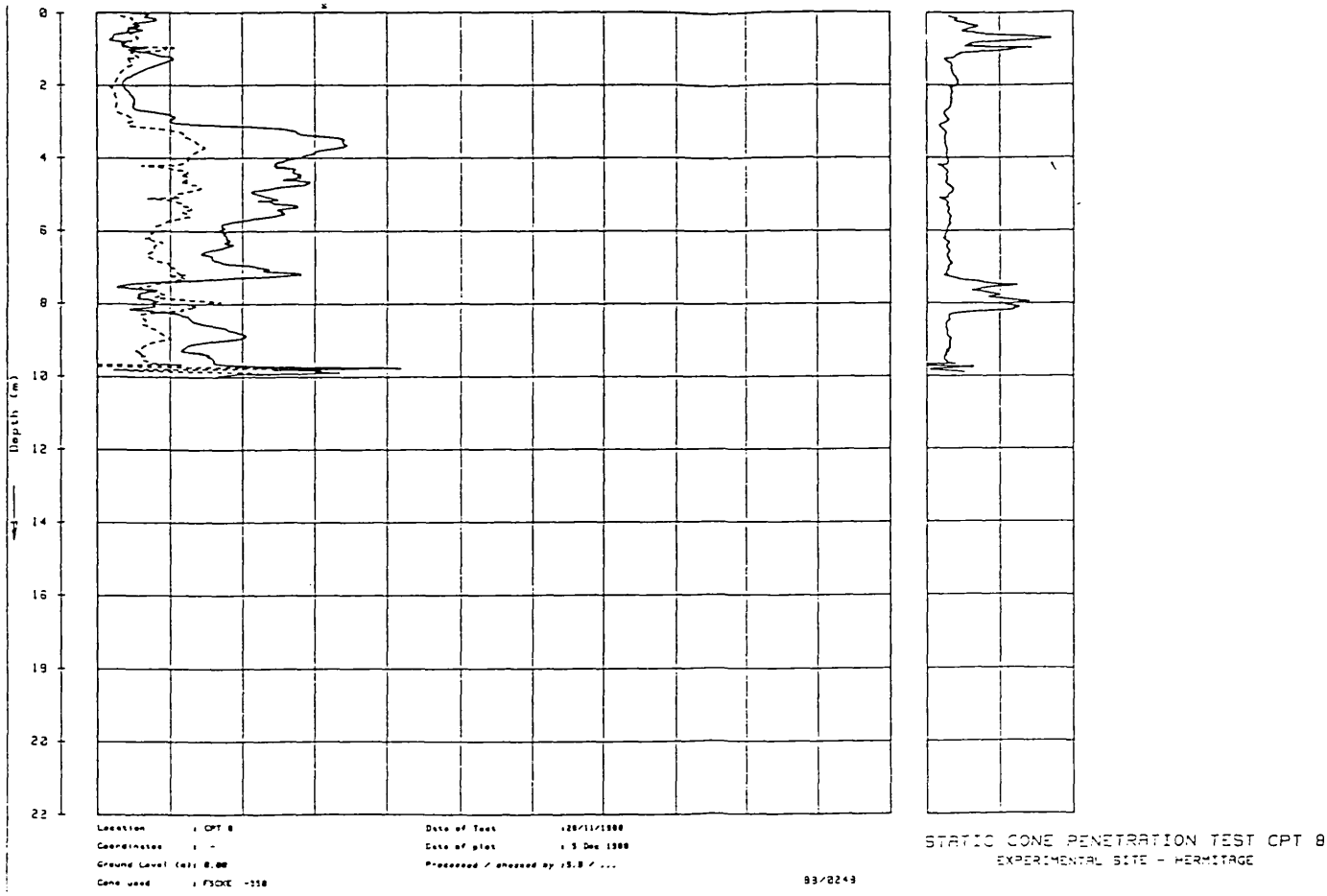

STATIC CONE PENETRATION TEST CPT 8
EXPERIMENTAL SITE - HERMITAGE

Appendix 8.2 (cont.)

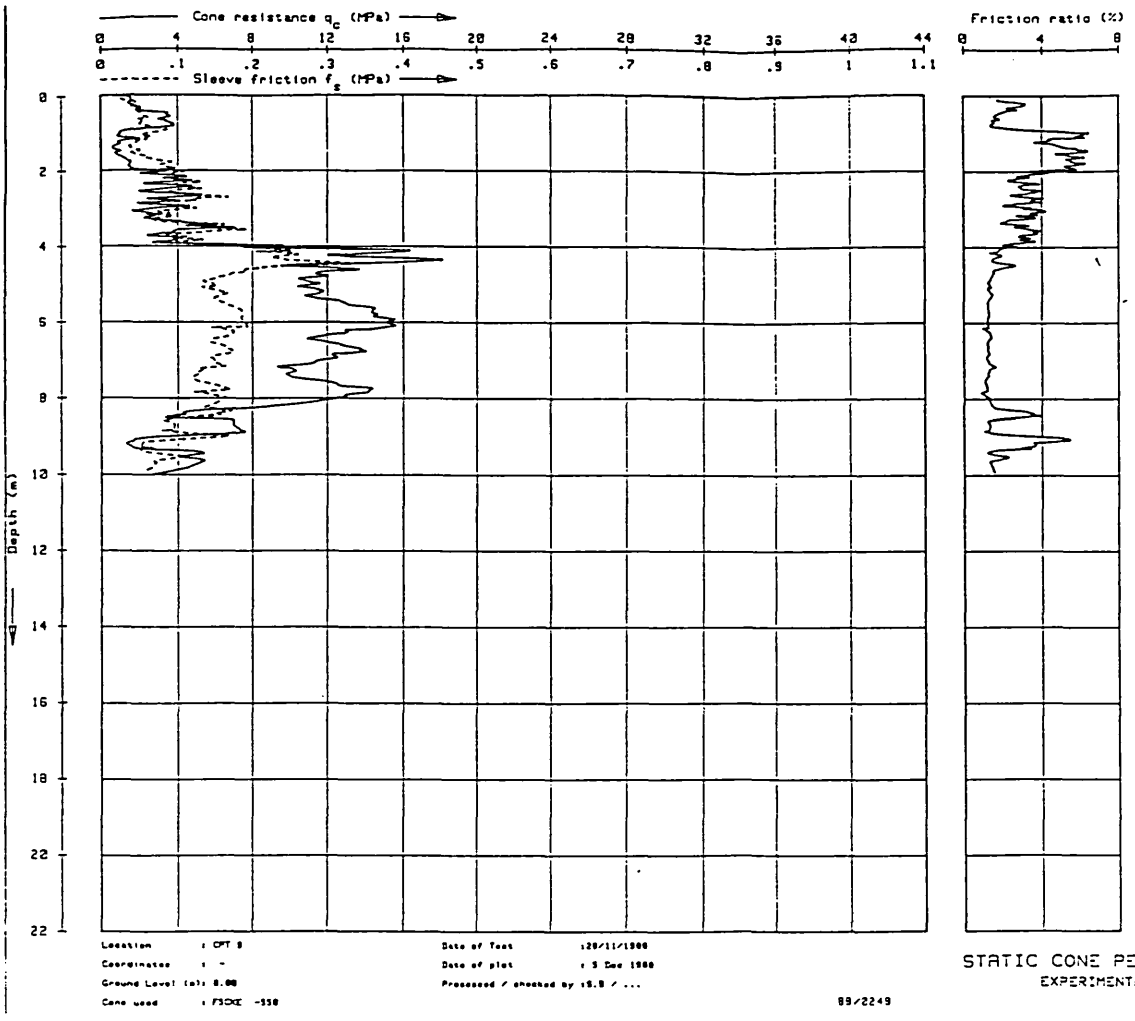

STATIC CONE PENETRATION TEST CPT 9
EXPERIMENTAL SITE - HERMITAGE

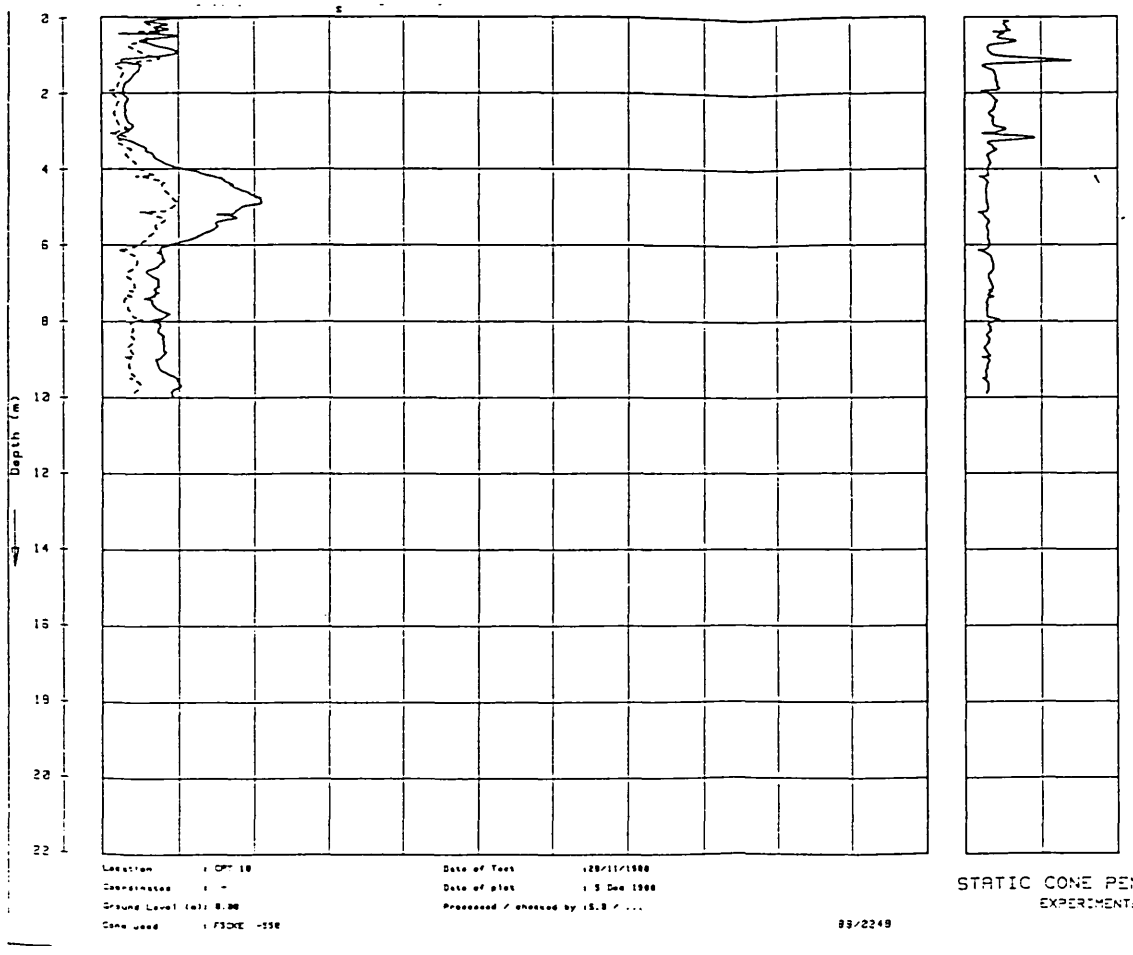

STATIC CONE PENETRATION TEST CPT 10
EXPERIMENTAL SITE - HERMITAGE

Appendix 8.2 (cont.)

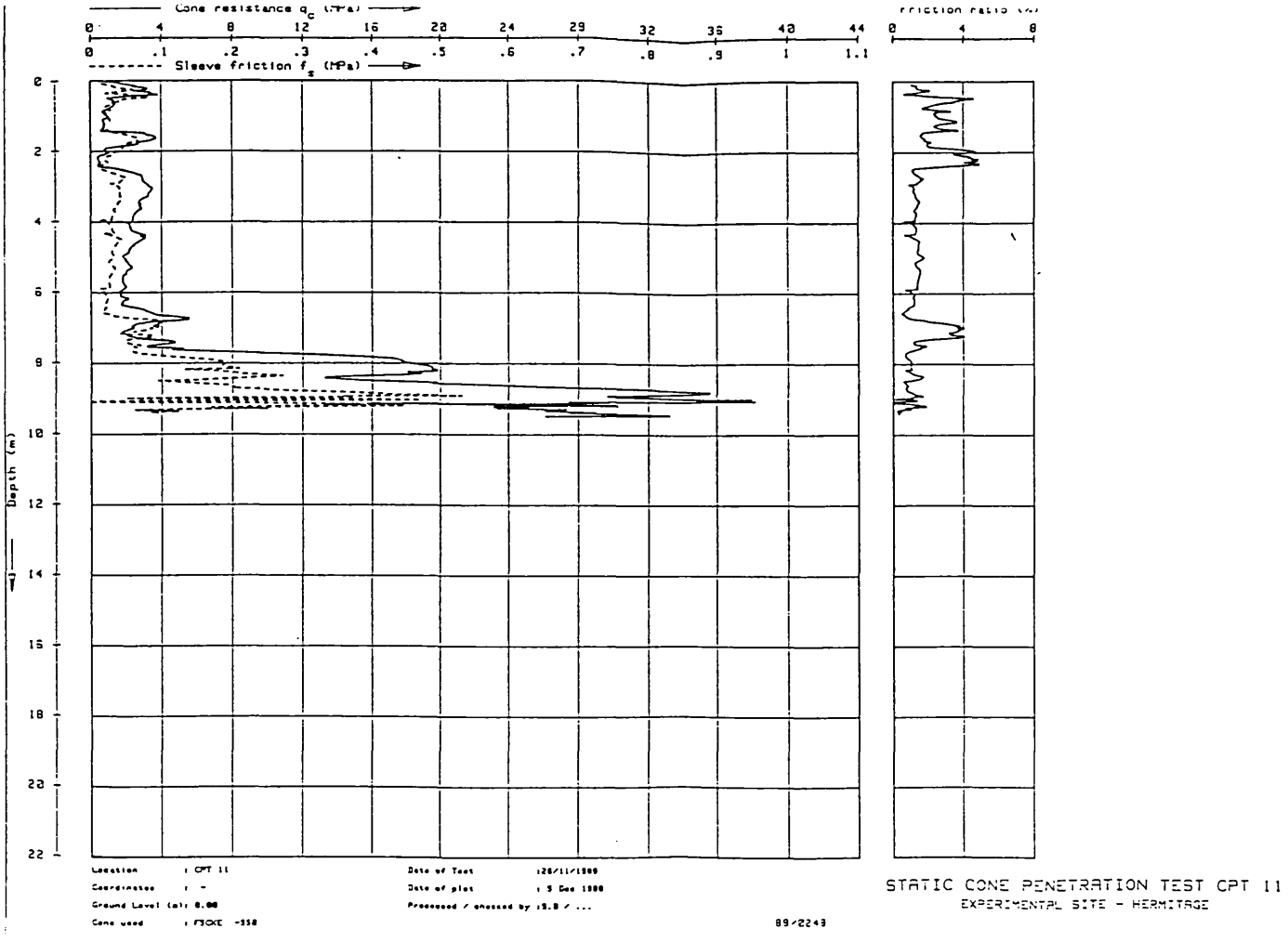

STATIC CONE PENETRATION TEST CPT 11
EXPERIMENTAL SITE - HERMITAGE

Appendix 8.2 (cont.)

IDEAL PROGRAM

```
C***  PROFILE- Version 2


C***  PROFILE- Version 2
C**********************************************
C***  PROGRAM PROFILE
C***  Version 2 - September 1987
C***  Written by David French
C**********************************************
$INSERT SYSCOM:KEYS.F
      INTEGER OUT,OUTFIL,OTBUFD
      DIMENSION INP(30)
      COMMON RNUM(501),POSN(501),DEPL(501),DEFLIN(501),SOIL(501)
      COMMON IFOB(3),REAC(2,3),BMLEN,BMWID,RL1,RL2,EI,SURG
      COMMON DELTA,PO,SEG,SPAN,JSTART,JSTOP,JPROF,J1,J2,J3,J4
      COMMON DAMP,ELEV,ULOAD,VDISP,ANG
      COMMON/FILES/INBUFD(12),OTBUFD(12),INFIL(16),OUTFIL(16),
     C             ITBUFD(12),ITTFIL(16),LDBUFD(12),LDFIL(16),
     C             IN,OUT,ITT,LD
      COMMON/ITER/NN,NNAR(250),AANG(250),KKAR(250),
     C            LLAR(250),FORC(250)
      INTEGER*4 IPASS
      DATA IPASS/'DJF '/
      IBEEP=7
      IN=0
      OUT=0
      ITT=0
      LD=0
      INFIL(1)='---'
      INFIL(2)='---'
      INFIL(3)='---'
      INFIL(4)='---'
      INFIL(5)='---'
      DO 5 I=6,16
       INFIL(I)='  '
5      CONTINUE
      OUTFIL(1)='---'
      OUTFIL(2)='---'
      OUTFIL(3)='---'
      OUTFIL(4)='---'
      OUTFIL(5)='---'
      OUTFIL(6)='---'
      DO 10 I=7,16
       OUTFIL(I)='  '
10     CONTINUE
      ITTFIL(1)='---'
      ITTFIL(2)='---'
      ITTFIL(3)='---'
      ITTFIL(4)='---'
      ITTFIL(5)='---'
      ITTFIL(6)='---'
      DO 15 I=7,16
       ITTFIL(I)='  '
15     CONTINUE
      LDFIL(1)='---'
      LDFIL(2)='---'
      LDFIL(3)='---'
      LDFIL(4)='---'
      DO 18 I=5,16
       LDFIL(I)='  '
18     CONTINUE
      ITBUFD(1)='IT'
      ITBUFD(2)='TO'
      ITBUFD(3)='UT'
      ITBUFD(4)='  '
      ITBUFD(5)='  '
      ITBUFD(6)='  '
      INBUFD(1)='PR'
      INBUFD(2)='OF'
      INBUFD(3)='IN'
      INBUFD(4)='  '
      INBUFD(5)='  '
      INBUFD(6)='  '
      OTBUFD(1)='PR'
      OTBUFD(2)='OF'
      OTBUFD(3)='OU'
      OTBUFD(4)='T '
      OTBUFD(5)='  '
      OTBUFD(6)='  '
      LDBUFD(1)='LD'
      LDBUFD(2)='OU'
      LDBUFD(3)='T '
      LDBUFD(4)='  '
      LDBUFD(5)='  '
      LDBUFD(6)='  '
C**********************
C***  Main menu
C**********************
20    CONTINUE
      CALL CLEAR
      WRITE(1,1000)
      WRITE(1,1010)
      WRITE(1,1020)
25    CONTINUE
      CALL LETTER(INP,30,LET)
      IF(LET.EQ.5) GOTO 999
      IF(LET.EQ.6) GOTO 100
      IF(LET.EQ.18) GOTO 800
      WRITE(1,9000) IBEEP
      CALL SLEEP@(0001000)
      GOTO 25
C**************************************
C***  File handling
C**************************************
100   CONTINUE
      CALL CLEAR
      WRITE(1,1100)
      WRITE(1,1110)(INFIL(I),I=1,16),(OUTFIL(I),I=1,16),
     W                (ITTFIL(I),I=1,16),(LDFIL(I),I=1,16)
      WRITE(1,1010)
      WRITE(1,1120)
      CALL LETTER(INP,30,LET)
      IF(LET.EQ.0)GOTO 20
      IF(LET.EQ.15)GOTO 300
      IF(LET.EQ.4)GOTO 200
      IF(LET.EQ.9)GOTO 400
      IF(LET.EQ.19)GOTO 500
      WRITE(1,9000)IBEEP
      CALL SLEEP@(0001000)
      GOTO 100
C**************************************
C***  Reading name of data file
C**************************************
200   CONTINUE
      IF(IN.EQ.1) CALL CLOS@A(30)
      IN=0
      CALL ATCH@@(IPASS,4,K@CURR,'      ',K@INFD,ICODE)
      CALL ATCH@@(INBUFD,12,K@CURR,'      ',K@ICUR,ICODE)
      WRITE(1,1200)(INFIL(I),I=1,16)
      CALL LETTER (INP,30,LET)
      IF(LET.EQ.0) GOTO 290
210   CONTINUE
      DO 230 I=1,16
       INFIL(I)=INP(I)
230    CONTINUE
220   CONTINUE
      CALL SRCH@@(K@EXST,INFIL,32,0,0,IC)
      IF(IC.EQ.0) GOTO 250
      WRITE(1,1210)(INFIL(I),I=1,16)
      CALL LETTER(INP,30,LET)
      IF(LET.EQ.5) GOTO 999
      GOTO 210
250   CONTINUE
      CALL OPEN@(K@RDWR,INFIL,32,30,1,ICODE)
      IF(ICODE.EQ.0) GOTO 260
      WRITE(1,9010)(INFIL(I),I=1,16)
      CALL BLEEP@(0001000)
      GOTO 200
260   CONTINUE
      CALL ATTDEV(9,7,30,128)
      IN=1
      GOTO 100
C**************************************
C***  Reading name of output file
C**************************************
300   CONTINUE
      IF(OUT.EQ.1) CALL CLOS@A(32)
      OUT=0
      CALL ATCH@@(IPASS,4,K@CURR,'      ',K@INFD,ICODE)
      CALL ATCH@@(OTBUFD,12,K@CURR,'      ',K@ICUR,ICODE)
      WRITE(1,1300)(OUTFIL(I),I=1,16)
      CALL LETTER (INP,30,LET)

C***  PROFILE- Version 2
```

```
310   CONTINUE
      DO 330 I=1,16
       OUTFIL(I)=INP(I)
330    CONTINUE
320   CONTINUE
      CALL SRCH$$(K$EXST,OUTFIL,32,0,0,IC)
      IF(IC.NE.0) GOTO 350
      WWRITE(1,1310)(OUTFIL(I),I=1,16)
      CALL LETTER (INP,30,LET)
      IF(LET.EQ.5) GOTO 999
      GOTO 310
350   CONTINUE
      CALL OPENF(K$RDWR,OUTFIL,32,32,1,ICODE)
      IF(ICODE.EQ.0) GOTO 360
      WWRITE(1,9020)(OUTFIL(I),I=1,16)
      CALL BLEEP$(0001000)
      GOTO 300
360   CONTINUE
      CALL ATTDEV(6,7,32,128)
      OUI=1
      GOTO 100
C***********************************************************
C***  Reading name of iteration file
C***********************************************************
400   CONTINUE
      IF(ITT.EQ.1) CALL CLOS$A(34)
      ITT=0
      CALL ATCH$$(IPASS,4,K$CURR,'      ',K$IMFD,ICODE)
      CALL ATCH$$(ITSUFD,12,K$CURR,'      ',K$ICUR,ICODE)
      WWRITE(1,1400)(ITTFIL(I),I=1,16)
      CALL LETTER (INP,30,LET)
      IF(LET.EQ.0) GOTO 420
410   CONTINUE
      DO 430 I=1,16
       ITTFIL(I)=INP(I)
430    CONTINUE
420   CONTINUE
      CALL SRCH$$(K$EXST,ITTFIL,32,0,0,IC)
      IF(IC.NE.0) GOTO 450
      WWRITE(1,1410)(ITTFIL(I),I=1,16)
      CALL LETTER (INP,30,LET)
      IF(LET.EQ.5) GOTO 999
      GOTO 410
450   CONTINUE
      CALL OPENF(K$RDWR,ITTFIL,32,34,1,ICODE)
      IF(ICODE.EQ.0) GOTO 460
      WWRITE(1,9020)(ITTFIL(I),I=1,16)
      CALL BLEEP$(0001000)
      GOTO 400
460   CONTINUE
      CALL ATTDEV(7,7,34,128)
      ITT=1
      GOTO 100
C***********************************************************
C***  Reading name of load-disp file
C***********************************************************
500   CONTINUE
      IF(LD.EQ.1) CALL CLOS$A(36)
      LD=0
      CALL ATCH$$(IPASS,4,K$CURR,'      ',K$IMFD,ICODE)
      CALL ATCH$$(LDSUFD,12,K$CURR,'      ',K$ICUR,ICODE)
      WWRITE(1,1500)(LDFIL(I),I=1,16)
      CALL LETTER (INP,30,LET)
      IF(LET.EQ.0) GOTO 520
510   CONTINUE
      DO 530 I=1,16
       LDFIL(I)=INP(I)
530    CONTINUE
520   CONTINUE
      CALL SRCH$$(K$EXST,LDFIL,32,0,0,IC)
      IF(IC.NE.0) GOTO 550
      WWRITE(1,1510)(LDFIL(I),I=1,16)
      CALL LETTER (INP,30,LET)
      IF(LET.EQ.5) GOTO 999
      GOTO 510
550   CONTINUE
      CALL OPENF(K$RDWR,LDFIL,32,36,1,ICODE)
      IF(ICODE.EQ.0) GOTO 560
      WWRITE(1,9020)(LDFIL(I),I=1,16)
      CALL BLEEP$(0001000)

C***  PROFILE- Version 2
```

```
      GOTO 500
560   CONTINUE
      CALL ATTDEV(8,7,36,128)
      LD=1
      GOTO 100
C***********************
C***  MAIN PROGRAM
C***********************
800   CONTINUE
      CALL INPUT
      CALL ITRATE
      CALL OUTPUT
C***********************
C***  END OF PROGRAM
C***********************
999   CONTINUE
      CALL CLOS$A(30)
      CALL CLOS$A(32)
      CALL CLOS$A(34)
      CALL CLOS$A(36)
      WWRITE(1,1900)
      CALL EXIT
C***********************************
C***  FORMAT STATEMENTS
C***********************************
1000  FORMAT('Welcome to the program PROFILE (Version 2, Sept 87)'/
     F       'Written by David French'//)
1010  FORMAT(/'Please select one of the following:')
1020  FORMAT(T5,'F - Enter/alter filenames'/
     F       T5,'R - Run the main program'/
     F       'Type E to exit the program')
1100  FORMAT('Option F : Enter/alter filenames'/
     F       '-- ------------ ------------'//)
1110  FORMAT('Current selection of filenames is :'//
     F       T5,'Data file :-',T25,'DJF>PROFIND>',16A2/
     F       T5,'Output file :-',T25,'DJF>PROFOUT>',16A2/
     F       T5,'Iteration file :-',T25,'DJF>ITTOUI>',16A2/
     F       T5,'Iteration file :-',T25,'DJF>LDOUT>',16A2)
1120  FORMAT(15,'D - Enter/alter data filename'/
     F       T5,'O - Enter/alter output filename'/
     F       T5,'I - Enter/alter iteration filename'/
     F       T5,'S - Load - disp curve'//
     F       'Type RETURN for main menu')
1200  FORMAT('Enter name of data file'/
     F       'type RETURN for default: ',16A2)
1210  FORMAT('This file does not exist: ',16A2/
     F       'Please re-enter: '//
     F       'Type E to exit the program')
1300  FORMAT('Enter name of output file'/
     F       'Type RETURN for default: ',16A2)
1310  FORMAT('This file already exists: ',16A2/
     F       'Please re-enter: '//
     F       'Type E to exit the program')
1400  FORMAT('Enter name of iteration file'/
     F       'Type RETURN for default: ',16A2)
1410  FORMAT('This file already exists: ',16A2/
     F       'Please re-enter: '//
     F       'Type E to exit the program')
1500  FORMAT('Enter name of load-disp file'/
     F       'Type RETURN for default: ',16A2)
1510  FORMAT('This file already exists: ',16A2/
     F       'Please re-enter: '//
     F       'Type E to exit the program')
1900  FORMAT(//'You have left the program PROFILE')
9000  FORMAT('Invalid entry - Please try again',A2)
9010  FORMAT('Error in opening data file',16A2)
9020  FORMAT('Error in opening output file',16A2)
      END
C***********************************
C*** SUBROUTINES
C***********************************
C***********************************************************
C***  Routine to read in data and initialise variables
C***********************************************************
      SUBROUTINE INPUT
      INTEGER OUI,OTBUFD,OUTFIL
      DIMENSION QUE85(501)
      COMMON RNUM(501),POSN(501),DEPL(501),DEFLIN(501),SOIL(501)
      COMMON IPOB(3),REAC(2,3),BMLEN,BMWID,RL1,RL2,EI,BUBO
      COMMON DELTA,PO,BEQ,SPAN,JBTART,JBTOP,JPROP,J1,J2,J3,J4
```

```
      COMMON DAMP,ELEV,ULOAD,UDISP,ANG
      COMMON/FILES/INSUFD(12),OTSUFD(12),INFIL(16),OUTFIL(16),
     C             ITSUFD(12),ITIFIL(16),LDSUFD(12),LOFIL(16),
     C             IN,OUT,ITT,LD
      COMMON/ITER/NN,NNAR(250),AANG(250),KKAR(250),
     C            LLAR(250),FORC(250)
      READ(5,*) BMLEN,BMWID,EI,SUBG,RL1,RL2,DELTA,PO,ELEV,NSTOP,
     R          IPOS(3),RDAMP
       X=0.0
       DO 10 J=1,501
        X=X+1.0
        RNUM(J)=X
        SOIL(J)=0.0
10      CONTINUE
       SEG=BMLEN/501
       RRL1=RL1/SEG
       RRL2=RL2/SEG
       IL1=INT(RRL1)
       IL2=INT(RRL2)
       IPOS(1)=IPOS(3)-IL1
       IPOS(2)=IPOS(3)+IL2
       JSTART=IPOS(1)
       JSTOP=IPOS(2)
       JPROP=IPOS(3)
       J1=JSTART-1
       J2=JSTOP+1
       J3=JPROP-1
       J4=JPROP+1
       DO 30 I=1,3
        REAC(1,I)=0.0
30      CONTINUE
       REAC(2,1)=0.0
       REAC(2,2)=DELTA
       REAC(2,3)=ELEV
       DO 40 J=1,501
        POSN(J)=(RNUM(J)*SEG)-(SEG/2)
40      CONTINUE
       POSN(J1)=POSN(J1)+(SEG/2)
       POSN(J2)=POSN(J2)-(0.5*SEG)
       SPAN=POSN(J2)-POSN(J1)
       RL1=POSN(JPROP)-POSN(J1)
       RL2=POSN(J2)-POSN(JPROP)
       DO 50 J=JSTART,JPROP
        QUESS(J)=((POSN(J)-POSN(J1))/(POSN(JPROP)-POSN(J1)))*REAC(2,3)
50      CONTINUE
       DO 60 J=J4,JSTOP
        QUESS(J)=((POSN(J)-POSN(JPROP))/(POSN(J2)-POSN(JPROP)))
     A           *(REAC(2,2)-REAC(2,3))
        QUESS(J)=QUESS(J)+REAC(2,3)
60      CONTINUE
       QUESS(J1)=0.0
       QUESS(J2)=REAC(2,2)
       DO 70 J=1,501
        DEFL(J)=QUESS(J)
70      CONTINUE
       DAMP=1.0
       CALL SPRCL2
C       DAMP=RDAMP
       ANG=0.0
       RETURN
       END
C*************************************************
C***  Routine to output results to file/screen
C*************************************************

      SUBROUTINE OUTPUT
      INTEGER OUT,OTSUFD,OUTFIL
      DIMENSION INP(30)
      COMMON RNUM(501),POSN(501),DEFL(501),DEFLIN(501),SOIL(501)
      COMMON IPOS(3),REAC(2,3),BMLEN,BMWID,RL1,RL2,EI,SUBG
      COMMON DELTA,PO,SEG,SPAN,JSTART,JSTOP,JPROP,J1,J2,J3,J4
      COMMON DAMP,ELEV,ULOAD,UDISP,ANG
      COMMON/FILES/INSUFD(12),OTSUFD(12),INFIL(16),OUTFIL(16),
     C             ITSUFD(12),ITIFIL(16),LDSUFD(12),LOFIL(16),
     C             IN,OUT,ITT,LD
      COMMON/ITER/NN,NNAR(250),AANG(250),KKAR(250),
     C            LLAR(250),FORC(250)
      COMMON/MOM/BHEAR(501),BMOMNT(501)
      CALL MOMENT
      IF(OUT.EQ.0) GOTO 10
      WRITE(6,3600)
      WRITE(6,3610)
      DO 20 J=1,501
       WRITE(6,3620) RNUM(J),POSN(J),DEFL(J),DEFLIN(J),SOIL(J),
     W BHEAR(J),BMOMNT(J)
20     CONTINUE
10    CONTINUE
      IF(ITT.EQ.0) GOTO 30
      WRITE(7,3700)
      WRITE(7,3710)
      DO 40 J=1,250
       WRITE(7,3720) NNAR(J),KKAR(J),LLAR(J),AANG(J),FORC(J)
40     CONTINUE
30    CONTINUE
      IF(LD.EQ.0) GOTO 50
      CALL SHAPE
50    CONTINUE
      CALL CLEAR
      WRITE(1,3000)
      WRITE(1,3010) BMLEN,RL1,RL2,EI,SUBG,DELTA,PO,SEG,SPAN,
     W              ELEV,BMWID,JSTART,JSTOP,NSTOP
      WRITE(1,3020)(IPOS(I),I=1,3)
      WRITE(1,3040)(REAC(1,J),J=1,3)
      WRITE(1,3050)(REAC(2,J),J=1,3)
      WRITE(1,3100)(OUTFIL(I),I=1,16)
      WRITE(1,3900)
      READ(1,*)
      RETURN
3000  FORMAT('PROFILE2 results'/
     F       '---------------')
3010  FORMAT('Beam length = ',F10.6,2X,'Length L1 = ',F10.6/
     F       'Length L2 = ',F10.6,2X,'EI value = ',F10.6/
     F       'Subgrade modulus = ',F10.6,2X,'Delta = ',F10.6/
     F       'Initial spring load = ',F10.6/
     F       'Segmental length = ',F10.6,2X,'Span length = ',F10.6/
     F       'ELEV = ',F10.6,2X,'BMWID = ',F10.6/
     F       'JSTART = ',I4,2X,'JSTOP = ',I4,2X,'NSTOP = ',I4)
3020  FORMAT('Reaction position numbers (Integer) : ',3(I4)/)
3040  FORMAT('Reactions : ',3(F10.6)/)
3050  FORMAT('Reaction elevations : ',3(F13.6)/)
3100  FORMAT('Array data held in DAT>PROFOUT> ',16A2)
3600  FORMAT('RNUM',11X,'POSN',11X,'DEFL',11X,'DEFLIN',9X,'SOIL',11X,
     F       'BHEAR',10X,'MOMENT',9X)
3610  FORMAT(6X,'No.',6X,6X,'m',8X,6X,'mm',7X,6X,'mm',7X,6X,'kN',7X,
     F       6X,'kN',7X,6X,'kNm',6X)
3620  FORMAT(7(F13.6))
3700  FORMAT('NNAR',11X,'KKAR',11X,'LLAR',11X,'MMAR',11X,
     F       'PROP',11X)
3710  FORMAT(4(6X,'No.',6X),6X,'kN',7X)
3720  FORMAT(3(I4),2(F13.10))
3900  FORMAT(//'RUN COMPLETED - Type RETURN to continue')
      END
C*************************************************
C***  Routine to define iterative scheme
C*************************************************
      SUBROUTINE ITRATE
      COMMON RNUM(501),POSN(501),DEFL(501),DEFLIN(501),SOIL(501)
      COMMON IPOS(3),REAC(2,3),BMLEN,BMWID,RL1,RL2,EI,SUBG
      COMMON DELTA,PO,SEG,SPAN,JSTART,JSTOP,JPROP,J1,J2,J3,J4
      COMMON DAMP,ELEV,ULOAD,UDISP,ANG
      COMMON/ITER/NN,NNAR(250),AANG(250),KKAR(250),
     C            LLAR(250),FORC(250)
      NN=0
      CALL ITRANG(0.1)
      CALL ITRELV(0.1)
      CALL ITRELV(0.01)
      RETURN
      END
C*************************************************
C***  Routine to iterate until propping force within
C***  specified limits
C*************************************************
      SUBROUTINE ITRPRP(RTPRP)
      COMMON RNUM(501),POSN(501),DEFL(501),DEFLIN(501),SOIL(501)
      COMMON IPOS(3),REAC(2,3),BMLEN,BMWID,RL1,RL2,EI,SUBG
      COMMON DELTA,PO,SEG,SPAN,JSTART,JSTOP,JPROP,J1,J2,J3,J4
      COMMON DAMP,ELEV,ULOAD,UDISP,ANG
      COMMON/ITER/NN,NNAR(250),AANG(250),KKAR(250),
     C            LLAR(250),FORC(250)
10    CONTINUE
```

```
      PRPOLD=REAC(1,3)
      CALL SPRCL2
      CALL DSPCL2
      CALL PRPCL2
      WRITE(1,9900)REAC(1,3)
9900  FORMAT('PROP= ',F10.6)
      NN=NN+1
      FORC(NN)=REAC(1,3)
      NNAR(NN)=NN
      KKAR(NN)=JSTART
      LLAR(NN)=JSTOP
      AANO(NN)=ANO
      PRCNT=ABS(((REAC(1,3)-PRPOLD)/REAC(1,3))*100)
      IF(PRCNT.LE.RTPRP) GOTO 50
      GOTO 10
50    CONTINUE
      RETURN
      END
C*****************************************************************
C***  Routine to iterate until prop angle within specified limits
C*****************************************************************
      SUBROUTINE ITRANG(RTANG)
      COMMON RNUM(501),POSN(501),DEFL(501),DEFLIN(501),SOIL(501)
      COMMON IPOS(3),REAC(2,3),BMLEN,BMWID,RL1,RL2,EI,SUBG
      COMMON DELTA,PO,SEG,SPAN,JSTART,JSTOP,JPROP,J1,J2,J3,J4
      COMMON DAMP,ELEV,ULOAD,UDISP,ANG
      COMMON/ITER/NN,NNAR(250),AANG(250),KKAR(250),
     C            LLAR(250),FORC(250)
10    CONTINUE
      ANGOLD=ANG
      CALL SPRCL2
      CALL DSPCL2
      CALL PRPCL2
      ANG=(DEFL(J4)-DEFL(J3))/(2*SEG)
      WRITE(1,9901)ANG,REAC(1,3)
9901  FORMAT('ANG= ',F15.10,'PROP= ',F15.10)
C       NN=NN+1
C       NNAR(NN)=NN
C       KKAR(NN)=JSTART
C       LLAR(NN)=JSTOP
C       FORC(NN)=REAC(1,3)
C       AANG(NN)=ANG
      PRCNT=ABS(((ANG-ANGOLD)/ANG)*100)
      IF(PRCNT.LE.RTANG)GOTO 50
      GOTO 10
50    CONTINUE
      WRITE(1,9902)
9902  FORMAT('Iteration completed')
      RETURN
      END
C*****************************************************
C***  Routine to adjust length L1
C*****************************************************
      SUBROUTINE ITRL1(ITL1,RTANG)
      COMMON RNUM(501),POSN(501),DEFL(501),DEFLIN(501),SOIL(501)
      COMMON IPOS(3),REAC(2,3),BMLEN,BMWID,RL1,RL2,EI,SUBG
      COMMON DELTA,PO,SEG,SPAN,JSTART,JSTOP,JPROP,J1,J2,J3,J4
      COMMON DAMP,ELEV,ULOAD,UDISP,ANG
      COMMON/ITER/NN,NNAR(250),AANG(250),KKAR(250),
     C            LLAR(250),FORC(250)
      INDIC=0
10    CONTINUE
      SLOPE=(DEFL(JSTART)-DEFL(J1))/SEG
      WRITE(1,9910)JSTART,SLOPE
9910  FORMAT('JSTART=',I4,'SLOPE=',F10.8)
      IF(SLOPE.GE.0.0) GOTO 20
      IF(INDIC.EQ.2)GOTO 12
      INDIC=1
      GOTO 15
12    CONTINUE
      INDIC=3
15    CONTINUE
      JSTART=JSTART+ITL1
      J1=JSTART-1
      GOTO 30
20    CONTINUE
      IF(INDIC.EQ.1) GOTO 100
      INDIC=2
      JSTART=JSTART-ITL1
      J1=JSTART-1
30    CONTINUE
      IPOS(1)=JSTART
      DO 40 J=1,501
       POSN(J)=(RNUM(J)*SEG)-SEG/2
40    CONTINUE
      POSN(J1)=POSN(J1)+SEG/2
      POSN(J2)=POSN(J2)-SEG/2
      SPAN=POSN(J2)-POSN(J1)
      RL1=POSN(JPROP)-POSN(J1)
      CALL ITRANG(RTANG)
      IF(INDIC.EQ.3) GOTO 100
      GOTO 10
100   CONTINUE
      RETURN
      END
C*****************************************************
C***  Routine to adjust cantilever length L2 until slope at
C***  free end = 0
C*****************************************************
      SUBROUTINE ITRCAN(ITL2,RTANG)
      COMMON RNUM(501),POSN(501),DEFL(501),DEFLIN(501),SOIL(501)
      COMMON IPOS(3),REAC(2,3),BMLEN,BMWID,RL1,RL2,EI,SUBG
      COMMON DELTA,PO,SEG,SPAN,JSTART,JSTOP,JPROP,J1,J2,J3,J4
      COMMON DAMP,ELEV,ULOAD,UDISP,ANG
      COMMON/ITER/NN,NNAR(250),AANG(250),KKAR(250),
     C            LLAR(250),FORC(250)
      INDIC=0
10    CONTINUE
      SLOPE=(DEFL(JSTOP)-DEFL(J2))/SEG
      IF(SLOPE.GT.0)GOTO 20
      IF(INDIC.EQ.2)GOTO 100
      INDIC=1
      JSTOP=JSTOP+ITL2
      J2=JSTOP+1
      GOTO 30
20    CONTINUE
      IF(INDIC.EQ.1)GOTO 40
      INDIC=2
      GOTO 50
40    CONTINUE
      INDIC=3
50    CONTINUE
      JSTOP=JSTOP-ITL2
      J2=JSTOP+1
30    CONTINUE
      IPOS(2)=JSTOP
      DO 80 J=1,501
       POSN(J)=(RNUM(J)*SEG)-SEG/2
80     CONTINUE
      POSN(J1)=POSN(J1)+SEG/2
      POSN(J2)=POSN(J2)-SEG/2
      SPAN=POSN(J2)-POSN(J1)
      CALL ITRANG(RTANG)
      WRITE(1,9966)JSTOP,SLOPE
9966  FORMAT('JSTOP= ',I4,'SLOPE= ',F10.8)
      IF(INDIC.EQ.3)GOTO 100
      GOTO 10
100   CONTINUE
      RL2=POSN(J2)-POSN(JPROP)
      RETURN
      END
C*****************************************************
C***  Routine to adjust prop elevation ELEV until deflection
C***  at free end = Delta
C*****************************************************
      SUBROUTINE ITRELV(RTELV)
      COMMON RNUM(501),POSN(501),DEFL(501),DEFLIN(501),SOIL(501)
      COMMON IPOS(3),REAC(2,3),BMLEN,BMWID,RL1,RL2,EI,SUBG
      COMMON DELTA,PO,SEG,SPAN,JSTART,JSTOP,JPROP,J1,J2,J3,J4
      COMMON DAMP,ELEV,ULOAD,UDISP,ANG
      INDIC=0
10    CONTINUE
      DIFF=DEFL(J2)-DELTA
      IF(DIFF.GT.0)GOTO 20
      IF(INDIC.EQ.2)GOTO 100
      INDIC=1
      ELEV=ELEV+RTELV
      GOTO 30
20    CONTINUE
      IF(INDIC.EQ.1)GOTO 40
```

```
      INDIC=2
      GOTO 50
40    CONTINUE
      INDIC=3
50    CONTINUE
      ELEV=ELEV-RTELV
30    CONTINUE
      CALL ITRCAN(5,0.2)
      CALL ITRL1(5,0.2)
      CALL ITRCAN(1,0.2)
      CALL ITRL1(1,0.2)
      CALL ITRCAN(1,0.2)
      CALL ITRL1(1,0.2)
      CALL ITRCAN(1,0.2)
      WRITE(1,9967)ELEV,DEFL(J2)
9967  FORMAT('ELEV= ',F10.6,'DEFL(J2)= ',F10.6)
      IF(INDIC.EQ.3)GOTO 100
      GOTO 10
100   CONTINUE
      REAC(2,3)=ELEV
      RETURN
      END
C*****************************************************************
C***  Routine to calculate loads due to a set of given
C***  displacements
C*****************************************************************
      SUBROUTINE SPRCL2
      DIMENSION SOLOLD(301),SOLNEW(301)
      COMMON RNUM(301),POSN(301),DEFL(301),DEFLIN(301),SOIL(301)
      COMMON IPOS(3),REAC(2,3),BMLEN,BMWID,RL1,RL2,EI,SUBQ
      COMMON DELTA,PO,SEQ,SPAN,JSTART,JSTOP,JPROP,J1,J2,J3,J4
      COMMON DAMP,ELEV,ULOAD,UDISP,ANG
      DO 10 J=JSTART,JSTOP
       SOLOLD(J)=SOIL(J)
10     CONTINUE
      DO 20 J=JSTART,JSTOP
       SOLNEW(J)=LCON52(DEFL(J),SUBQ,PO)*SEQ*BMWID
       SOIL(J)=(SOLNEW(J)-SOLOLD(J))*DAMP+SOLOLD(J)
20     CONTINUE
      DO 30 J=1,J1
       SOIL(J)=PO*BMWID*SEQ
30     CONTINUE
      DO 60 J=J2,301
       SOIL(J)=0.0
60     CONTINUE
      RETURN
      END
C*****************************************************************
C***  Routine to calculate propping force at position B
C*****************************************************************
      SUBROUTINE PRPCL2
      COMMON RNUM(301),POSN(301),DEFL(301),DEFLIN(301),SOIL(301)
      COMMON IPOS(3),REAC(2,3),BMLEN,BMWID,RL1,RL2,EI,SUBQ
      COMMON DELTA,PO,SEQ,SPAN,JSTART,JSTOP,JPROP,J1,J2,J3,J4
      COMMON DAMP,ELEV,ULOAD,UDISP,ANG
      SUMMT=0.0
      DO 10 J=JSTART,JSTOP
       SUMMT=SUMMT+(POSN(J)-POSN(J1))*SOIL(J)
10     CONTINUE
      REAC(1,3)=SUMMT/(POSN(JPROP)-POSN(J1))
      RETURN
      END
C*****************************************************************
C***  Routine to calculate deflection of propped cantilever
C***  A-B C due to set of soil loads
C*****************************************************************
      SUBROUTINE DSPCL2
      REAL MOM
      COMMON RNUM(301),POSN(301),DEFL(301),DEFLIN(301),SOIL(301)
      COMMON IPOS(3),REAC(2,3),BMLEN,BMWID,RL1,RL2,EI,SUBQ
      COMMON DELTA,PO,SEQ,SPAN,JSTART,JSTOP,JPROP,J1,J2,J3,J4
      COMMON DAMP,ELEV,ULOAD,UDISP,ANG
      THFOLD=0.0
      DO 10 J=1,301
       DEFL(J)=0.0
10     CONTINUE
      DO 20 J=1,J1
       DEFLIN(J)=0.0
20     CONTINUE
      DO 30 J=JSTART,J2
       DEFLIN(J)=((POSN(J)-POSN(J1))/RL1)*ELEV
30     CONTINUE
      JJ=J2+1
      DO 40 J=JJ,301
       DEFLIN(J)=DELTA
40     CONTINUE
C***
C***  Calculate deflection of simply supported beam A-B /
C***  Angle at B due to soil loads
C***
      THETB1=0.0
      DO 100 J=JSTART,J3
       A=POSN(J)-POSN(J1)
       THETB1=THETB1+BANG1(RL1,EI,SOIL(J),A)
       DO 110 JJ=JSTART,J3
        X=POSN(JJ)-POSN(J1)
        V1=DISP1(RL1,EI,SOIL(J),A,X)
        DEFL(JJ)=DEFL(JJ)-V1
110    CONTINUE
100   CONTINUE
C***
C***  Calculate deflection of cantilever B C / moment at B
C***  due to soil loads
C***
      MOM=0.0
      DO 130 J=J4,JSTOP
       A=POSN(J)-POSN(JPROP)
       MOM=MOM+BMOM2(SOIL(J),A)
       DO 160 JJ=J4,J2
        X=POSN(JJ)-POSN(JPROP)
        V3=DISP3(EI,SOIL(J),A,X)
        DEFL(JJ)=DEFL(JJ)-V3
160    CONTINUE
150   CONTINUE
C***
C***  Calculate deflection of simply supported beam A-B / angle
C***  at B due to moment at B
C***
      DO 200 J=JSTART,J3
       X=RL1-(POSN(J)-POSN(J1))
       V2=DISP2(RL1,EI,MOM,X)
       DEFL(J)=DEFL(J)+V2
200   CONTINUE
      THETB2=BANG2(RL1,EI,MOM)
C***
C***  Calculate deflection of cantilever B C due to rotation
C***  at B
C***
      THETB=((THETB1-THETB2)-THFOLD)*0.75+THFOLD
      THFOLD=THETB
      DO 250 J=J4,J2
       X=POSN(J)-POSN(JPROP)
       V4=DISP4(THETB,X)
       DEFL(J)=DEFL(J)+V4
250   CONTINUE
C***
C***  Add initial displacements
C***
      DO 300 J=1,301
       DEFL(J)=DEFL(J)+DEFLIN(J)
300   CONTINUE
      REAC(2,2)=DEFL(J2)
C      WRITE(1,9983)THETB
C9983  FORMAT('THETB= ',F10.8)
      RETURN
      END
C*****************************************************************
C***  Routine to calculate shear forces/bending moments in
C***  deflected beam
C*****************************************************************
      SUBROUTINE MOMENT
      DIMENSION ARM(301)
      COMMON RNUM(301),POSN(301),DEFL(301),DEFLIN(301),SOIL(301)
      COMMON IPOS(3),REAC(2,3),BMLEN,BMWID,RL1,RL2,EI,SUBQ
      COMMON DELTA,PO,SEQ,SPAN,JSTART,JSTOP,JPROP,J1,J2,J3,J4
      COMMON DAMP,ELEV,ULOAD,UDISP,ANG
      COMMON/MOM/SHEAR(301),BMOMNT(301)
      SUMSOL=0.0
      SUMMMT=0.0
```

```
      ARM(J)=POSN(J)-POSN(J1)
      BMOMNT(J)=BOIL(J)*ARM(J)
10    CONTINUE
      DO 20 J=JSTART,JSTOP
       SUMSOL=SUMSOL+BOIL(J)
       SUMMMT=SUMMMT+BMOMNT(J)
20    CONTINUE
      REAC(1,2)=(SUMMMT-REAC(1,3)*(POSN(JPROP)-POSN(J1)))/SPAN
      REAC(1,1)=SUMSOL-REAC(1,2)-REAC(1,3)
      DO 30 J=JSTART,JPROP
       SUMMMT=0.0
       SUMSOL=0.0
       DO 40 JJ=JSTART,J
        SUMMMT=SUMMMT-((ARM(J)-ARM(JJ))*BOIL(JJ))
        SUMSOL=SUMSOL-BOIL(JJ)
40     CONTINUE
       BMOMNT(J)=SUMMMT+REAC(1,1)*ARM(J)
       SHEAR(J)=SUMSOL+REAC(1,1)
30    CONTINUE
      DO 50 J=J4,JSTOP
       SUMMMT=0.0
       SUMSOL=0.0
       DO 60 JJ=JSTART,J
        SUMMMT=SUMMMT-((ARM(J)-ARM(JJ))*BOIL(JJ))
        SUMSOL=SUMSOL-BOIL(JJ)
60     CONTINUE
       BMOMNT(J)=SUMMMT+(REAC(1,1)*ARM(J))+(REAC(1,3)
     A           *(ARM(J)-ARM(JPROP)))
       SHEAR(J)=SUMSOL+REAC(1,1)+REAC(1,3)
50    CONTINUE
      DO 100 J=1,J1
       BMOMNT(J)=0.0
       SHEAR(J)=0.0
100   CONTINUE
      DO 110 J=J2,501
       BMOMNT(J)=0.0
       SHEAR(J)=0.0
110   CONTINUE
      RETURN
      END
C*****************************************************************
C***  Routine to plot load-displacement graph for
C***  displacement -10 - +40 mm
C*****************************************************************
      SUBROUTINE SHAPE
      INTEGER OU1,OTSUFD,OUTFIL
      DIMENSION X(61),Y(61)
      COMMON RNUM(501),POSN(501),DEFL(501),DEFLIN(501),BOIL(501)
      COMMON IPOS(3),REAC(2,3),BMLEN,BMWID,RL1,RL2,EI,SUBQ
      COMMON DELTA,PO,SEC,SPAN,JSTART,JSTOP,JPROP,J1,J2,J3,J4
      COMMON DAMP,ELEV,ULOAD,UDISP,ANG
      COMMON/FILES/INSUFD(12),OTSUFD(12),INFIL(16),OUTFIL(16),
     C             ITSUFD(12),ITIFIL(16),LDSUFD(12),LDFIL(16),
     C             IN,OUT,IT1,LD
      W=-11.0
      DO 10 J=1,61
      W=W+1.0
      X(J)=W
      Y(J)=LCONS3(W,SUBQ,PO)
10    CONTINUE
      WRITE(8,3800)
      WRITE(8,3810)
      DO 20 J=1,61
       WRITE(8,3820)X(J),Y(J)
20     CONTINUE
      WRITE(8,3830)
      XU1=UDISP
      YU1=ULOAD
      XU2=XU1-(YU1/450.0)*2.0
      YU2=0.0
      WRITE(8,3840)XU1,YU1,XU2,YU2
      WRITE(8,3830)
      RETURN
3800  FORMAT('Disp',11X,'Pressure',7X)
3810  FORMAT(6X,'mm',7X,6X,'kN/mm2',4X)
3820  FORMAT(2(F15.3))
3830  FORMAT('END OF CYCLE')
3840  FORMAT(2(F15.3)/2(F15.3))
      END
C*****************************************************************
C***  Function to calculate displacements due to cocentrated
C***  load on simply supported beam
C*****************************************************************
      FUNCTION DISP1(L,EI,P,A,X)
      REAL L
      B=L-A
      IF(X.GT.A) GOTO 10
      TERM1= L**2 - B**2 - X**2
      DISP1=((1000*P*B*X)/(6*L*EI))*TERM1
      GOTO 20
10    CONTINUE
      TERM1= L**2 - B**2 - X**2
      TERM2= (X-A)**3
      DISP1=((1000*P*B*X)/(6*L*EI)*TERM1) + (1000*P/(6*EI))*TERM2
20    CONTINUE
      RETURN
      END
C*****************************************************************
C***  Function to calculate displacements due to moment at end
C***  of  simply supported beam
C*****************************************************************
      FUNCTION DISP2(L,EI,M,X)
      REAL L,M
      TERM1=(2*L**2-3*L*X+X**2)
      DISP2=(1000*M*X*TERM1)/(6*L*EI)
      RETURN
      END
C*****************************************************************
C***  Function to calculate displacements due to concentrated
C***  load on cantilever
C*****************************************************************
      FUNCTION DISP3(EI,P,A,X)
      IF(X.GT.A)GOTO 10
      DISP3=(1000*P*X**2*(3*A-X))/(6*EI)
      GOTO 20
10    CONTINUE
      DISP3=(1000*P*A**2*(3*X-A))/(6*EI)
20    CONTINUE
      RETURN
      END
C*****************************************************************
C***  Function to calculate displacements at end of cantilever
C***  B C due to rotation at B
C*****************************************************************
      FUNCTION DISP4(ANG,X)
      DISP4=1000*ANG*X
      RETURN
      END
C*****************************************************************
C***  Funtion to calculate load required for given
C***  displacement on simply supported beam
C*****************************************************************
      FUNCTION PROP(L,EI,X,V)
      REAL L
      PROP=(0.001*V*6*L*EI)/(2*X**2*(L-X)**2)
      RETURN
      END
C*****************************************************************
C***  Function to calculate angle at end of simply supported
C***  bean due to intermediate concentrated load
C*****************************************************************
      FUNCTION BANG1(L,EI,P,A)
      REAL L
      B=L-A
      BANG1=(P*A*B*(L+A))/(6*L*EI)
      RETURN
      END
C*****************************************************************
C***  Function to calculate angle at end of simply supported
C***  beam due to moment applied at that end
C*****************************************************************
      FUNCTION BANG2(L,EI,M)
      REAL L,M
      BANG2=(M*L)/(3*EI)
      RETURN
      END
C*****************************************************************
C***  Function to calculate moment at B due to concentrated
C***  load on cantilever B-C
```

```
      FUNCTION BMOM2(P,X)
      BMOM2=P*X
      RETURN
      END
C*************************************************************
C***  Function to calculate soil pressure for given displacement
C*************************************************************
      FUNCTION LCONS1(DSP,C1,PO)
C       IF(DSP.LT.0)GOTO 10
C       LCONS1=(DSP*C1)+PO
C       GOTO 20
C10     CONTINUE
C       LCONS1=PO
C20     CONTINUE
        LCONS1=PO
      RETURN
      END
C*************************************************************
C***  Function to calculate soil pressure for given displacement
C*************************************************************
      FUNCTION LCONS2(DSP,C2,PO)
      IF(DSP.GT.10.0)GOTO 10
      LCONS2=((DSP/10)*PO*1)+PO
      GOTO 20
10    CONTINUE
      LCONS2=(PO*1)+PO
20    CONTINUE
      RETURN
      END
C*************************************************************
C***  Function to calculate soil pressure for given displacement
C*************************************************************
      FUNCTION LCONS3(DSP,C3,PO)
      IF(DSP.LT.0.0)GOTO 10
      IF(DSP.GT.20.0)GOTO 20
      LCONS3=450.0-(((20.0-DSP)/20.0)**5)*(450-PO)
      GOTO 30
10    CONTINUE
      LCONS3=PO
      GOTO 30
20    CONTINUE
      LCONS3=450
30    CONTINUE
      RETURN
      END
C*************************************************************
C***  Function to calculate soil pressure for given displacement
C***  (Unloading mode)
C*************************************************************
      FUNCTION VCONS1(DSP,ULOAD,UDISP)
      IF(DSP.LT.0.0)GOTO 10
      VCONS1=ULOAD-((UDISP-DSP)/2.0)*450.0
      GOTO 20
10    CONTINUE
      VCONS1=0.0
20    CONTINUE
      RETURN
      END
```

BLUNT PROGRAM

```
      COMMON DAMP,XXXX,ULOAD,UDISP
      COMMON/FILES/INSUFD(12),OTSUFD(12),INFIL(16),OUTFIL(16),
     C             ITSUFD(12),ITTFIL(16),LDSUFD(12),LNFIL(16),
     C             IN,OUT,ITT,LD
      COMMON/ITER/NN,MM,KK,LL,NNAR(100),MMAR(100),KKAR(100),
     C            LLAR(100),FORC(100)
      COMMON/MOM/SHEAR(501),BMOMNT(501)
      CALL MOMENT
      IF(OUT.EQ.0) GOTO 10
      WRITE(6,3600)
      WRITE(6,3610)
      DO 20 J=1,501
       WRITE(6,3620) RNUM(J),POSN(J),DEFL(J),DEFLIN(J),SOIL(J),
     W SHEAR(J),BMOMNT(J)
20     CONTINUE
10     CONTINUE
      IF(ITT.EQ.0) GOTO 30
      WRITE(7,3700)
      WRITE(7,3710)
      DO 40 J=1,100
       WRITE(7,3720) NNAR(J),KKAR(J),LLAR(J),MMAR(J),FORC(J)
40     CONTINUE
30    CONTINUE
      IF(LD.EQ.0) GOTO 50
      CALL SHAPE
50    CONTINUE
      CALL CLEAR
      WRITE(1,3000)
      WRITE(1,3010) BMLEN,RL1,RL2,EI,SUBQ,DELTA,PO,DPROP,SEQ,SPAN,
     W              XXXX,BMWID,JSTART,JSTOP,NSTOP
      WRITE(1,3020)(IPOS(I),I=1,3)
      WRITE(1,3030)(RPOS(I),I=1,3)
      WRITE(1,3040)(REAC(1,J),J=1,3)
      WRITE(1,3050)(REAC(2,J),J=1,3)
      WRITE(1,3100)(OUTFIL(I),I=1,16)
      WRITE(1,3900)
      READ(1,*)
      RETURN
3000  FORMAT('PROFILE results'/
     F       '---------------')
3010  FORMAT('Beam length = ',F10.3,2X,'Length L1 = ',F10.3/
     F       'Length L2 = ',F10.3,2X,'EI value = ',F10.3/
     F       'Subgrade modulus = ',F10.3,2X,'Delta = ',F10.3/
     F       'Initial spring load = ',F10.3,2X,'DPROP = ',F10.3/
     F       'Segmental length = ',F10.3,2X,'Span length = ',F10.3/
     F       'XXXX = ',F10.3,2X,'BMWID = ',F10.3/
     F       'JSTART = ',I4,2X,'JSTOP = ',I4,2X,'NSTOP = ',I4)
3020  FORMAT('Reaction position numbers (Integer) : ',3(I4)/)
3030  FORMAT('Reaction position numbers (Real) : ',3(F10.3)/)
3040  FORMAT('Reactions : ',3(F10.3)/)
3050  FORMAT('Reaction elevations : ',3(F15.3)/)
3100  FORMAT('Array data held in DJF>PROFOUT> ',16A2)
3600  FORMAT('RNUM',11X,'POSN',11X,'DEFL',11X,'DEFLIN',9X,'SOIL',11X,
     F       'SHEAR',10X,'MOMENT',9X)
3610  FORMAT(6X,'No.',6X,6X,'m',8X,6X,'mm',7X,6X,'mm',7X,6X,'kN',7X,
     F       6X,'kN',7X,6X,'kNm',6X)
3620  FORMAT(7(F15.3))
3700  FORMAT('NNAR',11X,'KKAR',11X,'LLAR',11X,'MMAR',11X,
     F       'PROP',11X)
3710  FORMAT(4(6X,'No.',6X),6X,'kN',7X)
3720  FORMAT(4(I4),F15.3)
3900  FORMAT(//'RUN COMPLETED - Type RETURN to continue')
      END
C*************************************************************
C***  Routine to define iterative scheme
C*************************************************************
      SUBROUTINE ITRATE
      COMMON RNUM(501),POSN(501),DEFL(501),DEFLIN(501),SOIL(501)
      COMMON IPOS(3),RPOS(3),REAC(2,3),BMLEN,BMWID,RL1,RL2,EI,SUBQ
      COMMON DELTA,PO,SEQ,SPAN,DPROP,JSTART,JSTOP,NSTOP
      COMMON DAMP,XXXX,ULOAD,UDISP
      COMMON/ITER/NN,MM,KK,LL,NNAR(100),MMAR(100),KKAR(100),
     C            LLAR(100),FORC(100)
      NN=0
      KK=0
      LL=0
      MM=0
      CALL ITRPRP(0.1)
      RETURN
      END
```

```
C*****************************************************
C***  Routine to iterate until propping force within
C***  specified limits
C*****************************************************
      SUBROUTINE ITRPRP(RTPRP)
      COMMON RNUM(501), POSN(501), DEFL(501), DEFLIN(501), SOIL(501)
      COMMON IPOS(3), RPOS(3), REAC(2,3), BMLEN, BMWID, RL1, RL2, EI, SUMG
      COMMON DELTA, PO, SEG, SPAN, DPROP, JSTART, JSTOP, NSTOP
      COMMON DAMP, XXXX, ULOAD, UDISP
      COMMON/ITER/NN, MM, KK, LL, NNAR(100), MMAR(100), KKAR(100),
     C            LLAR(100), FORC(100)
10    CONTINUE
      PRPOLD=REAC(1,3)
      CALL SPRCAL
      CALL DSPCAL
      CALL PRPCAL
      WRITE(1,9900)REAC(1,3)
9900  FORMAT('PROP= ',F10.3)
      NN=NN+1
      MM=MM+1
      FORC(NN)=REAC(1,3)
      NNAR(NN)=NN
      KKAR(NN)=KK
      LLAR(NN)=LL
      MMAR(NN)=MM
      PRCNT=ABS((REAC(1,3)-PRPOLD)/REAC(1,3))*100)
      IF(PRCNT.LE.RTPRP) GOTO 50
      GOTO 10
50    CONTINUE
      RETURN
      END
C*****************************************************
C***  Routine to adjust length L1
C*****************************************************
      SUBROUTINE ITRL1(ITL1,RTPRP)
      COMMON RNUM(501), POSN(501), DEFL(501), DEFLIN(501), SOIL(501)
      COMMON IPOS(3), RPOS(3), REAC(2,3), BMLEN, BMWID, RL1, RL2, EI, SUMG
      COMMON DELTA, PO, SEG, SPAN, DPROP, JSTART, JSTOP, NSTOP
      COMMON DAMP, XXXX, ULOAD, UDISP
      COMMON/ITER/NN, MM, KK, LL, NNAR(100), MMAR(100), KKAR(100),
     C            LLAR(100), FORC(100)
      INDIC=0
      J1=JSTART-1
10    CONTINUE
      SLOPE=(DEFL(JSTART)-DEFL(J1))/SEG
      WRITE(1,9910)JSTART, SLOPE
9910  FORMAT('JSTART=',I4,'SLOPE=',F10.5)
      IF(SLOPE.GE.0.0) GOTO 20
      IF(INDIC.EQ.2)GOTO 12
      INDIC=1
      GOTO 15
12    CONTINUE
      INDIC=3
15    CONTINUE
      JSTART=JSTART+ITL1
      J1=JSTART-1
      GOTO 30
20    CONTINUE
      IF(INDIC.EQ.1) GOTO 100
      INDIC=2
      JSTART=JSTART-ITL1
      J1=JSTART-1
30    CONTINUE
      IPOS(1)=JSTART
      RPOS(1)=RNUM(JSTART)
      SPAN=(RNUM(JSTOP)-RNUM(JSTART)+1)*SEG
      DO 40 J=1,501
       POSN(J)=(RNUM(J)*SEG)-SEG/2
40    CONTINUE
      POSN(J1)=POSN(J1)+SEG/2
      POSN(J2)=POSN(J2)-SEG/2
      DO 60 J=JSTART, JSTOP
       DEFLIN(J)=((((RNUM(J)-RNUM(JSTART))*SEG)+SEG/2)/SPAN)*DELTA
60     CONTINUE
      DEFLIN(J1)=0.0
      KK=JSTART
      CALL ITPPRP(RTPRP)
      FORC(NN)=REAC(1,3)
      NNAR(NN)=NN
      KKAR(NN)=KK
      LLAR(NN)=LL
      MMAR(NN)=MM
      IF(INDIC.EQ.3) GOTO 100
      GOTO 10
100   CONTINUE
      IL1=IPOS(3)-JSTART
      RL1=(RNUM(IL1)+0.5)*SEG
      RETURN
      END
C*****************************************************
C***  Routine to adjust length L2
C*****************************************************
      SUBROUTINE ITRL2(ITL2,RTPRP)
      COMMON RNUM(501), POSN(501), DEFL(501), DEFLIN(501), SOIL(501)
      COMMON IPOS(3), RPOS(3), REAC(2,3), BMLEN, BMWID, RL1, RL2, EI, SUMG
      COMMON DELTA, PO, SEG, SPAN, DPROP, JSTART, JSTOP, NSTOP
      COMMON DAMP, XXXX, ULOAD, UDISP
      COMMON/ITER/NN, MM, KK, LL, NNAR(100), MMAR(100), KKAR(100),
     C            LLAR(100), FORC(100)
      INDIC=0
      J2=JSTOP+1
10    CONTINUE
      SLOPE=(DEFL(JSTOP)-DEFL(J2))/SEG
      WRITE(1,9920)JSTOP, SLOPE
9920  FORMAT('JSTOP=',I4,'SLOPE=',F10.5)
      IF(SLOPE.LE.0.0) GOTO 20
      IF(INDIC.EQ.2)GOTO 100
      INDIC=1
      JSTOP=JSTOP+ITL2
      J2=JSTOP+1
      GOTO 30
20    CONTINUE
      IF(INDIC.EQ.1) GOTO 22
      INDIC=2
      GOTO 25
22    CONTINUE
      INDIC=3
25    CONTINUE
      JSTOP=JSTOP-ITL2
      J2=JSTOP+1
30    CONTINUE
      IPOS(2)=JSTOP
      RPOS(2)=RNUM(JSTOP)
      SPAN=(RNUM(JSTOP)-RNUM(JSTART)+1)*SEG
      DO 40 J=1,501
       POSN(J)=(RNUM(J)*SEG)-SEG/2
40    CONTINUE
      POSN(J1)=POSN(J1)+SEG/2
      POSN(J2)=POSN(J2)-SEG/2
      DO 60 J=JSTART, JSTOP
       DEFLIN(J)=((((RNUM(J)-RNUM(JSTART))*SEG)+SEG/2)/SPAN)*DELTA
60     CONTINUE
      DEFLIN(J2)=DELTA
      LL=JSTOP
      CALL ITRPRP(RTPRP)
      FORC(NN)=REAC(1,3)
      NNAR(NN)=NN
      KKAR(NN)=KK
      LLAR(NN)=LL
      MMAR(NN)=MM
      IF(INDIC.EQ.3) GOTO 100
      GOTO 10
100   CONTINUE
      IL2=JSTOP-IPOS(3)
      RL2=(RNUM(IL2)+0.5)*SEG
      RETURN
      END
C*****************************************************
C***  Routine to calculate loads due to a set of given
C***  displacements
C*****************************************************
      SUBROUTINE SPRCAL
      DIMENSION SOLOLD(501), SOLNEW(501)
      COMMON RNUM(501), POSN(501), DEFL(501), DEFLIN(501), SOIL(501)
      COMMON IPOS(3), RPOS(3), REAC(2,3), BMLEN, BMWID, RL1, RL2, EI, SUMG
      COMMON DELTA, PO, SEG, SPAN, DPROP, JSTART, JSTOP, NSTOP
      COMMON DAMP, XXXX, ULOAD, UDISP
      J1=JSTART-1
      J2=JSTOP+1
      JPROP=IPOS(3)
```

```
      DO 10 J=JSTART, JSTOP
       SOLOLD(J)=SOIL(J)
10     CONTINUE
      DO 20 J=1, JPROP
       SOLNEW(J)=LCONS3(DEFL(J), SUBG, PO)*SEG*BMWID
       SOIL(J)=(SOLNEW(J)-SOLOLD(J))*DAMP+SOLOLD(J)
20     CONTINUE
      J=J+1
      OLD=0.0
      MODE=0
100   CONTINUE
      DIFF=DEFL(J)-CLD
      IF(DIFF.LT.0.0)GOTO 200
      SOLNEW(J)=LCONS3(DEFL(J), SUBG, PO)*SEG*BMWID
      SOIL(J)=(SOLNEW(J)-SOLOLD(J))*DAMP + SOLOLD(J)
      IF(J.EQ.JSTOP)GOTO 300
      OLD=DEFL(J)
      J=J+1
      GOTO 100
200   CONTINUE
      MODE=1
      JJ=J
      ULOAD=SOIL(J)/(SCH*BMWID)
      UDISP=DEFL(J)
      DO 210 J=JJ, JSTOP
       SOLNEW(J)=UCONS1(DEFL(J), ULOAD, UDISP)*SEG*BMWID
       SOIL(J)=(SOLNEW(J)-SOLOLD(J))*DAMP + SOLOLD(J)
210    CONTINUE
      DO 250 J=1, J1
       SOIL(J)=PO*BMWID*SEG
250    CONTINUE
      DO 260 J=J2, 501
       SOIL(J)=UCONS1(DELTA, ULOAD, UDISP)*SEG*BMWID
260    CONTINUE
      GOTO 350
300   CONTINUE
      DO 310 J=1, J1
       SOIL(J)=PO*BMWID*SEG
310    CONTINUE
      DO 320 J=J2, 501
       SOIL(J)=LCONS3(DELTA, SUBG, PO)*BMWID*SEG
320    CONTINUE
350   CONTINUE
      RETURN
      END
C*****************************************************
C***  Routine to calculate propping force to give correct
C***  displacement at prop position
C*****************************************************
      SUBROUTINE PRPCAL
      COMMON RNUM(501), POSN(501), DEFL(501), DEFLIN(501), SOIL(501)
      COMMON IPOS(3), RPOS(3), REAC(2,3), BMLEN, BMWID, RL1, RL2, EI, SUBG
      COMMON DELTA, PO, SEG, SPAN, DPROP, JSTART, JSTOP, NSTOP
      COMMON DAMP, XXXX, ULOAD, UDISP
      JPROP=IPOS(3)
      DPROP=DEFL(JPROP)
      DIFF=REAC(2,3)-DPROP
      X=((RPOS(3)-RPOS(1))*SEG) + SEG/2
      P=PROP(SPAN, EI, X, DIFF)
      A=X
      DO 10 JJ=JSTART, JSTOP
       X=(RNUM(JJ)-RNUM(JSTART))*SEG+SEG/2
       V=DISP(SPAN, EI, P, A, X)
       DEFL(JJ)=DEFL(JJ)+V
10     CONTINUE
      REAC(1,3)=P
      DPROP=DEFL(IPOS(3))
      RETURN
      END
C*****************************************************
C***  Routine to calculate deflectio of simply supported
C***  beam due to set of given loads
C*****************************************************
      SUBROUTINE DSPCAL
      COMMON RNUM(501), POSN(501), DEFL(501), DEFLIN(501), SOIL(501)
      COMMON IPOS(3), RPOS(3), REAC(2,3), BMLEN, BMWID, RL1, RL2, EI, SUBG
      COMMON DELTA, PO, SEG, SPAN, DPROP, JSTART, JSTOP, NSTOP
      COMMON DAMP, XXXX, ULOAD, UDISP
      J1=JSTART-1
      J2=JSTOP+1
```